Stereocontrol of Excited-State Reactions Using Chiral Iridium Photocatalysts

By

Jesse Bertron Kidd

A dissertation submitted in partial fulfillment of

the requirements for the degree of

Doctor of Philosophy

(Chemistry)

at the

UNIVERSITY OF WISCONSIN–MADISON

2022

Date of final oral examination: January 26, 2022

The dissertation is approved by the following members of the Final Oral Committee:

Tehshik P. Yoon, Professor, Chemistry

John F. Berry, Professor, Chemistry

Clark R. Landis, Professor/Chair, Chemistry

Shannon S. Stahl, Steenbock Professor of Chemical Sciences, Chemistry

Stereocontrol of Excited-State Reactions Using Chiral Iridium Photocatalysts

Jesse Bertron Kidd

Under the supervision of Professor Tehshik P. Yoon

at the University of Wisconsin–Madison

Excited-state reactions offer mechanistically distinct pathways compared to thermal reactions, and thereby provide access to novel structural motifs that are of significant synthetic interest. This thesis details the use of a novel catalytic system designed to control the stereochemical outcome of [2+2] photocycloadditions. The intrinsic helical chirality of iridium(III) polypyridyl photocatalysts provides the key stereocontrol element; featuring a pyrazole ligand that efficiently orients a prochiral quinolone through hydrogen-bonding interactions to achieve excellent facial bias. In later work, this system was demonstrated to be useful in the enantioselective [2+2] cycloaddition between quinolones and maleimide. This reaction proceeds via Dexter energy transfer to free maleimide rather than the bound quinolone. We leveraged this unique mechanism to develop the first highly enantioselective Paternò–Büchi reaction. Optimization of this reaction required a chiral C_2-symmetric photocatalyst and slow addition of quinolone to suppress problematic racemic pathways. Lastly, the [2+2] photocycloaddition of vinyl boronate esters provided access to valuable building blocks in the synthesis of structurally diverse cyclobutanes.

Acknowledgments

At the beginning of graduate school, I expected my PI to teach me chemistry and to pointedly tell me when I am wrong. What I didn't anticipate from Tehshik was his emphasis to see the art and elegance in science. Throughout my training, he has always encouraged me to think creatively with scientific rigor, while not losing focus of the big picture narrative, the art. Perhaps this, more than anything, I will carry with me through my career. I am continually impressed by his patience and devotion to his students. Despite my constant trips to his office to present poorly structured ideas, Tehshik has always made time for insightful discussion with measured, clarifying responses.

Over the past six years, I've had the privilege of being part of the collegial atmosphere of the Chemistry Department at UW–Madison. The reason this department holds such a status is because of the brilliant and kind people here, beginning with the professors. I would like to extend a thank you to my committee members, Profs. John Berry, Clark Landis, and Shannon Stahl. They have had a profound effect on my graduate school experience through courses, seminars, casual conversations in the hallway, and their publications. I will sorely miss the innovative and unique environment at UW–Madison, but I look forward to the science that will result. Similarly, thank you to Profs. Nick Hill, Brian Esselman, and Matt Bowman to be the first people after I arrived at campus to give me confidence in my ability to do science.

The department here is privileged to have both world-class facilities, facility managers, and staff. Much of the success of the department wouldn't be possible without your continued support and devotion to your craft. I would like to thank Charlie Fry, Heike Hofstetter, Cathy Clewett, Martha Vestling, Ilia Guzei, and their assistants for your support. Without this, much of

the success of the department, including my own science, wouldn't be possible. I would also like to thank Karen Stephens for her invaluable guidance navigating graduation requirements.

I would like to extend a thank you to all Yoon group members, past and present. My time at UW–Madison has been an undoubtedly unique experience, for which I have benefited both in and outside of lab. The overabundance of affable goofballs in the group have made the daily grind of graduate school enjoyable. Additionally, my non-chemistry friends have been a welcomed source of relief during stressful times, reminding me that life exists outside of chemistry. Sam Cahoon and Steven Chapman have been invaluable in their camaraderie during our graduate school experiences. Thank you for your numerous discussions about both science and life. It was a privilege working with such a diverse crew on all my projects. Witnessing firsthand the meticulous scientific rigor of Kaz, diligent nature of Jian, Wes' detailed analytical thinking, and Spencer's resourceful creativity have all shaped my training as a scientist. I would be remiss without thanking my lab and office mates over the years. I would especially like to thank Evan, BJ, Sam Gockel, and Tahoe for the constant companionship on our daily coffee trips and occasional trek in the mountains.

Lastly, I want to acknowledge my family. Graduate school can be a somewhat stressful time, filled with ups and downs, but with your unending support I have made it to the end seemingly unscathed. Thank you to my big brother BJ, little sister Faith, Mom, Dad, and in-laws Tina and Bill for supporting me in following my passion and the many life lessons. Perhaps my biggest thanks should go to my wife Rachel. Thank you for the relentless love and support. You never stopped believing in me, even when I was unsure in myself. Over the years, you've integrated yourself as an irreplaceable group member and as such, I would like to congratulate you as well. We've both earned this.

Table of Contents

Abstract i

Acknowledgments ii

Table of Contents iv

List of Figures xi

List of Schemes xviii

List of Tables xxv

Chapter 1. Chiral Inorganic Photocatalyst Structures in Asymmetric Photochemical Synthesis 1

1.1 Introduction 2

1.2 Boron 7

1.3 Ruthenium 14

1.4 Lanthanides 19

1.5 Iridium 20

1.6 Rhodium 31

1.7 Nickel 43

1.8 Copper 45

1.9 Conclusion 53

1.10 References and Notes 55

Chapter 2. Enantioselective Excited-State Photoreactions Controlled by a Chiral Hydrogen-Bonding Iridium Sensitizer 68

2.1 Introduction 69

2.1.1 Asymmetric Secondary Photochemical Processes 69

2.1.2 Asymmetric Primary Photoreaction Processes 71

2.1.3 Asymmetric Primary Photoreactions using Transition Metal Sensitizers 76

2.2 Results and Discussion 80

2.2.1 Optimization of Hydrogen-Bonding Ligands 80

2.2.2 NMR Spectroscopy as a Tool for Optimization 82

2.2.3 Reaction Scope and Limitations 85

2.2.4 Mechanistic Investigations 88

2.3 Conclusion 92

2.4 Contributions 93

2.5 Experimental Procedures 93

2.5.1 General Information 93

2.5.2 Synthesis of Ligands 96

2.5.3 Synthesis of Iridium Complexes 104

2.5.4 Synthesis of Photocycloaddition Substrates 126

2.5.5 Reaction Optimization 153

2.5.6 Photosensitized [2+2] Cycloadditions 155

2.5.7 Determination of Absolute Stereochemistry 173

2.5.8 NMR Binding Experiments 174

2.5.9 Photophysical Measurements 182

2.5.10 Cyclic Voltammetry Data 186

2.5.11 Computational Studies 188

2.6 References and Notes 190

Chapter 3. Enantioselective Intermolecular Excited-State Photoreactions Using a Chiral Ir Triplet Sensitizer: Separating Association from Energy Transfer in Asymmetric Photocatalysis 202

3.1 Introduction 203

3.1.1 Stereocontrol of Excited-State Intermolecular Reactions 203

3.1.2 Hydrogen-Bonding Organic Photocatalysts 203

3.1.3 Chiral Lewis Acids 206

3.1.4 Prior Work 209

3.2 Results and Discussion 211

3.2.1 Optimization of Quinolone and Photocatalyst Structure 211

3.2.2 Reaction Scope and Limitations 213

3.2.3 Mechanistic Investigations 215

3.3 Conclusion and Future Directions 228

3.4 Contributions 230

3.5 Experimental Procedures 231

3.5.1 General Information 231

3.5.2 Synthesis of Photocatalysts 231

3.5.3 Synthesis of Substrates 239

3.5.4 Photosensitized [2+2] Cycloadditions 246

3.5.5 NMR Binding Experiments 259

3.5.6 Room Temperature Stern–Volmer Quenching Experiments 262

3.5.7 Kinetic Studies 263

3.5.8 Control Experiments 265

3.5.9 Transient Absorption Spectroscopy 266

3.5.10 Cyclic Voltammetry Data 271

3.5.11 Quantum yield of the parent reaction 273

3.5.12 Computational Studies 275

3.6 References and Notes 280

Chapter 4. Enantioselective Paternò–Büchi Reactions Enabled by a Chiral Iridium Photocatalyst 288

4.1 Introduction 289

4.1.1 Oxetanes in Medicinal Chemistry 289

4.1.2 Synthesis of Oxetanes 291

4.1.3 Stereocontrol of the Paternò–Büchi Reaction 293

4.1.4 Limitations in Current Enantioselective Photocatalytic Reactions 298

4.1.5 Prior Work and Mechanistic Hypothesis 300

4.2 Results and Discussion 301

4.2.1 Optimization of Reaction Conditions 301

4.2.2 Mechanistic Investigations as a Tool for Optimization 303

4.3 Conclusion and Outlook 311

4.4 Contributions 312

4.5 Experimental Procedures 313

4.5.1 General Information 313

4.5.2 Synthesis of Starting Materials 315

4.5.3 Photosensitized Cycloadditions 324

4.5.4 NMR Binding Experiments 336

4.5.5 Photophysical Measurements 339

4.5.6 Cyclic Voltammetry Data 345

4.6 References and Notes 348

Chapter 5. Construction of Complex Cyclobutane Building Blocks by Photosensitized [2+2] Cycloaddition of Vinyl Boronate Esters 357

5.1 Introduction 358

5.1.1 Strategies to Synthesize Cyclobutyl-Boronic Acid Derivatives 359

5.1.2 Photocycloadditions of Vinyl Boronate Esters and Prior Work 360

5.2 Results and Discussion 362

5.2.1 Compatibility of Boron Moieties 362

5.2.2 Reaction Scope 363

5.2.3 Diversification Reactions 364

5.2.4 Mechanistic Investigation 365

5.3 Conclusion 367

5.4 Contributions 367

5.5 Experimental Procedures 368

5.5.1 General Information 368

5.5.3 Photosensitized [2+2] Cycloadditions 391

5.5.4 Boronic Ester Functionalization 407

5.5.5 Mechanistic Studies 416

5.6 References and Notes 423

Appendix A. Investigation of Photosensitized Transposed Paternò–Büchi Reactions 431

A.1 Introduction 432

A.2 Results and Discussion 433

A.3 References 435

Appendix B. ^{1}H, ^{13}C, ^{19}F, and ^{11}B NMR Spectra of New Compounds 436

B.1 List of New Compounds for Chapter 2 437

B.2 List of New Compounds for Chapter 3 524

B.3 List of New Compounds for Chapter 4 576

B.4 List of New Compounds for Chapter 5 600

Appendix C. SFC and HPLC Chromatograms for New Compounds 662

Appendix D. X-Ray Crystallographic Data 713

D.1 X-Ray Data for Compound Λ-**2.32** 714

D.1.1 Data Collection 714

D.1.2 Structure Solution and Refinement 715

D.2 X-Ray Data for Compound **3.27f** 788

D.2.1 Data Collection 788

D.2.2 Structure Solution and Refinement 789

D.2.3 Summary 790

D.3 X-Ray Data for Compound Δ-**4.49f** 798

D.3.1 Data Collection 798

D.3.2 Structure Solution and Refinement 799

D.3.3 Summary 800

D.4 X-Ray Data for Compound **4.48i** 841

D.4.1 Data Collection 841

D.4.2 Structure Solution and Refinement 842

D.4.3 Summary 843

D.5 References 868

List of Figures

Chapter 1

Figure 1.1. Helical Chirality of Octahedral Transition-Metal Complexes 15

Figure 1.2. Chiral Bis(acetonitrile) Rh(III) Complexes 32

Chapter 2

Figure 2.1. Chiral-at-Metal Octahedral Catalysts Developed by Meggers 77

Figure 2.2. NMR Titration and Binding Plot of Λ-**2.30f** with Quinolone **2.28** at room temperature in CH_2Cl_2 83

Figure 2.3. Heat Map and Cyclometalating Ligand Optimization 84

Figure 2.4. UV-Vis absorption spectra for the association of quinolone **2.28a** and catalyst Λ-**2.32** 89

Figure 2.5. Investigation of N–H vs. N–Me Quinolones 90

Figure 2.6. Productive and Nonproductive Photocatalyst–Quinolone Adducts 91

Figure 2.7. A. Illustration of Dexter Energy Transfer **B.** Relevant Frontier Molecular Orbitals 92

Figure 2.8. NMR spectra of ligand **2.33**. 97

Figure 2.9. Representative ^1H NMR data for parent cycloadduct **2.29a** in different solvents. From top to bottom: C_6D_6, $(CD_3)_2CO$, $CDCl_3$. 156

Figure 2.10. Catalyst **2.30f** (**5f**) chemical shifts are not affected by concentration over the range examined during the titration. 174

Figure 2.11. (a) Quinolone **2.28a** chemical shifts show a slight dependence on concentration, particularly for NH (H1) and adjacent aryl CH (H8). 176

Figure 2.12. Titration of **2.28a** into **2.30f**, monitoring the chemical shift of the pyrazole NH in **2.30f**. 177

Figure 2.13. Measured and calculated binding isotherms for (a) **2.30f** in CD_2Cl_2 (b) **2.32** in CD_2Cl_2, and (c) **2.32** in 1:1 CD_2Cl_2:pentane. 178

Figure 2.14. Assignments and key correlations of (a) ^{1}H and ^{13}C NMR signals, (b) ^{19}F NMR signals, and (c) raw data for heat map of catalyst **2.30f**. 179

Figure 2.15. Titration data showing representative chemical shift changes for aryl protons. Line 1: **2.30f** only. 180

Figure 2.16. Measured and calculated binding isotherm for **2.32** with N–Me quinolone in CD_2Cl_2/pentane. 181

Figure 2.17. Absorption and emission data for iridium catalysts in CH_2Cl_2. Catalyst **2.30a**, 9.0×10^{-5} M. 183

Figure 2.18. Absorption data for representative quinolones in CH_2Cl_2. 184

Figure 2.19. Stern–Volmer experiment for the quenching of photoexcited catalyst **2.32** by quinolone **2.28a.** 185

Figure 2.20. Cyclic voltammograms of quinolone substrate **2.28a** and photocatalyst **2.32** with ferrocene added. 186

Chapter 3

Figure 3.1. Control Experiments 217

Figure 3.2. Time-Resolved Luminescence Experiments 220

Figure 3.3. DFT Optimized Structures of Hydrogen-bound Complexes for Λ–**3.28f** with **A.** Quinolone **3.25c** and **B.** Maleimide **3.26**. **C.** Gibbs Free Energy Changes During the Energy-Transfer Process. 223

Figure 3.4. Computationally Optimized Structures of Excited-State Ternary Complex [Ir–Q–M] 226

Figure 3.5. NMR titration of 3-O^{i}Pr quinolone **3.25c** to monitor dimerization. 259

Figure 3.6. NMR titration of **3.28f** with **3.25c**. 260

Figure 3.7. NMR titration of **3.28f** with maleimide. 261

Figure 3.8. Stern–Volmer Quenching Experiments between the photocalyst **3.28f** and substrates 262

Figure 3.9. Emission of photocalyst **3.28f** with different con. of quinolone **3.25c** (0, 1, 2, 3, 4 mM). 262

Figure 3.10. Stern–Volmer Quenching Experiments between the photocalyst **3.28f** and dimethyl fumarate 263

Figure 3.11. Zero order dependence on the concentration of **3.25c** 264

Figure 3.12. First-order dependence on the concentration of photocatalyst **3.28f** 264

Figure 3.13. First-order dependence on the concentration of maleimide 265

Figure 3.14. Transient absorption spectra for photocatalyst **3.28f** in CH_2Cl_2 at room temperature (left) and –78 °C at the indicated time delays after pulsed laser excitation at 440 nm 267

Figure 3.15. Left, titration of a 150 μM **3.28f** + 10 mM quinolone **3.25c** solution with increasing concentrations of maleimide **3.26** (**2**) (CH_2Cl_2). 268

Figure 3.16. Taped Schlenk tube 274

Figure 3.17. Absorbance of the photocatalyst **3.28f** solution. 275

Chapter 4

Figure 4.1. Oxetane-Containing Natural Products 289

Figure 4.2. Oxetanes as Versatile Tools in Medicinal Chemistry 290

Figure 4.3. NMR Titration Binding and Job Plot 304

Figure 4.4. Steady-State Luminescence Quenching Plots 305

Figure 4.5. Time-Resolved Luminescence Quenching Plots 307

Figure 4.6. The radiance spectra of the PR150-Kessil lamps used 314

Figure 4.7. Measured and calculated association constants for **4.49f** and **4.47** in toluene-*d*8/CD_2Cl_2 (2:1) 336

Figure 4.8. Measured and calculated association constants for **4.49f** and **4.44f** in toluene-*d*8/CD_2Cl_2 (2:1) 337

Figure 4.9. NMR titration of **4.47** with **4.44a**, probing for ground-state interactions 338

Figure 4.10. The absorbance and emission spectra of photocatalyst **4.49f**. 339

Figure 4.11. Absorbance and emission of **4.44f** sparged and under air 340

Figure 4.12. Absorbance spectra of **4.47** (top) and **4.44f** (middle) at varying concentrations 341

Figure 4.13. Steady-State Stern–Volmer experiment for the quenching of photoexcited catalyst **4.49f** by quinolone **4.47** (left) and **4.44f** (right) 342

Figure 4.14. Box diagram of the experimental setup for time-resolved emission studies 344

Figure 4.15. First-order decay of excited state α-ketoester substrates (left) and measured lifetimes (right) 344

Figure 4.16. Cyclic voltammograms of quinolone substrate **4.47** and α-ketoester **4.44f** with ferrocene added 345

Figure 4.17. Cyclic voltammograms of photocatalyst **4.49f** 346

Chapter 5

Figure 5.1. Cyclobutane Containing Natural Products and Medicines 358

Figure 5.2. Probing the Participation of the Vinyl Boronate Ester Triplet State 366

Figure 5.3. The emission spectrum of a H150 Blue Kessil lamp used for visible-light photoreactions. 369

Figure 5.4. Isomerization experiment of **5.35** (**28**) using photocatalyst **5.23** as a photosensitizer. 417

Figure 5.5. Isomerization experiment of **5.35** (**28**) using thioxanthone as a photosensitizer. 418

Figure 5.6. Isomerization experiment of **5.35** (**28**) using xanthone as a photosensitizer at 350 nm. 419

Figure 5.7. Stern–Volmer experiment for the quenching of photoexcited catalyst **5.23** by title substrate **5.24a**. 420

Figure 5.8. Stern–Volmer experiment for the quenching of photoexcited catalyst **5.23** by compound **5.35**. 421

Figure 5.9. Cyclic voltammogram of title substrate **5.24a** and with ferrocene added. 422

Appendix A

Figure A.1. Steady-State Stern–Volmer experiment for the quenching of photoexcited catalyst **4.49f** by benzophenone 434

Appendix D

Figure D.1. A molecular drawing of the Ir1 complex shown with 40% probability ellipsoids 716

Figure D.2. A molecular drawing of the Ir2 complex shown with 40% probability ellipsoids 717

Figure D.3. A molecular drawing of the B1 anion shown with 30% probability ellipsoids 718

Figure D.4. A molecular drawing of the B2 anion shown with 30% probability ellipsoids 719

Figure D.5. The content of the asymmetric unit shown with 30% probability ellipsoids. 720

Figure D.6. A molecular drawing of the $C_{31}H_{18}F_{10}IrN_6$ complex in Δ-**4.49f** shown with 50% probability ellipsoids. 801

Figure D.7. A molecular drawing highlighting the H-bonding interactions between the Ir complex and the two ether molecules in Δ-**4.49f** shown with 50% probability ellipsoids. 802

Figure D.8. A molecular drawing of the disordered ether molecule in Δ-**4.49f** shown with 50% probability ellipsoids. 803

Figure D.9. A molecular drawing of the $[C_{32}H_{12}BF_{24}]^-$ anion in Δ-**4.49f** shown with 50% probability ellipsoids. 804

Figure D.10. A molecular drawing of the $[C_{32}H_{12}BF_{24}]^-$ anion with 50% probability ellipsoids and all components of the disordered CF_3 groups shown. 805

Figure D.11. A molecular drawing of Δ-**4.49f** shown with 50% probability ellipsoids and selected atoms labeled. 806

Figure D.12. A molecular drawing of the first symmetry-independent molecule of **4.48i** shown with 50% probability ellipsoids. 844

Figure D.13. A molecular drawing of the second symmetry-independent molecule of **4.48i** shown with 50% probability ellipsoids. 845

Figure D.14. A molecular drawing of the two symmetry-independent molecule of **4.48i** superimposed. 846

Figure D.15. A molecular drawing of the asymmetric unit of **4.48i** shown with 50% probability ellipsoids. 847

List of Schemes

Chapter 1

Scheme 1.1. Racemic Photoreaction Processes 3

Scheme 1.2. Exciplex Formation 4

Scheme 1.3. General Mechanisms of Enantiocontrol by Chiral Inorganic Chromophores 5

Scheme 1.4. Primary Versus Secondary Photoreactions 6

Scheme 1.5. Bathochromic Shift of α,β-Unsaturated Carbonyls upon Lewis Acid Coordination 7

Scheme 1.6. Enantioselective [2+2] Photocycloadditions of Coumarins 8

Scheme 1.7. Enantioselective [2+2] Photocycloadditions of 5,6-Dihydro-4-pyridones 9

Scheme 1.8. Enantioselective [2+2] cycloaddition of 3-Alkenyloxy-2-cycloalkenones 11

Scheme 1.9. Intermolecular Enantioselective [2+2] Cycloaddition 11

Scheme 1.10. Enantioselective *ortho*-Photocycloaddition with Low Catalyst Loadings of Chiral Oxazaborolidine Lewis Acids 12

Scheme 1.11. Enantioselective Oxa-di-π-methane Rearrangement via a Singlet Excited State 13

Scheme 1.12. ON/OFF Photooxygenation Catalysis 14

Scheme 1.13. Enantioselective PET to $Co(acac)_3$ from Δ-$Ru(bpy)_3^{2+}$ 15

Scheme 1.14. Stereoselective PET to $Co(acac)_3$ with Chiral $Ru(bpy)_3^{2+}$ Photocatalysts 17

Scheme 1.15. Effect of Helical Chirality on Enantioselective PET and Photoderacemization of $Co(acac)_3$ 17

Scheme 1.16. Stereoselective PET to Chiral Methyl Viologens 18

Scheme 1.17. Atroposelective Synthesis of Binapthols 19

Scheme 1.18. Stereoselective Energy Transfer 19

Scheme 1.19. Enantioselective [2+2] Photocycloadditions Using Chiral Tb(III) Complexes 20

Scheme 1.20. Chiral-at-Metal Ir(III) Photocatalysts Used in Asymmetric Secondary Photoreactions 21

Scheme 1.21. Proposed Catalytic Cycle Using Chiral Bis(acetonitrile) Ir(III) Complexes 22

Scheme 1.22. Enantioselective Net-oxidative Mannich Reaction of 2-Acylimidazoles 23

Scheme 1.23. Enantioselective Couplings of Trifluoromethyl Ketyl Radicals and α-Aminoradicals 23

Scheme 1.24. Stereoselective Photoreactions using a Chiral Hydrogen-Bonding Ligand 24

Scheme 1.25. Enantioselective Alkylation using Supramolecular Iridium Photoaminocatalyst 25

Scheme 1.26. Enantioselective Intramolecular [2+2] Photocycloaddition with a Chiral Hydrogen-Bonding Iridium Photosensitizer 26

Scheme 1.27. Enantioselective [2+2] Photocycloaddition via Energy Transfer Rebound Mechanism 27

Scheme 1.28. Enantioselective Paternó–Büchi Reaction using a Chiral Iridium Photocatalyst 28

Scheme 1.29. Asymmetric 6π-Electrocyclization and [2+2] Photocycloaddition 28

Scheme 1.30. Asymmetric Photocatalysis Using Iridium-Chiral Borate Ion Pairs 29

Scheme 1.31. Cooperative Stereoinduction in Asymmetric Photocatalysis 30

Scheme 1.32: Asymmetric C–C Cross-Couplings Enabled by (η^3-allyl)Iridium(III) Photocatalyst 31

Scheme 1.33. Enantioselective α-Amination using Chiral-at-Metal Rhodium Photocatalysts 33

Scheme 1.34. Asymmetric Radical Additions Catalyzed by Chiral Rhodium Catalysts 34

Scheme 1.35. Lewis Acid Effects and Mode of Enantioinduction 35

Scheme 1.36. Enantioselective Radical–Radical Coupling Reaction of 2-Acyl-Imidazoles/Pyrazoles and α-Ketoesters 36

Scheme 1.37. Enantioconvergent Coupling of Racemic α-Chloroketones and *N*-Arylglycines 36

Scheme 1.38. Photocatalytic α-Deracemization of 2-Pyridylketones 37

Scheme 1.39. Enantioselective [3+2] Cycloaddition of Cyclopropyl Ketones with Alkenes and Alkynes 38

Scheme 1.40. Enantioselective Excited-State [2+2] Cycloaddition with Chiral Rhodium Complexes via Chromophore Activation 39

Scheme 1.41. Regio- and Enantioselective Formation of Head-to-Tail Cyclobutanes 40

Scheme 1.42. Enantioselective [2+2] Photocycloaddition of α,β-Unsaturated Sulfones 41

Scheme 1.43. Enantioselective [3+2] Photocycloaddition Between *N*-Cinnamoylpyrazoles and Vinylazides 42

Scheme 1.44. Enantioselective Hetero-Diels–Alder Reaction via Chromophore Activation 43

Scheme 1.45. Stereoselective Oxidation of β-Ketoesters by a Thioxanthone-Tethered Nickel Lewis Acid 44

Scheme 1.46. Asymmetric Radical Addition Enabled by Bifunctional Nickel Catalyst 45

Scheme 1.47. Enantioselective PET Using Chiral Cu(I) Complexes 46

Scheme 1.48. Asymmetric PET to Cobalt Complexes Using Chiral Cu(I) Complexes 46

Scheme 1.49. Application of Chromophore Activation to an Enantioselective 6π-Photoelectrocyclization 47

Scheme 1.50. Enantioconvergent Ullman C–N Coupling with a Chiral Phosphine–Cu(I) Catalyst 47

Scheme 1.51. Enantioselective Three-Component Coupling Using a Chiral Copper Photocatalyst 48

Scheme 1.52. Enantioselective Dual Carbofunctionalization of Styrenes 49

Scheme 1.53. Asymmetric Decarboxylative Alkynylation with Terminal Alkynes 50

Scheme 1.54. Visible Light Induced Enantioselective C(sp^3)-alkylation of Glycine Ester Derivatives 50

Scheme 1.55. Stereoselective Radical Addition Using a Dual-Purpose Copper Photocatalyst 51

Scheme 1.56. Stereoselective Radical Addition into Imines by a Bifunctional Copper Catalyst 52

Scheme 1.57. Asymmetric Aerobic Cross-Dehydrogenative Coupling 52

Scheme 1.58. Photoinduced Copper-Catalyzed Asymmetric C–O Cross-Coupling 53

Chapter 2

Scheme 2.1. Photochemically Generated Radical Using Dual-Catalytic Approach 70

Scheme 2.2. Examples of Downstream Asymmetric Secondary Photoreactions 71

Scheme 2.3. Photochemical deracemization via Exciplex Formation 73

Scheme 2.4. Enantioselective [2+2] Cycloaddition using Chiral Hydrogen-Bonding Photocatalyst 74

Scheme 2.5. Enantioselective [2+2] Cycloaddition Using Chiral Xanthone Photocatalyst 75

Scheme 2.6. Enantioselective [2+2] Photocycloaddition with Chiral Biaryl Thiourea 76

Scheme 2.7. Asymmetric Secondary Photoreaction using Chiral-at-Metal Photocatalyst 78

Chapter 3

Scheme 3.1. Enantioselective Intermolecular [2+2] of Pyridones and Acetylenedicarboxylates 204

Scheme 3.2. Intermolecular [2+2] Cycloaddition Catalyzed by a Thioxanthone Sensitizer 205

Scheme 3.3. Intermolecular [2+2] Cycloaddition Using Chromophore Activation 206

Scheme 3.4. Triplet Lowering Mechanism Enabled by Dual Catalytic Strategy 207

Scheme 3.5. Chromophore Activation Using Chiral Rhodium Lewis Acids 209

Scheme 3.6. Enantioselective Intramolecular [2+2] Cycloaddition Using Chiral Ir Photocatalyst 210

Scheme 3.7. Possible Mechanistic Scenarios 218

Scheme 3.8. Proposed Mechanism for the Enantioselective Intermolecular [2+2] Photocycloaddition 228

Chapter 4

Scheme 4.1. General Strategies for Oxetane Synthesis 291

Scheme 4.2. Initial Discovery and Generalized Mechanism of the Paternò–Büchi Reaction 292

Scheme 4.3. Regio- and Diastereoselectivity of the Paternò–Büchi Reaction 294

Scheme 4.4. Chiral Induction Using Chiral Carbonyl Substrates 295

Scheme 4.5. Chiral Induction Using Chiral Alkene Substrates 297

Scheme 4.6. Diastereoselective Paternò–Büchi Reaction Using Hydrogen–Bonding Template 298

Scheme 4.7. Paternò–Büchi Reaction and *ortho*-Photocycloaddition of 2-Napthaldehyde 299

Scheme 4.8. Divergent Photocatalytic Reactions of α-Ketoesters 300

Scheme 4.9. Mechanistic Hypothesis of an Enantioselective Catalytic Paternò–Büchi Reaction 301

Scheme 4.10. Possible Scalemic Product Forming Pathways 308

Scheme 4.11. Possible Racemic Pathways 310

Chapter 5

Scheme 5.1. Synthesis of Cyclobutyl Boronic Acid Derivatives 359

Scheme 5.2. Photochemical [2+2] Cycloadditions of Vinyl Boronate Ester Derivatives 360

Scheme 5.3. Photosensitized [2+2] Cycloadditions of Styrenes and 1,3-Dienes 361

Scheme 5.4. C–B Derivatization of **5.25a** into Highly Functionalized Cyclobutane Scaffolds 365

Appendix A

Scheme A.1. Proposed of Transposed Paternò–Büchi Reaction 432

Scheme A.2. Examples of Transposed Paternò–Büchi Reactions 433

Scheme A.3. Proof-of-Concept Transposed Paternò–Büchi Reactions 434

List of Tables

Chapter 2

Table 2.1. Optimization of Hydrogen-Bonding Ligand 81

Table 2.2. Quinolone Reaction Scope 86

Table 2.3. Alkene Scope 87

Table 2.4. Solvent screen with initial catalyst **2.30a** 153

Table 2.5. Effect of temperature in several different solvents 153

Table 2.6. Optimization with final catalyst **2.32**. 154

Table 2.7. Control experiments and scaled-up reaction 154

Table 2.8. Computed energies of the optimized geometries 189

Chapter 3

Table 3.1. Optimization Studies for the Intermolecular [2+2] Photocycloaddition 212

Table 3.2. Scope of Asymmetric Intermolecular [2+2] Cycloadditions 214

Table 3.3. Proof-of-Principle Experiments with Cinnamamides 230

Table 3.4. Parameters Extracted from Biexponential Equation and Equilibrium Constant at –78 °C in CH_2Cl_2 269

Table 3.5. Comparison of different functionals to evaluate triplet energies 277

Table 3.6. Comparison of experimental triplet energies with computed values for known Ir(III) photocatalysts 278

Chapter 4

Table 4.1. Optimization of the Chiral Photocatalyst Structure 302

Table 4.2. Effects of Sterics and Oxygen on Diastereoselectivity and Enantioselectivity 303

Table 4.3. Slow Addition Experiments and Final Optimization 311

Table 4.4. Evaluation of Chiral Photocatalyst Structure 324

Table 4.5. Evaluation of C_2-symmetric Photocatalysts 325

Table 4.6. Evaluation of Cyclometalating Ligand on pypz catalyst using **4.44g** 325

Table 4.7. Solvent Screen using **4.44g** and Λ-**4.49f** at –25 °C 326

Table 4.8. Effect of Solvent and Temperature 326

Chapter 5

Table 5.1. Examining Boron Moiety Compatibility for Triplet Sensitization with **5.23** 362

Table 5.2. Scope Studies for the Sensitized [2+2] Cycloaddition of Vinyl Boronate Esters 364

Appendix D

Table D.1. Crystal data and structure refinement for **2.32**. 721

Table D.2. Atomic coordinates (x 10^4) and equivalent isotropic displacement parameters (Å^{2}x 10^3) for **2.32**. 722

Table D.3. Bond lengths [Å] and angles [°] for **2.32** 736

Table D.4. Anisotropic displacement parameters (Å^{2}x 10^3) for **2.32**. 763

Table D.5. Hydrogen coordinates (x 10^4) and isotropic displacement parameters (Å^{2}x 10^3) for **2.32**. 768

Table D.6. Torsion angles [°] for **2.32** 772

Table D.7. Hydrogen bonds for **2.32** [Å and °]. 787

Table D.8. Crystal data and structure refinement for Yoon53. 790

Table D.9. Fractional Atomic Coordinates ($\times 10^4$) and Equivalent Isotropic Displacement Parameters ($Å^2 \times 10^3$) for Yoon53. 791

Table D.10. Anisotropic Displacement Parameters ($Å^2 \times 10^3$) for Yoon53. 792

Table D.11. Bond Lengths for Yoon53. 794

Table D.12. Bond Angles for Yoon53. 794

Table D.13. Hydrogen Bonds for Yoon53. 795

Table D.14. Torsion Angles for Yoon53. 795

Table D.15. Hydrogen Atom Coordinates ($Å \times 10^4$) and Isotropic Displacement Parameters ($Å^2 \times 10^3$) for Yoon53 797

Table D.16. Crystal data and structure refinement for Δ-**4.49f**. 807

Table D.17. Fractional Atomic Coordinates ($\times 10^4$) and Equivalent Isotropic Displacement Parameters ($Å^2 \times 10^3$) for Δ-**4.49f** 808

Table D.18. Anisotropic Displacement Parameters ($Å^2 \times 10^3$) for Δ-**4.49f** 815

Table D.19. Bond Lengths for Δ-**4.49f** 820

Table D.20. Bond Angles for Δ-**4.49f** 824

Table D.21. Hydrogen Bonds for Δ-**4.49f** 829

Table D.22. Torsion Angles for Δ-**4.49f** 829

Table D.23. Hydrogen Atom Coordinates ($Å \times 10^4$) and Isotropic Displacement Parameters ($Å^2 \times 10^3$) for Δ-**4.49f** 836

Table D.24. Atomic Occupancy for Δ-**4.49f** 839

Table D.25. Crystal data and structure refinement for **4.48i** 848

Table D.26. Fractional Atomic Coordinates ($\times 10^4$) and Equivalent Isotropic Displacement Parameters ($Å^2 \times 10^3$) for **4.48i** 849

Table D.27. Anisotropic Displacement Parameters ($Å^2 \times 10^3$) for **4.48i**. 852

Table D.28. Bond Lengths for **4.48i** 855

Table D.29. Bond Angles for **4.48i** 857

Table D.30. Hydrogen Bonds for **4.48i** 860

Table D.31. Torsion Angles for **4.48i** 861

Table D.32. Hydrogen Atom Coordinates ($Å \times 10^4$) and Isotropic Displacement Parameters ($Å^2 \times 10^3$) for **4.48i**. 865

Chapter 1. Chiral Inorganic Photocatalyst Structures in Asymmetric Photochemical Synthesis

Portions of this work have been published previously:

Genzink, M. J.; Kidd, J. B.; Swords, W. B.; Yoon, T. P. Chiral Photocatalyst Structures in Asymmetric Photochemical Synthesis. *Chem. Rev*. **2021**, https://doi.org/10.1021/acs.chemrev.1c00467

1.1 Introduction

The chirality of a molecule can have a profound influence on its biological and physical properties. Methods that produce enantiomerically enriched products from achiral starting materials are therefore of particular importance for the synthesis of a variety of materials, including drug molecules, agrochemicals, and polymers. The 2001 Nobel Prize for Chemistry, awarded for the development of the field of asymmetric catalysis, underscores the centrality of this problem in contemporary synthetic chemistry.[1–3] Several decades of sustained interest in enantioselective reaction method development has resulted in the elucidation of a large number of structurally diverse chiral catalyst architectures that effectively control stereochemical outcomes in almost every class of synthetically important transformation.

Photochemical reactions offer a conspicuous exception to this general trend. The emergence of general strategies for enantioselective catalytic photoreactions is a relatively recent development, and the variety of organic photoreactions that can be conducted in a highly enantioselective manner remains comparatively limited. This is despite the long fascination chemists have had with light-promoted reactions, both because of the distinctive reactive intermediates that are most readily available by photochemical activation, and because photochemical reactions often result in topologically complex molecular architectures that can be synthesized in no other way.[4–6] It stands to reason, therefore, that there exist complications specific to enantioselective catalytic photochemical reactions in comparison to better-established asymmetric ground-state reactions. Correspondingly, the chiral catalyst structures that have proven to be most effective in asymmetric photochemistry have often been structurally unique.

One central challenge common to all areas of asymmetric catalysis is the problematic participation of racemic background processes. Product-forming reaction pathways that occur

outside of the stereodifferentiating environment of a chiral catalyst necessarily result in racemic products. Thus, no matter how enantioselective a catalytic process might be, the enantioselectivity of the overall reaction is diminished if background processes are competitive. There are two features specific to photochemical activation that are uniquely challenging in this regard (Scheme 1.1). The first is the possibility of *competitive direct photoexcitation*. If an achiral substrate molecule directly absorbs light under the conditions of a catalytic photoreaction, the resulting photoexcited species can react to give racemic product prior to interacting with the chiral catalyst. Second, many of the most widely exploited photocatalytic systems operate via *collisional activation mechanisms*. When a photocatalyst activates an organic substrate by a diffusional photoinduced electron transfer (PET) or triplet energy-transfer (EnT) event, the encounter complex is typically short-lived. If dissociation of the deactivated photocatalyst and activated substrate is faster than the rate of subsequent bond formation, any chiral information associated with the photocatalyst cannot influence the stereochemical outcome of the reaction.

Scheme 1.1. Racemic Photoreaction Processes

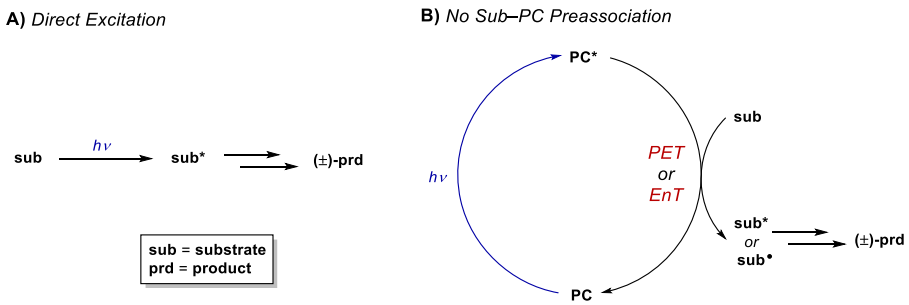

Thus, early investigations of catalytic asymmetric photochemistry that introduced chiral elements into well-studied organic sensitizers met with limited success.[7,8] Examples that resulted in measurable stereoinduction generally involved the formation of an exciplex, where a donor–acceptor interaction between the substrate and excited-state photocatalyst results in the formation of a longer-lived excited-state complex (Scheme 1.2). Because the exciplex extends the

lifetime of the encounter complex, product-formation can occur within the chiral environment of the photocatalyst. These studies provided a valuable proof-of-principle for the possibility of photocatalytic stereoinduction but suffered from low enantiomeric excess (ee) due to ill-defined substrate–catalyst interactions and relatively short exciplex lifetimes.

Scheme 1.2. Exciplex Formation

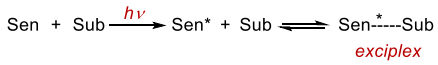

Expanding upon the concept of prolonging the interaction between the chiral catalysts and the substrate, a preassociation principle was originally articulated for macromolecular photoactive hosts by Inoue[9] and extended for small molecule asymmetric photocatalysis by Krische.[10] This principle argues that the participation of background product-forming pathways will be minimized when a chiral photocatalyst is capable of binding the substrate in the ground state. If the substrate in the complex is excited — either by direct excitation or sensitization — more readily than the free substrate, and if the rate of the photoreaction is faster than the rate of disassociation of the complex, then product formation will predominantly occur within the chiral environment of the photocatalyst with minimal competition from racemic background processes. Krische's seminal example utilized a chiral hydrogen-bonding domain appended to an organic photosensitizer as an effective catalyst to both ensure preassociation and to confer a kinetic advantage for the reaction, however, many other strategies have been reported since.

For more than a decade, the field of photochemical synthesis has experienced an exceptional growth of interest which is in part a result of the implementation of inorganic photocatalysts. These complexes, compared to their organic counterparts, are advantageous due to their widely varied and highly modular structures, which offer opportunities for unique reactivity. As such, many modes to control the stereochemical outcome of photochemical reactions have been uncovered.

These include *chromophore activation*, where coordination of a chiral catalyst to a substrate results in a new compound with altered light-absorbing properties; *association-induced PET*, where photon absorption is followed by a redox cascade generating reactive radicals that react with a ground-state activated substrate; and *organometallic photocatalysis*, where the formation of a new coordination complex engenders product-forming photochemical processes within the coordination sphere of the metal center (Scheme 1.3). The research area of asymmetric photochemistry has been the subject of several previous reviews.[11–20]

Scheme 1.3. General Mechanisms of Enantiocontrol by Chiral Inorganic Chromophores

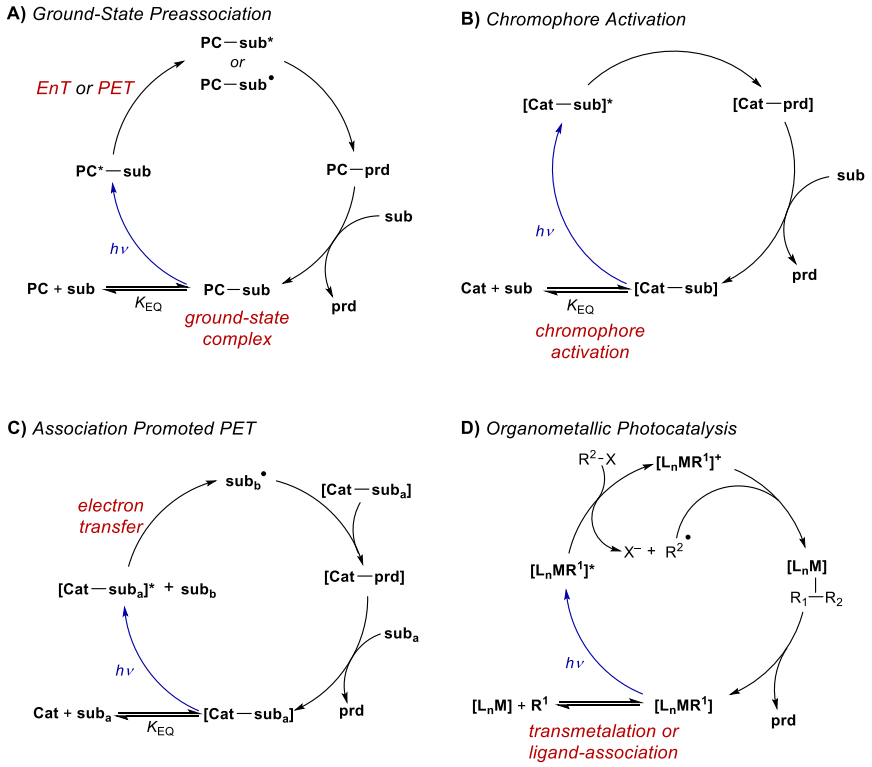

The term "photocatalysis" has been used in a somewhat ambiguous fashion throughout the literature of synthetic photochemistry. For the purposes of this review, we adopt a broad definition of photocatalysis and cover any enantioselective catalytic reaction where the stereoinducing chiral catalyst forms part of the light-absorbing complex, regardless of the photophysical properties of

the species in isolation. We exclude from this treatment dual-catalytic reactions where the chromophore and the chiral stereoinducing co-catalyst are separate molecular entities; this topic has been reviewed previously.[21] The scope of this review also excludes examples of chiral photo-activated complexes, in which photolysis of a precatalyst initiates a stereoselective thermal process.

There are also important distinctions that can be made among the mechanisms of photocatalytic reactions involving the nature of the reactive intermediates participating in the key bond-forming events. *Primary photoreactions* are those that involve bond-forming processes of organic compounds in their electronically excited states.[22] These are distinct from *secondary photoreactions*, in which the key bond-forming processes are those of photochemically generated reactive intermediates such as radicals or radical ions in their electronic ground states (Scheme 1.4). While the reactivity patterns available from primary and secondary photoreactions differ significantly, it can sometimes be challenging to unambiguously determine which is operative in a given photoreaction. This review thus covers both classes of photocatalytic reactions, and the organization of the topics centers on the central element of the inorganic chiral catalyst rather than on mechanistic considerations.

Scheme 1.4. Primary Versus Secondary Photoreactions

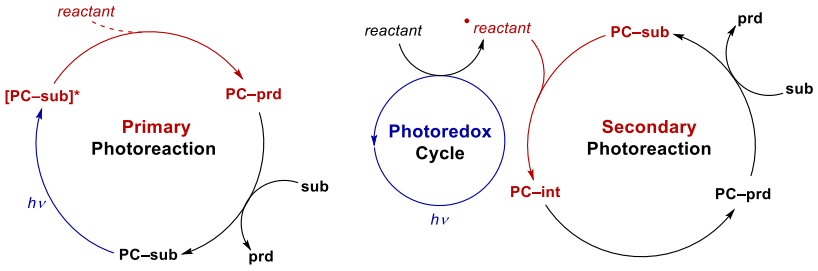

1.2 Boron

Lewis acids have been studied extensively for their ability to influence the outcomes of a wide range of ground-state transformations. Their effect on photochemical reactions has received considerably less attention. In 1910, Praetorius and Korn described a uranyl chloride accelerated [2+2] photodimerization of α,β-unsaturated ketones.[23] Alcock later showed that $SnCl_4$ exhibits a similar effect, suggesting that many Lewis acids might have a general effect in photochemical transformations.[24] In more recent work, Lewis and Barancyk performed a detailed study of the Lewis acid promoted [2+2] photocycloaddition of coumarin with 2,3-dimethyl-2-butene.[25,26] While little product was formed in the absence of Lewis acid, addition of 50 mol% of various Lewis acid catalysts led to a large enhancement of product formation. The most active catalyst tested was $AlBr_3$, which yielded complete conversion to the cycloadduct. Mechanistically, Lewis proposed that the binding of a Lewis acid alters the electronic structure of the enone, which in the case of coumarin manifests as a bathochromic shift in the complex's absorption profile (Scheme 1.5).

Scheme 1.5. Bathochromic Shift of α,β-Unsaturated Carbonyls upon Lewis Acid Coordination

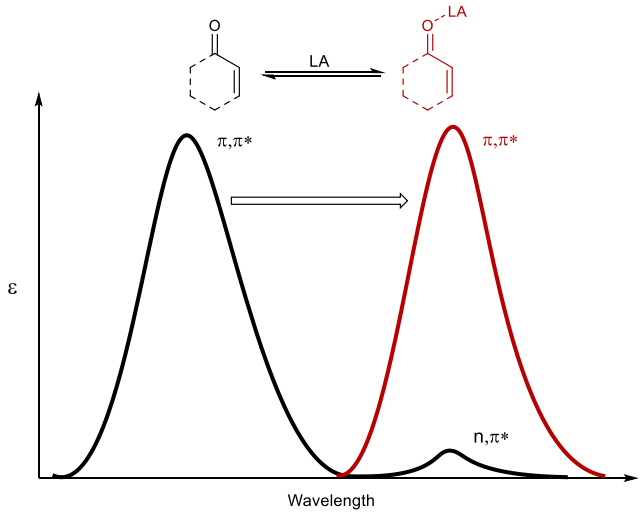

Bach has described this phenomenon as "chromophore activation"[27,28] and proposed that it could be exploited in the design of Lewis acid catalyzed asymmetric photoreactions. Irradiation at wavelengths that maximize the selective photoexcitation of a chiral catalyst–substrate complex over the free α,β-unsaturated carbonyl in solution ensures that reaction occurs within the chiral environment of the Lewis acid, while minimizing direct racemic photoreaction. The initial report demonstrating the feasibility of this concept examined the intramolecular photocycloaddition of coumarin **1.1** (Scheme 1.6).[29] The reaction proceeds sluggishly upon irradiation at 366 nm due to the low extinction coefficient of the coumarin. In line with the proposed chromophore activation mechanism, addition of simple boron or aluminum Lewis acids red-shift the (π,π*) absorption, greatly accelerating product formation upon irradiation, highlighting that Lewis acids can indeed increase photoreaction rates. Moreover, the use of chiral oxazaborolidine Lewis acid **1.3** provides the cycloadduct in 82% yield and a remarkable 62% ee, which could be increased to 82% ee at –75 °C.[30] At lower concentrations (20 mol%) of oxazaborolidine catalyst **1.3**, however, the ee was diminished due to direct excitation of the weak (n,π*) absorption of free coumarin.

Scheme 1.6. Enantioselective [2+2] Photocycloadditions of Coumarins

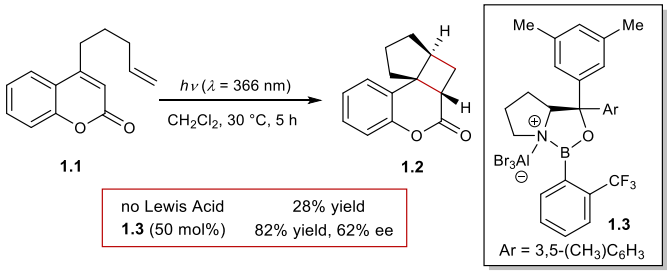

Mechanistic studies provided further insights into the origins of the catalytic effect.[31] When the coumarin substrate is irradiated in the absence of a Lewis acid, the cycloaddition is stereospecific, where starting from either the tethered (*E*) or (*Z*)-alkene leads to distinct diastereomers. This is consistent with reaction through a singlet excited state. Upon addition of a

Lewis acid, the quantum yield (Φ) of the photocycloaddition increases by an order of magnitude. Importantly, under these conditions the cycloaddition becomes stereoconvergent, indicating that the reaction proceeds through a triplet excited state. The Lewis acid promoted increase in efficiency was attributed to the presence of a heavy atom that facilitates intersystem crossing to the coumarin triplet excited state, which proceeds to the cycloadduct more efficiently than the shorter-lived singlet coumarin.

Exploring the generality of this strategy, Bach and coworkers investigated the enantioselective [2+2] photocycloaddition of the synthetically useful class of 5,6-dihydro-4-pyridones (Scheme 1.7).[32] In contrast to their previous work, enone **1.4** undergoes a more pronounced bathochromic shift when coordinated to a Lewis acid. The authors reasoned that this red shift in combination with a longer wavelength light source would enable selective excitation of the bound species, thus eliminating racemic background reactivity. This proved correct and yielded highly selective cycloadditions (up to 90% ee). In addition, one of the products (**1.6**) was utilized as a key intermediate in the total synthesis of (+)-lupinine and the formal synthesis of (+)-thermopsine.

Scheme 1.7. Enantioselective [2+2] Photocycloadditions of 5,6-Dihydro-4-pyridones

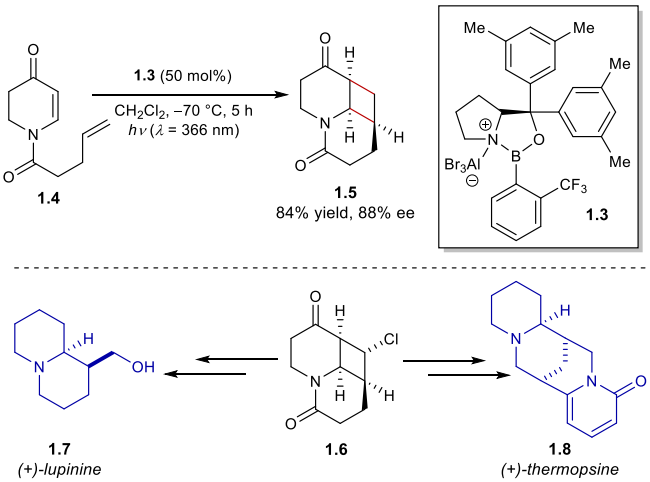

Despite the superficial similarities of coumarin **1.1** and dihydropyridone **1.4**, there are several intriguing differences in the mechanisms of their Lewis acid catalyzed [2+2] photocycloadditions. First, the dihydropyridone substrates undergo stereoconvergent cyclization with and without Lewis acid, consistent with the formation of a triplet excited state in both cases. In contrast to the coumarin substrates, the quantum yield of the dihydropyridone cycloaddition decreases from 0.23 to 4 x 10^{-3} in the presence of a Lewis acid. It is therefore surprising that high enantioselectivity is achieved given that after excitation, free pyridone cyclizes significantly more efficiently than catalyst-bound pyridone. However, this highlights the importance of the change in the absorption spectrum of the Lewis acid complex. Because almost all photons are absorbed by the Lewis acid-bound dihydropyridone upon irradiation at 366 nm, the relatively inefficient stereoselective cyclization still outcompetes the racemic direct excitation pathway. Bach's mechanistic proposals for both the coumarin and dihydropyridone cycloadditions were consistent with computational studies conducted by Dolg[33] and Chen.[34]

The ability to afford highly enantioenriched cyclobutane products from a chemo- and regioselective [2+2] photocycloaddition of simple cyclic enones and alkenes is a highly desirable goal. To this end, Bach and coworkers studied the enantioselective [2+2] photocycloaddition of 3-alkenyloxy-2-cycloalkenones (**1.9**) (Scheme 1.8).[35] For this [2+2] photocycloaddition, modified $AlBr_3$-activated oxazaborolidine **1.10** proved to be ideal, delivering the simple aliphatic cyclobutane products in nearly quantitative yield and up to 94% ee. The utility of these products was showcased through acid-catalyzed allylation and ring expansion reactions that afforded **1.14** and **1.15** without erosion of enantioselectivity.

Scheme 1.8. Enantioselective [2+2] cycloaddition of 3-Alkenyloxy-2-cycloalkenones

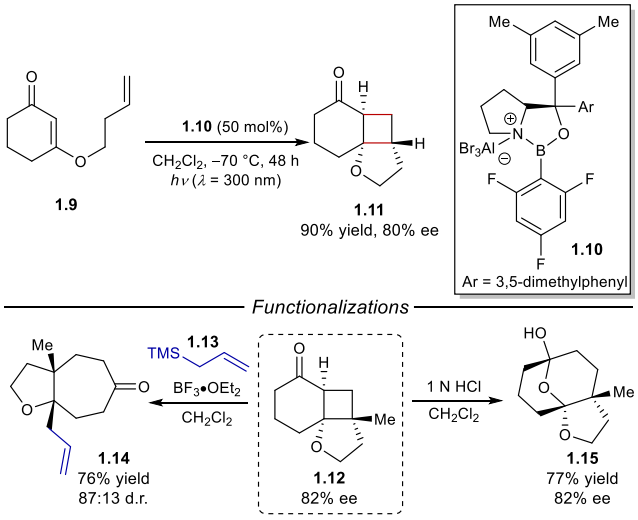

The intermolecular photocycloaddition of cyclohexanones with alkenes has played an important role in the history of total synthesis.[36] Bach and coworkers expanded the chromophore activation strategy to intermolecular cycloadditions of simple cyclohexenones with a range of terminal alkenes (Scheme 1.9).[37] The synthetic utility of the enantioenriched cyclobutane products was showcased in a concise 6-step synthesis of the enantiopure monoterpene (–)-grandisol. Interestingly, the uncatalyzed reaction affords a mixture of regioisomers, while the use of chiral Lewis acid **1.19** results in the exclusive formation of the head-to-tail regioisomer. This observation was rationalized as the result of increased polarization of the excited-state enone–Lewis acid complex, which improves the selectivity for initial bond formation.

Scheme 1.9. Intermolecular Enantioselective [2+2] Cycloaddition

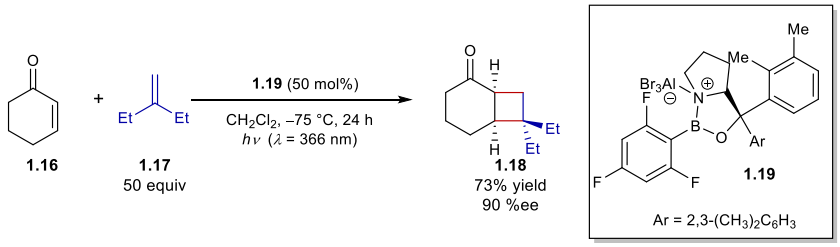

In each of the previous examples, coordination of a Lewis acid to an α,β-unsaturated carbonyl compound results in a bathochromic shift of the (π,π*) absorption band that typically overlaps with the (n,π*) absorption band of the free substrate. Consequently, relatively high catalyst loadings (50 mol%) are required to outcompete racemic uncatalyzed photoreaction of the free substrate. If however the (π,π*) absorption could be further shifted beyond the (n,π*) absorption, one might expect lower catalyst loadings to be effective. Bach noted that the addition of $EtAlCl_2$ to phenanthrene-9-carboxaldehyde **1.20** results in such a shift. When oxazaborolidine **1.22** was used to catalyze its photocycloaddition with tetramethylethylene (**1.21**), the corresponding *ortho*-photocycloadduct **1.23** was produced in high enantioselectivity (94% ee) using only 10 mol% of the catalyst (Scheme 1.10).[38]

Scheme 1.10. Enantioselective *ortho*-Photocycloaddition with Low Catalyst Loadings of Chiral Oxazaborolidine Lewis Acids

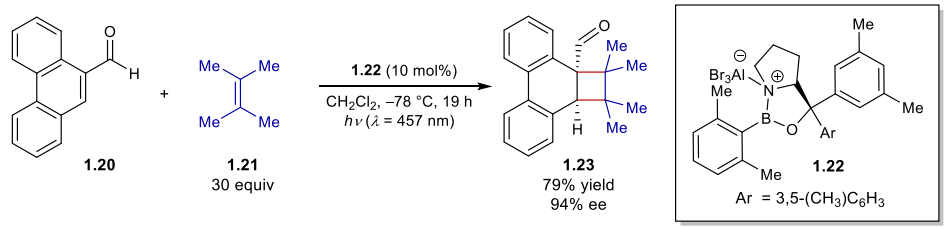

Many of the enone cycloadditions described above require a relatively slow, symmetry-forbidden $S_1(\pi,\pi^*) \rightarrow T_1(\pi,\pi^*)$ intersystem crossing (ISC) event.[39] The corresponding uncatalyzed photoreactions, on the other hand, involve a faster symmetry-allowed $S_1(n,\pi^*) \rightarrow T_1(\pi,\pi^*)$ ISC. In this scenario, the more efficient ISC of the free excited-state substrate further challenges the ability to outcompete the racemic background reaction. Thus, Bach and coworkers sought to optimize a photochemical enone reaction that occurs from the singlet excited state, removing the complication of slow ISC and in turn allowing for lower Lewis acid catalyst loading. Inspired by work of Griffiths [40] and more recent precedent by Ramamurthy, [41] they investigated the

oxa-di-π-methane rearrangement of 2,4-cyclohexadienone **1.25** to bicyclic ketone **1.26** (Scheme 1.11).[42] Indeed, this reaction was shown to proceed with high enantioselectivity (92–97% ee) at low chiral catalyst loadings (10 mol%). Computational experiments suggest that the population of the triplet hypersurface is minimized due to a conical intersection on the singlet surface.

Scheme 1.11. Enantioselective Oxa-di-π-methane Rearrangement via a Singlet Excited State

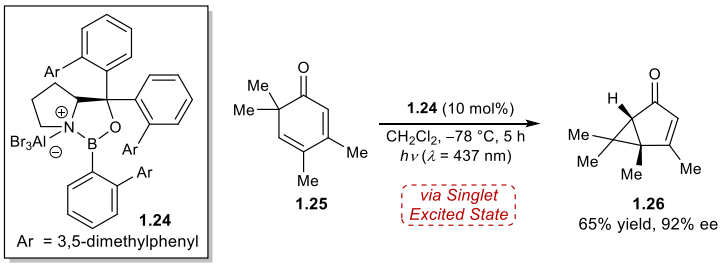

Coeffard recently described a chiral photocatalyst for stereoselective α-oxygenation reactions that includes boron in the photosensitizing unit.[43] The catalyst (**1.27**) consists of a BODIPY photosensitizer covalently tethered to a chiral cinchona alkaloid. The quinuclidine moiety of the catalyst is proposed to serve two roles. First, it activates 1,3-dicarbonyl substrate **1.28** through deprotonation and provides a chiral environment for the resulting enolate through hydrogen-bonding. Additionally, the lone pair of the unprotonated quinuclidine is a competent scavenger for $^1O_2$ when the substrate is not bound. As a result, the local concentration of photogenerated $^1O_2$ is enriched when the substrate is bound and depleted when it is not, further minimizing the possibility of racemic background oxygenation. In practice, this system catalyzed the formation of α-hydroxylation product **1.29** from the corresponding β-dicarbonyl substrate in 40% ee. Coeffard uses the term "on/off" photooxygenation to reflect the dual roles of the quinuclidine nitrogen (Scheme 1.12).

Scheme 1.12. ON/OFF Photooxygenation Catalysis

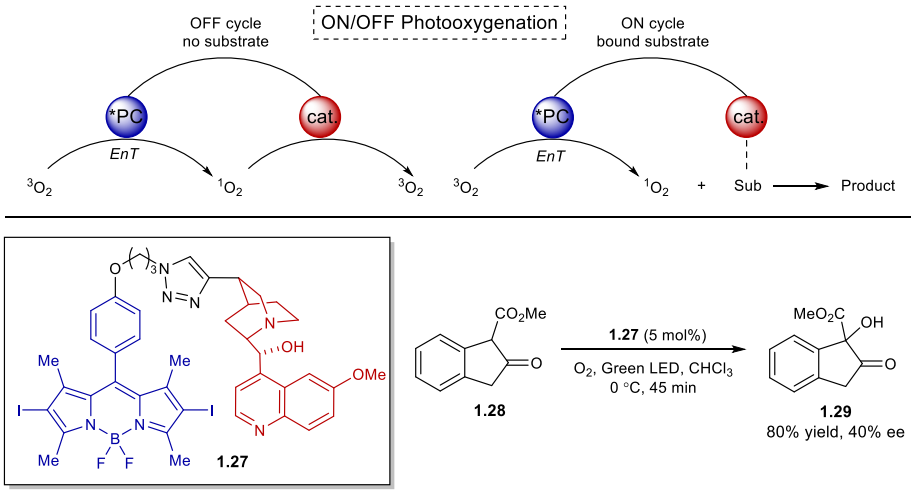

1.3 Ruthenium

Many structurally diverse photocatalysts have proven to be useful in a range of important transformations. Recent developments in the field of synthetic photochemistry, however, have centered on the use of transition-metal chromophores, including the canonical $Ru(bpy)_3^{2+}$ (bpy = 2,2'-bipyridine) photocatalyst. These complexes are attractive because they generally feature large molar extinction coefficients, high intersystem crossing quantum yields, and long-lived excited states. Moreover, the excited-state energies and redox properties of photoactive coordination complexes can often be readily tuned by modulating the structures of the supporting ligands without adversely affecting their photophysical properties. The homoleptic $Ru(bpy)_3^{2+}$ chromophore possesses D_3 symmetry and can be resolved into two enantiomeric forms, denoted as Λ or Δ (Figure 1.1).[44] Stereoinduction from the metal-centered stereochemistry of chiral coordination complexes has been the topic of significant recent interest.[45,46] Interestingly, despite their widespread use as synthetic photocatalysts, the study of chiral enantiopure transition metal chromophores in asymmetric photocatalysis was limited until quite recently.[47]

Figure 1.1. Helical Chirality of Octahedral Transition-Metal Complexes

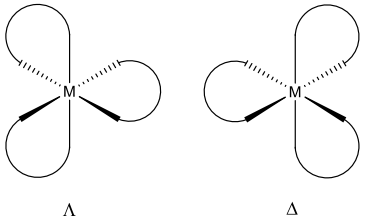

Early studies by Geselowitz and Taube demonstrated that ground-state, outer-sphere electron transfer from racemic $Co(edta)^{2-}$ (edta = ethylenediaminetetraacetate) to enantiomerically enriched $Os(bpy)_3^{3+}$ results in the formation of the oxidized Co(III) complex in 2.9% ee.[48] Similar effects were observed using other inorganic complexes of cobalt, iron, and ruthenium.[49] These studies provided proof-of-principle examples that the helical chirality of octahedral metal centers could be stereoinducing in electron-transfer processes. The first example of an enantioselective photoinduced electron transfer was reported in 1979 by Porter and Sparks, who found that enantioenriched Δ-$Ru(bpy)_3^{2+}$ preferentially reduces Λ-$Co(acac)_3$ (acac = acetylacetone) over the Δ enantiomer.[50] The relative rate constants (k_r) for the reduction of Λ- and Δ-$Co(acac)_3$ were determined to be 1.08:1 by monitoring the circular dichroism (CD) of the unreacted Co(III) starting material. Kobayashi and coworkers subsequently determined a similar ratio of 1.19:1 from luminescence quenching measurements (Scheme 1.13).[51] The analogous enantioselective photoreduction of $Co(oxox)_3^{3-}$ (oxox = oxalate) was studied by Kato, Kimura, and coworkers, with a maximum reported selectivity ratio of 1.32:1.[52]

Scheme 1.13. Enantioselective PET to $Co(acac)_3$ from Δ-$Ru(bpy)_3^{2+}$

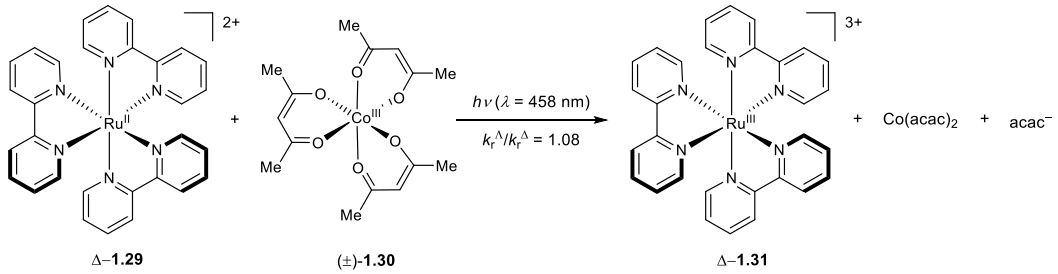

Although the stereochemical configuration of Δ- or Λ-Ru(bpy)$_3^{2+}$ is stable to electron transfer [53] and to heating, [54] photoracemization is known to occur from its excited state (Φ_{rac} = 2.88 x 10^{-4}).[55] Thus, the reported selectivity for the enantiodiscriminating electron transfer might be artificially diminished due to photoracemization of the catalyst over the course of the reaction. To minimize the influence of competitive photoracemization, Ohkubo and coworkers developed catalysts bearing stable chiral substituents on the bipyridine ligands. These complexes, Ru((–)-menbpy)$_3^{2+}$ (**1.32**) and Ru(PhEtbpy)$_3^{2+}$ (**1.33** and **1.34**), exhibit similar absorption and emission profiles, are slightly more oxidizing compared to Ru(bpy)$_3^{2+}$, and notably have racemization quantum yields substantially lower than Ru(bpy)$_3^{2+}$ (4.0 x 10^{-6} and 7.6 x 10^{-6}, respectively). [56] Ru(PhEtbpy)$_3^{2+}$ proved relatively unselective (1.05:1) for the reduction of Co(acac)$_3$. [57] On the other hand, Ru((–)-menbpy)$_3^{2+}$ preferentially quenches (k_q) Δ-Co(acac)$_3$ in a 1.33:1 ratio (Scheme 1.14).[58]

An investigation of the influence of the metal stereocenter revealed a significant impact (Scheme 1.15). Ohkubo prepared the diastereomerically pure Λ-Ru((–)-menbpy)$_3^{2+}$ isomer and showed that its selectivity for photoreduction of Co(acac)$_3$ was higher than that of the unresolved 1:1 mixture of Λ- and Δ-Ru((–)-menbpy)$_3^{2+}$ (Scheme 1.15).[58, 59] Thus, while some degree of selectivity is controlled by the chirality of the bipyridyl ligands and Ru metal center, the overall selectivity of the reaction is almost entirely driven by the macroscopic helicity of the complex. [60] Interestingly, the ee of the overall photoreduction (k_r) was found to be substantially larger than that of solely the electron-transfer quenching process (k_q). The authors proposed that while the Ru(III) species may be reduced by acac$^-$ or solvent to reform the ground-state Ru(II) photocatalyst, back electron transfer (BET) from Co(II) to Ru(III) is competitive and enantioselective. This strategy was used to develop a kinetic resolution of Co(acac)$_3$, achieving 39% ee at 40% conversion.[61]

Notably, in a later study Ohkubo discovered that the addition of exogenous acetylacetone (Hacac) had a beneficial effect on the selectivity of BET to reform Λ/Δ-Co(acac)$_3$; a remarkable $k_r^{\Delta}/k_r^{\Lambda}$ of 91.9 was obtained in the presence of 10 equiv of Hacac (Scheme 1.15).[62]

Scheme 1.14. Stereoselective PET to Co(acac)$_3$ with Chiral Ru(bpy)$_3^{2+}$ Photocatalysts

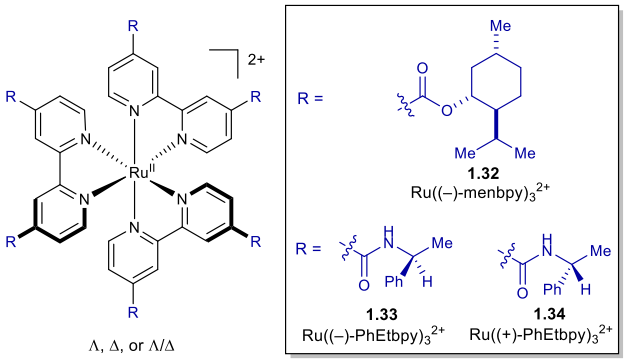

$$Ru(R_2bpy)_3^{2+} + Co(acac)_3 \xrightarrow[EtOH/H_2O\ (70\%\ v/v)]{h\nu\ (\lambda > 400\ nm)} Ru(R_2bpy)_3^{3+} + Co(acac)_2 + acac^-$$

Catalyst	$k_q^{\Delta}/k_q^{\Lambda}$
Λ/Δ-**1.32**	1.33
Λ-**1.33**	1.05
Δ-**1.34**	1.06

Scheme 1.15. Effect of Helical Chirality on Enantioselective PET and Photoderacemization of Co(acac)$_3$

$$Ru(menbpy)_3^{2+} + Co(acac)_3 \xrightarrow[90\%\ EtOH/H_2O]{h\nu\ (\lambda > 400\ nm)} Ru(menbpy)_3^{3+} + Co(acac)_2 + acac^-$$

Catalyst	$k_q^{\Delta}/k_q^{\Lambda}$	$k_r^{\Delta}/k_r^{\Lambda}$
Δ-**1.32**	1.28	14.7
Λ/Δ-**1.32** (1:1 d.r.)	1.14	1.67
Δ-**1.32**	–	91.9[a]

[a] 10 equiv of acetylacetone (Hacac) added.

Proposed Mechanism

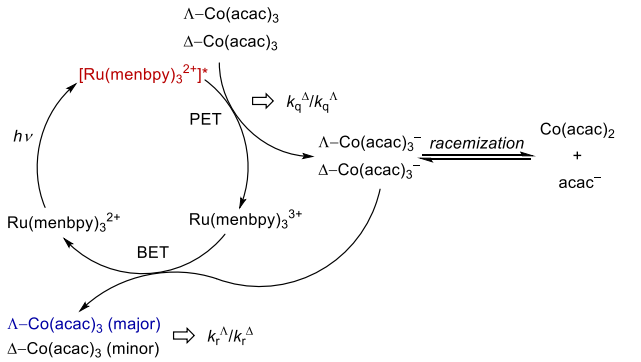

Methyl viologen, a pyridinium dication, is an efficient quencher of photoexcited $Ru(bpy)_3^{2+}$. Several groups have examined the effect of chiral viologens on the rate of electron transfer from Λ- and Δ-$Ru(bpy)_3^{2+}$. Using partially enantioenriched Λ- and Δ-$Ru(bpy)_3^{2+}$ Rau and Ratz studied the photoreduction of viologen **1.35**, finding a significant difference in the rate of quenching ($k_q^{\Lambda}/k_q^{\Delta} = 1.66$).[63,64] In related studies, Tsukahara and coworkers investigated selective quenching using viologens featuring chiral *sec*-arylethylamine units (Scheme 1.16).[65] Photoexcited Δ-$Ru(bpy)_3^{2+}$ is preferentially quenched by viologen (*S*,*S*)-**1.36** over its enantiomer ($k_q^{(S,S)}/k_q^{(R,R)} = 1.27$). Interestingly, the naphthyl substituted viologens (**1.37**, **1.38**) quench the photocatalyst by both static and dynamic pathways, the former arising from attractive π-π interactions with ground-state Δ-$Ru(bpy)_3^{2+}$. Despite this, viologens **1.37** and **1.38** quenched with lower stereoselectivity ($k_q^{(S,S)}/k_q^{(R,R)} = 1.16$ and 1.11 respectively).

Scheme 1.16. Stereoselective PET to Chiral Methyl Viologens

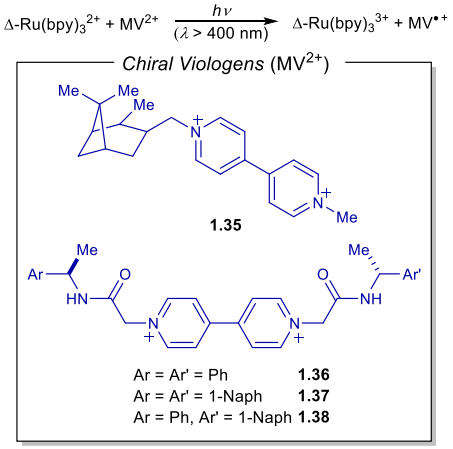

Ohkubo also demonstrated that the Δ-**1.32** enables the atroposelective synthesis of binaphthols (Scheme 1.17).[66,67] This reaction proceeds by initial oxidation of the photoexcited Δ-$Ru((-)\text{-menbpy})_3^{2+}$ by $Co(acac)_3$ to generate a Ru(III) complex, which subsequently oxidizes naphthol and initiates oxidative coupling to afford binaphthol in 16% ee.

Scheme 1.17. Atroposelective Synthesis of Binapthols

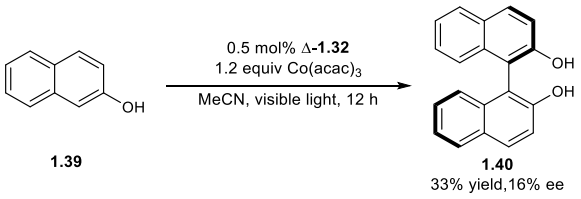

1.4 Lanthanides

Stereoselective energy transfer processes have also been investigated using chiral metal coordination complexes. Brittain observed that energy transfer between amino acid-bound Tb(III) and Eu(III) complexes exhibited different efficiencies depending on the enantiopurity of the amino acid ligand.[68,69] Later, Metcalf, Richardson, and coworkers investigated energy transfer from a racemic $Tb(dpa)_3^{3-}$ photocatalyst to enantiopure Δ-$Ru(phen)_3^{2+}$.[70] In these reactions, the Tb(III) complex absorbs UV light, and the resulting enantiomeric excited-state lanthanides are quenched by the enantiopure Ru(II) acceptor at different rates (Scheme 1.18). The stereoselectivity of the quenching process was monitored by observing the luminescence of the $[Tb(dpa)_3^{3-}]^*$ excited state, which exhibited a significant circular polarization (CP) consistent with preferential quenching of the Λ isomer by Δ-$Ru(phen)_3^{2+}$. Subsequent investigations examined chiral discrimination in energy transfer using complexes with varied metal centers[71–73] and their supporting ligands,[74,75] in which the highest selectivity ($k_q^{\Delta}/k_q^{\Lambda}$ = 7.21) was recorded for the quenching of photoexcited Δ- and Λ-$Eu(dpa)_3^{3-}$ by diastereomeric Δ-Co((*S*,*S*)-*trans*-1,2-cyclohexadiamine)$_3^{3+}$.[76]

Scheme 1.18. Stereoselective Energy Transfer

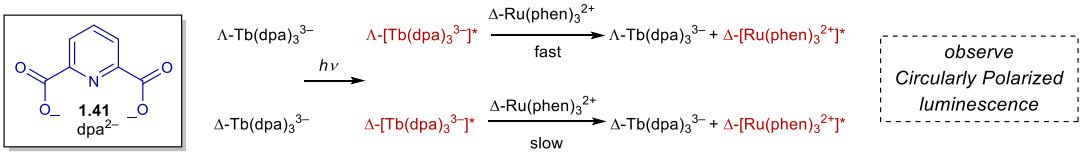

More recently, Liu and Feng disclosed a chromophore activation strategy using a chiral Tb(III) complex to promote [2+2]-photocycloadditions of 2-cinnamoylpyridine **1.42** in excellent

enantioselectivity (Scheme 1.19).[77] Mechanistic experiments revealed that addition of a mixture of $Tb(OTf)_3$ and chiral *N*,*N*'-dioxide ligand **1.44** to 2-cinnamoylpyridine **1.42** results in a bathochromic shift in the UV-Vis absorption spectrum, indicating the formation of a new photoactive species. The authors hypothesized that the rate of intersystem crossing of excited-state **1.42** is accelerated by paramagnetic and heavy-atom effects from Tb(III).

Scheme 1.19. Enantioselective [2+2] Photocycloadditions Using Chiral Tb(III) Complexes

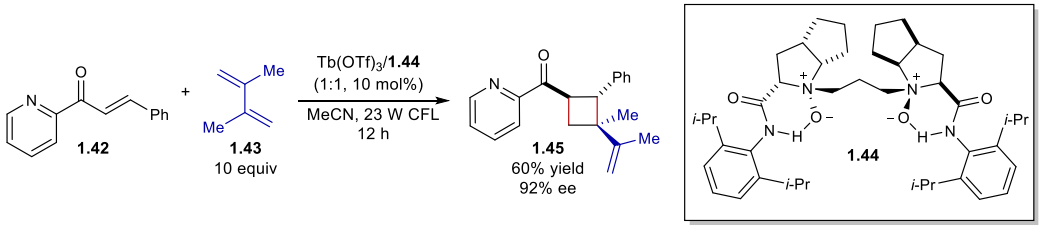

1.5 Iridium

Meggers pioneered the use of helically chiral iridium(III) polypyridyl complexes as enantioselective catalysts for a variety of synthetically important transformations. These catalysts can be easily prepared in stereochemically pure form using a chiral auxiliary approach[78] and have shown to be resistant to racemization.[79] Initial studies involved iridium complexes featuring ligands modified with organic functional groups that could act as organocatalysts, using the metal-centered stereocenter as a stereocontrolling element. These investigations resulted in the development of highly enantioselective transfer hydrogenations,[80] Friedel–Crafts alkylations,[81] sulfa-Michael and aza-Henry reactions,[82] and α-amination reactions.[83]

Cyclometallated Ir(III) complexes are among the most widely utilized photocatalysts in contemporary synthetic photochemistry. Meggers hypothesized that chiral-at-metal Ir(III) complexes could serve a dual purpose as both enantioselective catalysts and photocatalysts.[84] Chiral bis(acetonitrile) Ir(III) complex Λ-**1.46b** was designed to be a Lewis acid catalyst that becomes photoactive upon coordination of a bidentate Lewis basic substrate. Meggers' initial

investigations demonstrated that Λ-**1.46b** successfully mediates the highly enantioselective photoalkylation of 2-acylimidazolyl ketones with benzyl (**1.47**) and phenacyl bromide (**1.48**) radical precursors, yielding α-alkylated substrates in superb enantioselectivities up to 99% ee (Scheme 1.20). In subsequent work, Λ-**1.46b** and modified analogue Λ-**1.46c** proved to be effective chiral photocatalysts for enantioselective α-trichloromethylations[85] of both *N*-phenyl 2-acylimidazoles (**1.49**) and 2-acylpyridines (**1.50**) and α-perfluoroalkylations (**1.51**, **1.52**)[86] of 2-acylimidazoles. Moreover, Meggers later showed that similar stereocontrolled radical addition reactions could be carried out in a one-pot, two-step procedure where the chirality is induced during a dimethylpyrazole-accelerated asymmetric transfer hydrogenation reaction.[87,88]

Scheme 1.20. Chiral-at-Metal Ir(III) Photocatalysts Used in Asymmetric Secondary Photoreactions

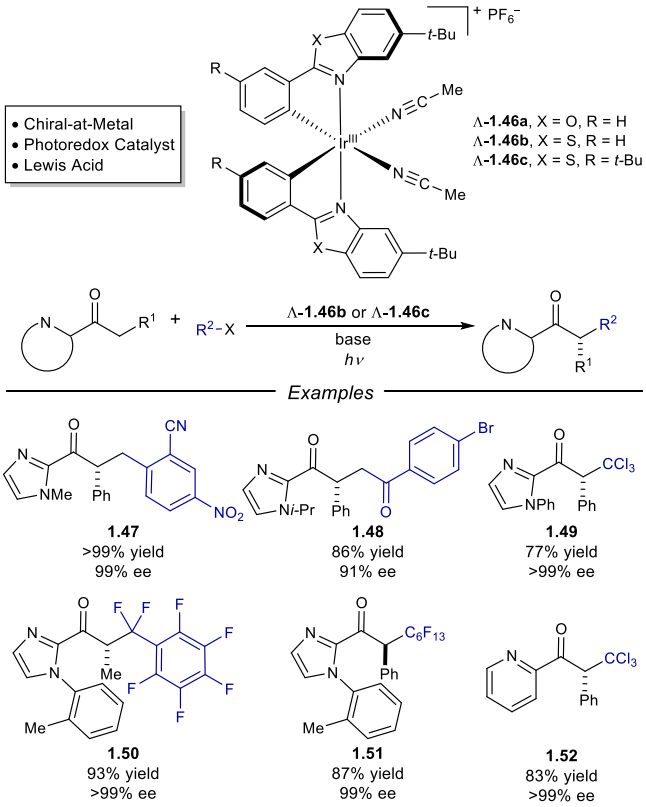

Several experiments were conducted to understand the mechanism of these reactions (Scheme 1.21). First, in many cases the benzothiazole complexes (Λ-**1.46b**) were found to provide superior asymmetric induction compared to the benzoxazole congeners (Λ-**1.46a**). This effect was attributed to the longer C–S bond distance, which results in an increase in the steric profile of the two *tert*-butyl groups proximal to the site of substrate coordination.[79,80] Second, X-ray crystallography verified that the substitutionally labile acetonitrile ligands are displaced by a bidentate substrate without loss of the stereochemical integrity of the metal center; deprotonation by an exogenous base affords the corresponding chiral enolate complex (**1.53**). Stern–Volmer luminescence quenching studies and electrochemical measurements were consistent with the role of this complex as the active photocatalyst that absorbs visible light to become a photoreductant capable of one-electron reduction of electron-deficient alkyl bromides. An Ir(III) Lewis acid catalyzed radical addition is followed by ketyl radical oxidation to reform the photoredox catalyst and provide the enantioenriched alkylation products. While a closed catalytic cycle was proposed, the possibility of a radical-chain mechanism was not ruled out.

Scheme 1.21. Proposed Catalytic Cycle Using Chiral Bis(acetonitrile) Ir(III) Complexes

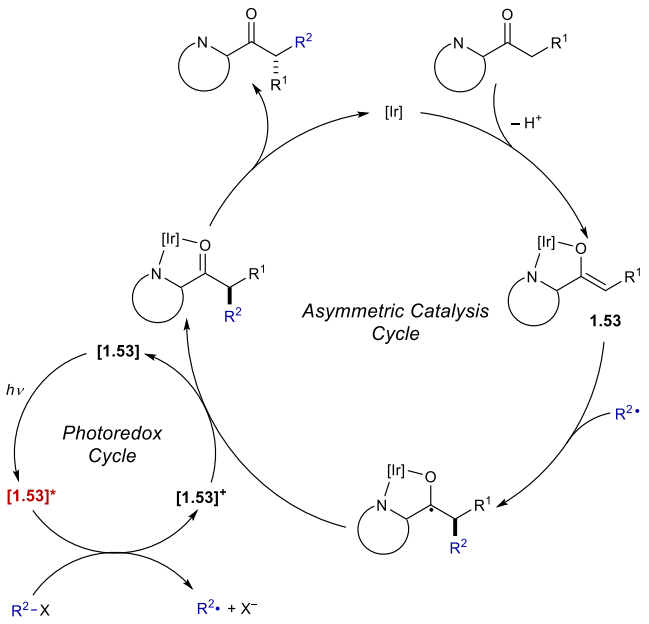

In subsequent work, Meggers reported that these substrate-bound chiral-at-metal complexes can also function as photooxidants, facilitating the desilylative oxidation of α-silyl amines (Scheme 1.22).[89] The resulting electron-rich α-aminoradicals undergo oxidation in the presence of oxygen to afford electrophilic iminium cations, which can react with the iridium enolate to afford Mannich adducts (**1.56**) in high enantioselectivity (97% ee). In this example, the Λ-**1.46a** catalyst proved to be superior to Λ-**1.46b** due to its increased oxidizing power. Nucleophilic α-aminoradicals can also be generated from deprotonation of photogenerated amine radical cations; Meggers demonstrated that these could engage in productive enantioselective radical–radical recombination with Ir-bound trifluoromethyl ketyl radicals to afford valuable 1,2-aminoalcohols (Scheme 1.23).[90]

Scheme 1.22. Enantioselective Net-oxidative Mannich Reaction of 2-Acylimidazoles

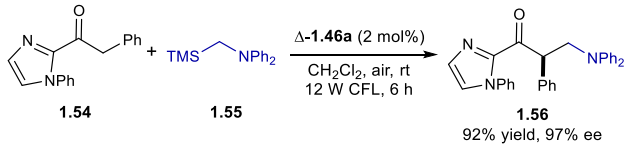

Scheme 1.23. Enantioselective Couplings of Trifluoromethyl Ketyl Radicals and α-Aminoradicals

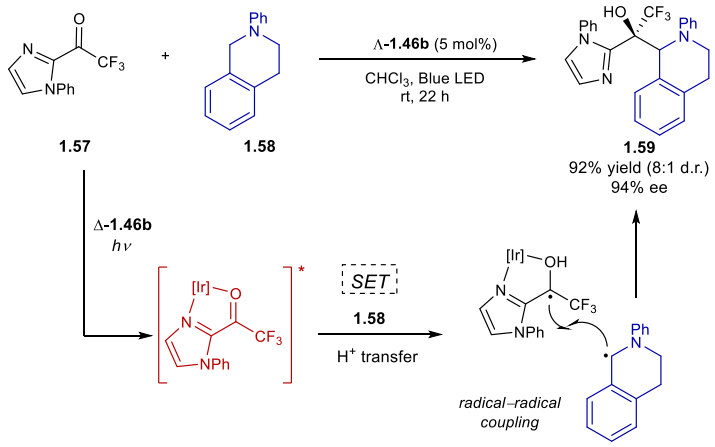

As previously discussed, Bach has studied the use of a Kemp's triacid derived chiral lactam functionalized with a xanthone or thioxanthone sensitizer to develop a variety of enantioselective

photoreactions. Bach recently prepared an iridium photocatalyst bearing a modified bipyridine ligand functionalized with a similar chiral lactam moiety and studied its ability to influence the stereochemistry of electron- and energy-transfer photoreactions (Scheme 1.24).[91] In contrast to the work of Meggers, however, the stereochemistry of the Ir(III) center was not controlled, and the photocatalytic assembly was used as a mixture of diastereomers. A model reductive cyclization of tertiary α-bromocarbonyl **1.60** unfortunately suffered from competitive hydrodebromination, and the expected cyclization product was formed in modest yields. The authors attributed the low enantioselectivity of this reaction (<10% ee) to a non-catalytic radical chain process. An energy-transfer reaction in which a chain mechanism is not feasible was more successful; the photosensitized rearrangement of spiroepoxide **1.64** afforded ketone **1.65** in 29% ee.

Scheme 1.24. Stereoselective Photoreactions using a Chiral Hydrogen-Bonding Ligand

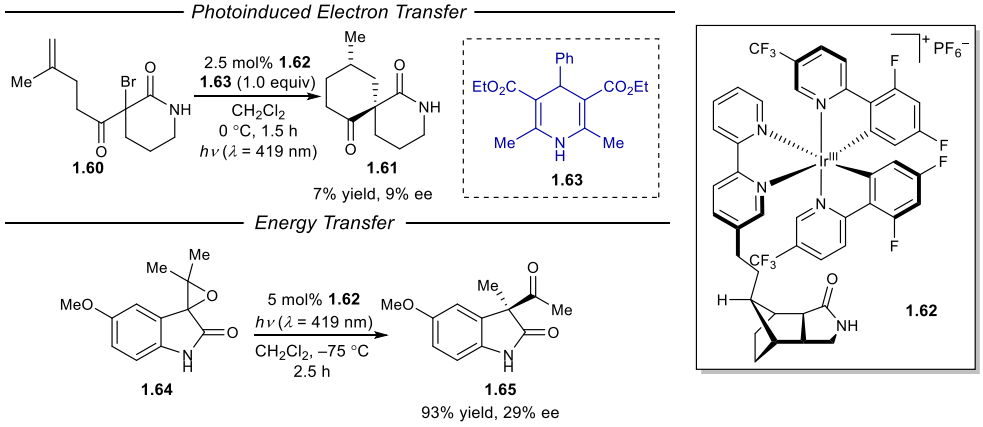

Inspired by MacMillan's seminal asymmetric organocatalytic photoredox alkylation,[Error! Bookmark not defined.] Ceroni, Lombardo, and Cozzi designed an alternate supramolecular photocatalyst that tethers an imidazolidinone organocatalyst to an iridium sensitizer (Scheme 1.25).[92] As in the previous example, the stereochemistry about the metal center was not controlled; instead, efficient enantiofacial bias relies solely upon the chirality of the amine catalyst. Under optimized conditions photocatalyst **1.69** afforded product **1.68** in 84% yield and 70% ee. Interestingly, the authors noted

lower yield and enantioselectivity (57% yield and 59% ee) when the corresponding organocatalyst and photocatalyst were separated into their individual components. This decreased performance demonstrates how controlling the spatial proximity of the independent catalysts can improve the efficiency of the overall process.

Scheme 1.25. Enantioselective Alkylation using Supramolecular Iridium Photoaminocatalyst

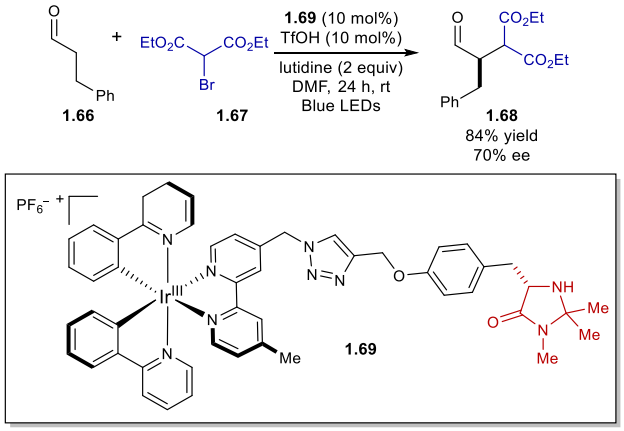

Inspired by Meggers' precedential work, Yoon and Baik developed chiral iridium photosensitizer Λ-**1.72** functionalized with a hydrogen-bonding domain that can control the enantioselectivity of an excited-state [2+2] photocycloaddition (Scheme 1.26).[93] The design of this photocatalyst incorporates a pyridylpyrazole ligand capable of recruiting quinolone substrate **1.70** through a secondary-sphere hydrogen-bonding interaction. Under optimal conditions, cyclobutane product **1.71** can be isolated in near quantitative yield and 91% ee. Interestingly, computational analysis revealed a stereochemical model involving an unusual hydrogen bond between the amide group of the quinolone and the N–H of the pyrazole moiety, in addition to a π–π interaction between the cyclometalated ligand on the photocatalyst and substrate. Importantly, these non-covalent interactions facilitate both the orbital overlap necessary for triplet energy transfer to the quinolone and rationalize the absolute stereoinduction observed in the intramolecular reaction with the pendant alkene. Further discussion of this work can be found in Chapter 2.

Scheme 1.26. Enantioselective Intramolecular [2+2] Photocycloaddition with a Chiral Hydrogen-Bonding Iridium Photosensitizer

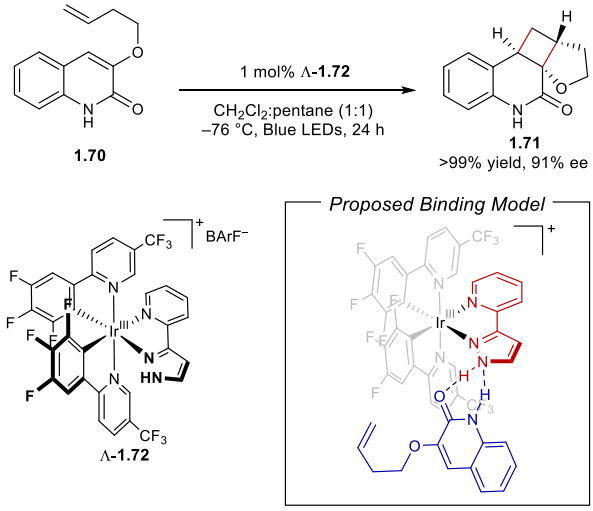

Following this report, Yoon, Baik, and Meyer extended this approach to the intermolecular [2+2] photocycloaddition of 3-isopropoxy quinolone **1.73** with maleimide **1.74**. The optimal conditions for this reaction involved modified chiral photocatalyst Λ-**1.76**, which results in the formation of cyclobutane **1.75** in high yield and 97% ee (Scheme 1.27).[94] Interestingly, a combination of NMR, steady-state luminescence quenching, and transient absorption studies revealed an unexpected mechanism in which the chiral photocatalyst selectively binds quinolone **207** but preferentially sensitizes maleimide **1.74** through a collisional energy-transfer process. The triplet excited state maleimide then reacts with the bound quinolone enantioselectively to form the product in a rebound-like mechanism. DFT calculations suggested that the lowest-energy binding interaction between the photocatalyst and quinolone was substantially different than in the intramolecular case, and that the favored binding geometry lacks the orbital overlap necessary for efficient intracomplex Dexter energy exchange. Consistent with this proposal, an N–Me quinolone (**1.77**) incapable of engaging in N–H-to-pyrazole hydrogen bonding affords reasonable enantioselectivity in this reaction. Further discussion of this work can be found in Chapter 3.

Scheme 1.27. Enantioselective [2+2] Photocycloaddition via Energy Transfer Rebound Mechanism

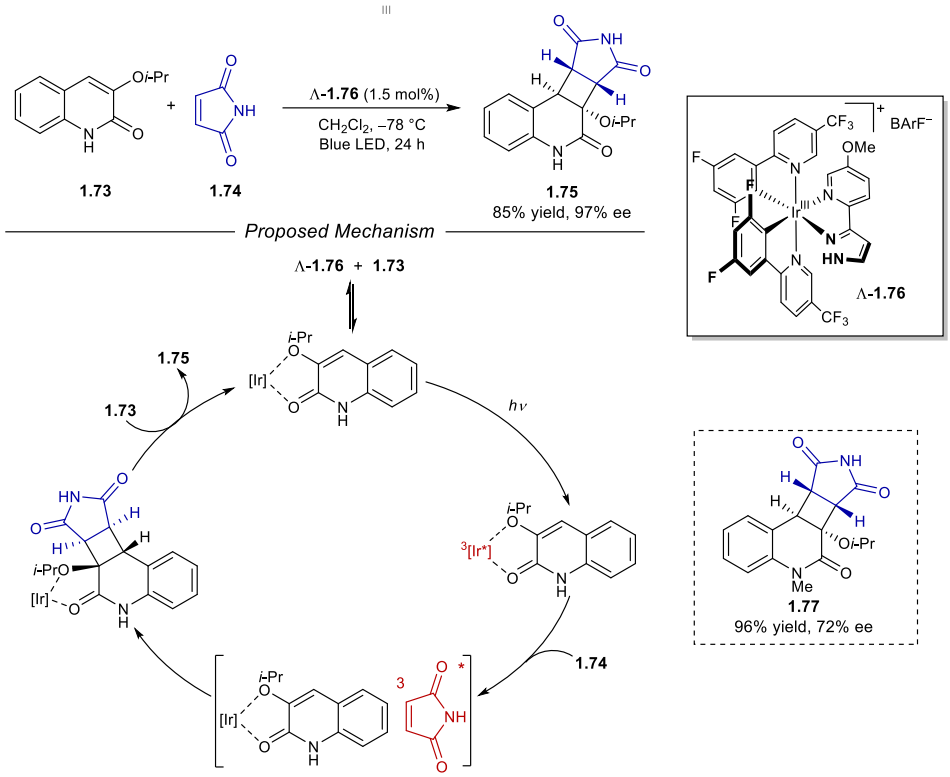

With this mechanistic finding in mind, Yoon and Wright applied this methodology toward the development of an enantioselective Paternó–Büchi reaction between quinolone **1.73** and α-ketoester **1.78** using C_2-symmetric photocatalyst Λ-**1.80** (Scheme 1.28). Mechanistic investigations revealed that both quinolone and **1.78** quench photoexcited Λ-**1.80**, however, time-resolved experiments demonstrated that **1.73** quenches via dynamic energy transfer, resulting in racemic [2+2] outside of the influence of the chiral environment. With this understanding, final optimized conditions were found by employing a slow addition of **1.73**, affording the oxetane in 98% ee. Further discussion of this work can be found in Chapter 4.

Scheme 1.28. Enantioselective Paternó–Büchi Reaction using a Chiral Iridium Photocatalyst

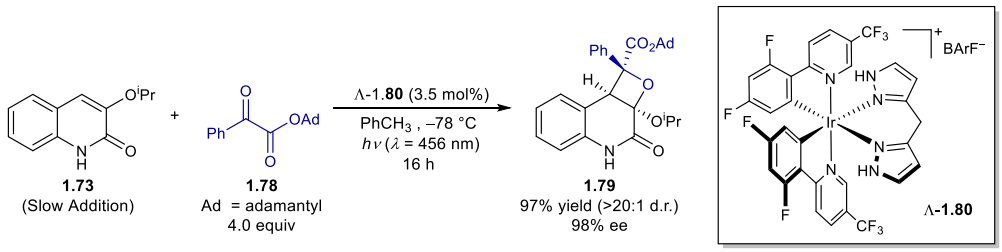

Yoon also demonstrated that the pyridylpyrazole ligand of the enantiopure iridium photocatalysts is a flexible hydrogen-bonding donor capable of recruiting and orienting various motifs for efficient enantiofacial bias. Chiral photocatalyst Λ-**1.84** was found to be optimal in promoting the 6π-electrocyclization of aniline substrate **1.81** and the [2+2] photocycloaddition of 2-cinnamoyl imidazole **1.85** with styrene in high enantioselectivity (Scheme 1.29).[95] Interestingly, modest enantioselectivity was observed when pyrazole and phenyl ketone substrates **1.82** and **1.83** were used.

Scheme 1.29. Asymmetric 6π-Electrocyclization and [2+2] Photocycloaddition

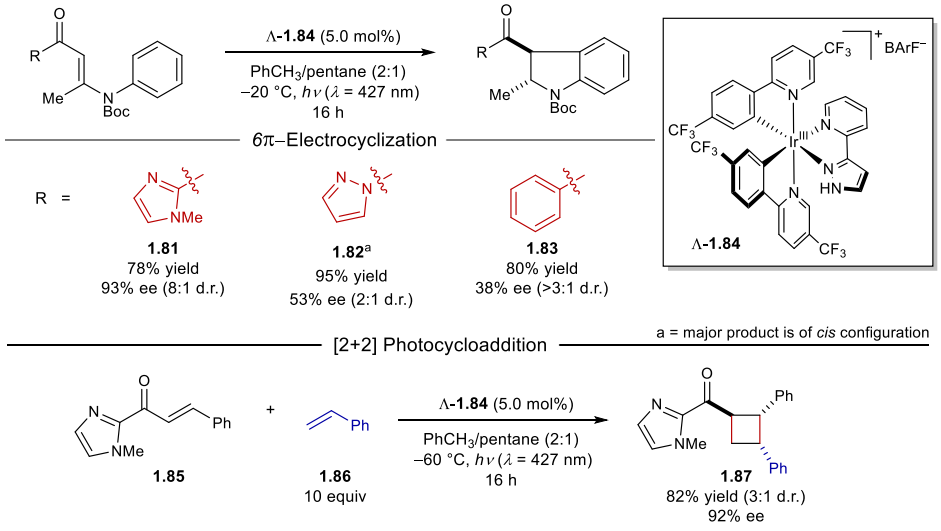

Based on their previous studies using tandem chiral Brønsted acid and Ir photoredox catalysis,[96] Ooi developed an asymmetric [3+2] photocycloaddition using a cationic iridium photocatalyst with a chiral hydrogen-bonding borate counteranion (Scheme 1.30).[97] This strategy

utilizes the ability of *N*-cyclopropylurea **1.88** to associate with chiral borate **1.91**. In addition to preorganizing the substrate within a stereodifferentiating environment, this complexation increases the rate of reaction, as a parallel reaction with the PF_6 salt of [*rac*-Ir(dFCF_3ppy)$_2$(dtbbpy)]$^+$ was significantly slower (<10% yield). Notably, the chirality of the cationic Ir center bore no influence on reaction selectivity, as the use of either the Δ- or Λ-isomer of the iridium photocatalyst produced essentially the same results. Photoinduced electron-transfer oxidation of the borate-bound urea substrate produces radical-ion pair **1.88⊂1.91** that reacts smoothly and selectively with α-substituted styrenes to provide the chiral cyclopentane products. This methodology was later shown to work equally well with α-substituted acrylates as the alkene partner.[98]

Scheme 1.30. Asymmetric Photocatalysis Using Iridium-Chiral Borate Ion Pairs

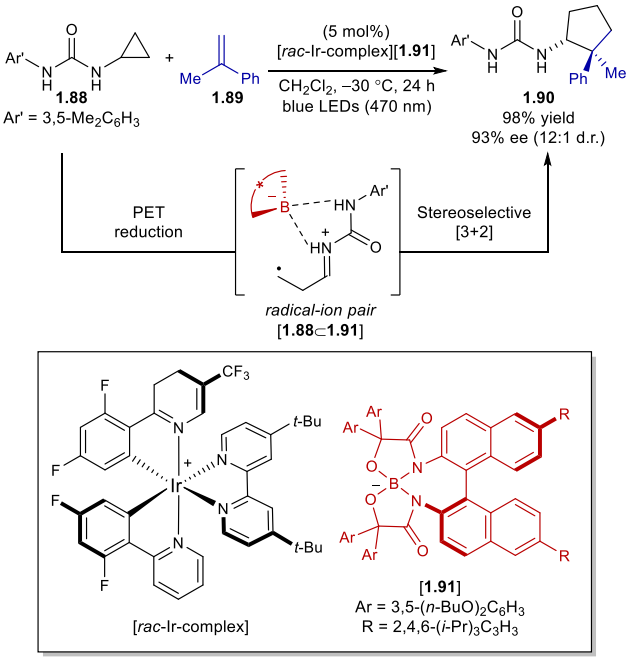

While the chirality of the iridium photocatalysts had no influence on the selectivity of the previous reaction, Yoon and Toste recently observed matched/mismatched rates of energy transfer to a chiral SPINOL–vinyl pyridine complex from the respective Δ or Λ enantiomers of photocatalyst **1.94**.[99] Under matched conditions, this system was found to react smoothly and

selectively with styrene to yield pyridyl cyclobutane **1.93** in 90% and 95% ee (Scheme 1.31). On the other hand, when Λ-**1.93** was employed, product formation was sluggish and exhibited lower enantioselectivity (45% ee). Mechanistic investigations ruled out the possibility of a ground-state association between the photocatalysts and the SPINOL–vinyl pyridine complex, suggesting that transient, diastereomeric excited-state complexes are responsible for the matched/mismatched effect.

Scheme 1.31. Cooperative Stereoinduction in Asymmetric Photocatalysis

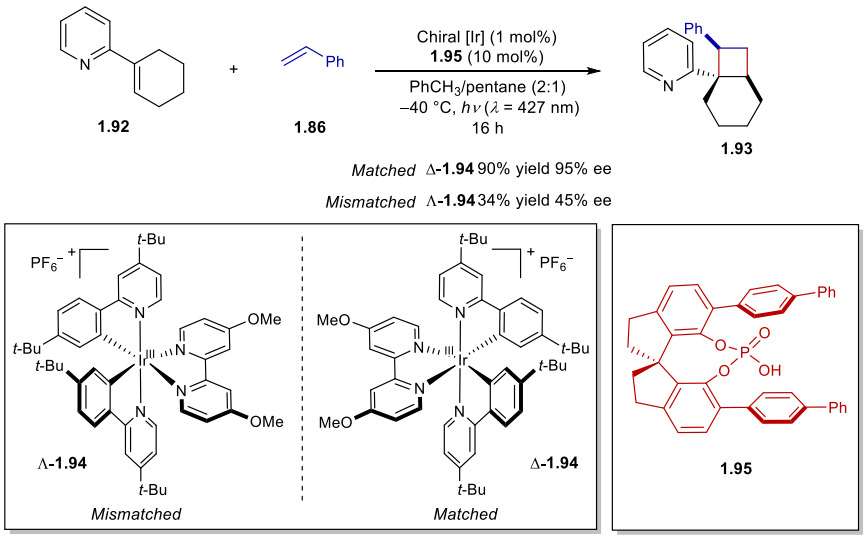

Recently, Melchiorre demonstrated that iridium catalyst **1.102**, a complex widely recognized as a privileged organometallic intermediate in enantioselective allylic substitutions,[100] is also a competent photoredox catalyst. Photoexcitation of the complex enables the oxidation of carbazoles functionalized with cleavable redox auxiliary (RA) groups (Scheme 1.32).[101] The resulting carbazole-stabilized radicals is captured by an (η^3-allyl)iridium(II) complex, which then undergoes stereodetermining reductive elimination to afford the alkyl–alkyl cross-coupled product in high yield and enantioselectivity. The intermediacy of a radical species resulting from PET by the iridium–allyl complex was evidenced from electrochemical and radical trap experiments.

Scheme 1.32: Asymmetric C–C Cross-Couplings Enabled by (η^3-allyl)Iridium(III) Photocatalyst

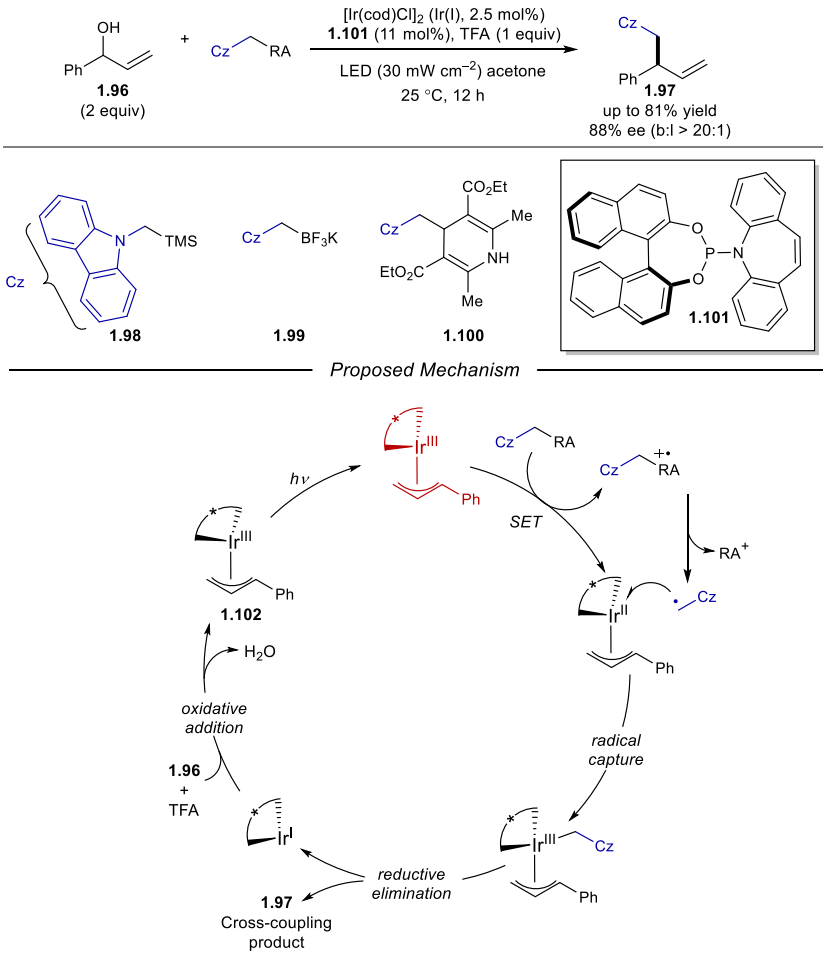

1.6 Rhodium

Ruthenium and Iridium based catalysts have received much of the attention when developing photoredox catalysts. In the previous section, Meggers demonstrated that iridium complexes that are stereogenic at the metal are configurationally stable to photochemical conditions and stereospecific substitution of the labile acetonitrile ligands. However versatile these catalysts are, they are limited to secondary photochemical reactions. In this context, Meggers has extended the protocol for the synthesis of enantiopure helically chiral metal complexes to several late transition metals. The Rh(III) complexes of this class have proven to be exceptionally effective

structures for both primary and secondary photoreactions (Figure 1.2). Many of these methods have utilized the Rh(III) complex as a non-photoactive chiral Lewis acid in tandem with exogenous photocatalysts;[102] the coverage of the literature in this section, however, is limited to examples in which the chiral Rh(III) fragment forms part of the light-absorbing chromophore.

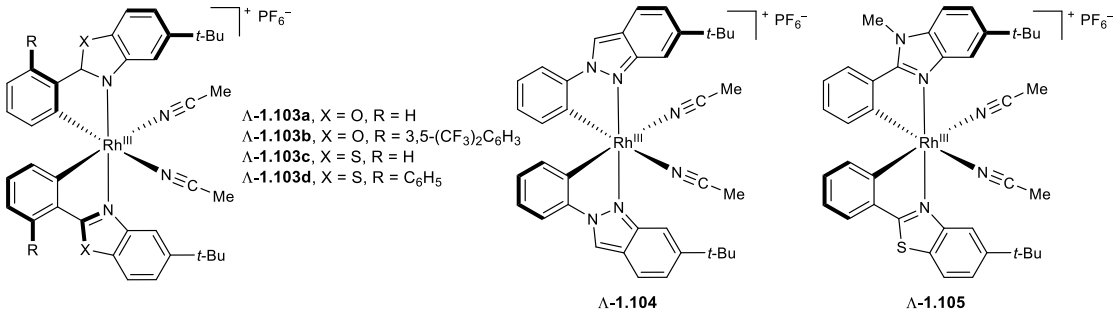

Figure 1.2. Chiral Bis(acetonitrile) Rh(III) Complexes

The first demonstration of chiral-at-rhodium Lewis acids in asymmetric photochemistry involved a study of the α-amination of *C*-acylimidazole substrates (Scheme 1.33). Meggers proposed that photoexcitation of the photocatalyst–substrate complex would promote reduction of ODN-carbamates (ODN = 2,4-dinitrophenylsulfonyloxy) producing electrophilic nitrogen-centered radicals. Reaction of the radicals with the chiral Rh–enolate complex in a stereoselective Lewis acid catalyzed chain process provides the α-aminoketone in nearly quantitative yield and 97% ee.[103] Interestingly, while Λ-**1.103a** is an excellent catalyst for this transformation, the chiral-at-iridium photocatalysts described previously proved ineffective. The improved reaction rate using Λ-**1.103a** was attributed to its faster rate of ligand exchange,[104] which can compensate for the short lifetimes of the highly reactive nitrogen-centered radicals. In line with results of studies using the analogous Ir(III) complexes, benzothiazole Λ-**1.103c** catalysts provided somewhat superior stereocontrol in comparison to the analogous benzoxazole complexes.[105]

Scheme 1.33. Enantioselective α-Amination using Chiral-at-Metal Rhodium Photocatalysts

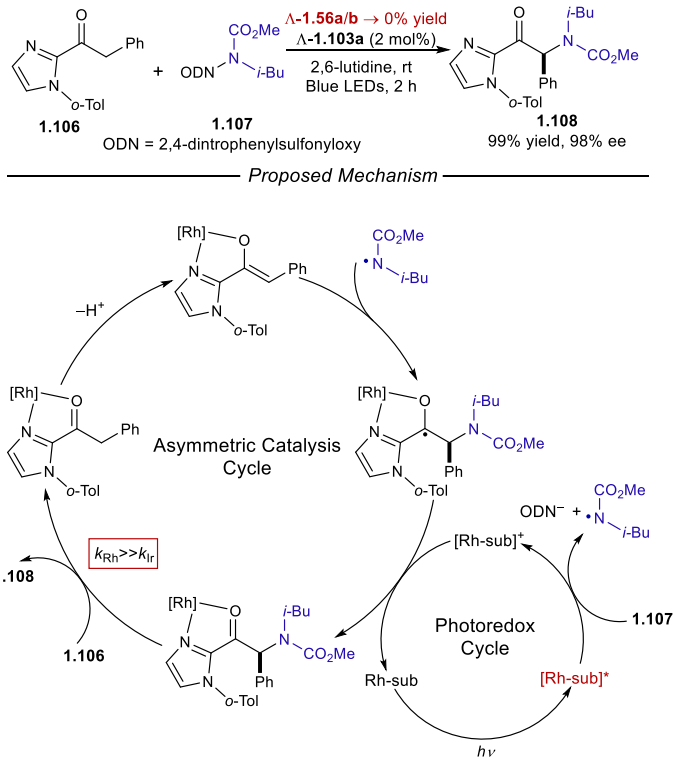

Chiral-at-rhodium photocatalysts have proven to be extremely versatile (Scheme 1.34). Notably, many of these reactions cannot be catalyzed by the first-generation iridium complexes. Meggers reported a photocatalytic oxidative coupling of enolates to photogenerated α-amino radicals that uses air as the terminal oxidant.[106] Kang independently developed the asymmetric radical conjugate addition of tetrahydroisoquinolone-derived α-amino radicals into rhodium complexed α,β-unsaturated 2-acylimidazoles.[107] Comparable reactivity was thereafter reported by Meggers using Hantzsch ester derivatives as alkyl radical sources.[108] Meggers later showed that a similar enantioselective α-amino radical conjugate addition could be initiated through photoinduced reductive decarboxylation of *O*-phthalimidyl protected amino acids.[109] More recently, Su and Kang established an asymmetric Giese addition of *p*-aminobenzyl radicals from

the corresponding carboxylic acids using chiral rhodium catalyst Λ-**1.103b**.[110] Finally, the synthesis and application of a chiral-at-metal novel bis-cyclometalated indazole catalyst Λ-**1.104** was useful in producing α-cyano radicals and controlling their facially-selective addition into rhodium enolates.[111]

Scheme 1.34. Asymmetric Radical Additions Catalyzed by Chiral Rhodium Catalysts

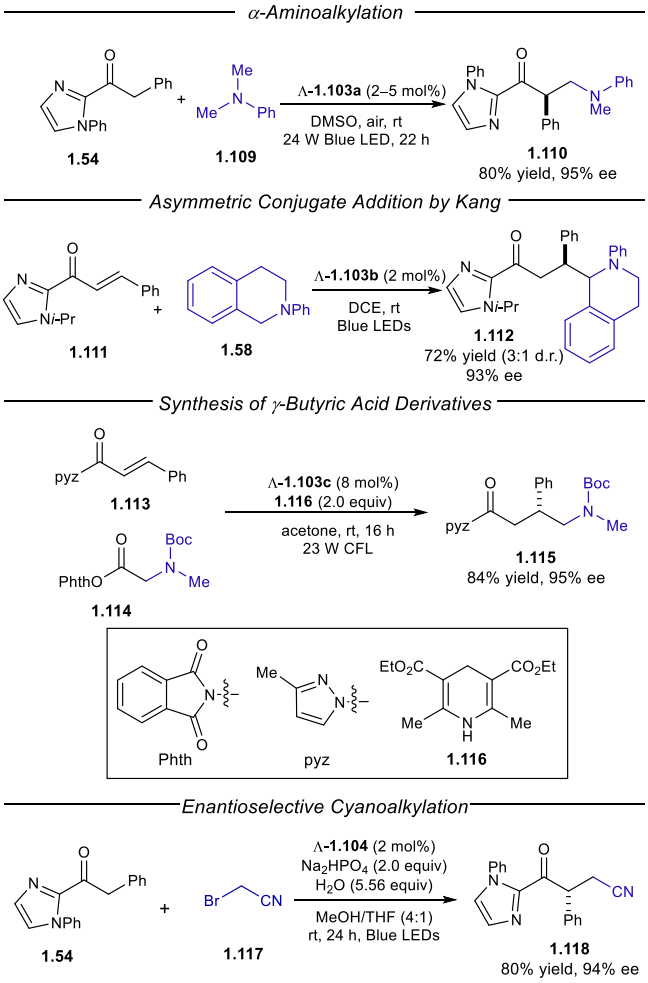

The mechanisms and origins of enantioselectivity using this class of Rh(III) photocatalysts (Scheme 1.35) has been studied by Meggers together with Wiest[112] revealing a strong rate enhancement induced by the rhodium catalyst to overcome competitive racemic reactivity. An X-ray crystal structure of a Rh(III)–enolate intermediate exposed a steric burden imposed by the *tert*-

butyl groups on the *Si* face of the prochiral substrate.[113] Additional DFT calculations performed in collaboration with Houk[114] suggest that distortions of the substrate–catalyst complex is a major contributor in controlling the enantioselectivity.

Scheme 1.35. Lewis Acid Effects and Mode of Enantioinduction

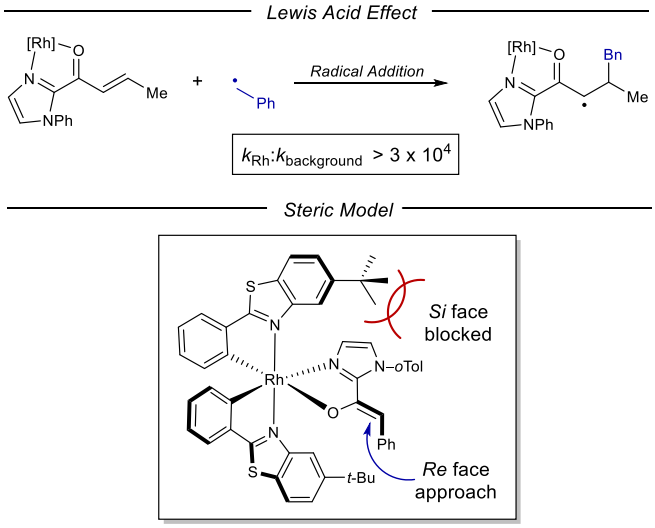

Enantioselective radical–radical coupling reactions can also be catalyzed by chiral Rh(III) photocatalysts. In 2017, Weist and Meggers reported the asymmetric β-C–H functionalization of 2-acylimidazoles (**1.118**) and 2-acylpyrazoles with α-ketoester **1.119** (Scheme 1.36).[115] The radical reactants in this process are generated by photoinduced electron transfer from the excited-state Rh(III)-enolate complex to the α-ketoester to afford ketyl radical and α-ketoradical intermediates. Radical coupling occurs with high diastereoselectivity and >90% ee. A complementary study resulted in a method for the stereoconvergent asymmetric coupling of racemic α-chloro-imidazol-2-yl-ketones with *N*-arylglycines (Scheme 1.37).[116] In this work the radical partners were generated by a photoinduced decarboxylation of the *N*-arylglycinate **1.122** and a concomitant photoreductive dehalogenation of the Rh(III)-ketone complex; radical–radical coupling of the resulting α-aminoradical and α-ketoradical affords chiral β-aminoketone **1.123** in high ee.

Scheme 1.36. Enantioselective Radical–Radical Coupling Reaction of 2-Acyl-Imidazoles/Pyrazoles and α-Ketoesters

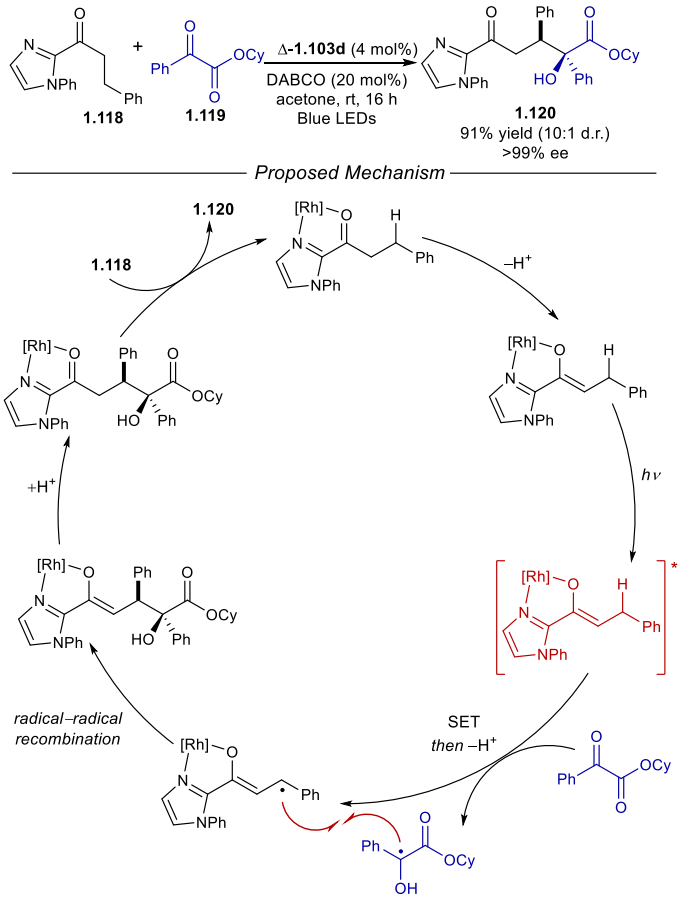

Scheme 1.37. Enantioconvergent Coupling of Racemic α-Chloroketones and *N*-Arylglycines

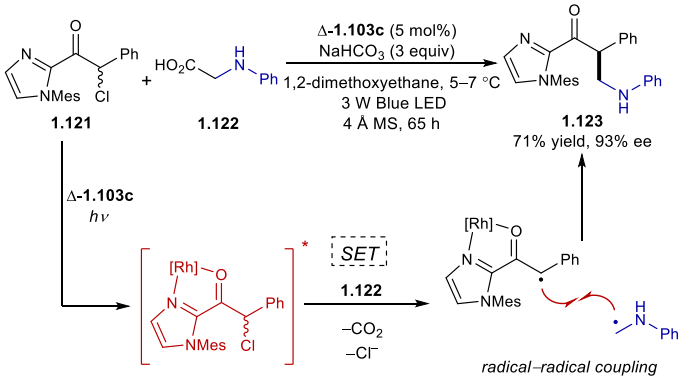

In addition to enantioconvergent cross-couplings, Meggers and Chen demonstrated that Rh(III) catalyst Λ-**1.104** in combination with a tertiary amine could accomplish a photochemical

deracemization of 2-pyridylketone **1.124** in 96% ee (Scheme 1.38).[117] A photochemically driven single-electron reduction of Rh-bound **1.124** by aniline **1.125** followed by HAT to the oxidized amine yields the achiral rhodium–enolate complex. Diastereoselective proton transfer provides the rhodium coordinated ketone as a single stereoisomer. This mechanistic separation was critical in circumventing the restriction of microscopic reversibility as the elementary steps for enolate formation are distinct from stereoselective protonation. (*R*)-**1.124** bound to Λ-**1.104** is destabilized compared to (*S*)-**1.124**, and thus iterative SET/HAT/protonation sequences selectively enhance (*R*)-**1.124**. Notably, the protonation step alone does not fully account for the enhanced stereoselectivity. Instead the selective association and photochemical activation of (*S*)-**1.124** facilitates the enrichment of (*R*)-**1.124**.

Scheme 1.38. Photocatalytic α-Deracemization of 2-Pyridylketones

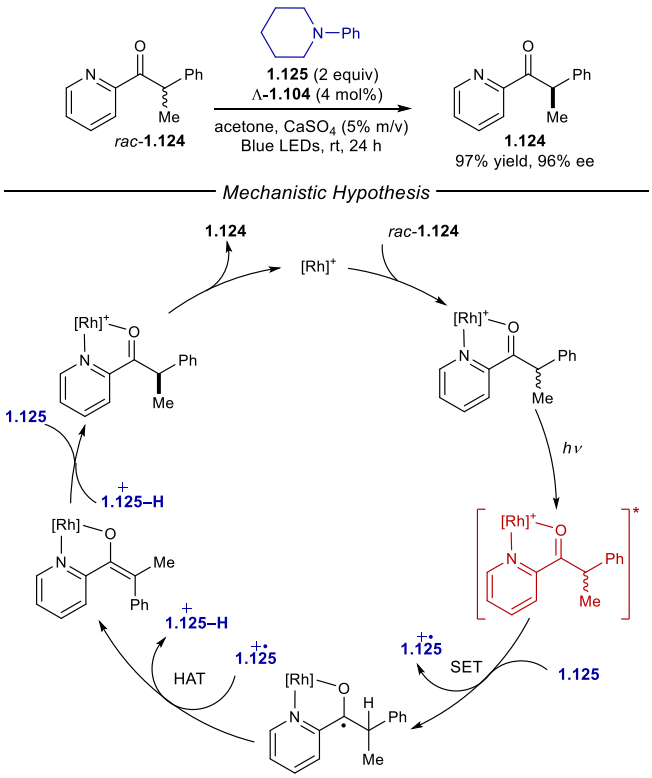

Meggers developed an asymmetric [3+2] photocycloaddition that also involves a chiral Rh(III) photocatalyst.[118] Cyclopropyl imidazolyl ketones react smoothly with a wide variety of alkenes and alkynes upon irradiation in the presence of the Rh(III) complex Λ-**1.103c** to afford highly enantioenriched cyclopentanes (**1.126**) and cyclopentenes (**1.127**, **1.128**) (Scheme 1.39).

Scheme 1.39. Enantioselective [3+2] Cycloaddition of Cyclopropyl Ketones with Alkenes and Alkynes

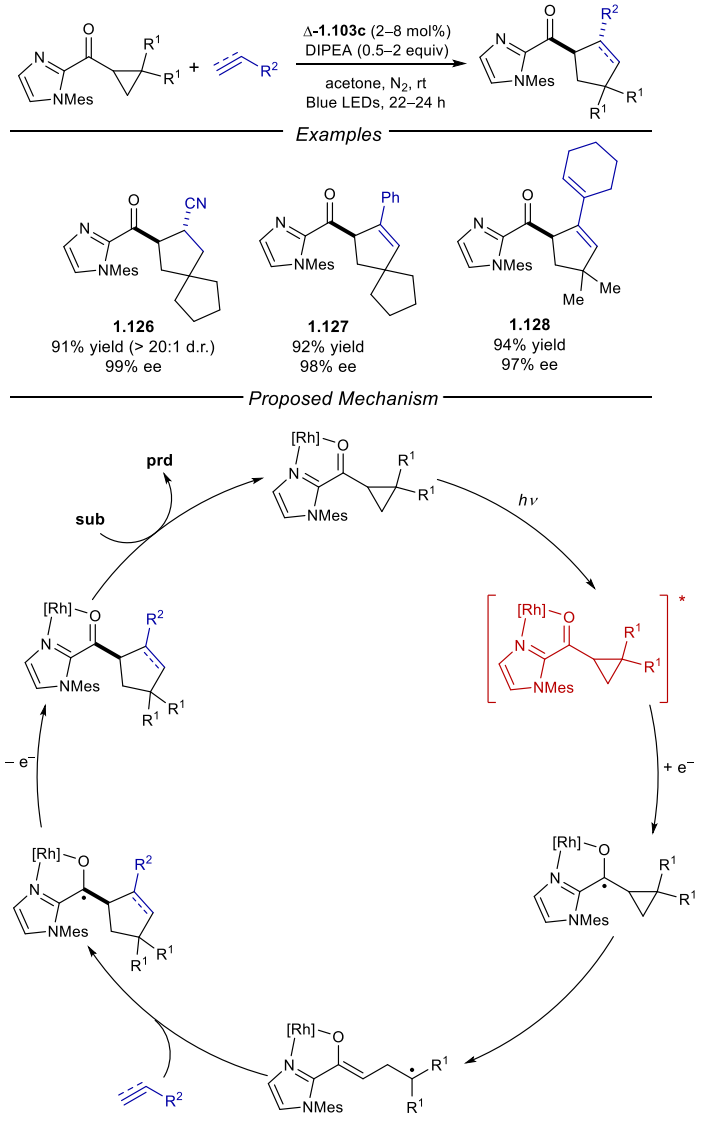

The mechanism of this reaction involves chromophore activation: complexation of the imidazolyl ketone to the Rh(III) Lewis acid results in a bathochromic shift that enables excitation by visible light. The Lewis acid activation also results in an anodic shift in the substrate reduction potential, facilitating formation of the ketyl radical by photoreduction.

Meggers and Wiest extended this concept to the enantioselective [2+2] photocycloaddition of chelating *N*-phenyl-cinnamoylimidazole **1.129** with alkenes (Scheme 1.40).[119] As in the previous example, the enhanced visible-light absorption of the substrate–catalyst complexation allows for the selective photoexcitation of the chiral catalyst-bound compound and suppresses racemic background reactivity. Notably, both isomers of the reacting alkene converged to provide the same cyclobutane stereoisomer ratio, suggesting that this reaction proceeds through a triplet

Scheme 1.40. Enantioselective Excited-State [2+2] Cycloaddition with Chiral Rhodium Complexes via Chromophore Activation

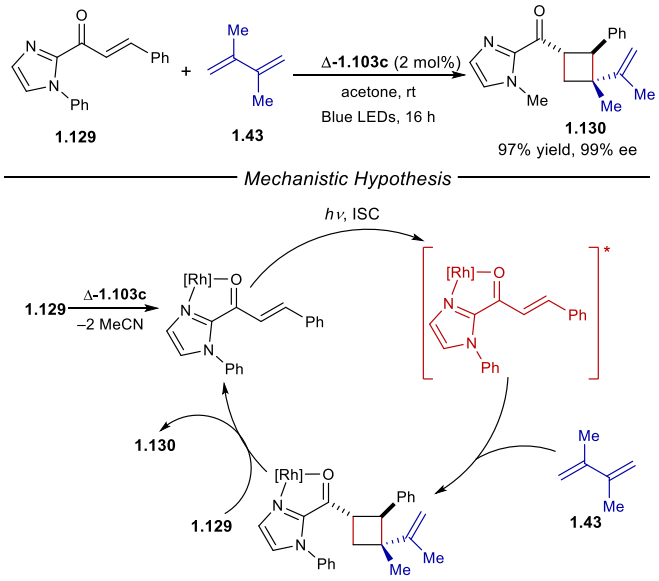

excited state. This hypothesis was computationally and spectroscopically validated, which revealed a localization of the triplet spin density across the substrate alkene carbons in the photoexcited Rh-substrate complex.[120] In later work, a novel non-C_2-symmetric tris-heteroleptic

Rh(III) complex (Λ-**1.105**) was also shown to be an efficient asymmetric catalyst for the [2+2] photocycloaddition of related substrates.[121]

This strategy was also applied to the enantioselective dearomative [2+2] photocycloaddition of benzofurans and benzothiofurans (**1.131**) with styrenes.[122] An *N*-acylpyrazole moiety was appended at the 2-position of the heteroaromatic substrate to facilitate coordination to the rhodium catalyst. The pyrazole moiety can also be cleaved without eroding the ee of the cycloadduct. Interestingly, this system exclusively produces the head-to-tail regioisomer rather than the tail-to-tail isomer that is commonly formed in the cycloaddition of two styrenic olefins. In collaboration with the Baik group, Meggers reported DFT calculations rationalizing the regiochemistry by considering the relative stability of the two possible regioisomeric 1,4-biradical intermediates. The intermediate of the major product benefits from captodative stabilization by the lone pair of the adjacent oxygen atom and the neighboring carbonyl group, leading to a free energy difference of over 5.0 kcal/mol (Scheme 1.41).

Scheme 1.41. Regio- and Enantioselective Formation of Head-to-Tail Cyclobutanes

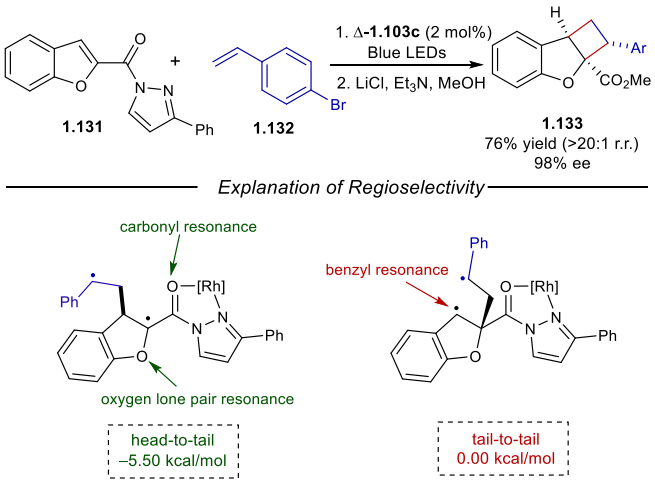

Bach recently demonstrated that Λ-**1.103c** can influence the stereochemistry of the [2+2] photocycloadditions of 2-benzimidazoyl styryl sulfone **1.134** (Scheme 1.42).[123] The sulfone

substrate binds to the chiral Lewis acid by chelation between the sulfone oxygen and the benzimidazole. During optimization, the authors noted an interesting dependence on the wavelength of the light source used. Longer wavelengths result in low sulfone conversion but higher ee. Irradiation at 420 nm resulted in the best compromise, affording product **1.135** in 41% yield and 77% ee.

Scheme 1.42. Enantioselective [2+2] Photocycloaddition of α,β-Unsaturated Sulfones

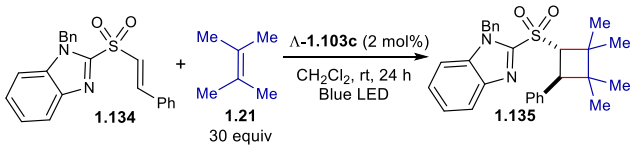

λ (nm)	yield	ee (%)
405	77%	40
420	41%	77
457	33%	79

This chromophore activation catalyst is also able to control the stereoselectivity of other classes of excited-state photoreactions. In 2017 the Meggers group reported a catalytic enantioselective synthesis of chiral 1-pyrroline **1.138** through a [3+2] cycloaddition between *N*-cinnamoylpyrazole **1.136** with vinylazide **1.137** (Scheme 1.43).[124] Mechanistic investigations indicate that the excited-state chiral catalyst–substrate complex reacts directly with ground-state vinylazide, rather than through bimolecular energy transfer, which could result in racemic reactivity. The resulting biradical intermediate undergoes N_2 extrusion followed by ring closure to form the enantioenriched product. Interestingly, the chiral Ir(III) analogues are unselective photocatalysts for this cycloaddition. DFT computations indicated that the excited state of the iridium–substrate complex is primarily localized on the metal center rather than the bound alkene. Meggers proposed that the Ir(III) catalyst functions primarily through bimolecular collisional Dexter energy transfer, which sensitizes unbound pyrazole and produces racemic cycloadduct.

Scheme 1.43. Enantioselective [3+2] Photocycloaddition Between *N*-Cinnamoylpyrazoles and Vinylazides

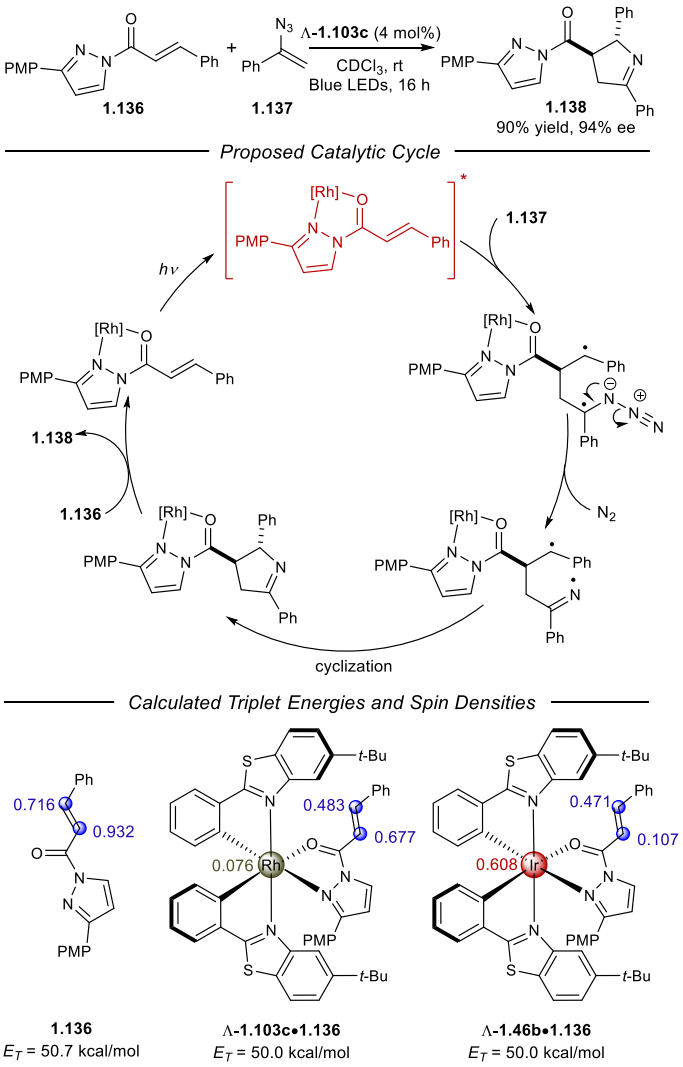

In subsequent work, Meggers and Houk reported a unique example of a catalyst–substrate adduct engaging in a visible light-initiated hydrogen atom transfer (HAT) reaction to form a bound radical intermediate (Scheme 1.44).[125] Consistent with previous results, a 2-acylpyrazole auxiliary was necessary for bidentate chelation to the helically chiral rhodium complex. Complexation of the substrate to the metal center constitutes the photoactive species, which upon excitation populates the alkene-centered triplet. This triplet diradical, which is near the aldehydic hydrogen

atom, undergoes hydrogen atom transfer and concomitant rearrangement to a ketene intermediate; this intramolecular HAT step is supported by DFT calculations. Finally, the rhodium-bound ground-state ketene engages in a hetero-Diels–Alder cycloaddition with an appended aldehyde to yield fused cyclopropane products in up to 99% ee.

Scheme 1.44. Enantioselective Hetero-Diels–Alder Reaction via Chromophore Activation

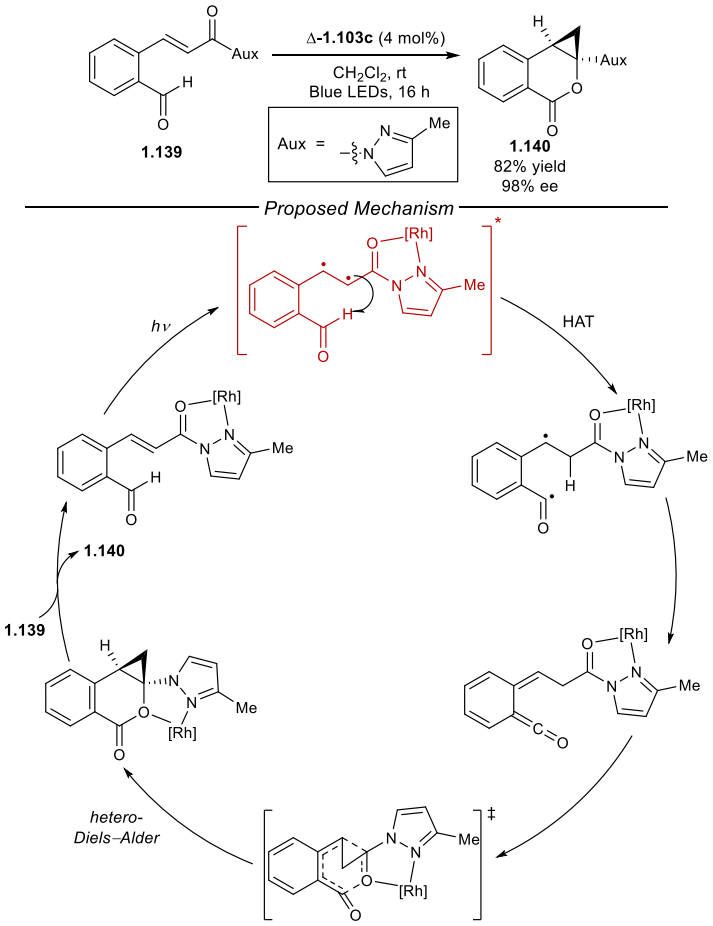

1.7 Nickel

The past decade of research in synthetic photochemistry has been dominated by the use of Ru(II) and Ir(III) complexes because of their tunability and attractive photophysical properties. The discovery of photocatalysts with similar efficacy based on less expensive, earth-abundant first-row transition-metal elements is an important challenge. Structurally analogous first-row

metal polypyridyl complexes, however, have very different photophysical properties and in general are not effective photocatalysts.[126] Hence, there are a few examples of chiral photocatalysts based on first-row transition metals.

In 2016, Xiao described the design of novel chiral BOX ligand **1.143** in which the central bridging carbon is functionalized with a thioxanthone substituent; the $Ni(acac)_2$ complex of this ligand was used to catalyze the enantioselective oxidation of β-ketoester **1.141** using oxygen as the terminal oxidant (Scheme 1.45).[127] The thioxanthone moiety acts as a sensitizer for the formation of singlet oxygen, while the Ni(II) center promotes enolization of the β-ketoester substrate and controls the facial selectivity of the C–O bond formation. The absorption and emission spectra of the ligand did not significantly change upon coordination of Ni(II), indicating that the photosensitizer operates independently of the Lewis acidic metal center. Luminescence quenching studies showed no quenching by the complexed substrate but did show a decrease in emission when oxygen was present. The excellent selectivity achieved was attributed to the dynamic steric profile of the covalently attached thioxanthone sensitizer. Interestingly, when the reaction is conducted with separated thioxanthone and Ni(II) BOX catalysts, the yield and ee are diminished, which was attributed to the reduced steric profile of the BOX ligand.

Scheme 1.45. Stereoselective Oxidation of β-Ketoesters by a Thioxanthone-Tethered Nickel Lewis Acid

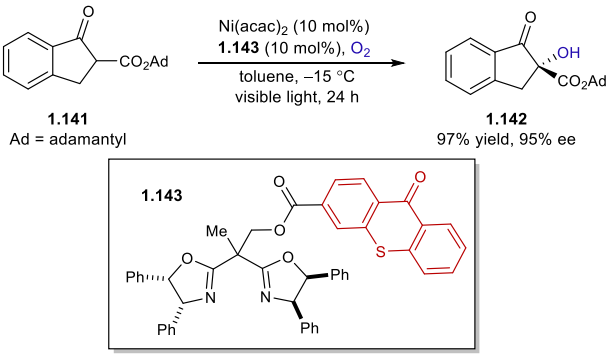

Shen described the use of a bifunctional Ni(II)-DBFOX complex that serves as both a competent photoredox catalyst and chiral Lewis acid catalyst for the asymmetric addition of α-amino radicals to α,β-unsaturated compounds (Scheme 1.46).[128] The identity of the catalytically relevant photocatalyst was not unambiguously determined but was proposed to either be the Ni(II)-DBFOX complex or its complex with substrate **1.144**, both of which absorbed significantly in the visible range. The luminescence of these complexes was readily quenched by addition of α-silylamine **1.145**, consistent with desilylative photooxidation to generate the key α-amino radical intermediate. While a quantum yield of 0.59 was measured, a radical chain cannot be ruled out based on this reaction's similarity to other literature.[129,130]

Scheme 1.46. Asymmetric Radical Addition Enabled by Bifunctional Nickel Catalyst

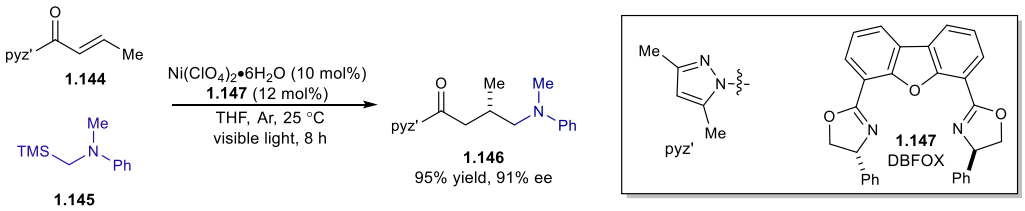

1.8 Copper

Chiral Cu(I) complexes have also been used as asymmetric photocatalysts; however, tetrahedral copper complexes readily undergo fast ligand exchange, which prevents the exploitation of any innate metal-centered chirality.[131] Thus, enantiocontrol requires the use of chiral ligands. Ohkubo achieved an enantiodiscriminating photoreduction of the racemic mixture of Λ- and Δ-Co(edta)$^-$ using the photocatalyst Cu(dmp)(diop)$^+$ (**1.148**), yielding an enantiomer ratio of 1.17:1 (Scheme 47).[132] Later studies focused on the use of chiral bpy ligands (**1.149**) that position the chiral information closer to the metal center. Under kinetic resolution conditions, 42%

ee was obtained at 10% conversion.[133] Both the counterion of the Co(II) complex and the edta^{4-} additive had an effect on the outcome of the reaction (Scheme 1.48).[134]

Scheme 1.47. Enantioselective PET Using Chiral Cu(I) Complexes

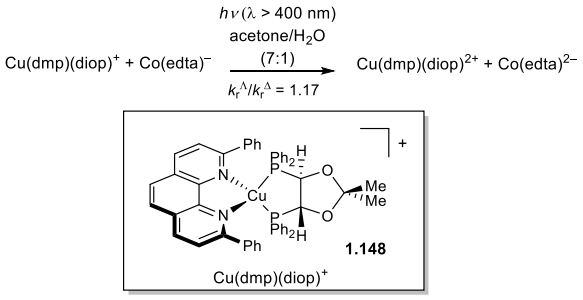

Scheme 1.48. Asymmetric PET to Cobalt Complexes Using Chiral Cu(I) Complexes

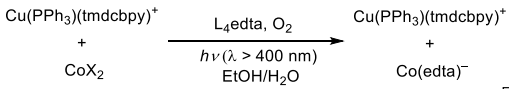

CoX_2	L_4edta	Yield	ee
$Co(OAc)_2$	H_4edta	28%	7%
$Co(OAc)_2$	Na_4edta	32%	–7%
$Co(NO_3)_2$	H_4edta	22%	9%
$Co(NO_3)_2$	Na_4edta	36%	5%
CoCl	H_4edta	0%	–
CoCl	Na_4edta	5%	nd

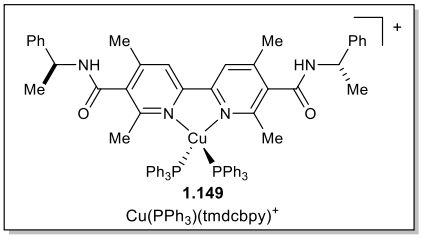

Bach observed that a Cu(II) catalyst bearing a chiral BOX ligand could influence the stereochemistry of the 6π-photoelectrocyclization of 2-aryloxycyclohexenone substrate **1.150** (Scheme 1.49).[135] Consistent with previous examples of chromophore activation, the copper Lewis acid induces a bathochromic shift in the absorption of the substrate, resulting in an intense (π,π*) absorption that overlaps with the weaker (n,π*) absorption of the non-coordinated substrate. The optimized conditions employed 50 mol% $Cu(ClO_4)_2 \cdot 6H_2O$ and 60 mol% of C_2-symmetric BOX ligand **1.152**, providing the photocyclized product in up to 40% ee. In addition to competitive absorption of by the unbound substrate, the lower enantioselectivity in this reaction is attributed to poor coordination of the ethereal oxonium when approaching the transition state of an ylide

intermediate. A second protocol in the same report was developed using a triplet sensitizer, thioxanthone, and visible light (419 nm) to obtain product in modest selectivity, up to 47% ee.

Scheme 1.49. Application of Chromophore Activation to an Enantioselective 6π-Photoelectrocyclization

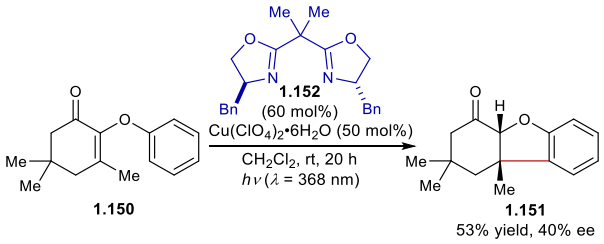

In 2012 Peters and Fu reported a Cu(I)-carbazolide complex capable of undergoing an ultraviolet light mediated Ullmann C–N coupling with aryl halides via a radical pathway.[136] These findings were followed by several reports describing the extension of this chemistry to alkyl halide electrophiles.[137–141] In 2016, a chiral phosphine–Cu(I) complex was shown to catalyze the

Scheme 1.50. Enantioconvergent Ullman C–N Coupling with a Chiral Phosphine–Cu(I) Catalyst

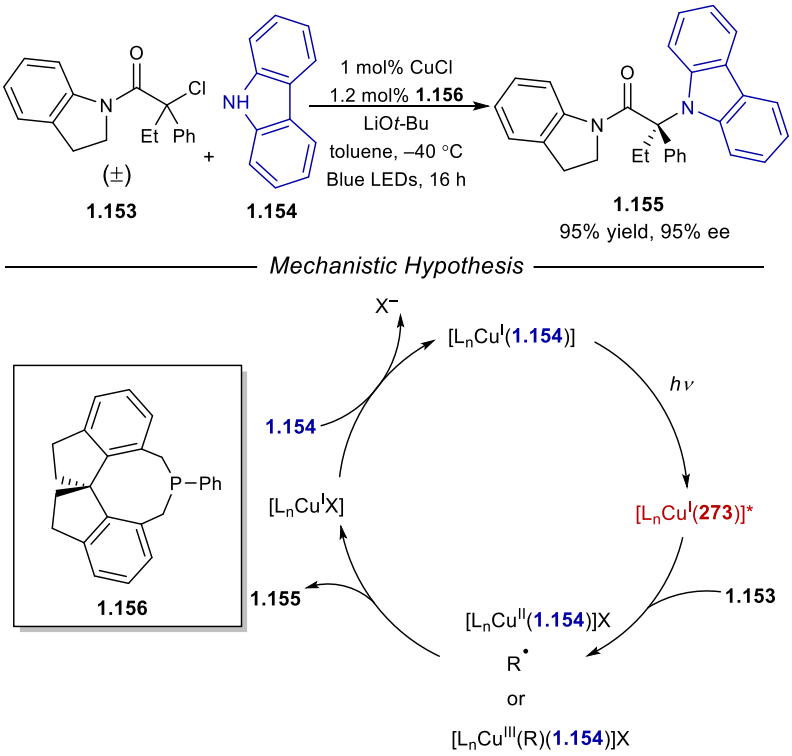

stereoconvergent coupling of carbazole **1.154** to racemic tertiary α-chloroamide **1.153**.[142] A kinetic resolution was ruled out because no enantioenrichment of the starting alkyl halide was observed after completion of the reaction (Scheme 1.50). Later efforts extended this methodology toward the asymmetric amidation of unactivated racemic alkyl chlorides.[143]

Xu and Wang reported a photocatalytic protocol for the asymmetric cyanofluoroalkylation of styrenic olefins utilizing a chiral BOX ligand (Scheme 1.51).[144] In contrast to the system developed by Fu and Peters, in this reaction, chiral phosphine ligands slowed product formation and did not result in any enantiomeric enrichment. A combination of UV-Vis and NMR experiments indicated that the active photocatalyst is formed in situ by the coordination of chiral BOX ligand **1.160** and ligand exchange to afford a (**1.160**)CuCN complex. The excited state of this species is a competent reductant (–2.24 V vs SCE) capable of generating the resultant alkyl-radical from the perfluoroalkyl iodide (–1.32 V vs SCE).

Scheme 1.51. Enantioselective Three-Component Coupling Using a Chiral Copper Photocatalyst

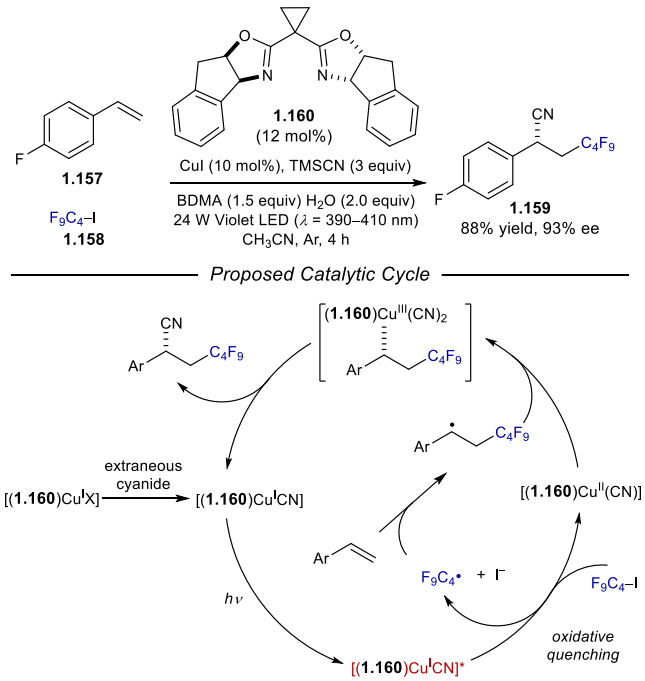

More recently, G. Zhang and D. Zhang described a photoinduced, copper-catalyzed, highly enantioselective dual carbofunctionalization of the same class of alkenes (Scheme 1.52).[145] UV-Vis experiments suggested that the photoactive catalyst is generated from the aggregation of the chiral *t*-Bu-BOPA ligand **1.161** and an alkyne nucleophile to the Cu(I)–acetylide species. Moreover, steady-state luminescence quenching indicated that this complex was effectively quenched by the alkyl halide coupling partner.

Scheme 1.52. Enantioselective Dual Carbofunctionalization of Styrenes

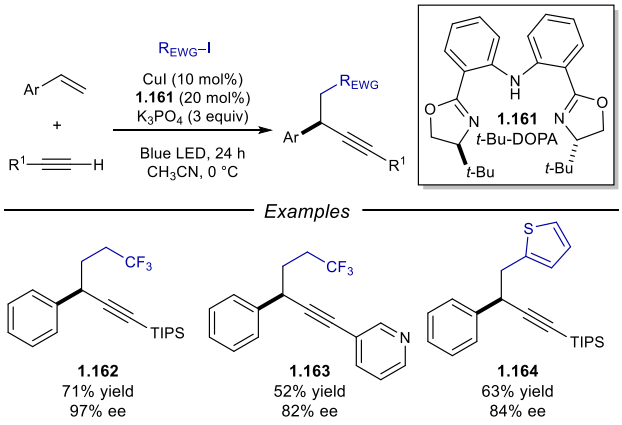

Liu reported a related approach for the asymmetric alkynylation of *N*-hydroxypthalimide (NHP)-type esters using a Cu(I)–acetylide complex ligated by cinchona alkaloid-derived *N*,*N*,*P*-ligand **1.168** as the photoreductant (Scheme 1.53).[146] Critical to their success was the use of naphthyl-NHP ester **1.165** to suppress the formation of the Glaser homocoupling product of terminal alkyne **1.166** and radical dimerization of **1.165**. The authors proposed this effect results from a decreased rate of quenching of the excited-state copper complex by **1.165** compared to commonly employed NHP esters. Finally, stoichiometric experiments demonstrated that in the absence of chiral ligand **1.168** only 10% of product **1.167** is formed, indicating that the ligand significantly improves the photocatalytic efficiency of the transformation.

Scheme 1.53. Asymmetric Decarboxylative Alkynylation with Terminal Alkynes

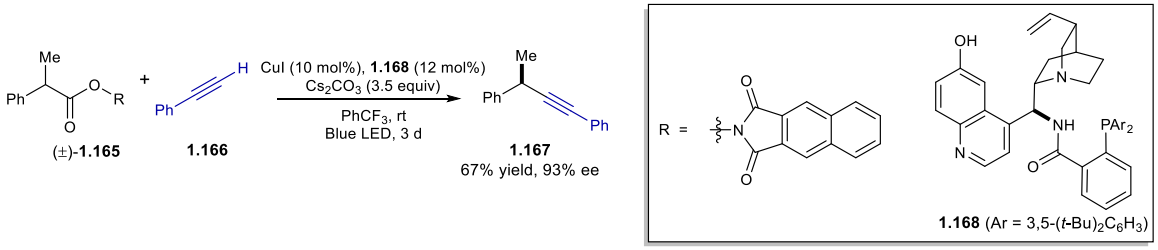

Subsequently, Xu and Wang reported the enantioselective C(sp^3)-alkylation of quinolinyl-appended glycinate ester **1.169** utilizing NHP ester **1.170** as an alkyl radical precursor (Scheme 1.54).[147] Similar to the previously discussed examples, coordination of substrate **1.169** to a chiral phosphine–Cu(I) complex results in the *in situ* generation of the photoactive catalyst. Oxidative quenching by ester **1.170** to form the corresponding alkyl radical is thermodynamically feasible. Under optimized conditions the cross-coupled product is produced in 88% yield and 94% ee.

Scheme 1.54. Visible Light Induced Enantioselective C(sp^3)-alkylation of Glycine Ester Derivatives

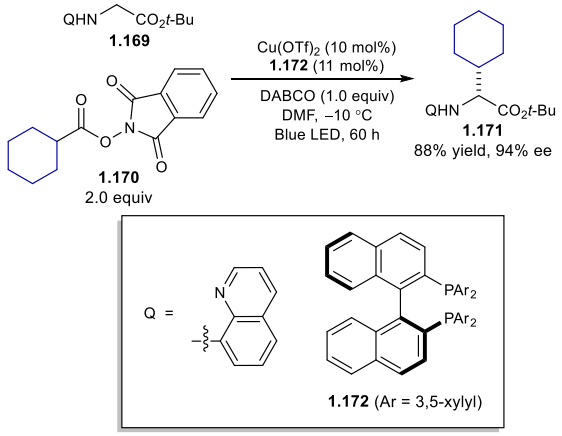

Seminal work by Kochi and co-workers[148] demonstrated that upon irradiation with UV light $CuCl_2$ undergoes homolysis to afford the corresponding Cl• and Cu(I)–Cl complex. In direct contrast with the photochemistry of Cu(I)X complexes, these Cu(II)X_2 catalysts operate through a

LMCT,[149–152] rather than a MLCT, which have been shown to mediate oxidative transformations. While examples of this type of reaction are limited, asymmetric variants are even rarer. In 2018, Gong reported that a Cu(II) complex ligated by BOX ligand **1.176** enables the photoinduced alkylation of imine **1.173** to afford enantioenriched tetrasubstituted carbon centers in up to 98% ee (Scheme 1.55).[153] Mechanistically, the authors suggest a fast transmetallation to form a Cu(II)–alkyl complex that is proposed to undergo a ligand-to-metal charge transfer (LMCT) photoexcitation and subsequent homolysis to liberate the alkyl radical. This nucleophilic radical undergoes addition to the coordinated imine substrate, which produces a nitrogen-centered radical that is stabilized by Cu(II). This species can be reduced by the Cu(I)–**1.176** complex.

Scheme 1.55. Stereoselective Radical Addition Using a Dual-Purpose Copper Photocatalyst

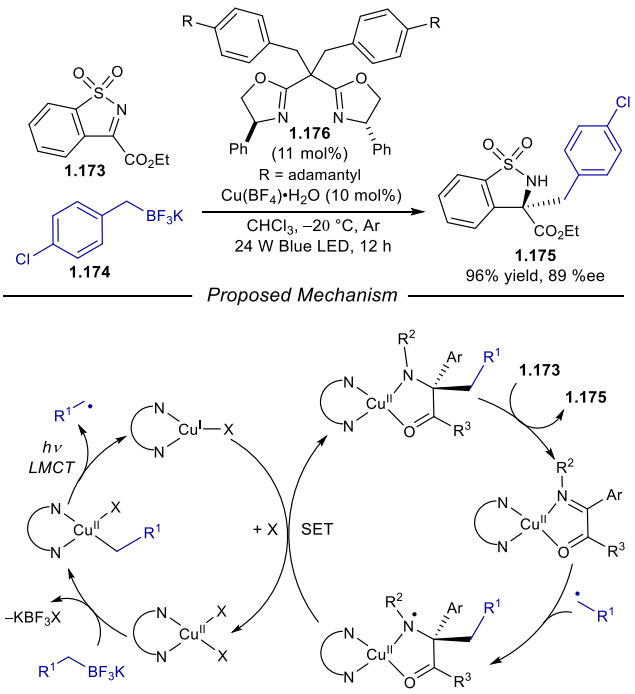

Following this study, Gong reported that chiral Cu(II)–BOX complexes enable the related addition of α-amino radicals to acyclic imine derivative **1.177** to afford highly desired enantioenriched vicinal diamine compounds (**1.179**) (Scheme 1.56).[154] While the Cu(II)–BOX

complex acts as both a photoredox catalyst and Lewis acid producing the alkyl radical and coordinating the prochiral imine, the mechanism of this reaction differs from the previous example because the α-TMS aniline radical precursor is proposed to be directly oxidized by a PET process, rather than by transmetallation and LMCT homolysis.

Scheme 1.56. Stereoselective Radical Addition into Imines by a Bifunctional Copper Catalyst.

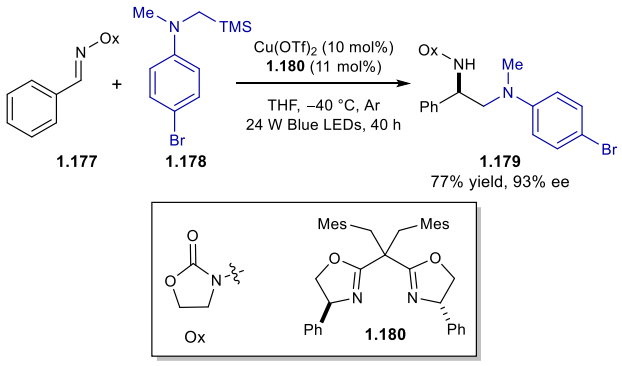

In later work, Gong extended this methodology to the asymmetric cross-dehydrogenative coupling of 2-acylimidazole **1.181** with xanthene derivatives, utilizing O_2 as a terminal oxidant, to produce **1.183** in good yield and excellent enantioselectivity (Scheme 1.57).[155] Electrochemical and spectroscopic experiments revealed the Cu(II)–BOX complex as the photoactive species, initiating the reaction via oxidation of xanthene **1.182**. Furthermore, this complex serves to preorganize **1.181** resulting in efficient stereofacial bias.

Scheme 1.57. Asymmetric Aerobic Cross-Dehydrogenative Coupling

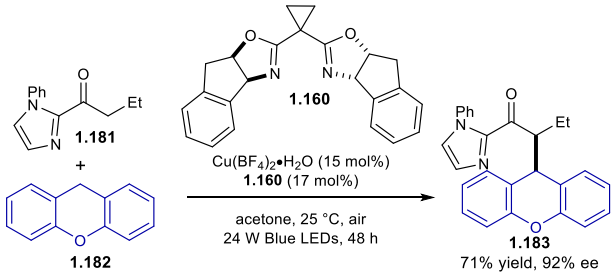

More recently, Chen, Xiao, and Guan reported an enantioselective C–O cross-coupling of 1,3-dienes and readily available oxime esters catalyzed by Cu(I)–BOX under irradiation with

purple light (Scheme 1.58).[156] This photocatalyst serves a dual role in generating an alkyl radical via reduction of oxime ester **1.184** and as the source of asymmetric induction in the C–O bond formation. Interestingly, this reaction heavily favors 1,2-addition rather than 1,4-substitution. DFT computations revealed a thermodynamic and kinetic preference for the formation of a π-allylcopper complex over the competing π-benzylcopper complex, leading to the experimentally observed 1,2-adduct.

Scheme 1.58. Photoinduced Copper-Catalyzed Asymmetric C–O Cross-Coupling

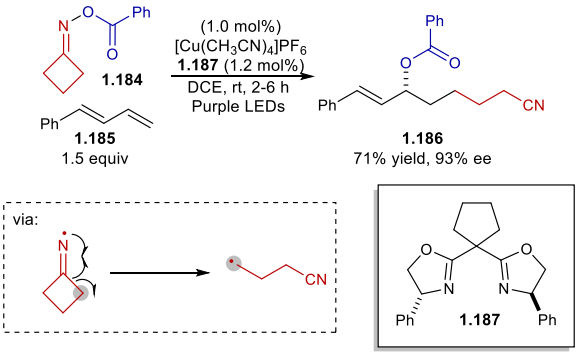

1.9 Conclusion

After several decades of relatively slow development, there has been a recent, rapid increase in the pace of discovery of photocatalytic reactions that deliver enantioselectivities on par with those obtained in modern ground-state asymmetric catalytic reactions. In many cases, chiral photocatalyst structures have been developed by adapting catalyst classes originally designed for use in ground-state transformations. Several of these show promise to become privileged scaffolds within asymmetric photochemistry as well, including phosphine- and oxazoline-ligated complexes and oxazaborolidine catalysts investigated by Bach. Various photocatalyst structures unique to excited-state reactions have also been created to address the specific challenges relevant in asymmetric photochemistry. Many of these incorporate a chiral moiety into the structure of a

known photosensitizing moiety. Examples include the chiral transition metal photocatalysts developed by Meggers and further expanded by the Yoon group.

While the structures of these photocatalysts are diverse, and the mechanisms by which they operate varied, a common design principle across multiple catalyst classes is the requirement for ground-state association of the substrate to the photocatalyst prior to excitation. This preassociation is one way to ensure that the catalyst meets the criteria described above. Preassociation sets the substrate within the chiral environment of the catalyst, and in most cases increases the rate of the enantioselective transformation over any competitive racemic background reactivity.

The field of asymmetric photochemistry is poised for significant development over the next few decades. Despite the impressive advances that have emerged in this area in recent years, many challenges remain unsolved, perhaps most important of which is the need for generality. Some photocatalyst structures show promise to develop into privileged structures for enantioselective photochemical synthesis, catalyzing a number of highly enantioselective organic photoreactions with selectivities over 90% ee. These structures, however, are exceptional, and continued investigations are required to both establish their generality and to identify other classes of privileged asymmetric photocatalysts. While asymmetric photoreactions have the potential to greatly expedite the synthesis of complex products in unexplored areas of chemical diversity space, the continued development of more general methods is required before these reactions are used routinely by non-photochemists. We expect that the insights gained in research in this field to date will provide a solid foundation for continued transformative innovation.

1.10 References and Notes

[1] Sharpless, K. B. Searching for New Reactivity (Nobel Lecture). *Angew. Chem. Int. Ed.* **2002**, *41*, 2024–2032.

[2] Noyori, R. Asymmetric Catalysis: Science and Opportunities (Nobel Lecture 2001). *Adv. Synth. Catal.* **2003**, *345*, 15–32.

[3] Knowles, W. S. Asymmetric Hydrogenations (Nobel Lecture 2001). *Adv. Synth. Catal.* **2003**, *345*, 3–13.

[4] Ciamician, G. The Photochemistry of the Future. *Science* **1912**, *36*, 385–394.
[5] Roth, H. D. The Beginnings of Organic Photochemistry. *Angew. Chem. Int. Ed.* **1989**, *28*, 1193–1207.

[6] Inoue, Y.; Ramamurthy, V. *Molecular and Supramolecular Photochemistry, Volume 11: Chiral Photochemistry*; Marcel Dekker, **2004**.

[7] Inoue, Y. Asymmetric Photochemical Reactions in Solution. *Chem. Rev.* **1992**, *92*, 741–770.

[8] Sherbrook, E. M.; Yoon, T. P. Asymmetric Catalysis of Triplet-State Photoreactions. In *Specialist Periodical Reports: Photochemistry*; Albini, A., Protti, S., Eds.; Royal Society of Chemistry: Croydon, UK, 2019; Vol. *46*, pp 432−448.

[9] Inoue, Y.; Dong, F.; Yamamoto, K.; Tong, L. H.; Tsuneishi, H.; Hakushi, T.; Tai, A. Inclusion-Enhanced Optical Yield and *E*/*Z* Ratio in Enantiodifferentiating Photoisomerization of Cyclooctene Included and Sensitized by β-Cyclodextrin Monobenzoate. *J. Am. Chem. Soc.* **1995**, *117*, 11033–11034.

[10] Cauble, D. F.; Lynch, V.; Krische, M. J. Studies on the Enantioselective Catalysis of Photochemically Promoted Transformations: "Sensitizing Receptors" as Chiral Catalysts. *J. Org. Chem.* **2003**, *68*, 15–21.

[11] Griesbeck, A. G.; Meierhenrich, U. J. Asymmetric Photochemistry and Photochirogenesis. *Angew. Chem. Int. Ed.* **2002**, *41*, 3147–3154.

[12] Yang, C.; Inoue, Y. Supramolecular Photochirogenesis. *Chem. Soc. Rev.* **2014**, *43*, 4123–4143
[13] Brimioulle, R.; Lenhart, D.; Maturi, M. M.; Bach, T. Enantioselective Catalysis of Photochemical Reactions. *Angew. Chem. Int. Ed.* **2015**, *54*, 3872–3890.

[14] Garrido-Castro, A. F. Asymmetric Induction in Photocatalysis – Discovering a New Side to Light-Driven Chemistry. *Tetrahedron Lett.* **2018**, *59*, 1286–1294.

[15] Rao, M.; Wu, W.; Yang, C. Recent Progress on the Enantioselective Excited-State Photoreactions by Pre-Arrangement of Photosubstrate(s). *Green Synth. Catal.* **2021**, *2*, 131–144.

[16] Rigotti, T.; Alemán, J. Visible Light Photocatalysis – From Racemic to Asymmetric Activation Strategies. *Chem. Commun*. **2020**, *56*, 11169–11190.

[17] Nijland, A.; Harutyunyan, S. R. Light on the Horizon? Catalytic Enantioselective Photoreactions. Catal. Sci. Technol. **2013**, *3*, 1180–1189.

[18] Zhao, J.-J.; Zhang, H.-H.; Yu, S. Enantioselective Radical Functionalization of Imines and Iminium Intermediates via Visible-Light Photoredox Catalysis. *Synthesis* **2021**, *53*, 1706–1718.

[19] Prentice, C.; Morrisson, J.; Smith, A. D.; Zysman-Coleman, E. Recent Developments in Enantioselective Photocatalysis. **2020**, *16*, 2363–2441.

[20] Hong, B.-C. Enantioselective Synthesis Enabled by Visible Light Photocatalysis. *Org. Biomol. Chem.* **2020**, *18*, 4298–4353.

[21] Skubi, K. L.; Blum, T. R.; Yoon, T. P. Dual Catalysis Strategies in Photochemical Synthesis. *Chem. Rev*. **2016**, *116*, 10035–10074.

[22] Turro, N. J. Organic Photochemistry–An Overview. In *Modern Molecular Photochemistry*; Benjamin/Cummings: Menlo Park, CA, 1978; Chapter 1, pp 1−16

[23] Praetorius, P.; Korn, F. *Ber. Dtsch. Chem. Ges*. **1910**, *43*, 2744–2746.

[24] Alcock, N. W.; Herron, N.; Kemp, T. J.; Shoppee, C. W. Orientation of Photo-Dimerization by Metal Ions: The Crystal Structure of Bis(dibenzylideneacetone)uranyl Dichloride. *J. Chem. Soc., Chem. Commun*. **1975**, 785–786.

[25] Lewis, F. D.; Howard, D. K.; Oxman, J. D. Lewis Acid Catalysis of Coumarin Photodimerization. *J. Am. Chem. Soc*. **1983**, *105*, 3344–3345.

[26] Lewis, F. D.; Barancyk, S. V. Lewis Acid Catalysis of Photochemical Reactions. 8. Photodimerization and Cross-Cycloaddition of Coumarin. *J. Am. Chem. Soc.* **1989**, *111*, 8653–8661.

[27] Brenninger, C.; Jolliffe, J. D.; Bach, T. Chromophore Activation of α,β-Unsaturated Carbonyl Compounds and Its Application to Enantioselective Photochemical Reactions. *Angew. Chem. Int. Ed*. **2018**, *57*, 14338 – 14349.

[28] Schwinger, D. P.; Bach, T. Chiral 1,3,2-Oxazaborolidine Catalysts for Enantioselective Photochemical Reactions. *Acc. Chem. Res.* **2020**, *53*, 1933−1943.

[29] Guo, H.; Herdtweck, E.; Bach, T. Enantioselective Lewis Acid Catalysis in Intramolecular [2+2] Photocycloaddition Reactions of Coumarins. *Angew. Chem. Int. Ed*. **2010**, *49*, 7782–7785.

[30] Brimioulle, R.; Guo, H.; Bach, T. Enantioselective Intramolecular [2+2] Photocycloaddition Reactions of 4-Substituted Coumarins Catalyzed by a Chiral Lewis Acid. *Chem. - A Eur. J.* **2012**, *18*, 7552–7560.

[31] Brimioulle, R.; Bauer, A.; Bach, T. Enantioselective Lewis Acid Catalysis in Intramolecular [2 + 2] Photocycloaddition Reactions: A Mechanistic Comparison between Representative Coumarin and Enone Substrates. *J. Am. Chem. Soc.* **2015**, *137*, 5170–5176.

[32] Brimioulle, R.; Bach, T. Enantioselective Lewis Acid Catalysis of Intramolecular Enone [2+2] Photocycloaddition Reactions. *Science* **2013**, *342*, 840–843.

[33] Wang, H.; Cao, X.; Chen, X.; Fang, W.; Dolg, M. Regulatory Mechanism of the Enantioselective Intramolecular Enone [2+2] Photocycloaddition Reaction Mediated by a Chiral Lewis Acid Catalyst Containing Heavy Atoms. *Angew. Chem. Int. Ed.* **2015**, *54*, 14295–14298.

[34] Wang, H.; Fang, W. H.; Chen, X. Mechanism of the Enantioselective Intramolecular [2 + 2] Photocycloaddition Reaction of Coumarin Catalyzed by a Chiral Lewis Acid: Comparison with Enone Substrates. *J. Org. Chem.* **2016**, *81*, 7093–7101.

[35] Brimioulle, R.; Bach, T. [2+2] Photocycloaddition of 3-Alkenyloxy-2-cycloalkenones: Enantioselective Lewis Acid Catalysis and Ring Expansion. *Angew. Chem. Int. Ed.* **2014**, *53*, 12921–12924.

[36] Bach, T.; Hehn, J. Photochemical Reactions as Key Steps in Natural Product Synthesis. *Angew. Chem. Int. Ed.* **2011**, *50*, 1000–1045.

[37] Poplata, S.; Bach, T. Enantioselective Intermolecular [2+2] Photocycloaddition Reaction of Cyclic Enones and Its Application in a Synthesis of (–)-Grandisol. *J. Am. Chem. Soc.* **2018**, *140*, 3228–3231.

[38] Stegbauer, S.; Jandl, C.; Bach, T. Enantioselective Lewis Acid Catalyzed *ortho* Photocycloaddition of Olefins to Phenanthrene-9-carboxaldehydes. *Angew. Chem. Int. Ed.* **2018**, *57*, 14593−14596.

[39] El-Sayed, M. A. Triplet state. Its Radiative and Nonradiative Properties. *Acc. Chem. Res.* **1968**, *1*, 8−16.

[40] Griffiths, J.; Hart, H. A New General Photochemical Reaction of 2,4-Cyclohexadienones. *J. Am. Chem. Soc.* **1968**, *90*, 5296−5298.

[41] Uppili, S.; Ramamurthy, V. Enhanced Enantio- and Diastereoselectivities via Confinement: Photorearrangement of 2,4-Cyclohexadienones Included in Zeolites. *Org. Lett.* **2002**, *4*, 87−90.

[42] Leverenz, M.; Merten, C.; Dreuw, A.; Bach, T. Lewis Acid Catalyzed Enantioselective Photochemical Rearrangements on the Singlet Potential Energy Surface. *J. Am. Chem. Soc.* **2019**, *141*, 20053–20057.

[43] Fischer, J.; Mele, L.; Serier-Brault, H.; Nun, P.; Coeffard, V. Controlling Photooxygenation with a Bifunctional Quinine-BODIPY Catalyst: Towards Asymmetric Hydroxylation of β-Dicarbonyl Compounds. *Eur. J. Org. Chem.* **2019**, *37*, 6352–6358

[44] Werner, A. Zur Kenntnis des Asymmetrischen Kobaltatoms. I. *Chem. Ber.* **1911**, *44*, 1887–1898.

[45] Bauer, E. B. Chiral-at-Metal Complexes and Their Catalytic Applications in Organic Synthesis. *Chem. Soc. Rev.* **2012**, *41*, 3153–3167.

[46] Cao, Z.-Y.; Brittain, W. D. G.; Fossey, J. S.; Zhou, F. Recent Advances in the use of Chiral Metal Complexes with Achiral Ligands for Application in Asymmetric Catalysis. *Catal. Sci. Technol.* **2015**, *5*, 3441–3451.

[47] For a more comprehensive account on the early works of asymmetric photochemistry using chiral transition metal complexes see: Skubi, K. L. New Strategies for Catalytic Stereocontrol in Photochemical Synthesis. Ph. D. Thesis, University of Wisconsin–Madison, WI, 2017

[48] Geselowitz, D. A.; Taube, H. Stereoselectivity in Electron-Transfer Reactions. *J. Am. Chem. Soc.* **1980**, *102*, 4525–4526.

[49] Lappin, A. G.; Marusak, R. A. Stereoselectivity in Electron Transfer Reactions Involving Metal Ion Complexes. *Coord. Chem. Rev.* **1991**, *109*, 125–180.

[50] Porter, G. B.; Sparks, R. H. Generation of Optical Activity by Photoinduced Chiroselective Electron Transfer. *J. Chem. Soc., Chem. Commun.* **1979**, 1094–1095.

[51] Kaizu, Y.; Mori, T.; Kobayashi, H. Photoinduced Electron-Transfer Reactions between Optical Isomers. *J. Phys. Chem.* **1985**, *89*, 332–335.

[52] Kato, M.; Sasagawa, T.; Ishihara, Y.; Yamada, S.; Fujitani, S.; Kimura, M. Stereoselective Photosensitized Decomposition of Tris(oxalate)cobaltate(III) and Tris(acetylacetanato)cobalt(III) by Tris(2,2'-bipyridine)ruthenium(II). *J. Chem. Soc., Dalton Trans.* **1994**, 583–587.

[53] Dwyer, F. P.; Gyarfas, E. C. The Chemistry of Ruthenium. Part VI. The Existence of the Tris-*o*-Phenanthroline Ruthenium II and Tris-*o*-Phenanthroline Ruthenium III Ions in Enantiomorphous Forms. *Proc. Royal Soc. N. S. W.* **1949**, *83*, 170–173.

[54] Brandt, W. W.; Dwyer, F. P.; Gyarfas, E. C. Chelate Complexes of 1,10-Phenanthroline and Related Compounds. *Chem. Rev.* **1954**, *54*, 959–1017.

[55] Porter, G. B.; Sparks, R. H. Photoracemization of Ru(bipyridine)$_3^{2+}$. *J. Photochem.* **1980**, *13*, 123–131.

[56] Ohkubo, K.; Hamada, T.; Ishida, H. Novel Enantioselective Photocatalysis by Chiral, Helical Ruthenium(II) Complexes. *J. Chem. Soc., Chem. Commun.* **1993**, 1423–1425.

[57] Ohkubo, K.; Ishida, H.; Hamada, T.; Inaoka, T. Enantioselective Electron Transfer Reaction Catalyzed by a Novel Photosensitizer, $[Ru(S(-) \text{ or } R(+)\text{-PhEt*bpy})_3]^{2+}$. *Chem. Lett.* **1989**, *18*, 1545–1548.

[58] Ohkubo, K.; Hamada, T.; Inaoka, T.; Ishida, H. Photoinduced Enantioselective and Catalytic Reduction of $Co(acac)_3$ with a Chiral Ruthenium Photosensitizer. *Inorg. Chem.* **1989**, *28*, 2021–2022.

[59] Ohkubo, K.; Hamada, T.; Ishida, H.; Fukushima, M.; Watanabe, M. Stereoselective Molecular Recognition of Enantiomeric Cobalt(III) Complexes by Novel Photosensitizers of Helical Ruthenium(II) Complexes. *J. Mol. Catal.* **1994**, *89*, L5–L10.

[60] Ohkubo, K.; Hamada, T.; Watanabe, M. Novel Photoinduced Asymmetric Synthesis of Λ-$Co[(acac)_3]$from $Co(acac)_2(H_2O)_2$ and Hacac Catalysed by Racemic Complexes of Δ- and Λ-$[Ru(menbpy)_3]^{2+}$ {menbpy = 4,4'-Di[(1*R*,2*S*,5*R*)-(–)-menthoxycarbonyl)]-2,2'-bipyridine; Hacac = Pentane-2,4-dione}. *J. Chem. Soc., Chem. Commun*. **1993**, 1070–1072.

[61] Ohkubo, K.; Hamada, T.; Ishida, H.; Fukushima, M.; Watanabe, M.; Kobayashi, H. Stereoselective Photocatalysis of Helical Ruthenium(II) Complexes in the Reduction of Racemic Tris(acetylacetonato)cobalt(III). *J. Chem. Soc., Dalton Trans.* **1994**, 239–241.

[62] Ohkubo, K.; Fukushima, M.; Ohta, H.; Usui, S. Extremely High Stereoselectivity of Novel Helical Ruthenium(II) Complexes for Photoinduced Reduction of Racemic-$[Co(acac)_3]$ (Hacac = Pentane-2,4-dione). *J. Photochem. Photobiol. A* **1996**, *95*, 137–140.

[63] Rau, H.; Ratz, R. Asymmetry of Emission Quenching and Product Formation in an Asymmetrically Sensitized Photoreaction. *Angew. Chem. Int. Ed.* **1983**, *22*, 550–551.

[64] Wörner, M.; Greiner, G.; Rau, H. Asymmetric Electron Transfer from a Chiral Ru Complex Donor to an Atropisomeric Chiral 2,2'-Bipyridine Acceptor. *J. Phys. Chem.* **1995**, *99*, 14161–14166.

[65] Tsukahara, K.; Kaneko, J.; Miyaji, T.; Hara, T.; Kato, M.; Kimura, M. Stereoselective Luminescence Quenching in the Complex of Excited Triplet State of Δ-Tris(2,2'-bipyridine)ruthenium(II) with Optically Active Viologens in an Aqueous Solution. *Chem. Lett.* **1997**, *26*, 6455–456.

[66] Hamada, T.; Ishida, H.; Usui, S.; Watanabe, Y.; Tsumura, K.; Ohkubo, K. A Novel Photocatalytic Asymmetric Synthesis of (*R*)-(+)-1,1'-Bi-2-naphthol Derivatives by Oxidative Coupling of 3-Substituted-2-naphthol with Δ-$[Ru(menbpy)_3^{2+}]$ [menbpy = 4,4'-di(1*R*,2*S*,5*R*)-(–)-menthoxycarbonyl-2,2'-bipyridine], which Possesses Molecular Helicity. *J. Chem. Soc., Chem. Commun*. **1993**, 909–911.

[67] Hamada, T.; Ishida, H.; Usui, S.; Tsumura, K.; Ohkubo, K. Enantioselective and Photocatalytic Oxidation of 1,1'-Bi-2-naphthol with a Chiral Ruthenium Complex which Includes Molecular Helicity. *J. Mol. Catal.* **1994**, *88*, L1–L5.

[68] Brittain, H. G. Intermolecular Energy Transfer between Lanthanide Complexes in Aqueous Solution. 4. Stereoselectivity in the Transfer from Terbium(III) to Europium(III) Complexes of Aspartic Acid. *Inorg. Chem.* **1979**, *18*, 1740–1745.

[69] Brittain, H. G. Intermolecular Energy Transfer Between Lanthanide Complexes in Aqueous Solution—V: Stereoselectivity in the Transfer from Terbium(III) to Europium(III) Complexes of Malic Acid. *J. Inorg. Nucl. Chem.* **1979**, *41*, 721–724.

[70] Metcalf, D. H.; Snyder, S. W.; Wu, S.; Hilmes, G. L.; Riehl, J. P.; Demas, J. N.; Richardson, F. S. Excited-State Chiral Discrimination Observed by Time-Resolved Circularly Polarized Luminescence Measurements. *J. Am. Chem. Soc.* **1989**, *111*, 3082–3083.

[71] Metcalf, D. H.; Snyder, S. W.; Demas, J. N.; Richardson, F. S. Chiral Discrimination in Electronic Energy-Transfer Processes between Dissymmetric Metal Complexes in Solution. Time-Resolved Chiroptical Luminescence Measurements of Enantioselective Excited-State Quenching Kinetics. *J. Am. Chem. Soc.* **1990**, *112*, 5681–5695.

[72] Richardson, F. S.; Metcalf, D. H.; Glover, D. P. Intermolecular Chiral Recognition Probed by Enantioselective Quenching Kinetics. A Mechanistic Model for Dissymmetric Metal Complexes in Solution. *J. Phys. Chem.* **1991**, *95*, 6249–6259.

[73] Metcalf, D. H.; Bolender, J. P.; Driver, M. S.; Richardson, F. S. Chiral Discrimination in Electronic Energy Transfer between Dissymmetric Lanthanide(III) and Cobalt(III) Complexes in Solution. Effects of Ligand Size, Shape, and Configuration in the Acceptor Complexes. *J. Phys. Chem.* **1993**, *97*, 553–564.

[74] Metcalf, D. H.; Stewart, J. M. McD.; Snyder, S. W.; Grisham, C. M. Chiral Recognition between Dissymmetric $Ln(dpa)_3^{3-}$ and Co(III)-Nucleotide Complexes in Aqueous Solution. Enantioselective Luminescence Quenching as a Probe of Intermolecular Chiral Discrimination. *Inorg. Chem.* **1992**, *31*, 2445–2455.

[75] Meskers, S. C. J.; Dekkers, H. P. J. M. Enantioselective Excited-State Quenching of Racemic Tb (III) and Eu (III) Tris (pyridine-2,6-dicarboxylate) by Vitamin B_{12} Derivatives. *Spectrochim. Acta A.* **1999**, *55*, 1857–1874.

[76] Bolender, J. P.; Metcalf, D. H.; Richardson, F. S. Chirality-Dependent Intermolecular Interactions Probed by Time-Resolved Chiroptical Luminescence Measurements of Enantio-differential Excited-State Quenching Kinetics. *Chem Phys. Lett.* **1993**, *213*, 131–138.

[77] Yu, H.; Dong, S.; Yao, Q.; Chen, L.; Zhang, D.; Liu, X.; Feng, X. Enantioselective [2+2] Photocycloaddition Reactions of Enones and Olefins with Visible Light Mediated by *N*,*N*'-Dioxide–Metal Complexes. *Chem. Eur. J.* **2018**, *24*, 19361–19367.

[78] Ma, J.; Zhang, X.; Huang, X.; Luo, S.; Meggers, E. Preparation of Chiral-at-Metal Catalysts and Their use in Asymmetric Photoredox Chemistry. *Nat. Protoc.* **2018**, *13*, 605–632.

[79] Zhang, L.; Meggers, E. Steering Asymmetric Lewis Acid Catalysis Exclusively with Octahedral Metal-Centered Chirality. *Acc. Chem. Res.* **2017**, *50*, 320−330.

[80] Chen, L.-A.; Xu, W.; Huang, B.; Ma, J.; Wang, L.; Xi, J.; Harms,K.; Gong, L.; Meggers, E. Asymmetric Catalysis with an Inert Chiral-at-Metal Iridium Complex. *J. Am. Chem. Soc.* **2013**, *135*, 10598−10601.

[81] Chen, L.-A.; Tang, X.; Xi, J.; Xu, W.; Gong, L.; Meggers, E. Chiral-at-Metal Octahedral Iridium Catalyst for the Asymmetric Construction of an All-Carbon Quaternary Stereocenter. *Angew. Chem. Int. Ed.* **2013**, *52*, 14021−14025.

[82] Ma, J.; Ding, X.; Hu, Y.; Huang, Y.; Gong, L.; Meggers, E. Metal-Templated Chiral Brønsted Base Organocatalysis. *Nat. Commun.* **2014**, *5*, 4531.

[83] Huo, H.; Fu, C.; Wang, C.; Harms, K.; Meggers, E. Metal-Templated Enantioselective Enamine/H-Bonding Dual Activation Catalysis. *Chem. Commun.* **2014**, *50*, 10409−104111.

[84] Huo, H.; Shen, X.; Wang, C.; Zhang, L.; Röse, P.; Chen, L. A.; Harms, K.; Marsch, M.; Hilt, G.; Meggers, E. Asymmetric Photoredox Transition-Metal Catalysis Activated by Visible Light. *Nature* **2014**, *515*, 100–103.

[85] Huo, H.; Wang, C.; Harms, K.; Meggers, E. Enantioselective, Catalytic Trichloromethylation through Visible-Light-Activated Photoredox Catalysis with a Chiral Iridium Complex. *J. Am. Chem. Soc.* **2015**, *137*, 9551–9554.

[86] Huo, H.; Huang, X.; Shen, X.; Harms, K.; Meggers, E. Visible-Light-Activated Enantioselective Perfluoroalkylation with a Chiral Iridium Photoredox Catalyst. *Synlett* **2016**, *27*, 749–753.

[87] Zhang, X.; Qin, J.; Huang, X.; Meggers, E. Sequential Asymmetric Hydrogenation and Photoredox Chemistry with a Single Catalyst. *Org. Chem. Front.* **2018**, *5*, 166–170.

[88] Zhang, X.; Qin, J.; Huang, X.; Meggers, E. One-Pot Sequential Photoredox Chemistry and Asymmetric Transfer Hydrogenation with a Single Catalyst. *Eur. J. Org. Chem.* **2018**, *2018*, 571–577.

[89] Wang, C.; Zheng, Y.; Huo, H.; Röse, P.; Zhang, L.; Harms, K.; Hilt, G.; Meggers, E. Merger of Visible Light Induced Oxidation and Enantioselective Alkylation with a Chiral Iridium Catalyst. *Chem. - Eur. J.* **2015**, *21*, 7355–7359.

[90] Wang, C.; Qin, J.; Shen, X.; Riedel, R.; Harms, K.; Meggers, E. Asymmetric Radical-Radical Cross-Coupling through Visible-Light-Activated Iridium Catalysis. *Angew. Chem. Int. Ed.* **2016**, *55*, 685–688.

[91] Böhm, A.; Bach, T. Synthesis of Supramolecular Iridium Catalysts and Their Use in Enantioselective Visible-Light-Induced Reactions. *Synlett* **2016**, *27*, 1056–1060.

[92] Gualandi, A.; Calogero, F.; Martinelli, A.; Quintavalla, A.; Marchini, M.; Ceroni, P.; Lombardo, M.; Cozzi, P. G. A Supramolecular Bifunctional Iridium Photocatalyst for the Enantioselective Alkylation of Aldehydes. *Dalton Trans.* **2020**, *49*, 14497–14505.

[93] Skubi, K. L.; Kidd, J. B.; Jung, H.; Guzei, I. A.; Baik, M. H.; Yoon, T. P. Enantioselective Excited-State Photoreactions Controlled by a Chiral Hydrogen-Bonding Iridium Sensitizer. *J. Am. Chem. Soc.* **2017**, *139*, 17186–17192.

[94] Zheng, J.; Swords, W. B.; Jung, H.; Skubi, K. L.; Kidd, J. B.; Meyer, G. J.; Baik, M. H.; Yoon, T. P. Enantioselective Intermolecular Excited-State Photoreactions Using a Chiral Ir Triplet Sensitizer: Separating Association from Energy Transfer in Asymmetric Photocatalysis. *J. Am. Chem. Soc.* **2019**, *141*, 13625–13634.

[95] Swords, W. B.; Yoon, T. P. Chiral-at-Ir Photosensitized Asymmetric 6π-Elecrocyclization. *Manuscript in Preparation*.

[96] Uraguchi, D.; Kinoshita, N.; Kizu, T.; Ooi, T. Synergistic Catalysis of Ionic Brønsted Acid and Photosensitizer for a Redox Neutral Asymmetric α-Coupling of *N*-Arylaminomethanes with Aldimines. *J. Am. Chem. Soc.* **2015**, *137*, 13768–13771.

[97] Uraguchi, D.; Kimura, Y.; Ueoka, F.; Ooi, T.; Urea as a Redox-Active Directing Group under Asymmetric Photocatalysis of Iridium-Chiral Borate Ion Pairs. *J. Am. Chem. Soc.* **2020**, *142*, 19462–19467.

[98] Kimura, Y.; Uraguchi, D.; Ooi, T. Catalytic Asymmetric Synthesis of 5-Membered Alicyclic α-Quaternary β-amino acids *via* [3+2]-photocycloaddition of α-substituted acrylates. *Org. Biomol. Chem.* **2021**, *19*, 1744–1747.

[99] Chapman, S. J.; Swords, W. B.; Son, M.; Park, Y.; Le, C.; Guzei, I. A.; Toste, D.; Baik, M. -H.; Yoon, T, P. Cooperative Stereoinduction in Asymmetric Photocatalysis. *Manuscript in Submission*.

[100] Rössler, S. L., Petrone, D. A. & Carreira, E. M. Iridium-catalyzed Asymmetric Synthesis of Functionally Rich Molecules Enabled by (Phosphoramidite,olefin) Ligands. *Acc. Chem. Res.* **2019**, *52*, 2657–2672.

[101] Crisenza, G. E. M.; Faraone, A.; Gandolfo, E.; Mazzarella, D.; Melchiorre, P. Catalytic Asymmetric C–C Cross-couplings Enabled by Photoexcitation. *Nat. Chem.* **2021**, *13*, 575–580.
[102] Huang, X.; Meggers, E. Asymmetric Photocatalysis with Bis-Cyclometalated Rhodium Complexes. *Acc. Chem. Res.* **2019**, *52*, 833–847.

[103] Shen, X.; Harms, K.; Marsch, M.; Meggers, E. A Rhodium Catalyst Superior to Iridium Congeners for Enantioselective Radical Amination Activated by Visible Light. *Chem. - Eur. J.* **2016**, *22*, 9102–9105.

[104] Wang, C.; Chen, L.-A.; Huo, H.; Shen, X.; Harms, K.; Gong, L.; Meggers, E. Asymmetric Lewis Acid Catalysis Directed by Octahedral Rhodium Centrochirality. *Chem. Sci.* **2015**, *6*, 1094−1100.

[105] Ma, J.; Shen, X.; Harms, K.; Meggers, E. Expanding the Family of Bis-cyclometalated Chiral-at-Metal Rhodium(III) Catalysts with a Benzothiazole Derivative. *Dalton Trans.* **2016**, *45*, 8320−8323.

[106] Tan, Y.; Yuan, W.; Gong, L.; Meggers, E. Aerobic Asymmetric Dehydrogenative Cross-Coupling between Two C_{sp3}—H Groups Catalyzed by a Chiral-at-Metal Rhodium Complex. *Angew. Chem. Int. Ed.* **2015**, *54*, 13045–13048.

[107] Lin, S. X.; Sun, G. J.; Kang, Q. A Visible-Light-Activated Rhodium Complex in Enantioselective Conjugate Addition of α-Amino Radicals with Michael Acceptors. *Chem. Commun.* **2017**, *53*, 7665–7668.

[108] de Assis, F. F.; Huang, X.; Akiyama, M.; Pilli, R. A.; Meggers, E. Visible-Light-Activated Catalytic Enantioselective β-Alkylation of α,β-Unsaturated 2-Acyl Imidazoles Using Hantzsch Esters as Radical Reservoirs. *J. Org. Chem.* **2018**, *83*, 10922–10932.

[109] Ma, J.; Lin, J.; Zhao, L.; Harms, K.; Marsch, M.; Xie, X.; Meggers, E. Synthesis of β-Substituted γ-Aminobutyric Acid Derivatives through Enantioselective Photoredox Catalysis. *Angew. Chem. Int. Ed.* **2018**, *57*, 11193–11197.

[110] Chen, L.; Hu, L.; Du, Y.; Su, W.; Kang, Q. Asymmetric Photoinduced Giese Radical Addition Enabled by a Single Chiral-at-Metal Rhodium Complex. *Chin. J. Org. Chem.* **2020**, *40*, 3944–3952.

[111] Steinlandt, P. S.; Zuo, W.; Harms, K.; Meggers, E. Bis-Cyclometalated Indazole Chiral-at-Rhodium Catalyst for Asymmetric Photoredox Cyanoalkylations. *Chem. - Eur. J.* **2019**, *25*, 15333–15340.

[112] Tutkowski, B.; Meggers, E.; Wiest, O. Understanding Rate Acceleration and Stereoinduction of an Asymmetric Giese Reaction Mediated by a Chiral Rhodium Catalyst. *J. Am. Chem. Soc.* **2017**, *139*, 8062–8065.

[113] Huang, X.; Webster, R. D.; Harms, K.; Meggers, E. Asymmetric Catalysis with Organic Azides and Diazo Compounds Initiated by Photoinduced Electron Transfer. *J. Am. Chem. Soc.* **2016**, *138*, 12636−12642.

[114] Chen, S.; Huang, X.; Meggers, E.; Houk, K. N. Origins of Enantioselectivity in Asymmetric Radical Additions to Octahedral Chiral-at-Rhodium Enolates: A Computational Study. *J. Am. Chem. Soc.* **2017**, *139*, 17902–17907.

[115] Ma, J.; Rosales, A. R.; Huang, X.; Harms, K.; Riedel, R.; Wiest, O.; Meggers, E. Visible-Light-Activated Asymmetric β-C–H Functionalization of Acceptor-Substituted Ketones with 1,2-Dicarbonyl Compounds. *J. Am. Chem. Soc.* **2017**, *139*, 17245–17248.

[116] Zhou, Z.; Nie, X.; Harms, K.; Riedel, R.; Zhang, L.; Meggers, E. Enantioconvergent Photoredox Radical-Radical Coupling Catalyzed by a Chiral-at-Rhodium Complex. *Sci. China Chem.* **2019**, *62*, 1512–1518.

[117] Zhang, C.; Gao, A. Z.; Nie, X.; Ye, C. -X.; Ivlev, S.; Chen.; Meggers, E. Catalytic α-Deracemization of Ketones Enabled by Photoredox Deprotonation and Enantioselective Protonation. *J. Am. Chem. Soc.* https://doi.org/10.1021/jacs.1c06637.

[118] Huang, X.; Lin, J.; Shen, T.; Harms, K.; Marchini, M.; Ceroni, P.; Meggers, E. Asymmetric [3+2] Photocycloadditions of Cyclopropanes with Alkenes or Alkynes through Visible-Light Excitation of Catalyst-Bound Substrates. *Angew. Chem. Int. Ed.* **2018**, *57*, 5454–5458.

[119] Huang, X.; Quinn, T. R.; Harms, K.; Webster, R. D.; Zhang, L.; Wiest, O.; Meggers, E. Direct Visible-Light-Excited Asymmetric Lewis Acid Catalysis of Intermolecular [2+2] Photocycloadditions. *J. Am. Chem. Soc.* **2017**, *139*, 9120–9123.

[120] Jung, H.; Hong, M.; Marchini, M.; Villa, M.; Steinlandt, P. S.; Huang, X.; Hemming, M.; Meggers, E.; Ceroni, P.; Park, J.; Baik, M. –H. Understanding the Mechanism of Direct Visible-light-activated [2+2] Cycloadditions Mediated by Rh and Ir photocatalysts: Combined Computational and Spectroscopic Studies. *Chem. Sci.* **2021,** *12*, 9673–9681.

[121] Grell, Y.; Hong, Y.; Huang, X.; Mochizuki, T.; Xie, X.; Harms, K.; Meggers, E. Chiral-at-Rhodium Catalyst Containing Two Different Cyclometalating Ligands. *Organometallics* **2019**, *38*, 3948–3954.

[122] Hu, N.; Jung, H.; Zheng, Y.; Lee, J.; Zhang, L.; Ullah, Z.; Xie, X.; Harms, K.; Baik, M. H.; Meggers, E. Catalytic Asymmetric Dearomatization by Visible-Light-Activated [2+2] Photocycloaddition. *Angew. Chem. Int. Ed.* **2018**, *57*, 6242–6246.

[123] Jeremias, N.; Mohr, L. –M.; Bach, T. Intermolecular [2+2] Photocycloaddition of α,β-Unsaturated Sulfones: Catalyst-Free Reaction and Catalytic Variants. *Org. Lett.* **2021**, *23*, 5674–5678.

[124] Huang, X.; Li, X.; Xie, X.; Harms, K.; Riedel, R.; Meggers, E. Catalytic Asymmetric Synthesis of a Nitrogen Heterocycle through Stereocontrolled Direct Photoreaction from Electronically Excited State. *Nat. Commun.* **2017**, *8*, 2245.

[125] Zhang, C.; Chen, S.; Ye, C.; Harms, K.; Zhang, L.; Houk, K. N.; Meggers, E. Asymmetric Photocatalysis by Intramolecular Hydrogen-Atom Transfer in Photoexcited Catalyst–Substrate Complex. *Angew. Chem. Int. Ed.* **2019**, *58*, 14462–14466.

[126] Woodhouse, M.; McCusker, J. K. Mechanistic Origin of Photoredox Catalysis Involving Iron(II) Polypyridyl Chromophores. *J. Am. Chem. Soc.* **2020**, *142*, 16229−16233.

[127] Ding, W.; Lu, L. Q.; Zhou, Q. Q.; Wei, Y.; Chen, J. R.; Xiao, W. J. Bifunctional Photocatalysts for Enantioselective Aerobic Oxidation of β-Ketoesters. *J. Am. Chem. Soc.* **2017**, *139*, 63–66.

[128] Shen, X.; Li, Y.; Wen, Z.; Cao, S.; Hou, X.; Gong, L. A Chiral Nickel DBFOX Complex as a Bifunctional Catalyst for Visible-Light-Promoted Asymmetric Photoredox Reactions. *Chem. Sci.* **2018**, *9*, 4562–4568.

[129] Ruiz Espelt, L.; Wiensch, E. M.; Yoon, T. P. Brønsted Acid Cocatalysts in Photocatalytic Radical Addition of α-Amino C–H Bonds across Michael Acceptors. *J. Org. Chem.* **2013**, *78*, 4107–4114.

[130] Ruiz Espelt, L.; McPherson, I. S.; Wiensch, E. M.; Yoon, T. P. Enantioselective Conjugate Additions of α-Amino Radicals via Cooperative Photoredox and Lewis Acid Catalysis. *J. Am. Chem. Soc.* **2015**, *137*, 2452–2455.

[131] Endo, K.; Liu, Y.; Ube, H.; Nagata, K.; Shionoya, M. Asymmetric Construction of Tetrahedral Chiral Zinc with High Configurational Stability and Catalytic Activity. *Nat. Commun.* **2020**, *11*, 6263.

[132] Sakaki, S.; Satoh, T.; Ohkubo, K. Stereo-Selective Photo-Induced Electron Transfer Reaction from [Cu(dmp)((*R*, *R*)-diop)]$^{+}$ ((*R*, *R*)-Diop = (*R*, *R*)-2,3-*o*-Isopropylidene-2,3-dihdydroxy-1,4-bis(diphenylphosphino)butane, dmp = 2,9-Dimethyl-1,10-phenanthroline) to [Co(edta)]$^{-}$. *New J. Chem.* **1986**, *10*, 145–147.

[133] Sakaki, S.; Ishikura, H.; Kuraki, K.-I.; Tanaka, K.-J.; Satoh, T.; Arai, T.; Hamada, T. Synthesis of a New Chiral Copper(I) Complex and its Application to Stereoselective Photoreduction of [Co(edta)]$^{-}$ (H_4edta = Ethylenedinitrioltetraacetic Acid). *J. Chem. Soc., Dalton Trans.* **1997**, 1815–1820.

[134] Sakaki, S.; Horita, R.; Kuraki, K.; Hamada, T. Photoasymmetric Synthesis of [Co(edta)]$^{-}$ from Co(II) Salt and L_4edta (L = H^{+} or Na^{+}), using a Chiral Cu(I) Complex. *Chem. Lett.* **1998**, *27*, 827–828.

[135] Edtmüller, V.; Pöthig, A.; Bach, T. Enantioselective Photocyclisation Reactions of 2-Aryloxycyclohex-2-enones Mediated by a Chiral Copper-Bisoxazoline Complex. *Tetrahedron* **2017**, *73*, 5038–5047.

[136] Creutz, S. E.; Lotito, K. J.; Fu, G. C.; Peters, J. C. Photoinduced Ullmann C–N Coupling: Demonstrating the Viability of a Radical Pathway. *Science* **2012**, *338*, 647–651.

[137] Uyeda, C.; Tan, Y.; Fu, G. C.; Peters, J. C. A New Family of Nucleophiles for Photoinduced, Copper-Catalyzed Cross-Couplings via Single-Electron Transfer: Reactions of Thiols with Aryl Halides Under Mild Conditions (0 °C). *J. Am. Chem. Soc.* **2013**, *135*, 9548–9552.

[138] Tan, Y.; Muñoz-Molina, J. M.; Fu, G. C.; Peters, J. C. Oxygen Nucleophiles as Reaction Partners in Photoinduced, Copper-Catalyzed Cross-Couplings: *O*-Arylations of Phenols at Room Temperature. *Chem. Sci.* **2014**, *5*, 2831–2835.

[139] Ahn, J. M.; Peters, J. C.; Fu, G. C. Design of a Photoredox Catalyst that Enables the Direct Synthesis of Carbamate-Protected Primary Amines via Photoinduced, Copper-Catalyzed *N*-Alkylation Reactions of Unactivated Secondary Halides. *J. Am. Chem. Soc.* **2017**, *139*, 18101–18106.

[140] Matier, C. D.; Schwaben, J.; Peters, J. C.; Fu, G. C. Copper-Catalyzed Alkylation of Aliphatic Amines Induced by Visible Light. *J. Am. Chem. Soc.* **2017**, *139*, 17707–17710.

[141] Zhao, W.; Wurz, R. P.; Peters, J. C.; Fu, G. C. Photoinduced, Copper-Catalyzed Decarboxylative C–N Coupling to Generate Protected Amines: An Alternative to the Curtius Rearrangement. *J. Am. Chem. Soc.* **2017**, *139*, 12153–12156.

[142] Kainz, Q. M.; Matier, C. D.; Bartoszewicz, A.; Zultanski, S. L.; Peters, J. C.; Fu, G. C. Asymmetric Copper-Catalyzed C–N Cross-Couplings Induced by Visible Light. *Science* **2016**, *351*, 681–684.

[143] Chen, C.; Peters, J. C.; Fu, G. C. Photoinduced Copper-Catalysed Asymmetric Amidation via Ligand Cooperativity. *Nature* **2021**, *596*, 250–256.

[144] Guo, Q.; Wang, M.; Peng, Q.; Huo, Y.; Liu, Q.; Wang, R.; Xu, Z. Dual-Functional Chiral Cu-Catalyst-Induced Photoredox Asymmetric Cyanofluoroalkylation of Alkenes. *ACS Catal.* **2019**, *9*, 4470–4476.

[145] Zhang, Y.; Sun, Y.; Chen, B.; Xu, M.; Li, C.; Zhang, D.; Zhang, G. Copper-Catalyzed Photoinduced Enantioselective Dual Carbofunctionalization of Alkenes. *Org. Lett.* **2020**, *22*, 1490–1494.

[146] Xia, H. -D.; Li, Z. -L.; Gu, Q. -S.; Dong, X. -Y.; Fang, J. -H.; Du, X. -Y.; Wang, L. -L.; Liu, X. -Y. Photoinduced Copper-Catalyzed Asymmetric Decarboxylative Alkynlation with Terminal Alkynes. *Angew. Chem. Int. Ed.* **2020**, *59*, 16926–16932.

[147] Qi, R.; Wang, C.; Huo, Y.; Chai, H.; Wang, H.; Ma, Z.; Liu, L.; Wang, R.; Xu, Z. Visible Light Induced Cu–Catalyzed Asymmetric C(sp^3)–H Alkylation. https://doi.org/10.1021/jacs.1c05890.

[148] J. K. Kochi, Photolyses of metal compounds: Cupric chloride in organic media. *J. Am. Chem. Soc.*, **1962**, *84*, 2121–2127.

[149] J. -J. Guo et al., Photocatalytic C-C bond cleavage and amination of cycloalkanols by cerium(III) chloride complex. *Angew. Chem. Int. Ed.* **2016**, *55*, 15319–15322.

[150] A. Hu, J.-J. Guo, H. Pan, Z. Zuo, Selective functionalization of methane, ethane, and higher alkanes by cerium photocatalysis. *Science* **2018**, *361*, 668–672.

[151] A. Hossain et al., Visible-light-accelerated copper(II)-catalyzed regio- and chemoselective oxo-azidation of vinyl arenes. *Angew. Chem. Int. Ed.* **2018**, *57*, 8288–8292.

[152] Treacy, S. M.; Rovis, T. *J. Am. Chem. Soc.* **2021**, DOI: 10.1021/jacs.1021c00687

[153] Li, Y.; Zhou, K.; Wen, Z.; Cao, S.; Shen, X.; Lei, M.; Gong, L. Copper(II)-Catalyzed Asymmetric Photoredox Reactions: Enantioselective Alkylation of Imines Driven by Visible Light. *J. Am. Chem. Soc.* **2018**, *140*, 15850–15858.

[154] Han, B.; Li, Y.; Yu, Y.; Gong, L. Photocatalytic Enantioselective α-Aminoalkylation of Acyclic Imine Derivatives by a Chiral Copper Catalyst. *Nat. Commun.* **2019**, *10*. 3804.

[155] Zhou, K.; Yu, Y.; Lin, Y. -M.; Li, Y.; Gong, L. Copper-catalyzed Aerobic Asymmetric Cross-dehydrogenative Coupling of C(sp^3)–H Bonds Driven by Visible Light. *Green Chem.* **2020**, *22*, 4597–4603.

[156] Chen, J.; Liang, Y. -J.; Wang, P. -Z.; Li, G. -Q.; Zhang, B.; Qian, H.; Huan, X. -D.; Guan, W.; Xiao, W. -J.; Chen, J. -R. Photoinduced Copper -Catalyzed Asymmetric C–O Cross-Coupling. https://doi.org/10.1021/jacs.1c06535.

Chapter 2. Enantioselective Excited-State Photoreactions Controlled by a Chiral Hydrogen-Bonding Iridium Sensitizer

Portions of this work have been published previously:

Skubi, K. L.; Kidd, J. B.; Jung, H.; Guzei, I. A.; Baik, M. -H.; Yoon, T. P. Enantioselective Excited-State Photoreactions Controlled by a Chiral Hydrogen-Bonding Iridium Sensitizer. *J. Am. Chem. Soc.* **2017**, *138*, 17186–17192.

2.1 Introduction

Recently, photochemistry has emerged as a powerful tool in the generation of reactive intermediates that can aid in the synthesis of complex molecular architectures that cannot be accessed by other means.[1–3] Perhaps this is best exemplified by the canonical [2+2] photocycloaddition between two alkenes. In the ground state, this cycloaddition is a symmetry-forbidden process as predicted by the Woodward–Hoffman rules. However, upon the promotion of one of the alkenes to its electronically excited state, the [2+2] can proceed, affording structurally rich cyclobutanes. Additionally, in the past fifty years considerable efforts have been directed toward the design of strategies and methods to control the absolute stereochemistry of organic transformations. The field of photochemical synthesis, however, has remained a conspicuous outlier to this trend. Central to this challenge is the suppression of racemic background processes, reaction pathways that form the product outside of the influence of a stereodifferentiating environment. This difficulty overlaps with the utility of photochemistry to activate small molecules to generate highly energetic intermediates that are typically short lived, positing that the bimolecular interception of these transient species by a chiral catalyst extremely unlikely. Thus, successful strategies have relied upon the generation of the reactive intermediate within a well-defined chiral environment to bias the stereochemistry of subsequent bond formation.

2.1.1 Asymmetric Secondary Photochemical Processes

The vast majority of successful stereocontrolled photoreactions proceed by photoredox catalysis, in which the generation of radical or radical ion intermediates occurs through photoinduced electron transfer (PET). These processes are termed secondary photochemical reactions, in that the key bond formation arises from a photochemically generated intermediate in

its ground state.[45] In these transformations the stereochemical controller is often coupled to the generation of the key reactive intermediates. For example, in 2014 our group published on the enantioselective [2+2] cycloaddition of enones (Scheme 2.1).[6] This reaction advances through the reduction of Lewis acid coordinated enone **2.1** by photoexcited $Ru(bpy)_3^{2+}$ to afford the corresponding radical anion within the steric influence imparted by the chiral Lewis acid. Importantly, the Lewis acid is dual-purposed, activating the enone for reduction upon binding and imparting stereocontrol over the subsequent C–C bond formation. Other noteworthy examples of this strategy include reports by Knowles using a chiral Brønsted acid to aid in the generation ketyl radicals by proton coupled electron transfer[7] and a more recent example by Ooi that utilized a chiral borate to bind a *N*-cyclopropyl urea, enabling its reduction by PET.[8,9]

Scheme 2.1. Photochemically Generated Radical Using Dual-Catalytic Approach

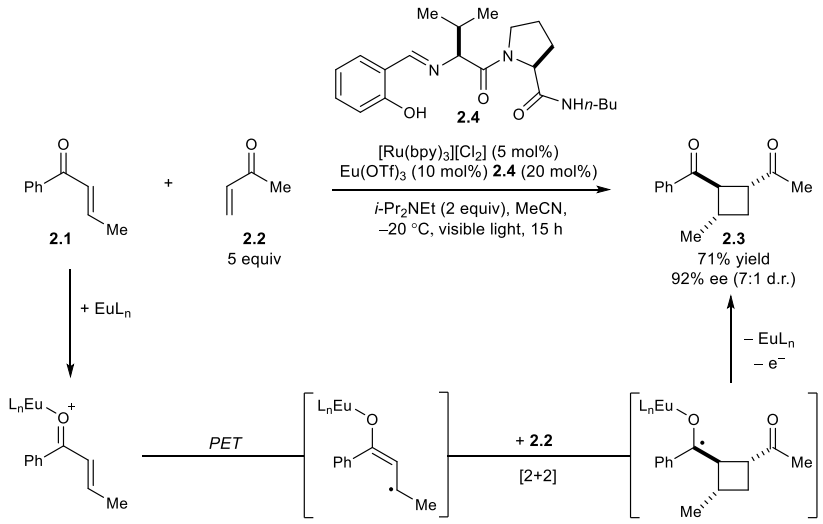

A complementary strategy to render a photoredox reaction asymmetric is by employing a chiral catalyst in a downstream process, after the photochemical activation step (Scheme 2.2). In many cases, the chiral controller is spatially separated from the molecule that undergoes electron transfer with the photocatalyst. For example, we recently demonstrated that α-amino radicals,

generated by oxidation and concomitant mesolytic cleavage, can react with chiral Lewis acid bound Michael acceptors with good enantiofacial bias.[10] In this instance, the Lewis acid accelerates the rate of addition of the radical, outcompeting the parallel racemic reaction.[11] Furthermore, metallophotoredox catalysis has developed as a valuable cross-coupling strategy by merging the benefits of photoredox catalysis with organotransition metal chemistry.[12–15] In some of these works, an alkyl radical can undergo facile recombination with nickel intermediates followed by elementary steps to afford the cross-coupled product. The stereochemical outcome of these transformations can thus be controlled by the use of optically active ligands coordinated to the metal center.[16–19]

Scheme 2.2. Examples of Downstream Asymmetric Secondary Photoreactions

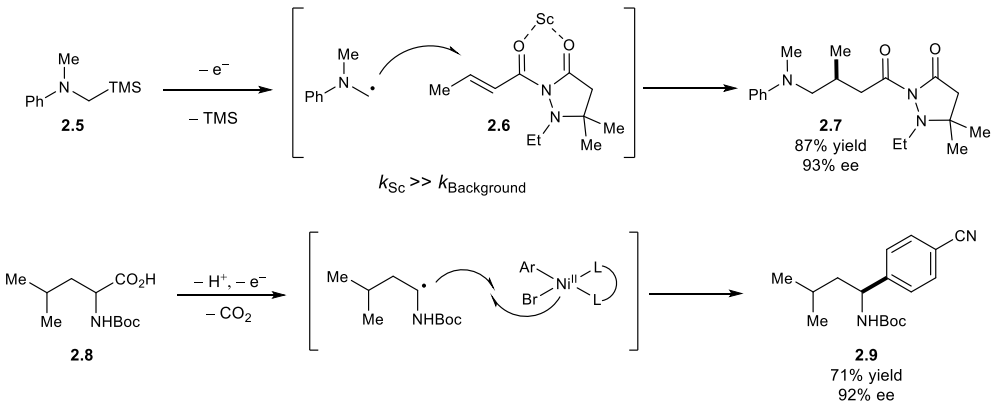

2.1.2 Asymmetric Primary Photoreaction Processes

Although substantial progress has been made in the stereocontrol of secondary photochemical processes that involve ground states, the same level of control for primary photoreactions have been considerably less developed. Primary photochemical reactions occur when the key bond forming steps arise directly from an electronically excited-state molecule. Compared to the open-shell intermediates discussed above, excited-state species are also subject

to vanishingly short lifetimes. However, these high-energy intermediates are additionally prone to relaxation to their ground state, most commonly accomplished by rapid unimolecular pathways such as fluorescence, phosphorescence, *E*/*Z* isomerization and internal conversion.

As discussed in Chapter 1, key to the development of asymmetric photochemical protocols is the suppression background racemic processes. Specifically problematic to enantioselective primary photoreactions is the potential of direct excitation of the substrate, which can lead to its reaction prior to an interaction with a chiral catalyst. To avoid this background excitation, a chiral photocatalyst can be employed to absorb photons at a wavelength that is substantially different from that of the substate. Subsequent energy transfer from the photoexcited catalyst to the organic molecule yields its excited state. This energy transfer mechanism proceeds by a collisional activation event in which the encounter complex is typically short lived. Thus, early investigations in this field postulated that if the interaction in this encounter complex could be prolonged, stereoinduction could be possible.

In 1965, Hammond was the first to demonstrate this proof-of-principle using chiral naphthylamide catalyst **2.12** to deracemize and reach a photostationary state of 1,2-diphenyl cyclopropane **2.10** in 7% ee (Scheme 2.3).[20–22] The interconversion of (*R*)- and (*S*)-**2.10** likely occurs via bond cleavage of the excited-state cyclopropane to the corresponding 1,3-diradical followed by ring closure. The chiral arene in this reaction imparts its chiral information through the formation of an exciplex,[23] an electronically excited bimolecular complex between two species that are not associated in the ground state but rather exclusively interact in the excited state. Notably, activation by exciplex formation is mechanistically distinct from energy transfer, wherein the exciton is shared, rather than transferred, across the sensitizer and substrate.

Scheme 2.3. Photochemical deracemization via Exciplex Formation

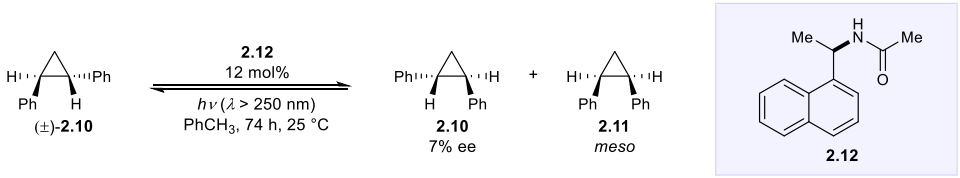

Many variations of this concept have been reported since then including the deracemization of sulfoxides[24] and allenes,[25] the enantioselective isomerization of (*E*)-cyclooctene to optically active (*Z*)-cyclooctene,[26] and a triplex activated Diels–Alder cycloaddition catalyzed by an axially chiral cyanoarene.[27] However valuable these proof-of-concept examples are, the majority rarely achieve selectivity above 20% ee due to ill-defined substrate–catalyst interactions and relatively short exciplex lifetimes. Since then, a guiding strategy for most highly enantioselective photoreactions has relied upon a preassociation principle that was originally articulated by Inoue[28] and later expanded to small molecule catalysis by Krische.[29] This principle argues that racemic background pathways will be minimized when the chiral catalyst can organize and orient the substrate in the ground state within a well-defined stereodifferentiating environment. Secondly, this catalyst must confer a kinetic advantage for the photoreaction — either by direct excitation or sensitization — once the substrate is bound. Lastly, if the rate of the reaction is faster than the rate of dissociation of the complex then product formation will predominantly occur within the influence of the chiral catalyst.

To satisfy these criteria, Krische designed a catalyst bearing a chiral hydrogen-bonding domain capable of recruiting quinolone **2.13**. Strategically embedded within catalyst **2.15** is a benzophenone triplet sensitizer, thereby creating a binding-induced rate enhancement due to the distance dependence on energy transfer. With superstiochiometric loadings of **2.15**, the [2+2]

photocycloaddition of the quinolone was promoted in 21% ee (Scheme 2.4). Photocatalyst **2.15** could be reduced to 25 mol% without significant erosion of enantioselectivity (19% ee). These results imply that the **2.15** is efficient at binding and sensitizing **2.13** for its cycloaddition, however, is a poor catalyst for enantiofacial bias.

Scheme 2.4. Enantioselective [2+2] Cycloaddition using Chiral Hydrogen-Bonding Photocatalyst

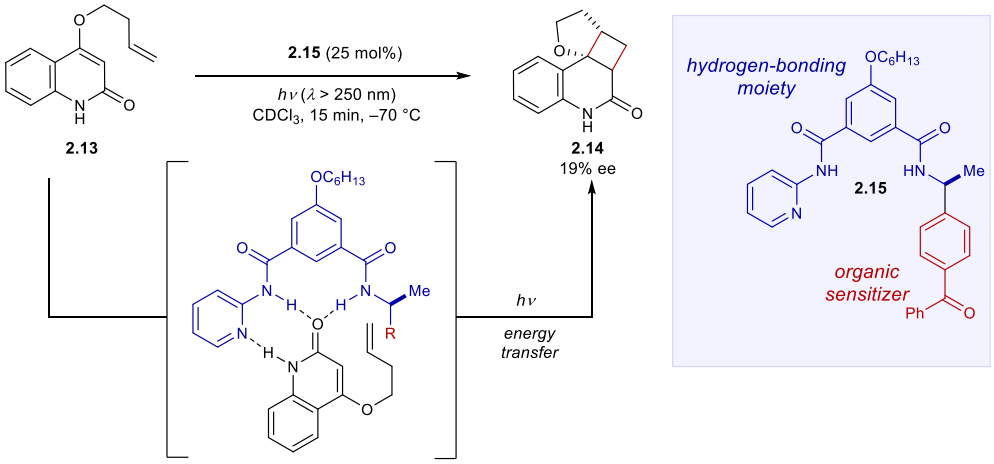

A similar strategy was later utilized by Bach with a chiral hydrogen-bonding controller, derived from Kemp's triacid,[30] in which previous adaptations lacking a photosensitizer were used as a stoichiometric template for a wide assortment of photoreactions.[31–38] In contrast to Krische's design, this catalyst incorporated a rigid cyclohexyl backbone into the binding site and a planar benzoxazole fused to a xanthone photocatalyst, restricting its conformational flexibility. In 2009, Bach applied this scaffold to the same [2+2] photocycloaddition of quinolone **2.13**, affording the regioisomeric products **2.14** and **2.16** (Scheme 2.5).[39] In this system, xanthone-containing catalyst **2.17** efficiently absorbs light at 366 nm, whereas the quinolone has a much lower extinction coefficient at the same wavelength. Consequently, if a nearly monochromatic light source centered at 366 nm is employed, minimal racemic reaction by direct excitation of the quinolone can occur.

Thus, Bach used this strategy to selectively generate the excited state of **2.13** only when bound to the chiral catalyst, via energy transfer, affording **2.14** in 92% ee. Notably, compared to Bach's previous work decreasing the catalytic amount of **2.17** did not result in a significant drop in ee. This methodology was subsequently extended toward intermolecular reactions of related pyridones.[40] Lastly, the use of an even further red-shifted thioxanthone catalyst was shown to be proficient at minimizing background reaction[41,42] and photochemical deracemizations.[43–48]

Scheme 2.5. Enantioselective [2+2] Cycloaddition Using Chiral Xanthone Photocatalyst

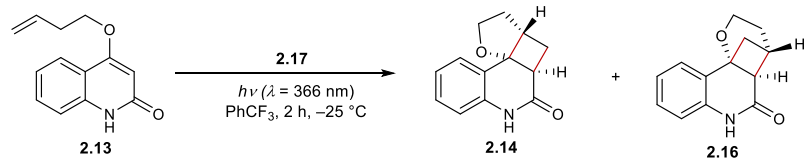

2.17	conversion	r.r.	ee (**2.14**)	ee (**2.16**)
20%	73%	78:21	94%	94%
10%	64%	78:22	92%	90%
5%	50%	78:22	90%	ND

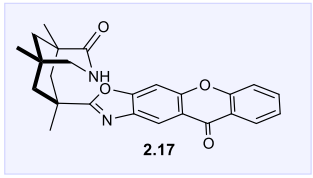

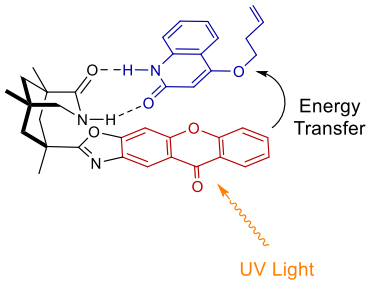

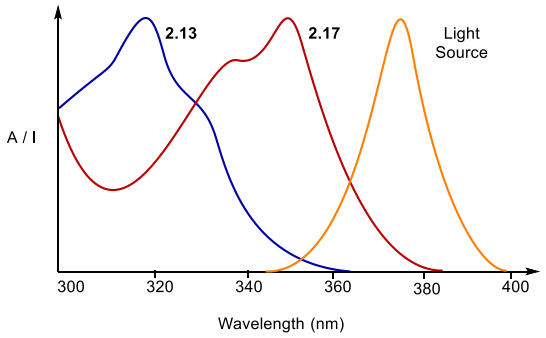

Sibi, and Sivaguru reported a similar approach for the enantioselective [2+2] photocycloaddition of alkene-tethered coumarin substrate **2.18** using a hydrogen-bonding chiral thiourea catalyst to efficiently organize the substrate (Scheme 2.6).[49] However, in this system both the catalyst and substrate are able to absorb the irradiation wavelength of the light source leading to significant amounts of background reaction at lower catalyst loadings. Subsequent studies

focused on the interactions between the chiral thiourea and coumarin.[50,51] This methodology was later applied to an enantioselective 6π-electrocyclization of acrylanilides.[52]

Scheme 2.6. Enantioselective [2+2] Photocycloaddition with Chiral Biaryl Thiourea

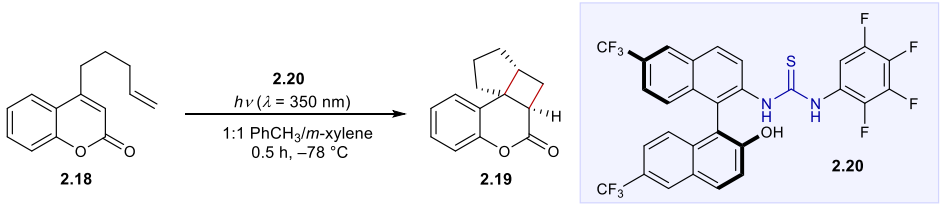

2.20	Time	conversion	ee
100 mol%	0.5 h	100 %	96%
10 mol%	0.5 h	100%	94%
1 mol%	0.5 h	48%	77%
0	4 h	12%	0

2.1.3 Asymmetric Primary Photoreactions using Transition Metal Sensitizers

All the previously discussed exampled have utilized organic chromophores as the sensitizer. However, the photophysical properties of small organic molecules are relatively sensitive to small structural and electronic perturbations.[53,54] Thus, the optimization of such systems can be quite challenging because changes to the catalyst structure beneficial for stereoselectivity may also harm its photochemical performance. In contrast to many organic chromophores, transition metal photocatalysts, exemplified by $Ru(bpy)_3^{2+}$ and $Ir(ppy)_3$, typically exhibit favorable photophysical properties such as large extinction coefficients in the visible region, high intersystem crossing quantum yields, and long-lived excited states. Moreover, these inorganic frameworks do not suffer from photobleaching after extended periods of irradiation as opposed to their organic counterparts. Lastly, alterations to the supporting ligands of these complexes can have large impacts on its redox potentials and triplet energy while minimally impacting the photophysical properties that are vital for effective photocatalysis.[55] For these

reasons, ligand-modified $Ru(bpy)_3^{2+}$ and $Ir(ppy)_3$ analogues have become ubiquitous photoredox catalysts ranging in applications from dye-sensitized solar cells to organic synthesis.[56]

The synthetic community has employed similar transition metal chromophores, such as the common $Ir(dF(CF_3)ppy)_2(dtbbpy)^+$, to perform various primary photochemical process via triplet energy transfer. These excited-state reaction types include cycloaddition,[57–59] aziridination,[60] isomerization,[61] cross-coupling,[62–64] and formal C–H amination.[65,66] Additionally, these octahedral complexes possess D_3 symmetry and thus have intrinsic helical chirality about the metal center. We wondered however, if these enantiopure complexes could offer a unique mode of enantioinduction, distinct from the point- and axially-chiral photocatalysts mentioned above, while providing sufficient stereodiscrimination to afford highly enantioselective primary photoreactions.

To this end, we were inspired by the pioneering work performed by Meggers, who demonstrated that iridium(III) polypyridyl complexes, shown in Figure 2.1, could easily be prepared in stereochemically pure form using a chiral auxiliary approach.[67] Furthermore, early investigations determined that the metal-centered stereogenecity could be utilized as a proficient chiral scaffold for the development of highly enantioselective transfer hydrogenations,[68] Friedel–Crafts alkylations,[69] sulfa-Michael and aza-Henry additions,[70] and α-amination reactions.[71]. These

Figure 2.1. Chiral-at-Metal Octahedral Catalysts Developed by Meggers

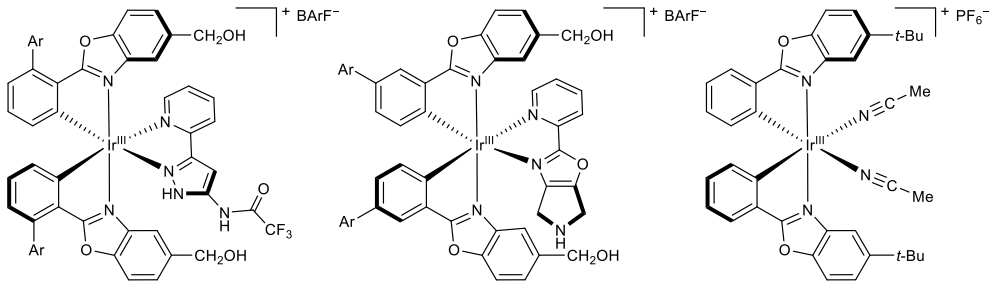

catalysts incorporated a bidentate L_2-type ligands bearing hydrogen-bonding (**2.21**) or basic amine motifs (**2.22**) as catalytic functional groups. Meggers later described the use of a chiral-at-metal bis(acetonitrile) complex (**2.23**) as controllers for Lewis acid[72,73] and organotransition catalysis.[74]

Of interest to our research, Meggers reported that chiral iridium complex **2.23** can serve as both a chiral Lewis acid and a competent photocatalyst to effect the transformation of **2.24** to **2.26** (Scheme 2.7).[75] The reaction advances by formation of iridium–enolate complex **2.27** that can

Scheme 2.7. Asymmetric Secondary Photoreaction using Chiral-at-Metal Photocatalyst

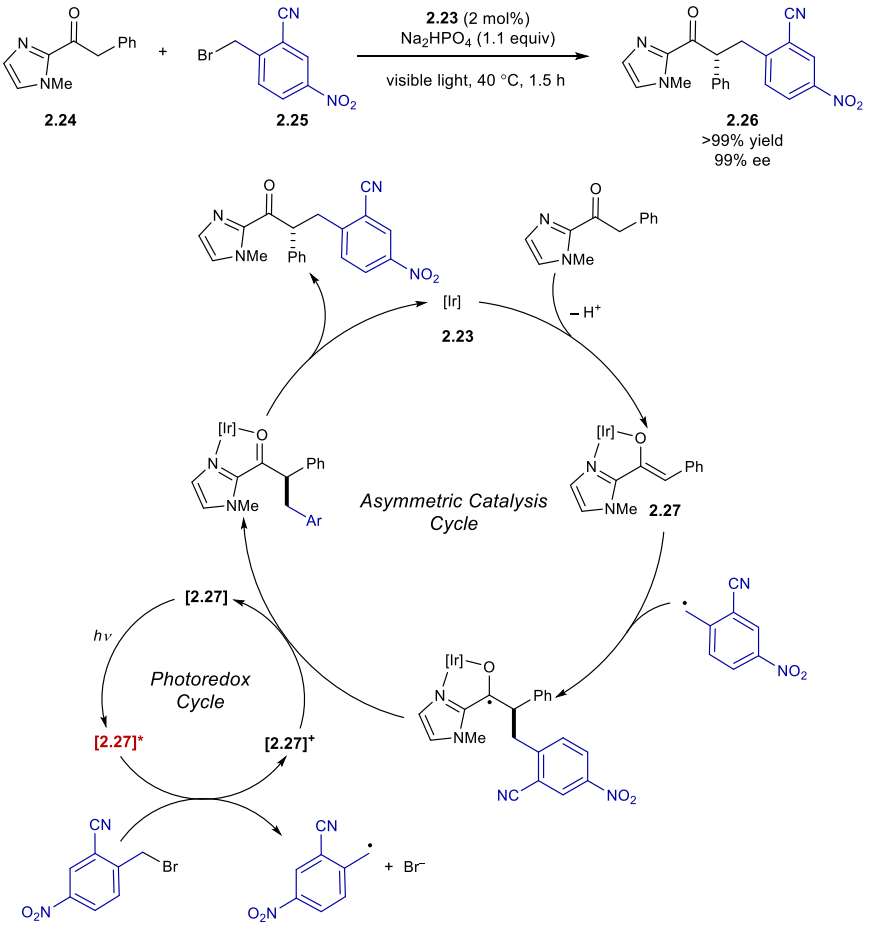

absorb visible light, which subsequently enables reduction of **2.25** by PET to the resulting radical. This open-shell species then reacts with another equivalent of chiral enolate to afford the product

up to 99% ee. This methodology has proven to be quite broad, applicable to numerous asymmetric transformations of similarly generated radicals with and without exogenous photocatalyst.[76]

However, these reactions are secondary photochemical processes, and at the time we began these investigations, there were no reports of an enantioselective organic transformation using a chiral organometallic complex as a triplet photosensitizer.[77,78] The catalysts designed by Meggers require inner-sphere coordination of the substrate to achieve high stereocontrol. However, this strong binding interaction limits the types of substrates amenable to this methodology and can result in large electronic perturbations of the overall complex, thus risking affects to its photophysical properties (*vide infra*). We were therefore interested in determining if an enantiopure, chiral-at-metal photocatalyst bearing a ligand capable of non-covalent interactions could preorganize an organic substrate prior to triplet energy transfer and control the absolute stereochemistry of the following product forming steps.

2.2 Results and Discussion

2.2.1 Optimization of Hydrogen-Bonding Ligands

Our preliminary investigations (Table 2.1) were based on three central premises. First, we elected to study 3-alkoxyquinolone **2.28** as a model substrate because its triplet energy is computationally estimated to be ~55 kcal/mol, easily within a range accessible using common iridium(III) complexes previously studied in our laboratory. It is also similar in structure to the quinolones and coumarins that are the optimal substrates for previously reported chiral organic photosensitizers (*vide supra*), which provides an opportunity to directly compare the effectiveness of these photocatalysts. Second, iridium(III) photocatalysts bearing electron-deficient cyclometalated phenylpyridine ligands can possess quite high-energy triplet excited states. Thus, we adapted the synthetic route developed by Meggers to prepare enantiopure complexes of general structure Λ-**2.30** that we hoped would have a triplet energy sufficient to sensitize **2.28**. Finally, Meggers has reported a range of chiral-at-metal complexes bearing L_2 ligands functionalized with Brønsted acidic moieties that serve as highly effective hydrogen-bonding asymmetric catalysts in non-photochemical applications. We hoped that a heterocyclic ligand previously utilized to activate nitroalkenes[68,69] might similarly be proficient at binding **2.28** within the stereoinducing environment defined by the octahedral Ir stereocenter. In our initial experiments, irradiation of **2.28** with blue LEDs in the presence of 1 mol% of Ir catalyst Λ-**2.30a** at –70 °C resulted in the formation of **2.29** in 49% ee (Table 1), confirming the validity of our design plan.

Table 2.1. Optimization of Hydrogen-Bonding Ligand

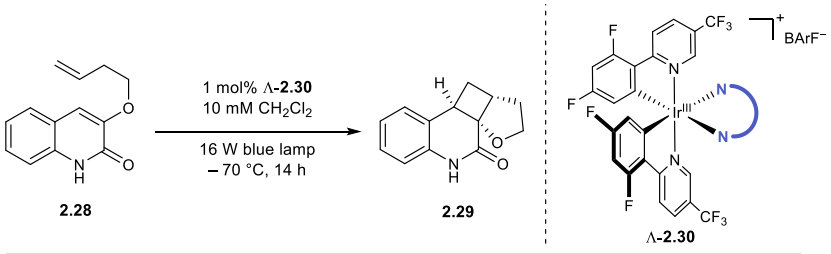

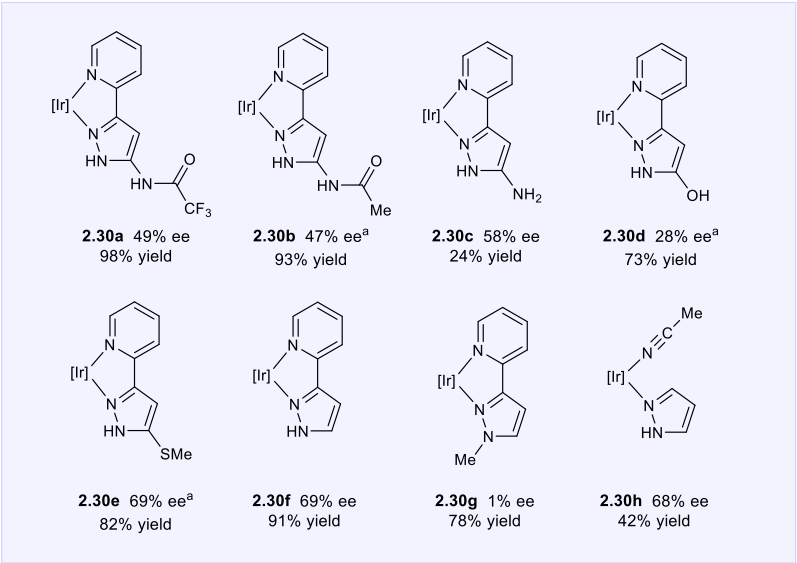

[a] Conducted with Δ-**2.30**. Sign of ee value is corrected for the absolute stereochemistry of the catalyst.

Next, we interrogated the role the acidic trifluoroacetamide N–H bond plays as a H-bond donor (Table 2.1). We replaced the trifluoroacetamide moiety with a variety of other groups bearing hydrogen bond donors (Λ-**2.30b-d**), but surprisingly, there was no clear correlation between pK_a and the ee of the cycloadduct. This suggests that the presence of this hydrogen bond-donating substituent on the pyrazole ring is likely not critical for binding the substrate. Consistent with this hypothesis, an analogue bearing a thioether substituent (Λ-**2.30e**) incapable of donating a hydrogen bond provided improved ee. Moreover, a complex featuring an unsubstituted pyridylpyrazole ligand provided both faster rate and high ee (Λ-**2.30f**). We found that the pyrazole moiety is necessary and sufficient for this level of enantiocontrol. A complex in which the critical

N–H of the pyridylpyrazole ligand is blocked with a methyl group (Λ-**2.30g**) provided no enantioinduction. In contrast, the use of a complex bearing a monodentate pyrazole ligand and an acetonitrile ligand (Λ-**2.30h**) afforded almost the same ee as the optimal catalyst with a bidentate pyridylpyrazole ligand, albeit with slightly diminished reactivity.

2.2.2 NMR Spectroscopy as a Tool for Optimization

After surveying the structures of hydrogen-bonding ligands, the binding interaction between the catalyst and substrate was not understood or its stereoinduction, and the enantioselectivity had plateaued at 70%. Thus, we chose to further investigate this system using NMR spectroscopy to provide both a quantitative and qualitative understanding of the association of quinolone **2.28** to photocatalyst Λ-**2.30f**. Firstly, we found that the resonances of the chemical shifts of **2.28** was dependent on the concentration of the sample, consistent with the well-known propensity of quinolones to form hydrogen-bonding homodimers. The dimerization equilibrium was found by monitoring the chemical shift of the N–H proton, which deshielded, with increasing [**2.28**]. Analyzing the data resulting in a value of $K_{dim} = 95 \pm 8.5\ M^{-1}$ when CD_2Cl_2 was the solvent. Control experiments using photocatalyst Λ-**2.30f** found that its chemical shifts were independent of concentration, and therefore does not self-associate.

Next, the binding interaction between **2.28** and Λ-**2.30f** was investigated by monitoring the chemical shift of the pyrazole N–H, resulting in a dramatic downfield shift upon the addition of quinolone substrate. These data were fit to a 1:1 binding model and we obtained an associate constant of 500 M^{-1}. While performing this titration study, we observed that the chemical shifts of other NMR active nuclei also changed over the course of the titration (Figure 2.2). These observations suggested a strategy for further optimization of the chiral photocatalyst. We reasoned

that large changes in chemical shift at various positions on the catalyst would likely correlate to close contacts with the substrate. Thus, modification at those positions associated with the largest chemical shift changes might be expected to have a substantial impact on the enantioselectivity of the catalyst.

Figure 2.2. NMR Titration and Binding Plot of Λ-**2.30f** with Quinolone **2.28** at room temperature in CH_2Cl_2

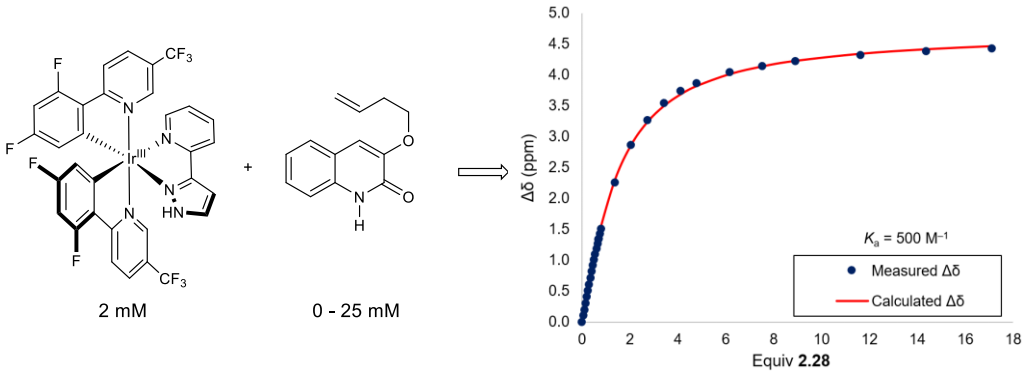

These chemical shift changes are graphically summarized in Figure 2.3. Several features of this heat map warrant comment. First, while the pyrazole moiety itself is strongly affected by association of the substrate, consistent with its critical role in binding, its pyridyl substituent is not strongly impacted. This is consistent with the empirical observation that a complex lacking the pyridyl group nevertheless provides high ee (Table 2.1, Λ-**2.30h**). Second, most of the significant changes in chemical shift are localized to one of the two cyclometalating phenylpyridine ligands; the other is comparatively unaffected. Moreover, the magnitude of the chemical shifts on the cyclometalating phenyl moiety are generally larger than on the pyridyl group. Thus, it seems reasonable to suppose that alteration of the cyclometalating ligands, and specifically the substituents about the phenyl ring, should have a large impact on the enantioselectivity of the photocycloaddition.

Optimization studies varying the structure of the cyclometalating ligands are in good agreement with this expectation (Figure 2.3). Modest changes to the fluorination pattern on the phenyl group result in large increases in enantioselectivity, albeit at the cost of reaction rate. Photocatalyst structure Λ-**2.31**, that bears a 2,4-F/CF_3(CF_3)ppy cyclometalating ligand, yields the product in 76% with an improved selectivity at 75% ee. Trifluorinated photocatalyst Λ-**2.32** resulted in a substantial increase to 89% ee for the cycloaddition reaction. Using this photocatalyst structure, we further probed its binding interaction with the substrate which exhibits a significantly larger association constant K_a = 3000 M^{-1}. This suggests that stronger binding between the catalyst and substrate might be responsible for the heightened selectivity.

Figure 2.3. Heat Map and Cyclometalating Ligand Optimization

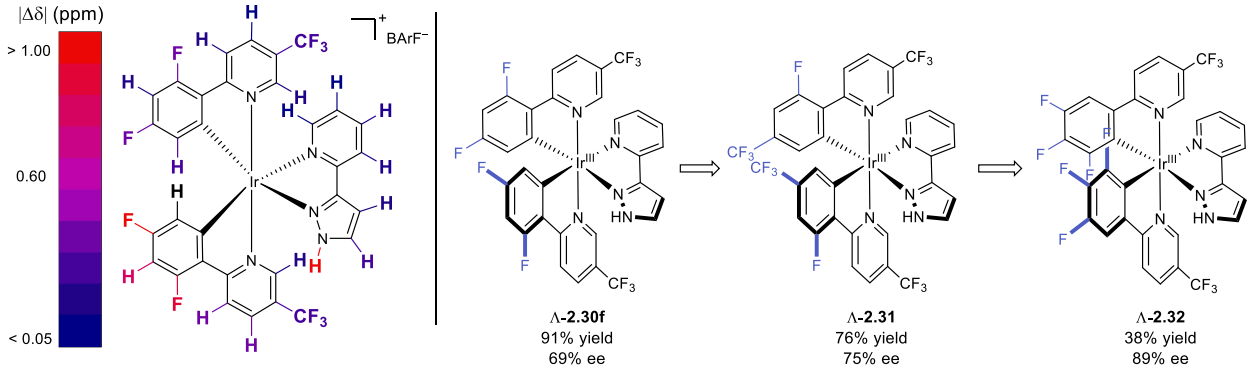

Given the sensitivity of hydrogen bonding interactions to solvent dielectric, we wondered if the substrate–catalyst interaction might be strengthened by reducing the solvent polarity. Indeed, conducting the reaction in 1:1 CH_2Cl_2:pentane resulted in an increase in the measured binding constant to K_a = 19000 M^{-1} and the formation of cycloadduct **2.29** in quantitative yield and 91% ee. Complex Λ-**2.32** is an exceptionally effective asymmetric photocatalyst; it provides high ee's at catalyst loadings considerably lower than the optimal conditions reported for chiral organic photosensitizers.[41,49] As a demonstration of this point, we conducted a [2+2] cycloaddition using

only 0.1 mol% of Λ-**2.32**. Although this led to the formation of **2.29** at diminished rate (38% yield at 24 h), there was negligible effect on enantioselectivity (88% ee). These results underscore the remarkable photocatalytic properties of this family of Ir(III) photosensitizers, which generally provide superior reactivity compared to classical organic sensitizers.

2.2.3 Reaction Scope and Limitations

A brief examination of substrates (Table 2.2) demonstrates that structurally related quinolones can also provide excellent yield and high ee in this transformation. Chloro - and bromo-substituted quinolones behave comparably to the parent substrate (**2.29b** and **2.29c**), while an iodinated substrate exhibited diminished ee (**2.29d**) due to an uncatalyzed background reaction arising from direct excitation. However, only trace amounts of de-iodinated product were observed under our conditions, consistent with the low energy of the visible light utilized in this procedure. Electron-poor (**2.29e**) and electron-rich (**2.29f**, **2.29g**) quinolones also react in high yields and good enantioselectivities. Substitution of a chlorine at the 8-position of the quinolone (**2.29i**) results in a dramatic drop to 20% ee, presumably because this large substituent interferes with the critical hydrogen bonding contact necessary for catalyst binding. In contrast, the smaller 8-fluoroquinolone (**2.29j**) exhibits only a slight decrease in enantioselectivity compared to **2.29a**. We also tested substrates in which the amidyl N–H moiety is either blocked with an alkyl substituent (**2.29k**) or replaced by an oxygen that is incapable of donating a hydrogen bond (**2.29l**). In both cases, these substrates give good yields but negligible ee. This suggests that the quinolone N–H bond plays a critical role in organizing the substrate relative to the stereodetermining Ir ligand sphere, but that it is not important for the success of the sensitized cycloaddition itself.

Table 2.2. Quinolone Reaction Scope

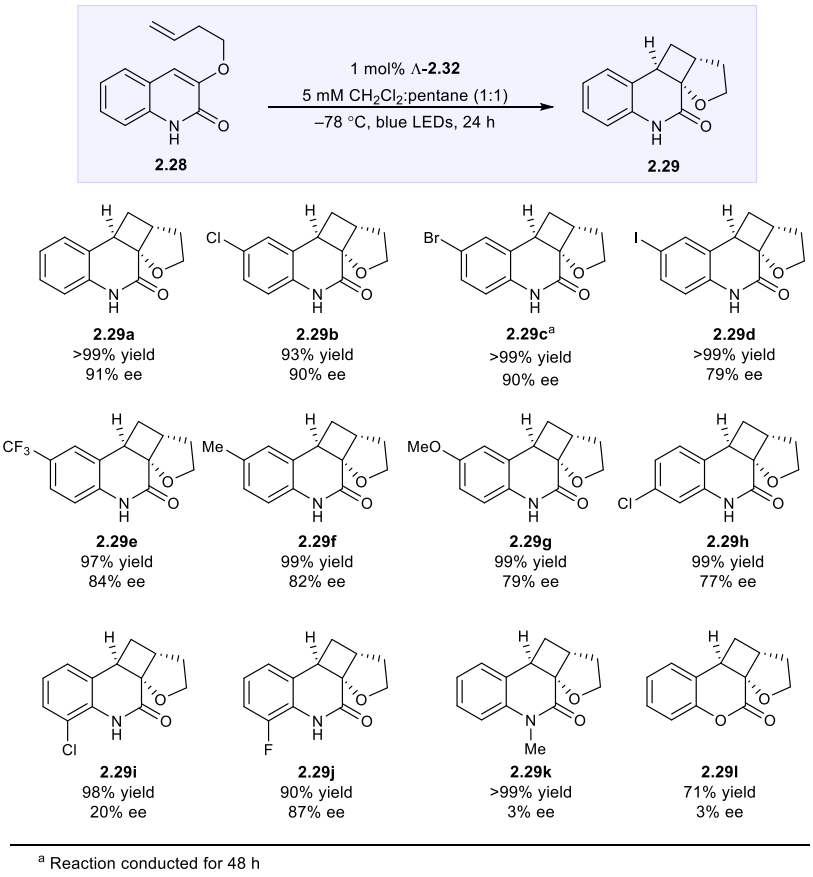

Intriguingly, the enantiomeric excess of this system is remarkably sensitive to changes of the pendant alkene (Table 2.3). Both a methyl substitution at the alpha position (**2.29m**) and *gem*-dimethyl substrate **2.29n** resulted in diminished selectivity to 68% ee and 69% ee respectively. Products (**2.29o**) were synthesized from both the (*E*) and (*Z*) 3-hexene starting materials in identical yield and diastereoselectivity albeit with a slight decrease in ee. Styrenyl-tethered quinolone **2.29p** resulted in substantially lower enantioselectivity A pendant Michael acceptor, which could disrupt the primary mode of binding, resulted in cyclobutane **2.29q** with excellent yield and diastereoselectivity, albeit with poor enantioselectivity.

Table 2.3. Alkene Scope

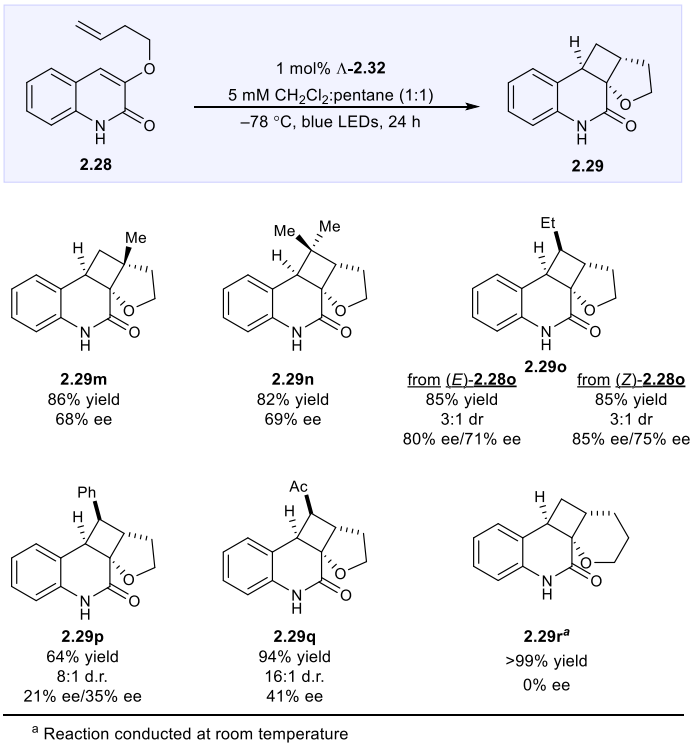

Lengthening the tether by one methylene unit to afford the six-membered ring product **2.29r** resulted in a lack of reactivity at cryogenic temperatures. At room temperature, quantitative yield was observed, but without any enantiomeric excess (compared to 43% ee for the parent substrate **2.29a**). The erosion of selectivity seen in **2.29r** can be explained by the enhanced degrees of freedom of the tether and intrinsically slower kinetics observed in six-exo-trig *vs*. five-exo-trig cyclizations.[79] It's possible that slower rates of cyclization could lead to an increase in the substrate's excited-state lifetime. Thus, if the lifetime of the activated substrate has increased, the probability of subsequent bond formation following dissociation from the deactivated catalyst's stereochemical influence would increase, resulting in a lowering of ee. This hypothesis is consistent with observations made by Bach and coworkers.[80]

2.2.4 Mechanistic Investigations

The design strategy for the development of Ir complex Λ-**2.32** was premised upon the ability of similar octahedral Ir polypyridyl complexes to catalyze a wide variety of primary photoreactions, including cycloadditions, via triplet energy transfer. However, we also considered several mechanistic alternatives for this reaction.

First, we examined the possibility that the [2+2] cycloaddition might be initiated by photoinduced electron transfer, rather than energy transfer. Electrochemical studies in CH_2Cl_2 indicate a substrate oxidation potential of +1.59 V and reduction potential of <–1.7 V vs. SCE, both of which lie well outside the potentials of the photoexcited catalyst (+1.27 V and –0.78 V, respectively). Thus, photoinduced electron transfer to or from the photocatalyst is not thermodynamically feasible. Second, control experiments indicate that no reaction occurs in the absence of photocatalyst or in the dark, ruling out alternative mechanisms involving either direct excitation of **2.28a** or a purely thermal process in which the iridium catalyst serves as a chiral Brønsted acid.

Finally, Meggers recently reported that a chiral-at-metal Rh Lewis acid is capable of catalyzing the [2+2] photocycloadditions of enones with excellent enantioselectivity.[81] The optimal Rh catalyst for this reaction, however, was not proposed to behave as a triplet sensitizer. Instead, Meggers showed that the rhodium center forms an association complex with the substrate, in a manner analogous to the Lewis acid catalyzed photocycloaddition methods described by Bach.[82] The key enabling feature of this reaction is the appearance of a strong, long-wavelength feature in the UV-vis spectrum of the Rh–substrate complex that is significantly enhanced relative to the sum of the individual spectra of the catalyst and substrate. We conducted an analogous UV-vis absorption experiment using Ir catalyst Λ-**2.32** and quinolone **2.28a** (Figure 2.4). While there

is a subtle bathochromic shift in the absorption spectrum of Λ-**2.32** upon addition of a 20-fold excess of **2.28a**, the effect is comparatively modest. Moreover, the fact that Λ-**2.32** remains an effective photocatalyst for cycloaddition of substrates that cannot form the same hydrogen-bonded complex as **2.28a** (Table 2.2, **2.28k** and **2.28l**) indicates that pre-association is not critical for photoactivation to occur, and that a different mechanism is likely operative.

Figure 2.4. UV-Vis absorption spectra for the association of quinolone **2.28a** and catalyst Λ-**2.32**

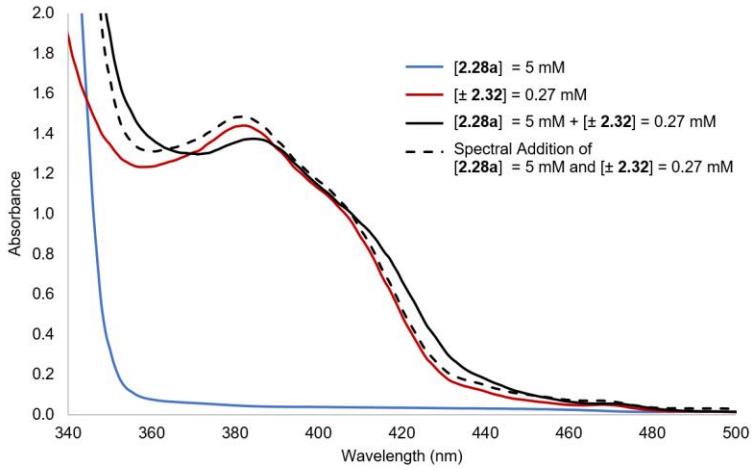

Thus, the available experimental evidence suggests that a Dexter energy transfer mechanism is operative. The emission maximum of our catalyst is 480 nm, corresponding to a triplet energy of 59.6 kcal/mol. We computationally estimated the substrate triplet energy as 55.0 kcal/mol, which indicates that the state change associated with triplet energy transfer from the photocatalyst to Λ-**2.32** would be exergonic. Xanthone-sensitized [2+2] cycloadditions of quinolones have been studied extensively by Bach, who proposed an analogous mechanism.[83,84] Finally, independent experiments with stereochemically defined (*E*)-**2.28o** and (*Z*)-**2.28o** converge to the same diastereomeric ratio, consistent with a stepwise triplet cycloaddition in which bond rotation occurs faster than radical recombination, rather than a concerted singlet process.

Lastly, a model for stereoinduction was pursued using experimental and theoretical methods. From NMR titration experiments it was clear that the N–H of the amide was critical for binding to the catalyst, nonetheless we were intrigued by the nearly racemic reactivity of N–Me quinolone **2.28k** and decided to investigate further. Our initial hypothesis was that without the N–H the substrate can no longer bind and orient itself to the chiral catalyst, causing the lack of enantioselectivity. If our hypothesis is correct the title substrate **2.28a**, which strongly binds to the photocatalyst, should exhibit a proximity-induced rate enhancement, and thus react substantialy faster compared to **2.28k**. Under optimized reaction conditions a competition experiment was conducted, in which both substrates are in the same pot (Figure 2.5). After 30 min substrate **2.28a** was found to convert to the product at nearly the same rate as the methylated substrate. Relatedly, steady-state luminescence quenching experiments were performed to measure their independent quenching rates. To our surprise, both **2.28a** and **2.28k** was found to exhibit similar K_{SV} values.

Figure 2.5. Investigation of N–H vs. N–Me Quinolones

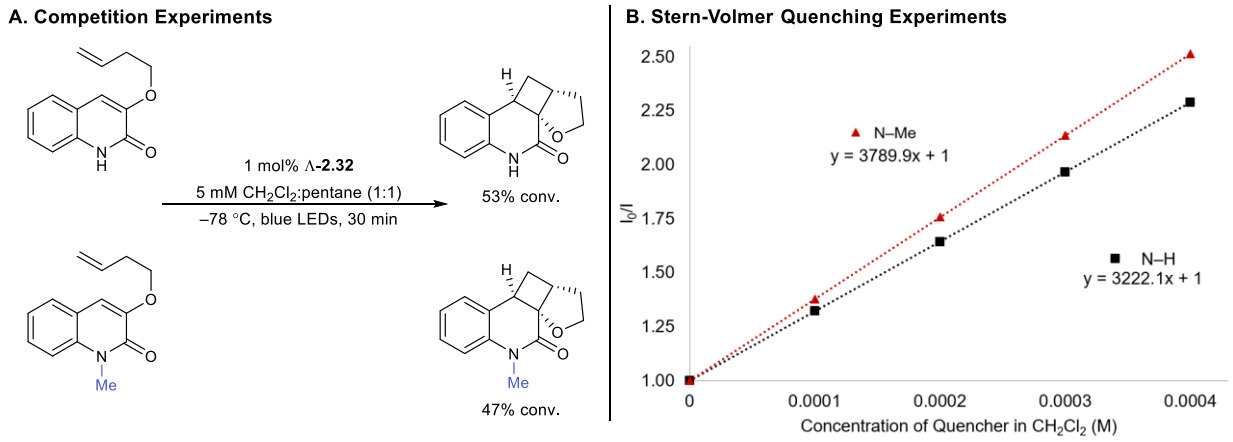

Finally, an NMR titration of Λ-**2.32** with the N–Me substrate indicated that indeed a binding interaction occurs on the same order of magnitude, K_a = 16,000 M^{-1}, presumably via a hydrogen bond with the electron-rich oxygen atom of the amide and N–H of the pyrazole unit.

This was a shocking result given our initial design of this system. Despite the catalyst being engineered for two-point binding with the amide of the title substrate **2.28a**, the N–Me substrate that is lacking any hydrogen–bond donor was shown to bind with comparative affinity. This is interesting given the context that the N–Me substrate is absent of enantiomeric excess.

In collaboration with the Baik group, the interaction between Λ-**2.32** and **2.28a** was investigated computationally. DFT calculations demonstrate that an association between these two species was thermodynamically favorable, and several hydrogen-bonding adducts were found to coexist in a dynamic equilibrium. In particular, a catalyst–substrate complex was found that is in accord with the experimental observations outlined above (Figure 2.6). This model correctly predicts the absolute stereochemical outcome of the reaction, in which association blocks the *Si* face of the reacting alkene. Interestingly, there is an unusual N–H-π interaction between the quinolone amide and the pyrazole group that stabilizes this conformation and is consistent with the observation that the N–H of the quinolone is necessary to achieve enantioselectivity (*cf.* **2.28k**, **2.28l**).

Figure 2.6. Productive and Nonproductive Photocatalyst–Quinolone Adducts

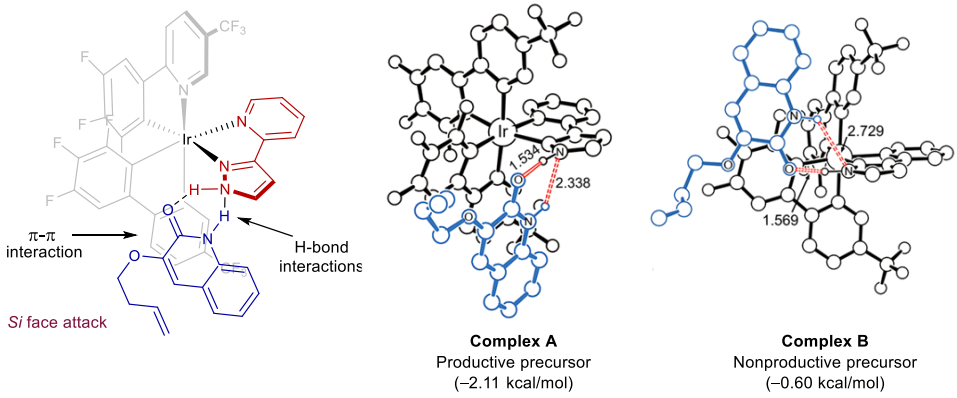

As hypothesized, a strong H-bonding interaction between the pyrazole and the quinolone carbonyl establishes the main contact, but an important π–π interaction between the substrate and cyclometalating ligand is also formed. This interaction not only increases net stabilization but also explains the large changes in chemical shift of the cyclometalated ligand observed in the NMR titration experiments. Importantly, this π–π interaction may promote efficient symmetry matched orbital overlap between the triplet excited state of the Ir sensitizer (donor) and the π orbital fragment of the substrate (acceptor), enabling energy transfer (Figure 2.7).

Figure 2.7. A. Illustration of Dexter Energy Transfer **B.** Relevant Frontier Molecular Orbitals

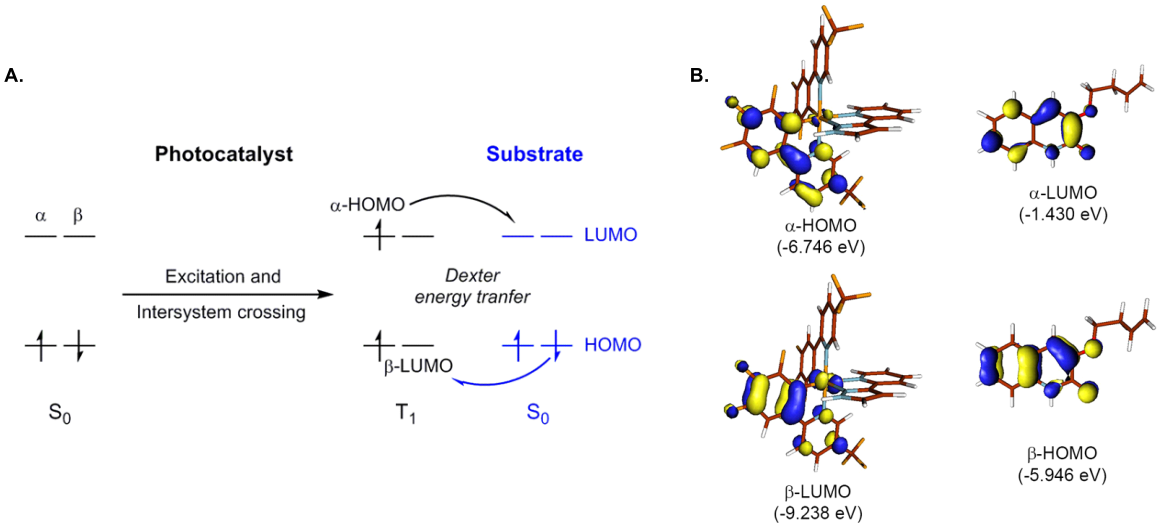

2.3 Conclusion

In this chapter, we have outlined the development of a highly effective chiral triplet sensitizer that combines the exceptional photochemical properties of transition metal coordination complexes with a hydrogen bonding domain to orient the organic substrate. Notably, the robust photophysical properties of iridium(III) polypyridyl complexes enabled considerable optimization of both the cyclometalating phenylpyridine and L_2 pyridylpyrazole ligands. The flexibility of this

strategy led us to discover an enantioselective catalyst that exploits an unexpected π–π interaction and unusual N–H to π hydrogen bond, rather than any direct inner-sphere substrate–catalyst association. The optimal complex can be utilized at catalyst loadings two orders of magnitude lower than current state of the art chiral organic photosensitizers. We believe this constitutes an attractive new approach to stereocontrol in excited state photoreactions, which have historically proven to be a formidable synthetic challenge. Further exploration of these design principles is a continuing theme of research in our laboratory.

2.4 Contributions

Dr. Kazimer L. Skubi performed the optimization of this system, measured the association constant for Λ-**2.30f**, and performed the syntheses of the photocatalysts, substrates, and cycloadducts **2.29a-j**. Computational experiments were conducted by Hoimin Jung and Prof. Mu-Hyun Baik. Dr. Ilia A. Guzei collected and analyzed X-ray crystallographic data. Prof. Tehshik P. Yoon provided expertise, resources, and funding for researchers.

2.5 Experimental Procedures

2.5.1 General Information

2.5.1.a Reagent Preparation

Ethyl 3-oxo-3-(pyridin-2-yl)propanoate (**2.41**),[85] 3,3-bis(methylthio)-1-(pyridin-2-yl)prop-2-en-1-one (**2.43)**,[86] 5-trifluoromethylisatin (**2.57**),[87] 3-methylbut-3-en-1-yl 4-methylbenzenesulfonate (**2.58**),[88] (*E*)-hex-3-en-1-yl 4-methylbenzenesulfonate (**2.59**),[89] (*Z*)-hex-3-en-1-yl 4-methylbenzenesulfonate (**2.60**),[90] and (E)-(4-bromobut-1-en-yl)benzene (**2.61**)[91] were prepared as previously described. Racemic photocatalyst [Ir(dF(CF_3)ppy)$_2$(dtbbpy)] [PF_6] was synthesized following the published route.[92] DBU (1,8-Diazabicyclo[5.4.0]undec-7-ene) was purchased from

Oakwood Chemical and distilled prior to use, discarding the forerun. $Pd(PPh_3)_4$ was purchased from Strem Chemical. $IrCl_3 \cdot xH_2O$ was provided by a generous gift from Sigma Aldrich. All other reagents were purchased from commercial suppliers and used without additional purification. Except in the case of aqueous reactions, all reaction glassware was flame- or oven-dried prior to use. Flash column chromatography was carried out with Purasil 60 Å silica gel (230–400 mesh).

2.5.1.b Product Characterization

^1H, $^{13}C\{^1H\}$, and $^{19}F\{^1H\}$ NMR spectra were obtained using a Bruker Avance-400, Avance-500, or Avance-600 spectrometer with DCH, Prodigy, BBFO+, or TCI-F probes. ^1H spectra were internally referenced to tetramethyl silane (0.00 ppm) or the residual protio-solvent peak in acetone-d_6 or DMSO-d_6. $^{13}C\{^1H\}$ spectra were internally referenced to $CDCl_3$ (77.16 ppm) or DMSO-d_6 (39.52 ppm). $^{19}F\{^1H\}$ spectra were absolute referenced to the corresponding ^1H spectra using the method described by Harris.[93,94] Multiplicities are defined using the following abbreviations: s (singlet), d (doublet), t (triplet), q (quartet), p (pentet), sext (sextet), sept (septet), br. (broad), app. (apparent). Diastereomeric ratios for iridium catalysts **2.50–2.53** were determined from ^1H NMR spectra of purified material. Diastereomeric ratios for cycloadducts were determined from ^1H NMR spectra of the crude reaction mixture. The spectrometers used for this work are supported by the NSF (CHE-1048642, CHE-0342998, CHE-9208463), NIH (S10 OD012245, S10 RR13866-01), and a generous gift from Paul J. and Margaret M. Bender.

Mass spectrometry was performed with a Thermo Q Exactive™ Plus. This instrumentation is supported by the NIH (1S10 OD020022-1) and the University of Wisconsin.

Enantiomeric excesses were determined for isolated, purified material using either chiral SFC (Waters/Thar Investigator) or chiral HPLC (Waters Alliance), Daicel CHIRALCEL® columns and Chromasolv®-grade solvents.

IR spectra were obtained using a Bruker Alpha Platinum spectrometer (powder or thin film). Melting points were obtained using a Stanford Research Systems DigiMelt apparatus, and are uncorrected.

Optical rotations were measured using a Rudolph Research Autopol III polarimeter at room temperature.

UV-Vis absorption spectra were acquired using a Varian Cary® 50 UV-visible spectrophotometer with a scan rate of 300 nm/min. UV-Vis emission spectra were acquired on Hitachi F-4500 fluorescence spectrophotometer.

Cyclic voltammograms were acquired using a Pine Research WaveNow potentiostat/galvanostat.

2.5.2 Synthesis of Ligands

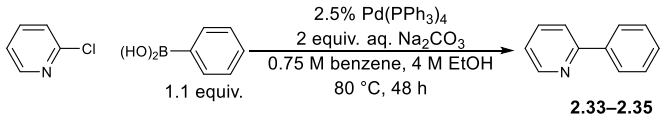

General Procedure 2.A: Phenylpyridine (ppy) ligands were prepared based on the procedure described by Malliaras, Bernhard, and coworkers.[92] A 50 mL round-bottomed flask was charged with chloropyridine (5.00 mmol, 1.0 equiv.) and arylboronic acid (5.50 mmol, 1.1 equiv.), followed by $Pd(PPh_3)_4$ (0.125 mmol, 0.025 equiv.). Benzene (6.7 mL, 0.75 M with respect to substrate) was added, followed by 2 M aq. Na_2CO_3 (10.0 mmol, 2.0 equiv.) and EtOH (1.25 mL, 4 M with respect to substrate). The solution was stirred vigorously and sparged for 5 min with N_2, resulting in a slight lightening of color. Following this, the mixture was heated at reflux (80 °C) under N_2 and maintained at this temperature for 2 d. The reaction was then cooled to room temperature and H_2O (6 mL/mmol substrate) was added. The mixture was extracted three times into an equal volume of CH_2Cl_2 and the combined organic layers were concentrated *in vacuo*. The residue was passed through a short plug of silica gel with CH_2Cl_2, affording a colorless oil or white solid. In most cases, this crude material was sufficiently pure to proceed to the next step; we have found that small amounts (< 10%) of PPh_3 or unreacted coupling partner do not interfere in the subsequent cyclometalation. However, spectroscopically pure material could be obtained by flash column chromatography on silica gel.

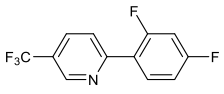

2-(2,4-Difluorophenyl)-5-(trifluoromethyl)pyridine (dF(CF_3)ppy, **2.33**): Prepared according to General Procedure 2.A using 2-chloro-5-(trifluoromethyl)pyridine (908 mg, 5.00 mmol, 1.0 equiv.), 2,4-difluorophenylboronic acid (868 mg, 5.50 mmol, 1.1 equiv.), and $Pd(PPh_3)_4$ (152 mg, 0.132 mmol, 0.026 equiv.). Following

workup, the product was purified by flash column chromatography on silica gel (33:67 CH_2Cl_2:hexanes) to afford a white solid (947 mg, 3.65 mmol, 73% yield). Chemical shifts were consistent with the original report,[92] but several key features of the spectra require reassignment.

First, the protons with chemical shifts 8.10 (8.12) and 7.04 (7.05) ppm were originally assigned as Phenyl-H_5 and Phenyl-H_6, respectively. Based on the magnitude of the smaller coupling, we propose the reverse assignment. A decoupled $^1H\{^{19}F\}$ spectrum (Figure S1) corroborates our assignment, as the upfield signal retains both an *ortho* and *meta* coupling, while the downfield peak collapses into a doublet.

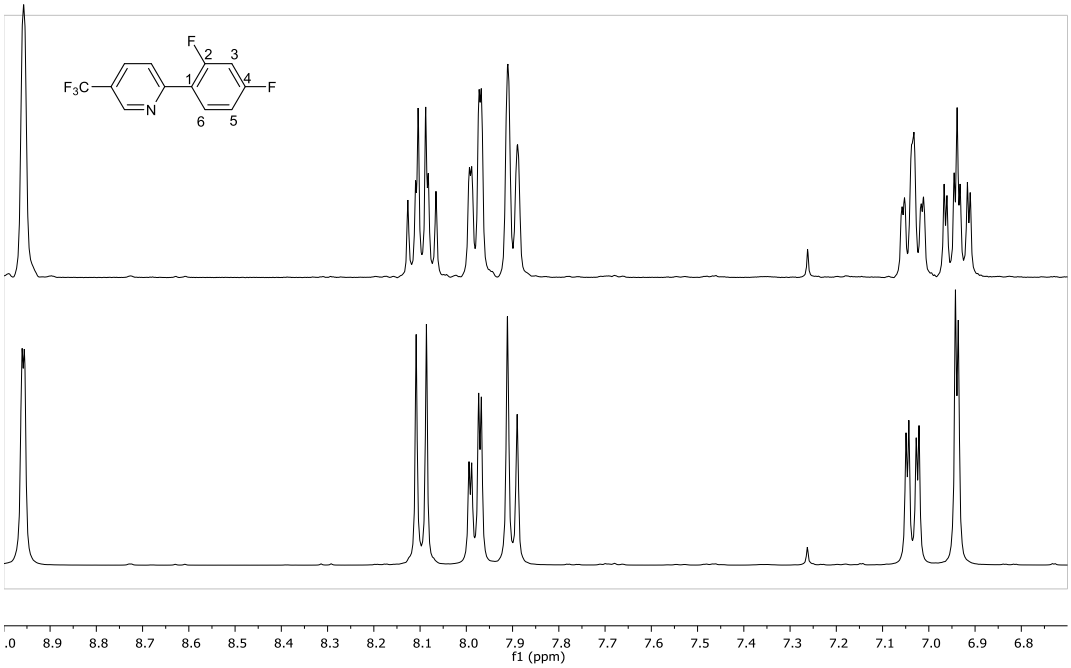

Figure 2.8. NMR spectra of ligand **2.33**. Top: Standard ^1H NMR. Bottom: $^1H\{^{19}F\}$ NMR with adiabatic decoupling (decoupler offset = –90 ppm).

Second, in the ^{13}C NMR spectrum, the four signals at δ 165.2, 163.2, 162.2, and 160.2 ppm were originally assigned as four different carbons. Instead, we propose that these are two doublets of doublets, the large coupling constants of which are consistent with one-bond carbon–fluorine coupling. The remaining two signals are: (1) a low-intensity doublet of doublets at 122.57 ppm corresponding to the quaternary carbon on the phenyl ring, and (2) a quartet at 123.69 ppm assigned as the CF_3 group.

These reassignments were utilized in the titration studies.

Our revised spectral data are as follows:

^{1}H NMR (500 MHz, $CDCl_3$) δ 8.96 (s, 1H), 8.10 (td, *J* = 8.8, 6.5 Hz, 1H), 7.99 (dd, *J* = 8.4, 2.3 Hz, 1H), 7.91 (d, *J* = 8.3 Hz, 1H), 7.04 (dddd, *J* = 8.7, 7.6, 2.5, 1.0 Hz, 1H), 6.95 (ddd, *J* = 11.3, 8.7, 2.5 Hz, 1H).

^{13}C NMR (126 MHz, $CDCl_3$) δ 164.02 (dd, *J* = 252.9, 12.2 Hz), 161.07 (dd, *J* = 253.7, 12.1 Hz), 155.88, 146.71 (q, *J* = 4.1 Hz), 133.88 (q, *J* = 3.5 Hz), 132.58 (dd, *J* = 9.8, 4.1 Hz), 125.27 (q, *J* = 33.2 Hz), 123.78 (d, *J* = 10.9 Hz), 123.69 (q, *J* = 272.2 Hz), 122.57 (dd, *J* = 11.3, 3.6 Hz), 112.40 (dd, *J* = 21.2, 3.6 Hz), 104.77 (dd, *J* = 26.9, 25.4 Hz).

^{19}F NMR (377 MHz, $CDCl_3$) δ –62.42 (s, 3F), –107.24 (d, *J* = 9.4 Hz, 1F), –112.08 (d, *J* = 9.1 Hz, 1F).

HRMS (ASAP-MS[95]) calculated for $[C_{12}H_7F_5N]^+$ ($[M+H]^+$). Requires *m/z* 260.0493; found *m/z* 260.0492.

IR (ATR, powder): 3046, 1601, 1327, 1119, 1082 cm^{-1}.

M.P. 61.8–62.8 °C.

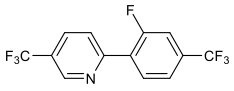

2-(2-Fluoro-4-(trifluoromethyl)phenyl)-5-(trifluoromethyl)pyridine (2,4-F/CF_3(CF_3)ppy, **2.34**): Prepared according to General Procedure 2.A using 2-chloro-5-(trifluoromethyl)pyridine (905 mg, 4.99 mmol, 1.0 equiv.), 2-fluoro-4-(trifluoromethyl)phenylboronic acid (1.146 g, 5.51 mmol, 1.1 equiv.), and $Pd(PPh_3)_4$ (153 mg, 0.132 mmol, 0.026 equiv.). Following workup, the product was purified by flash column chromatography on silica gel (20:80 CH_2Cl_2:hexanes) to afford a white solid (1.145 g, 3.70 mmol, 74% yield).

^{1}H NMR (500 MHz, $CDCl_3$) δ 9.01 (s, 1H), 8.22 (t, *J* = 7.9 Hz, 1H), 8.04 (dd, *J* = 8.4, 2.3 Hz, 1H), 7.99 (d, *J* = 8.3 Hz, 1H), 7.58 (d, *J* = 8.2 Hz, 1H), 7.48 (dd, *J* = 11.1, 1.7 Hz, 1H).

^{13}C NMR (126 MHz, $CDCl_3$) δ 160.39 (d, *J* = 253.2 Hz), 155.22, 146.95 (q, *J* = 4.1 Hz), 134.06 (q, *J* = 3.5 Hz), 133.59 (qd, *J* = 33.7, 8.4 Hz), 132.25 (d, *J* = 2.9 Hz), 129.51 (d, *J* = 11.4 Hz), 126.08 (q, *J* = 33.1 Hz), 124.38 (d, *J* = 10.6 Hz), 123.55 (q, *J* = 272.3 Hz), 123.20 (qd, *J* = 272.7, 2.6 Hz), 121.70 (p, *J* = 3.8 Hz), 114.17 (dq, *J* = 26.4, 3.8 Hz).

^{19}F NMR (377 MHz, $CDCl_3$) δ –62.49 (s, 3F), –62.99 (s, 3F), –114.36 (s, 1F).

HRMS (ASAP-MS) calculated for $[C_{13}H_7F_7N]^+$ ($[M+H]^+$). Requires *m/z* 310.0461; found *m/z* 310.0457.

IR (ATR, powder): 3087, 1606, 1583, 1509, 1426, 1389, 1318, 1167, 1119, 1083 cm^{-1}.

M.P. 36.4–37.7 °C.

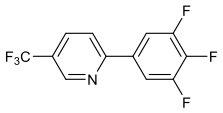

5-(Trifluoromethyl)-2-(3,4,5-trifluorophenyl)pyridine (tF(CF_3)ppy, **2.35**): Prepared according to General Procedure 2.A using 2-chloro-5-(trifluoromethyl)pyridine (907 mg, 5.00 mmol, 1.0 equiv.), 3,4,5-trifluorobenzeneboronic acid (977 mg, 5.55 mmol, 1.1 equiv.), and $Pd(PPh_3)_4$ (146 mg, 0.126 mmol, 0.025 equiv.). Following

workup, the product was purified by flash column chromatography on silica gel (20:80 CH_2Cl_2:hexanes) to afford a white solid (1.165 g, 4.20 mmol, 84% yield).

^{1}H NMR (500 MHz, $CDCl_3$) δ 8.94 (s, 1H), 8.02 (dd, *J* = 8.3, 2.3 Hz, 1H), 7.78 (d, *J* = 8.3 Hz, 1H), 7.76 – 7.69 (m, 2H).

^{13}C NMR (126 MHz, $CDCl_3$) δ 157.21, 151.79 (ddd, *J* = 250.4, 10.2, 4.0 Hz), 146.95 (q, *J* = 4.0 Hz), 141.21 (dt, *J* = 255.8, 15.5 Hz), 134.53 (q, *J* = 3.5 Hz), 133.93 (td, *J* = 7.4, 4.3 Hz), 125.97 (q, *J* = 33.2 Hz), 123.58 (q, *J* = 272.3 Hz), 119.69, 111.71 – 111.39 (m).

^{19}F NMR (377 MHz, $CDCl_3$) δ –62.43 (s, 3F), –133.09 (d, *J* = 20.4 Hz, 2F), –157.88 (t, *J* = 20.4 Hz, 1F).

HRMS (ASAP-MS) calculated for $[C_{12}H_6F_6N]^+$ ($[M+H]^+$). Requires *m/z* 278.0399; found *m/z* 278.0395.

IR (ATR, powder): 3100, 1606, 1529, 1484, 1362, 1323, 1131, 1078, 1041, 1010, 841, 760 cm^{-1}.

M.P. 52.8–53.9 °C.

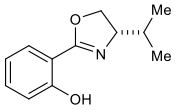

(*S*)-2-(4-Isopropyl-4,5-dihydrooxazol-2-yl)phenol (*i*-PrHBO, **2.36**):

[Note: 2-hydroxybenzonitrile is a toxic and irritating powder. Exercise caution!]

Prepared according to a procedure modified from Bolm and coworkers.[96] $ZnCl_2$ (79.5 mg, 0.583 mmol, 0.05 equiv.) was added to a 100 mL round-bottomed flask, placed under vacuum, and melted with a Bunsen burner. Upon cooling and backfilling with N_2, the oil resolidified and chlorobenzene (34 mL) was added to the flask. L-Valinol (1.74 g, 16.9 mmol, 1.5 equiv.) was added, followed by 2-hydroxybenzonitrile (1.36 g, 11.4 mmol, 1.0 equiv.). The solution was heated at reflux (150 °C) under N_2 and maintained at this temperature for 24 h. Following this period, the majority of chlorobenzene was removed by short-path distillation under reduced pressure. The crude residue was purified by flash column chromatography on silica gel (6:94 EtOAc:hexanes)

to afford a colorless oil (2.12 g, 10.3 mmol, 90% yield). Spectral data were fully consistent with previously reported values.[96]

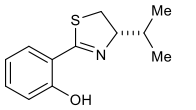

(*S*)-2-(4-Isopropyl-4,5-dihydrothiazol-2-yl)phenol (i-PrHBT, **2.37**): Prepared as described by Meggers.[97] Spectral data were consistent with those reported previously.[98]

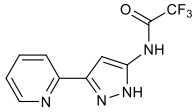

2,2,2-Trifluoro-*N*-(3-(pyridin-2-yl)-1*H*-pyrazol-5-yl)acetamide (5'-NHTFApypz, **2.38**): Prepared as described by Meggers.[98]

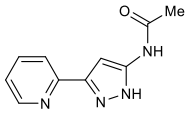

***N*-(3-(Pyridin-2-yl)-1*H*-pyrazol-5-yl)acetamide** (5'-NHAcpypz, **2.39**): Prepared as described by Halcrow.[99]

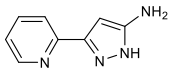

3-(Pyridin-2-yl)-1*H*-pyrazol-5-amine (5'-NH_2pypz, **2.40**): Prepared as described by Halcrow.[99]

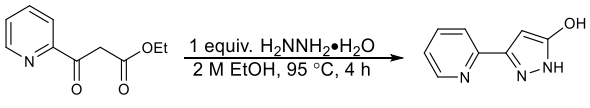

2.41 **2.42**

3-(Pyridin-2-yl)-1*H*-pyrazol-5-ol (5'-OHpypz, **2.42**)[100]: A round-bottomed flask was charged with β-ketoester **2.41**[85] (548 mg, 2.84 mmol, 1.0 equiv.), EtOH (1.4 mL), and $H_2NNH_2•H_2O$ (140 μL, 2.89 mmol, 1.0 equiv.). The mixture was heated at reflux (95 °C) under N_2, forming a milky white slurry. After 4 h, the reaction was cooled to room temperature and concentrated. The crude solid was isolated by suction filtration on a frit, rinsed with hexanes, and dried under high vacuum to give **2.42** as a pale tan solid (422 mg, 2.62 mmol, 92% yield). This material decomposed slowly over several weeks at room temperature.

^{1}H NMR (**2.40**, 500 MHz, DMSO-d_6) δ 12.20 (br. s, 1H), 10.04 (br. s, 1H), 8.55 (d, J = 4.7 Hz, 1H), 7.81 (td, J = 7.7, 1.8 Hz, 1H), 7.75 (d, J = 7.9 Hz, 1H), 7.28 (ddd, J = 7.4, 4.8, 1.2 Hz, 1H), 6.06 (s, 1H).

^{13}C NMR (**2.42**, 126 MHz, DMSO-d_6) δ 160.90, 149.26, 149.16, 143.18, 135.72, 122.61, 119.37, 87.82.

^{1}H NMR (**2.42•HCl**,[100] 500 MHz, DMSO-d_6) δ 11.26 (br. s, 2H), 8.63 (d, *J* = 4.6 Hz, 1H), 8.21 (t, *J* = 7.8 Hz, 1H), 8.13 (d, *J* = 8.0 Hz, 1H), 7.61 (t, *J* = 6.4 Hz, 1H), 6.38 (s, 1H).

^{13}C NMR (**2.42•HCl**,[100] 126 MHz, DMSO-d_6) δ 158.40, 146.84, 145.10, 142.34, 141.93, 124.05, 121.38, 87.50.

HRMS (ESI$^+$) calculated for $[C_8H_8N_3O]^+$ ([M+H]$^+$). Requires *m/z* 162.0662; found *m/z* 162.0661.

IR (ATR, powder): 2978, 2704, 2621, 2560, 1588, 1539, 1504, 1476, 1006, 740 cm^{-1}.

M.P. 217.8–219.7 °C.

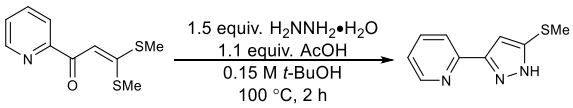

2.43 **2.44**

2-(5-(Methylthio)-1*H*-pyrazol-3-yl)pyridine (5'-SMepypz, **2.44**)[100]: A round-bottomed flask was charged with dithioketene acetal **2.43**[86] (1.014 g, 4.50 mmol, 1.0 equiv.), *t*-BuOH (30 mL), AcOH (280 µL, 4.89 mmol, 1.1 equiv.), and $H_2NNH_2•H_2O$ (330 µL, 6.80 mmol, 1.5 equiv.). The solution was heated at reflux (100 °C) under N_2 for 2 h. Following this period, the reaction was cooled to room temperature, poured into 30 mL H_2O, and extracted 2 x 30 mL into EtOAc. The combined organic layers were washed with 50 mL brine, dried over Na_2SO_4, filtered, and concentrated to a brown oil. This crude residue was purified by flash column chromatography on silica gel (33:67 acetone:hexanes), affording **2.44** as a pale tan powder (663 mg, 3.47 mmol, 77% yield).

^{1}H NMR (**2.44**, 500 MHz, $CDCl_3$) δ 11.96 (br. s, 1H), 8.68 (ddd, *J* = 4.9, 1.7, 1.0 Hz, 1H), 7.76 (td, *J* = 7.7, 1.8 Hz, 1H), 7.65 (br. d, *J* = 7.8 Hz, 1H), 7.26 (ddd, *J* = 7.6, 4.9, 1.2 Hz, 1H), 6.70 (s, 1H), 2.58 (s, 3H).

^{13}C NMR (**2.44**, 126 MHz, $CDCl_3$) δ 149.65, 148.18, 137.27, 123.27, 120.28, 103.93, 16.75.

^{1}H NMR (**2.44**•HCl,[100] 500 MHz, DMSO-d_6) δ 14.26 (br. s, 2H), 8.74 (d, *J* = 5.2 Hz, 1H), 8.56 (td, *J* = 8.3, 1.5 Hz, 1H), 8.44 (d, *J* = 8.1 Hz, 1H), 7.90 (t, *J* = 6.74 Hz, 1H), 7.55 (s, 1H), 2.55 (s, 3H).

^{13}C NMR (**2.44**•HCl,[100] 126 MHz, DMSO-d_6) δ 146.15, 144.65, 142.89, 141.95, 139.96, 125.36, 123.07, 107.13, 17.29.

HRMS (ESI$^+$) calculated for $[C_9H_{10}N_3S]^+$ ($[M+H]^+$). Requires *m/z* 192.0590; found *m/z* 192.0589.

IR (ATR, powder): 3225, 3118, 2996, 2921, 1593, 1561, 1444, 776 cm^{-1}.

M.P. 95.4–97.2 °C.

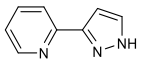

2-(1*H*-Pyrazol-3-yl)pyridine (pypz, **2.45**): Prepared as described by Thiel.[101]

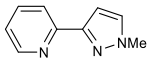

2-(1-Methyl-1*H*-pyrazol-3-yl)pyridine (1'-Mepypz, **2.46**): A 50 mL round bottom flask was charged with pypz (**2.45**) (183 mg, 1.26 mmol, 1.0 equiv.) and THF (13 mL). NaH (60 wt%, 304 mg, 7.60 mmol, 6.0 equiv.) was added, and the heterogeneous suspension was stirred for 1 hour under N_2. MeI (160 µL, 2.57 mmol, 2.0 equiv.) was added by syringe, and the mixture was stirred for 16 h. Following this period, the reaction was quenched with MeOH, then concentrated *in vacuo*. H_2O and EtOAc were added, and the mixture was extracted twice into EtOAc. The combined organics were dried over Na_2SO_4, filtered, and concentrated. This crude residue was passed through a silica plug with 10:90 MeOH:CH_2Cl_2, then concentrated to a yellow oil (222 mg, 1.39 mmol, quant.).

^{1}H NMR (400 MHz, $CDCl_3$) δ 8.63 (d, *J* = 4.0 Hz, 1H), 7.90 (dt, *J* = 8.1, 1.1 Hz, 1H), 7.70 (td, *J* = 7.7, 1.8 Hz, 1H), 7.41 (d, *J* = 2.3 Hz, 1H), 7.18 (ddd, *J* = 7.5, 4.9, 1.2 Hz, 1H), 6.86 (d, *J* = 2.3 Hz, 1H), 3.98 (s, 3H).

^{13}C NMR (126 MHz, $CDCl_3$) δ 152.40, 151.83, 149.58, 136.64, 131.66, 122.39, 120.00, 104.52, 39.35.

HRMS (ESI^+) calculated for $[C_9H_{10}N_3]^+$ ($[M+H]^+$). Requires *m/z* 160.0869; found *m/z* 160.0867.

IR (ATR, thin film): 3223, 3117, 3048, 2993, 2925, 1592, 1563, 768 cm^{-1}.

2.5.3 Synthesis of Iridium Complexes

2.5.3.a Synthesis and Resolution of Neutral Iridium Complexes

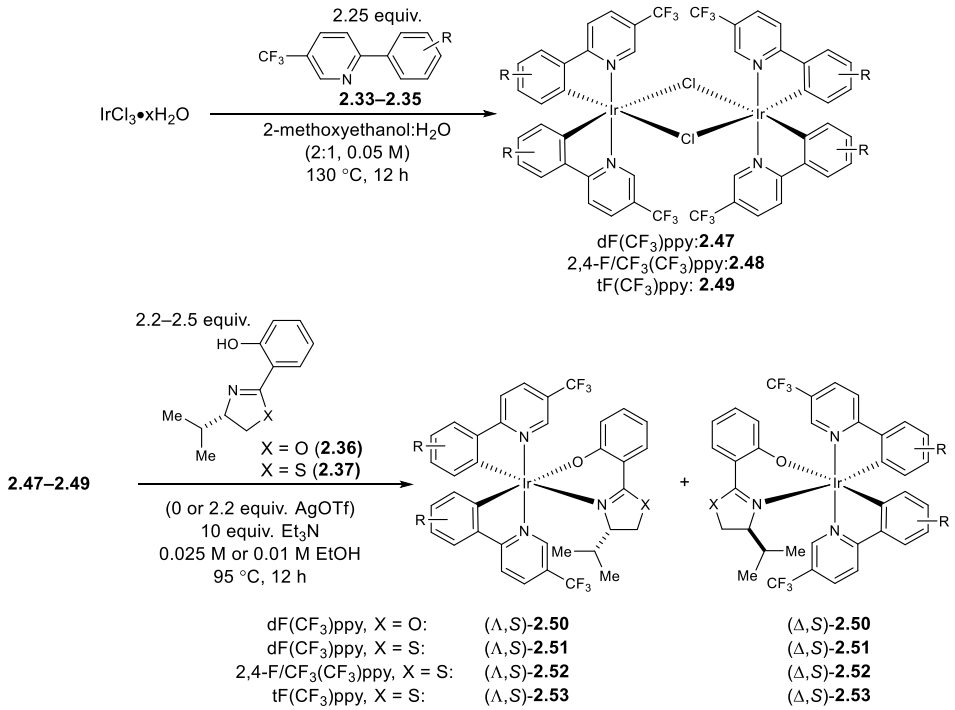

General Procedure 2.B: Resolved iridium diastereomers were prepared using a modification of the procedure reported by Meggers.[97,98] A round-bottomed flask was charged with $IrCl_3$•xH_2O (1.00 mmol, 1.0 equiv.), ppy ligand (2.25 mmol, 2.25 equiv.) and a 2:1 mixture of 2-methoxyethanol:water (20 mL total, 0.05 M with respect to $IrCl_3$). The solution was heated at reflux (130 °C) under N_2 overnight. After cooling to room temperature, H_2O was added, resulting

in precipitation. The resulting solid was isolated by suction filtration on a frit and rinsed with H_2O and hexanes before drying under vacuum. Crude iridium dimer **2.47–2.49** (mass corrected for residual 2-methoxyethanol) was not further purified or characterized, but was directly subjected to one of the following two cleavage reactions.

General Procedure 2.B-1:[98] The iridium dimer **2.47–2.49** (1.0 equiv.) was added to a round-bottomed flask, along with EtOH (0.025 M), *i*-PrHBO (**2.36**) (2.5 equiv.), and Et_3N (10.0 equiv.). The mixture was heated at reflux (95 °C) under N_2 overnight. Following this period, the solvent was removed *in vacuo* and the diastereomers were separated by flash column chromatography on silica gel.

General Procedure 2.B-2:[97] The iridium dimer **2.47–2.49** (1.0 equiv.) was added to a round-bottomed flask, along with EtOH (0.01 M), AgOTf (2.2 equiv.), *i*-PrHBT (**2.37**) (2.2 equiv.), and Et_3N (10.0 equiv.). The mixture was heated at reflux (95 °C) under N_2 overnight. Following this period, the solvent was removed *in vacuo* and the residue was passed through a short plug of silica with CH_2Cl_2 or EtOAc to remove silver salts. The two iridium diastereomers were then separated by flash column chromatography on silica gel.

Final isolation of each diastereomer was best accomplished by repeated reconcentration from roughly 2 mL of CH_2Cl_2/pentane with increasing concentrations of the latter. Rotary evaporation proved problematic, and instead, a gentle stream of nitrogen was used to concentrate the sample. This process was repeated until a solid powder formed, which was subsequently dried under high vacuum.[102]

$Ir(dF(CF_3)ppy)_2$(*i*-PrHBO) (**2.50**): Prepared according to General Procedure 2.B using $IrCl_3$ (1.000g, 3.35 mmol, 1.0 equiv.) and **2.33** (1.954 g, 7.54 mmol, 2.25 equiv.). Iridium dimer **2.47** was isolated as a yellow powder (2.184 g, 1.47 mmol, 88% crude yield) and carried on without

further purification. The cleavage was performed according to General Procedure 2.B-1 with **2.36** (759 mg, 3.70 mmol, 2.5 equiv.) and Et_3N (2.1 mL, 15 mmol, 10.3 equiv.). Following workup, the diastereomers were separated by flash column chromatography on silica gel (9:91 EtOAc:hexanes). Combined yield: 1.366 g, 1.50 mmol, 51% yield from **2.47**; 45% yield from $IrCl_3$.

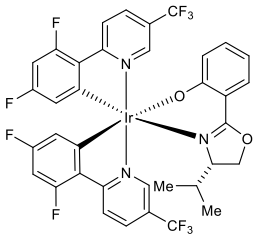

(*S*),Λ-**2.50**: Isolated as a yellow-orange powder (609 mg, 0.67 mmol, 23% yield from **2.47**; 20% yield from $IrCl_3$). >98:2 dr.

^{1}H NMR (500 MHz, $CDCl_3$) δ 9.36 (s, 1H), 8.64 (s, 1H), 8.42 (dd, *J* = 8.9, 2.2 Hz, 1H), 8.33 (dd, *J* = 8.8, 3.1 Hz, 1H), 8.03 (dd, *J* = 8.7, 2.2 Hz, 1H), 7.89 (dd, *J* = 8.8, 2.1 Hz, 1H), 7.61 (dd, *J* = 8.2, 1.9 Hz, 1H), 7.14 (ddd, *J* = 8.7, 6.9, 1.9 Hz, 1H), 6.63 (dd, *J* = 8.6, 1.1 Hz, 1H), 6.46 – 6.38 (m, 3H), 5.83 (dd, *J* = 8.5, 2.3 Hz, 1H), 5.45 (dd, *J* = 8.6, 2.3 Hz, 1H), 4.34 (dd, *J* = 9.4, 3.8 Hz, 1H), 4.25 (t, *J* = 9.3 Hz, 1H), 3.84 (dt, *J* = 9.3, 3.5 Hz, 1H), 0.53 (app. pd, *J* = 7.1, 2.9 Hz, 1H), 0.40 (d, *J* = 6.9 Hz, 3H), 0.14 (d, *J* = 6.9 Hz, 3H).

^{19}F NMR (377 MHz, $CDCl_3$) δ –62.40 (s, 3F), –62.70 (s, 3F), –104.88 (d, *J* = 11.6 Hz, 1F), –104.94 (d, *J* = 11.6 Hz, 1F), –108.46 (d, *J* = 11.6 Hz, 1F), –108.83 (d, *J* = 11.5 Hz, 1F).

HRMS (ESI^+) calculated for $[C_{36}H_{25}F_{10}IrN_3O_2]^+$ ($[M+H]^+$). Requires *m/z* 912.1388; found *m/z* 912.1397.

IR (ATR, thin film): 3069, 2966, 1605, 1569, 1330, 1139 cm^{-1}.

$[\alpha]_D^{22}$: +413.3° (*c*0.79, CH_2Cl_2).

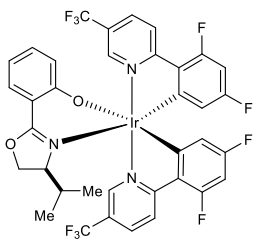

(*S*),Δ-**2.50:** Isolated as a yellow-orange powder (757 mg, 0.83 mmol, 28% yield from **2.47**; 25% yield from $IrCl_3$). >98:2 dr.

^{1}H NMR (500 MHz, $CDCl_3$) δ 9.21 (s, 1H), 8.78 (s, 1H), 8.42 (dd, *J* = 8.5, 2.2 Hz, 1H), 8.35 (dd, *J* = 8.7, 2.9 Hz, 1H), 8.04 (dd, *J* = 8.8, 2.2 Hz, 1H),

7.90 (dd, *J* = 8.8, 2.1 Hz, 1H), 7.52 (dd, *J* = 8.1, 1.9 Hz, 1H), 7.09 (ddd, *J* = 8.7, 6.9, 1.9 Hz, 1H), 6.51 (dd, *J* = 8.7, 1.2 Hz, 1H), 6.47 – 6.38 (m, 3H), 5.92 (dd, *J* = 8.5, 2.3 Hz, 1H), 5.53 (dd, *J* = 8.5, 2.3 Hz, 1H), 4.33 (dd, *J* = 9.1, 3.7 Hz, 1H), 3.80 (t, *J* = 9.3 Hz, 1H), 3.01 (ddd, *J* = 9.5, 3.7, 2.0 Hz, 1H), 1.58 (septd, *J* = 6.7, 1.8 Hz, 1H), 0.86 (d, *J* = 6.8 Hz, 3H), 0.37 (d, *J* = 7.0 Hz, 3H).

^{19}F NMR (377 MHz, $CDCl_3$) δ –62.18 (s, 3F), –62.20 (s, 3F), –105.22 (d, *J* = 11.5 Hz, 1F), –105.50 (d, *J* = 11.5 Hz, 1F), –108.49 (d, *J* = 11.5 Hz, 1F), –109.04 (d, *J* = 11.4 Hz, 1F).

HRMS (ESI^+) calculated for $[C_{36}H_{25}F_{10}IrN_3O_2]^+$ ($[M+H]^+$). Requires *m/z* 912.1388; found *m/z* 912.1394.

IR (ATR, thin film): 3065, 2965, 1604, 1568, 1330, 1138 cm^{-1}.

$[\boldsymbol{\alpha}]_{\mathbf{D}}^{\mathbf{22}}$: +161.5° (*c*1.08, CH_2Cl_2).

Ir(dF(CF_3)ppy)$_2$(*i*-PrHBT) (**2.51**): Prepared according to General Procedure 2.B using $IrCl_3$ (748 mg, 2.51 mmol, 1.0 equiv.) and **2.33** (1.458 g, 5.63 mmol, 2.2 equiv.). Iridium dimer **2.47** was isolated as a yellow powder (1.631 g, 1.10 mmol, 87% crude yield) and carried on without further purification. The cleavage was performed according to General Procedure B-2 with AgOTf (633 mg, 2.46 mmol, 2.2 equiv.), **2.37** (532 mg, 2.40 mmol, 2.2 equiv.) and Et_3N (1.5 mL, 11 mmol, 10 equiv.). Following workup, the diastereomers were separated by flash column chromatography on silica gel (9:91 EtOAc:hexanes). Combined yield: 1.400 g, 1.51 mmol, 69% yield from **2.47**; 60% yield from $IrCl_3$.

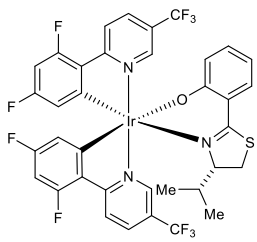

(*S*),Λ-**2.51**: Isolated as an orange powder (696 mg, 0.749 mmol, 34% yield from **2.47**; 30% yield from $IrCl_3$). >98:2 dr.

^{1}H NMR (500 MHz, $CDCl_3$) δ 9.40 (s, 1H), 8.62 (s, 1H), 8.44 (dd, *J* = 8.8, 2.3 Hz, 1H), 8.30 (dd, *J* = 8.7, 3.3 Hz, 1H), 8.04 (dd, *J* = 8.7, 2.2 Hz, 1H),

7.88 (dd, *J* = 8.8, 2.1 Hz, 1H), 7.43 (dd, *J* = 8.1, 1.8 Hz, 1H), 7.13 (ddd, *J* = 8.6, 6.8, 1.8 Hz, 1H), 6.63 (dd, *J* = 8.6, 1.2 Hz, 1H), 6.47 – 6.36 (m, 3H), 5.80 (dd, *J* = 8.5, 2.3 Hz, 1H), 5.39 (dd, *J* = 8.6, 2.3 Hz, 1H), 4.29 (dt, *J* = 9.9, 2.0 Hz, 1H), 3.31 (dd, *J* = 11.7, 9.8 Hz, 1H), 3.05 (dd, *J* = 11.8, 1.8 Hz, 1H), 0.48 – 0.40 (m, 1H), 0.39 (d, *J* = 6.5 Hz, 3H), 0.36 (d, *J* = 6.6 Hz, 3H).

^{19}F NMR (377 MHz, $CDCl_3$) δ –62.39 (s, 3F), –62.73 (s, 3F), –104.69 (d, *J* = 11.6 Hz, 1F), –104.88 (d, *J* = 11.6 Hz, 1F), –108.31 (d, *J* = 11.6 Hz, 1F), –108.71 (d, *J* = 11.6 Hz, 1F).

HRMS (ESI^+) calculated for $[C_{36}H_{25}F_{10}IrN_3OS]^+$ ($[M+H]^+$). Requires *m/z* 928.1159; found *m/z* 928.1165.

IR (ATR, thin film): 3068, 2962, 1602, 1563, 1330, 1140 cm^{-1}.

$[\boldsymbol{\alpha}]_{\mathbf{D}}^{\mathbf{22}}$: +435.2° (*c*1.00, CH_2Cl_2).

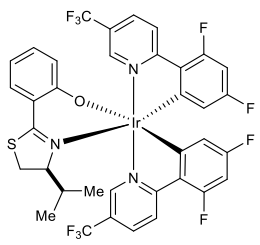

(*S*),Δ-**2.51**: Isolated as a yellow powder (704 mg, 0.758 mmol, 34% yield from **2.47**; 30% yield from $IrCl_3$). 95:5 dr.

^{1}H NMR (500 MHz, $CDCl_3$) δ 9.37 (s, 1H), 8.64 (s, 1H), 8.47 (dd, *J* = 8.8, 2.3 Hz, 1H), 8.29 (dd, *J* = 8.7, 2.8 Hz, 1H), 8.07 (dd, *J* = 8.8, 2.2 Hz, 1H), 7.83 (dd, *J* = 8.7, 2.1 Hz, 1H), 7.28 (dd, *J* = 7.9, 1.8 Hz, 1H), 7.01 (ddd, *J* = 8.6, 7.0, 1.8 Hz, 1H), 6.47 – 6.37 (m, 4H), 5.92 (dd, *J* = 8.5, 2.3 Hz, 1H), 5.47 (dd, *J* = 8.4, 2.3 Hz, 1H), 3.43 (dt, *J* = 9.8, 1.7 Hz, 1H), 3.03 (dd, *J* = 11.5, 1.6 Hz, 1H), 2.87 (dd, *J* = 11.4, 9.8 Hz, 1H), 1.86 (septd, *J* = 6.9, 1.4 Hz, 1H), 0.98 (d, *J* = 6.9 Hz, 3H), 0.31 (d, *J* = 6.9 Hz, 3H).

^{19}F NMR (377 MHz, $CDCl_3$) δ –62.05 (s, 3F), –62.40 (s, 3F), –105.03 (d, *J* = 11.5 Hz, 1F), –105.55 (d, *J* = 11.5 Hz, 1F), –108.24 (d, *J* = 11.5 Hz, 1F), –109.12 (d, *J* = 11.5 Hz, 1F).

HRMS (ESI^+) calculated for $[C_{36}H_{25}F_{10}IrN_3OS]^+$ ($[M+H]^+$). Requires *m/z* 928.1159; found *m/z* 928.1169.

IR (ATR, thin film): 3306, 2964, 1600, 1564, 1328, 1137 cm^{-1}.

$[\alpha]_D^{22}$: +414.6° (*c*0.81, CH_2Cl_2).

Ir(2,4-F/CF_3(CF_3)ppy)$_2$(*i*-PrHBT) (**2.52**): Prepared according to General Procedure 2.B using $IrCl_3$ (300 mg, 1.00 mmol, 1.0 equiv.) and **234** (698 mg, 2.26 mmol, 2.3 equiv.). Iridium dimer **2.48** was isolated as a yellow powder (650 mg (641 mg corrected), 0.380 mmol, 76% crude yield) and carried on without further purification. The cleavage was performed according to General Procedure 2.B-2 with AgOTf (211 mg, 0.821 mmol, 2.2 equiv.), **2.37** (186 mg, 0.840 mmol, 2.2 equiv.) and Et_3N (530 µL, 3.81 mmol, 10.0 equiv.). Following workup, the diastereomers were separated by flash column chromatography on silica gel (10:90 EtOAc:hexanes). Combined yield: 526 mg, 0.511 mmol, 67% yield from **2.48**; 51% yield from $IrCl_3$.

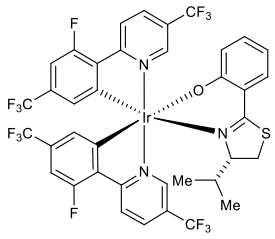

(*S*),Λ-**2.52**: Isolated as an orange powder (223 mg, 0.217 mmol, 29% yield from **2.48**; 22% yield from $IrCl_3$). >98:2 dr.

^{1}H NMR (500 MHz, $CDCl_3$) δ 9.47 (s, 1H), 8.71 (s, 1H), 8.59 (dd, *J* = 8.7, 2.5 Hz, 1H), 8.44 (dd, *J* = 8.7, 3.4 Hz, 1H), 8.13 (dd, *J* = 8.7, 2.1 Hz, 1H), 7.97 (dd, *J* = 8.7, 2.1 Hz, 1H), 7.44 (dd, *J* = 8.2, 1.8 Hz, 1H), 7.14 (ddd, *J* = 8.6, 6.9, 1.8 Hz, 1H), 6.89 (dd, *J* = 9.0, 0.8 Hz, 1H), 6.86 (dd, *J* = 9.0, 0.9 Hz, 1H), 6.63 (dd, *J* = 8.6, 1.2 Hz, 1H), 6.40 (ddd, *J* = 8.1, 6.9, 1.2 Hz, 1H), 6.35 (s, 1H), 5.85 (s, 1H), 4.22 (dt, *J* = 9.8, 1.9 Hz, 1H), 3.32 (dd, *J* = 11.8, 9.8 Hz, 1H), 3.05 (dd, *J* = 11.8, 1.8 Hz, 1H), 0.41 – 0.37 (m, 4H), 0.33 – 0.28 (m, 3H).

^{19}F NMR (377 MHz, $CDCl_3$) δ –62.58 (s, 3F), –62.90 (s, 3F), –63.19 (s, 3F), –63.28 (s, 3F), –110.79 (s, 1F), –111.33 (s, 1F).

HRMS (ESI^+) calculated for $[C_{38}H_{25}F_{14}IrN_3OS]^+$ ($[M+H]^+$). Requires *m/z* 1028.1095; found *m/z* 1028.1097.

IR (ATR, thin film): 3065, 2964, 1679, 1555, 1283, 1092, 1012 cm^{-1}.

$[\alpha]_D^{22}$: +356.3° (*c*0.82, CH_2Cl_2).

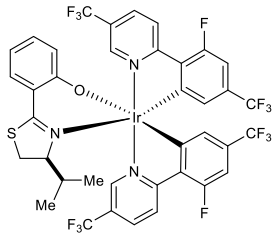

(*S*),Δ-**2.52**: Isolated as an orange powder (303 mg, 0.294 mmol, 39% yield from **2.48**; 30% yield from $IrCl_3$). 98:2 dr, but this material was contaminated with significant amounts of another species.

^{1}H NMR (500 MHz, $CDCl_3$) δ 9.44 (s, 1H), 8.73 (s, 1H), 8.62 (dd, *J* = 8.7, 2.5 Hz, 1H), 8.43 (dd, *J* = 8.7, 3.1 Hz, 1H), 8.15 (dd, *J* = 8.8, 2.1 Hz, 1H), 7.92 (dd, *J* = 8.7, 2.0 Hz, 1H), 7.29 (dd, *J* = 8.0, 1.8 Hz, 1H), 7.02 (ddd, *J* = 8.7, 7.0, 1.8 Hz, 1H), 6.89 (dd, *J* = 7.5, 1.6 Hz, 1H), 6.87 (dd, *J* = 7.7, 1.6 Hz, 1H), 6.49 (s, 1H), 6.45 (ddd, *J* = 8.0, 7.0, 1.2 Hz, 1H), 6.38 (dd, *J* = 8.5, 1.1 Hz, 1H), 5.94 (s, 1H), 3.37 (dt, *J* = 9.8, 1.6 Hz, 1H), 3.02 (dd, *J* = 11.5, 1.6 Hz, 1H), 2.87 (dd, *J* = 11.5, 9.8 Hz, 1H), 1.78 (septd, *J* = 6.8, 1.4 Hz, 1H), 0.99 (d, *J* = 6.9 Hz, 3H), 0.22 (d, *J* = 7.0 Hz, 3H).

^{19}F NMR (377 MHz, $CDCl_3$) δ –62.21 (s, 3F), –62.54 (s, 3F), –63.26 (s, 3F), –63.28 (s, 3F), –110.59 (s, 1F), –111.74 (s, 1F).

HRMS (ESI^+) calculated for $[C_{38}H_{25}F_{14}IrN_3OS]^+$ ($[M+H]^+$). Requires *m/z* 1028.1095; found *m/z* 1028.1098.

IR (ATR, thin film): 3438, 3143, 3065, 2964, 1679, 1555, 1283, 1092, 1012 cm^{-1}.

$[\alpha]_D^{22}$: +392.2° (*c*0.70, CH_2Cl_2).

Ir(tF(CF_3)ppy)$_2$(*i*-PrHBT) (**2.53**): Prepared according to General Procedure 2.B using $IrCl_3$ (302 mg, 1.01 mmol, 1.0 equiv.) and **2.35** (627 mg, 2.26 mmol, 2.3 equiv.). Iridium dimer **2.49** did not readily precipitate from the reaction, so instead the crude mixture was concentrated to an oil (1.254 g), which was carried on without further purification. The cleavage was performed according to General Procedure 2.B-2 with AgOTf (281 mg, 1.09 mmol, 2.2 equiv.), **2.37** (245 mg, 1.11 mmol,

2.2 equiv.) and Et_3N (700 µL, 5.02 mmol, 10.0 equiv.). Following workup, the diastereomers were separated by flash column chromatography on silica gel (15:85 EtOAc:hexanes). Combined yield: 649 mg, 0.673 mmol, 67% yield from $IrCl_3$.

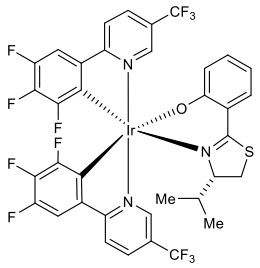

(*S*),Λ-**2.53**: Isolated as a yellow-orange powder (288 mg, 0.298 mmol, 29% yield from $IrCl_3$). >98:2 dr.

^{1}H NMR (500 MHz, $CDCl_3$) δ 9.32 (s, 1H), 8.61 (s, 1H), 8.01 (dd, *J* = 8.6, 2.1 Hz, 1H), 7.87 – 7.82 (m, 2H), 7.72 (d, *J* = 8.6 Hz, 1H), 7.47 (ddd, *J* = 9.9, 6.2, 1.4 Hz, 1H), 7.45 (dd, *J* = 8.2, 1.7 Hz, 1H), 7.33 (ddd, *J* = 10.4, 6.3, 1.6 Hz, 1H), 7.15 (ddd, *J* = 8.6, 6.8, 1.8 Hz, 1H), 6.66 (dd, *J* = 8.6, 1.2 Hz, 1H), 6.41 (ddd, *J* = 8.1, 6.9, 1.2 Hz, 1H), 4.34 (dt, *J* = 9.9, 1.9 Hz, 1H), 3.37 (dd, *J* = 11.8, 9.7 Hz, 1H), 3.07 (dd, *J* = 11.8, 1.6 Hz, 1H), 0.47 – 0.39 (m, 1H), 0.37 (d, *J* = 6.6 Hz, 3H), 0.35 (d, *J* = 6.6 Hz, 3H).

^{19}F NMR (377 MHz, $CDCl_3$) δ –62.45 (s, 3F), –62.80 (s, 3F), –126.61 (dd, *J* = 23.9, 4.0 Hz, 1F), –130.52 (dd, *J* = 23.5, 5.0 Hz, 1F), –142.93 (dd, *J* = 19.6, 4.9 Hz, 1F), –143.24 (dd, *J* = 19.3, 4.0 Hz, 1F), –155.45 (dd, *J* = 24.2, 19.5 Hz, 1F), –155.95 (dd, *J* = 23.5, 19.5 Hz, 1F).

HRMS (ESI^+) calculated for $[C_{36}H_{23}F_{12}IrN_3OS]^+$ ($[M+H]^+$). Requires *m/z* 964.0971; found *m/z* 964.0967.

IR (ATR, thin film): 2923, 1608, 1558, 1524, 1470, 1438, 1327, 1137, 830 cm^{-1}.

$[\boldsymbol{\alpha}]_{\mathbf{D}}^{\mathbf{22}}$: +323.7° (*c*0.86, CH_2Cl_2).

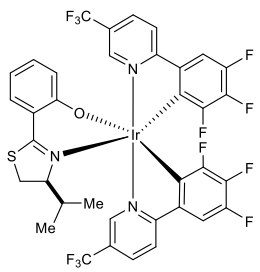

(*S*),Δ-**2.53**: Isolated as a yellow-orange powder (361 mg, 0.374 mmol, 37% yield from $IrCl_3$). 98:2 dr.

^{1}H NMR (500 MHz, $CDCl_3$) δ 9.34 (s, 1H), 8.62 (s, 1H), 8.05 (dd, *J* = 8.7, 2.1 Hz, 1H), 7.89 (d, *J* = 8.5 Hz, 1H), 7.81 (dd, *J* = 8.6, 2.0 Hz, 1H), 7.72 (d, *J* = 8.5 Hz, 1H), 7.50 (ddd, *J* = 10.2, 6.3, 1.5 Hz, 1H), 7.36 (ddd, *J* = 10.3, 6.2, 1.5 Hz, 1H), 7.30

(dd, J = 8.0, 1.8 Hz, 1H), 7.03 (ddd, J = 8.6, 7.0, 1.8 Hz, 1H), 6.46 (ddd, J = 8.0, 7.1, 1.1 Hz, 1H), 6.39 (dd, J = 8.6, 1.1 Hz, 1H), 3.42 (dt, J = 9.9, 1.6 Hz, 1H), 3.04 (dd, J = 11.5, 1.4 Hz, 1H), 2.83 (dd, J = 11.5, 9.8 Hz, 1H), 1.81 (sept, J = 6.2 Hz, 1H), 1.04 (d, J = 6.8 Hz, 3H), 0.30 (d, J = 7.0 Hz, 3H).

^{19}F NMR (377 MHz, $CDCl_3$) δ –62.06, –62.42, –124.89 (dd, J = 24.3, 4.3 Hz), –129.36 (dd, J = 23.7, 4.8 Hz), –143.04 (dd, J = 19.4, 4.9 Hz), –143.20 (dd, J = 19.4, 4.4 Hz), –155.87 (dd, J = 23.7, 19.4 Hz), –156.14 (dd, J = 24.4, 19.6 Hz).

HRMS (ESI$^+$) calculated for $[C_{36}H_{23}F_{12}IrN_3OS]^+$ ($[M+H]^+$). Requires *m/z* 964.0971; found *m/z* 964.0968.

IR (ATR, thin film): 3059, 2963, 1608, 1562, 1529, 1470, 1260, 1136, 782 cm^{-1}.

$[\boldsymbol{\alpha}]_{\mathbf{D}}^{\mathbf{22}}$: +313.1° (*c*0.81, CH_2Cl_2).

2.5.3.b Synthesis of Enantiopure Cationic Iridium Complexes

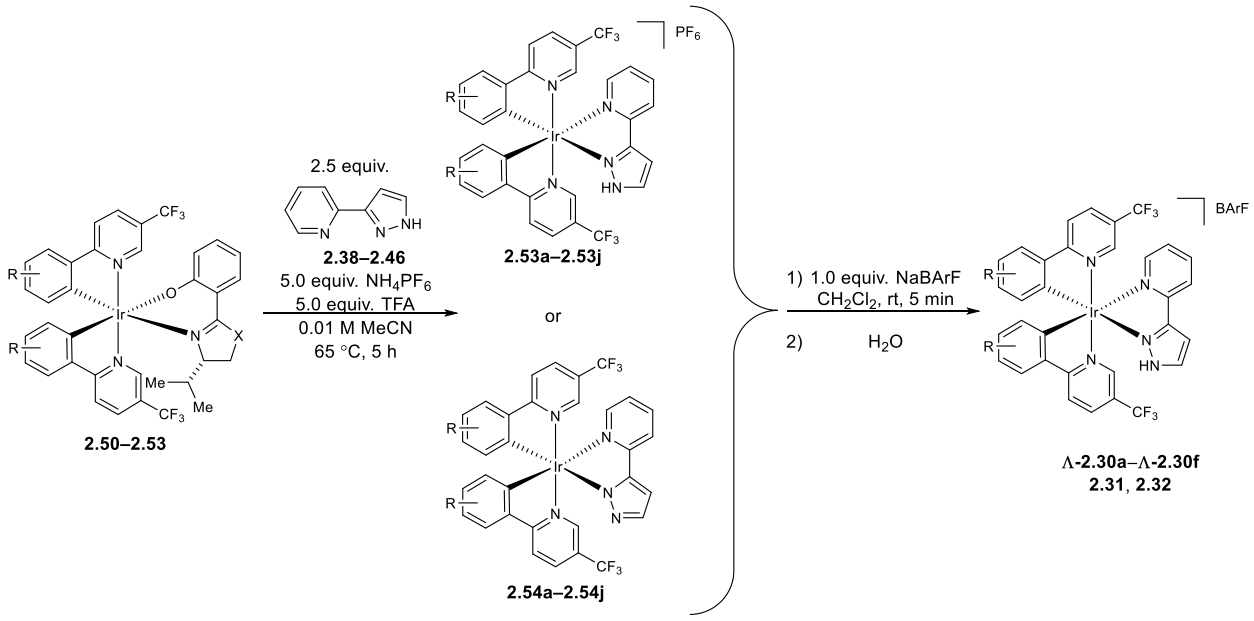

General Procedure 2.C: Based on a modification of the method by Meggers.[9898] A round-bottomed flask was charged with **2.50–2.53** (0.080 mmol, 1.0 equiv.), NH_4PF_6 (0.40 mmol, 5.0 equiv.), pyridyl pyrazole ligand (**2.38–2.46**) (0.20 mmol, 2.5 equiv.) and dry MeCN (8 mL, 0.01 M with respect to Ir), then placed under a nitrogen atmosphere. Trifluoroacetic acid (0.40 mmol, 5.0 equiv.) was added by syringe, and the solution was heated to 65 °C in the dark. After 5 h, the mixture was cooled and directly concentrated *in vacuo*. The crude residue was purified by flash column chromatography on silica gel to afford either iridium complex **2.53** or **2.54**, which was carried on without further characterization.

Note: In many cases, the products formed were neutral iridium complexes (**2.53**) rather than the expected cationic species (**2.54**). No pyrazole N–H proton is visible in the ^{1}H NMR spectra of these intermediates, but such a signal is otherwise observed in the final cationic complexes Λ-**2.30a**–**f**, Λ-**2.31**, and Λ-**2.32**. Furthermore, both ^{19}F NMR and X-ray crystallographic data show

the absence of a PF_6 counterion. These results are most consistent with deprotonation of the pyrazole N–H to form an anionic ligand, and thus neutral complex. For example, characterization data for **S23f 2.54f** are as follows:

^{1}H NMR (400 MHz, $CDCl_3$) δ 8.39 (dd, *J* = 8.8, 3.2 Hz, 1H), 8.33 (dd, *J* = 8.7, 2.8 Hz, 1H), 7.88 (td, *J* = 7.3, 6.2, 2.0 Hz, 2H), 7.79 (d, *J* = 4.3 Hz, 2H), 7.77 (s, 1H), 7.74 (d, *J* = 2.0 Hz, 1H), 7.68 (d, *J* = 5.6 Hz, 1H), 7.57 (s, 1H), 7.03 (app. sext, *J* = 4.5 Hz, 1H), 6.77 (d, *J* = 2.0 Hz, 1H), 6.54 (ddd, *J* = 12.0, 9.1, 2.3 Hz, 1H), 6.47 (ddd, *J* = 11.9, 9.1, 2.3 Hz, 1H), 5.81 (dd, *J* = 8.1, 2.3 Hz, 1H), 5.73 (dd, *J* = 8.5, 2.3 Hz, 1H).

^{19}F NMR (377 MHz, $CDCl_3$) δ –62.78 (s, 3F), –104.03 (d, *J* = 11.9 Hz, 1F), –104.04 (d, *J* = 11.9 Hz, 1F), –107.62 (d, *J* = 11.7 Hz, 1F), –108.46 (d, *J* = 11.7 Hz, 1F).

X-Ray: See Appendix XX.

Although the electronic environment of both pyrazole and cyclometalating ppy ligands appear to influence the protonation state, these outcomes could not be predicted *a priori*, and thus all reactions were conducted using NH_4PF_6 as described above. Regardless of which complex was formed in the first step, the following reaction could be performed without issue.

The neutral (**5.53**) or cationic (**5.54**) iridium complex (1.0 equiv.) was dissolved in a minimal amount of CH_2Cl_2 and NaBArF (1.0 equiv.) was added. After stirring for 5 min at room temperature, the mixture was washed with two large portions of water (roughly 5 times the volume of organic solvent). A significant emulsion often formed during this process, which necessitated removal of the aqueous layer by pipette. The organic phase was then dried by repeatedly passing it through small plugs of Celite® until homogeneous. This filtrate was then concentrated *in vacuo* and reconcentrated from CH_2Cl_2/pentane using the same technique as described in General

Procedure 2.B to afford cationic iridium complexes Λ-**2.30a**–**f**, Λ-**2.31**, and Λ-**2.32** as crystalline powders.

Note: In order to maximize use of the resolved auxiliary compounds **2.50**–**2.53** both diastereomers were employed in subsequent reactions. Specifically, catalysts **2.30a**, **2.30c**, **2.30f**, **2.30g**, **2.30h**, **2.31**, and **2.32** were synthesized as the Λ enantiomer, while complexes **2.30b**, **2.30d**, and **2.30e** were prepared with Δ stereochemistry. In all cases, Λ catalysts favored one enantiomer of the cyclobutane product, and Δ catalysts favored the other. Thus, the ee values listed in the main text are sign-corrected for the absolute configuration of the catalyst used.

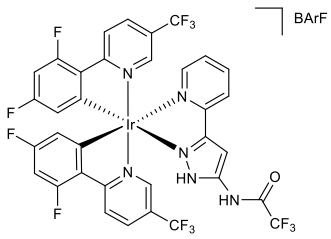

Λ-[Ir(dF(CF$_3$)ppy)$_2$(5'-NHTFApypz)][BArF] (**2.30a**): Prepared according to General Procedure 2.C using (*S*), Λ-**2.51** (109 mg, 0.117 mmol, 1.0 equiv.) NH_4PF_6 (96.1 mg, 0.590 mmol, 5.0 equiv.), **2.38** (74.1 mg, 0.289 mmol, 2.5 equiv.) and trifluoroacetic acid (45 µL, 0.588 mmol, 5.0 equiv.) Following workup, the crude residue was purified by flash column chromatography on silica gel (gradient, 25:75 to 40:60 EtOAc:hexanes) to afford neutral iridium complex **2.54a** as a yellow solid (92.7 mg, 0.0962 mmol), which was carried on without further purification or characterization. This material was treated with NaBArF (85.2 mg, 0.961 mmol, 1.0 equiv.) according to General Procedure 2.C, providing the final iridium catalyst **2.30a** as a yellow powder (150 mg, 0.0821 mmol, 85% yield; 70% over two steps).

^{1}H NMR (500 MHz, $CDCl_3$) δ 11.51 (s, 1H), 9.22 (s, 1H), 8.49 (app. dt, *J* = 8.7, 3.2 Hz, 2H), 8.07 (app. td, *J* = 8.1, 7.3, 2.0 Hz, 2H), 7.82 (d, *J* = 5.0 Hz, 1H), 7.72 (s, 8H), 7.66 (s, 1H), 7.61 (td, *J* = 7.8, 1.5 Hz, 1H), 7.46 (s, 5H*), 7.37 (d, *J* = 7.9 Hz, 1H), 7.34 (ddd, *J* = 7.7, 5.5, 1.3 Hz, 1H), 6.68 (app. ddt, *J* = 12.2, 8.8, 2.8 Hz, 2H), 6.16 (d, *J* = 1.6 Hz, 1H), 5.66 (dd, *J* = 7.8, 2.3 Hz, 1H), 5.57 (dd, *J* = 7.9, 2.3 Hz, 1H). * = Partial overlap between catalyst proton and BArF singlet.

^{19}F NMR (377 MHz, $CDCl_3$) δ –62.51 (s, 24F), –62.94 (s, 3F), –63.23 (s, 3F), –75.30 (s, 3F), –100.18 (d, *J* = 13.0 Hz, 1F), –100.21 (d, *J* = 13.0 Hz, 1F), –105.09 (d, *J* = 13.0 Hz, 1F), –105.16 (d, *J* = 13.0 Hz, 1F).

HRMS (ESI^+) calculated for $[C_{34}H_{17}F_{13}IrN_6O]^+$ ($[M]^+$). Requires *m/z* 963.0857; found *m/z* 963.0863.

IR (ATR, thin film): 3682, 3380, 3085, 1602, 1355, 1330, 1276, 1118 cm^{-1}.

$[\alpha]_D^{22}$: +161.3° (*c*0.79, CH_2Cl_2).

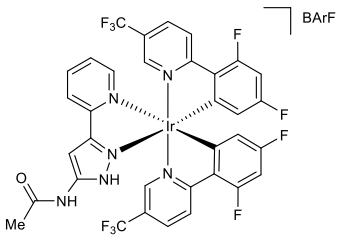

Δ-[Ir(dF(CF_3)ppy)$_2$(5'-NHAcpypz)][BArF] (**2.30b**): Prepared according to General Procedure 2.C using (*S*), Δ-**2.50** (75.0 mg, 0.0822 mmol, 1.0 equiv.) NH_4PF_6 (65.0 mg, 0.399 mmol, 4.9 equiv.), **2.39** (42.4 mg, 0.210 mmol, 2.6 equiv.) and trifluoroacetic acid (31 µL, 0.405 mmol, 4.9 equiv.) Following workup, the crude residue was purified by flash column chromatography on silica gel (33:67 acetone:hexanes) to afford neutral iridium complex **2.54b** as a yellow solid, which was carried on without further purification or characterization. This material was treated with NaBArF (72.9 mg, 0.0823 mmol, 1.0 equiv.) according to General Procedure 2.C, providing the final iridium catalyst **2.30b** as a yellow powder (85.3 mg, 0.0481 mmol, 59% yield over two steps).

^{1}H NMR (500 MHz, $CDCl_3$) δ 11.89 (s, 1H), 8.47 (app. td, *J* = 9.9, 3.0 Hz, 2H), 8.06 (app. dt, *J* = 8.8, 2.0 Hz, 2H), 7.81 (d, *J* = 5.1 Hz, 1H), 7.75 – 7.71 (m, 9H*), 7.69 (td, *J* = 7.9, 1.6 Hz, 1H), 7.63 (s, 1H), 7.49 (s, 1H), 7.48 (s, 4H), 7.37 (d, *J* = 8.0 Hz, 1H), 7.34 (ddd, *J* = 7.7, 5.5, 1.3 Hz, 1H), 6.66 (app. ddt, *J* = 11.6, 8.7, 2.4 Hz, 2H), 5.71 (d, *J* = 1.7 Hz, 1H), 5.65 (dd, *J* = 7.9, 2.3 Hz, 1H), 5.61 (dd, *J* = 7.9, 2.3 Hz, 1H), 2.09 (s, 3H). * = Partial overlap between catalyst proton and BArF singlet.

^{19}F NMR (377 MHz, $CDCl_3$) δ –62.50 (s, 24F), –63.01 (s, 3F), –63.23 (s, 3F), –100.67 (d, *J* = 12.8 Hz, 1F), –100.80 (d, *J* = 12.9 Hz, 1F), –105.44 (d, *J* = 12.8 Hz, 1F), –105.59 (d, *J* = 12.9 Hz, 1F).

HRMS (ESI^+) calculated for $[C_{34}H_{20}F_{10}IrN_6O]^+$ ($[M]^+$). Requires *m/z* 909.1139; found *m/z* 909.1137.

IR (ATR, thin film): 3691, 3449, 3354, 3087, 1598, 1355, 1330, 1276, 1118 cm^{-1}.

$[\alpha]_D^{22}$: –183.8° (*c*0.94, CH_2Cl_2).

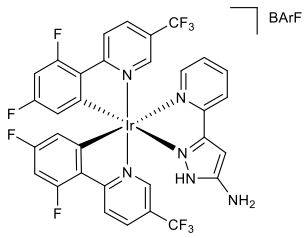

Λ-[Ir(dF(CF_3)ppy)$_2$(5'-NH_2pypz)][BArF] (**2.30c**): Prepared according to General Procedure 2.C using (*S*), Λ-**2.50** (74.4 mg, 0.0815 mmol, 1.0 equiv.) NH_4PF_6 (67.7 mg, 0.415 mmol, 5.1 equiv.), **2.40** (32.9 mg, 0.205 mmol, 2.5 equiv.) and trifluoroacetic acid (31 µL, 0.405 mmol, 5.0 equiv.) Following workup, the crude residue was purified by flash column chromatography on silica gel (gradient, 40:60 to 50:50 acetone:hexanes) to afford cationic iridium complex **2.53c** as a yellow solid, which was carried on without further purification or characterization. This material was treated with NaBArF (72.2 mg, 0.0815 mmol, 1.0 equiv.) according to General Procedure 2.C, providing the final iridium catalyst **2.30c** as a dull yellow-brown powder (92.8 mg, 0.0536 mmol, 66% yield over two steps).

^{1}H NMR (500 MHz, $CDCl_3$) δ 9.33 (s, 1H), 8.45 (app. td, *J* = 8.8, 3.0 Hz, 2H), 8.05 (app. td, *J* = 8.3, 2.1 Hz, 2H), 7.85 – 7.80 (m, 2H), 7.69 (s, 11H), 7.68 (s, 1H), 7.64 – 7.61 (m, 1H), 7.55 (s, 1H), 7.48 (s, 5H), 7.36 – 7.32 (m, 1H), 6.64 (app. tdd, *J* = 12.0, 8.9, 2.3 Hz, 2H), 5.79 (d, *J* = 2.0 Hz, 1H), 5.65 (dd, *J* = 7.9, 2.3 Hz, 1H), 5.62 (dd, *J* = 8.0, 2.3 Hz, 1H), 4.01 (br. s, 2H).

^{19}F NMR (377 MHz, $CDCl_3$) δ –62.49 (s, 24F), –63.04 (s, 3F), –63.15 (s, 3F), –100.77 (d, *J* = 12.8 Hz, 1F), –101.45 (d, *J* = 12.4 Hz, 1F), –105.52 (d, *J* = 12.9 Hz, 1F), –105.82 (d, *J* = 12.5 Hz, 1F).

HRMS (ESI^+) calculated for $[C_{32}H_{18}F_{10}IrN_6]^+$ ($[M]^+$). Requires *m/z* 867.1034; found *m/z* 867.1036.

IR (ATR, thin film): 3689, 3493, 3440, 3402, 3150, 3084, 1602, 1355, 1330, 1275, 1117 cm^{-1}.

$[\alpha]_D^{22}$: +191.7° (*c*0.53, CH_2Cl_2).

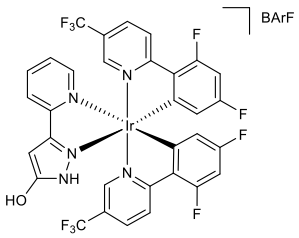

Δ-[Ir(dF(CF_3)ppy)$_2$(5'-OHpypz)][BArF] (**2.30d**): Prepared according to General Procedure 2.C using (*S*), Δ-**2.50** (70.0 mg, 0.0767 mmol, 1.0 equiv.) NH_4PF_6 (64.9 mg, 0.398 mmol, 5.2 equiv.), **2.42** (32.1 mg, 0.199 mmol, 2.6 equiv.) and trifluoroacetic acid (31 µL, 0.405 mmol, 5.3 equiv.) Following workup, the crude residue was purified by flash column chromatography on silica gel (gradient, 6:94 to 10:90 MeOH:CH_2Cl_2) to afford neutral iridium complex **2.54d** as an orange solid, which was carried on without further purification or characterization. This material was treated with NaBArF (69.7 mg, 0.0786 mmol, 1.0 equiv.) according to General Procedure 2.C, providing the final iridium catalyst **2.30d** as a yellow powder (81.8 mg, 0.0472 mmol, 62% yield over two steps).

^{1}H NMR (500 MHz, $CDCl_3$) δ 9.33 (br. s, 1H), 8.44 (app. td, *J* = 9.8, 3.0 Hz, 2H), 8.04 (dd, *J* = 8.8, 2.0 Hz, 1H), 8.00 (dd, *J* = 8.7, 1.3 Hz, 1H), 7.81 (dd, *J* = 5.4, 1.3 Hz, 1H), 7.73 – 7.67 (m, 8H*), 7.67 (s, 1H), 7.57 – 7.52 (m, 2H), 7.46 (s, 4H), 7.29 (ddd, *J* = 7.2, 5.6, 1.3 Hz, 1H), 6.65 (ddd, *J* = 12.3, 9.2, 2.7 Hz, 1H), 6.60 (ddd, *J* = 11.5, 9.3, 2.6 Hz, 1H), 5.84 (s, 1H), 5.63 (app. ddd, *J* = 7.6, 4.9, 2.3 Hz, 2H). * = Partial overlap between catalyst proton and BArF singlet.

^{19}F NMR (377 MHz, $CDCl_3$) δ –62.53 (s, 24F), –63.00 (s, 3F), –63.12 (s, 3F), –100.95 (d, *J* = 12.8 Hz, 1F), –101.63 (d, *J* = 12.0 Hz, 1F), –105.59 (d, *J* = 12.7 Hz, 1F), –106.00 (d, *J* = 11.9 Hz, 1F).

HRMS (ESI^+) calculated for $[C_{32}H_{17}F_{10}IrN_5O]^+$ ($[M]^+$). Requires *m/z* 868.0874; found *m/z* 868.0878.

IR (ATR, thin film): 3677, 3437, 3093, 1601, 1354, 1330, 1273, 1112 cm^{-1}.

$[\alpha]_D^{22}$: –186.3° (*c*0.60, CH_2Cl_2).

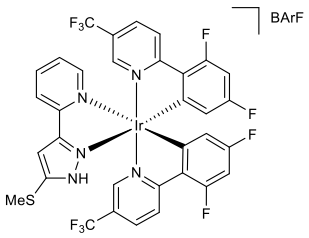

Δ-[Ir(dF(CF_3)ppy)$_2$(5-SMepypz)][BArF] (**2.30e**): Prepared according to General Procedure 2.C using (*S*), Δ-**2.50** (74.2 mg, 0.0812 mmol, 1.0 equiv.) NH_4PF_6 (67.5 mg, 0.414 mmol, 5.1 equiv.), **2.44** (39.5 mg, 0.207 mmol, 2.5 equiv.) and trifluoroacetic acid (31 µL, 0.405 mmol, 5.0 equiv.) Following workup, the crude residue was purified by flash column chromatography on silica gel (gradient, 2:98 to 3:97 MeOH:CH_2Cl_2) to afford neutral iridium complex **2.54e** as a yellow solid, which was carried on without further purification or characterization. This material was treated with NaBArF (73.0 mg, 0.0824 mmol, 1.0 equiv.) according to General Procedure 2.C, providing the final iridium catalyst **2.30e** as a yellow powder (105 mg, 0.0596 mmol, 73% yield over two steps).

^{1}H NMR (500 MHz, $CDCl_3$) δ 10.12 (s, 1H), 8.46 (app. ddd, *J* = 13.0, 8.7, 3.1 Hz, 2H), 8.05 (app. ddd, *J* = 11.2, 8.8, 2.1 Hz, 2H), 7.84 (dt, *J* = 5.5, 1.3 Hz, 1H), 7.75 – 7.72 (m, 2H), 7.69 (s, 9H), 7.54 – 7.51 (m, 2H), 7.47 (s, 4H), 7.31 (td, *J* = 5.4, 3.8 Hz, 1H), 6.79 (d, *J* = 1.9 Hz, 1H), 6.66 (app. dddd, *J* = 12.3, 8.8, 5.3, 2.3 Hz, 2H), 5.66 (dd, *J* = 7.9, 2.3 Hz, 1H), 5.59 (dd, *J* = 7.9, 2.3 Hz, 1H), 2.46 (s, 3H).

^{19}F NMR (377 MHz, $CDCl_3$) δ –62.51 (s, 24F), –63.12 (s, 3F), –63.18 (s, 3F), –100.23 (d, *J* = 13.0 Hz, 1F), –100.87 (d, *J* = 12.8 Hz, 1F), –105.16 (d, *J* = 13.1 Hz, 1F), –105.39 (d, *J* = 12.8 Hz, 1F).

HRMS (ESI^+) calculated for $[C_{33}H_{19}F_{10}IrN_5S]^+$ ($[M]^+$). Requires *m/z* 898.0802; found *m/z* 898.0806.

IR (ATR, thin film): 3689, 3422, 3084, 1603, 1354, 1329, 1273, 1114 cm^{-1}.

$[\alpha]_D^{22}$: –199.0° (*c*1.15, CH_2Cl_2).

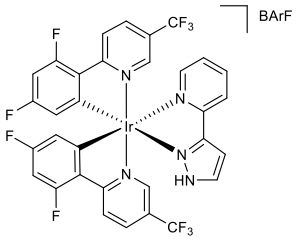

Λ-[Ir(dF(CF_3)ppy)$_2$(pypz)][BArF] (**2.30f**): Prepared according to General Procedure 2.C using (*S*), Λ-**2.50** (75.8 mg, 0.0830 mmol, 1.0 equiv.) NH_4PF_6 (68.1 mg, 0.418 mmol, 5.0 equiv.), **2.45** (30.9 mg, 0.213 mmol, 2.6 equiv.) and trifluoroacetic acid (31 µL, 0.405 mmol, 4.9 equiv.) Following workup, the crude residue was purified by flash column chromatography on silica gel (40:60 acetone:hexanes) to afford neutral iridium complex **2.54f** as a yellow solid, which was carried on without further purification. This material was treated with NaBArF (72.9 mg, 0.0823 mmol, 1.0 equiv.) according to General Procedure 2.C, providing the final iridium catalyst **2.30f** as a yellow-green powder (101 mg, 0.0588 mmol, 71% yield over two steps).

^{1}H NMR (500 MHz, $CDCl_3$) δ 10.44 (s, 1H), 8.47 (app. ddd, *J* = 9.1, 6.5, 3.1 Hz, 2H), 8.06 (app. td, *J* = 9.0, 2.1 Hz, 2H), 7.88 – 7.83 (m, 2H), 7.75 – 7.72 (m, 1H), 7.70 (s, 9H), 7.54 (s, 1H), 7.46 (s, 5H*), 7.43 (s, 1H), 7.38 (ddd, *J* = 7.5, 5.7, 1.3 Hz, 1H), 6.71 – 6.62 (m, 3H), 5.65 (dd, *J* = 7.9, 2.3 Hz, 1H), 5.62 (dd, *J* = 7.9, 2.3 Hz, 1H). * = Partial overlap between catalyst proton and BArF singlet.

^{19}F NMR (377 MHz, $CDCl_3$) δ –62.52 (s, 28F), –63.17 (s, 3F), –63.20 (s, 3F), –100.29 (d, *J* = 13.0 Hz, 1F), –100.90 (d, *J* = 12.2 Hz, 1F), –105.22 (d, *J* = 12.9 Hz, 1F), –105.44 (d, *J* = 12.4 Hz, 1F).

HRMS (ESI^+) calculated for $[C_{32}H_{17}F_{10}IrN_5]^+$ ($[M]^+$). Requires *m/z* 852.0925; found *m/z* 852.0929.

IR (ATR, thin film): 3697, 3438, 3150, 3091, 1604, 1355, 1330, 1277, 1121 cm^{-1}.

$[\alpha]_D^{22}$: +194.5° (*c*0.66, CH_2Cl_2).

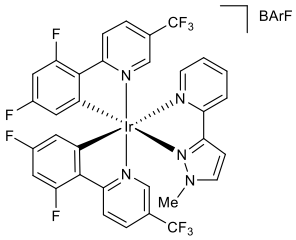

Λ-[Ir(dF(CF_3)ppy)$_2$(1'-Mepypz)][BArF] (**2.30g**): Prepared according to General Procedure 2.C using (*S*), Λ-**2.50** (76.2 mg, 0.0835 mmol, 1.0 equiv.) NH_4PF_6 (67.6 mg, 0.415 mmol, 5.0 equiv.), **2.46** (36.2 mg, 0.227 mmol, 2.7 equiv.) and trifluoroacetic acid (31 µL, 0.405 mmol, 4.9 equiv.) Following workup, the crude residue was purified by flash column chromatography on silica gel (3:97 MeOH:CH_2Cl_2) to afford cationic iridium complex **2.53g** as a yellow solid, which was carried on without further purification or characterization. This material was treated with NaBArF (72.8 mg, 0.0840 mmol, 1.0 equiv.) according to General Procedure 2.C, providing the final iridium catalyst **2.30g** as a yellow powder (82.1 mg, 0.474 mmol, 57% yield over two steps).

^{1}H NMR (500 MHz, $CDCl_3$) δ 8.51 (dd, *J* = 8.8, 3.1 Hz, 1H), 8.47 (dd, *J* = 8.8, 3.1 Hz, 1H), 8.09 (dd, *J* = 8.9, 2.0 Hz, 1H), 8.06 (dd, *J* = 8.8, 1.7 Hz, 1H), 7.84 (td, *J* = 7.8, 1.6 Hz, 1H), 7.76 (d, *J* = 5.5 Hz, 1H), 7.73 – 7.68 (m, 9H*), 7.50 (s, 1H), 7.49 (s, 1H), 7.46 (s, 4H), 7.33 (ddd, *J* = 7.6, 5.5, 1.4 Hz, 1H), 7.16 (d, *J* = 2.7 Hz, 1H), 6.67 (ddd, *J* = 11.8, 8.8, 2.1 Hz, 1H), 6.63 (ddd, *J* = 12.0, 8.7, 2.1 Hz, 1H), 6.56 (d, *J* = 2.7 Hz, 1H), 5.62 (dd, *J* = 7.9, 2.3 Hz, 1H), 5.53 (dd, *J* = 7.9, 2.3 Hz, 1H), 3.22 (s, 3H). * = Partial overlap between catalyst proton and BArF singlet.

^{19}F NMR (377 MHz, $CDCl_3$) δ –62.56 (s, 25F), –63.19 (s, 3F), –63.23 (s, 3F), –99.82 (d, *J* = 13.0 Hz, 1F), –100.28 (d, *J* = 12.7 Hz, 1F), –104.96 (d, *J* = 13.1 Hz, 1F), –105.01 (d, *J* = 13.0 Hz, 1F).

HRMS (ESI^+) calculated for $[C_{33}H_{19}F_{10}IrN_5]^+$ ($[M]^+$). Requires *m/z* 866.1081; found *m/z* 866.1088.

IR (ATR, thin film): 3150, 3087, 1605, 1356, 1331, 1277, 1121 cm^{-1}.

$[\boldsymbol{\alpha}]_{\mathbf{D}}^{\mathbf{22}}$: +175.5° (*c*0.80, CH_2Cl_2).

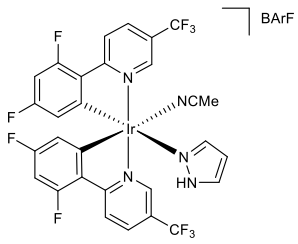

Λ-[Ir(dF(CF_3)ppy)$_2$(pyz)(MeCN)][BArF] (**2.30h**): Prepared according to General Procedure 2.C using (*S*), Λ-**2.50** (75.3 mg, 0.0825 mmol, 1.0 equiv.) NH_4PF_6 (70.5 mg, 0.433 mmol, 5.2 equiv.), pyrazole (28.0 mg, 0.411 mmol, 5.0 equiv.) and trifluoroacetic acid (31 µL, 0.405 mmol, 4.9 equiv.) Following workup, the crude residue was purified by flash column chromatography on silica gel (50:50 acetone:hexanes) to afford cationic iridium complex **2.53h** as a yellow solid, which was carried on without further purification or characterization. This material was treated with NaBArF (72.9 mg, 0.0823 mmol, 1.0 equiv.) according to General Procedure 2.C, providing the final iridium catalyst **2.30h** as a yellow powder (52.8 mg, 0.0314 mmol, 38% yield over two steps).

^{1}H NMR (500 MHz, $CDCl_3$) δ 8.99 (s, 1H), 8.50 (app. dd, *J* = 8.8, 3.2 Hz, 2H), 8.26 (s, 1H), 8.14 (app. dt, *J* = 8.7, 2.3 Hz, 2H), 7.68 (s, 10H), 7.54 (d, *J* = 3.2 Hz, 1H), 7.49 (s, 5H), 7.48 – 7.46 (m, 1H), 7.39 (d, *J* = 2.0 Hz, 1H), 6.65 (ddd, *J* = 11.3, 7.5, 2.1 Hz, 1H), 6.61 (ddd, *J* = 11.3, 7.6, 2.4 Hz, 1H), 6.50 (dd, *J* = 2.9, 2.2 Hz, 1H), 5.55 (app. ddd, *J* = 8.0, 5.5, 2.3 Hz, 2H), 2.49 (d, *J* = 1.1 Hz, 3H).

^{19}F NMR (377 MHz, $CDCl_3$) δ –62.47 (s, 28F), –62.67 (s, 3F), –63.03 (s, 3F), –100.91 (d, *J* = 12.8 Hz, 1F), –101.08 (d, *J* = 12.9 Hz, 1F), –105.72 (d, *J* = 12.8 Hz, 1F), –105.86 (d, *J* = 12.9 Hz, 1F).

HRMS (ESI^+) calculated for $[C_{29}H_{17}F_{10}IrN_5]^+$ ($[M]^+$). Requires *m/z* 818.0948; found *m/z* 818.0945.

IR (ATR, thin film): 3696, 3639, 3364, 2924, 1609, 1356, 1277, 1117 cm^{-1}.

$[\alpha]_D^{22}$: +48.5° (*c*0.94, CH_2Cl_2).

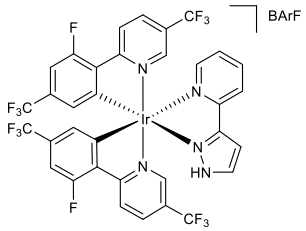

Λ-[Ir(2,4-F/CF_3(CF_3)ppy)$_2$(pypz)][BArF] (**2.31**): Prepared according to General Procedure 2.C using (*S*),Λ-**2.52** (83.0 mg, 0.0807 mmol, 1.0 equiv.), NH_4PF_6 (66.8 mg, 0.410 mmol, 5.1 equiv.), **2.45** (28.9 mg, 0.199 mmol, 2.5 equiv.) and trifluoroacetic acid (31 µL, 0.40 mmol, 5.0 equiv.) Following workup, the crude residue was purified by flash column chromatography on silica gel (6:94 MeOH:CH_2Cl_2) to afford neutral iridium complex **2.54i** as a yellow solid (76.3 mg, 0.0801 mmol), which was carried on without further purification or characterization. This material was treated with NaBArF (70.9 mg, 0.0800 mmol, 1.0 equiv.) according to General Procedure 2.C, providing the final iridium catalyst **2.31** as a yellow powder (117 mg, 0.0644 mmol, 80% yield; 80% over two steps).

^{1}H NMR (500 MHz, $CDCl_3$) δ 10.45 (br. s, 1H), 8.60 (app. ddd, *J* = 9.3, 6.1, 3.3 Hz, 2H), 8.13 (app. td, *J* = 8.6, 2.0 Hz, 2H), 7.84 (td, *J* = 7.8, 1.5 Hz, 1H), 7.78 – 7.74 (m, 2H), 7.69 (s, 8H), 7.66 (s, 1H), 7.54 (s, 1H), 7.44 (s, 4H), 7.42 (d, *J* = 2.9 Hz, 1H), 7.36 (ddd, *J* = 7.7, 5.5, 1.3 Hz, 1H), 7.13 (app. td, *J* = 11.1, 10.3, 1.6 Hz, 2H), 6.70 (d, *J* = 2.9 Hz, 1H), 6.12 (d, *J* = 0.7 Hz, 1H), 6.08 (d, *J* = 0.7 Hz, 1H).

^{19}F NMR (377 MHz, $CDCl_3$) δ –62.55 (s, 24F), –63.39 (s, 6F), –63.57, (s, 3F), –63.58 (s, 3F), –107.63 (s, 1F), –107.83 (s, 1F).

HRMS (ESI^+) calculated for $[C_{34}H_{17}F_{14}IrN_5]^+$ ($[M]^+$). Requires *m/z* 952.0861; found *m/z* 952.0859.

IR (ATR, thin film): 3438, 3143, 1613, 1355, 1324, 1277, 1122, 1095, 936 cm^{-1}.

$[\alpha]_D^{22}$: +239.4° (*c*0.77, CH_2Cl_2).

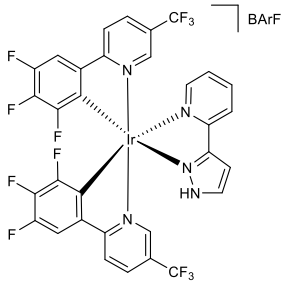

Λ-[Ir(tF(CF_3)ppy)$_2$(pypz)][BArF] (**2.32**): Prepared according to a modification of General Procedure 2.C. The standard reaction conditions gave an inseparable mixture of desired product and an impurity which we have tentatively assigned the bis(acetonitrile) iridium complex. To ensure full conversion in this ligand exchange, increased equivalences of most reagents were employed, and the reaction was run for 24 h. Modified amounts are as follows: (*S*), Λ-**2.53** (144 mg, 0.149 mmol, 1.0 equiv.) NH_4PF_6 (124.7 mg, 0.765 mmol, 5.1 equiv.), **2.45** (109.7 mg, 0.756 mmol, 5.1 equiv.) and trifluoroacetic acid (120 µL, 1.56 mmol, 10.5 equiv.) Following workup after 24 h (rather than the typical 5 h), the crude residue was purified by flash column chromatography on silica gel (30:70 acetone:hexanes) to afford neutral iridium complex **2.54j** as a yellow solid (104 mg, 0.117 mmol), which was carried on without further purification or characterization. This material was treated with NaBArF (104 mg, 0.117 mmol, 1.0 equiv.) according to General Procedure 2.C, providing the final iridium catalyst **2.32** as a yellow powder (162 mg, 0.0924 mmol, 79% yield; 62% over two steps).

^{1}H NMR (500 MHz, $CDCl_3$) δ 10.52 (s, 1H), 8.01 (app. td, *J* = 8.5, 2.0 Hz, 2H), 7.92 (d, *J* = 5.4 Hz, 1H), 7.88 (d, *J* = 4.6 Hz, 1H), 7.88 – 7.83 (m, 2H), 7.74 – 7.68 (m, 9H*), 7.53 (app. dd, *J* = 9.6, 6.0 Hz, 2H), 7.47 (s, 1H), 7.45 (s, 4H), 7.42 (dd, *J* = 2.9, 1.6 Hz, 1H), 7.40 (ddd, *J* = 7.7, 5.6,

1.4 Hz, 1H), 7.36 (s, 1H), 6.63 (dd, *J* = 3.0, 1.8 Hz, 1H). * = Partial overlap between catalyst proton and BArF singlet.

^{19}F NMR (377 MHz, $CDCl_3$) δ –62.53 (s, 25F), –63.26 (s, 3F), –63.31 (s, 3F), –126.98 (dd, *J* = 22.7, 5.9 Hz, 1F), –127.34 (dd, *J* = 22.6, 5.9 Hz, 1F), –138.17 (dd, *J* = 19.5, 6.0 Hz, 1F), –138.33 (dd, *J* = 19.4, 5.8 Hz, 1F), –151.34 (dd, *J* = 22.5, 19.3 Hz, 1F), –151.87 (dd, *J* = 22.6, 19.5 Hz, 1F).

HRMS (ESI^+) calculated for $[C_{32}H_{15}F_{12}IrN_5]^+$ ($[M]^+$). Requires *m/z* 888.0736; found *m/z* 888.0743.

IR (ATR, powder): 3435, 2923, 2854, 1616, 1478, 1353, 1274, 1117, 674 cm^{-1}.

$[\boldsymbol{\alpha}]_{\mathbf{D}}^{\mathbf{22}}$: +142.7° (*c*0.81, CH_2Cl_2).

2.5.3.c Synthesis of Racemic Cationic Iridium Complexes

Racemic catalysts **2.30f** and **2.32** were used for the NMR titration and binding studies, as well as electrochemical measurements. These complexes were synthesized by treating the dimer (**2.47** or **2.49**) with **2.45**, following literature procedure. Spectroscopic data were identical to those obtained for the enantiopure compounds (see above).

2.5.4 Synthesis of Photocycloaddition Substrates

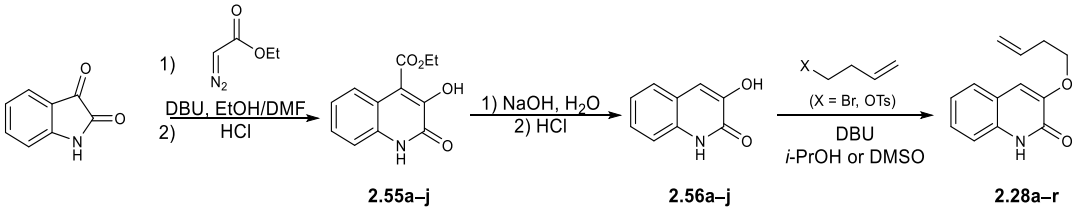

The majority of quinolone substrates were prepared by Eistert ring expansion of the corresponding isatin, followed by hydrolysis, decarboxylation, and alkylation with the desired tether.

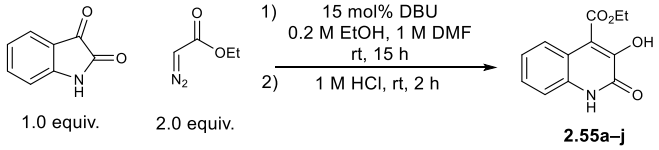

General Procedure 2.D: Adapted from a procedure reported by Candeias, Gois, and coworkers.[103] A 250 mL round bottom flask was charged with isatin (10 mmol, 1.0 equiv.), a 5:1 mixture of EtOH:DMF (60 mL total, 0.17 M with respect to substrate) and stirred at room temperature under N_2. DBU (1.5 mmol, 0.15 equiv.) was added quickly dropwise, generally resulting in a darkening of color. Ethyl diazoacetate (85 wt%, 20. mmol, 2.0 equiv.) was then added, and the mixture was stirred at room temperature for 15 h. Following this period, the reaction was concentrated *in vacuo* to remove most of the ethanol. Aqueous 1 M HCl (35 mL) was added slowly, resulting in vigorous evolution of N_2. After 2 h of stirring, the resultant precipitate was collected by suction filtration, rinsed with H_2O (2 x 20 mL) and Et_2O (2 x 20 mL), then dried under high vacuum to give the 3-hydroxyquinolone ethyl ester **2.55** without the need for further purification.

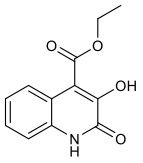

Ethyl 3-hydroxy-2-oxo-1,2-dihydroquinoline-4-carboxylate (**2.55a**): Prepared according to General Procedure 2.D using isatin (1.474 g, 10.0 mmol, 1.0 equiv.), DBU (230 μL, 1.54 mmol, 0.15 equiv.), and ethyl diazoacetate (2.5 mL, 20.2 mmol, 2.0 equiv.). The product was isolated as a light beige powder (1.836 g, 7.87 mmol, 79% yield).

^{1}H NMR (500 MHz, DMSO-d_6) δ 12.31 (s, 1H), 10.24 (s, 1H), 7.39 – 7.34 (m, 2H), 7.32 (d, J = 7.6 Hz, 1H), 7.19 (ddd, J = 8.3, 6.9, 1.4 Hz, 1H), 4.39 (q, J = 7.1 Hz, 2H), 1.32 (t, J = 7.1 Hz, 3H).

^{13}C NMR (126 MHz, DMSO-d_6) δ 165.31, 157.89, 143.63, 132.98, 127.01, 123.24, 122.70, 117.10, 116.87, 115.41, 61.30, 14.11.

HRMS (ESI$^-$) calculated for $[C_{12}H_{10}NO_4]^-$ ([M–H]$^-$). Requires *m/z* 232.0615; found *m/z* 232.0613.

IR (ATR, powder): 3075, 2988, 2876, 1729, 1643, 1616, 1566, 1401, 1306, 1267, 1230, 1185, 1158 cm^{-1}.

M.P. 226.4–229.4 °C.

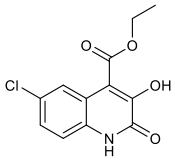

Ethyl 6-chloro-3-hydroxy-2-oxo-1,2-dihydroquinoline-4-carboxylate (**2.55b**): Prepared according to General Procedure 2.D using 5-chloroisatin (1.817 g, 10.0 mmol, 1.0 equiv.), DBU (230 μL, 1.54 mmol, 0.15 equiv.), and ethyl diazoacetate (2.5 mL, 20.2 mmol, 2.0 equiv.). The product was isolated as a light beige powder (2.106 g, 7.86 mmol, 79% yield).

^{1}H NMR (500 MHz, DMSO-d_6) δ 12.45 (s, 1H), 10.59 (s, 1H), 7.44 – 7.39 (m, 2H), 7.32 (d, J = 8.5 Hz, 1H), 4.41 (q, J = 7.1 Hz, 2H), 1.32 (t, J = 7.1 Hz, 3H).

^{13}C NMR (126 MHz, DMSO-d_6) δ 164.86, 157.67, 145.29, 131.70, 126.87, 126.71, 122.25, 118.56, 117.30, 115.31, 61.49, 14.07.

HRMS (ESI$^-$) calculated for $[C_{12}H_9ClNO_4]^-$ ([M–H]$^-$). Requires *m/z* 266.0226; found *m/z* 266.0226.

IR (ATR, powder): 3258, 2984, 1720, 1659, 1313, 1270, 1241, 1198 cm^{-1}.

M.P. 219.1–220.9 °C.

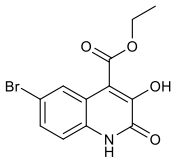

Ethyl 6-bromo-3-hydroxy-2-oxo-1,2-dihydroquinoline-4-carboxylate (**2.55c**): Prepared according to General Procedure 2.D using 5-bromoisatin (2.264 g, 10.0 mmol, 1.0 equiv.), DBU (230 µL, 1.54 mmol, 0.15 equiv.), and ethyl diazoacetate (2.5 mL, 20.2 mmol, 2.0 equiv.). The product was isolated as a tan powder (2.786 g, 8.92 mmol, 89% yield).

^{1}H NMR (500 MHz, DMSO-d_6) δ 12.45 (s, 1H), 10.60 (s, 1H), 7.58 – 7.48 (m, 2H), 7.27 (d, *J* = 9.1 Hz, 1H), 4.40 (q, *J* = 7.0 Hz, 2H), 1.32 (t, *J* = 7.1 Hz, 3H).

^{13}C NMR (126 MHz, DMSO-d_6) δ 164.86, 157.67, 145.23, 132.02, 129.57, 125.16, 119.03, 117.57, 115.20, 114.57, 61.49, 14.07.

HRMS (ESI$^-$) calculated for $[C_{12}H_9BrNO_4]^-$ ([M–H]$^-$). Requires *m/z* 309.9720; found *m/z* 309.9720.

IR (ATR, powder): 3493, 3146, 2984, 2924, 1658, 1538, 1322, 1275, 1201 cm^{-1}.

M.P. 217.8–218.9 °C.

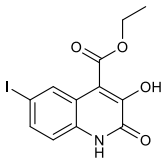

Ethyl 3-hydroxy-6-iodo-2-oxo-1,2-dihydroquinoline-4-carboxylate (**2.55d**): Prepared according to General Procedure 2.D using 6-iodoisatin (2.731 g, 10.0 mmol, 1.0 equiv.), DBU (230 µL, 1.54 mmol, 0.15 equiv.), and ethyl diazoacetate (2.5 mL, 20.2 mmol, 2.0 equiv.). The product was isolated as a beige powder (3.361 g, 9.36 mmol, 94% yield).

^{1}H NMR (500 MHz, DMSO-d_6) δ 12.42 (s, 1H), 10.55 (s, 1H), 7.69 – 7.65 (m, 2H), 7.13 (d, J = 8.3 Hz, 1H), 4.40 (q, J = 7.1 Hz, 2H), 1.32 (t, J = 7.1 Hz, 3H).

^{13}C NMR (126 MHz, DMSO-d_6) δ 164.90, 157.68, 144.87, 135.15, 132.40, 131.08, 119.43, 117.64, 115.12, 86.34, 61.45, 14.08.

HRMS (ESI$^-$) calculated for $[C_{12}H_9INO_4]^-$ ([M–H]$^-$). Requires *m/z* 357.9582; found *m/z* 357.9581.

IR (ATR, powder): 3147, 2985, 2918, 1691, 1651, 1401, 1318, 1274, 1227, 1194 cm^{-1}.

M.P. 236.9–237.9 °C.

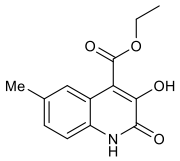

Ethyl 3-hydroxy-6-methyl-2-oxo-1,2-dihydroquinoline-4-carboxylate (**2.55f**): Prepared according to General Procedure 2.D using 5-methylisatin (1.615 g, 10.0 mmol, 1.0 equiv.), DBU (230 μL, 1.54 mmol, 0.15 equiv.), and ethyl diazoacetate (2.5 mL, 20.2 mmol, 2.0 equiv.). The product was isolated as a pale brown powder (1.857 g, 7.51 mmol, 75% yield).

^{1}H NMR (500 MHz, DMSO-d_6) δ 12.23 (s, 1H), 10.15 (s, 1H), 7.24 – 7.17 (m, 2H), 7.13 (s, 1H), 4.39 (q, J = 7.1 Hz, 2H), 2.32 (s, 3H), 1.32 (t, J = 7.1 Hz, 3H).

^{13}C NMR (126 MHz, DMSO-d_6) δ 165.38, 157.70, 143.58, 131.71, 130.95, 128.22, 122.79, 117.02, 116.77, 115.34, 61.25, 20.69, 14.12.

HRMS (ESI$^-$) calculated for $[C_{13}H_{12}NO_4]^-$ ([M–H]$^-$). Requires *m/z* 246.0772; found *m/z* 246.0770.

IR (ATR, powder): 3486, 3155, 2918, 1657, 1543, 1500, 1322, 1286, 1206 cm^{-1}.

M.P. 193.2–196.0 °C.

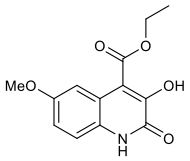

Ethyl 3-hydroxy-6-methoxy-2-oxo-1,2-dihydroquinoline-4-carboxylate (**2.55g**): Prepared according to General Procedure 2.D using 5-methoxyisatin (1.771 g, 10.0 mmol, 1.0 equiv.), DBU (230 μL, 1.54 mmol, 0.15 equiv.), and ethyl diazoacetate (2.5 mL, 20.2 mmol, 2.0 equiv.). The product was isolated as a fine brown powder (2.113 g, 8.03 mmol, 80% yield).

^{1}H NMR (500 MHz, DMSO-d_6) δ 12.21 (s, 1H), 10.24 (s, 1H), 7.26 (d, J = 9.0 Hz, 1H), 7.03 (dd, J = 8.9, 2.7 Hz, 1H), 6.81 (d, J = 2.7 Hz, 1H), 4.40 (q, J = 7.1 Hz, 2H), 3.75 (s, 3H), 1.33 (t, J = 7.1 Hz, 3H).

^{13}C NMR (126 MHz, DMSO-d_6) δ 165.26, 157.23, 154.78, 144.46, 127.30, 117.85, 116.73, 116.29, 115.44, 105.63, 61.24, 55.32, 14.14.

HRMS (ESI$^-$) calculated for $[C_{13}H_{12}NO_5]^-$ ([M–H]$^-$). Requires m/z 262.0721; found m/z 262.0719.

IR (ATR, powder): 3165, 2982, 2830, 1662, 1613, 1500, 1467, 1418, 1290, 1184, 1018 cm^{-1}.

M.P. 203.7–206.1 °C.

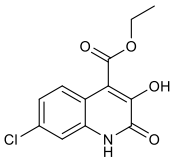

Ethyl 7-chloro-3-hydroxy-2-oxo-1,2-dihydroquinoline-4-carboxylate (**2.55h**): Due to incomplete conversion even at extended timepoints, a modified procedure was employed. The reaction was conducted according to General Procedure 2.D, using 6-chloroisatin (1.816 g, 10.0 mmol, 1.0 equiv.), DBU (230 μL, 1.54 mmol, 0.15 equiv.), and ethyl diazoacetate (2.5 mL, 20.2 mmol, 2.0 equiv.). After 15 h, another portion of ethyl diazoacetate (1.0 mL, 8.1 mmol, 0.8 equiv.) was added, and the reaction stirred for an additional 19 h. The crude mixture was worked up according to General Procedure D, affording the product as a beige powder (2.094 g, 7.82 mmol, 78% yield).

^{1}H NMR (500 MHz, DMSO-d_6) δ 12.40 (s, 1H), 10.48 (s, 1H), 7.40 (d, J = 8.6 Hz, 1H), 7.34 (d, J = 2.1 Hz, 1H), 7.24 (dd, J = 8.6, 2.1 Hz, 1H), 4.39 (q, J = 7.1 Hz, 2H), 1.32 (t, J = 7.1 Hz, 3H).

^{13}C NMR (126 MHz, DMSO-d_6) δ 164.97, 157.87, 144.20, 133.87, 131.12, 125.10, 122.76, 116.19, 116.09, 114.66, 61.44, 14.08.

HRMS (ESI$^-$) calculated for $[C_{12}H_9ClNO_4]^-$ ([M–H]$^-$). Requires *m/z* 266.0226; found *m/z* 266.0226.

IR (ATR, powder): 2992, 2851, 1686, 1651, 1537, 1327, 1280, 1216, 1151, 1014 cm^{-1}.

M.P. 197.6–200.3 °C.

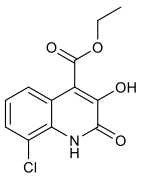

Ethyl 8-chloro-3-hydroxy-2-oxo-1,2-dihydroquinoline-4-carboxylate (**2.55i**): Prepared according to General Procedure 2.D using 7-chloroisatin (1.814, 10.0 mmol, 1.0 equiv.), DBU (230 μL, 1.54 mmol, 0.15 equiv.), and ethyl diazoacetate (2.5 mL, 20.2 mmol, 2.0 equiv.). The product was isolated as a light mauve powder (2.202 g, 8.23 mmol, 82% yield).

^{1}H NMR (500 MHz, DMSO-d_6) δ 11.68 (s, 1H), 10.64 (s, 1H), 7.52 (dd, J = 7.8, 1.2 Hz, 1H), 7.33 (dd, J = 8.1, 1.3 Hz, 1H), 7.21 (t, J = 8.0 Hz, 1H), 4.40 (q, J = 7.1 Hz, 2H), 1.32 (t, J = 7.1 Hz, 3H).

^{13}C NMR (126 MHz, DMSO-d_6) δ 164.95, 158.25, 144.27, 129.42, 127.35, 123.43, 122.46, 118.89, 118.82, 116.80, 61.56, 14.08.

HRMS (ESI$^-$) calculated for $[C_{12}H_9ClNO_4]^-$ ([M–H]$^-$). Requires *m/z* 266.0226; found *m/z* 266.0225.

IR (ATR, powder): 3171, 2988, 1735, 1648, 1618, 1565, 1480, 1294, 1255, 1186, 1033 cm^{-1}.

M.P. 165.7–167.7 °C.

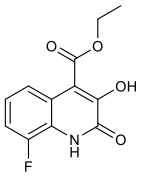

Ethyl 8-fluoro-3-hydroxy-2-oxo-1,2-dihydroquinoline-4-carboxylate (**2.55j**): Prepared according to a slight modification of General Procedure 2.D using 7-fluoroisatin (1.652 g, 10.0 mmol, 1.0 equiv.), DBU (230 µL, 1.54 mmol, 0.15 equiv.), and ethyl diazoacetate (2.5 mL, 20.2 mmol, 2.0 equiv.). Instead of the typical EtOH/DMF solvent mixture, only ethanol (100 mL) was used. Following workup, the product was isolated as a beige powder (2.045 g, 8.14 mmol, 81% yield).

^{1}H NMR (500 MHz, DMSO-d_6) δ 12.37 (s, 1H), 10.55 (s, 1H), 7.28 (ddd, J = 11.0, 5.8, 3.5 Hz, 1H), 7.21 – 7.15 (m, 2H), 4.39 (q, J = 7.1 Hz, 2H), 1.32 (t, J = 7.1 Hz, 3H).

^{13}C NMR (126 MHz, DMSO-d_6) δ 164.94, 157.89, 149.03 (d, J = 245.6 Hz), 144.62, 122.78 (d, J = 7.4 Hz), 121.59 (d, J = 14.3 Hz), 119.33 (d, J = 3.2 Hz), 119.04 (d, J = 3.5 Hz), 116.45 (d, J = 2.5 Hz), 112.41 (d, J = 17.3 Hz), 61.46, 14.08.

^{19}F NMR (377 MHz, DMSO-d_6) δ –130.12.

HRMS (ESI$^-$) calculated for $[C_{12}H_9FNO_4]^-$ ([M–H]$^-$). Requires *m/z* 250.0521; found *m/z* 250.0523.

IR (ATR, powder): 3132, 3009, 2902, 2847, 1677, 1593, 1552, 1490, 1325, 1263, 1239, 1213, 1023 cm^{-1}.

M.P. 195.3–196.3 °C.

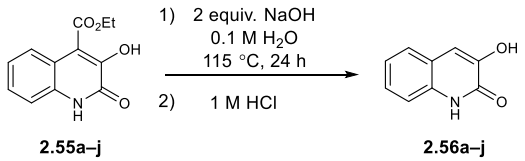

2.55a–j **2.56a–j**

General Procedure 2.E: Adapted from a procedure originally reported by Candeias, Gois, and coworkers.[103] NaOH (14 mmol, 2 equiv.) was added to a 250 mL round bottom flask and dissolved

in H_2O (70 mL, 0.1 M with respect to substrate). The appropriate hydroxyquinolone ethyl ester **2.55** (7.0 mmol, 1 equiv.) was then added, and the solution brought to 115 °C (reflux), stirring vigorously for 24 h. After cooling, the reaction was acidified to pH 2 using 1 M HCl (ca. 20 mL). The resulting slurry was collected by suction filtration on a frit, rinsed with water (2 x 20 mL) and Et_2O (2 x 20 mL), then dried under high vacuum to afford the decarboxylated hydroxyquinolone **S25**.

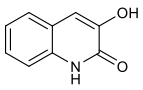

3-Hydroxyquinolin-2(1*H*)-one (**2.56a**): Prepared according to General Procedure 2.E using **2.55a** (2.334 g, 10.0 mmol, 1.0 equiv.) and NaOH (804 mg, 20.1 mmol, 2.0 equiv.). The product was isolated as a white powder (1.495 g, 9.28 mmol, 93% yield).

^{1}H NMR (500 MHz, DMSO-d_6) δ 12.00 (s, 1H), 9.45 (s, 1H), 7.48 (d, J = 7.8 Hz, 1H), 7.32 – 7.23 (m, 2H), 7.12 (ddd, J = 8.1, 6.8, 1.6 Hz, 1H), 7.08 (s, 1H).

^{13}C NMR (126 MHz, DMSO-d_6) δ 158.54, 146.20, 133.51, 126.25, 125.78, 122.03, 120.69, 114.69, 112.40.

HRMS (ESI$^+$) calculated for $[C_9H_8NO_2]^+$ ($[M+H]^+$). Requires *m/z* 162.0550; found *m/z* 162.0549.

IR (ATR, powder): 3269, 3156, 3055, 3000, 1656, 1615, 1571, 1398, 1286, 1246, 1182 cm^{-1}.

M.P. > 260 °C.

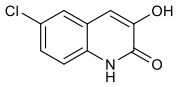

6-Chloro-3-hydroxyquinolin-2(1*H*)-one (**2.56b**): Prepared according to General Procedure 2.E using **2.55b** (1.876, 7.01 mmol, 1.0 equiv.) and NaOH (560 mg, 14.0 mmol, 2.0 equiv.). The product was isolated as a cream-colored powder (1.269 g, 6.49 mmol, 93% yield).

^{1}H NMR (500 MHz, DMSO-d_6) δ 12.12 (s, 1H), 9.75 (s, 1H), 7.60 (d, J = 2.3 Hz, 1H), 7.31 (dd, J = 8.7, 2.4 Hz, 1H), 7.25 (d, J = 8.7 Hz, 1H), 7.07 (s, 1H).

^{13}C NMR (126 MHz, DMSO-d_6) δ 158.31, 147.22, 132.21, 126.01, 125.94, 124.68, 122.25, 116.44, 111.41.

HRMS (ESI$^-$) calculated for $[C_9H_5ClNO_2]^-$ ([M–H]$^-$). Requires *m/z* 194.0014; found *m/z* 194.0016.

IR (ATR, powder): 3087, 3024, 2921, 2852, 1640, 1608, 1570, 1434, 1395, 1212, 1189 cm^{-1}.

M.P. > 260 °C.

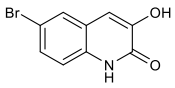

6-Bromo-3-hydroxyquinolin-2(1*H*)-one (**2.56c**): Prepared according to General Procedure 2.E using **2.55c** (2.186, 7.00 mmol, 1.0 equiv.) and NaOH (558 mg, 14.0 mmol, 2.0 equiv.). The product was isolated as a light brown powder, which contained 21 mol% unreacted starting material by NMR analysis. Representative ^{1}H and ^{13}C data are provided below, but no additional characterization was performed. Instead, the crude material (1.629 g, 1.211 g corrected, 5.04 mmol, 72% yield) was carried on to the subsequent alkylation reaction without further purification.

^{1}H NMR (500 MHz, DMSO-d_6) δ 12.12 (s, 1H), 9.75 (s, 1H), 7.74 (s, 1H), 7.42 (d, J = 8.6 Hz, 1H), 7.19 (d, J = 8.6 Hz, 1H), 7.07 (s, 1H).

^{13}C NMR (126 MHz, DMSO-d_6) δ 158.31, 147.15, 132.54, 128.69, 127.65, 122.77, 116.73, 113.81, 111.33.

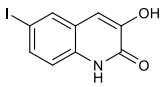

3-Hydroxy-6-iodoquinolin-2(1*H*)-one (**2.56d**): Prepared according to General Procedure 2.E using **2.55d** (2.512 g, 6.99 mmol, 1.0 equiv.) and NaOH (561 mg, 14.0 mmol, 1.0 equiv.). The product was isolated as a tan powder, which contained 12 mol% of an unidentified impurity by NMR analysis. Representative ^{1}H, ^{13}C, and HRMS data are provided below, but no additional characterization was performed. Instead, the crude material (1.994 g,

1.704 g corrected, 5.94 mmol, 85% yield) was carried on to the subsequent alkylation reaction without further purification.

^{1}H NMR (500 MHz, DMSO-d_6) δ 12.09 (br. s, 1H), 9.75 (br. s, 1H), 7.89 (d, J = 1.8 Hz, 1H), 7.56 (dd, J = 8.4, 1.9 Hz, 1H), 7.08 – 7.03 (m, 2H).

^{13}C NMR (126 MHz, DMSO-d_6) δ 158.36, 146.93, 134.22, 133.63, 132.93, 123.26, 116.89, 111.17, 85.46.

HRMS (ESI$^-$) calculated for $[C_9H_5INO_2]^-$ ([M–H]$^-$). Requires *m/z* 285.9370; found *m/z* 285.9372.

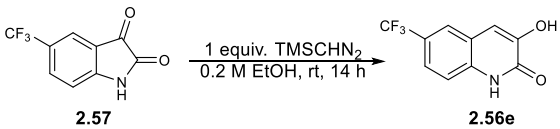

2.57 **2.56e**

3-Hydroxy-6-(trifluoromethyl)quinolin-2(1*H*)-one (**2.56e**): [Note: **Trimethylsilyldiazomethane is extremely toxic and should be handled with great caution!**] Prepared according to the general method of Arnold, LaVoie, and coworkers.[104] A round-bottomed flask was charged with **2.57** (1.995 g, 9.27 mmol, 1.0 equiv.) and EtOH (50 mL). Trimethylsilyldiazomethane (2 M in Et_2O, 4.6 mL, 9.3 mmol, 1.0 equiv.) was added cautiously via syringe, followed by Et_3N (2.6 mL, 18.7 mmol, 2.0 equiv.). The solution was stirred at room temperature under N_2 for 14 h, then diluted with Et_2O and concentrated to a brown oil (2.04 g, 1.76 g corrected for residual Et_3N and Et_2O), which was carried on to the subsequent alkylation reaction (see **2.28e**, below) without further purification or characterization.

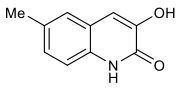

3-Hydroxy-6-methylquinolin-2(1*H*)-one (**2.56f**): Prepared according to General Procedure 2.E using **2.55f** (1.731 g, 7.00 mmol, 1.0 equiv.) and NaOH (562 mg, 14.1 mmol, 2.0 equiv.). The product was isolated as a beige powder (914 mg, 5.22 mmol, 74% yield).

^{1}H NMR (500 MHz, DMSO-d_6) δ 11.92 (s, 1H), 9.37 (s, 1H), 7.28 (s, 1H), 7.15 (d, J = 8.3 Hz, 1H), 7.11 (d, J = 8.2 Hz, 1H), 7.02 (s, 1H), 2.31 (s, 3H).

^{13}C NMR (126 MHz, DMSO-d_6) δ 158.38, 146.20, 131.46, 130.89, 127.45, 125.44, 120.64, 114.61, 112.19, 20.52.

HRMS (ESI$^-$) calculated for $[C_{10}H_8NO_2]^-$ ([M–H]$^-$). Requires *m/z* 174.0561; found *m/z* 174.0560.

IR (ATR, powder): 3150, 3019, 2976, 1653, 1614, 1574, 1371, 1280, 1235, 1188 cm^{-1}.

M.P. 225.9–232.0 °C.

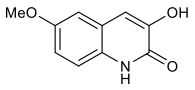

3-Hydroxy-6-methoxyquinolin-2(1*H*)-one (**2.56g**): Prepared according to General Procedure 2.E using **2.55g** (1.844 g, 7.00 mmol, 1.0 equiv.) and NaOH (559 mg, 14.0 mmol, 2.0 equiv.). The product was isolated as a light brown powder, which contained 15 mol% of an unidentified impurity by NMR analysis. Representative ^{1}H, ^{13}C, and HRMS data are provided below, but no additional characterization was performed. Instead, the crude material (858 mg, 730 mg corrected, 3.82 mmol, 55% yield) was carried on to the subsequent alkylation reaction without further purification.

^{1}H NMR (500 MHz, DMSO-d_6) δ 11.89 (s, 1H), 9.42 (s, 1H), 7.17 (d, J = 8.8 Hz, 1H), 7.06 – 7.02 (m, 2H), 6.92 (dd, J = 8.9, 2.8 Hz, 1H), 3.75 (s, 3H).

^{13}C NMR (126 MHz, DMSO-d_6) δ 158.40, 154.95, 147.11, 128.30, 121.99, 116.35, 115.51, 112.63, 108.25, 55.77.

HRMS (ESI$^-$) calculated for $[C_{10}H_8NO_3]^-$ ([M–H]$^-$). Requires *m/z* 190.0510; found *m/z* 190.0511.

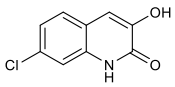

7-Chloro-3-hydroxyquinolin-2(1*H*)-one (**2.56h**): Prepared according to General Procedure 2.E using **2.55h** (1.873 g, 7.00 mmol, 1.0 equiv.) and NaOH (560 mg, 14.0 mmol, 2.0 equiv.). The product was isolated as a pale yellow powder (1.197 g, 6.12 mmol, 87% yield).

^{1}H NMR (500 MHz, DMSO-d_6) δ 12.09 (s, 1H), 9.67 (s, 1H), 7.52 (d, J = 8.4 Hz, 1H), 7.27 (d, J = 2.1 Hz, 1H), 7.16 (dd, J = 8.4, 2.1 Hz, 1H), 7.10 (s, 1H).

^{13}C NMR (126 MHz, DMSO-d_6) δ 158.43, 146.49, 134.37, 130.35, 127.46, 122.08, 119.64, 113.93, 111.96.

HRMS (ESI$^-$) calculated for $[C_9H_5ClNO_2]^-$ ([M–H]$^-$). Requires *m/z* 194.0014; found *m/z* 194.0014.

IR (ATR, powder): 3167, 3066, 2983, 2835, 1658, 1615, 1571, 1271, 1225 cm^{-1}.

M.P. > 260 °C.

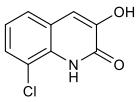

8-Chloro-3-hydroxyquinolin-2(1*H*)-one (**2.56i**): Prepared according to General Procedure 2.E using **2.55i** (1.873 g, 7.00 mmol, 1.0 equiv.) and NaOH (561 mg, 14.0 mmol, 2.0 equiv.). The product was isolated as a beige powder (1.059 g, 5.41 mmol, 77% yield).

^{1}H NMR (500 MHz, DMSO-d_6) δ 7.26 (dd, J = 7.8, 1.3 Hz, 1H), 7.17 (dd, J = 7.8, 1.3 Hz, 1H), 6.97 (t, J = 7.8 Hz, 1H), 6.71 (s, 1H), 5.32 (br. s, 2H).

^{13}C NMR (126 MHz, DMSO-d_6) δ 162.03, 152.65, 128.55, 125.21, 123.03, 123.00, 121.95, 118.20, 108.85.

HRMS (ESI$^-$) calculated for $[C_9H_5ClNO_2]^-$ ([M–H]$^-$). Requires *m/z* 194.0014; found *m/z* 194.0014.

IR (ATR, powder): 3552, 3347, 3175, 3025, 1671, 1645, 1607, 1485, 1276 cm^{-1}.

M.P. > 260 °C.

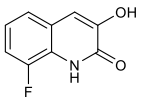

8-Fluoro-3-hydroxyquinolin-2(1*H*)-one (2.56j): Prepared according to General Procedure 2.E using **2.55j** (1.759 g, 7.00 mmol, 1.0 equiv.) and NaOH (561 mg, 14.0 mmol, 2.0 equiv.). The product was isolated as a beige powder (1.011 g, 5.64 mmol, 81% yield).

^{1}H NMR (500 MHz, DMSO-d_6) δ 11.80 (br. s, 1H), 10.21 (br. s, 1H), 7.31 (d, J = 7.7 Hz, 1H), 7.17 (dd, J = 11.1, 8.0 Hz, 1H), 7.14 – 7.06 (m, 2H).

^{13}C NMR (126 MHz, DMSO-d_6) δ 158.49, 148.78 (d, J = 244.5 Hz), 147.28 , 123.07 (d, J = 3.4 Hz), 122.06 (d, J = 7.2 Hz), 121.86 (d, J = 13.6 Hz), 121.53 (d, J = 3.3 Hz), 111.96 (d, J = 2.7 Hz), 111.57 (d, J = 17.3 Hz).

^{19}F NMR (377 MHz, DMSO-d_6) δ –131.44.

HRMS (ESI$^-$) calculated for $[C_9H_5FNO_2]^-$ ($[M–H]^-$). Requires m/z 178.0310; found m/z 178.0309.

IR (ATR, powder): 3411, 3135, 2985, 1668, 1640, 1283 cm^{-1}.

M.P. 238.2–239.8 °C.

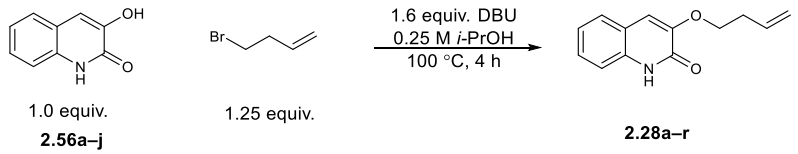

General Procedure 2.F (alkylation with bromides): Adapted from a procedure reported by Bach and coworkers.[105] A 100 mL round-bottomed flask was charged with 3-hydroxyquinolone **2.56** (4.0 mmol, 1.0 equiv.) and *i*-PrOH (16 mL, 0.25 M with respect to substrate). DBU (6.4 mmol, 1.6 equiv.) was then added to this slurry, generally resulting in a change in color and heterogeneity. Next, the alkyl bromide (5.0 mmol, 1.25 equiv.) was added dropwise, and the solution was heated at reflux (100 °C) under N_2 for 4 h. Following this period, the mixture was cooled to room temperature and concentrated *in vacuo*. The crude residue was dissolved in CH_2Cl_2 (60 mL) and sequentially washed with 1 M NaOH (30 mL) and 0.1 M HCl (30 mL). The organic phase was dried over Na_2SO_4, filtered, and concentrated to a semisolid. The crude product was purified by flash column chromatography on silica gel to afford the alkylated quinolone.

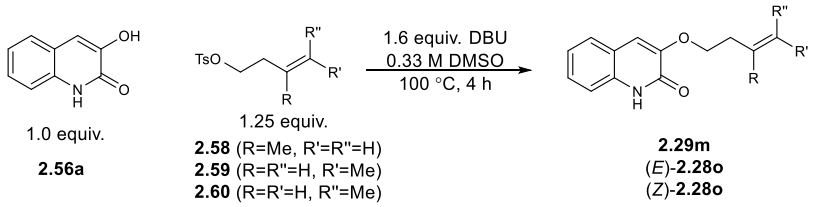

General Procedure 2.G (alkylation with tosylates): A 100 mL round-bottomed flask was charged with 3-hydroxyquinolone **2.56a** (2.0 mmol, 1.0 equiv.) and DMSO (6 mL, 0.33 M with respect to the substrate). DBU (3.12 mmol, 1.6 equiv.) was then added to the slurry, generally resulting in change of color and hetereogeneity. Next, the alkyl tosylate **2.58**–**2.60** (2.5 mmol, 1.25 equiv.) was added dropwise, and the solution was heated to 100 °C under N_2 for 4 h. Following this period, the mixture was cooled to room temperature and diluted with CH_2Cl_2 (25 mL). The combined organic layers were sequentially washed with 1 M NaOH (25 mL), 0.25 M HCl (25 mL), and brine (25 mL), then dried over Na_2SO_4, filtered, and concentrated *in vacuo*. The crude product was purified by flash column chromatography on silica gel to afford the alkylated quinolone.

General note for compounds **2.56**, **2.28**, and **2.29**: In relatively nonpolar solvents such as chloroform, analyte concentration has an appreciable effect on the chemical shifts of the quinolone protons, most dramatically on H1 (NH) and H8. We ascribe this behavior to the formation of hydrogen-bonded dimers, the extent of which will vary depending on concentration. Thus, it is not usual for different samples to give slightly different ^{1}H NMR spectra, especially in the aromatic region.

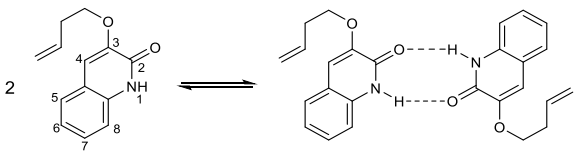

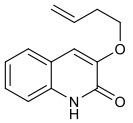

3-(But-3-en-1-yloxy)quinolin-2(1*H*)-one (**2.28a**): Prepared according to General Procedure 2.F using **2.56a** (1.124 g, 6.97 mmol, 1.0 equiv.), DBU (1.7 mL, 11 mmol, 1.5 equiv.), and 4-bromo-1-butene (890 µL, 8.8 mmol, 1.25 equiv.). Following workup, the crude residue was purified by flash column chromatography (6:94 MeOH:CH_2Cl_2, dry load) to afford a white powder (1.015 g, 4.72 mmol, 63% yield).

^{1}H NMR (500 MHz, $CDCl_3$) δ 10.80 (s, 1H), 7.48 (dd, *J* = 7.9, 1.4 Hz, 1H), 7.37 (ddd, *J* = 8.4, 7.1, 1.4 Hz, 1H), 7.31 (d, *J* = 8.1 Hz, 1H), 7.21 (ddd, *J* = 8.2, 7.1, 1.2 Hz, 1H), 7.00 (s, 1H), 5.95 (ddt, *J* = 17.1, 10.3, 6.8 Hz, 1H), 5.23 (dq, *J* = 17.2, 1.6 Hz, 1H), 5.16 (dq, *J* = 10.2, 1.3 Hz, 1H), 4.13 (t, *J* = 7.1 Hz, 2H), 2.72 (qt, *J* = 7.0, 1.4 Hz, 2H).

^{13}C NMR (126 MHz, $CDCl_3$) δ 159.91, 147.95, 133.85, 133.69, 127.57, 126.28, 123.03, 120.42, 117.70, 116.09, 113.31, 68.37, 33.24.

HRMS (ESI^-) calculated for $[C_{13}H_{12}NO_2]^-$ ($[M–H]^-$). Requires *m/z* 214.0874; found *m/z* 214.0875.

IR (ATR, thin film): 3062, 3004, 2945, 2862, 1653, 1610, 1571, 1436, 1230, 1185, 904, 723 cm^{-1}.

M.P. 179.1–181.0 °C.

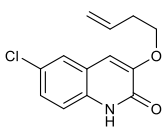

3-(But-3-en-1-yloxy)-6-chloroquinolin-2(1*H*)-one (**2.28b**): Prepared according to General Procedure 2.F using **2.56b** (781 mg, 3.99 mmol, 1.0 equiv.), DBU (960 µL, 6.4 mmol, 1.6 equiv.), and 4-bromo-1-butene (510 µL, 5.0 mmol, 1.3 equiv.). Following workup, the crude residue was purified by flash column chromatography (40:60 acetone:hexanes) to afford a beige powder (579 mg, 2.32 mmol, 58% yield).

^{1}H NMR (500 MHz, $CDCl_3$) δ 12.51 (s, 1H), 7.45 (d, *J* = 2.2 Hz, 1H), 7.42 (d, *J* = 8.6 Hz, 1H), 7.31 (dd, *J* = 8.7, 2.2 Hz, 1H), 6.90 (s, 1H), 5.94 (ddt, *J* = 17.1, 10.2, 6.8 Hz, 1H), 5.23 (dq, *J* = 17.1, 1.6 Hz, 1H), 5.16 (dq, *J* = 10.3, 1.3 Hz, 1H), 4.12 (t, *J* = 7.1 Hz, 2H), 2.71 (qt, *J* = 7.1, 1.0 Hz, 2H).

^{13}C NMR (126 MHz, $CDCl_3$) δ 159.68, 148.72, 133.62, 132.05, 128.34, 127.68, 125.39, 121.61, 117.89, 117.54, 111.96, 68.49, 33.14.

HRMS (ESI$^-$) calculated for $[C_{13}H_{11}ClNO_2]^-$ ([M–H]$^-$). Requires *m/z* 248.0484; found *m/z* 248.0484.

IR (ATR, thin film): 3170, 3063, 2923, 1662, 1612, 1573, 1420, 1270, 1225, 1190 cm^{-1}.

M.P. 146.2–147.8 °C.

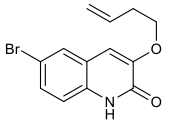

6-Bromo-3-(but-3-en-1-yloxy)quinolin-2(1*H*)-one (**2.28c**): Prepared according to General Procedure 2.F using crude **2.56c** (1.211 g corrected, 5.04 mmol, 1.0 equiv.), DBU (1.2 mL, 8.0 mmol, 1.6 equiv.), and 4-bromo-1-butene (640 µL, 6.3 mmol, 1.3 equiv.). Following workup, the crude residue was purified by flash column chromatography (40:60 acetone:hexanes) to afford a beige powder (733 mg, 2.49 mmol, 49% yield, 36% yield from **2.55c**).

^{1}H NMR (500 MHz, $CDCl_3$) δ 12.28 (s, 1H), 7.61 (d, *J* = 2.1 Hz, 1H), 7.45 (dd, *J* = 8.7, 2.1 Hz, 1H), 7.34 (d, *J* = 8.6 Hz, 1H), 6.91 (s, 1H), 5.94 (ddt, *J* = 17.1, 10.3, 6.8 Hz, 1H), 5.23 (dq, *J* = 17.2, 1.6 Hz, 1H), 5.17 (dq, *J* = 10.3, 1.3 Hz, 1H), 4.12 (t, *J* = 7.1 Hz, 2H), 2.72 (qt, *J* = 7.0, 1.4 Hz, 2H).

^{13}C NMR (126 MHz, $CDCl_3$) δ 159.60, 148.71, 133.61, 132.39, 130.39, 128.49, 122.12, 117.91, 117.68, 115.79, 111.86, 68.52, 33.14.

HRMS (ESI$^-$) calculated for $[C_{13}H_{11}BrNO_2]^-$ ([M–H]$^-$). Requires *m/z* 291.9979; found *m/z* 291.9981.

IR (ATR, thin film): 3168, 3062, 2922, 1666, 1612, 1572, 1419, 1272, 1226, 1192 cm^{-1}.

M.P. 169.4–170.4 °C.

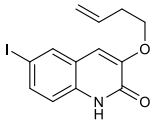

3-(But-3-en-1-yloxy)-6-iodoquinolin-2(1*H*)-one (**2.28d**): Prepared according to General Procedure 2.F using crude **2.56d** (1.704 g corrected, 5.94 mmol, 1.0 equiv.), DBU (1.45 mL, 9.7 mmol, 1.6 equiv.), and 4-bromo-1-butene (750 µL, 7.4 mmol, 1.3 equiv.). Following workup, the crude residue was purified by flash column chromatography (35:65 acetone:hexanes), then triturated with pentane to afford a beige powder (733 mg, 2.15 mmol, 36% yield, 31% yield from **2.55d**).

^{1}H NMR (500 MHz, $CDCl_3$) δ 12.17 (s, 1H), 7.81 (d, *J* = 1.9 Hz, 1H), 7.61 (dd, *J* = 8.5, 1.9 Hz, 1H), 7.21 (d, *J* = 8.6 Hz, 1H), 6.88 (s, 1H), 5.94 (ddt, *J* = 17.0, 10.2, 6.7 Hz, 1H), 5.23 (dq, *J* = 17.2, 1.6 Hz, 1H), 5.16 (dq, *J* = 10.3, 1.3 Hz, 1H), 4.12 (t, *J* = 7.1 Hz, 2H), 2.71 (qt, *J* = 6.8, 1.3 Hz, 2H).

^{13}C NMR (126 MHz, $CDCl_3$) δ 159.59, 148.51, 135.96, 134.67, 133.61, 132.94, 122.63, 117.91, 117.85, 111.67, 86.02, 68.51, 33.13.

HRMS (ESI^-) calculated for $[C_{13}H_{11}INO_2]^-$ ($[M–H]^-$). Requires *m/z* 339.9840; found *m/z* 339.9840.

IR (ATR, thin film): 3162, 3054, 2915, 1657, 1609, 1569, 1416, 1274, 1224, 1191 cm^{-1}.

M.P. 147.9–149.3 °C.

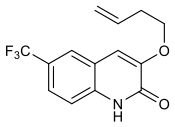

3-(But-3-en-1-yloxy)-6-(trifluoromethyl)quinolin-2(1*H*)-one (**2.28e**): Prepared according to General Procedure 2.F using crude **2.56e** (1.76 g (corrected), 7.68 mmol, 1.0 equiv.), DBU (1.8 mL, 12.0 mmol, 1.6 equiv.), and 4-bromo-1-butene (1.0 mL, 9.9 mmol, 1.3 equiv.). Following workup, the crude residue was purified by flash column chromatography (gradient, 25:75 to 50:50 EtOAc:hexanes), providing a light brown solid. This

was recrystallized from EtOAc/hexanes to afford a pale pink powder (488 mg, 1.72 mmol, 22% yield from 5-trifluoromethylisatin).

^{1}H NMR (500 MHz, $CDCl_3$) δ 11.17 (s, 1H), 7.78 (s, 1H), 7.59 (dd, *J* = 8.5, 1.6 Hz, 1H), 7.42 (d, *J* = 8.5 Hz, 1H), 7.03 (s, 1H), 5.95 (ddt, *J* = 17.1, 10.3, 6.8 Hz, 1H), 5.24 (dq, *J* = 17.2, 1.6 Hz, 1H), 5.17 (dq, *J* = 10.3, 1.4 Hz, 1H), 4.15 (t, *J* = 7.1 Hz, 2H), 2.73 (qt, *J* = 6.8, 1.3 Hz, 2H).

^{13}C NMR (126 MHz, $CDCl_3$) δ 159.78, 148.98, 135.50, 133.54, 125.49 (q, *J* = 32.8 Hz), 124.23 (q, *J* = 271.7 Hz), 124.05 (q, *J* = 3.3 Hz), 123.85 (q, *J* = 4.0 Hz), 120.17, 118.00, 116.36, 112.48, 68.62, 33.13.

^{19}F NMR (377 MHz, $CDCl_3$) δ –61.79.

HRMS (ESI$^-$) calculated for $[C_{14}H_{11}F_3NO_2]^-$ ([M–H]$^-$). Requires *m/z* 282.0747; found *m/z* 282.0747.

IR (ATR, powder): 3010, 2846, 1683, 1584, 1329, 1278, 1228, 1196, 1112, 1068, 905 cm^{-1}.

M.P. 177.4–178.1 °C.

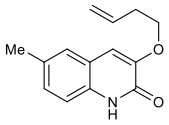

3-(But-3-en-1-yloxy)-6-methylquinolin-2(1*H*)-one (**2.28f**): Prepared according to General Procedure 2.F using **2.56f** (701 mg, 4.00 mmol, 1.0 equiv.), DBU (960 µL, 6.4 mmol, 1.6 equiv.), and 4-bromo-1-butene (510 µL, 5.0 mmol, 1.3 equiv.). Following workup, the crude residue was purified by flash column chromatography (gradient, 50:50 to 60:40 acetone:hexanes) to afford a beige powder (457 mg, 1.99 mmol, 50% yield).

^{1}H NMR (500 MHz, $CDCl_3$) δ 11.58 (s, 1H), 7.29 (d, *J* = 8.3 Hz, 1H), 7.27 (s, 1H), 7.19 (dd, *J* = 8.3, 1.8 Hz, 1H), 6.96 (s, 1H), 5.96 (ddt, *J* = 17.1, 10.2, 6.8 Hz, 1H), 5.23 (dq, *J* = 17.1, 1.6 Hz, 1H), 5.15 (dq, *J* = 10.2, 1.3 Hz, 1H), 4.13 (t, *J* = 7.2 Hz, 2H), 2.72 (qt, *J* = 7.0, 1.3 Hz, 2H), 2.40 (s, 3H).

^{13}C NMR (126 MHz, $CDCl_3$) δ 159.48, 148.03, 133.90, 132.57, 131.56, 128.92, 126.14, 120.39, 117.69, 115.70, 113.11, 68.35, 33.26, 21.14.

HRMS (ESI^-) calculated for $[C_{14}H_{14}NO_2]^-$ ($[M–H]^-$). Requires *m/z* 228.1030; found *m/z* 228.1030.

IR (ATR, thin film): 2978, 2920, 2864, 1654, 1611, 1580, 1232, 1197, 911, 727 cm^{-1}.

M.P. 173.0–174.4 °C.

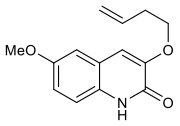

3-(But-3-en-1-yloxy)-6-methoxyquinolin-2(1*H*)-one (**2.28g**): Prepared according to General Procedure F using crude **2.56g** (730 mg, 3.82 mmol, 1.0 equiv.), DBU (910 µL, 6.1 mmol, 1.6 equiv.), and 4-bromo-1-butene (490 µL, 4.8 mmol, 1.3 equiv.). Following workup, the crude residue was purified by flash column chromatography (gradient, 40:60 to 50:50 acetone:hexanes) to afford a light brown powder (538 mg, 2.19 mmol, 58% yield, 31% yield from **2.55g**).

^{1}H NMR (500 MHz, $CDCl_3$) δ 11.71 (s, 1H), 7.33 (d, *J* = 8.9 Hz, 1H), 7.00 (dd, *J* = 8.9, 2.7 Hz, 1H), 6.97 (s, 1H), 6.93 (d, *J* = 2.7 Hz, 1H), 5.95 (ddt, *J* = 17.1, 10.2, 6.8 Hz, 1H), 5.23 (dq, *J* = 17.1, 1.6 Hz, 1H), 5.16 (dq, *J* = 10.3, 1.3 Hz, 1H), 4.13 (t, *J* = 7.2 Hz, 2H), 3.85 (s, 3H), 2.73 (qt, *J* = 7.0, 1.4 Hz, 2H).

^{13}C NMR (126 MHz, $CDCl_3$) δ 159.07, 155.62, 148.50, 133.85, 128.08, 121.21, 117.72, 117.12, 116.46, 112.92, 108.27, 68.39, 55.79, 33.24.

HRMS (ESI^-) calculated for $[C_{14}H_{14}NO_3]^-$ ($[M–H]^-$). Requires *m/z* 244.0979; found *m/z* 244.0979.

IR (ATR, thin film): 3149, 3056, 2935, 1656, 1619, 1503, 1422, 1284, 1227, 1208, 870 cm^{-1}.

M.P. 168.0–169.3 °C.

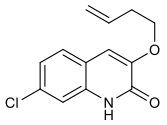

3-(But-3-en-1-yloxy)-7-chloroquinolin-2(1*H*)-one (**2.28h**): Prepared according to General Procedure 2.F using **2.56h** (784 mg, 4.01 mmol, 1.0 equiv.), DBU (960 µL, 6.4 mmol, 1.6 equiv.), and 4-bromo-1-butene (510 µL, 5.0 mmol, 1.3 equiv.). Following workup, the crude residue was purified by flash column chromatography (35:65 acetone:hexanes) to afford a beige powder (581 mg, 2.33 mmol, 58% yield).

^{1}H NMR (500 MHz, $CDCl_3$) δ 12.22 (s, 1H), 7.47 (d, *J* = 1.9 Hz, 1H), 7.39 (d, *J* = 8.4 Hz, 1H), 7.16 (dd, *J* = 8.4, 2.0 Hz, 1H), 6.98 (s, 1H), 5.95 (ddt, *J* = 17.1, 10.3, 6.8 Hz, 1H), 5.24 (dq, *J* = 17.2, 1.6 Hz, 1H), 5.17 (dq, *J* = 10.3, 1.3 Hz, 1H), 4.13 (t, *J* = 7.1 Hz, 2H), 2.73 (qt, *J* = 7.0, 1.3 Hz, 2H).

^{13}C NMR (126 MHz, $CDCl_3$) δ 159.84, 147.99, 134.29, 133.69, 133.42, 127.42, 123.68, 118.99, 117.86, 115.65, 112.74, 68.52, 33.21.

HRMS (ESI^-) calculated for $[C_{13}H_{11}ClNO_2]^-$ ($[M–H]^-$). Requires *m/z* 248.0484; found *m/z* 248.0484.

IR (ATR, thin film): 3070, 3008, 2936, 2843, 1653, 1610, 1570, 1405, 1266, 1222, 1191 cm^{-1}.

M.P. 173.2–175.4 °C.

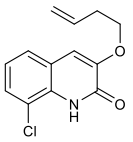

3-(But-3-en-1-yloxy)-8-chloroquinolin-2(1*H*)-one (**2.28i**): Prepared according to General Procedure 2.F using **2.56i** (783 mg, 4.00 mmol, 1.0 equiv.), DBU (960 µL, 6.4 mmol, 1.6 equiv.), and 4-bromo-1-butene (510 µL, 5.0 mmol, 1.3 equiv.). Following workup, the crude residue was purified by flash column chromatography (30:70 acetone:hexanes) to afford a beige powder (301 mg, 1.21 mmol, 30% yield).

^{1}H NMR (500 MHz, $CDCl_3$) δ 9.16 (s, 1H), 7.42 – 7.37 (m, 2H), 7.13 (t, *J* = 7.9 Hz, 1H), 6.92 (s, 1H), 5.93 (ddt, *J* = 17.0, 10.2, 6.7 Hz, 1H), 5.21 (dq, *J* = 17.2, 1.6 Hz, 1H), 5.15 (dq, *J* = 10.3, 1.3 Hz, 1H), 4.11 (t, *J* = 7.1 Hz, 2H), 2.70 (qt, *J* = 7.0, 1.4 Hz, 2H).

^{13}C NMR (126 MHz, $CDCl_3$) δ 157.73, 149.02, 133.60, 129.81, 127.27, 125.28, 123.25, 121.61, 118.90, 117.84, 111.94, 68.57, 33.15.

HRMS (ESI$^-$) calculated for $[C_{13}H_{11}ClNO_2]^-$ ([M–H]$^-$). Requires *m/z* 248.0484; found *m/z* 248.0484.

IR (ATR, thin film): 3174, 3122, 3052, 2934, 2877, 1651, 1606, 1295, 1181, 907, 858, 728 cm^{-1}.

M.P. 111.5–113.6 °C.

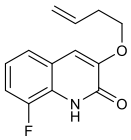

3-(But-3-en-1-yloxy)-8-fluoroquinolin-2(1*H*)-one (**2.28j**): Prepared according to General Procedure 2.F using **2.56j** (714 mg, 3.99 mmol, 1.0 equiv.), DBU (960 µL, 6.4 mmol, 1.6 equiv.), and 4-bromo-1-butene (510 µL, 5.0 mmol, 1.3 equiv.). Following workup, the crude residue was purified by flash column chromatography (gradient, 20:80 to 100:0 EtOAc:hexanes) to afford a white, highly crystalline powder (404 mg, 1.73 mmol, 43% yield).

^{1}H NMR (500 MHz, $CDCl_3$) δ 9.45 (s, 1H), 7.26 – 7.24 (m, 1H), 7.15 – 7.10 (m, 2H), 6.95 (d, *J* = 1.4 Hz, 1H), 5.94 (ddt, *J* = 17.0, 10.2, 6.7 Hz, 1H), 5.22 (dq, *J* = 17.2, 1.6 Hz, 1H), 5.15 (dq, *J* = 10.3, 1.3 Hz, 1H), 4.11 (t, *J* = 7.1 Hz, 2H), 2.70 (qt, *J* = 7.0, 1.4 Hz, 2H).

^{13}C NMR (126 MHz, $CDCl_3$) δ 157.66, 149.20, 149.17 (d, *J* = 244.8 Hz), 133.68, 122.77 (d, *J* = 7.2 Hz), 122.33 (d, *J* = 12.8 Hz), 122.27 (d, *J* = 2.7 Hz), 121.87 (d, *J* = 3.5 Hz), 117.82, 112.67 (d, *J* = 17.1 Hz), 111.89 (d, *J* = 2.7 Hz), 68.51, 33.18.

^{19}F NMR (377 MHz, $CDCl_3$) δ –135.72.

HRMS (ESI$^-$) calculated for $[C_{13}H_{11}FNO_2]^-$ ([M–H]$^-$). Requires *m/z* 232.0779; found *m/z* 232.0779.

IR (ATR, thin flim): 3174, 3132, 3068, 3005, 2914, 2860, 1656, 1613, 1581, 1252, 1185 cm^{-1}.

M.P. 158.3–159.7 °C.

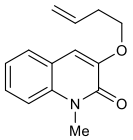

3-(But-3-en-1-yloxy)-1-methylquinolin-2(1*H*)-one (**2.28k**): A 50 mL round-bottomed flask was charged with **2.28a** (219 mg, 1.00 mmol, 1.0 equiv.) and DMF (1.50 mL). NaH (60 wt%, 44 mg, 1.2 mmol, 1.2 equiv.) was added, and the heterogeneous suspension was stirred for 2 h under N_2. MeI (75 µL, 1.2 mmol, 1.2 equiv.) was added by syringe, and the mixture was stirred for 16 h. H_2O and EtOAc were added, and the mixture was extracted twice into EtOAc. The combined organics were washed with brine, dried over Na_2SO_4, filtered, and concentrated *in vacuo* to afford a beige powder (164 mg, 0.715 mmol, 71% yield).

^{1}H NMR (500 MHz, $CDCl_3$) δ 7.48 (dd, *J* = 7.8, 1.5 Hz, 1H), 7.43 (ddd, *J* = 8.6, 7.2, 1.5 Hz, 1H), 7.32 (d, *J* = 8.4 Hz, 1H), 7.22 (td, *J* = 7.5, 1.0 Hz, 1H), 6.9 (s, 1H), 5.94 (ddt, *J* = 17.0, 10.2, 6.7 Hz, 1H), 5.21 (dq, *J* = 17.2, 1.5 Hz, 1H), 5.13 (d, *J* = 10.1 Hz, 1H), 4.09 (t, *J* = 7.0 Hz, 2H), 3.77 (s, 3H), 2.69 (q, *J* = 6.9 Hz, 2H).

^{13}C NMR (126 MHz, $CDCl_3$) δ 158.32, 147.79, 135.60, 133.97, 127.57, 127.29, 122.67, 120.73, 117.59, 113.98, 111.45, 68.26, 33.28, 30.09.

HRMS (ESI^+) calculated for $[C_{14}H_{16}NO_2]^+$ ($[M+H]^+$). Requires *m/z* 230.1176; found *m/z* 230.1175.

IR (ATR, powder): 3068, 2940, 1646, 1592 cm^{-1}.

M.P. 83.0–86.7 °C.

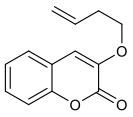

3-(But-3-en-1-yloxy)-2*H*-chromen-2-one (**2.28l**): Prepared according to General Procedure 2.F using 3-hydroxycoumarin (649 mg, 4.00 mmol, 1.0 equiv.), DBU (960 µL, 6.4 mmol, 1.6 equiv.), and 4-bromo-1-butene (510 µL, 5.0 mmol, 1.3 equiv.). Following workup, the crude residue was purified by flash column chromatography (20:80 EtOAc:hexanes) to afford a white powder (635 mg, 2.94 mmol, 73% yield).

^{1}H NMR (500 MHz, $CDCl_3$) δ 7.41 – 7.35 (m, 2H), 7.30 (app. d, *J* = 8.3 Hz, 1H), 7.25 (td, *J* = 7.5, 1.2 Hz, 1H), 6.84 (s, 1H), 5.92 (ddt, *J* = 17.1, 10.3, 6.7 Hz, 1H), 5.21 (dq, *J* = 17.2, 1.6 Hz, 1H), 5.15 (dq, *J* = 10.2, 1.3 Hz, 1H), 4.08 (t, *J* = 6.9 Hz, 2H), 2.66 (qt, *J* = 6.9, 1.3 Hz, 2H).

^{13}C NMR (126 MHz, $CDCl_3$) δ 157.64, 149.69, 143.98, 133.53, 128.57, 126.50, 124.79, 119.83, 117.93, 116.41, 113.70, 68.75, 33.14.

HRMS (ESI^+) calculated for $[C_{13}H_{13}O_3]^+$ ($[M+H]^+$). Requires *m/z* 217.0859; found *m/z* 217.0860.

IR (ATR, thin film): 3077, 3001, 2922, 1724, 1626, 1301, 1147, 1114, 748 cm^{-1}.

M.P. 61.7–63.6 °C.

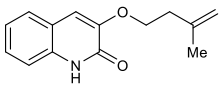

3-((3-Methylbut-3-en-1-yl)oxy)quinolin-2(1*H*)-one (**2.28m**): Prepared according to General Procedure 2.G using **2.56a** (243 mg, 1.51 mmol, 1.0 equiv.), tosylate **2.58** (400 µL, 1.9 mmol, 1.25 equiv.), and DBU (350 µL, 2.3 mmol, 1.6 equiv.). Following workup, the crude residue was purified by flash column chromatography (6:94 MeOH:CH_2Cl_2) to afford a white powder (209 mg, 0.912 mmol, 60% yield.

^{1}H NMR (500 MHz, $CDCl_3$) δ 10.80 (s, 1H), 7.48 (dd, *J* = 7.9, 1.4 Hz, 1H), 7.37 (ddd, *J* = 8.3, 7.1, 1.3 Hz, 1H), 7.30 (d, *J* = 8.3 Hz, 1H), 7.21 (ddd, *J* = 8.1, 7.2, 1.2 Hz, 1H), 7.01 (s, 1H), 4.89 (t, *J* = 1.6 Hz, 1H), 4.85 (s, 1H), 4.20 (t, *J* = 7.4 Hz, 2H), 2.68 (t, *J* = 7.3 Hz, 2H), 1.86 (s, 3H).

^{13}C NMR (126 MHz, $CDCl_3$) δ 159.23, 148.15, 141.80, 133.49, 127.60, 126.47, 123.08, 120.46, 115.47, 113.04, 112.54, 67.84, 36.77, 23.17.

HRMS (ESI^-) calculated for $[C_{14}H_{14}NO_2]^-$ ($[M–H]^-$) Requires *m/z* 228.1030; found *m/z* 228.1030.

IR (ATR, powder): 2858, 1660, 1611, 1575 cm^{-1}.

M.P. 145.8–147.9 °C.

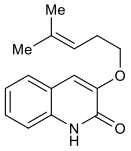

3-((4-Methylpent-3-en-1-yl)oxy)quinolin-2(1*H*)-one (**2.28n**): Prepared according to General Procedure 2.F using **2.56a** (506 mg, 3.14 mmol, 1.0 equiv.), DBU (740 µL,

5.0 mmol, 1.6 equiv.), and 5-bromo-2-methyl-2-pentene (645 mg, 3.96 mmol, 1.3 equiv.). Following workup, the crude residue was purified by flash column chromatography (3:97 MeOH:CH_2Cl_2) to afford a tan powder (486 mg, 2.00 mmol, 64% yield).

^{1}H NMR (500 MHz, $CDCl_3$) δ 12.36 (s, 1H), 7.49 (d, *J* = 8.3 Hz, 1H), 7.46 (d, *J* = 8.0 Hz, 1H), 7.36 (td, *J* = 7.7, 1.4 Hz, 1H), 7.19 (td, *J* = 7.6, 1.1 Hz, 1H), 7.02 (s, 1H), 5.25 (app. tt, *J* = 7.3, 1.2 Hz, 1H), 4.05 (t, *J* = 7.6 Hz, 2H), 2.67 (q, *J* = 7.5 Hz, 2H), 1.75 (s, 3H), 1.70 (s, 3H).

^{13}C NMR (126 MHz, $CDCl_3$) δ 159.99, 148.04, 135.24, 133.62, 127.44, 126.22, 122.99, 120.51, 118.85, 116.13, 113.01, 68.65, 27.89, 25.90, 18.03.

HRMS (ESI$^-$) calculated for $[C_{15}H_{16}NO_2]^-$ ($[M–H]^-$) Requires *m/z* 242.1187; found *m/z* 242.1190.

IR (ATR, powder): 2861, 1657, 1610, 1575 cm^{-1}.

M.P. 146.8–148.7 °C.

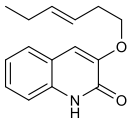

(*E*)-3-(Hex-3-en-1-yloxy)quinolin-2(1*H*)-one ((*E*)-**2.28o**): Prepared according to General Procedure 2.G using **2.56a** (248 mg, 1.54 mmol, 1.0 equiv.), tosylate **2.59** (404 µL, 1.87 mmol, 1.25 equiv.), and DBU (350 µL, 2.3 mmol, 1.6 equiv.). Following workup, the crude residue was purified by flash column chromatography (6:94 MeOH:CH_2Cl_2) to afford a light yellow powder (220 mg, 0.885 mmol, 59% yield).

^{1}H NMR (500 MHz, $CDCl_3$) δ 11.32 (s, 1H), 7.47 (d, *J* = 7.8 Hz, 1H), 7.37 (app. d, *J* = 4.0 Hz, 2H), 7.23 – 7.17 (m, 1H), 7.01 (s, 1H), 5.67 (dt, *J* = 15.0, 6.4 Hz, 1H), 5.53 (dt, *J* = 15.4, 6.9 Hz, 1H), 4.09 (t, *J* = 7.3 Hz, 2H), 2.66 (q, *J* = 6.9 Hz, 2H), 2.06 (p, *J* = 7.2 Hz, 2H), 1.00 (t, *J* = 7.5 Hz, 3H).

^{13}C NMR (126 MHz, $CDCl_3$) δ 159.51, 148.15, 135.62, 133.51, 127.52, 126.37, 123.83, 123.05, 120.51, 115.69, 113.02, 69.03, 32.13, 25.83, 13.86.

HRMS (ESI$^-$) calculated for $[C_{15}H_{16}NO_2]^-$ ($[M–H]^-$) Requires *m/z* 242.1187; found *m/z* 242.1189.

IR (ATR, powder): 2959, 2857, 1662, 1611, 1575 cm^{-1}.

M.P. 136.8–137.5 °C.

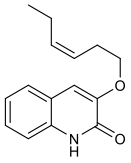

(*Z*)-3-(hex-3-en-1-yloxy)quinolin-2(1*H*)-one ((*Z*)-**2.28o**): Prepared according to General Procedure 2.G using **2.56a** (329 mg, 2.04 mmol, 1.0 equiv.), tosylate **2.60** (538 µL, 2.50 mmol, 1.25 equiv.), and DBU (466 µL, 3.12 mmol, 1.6 equiv.). Following workup, the crude residue was purified by flash column chromatography (6:94 MeOH:CH_2Cl_2) to afford a light yellow powder (301 mg, 1.24 mmol, 61% yield).

^{1}H NMR (500 MHz, $CDCl_3$) δ 12.02 (s, 1H), 7.47 (dd, *J* = 7.9, 1.3 Hz, 1H), 7.44 (d, *J* = 8.6 Hz, 1H), 7.37 (ddd, *J* = 8.0, 7.0, 1.2 Hz, 1H), 7.20 (td, *J* = 7.6, 1.1 Hz, 1H), 7.01 (s, 1H), 5.59 (dtt, *J* = 10.8, 7.2, 1.5 Hz, 1H), 5.47 (dtt, *J* = 10.8, 7.2, 1.5 Hz, 1H), 4.08 (t, *J* = 7.4 Hz, 2H), 2.73 (qd, *J* = 7.3, 1.6 Hz, 2H), 2.14 (pd, *J* = 7.5, 1.5 Hz, 2H), 1.02 (t, *J* = 7.5 Hz, 3H).

^{13}C NMR (126 MHz, $CDCl_3$) δ 159.81, 148.05, 135.15, 133.62, 127.52, 126.30, 123.32, 123.03, 120.48, 115.97, 113.04, 68.57, 27.05, 20.88, 14.43.

HRMS (ESI^-) calculated for $[C_{15}H_{16}NO_2]^-$ ($[M–H]^-$) Requires *m/z* 242.1187; found *m/z* 242.1189.

IR (ATR, powder): 2959, 2857, 1662, 1611, 1575 cm^{-1}.

M.P. 121.5–122.9 °C.

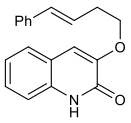

(**2.28p**): Prepared according to General Procedure 2.F using **2.56a** (0.3260g, 2.00 mmol, 1.0 equiv.), DBU (0.466 mL, 3.12 mmol, 1.56 equiv.), and **2.61** (.466 mL, 2.50 mmol, 1.25 equiv.). Following workup, the crude residue was purified by flash column chromatography (2:3 hexanes:EtOAc, dry load) to afford a white powder (186.1 mg, 0.64 mmol, 32% yield).

^{1}H NMR (500 MHz, $CDCl_3$) δ 10.61 (s, 1H), 7.48 (d, *J* = 7.9 Hz, 0H), 7.41 – 7.34 (m, 3H), 7.30 (dt, *J* = 8.2, 6.2 Hz, 4H), 7.25 – 7.18 (m, 2H), 7.02 (s, 1H), 6.58 (d, *J* = 16.1 Hz, 1H), 6.34 (dt, *J* = 15.8, 7.0 Hz, 1H), 4.20 (t, *J* = 7.1 Hz, 2H), 2.88 (qd, *J* = 7.1, 1.4 Hz, 2H).

^{13}C NMR (126 MHz, $CDCl_3$) δ 158.95, 148.00, 137.18, 133.33, 132.73, 128.52, 127.50, 127.32, 126.36, 126.13, 125.20, 122.94, 120.28, 115.21, 113.03, 68.52, 32.46.

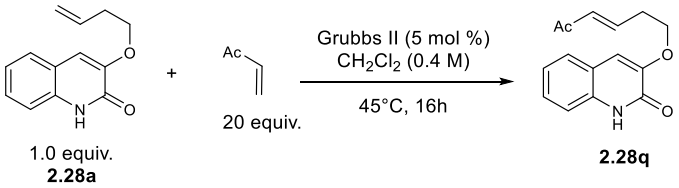

(**2.28q**): A 10 mL round-bottomed flask was charged with **2.28a** (.4305g, 2.00 mmol, 1.0 equiv.), Grubbs Generation II catalyst (8.5 mg, 0.10 mmol, 0.05 equiv.), freshly distilled methyl vinyl ketone (40 mmol, 3.25 mL, 20 equiv.) and CH_2Cl_2 (0.40 M relative to **2.28a**). The resulting brown slurry was heated to 45ºC, becoming homogenous, under N_2 for 16 h. Following this the brown mixture was concentrated *in vacuo*. The crude product was purified by flash column chromatography on silica gel (25:75 Hexanes: Ethyl Acetate) to afford **2.28q** as a metallic colored solid (158.1 mg, 0.61 mmol, 30% yield).

^{1}H NMR (500 MHz, $CDCl_3$) δ 12.07 (s, 1H), 7.49 (d, *J* = 7.6 Hz, 1H), 7.44 (d, *J* = 8.1 Hz, 1H), 7.39 (td, *J* = 7.7, 1.3 Hz, 1H), 7.21 (td, *J* = 7.6, 1.2 Hz, 1H), 7.05 (s, 1H), 6.94 (dt, *J* = 16.0, 6.8 Hz, 1H), 6.25 (dt, *J* = 16.1, 1.6 Hz, 1H), 4.23 (t, *J* = 6.6 Hz, 2H), 2.89 (qd, *J* = 6.7, 1.6 Hz, 2H), 2.29 (s, 3H).

^{13}C NMR (126 MHz, $CDCl_3$) δ 198.34, 159.48, 147.53, 142.86, 133.65, 133.26, 127.73, 126.28, 123.01, 120.05, 115.78, 113.80, 67.05, 31.77, 26.97.

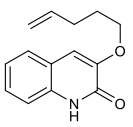

(**2.28r**): Prepared according to General Procedure 2.F using **2.28a** (321.3 mg, 2.00 mmol, 1.0 equiv.), DBU (0.466 mL, 3.12 mmol, 1.56 equiv.), and 5-bromo-1-

pentene (466 µL, 2.50 mmol, 1.25 equiv.). Following workup, the crude residue was purified by flash column chromatography (15:1 CH_2Cl_2:MeOH) to afford a colorless powder (290.3 mg, 1.26 mmol, 63% yield).

^{1}H NMR (500 MHz, $CDCl_3$) δ 10.73 (s, 1H), 7.48 (d, *J* = 7.8 Hz, 1H), 7.37 (leaning t, *J* = 7.8 Hz, 1H), 7.30 (d, *J* = 8.02 Hz, 1H), 7.21 (t, *J* = 7.6 1H), 6.98 (s, 1H), 5.88 (ddt, *J* = 16.9, 10.0, 6.6 Hz, 1H), 5.10 (ddd, *J* = 17.1, 1.8 Hz, 1.81 Hz, 1H), 5.03 (ddd, *J* = 10.2, 2.1, 1.0 Hz, 1H), 4.09 (t, *J* = 6.7 Hz, 2H), 2.31 (q, *J* = 7.4 Hz, 1H), 2.06 (p, *J* = 7.0 Hz, 2H).

^{13}C NMR (126 MHz, $CDCl_3$) δ 159.05, 148.15, 137.53, 133.25, 127.35, 126.28, 122.90, 120.36, 115.44, 115.25, 112.60, 68.25, 30.01, 27.74.

2.5.5 Reaction Optimization

Table 2.4. Solvent screen with initial catalyst **2.30a**. Yields determined by ^{1}H NMR analysis of crude reactions using TMSPh as an external standard. Enantiomeric excesses determined by chiral SFC of isolated material.

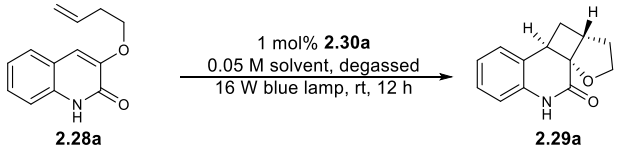

2.28a **2.29a**

Entry	Solvent	Yield	ee	RSM
1	Hexanes	96%	5%	16%
2	Et_2O	95%	–1%	1%
3	THF	100%	–3%	0
4	$PhCH_3$	96%	7%	0
5	$PhCF_3$	92%	9%	2%
6	CH_2Cl_2	97%	7%	0

Entry	Solvent	Yield	ee	RSM
7	$CHCl_3$	98%	8%	0
8	1,2-DCE	97%	10%	0
9	CCl_4	93%	6%	2%
10	MeCN	93%	0%	4%
11	Acetone	88%	–1%	0
12	EtOH	quant.	–1%	0

Table 2.5. Effect of temperature in several different solvents. Yields determined by ^{1}H NMR analysis of crude reactions using TMSPh as an external standard. Enantiomeric excesses determined by chiral SFC of isolated material.

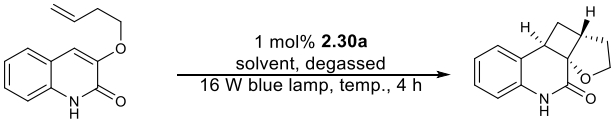

2.28a **2.29a**

Entry	Solvent ([2.28])	Time	Temp.	Yield	ee	RSM
1	CH_2Cl_2 (0.01 M)	12 h	rt	95%	8%	0
2	CH_2Cl_2 (0.05 M)	12 h	0 °C	98%	9%	0
3	1,2-DCE (0.01 M)	12 h	–30 °C	99%	17%	0
4	CH_2Cl_2 (0.01 M)	4 h	–70 °C	95%	40%	0
5	Hexanes (0.01 M)	4 h	–70 °C	0	--	96%
6	Et_2O (0.01 M)	4 h	–70 °C	2%	nd	94%
7	MTBE (0.01 M)	4 h	–70 °C	4%	nd	77%

Table 2.6. Optimization with final catalyst **2.32**. Yields determined by ^{1}H NMR analysis of crude reactions using TMSPh as an external standard. Enantiomeric excesses determined by chiral SFC of isolated material. [a] Reaction degassed.

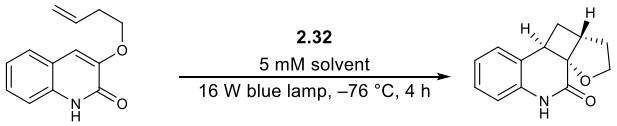

2.28a **2.29a**

Entry	Solvent	6b	Yield	ee	RSM
1	CH_2Cl_2	1 mol%	23%	87%	77%
2	CH_2Cl_2	2 mol%	70%	86%	17%
3	CH_2Cl_2	3 mol%	76%	87%	2%
4	3:1 CH_2Cl_2:pentane	1 mol%	78%	87%	16%
5	2:1 CH_2Cl_2:pentane	1 mol%	44%	92%	48%
6	1:1 CH_2Cl_2:pentane	1 mol%	49%	93%	44%
7	1:2 CH_2Cl_2:pentane	1 mol%	36%	92%	58%
8[a]	1:1 CH_2Cl_2:pentane	1 mol%	50%	90%	43%

Table 2.7. Control experiments and scaled-up reaction. Unless otherwise noted, yields were determined by ^{1}H NMR analysis of crude reactions using TMSPh as an external standard and enantiomeric excesses were determined by chiral SFC or HPLC of isolated material. [a] Isolated yield.

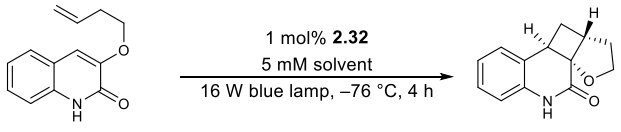

2.28a **2.29a**

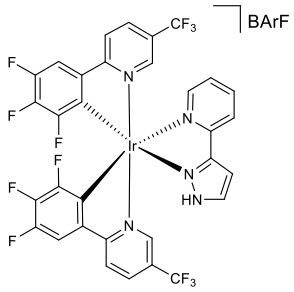

2.32

Entry	Deviation from Standard	Yield	ee	RSM
1	none	49%	93%	44%
2	no photocatalyst	0	--	102%
3	no light	0	--	101%
4	0.1 mol% **2.32**, 24 h	38%	88%	60%
5[a]	0.25 mmol scale, 24 h	100%	91%	0

2.5.6 Photosensitized [2+2] Cycloadditions

2.5.6.a Racemic [2+2] Cycloadditions

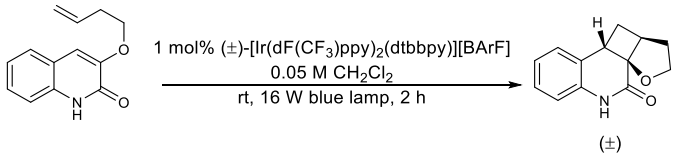

General Procedure 2.H: A 2 dram vial was charged with substrate **2.28** (46 µmol, 1.0 equiv.), (±)-[Ir(dF(CF_3)ppy)$_2$(dtbbpy)][PF_6] (0.46 µmol, 0.01 equiv.), and dry CH_2Cl_2 (920 µL, 0.05 M with respect to substrate). The solution was irradiated by a 16 W blue LED lamp for two h at room temperature, then concentrated *in vacuo*. Purification by silica gel chromatography provided racemic cyclobutane, which was used to develop and calibrate chiral HPLC methods. All characterization and spectroscopic data are reported for the enantioenriched species described in Section 2.5.6b.

2.5.6.b Enantioselective [2+2] Cycloadditions

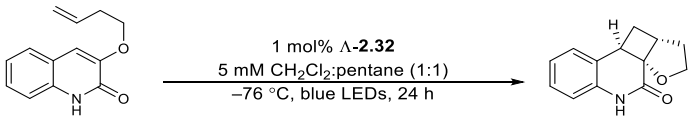

General Procedure 2.I: A 100 mL pear flask was charged with substrate **2.28** (0.25 mmol, 1.0 equiv.), photocatalyst **2.32** (2.5 µmol, 0.01 equiv.), dry CH_2Cl_2 (25 mL) and pentane (25 mL). The mixture was sonicated if necessary to ensure full dissolution of the substrate. The solution was then cooled to –76 °C in an acetone bath and maintained at this temperature using an immersion cryotrol. Irradiation was carried out with two 16 W blue LED lamps for a duration of 24 h. Following this period, the reaction was warmed to room temperature and the solvent was removed *in vacuo*. Purification of the crude mixture by flash column chromatography provided the cyclobutane product.

Note: As with the cycloaddition substrates **2.28**, we observed small changes in arene chemical shifts depending on sample concentration, which we attribute to quinolone dimerization by hydrogen bonding. In some cases, the N–H and even some aromatic C–H peaks have shoulders that are needed for the full integration value. Again, we ascribe this to chemically distinct free and dimerized quinolone. Notably, these features disappear in other solvents such as $(CD_3)_2CO$, and only a single species is observed in the ^1H NMR spectrum (Figure 2.9).

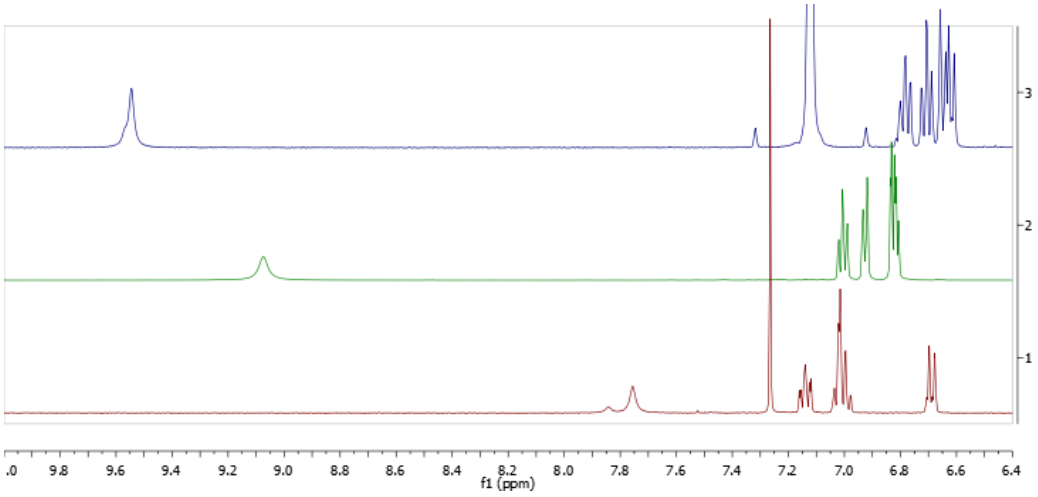

Figure 2.9. Representative ^1H NMR data for parent cycloadduct **2.29a** in different solvents. From top to bottom: C_6D_6, $(CD_3)_2CO$, $CDCl_3$.

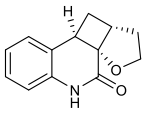

(1a*R*,4a*S*,10b*R*)-1,1a,2,3,6,10b-Hexahydro-5*H*-furo[2',3':1,4]cyclobuta[1,2-*c*]quinolin-5-one (**2.29a**): Prepared according to General Procedure 2.I using **2.28a** (53.6 mg, 0.249 mmol, 1.0 equiv.) and Λ-**2.32** (4.4 mg, 2.5 μmol, 0.010 equiv.). The crude residue was purified by flash column chromatography on silica gel (EtOAc) to afford the cycloadduct as a white powder (53.6 mg, 0.249 mmol, 100% yield). 91% ee.

^1H NMR (500 MHz, $CDCl_3$) δ 7.77 (s, 1H), 7.14 (ddd, *J* = 8.3, 6.6, 2.7 Hz, 1H), 7.03 – 6.96 (m, 2H), 6.70 (d, *J* = 7.9 Hz, 1H), 4.53 (ddd, *J* = 8.9, 7.8, 2.8 Hz, 1H), 4.32 (td, *J* = 9.3, 6.0 Hz, 1H),

3.65 (dd, *J* = 9.9, 5.9 Hz, 1H), 3.36 (app. qt *J* = 7.5, 1.3 Hz, 1H), 2.26 (ddd, *J* = 12.5, 9.9, 5.4 Hz, 1H), 2.21 – 2.09 (m, 2H), 1.84 (dddd, *J* = 12.6, 6.0, 2.8, 1.8 Hz, 1H).

^{13}C NMR (126 MHz, $CDCl_3$) δ 169.11, 135.15, 128.24, 127.70, 125.58, 123.84, 115.87, 81.97, 70.87, 45.45, 40.39, 32.88, 31.47.

HRMS (ESI^+) calculated for $[C_{13}H_{14}NO_2]^+$ ($[M+H]^+$). Requires *m/z* 216.1019; found *m/z* 216.1017.

IR (ATR, thin film): 3214, 3062, 2971, 2927, 2862, 1674, 1593, 1492, 1389, 1125, 755 cm^{-1}.

M.P. 169.8–171.7 °C.

$[\alpha]_D^{22}$: +115.7° (*c*1.08, CH_2Cl_2).

$[\alpha]_D^{22}$: +109.7° (*c*1.03, MeOH).

HPLC: Daicel CHIRALCEL® OD-H, 70% *i*-PrOH, 30% hexanes, 1 mL/min, 258.1 nm; t_1 = 8.0 min, t_2 = 12.7 min; Area% = 95.31 : 4.69 (91% ee).

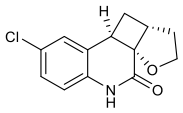

(1a*R*,4a*S*,10b*R*)-9-Chloro-1,1a,2,3,6,10b-hexahydro-5*H*-furo[2',3':1,4]cyclobuta [1,2-*c*]quinolin-5-one (**2.29b**): Prepared according to General Procedure 2.I using **2.28b** (62.4 mg, 0.250 mmol, 1.0 equiv.) and Λ-**2.32** (4.4 mg, 2.5 µmol, 0.01 equiv.). The crude residue was purified by flash column chromatography on silica gel (75:25 EtOAc:hexanes) to afford the cycloadduct as a white powder (58.3 mg, 0.233 mmol, 93% yield). 90% ee.

^{1}H NMR (500 MHz, $CDCl_3$) δ 8.47 (s, 1H), 7.11 (dd, *J* = 8.5, 2.3 Hz, 1H), 6.99 (d, *J* = 2.3 Hz, 1H), 6.72 (d, *J* = 8.5 Hz, 1H), 4.53 (ddd, *J* = 8.9, 7.8, 2.9 Hz, 1H), 4.32 (td, *J* = 9.3, 6.0 Hz, 1H), 3.61 (dd, *J* = 10.1, 5.9 Hz, 1H), 3.36 (app. qt, *J* = 7.7, 1.4 Hz, 1H), 2.26 (ddd, *J* = 12.6, 10.1, 5.5 Hz, 1H), 2.22 – 2.10 (m, 2H), 1.85 (dddd, *J* = 12.6, 5.9, 2.8, 1.8 Hz, 1H).

^{13}C NMR (126 MHz, $CDCl_3$) δ 168.98, 133.84, 128.64, 128.10, 127.75, 127.19, 117.17, 81.56, 70.97, 45.54, 40.25, 32.85, 31.32.

HRMS (ESI$^+$) calculated for $[C_{13}H_{13}ClNO_2]^+$ ($[M+H]^+$). Requires *m/z* 250.0629; found *m/z* 250.0632.

IR (ATR, thin film): 3114, 3046, 2926, 2861, 1680, 1489, 1375, 1092, 727 cm^{-1}.

M.P. 224.4–225.5 °C.

$[\boldsymbol{\alpha}]_{\mathbf{D}}^{\mathbf{22}}$: +133.4° (*c*0.88, CH_2Cl_2).

HPLC: Daicel CHIRALCEL® OD-H, 70% *i*-PrOH, 30% hexanes, 1 mL/min, 261.6 nm; t_1 = 5.5 min, t_2 = 8.6 min; Area% = 4.95 : 95.05 (90% ee).

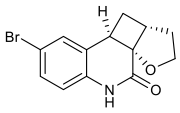

(1a*R*,4a*S*,10b*R*)-9-Bromo-1,1a,2,3,6,10b-hexahydro-5*H*-furo[2',3':1,4]cyclobuta[1,2-*c*]quinolin-5-one (**2.29c**): Prepared according to General Procedure 2.I using **2.28c** (73.3 mg, 0.249 mmol, 1.0 equiv.) and Λ-**2.32** (4.5 mg, 2.6 µmol, 0.01 equiv.). The crude residue was purified by flash column chromatography on silica gel (75:25 EtOAc:hexanes) to afford the cycloadduct as a cream-colored powder (73.8 mg, 0.251 mmol, quant.). 90% ee.

^{1}H NMR (500 MHz, $CDCl_3$) δ 8.87 (s, 1H), 7.24 (dd, *J* = 8.4, 2.2 Hz, 1H), 7.13 (d, *J* = 2.1 Hz, 1H), 6.71 (d, *J* = 8.4 Hz, 1H), 4.53 (ddd, *J* = 8.9, 7.8, 2.8 Hz, 1H), 4.32 (td, *J* = 9.3, 5.9 Hz, 1H), 3.61 (dd, *J* = 10.1, 6.0 Hz, 1H), 3.36 (app. qt, *J* = 7.5, 1.6 Hz, 1H), 2.26 (ddd, *J* = 12.7, 10.1, 5.4 Hz, 1H), 2.22 – 2.10 (m, 2H), 1.85 (dddd, *J* = 12.6, 5.9, 2.7, 1.7 Hz, 1H).

^{13}C NMR (126 MHz, $CDCl_3$) δ 169.22, 134.37, 130.93, 130.62, 127.56, 117.71, 116.02, 81.55, 70.95, 45.58, 40.16, 32.85, 31.35.

HRMS (ESI$^+$) calculated for $[C_{13}H_{13}BrNO_2]^+$ ($[M+H]^+$). Requires *m/z* 294.0124; found *m/z* 294.0125.

IR (ATR, thin film): 3238, 3079, 2933, 1683, 1489 cm^{-1}.

M.P. 223.3–227.5 °C.

$[\alpha]_D^{22}$: +118.4° (*c*1.11, CH_2Cl_2).

$[\alpha]_D^{22}$: +108.7° (*c*1.08, MeOH).

HPLC: Daicel CHIRALCEL® OD-H, 70% *i*-PrOH, 30% hexanes, 1 mL/min, 262.8 nm; t_1 = 5.6 min, t_2 = 9.2 min; Area% = 5.15 : 94.85 (90% ee).

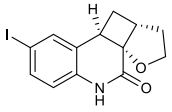

(1a*R*,4a*S*,10b*R*)-9-Iodo-1,1a,2,3,6,10b-hexahydro-5*H*-furo[2',3':1,4]cyclobuta[1,2-*c*]quinolin-5-one (**2.29d**): Prepared according to General Procedure 2.I using **2.28d** (85.3 mg, 0.250 mmol, 1.0 equiv.) and Λ-**2.32** (4.6 mg, 2.6 µmol, 0.01 equiv.). The crude residue was purified by flash column chromatography on silica gel (75:25 EtOAc:hexanes) to afford the cycloadduct as a white powder (84.9 mg, 0.249 mmol, 100% yield). 79% ee.

^{1}H NMR (500 MHz, $CDCl_3$) δ 8.63 (s, 1H), 7.43 (dd, *J* = 8.4, 1.9 Hz, 1H), 7.32 (d, *J* = 2.0 Hz, 1H), 6.57 (d, *J* = 8.3 Hz, 1H), 4.52 (ddd, *J* = 9.0, 7.8, 2.8 Hz, 1H), 4.31 (td, *J* = 9.3, 6.0 Hz, 1H), 3.60 (dd, *J* = 10.1, 5.9 Hz, 1H), 3.35 (app. qt, *J* = 7.2, 1.2 Hz, 1H), 2.25 (ddd, *J* = 12.7, 10.0, 5.5 Hz, 1H), 2.20 – 2.09 (m, 2H), 1.84 (dddd, *J* = 12.5, 5.9, 2.8, 1.7 Hz, 1H).

^{13}C NMR (126 MHz, $CDCl_3$) δ 169.10, 136.87, 136.50, 135.05, 127.95, 117.95, 86.29, 81.59, 70.96, 45.59, 40.01, 32.84, 31.36.

HRMS (ESI$^-$) calculated for $[C_{13}H_{11}INO_2]^-$ ($[M–H]^-$). Requires *m/z* 339.9840; found *m/z* 339.9842.

IR (ATR, thin film): 3225, 3069, 2940, 2871, 1680, 1487 cm^{-1}.

M.P. 247.2–248.8 °C.

$[\alpha]_D^{22}$: +120.0° (*c*0.75, CH_2Cl_2).

HPLC:[106] Daicel CHIRALCEL® OD-H, 70% *i*-PrOH, 30% hexanes, 1 mL/min, 266.4 nm; t_1 = 5.6 min, t_2 = 9.9 min; Area% = 10.71 : 89.29 (79% ee).

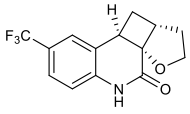

(1a*R*,4a*S*,10b*R*)-9-(Trifluoromethyl)-1,1a,2,3,6,10b-hexahydro-5*H*-furo[2',3':1,4]cyclobuta[1,2-*c*]quinolin-5-one (**2.29e**): Prepared according to General Procedure 2.I using **2.28e** (70.3 mg, 0.248 mmol, 1.0 equiv.) and Λ-**2.32** (4.4 mg, 2.5 µmol, 0.01 equiv.). The crude residue was purified by flash column chromatography on silica gel (75:25 EtOAc:hexanes) to afford the cycloadduct as a white powder (68.5 mg, 0.242 mmol, 97% yield). 84% ee.

^{1}H NMR (500 MHz, $CDCl_3$) δ 8.85 (s, 1H), 7.40 (d, *J* = 8.3 Hz, 1H), 7.27 (s, 1H), 6.89 (d, *J* = 8.3 Hz, 1H), 4.54 (ddd, *J* = 9.1, 7.8, 2.9 Hz, 1H), 4.34 (td, *J* = 9.3, 6.0 Hz, 1H), 3.69 (dd, *J* = 10.2, 5.9 Hz, 1H), 3.39 (app. qt, *J* = 7.7, 1.3 Hz, 1H), 2.31 (ddd, *J* = 12.7, 10.0, 5.4 Hz, 1H), 2.25 – 2.11 (m, 2H), 1.88 (dddd, *J* = 12.5, 5.8, 2.7, 1.7 Hz, 1H).

^{13}C NMR (126 MHz, $CDCl_3$) δ 169.45, 138.15 (d, *J* = 1.4 Hz), 126.00 (q, *J* = 32.8 Hz), 125.95, 125.50 (q, *J* = 3.7 Hz), 124.99 (q, *J* = 3.7 Hz), 124.09 (q, *J* = 271.6 Hz), 116.22, 81.61, 71.07, 45.77, 40.19, 32.88, 31.35.

^{19}F NMR (377 MHz, $CDCl_3$) δ –62.06.

HRMS (ESI$^-$) calculated for $[C_{14}H_{11}F_3NO_2]^-$ ($[M–H]^-$). Requires *m/z* 282.0747; found *m/z* 282.0749.

IR (ATR, thin film): 3230, 3143, 3086, 2975, 2942, 2863, 1688, 1621, 1606, 1516, 1383, 1248, 1190, 1165, 1114, 1089, 1075, 904, 832, 734 cm^{-1}.

M.P. 216.0–216.8 °C.

$[\alpha]_D^{22}$: +97.7° (*c*0.71, CH_2Cl_2).

HPLC: Daicel CHIRALCEL® OD-H, 70% *i*-PrOH, 30% hexanes, 1 mL/min, 260.4 nm; t_1 = 4.3 min, t_2 = 7.9 min; Area% =7.97 : 92.03 (84% ee).

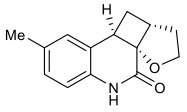

(1a*R*,4a*S*,10b*R*)-9-Methyl-1,1a,2,3,6,10b-hexahydro-5*H*-furo[2',3':1,4]cyclobuta [1,2-*c*]quinolin-5-one (**2.29f**): Prepared according to General Procedure 2.I using **2.28f** (57.0 mg, 0.249 mmol, 1.0 equiv.) and Λ-**2.32** (4.4 mg, 2.5 µmol, 0.01 equiv.). The crude residue was purified by flash column chromatography on silica gel 75:25 EtOAc:hexanes) to afford the cycloadduct as a white solid (56.2 mg, 0.245 mmol, 99% yield). 82% ee.

^{1}H NMR (500 MHz, $CDCl_3$) δ 7.91 (s, 1H), 6.94 (dd, *J* = 8.0, 1.8 Hz, 1H), 6.81 (s, 1H), 6.61 (d, *J* = 8.0 Hz, 1H), 4.52 (ddd, *J* = 8.9, 7.8, 2.7 Hz, 1H), 4.31 (td, *J* = 9.3, 6.0 Hz, 1H), 3.60 (dd, *J* = 10.1, 5.8 Hz, 1H), 3.34 (app. qt, *J* = 7.7, 1.6 Hz, 1H), 2.27 (s, 3H), 2.24 (ddd, *J* = 12.6, 10.1, 5.6 Hz, 1H), 2.21 – 2.07 (m, 2H), 1.83 (dddd, *J* = 12.5, 6.0, 2.8, 1.7 Hz, 1H).

^{13}C NMR (126 MHz, $CDCl_3$) δ 168.81, 133.38, 132.66, 128.73, 128.26, 125.42, 115.59, 82.02, 70.85, 45.33, 40.39, 32.86, 31.51, 20.87.

HRMS (ESI^+) calculated for $[C_{14}H_{16}NO_2]^+$ ($[M+H]^+$). Requires *m/z* 230.1176; found *m/z* 230.1177.

IR (ATR, thin film): 3208, 3064, 2930, 2866, 1674, 1508, 1386, 1092, 730 cm^{-1}.

M.P. 197.9–200.1 °C.

$[\alpha]_D^{22}$: +119.0° (*c*0.96, CH_2Cl_2).

HPLC:[107] Daicel CHIRALCEL® OD-H, 70% *i*-PrOH, 30% hexanes, 1 mL/min, 261.6 nm; t_1 = 6.5 min, t_2 = 7.7 min; Area% = 8.92 : 91.08 (82% ee).

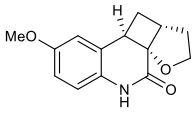

(1a*R*,4a*S*,10b*R*)-9-Methoxy-1,1a,2,3,6,10b-hexahydro-5*H*-furo[2',3':1,4]cyclobuta [1,2-*c*]quinolin-5-one (**2.29g**): Prepared according to General Procedure 2.I using **2.28g** (61.4 mg, 0.250 mmol, 1.0 equiv.) and Λ-**2.32** (4.5 mg, 2.6 µmol, 0.01 equiv.). The crude residue was purified by flash column chromatography on silica gel (EtOAc) to afford the cycloadduct as a light beige powder (60.7 mg, 0.247 mmol, 99% yield). 79% ee.

^{1}H NMR (500 MHz, $CDCl_3$) δ 8.00 (s, 1H), 6.70 (dd, *J* = 8.7, 2.7 Hz, 1H), 6.66 (d, *J* = 8.6 Hz, 1H), 6.55 (d, *J* = 2.6 Hz, 1H), 4.52 (ddd, *J* = 8.9, 7.8, 2.8 Hz, 1H), 4.31 (td, *J* = 9.3, 5.9 Hz, 1H), 3.76 (s, 3H), 3.62 (dd, *J* = 10.1, 5.9 Hz, 1H), 3.34 (app. qt, *J* = 7.6, 1.5 Hz, 1H), 2.25 (ddd, *J* = 12.5, 10.0, 5.4 Hz, 1H), 2.21 – 2.09 (m, 2H), 1.83 (dddd, *J* = 12.6, 6.0, 2.8, 1.8 Hz, 1H).

^{13}C NMR (126 MHz, $CDCl_3$) δ 168.53, 156.12, 128.74, 126.72, 116.65, 113.37, 113.16, 81.76, 70.84, 55.71, 45.17, 40.69, 32.86, 31.40.

HRMS (ESI^+) calculated for $[C_{14}H_{16}NO_3]^+$ ($[M+H]^+$). Requires *m/z* 246.1125; found *m/z* 246.1126.

IR (ATR, thin film): 3211, 3066, 2940, 1674, 1506, 1245 cm^{-1}.

M.P. 159.0–160.3 °C.

$[\boldsymbol{\alpha}]_{\mathbf{D}}^{\mathbf{22}}$: +114.0° (*c*0.83, CH_2Cl_2).

HPLC: Daicel CHIRALCEL® OD-H, 70% *i*-PrOH, 30% hexanes, 1 mL/min, 265.2 nm; t_1 = 6.2 min, t_2 = 8.5 min; Area% = 10.59 : 89.41 (79% ee).

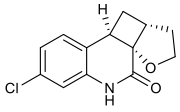

(1a*R*,4a*S*,10b*R*)-8-Chloro-1,1a,2,3,6,10b-hexahydro-5*H*-furo[2',3':1,4]cyclobuta [1,2-*c*]quinolin-5-one (**2.29h**): Prepared according to General Procedure 2.I using **2.28h** (62.3 mg, 0.250 mmol, 1.0 equiv.) and Λ-**2.32** (4.4 mg, 2.5 µmol, 0.01 equiv.). The crude residue was purified by flash column chromatography on silica gel

(75:25 EtOAc:hexanes) to afford the cycloadduct as a white powder (61.9 mg, 0.248 mmol, 99% yield). 77% ee.

^{1}H NMR (500 MHz, $CDCl_3$) δ 8.48 (s, 1H), 6.96 (dd, *J* = 8.2, 1.9 Hz, 1H), 6.93 (d, *J* = 7.9 Hz, 1H), 6.79 (d, *J* = 1.9 Hz, 1H), 4.53 (ddd, *J* = 8.9, 7.8, 2.9 Hz, 1H), 4.32 (td, *J* = 9.3, 6.0 Hz, 1H), 3.61 (dd, *J* = 9.9, 5.9 Hz, 1H), 3.36 (app. qt, *J* = 7.7, 1.3 Hz, 1H), 2.26 (ddd, *J* = 12.5, 10.0, 5.4 Hz, 1H), 2.22 – 2.15 (m, 1H), 2.10 (ddd, *J* = 12.6, 9.2, 5.9 Hz, 1H), 1.85 (dddd, *J* = 12.6, 6.1, 2.9, 1.8 Hz, 1H).

^{13}C NMR (126 MHz, $CDCl_3$) δ 169.23, 136.34, 133.16, 129.42, 124.05, 123.84, 115.82, 81.72, 71.01, 45.55, 39.94, 32.86, 31.44.

HRMS (ESI^+) calculated for $[C_{13}H_{13}ClNO_2]^+$ ($[M+H]^+$). Requires *m/z* 250.0629; found *m/z* 250.0631.

IR (ATR, thin film): 3231, 3060, 2967, 2868, 1685, 1587, 1486, 1395, 1088 cm^{-1}.

M.P. 206.2–207.7 °C.

$[\alpha]_D^{22}$: +102.1° (*c*1.06, CH_2Cl_2).

HPLC: Daicel CHIRALCEL® OD-H, 70% *i*-PrOH, 30% hexanes, 1 mL/min, 261.6 nm; t_1 = 5.3 min, t_2 = 8.3 min; Area% = 11.28 : 88.72 (77% ee).

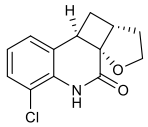

(1a*R*,4a*S*,10b*R*)-7-Chloro-1,1a,2,3,6,10b-hexahydro-5*H*-furo[2',3':1,4]cyclobuta[1,2-*c*] quinolin-5-one (**2.29i**): Prepared according to General Procedure 2.I using **2.28i** (62.4 mg, 0.250 mmol, 1.0 equiv.) and Λ-**2.32** (4.3 mg, 2.5 µmol, 0.01 equiv.). The crude residue was purified by flash column chromatography on silica gel (gradient, 40:60 to 50:50 EtOAc:hexanes) to afford the cycloadduct as a pale yellow powder (60.9 mg, 0.244 mmol, 98% yield). 20% ee.

^{1}H NMR (500 MHz, $CDCl_3$) δ 7.93 (s, 1H), 7.25 – 7.19 (m, 1H), 6.97 – 6.90 (m, 2H), 4.53 (ddd, *J* = 9.0, 7.8, 2.8 Hz, 1H), 4.32 (td, *J* = 9.3, 6.0 Hz, 1H), 3.67 (ddd, *J* = 10.1, 5.8, 1.4 Hz, 1H), 3.38 (app. qt, *J* = 7.7, 1.4 Hz, 1H), 2.28 (ddd, *J* = 12.7, 10.1, 5.5 Hz, 1H), 2.23 – 2.08 (m, 2H), 1.85 (dddd, *J* = 12.7, 6.0, 2.8, 1.8 Hz, 1H).

^{13}C NMR (126 MHz, $CDCl_3$) δ 168.25, 131.98, 127.87, 127.29, 126.78, 123.96, 119.59, 81.92, 71.01, 45.59, 40.61, 32.82, 31.44.

HRMS (ESI^+) calculated for $[C_{13}H_{13}ClNO_2]^+$ ($[M+H]^+$). Requires *m/z* 250.0629; found *m/z* 250.0631.

IR (ATR, thin film): 3388, 3237, 3085, 2941, 2868, 1692, 1481, 1372, 1093 cm^{-1}.

M.P. 109.7–112.1 °C.

$[\alpha]_D^{22}$: +30.1° (*c*0.81, CH_2Cl_2).

HPLC: Daicel CHIRALCEL® OD-H, 70% *i*-PrOH, 30% hexanes, 1 mL/min, 258.1 nm; t_1 = 5.6 min, t_2 = 7.1 min; Area% = 39.92 : 60.08 (20% ee).

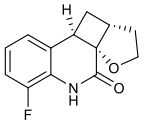

(1a*R*,4a*S*,10b*R*)-7-Fluoro-1,1a,2,3,6,10b-hexahydro-5*H*-furo[2',3':1,4]cyclobuta[1,2-*c*]quinolin-5-one (**2.29j**): Prepared according to General Procedure 2.I using **2.28j** (57.9 mg, 0.248 mmol, 1.0 equiv.) and Λ**-2.32** (4.3 mg, 2.5 µmol, 0.01 equiv.). The crude residue was purified by flash column chromatography on silica gel (gradient, 50:50 to 67:33 EtOAc:hexanes) to afford the cycloadduct as a cream-colored powder (52.2 mg, 0.224 mmol, 90% yield). 87% ee.

^{1}H NMR (500 MHz, $CDCl_3$) δ 7.63 (s, 1H), 6.98 – 6.90 (m, 2H), 6.83 – 6.77 (m, 1H), 4.53 (ddd, *J* = 8.9, 7.8, 2.8 Hz, 1H), 4.32 (td, *J* = 9.3, 6.0 Hz, 1H), 3.68 (dd, *J* = 10.0, 5.8 Hz, 1H), 3.38 (app. qt, *J* = 7.7, 1.4 Hz, 1H), 2.28 (ddd, *J* = 12.6, 10.0, 5.6 Hz, 1H), 2.23 – 2.11 (m, 2H), 1.85 (dddd, *J* = 12.6, 6.0, 2.8, 1.7 Hz, 1H).

^{13}C NMR (126 MHz, $CDCl_3$) δ 167.81, 149.50 (d, *J* = 243.6 Hz), 127.60 (d, *J* = 1.3 Hz), 123.98 (d, *J* = 11.7 Hz), 123.55 (d, *J* = 7.6 Hz), 123.43 (d, *J* = 3.5 Hz), 113.63 (d, *J* = 18.3 Hz), 81.85, 71.01, 45.53, 40.53 (d, *J* = 2.3 Hz), 32.80, 31.46.

^{19}F NMR (377 MHz, $CDCl_3$) δ –135.44.

HRMS (ESI^+) calculated for $[C_{13}H_{13}FNO_2]^+$ ($[M+H]^+$). Requires *m/z* 234.0925; found *m/z* 234.0926.

IR (ATR, thin film): 3216, 3093, 2931, 2864, 1686, 1499, 1376, 1246, 1105, 727 cm^{-1}.

M.P. 141.4–143.4 °C.

$[\alpha]_D^{22}$: +144.1° (*c*0.97, CH_2Cl_2).

HPLC: Daicel CHIRALCEL® OD-H, 70% *i*-PrOH, 30% hexanes, 1 mL/min, 253.3 nm; t_1 = 6.9 min, t_2 = 8.4 min; Area% = 6.41 : 93.59 (87% ee).

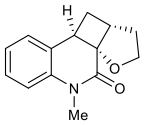

(1a*R*,4a*S*,10b*R*)-6-Methyl-1,1a,2,3,6,10b-hexahydro-5*H*-furo[2',3':1,4]cyclobuta[1,2-*c*]quinolin-5-one (**2.29k**): Prepared according to General Procedure 2.I using **2.28k** (57.1 mg, 0.249 mmol, 1.0 equiv.) and Λ-**2.32** (4.5 mg, 2.6 µmol, 0.01 equiv.). The crude residue was purified by flash column chromatography on silica gel (50:50 EtOAc:hexanes) to afford the cycloadduct as a pale yellow semisolid (57.6 mg, 0.251 mmol, quant.). 3% ee.

^{1}H NMR (500 MHz, $CDCl_3$) δ 7.23 (ddd, *J* = 8.6, 6.2, 3.1 Hz, 1H), 7.06 – 7.01 (m, 2H), 6.98 (d, *J* = 8.2 Hz, 1H), 4.50 (ddd, *J* = 8.9, 7.8, 3.5 Hz, 1H), 4.31 (td, *J* = 8.9, 6.2 Hz, 1H), 3.62 (dd, *J* = 9.6, 6.0 Hz, 1H), 3.40 (s, 3H), 3.24 (app. q, *J* = 7.4 Hz, 1H), 2.27 – 2.15 (m, 2H), 2.08 (ddd, *J* = 12.3, 9.0, 5.9 Hz, 1H), 1.83 (dddd, *J* = 12.3, 6.0, 3.5, 2.1 Hz, 1H).

^{13}C NMR (126 MHz, $CDCl_3$) δ 168.32, 138.11, 128.44, 127.57, 126.54, 123.39, 114.79, 81.46, 70.96, 45.26, 39.57, 32.93, 31.29, 29.80.

HRMS (ESI$^+$) calculated for $[C_{14}H_{16}NO_2]^+$ ($[M+H]^+$). Requires *m/z* 230.1176; found *m/z* 230.1176.

IR (ATR, thin film): 2938, 2867, 1669, 1467, 1369, 1082, 1041, 756 cm^{-1}.

$[\alpha]_D^{22}$: –3.0° (*c*1.62, CH_2Cl_2).

HPLC: Daicel CHIRALCEL® OD-H, 70% *i*-PrOH, 30% hexanes, 1 mL/min, 260.4 nm; t_1 = 7.7 min, t_2 = 9.0 min; Area% = 48.48 : 51.52 (3% ee).

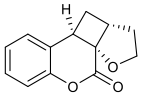

(1a*R*,4a*S*,10b*R*)-1,1a,2,10b-Tetrahydro-3*H*,5*H*-furo[2',3':1,4]cyclobuta[1,2-*c*]chromen-5-one (**2.29l**): Prepared according to General Procedure 2.I using **2.28l** (54.3 mg, 0.251 mmol, 1.0 equiv.) and Λ-**2.32** (4.5 mg, 2.6 µmol, 0.01 equiv.). The crude residue was purified by flash column chromatography on silica gel (25:75 EtOAc:hexanes) to afford the cycloadduct as an off-white powder (38.5 mg, 0.178 mmol, 71% yield). 3% ee.

^{1}H NMR (500 MHz, $CDCl_3$) δ 7.25 (td, *J* = 7.8, 1.8 Hz, 1H), 7.14 (td, *J* = 7.4, 1.2 Hz, 1H), 7.09 (d, *J* = 7.4 Hz, 1H), 7.04 (d, *J* = 8.2 Hz, 1H), 4.55 (ddd, *J* = 8.8, 8.0, 3.0 Hz, 1H), 4.38 (td, *J* = 9.1, 6.2 Hz, 1H), 3.58 (dd, *J* = 9.5, 4.2 Hz, 1H), 3.44 (app. qt, *J* = 7.7, 1.4 Hz, 1H), 2.37 (ddd, *J* = 12.5, 9.3, 6.5 Hz, 1H), 2.20 – 2.09 (m, 2H), 1.90 (dddd, *J* = 12.6, 6.1, 2.9, 1.4 Hz, 1H).

^{13}C NMR (126 MHz, $CDCl_3$) δ 166.80, 149.82, 128.53, 128.45, 125.27, 124.89, 117.58, 81.32, 71.60, 44.94, 38.77, 32.34, 32.22.

HRMS (ESI$^+$) calculated for $[C_{13}H_{13}O_3]^+$ ($[M+H]^+$). Requires *m/z* 217.0859; found *m/z* 217.0861.

IR (ATR, thin film): 2942, 2873, 1761, 1246, 1175, 1156, 1066, 759 cm^{-1}.

M.P. 92.0–93.8 °C.

$[\alpha]_D^{22}$: +10.4° (*c*0.77, CH_2Cl_2).

HPLC: Daicel CHIRALCEL® OD-H, 70% *i*-PrOH, 30% hexanes, 1 mL/min, 277.1 nm; t_1 = 4.3 min, t_2 = 8.5 min; Area% = 51.33 : 48.67 (3% ee).

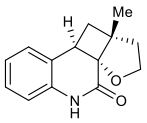

(1a*R*,4a*R*,10b*R*)-1a-Methyl-1,1a,2,3,6,10b-hexahydro-5*H*-furo[2',3':1,4]cyclobuta[1,2-*c*]quinolin-5-one (**2.29m**): Prepared according to General Procedure 2.I using **2.28m** (57.2 mg, 0.250 mmol, 1.0 equiv.) and Λ-**2.32** (4.4 mg, 2.5 µmol, 0.01 equiv.). The crude residue was purified by flash column chromatography on silica gel (75:25 EtOAc:hexanes) to afford the cycloadduct as a white powder (49.0 mg, 0.215 mmol, 86% yield). 68% ee.

^{1}H NMR (400 MHz, $CDCl_3$) δ 7.76 (s, 1H), 7.14 (ddd, *J* = 8.5, 7.2, 2.0 Hz, 1H), 7.05 – 6.97 (m, 2H), 6.69 (dd, *J* = 7.9, 1.0 Hz, 1H), 4.46 (ddd, *J* = 9.2, 6.1, 3.8 Hz, 1H), 4.25 (td, *J* = 9.1, 7.0 Hz, 1H), 3.57 (dd, *J* = 10.2, 5.6 Hz, 1H), 2.53 (dd, *J* = 12.4, 10.2 Hz, 1H), 1.90 – 1.84 (m, 2H), 1.80 (dd, *J* = 12.3, 5.6 Hz, 1H), 1.30 (s, 3H).

^{13}C NMR (126 MHz, $CDCl_3$) δ 166.92, 135.02, 128.32, 127.60, 126.05, 123.88, 115.56, 84.19, 69.70, 52.14, 40.40, 38.86, 38.24, 22.57.

HRMS (ESI^+) calculated for $[C_{14}H_{16}NO_2]^+$ ($[M+H]^+$). Requires *m/z* 230.1176; found *m/z* 230.1175.

IR (ATR, powder): 3194, 3074, 2915, 2860, 1674, 1589 cm^{-1}.

M.P. 146.9–150.3 °C.

$[\alpha]_D^{22}$: +39° (*c*0.86, CH_2Cl_2).

HPLC: Daicel CHIRALCEL® OD-H, 70% *i*-PrOH, 30% hexanes, 1 mL/min, 258.1 nm; t_1 = 5.9 min, t_2 = 19.3 min; Area% = 84.04 : 15.96 (68% ee).

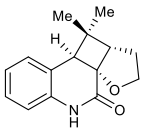

(1a*S*,4a*S*,10b*R*)-1,1-Dimethyl-1,1a,2,3,6,10b-Hexahydro-5*H*-furo[2',3':1,4]cyclobuta [1,2-*c*]quinolin-5-one (**2.29n**): Prepared according to General Procedure 2.I using **2.28n** (59.1 mg, 0.250 mmol, 1.0 equiv.) and Λ-**2.32** (4.2 mg, 2.4

μmol, 0.01 equiv.). The crude residue was purified by flash column chromatography on silica gel (75:25 EtOAc:hexanes) to afford the cycloadduct as a pale beige powder (48.7 mg, 0.205 mmol, 82% yield). 69% ee.

^{1}H NMR (500 MHz, $CDCl_3$) δ 7.99 (s, 1H), 7.15 (td, *J* = 7.7, 1.5 Hz, 1H), 6.98 (td, *J* = 7.4, 1.1 Hz, 1H), 6.91 (d, *J* = 7.4 Hz, 1H), 6.73 (dd, *J* = 7.9, 1.1 Hz, 1H), 4.45 (ddd, *J* = 9.1, 7.8, 3.1 Hz, 1H), 4.15 (td, *J* = 9.3, 6.5 Hz, 1H), 3.29 (s, 1H), 2.94 (app. dt, *J* = 8.9, 2.1 Hz, 1H), 2.17 – 2.02 (m, 2H), 1.16 (s, 3H), 0.81 (s, 3H).

^{13}C NMR (126 MHz, $CDCl_3$) δ 170.01, 136.35, 128.56, 127.85, 123.59, 121.65, 115.53, 78.33, 71.00, 56.55, 50.50, 34.93, 27.81, 26.45, 24.74.

HRMS (ESI^+) calculated for $[C_{15}H_{18}NO_2]^+$ ($[M+H]^+$). Requires *m/z* 244.1332; found *m/z* 244.1331.

IR (ATR, powder): 3213, 2955, 2923, 1677, 1594 cm^{-1}.

M.P. 145.5–148.3 °C.

$[\alpha]_D^{22}$: –3.9° (*c*0.97, CH_2Cl_2).

$[\alpha]_D^{22}$: +7.9° (*c*0.98, MeOH).

HPLC: Daicel CHIRALCEL® OD-H, 70% *i*-PrOH, 30% hexanes, 1 mL/min, 259.3 nm; t_1 = 6.4 min, t_2 = 9.2 min; Area% = 84.50 : 15.50 (69% ee).

(1*S*,1a*S*,4a*S*,10b*R*)-1-Ethyl-1,1a,2,3,6,10b-hexahydro-5*H*-furo[2',3':1,4]cyclobuta[1,2-*c*]quinolin-5-one (*trans*-**2.29o**) and **(1*R*,1a*S*,4a*S*,10b*R*)-1-ethyl-1,1a,2,3,6,10b-hexahydro-5*H*-furo[2',3':1,4]cyclobuta [1,2-*c*]quinolin-5-one** (*cis*-**2.29o**).

Experiment 1: Prepared according to General Procedure 2.I using (*E*)-**2.28o** (61.8 mg, 0.250 mmol, 1.0 equiv.) and Λ-**2.32** (4.7 mg, 2.7 μmol, 0.01 equiv.). The crude residue was purified by flash column chromatography on silica gel (60:40 EtOAc:hexanes) to afford the diastereomeric

mixture of cycloadducts as a white powder (52.4 mg, 0.215 mmol, 85% yield, 3:1 d.r.). 80% ee (major); 71% ee (minor).

Experiment 2: Prepared according to General Procedure 2.I using (*Z*)-**2.28o** (61.2 mg, 0.250 mmol, 1.0 equiv.) and Λ-**2.32** (4.2 mg, 2.4 µmol, 0.01 equiv.). The crude residue was purified by flash column chromatography on silica gel (60:40 EtOAc:hexanes) to afford the diastereomeric mixture of cycloadducts as a white powder (52.2 mg, 0.215 mmol, 85% yield, 3:1 d.r.). 85% ee (major); 75% ee (minor). Characterization data are reported for the mixture of diastereomers.

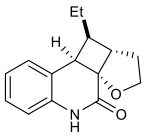

(1*S*,1a*S*,4a*S*,10b*R*)-1-Ethyl-1,1a,2,3,6,10b-hexahydro-5*H*-furo[2',3':1,4]cyclobuta[1,2-*c*]quinolin-5-one (*trans*-**2.29o**)

^{1}H NMR (500 MHz, $CDCl_3$) δ 7.72 (s, 1H), 7.14* (td, *J* = 7.6, 1.1 Hz, 1H), 6.96* (td, *J* = 7.4, 1.0 Hz, 1H), 6.94 (br. d, *J* = 7.5 Hz, 1H), 6.68 (dd, *J* = 8.0, 0.7 Hz, 1H), 4.45 (ddd, *J* = 8.8, 7.9, 2.5 Hz, 1H), 4.43 (ddd, *J* = 9.9, 9.5, 5.9 Hz, 1H), 3.78 (d, *J* = 9.9 Hz, 1H), 2.89 (ddt, *J* = 8.1, 5.3, 1.5 Hz, 1H), 2.26 – 2.09* (m, 2H), 1.82 (dddd, *J* = 12.6, 5.9, 2.3, 1.8 Hz, 1H), 1.23 (dqd, *J* = 14.1, 7.2, 4.5 Hz, 1H), 0.87* (m, 1H), 0.79 (t, *J* = 7.2 Hz, 3H). * = overlapped with minor diastereomer.

^{13}C NMR (126 MHz, $CDCl_3$) δ 169.19, 136.35, 129.73, 127.74, 123.20, 121.06, 115.45, 80.02, 70.97, 52.46, 43.47, 41.82, 32.98, 24.99, 11.20.

HRMS (ESI^+) calculated for $[C_{15}H_{18}NO_2]^+$ ($[M+H]^+$). Requires *m/z* 244.1332; found *m/z* 244.1331.

IR (ATR, powder): 3199, 3065, 2868, 1672, 1591 cm^{-1}.

M.P. 134.0–136.9 °C.

$[\alpha]_D^{22}$: +31.9° (*c*0.52, CH_2Cl_2).

HPLC: Daicel CHIRALCEL® OD-H, 10% *i*-PrOH, 90% MTBE, 1 mL/min, 256.9 nm; t_1 = 9.1 min, t_2 = 21.2 min; Area% = 71.02 : 5.78 (85% ee).

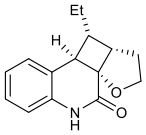

(1*R*,1a*S*,4a*S*,10b*R*)-1-Ethyl-1,1a,2,3,6,10b-hexahydro-5*H*-furo[2',3':1,4]cyclobuta[1,2-*c*]quinolin-5-one (*cis*-**2.29o**)

^{1}H NMR (500 MHz, $CDCl_3$) δ 7.82 (s, 1H), 7.14* (td, *J* = 7.6, 1.1 Hz, 1H), 7.01 (dd, *J* = 7.6, 1.3 Hz, 1H), 6.96* (td, *J* = 7.4, 1.0 Hz, 1H), 6.71 (dd, *J* = 8.0, 0.8 Hz, 1H), 4.42 (ddd, *J* = 8.9, 7.6, 4.3 Hz, 1H), 4.15 (td, *J* = 8.7, 6.8 Hz, 1H), 3.36 (ddt, *J* = 9.0, 3.1, 1.1 Hz, 1H), 3.20 (d, *J* = 8.1 Hz, 1H), 2.26 – 2.00* (m, 3H), 1.48 – 1.68 (m, 2H), 0.91* (t, *J* = 7.5 Hz, 3H). * = overlapped with major diastereomer.

^{13}C NMR (126 MHz, $CDCl_3$) δ 169.72, 135.37, 127.92, 127.68, 124.80, 123.74, 115.71, 79.56, 71.74, 48.36, 47.28, 40.47, 26.64, 23.45, 11.98.

HPLC: Daicel CHIRALCEL® OD-H, 10% *i*-PrOH, 90% MTBE, 1 mL/min, 256.9 nm; t_1 = 8.3 min, t_2 = 17.9 min; Area% = 20.30 : 2.90 (75% ee).

The relative stereochemistry of these two diastereomers was determined by 1D selective NOE experiments.

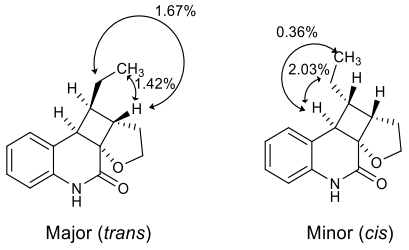

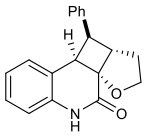

(**2.29p**) Prepared according to General Procedure 2.I using **2.28p** (13.5 mg, 0.046 mmol, 1.0 equiv.) and Λ-**2.32** (0.7 mg, 0.46 µmol, 0.01 equiv.). The crude residue was purified by flash column chromatography on silica gel (3:1 EtOAc:hexanes) to afford the diastereomeric mixture of cycloadducts as a white powder (42% yield, 8:1 d.r.). 21% ee (major); 35% ee (minor). Characterization data are reported for the mixture of diastereomers.

^{1}H NMR (400 MHz, $CDCl_3$) δ 8.61 (s, 1H), 7.13 – 7.04 (m, 3H), 6.99 – 6.91 (m, 3H), 6.69 (d, *J* = 7.9 Hz, 1H), 6.59 (t, *J* = 7.5 Hz, 1H), 6.27 (d, *J* = 7.6 Hz, 1H), 4.65 (td, *J* = 8.5, 2.5 Hz, 1H), 4.48 (td, *J* = 9.4, 6.0 Hz, 1H), 4.06 (d, *J* = 10.2 Hz, 1H), 3.70 (dd, *J* = 10.0, 6.6 Hz, 1H), 3.60 (leaning q, *J* = 7.4 Hz, 1H), 2.24 (ddt, *J* = 12.7, 9.8, 7.9 Hz, 1H), 1.98 (ddd, *J* = 13.2, 6.4, 2.4 Hz, 1H).

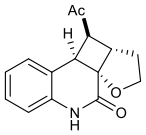

(**2.29q**) Prepared according to General Procedure 2.I using **2.28q** (63.6 mg, 0.25 mmol, 1.0 equiv.) and Λ-**2.32** (4.8 mg, 2.50 µmol, 0.01 equiv.). The crude residue was purified by flash column chromatography on silica gel (EtOAc) to afford the diastereomeric mixture of cycloadducts as a white powder (60.4 mg, 94% yield, 16:1 d.r.). 41% ee (major). Characterization data are reported for the mixture of diastereomers

^{1}H NMR (500 MHz, $CDCl_3$) δ 8.17 (s, 1H), 7.15 (*app*. ddd, *J* = 8.4, 6.4, 2.6 Hz, 1H), 7.00 – 6.93 (m, 2H), 6.72 (d, *J* = 8.6 Hz, 1H), 4.52 (ddd, *J* = 9.2, 7.7, 3.1 Hz, 1H), 4.27 (td, *J* = 9.3, 6.1 Hz, 1H), 4.15 – 4.10 (m, 1H), 3.73 (*app*. dddt, *J* = 8.3, 5.0, 3.2, 1.5 Hz, 1H), 3.39 (dd, *J* = 10.9, 4.9 Hz, 1H), 2.28 (dtd, *J* = 12.8, 9.1, 7.8 Hz, 1H), 1.83–1.90 (m, 4H).

^{13}C NMR (126 MHz, $CDCl_3$) δ 206.34, 168.03, 136.53, 128.69, 128.50, 123.21, 118.87, 116.14, 79.49, 70.89, 51.41, 45.40, 44.19, 31.95, 31.28.

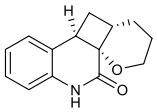

(**2.29r**): Prepared according to General Procedure 2.I using **2.28r** (58.4 mg, 0.25 mmol, 1.0 equiv.) and Λ-**2.32** (4.3 mg, 2.4 µmol, 0.01 equiv.). The crude residue was purified by flash column chromatography on silica gel (75:25 EtOAc:hexanes) to afford the cycloadduct as a pale beige powder (>98% yield). 0% ee

^{1}H NMR (500 MHz,$CDCl_3$) δ 8.15 (s, 1H), 7.18 – 7.10 (m, 2H), 7.01 (td, *J* = 7.5, 1.2 Hz, 1H), 6.74 (d, *J* = 1.1 Hz, 1H), 4.33 – 4.24 (m, 1H), 3.95 (dtd, *J* = 10.7, 3.6, 1.8 Hz, 1H), 3.60 (dd, *J* =

8.7, 4.2 Hz, 1H), 2.84 (tt, J = 8.5, 5.0 Hz, 1H), 2.69 (dt, J = 10.9, 8.4 Hz, 1H), 1.98 – 1.83 (m, 3H), 1.67 – 1.53 (m, 3H).

^{13}C NMR (126 MHz, $CDCl_3$) δ 170.25, 135.69, 128.70, 127.56, 125.23, 123.43, 115.34, 73.41, 64.59, 39.80, 34.98, 30.99, 23.88, 20.89.

2.5.7 Determination of Absolute Stereochemistry

The absolute stereochemistry of the cycloadducts was determined by comparison to the literature.[105] The optical rotations of **2.29a**, **2.2c**, and **2.29l** are in good agreement with those reported by Bach for the (+)-enantiomer. In addition, an X-ray quality crystal of cycloadduct **2.29c** was grown by vapor diffusion of pentane into a solution of **2.29c** in CH_2Cl_2. Its crystal structure (including absolute configuration) was identical to the compound reported by Bach (CCDC SEYYUS). All other cycloadducts were assigned by analogy.

The absolute configuration of iridium catalyst Λ-**2.32** was determined by crystallography. X-ray quality crystals were grown by liquid-liquid diffusion of pentane into a solution of Λ-**2.32** in chloroform. The crystal structure of this complex (Appendix D) confirmed that **2.32** was the Λ enantiomer. Based on Meggers' work, we can assume that ligand exchange from **2.50–2.53** is stereospecific,[98] allowing us to assign all other iridium complexes by analogy. In agreement with Meggers, we also found that the first eluting diastereomer of **2.50–2.53** possessed Λ stereochemistry at the metal center, while the second eluting diastereomer had Δ stereochemistry. These data are also consistent with the optical rotations of the catalysts (all Λ-**2.30** complexes gave + rotation; all Δ-**2.30** complexes gave – rotation) and the products of [2+2] cycloaddition (all Λ catalysts gave + cycloadducts; all Δ catalysts gave – cycloadducts).

2.5.8 NMR Binding Experiments

Association constants for the binding of quinolone **2.28a** to the Ir catalysts were determined through NMR titration studies.

Dimerization Studies of 2.30f and 2.28a. First, we investigated whether the chemical shifts associated with catalyst **2.30f** (**5f**) or quinolone **2.28a** might be concentration dependent. Control experiments showed that the ^{1}H chemical shifts of **2.30f** do not vary over the range of concentrations used in the titration (Figure 2.10). We therefore made the assumption that **2.30f** does not have a significant propensity towards self-association.

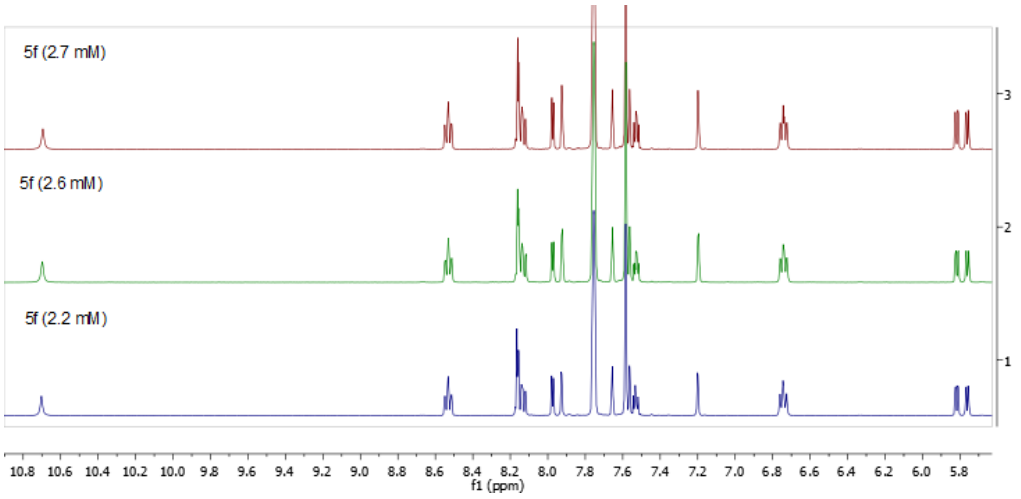

Figure 2.10. Catalyst **2.30f** (**5f**) chemical shifts are not affected by concentration over the range examined during the titration.

However, the chemical shifts of quinolone **2.28a** exhibit a dependence on concentration (Figure 2.11). This is consistent with the well-known propensity of quinolones to the form hydrogen-bound homodimers. The equilibrium constant for homodimerization (K_{dim}) was determined by NMR titration. A stock solution of **2.28a** (2.0 mg, 9.30 µmol, 1.0 equiv.) in CD_2Cl_2 (2 mL) was prepared, and 450 µL was transferred to an NMR tube. Next, a separate stock solution of **2.28a** (14.5 mg in

1.0 mL CD_2Cl_2) was prepared, and increasing amounts of this solution were titrated into the former solution, acquiring ^1H NMR spectra between each titration (Figure S4 XXB). The chemical shift of the NH (H1), which shifted downfield, was monitored and analyzed using the method described by Bach,[108] resulting in a value of K_{dim} = 95 ± 8.5 M^{-1}. An analogous titration conducted in CD_2Cl_2:pentane provided a value of K_{dim} = 110 ± 32 M^{-1}.

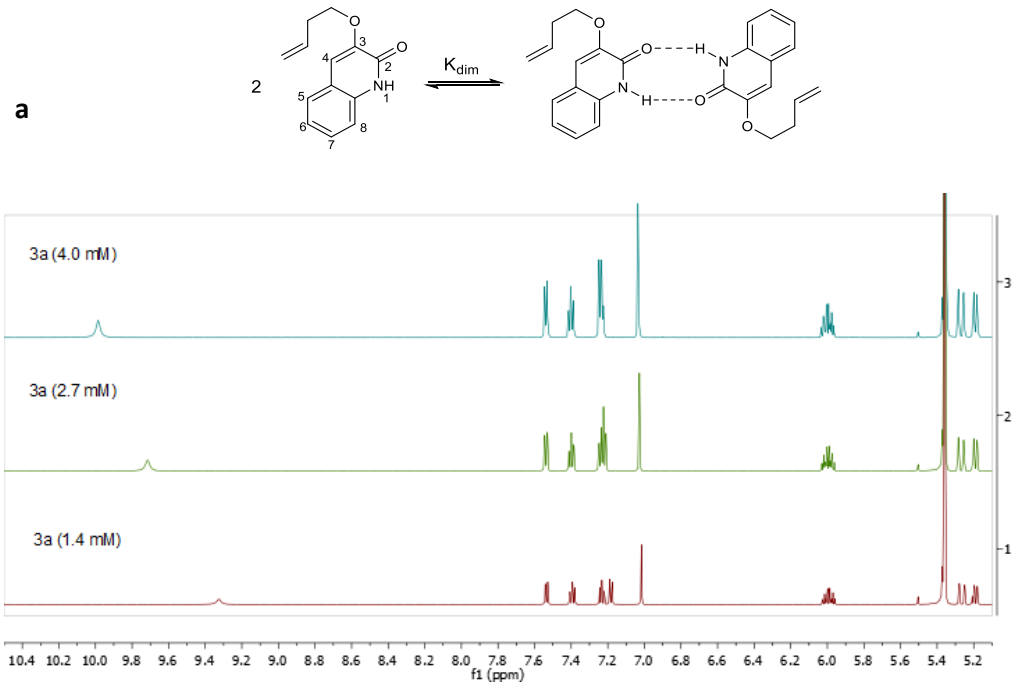

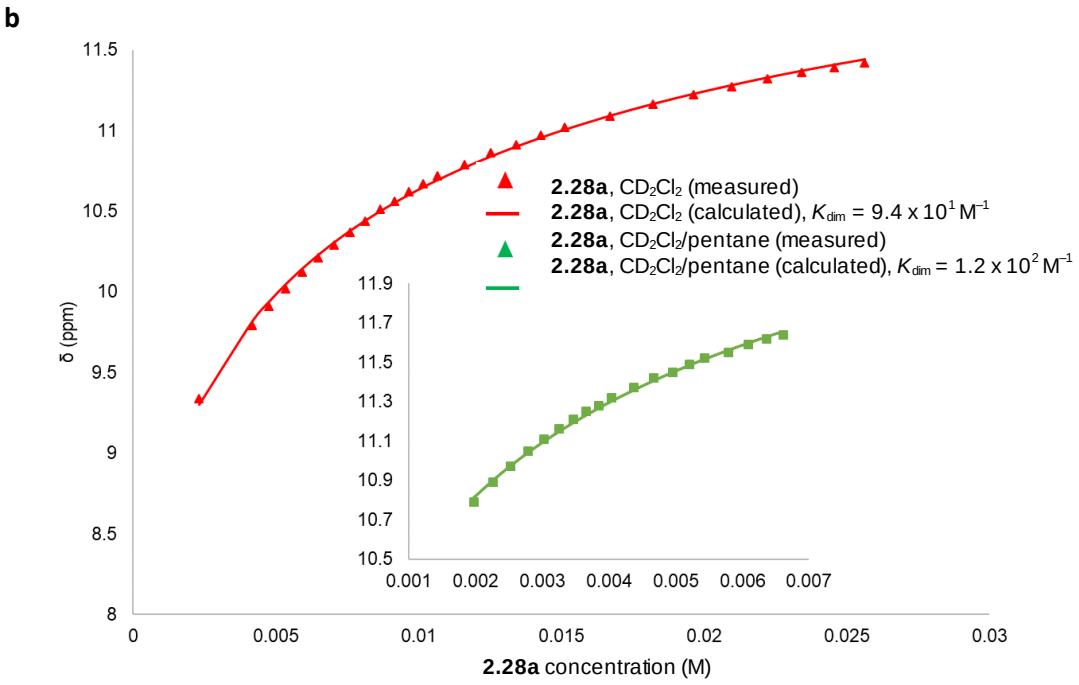

Figure 2.11. (a) Quinolone **2.28a** chemical shifts show a slight dependence on concentration, particularly for NH (H1) and adjacent aryl CH (H8). (b) Measured and calculated binding isotherms for the dimerization of **2.28a** in CD_2Cl_2 and in 1:1 CD_2Cl_2:pentane.

Titration Study of (±)-2.30f with 2.28a. A solution of (±)-**2.30f** (1.6 mg, 0.93 µmol, 1.0 equiv.) in CD_2Cl_2 (450 µL) was transferred to an NMR tube. Separately, a stock solution of **2.28a** (20.6 mg in 1.5 mL CD_2Cl_2) was prepared, and increasing amounts of this solution were titrated into the catalyst solution, acquiring ^{1}H NMR spectra between each titration (Figure 2.12). The experiment was repeated with fresh stock solutions to further probe the low-concentration region. The titration was quantified by monitoring the chemical shift of the NH proton in the catalyst, which moved downfield with increasing [**2.28a**]. Analogous experiments were also performed for (±)-**2.32** in both CD_2Cl_2 and 1:1 CD_2Cl_2:pentane.

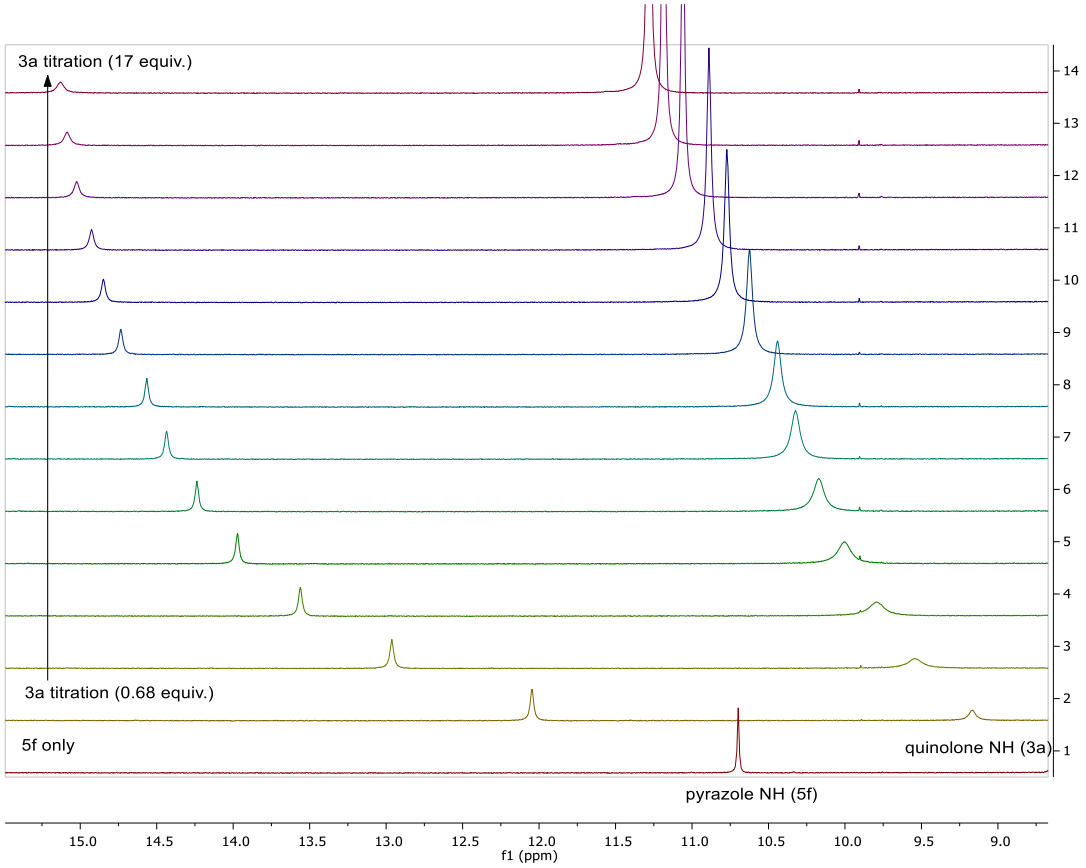

Figure 2.12. Titration of **2.28a** into **2.30f**, monitoring the chemical shift of the pyrazole NH in **2.30f**. Line 1: **2.30f** only. Lines 2–14: Titration of **2.28a**, increasing going upwards.

These data were fit to a 1:1 binding model, after correcting for the dimerization of **2.28a**, following the method developed by Thordarson.[109] Microsoft Excel was used to alter K_a in order to minimize the error between calculated and experimental chemical shifts. This provided the K_a values and binding isotherms shown in Figure 2.13.

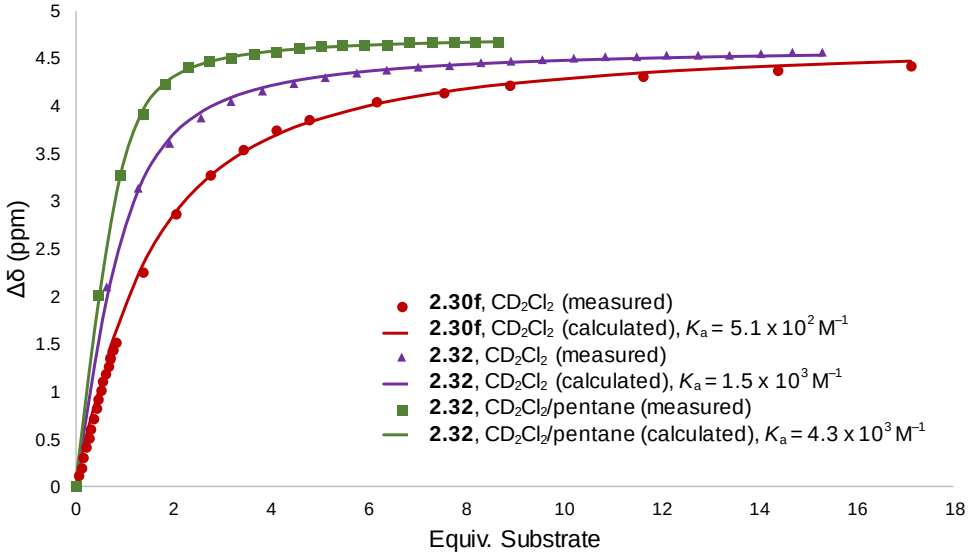

Figure 2.13. Measured and calculated binding isotherms for (a) **2.30f** in CD_2Cl_2 (b) **2.32** in CD_2Cl_2, and (c) **2.32** in 1:1 CD_2Cl_2:pentane.

Heat Map. The data shown in Figure 2.3 and Figure 2.14c were derived by comparing the initial and final chemical shifts of each proton over the course of the titration (Figure 2.15). For assignments, we made the initial assumption that the aryl protons that were most perturbed by binding were those on the same face as the pyrazole, i.e., on the bottom dF(CF_3)ppy ligand as drawn. Using these data, we were able to assign all of the protons and some of the carbons[102] in the complex, starting from H_O/H_N and working outwards using a combination of 1D and 2D experiments. The key assignment to connect the pyridine ring came from a selective HMBC, which shows correlation between the ipso carbon of the benzene ring (C1, 126.77) and H_C, H_O, and H_P. The analogous contacts in the other ligand (C1', 126.64 to H_B, H_N, H_Q) unambiguously differentiates the top and bottom ligands.

We next performed several HOESY experiments, but were unable to obtain sufficient signal at the low concentrations needed to achieve good separation of the proton signals. A separate

sample of **2.30f** only (significantly more concentrated) gave good signals in the HOESY, but only H_P and H_Q were resolved, allowing the assignment of F_{IV} and F_V. The two pairs of aryl fluoride doublets have essentially identical coupling constants, so simple 1D analysis was unable to differentiate the two. However, a ^{19}F-^{19}F COSY of the titrated complex allowed facile assignment of F_{VI} and F_{VII}. Lastly, these experiments were unable to assign the two CF_3 groups. In principle, this should be possible by ^{19}F-^{13}C HSQC, but correlating the attached carbon to other signals in the pyridine ring by ^{1}H-^{13}C HMBC is challenging due to the large coupling of the CF_3 group.

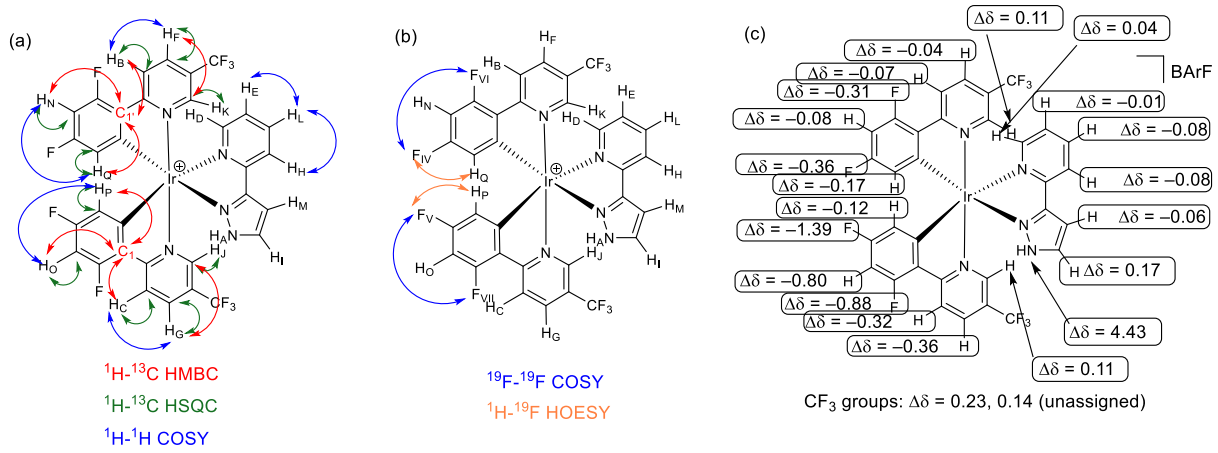

Figure 2.14. Assignments and key correlations of (a) ^{1}H and ^{13}C NMR signals, (b) ^{19}F NMR signals, and (c) raw data for heat map of catalyst **2.30f**. Other correlations are omitted for clarity. All other assignments were made using coupling or chemical shift arguments based upon the simple 1D ^{1}H or ^{19}F spectra. The values in (c) represent the change in chemical shift between the first and last titration data point.

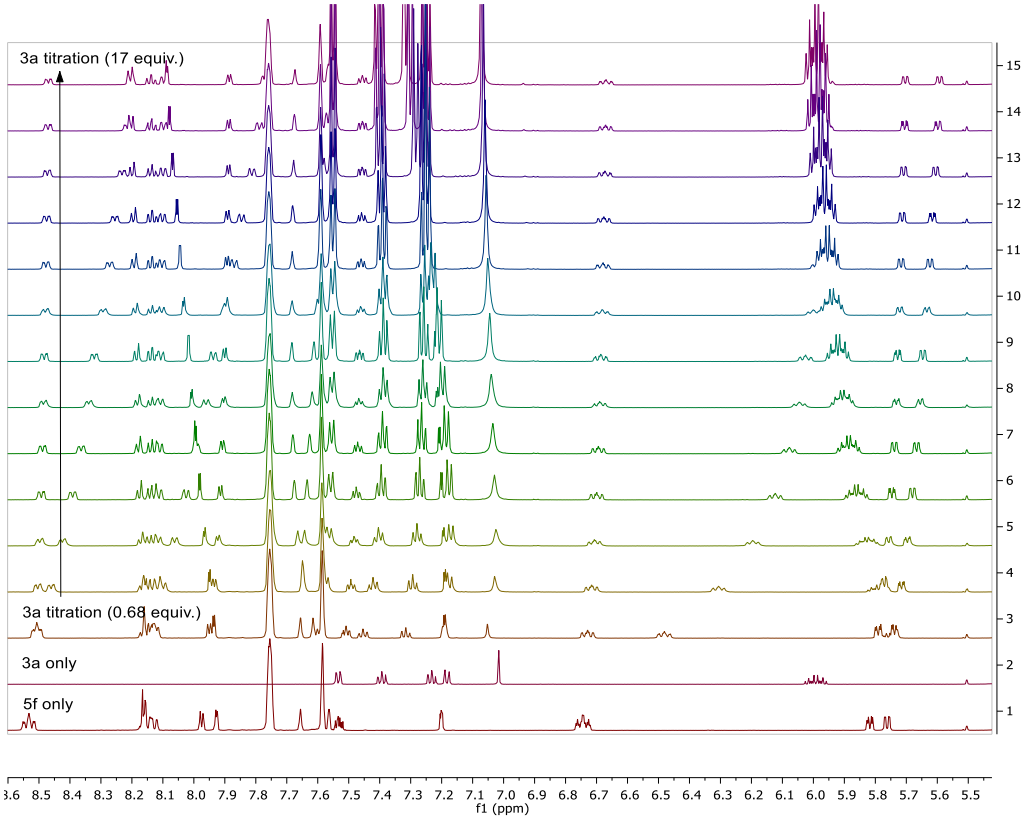

Figure 2.15. Titration data showing representative chemical shift changes for aryl protons. Line 1: **2.30f** only. Line 2: **2.28a** only. Lines 3–15: Titration of **2.28a**, increasing going upwards.

Titration Study of (±)-2.32 with N–Me substrate. A solution of (±)-**2.32** (1.8 mg, 1.00 µmol, 1.0 equiv.) in CD_2Cl_2/pentane (450 µL) was transferred to an NMR tube. Separately, a stock solution of N–Me quinolone (7.17 mg in 2.0 mL CD_2Cl_2/pentane) was prepared and increasing amounts of this solution were titrated into the catalyst solution, acquiring ^1H NMR spectra between each titration (Figure 2.16). The titration was quantified by monitoring the chemical shift of the NH proton in the catalyst, which moved downfield with increasing [quinolone]. Analogous experiments were also performed for (±)-**2.32** in both CD_2Cl_2 and 1:1 CD_2Cl_2:pentane with **2.28k**.

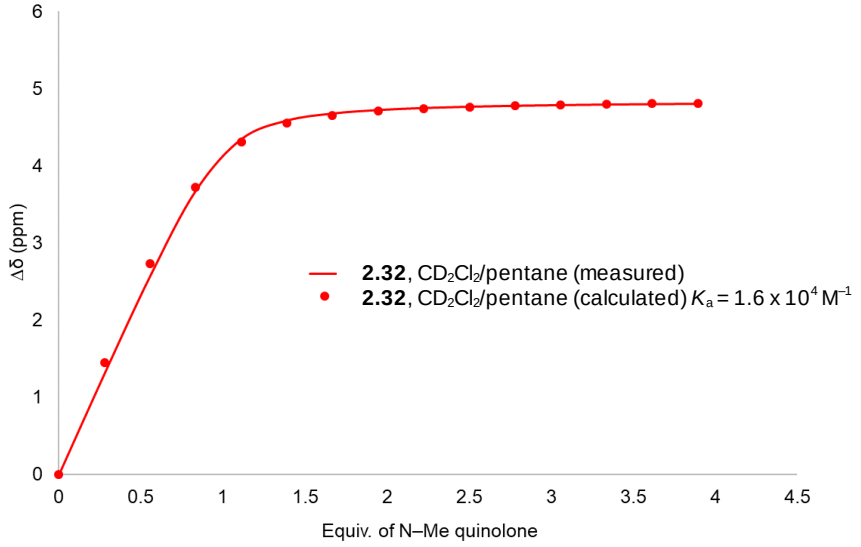

Figure 2.16. Measured and calculated binding isotherm for **2.32** with N–Me quinolone in CD_2Cl_2/pentane.

2.5.9 Photophysical Measurements

2.5.9.a. Absorption and Emission Spectra

Figure 2.17 shows UV-Vis absorption spectra for three representative catalysts: **2.30a**, **2.30f**, and **2.32** at similar concentrations in CH_2Cl_2**.** For the emission experiments, higher concentrations and different slit widths were necessary in order to obtain sufficient signal-to-noise ratios. Thus, the magnitude of emission intensities should not be compared between these three catalysts. Triplet energies were calculated from $\lambda_{max,}$ values for emission.

UV-Vis absorption spectra of several substrates (**2.28a**, **2.28b**, **2.28d**, **2.28g**) in CH_2Cl_2 are shown in Figure 2.18. The low concentration data show fine structure in the UV, while the high concentration data show the absorption profile at the reaction concentration of 5 mM. Substrate **2.28g** exhibits an anomalously large bathochromic shift and tail into the visible region, which may enable an uncatalyzed process to occur. Iodide **2.28d** does not have a substantially different absorbance than other quinolones, but we hypothesize that the heavy iodine atom may facilitate intersystem crossing, leading to a similar uncatalyzed background reaction

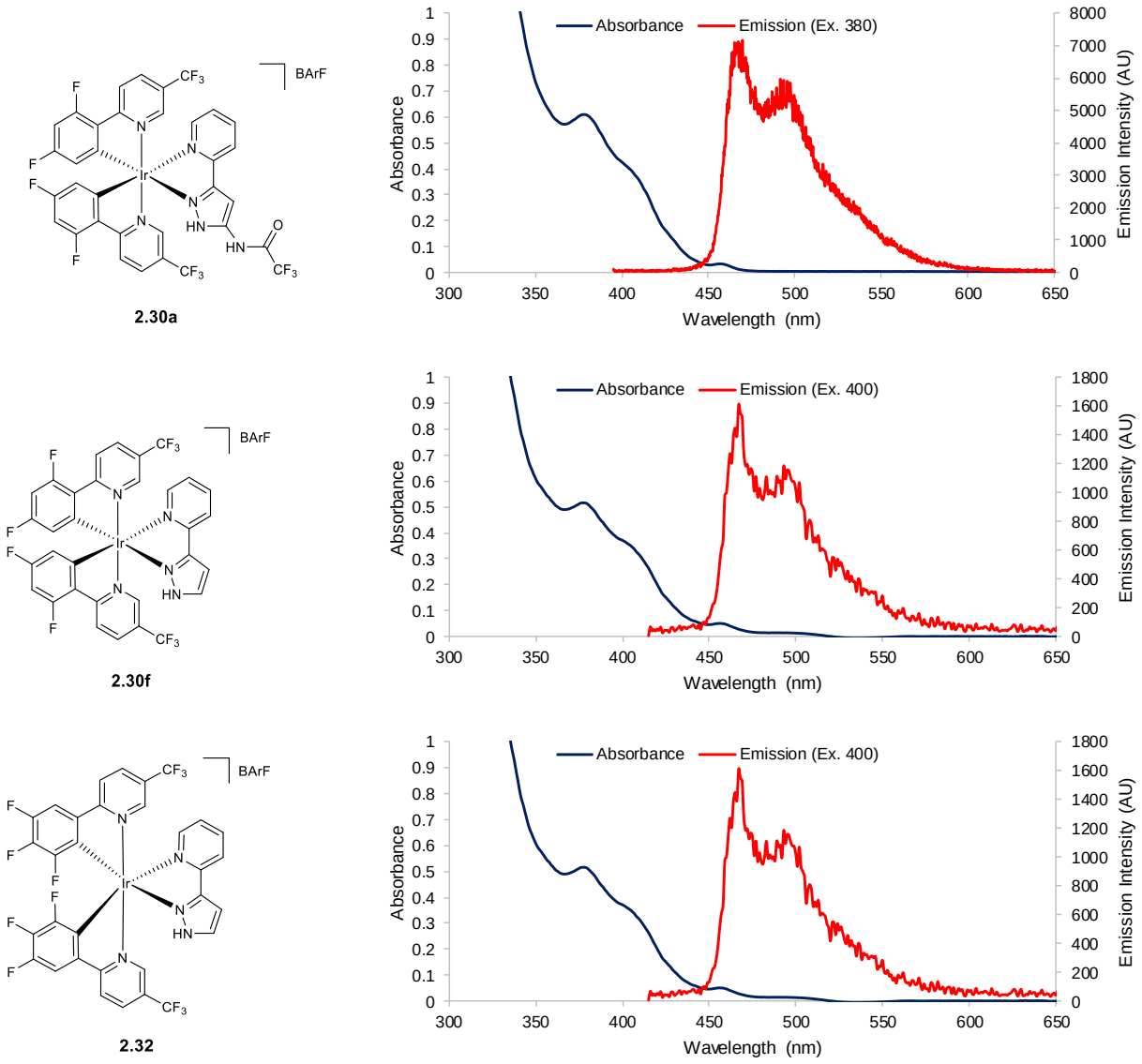

Figure 2.17. Absorption and emission data for iridium catalysts in CH_2Cl_2. Catalyst **2.30a**, 9.0 x 10^{-5} M. Catalyst **2.30f**, 8.0 x 10^{-5} M. Catalyst **2.32**, 8.0 x 10^{-5} M.

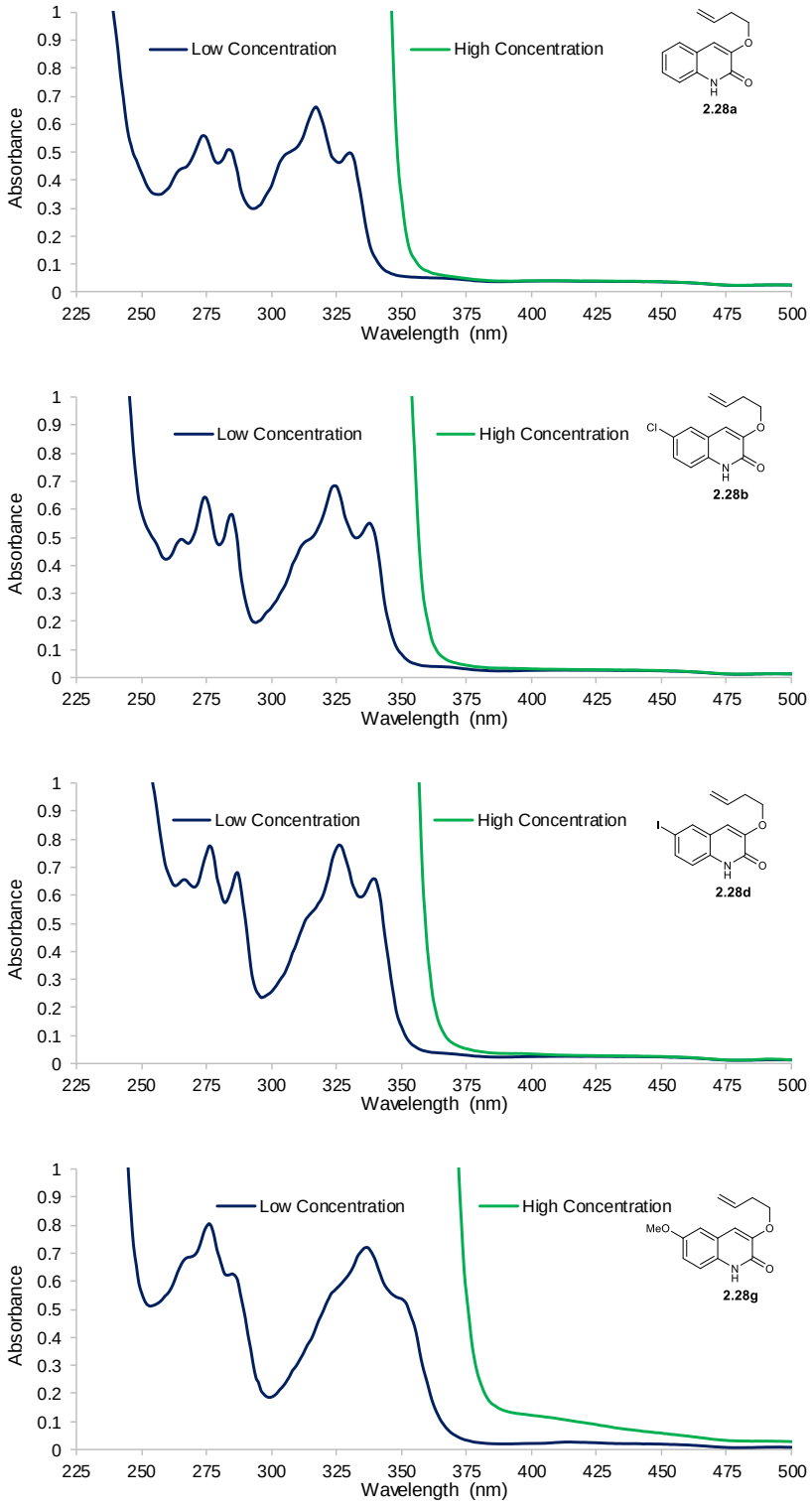

Figure 2.18. Absorption data for representative quinolones in CH_2Cl_2. Low concentration = 5 x 10^{-5} M. High concentration = 5 x 10^{-3} M.

2.5.9.b Stern–Volmer Quenching Experiments

Stern–Volmer experiments were conducted as previously described.[110] Five separate solutions were prepared containing (±)-**2.32** (4.3×10^{-5} M) and **2.28a** (ranging from 0 to 5.5×10^{-4} M) in CH_2Cl_2, and each was sparged with N_2 for 15 min. The solutions were irradiated at 400 nm, and the emission intensity (I) at 480 nm was compared to the initial emission intensity (I_0) at the same wavelength. These data result in a linear Stern–Volmer relationship, consistent with the proposed mechanism in which the photoexcited catalyst is quenched by substrate.

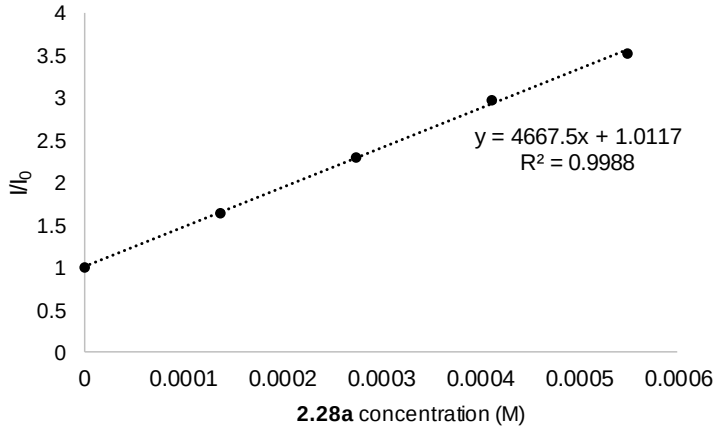

Figure 2.19. Stern–Volmer experiment for the quenching of photoexcited catalyst **2.32** by quinolone **2.28a**.

2.5.10 Cyclic Voltammetry Data

Cyclic voltammetry experiments were performed in CH_2Cl_2 with analyte (1 mM) and $[(n\text{-}Bu)_4N]^+[PF_6]^-$ (100 mM) using a glassy carbon working electrode, platinum wire counter electrode, a $Ag/AgNO_3$ MeCN reference electrode, and a scan rate of 50 mV/s. Ferrocene was added as an internal reference to SCE. As the redox events for both substrate and catalyst were irreversible, half-peak potentials were estimated from the voltammograms (Figure 2.20).

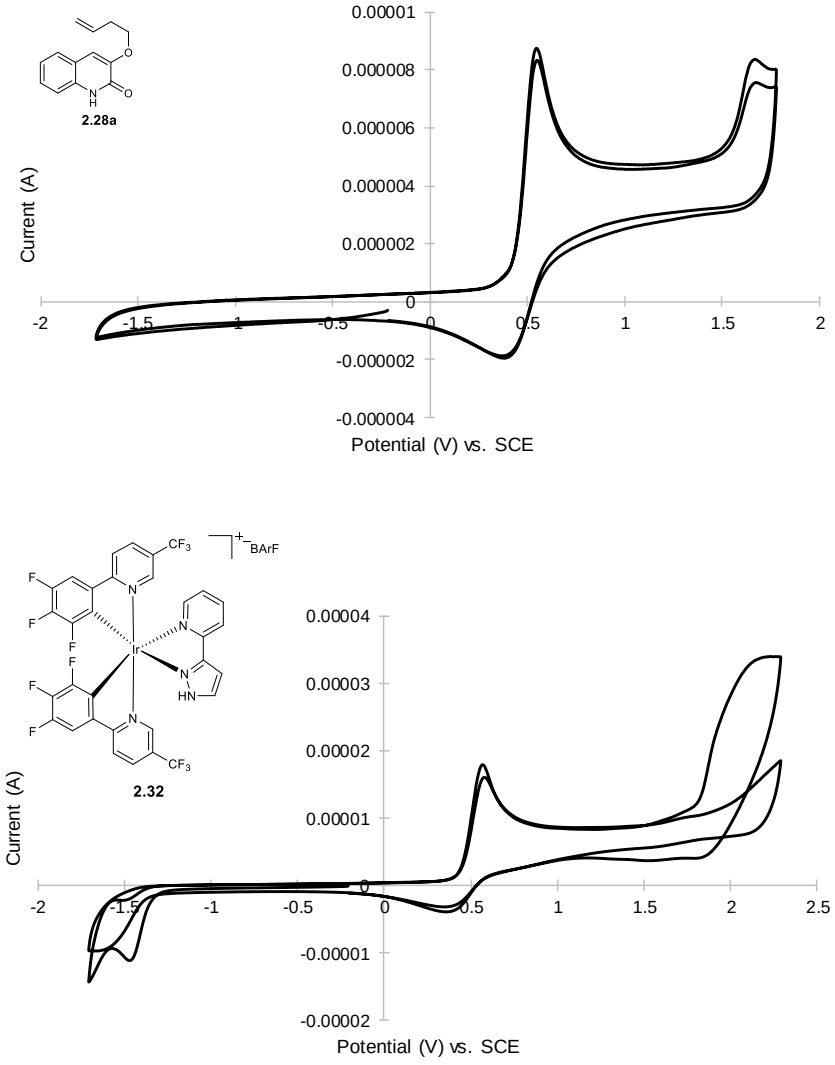

Figure 2.20. Cyclic voltammograms of quinolone substrate **2.28a** and photocatalyst **2.32** with ferrocene added.

Quinolone **2.28a**: **2.28a/2.28a**$^{\bullet-}$ $E_{p/2} < -1.7$ V vs. SCE in CH_2Cl_2
2.28a$^{\bullet+}$**/2.28a** $E_{p/2} = +1.59$ V vs. SCE in CH_2Cl_2

Iridium Catalyst **2.32**: Ir^{III}/Ir^{II} $E_{p/2} = -1.42$ V vs. SCE in CH_2Cl_2
Ir^{IV}/Ir^{III} $E_{p/2} = +1.79$ V vs. SCE in CH_2Cl_2

The excited state redox potentials of iridium catalyst **2.32** were computed from the Rehm–Weller equation[111,112] using the ground state potentials obtained above and the energy gap between zero vibrational levels of the ground and excited states ($E_{0,0}$). The latter value was approximated as the wavelength at which emission is 10% of its maximum.[113–115] This provides a generous estimate for the excited state redox potentials, demonstrating that photoinduced electron transfer is endergonic even under limiting conditions.

$E(Ir^{III*}/Ir^{II}) = E(Ir^{III}/Ir^{II}) + E_{0,0}$
$= -1.42$ V + 2.69 V
$= +1.27$ V vs. SCE in CH_2Cl_2

$E(Ir^{IV}/Ir^{III*}) = E(Ir^{IV}/Ir^{III}) - E_{0,0}$
$= 1.91$ V – 2.69 V
$= -0.78$ V vs. SCE in CH_2Cl_2

2.5.11 Computational Studies

2.5.11.a General Information

All computations were performed using density functional theory[116] (DFT) in Jaguar 9.1 suite.[117] Geometry optimizations were executed with B3LYP-D3[118–120] levels of theory and 6-31G** basis set.[121] Ir metal was evaluated with Los Alamos LACVP[122–124] basis set, which reflects the relativistic effective core potentials. The energies of optimized geometries were re-evaluated with M06-D3[120,125] levels of theory and cc-pVTZ(-f)[126] basis set, which is a high quality triple-ζ basis set. Ir metal was calculated with LACV3P** basis set, with the decontracted LACVP exponents to match with the triple-ζ functions of the main group elements. Vibrational frequencies were computed with the optimized geometries at the same level as the geometry optimizations. Finally, solvation correction energies were evaluated by using the self-consistent reaction field (SCRF) approximations,[127–129] which solve the linearized Poisson-Boltzmann equations with the proper dielectric constants (ε=9.08 for dichloromethane). The solution phase Gibbs free energies were computed as follows:

$$G(Sol) = G(gas) + G^{solv} \quad (1)$$

$$G(gas) = H(gas) - TS(gas) \quad (2)$$

$$H(Gas) = E(SCF) + ZPE \quad (3)$$

$$\Delta G(Sol) = \Sigma G(Sol) \text{ for products} - \Sigma G(Sol) \text{ for reactants} \quad (4)$$

G(Sol) is the solvation corrected Gibbs free energy from gas phase free energy G(gas); H(gas) is the enthalpy in the gas phase; T is the temperature (298.15 K); S(gas) is the entropy in the gas phase; E(SCF) is the electronic energy converged from the self-consistent field method; ZPE is the vibrational zero-point energy; and S for the vibrational entropy correction. Note that here

entropy refers specifically to the vibrational/rotational/translational entropy of the solute(s). The solvent entropies are implicitly included in the continuum model.

2.5.11.b Energies, Coordinates, and Vibrational Frequencies of Optimized Structures

Table 2.8. Computed energies of the optimized geometries

	E(SCF)/(eV)	**ZPE/(kcal/mol)**	**S(gas)/(cal/mol)**	**G(solv)/(kcal/mol)**
	cc-pVTZ(-f)/LACV3P**	6-31G**/LACVP**	6-31G**/LACVP**	6-31G**/LACVP**
2.32	-76307.336	267.44	244.410	-45.07
2.32*	-76304.797	265.14	257.940	-44.96
2.28a	-19268.947	147.83	119.120	-11.79
Complex A	-95577.617	416.38	318.307	-42.80
Complex B	-95577.531	416.13	316.899	-43.45

For the complete listing of Cartesian coordinates and vibrational fequencies of the optimized geometries for the substrate, photocatalyst, and complexes please see the supplementary information of: Skubi, K. L.; Kidd, J. B.; Jung, H.; Guzei, I. A.; Baik, M. -H.; Yoon, T. P. Enantioselective Excited-State Photoreactions Controlled by a Chiral Hydrogen-Bonding Iridium Sensitizer. *J. Am. Chem. Soc.* **2017**, *138*, 17186–17192.

2.6 References and Notes

[1] Iriondo-Alberdi, J.; Greaney, M. F. Photocycloaddition in Natural Product Synthesis. *Eur. J. Org. Chem.* **2007**, 4801–4815.

[2] Hoffmann, N. Photochemical Reactions as Key Steps in Organic Synthesis. *Chem. Rev.* **2008**, *108*, 1052–1103.

[3] Bach, T.; Hehn, J. P. Photochemical Reactions as Key Steps in Natural Product Synthesis. *Angew. Chem. Int. Ed.* **2011**, *50*, 1000–1046.

[4] Turro, N. J. *Modern Molecular Photochemistry*: Benjamin/Cummings, 1978; pp 1–16.
[5] Verhoven, J. W. Glossary of Terms Used in Photochemistry. *Pure Appl. Chem.* **1996**, *68*, 2223–2286.

[6] Du, J.; Skubi, K. L.; Schultz, D. M.; Yoon, T. P. A Dual-Catalysis Approach to Enantioselective [2+2] Photocycloadditions Using Visible Light. *Science* **2014**, *344*, 392–396.

[7] Rono, L. J.; Yayla, H. G.; Wang, D. Y.; Armstrong, M. F.; Knowles, R. R. Enantioselective Photoredox Catalysis Enabled by Proton-Coupled Electron Transfer: Development of an Asymmetric Aza-Pinacol Cyclization. *J. Am. Chem. Soc.* **2013**, *135*, 17735–17738.

[8] Uraguchi, D.; Kimura, Y.; Ueoka, F.; Ooi, T.; Urea as a Redox-Active Directing Group under Asymmetric Photocatalysis of Iridium-Chiral Borate Ion Pairs. *J. Am. Chem. Soc.* **2020**, *142*, 19462–19467.

[9] Kimura, Y.; Uraguchi, D.; Ooi, T. Catalytic Asymmetric Synthesis of 5-Membered Alicyclic α-Quaternary β-amino acids *via* [3+2]-photocycloaddition of α-substituted acrylates. *Org. Biomol. Chem.* **2021**, *19*, 1744–1747.

[10] Ruiz Espelt, L.; McPherson, I. S.; Wiensch, E. M.; Yoon, T. P. Enantioselective Conjugate Additions of α-Amino Radicals via Cooperative Photoredox and Lewis Acid Catalysis. *J. Am. Chem. Soc.* **2015**, *137*, 2452–2455.

[11] An analogous effect has been studied using chiral-at-metal photocatalytic systems. Tutkowski, B.; Meggers, E.; Wiest, O. Understanding Rate Acceleration and Stereoinduction of an Asymmetric Giese Reaction Mediated by a Chiral Rhodium Catalyst. *J. Am. Chem. Soc.* **2017**, *139*, 8062–8065.

[12] Tellis, J. C.; Kelly, C. B.; Primer, D. N.; Jouffroy, M.; Patel, N. R.; Molander, G. A. Single-Electron Transmetalation via Photoredox/Nickel Dual Catalysis: Unlocking a New Paradigm for sp3–sp2 Cross-Coupling. *Acc. Chem. Res.* **2016**, *49*, 1429–1439.

[13] Twilton, J.; Le, C.; Zhang, P.; Shaw, M. H.; Evans, R. W.; MacMillan, D. W. C. The merger of transition metal and photocatalysis. *Nat. Rev. Chem.* **2017**, *1*, 0052.

[14] Tellis, J. C.; Primer, D. N.; Molander, G. A. Single-Electron Transmetalation in Organoboron Cross-Coupling by Photoredox/Nickel Dual Catalysis. *Science* **2014**, *345*, 433–436.

[15] Zuo, Z.; Ahneman, D. T.; Chu, L.; Terrett, J. A.; Doyle, A. G.; MacMillan, D. W. C. Merging photoredox with nickel catalysis: Coupling of α-carboxyl sp3 -carbons with aryl halides. *Science* **2014**, *345*, 437–440.

[16] Gutierrez, O.; Tellis, J. C.; Primer, D. N.; Molander, G. A.; Kozlowski, M. C. Nickel-Catalyzed Cross-Coupling of Photoredox-Generated Radicals: Uncovering a General Manifold for Stereoconvergence in Nickel-Catalyzed Cross-Couplings. *J. Am. Chem. Soc.* **2015**, *137*, 4896–4899.

[17] Zuo, Z.; Cong, H.; Li, W.; Choi, J.; Fu, G. C.; MacMillan, D. W. C. Enantioselective Decarboxylative Arylation of α-Amino Acids via the Merger of Photoredox and Nickel Catalysis. *J. Am. Chem. Soc.* **2016**, *138*, 1832–1835.

[18] Stache, E. E.; Rovis, T.; Doyle, A. G. Dual Nickel- and Photoredox-Catalyzed Enantioselective Desymmetrization of Cyclic *meso*-Anhydrides. *Angew. Chem. Int. Ed.* **2017**, *56*, 3679–3683.

[19] Lipp, A.; Badir, S. O.; Molander, G. A. Stereoinduction in Metallophotoredox Catalysis. *Angew. Chem. Int. Ed.* **2021**, *60*, 1714–1726.

[20] Hammond, G. S.; Cole, R. S. Asymmetric Induction During Energy Transfer. *J. Am. Chem. Soc.* **1965**, *87*, 3256–3257.

[21] Aratani, T.; Nakanisi, Y.; Nozaki, H. The Absolute Configuration of *cis*-2-Phenylcyclopropanecarboxylic Acid. *Tetrahedron Lett.* **1969**, *10*, 1809–1810.

[22] Aratani, T.; Nakanisi, H.; Nozaki, H. The Absolute Configuration of cis-2-Phenylcyclopropanecarboxylic Acid and Related Compounds. *Tetrahedron*, **1970**, *26*, 1675–1684.

[23] Murov, S. L.; Cole, R. S.; Hammond, G. S. Mechanisms of Photochemical Reactons in Solution. LIV. A New Mechanism for Photosensitization. *J. Am. Chem. Soc.* **1968**, *90*, 2957–2958.

[24] Balavoine, G.; Jugé, S.; Kagan, H. B. Photoactivation Optique du Methyl *p*-Tolyl Sulfoxide Racemique par Emploi d'un Sensibilisateur Chiral. *Tetrahedron Lett.* **1973**, *14*, 4159–4162.

[25] Drucker, C. S.; Toscano, V. G.; Weiss, R. G. A General Method for the Determination of Steric Effects during Collisional Energy Transfer. Partial Photoresolution of Penta-2,3-Diene. *J. Am. Chem. Soc.* **1973**, *95*, 6482–6484.

[26] For a broad overview, see: Inoue, Y. Enantiodifferentiating Photosensitized Reactions. In *Molecular and Supramolecular Photochemistry, Vol. 11: Chiral Photochemistry*; Inoue, Y.; Ramamurthy, V., Eds.; Marcel Dekker: New York, NY, 2004; pp 129–177.

[27] Vondenhof, M.; Mattay, J. 1,1'-Binaphthalene-2,2'-Dicarbonitrile in Photochemically Sensitized Enantiodifferentiating Isomerizations. *Chem. Ber.* **1990**, *123*, 2457–2459.

[28] Inoue, Y.; Dong, F.; Yamamoto, K.; Tong, L. H.; Tsuneishi, H.; Hakushi, T.; Tai, A. Inclusion-Enhanced Optical Yield and *E*/*Z* Ratio in Enantiodifferentiating Photoisomerization of Cyclooctene Included and Sensitized by *β*-Cyclodextrin Monobenzoate. *J. Am. Chem. Soc.* **1995**, *117*, 11033–11034.

[29] Cauble, D. F.; Lynch, V.; Krische, M. J. Studies on the Enantioselective Catalysis of Photochemically Promoted Transformations: "Sensitizing Receptors" as Chiral Catalysts. *J. Org. Chem.* **2003**, *68*, 15–21.

[30] Kemp, D. S.; Petrakis, K. S. Synthesis and Conformational Analysis of *cis,cis*-1,3,5-Trimethylcyclohexane-1,3,5-tricarboxylic Acid. *J. Org. Chem.* **1981**, *46*, 5140–5143.

[31] Bach, T.; Bergmann, H.; Harms, K. High Facial Diastereoselectivity in the Photocycloaddition of a Chiral Aromatic Aldehyde and an Enamide Induced by Intermolecular Hydrogen Bonding. *J. Am. Chem. Soc.* **1999**, *121*, 10650–10651.

[32] Bach, T.; Bergmann, H.; Harms, K. Enantioselective Intramolecular [2+2]-Photocycloaddition Reaction in Solution. *Angew. Chem. Int. Ed.* **2000**, *39*, 2302–2304.

[33] Bach, T.; Bergmann, H.; Grosch, B.; Harms, K. Highly Enantioselective Intra- and Intermolecular [2+2] Photocycloaddition Reactions of 2-Quinolones Mediated by a Chiral Lactam Host: Host–Guest Interactions, Product Configuration, and the Origin of the Stereoselectivity in Solution. *J. Am. Chem. Soc.* **2002**, *124*, 7982–7990.

[34] Bach, T.; Bergmann, H. Enantioselective Intermolecular [2+2]-Photocycloaddition Reactions of Alkenes and a 2-Quinolone in Solution. *J. Am. Chem. Soc.* **2000**, *122*, 11525–11526.

[35] Grosch, B.; Orlebar, C. N.; Herdtweck, E.; Massa, W.; Bach, T. Highly Enantioselective Diels–Alder Reactions of a Photochemically Generated *o*-Quinodimethane with Olefins. *Angew. Chem. Int. Ed.* **2003**, *42*, 3693–3696.

[36] Bach, T.; Bergmann, H.; Harms, K. Enantioselective Photochemical Reactions of 2-Pyridones in Solution. *Org. Lett.* **2001**, *3*, 601–603.

[37] Bach, T.; Aechtner, T.; Neumüller, B. Intermolecular Hydrogen Binding of a Chiral Host and a Prochiral Imidazolidinone: Enantioselective Norrish–Yang Cyclisation in Solution. *Chem. Commun.* **2001**, 607–608.

[38] Bach, T.; Grosch, B.; Strassner, T.; Herdtweck, E. Enantioselective [6π]-Photocyclization Reaction of an Acrylanilide Mediated by a Chiral Host. Interplay between Enantioselective Ring Closure and Enantioselective Protonation. *J. Org. Chem.* **2003**, *68*, 1107–1116.

[39] Müller, C.; Bauer, A.; Bach, T. Light-Driven Enantioselective Organocatalysis. *Angew. Chem. Int. Ed.* **2009**, *48*, 6640–6642.

[40] Maturi, M. M.; Bach, T. Enantioselective Catalysis of the Intermolecular [2+2] Photo-cycloaddition
between 2-Pyridones and Acetylenedicarboxylates. *Angew. Chem. Int. Ed.* **2014**, *53*, 7661–7664.

[41] Alonso, R.; Bach, T. A Chiral Thioxanthone as an Organocatalyst for Enantioselective [2+2] Photocycloaddition Reactions Induced by Visible Light. *Angew. Chem. Int. Ed.* **2014**, *53*, 4368–4371.

[42] Tröster, A.; Alonso, R.; Bauer, A.; Bach, T. Enantioselective Intermolecular [2 + 2] Photocycloaddition Reactions of 2(1*H*)-Quinolones Induced by Visible Light Irradiation. *J. Am. Chem. Soc.* **2016**, *138*, 7808–
7811.

[43] Hölzl-Hobmeier, A.; Bauer, A.; Silva, A. V.; Huber, S. M.; Bannwarth, C.; Bach, T. Catalytic Deracemization of Chiral Allenes by Sensitized Excitation with Visible Light. *Nature*, **2018**, *564*, 240–243.

[44] Plaza, M.; Jandl, C.; Bach, T. Photochemical Deracemization of Allenes and Subsequent Chirality Transfer. *Angew. Chem. Int. Ed.* **2020**, *59*, 12785–12788.

[45] Plaza, M.; Großkopf, J.; Breitenlechner, S.; Bannwarth, C.; Bach, T. Photochemical Deracemization of Primary Allene Amides by Triplet Energy Transfer: A Combined Synthetic and Theoretical Study. *J. Am. Chem. Soc.* **2021**, *143*, 11209–11217.

[46] Wimberger, L.; Kratz, T.; Bach, T. Photochemical Deracemization of Chiral Sulfoxides Catalyzed by a Hydrogen-Bonding Xanthone Sensitizer. *Synthesis* **2019**, *51*, 4417–4424.

[47] Tröster, A.; Bauer, A.; Jandl, C.; Bach, T. Enantioselective Visible-Light-Mediated Formation of 3-Cyclopropylquinolones by Triplet-Sensitized Deracemization. *Angew. Chem. Int. Ed.* **2019**, *58*, 3538–3541.

[48] Li, X.; Kutta, R. J.; Jandl, C.; Bauer, A.; Nuernberger, P.; Bach, T. Photochemically Induced Ring Opening of Spirocyclopropyl Oxindoles: Evidence for a Triplet 1,3-Diradical Intermediate and Deracemization by a Chiral Sensitizer. *Angew. Chem. Int. Ed.* **2020**, *59*, 21640–21647.

[49] Vallavoju, N.; Selvakumar, S.; Jockusch, S.; Sibi, M. P.; Sivaguru, J. Enantioselective Organo-Photocatalysis Mediated by Atropisomeric Thiourea Derivatives. *Angew. Chem. Int. Ed.* **2014**, *53*, 5604–5608.

[50] Vallavoju, N.; Selvakumar, S.; Jockusch, S.; Prabhakaran, M. T.; Sibi, M. P.; Sivaguru, J. Evaluating Thiourea Architecture for Intramolecular [2+2] Photocycloaddition of 4-Alkenylcoumarins. *Adv. Synth. Catal.* **2014**, *356*, 2763–2768.

[51] Vallavoju, N.; Selvakumar, S.; Pemberton, B. C.; Jockusch, S.; Sibi, M. P.; Sivaguru, J. Organophotocatalysis: Insights into the Mechanistic Aspects of Thiourea-Mediated Intermolecular [2+2] Photocycloadditions. *Angew. Chem. Int. Ed.* **2016**, *55*, 5446–5451.

[52] Raghunathan, R.; Jockusch, S.; Sibi, M. P.; Sivaguru, J. Evaluating Thiourea/Urea Catalyst for Enantioselective 6π-Photocyclization of Acrylanilides. *J. Photochem. Photobiol. A* **2016**, *331*, 84–88.

[53] Ueno, T.; Urano, Y.; Setsukinai, K.-I.; Takakusa, H.; Kojima, H.; Kikuchi, K.; Ohkubo, K.; Fukuzumi, S.; Nagano, T. Rational Principles for Modulating Fluorescence Properties of Fluorescein. *J. Am. Chem. Soc.* **2004**, *126*, 14079–14085.

[54] Choi, E. J.; Kim, E.; Lee, Y.; Jo, A.; Park, S. B. Rational Perturbation of the Fluorescence Quantum Yield in Tunable and Predictable Fluorophores (Seoul-Fluors) by a Synthetic Method Involving C–H Activation. *Angew. Chem. Int. Ed.* **2014**, *53*, 1346–1350.

[55] Kalyanasundaram, K. Photophysics, photochemistry and solar energy conversion with tris(bipyridyl)ruthenium(II) and its analogues. *Coord. Chem. Rev.* **1982**, *46*, 159–244.

[56] Juris, A.; Balzani, V.; Barigelletti, F.; Campagna, S.; Belser, P.; von Zelewsky, A. Ru(II) Polypyridine Complexes - Photophysics, Photochemistry, Electrochemistry, and Chemiluminescence. *Coord. Chem. Rev.* **1988**, *84*, 85–277.

[57] Lu, Z.; Yoon, T. P. Visible Light Photocatalysis of [2+2] Styrene Cycloadditions by Energy Transfer. *Angew. Chem. Int. Ed.* **2012**, *51*, 10329–10332.

[58] Zou, Y.-Q.; Duan, S.-W.; Meng, X.-G.; Hu, X.-Q.; Gao, S.; Chen, J.-R.; Xiao, W.-J. Visible light induced intermolecular [2+2]-cycloaddition reactions of 3-ylideneoxindoles through energy transfer pathway. *Tetrahedron* **2012**, *68*, 6914–6919.

[59] Hurtley, A. E.; Lu, Z.; Yoon, T. P. [2+2] Cycloaddition of 1,3-Dienes by Visible Light Photocatalysis. *Angew. Chem. Int. Ed.* **2014**, *53*, 8991–8994.

[60] Scholz, S. O.; Farney, E. P.; Kim, S.; Bates, D. M.; Yoon, T. P. Spin-Selective Generation of Triplet Nitrenes: Olefin Aziridination through Visible-Light Photosensitization of Azidoformates. *Angew. Chem. Int. Ed.* **2016**, *55*, 2239–2242.

[61] Singh, K.; Staig, S. J.; Weaver, J. D. Facile Synthesis of *Z*-Alkenes via Uphill Catalysis. *J. Am. Chem. Soc.* **2014**, *136*, 5275–5278.

[62] Yoo, W.-J.; Tsukamoto, T.; Kobayashi, S. Visible Light-Mediated Ullmann-Type C–N Coupling Reactions of Carbazole Derivatives and Aryl Iodides. *Org. Lett.* **2015**, *17*, 3640–3642.

[63] Heitz, D. R.; Tellis, J. C.; Molander, G. A. Base-Free Photoredox/Nickel Dual-Catalytic Cross-Coupling of Ammonium Alkylsilicates. *J. Am. Chem. Soc.* **2016**, *138*, 12715–12718.

[64] Welin, E. R.; Le, C.; Arias-Rotondo, D. M.; McCusker, J. K.; MacMillan, D. W. C. Photosensitized, energy transfer-mediated organometallic catalysis through electronically excited nickel(II). *Science* **2017**, *355*, 380–385.

[65] Farney, E. P.; Yoon, T. P. Visible-Light Sensitization of Vinyl Azides by Transition-Metal Photocatalysis. *Angew. Chem. Int. Ed.* **2014**, *53*, 793–797.

[66] Xia, X.-D.; Xuan, J.; Wang, Q.; Lu, L.-Q.; Chen, J.-R.; Xiao, W.-J. Synthesis of 2-Substituted Indoles through Visible Light-Induced Photocatalytic Cyclizations of Styryl Azides. *Adv. Synth. Catal.* **2014**, *356*, 2807–2812.

[67] Ma, J.; Zhang, X.; Huang, X.; Luo, S.; Meggers, E. Preparation of Chiral-at-Metal Catalysts and Their use in Asymmetric Photoredox Chemistry. *Nat. Protoc.* **2018**, *13*, 605–632.

[68] Chen, L.-A.; Xu, W.; Huang, B.; Ma, J.; Wang, L.; Xi, J.; Harms, K.; Gong, L.; Meggers, E. Asymmetric Catalysis with an Inert Chiral-at-Metal Iridium Complex. *J. Am. Chem. Soc.* **2013**, *135*, 10598−10601.

[69] Chen, L.-A.; Tang, X.; Xi, J.; Xu, W.; Gong, L.; Meggers, E. Chiral-at-Metal Octahedral Iridium Catalyst for the Asymmetric Construction of an All-Carbon Quaternary Stereocenter. *Angew. Chem. Int. Ed.* **2013**, *52*, 14021−14025.

[70] Ma, J.; Ding, X.; Hu, Y.; Huang, Y.; Gong, L.; Meggers, E. Metal-Templated Chiral Brønsted Base Organocatalysis. *Nat. Commun.* **2014**, *5*, 4531.

[71] Huo, H.; Fu, C.; Wang, C.; Harms, K.; Meggers, E. Metal-Templated Enantioselective Enamine/H-Bonding Dual Activation Catalysis. *Chem. Commun.* **2014**, *50*, 10409−104111.

[72] Huo, H.; Fu, C.; Harms, K.; Meggers, E. Asymmetric Catalysis with Substitutionally Labile yet Stereochemically Stable Chiral-at-Metal Iridium(III) Complex. *J. Am. Chem. Soc.* **2014**, *136*, 2990–2993.

[73] Shen, X.; Huo, H.; Wang, C.; Zhang, B.; Harms, K.; Meggers, E. Octahedral Chiral-at-Metal Iridium Catalysts: Versatile Chiral Lewis Acids for Asymmetric Conjugate Additions. *Chem. Eur. J.* **2015**, *21*, 9720–9726.

[74] Tian, C.; Gong, L.; Meggers, E. Chiral-at-metal iridium complex for efficient enantioselective transfer hydrogenation of ketones. *Chem. Commun.* **2016**, *52*, 4207–4210.

[75] Huo, H.; Shen, X.; Wang, C.; Zhang, L.; Röse, P.; Chen, L. A.; Harms, K.; Marsch, M.; Hilt, G.; Meggers, E. Asymmetric Photoredox Transition-Metal Catalysis Activated by Visible Light. *Nature* **2014**, *515*, 100–103.

[76] Zhang, L.; Meggers, E. Steering Asymmetric Lewis Acid Catalysis Exclusively with Octahedral Metal-Centered Chirality. *Acc. Chem. Res.* **2017**, *50*, 320–330.

[77] Chiral Lanthanide complexes have been shown to perform asymmetric energy transfer to inorganic scaffolds. Notably, this examples focus on the stereoselective energy transfer toa racemic mixture, rather than the creation of a new stereocenter from an achiral molecule. For more information on this subject, see chapter 1.

[78] A notable example was demonstrated by our group using *rac*-$[Ru(bpy)_3][PF_6]$ to perform triplet energy transfer to chiral Lewis acid bound 2'-hydroxychalcones effect the stereochemical outcome of its [2+2] cycloaddition with alkenes. In this reaction the pre-complexation of a BOX-ligated Scandium to the starting material lowers the chalcone's triplet energy, activation it for energy transfer. For more information, see: Blum, T. R.; Miller, Z. D.; Bates, D. M.; Guzei, I. A.; Yoon, T. P. Enantioselective photochemistry through Lewis acid–catalyzed triplet energy transfer. *Science* **2016**, *354*, 1391–1395.

[79] Baldwin, J. E. Rules for Ring Closure. *J.C.S. Chem. Comm.* **1976**, 734–736.

[80] Müller, C.; Bauer, A.; Maturi, M. M.; Cuquerella, M. C.; Miranda, M. A.; Bach, T. Enantioselective Intramolecular [2+2] Photocycloaddition Reactions of 4-Substituted Quinolones Catalyzed by a Chiral Sensitizer with a Hydrogen-Bonding Motif. *J. Am. Chem. Soc.* **2011**, *133*, 16689–16697.

[81] Huang, X.; Quinn, T. R.; Harms, K.; Webster, R. D.; Zhang, L.; Wiest, O.; Meggers, E. Direct Visible-Light-Excited Asymmetric Lewis Acid Catalysis of Intermolecular [2+2] Photocycloadditions. *J. Am. Chem. Soc.* **2017**, *139*, 9120–9123.

[82] For a review, see: Brenninger, C.; Jolliffe, J. D.; Bach, T. Chromophore Activation of α,β-Unsaturated Carbonyl Compounds and Its Application to Enantioselective Photochemical Reactions. *Angew. Chem. Int. Ed.* **2018**, *57*, 14338 – 14349.

[83] Maturi, M. M.; Wenninger, M.; Alonso, R.; Bauer, A.; Pöthig, A.; Riedle, E.; Bach, T. Intramolecular [2+2] Photocycloaddition of 3- and 4-(But-3-enyl)oxyquinolones: Influence of the Alkene Substitution Pattern, Photophysical Studies, and Enantioselective Catalysis by a Chiral Sensitizer. *Chem. Eur. J.* **2013**, *19*, 7461–7472.

[84] Bauer, A.; Alonso Ruiz, R. "Templated Enantioselective Photocatalysis." In *Chemical Photocatalysis*; König, B., Ed.; De Gruyter: Berlin, 2013; pp 67–90.

[85] Prepared by crossed Claisen condensation following the procedure of Bunting and Kanter (Acidity and Tautomerism of β-Keto Esters and Amides in Aqueous Solution. *J. Am. Chem. Soc.* **115**, 11705–11715 (1993)), which provided an 80:20 mixture of keto and enol tautomers. The chemical shifts of the major (keto) isomer were consistent with those in the literature (Alves, M.

J.; Fortes, A. G.; Lemos, A.; Martins, C. Ethyl 3-(2-Pyridyl)-2H-azirine-2-carboxylate: Synthesis and Reaction with Dienes. *Synthesis* **4**, 0555–0558 (2005)).

[86] Potts, K. T.; Ralli, P.; Theodoridis, G.; Winslow, P. 2,2' : 6',2'-Terpyridine. *Org. Synth.* **64**, 189 (1986).

[87] Hewawasam, P.; Meanwell, N. A. A General Method for the Synthesis of Isatins: Preparation of Regiospecifically Functionalized Isatins from Anilines. *Tetrahedron Lett.* **35**, 7303–7306 (1994).

[88] Ghosh, A. K. & Nicponski, D. R. Cu(II)-Catalyzed Olefin Migration and Prins Cyclization : Highly Diastereoselective Synthesis of Substituted Tetrahydropyrans. *Org. Lett.* **13**, 4328–4331 (2011).

[89] Shi, W.; Nacev, B. A.; Aftab, B. T.; Head, S.; Rudin, C. M.; Liu, J. O. Itraconazole Side Chain Analogues: Structure-Activity Relationship Studies for Inhibition of Endothelial Cell Proliferation, Vascular Endothelial Growth Factor Receptor 2 (VEGFR2) Glycosylation, and Hedgehog Signaling. *J. Med. Chem.* **54**, 7363–7374 (2011).

[90] Kim, S., Lawson, J. A., Pratico, D., Fitzgerald, A. & Rokach, J. The first total synthesis of $iPF_{4\alpha}$-VI and its deuterated analog. *Tetrahedron Lett.* **43**, 2801–2805 (2002).

[91] McCormick, J. P.; Barton, Donald, L. Synthetic applications of metal halides. Conversion of cyclopropylmethanols into homoallylic halides. *J. Org. Chem.* **1980**, *45*, 2566–-2570.
[92] Lowry, M. S.; Goldsmith, J. I.; Slinker, J. D.; Rohl, R.; Pascal, R. A., Jr.; Malliaras, G. G.; Bernhard, S. Single-Layer Electroluminescent Devices and Photoinduced Hydrogen Production from an Ionic Iridium(III) Complex. *Chem. Mater.* **17**, 5712–5719 (2005).

[93] Harris, R. K.; Becker, E. D.; de Menezes, S. M. C.; Goodfellow, R.; Granger, P. NMR Nomenclature. Nuclear Spin Properties and Conventions for Chemical Shifts. *Pure Appl. Chem.* **73**, 1795–1818 (2001).

[94] Harris, R. K.; Becker, E. D.; de Menezes, S. M. C.; Granger, P.; Hoffman, R. E.; Zilm, K. W. Further Conventions for NMR Shielding and Chemical Shifts. *Pure Appl. Chem.* **80**, 59–84 (2008).

[95] McEwen, C. N.; McKay, R. G.; Larsen, B. S. Analysis of Solids, Liquids, and Biological Tissues Using Solids Probe Introduction at Atmospheric Pressure on Commercial LC/MS Instruments. *Anal. Chem.* **77**, 7826–7831 (2005).

[96] Bolm, C.; Weickhardt, K.; Zehnder, M.; Ranff, T. Synthesis of Optically Active Bis(2-oxazolines): Crystal Structure of a 1,2-Bis(2-oxazolinyl)benzene•ZnCl2 Complex. *Chem. Ber.* **124**, 1173–1180 (1991).

[97] Shen, X.; Huo, H.; Wang, C.; Zhang, B.; Harms, K.; Meggers, E. Octahedral Chiral-at-Metal Iridium Catalysts: Versatile Chiral Lewis Acids for Asymmetric Conjugate Additions. *Chem. Eur. J.* **21**, 9720–9726 (2015).

[98] Chen, L.-A.; Xu, W.; Huang, B.; Ma, J.; Wang, L.; Xi, J.; Harms, K.; Gong, L.; Meggers, E. Asymmetric Catalysis with an Inert Chiral-at-Metal Iridium Complex. *J. Am. Chem. Soc.* **135**, 10598–10601 (2013).

[99] Pask, C. M.; Camm, K. D.; Kilner, C. A.; Halcrow, M. A. Synthesis of a new series of ditopic proligands for metal salts: Differing regiochemistry of electrophilic attack at 3{5}-amino-5{3}-(pyrid-2-yl)-1H-pyrazole. *Tetrahedron Lett.* **47**, 2531–2534 (2006).

[100] Note that the ^{13}C NMR spectra of several hydrogen bonding ligands appear to have fewer than the expected number of ^{13}C signals. Close examination shows several extremely broad carbon peaks, presumably due to tautomerization of the pyrazole occurring on the NMR timescale. Our attempts to alter this process by changing solvent or temperature were ineffective, but we found that the corresponding HCl salts exhibited clean, sharp, and well-resolved ^{13}C signals. For these compounds, ^{1}H and ^{13}C data are provided for the salt (or both), but other characterization data are for the free base.

A general procedure for protonation is as follows: A 2 dram vial was charged with free base (0.25 mmol, 1.0 equiv.) and CH_2Cl_2 (2.5 mL). After sonication, etheral HCl (2 M in Et_2O, 125 µL, 1.0 equiv.) was added, resulting in immediate precipitation of a solid. After stirring for several minutes, the solvent was removed by rotary evaporation, leaving the corresponding HCl salt as a powder.

[101] Pleier, A.-K.; Glas, H.; Grosche, M.; Sirsch, P.; Thiel, W. R. Microwave Assisted Synthesis of 1-Aryl-3-dimethylaminoprop-2-enones: A Simple and Rapid Access to 3(5)-Arylpyrazoles. *Synthesis* **1**, 55–62 (2001).

[102] Note that ^{13}C NMR spectra are not reported for these compounds. Strong coupling with the highly fluorinated ppy ligands results in low signal-to-noise ratios and complicated spectra. This is further exacerbated by the pseudo-C_2 equivalence of the complexes, which results in doubled signals for all ppy nuclei. Two-dimensional NMR data can be used to corroborate assignments (see Section 8), but interpretation of simple 1D ^{13}C spectra is impractical.

[103] Paterna, R.; André, V.; Duarte, M. T.; Veiros, L. F.; Candeias, N. R.; Gois, P. M. P. Ring-expansion reaction of isatins with ethyl diazoacetate catalyzed by dirhodium(II)/DBU metal-organic system: En route to viridicatin alkaloids. *Eur. J. Org. Chem.* **28**, 6280–6290 (2013).

[104] Sagong, H. Y.; Parhi, A.; Bauman, J. D.; Patel, D.; Vijayan, R. S. K.; Das, K.; Arnold, E.; LaVoie, E. J. 3-Hydroxyquinolin-2(1H)-ones As Inhibitors of Influenza A Endonuclease. *ACS Med. Chem. Lett.* **4**, 547–550 (2013).

[105] Maturi, M. M.; Wenninger, M.; Alonso, R.; Bauer, A.; Pöthig, A.; Riedle, E.; Bach, T. Intramolecular [2+2] Photocycloaddition of 3- and 4-(But-3- enyl)oxyquinolones: Influence of

the Alkene Substitution Pattern, Photophysical Studies, and Enantioselective Catalysis by a Chiral Sensitizer. *Chem. Eur. J.* **19**, 7461–7472 (2013).

[106] When synthesizing the racemic standard, the conditions in General Procedure H gave roughly 25% of de-iodinated product alongside the desired cyclobutane. These species could not be readily separated. To circumvent this problem, we synthesized racemic cyclobutane using the asymmetric conditions (General Procedure I), but with (±)-**6**.

[107] When synthesizing the racemic standard, the conditions in General Procedure H gave small amounts of a species consistent with benzylic oxidation of the methyl group. This side product could not be readily separated. To circumvent this problem, we synthesized racemic cyclobutane using the asymmetric conditions (General Procedure I), but with (±)-**6**.

[108] Bakowski, A.; Dressel, M.; Bauer, A.; Bach, T. *Org. Biomol. Chem.* **2011**, *9*, 3516.

[109] Thordarson, P. Determining association constants from titration experiments in supramolecular chemistry. *Chem. Soc. Rev.* **40**, 1305–1323 (2011).

[110] Cismesia, M. A.; Yoon, T. P. Characterizing chain processes in visible light photoredox catalysis. *Chem. Sci.* **6**, 5426–5434 (2015).

[111] Rehm, D.; Weller, A. Kinetics of Fluorescence Quenching by Electron and H–Atom Transfer. *Isr. J. Chem.* **8**, 259–271 (1970).

[112] Ballardini, R.; Varani, G.; Indelli, M. T.; Scandola, F.; Balzani, V. Free Energy Correlation of Rate Constants for Electron Transfer Quenching of Excited Transition Metal Complexes. *J. Am. Chem. Soc.* **100**, 7219–7223 (1978).

[113] McClure, L. J.; Ford, P. C. Ligand Macrocycle Effects on the Photophysical Properties of Rhodium(III) Complexes. A Detailed Investigation of cis- and trans-Dicyano(l14,8,11-tetraazacyclotetradecane)rhodium(III) and Related Species. *J. Phys. Chem.* **96**, 6640–6650 (1992).

[114] Døssing, A.; Ryu, C. K.; Kudo, S.; Ford, P. C. Competitive Bimolecular Electron- and Energy-Transfer Quenching of the Excited State(s) of the Tetranuclear Copper(I) Cluster $Cu_4I_4py_4$. Evidence for Large Reorganization Energies in an Excited-State Electron Transfer. *J. Am. Chem. Soc.* **115**, 5132–5137 (1993).

[115] Zhu, Q.; Gentry, E. C.; Knowles, R. R. Catalytic Carbocation Generation Enabled by the Mesolytic Cleavage of Alkoxyamine Radical Cations. *Angew. Chem. Int. Ed.* **55**, 9969–9973 (2013).

[116] Parr, R. G.; Yang, W. *Density Functional Theory of Atoms and Molecules*. (Oxford University Press: New York, 1989).

[117] Bochevarov, A. D.; Harder, E.; Hughes, T. F.; Greenwood, J. R.; Braden, D. A.; Philipp, D. M.; Rinaldo, D.; Halls, M. D.; Zhang, J.; Friesner, R. A. Jaguar: A High-Performance Quantum Chemistry Software Program with Strengths in Life and Materials Sciences. *Int. J. Quantum Chem.* **113**, 2110–2142 (2013).

[118] Becke, A. D. Density-functional thermochemistry. III. The role of exact exchange. *J. Chem. Phys.* **98**, 5648–5652 (1993).

[119] Lee, C. T.; Yang, W.; Parr, R. G. Development of the Colle-Salvetti correlation-energy formula into a functional of the electron density. *Phys. Rev. B* **37**, 785–789 (1988).

[120] Grimme, S.; Antony, J.; Ehrlich, S.; Krieg, H. A consistent and accurate ab initio parametrization of density functional dispersion correction (DFT-D) for the 94 elements H-Pu. *J. Chem. Phys.* **2010**, *132*, 154104.

[121] Ditchfield, R.; Hehre, W. J.; Pople, J. A. Self-Consistent Molecular-Orbital Methods. IX. An Extended Gaussian-Type Basis for Molecular-Orbital Studies of Organic Molecules. *J. Chem. Phys.* **54**, 724–728 (1971).

[122] Hay, P. J.; Wadt, W. R. *Ab initio* effective core potentials for molecular calculations. Potentials for the transition metal atoms Sc to Hg. *J. Chem. Phys.* **82**, 270–283 (1985).

[123] Wadt, W. R.; Hay, P. J. Ab initio effective core potentials for molecular calculations. Potentials for main group elements Na to Bi. *J. Chem. Phys.* **82**, 284–298 (1985).

[124] Hay, P. J.; Wadt, W. R. *Ab initio* effective core potentials for molecular calculations. Potentials for K to Au including the outermost core orbitals. *J. Chem. Phys.* **82**, 299–310 (1985).

[125] Zhao, Y.; Truhlar, D. G. The M06 suite of density functionals for main group thermochemistry, thermochemical kinetics, noncovalent interactions, excited states, and transition elements: two new functionals and systematic testing of four M06-class functionals and 12 other functionals. *Theor. Chem. Acc.* **120**, 215–241 (2008).

[126] Dunning, T. H., Jr. Gaussian basis sets for use in correlated molecular calculations. I. The atoms boron through neon and hydrogen. *J. Chem. Phys.* **90**, 1007–1023 (1989).

[127] Marten, B.; Kim, K.; Cortis, C.; Friesner, R. A.; Murphy, R. B.; Ringnalda, M. N.; Sitkoff, D.; Honig, B. New Model for Calculation of Solvation Free Energies: Correction of Self-Consistent Reaction Field Continuum Dielectric Theory for Short-Range Hydrogen-Bonding Effects. *J. Phys. Chem.* **100**, 11775–11788 (1996).

[128] Edinger, S. R.; Cortis, C.; Shenkin, P. S.; Friesner, R. A. Solvation Free Energies of Peptides: Comparison of Approximate Continuum Solvation Models with Accurate Solution of the Poisson-Boltzmann Equation. *J. Phys. Chem. B* **101**, 1190–1197 (1997).

[129] Friedrichs, M.; Zhou, R. H.; Edinger, S. R.; Friesner, R. A. Poisson-Boltzmann Analytical Gradients for Molecular Modeling Calculations. *J. Phys. Chem. B* **103**, 3057–3061 (1999).

Chapter 3. Enantioselective Intermolecular Excited-State Photoreactions Using a Chiral Ir Triplet Sensitizer: Separating Association from Energy Transfer in Asymmetric Photocatalysis

Portions of this work have been published previously:

Zheng, J.; Swords, W. B.; Jung, H.; Skubi, K. L.; Kidd, J. B.; Meyer, G. J.; Baik, M. –H.; Yoon, T. Enantioselective Intermolecular Excited-State Photoreactions Using a Chiral Ir Triplet Sensitizer: Separating Association from Energy Transfer. *J. Am. Chem. Soc.*, **2019**, *141*, 13625-13634.

3.1 Introduction

3.1.1 Stereocontrol of Excited-State Intermolecular Reactions

Asymmetric catalysis has been a central theme in synthetic organic chemistry for many decades. However, enantioselective catalysis of photochemical reactions has only recently been proven to be feasible.[1–4] The central challenges in asymmetric excited-state photochemistry derive from the existence of unimolecular relaxation pathways that provide a rapid mechanism for deactivation of the key reactive intermediates in photochemical reactions. The intrinsic lifetimes of these electronically excited intermediates are generally quite short (ps to ns), and thus their ability to engage in bimolecular interactions, either with chiral enantiocontrolling catalysts or with other reaction partners, is usually limited.[5] The literature of asymmetric excited-state photoreactions has consequently been dominated by intramolecular transformations, where local proximity effects enable product-forming reactions to compete with unproductive relaxation. Only a handful of known asymmetric catalytic photocycloaddition reactions are effective in an intermolecular context.

3.1.2 Hydrogen-Bonding Organic Photocatalysts

All examples of highly enantioselective excited-state photoreactions reported to date rely upon strong ground-state preassociation between the organic substrate and a chiral catalyst prior to its excitation. Arguably the most successful general strategies to date have involved chiral photosensitizers functionalized with a hydrogen-bonding domain that organizes the substrate proximal to a sensitizing organic chromophore such as an aromatic ketone[6] or binaphthyl unit.[7] This design principle ensures that the electronically excited intermediate is generated exclusively within the stereodifferentiating environment of the chiral catalyst. Additionally, this approach

obviates the need to intercept a fleeting excited-state intermediate with a low-concentration chiral catalyst, thereby circumventing one underlying limitation of excited-state photoreactions.[2,8]

Bach pioneered such a system using a chiral catalyst **3.4**, bearing a hydrogen-bonding motif to preorganize a substrate, prior to its sensitization by an appended xanthone photocatalyst.[9,10] In 2014, this catalyst was applied to the design of an intermolecular [2+2] cyclization of pyridones with acetylenedicarboxylates to afford cyclobutene products in enantiomeric excess up to 92% (Scheme 3.1).[11] At –25 °C, the enantioselectivity of the photoreaction was found to positively correlate with the excess of alkyne **3.2**, plateauing at 50 equiv. It was proposed that higher concentrations of the alkyne coupling partner increase the rate of the bimolecular reaction while suppressing the likelihood of racemic cyclization with **3.2** following dissociation of excited-state **3.1** from **3.4**. The same phenomenon was suspected of the photochemical rearrangement of spirooxindole epoxides, in which poor selectivity (up to 33% ee) is believed to arise from a slow rate of rearrangement relative to substrate dissociation.[12]

Scheme 3.1. Enantioselective Intermolecular [2+2] of Pyridones and Acetylenedicarboxylates

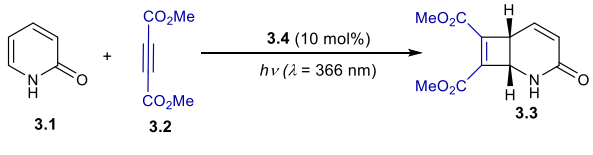

c (mM)	temp.	TFT/HFX	t (h)	**3.2** (equiv)	yield	ee
10	–25 °C	1:0	2	10	42%	22%
10	–25 °C	1:0	1	50	40%	42%
10	–25 °C	1:0	1	100	42%	42%
20	–25 °C	1:0	3	100	61%	44%
20	–65 °C	1:2	1	50	55%	48%

Although catalyst **3.4** was successful in the development of several asymmetric photoreactions (see Chapter 2.1.2), there were several problems that posed limitations in improving this methodology. Firstly, the xanthone chromophore is exceptionally active toward

hydrogen-atom abstraction in toluene, photobleaching in less than 10 minutes under irradiation with 366 nm light, limiting the choice of reaction solvents.[13] This catalyst also does not significantly absorb in the visible region, necessitating irradiation at shorter wavelengths that have a greater possibility of photoexciting unbound substrate. The Bach group found that the replacement of this chromophore with thioxanthone solves both problems: it has higher stability under irradiation in toluene and possesses high molar absorptivity coefficients in the visible. Moreover, catalyst **3.10** was shown to be a proficient chiral controller of a sufficiently high triplet energy (64 kcal/mol) to promote the intramolecular [2+2] cycloaddition of alkene-tethered quinolones affording the cycloadducts in up to 96% ee.[13]

Scheme 3.2. Intermolecular [2+2] Cycloaddition Catalyzed by a Thioxanthone Sensitizer

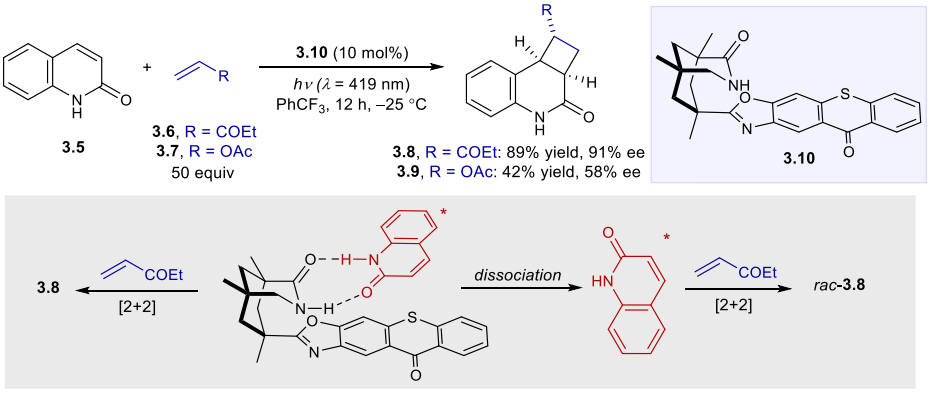

Subsequently, this thioxanthone photocatalyst was applied to the intermolecular [2+2] cycloaddition of quinolone **3.5** with a variety of alkene coupling partners to yield the corresponding cyclobutane products in enantioselectivities up to 95% (Scheme 3.2).[14] However, the alkene partner was limited to abundantly available olefins due to the large excess necessary to achieve high enantioselectivity. Similar to the previous example, 50 equiv of the coupling partner were needed to ensure cyclization prior to dissociation of the sensitized quinolone from the influence of the chiral catalyst. From this analysis, a slower-reacting alkene should exhibit lower

enantioselectivity. Correspondingly, vinyl acetate reacts an order of magnitude slower than ethyl vinyl ketone and consequently afforded products in substantially lower ee (58% ee vs. 91% ee).

3.1.3 Chiral Lewis Acids

An alternative strategy to control the stereochemical outcome of a primary photoreaction involves the use of a chiral Lewis acid. Early work by the Bach group demonstrated that chiral $AlBr_3$-activated oxazaborolidine Lewis acids are capable of inducing a bathochromic shift of the (π,π*) absorption band upon complexation with α,β-unsaturated carbonyl substrates.[15,16] Bach termed this phenomenon "chromophore activation" and proposed that it could be exploited in the design of asymmetric photoreactions by selective excitation of the catalyst–substrate complex. This ensures the generation of the excited-state intermediate within the influence of the chiral catalyst, while minimizing direct racemic photoreaction. Indeed, chromophore activation was found to be an effective method for the enantiocontrol for a variety of intramolecular photoreactions.[17]

Bach and coworkers applied this design strategy to intermolecular cycloadditions of simple cyclohexanones with terminal alkenes, achieving excellent enantioselectivities in up to 91% (Scheme 3.3).[18] However, high loadings (50 mol%) of chiral Lewis acid **3.14** was necessary to outcompete fast racemic reaction that stems from direct photoexcitation of cyclohexenone.

Scheme 3.3. Intermolecular [2+2] Cycloaddition Using Chromophore Activation

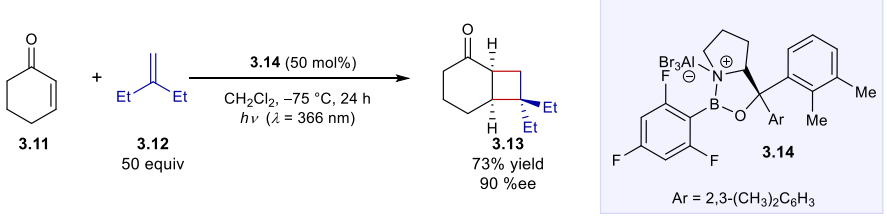

Moreover, despite the synthetic utility of this methodology,[19] the practicality of the photocycloaddition is restricted to the use of simple, feedstock olefins in high excess (50 equiv).

Recently, the synthetic community has been interested in the ability of transition metal complexes to serve as triplet sensitizers in organic photoreactions.[20–25] We have argued that these complexes feature several key advantages over organic chromophores: these complexes strongly absorb visible light, minimizing the direct excitation of organic substrates, they possess superior chemical stability and longer excited-state lifetimes, and they can tolerate substantial structural modifications that facilitate the tuning of the structural and photophysical properties necessary for effective photocatalysis. In 2016, our group reported a dual catalytic strategy employing both a transition metal photosensitizer and a chiral PyBox–ligated scandium Lewis acid to enable the excited-state [2+2] cycloaddition of 2'-hydroxychalcones and dienes[26] — and later styrenes[27] — affording the cyclobutene products in high ee (Scheme 3.4). Similar to the change in photophysics

Scheme 3.4. Triplet Lowering Mechanism Enabled by Dual Catalytic Strategy

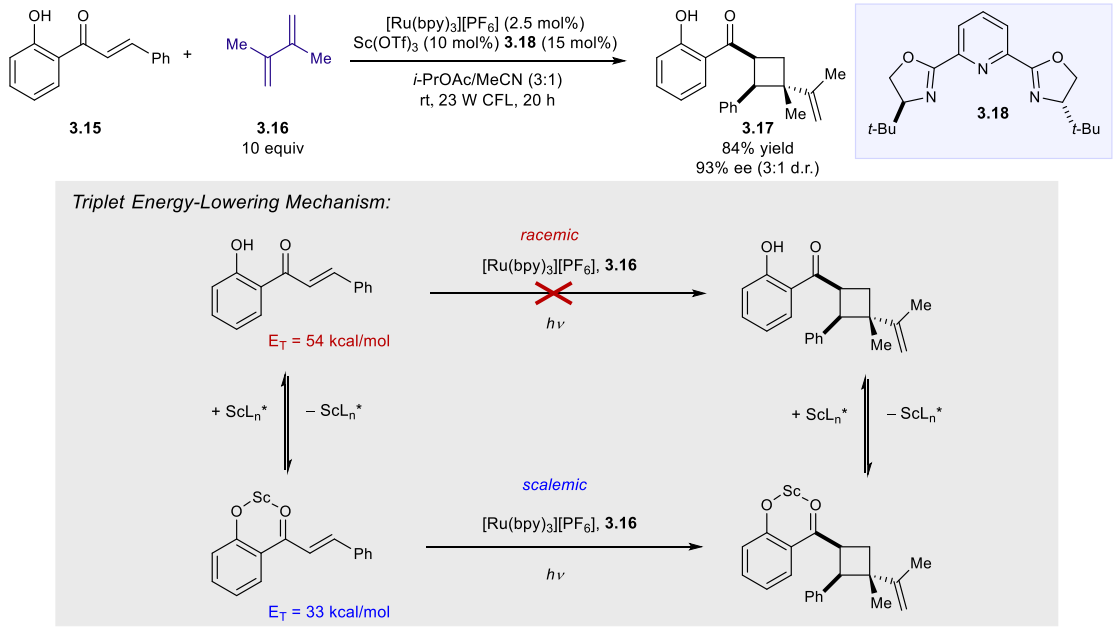

observed in chromophore activation protocols, the crux of this method hinges on the complexation of the Lewis acid to the chalcone substrate, lowering its triplet energy, rendering Dexter energy transfer from photoexcited $Ru(bpy)_3(PF_6)$ thermodynamically feasible. Photoactivation of the substrate in this manner generates its excited state within a chiral environment while minimizing the rate of background reaction.

Meggers has developed a family of enantiopure, helically chiral Ir and Rh organometallic complexes that serve as photocatalysts in a remarkable variety of highly stereoselective transformations.[28–30] While most of these have been photoredox reactions,[31–36] in which the key bond-forming steps are ground-state radical reactions, recent efforts have also demonstrated that chiral-at-metal Rh Lewis acids offer exceptional chiral environments for photoreactions of electronically excited organic intermediates as well (Scheme 3.5).[37–39] These chiral Lewis acids, similar to the oxazaborolidines utilized by Bach, slow racemic photoreaction through the selective excitation of the catalyst–substrate adduct by a chromophore activation mechanism.[40]

While these examples demonstrate proof-of-principle of enantioselective intermolecular primary photoreactions they are not without significant drawbacks. When a hydrogen-bonding organic photocatalyst is used, a large excess of alkene coupling partner is required to counteract the rate of dissociation of the substrate from the chiral catalyst, limiting the methods' practicality. Moreover, the (thio)xanthone photocatalyst is highly specialized, in which small structural or electronic perturbations can lead to large changes in its photophysics, restricting its broad applicability as a chiral catalyst. When Lewis acids are employed instead, substrates are limited to those that exhibit substantial photophysical changes upon binding which is accompanied by careful balancing of the absorption profiles of the bound and unbound substrate and the irradiation wavelength.

Scheme 3.5. Chromophore Activation Using Chiral Rhodium Lewis Acids

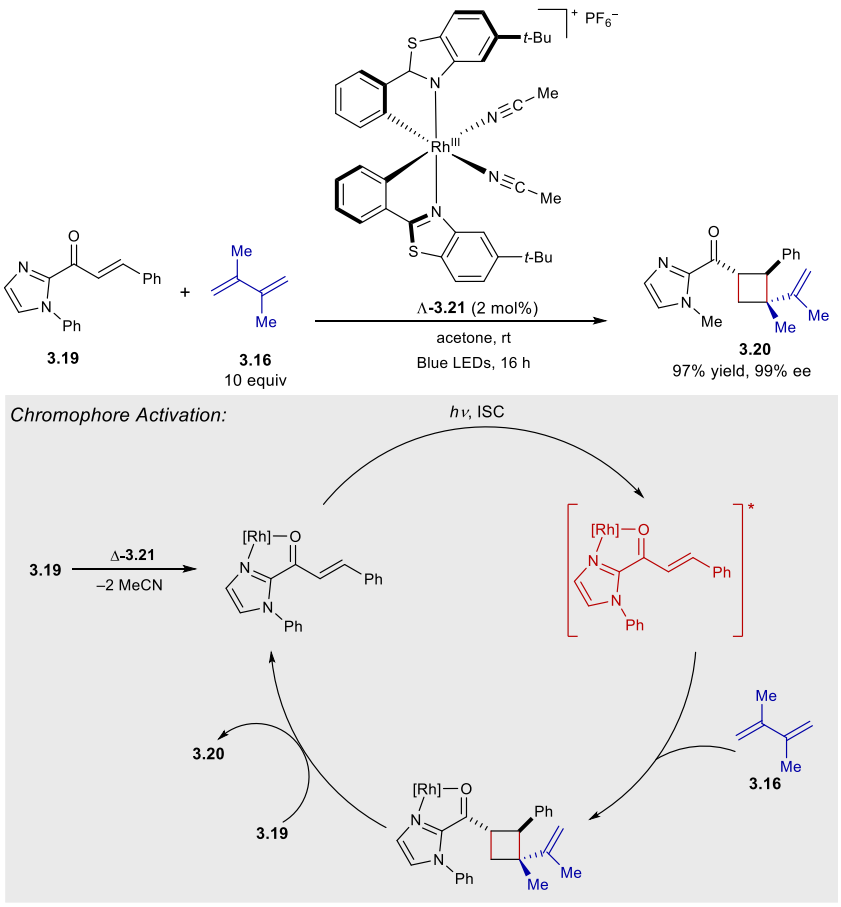

3.1.4 Prior Work

We recently reported that an Ir complex bearing a pyridylpyrazole hydrogen-bonding domain can be used as an asymmetric triplet sensitizer, enabling the exceptionally efficient and highly enantioselective catalysis of [2+2] photocycloadditions of quinolones (Scheme 3.6).[41] The structure of the Ir complex can be tuned for optimal reactivity without deleteriously impacting its ability to act as a triplet sensitizer, which suggests that this family of hydrogen-bonding organometallic photosensitizers might offer an important complement to conceptually similar chiral organic photosensitizers. Consistent with the criteria outlined in chapter 2 for rendering a primary photoreaction asymmetric, the quinolone **3.22** was found to bind with the iridium

photocatalyst in the ground state, prior to sensitization via an intracomplex Dexter energy transfer (DET). This ensures that the enantiodetermining bond formation occurs within the chiral environment induced by the catalyst.

Scheme 3.6. Enantioselective Intramolecular [2+2] Cycloaddition Using Chiral Ir Photocatalyst

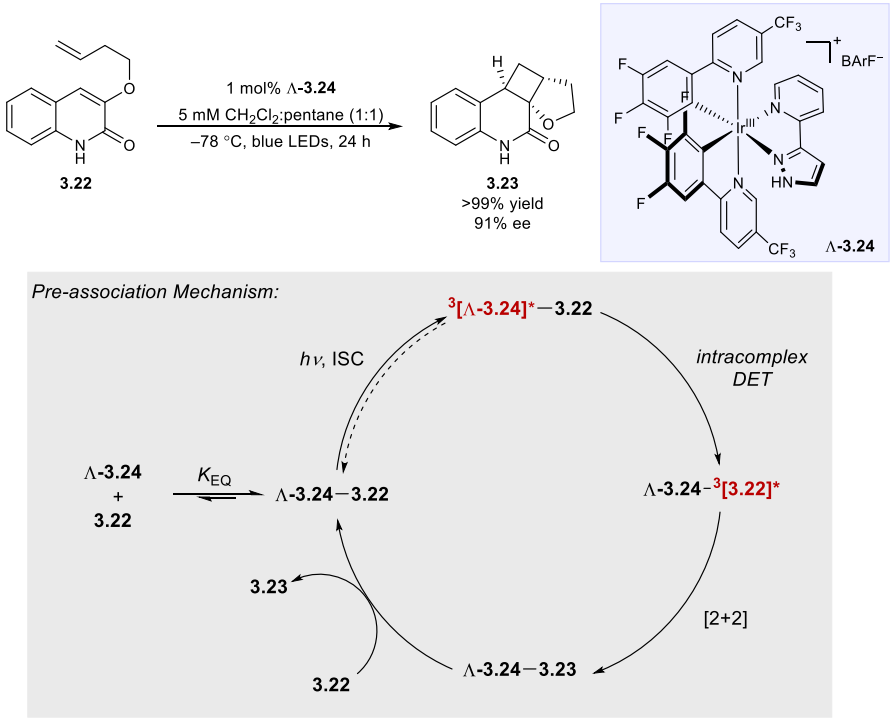

However, the scope of the reaction was limited to intramolecular cycloaddition reactions. Herein, we describe studies that led to the development of a highly enantioselective intermolecular [2+2] photocycloaddition reaction using a structurally modified chiral Ir sensitizer. Importantly, photoluminescence quenching and transient absorption studies suggest that, in contrast to the above work from our group and others, the excited-state reactant is generated *outside* of the binding domain of the chiral sensitizer. The identification of this novel mechanism contradicts the long-standing principle that has informed previous approaches to enantioselective catalysis of excited-

state photoreactions and suggests a new and potentially more general strategy for asymmetric photocatalysis.

3.2 Results and Discussion

3.2.1 Optimization of Quinolone and Photocatalyst Structure

Our studies began by screening the reaction of 3-*n*-butoxyquinolone (**3.25a**) and 5 equiv of maleimide (**3.26**) upon visible light irradiation at –78 °C in the presence of Ir complex Λ-**3.28a**, which had proven to be the optimal photocatalyst for the intramolecular cycloaddition (Table 3.1, entry 1). However, the rate of this probe reaction was prohibitively slow, consistent with the general trend that intermolecular photocycloadditions are substantially less efficient than intramolecular reactions. The rate could be improved by conducting the reaction at ambient temperature; however, the product was formed with negligible ee (entry 2). Because the iridium center defines the stereogenic unit of this photocatalyst, we speculated that the identity of both the cyclometalating phenylpyridine (ppy) and hydrogen-bonding ligands would have a substantial impact on enantioinduction. Indeed, alterations to the ppy ligand had a pronounced impact on ee, with ligand **A4** providing the cycloadduct in 19% ee (entry 5). The structure of the hydrogen-bonding ligand had less of an effect, although methoxy-substituted ligand **B3** afforded a modest improvement in ee (entry 7). The identity of the 3-alkoxy group on the quinolone substrate had a much larger impact on stereoselectivity. Methoxy quinolone **3.25b** provided significantly higher ee without loss of reactivity (entry 8), and isopropoxy-substituted analogue **3.25c** offered both higher yield and ee (entry 9). Because of this increased reactivity, we were able to lower the temperature to –78°C and achieve complete conversion to cycloadduct **3.25c** in 97% ee (entry 10). Finally, control experiments revealed that product formation required both light and photocatalyst,

validating the photocatalytic nature of this reaction (entries 11 and 12). Under these optimized conditions we measured a quantum yield of 1.3% for the optimized reaction between **3.25c** and **3.26**.

Table 3.1. Optimization Studies for the Intermolecular [2+2] Photocycloaddition

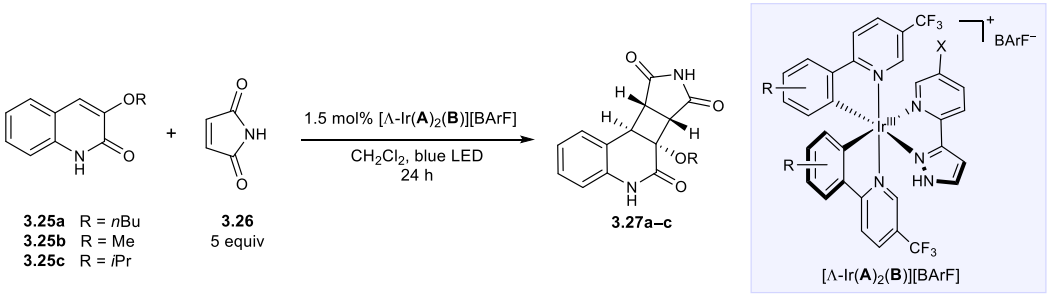

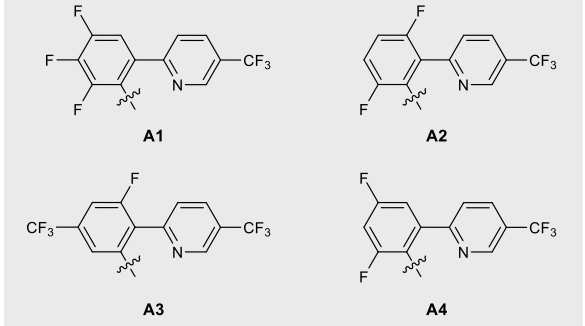

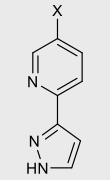

B1 X = H
B2 X = CF_3
B3 X = OMe

entry	quinolone	photocatalyst	temp.	yield	ee
1	**3.25a**	**3.28a** [Λ-Ir(**A1**)$_2$(**B1**)][BArF]	–78 °C	14%	--
2	**3.25a**	**3.28a** [Λ-Ir(**A1**)$_2$(**B1**)][BArF]	23 °C	60%	2%
3	**3.25a**	**3.28b** [Λ-Ir(**A2**)$_2$(**B1**)][BArF]	23 °C	74%	12%
4	**3.25a**	**3.28c** [Λ-Ir(**A3**)$_2$(**B1**)][BArF]	23 °C	63%	1%
5	**3.25a**	**3.28d** [Λ-Ir(**A4**)$_2$(**B1**)][BArF]	23 °C	60%	19%
6	**3.25a**	**3.28e** [Λ-Ir(**A4**)$_2$(**B2**)][BArF]	23 °C	55%	10%
7	**3.25a**	**3.28f** [Λ-Ir(**A4**)$_2$(**B3**)][BArF]	23 °C	54%	21%
8	**3.25b**	**3.28f** [Λ-Ir(**A4**)$_2$(**B3**)][BArF]	23 °C	52%	44%
9	**3.25c**	**3.28f** [Λ-Ir(**A4**)$_2$(**B3**)][BArF]	23 °C	72%	51%
10	**3.25c**	**3.28f** [Λ-Ir(**A4**)$_2$(**B3**)][BArF]	–78 °C	85%	97%
11[b]	**3.25c**	**3.28f** [Λ-Ir(**A4**)$_2$(**B3**)][BArF]	–78 °C	0%	--
12	**3.25c**	none	–78 °C	0%	--

[a] Reactions conducted using 0.20 mmol of quinolone and 5 equiv maleimide with a 15 W LED lamp unless otherwise noted. [b] Reaction conducted in the dark.

3.2.2 Reaction Scope and Limitations

Experiments probing the scope of this reaction are summarized in Table 3.2. First, we verified that the identity of the 3-alkoxy substituent is critical for the success of the enantioselective photocycloaddition. Both 3-*n*-butoxy and 3-methoxy quinolones reacted with lower ee (**3.27a** and **3.27b**), and quinolones lacking this 3-substituent failed to react at all (**3.27d**). The reaction, however, proved less sensitive to substitutions at other positions on the quinolone ring. We examined the effect of substitution at the 6-position of the quinolone and found that substrates bearing alkyl, halogen, and alkoxy groups all reacted to afford [2+2] cycloadducts in high enantioselectivity and good diastereoselectivity (**3.27g**–**i**), although electron-rich 6-methoxyquinolone reacted sluggishly and required longer reaction times to afford reasonable yields of the cycloadduct (**3.27i**). The product of cycloaddition with 6-iodoquinoline (**3.27f**) was highly crystalline, and X-ray analysis of this compound enabled us to assign the absolute and relative configuration of the product.[42] Substitution at the 7-position of the quinolone had minimal effect on the success of the cycloaddition (**3.27j**, **3.27k**). Substitutions proximal to the reacting C=C bond of the quinolone, either at the 5-position (**3.27l**) or directly on the alkene (**3.27m**) did not significantly impact the enantioselectivity of the reaction, although the diastereoselectivity of these reactions was somewhat diminished. Interestingly, substitution at the 8-position of the quinolone with a chlorine has a negatively impacted ee (**3.27n**) and was not restored upon incorporation of a smaller fluorine substituent at the same position (**3.27o**).

Table 3.2. Scope of Asymmetric Intermolecular [2+2] Cycloadditions[a]

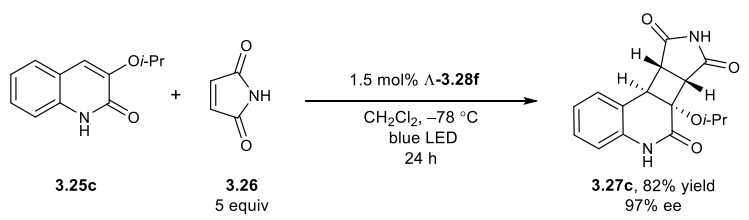

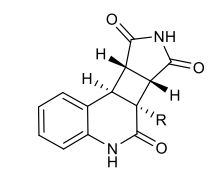

3.27a, (R = *n*-Bu)
14% yield,[b] 7% ee
3.27b, (R = OMe)
30% yield,[b] 70% ee
3.27d, (R = H)
0% yield[b]

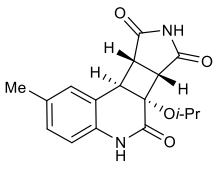

3.27e, 99% yield
96% ee

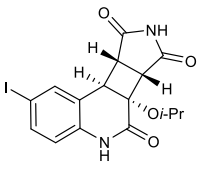

3.27f, 67% yield
99% ee (9:1 d.r.)

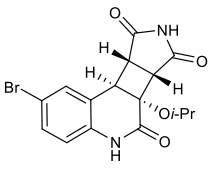

3.27g, 71% yield
95% ee (9:1 d.r.)

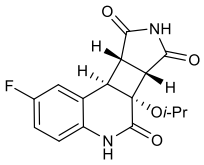

3.27h, 77% yield
90% ee

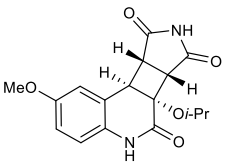

3.27i, 60% yield[c]
94% ee

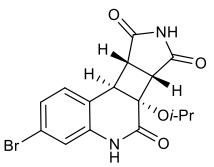

3.27j, 92% yield
93% ee

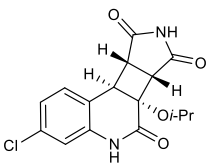

3.27k, 85% yield
97% ee

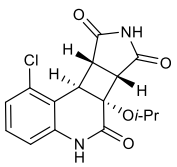

3.27l, 99% yield
99% ee (6:1 d.r.)

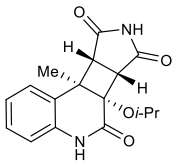

3.27m, 78% yield
87% ee (5:1 d.r.)

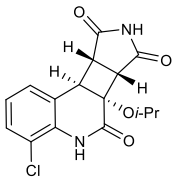

3.27n, 74% yield
51% ee

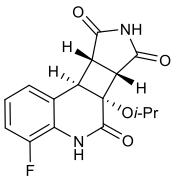

3.27o, 79% yield
14% ee (8:1 d.r.)

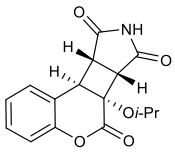

3.27p, 87% yield
7% ee

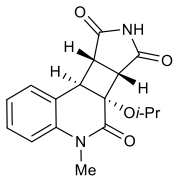

3.27q, 96% yield
72% ee (3:1 d.r.)

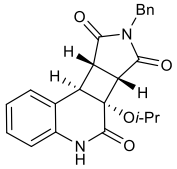

3.27r, 63% yield
88% ee

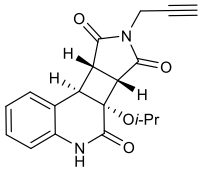

3.27s, 61% yield
97% ee

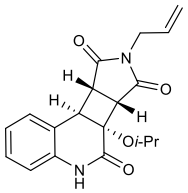

3.27t, 44% yield
84% ee

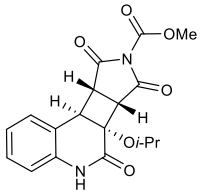

3.27u, 76% yield
99% ee

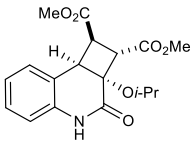

3.27v, 60% yield
61% ee (7:1 d.r.)

[a] Isolated yields are reported except where noted. Diastereomer ratoes were determined by ^{1}H NMR analysis and are >10:1 unless noted. Reactions conducted using 0.20 mmol quinolone, 5 equiv maleimide, and 1.5 mol% photocatalyst in CH_2Cl_2, irradiating with a blue LED unless otherwise noted. [b] Yield determined by ^{1}H NMR analysis. [c] Reaction conducted for 48 h.

The dependence of the N–H amide, for both the quinolone and maleimide, on enantioselectivity was examined. Notably, coumarin **3.27p** resulted in a substantial loss of ee, meanwhile the methylated quinolone forms product **3.27q** in 72% ee. Substitution at the nitrogen

atom of the maleimide was found to not be critical for selectivity as a range of reactions partners *N*-alkyl, propargyl, allyl, and carbamoyl (**3.27r-u**) afforded high enantioselectivity. Next, we found that cyclic maleimide could be replaced with dimethyl fumarate to afford the diester cyclobutane product **3.27v** in good yield and ee, demonstrating the potential generality of this methodology.

3.2.3 Mechanistic Investigations

Most of the observations made during the scope study were consistent with the analogous investigations of the intramolecular photocycloaddition.[41] There were, however, some surprising discrepancies. For instance, we had previously observed that modification of the 8-position, which is proximal to the catalyst-binding amide motif, had a pronounced deleterious effect on ee (**3.27n**). In the present system, however, the enantioselectivity was not rescued upon incorporation of a small fluorine substituent at this position (**3.27o**), as it was in the intramolecular reaction. Most notably, *N*-methylquinolone, which reacted without stereoselectivity in the intramolecular reaction, nevertheless provided good ee in this intermolecular context (**3.27q**). In our previous work, we had proposed that the quinolone N-H was necessary to ensure the proper orientation of the reactant with the Ir photocatalyst. The observation that *N*-methylated quinolone reacts to afford **3.27q** in 72% ee suggests that the product-forming catalyst–substrate complex must possess some differences compared to the intramolecular system we reported previously.

We first considered the possibility that the catalyst might bind principally to the other reaction partner, maleimide, and not the quinolone. However, an NMR titration study indicates that the ground-state hydrogen-bonding interaction of catalyst Λ–**3.28f** with maleimide is negligible ($K_a = 24\ M^{-1}$) at room temperature compared to its interaction with quinolone **3.25c** ($K_a = 603\ M^{-1}$). These results suggest that a catalyst–maleimide interaction is likely not critical for this

reaction to occur. Indeed, the ee remained high in reactions between **3.25c** and a range of alternate reaction partners, (**3.27r**–**v**), that could not participate in H–bonding interactions similar to **3.25c**. These experiments support the contention that there is a specific binding interaction between the catalyst and the quinolone but not with its reaction partner in the product-forming complex. An analysis of the kinetics of this photoreaction are also consistent with this hypothesis. We observe a first-order dependence on the photocatalyst and maleimide **3.26** but a zero-order dependence on quinolone **3.25c**. Thus, we concluded from these collected data that the principal binding interaction was between the Ir photocatalyst and the quinolone substrate, similar to the intramolecular reaction, and that the differences in reaction scope likely arise from subtle changes in the geometry of the hydrogen-bound complex.

Luminescence measurements, on the other hand, suggested that the maleimide might play a critical role in the photoactivation mechanism. Stern–Volmer quenching studies were conducted to measure the rate of energy transfer from triplet-state photocatalyst Λ–**3.28f** to both reaction partners. These studies indicated that **3.25c** is a modest quencher of Λ–**3.28f*** with a calculated Stern–Volmer constant of K_{SV} = 47 M^{-1}. This value is substantially lower than both K_{SV} for quenching of Λ–**3.28f*** by maleimide (1900 M^{-1}) and for the optimal intramolecular catalyst–substrate pair of Λ–**3.28a** + **3.25w** (K_{SV} = 3200 M^{-1}).[41] This observation encouraged us to wonder whether the role of the photocatalyst might not be to activate the bound quinolone, which is a poor excited-state quencher, but rather to sensitize the maleimide, which exhibits much faster quenching dynamics.

As a test of this hypothesis, we examined the reaction of alkene-functionalized quinolone **3.25w** using photocatalyst Λ–**3.28f** (Figure 3.1). In the absence of added maleimide, we observe the formation of intramolecular cyclization product **3.32** in 13% yield after 24 h of irradiation.

Thus, Λ–**3.28f** is a competent catalyst for the intramolecular photocycloaddition, albeit a relatively inefficient one. When the reaction is conducted in the presence of maleimide, however, the formation of **3.32** is suppressed, and we exclusively observe formation of intermolecular maleimide adduct **3.27w** in 24% yield.

Figure 3.1. Control Experiments

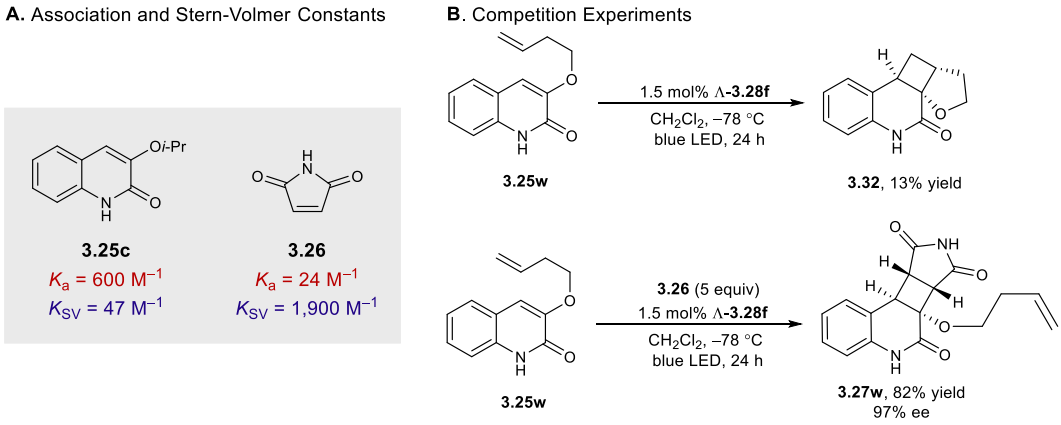

We considered three limiting scenarios to explain the overall rate law derived for this reaction, the Stern–Volmer studies, and the outcome of the competition study. These hypotheses are outlined in Scheme 3.7. First, we believe that the collective data are most consistent with a scenario in which the exciton is initially localized on the Ir component of the complex and then transferred to maleimide via an intermolecular energy-transfer process (eq **A**). This would be a surprising and, to the best of our knowledge, unprecedented example of a highly enantioselective triplet-state photoreaction that does not involve photosensitization of a catalyst-bound substrate. Next, we also considered an alternate model in which the initially formed Ir-localized triplet state undergoes intramolecular energy transfer to generate a quinolone-localized triplet state (eq **B**). In order to explain the competition experiments in Figure 3.1B, this scenario would require a

preference for triplet quinolone to react with an electron-deficient maleimide over a tethered aliphatic alkene and that the *inter*molecular process out-competes an *intra*molecular one.

Finally, we considered a third possibility in which the excited-state Ir–quinolone complex might form a charge-transfer complex, in which the exciton is distributed over both the Ir and quinolone units, and thereafter react with maleimide in a product-forming step (eq **C**). This process would be analogous to the "triplex mechanism" proposed by Schuster for enantioselective [4+2] cycloadditions catalyzed by dicyanobinapthyl chromophores as chiral photocatalysts.[43–45] However, the luminescence spectrum of the photocatalyst does not change significantly upon addition of increasing quantities of quinolone **3.25c**. There is, therefore, no spectroscopic evidence to support the formation of a new triplet state with any significant excited-state delocalization onto the quinolone unit.

Scheme 3.7. Possible Mechanistic Scenarios

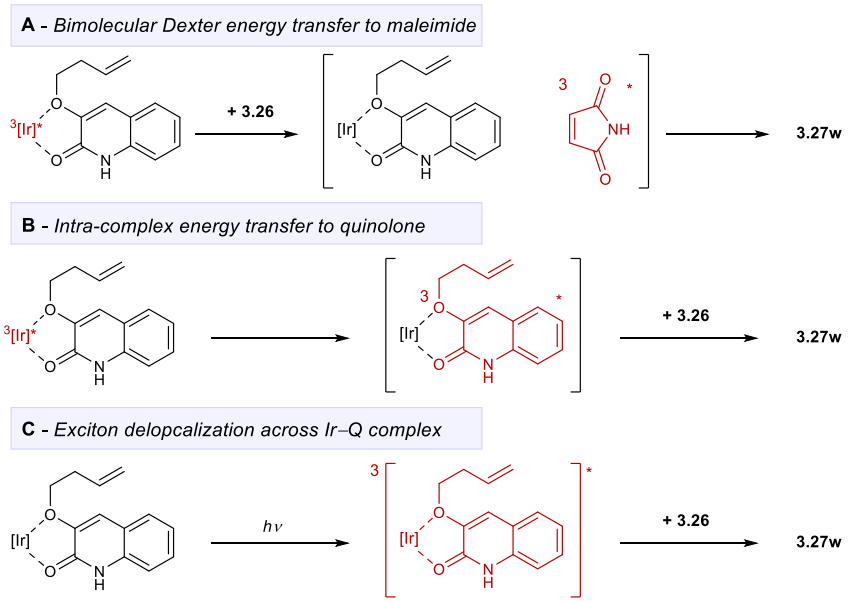

In order to differentiate among these possibilities, we next performed transient absorption spectroscopic experiments. Photoexcitation of a 150 μM solution of the iridium photocatalyst in

CH_2Cl_2 by a 532 nm laser (7 ns full-width at half-max) produced the long-lived iridium triplet excited state (^{3}[Ir*]), which showed absorption from 350–550 nm (see section 3.5). The feature at 370 nm decayed with first-order kinetics, and a single exponential fit provided an excited-state lifetime of 4.4 μs. This lifetime was in good agreement with the decay of the photoluminescence monitored at 580 nm. Cooling the sample to –78 °C produced minor changes in the absorption difference spectrum and a negligible change in the photoluminescence lifetime (τ_{-78} = 4.3 μs.) This lifetime was insensitive to the addition of up to 10 mM of quinolone **3.25c**, indicating that dynamic energy transfer to quinolone cannot compete kinetically with excited-state decay. In contrast, the addition of maleimide **3.26** to the iridium photocatalyst at –78 °C produced a significant decrease in the lifetime of the ^{3}[Ir*] excited state (500 ns with 10 mM **3.26**, Figure 3.2A).

These results are fully consistent with the conclusions of the luminescence experiments conducted at room temperature: (*1*) binding of quinolone does not significantly perturb the photophysics of the Ir triplet, which is inconsistent with formation of a triplet exciplex required in Scheme 3.7C; (*2*) the quinolone substrate does not undergo energy transfer with the iridium photocatalyst which is inconsistent with the model depicted in Scheme 3.7B; and (*3*) only the maleimide is a competent quencher of the ^{3}[Ir*] excited state, in agreement with the model proposed in Scheme 3.7A. However, transient absorption experiments also provided us with an opportunity to interrogate the decay of the triplet excited-state photocatalyst in the presence of both reaction partners. Based on the equilibrium constant for the formation of the hydrogen-bound catalyst–quinolone complex [Ir-Q], a solution of iridium photocatalyst Λ–**3.28f** and quinolone **3.25c** was prepared with quinolone concentrations large enough to ensure that >95% of the iridium photocatalyst was bound to quinolone. As noted above, the lifetime of the iridium excited state was unaffected by the bound quinolone. The addition of maleimide **3.26** did quench the ^{3}[Ir*-Q]

excited-state, but the rate of quenching was significantly attenuated compared to the free iridium: we observed only a 2-fold decrease in the excited-state lifetime (4.3 → 2.2 μs) after the addition of 14 mM **3.26**. A Stern–Volmer analysis was linear and provided a K_{SV} of 130 M^{-1}, which corresponds to a bimolecular quenching rate constant of $k_q = 3.0 \times 10^7\ M^{-1}\ s^{-1}$. We note that there was no evidence for static quenching by the quinolone within the [Ir-Q] complex. Any small, unmeasurable static quenching by quinolone would not be kinetically competitive with the maleimide quenching, and thus not be a significant mechanistic pathway for the reported reaction.

Figure 3.2. Time-Resolved Luminescence Experiments

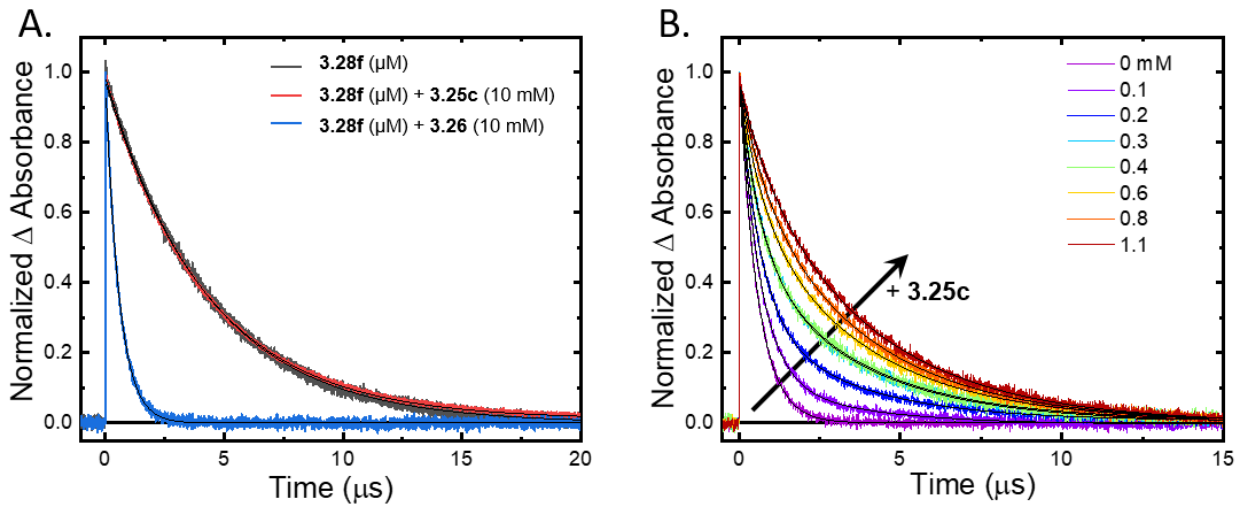

At lower concentrations of quinolone **3.25c**, the ^{3}[Ir*] absorbance decayed with biexponential kinetics in the presence of 10 mM maleimide. The two lifetimes were independent of the quinolone concentration, with the short lifetime, $\tau_1 \sim 680$ ns, consistent with the previously obtained lifetime for energy transfer quenching of a free iridium photocatalyst by maleimide, and the long decay, $\tau_2 \sim 3.4$ μs, aligning with the expected lifetime for maleimide quenching of the [^{3}Ir*-Q] complex. The presence of these two decays at –78 °C can be rationalized as a consequence of a slow rate of association and dissociation of the quinolone-iridium complex at lower

temperatures. In order to measure the strength of this binding interaction, a solution of the iridium photocatalyst and 10 mM concentration of maleimide **3.26** was titrated with increasing concentrations of quinolone **3.25c**. An analysis of the preexponential factors from biexponential fits to the single wavelength kinetics allowed us to estimate the equilibrium constant for the hydrogen bound [Ir-Q] complex at –78 °C ($K_{eq,-78}$ = 3,400 ± 900 M^{-1}). Hydrogen bonds typically increase in strength with decreased temperature, which agrees with the increased binding constant at –78 °C versus room temperature.

The combination of transient absorption and photoluminescence quenching experiments, however, does not establish exactly which species are involved in C–C bond-forming process. The triplet maleimide may react with the quinolone present within the same [Ir-Q] complex that was quenched, or the maleimide could escape the solvent cage and undergo a bimolecular reaction with a different [Ir-Q] complex. Attempts to observe the triplet maleimide complex by transient absorption spectroscopy were unsuccessful. However, two details support the proposed caged reaction mechanism. First, the concentration of free quinolone is nearly two orders of magnitude larger than that of hydrogen bound quinolone. Thus, if triplet maleimide escapes the solvent cage, one would expect it to react readily with free quinolone and produce a racemic mixture. This expectation is inconsistent with the highly enantioselective transformation observed. Second, triplet maleimide has a lifetime of 170 ns and undergoes rapid self-reaction near the diffusion limit, 10^9–10^{10} M^{-1} s^{-1}.[46] Under the initial reaction conditions, the concentration of maleimide is 5-fold higher than quinolone and more than 100-fold higher than the [Ir-Q] complex. Thus, any triplet maleimide that escapes the solvent cage would be expected to rapidly dimerize before encountering an [Ir-Q] complex. The maleimide dimers are difficult to unambiguously identify in the reaction mixtures of most of the experiments summarized in Table 3.2. We were, however, able

to quantify the formation of 8% of *N*-benzyl maleimide dimer along with intermolecular cycloadduct **3.27r**. Thus, it is clear that triplet maleimide is being generated during the course of these photoreactions, but that the rate of dimerization is relatively slow compared to the rate of the reaction with [Ir-Q]. This would be consistent with a scenario in which maleimide is formed via triplet energy transfer, but the majority of [2+2] cycloaddition occurs before the triplet maleimide can escape the solvent cage.

The transient absorption data therefore show that energy transfer occurs exclusively through an intermolecular interaction with maleimide. These results rule out the mechanistic proposal depicted in Scheme 3.7B: there is essentially no population of triplet quinolone under the reaction conditions. Instead, the conclusions from these studies support the mechanism shown in Scheme 3.7A, in which a *bimolecular, collisional energy transfer process is substantially faster than an analogous intramolecular event.* This is a surprising result. It is well appreciated that Dexter energy transfer exhibits a strong distance dependence, which seems incongruous to the finding that the Ir photocatalyst binds quinolone but sensitizes unbound maleimide. On the other hand, investigations of intramolecular energy transfer processes conducted by Speiser demonstrated that the rate of Dexter energy transfer can also exhibit a strong dependence on the relative orientations of the interacting chromophores[47,48] We wondered whether a similar explanation could be invoked to rationalize these findings.

We therefore further interrogated this reaction using density functional theory (DFT) to model the parent reaction between quinolone **3.25c** and maleimide. In our previous computational studies of the intramolecular version of this cycloaddition, we found that key to engineering an efficient triplet energy-transfer event is maximizing the overlap between orbitals that are involved in the double electron transfer on the cyclometalating ligand and the coordinated substrate. For the

present intermolecular reaction system, however, Stern–Volmer quenching experiments and transient absorption data showed that the energy transfer to the bound quinolone substrate is not facile. Instead, the intermolecular activation of maleimide is more effective. Figure 3.3 summarizes the DFT-calculated energy differences of all plausible donor-acceptor pairs. Extensive sampling of possible donor-acceptor geometries revealed four relevant structures for the [Ir-Q] complex and two structures for the [Ir-M] adduct, shown in Figure 3.3.

Figure 3.3. DFT Optimized Structures of Hydrogen-bound Complexes for Λ–**3.28f** with **A.** Quinolone **3.25c** and **B.** Maleimide **3.26**. **C.** Gibbs Free Energy Changes During the Energy-Transfer Process.

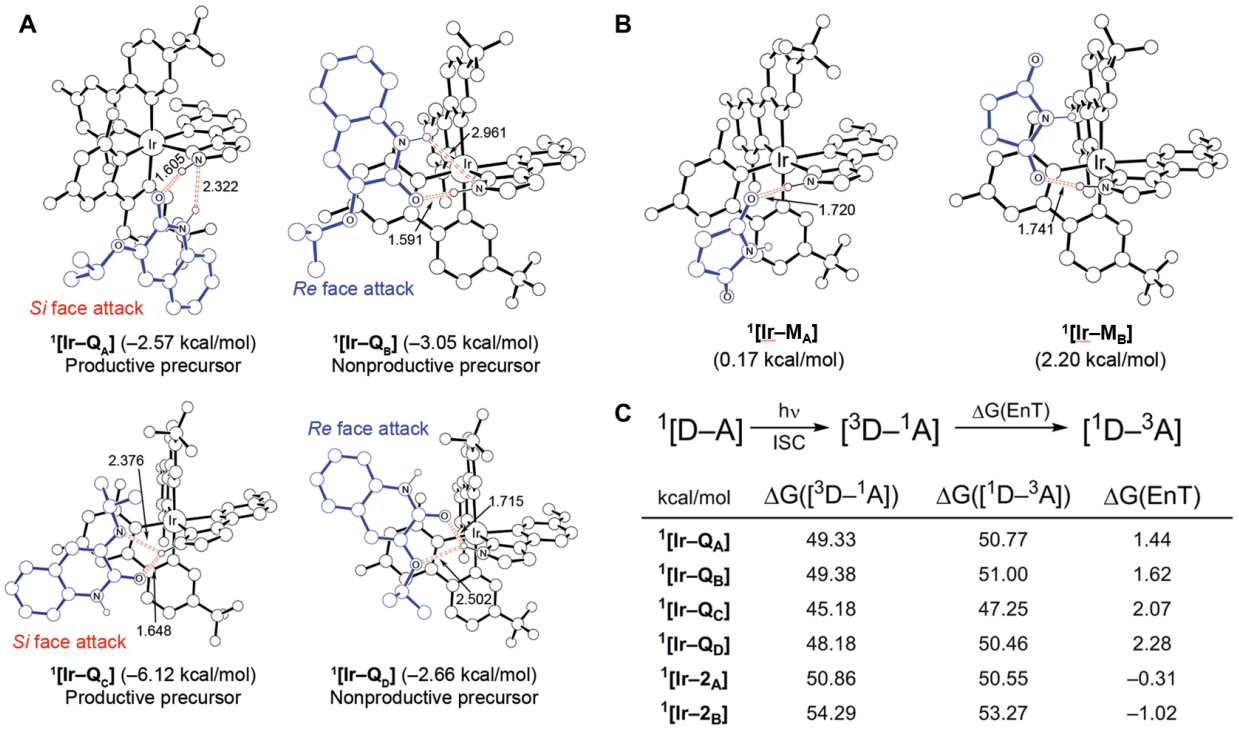

kcal/mol	ΔG([^{3}D–^{1}A])	ΔG([^{1}D–^{3}A])	ΔG(EnT)
^{1}[Ir–Q_A]	49.33	50.77	1.44
^{1}[Ir–Q_B]	49.38	51.00	1.62
^{1}[Ir–Q_C]	45.18	47.25	2.07
^{1}[Ir–Q_D]	48.18	50.46	2.28
^{1}[Ir–2_A]	50.86	50.55	–0.31
^{1}[Ir–2_B]	54.29	53.27	–1.02

In analogy to our previous work,[41] encounter complexes **^{1}[Ir-Q_A]**, and **^{1}[Ir-Q_B]** feature non-classical hydrogen bonds between the pyrazole N–H group and the oxygen and N–H functionalities of the quinolone substrate. Among these four possible adducts, **^{1}[Ir-Q_C]** was most

stable at a relative binding energy of –6.1 kcal/mol, which is in good agreement with the experimentally observed sense of the stereoinduction, although the absolute value of the binding energy estimate is not consistent with the measured association constant. Given the many approximations about the unbound state and the crude way solvation is treated, we cannot expect a quantitatively reliable prediction of the binding energy. Moreover, because the entropic penalty is temperature-dependent, this inconsistency might also be due to an overestimation of the entropy correction at the reaction temperature. Nonetheless, these computed energies are useful for comparing the stabilities of different geometries, as significant error-cancellation is expected.

We find notable differences in the optimal binding structure, **^{1}[Ir-Q$_C$]**, compared to the optimal complex involved in the intramolecular [2+2] cycloaddition.[41] Previously, we had found that the quinoline N–H moiety engages in a non-classical hydrogen bond to the pyrazole nitrogen, which aligns the quinolone to maximize the orbital overlap with the cyclometalating ligand. In the present case, the encounter complex adopts a different geometry because the tether carrying the olefin fragment is not present and the main hydrogen-bonding feature is between the pyrazole N–H and the oxygen atoms of **3.25c**, as shown in Figure 3.3. Importantly, this quinolone binding mode minimizes the potential for orbital overlap between it and the photocatalyst ligands and thus suggests that energy transfer within the complex might not be facile. The calculated optimal binding geometry, however, is in good agreement with the unexpected experimental observation that the photoreaction of *N*-methyl quinolone substrate (**3.25q**) shows good ee, implying that the quinolone N–H bond is no longer critical. Compared to this intermediate, the binding of maleimide is predicted to be much less favored: the two lowest energy structures being **^{1}[Ir-M$_A$]** and **^{1}[Ir-M$_B$]** have binding energies of 0.2 and 2.2 kcal/mol, respectively. Thus, our calculations predict that the

[Ir–2] encounter complexes should be much harder to detect experimentally, which is also in good agreement with the NMR titration experiments.

Using the singlet ground state structures of the encounter complexes, the energies of two triplet states denoted [^{3}Ir-^{1}Q] and [^{1}Ir-^{3}Q] can be calculated, which in turn allows for estimating the energy of the triplet energy transfer from the photocatalyst to the bound substrates (Figure 3.3C). Interestingly, these calculations reveal that the triplet energy transfer in **^{1}[Ir-M$_B$]** is easiest at –1.0 kcal/mol. In contrast, the energy transfer to the quinolone substrate is slightly uphill with energy requirement of +1.4 to +2.3 kcal/mol for the triplet energy transfer. These results agree with the Stern–Volmer quenching experiments and offers a rationale for the relatively low rate of triplet energy transfer to the quinolone compared to maleimide, as the rate of triplet energy transfer is generally dependent on the thermodynamic driving force.

Under the employed experimental conditions, however, the concentration of the quinolone compared to the photocatalyst is high, and practically all of the Ir complexes will be bound to a quinolone substrate.[49] Thus, the direct triplet sensitization from a free Ir catalyst to maleimide as outlined above is unlikely to be kinetically relevant. We wondered if a transient three-component complex **[Ir-Q-M]** might be responsible for the triplet energy transfer (Figure 3.4). We located a 3-component adduct with maleimide bound to **[^{3}Ir-^{1}Q$_C$]**. Notably, this arrangement exhibits a π-π stacking interaction between maleimide and the cyclometalating phenylpyridine ligand of the Ir-catalyst. Such a favorable non-covalent interaction was not possible with the free photocatalyst. We speculate that this arrangement allows for the appropriate orbital overlap necessary that would enable rapid Dexter energy transfer between the triplet Ir complex and maleimide.

Using the calculated structure of the singlet ground state **[Ir-Q-M]**, three triplet states denoted **[^{3}Ir-^{1}Q-^{1}M]**, **[^{1}Ir-^{3}Q-^{1}M]** and **[^{1}Ir-^{1}Q-^{3}M]** were optimized, and their structures and

energies are shown in Figure 3.4. The Mulliken spin density values are helpful in identifying which state corresponds to which conceptual triplet and are given in the supporting information. Interestingly, the quinolone in the **[^{1}Ir-^{3}Q-^{1}M]** state shows an elongated C=C double bond of 1.472 Å, which is 0.103 Å longer than in **[^{3}Ir-^{1}Q-^{1}M]**. Similarly, the C=C double bond of maleimide was elongated to 1.472 Å from 1.349 Å in **[^{3}Ir-^{1}Q-^{1}M]**. These structural features are indicative of triplet formation in the respective substrates, as a result of the Dexter energy transfer event. These calculations strongly suggest that the fully delocalized exciplex, as shown in Scheme 3.7C, is unlikely to exist. The metal and ligand-based orbitals do not mix strongly enough justify such a delocalized state and our calculations show significant preference for the localized states, consistent with the experimental observations discussed above.

Figure 3.4. Computationally Optimized Structures of Excited-State Ternary Complex [Ir–Q–M]

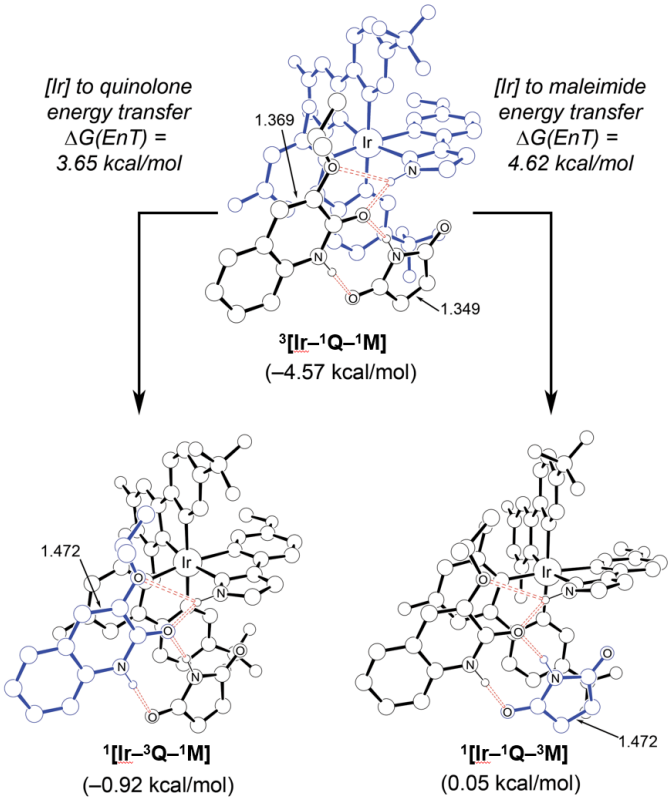

Our calculations suggest that the energy required to access the two possible reactive triplet species is 3.7 kcal/mol for quinolone and 4.6 kcal/mol for maleimide. However, the rate of Dexter energy transfer depends upon the degree of orbital overlap between the photocatalyst and the triplet acceptors. The arrangement that ^{1}**[Ir-Q$_{C}$]** possesses does not show a strong π-π interaction between the quinolone and the cyclometalating ligand of the photocatalyst, which is a notably different feature from what we had found in the intramolecular [2+2] case. As illustrated in Figure 3.4, the position of the quinolone does not change significantly upon maleimide attachment. Therefore, we expect the Dexter energy transfer to the quinolone unit to be still inefficient. The maleimide, on the other hand, can approach the excited-state photocatalyst from many different trajectories, and in the optimized ternary encounter complex [^{3}**Ir-**^{1}**Q-**^{1}**M**] the maleimide interacts directly with the cyclometalating ligand, appropriately positioning these components to participate in the Dexter energy transfer (DET) and become the triplet state that triggers the intermolecular [2+2] cycloaddition. Note that this geometry is only one reasonable arrangement for the energy transfer; there may exist many other binding modes that can remotely activate the maleimide into its triplet state.

Thus, computational evidence provides a model that explains the differences in substrate scope between this newly discovered intermolecular reaction and the analogous intermolecular system previously reported by our group: the reactive binding conformation of the quinolone substrate is quite different and involves a different set of hydrogen-bonding interactions with the photocatalyst pyridylpyrazole unit. More importantly, this binding mode also minimizes π overlap between the photocatalyst and the quinolone that would be necessary for efficient Dexter energy transfer, leaving maleimide sensitization as the dominant reaction pathway in this cycloaddition.

3.3 Conclusion and Future Directions

In conclusion, we have developed a highly enantioselective intermolecular [2+2] photocycloaddition using a chiral hydrogen-bonding Ir complex as a triplet sensitizer. A combination of synthetic, kinetic, spectroscopic, and computational studies suggest an unusual mode of asymmetric photocatalysis, outlined in Scheme 3.8. The quinolone substrate associates to the pyrazole moiety of iridium complex Λ–**3.28f** to produce the resting state of the photocatalytic cycle. The bidentate hydrogen-bonding interaction enforces a geometry that prevents overlap between the π molecular orbitals of the catalyst and quinolone that would enable Dexter energy transfer to occur. Thus upon excitation, the photocatalyst preferentially undergoes bimolecular energy transfer with maleimide **3.26**. The resulting triplet state maleimide reacts with the quinolone within the stereodifferentiating influence of the Ir stereocenter, affording cycloadduct **3.25c** in high ee.

Scheme 3.8. Proposed Mechanism for the Enantioselective Intermolecular [2+2] Photocycloaddition

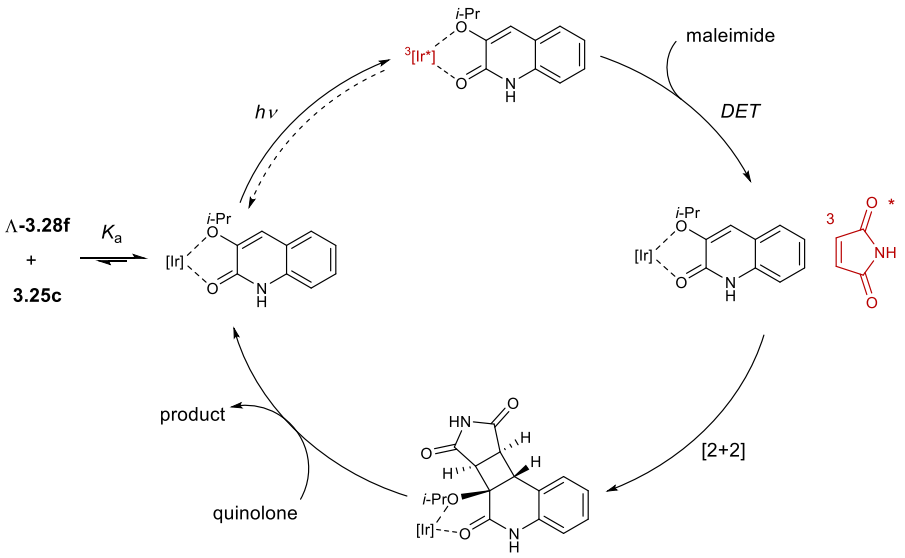

These studies suggest that highly enantioselective excited-state photoreactions are feasible even when there is no strong ground-state preassociation between the chiral catalyst and the sensitized organic substrate. This conclusion contradicts a central axiom of asymmetric photochemistry, which has long posited that such preassociations are necessary to ensure that highly reactive excited-state intermediates remain closely associated with the chiral catalyst throughout the photoexcitation and bond-forming processes. The potential implications of this work are highly significant for a variety of reasons. First, the discovery of this unexpected mechanism of substrate activation suggests that a similar principle might be utilized in the development of other highly enantioselective excited-state photoreactions. As such we wondered if perhaps this mechanism could enable the asymmetric [2+2] photocycloaddition of other classes of amides, such as cinnamamides, in the place of the quinolone starting material (Table 3.3). Validating our hypothesis, chiral photocatalyst Λ–**3.28f** was found to promote the cycloaddition of cinnamamide **3.29a** and *N*-methyl maleimide **3.30** in good yield and 7% ee. Next, enabled by the ease of preparation of these substrates, we investigated the effect that the pK_a of the amide has on the enantioselectivity in this system. Anilinyl-amide **3.29b** afforded the highest selectivity observed at 44%, while further increasing the acidity of the N–H resulted in a loss of ee (entry 3). Lastly, unlike the title photocycloaddition above, conducting this reaction under cryogenic conditions had a negative impact on ee, albeit increasing the diastereoselectivity of the cycloaddition. These experiments demonstrate that this methodology isn't limited to specialized quinolones but holds potential to be widely applicable, warranting further investigation.

Table 3.3. Proof-of-Principle Experiments with Cinnamamides

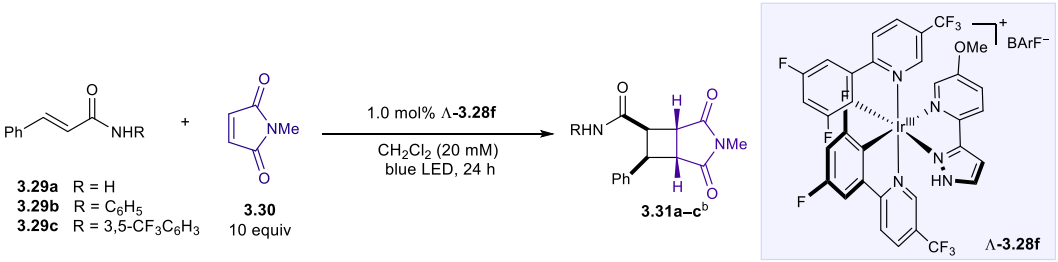

entry	cinnamamide	temp.	yield	d.r.	ee
1	**3.29a**	0 °C	54%	2.5:1	7%
2	**3.29b**	0 °C	42%	2:1	44%
3	**3.29c**	0 °C	56%	10:1	14%
4	**3.29b**	–78 °C	30%	10:1	25%

[a] Isolated yields are reported except where noted. Diastereomer ratios were determined by ^{1}H NMR analysis. [b] The absolute and relative stereochemistry of the products are undetermined.

More broadly, the work covered in this chapter highlights that subtly different photocatalytic methodologies have multiple reactivity pathways available to them and can proceed via entirely different mechanisms. The results of our comprehensive kinetic, spectroscopic, and computational studies underscore the importance of mechanistic investigations in the field of synthetic organic photochemistry.

3.4 Contributions

Dr. Jian Zheng conducted the optimization of this system, electrochemical and steady-state spectroscopic experiments, and the synthesis of the photocatalysts, substrates, and cycloadducts with the aid of Hoimin Jung. Time resolved luminescence experiments and analysis was conducted by Dr. Wesley B. Swords and Prof. Gerald J. Meyer. Dr. Kazimer L. Skubi performed the initial proof-of-principle intermolecular reactions. Computational experiments were conducted by Hoimin Jung and Prof. Mu-Hyun Baik. Dr. Ilia A. Guzei collected and analyzed X-ray crystallographic data. Prof. Tehshik P. Yoon provided expertise, resources, and funding for researchers.

3.5 Experimental Procedures

3.5.1 General Information

All reagents were purchased from commercial suppliers and used without additional purification unless otherwise noted. Flash column chromatography was carried out with Purasil 60 Å silica gel (230–400 mesh). ^{1}H, ^{13}C, and ^{19}F NMR spectra were obtained using a Bruker Avance-400, Avance-500, or Avance-600 spectrometer with DCH, Prodigy, BBFO+, or TCI-F probes. ^{1}H spectra were internally referenced to tetramethyl silane or the residual protio-solvent peak in $CDCl_3$, CD_3OD, DMSO-d_6, or acetone-d_6. Enantiomeric excesses were determined for isolated, purified material using either chiral SFC (Waters/TharInvestigator) or chiral HPLC (Waters Alliance), Daicel CHIRALCEL® columns and Chromasolv®-grade solvents. IR spectra were obtained using a Bruker Alpha Platinum spectrometer (powder or thin film). Melting points were obtained using a Stanford Research Systems DigiMeltapparatus, and are uncorrected. Optical rotations were measured using a Rudolph Research Autopol III polarimeter at room temperature. UV-Vis emission spectra were acquired on ISS PC1 photon-counting fluorometer. The spectrometers used for this work are supported by the NSF (CHE-1048642, CHE-0342998, CHE-9208463), NIH (S10 OD012245, S10 RR13866-01), and a generous gift from Paul J. and Margaret M. Bender. Mass spectrometry was performed with a Thermo Q Exactive™ Plus. This instrumentation is supported by the NIH (1S10 OD020022-1) and the University of Wisconsin.

3.5.2 Synthesis of Photocatalysts

3.5.2.a Synthesis of Ligands

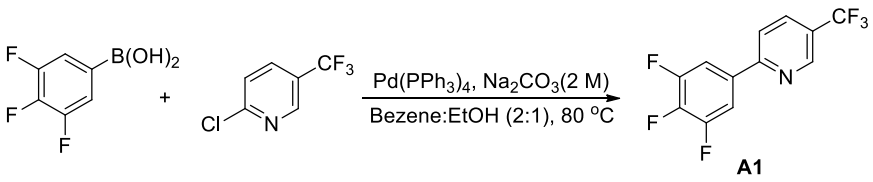

A1

Phenylpyridine (ppy) ligands were prepared based on a known procedure.[50] A 50 mL flask was charged with chloropyridine (5.00 mmol, 1.0 equiv.) and arylboronic acid (5.50 mmol, 1.1 equiv.), followed by $Pd(PPh_3)_4$ (0.125 mmol, 0.025 equiv.). Benzene (6.7 mL) was added, followed by 2 M aq. Na_2CO_3 (10.0 mmol, 2.0 equiv.) and EtOH (1.25 mL). Then the mixture was heated at 80 °C under N_2 and maintained at this temperature for 2 d. The reaction was then cooled to room temperature and diluted by 6 mL H_2O. The crude was extracted by EtOAc (10 mL X 3). Then the organic layers were combined, dried with $MgSO_4$, filtered and concentrated, and the residue was further purified by flash column chromatography (EtOAc:Hexanes = 1:10) to afford the pure product.

5-(Trifluoromethyl)-2-(3,4,5-trifluorophenyl)pyridine (A1): Prepared as described before. Spectral data were consistent with those reported previously.[51]

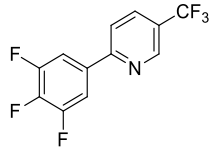

A1

2-(2,5-Difluorophenyl)-5-(trifluoromethyl)pyridine (A2): 1.12 g, 86% yield, white solid; ^{1}H NMR (400 MHz, $CDCl_3$) δ 8.98 (s, 1H), 8.05 – 7.94 (m, 2H), 7.82 (ddd, *J* = 9.1, 6.1, 3.0 Hz, 1H), 7.22 – 7.08 (m, 2H). ^{13}C NMR (126 MHz, $CDCl_3$) δ 160.00 (dd, *J* = 243.0, 2.2 Hz), 156.75 (dd, *J* = 246.9, 2.4 Hz), 155.47 – 155.24 (m), 146.64 (q, *J* = 4.0 Hz), 133.85 (q, *J* = 3.1 Hz), 127.24 (dd, *J* = 13.4, 7.9 Hz), 125.60 (q, *J* = 33.1 Hz), 123.92 (d, *J* = 11.8 Hz), 123.49 (q, *J* = 272.2 Hz), 118.04 (dd, *J* = 24.4, 9.1 Hz), 117.69 (dd, *J* = 26.2, 8.4 Hz), 117.28 (dd, *J* = 25.7, 3.0 Hz). ^{19}F NMR (377 MHz, $CDCl_3$) δ –62.41 (s, 3F), –117.92 (d, *J* = 18.2 Hz, 1F), –122.23 (d, *J* = 18.2 Hz, 1F). IR (thin film): 3080, 2927, 1604, 1569, 1500, 1475, 1326, 1129, 817, 757 cm^{-1}; HRMS (ESI): $[M+H]^+$ calculated for $C_{12}H_7F_5N^+$ *m/z* 260.0493, found *m/z* 260.0490; mp = 65.2–65.4 °C.

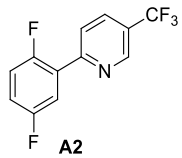

A2

2-(2-Fluoro-4-(trifluoromethyl)phenyl)-5-(trifluoromethyl)pyridine (A3): Prepared as described before. Spectral data were consistent with those reported previously.[51]

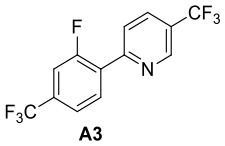

A3

2-(3,5-Difluorophenyl)-5-(trifluoromethyl)pyridine (A4): 1.2 g, 93% yield, pale yellow solid; ^{1}H NMR (500 MHz, $CDCl_3$) δ 8.97 – 8.93 (m, 1H), 8.02 (dd, *J* = 8.4, 2.0 Hz, 1H), 7.81 (d, *J* = 8.3 Hz, 1H), 7.63 – 7.56 (m, 2H), 6.92 (tt, *J* = 8.6, 2.3 Hz, 1H).^{13}C NMR (126 MHz, $CDCl_3$) δ 163.48 (dd, *J* = 248.8, 12.6 Hz), 158.07 – 157.85 (m), 146.80 (q, *J* = 3.9 Hz), 141.11 (t, *J* = 9.3 Hz), 134.32 (q, *J* = 3.5 Hz), 125.94 (q, *J* = 33.2 Hz), 123.48 (q, *J* = 272.3 Hz), 120.02 – 119.98 (s), 110.40 – 110.01 (m), 105.33 (t, *J* = 25.4 Hz).^{19}F NMR (377 MHz, $CDCl_3$) δ –62.38(s, 3F),–108.75 (s, 2F). IR (thin film): 3101, 1598, 1570, 1323, 1125, 839 cm^{-1}; HRMS (ESI): $[M+H]^+$ calculated for $C_{12}H_7F_5N^+$ requires *m/z* 260.0493, found *m/z* 260.0491; mp = 52–54 °C.

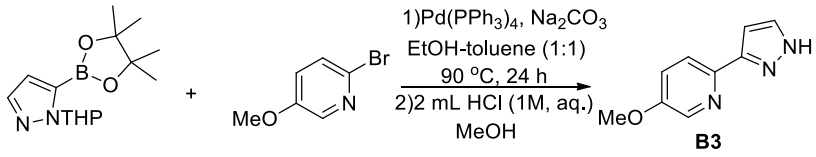

B3

Pyrazolpyridine (pzpy) ligands were prepared based on a known procedure.[52] A 25 mL flask was charged with 2-bromo-5-methoxypyridine (1.20 mmol, 1.2 equiv.) and 1-(tetrahydro-2*H*-pyran-2-yl)-5-(4,4,5,5-tetramethyl-1,3,2-dioxaborolan-2-yl)-1*H*-pyrazole (1.0 mmol, 1.0 equiv.), followed by $Pd(PPh_3)_4$ (0.025 mmol, 0.025 equiv.). Toluene (1.0 mL) was added, followed by 1.5 mL 2 M aq. Na_2CO_3 (3 mmol, 3.0 equiv.) and EtOH (1.0 mL). Then the mixture was heated at 90 °C under N_2 and maintained at this temperature for 24 h. The reaction was then cooled to 0 °C and diluted

with 6 mL H_2O. The crude was extracted into EtOAc (10 mL X 3) at RT. Then the organic layers were combined and concentrated, and the residue was dissolved in 2 mL MeOH, followed by 2 mL HCl (1M, aq.). After stirring for 5 h at RT, the crude was quenched with 3 mL NaOH (2 M, aq.).

The reaction was then diluted with 6 mL H_2O and the crude was extracted into EtOAc (10 mL X 3). Then the organic layers were combined, dried with $MgSO_4$, filtered and concentrated, and the residue was further purified by flash column chromatography (EtOAc:Hexanes = 1:1) to afford the pure product.

2-(1*H*-Pyrazol-3-yl)-5-(trifluoromethyl)pyridine (B2): Prepared as described before. Spectral data were consistent with those reported previously.[52]

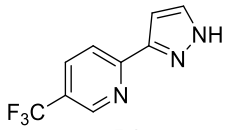

B2

5-Methoxy-2-(1*H*-pyrazol-3-yl)pyridine (B3): (Note: the ligand appears to have fewer than the expected number of signals in the ^{13}C NMR. This phenomenon is consistent with previously-reported results. We found that the HCl salt gave better data.):

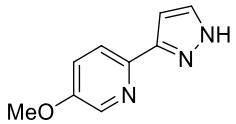

B3

143.4 mg, 82% yield, white solid; ^1H NMR (500 MHz, $CDCl_3$) δ 8.39 (d, *J* = 2.8 Hz, 1H), 7.70 (d, *J* = 8.7 Hz, 1H), 7.65 (d, *J* = 1.9 Hz, 1H), 7.25 (dd, *J* = 8.7, 2.9 Hz, 1H), 6.71 (d, *J* = 1.9 Hz, 1H), 3.89 (s, 3H). ^1H NMR (**B3·HCl**, 500 MHz, DMSO-d_6) δ 9.68 (s, 2H), 8.35 (d, *J* = 2.8 Hz, 1H), 8.23 (d, *J* = 8.9 Hz, 1H), 8.02 – 7.95 (m, 1H), 7.95 – 7.91 (m, 1H), 7.16 (s, 1H), 3.97 (s, 3H). ^{13}C NMR (**B3·HCl**, 126 MHz, DMSO-d_6) δ 156.56, 143.61 , 140.00 , 132.41 , 131.18 , 129.30 , 124.13 , 105.30 , 57.41. IR (thin film): 3171, 2943, 2840, 1571, 1486, 1459, 1272, 1230, 1026, 836, 786 cm^{-1}; HRMS (ESI): $[M+H]^+$ calculated for $C_9H_{10}N_3O^+$ requires *m/z* 176.0818, found *m/z* 176.0817; mp = 105–107 °C;

(*S*)-2-(4-Isopropyl-4,5-dihydrothiazol-2-yl)phenol (ⁱPrHBT):Prepared as described before and

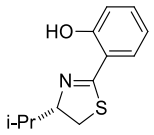

the spectral data were consistent with those reported previously.[53]

3.5.2.b Synthesis of Iridium Complexes

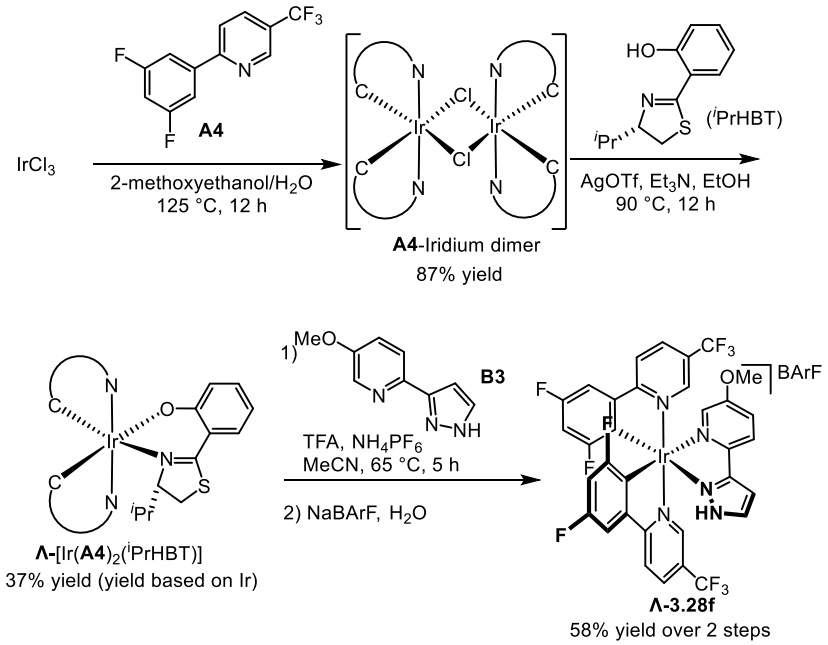

The iridium complexes were prepared following the procedure reported by our group.[51]

Step 1: A flask was charged with a stir bar, $IrCl_3 \cdot xH_2O$ (2.00 mmol, 1.0 equiv.), ppy ligand (2.25 mmol, 2.25 equiv.) and 36 mL co-solvent($V_{2\text{-methoxyethanol}}$:$V_{H2O}$ = 2:1). The solution was heated at 125 °C under N_2 overnight. After cooling to room temperature, 100 mL H_2O was added, resulting in precipitation. The resulting solid was isolated by suction filtration on a frit and rinsed with H_2O and hexanes before drying under vacuum. The crude iridium dimer was carried on to the following steps without further purification.

Step 2: The iridium dimer (0.6 mmol, 1.0 equiv.) was added to a round-bottomed flask, along with EtOH (60 mL), ⁱPrHBT (2.2 equiv.), AgOTf (2.2 equiv.) and Et_3N (10.0 equiv.). The mixture was

heated at 90 °C under N_2 overnight. After cooling to RT, the solvent was removed *in vacuo* and the diastereomers were separated by flash column chromatography to afford the pure product, which was assigned as the(*S*), Λ-diastereomer by analogy to the compounds reported before.[51]

Step 3: A round-bottomed flask was charged with the (*S*),Λ-iridium complex (0.08 mmol, 1 equiv.), NH_4PF_6 (0.40 mmol, 5.0 equiv.), pyridyl pyrazole ligand (0.20 mmol, 2.5 equiv.) and dry MeCN (8 mL), then placed under a nitrogen atmosphere. Trifluoroacetic acid (0.40 mmol, 5.0 equiv.) was added by syringe, and the solution was heated at 65 °C in the dark. After 5 h, the mixture was cooled to RT and concentrated. The crude residue was purified by flash column chromatography on silica gel (CH_2Cl_2) to afford the pure PF_6 salt, which was carried on without further characterization. This material was dissolved in 1 mL CH_2Cl_2 and NaBArF (1.0 equiv.) was added. After stirring for 5 min at room temperature, the mixture was washed with H_2O (3 mL X 3). The final photocatalyst was purified by flash column chromatography (CH_2Cl_2).[54]

(*S*),Λ-[Ir(**A2**)$_2$(^{i}PrHBT)]: 342.7 mg, 46% yield, yellow solid; ^{1}H NMR (400 MHz, $CDCl_3$) δ 9.37 (s, 1H), 8.67 (s, 1H), 8.42 (dd, *J* = 8.7, 2.8 Hz, 1H), 8.34 (dd, *J* = 8.7, 3.9 Hz, 1H), 7.98 (dd, *J* = 8.7, 1.5 Hz, 1H), 7.84 (d, *J* = 8.8 Hz, 1H), 7.43 (dd, *J* = 8.2, 1.6 Hz, 1H), 7.15 (ddd, *J* = 8.6, 6.9, 1.7 Hz, 1H), 6.68 (dd, *J* = 8.6, 0.9 Hz, 1H), 6.66 – 6.53 (m, 2H), 6.50 – 6.31 (m, 3H), 4.37 (d, *J* = 10.3 Hz, 1H), 3.35 (dd, *J* = 11.7, 9.7 Hz, 1H), 3.06 (dd, *J* = 11.7, 1.3 Hz, 1H), 0.57 – 0.45 (m, 1H), 0.36 (d, *J* = 6.9 Hz, 3H), 0.33 (d, *J* = 6.9 Hz, 3H). ^{19}F NMR (377 MHz, $CDCl_3$) δ –62.47 (s, 3F), –62.80 (s, 3F), –109.17 (d, *J* = 22.1 Hz, 1F), –112.62 (d, *J* = 21.6 Hz, 1F), –117.89 (d, *J* = 21.6 Hz, 1F, –118.26 (d, *J* = 22.1 Hz, 1F). IR (thin film): 2960, 1605, 1553, 1523, 1329, 1139, 1092, 924, 848 cm^{-1}; HRMS (ESI): $[M+H]^+$ calculated for $C_{36}H_{25}F_{10}IrN_3OS^+$ requires *m/z* 930.1182; found *m/z* 930.1190; $[\alpha]_{22}^{D}$+478.9º (*c*0.73, CH_2Cl_2).

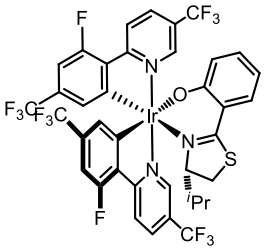

(*S*),Λ-[Ir(**A3**)$_2$(*i*PrHBT)]: Prepared as described before. Spectral data were consistent with the previous report.[51]

(*S*),Λ-[Ir(**A4**)$_2$(*i*PrHBT)]: 273.6 mg, 37% yield, yellow solid; ^{1}H NMR (400 MHz, $CDCl_3$) δ 9.35 (s, 1H), 8.65 (d, *J* = 0.5 Hz, 1H), 7.99 (dd, *J* = 8.6, 1.8 Hz, 1H), 7.89 (d, *J* = 8.5 Hz, 1H), 7.85 (dd, *J* = 8.7, 1.6 Hz, 1H), 7.79 (d, *J* = 8.6 Hz, 1H),7.44 (dd, *J* = 8.2, 1.7 Hz, 1H), 7.34 (dd, *J* = 9.0, 2.3 Hz, 1H), 7.22 (dd, *J* = 9.2, 2.3 Hz, 1H), 7.15 (ddd, *J* = 8.6, 6.9, 1.7 Hz, 1H), 6.67 (dd, *J* = 8.6, 1.0 Hz, 1H), 6.42 – 6.31 (m, 2H), 6.25 (td, *J* = 9.5, 2.3 Hz, 1H), 4.40 – 4.34 (m, 1H), 3.35 (dd, *J* = 11.7, 9.8 Hz, 1H), 3.06 (dd, *J* = 11.8, 1.4 Hz, 1H), 0.52 – 0.39 (m, 1H), 0.35 (d, *J* = 6.8 Hz, 3H), 0.31 (d, *J* = 6.8 Hz, 3H). ^{19}F NMR (377 MHz, $CDCl_3$) δ –62.39 (s, 3F), –62.73 (s, 3F), –100.53 (d, *J* = 5.8 Hz, 1F), –103.91 (d, *J* = 6.4 Hz, 1F), –119.68 (d, *J* = 6.3 Hz, 1F), –120.07 (d, *J* = 5.9 Hz, 1F).IR (thin film): 3068, 2960, 1606, 1556, 1524, 1464, 1435, 1323, 1134, 1085, 991, 844, 743 cm^{-1}; HRMS (ESI): $[M+H]^+$ calculated for $C_{36}H_{25}F_{10}IrN_3OS^+$ requires *m/z* 930.1182; found *m/z* 930.1182; $[\alpha]_{22}^{D}$: +360° (*c*1.15, CH_2Cl_2).

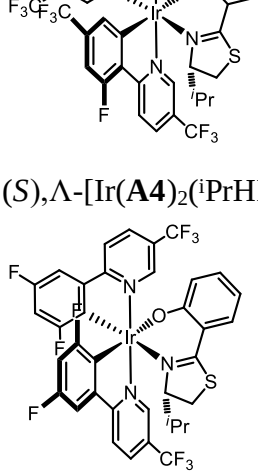

Λ-**3.28a**: Prepared as described before. Spectral data match the previous report.[51]

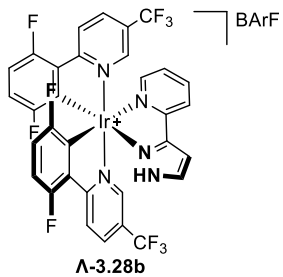

Λ-**3.28b**

Λ-**3.28b**:116.4 mg, 78% yield, pale yellow solid; ^{1}H NMR (400 MHz, $CDCl_3$) δ 11.15 (s, 1H), 8.53 – 8.38 (m, 2H), 7.99 (t, *J* = 9.1 Hz, 2H), 7.94 – 7.85 (m, 2H), 7.77 (d, *J* = 7.9 Hz, 1H), 7.71 (s, 8H), 7.54 (s, 1H), 7.46 (m, 5H), 7.43 – 7.35 (m, 2H), 6.92 – 6.78 (m, 2H), 6.71 – 6.58 (m, 3H). ^{19}F NMR (377 MHz, $CDCl_3$) δ –62.50 (s, 24F), –63.30 (s, 3F), –63.34 (s, 3F), –109.69 (d, *J* = 21.4 Hz, 1F), –110.11 (d, *J* = 21.5 Hz, 1F), –115.17 (d, *J* = 21.4 Hz,

1F), –115.31 (d, *J* = 21.5 Hz, 1F). IR (thin film): 2928, 1613, 1455, 1355, 1329, 1275, 1119, 675 cm^{-1}; HRMS (ESI): $[M]^+$ calculated for $C_{32}H_{17}F_{10}IrN_5^+$ requires *m/z* 854.0948; found *m/z* 854.0951; $[\alpha]_{22}^{D}$ +124.8º (*c*0.66, CH_2Cl_2).

Λ-**3.28c**: Prepared as described before. Spectral data match the previous report.[51]

Λ-**3.28d**:70.2 mg, 25% yield, yellow solid; ^{1}H NMR (400 MHz, $CDCl_3$) δ 10.87 (s, 1H), 8.03 – 7.97 (m, 2H), 7.96 – 7.89 (m, 3H), 7.86 (td, *J* = 7.8, 1.5 Hz, 1H),7.74 (d, *J* = 8.1 Hz, 1H), 7.70 (s, 8H), 7.52 (s, 1H), 7.48 – 7.43 (m, 5H), 7.43 – 7.34 (m, 4H), 6.66 (s, 1H), 6.58 – 6.48 (m, 1H). ^{19}F NMR (377 MHz, $CDCl_3$) δ –62.49 (s, 24F), –63.22 (s, 3F), –63.26 (s, 3F), –100.97 (d, *J* = 6.8 Hz, 1F), –101.36 (d, *J* = 7.0 Hz, 1F), –115.14 (d, *J* = 6.9 Hz, 1F), –115.24 (d, *J* = 6.8 Hz, 1F). IR (thin film): 1613, 1392, 1354, 1327.37, 1273, 1118, 996, 889, 673 cm^{-1}; HRMS (ESI): $[M]^+$ calculated for $C_{32}H_{17}F_{10}IrN_5^+$ requires *m/z* 854.0948; found *m/z* 854.0940;$[\alpha]_{22}^{D}$: +130º (*c*0.75, CH_2Cl_2).

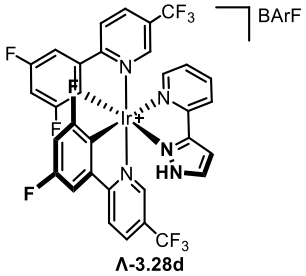

Λ-3.28d

Λ-**3.28e**: 142.7 mg, >99% yield, yellow solid; ^{1}H NMR (400 MHz, $CDCl_3$) δ 10.51 (s, 1H), 8.12 – 8.01 (m, 4H), 7.99 – 7.94 (m, 2H), 7.76 – 7.65 (m, 9H), 7.46 (s, 4H), 7.44 – 7.42 (m, 2H), 7.41 (s, 1H), 7.38 – 7.36 (m, 1H), 7.35 (s, 1H), 6.63 – 6.49 (m, 3H). ^{19}F NMR (377 MHz, $CDCl_3$) δ -62.51(s, 24F), -63.00(s, 3F), -63.26(s, 3F), -63.37(s, 3F), -101.17 (d, *J* = 7.4 Hz, 1F), -101.19 (d, *J* = 6.8 Hz, 1F), -114.04 (d, *J* = 7.1 Hz, 1F), -114.58 (d, *J* = 6.9 Hz, 1F). IR (thin film): 1616, 1355, 1327, 1275, 1116, 888, 673 cm^{-1}; HRMS (ESI): $[M]^+$ calculated for $C_{33}H_{16}F_{13}IrN_5^+$ requires *m/z* 922.0822; found *m/z* 922.0816; $[\alpha]_{22}^{D}$: +66.7º (*c*0.83, CH_2Cl_2).

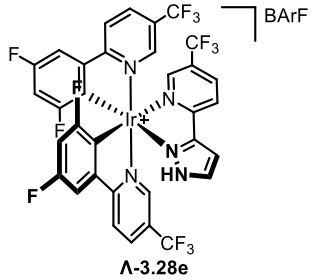

Λ-3.28e

Λ-**3.28f**: 81.2 mg, 58% yield, yellow solid; ^{1}H NMR (400 MHz, $CDCl_3$) δ 12.29 (br. s, 1H), 7.98

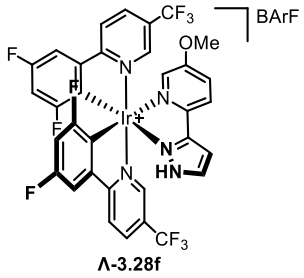

Λ-3.28f

– 7.85 (m, 4H), 7.75 – 7.66 (m, 9H), 7.58 (s, 1H), 7.53 – 7.48 (m, 3H), 7.46 (s, 4H), 7.38 – 7.32 (m, 2H), 7.30 (dd, *J* = 8.9, 2.7 Hz, 1H), 6.63 (d, *J* = 2.8 Hz, 1H), 6.50 (td, *J* = 9.1, 2.2 Hz, 1H), 6.41 (td, *J* = 9.1, 2.2 Hz, 1H), 3.66 (s, 3H). ^{19}F NMR (377 MHz, $CDCl_3$) δ –62.51 (s, 24F), –63.13 (s, 3F), –63.23 (s, 3F), –101.00 (d, *J* = 6.8 Hz, 1F), –101.25 (d, *J* = 6.9 Hz, 1F), –115.15 (d, *J* = 7.0 Hz, 1F), –115.49 (d, *J* = 6.8 Hz, 1F). IR (thin film): 2924, 1612, 1571, 1393, 1354, 1327, 1275, 1123, 1092, 889, 842, 674 cm^{-1}; HRMS (ESI): $[M]^+$calculated for $C_{33}H_{19}F_{10}IrN_5O^+$ requires *m/z* 884.1054; found *m/z* 884.1052; $[\alpha]_{22}^{D}$: +136° (*c*0.97, CH_2Cl_2).

Racemic (±)-**3.28f** was synthesized according to a literature procedure.[50] Spectral data were consistent with the enantiopure material prepared by our method.

3.5.3 Synthesis of Substrates

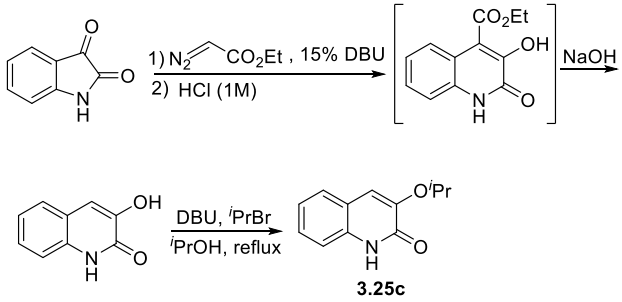

3.25c

Substituted 3-alkoxyquinolones were prepared by the route shown above, following known procedures unless otherwise noted. A 25 mL flask was charged with substituted 3-hydroxyquinolone (2.0 mmol, 1.0 equiv.), ^{i}PrOH (10 mL, 0.25 M with respect to substrate), DBU (3.12 mmol, 1.56 equiv.), and ^{i}PrBr (2.5 mmol, 1.25 equiv.), then heated at 95 °C under N_2 overnight. Following this period, the mixture was cooled to room temperature and concentrated *in*

vacuo. The crude residue was subjected to flash column chromatography (EtOAc:Hexanes = 2:1) to afford the 3-O^{i}Pr quinolone.

3-Butoxyquinolin-2(1*H*)-one (3.25a): Prepared as described before and the spectral data were consistent with those reported previously.[55]

3-Methoxyquinolin-2(1*H*)-one(3.25b): Prepared as described before[56] and the spectral data were consistent with those reported previously.[57]

3-Isopropoxyquinolin-2(1*H*)-one (3.25c): 71% yield, white solid; ^{1}H NMR (400 MHz, $CDCl_3$) δ

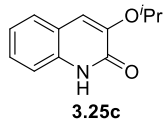

3.25c

12.74 (s, 1H), 7.52 (d, *J* = 8.1 Hz, 1H), 7.45 (d, *J* = 7.8 Hz, 1H), 7.37 – 7.30 (m, 1H), 7.21 – 7.13 (m, 1H), 7.02 (s, 1H), 4.68 (hept, *J* = 6.1 Hz, 1H), 1.47 (d, *J* = 6.1 Hz, 6H). ^{13}C NMR (101 MHz, $CDCl_3$) δ 160.53, 146.73, 133.59, 127.25, 126.02, 122.76, 120.45, 116.15, 114.71, 71.14, 21.63. IR (thin film): 3170, 3058, 2975, 1657, 1611, 1574, 1432, 1192, 1114, 754 cm^{-1}; HRMS (ESI): $[M+H]^+$ calculated for $C_{12}H_{14}NO_2^+$ *m/z* 204.1019, found *m/z* 204.1018; mp = 151–153 ºC.

3-Isopropoxy-6-methylquinolin-2(1*H*)-one (3.25e): 30%yield, white solid; ^{1}H NMR (400 MHz,

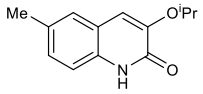

3.25e

$CDCl_3$) δ 11.27 (br. s, 1H), 7.29 – 7.26 (m, 2H), 7.20 (dd, *J* = 8.3, 1.4 Hz, 1H), 6.97 (s, 1H), 4.69 (hept, *J* = 6.1 Hz, 1H), 2.43 (s, 3H), 1.49 (d, *J* = 6.1 Hz, 6H). ^{13}C NMR (101 MHz, $CDCl_3$) δ 159.75, 146.85, 132.33, 131.31, 128.64, 125.95, 120.41, 115.42, 114.39, 71.08, 21.61, 21.00. IR (thin film): 3158 2979, 1656, 1613, 1579, 1232, 1110, 601 cm^{-1}; HRMS (ESI): $[M+H]^+$ calculated for $C_{13}H_{16}NO_2^+$ *m/z* 218.1176, found *m/z* 218.1173; mp = 155–157 ºC.

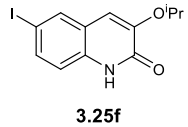

3.25f

6-Iodo-3-isopropoxyquinolin-2(1*H*)-one (3.25f): 63% yield, white solid;^{1}H NMR (500 MHz, $CDCl_3$) δ 12.00 (s, 1H), 7.83 (d, *J* = 1.6 Hz, 1H), 7.63 (dd, *J* = 8.5, 1.6 Hz, 1H), 7.21 (d, *J* = 8.6 Hz, 1H), 6.90 (s, 1H), 4.68 (hept, *J* = 6.1 Hz, 1H), 1.50 (d, *J* =

6.1 Hz, 6H). ^{13}C NMR (126 MHz, $CDCl_3$) δ 159.93, 147.38, 135.64, 134.45, 132.66, 122.69, 117.64, 112.65, 85.77, 71.42, 21.53. IR (thin film): 2980, 2904, 1663, 1609, 1568, 1273, 1227, 938, 720 cm^{-1}; HRMS (ESI): $[M+H]^+$ calculated for $C_{12}H_{13}INO_2^+$ *m/z* 329.9986, found *m/z* 329.9982; mp = 212–214 ºC.

6-Bromo-3-isopropoxyquinolin-2(1*H*)-one (3.25g): 36% yield, white solid; ^{1}H NMR (400 MHz, $CDCl_3$) δ 12.27 (s, 1H), 7.61 (d, *J* = 2.0 Hz, 1H), 7.46 – 7.32 (m, 2H), 6.90 (s, 1H), 4.67 (hept, *J* = 6.1Hz, 1H),1.48 (d, *J* = 6.1 Hz, 6H). ^{13}C NMR (101 MHz, $CDCl_3$) δ 160.03, 147.56, 132.14, 130.05, 128.25, 122.17, 117.56, 115.54, 112.83, 71.42, 21.53. IR (thin film): 2982, 2916, 1666, 1612, 1570, 1418, 1270, 938, 722 cm^{-1}; HRMS (ESI): $[M+H]^+$ calculated for $C_{12}H_{13}BrNO_2^+$ *m/z* 282.0124, found *m/z* 282.0125; mp = 192–194 ºC.

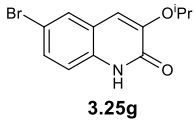

3.25g

6-Fluoro-3-isopropoxyquinolin-2(1*H*)-one (3.25h): 50% yield, white solid; ^{1}H NMR (500 MHz, $CDCl_3$) δ 11.71 (s, 1H), 7.38 (dd, *J* = 8.9, 4.7 Hz, 1H), 7.17 (dd, *J* = 8.9, 2.6 Hz, 1H), 7.12 (td, *J* = 8.6, 2.7 Hz, 1H), 6.95 (s, 1H), 4.70 (hept, *J* = 6.1Hz, 1H),1.51 (d, *J* = 6.1 Hz, 6H). ^{13}C NMR (126 MHz, $CDCl_3$) δ 159.62 (s), 158.56 (d, *J* = 241.2 Hz), 147.78 (s), 129.72 (s), 121.45 (d, *J* = 9.2 Hz), 117.12 (d, *J* = 8.7 Hz), 115.24 (d, *J* = 24.5 Hz), 113.27 (d, *J* = 3.1 Hz), 111.11 (d, *J* = 23.3 Hz), 71.38 (s), 21.55 (s). ^{19}F NMR (377 MHz, $CDCl_3$) δ –119.91(s, 1F). IR (thin film): 2988, 2947, 2866, 1660, 1622, 1583, 1521, 1422, 1272, 950, 852, 603 cm^{-1}; HRMS (ESI): $[M+H]^+$ calculated for $C_{12}H_{13}FNO_2^+$, *m/z* 222.0925, found *m/z* 222.0922; mp = 158–160 ºC.

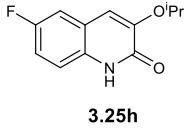

3.25h

3-Isopropoxy-6-methoxyquinolin-2(1*H*)-one (3.25i): 38% yield, white solid; ^{1}H NMR (400 MHz, $CDCl_3$) δ 12.08 (s, 1H), 7.37 (d, *J* = 8.8, 1H), 6.99 (dd, *J* = 8.9, 2.7 Hz, 1H), 6.97 (s, 1H), 6.91 (d, *J* = 2.6 Hz, 1H), 4.68 (hept, *J* = 6.1 Hz, 1H), 3.85 (s, 3H), 1.48 (d, *J* = 6.1 Hz, 6H). ^{13}C NMR (101 MHz, $CDCl_3$) δ 159.64, 155.42, 147.27, 127.94,

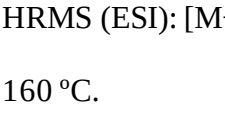

3.25i

121.22, 117.17, 116.23, 114.26, 107.90, 71.15, 55.65, 21.63. IR (thin film): 2978, 2929, 2839, 1654, 1615, 1576, 1501, 1421, 1283, 1216, 1185, 1109, 596 cm^{-1}; HRMS (ESI): $[M+H]^+$ calculated for $C_{13}H_{16}NO_3^+$ *m/z* 234.1125, found *m/z* 234.1122; mp = 170–172 ºC.

7-Bromo-3-isopropoxyquinolin-2(1*H*)-one (3.25j): 48% yield, white solid; ^1H NMR (500 MHz, $CDCl_3$) δ 12.22 (s, 1H), 7.56 (d, *J* = 1.3 Hz, 1H), 7.25 – 7.18 (m, 2H), 6.88 (s, 1H), 4.60 (hept, *J* = 6.1 Hz, 1H), 1.41 (d, *J* = 6.1 Hz, 6H). ^{13}C NMR (126 MHz, $CDCl_3$) δ 160.23, 146.99, 134.27, 127.34, 126.17, 120.88, 119.39, 118.44, 113.92, 71.44, 21.58. IR (thin film): 2977, 2931, 2839, 1659, 1607, 1565, 1400, 1374, 1262, 1189, 937, 872 cm^{-1}; HRMS (ESI): $[M+H]^+$ calculated for $C_{12}H_{13}BrNO_2^+$ *m/z* 282.0124, found *m/z* 282.0123; mp = 225–227 ºC.

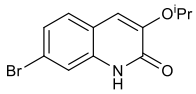

3.25j

7-Chloro-3-isopropoxyquinolin-2(1*H*)-one (3.25k): 13% yield, white solid; ^1H NMR (500 MHz, $CDCl_3$) δ 11.44 (s, 1H), 7.43 – 7.39 (m, 2H), 7.18 (dd, *J* = 8.4, 1.9 Hz, 1H), 6.98 (s, 1H), 4.70 (hept, *J* = 6.1 Hz, 1H), 1.51 (d, *J* = 6.1 Hz, 6H). ^{13}C NMR (126 MHz, $CDCl_3$) δ 159.86, 146.90, 133.98, 133.10, 127.32, 123.44, 119.03, 115.19, 113.79, 71.41, 21.58. IR (thin film): 2978, 2933, 1663, 1609, 1568, 1402, 1376, 1262, 1190, 943, 873, 627 cm^{-1}; HRMS (ESI): $[M+H]^+$ calculated for $C_{12}H_{13}ClNO_2^+$ *m/z* 238.0629, found *m/z* 238.0627; mp = 231–233 ºC.

3.25k

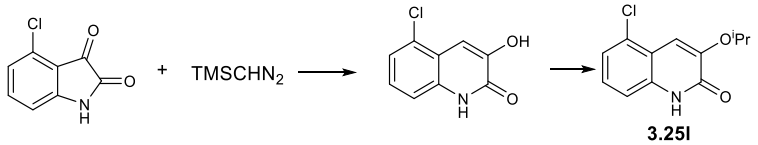

3.25l

5-Chloro-3-isopropoxyquinolin-2(1*H*)-one (3.25l): 33% yield from 5-chloro-3-hydroxyquinolin-2(1*H*) -one[56], white solid; ^1H NMR (500 MHz, $CDCl_3$) δ 11.37 (s, 1H), 7.31 (s, 1H), 7.24 –7.19 (m, 3H), 4.70 (hept, *J* = 6.1 Hz, 1H), 1.44 (d, *J* = 6.1 Hz, 6H). ^{13}C NMR (126

MHz, $CDCl_3$) δ 159.59, 147.67, 134.23, 130.36, 127.37, 123.39, 118.56, 114.42, 110.29, 71.54, 21.49. IR (thin film): 2980, 2902, 1662, 1605, 1571, 1431, 1237, 1177, 786 cm^{-1}; HRMS (ESI): $[M+H]^+$ calculated for $C_{12}H_{13}ClNO_2^+$ *m/z* 238.0629, found *m/z* 238.0627; mp = 209–211 ºC.

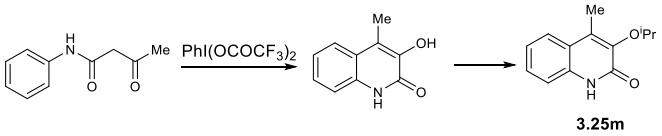

3.25m

3-Isopropoxy-4-methyl quinolin-2(1*H*)-one (3.25m): 34% yield from 3-hydroxy-4-methylquinolin- 2(1*H*)-one[58], white solid; ^1H NMR (400 MHz, $CDCl_3$) δ 12.26 (s, 1H), 7.66 (d, *J* = 8.4 Hz, 1H), 7.47 – 7.39 (m, 2H), 7.36 – 7.16 (m, 1H), 4.97 (hept, *J* = 6.2 Hz, 1H), 2.47 (s, 3H), 1.38 (d, *J* = 6.2 Hz, 6H). ^{13}C NMR (101 MHz, $CDCl_3$) δ 160.87, 143.82, 135.47, 135.17, 128.36, 124.28, 122.47, 121.23, 115.93, 74.01, 22.74, 12.10. IR (thin film): 2974, 2861, 1656, 1612, 1566, 1501, 1434, 1276, 1208, 743 cm^{-1}; HRMS (ESI): $[M+H]^+$ calculated for $C_{13}H_{16}NO_2^+$ *m/z* 218.1176, found *m/z* 218.1174; mp = 155–158 ºC.

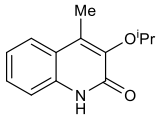

3.25m

8-Chloro-3-isopropoxyquinolin-2(1*H*)-one (3.25n): 4% yield, white solid; ^1H NMR (500 MHz, $CDCl_3$) δ 9.07 (s, 1H),δ 7.33 (dd, *J* = 7.9, 1.2 Hz, 1H), 7.31 (d, *J* = 8.0 Hz, 1H), 7.06 (t, *J* = 7.9 Hz, 1H), 6.84 (s, 1H), 4.60 (hept, *J* = 6.1 Hz, 1H), 1.39 (d, *J* = 6.1 Hz, 6H). ^{13}C NMR (126 MHz, $CDCl_3$) δ 158.20, 147.82, 129.58, 126.98, 125.05, 123.06, 121.70, 118.75, 112.91, 71.42, 21.51. IR (thin film): 3057, 2978, 2932, 1657, 1608, 1562, 1479, 1380, 1292, 1249, 1108, 930, 835 cm^{-1}; HRMS (ESI): $[M+H]^+$ calculated for $C_{12}H_{13}ClNO_2^+$ *m/z* 238.0629, found *m/z* 238.0626; mp = 136–138 ºC.

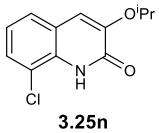

3.25n

8-Fluoro-3-isopropoxyquinolin-2(1*H*)-one (3.25o): 29% yield, white solid; ^1H NMR (500 MHz, $CDCl_3$) δ 9.45 (s, 1H), 7.26 – 7.21 (m, 1H), 7.15 – 7.07 (m, 2H), 6.94 (s, 1H), 4.66 (hept, *J* = 6.1 Hz, 1H), 1.46 (d, *J* = 6.1 Hz, 6H). ^{13}C NMR (126 MHz, $CDCl_3$) δ

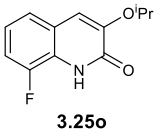

3.25o

158.10 (s), 149.02 (d, J = 244.7 Hz), 147.96 (s), 122.55 (d, J = 7.3 Hz), 122.33 (d, J = 2.9 Hz), 122.05 (d, J = 13.4 Hz), 121.63 (d, J = 3.6 Hz), 112.96 (d, J = 2.7 Hz), 112.35 (d, J = 17.2 Hz), 71.34 (s), 21.51 (s). ^{19}F NMR (377 MHz, $CDCl_3$) δ –135.99 (s, 1F). IR (thin film): 2974, 2484, 1643, 1606, 1576, 1489, 1437, 1257, 1236, 1105, 868, 791, 531 cm^{-1}; HRMS (ESI): $[M+H]^+$ calculated for $C_{12}H_{13}FNO_2^+$ *m/z* 222.0925,found *m/z* 222.0922; mp = 175–176 ºC.

3-Isopropoxy-2*H*-chromen-2-one (3.25p): 82% yield from 3-hydroxycoumarin, white solid; ^{1}H NMR (500 MHz, $CDCl_3$) δ 7.33 – 7.27 (m, 2H), 7.22 (d, J = 8.2 Hz, 1H), 7.17 (td, J = 7.5, 1.2 Hz, 1H), 6.76 (s, 1H), 4.54 (hept, J = 6.1 Hz, 1H), 1.36 (d, J = 6.1 Hz, 6H). ^{13}C NMR (126 MHz, $CDCl_3$) δ 158.12, 149.53, 142.67, 128.34, 126.30, 124.60, 119.90, 116.24, 115.13, 71.85, 21.50. IR (thin film): 3068, 2978, 2932, 1728, 1621, 1453, 1295, 1134, 1107, 930, 755 cm^{-1}; HRMS (ESI): $[M+H]^+$ calculated for $C_{12}H_{13}O_3^+$ *m/z* 205.0859, found *m/z* 205.0857; mp = 71–73 ºC.

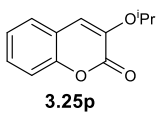

3.25p

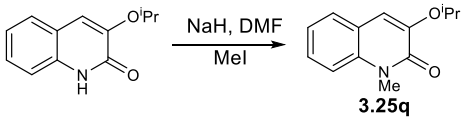

3.25q

3-Isopropoxy-1-methylquinolin-2(1*H*)-one(3.25q) was prepared from **3.25c** following a known method[51]: 98% yield, colorless oil; ^{1}H NMR (500 MHz, $CDCl_3$) δ 7.47 (dd, J = 7.7, 1.1 Hz, 1H), 7.42 (ddd, J = 8.7, 7.3, 1.4 Hz, 1H), 7.31 (d, J = 8.4 Hz, 1H), 7.22 (t, J = 7.5 Hz, 1H), 6.91 (s, 1H), 4.64 (hept, J = 6.1 Hz, 1H), 3.77 (s, 3H), 1.44 (d, J = 6.1 Hz, 6H). ^{13}C NMR (126 MHz, $CDCl_3$) δ 158.77, 146.59, 135.48, 127.34, 127.09, 122.44, 120.78, 113.80, 113.09, 71.01, 29.98, 21.64. IR (thin film): 2978, 1650, 1600, 1462, 1238, 1115, 751 cm^{-1}; HRMS (ESI): $[M+H]^+$ calculated for $C_{13}H_{16}NO_2^+$ *m/z* 218.1176, found *m/z* 218.1172.

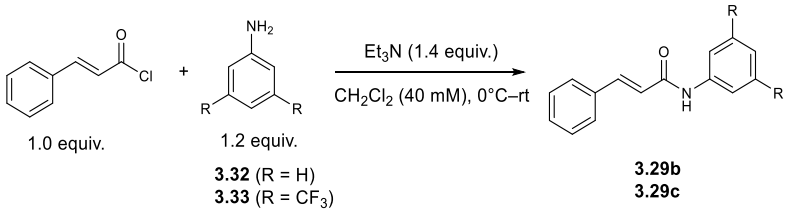

General Procedure 3.A: To a stirring solution of aniline **3.32** or **3.33** (2.6 mmol, 1.3 equiv.) and Et_3N (2.8 mmol, 1.4 equiv.) in CH_2Cl_2 (40 mL) was added cinnamoyl chloride (2.0 mmol, 1.0 equiv.) slowly at 0ºC. The reaction was allowed to warm to room temperature and stirred for 3 h. Following this this mixture was washed concomitantly with 10 mL 2M HCl, 10 mL H_2O, and 10 mL 2M K_2CO_3. The organic layer was dried using $MgSO_4$ and concentrated *in vacuo*. The crude product was purified by flash column chromatography on silica gel to afford the cinnamamide.

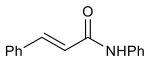

(**3.29b**): Prepared according to General Procedure 3.A using **3.32** (0.182 mL, 2.6 mmol, 1.3 equiv.), Et_3N (0.4 mL, 2.80 mmol, 1.4 equiv.), and cinnamoyl chloride (317.4 mg, 2.00 mmol, 1.0 equiv.). Following workup, the crude residue was purified by flash column chromatography (CH_2Cl_2) to afford a colorless powder (434.8 mg, 1.94 mmol, 93% yield).

^{1}H NMR (500 MHz, $CDCl_3$) δ 7.76 (d, *J* = 15.5 Hz, 1H), 7.63 (d, *J* = 7.9 Hz, 2H), 7.52 (dd, *J* = 6.6, 2.9 Hz, 2H), 7.46 (s, 1H), 7.39 – 7.33 (m, 5H), 7.13 (t, *J* = 7.4 Hz, 1H), 6.57 (d, *J* = 15.5 Hz, 1H).

^{13}C NMR (126 MHz, $CDCl_3$) δ 163.91, 142.44, 137.97, 134.57, 129.97, 129.07, 128.87, 127.94, 124.43, 120.78, 119.90.

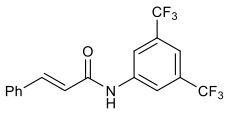

(**3.29c**): Prepared according to General Procedure 3.A using **3.33** (0.5957 g, 2.6 mmol, 1.3 equiv.), Et_3N (0.4 mL, 2.80 mmol, 1.4 equiv.), and cinnamoyl chloride (330.0 mg, 2.00 mmol, 1.0 equiv.). Following workup, the crude residue was purified by

flash column chromatography (4:1 pentane:Et_2O) to afford a colorless powder (134.8 mg, 0.38 mmol, 19% yield).

^{1}H NMR (400 MHz, $CDCl_3$) δ 8.15 (s, 2H), 7.82 (d, *J* = 15.5 Hz, 1H), 7.63 (s, 1H), 7.59 – 7.52 (m, 3H), 7.46 – 7.39 (m, 3H), 6.54 (d, *J* = 15.5 Hz, 1H).

^{13}C NMR (126 MHz, $CDCl_3$) δ 164.24, 144.25, 139.38, 134.02, 132.43 (q, *J* = 33.5 Hz), 130.58, 129.01, 128.12, 123.03 (q, *J* = 272.8 Hz), 119.50 (q, *J* = 3.7 Hz), 119.36, 117.62 (*app*. p, *J* = 3.8 Hz).

3.5.4 Photosensitized [2+2] Cycloadditions

3.5.4.a Racemic [2+2] Cycloadditions

A 12 mL vial was charged with substrate (0.1 mmol, 1.0 equiv.), (±)-**3.28f** (0.0015 mmol, 1.5 mol%), maleimide (0.5 mmol, 5 equiv.) and dry CH_2Cl_2 (5 mL). The mixture was irradiated with a 16 W blue LED lamp or 15 W blue LED lamp for 14–24 h at room temperature, then concentrated *in vacuo*. Purification by silica gel chromatography (EtOAc:Hexanes = 2:1) provided racemic cyclobutane.

3.5.4.b Enantioselective [2+2] Cycloadditions

A 25 mL Schlenk tube was charged with a magnetic stir bar, substrate (0.2 mmol, 1.0 equiv.), (Λ)-**3.28f** (0.003 mmol, 1.5 mol%), maleimide (1 mmol, 5 equiv.) and dry CH_2Cl_2 (10 mL). The mixture was irradiated with a 15 W blue LED lamp for 24 h at –78 °C, then the mixture was concentrated *in vacuo*. The residue was purified by silica gel column chromatography (EtOAc:Hexanes = 2:1 or EtOAc:CH_2Cl_2 = 1:1) to afford the target [2+2] cycloadduct. In cases where a mixture of diastereomers were formed, these products could not be separated by flash column chromatography. Instead, we found that the minor product could be removed by washing

with $CHCl_3$. The resulting residue, which was the major diastereomer, was used for further characterization.

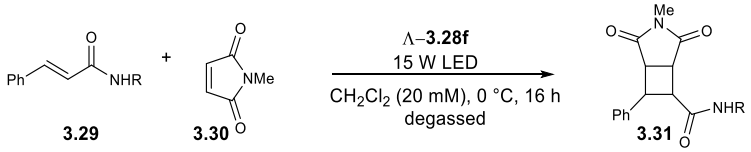

General Procedure 3.B: A Schlenk tube was charged with substrate **2.29** (67 µmol, 1.0 equiv.), *N*-methylmaleimide (0.67 mmol, 10 equiv.) **3.28f** (0.67 µmol, 0.01 equiv.), dry CH_2Cl_2 (3 mL, 20 mM with respect to substrate), and degassed by three *freeze-pump-thaw* (4 min.) cycles. The solution was irradiated by a 15 W blue LED lamp for 16 h at 0 °C, then concentrated *in vacuo*. Purification by silica gel chromatography provided racemic cyclobutane, which was used to develop and calibrate chiral HPLC methods. All characterization and spectroscopic data are reported for the enantioenriched species.

(6a*R*,6b*S*,9a*S*,9b*R*)-6a-Butoxy-9a,9b-dihydro-5*H*-pyrrolo[3',4':3,4]cyclobuta[1,2-*c*]quinoline-6,7,9(6a*H*,6b*H*,8*H*)-trione (3.27a): 14% NMR yield, 7% ee (HPLC, Daicel CHIRALPAK® AD-H, Gradient 5% ^{i}PrOH (95% Hexane) to 40% ^{i}PrOH (60% Hexane), 1.0 mL/min, 221 nm; t_1 = 11.44 min, t_2 = 14.79 min); ^{1}H NMR (500 MHz, CD_3OD) δ 7.19 – 7.11 (m, 2H), 6.97 (td, *J* = 7.5, 1.0 Hz, 1H), 6.82 (d, *J* = 7.9 Hz, 1H), 3.78 (d, *J* = 5.6 Hz, 1H), 3.61 (dd, *J* = 6.5, 1.2 Hz, 1H), 3.38 (dt, *J* = 8.7, 6.2 Hz, 1H), 3.26 (dt, *J* = 8.7, 6.7 Hz, 1H), 2.77 (dd, *J* = 6.4, 5.7 Hz, 1H), 1.46 – 1.33 (m, 2H), 1.31 – 1.17 (m, 2H), 0.77 (t, *J* = 7.4 Hz, 3H). ^{13}C NMR (126 MHz, CD_3OD) δ 179.84, 174.84, 167.41, 135.69, 128.66, 127.86, 123.76, 121.23, 115.63, 73.16, 64.83, 48.39, 47.18, 41.10, 31.39, 18.75, 12.73. IR (thin film): 3238, 2958, 1773, 1716, 1679, 1598, 1338, 1182, 760 cm^{-1}; HRMS (ESI): $[M+NH_4]^+$ calculated for $C_{17}H_{22}N_3O_4^+$ *m/z* 332.1605, found *m/z* 332.1599; mp = 233–235 ºC.

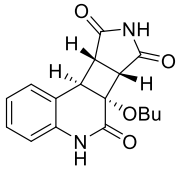

3.27a

(6a*R*,6b*S*,9a*S*,9b*R*)-6a-Methoxy-9a,9b-dihydro-5*H*-pyrrolo[3',4':3,4]cyclobuta[1,2-*c*]quinoline-6,7,9(6a*H*,6b*H*,8*H*)-trione (3.27b): 30% NMR yield, 70% ee (HPLC, Daicel CHIRALPAK® AD-H, Gradient 5% ^{i}PrOH (95% Hexane) to 40% ^{i}PrOH (60% Hexane), 1.0 mL/min, 277.4 nm; t_1 = 13.64 min, t_2 = 15.54 min); ^{1}H NMR (500 MHz, CD_3OD) δ 7.27 – 7.21 (m, 2H), 7.07 (td, *J* = 7.6, 0.8 Hz, 1H), 6.92 (d, *J* = 7.9 Hz, 1H), 3.93 (d, *J* = 5.5 Hz, 1H), 3.70 (dd, *J* = 6.5, 1.0 Hz, 1H), 3.26 (s, 3H), 2.85 (dd, *J* = 6.3, 5.8 Hz, 1H). ^{13}C NMR (126 MHz, CD_3OD) δ 179.80, 174.92, 167.08, 135.65, 128.66, 127.84, 123.79, 121.26, 115.65, 73.74, 51.97, 48.20, 46.58, 40.96. IR (thin film): 3231, 3086, 1771, 1713, 1679, 1600, 1494, 1341, 1183, 761 cm^{-1}; HRMS (ESI): $[M+NH_4]^+$ calculated for $C_{14}H_{16}N_3O_4^+$ *m/z* 290.1135, found *m/z* 290.1134; mp > 260 ºC.

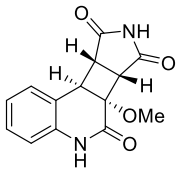

3.27b

(6a*R*,6b*S*,9a*S*,9b*R*)-6a-Isopropoxy-9a,9b-dihydro-5*H*-pyrrolo[3',4':3,4]cyclobuta[1,2-*c*]quinoline-6,7,9(6a*H*,6b*H*,8*H*)-trione (3.27c): 82% yield, white solid, 97% ee (SFC, Daicel CHIRALPAK® AD-H, isocratic 20% MeOH, 3.0 mL/min, 221 nm; t_1 = 4.03 min, t_2 = 5.58 min). ^{1}H NMR (400 MHz, CD_3OD) δ 7.16 (td, *J* = 7.8, 1.4 Hz, 1H), 7.12 (d, *J* = 7.6 Hz, 1H), 6.97 (td, *J* = 7.6, 1.1 Hz, 1H), 6.85 (d, *J* = 7.6 Hz, 1H), 3.82 (d, *J* = 5.8 Hz, 1H), 3.71 (hept, *J* = 6.1 Hz, 1H), 3.58 (dd, *J* = 6.5, 1.2 Hz, 1H), 2.74 (dd, *J* = 6.4, 5.9 Hz, 1H), 1.00 (d, *J* = 6.1 Hz, 3H), 0.93 (d, *J* = 6.1 Hz, 3H). ^{13}C NMR (126 MHz, CD_3OD) δ 179.89, 174.92, 168.61, 135.77, 128.76, 127.91, 123.83, 121.22, 115.71, 72.78, 69.25, 49.32, 48.48, 40.83, 22.52, 22.09.IR (thin film): 3233, 1719, 1668, 1595, 1387, 1120, 1086 cm^{-1}; HRMS (ESI): $[M+NH_4]^+$ calculated for $C_{16}H_{20}N_3O_4^+$ *m/z* 318.1448, found *m/z* 318.1445; mp = 152–154 ºC; $[\alpha]_{22}^{D}$ –91.8º (*c*0.305, CH_3OH).

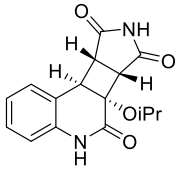

3.27c

(6a*R*,6b*S*,9a*S*,9b*R*)-6a-Isopropoxy-2-methyl-9a,9b-dihydro-5*H*-

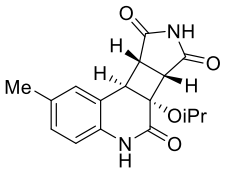

3.27e

pyrrolo[3',4':3,4]cyclobuta[1,2-*c*]quinoline-6,7,9(6a*H*,6b*H*,8*H*)-trione (3.27e): >99% yield, white solid, 97% ee (SFC, Daicel CHIRALPAK® OJ-H, isocratic 20% MeOH, 3.0 mL/min, 221 nm; t_1 = 3.27 min, t_2 = 4.42 min). ^{1}H NMR (500 MHz, CD_3OD) δ 7.10 (dd, *J* = 8.1, 1.2 Hz, 1H), 7.06 (s, 1H), 6.86 (d, *J* = 8.1 Hz, 1H), 3.89 (d, *J* = 5.8 Hz, 1H), 3.82 (hept, *J* = 6.1 Hz, 1H), 3.69 (dd, *J* = 6.5, 1.2 Hz, 1H), 2.84 (dd, *J* = 6.5, 5.8 Hz, 1H), 2.31 (s, 3H), 1.12 (d, *J* = 6.1 Hz, 3H), 1.05 (d, *J* = 6.1 Hz, 3H). ^{13}C NMR (126 MHz, CD_3OD) δ 179.98, 174.91, 168.48, 133.72, 133.28, 129.23, 128.20, 121.07, 115.59, 72.76, 69.19, 49.32, 48.56, 40.87, 22.49, 22.03, 19.31. IR(thin film): 3207, 2975, 1772, 1711, 1671, 1509, 1335, 1115, 821, 731 cm^{-1}; HRMS (ESI): $[M+NH_4]^+$ calculated for $C_{17}H_{22}N_3O_4^+$ *m/z* 332.1605, found *m/z* 332.1601; mp = 155–156 ºC; $[\alpha]_{22}^{D}$+44º (*c*0.25, CH_3OH).

(6a*R*,6b*S*,9a*S*,9b*R*)-2-Iodo-6a-isopropoxy-9a,9b-dihydro-5*H*-

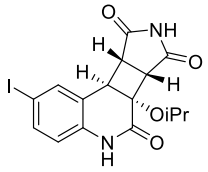

3.27f

pyrrolo[3',4':3,4]cyclobuta[1,2-*c*]quinoline-6,7,9(6a*H*,6b*H*,8*H*)-trione (3.27f): 67% yield, 9:1 d.r., white solid, 99% ee (SFC, Daicel CHIRALPAK® OD-H, isocratic 20% MeOH, 3.0 mL/min, 221 nm; t_1 = 10.28 min, t_2 = 11.34 min). ^{1}H NMR (500 MHz, CD_3OD) δ 7.66 – 7.52 (m, 2H), 6.83 – 6.71 (m, 1H), 3.95 (d, *J* = 6.1 Hz, 1H), 3.83 (hept, *J* = 6.1 Hz, 1H), 3.69 (dd, *J* = 6.1, 1.0 Hz, 1H), 2.89 (t, *J* = 6.1 Hz, 1H), 1.12 (d, *J* = 6.1 Hz, 3H), 1.06 (d, *J* = 6.1 Hz, 3H). ^{13}C NMR (126 MHz, CD_3OD) δ 179.69, 174.70, 168.37, 137.66, 136.54, 135.78, 123.63, 117.63, 85.69, 72.52, 69.36, 49.34, 47.68, 40.66, 22.47, 22.04. IR (thin film): 3057, 2945, 1723,1690, 1609, 1353, 1226, 1067, 867 cm^{-1}; HRMS (ESI): $[M+NH_4]^+$ calculated for $C_{16}H_{19}IN_3O_4^+$ *m/z* 444.0415, found *m/z* 444.0408; mp = 230–233 ºC; $[\alpha]_{22}^{D}$–24º (*c*0.28, CH_3OH).

(6a*R*,6b*S*,9a*S*,9b*R*)-2-Bromo-6a-isopropoxy-9a,9b-dihydro-5*H*-

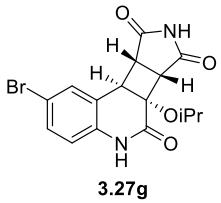

3.27g

pyrrolo[3',4':3,4]cyclobuta[1,2-*c*]quinoline-6,7,9(6a*H*,6b*H*,8*H*)-trione (3.27g): 71% yield, 9:1 d.r., white solid, 95% ee (SFC, Daicel CHIRALPAK® OD-H, isocratic 20% MeOH, 3.0 mL/min, 221 nm; t_1 = 8.23 min, t_2 = 9.00 min). ^{1}H NMR (500 MHz, CD_3OD) δ 7.44–7.40 (m, 2H), 6.98 – 6.80 (m, 1H), 3.98 (d, *J* = 5.8 Hz, 1H), 3.83 (hept, *J* = 6.1 Hz, 1H), 3.71 (dd, *J* = 6.6, 1.0 Hz, 1H), 2.91 (t, *J* = 6.2 Hz, 1H), 1.11 (d, *J* = 6.1 Hz, 3H), 1.06 (d, *J* = 6.1 Hz, 3H). ^{13}C NMR (126 MHz, CD_3OD) δ 179.65, 174.72, 168.37, 135.18, 131.62, 130.61, 123.39, 117.47, 115.71, 72.48, 69.37, 49.34, 47.81, 40.64, 22.49, 22.07.IR(thin film): 3217, 2974, 2928, 1775, 1715, 1677, 1490, 1341, 1182 cm^{-1}; HRMS (ESI): $[M+NH_4]^+$ calculated for $C_{16}H_{19}BrN_3O_4^+$ *m/z* 396.0553, found *m/z* 396.0549; mp = 223–225 ºC; $[\alpha]_{22}^{D}$+43º (*c*0.23, CH_3OH)

(6a*R*,6b*S*,9a*S*,9b*R*)-2-Fluoro-6a-isopropoxy-9a,9b-dihydro-5*H*-

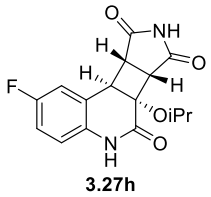

3.27h

pyrrolo[3',4':3,4]cyclobuta[1,2-*c*]quinoline-6,7,9(6a*H*,6b*H*,8*H*)-trione (3.27h): 77% yield, white solid, 90% ee (SFC, Daicel CHIRALPAK® OJ-H, isocratic 20% MeOH, 3.0 mL/min, 221 nm; t_1 = 2.65 min, t_2 = 4.22 min). ^{1}H NMR (500 MHz, CD_3OD) δ 7.08 – 7.01 (m, 2H), 6.98 (dd, J=8.3, 4.8 Hz 1H), 3.97 (d, *J* = 5.8 Hz, 1H), 3.83 (hept, *J* = 6.1 Hz, 1H), 3.70 (dd, *J* = 6.5, 1.1 Hz, 1H),2.90 (t, *J* = 6.4 Hz, 1H), 1.12 (d, *J* = 6.1 Hz, 3H), 1.06 (d, *J* = 6.1 Hz, 3H). ^{13}C NMR (126 MHz, CD_3OD) δ 179.67 (s), 174.78 (s), 168.25 (s), 159.04 (d, *J* = 242.3 Hz), 132.23 (d, *J* = 2.6 Hz), 122.99 (d, *J* = 7.6 Hz), 117.15 (d, *J* = 8.2 Hz), 115.33 (d, *J* = 23.2 Hz), 114.37 (d, *J* = 23.6 Hz), 72.34 (s), 69.32 (s), 49.32 (s), 48.15 (d, *J* = 0.9 Hz), 40.63 (s), 22.44 (s), 22.05 (s). ^{19}F NMR (377 MHz, CD_3OD) δ –120.52 (s, 1F). IR (thin film): 3231, 2977, 1718, 1670, 1502, 1236, 1017, 658 cm^{-1}; HRMS (ESI): $[M+NH_4]^+$

calculated for $C_{16}H_{19}FN_3O_4^+$ *m/z* 336.1354, found *m/z* 336.1347; mp = 154–156 ºC; $[\alpha]_{22}^{D}$+12º (*c*0.39, CH_3OH).

(6a*R*,6b*S*,9a*S*,9b*R*)-6a-Isopropoxy-2-methoxy-9a,9b-dihydro-5*H*-pyrrolo[3',4':3,4]cyclobuta[1,2-*c*]quinoline-6,7,9(6a*H*,6b*H*,8*H*)-trione (3.27i): 60% yield, white solid, 94% ee (SFC, Daicel CHIRALPAK® OJ-H, isocratic 20% MeOH, 3.0 mL/min, 221 nm; t_1 = 3.19 min, t_2 = 5.07 min). ^{1}H NMR (500 MHz, CD_3OD) δ 6.79 (d, *J* = 8.7 Hz, 1H), 6.74 (dd, *J* = 8.7, 2.7 Hz, 1H), 6.70 (d, *J* = 2.7 Hz, 1H), 3.80 (d, *J* = 5.8 Hz, 1H), 3.71 (hept, *J* = 6.1 Hz, 1H), 3.67 (s, 3H), 3.57 (dd, *J* = 6.5, 1.2 Hz, 1H), 2.75 (t, *J* = 6.4 Hz, 1H), 1.00 (d, *J* = 6.1 Hz, 3H), 0.93 (d, *J* = 6.1 Hz, 3H). ^{13}C NMR (126 MHz, CD_3OD) δ 179.98, 174.87, 168.10, 156.50, 129.05, 122.30, 116.81, 114.45, 112.64, 72.59, 69.21, 54.67, 49.27, 48.66, 40.80, 22.49, 22.05. IR (thin film): 3233, 2973, 1711, 1669, 1505, 1241, 815, 568 cm^{-1}; HRMS (ESI): $[M+NH_4]^+$ calculated for $C_{17}H_{22}N_3O_5^+$ *m/z* 348.1554, found *m/z* 348.1549; mp = 166–168 ºC; $[\alpha]_{22}^{D}$+51º (*c*0.80, acetone).

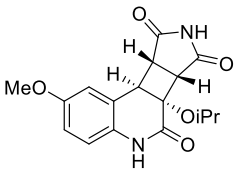

3.27i

(6a*R*,6b*S*,9a*S*,9b*R*)-3-Bromo-6a-isopropoxy-9a,9b-dihydro-5*H*-pyrrolo[3',4':3,4]cyclobuta[1,2-*c*]quinoline-6,7,9(6a*H*,6b*H*,8*H*)-trione (3.27j): 92% yield, white solid, 93% ee (SFC, Daicel CHIRALPAK® OD-H, isocratic 20% MeOH, 3.0 mL/min, 221 nm; t_1 = 8.61 min, t_2 = 9.98 min). ^{1}H NMR (500 MHz, CD_3OD) δ 7.24 (dd, *J* = 8.1, 1.9 Hz, 1H), 7.16 (d, *J* = 8.1 Hz, 1H), 7.15 (d, *J* = 1.8 Hz, 1H),3.93 (d, *J* = 5.8 Hz, 1H), 3.84 (hept, *J* = 6.1 Hz, 1H), 3.70 (dd, *J* = 6.5, 1.1 Hz, 1H), 2.89 (dd, *J* = 6.5, 5.8 Hz, 1H), 1.12 (d, *J* = 6.1 Hz, 3H), 1.06 (d, *J* = 6.1 Hz, 3H). ^{13}C NMR (126 MHz, CD_3OD) δ 179.65, 174.75, 168.49, 137.39, 129.60, 126.46, 121.84, 120.36, 118.40, 72.58, 69.36, 49.31, 47.90, 40.62, 22.46, 22.07. IR (thin film): 3205, 2974, 1775, 1714, 1680, 1328, 1124,

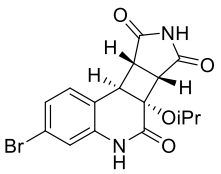

3.27j

1094, 719 cm^{-1}; HRMS (ESI): $[M+NH_4]^+$ calculated for $C_{16}H_{19}BrN_3O_4^+$ *m/z* 396.0554, found *m/z* 396.0548; mp > 260 ºC; $[\alpha]_{22}^{D}$+29º (*c*0.55, CH_3OH).

(6a*R*,6b*S*,9a*S*,9b*R*)-3-Chloro-6a-isopropoxy-9a,9b-dihydro-5*H*-

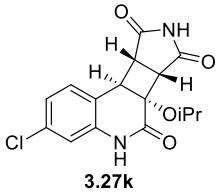

3.27k

pyrrolo[3',4':3,4]cyclobuta[1,2-*c*]quinoline-6,7,9(6a*H*,6b*H*,8*H*)-trione (3.27k): 85% yield, white solid, 97% ee (SFC, Daicel CHIRALPAK® OD-H, isocratic 20% MeOH, 3.0 mL/min, 221 nm; t_1 = 7.14 min, t_2 = 7.92 min). ^{1}H NMR (500 MHz, CD_3OD) δ 7.23 (d, *J* = 8.2 Hz, 1H), 7.08 (dd, *J* = 8.2, 2.0 Hz, 1H), 7.00 (d, *J* = 2.0 Hz, 1H), 3.95 (d, *J* = 5.9 Hz, 1H), 3.83 (hept, *J* = 6.1 Hz, 1H), 3.70 (dd, *J* = 6.4, 1.2 Hz, 1H), 2.89 (dd, *J* = 6.4, 5.9 Hz, 1H), 1.12 (d, *J* = 6.1 Hz, 3H), 1.05 (d, *J* = 6.1 Hz, 3H). ^{13}C NMR (126 MHz, CD_3OD) δ 179.71, 174.81, 168.54, 137.23, 134.17, 129.40, 123.48, 119.92, 115.50, 72.62, 69.37, 49.30, 47.82, 40.72, 22.48, 22.09. IR (thin film): 3196, 2975, 1728, 1675, 1587, 1358, 1211, 1080, 763 cm^{-1}; HRMS (ESI): $[M+NH_4]^+$ calculated for $C_{16}H_{19}ClN_3O_4^+$ *m/z* 352.1059, found *m/z* 352.1052; mp = 233–235 ºC; $[\alpha]_{22}^{D}$–21º (*c*0.29, CH_3OH).

(6a*R*,6b*S*,9a*S*,9b*R*)-1-Chloro-6a-isopropoxy-9a,9b-dihydro-5*H*-

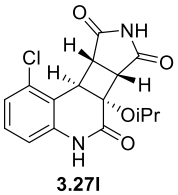

3.27l

pyrrolo[3',4':3,4]cyclobuta[1,2-*c*]quinoline-6,7,9(6a*H*,6b*H*,8*H*)-trione (3.27l): 99% yield, 6:1 d.r., white solid, 99% ee (SFC, Daicel CHIRALPAK® OD-H, isocratic 20% MeOH, 3.0 mL/min, 221 nm; t_1 = 7.13 min, t_2 = 10.17 min). ^{1}H NMR (500 MHz, CD_3OD) δ 7.28 (t, *J* = 8.1 Hz, 1H), 7.17 (dd, *J* = 8.1, 0.6 Hz, 1H), 6.92 (dd, *J* = 8.1, 0.6 Hz, 1H), 4.15 (dd, *J* = 5.8, 0.9 Hz, 1H), 3.84 (hept, *J* = 6.1 Hz, 1H), 3.76 (dd, *J* = 6.5, 0.9 Hz, 1H), 2.94 (dd, *J* = 6.5, 5.8 Hz, 1H), 1.14 (d, *J* = 6.1 Hz, 3H), 1.06 (d, *J* = 6.1 Hz, 3H). ^{13}C NMR (126 MHz, CD_3OD) δ 178.82, 174.61, 168.01, 137.57, 133.55, 129.80, 124.10, 119.09, 114.39, 72.51, 69.48, 49.63, 46.19, 40.55, 22.35, 22.15. IR (thin film): 3211, 3068, 2978, 1772, 1712, 1678, 1585, 1334, 1181, 785, 733 cm^{-1}; HRMS (ESI): $[M+NH_4]^+$ calculated for

$C_{16}H_{19}ClN_3O_4^+$ *m/z* 352.1059, found *m/z* 352.1055; mp = 248–250 ºC; $[\alpha]_{22}^{D}$+106º (*c*0.28, CH_3OH).

(6a*S*,6b*S*,9a*R*,9b*R*)-6a-Isopropoxy-9b-methyl-9a,9b-dihydro-5*H*-

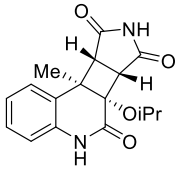

3.27m

pyrrolo[3',4':3,4]cyclobuta[1,2-*c*]quinoline-6,7,9(6a*H*,6b*H*,8*H*)-trione (3.27m): 78% yield, 5:1 d.r., white solid, 85% ee (SFC, Daicel CHIRALPAK® AD-H, isocratic 20% MeOH, 3.0 mL/min, 221 nm; t_1 = 5.13 min, t_2 = 6.73 min). ^{1}H NMR (500 MHz, CD_3OD) δ 7.33 (dd, *J* = 7.8, 1.2 Hz, 1H), 7.25 (td, *J* = 7.8, 1.2 Hz, 1H), 7.11 (td, *J* = 7.8, 1.2 Hz, 1H), 6.93 (dd, *J* = 7.8, 1.2 Hz, 1H), 4.07 (hept, *J* = 6.1 Hz, 1H), 3.72 (d, *J* = 7.0 Hz, 1H), 2.94 (d, *J* = 7.0 Hz, 1H), 1.65 (s, 3H), 1.19 (d, *J* = 6.1 Hz, 3H), 1.03 (d, *J* = 6.1 Hz, 3H). ^{13}C NMR (126 MHz, CD_3OD) δ 178.06, 175.69, 168.30, 134.74, 128.39, 127.65, 125.68, 124.00, 115.70, 75.30, 69.54, 49.17, 48.07, 45.29, 22.32, 22.32, 16.86. IR (thin film): 3121, 3064, 2978, 1771, 1707, 1658, 1589, 1384, 1339, 1162, 851, 772 cm^{-1}; HRMS (ESI): $[M+NH_4]^+$ calculated for $C_{17}H_{22}N_3O_4^+$ *m/z* 332.1605, found *m/z* 332.1600; mp = 260–261 ºC; $[\alpha]_{22}^{D}$+57º (*c*0.46, CH_3OH).

(6a*R*,6b*S*,9a*S*,9b*R*)-4-Chloro-6a-isopropoxy-9a,9b-dihydro-5*H*-

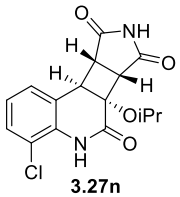

3.27n

pyrrolo[3',4':3,4]cyclobuta[1,2-*c*]quinoline-6,7,9(6a*H*,6b*H*,8*H*)-trione (3.27n): 74% yield, white solid, 51% ee (SFC, Daicel CHIRALPAK® OD-H, isocratic 20% MeOH, 3.0 mL/min, 221 nm; t_1 = 5.9 min, t_2 = 6.56 min). ^{1}H NMR (500 MHz, CD_3OD) δ 7.40 (dd, *J* = 7.8, 1.2 Hz, 1H), 7.22 (d, *J* = 7.8 Hz, 1H), 7.09 (t, *J* = 7.8 Hz, 1H), 4.00 (d, *J* = 6.5 Hz, 1H), 3.86 (hept, *J* = 6.1 Hz, 1H), 3.74 (dd, *J* = 6.5, 1.0 Hz, 1H), 2.92 (t, *J* = 6.5 Hz, 1H), 1.12 (d, *J* = 6.1 Hz, 3H), 1.06 (d, *J* = 6.1 Hz, 3H). ^{13}C NMR (126 MHz, CD_3OD) δ 179.51, 174.72, 168.50, 132.51, 129.17, 126.84, 124.31, 123.20, 119.69, 72.84, 69.51, 49.29, 48.41, 40.55, 22.44, 22.15. IR (thin film): 3168, 3088, 2980, 1773, 1707, 1679, 1479, 1341, 1183,

793, 698, cm^{-1}; HRMS (ESI): $[M+NH_4]^+$ calculated for $C_{16}H_{19}ClN_3O_4^+$ *m/z* 352.1059, found *m/z* 352.1055; mp = 199–201 ºC; $[\alpha]_{22}^{D}$+28º (*c*1.08, CH_3OH).

(6a*R*,6b*S*,9a*S*,9b*R*)-4-Fluoro-6a-isopropoxy-9a,9b-dihydro-5*H*-

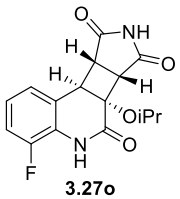

3.27o

pyrrolo[3',4':3,4]cyclobuta[1,2-*c*]quinoline-6,7,9(6a*H*,6b*H*,8*H*)-trione (3.27o): 79% yield, white solid, 14% ee (SFC, Daicel CHIRALPAK® OD-H, isocratic 20% MeOH, 3.0 mL/min, 221 nm; t_1 = 4.62 min, t_2 = 5.01 min). ^{1}H NMR (500 MHz, CD_3OD) δ 7.17 – 7.05 (m, 3H), 4.00 (d, *J* = 5.8 Hz, 1H), 3.86 (hept, *J* = 6.1 Hz, 1H), 3.73 (dd, *J* = 6.5, 1.2 Hz, 1H), 2.92 (dd, *J* = 6.5, 5.8 Hz, 1H), 1.13 (d, *J* = 6.1 Hz, 3H), 1.06 (d, *J* = 6.1 Hz, 3H). ^{13}C NMR (126 MHz, CD_3OD) δ 179.60 (s), 174.75 (s), 168.20 (s), 149.82 (d, *J* = 245.0 Hz), 124.25 (d, *J* = 12.5 Hz), 123.90 (d, *J* = 7.5 Hz), 123.42 (d, *J* = 2.2 Hz), 123.40 (d, *J* = 3.6 Hz), 114.84 (d, *J* = 18.6 Hz), 72.70 (s), 69.42 (s), 49.35 (s), 48.23 (d, *J* = 2.4 Hz), 40.69 (s), 22.45 (s), 22.11 (s). ^{19}F NMR (377 MHz, CD_3OD) δ –133.88 (s, 1F).IR (thin film): 3191, 2976, 1778, 1716, 1665, 1499, 1339, 1213, 1120, 787 cm^{-1}; HRMS (ESI): $[M+NH_4]^+$ calculated for $C_{16}H_{19}FN_3O_4^+$ *m/z* 336.1354, found *m/z* 336.1352; mp > 260 ºC; $[\alpha]_{22}^{D}$ +11º (*c*0.35, acetone).

(6a*R*,6b*S*,9a*S*,9b*R*)-6a-Isopropoxy-9a,9b-dihydrochromeno[3',4':3,4]cyclobuta[1,2-

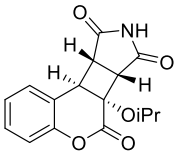

3.27p

***c*]pyrrole-6,7,9(6a*H*,6b*H*,8*H*)-trione (3.27p)**: 87% yield, white solid, 7% ee (SFC, Daicel CHIRALPAK®OD-H, isocratic 20% MeOH, 3.0 mL/min, 221 nm; t_1 = 3.97 min, t_2 = 5.28 min). ^{1}H NMR (500 MHz, CD_3OD) δ 7.43 – 7.38 (m, 1H), 7.35 (d, *J* = 7.6 Hz, 1H), 7.26 (td, *J* = 7.5, 0.9 Hz, 1H), 7.14 (d, *J* = 8.2 Hz, 1H), 4.05 (d, *J* = 5.1 Hz, 1H), 3.90 (hept, *J* = 6.1 Hz, 1H), 3.79 (dd, *J* = 6.6, 1.1 Hz, 1H), 3.01 (dd, *J* = 6.6, 5.1 Hz, 1H), 1.13 (d, *J* = 6.1 Hz, 3H), 1.10 (d, *J* = 6.1 Hz, 3H). ^{13}C NMR (126 MHz, CD_3OD) δ 179.10, 174.28, 166.58, 150.18, 129.62, 128.33, 125.47, 120.51, 116.97, 72.84, 70.29, 49.08, 45.72, 41.99, 22.30, 21.90. IR (thin film): 2974, 2927, 1761, 1703, 1586, 1262, 1228, 1168, 768 cm^{-1}; HRMS (ESI):

$[M+NH_4]^+$ calculated for $C_{16}H_{19}N_2O_5^+$ *m/z* 319.1286, found *m/z* 319.1283; mp > 260 ºC; $[\alpha]_{22}^{D}$ +6º (*c*0.56, acetone).

(6a*R*,6b*S*,9a*S*,9b*R*)-6a-Isopropoxy-5-methyl-9a,9b-dihydro-5*H*-

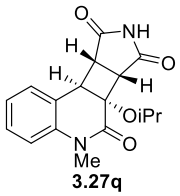

3.27q

pyrrolo[3',4':3,4]cyclobuta[1,2-*c*]quinoline-6,7,9(6a*H*,6b*H*,8*H*)-trione (3.27q): 96% yield, 3:1 d.r., white solid, 72% ee (SFC, Daicel CHIRALPAK® OD-H, isocratic 20% MeOH, 3.0 mL/min, 221 nm; t_1 = 4.67 min, t_2 = 5.89 min). ^{1}H NMR (500 MHz, $CDCl_3$) δ 8.86 (s, 1H), 7.36 (t, *J* = 7.9 Hz, 1H), 7.24 (d, *J* = 7.1 Hz, 1H), 7.12 (t, *J* = 7.4 Hz, 1H), 7.07 (d, *J* = 8.3 Hz, 1H), 3.96 – 3.83 (m, 3H), 3.49 (s, 3H), 2.88 (t, *J* = 6.2 Hz, 1H), 1.12 (d, *J* = 6.1 Hz, 3H), 1.00 (d, *J* = 6.1 Hz, 3H). ^{13}C NMR (126 MHz, $CDCl_3$) δ 177.91, 173.29, 167.35, 138.17, 129.31, 128.96, 124.22, 121.54, 115.16, 77.26, 72.59, 69.79, 49.46, 48.97, 40.07, 30.46, 23.45. IR (thin film): 3135, 3079, 2973, 1772, 1722, 1635, 1591, 1466, 1332, 1128, 808, 763 cm^{-1}; HRMS (ESI): $[M+NH_4]^+$ calculated for $C_{17}H_{22}N_3O_4^+$ *m/z* 332.1605, found *m/z* 332.1599; mp = 237–239 ºC; $[\alpha]_{22}^{D}$ +43º (*c*0.63, acetone).

(6a*R*,6b*S*,9a*S*,9b*R*)-8-Benzyl-6a-isopropoxy-9a,9b-dihydro-5*H*-

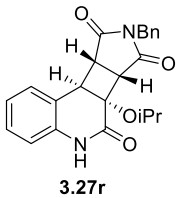

3.27r

pyrrolo[3',4':3,4]cyclobuta[1,2-*c*]quinoline-6,7,9(6a*H*,6b*H*,8*H*)-trione (3.27r): 63% yield, white solid, 88% ee (SFC, Daicel CHIRALPAK® OD-H, isocratic 20% MeOH, 3.0 mL/min, 221 nm; t_1 = 6.35 min, t_2 = 7.51 min). ^{1}H NMR (500 MHz, Acetone-d_6) δ 9.72 (s, 1H), 7.42 (d, *J* = 7.4 Hz, 2H), 7.34 (t, *J* = 7.4 Hz, 2H), 7.31 – 7.25 (m, 2H), 7.16 (d, *J* = 7.4 Hz, 1H), 7.09 – 7.02 (m, 2H), 4.75 (d, *J* = 14.7 Hz, 1H), 4.68 (d, *J* = 14.7 Hz, 1H), 3.88 (hept, *J* = 6.1 Hz, 1H), 3.80 (d, *J* = 6.6 Hz, 1H), 3.76 (d, *J* = 5.7 Hz, 1H), 3.02 (t, *J* = 6.2 Hz, 1H), 1.06 (d, *J* = 6.1 Hz, 3H), 0.95 (d, *J* = 6.1 Hz, 3H). ^{13}C NMR (126 MHz, Acetone-d_6) δ 177.15, 172.66, 167.11, 136.61, 136.50, 128.89, 128.43, 128.21, 127.88, 127.47, 123.50, 121.02, 115.78, 73.20, 69.03, 48.48, 47.91, 41.89, 39.38, 22.97, 22.82. IR (thin film):

3072, 2977, 2926, 1773, 1699, 1673, 1593, 1380, 1339, 1117, 765 cm^{-1}; HRMS (ESI): $[M+NH_4]^+$ calculated for $C_{23}H_{26}N_3O_4^+$ *m/z* 408.1918, found *m/z* 408.1914; mp = 213–215 ºC; $[\alpha]_{22}^{D}$+20º (*c*0.61, CH_3OH).

Dimer of NBn-maleimide: Spectral data were consistent with the previous report.[59]

(6a*R*,6b*S*,9a*S*,9b*R*)-6a-Isopropoxy-8-(prop-2-yn-1-yl)-9a,9b-dihydro-5*H*-

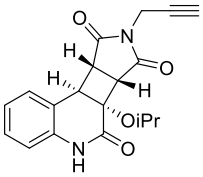

3.27s

pyrrolo[3',4':3,4]cyclobuta[1,2-*c*]quinoline-6,7,9(6a*H*,6b*H*,8*H*)-trione (3.27s): 61% yield, white solid, 97% ee (HPLC, Daicel CHIRALPAK®OD-H, Gradient 5% *i*PrOH (95% Hexane) to 40% *i*PrOH (60% Hexane), 1.0 mL/min, 221 nm; t_1 = 22.31 min, t_2 = 26.46 min). ^{1}H NMR (500 MHz, CD_3OD) δ 7.29 (td, *J* = 7.8, 1.4 Hz, 1H), 7.23 (d, *J* = 7.5 Hz, 1H), 7.11 (td, *J* = 7.5, 1.1 Hz, 1H), 6.98 (d, *J* = 8.0 Hz, 1H), 4.40 – 4.29 (m, 2H), 3.84 (d, *J* = 5.7 Hz, 1H), 3.81 (hept, *J* = 6.3 Hz, 1H), 3.76 (dd, *J* = 6.6, 1.2 Hz, 1H),2.99 (dd, *J* = 6.5, 5.8 Hz, 1H), 2.67 (t, *J* = 2.5 Hz, 1H), 1.11 (d, *J* = 6.1 Hz, 3H), 1.04 (d, *J* = 6.1 Hz, 3H). ^{13}C NMR (126 MHz, CD_3OD) δ 176.79, 172.06, 168.32, 135.81, 128.86, 127.92, 123.88, 120.89, 115.76, 76.55,72.97, 71.14, 69.29, 47.88, 47.73, 39.45, 27.40, 22.58, 21.99. IR (thin film): 3271, 2977, 2925, 1779, 1708, 1674, 1595, 1380, 1325, 1174, 732 cm^{-1}; HRMS (ESI): $[M+NH_4]^+$ calculated for $C_{19}H_{22}N_3O_4^+$ *m/z* 356.1605, found *m/z* 356.1599; mp = 177–179 ºC; $[\alpha]_{22}^{D}$+17º (*c*0.63, CH_3OH).

(6a*R*,6b*S*,9a*S*,9b*R*)-8-Allyl-6a-isopropoxy-9a,9b-dihydro-5*H*-

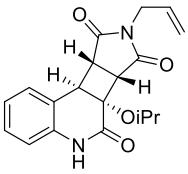

3.27t

pyrrolo[3',4':3,4]cyclobuta[1,2-*c*]quinoline-6,7,9(6a*H*,6b*H*,8*H*)-trione (3.27t): 44% yield, white solid, 84% ee (SFC, Daicel CHIRALPAK® OD-H, isocratic 20% MeOH, 3.0 mL/min, 221 nm; t_1 = 3.62 min, t_2 = 4.04 min). ^{1}H NMR (500 MHz, CD_3OD) δ 7.17 (td, *J* = 7.8, 1.4 Hz, 1H), 7.11 (d, *J* = 7.6 Hz, 1H), 6.98 (td, *J* = 7.5, 1.1 Hz, 1H), 6.85 (d, *J* = 8.0 Hz, 1H), 5.77 (ddt, *J* = 17.1, 10.8, 5.5 Hz, 1H), 5.18 (dq, *J* = 17.2, 1.5

Hz, 1H), 5.09 (dq, *J* = 10.4, 1.2 Hz, 1H), 4.06 (dt, *J* = 5.5, 1.4 Hz, 2H), 3.75 – 3.66 (m, 2H), 3.63 (dd, *J* = 6.6, 1.2 Hz, 1H), 2.84 (dd, *J* = 6.6, 5.6 Hz, 1H), 0.99 (d, *J* = 6.1 Hz, 3H), 0.91 (d, *J* = 6.1 Hz, 3H). ^{13}C NMR (126 MHz, CD_3OD) δ 177.86, 173.05, 168.35, 135.75, 130.91, 128.80, 127.94, 123.87, 121.01, 116.53, 115.73, 72.97, 69.30, 48.13, 47.89, 40.45, 39.53, 22.53, 22.02. IR (thin film): 2973, 2920, 1692, 1593, 1373, 1319, 1245, 1189, 1076, 762 cm^{-1}; HRMS (ESI): $[M+NH_4]^+$ calculated for $C_{19}H_{24}N_3O_4^+$ *m/z* 358.1761, found *m/z* 358.1757; mp = 190–192 ºC; $[\alpha]_{22}^{D}$+34º (*c*0.50, CH_3OH).

(6a*R*,6b*S*,9a*S*,9b*R*)-Methyl-6a-isopropoxy-6,7,9-trioxo-6,6a,6b,7,9,9a-hexahydro-5*H*-

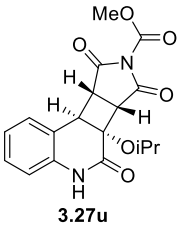

3.27u

pyrrolo[3',4':3,4]cyclobuta[1,2-*c*]quinoline-8(9b*H*)-carboxylate (3.27u): 76% yield, white solid, 99% ee (SFC, Daicel CHIRALPAK® OD-H, isocratic 20% MeOH, 3.0 mL/min, 221 nm; t_1 = 2.17 min, t_2 = 3.77 min). ^{1}H NMR (500 MHz, $CDCl_3$) δ 9.60 (s, 1H), 7.23 (td, *J* = 7.8, 1.3 Hz, 1H), 7.15 (d, *J* = 7.4 Hz, 1H), 7.03 (td, *J* = 7.5, 1.0 Hz, 1H), 6.93 (d, *J* = 7.8 Hz, 1H), 3.97 (s, 3H), 3.93 – 3.84 (m, 2H), 3.81 (dd, *J* = 6.8, 1.2 Hz, 1H), 2.96 (dd, *J* = 6.7, 5.9 Hz, 1H), 1.10 (d, *J* = 6.1 Hz, 3H), 0.98 (d, *J* = 6.1 Hz, 3H). ^{13}C NMR (126 MHz, $CDCl_3$) δ 172.94, 168.02, 167.99, 149.01, 135.15, 129.64, 128.49, 124.79, 119.98, 116.51, 73.30, 70.19, 55.17, 49.05, 47.77, 39.46, 23.52, 23.34. IR (thin film): 3063, 2978, 1812, 1768, 1723, 1676, 1595, 1310, 1252, 731 cm^{-1}; HRMS (ESI): $[M+NH_4]^+$ calculated for $C_{18}H_{22}N_3O_6^+$ *m/z* 376.1503, found *m/z* 376.1498; mp = 179–181 ºC; $[\alpha]_{22}^{D}$+17º (*c*0.63, CH_3OH).

(1*R*,2*S*,2a*R*,8b*R*)-Dimethyl-2a-isopropoxy-3-oxo-1,2,2a,3,4,8b-

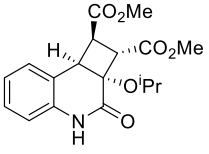

3.27v

hexahydrocyclobuta[*c*]quinoline-1,2-dicarboxylate (3.27v): 60% yield, 7:1 d.r., white solid, 61% ee (SFC, Daicel CHIRALPAK® OD-H, isocratic 20% MeOH, 3.0 mL/min, 221 nm; t_1 = 2.59 min, t_2 = 3.22 min). ^{1}H NMR (500 MHz, CD_3OD) δ 7.23 (td, *J* = 7.8, 1.4 Hz, 1H), 7.17 (d, *J* = 7.1 Hz, 1H), 7.04 (td, *J* = 7.5, 1.1 Hz, 1H),

6.89 (d, *J* = 7.9 Hz, 1H), 4.37 (d, *J* = 11.7 Hz, 1H), 3.95 (dd, *J* = 4.3, 1.1 Hz, 1H), 3.84 – 3.75 (m, 5H), 3.26 (s, 3H), 1.07 (d, *J* = 6.1 Hz, 3H), 1.05 (d, *J* = 6.1 Hz, 3H). ^{13}C NMR (126 MHz, CD_3OD) δ 171.41, 170.29, 169.06, 136.89, 128.66, 128.54, 123.12, 119.49, 115.49, 73.87, 68.69, 51.24, 50.72, 48.66, 44.99, 39.75, 22.71, 22.00. IR(thin film): 3215, 3063, 2979, 1728, 1680, 1595, 1301, 1168, 1116, 758 cm^{-1}; HRMS (ESI): $[M+NH_4]^+$ calculated for $C_{18}H_{25}N_2O_6^+$ *m/z* 365.1707, found *m/z* 365.1701; mp= 130–132 ºC; $[\alpha]_{22}^{D}$ –3º (*c*0.78, CH_3OH).

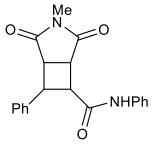

(**3.31b**): Prepared according to General Procedure 3.B using **3.29b** (15.5 mg, 0.067 mmol, 1.0 equiv.), *N*-methylmaleimide (74.2 mg, 0.67 mmol, 10 equiv.) and **3.28f** (1.5 mg, 0.67 µmol, 0.01 equiv.). The crude residue was purified by flash column chromatography on silica gel (1:1 EtOAc:pentane) to afford the cycloadduct as a white powder (34% yield). 34% ee.

^{1}H NMR (500 MHz,$CDCl_3$) δ 7.51 (d, *J* = 8.4 Hz, 2H), 7.38 – 7.27 (m, 6H), 7.15 (d, *J* = 6.8 Hz, 2H), 4.53 (dd, *J* = 10.7, 7.3 Hz, 1H), 3.77 (dd, *J* = 10.8, 6.8 Hz, 1H), 3.65 (dd, *J* = 6.8, 4.6 Hz, 1H), 3.46 (dd, *J* = 7.3, 4.7 Hz, 1H), 2.98 (s, 3H).

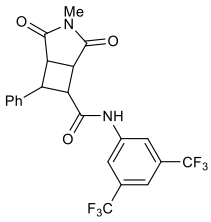

(**3.31c**): Prepared according to General Procedure 3.B using **3.29c** (9.8 mg, 0.028 mmol, 1.0 equiv.), *N*-methylmaleimide (31.1 mg, 0.28 mmol, 10 equiv.) and **3.28f** (0.6 mg, 0.28 µmol, 0.01 equiv.). The crude residue was purified by flash column chromatography on silica gel (2:3 EtOAc:pentane) to afford the cycloadduct as a pale beige powder (17% yield). 14% ee.

^{1}H NMR (500 MHz,$CDCl_3$) δ 7.99 (s, 2H), 7.57 (s, 2H), 7.32 – 7.21 (m, 3H), 7.07 (d, *J* = 7.2 Hz, 2H), 4.47 (dd, *J* = 10.8, 7.4 Hz, 1H), 3.72 (dd, *J* = 10.8, 6.8 Hz, 1H), 3.58 (dd, *J* = 6.8, 4.7 Hz, 1H), 3.42 (ddd, *J* = 7.3, 4.7, 0.9 Hz, 1H), 2.93 (s, 3H).

3.5.5 NMR Binding Experiments

The binding constants were determined through NMR titration studies.[51]

Binding between 3.28f and 3.25c quinonlone

It was found that 3-O*i*Pr quinolone **3.25c** readily dimerizes in solution. This process was analyzed using the method described by Bach,[60] resulting in a value of $K_{dim} = 103 \pm 8$.

A stock solution of 3-O*i*Pr quinolone **3.25c** (2.9 mg in 4 mL CD_2Cl_2) was prepared, and 0.45 mL was transferred to a NMR tube. Next, another stock solution of **3.25c** (5.6 mg in 1.5 mL CD_2Cl_2) was prepared. Increasing amounts of this solution were titrated into the former solution, acquiring ^{1}H NMR spectra for each titration (Figure 3.5).

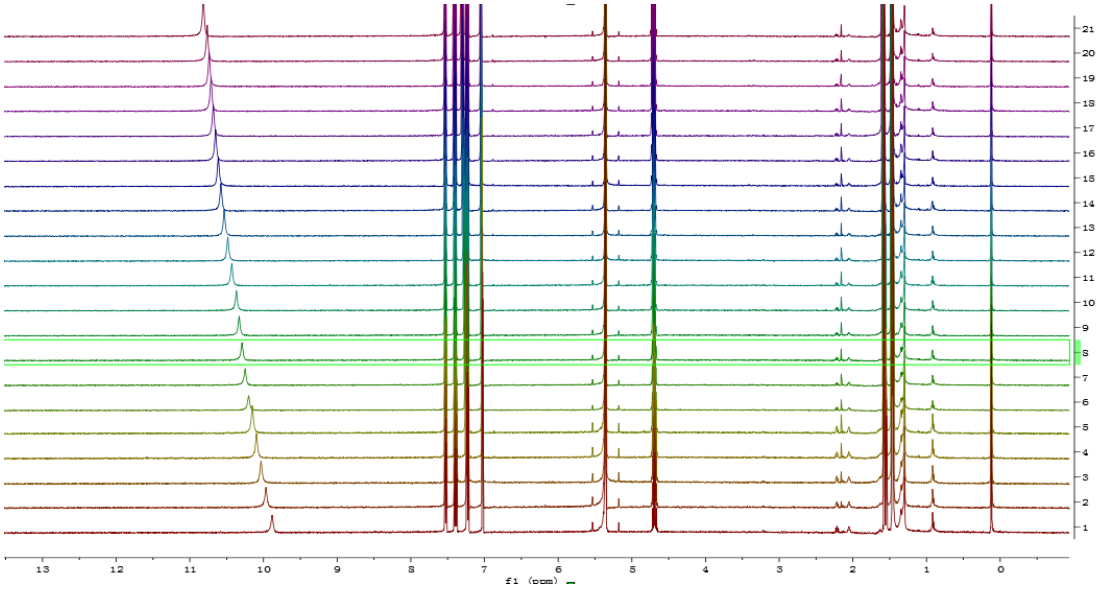

Figure 3.5. NMR titration of 3-O*i*Pr quinolone **3.25c** to monitor dimerization.

Similarly, we also performed the titration of **3.28f** with 3-O*i*Pr quinolone **3.25c**. The binding between **3.28f** and **3.25c** was analyzed using the method described by Thordarson,[61] resulting in a value of $K_a = 603 \pm 30$.

A stock solution (**A**) of **3.28f** (2.2 mg in 2 mL CD_2Cl_2) was prepared, and 0.45 mL was transferred to an NMR tube. Next, another stock solution of **3.25c** (5.6 mg in 1.0 mL **A**) was prepared, and

increasing amounts of this solution were titrated into the former solution, acquiring ^{1}H NMR spectra for each titration (Figure 3.6).

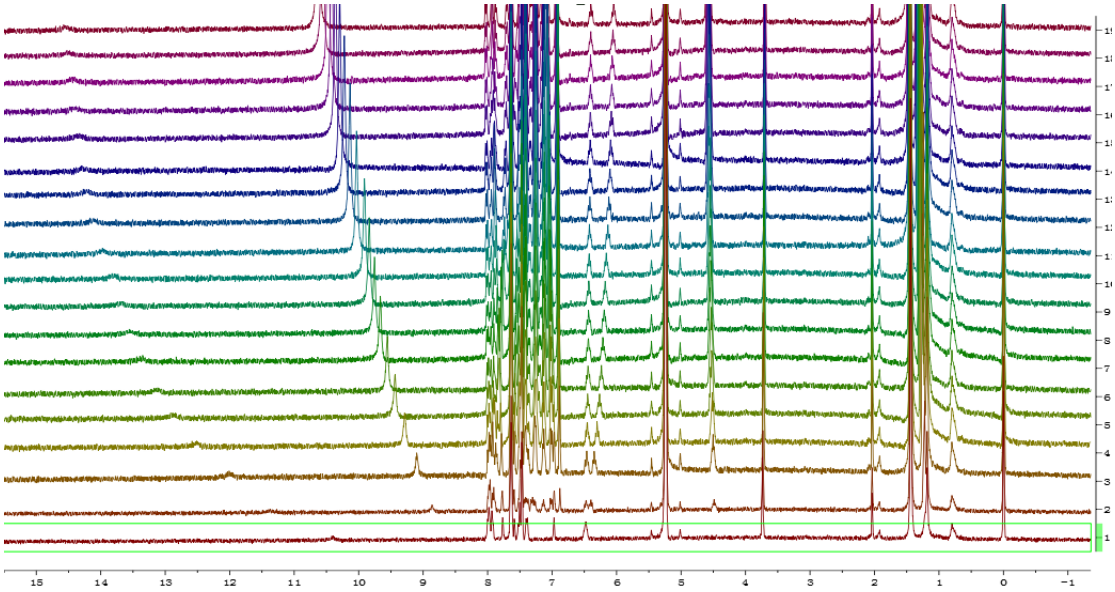

Figure 3.6. NMR titration of **3.28f** with **3.25c**.

We carried out a similar titration experiment for the binding between **3.28f** and maleimide, resulting in a value of $K_a = 24 \pm 3.8$.

A stock solution (**B**) of **3.28f** (1.8 mg in 2 mL CD_2Cl_2) was prepared, and 0.45 mL was transferred to a NMR tube. Next, another stock solution of **3.25c** (10.8 mg in 1.0 mL **B**) was prepared. Increasing amounts of this solution were titrated into the former solution, acquiring ^{1}H NMR spectra for each titration (Figure 3.7).

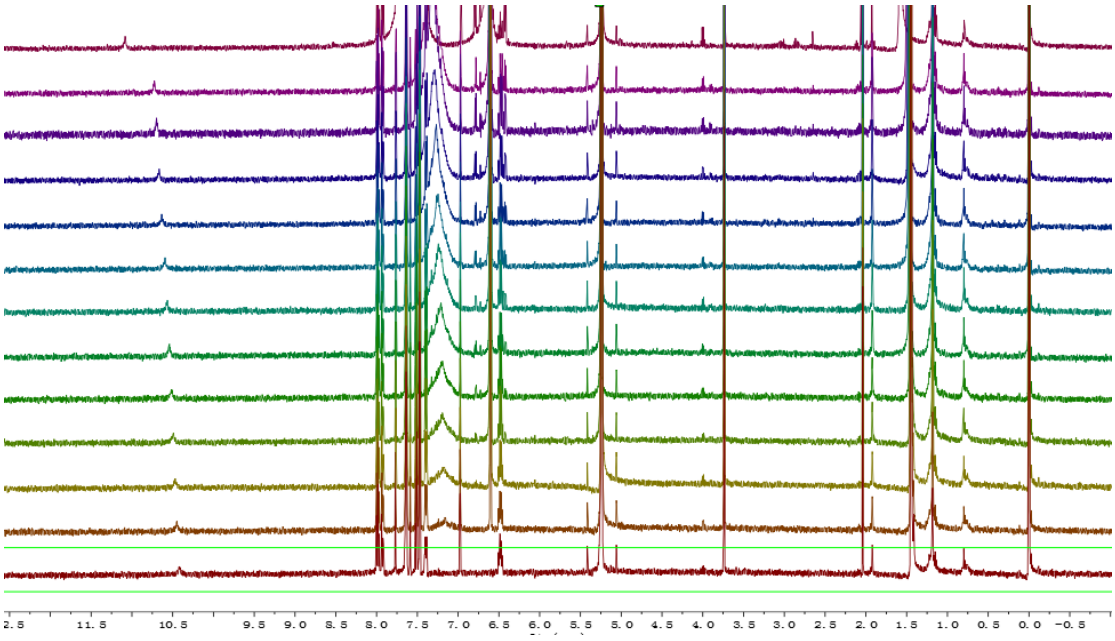

Figure 3.7. NMR titration of **3.28f** with maleimide.

3.5.6 Room Temperature Stern–Volmer Quenching Experiments

Stern–Volmer quenching experiments were conducted following a known report.[62]

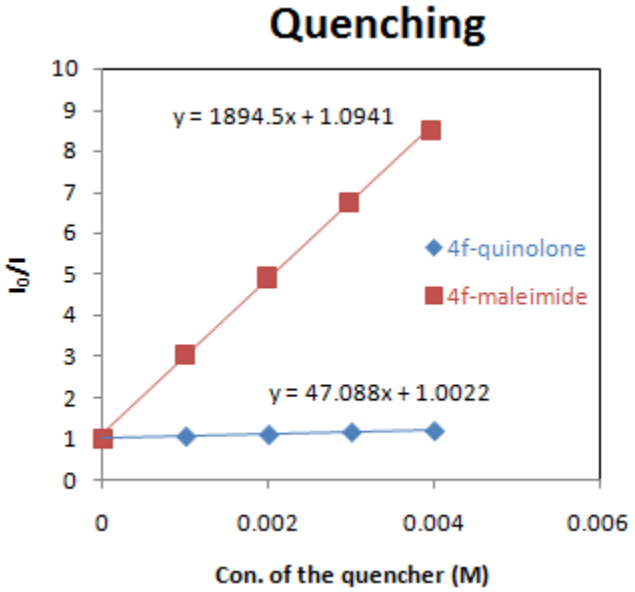

Figure 3.8. Stern–Volmer Quenching Experiments between the photocalyst **3.28f** and substrates

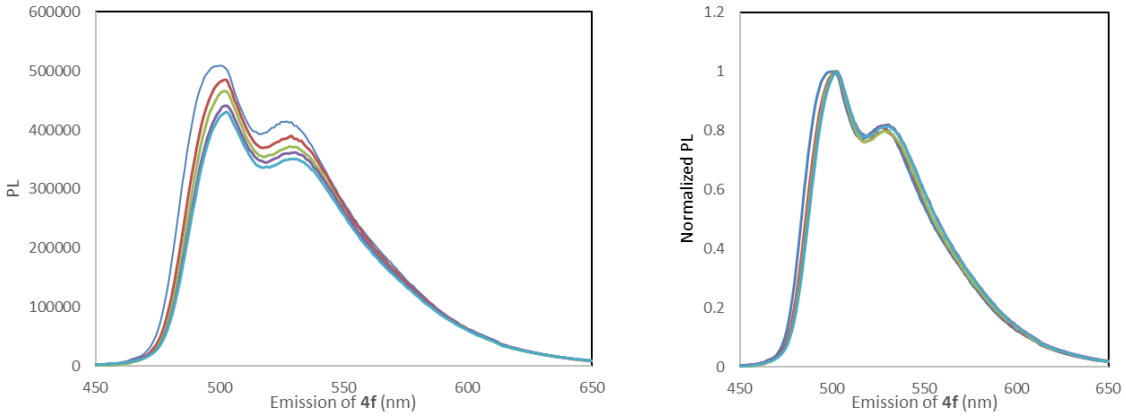

Figure 3.9. Emission of photocalyst **3.28f** with different con. of quinolone **3.25c** (0, 1, 2, 3, 4 mM).

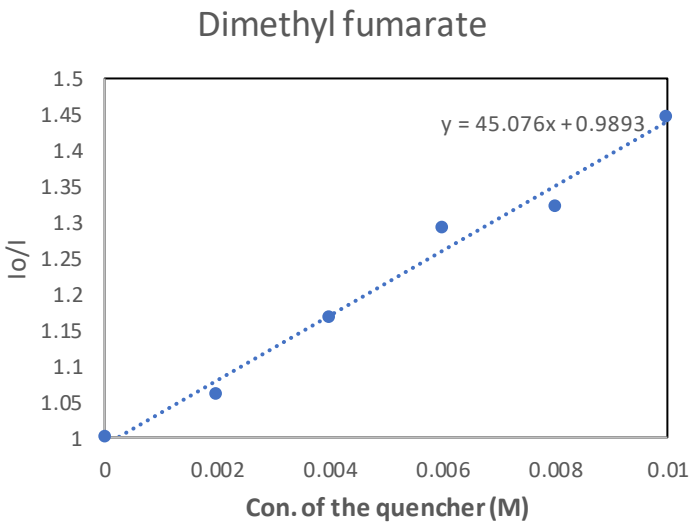

Figure 3.10. Stern–Volmer Quenching Experiments between the photocalyst **3.28f** and dimethyl fumarate

3.5.7 Kinetic Studies

Our kinetic studies focused on the cycloaddition between **3.25c** and maleimide **3.26**. With the optimized reaction conditions, the kinetics of the reaction were monitored by ^{1}H NMR. Each reaction was monitored to roughly 6%–11% conversion, and rate constants were calculated for each reaction using the method of initial rates.

3.5.7.a Reaction rate dependence on the concentration of quinolone 3.25c

The reactions were conducted using the procedure described above (section 3.5.4.b). The results displayed in Figure 3.11 show that the reaction rate exhibits a zero-order dependence on the concentration of quinolone **3.25c**.

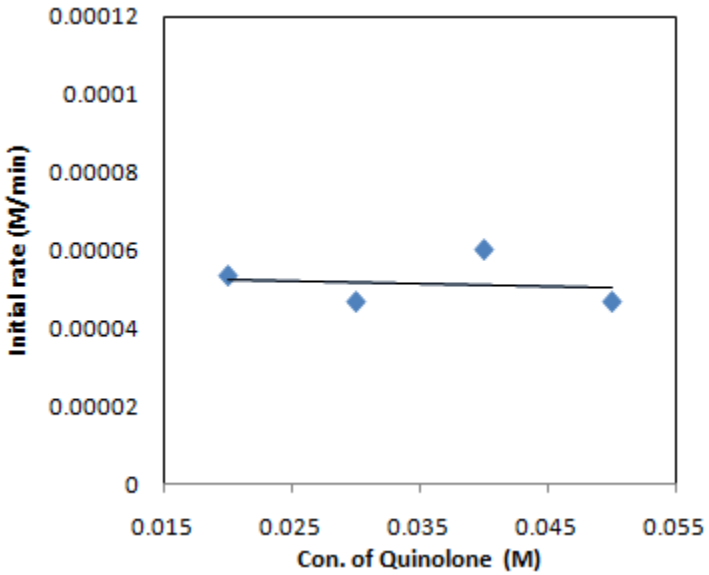

Figure 3.11. Zero order dependence on the concentration of **3.25c**

3.5.7.b Reaction rate dependence on the concentration of photocatalyst 3.28f

The reactions were conducted using the procedure described above (section 3.5.4.b). The results displayed in Figure 3.12 show that the reaction rate exhibits a first-order dependence on the concentration of photocatalyst **3.28f**.

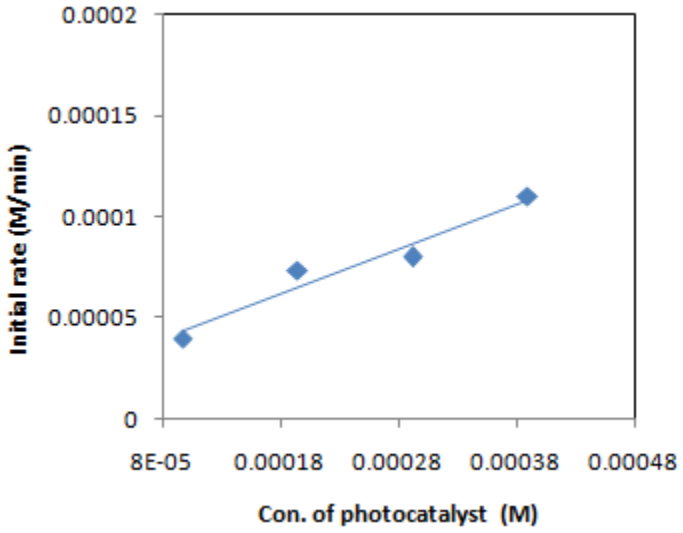

Figure 3.12. First-order dependence on the concentration of photocatalyst **3.28f**

3.5.7.c Reaction rate dependence on the concentration of maleimide 3.26

The reactions were conducted using the procedure described above (section 3.5.4.b). The results displayed in Figure 3.13 show that the reaction rate exhibits a first-order dependence on the concentration of maleimide.

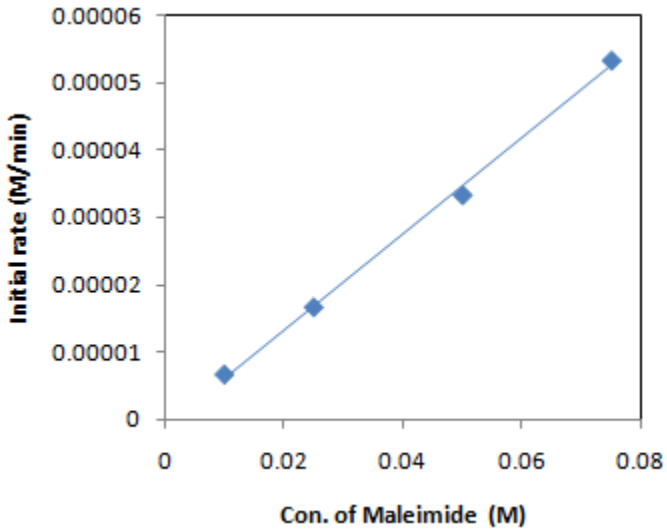

Figure 3.13. First-order dependence on the concentration of maleimide

3.5.8 Control Experiments

These cycloadditions were performed according to the standard procedure described above (section 3.5.4.b).

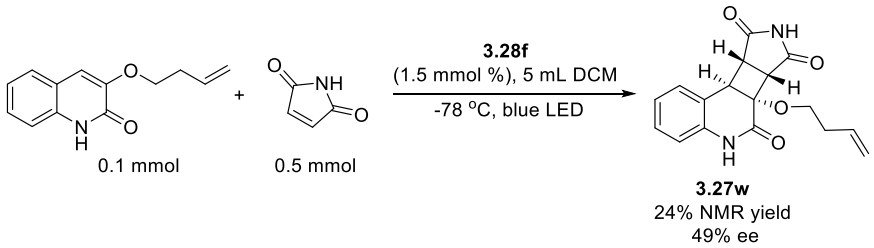

(6a*R*,6b*S*,9a*S*,9b*R*)-6a-(but-3-en-1-yloxy)-9a,9b-dihydro-5*H*-pyrrolo[3',4':3,4]cyclobuta[1,2-*c*]quinoline-6,7,9(6a*H*,6b*H*,8*H*)-trione (3.27w): white solid, 49% ee (HPLC, Daicel

CHIRALPAK® AD-H, Gradient5% iPrOH (95% Hexane) to 50% ^{i}PrOH (50% Hexane), 1.0 mL/min, 287 nm; t_1 = 12.95 min, t_2 = 16.69 min); ^{1}H NMR (500 MHz, CD_3OD) δ 7.15 (td, *J* = 7.7, 1.2 Hz, 1H), 7.12 (d, *J* = 7.5 Hz, 1H), 6.97 (td, *J* = 7.5, 0.8 Hz, 1H), 6.82 (d, *J* = 7.9 Hz, 1H), 5.67 (ddt, *J* = 17.1, 10.3, 6.8 Hz, 1H), 4.93 (dq, *J* = 17.2, 1.7 Hz, 1H), 4.90 – 4.86 (m, 1H), 3.79 (d, *J* = 5.6 Hz, 1H), 3.62 (dd, *J* = 6.5, 1.1 Hz, 1H), 3.47 (dt, *J* = 8.7, 6.4 Hz, 1H), 3.30 (dt, *J* = 8.6, 7.0 Hz, 1H), 2.77 (dd, *J* = 6.4, 5.7 Hz, 1H), 2.19 – 2.12 (m, 2H). ^{13}C NMR (126 MHz, CD_3OD) δ 179.76, 174.85, 167.16, 135.68, 134.49, 128.68, 127.88, 123.77, 121.10, 115.79, 115.63, 73.14, 64.81, 48.36, 47.21, 41.03, 33.74. IR (thin film): 3072, 2922, 2854, 1772, 1714, 1676, 1596, 1494, 1337, 1248, 1183, 759 cm^{-1}; HRMS (ESI): $[M+NH_4]^+$ calculated for $C_{17}H_{20}N_3O_4^+$ *m/z* 330.1448, found *m/z* 330.1446; mp = 246–248 ºC.

3.5.9 Transient Absorption Spectroscopy

Transient absorption spectra and single wavelength kinetic data were obtained on a home-built apparatus described previously.[63] Briefly, samples were excited by a frequency tripled Q-switched, pulsed Nd:YAG laser (Quantel USA (BigSky) Brilliant B) coupled to an optical parametric oscillator (OPO, Opotek, Inc.) to provide an excitation wavelength of 440 nm (7 ns full width at half-maximum). The laser power was controlled through the Q-switch delay and maintained between 3 – 4 mJ/pulse. The beam was directed through a 355 nm and 532 nm notch filter and directed to the sample by three silver mirrors. A 150 W xenon arc lamp (Applied Photophysics), pulsed with 70 V, served as the probe beam and was positioned orthogonal to the excitation laser. Detection was achieved with a monochromator (SPEX 1702/04) optically coupled to an R928 photomultiplier tube (Hamamatsu). Transient data were acquired on a computer-interfaced digital oscilloscope (LeCroy 9450, Dual 350 MHz) with 2.5 ns resolution terminated at 50 Ω. Full

transient absorption spectra were recorded with a resolution of 10 nm between 350 and 550 nm. Single wavelength kinetic analysis was performed in Origin2018 (Originlab) with least-squares error minimization accomplished using the Levenberg–Marquardt iteration method

Samples for measurement were prepared in dichloromethane in a 1 cm^2 cuvette affixed with a 24/40 ground glass joint (Quark Glass) and sparged with argon for 10 min. For the equilibrium constant and Stern–Volmer titrations, the titrant was prepared as a more concentrated stock solution in the same mixture of photocatalyst and substrate as required to keep the overall concentrations constant throughout the titration. This stock solution was sparged with argon and titrated into the cuvette with a Hamilton syringe.

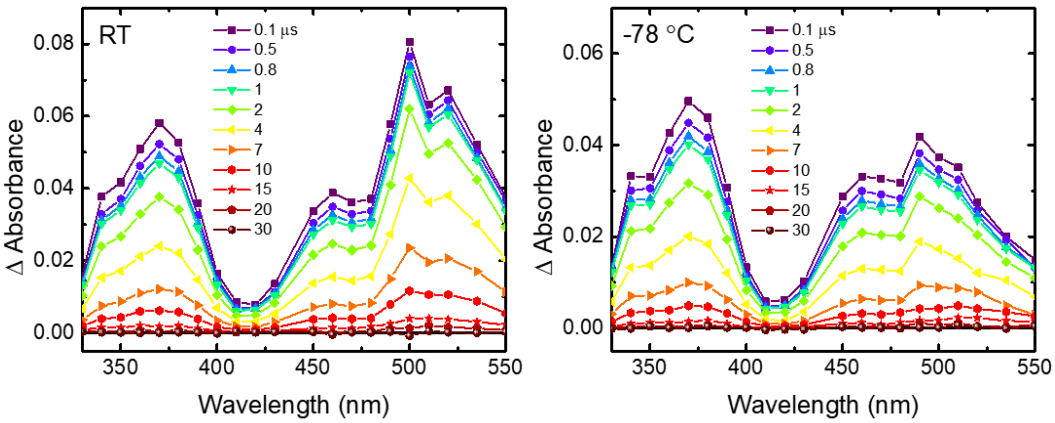

Figure 3.14. Transient absorption spectra for photocatalyst **3.28f** in CH_2Cl_2 at room temperature (left) and –78 °C at the indicated time delays after pulsed laser excitation at 440 nm

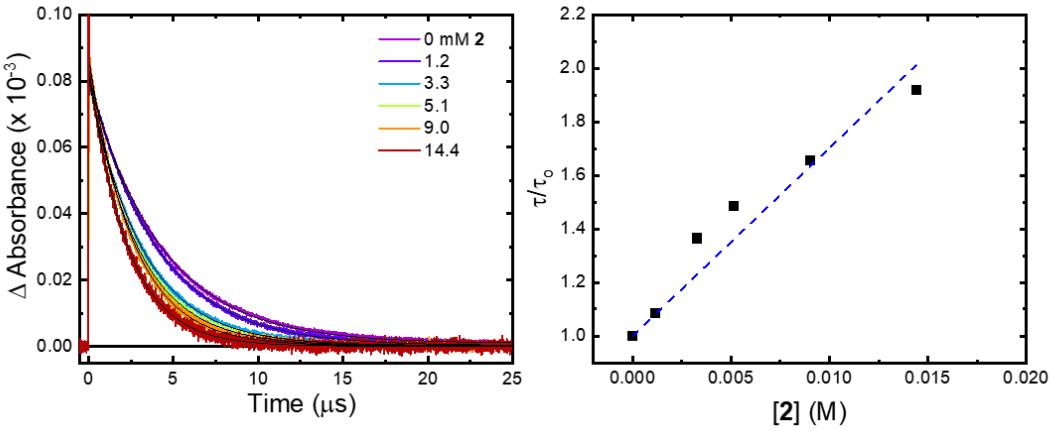

Figure 3.15. Left, titration of a 150 μM **3.28f** + 10 mM quinolone **3.25c** solution with increasing concentrations of maleimide **3.26** (**2**) (CH_2Cl_2). The kinetic data were fit with a single exponential, black lines. Right, Stern–Volmer quenching analysis of the photoexcited [Ir-Q] complex lifetime (τ) with increasing maleimide concentrations. Blue dashed line shows a linear best fit from which a Stern–Volmer constant of K_{SV} = 130 M^{-1} and a bimolecular quenching rate constant of k_q = 3.0 x 10^7 M^{-1} S^{-1} were extracted.

Table 3.4. Parameters Extracted from Biexponential Equation and Equilibrium Constant at –78 °C in CH_2Cl_2.

Quinolone (mM)	A_1	τ_1 (x 10^{-9} s)	A_2	τ_2 (x 10^{-6} s)	$K_{EQ.-78}$
0	0.067	570	[a]	[a]	[a]
0.11	0.064	620	0.010	3.09	1800
0.22	0.051	620	0.023	3.15	2600
0.32	0.039	660	0.038	3.44	3900
0.41	0.035	620	0.038	3.33	3100
0.59	0.027	680	0.051	3.55	3900
0.82	0.021	770	0.058	3.60	3900
1.13	0.015	930	0.066	3.76	4400
average	-	-	-	-	3400 ± 900

[a]At 0 equivalents of quinoline the quenching of the iridium excited state was first-order and modeled by a single exponential.

To estimate the equilibrium constant between the iridium photocatalyst (Ir) and quinolone **3.25c** (Q) at –78 °C in CH_2Cl_2 (eqn 1), the kinetic data reported in the manuscript were modeled by a biexponential decay (eqn 2), where A_1 and A_2 are the preexponential constants and τ_1 and τ_2 are the excited-state lifetimes of the free iridium photocatalyst ($[Ir]_{free}$) and quinolone bound photocatalyst ([Ir–Q]) respectively, Table S1. The concentrations of maleimide 2 (10 mM) and the iridium photocatalyst (150 μM) were kept constant throughout the titration. Quinolone **3.25c** was titrated into this solution from a more concentrated stock solution (3.6 mM). It was assumed that the difference in extinction coefficient of photoexcited $[Ir]_{free}$ ($[Ir]^*_{free}$) and [Ir–Q] ([Ir–Q]*) was

negligible at 370 nm and therefore the preexponential constants were proportional to the concentrations of the two excited-state species.

$$[\mathrm{Ir}]_{\mathrm{free}} + \mathrm{Q} \rightleftharpoons [\mathrm{Ir}\text{–}\mathrm{Q}] \qquad \text{eqn 1}$$

$$\Delta A = A_1 e^{-t/\tau_1} + A_2 e^{-t/\tau_2} \qquad \text{eqn 2}$$

To convert A_1 and A_2 to the relative equilibrium concentrations of the individual compounds ($[\mathrm{Ir}]_{\mathrm{free}}$, [Ir–Q], and Q_{eq}), the mole fractions were calculated via equations 3 and 4. The relative concentrations at equilibrium could then be calculated from the known initial concentrations of the iridium photocatalyst ($[\mathrm{Ir}]_0$) and quinolone ($[\mathrm{Q}]_0$), eqns 5–7.

$$\chi_{[Ir]_{free}} = \frac{A_1}{A_1 + A_2} \qquad \text{eqn 3}$$

$$\chi_{[Ir\text{–}Q]} = \frac{A_2}{A_1 + A_2} \qquad \text{eqn 4}$$

$$[Ir]_{free} = \chi_{[Ir]_{free}} * [Ir]_0 \qquad \text{eqn 5}$$

$$[Ir\text{–}Q] = \chi_{[Ir\text{–}Q]} * [Ir]_0 \qquad \text{eqn 6}$$

$$[Q]_{eq} = [Q]_0 - [Ir\text{–}Q] \qquad \text{eqn 7}$$

Finally, the equilibrium constant ($K_{\mathrm{EQ},-78}$) was estimated from the calculated equilibrium concentrations, eqn 8. This was performed for each addition of quinolone and the equilibrium constants were averaged and standard deviation calculated to provide K_{EQ} = 3,400 ± 900. An outlier test was performed with no outlier found.

$$K_{EQ,-78} = \frac{[Ir\text{–}Q]}{[Ir]_{free} * [Q]_{eq}} \qquad \text{eqn 8}$$

As shown in Table S1, the lifetimes assigned to $[\mathrm{Ir}]_{\mathrm{free}}$ (τ_1) and [Ir–Q] (τ_2) increase with the quinolone concentration. This result is consistent with the potential for heterodimerization between the quinolone and maleimide ([Q–M]) that reduces the concentration of maleimide available to quench the photoexcited iridium and [Ir–Q] complex. Along with heterodimerization,

we have shown that quinolone homodimerizes at room temperature, which would also be expected to affect the calculated $[Q]_{eq}$ concentration. Taken together, these competitive association processes prevent accurate determinization of the equilibrium constant. However, the qualitative conclusion can be made that the binding constant between the iridium complex and quinolone is larger at –78 °C than at room temperature.

3.5.10 Cyclic Voltammetry Data

Cyclic voltammetry experiments were performed in a standard three electrode setup in CH_2Cl_2 with the indicated analyte (1 mM) and $TBAPF_6$ (0.1 M) using a glassy carbon working electrode, platinum wire counter electrode, and a $Ag/AgNO_3$ (MeCN) reference electrode at a scan rate of 50 mV/s. The potentials were referenced to SCE through an external ferrocene standard ($Fc^{+/0}$ = 460 mV vs. SCE).[64] All the analytes showed irreversible reduction and oxidation. Half-peak potentials were estimated from the voltammograms.

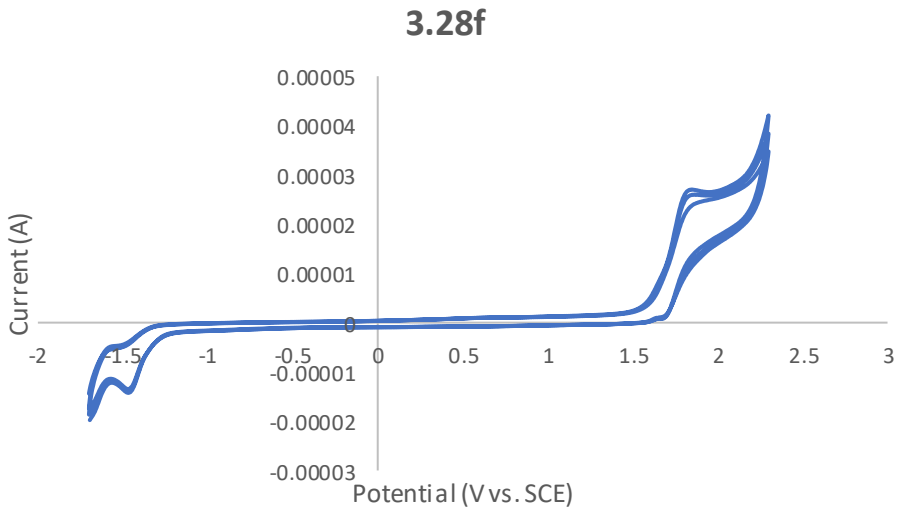

3.28f:

$E_{p/2}(Ir^{III}/Ir^{II}) = -1.36$ V vs. SCE in CH_2Cl_2
$E_{p/2}(Ir^{IV}/Ir^{III}) = +1.71$ V vs. SCE in CH_2Cl_2

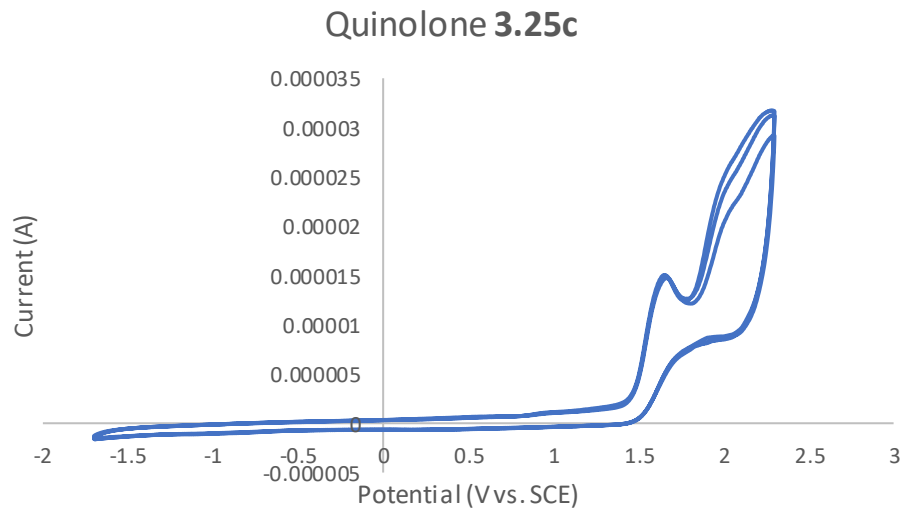

Quinolone **3.25c**:

$E_{p/2}$ **(3.25c /3.25c$^{\bullet-}$)** < -1.69 V vs. SCE in CH_2Cl_2
$E_{p/2}$ **(3.25c $^{\bullet+}$/3.25c)** $= +1.54$ V vs. SCE in CH_2Cl_2

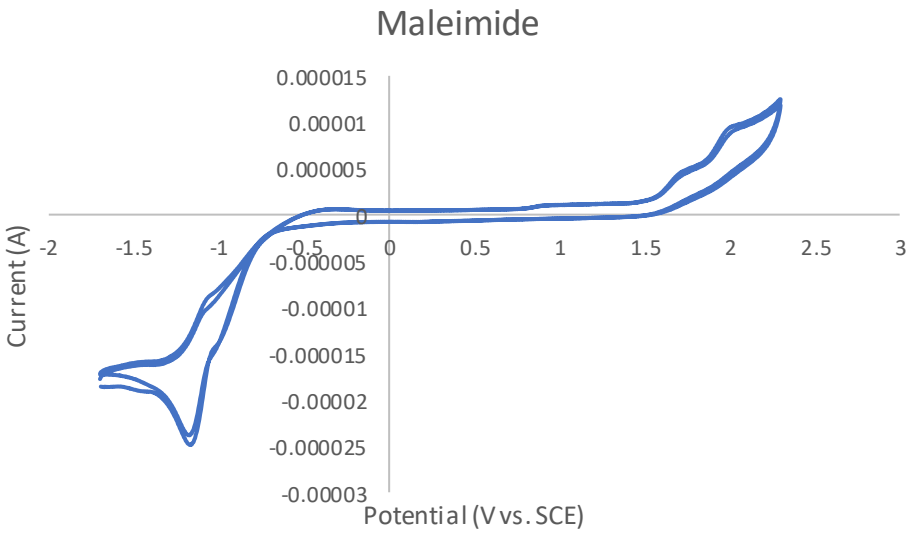

Maleimide **3.26**:

$$E_{p/2}\ (\mathbf{3.26/3.26^{\bullet -}}) = -1.09 \text{ V vs. SCE in } CH_2Cl_2$$
$$E_{p/2}\ (\mathbf{3.26^{\bullet +}/3.26}) = +1.64 \text{ V vs. SCE in } CH_2Cl_2$$

The excited-state redox potentials of photocatalyst **3.28f** were calculated through equations below[65,66] using the ground state potentials above and the Gibbs free energy change for the S_0 to T_1 transition (ΔG_{ES}) estimated as the energy at 10% of the PL maxima.[67,68,69] This provides a generous estimate for the excited-state redox potentials, and demonstrates that photoinduced electron transfer is endergonic in our reactions.

$E_{p/2}\ (Ir^{III*}/Ir^{II}) = E_{p/2}\ (Ir^{III}/Ir^{II}) + \Delta G_{ES} = -1.36 \text{ V} + 2.61 \text{ V} = +1.25 \text{ V vs. SCE in } CH_2Cl_2$

$E_{p/2}\ (Ir^{IV}/Ir^{III*}) = E_{p/2}\ (Ir^{IV}/Ir^{III}) - \Delta G_{ES} = 1.71 \text{ V} - 2.61 \text{ V} = -0.90 \text{ V vs. SCE in } CH_2Cl_2$

3.5.11 Quantum yield of the parent reaction

Determination of the light intensity at 436 nm: The intensity of the 436 nm blue LED light source used in these studies was determined as previously reported.[70,71,72,73] A 0.15 M solution of potassium ferrioxalate was prepared by dissolving 2.21 g of potassium ferrioxalate hydrate in 30 mL H_2SO_4 (0.05 M). A buffered solution of phenanthroline was prepared by dissolving 50 mg phenanthroline and 11.25 g sodium acetate in 50 mL H_2SO_4 (0.5 M). Both solutions were stored in the dark. Next, a Schlenk tube was completely covered in black tape except for a small hole near the base (see Figure 3.16). The prepared tube was charged with 5 mL of the ferrioxalate solution and irradiated for 10 seconds. This solution was treated with 0.875 mL buffered phenanthroline solution and stirred for 1 h in dark to allow the ferrous ions to completely coordinate to the phenanthroline. The absorbance of the resulting solution was measured at 510

nm. A non-irradiated sample was also prepared and the absorbance was measured at 510 nm. Finally, the conversion of ferrioxalate was calculated as below:

mol Fe^{2+}= V • ΔA/(l • ε) = 0.005875 L •(0.698881-0.097828)/(1 •11,100) = 3.18×10^{-7} mol

where V is the total volume (0.005875 L) of the solution after addition of phenanthroline, ΔA is the difference in absorbance at 510 nm between the irradiated and non-irradiated solutions, l is the path length (1.000 cm), and ε is the molar absorptivity at 510 nm (11,100 L mol^{-1} cm^{-1}).[71]

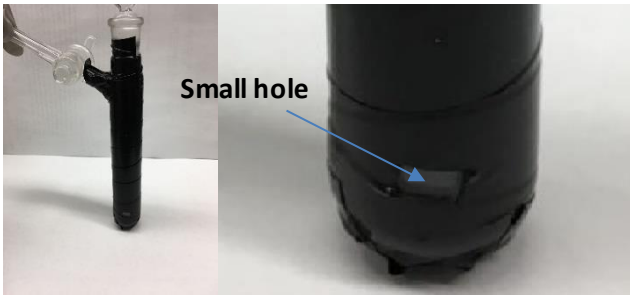

Figure 3.16. Taped Schlenk tube

The photon flux was calculated as follows:

photon flux = mol Fe^{2+} /(Φ • t • f) = 3.18×10^{-7}/(1.01 • 10 • 0.99833) = 3.15×10^{-8} einstein s^{-1}

where Φ is the quantum yield for the ferrioxalate actinometer (1.01 for a 0.15 M solution),[71] t is the time (10 s), and f is the fraction of light absorbed at λ = 436 nm (0.99833)[2].

Determination of quantum yield: The parent reaction was conducted in the same taped Schlenk tube at the optimal conditions in 0.1 mmol scale. After irradiation for 6 h, the yield of product was determined by ^{1}H NMR (6% yield). The quantum yield was determined as below.

Φ = mol product/(flux • t • f) = (6%•0.1 • 10^{-3})/(3.15×10^{-8}•21600•0.691) = 1.3×10^{-2}

Where Φ is the quantum yield for the reaction, t is the reaction time (21600 s), and f is 0.691 (*vide infra*) for the photocatalyst.

Determination of fraction of light absorbed at 436 nm for the photocatalyst 3.28f: The absorbance of the photocatalyst solution at 436 nm was measured to be 0.5094453692. The fraction of light absorbed (f) by this solution was calculated as below, where A is the measured absorbance at 436 nm.

$$f = 1 - 10^{-A} = 1 - 10^{-0.5094453692} = 0.691$$

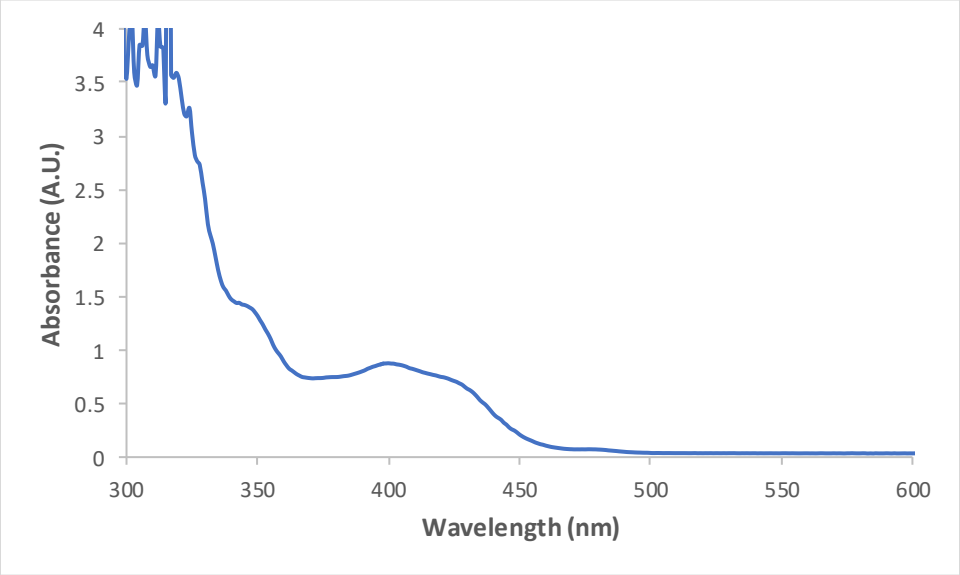

Figure 3.17. Absorbance of the photocatalyst **3.28f** solution.

3.5.12 Computational Studies

3.5.12.a General Information

All calculations were done using density functional theory[74] (DFT) implemented in Jaguar 9.1 suite of program.[75] Geometry of all structures were optimized with B3LYP-D3[76,77,78] levels of theory and 6-31G** basis set.[79] For the Ir metal center, Los Alamos LACVP[80,81,82] basis set was applied. The single point energies of all optimized structures were re-evaluated using triple-ζ quality of basis set, cc-pVTZ(-f),[83] where Ir metal was evaluated with LACV3P** basis set. Vibrational frequencies were calculated using the optimized structures at the same level as the

geometry optimizations. Solvation correction energies were derived from the self-consistent reaction field (SCRF) approximations,[84,85,86] which is the solution for the linearized Poisson-Boltzmann equations with the proper dielectric constants (ε=9.08 for dichloromethane). Finally, the solution phase Gibbs free energies were computed as follows:

$$G(Sol) = G(gas) + G^{solv} \quad (1)$$

$$G(gas) = H(gas) - TS(gas) \quad (2)$$

$$H(Gas) = E(SCF) + ZPE \quad (3)$$

$$\Delta G(Sol) = \Sigma G(Sol) \text{ for products} - \Sigma G(Sol) \text{ for reactants} \quad (4)$$

G(Sol) is the solvation corrected Gibbs free energy; G(gas) is the gas phase free energy; H(gas) is the enthalpy in the gas phase; T is the temperature (191.15 K); S(gas) is the entropy in the gas phase; E(SCF) is the electronic energy converged from the self-consistent field method; ZPE is the vibrational zero-point energy; and S for the vibrational entropy correction. Note that here entropy refers specifically to the vibrational/rotational/translational entropy of the solute(s). The solvent entropies are implicitly included in the continuum model.

3.5.12.b Benchmark calculations to evaluate triplet energies

Before we evaluate the triplet energies of molecules using DFT, we tested popular functionals to mimic the current system. Hence, B3LYP-D3, M06 and BH and HLYP levels were adopted for evaluation of triplet energies of photocatalyst (**3.28f**), maleimide (**3.26**), and quinolone substrate (**3.25c**). As summarized in Table 3.5, both B3LYP-D3 and BHandHLYP are closer to the experimental estimates, whereas the M06 functional severely underestimates the singlet-triplet gap.

Table 3.5. Comparison of different functionals to evaluate triplet energies.

Triplet energy (kcal/mol)	ΔG(**^{3}3.28f**) - ΔG(**^{1}3.28**) (Photocatalyst)	ΔG(**^{3}3.26**) - ΔG(**^{1}3.26**) (maleimide)	ΔG(**^{3}3.25c**) - ΔG(**^{1}3.25c**) (quinolone)
B3LYP-D3	53.14	64.42	55.44
M06	47.73	67.96	56.37
BH and HLYP	66.33	77.94	54.88
Experimental	~60 kcal/mol		

Additionally, to be sure that our computational level is high enough to mimic triplet state molecules, we further evaluated the triplet energies of known photocatalysts.[87] As shown in Table 3.6, the experimental values and computational estimations match in both qualitative and quantitative manners.

Table 3.6. Comparison of experimental triplet energies with computed values for known Ir(III) photocatalysts

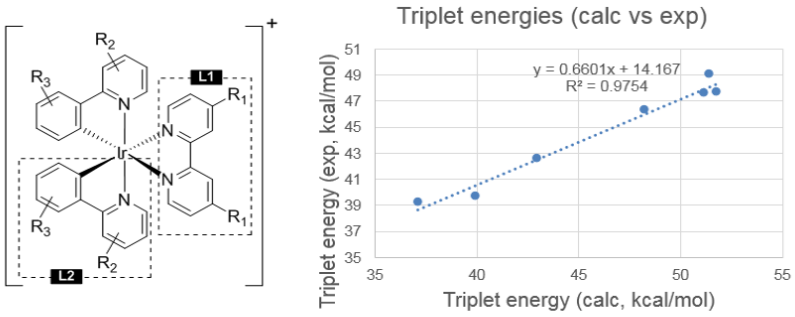

L1	L2	E_T (exp, kcal/mol)	E_T (calc, kcal/mol)
5,5'-Me_2bpy	ppy	49.0	51.39
4,4'-$(MeO)_2$bpy	ppy	47.7	51.78
4,4'-Me_2bpy	ppy	47.6	51.16
bpy	ppy	46.3	48.25
4,4'-Cl_2bpy	ppy	42.6	43.00
4,4'-$(CO_2Me)_2$bpy	ppy	39.7	39.92
4,4'-$(F_3C)_2$bpy	ppy	39.2	37.09

3.5.12.c Conformers for encounter complexes

To evaluate the energies of possible encounter complexes for donor-acceptor pairs ([Ir-Q] and [Ir-2]), various of conformations were optimized and compared. For [Ir-Q] complexes, since N–H bond in the pyrazole ring participates in the hydrogen bonds, we can consider two major hydrogen bond donor-acceptor pairs, where quinolone substrate possess two hydrogen bond acceptors and one hydrogen bond donor. Additionally, the two possible facial approaches give four major encounter complexes **[Ir-Q_A], [Ir-Q_B], [Ir-Q_C],** and **[Ir-Q_D]**. For **[Ir-Q_A]** and **[Ir-Q_B]**, encounter complex containing a non-classical hydrogen bond was observed, where two $N_{pyrazole}$–H to O=C_Q an O–C_Q hydrogen bonds were found for **[Ir-Q_C],** and **[Ir-Q_D]**. For [Ir-M], since there is only one

hydrogen bond donor in maleimide, two facial approaches were considered. (**[Ir-M_A]** and **[Ir-M_B]**)

For [Ir-Q] complexes, the conformation of isopropyl group tethered on the quinolone was also considered. Three major conformations showing the staggered relationship were optimized, and the geometry showing the lowest energy was chosen for the energy comparison.

For complete listing of Mulliken spin densities, energies, coordinates, and vibrational frequencies of optimized structures please see the supplementary information of: Zheng, J.; Swords, W. B.; Jung, H.; Skubi, K. L.; Kidd, J. B.; Meyer, G. J.; Baik, M. –H.; Yoon, T. Enantioselective Intermolecular Excited-State Photoreactions Using a Chiral Ir Triplet Sensitizer: Separating Association from Energy Transfer. *J. Am. Chem. Soc*., **2019**, *141*, 13625-13634.

3.6 References and Notes

[1] Inoue, Y. Asymmetric Photochemical Reactions in Solution. *Chem. Rev*. **1992**, *92*, 741–770.

[2] Inoue, Y.; Ramamurthy, V. *Molecular and Supramolecular Photochemistry, Volume 11: Chiral Photochemistry,* Marcel Dekker, New York, NY, **2004**.

[3] Brimioulle, R.; Lenhart, D.; Maturi, M. M.; Bach, T. Enantioselective Catalysis of Photochemical Reactions. *Angew. Chem. Int. Ed.* **2015**, *54*, 3872–3890.

[4] Sherbrook, E. M.; Yoon, T. P. Asymmetric Catalysis of Triplet-State Photoreactions. In *Specialist Periodical Reports: Photochemistry*; Albini, A., Protti, S., Eds.; Royal Society of Chemistry: Croydon, 2019; Vol. 46, pp 432–448.

[5] Eaton, P. E. Photochemical Reactions of Simple Alicyclic Enones. *Acc. Chem. Res.* **1967**, *1*, 50–57.

[6] Burg, F.; Bach, T. Lactam Hydrogen Bonds as Control Elements in Enantioselective Transition-Metal-Catalyzed and Photochemical Reactions. *J. Org. Chem.* **2019**, *84*, 8815–8836.

[7] Vallavoju, N.; Selvakumar, S.; Jockusch, S.; Sibi, M. P.; Sivaguru, J. "Enantioselective organo-photocatalysis mediated by atropisomeric thiourea derivatives", *Angew. Chem. Int. Ed*. **2014**, 53, 5604–5608.

[8] Cauble, D. F.; Lynch, V.; Krische, M. J. "Studies on the Enantioselective Catalysis of Photochemically Promoted Transformations: 'Sensitizing Receptors' as Chiral Catalysts", *J. Org. Chem*. **2003**, *68*, 15–21.

[9] Müller, C.; Bauer, A.; Bach, T. Light-driven enantioselective organocatalysis. *Angew. Chem. Int. Ed*. **2009**, *48*, 6640–6642.

[10] Müller, C.; Bauer, A.; Maturi, M. M.; Consuelo Cuquerella, M.; Miranda, M. A.; Bach, T. Enantioselective Intramolecular [2 + 2]-Photocycloaddition Reactions of 4-Substituted Quinolones Catalyzed by a Chiral Sensitizer with a Hydrogen-Bonding Motif. *J. Am. Chem. Soc*. **2011**, *133*, 16689–16697.

[11] Maturi, M. M.; Bach, T. Enantioselective Catalysis of the Intermolecular [2+2] Photocycloaddition between 2-Pyridones and Acetylenedicarboxylates. *Angew. Chem. Int. Ed*. **2014**, *53*, 7661–7664.

[12] Maturi, M. M.; Pöthig, A.; Bach, T. Enantioselective Photochemical Rearrangements of Spirooxindole Epoxides Catalyzed by a Chiral Bifunctional Xanthone. *Aust. J. Chem.* **2015**, *68*, 1682–1692.

[13] Alonso, R.; Bach, T. A Chiral Thioxanthone as an Organocatalyst for Enantioselective [2+2] Photocycloaddition Reactions Induced by Visible Light. *Angew. Chem. Int. Ed.* **2014**, *53*, 4368–4371.

[14] Tröster, A.; Alonso, R.; Bauer, A.; Bach, T. Enantioselective Intermolecular [2 + 2] Photocycloaddition Reactions of 2(1*H*)-Quinolones Induced by Visible Light Irradiation. *J. Am. Chem. Soc.* **2016**, *138*, 7808–7811.

[15] Brenninger, C.; Jolliffe, J. D.; Bach, T. Chromophore Activation of α,β-Unsaturated Carbonyl Compounds and Its Application to Enantioselective Photochemical Reactions. *Angew. Chem. Int. Ed.* **2018**, *57*, 14338 – 14349.

[16] Schwinger, D. P.; Bach, T. Chiral 1,3,2-Oxazaborolidine Catalysts for Enantioselective Photochemical Reactions. *Acc. Chem. Res.* **2020**, *53*, 1933−1943.

[17] For a more detailed analysis of this work see chapter 1.2.

[18] Poplata, S.; Bach, T. Enantioselective Intermolecular [2+2] Photocycloaddition Reaction of Cyclic Enones and Its Application in a Synthesis of (–)-Grandisol. *J. Am. Chem. Soc.* **2018**, *140*, 3228–3231.

[19] Bach, T.; Hehn, J. Photochemical Reactions as Key Steps in Natural Product Synthesis. *Angew. Chem. Int. Ed.* **2011**, *50*, 1000–1045.

[20] Lu, Z.; Yoon, T. P. Visible light photocatalysis of [2+2] styrene cycloadditions by energy transfer. *Angew. Chem. Int. Ed.* **2012**, *51*, 10329–10332.

[21] Zou, Y. Q.; Duan, S. W.; Meng, X. G.; Hu, X. Q.; Gao, S.; Chen, J. R.; Xiao, W. J. Visible light induced intermolecular [2+2]-cycloaddition reactions of 3-ylideneoxindoles through energy transfer pathway. *Tetrahedron* **2012**, *68*, 6914–6919.

[22] Hurtley, A. E.; Lu, Z.; Yoon, T. P. Cycloaddition of 1,3-dienes by visible light photocatalysis. *Angew. Chem. Int. Ed.* **2014**, *53*, 8991–8994.

[23] Farney, E. P.; Yoon, T. P. Visible-light sensitization of vinyl azides by transition-metal photocatalysis. *Angew. Chem. Int. Ed.* **2014**, *53*, 793–797.

[24] Xia, X. D.; Xuan, J.; Wang, Q.; Lu, L. Q.; Chen, J. R.; Xiao, W. J. Synthesis of 2-Substituted Indoles through Visible Light-Induced Photocatalytic Cyclizations of Styryl Azides. *Adv. Synth. Catal.* **2014**, *356*, 2807–2812.

[25] Scholz, S. O.; Farney, E. P.; Kim, S.; Bates, D. M.; Yoon, T. P. Spin-selective generation of triplet nitrenes: Olefin aziridination through visible-light photosensitization of azidoformates. *Angew. Chem. Int. Ed.* **2016**, *55*, 2239–2242.

[26] Blum, T. R.; Miller, Z. D.; Bates, D. M.; Guzei, I. A.; Yoon, T. P. Enantioselective Photochemistry through Lewis Acid-Catalyzed Triplet Energy Transfer. *Science* **2016**, *354*, 1391–1395.

[27] Miller, Z. D.; Lee, B. J.; Yoon, T. P. Enantioselective Crossed Photocycloadditions of Styrenic Olefins by Lewis Acid Catalyzed Triplet Sensitization. *Angew. Chem. Int. Ed.* **2017**, *56*, 11891–11895.

[28] Gong, L.; Chen, L.-A.; Meggers, E. Asymmetric Catalysis Mediated by the Ligand Sphere of Octahedral Chiral-at-Metal Complexes. *Angew. Chem. Int. Ed.* **2014**, *53*, 10868–10874.

[29] Zhang, L.; Meggers, E. Steering Asymmetric Lewis Acid Catalysis Exclusively with Octahedral Metal-Centered Chirality. *Acc. Chem. Res.* **2017**, *50*, 320–330.

[30] Huang, X.; Meggers, E. Asymmetric Photocatalysis with Bis-Cyclometalated Rhodium Complexes. *Acc. Chem. Res.* **2019**, *52*, 833–847.

[31] Huo, H.; Shen, X.; Wang, C.; Zhang, L.; Rose, P.; Chen, L.-A.; Harms, K.; Marsche, M.; Hilt, G.; Meggers, E. Asymmetric photoredox transition-metal catalysis activated by visible light. *Nature* **2014**, *515*, 100–103.

[32] Huo, H.; Wang, C.; Harms, K.; Meggers, E. Enantioselective, Catalytic Trichloromethylation through Visible-Light-Activated Photoredox Catalysis with a Chiral Iridium Complex. *J. Am. Chem. Soc.* **2015**, *137*, 9551–9556.

[33] Wang, C.; Zheng, Y.; Huo, H.; Röse, P.; Zhang, L.; Harms, K.; Hilt, G.; Meggers, E. Merger of Visible Light Induced Oxidation and Enantioselective Alkylation with a Chiral Iridium Catalyst. *Chem. Eur. J.* **2015**, *21*, 7355–7359.

[34] Wang, C.; Qin, J.; Shen, X.; Riedel, R.; Harms, K.; Meggers, E. Asymmetric Radical-Radical Cross-Coupling through Visible-Light-Activated Iridium Catalysis. *Angew. Chem. Int. Ed.* **2016**, *55*, 685–688.

[35] Ma, J. J.; Rosales, A. R.; Huang, X. Q.; Harms, K.; Riedel, R.; Wiest, O.; Meggers, E. Visible-Light-Activated Asymmetric β-C–H Functionalization of Acceptor-Substituted Ketones with 1,2-Dicarbonyl Compounds. *J. Am. Chem. Soc.* **2017**, *139*, 17245–17248.

[36] Huang, X.; Lin, J.; Shen, T.; Harms, K.; Marchini, M.; Ceroni, P.; Meggers, E. Asymmetric [3+2] Photocycloadditions of Cyclopropanes with Alkenes or Alkynes through Visible-Light Excitation of Catalyst-Bound Substrates. *Angew. Chem. Int. Ed.* **2018**, *57*, 5454–5458.

[37] Huang, X.; Quinn, T. R.; Harms, K.; Webster, R. D.; Zhang, L.; Wiest, O.; Meggers, E. Direct Visible-Light-Excited Asymmetric Lewis Acid Catalysis of Intermolecular [2+2] Photocycloadditions. *J. Am. Chem. Soc.* **2017**, *139*, 9120–9123.

[38] Hu, N.; Jung, H.; Zheng, Y.; Lee, J.; Zhang, L.; Ullah, Z.; Xie, X.; Harms, K.; Baik, M.-H.; Meggers, E. Catalytic Asymmetric Dearomatization by Visible-Light-Activated [2+2] Photocycloaddition. *Angew. Chem. Int. Ed*. **2018**, *57*, 6242–6246.

[39] Grell, Y.; Hong, Y.; Huang, X.; Mochizuki, T.; Xie, X.; Harms, K.; Meggers, E. Chiral-at-Rhodium Catalyst Containing Two Different Cyclometalating Ligands. *Organometallics* **2019**, *38*, 3948–3954

[40] Jung, H.; Hong, M.; Marchini, M.; Villa, M.; Steinlandt, P. S.; Huang, X.; Hemming, M.; Meggers, E.; Ceroni, P.; Park, J.; Baik, M. –H. Understanding the Mechanism of Direct Visible-light-activated [2+2] Cycloadditions Mediated by Rh and Ir photocatalysts: Combined Computational and Spectroscopic Studies. *Chem. Sci.* **2021,** *12*, 9673–9681.

[41] Skubi, K. L.; Kidd, J. B.; Jung, H.; Guzei, I. A.; Baik, M. H.; Yoon, T. P. Enantioselective Excited-State Photoreactions Controlled by a Chiral Hydrogen-Bonding Iridium Sensitizer. *J. Am. Chem. Soc.* **2017**, *139*, 17186–17192.

[42] CCDC-1897932 and CCDC-1897933 contain the supplementary crystallographic data for **3.27e** and **3.27v**, respectively. These data can be obtained free of charge from the Cambridge Crystallographic Data Centre.

[43] Calhoun, G. C.; Schuster, G. B. Radical cation and triplex Diels-Alder reactions of 1,3-cyclohexadiene. *J. Am. Chem. Soc.* **1984**, *106*, 870–871.

[44] Kim, J. I.; Schuster. G. B. Enantioselective catalysis of the triplex Diels-Alder reaction: addition of *trans*-□-methylstyrene to 1,3-cyclohexadiene photosensitized with (-)-1,1'-bis(2,4-dicyanonaphthalene). *J. Am. Chem. Soc.* **1990**, *112*, 9635–9637.

[45] Kim, J. I.; Schuster, G. B. Enantioselective catalysis of the triplex Diels-Alder reaction: a study of scope and mechanism. *J. Am. Chem. Soc.* **1992**, *114*, 9309–9317.

[46] Von Sonntag, J.; Beckert, D.; Knolle, W.; Mehnert, R. Electron transfer as the initiation mechanism of photocurable maleimide–vinyl ether based resins. *Radiat. Phys. Chem*, **1999**, *55*, 609–613.

[47] Levy, S. T.; Rubin, M. B.; Speiser, S. Photophysics of Cyclic α-Diketone-Aromatic Ring Bichromophoric Molecules. Structures, Spectra, and Intramolecular Electronic Energy Transfer." *J. Am. Chem. Soc*. **1992**, *114*, 10747–10756.

[48] Levy, S.; Speiser, S. Calculation of the Exchange Integral for Short Range Intramolecular Electronic Energy Transfer in Bichromophoric Molecules. *J. Chem. Phys.* **1992**, *96,* 3585–3593.

[49] The experimentally determined association constant suggests that 99% of the Ir photocatalysts are bound to quinolone under initial reaction concentrations at –78 °C.

[50] Lowry, M. S.; Goldsmith, J. I.; Slinker, J. D.; Rohl, R.; Pascal, R. A.; Malliaras, G. G.; Bernhard, S. Single-Layer Electroluminescent Devices and Photoinduced Hydrogen Production from an Ionic Iridium(III) Complex. *Chem. Mater.* **2005,** *17*, 5712-5719.

[51] Skubi, K. L.; Kidd, J. B.; Jung, H.; Guzei, I. A.; Baik, M. H.; Yoon, T. P. Enantioselective Excited-State Photoreactions Controlled by a Chiral Hydrogen-Bonding Iridium Sensitizer. *J. Am. Chem. Soc.* **2017,** *139*, 17186-17192.

[52] Suzuki, R.; Nozawa, D.; Futamura, A.; Nishikawa-Shimono, R.; Abe, M.; Hattori, N.; Ohta, H.; Araki, Y.; Kambe, D.; Ohmichi, M.; Tokura, S.; Aoki, T.; Ohtake, N.; Kawamoto, H. Discovery and in vitro and in vivo profiles of N-ethyl-N-[2-[3-(5-fluoro-2-pyridinyl)-1H-pyrazol-1-yl]ethyl]-2-(2H-1,2,3-triazol-2-yl) -benzamide as a novel class of dual orexin receptor antagonist. *Biorg. Med. Chem.* **2015,** *23*, 1260-1275.

[53] Chen, L.-A.; Xu, W.; Huang, B.; Ma, J.; Wang, L.; Xi, J.; Harms, K.; Gong, L.; Meggers, E., Asymmetric Catalysis with an Inert Chiral-at-Metal Iridium Complex. *J. Am. Chem. Soc.* **2013,** *135*, 10598-10601

[54] *It should be noted that ^{13}C NMR spectra are not reported for these chiral compounds. Strong couplings with the highly fluorinated ppy ligands resulted in low signal-to-noise ratios and complicated spectra.*

[55] Maturi, M. M.; Wenninger, M.; Alonso, R.; Bauer, A.; Pöthig, A.; Riedle, E.; Bach, T. Intramolecular [2+2] Photocycloaddition of 3- and 4-(But-3-enyl)oxyquinolones: Influence of the Alkene Substitution Pattern, Photophysical Studies, and Enantioselective Catalysis by a Chiral Sensitizer. *Chem..Eur. J.* **2013,** *19*, 7461-7472

[56] Duplantier, A. J.; Becker, S. L.; Bohanon, M. J.; Borzilleri, K. A.; Chrunyk, B. A.; Downs, J. T.; Hu, L.-Y.; El-Kattan, A.; James, L. C.; Liu, S.; Lu, J.; Maklad, N.; Mansour, M. N.; Mente, S.; Piotrowski, M. A.; Sakya, S. M.; Sheehan, S.; Steyn, S. J.; Strick, C. A.; Williams, V. A.; Zhang, L. Discovery, SAR, and Pharmacokinetics of a Novel 3-Hydroxyquinolin-2(1H)-one Series of Potent d-Amino Acid Oxidase (DAAO) Inhibitors. *J. Med. Chem.* **2009,** *52*, 3576-3585.

[57] Manley, P. J.; Bilodeau, M. T. A New Synthesis of Naphthyridinones and Quinolinones: Palladium-Catalyzed Amidation of o-Carbonyl-Substituted Aryl Halides. *Org. Lett.* **2004,** *6*, 2433-2435.

[58] Yuan, Y.; Yang, R.; Zhang-Negrerie, D.; Wang, J.; Du, Y.; Zhao, K. One-Pot Synthesis of 3-Hydroxyquinolin-2(1H)-ones from N-Phenylacetoacetamide via $PhI(OCOCF_3)_2$-Mediated α-

Hydroxylation and H_2SO_4-Promoted Intramolecular Cyclization. *J. Org. Chem.* **2013,** *78*, 5385-5392

[59] Skalenko, Y. A.; Druzhenko, T. V.; Denisenko, A. V.; Samoilenko, M. V.; Dacenko, O. P.; Trofymchuk, S. A.; Grygorenko, O. O.; Tolmachev, A. A.; Mykhailiuk, P. K., [2+2]-Photocycloaddition of N-Benzylmaleimide to Alkenes As an Approach to Functional 3-Azabicyclo[3.2.0]heptanes. *J. Org. Chem.* **2018,** *83*, 6275-6289.

[60] Bakowski, A.; Dressel, M.; Bauer, A.; Bach, T., Enantioselective radical cyclisation reactions of 4-substituted quinolones mediated by a chiral template. *Org. Biomol. Chem.* **2011,** *9*, 3516-3529

[61] Thordarson, P. Determining association constants from titration experiments in supramolecular chemistry. *Chem. Soc. Rev.* **2011,** *40*, 1305-1323.

[62] Cismesia, M. A.; Yoon, T. P. Characterizing chain processes in visible light photoredox catalysis. *Chem. Sci.* **2015,** *6*, 5426-5434.

[63] Argazzi, R.; Bignozzi, C. A.; Heimer, T. A.; Castellano, F. N.; Meyer, G. J.,Enhanced Spectral Sensitivity from Ruthenium(II) Polypyridyl Based Photovoltaic Devices. *Inorg. Chem.* **1994,** *33*, 5741-5749.

[64] Connelly, N. G.; Geiger, W. E., Chemical Redox Agents for Organometallic Chemistry. *Chem. Rev.* **1996,** *96*, 877-910.

[65] Rehm, D.; Weller, A. Kinetics of Fluorescence Quenching by Electron and H-Atom Transfer. *Isr. J. Chem.* **1970**, *8*, 259–271.

[66] Ballardini, R.; Varani, G.; Indelli, M. T.; Scandola, F.; Balzani, V. Free energy correlation of rate constants for electron transfer quenching of excited transition metal complexes. *J. Am. Chem. Soc.* **1978**, *100*, 7219–7223.

[67] McClure, L. J.; Ford, P. C. Ligand macrocycle effects on the photophysical properties of rhodium(III) complexes: a detailed investigation of cis- and trans-dicyano(1,4,8,11-tetraazacyclotetradecane)rhodium(III) and related species. *J. Phys. Chem.* **1992**, *96*, 6640–6650.

[68] Døssing, A.; Ryu, C. K.; Kudo, S.; Ford, P. C. Competitive bimolecular electron- and energy-transfer quenching of the excited state(s) of the tetranuclear copper(I) cluster Cu4I4py4. Evidence for large reorganization energies in an excited-state electron transfer. *J. Am. Chem. Soc.* **1993**, *115*, 5132–5137.

[69] Zhu, Q.; Gentry, E. C.; Knowles, R. R. Catalytic Carbocation Generation Enabled by the Mesolytic Cleavage of Alkoxyamine Radical Cations. *Angew. Chem., Int. Ed.* **2016**, *55*, 9969–9973.

[70] Cismesia, M. A.; Yoon, T. P., Characterizing chain processes in visible light photoredox catalysis. *Chem. Sci.* **2015,** *6*, 5426-5434.

[71] Hatchard, C. G.; Parker, C. A. *Proc. Roy. Soc. (London)* **1956**, *A235*, 518–536.

[72] Kuhn, H. J.; Braslavsky, S. E.; Schmidt, R. *Pure Appl. Chem.* **2004**, *76*, 2105–2146.

[73] Monalti, M. *et. al.* Chemical Actinometry. *Handbook of Photochemistry,* 3rd Ed; Taylor & Francis Group, LLC. Boca Raton, FL, **2006**, 601–616.

[74] Parr, R. G.; Yang, W. *Density Functional Theory of Atoms and Molecules*. (Oxford University Press: New York, 1989).

[75] Bochevarov, A. D.; Harder, E.; Hughes, T. F.; Greenwood, J. R.; Braden, D. A.; Philipp, D. M.; Rinaldo, D.; Halls, M. D.; Zhang, J.; Friesner, R. A. Jaguar: A High-Performance Quantum Chemistry Software Program with Strengths in Life and Materials Sciences. *Int. J. Quantum Chem.* **2013**, *113*, 2110–2142.

[76] Becke, A. D. Density-functional thermochemistry. III. The role of exact exchange. *J. Chem. Phys.* **1993**, *98,* 5648–5652.

[77] Lee, C. T.; Yang, W.; Parr, R. G. Development of the Colle-Salvetti correlation-energy formula into a functional of the electron density. *Phys. Rev. B* **1988**, *37*, 785–789.

[78] Grimme, S.; Antony, J.; Ehrlich, S.; Krieg, H. A consistent and accurate ab initio parametrization of density functional dispersion correction (DFT-D) for the 94 elements H-Pu. *J. Chem. Phys.* **2010**, *132*, 154104.

[79] Ditchfield, R.; Hehre, W. J.; Pople, J. A. Self-Consistent Molecular-Orbital Methods. IX. An Extended Gaussian-Type Basis for Molecular-Orbital Studies of Organic Molecules. *J. Chem. Phys.* **1971**, *54*, 724–728.

[80] Hay, P. J.; Wadt, W. R. *Ab initio* effective core potentials for molecular calculations. Potentials for the transition metal atoms Sc to Hg. *J. Chem. Phys.* **1985**, *82*, 270–283.

[81] Wadt, W. R.; Hay, P. J. Ab initio effective core potentials for molecular calculations. Potentials for main group elements Na to Bi. *J. Chem. Phys.* **1985**, *82*, 284–298.

[82] Hay, P. J.; Wadt, W. R. Ab initio effective core potentials for molecular calculations. Potentials for K to Au including the outermost core orbitals. *J. Chem. Phys.* **1985**, *82*, 299–310.

[83] Dunning, T. H., Jr. Gaussian basis sets for use in correlated molecular calculations. I. The atoms boron through neon and hydrogen. *J. Chem. Phys.* **1989**, *90*, 1007–1023.

[84] Marten, B.; Kim, K.; Cortis, C.; Friesner, R. A.; Murphy, R. B.; Ringnalda, M. N.; Sitkoff, D.; Honig, B. New Model for Calculation of Solvation Free Energies: Correction of Self-Consistent Reaction Field Continuum Dielectric Theory for Short-Range Hydrogen-Bonding Effects. *J. Phys. Chem.* **1996**, *100*, 11775–11788.

[85] Edinger, S. R.; Cortis, C.; Shenkin, P. S.; Friesner, R. A. Solvation Free Energies of Peptides: Comparison of Approximate Continuum Solvation Models with Accurate Solution of the Poisson-Boltzmann Equation. *J. Phys. Chem. B* **1997**, *101*, 1190–1197.

[86] Friedrichs, M.; Zhou, R. H.; Edinger, S. R.; Friesner, R. A. Poisson-Boltzmann Analytical Gradients for Molecular Modeling Calculations. *J. Phys. Chem. B* **1999**, *103*, 3057–3061.

[87] Welin, E. R.; Le, C.; Arias-Rotondo, D. M.; McCusker, J. K.; MacMillan, D. W. C. Photosensitized, energy transfer-mediated organometallic catalysis through electronically excited nickel(II). *Science* **2017**, *355*, 380–385.

Chapter 4. Enantioselective Paternò–Büchi Reactions Enabled by a Chiral Iridium Photocatalyst

4.1 Introduction

4.1.1 Oxetanes in Medicinal Chemistry

In the early stages of a drug discovery process, the physicochemical and pharmacokinetic properties of a compound are investigated in parallel with target affinity and selectivity, often improving the transition from lead hits to in vivo profiling of potential drug candidates. Nonetheless, the optimization of these properties presents a considerable challenge in medicinal chemistry. As such, chemical fragments that modulate a compound's properties in a predictable manner are of significant interest. Oxetanes are four-membered oxygen-containing heterocycles, which are featured in various natural products that exhibit promising biological activity (Figure 4.1). These oxetanes have recently been identified as such a motif in drug discovery.[1]

Figure 4.1. Oxetane-Containing Natural Products

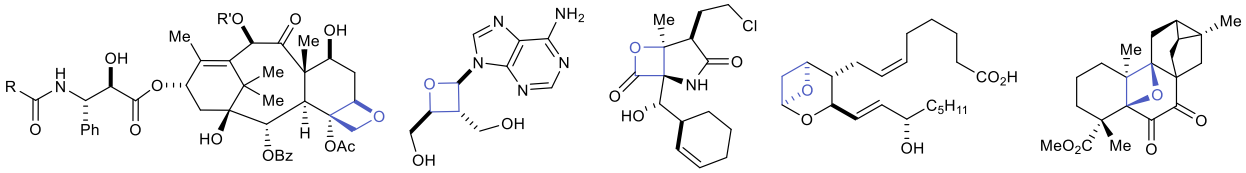

4.1: R = Ph, R' = Ac, Paclitaxel (Taxol
4.2: R = O*t*Bu, R' = H, Taxotere (Docetaxel)

4.3
Oxetanocin A
antiretroviral

4.4
Marizomib
protease inhibitor

4.5
Thromboxane A_2
vasoconstrictor

4.6
Mitrephorone A
neuron growth

During the development of a drug, it is common to inhibit metabolic degradation of exposed sites, such as methylene groups, by the incorporation of a *gem*-dimethyl unit that serves to shield nearby functional groups.[2] However, this perturbation can result in a substantial and often undesired increase in lipophilicity (log*D* and log*P*) that frequently correlates to shorter in vivo half-lives. Relatedly, carbonyl compounds are also ubiquitous constituents in medicines, in part due to their presence in feedstock building blocks and their ample synthetic utility. Highly reactive carbonyl groups such as aldehydes, acid halides, and Michael acceptors, however, are problematic

in drug discovery. Additionally, more chemically stable functional groups such as amides and esters are prone to hydrolysis by numerous enzymes, and ketones bearing α-stereocenters are susceptible to epimerization. Oxetanes are structural alternatives that offer increased metabolic stability without negatively impacting lipophilicity while retaining H–bond acceptor affinity owing to the Lewis basicity of the oxygen-atom lone pair (Figure 4.2).[1,3] Thus, oxetanes have been of significant interest in contemporary medicinal chemistry and provide unique opportunities

Figure 4.2. Oxetanes as Versatile Tools in Medicinal Chemistry. Reproduced from ref 1.

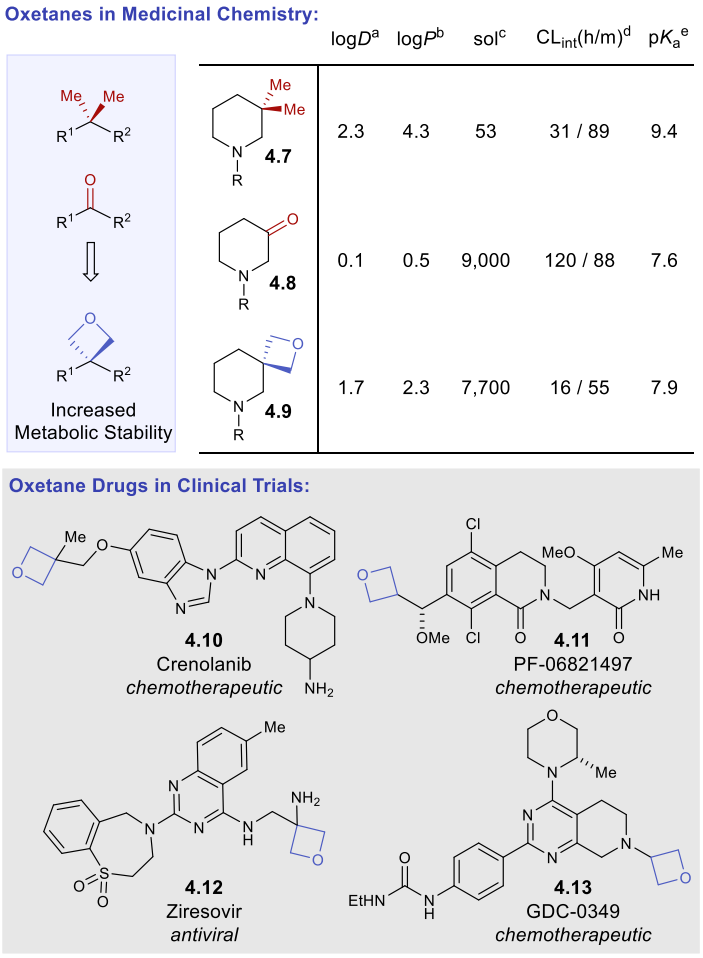

	log*D*[a]	log*P*[b]	sol[c]	CL_{int}(h/m)[d]	pK_a[e]
4.7	2.3	4.3	53	31 / 89	9.4
4.8	0.1	0.5	9,000	120 / 88	7.6
4.9	1.7	2.3	7,700	16 / 55	7.9

R = piperonyl; [a] Logarithm of *n*-octanol/water distribution coefficient at pH 7.4. [b] Intrinsic lipophilicity of the neutral base. [c] molar solubility (μmol/L). [d] Intrinsic clearance, measured in human (h) and mouse (m) liver microsomes. [e] pKa of the protonated piperadine.

to tune the physicochemical and pharmacokinetic properties of bioactive molecules, evidenced by numerous non-taxol derived oxetane-containing drugs that have been submitted into clinical trials within the last decade, Figure 4.2.[4–10]

4.1.2 Synthesis of Oxetanes

Intrinsic ring strain (25.3 kcal/mol)[11,12] and kinetically slower cyclization imposes fundamental constraints in the synthesis of oxetanes compared to three-, five-, and six-membered cyclic ether analogues[13]. Hence, there exist relatively few strategies to form these heterocycles (Scheme 4.1). Most commonly these methods rely on the preactivation of starting materials via the incorporation of leaving groups to promote ether cyclization.[14,15] Relatedly, intramolecular haloetherification via halonium ion intermediates by a 4-exo-trig cyclization has been shown to be viable strategy.[16,17] Triflate-appended saccharides have also been extensively utilized to afford enantio- and diastometrically enriched oxetanes by ring contraction.[18,19] On the other hand, Corey-Chaykovsky sulfonium ylides offer an alternative route by the ring expansion of readily prepared epoxides.[20] Despite the usefulness of these approaches, oxetanes remain an underdeveloped area

Scheme 4.1. General Strategies for Oxetane Synthesis

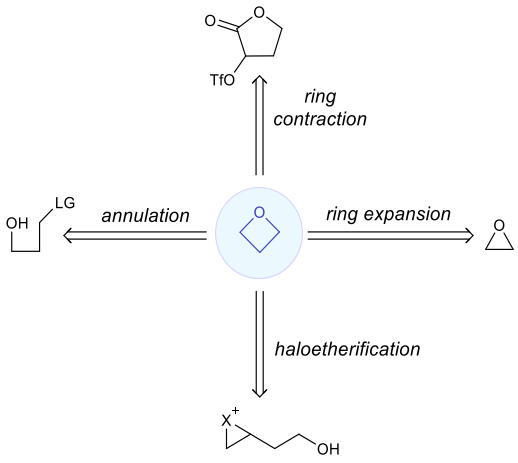

of chemical space as their synthesis remain restricted to activated starting materials and classical polar mechanisms that limit their applicability toward to synthesis of complex, polysubstituted oxetanes.

Arguably, the most efficient method for the synthesis of oxetanes is through the direct [2+2] photocycloaddition of carbonyl and alkene moieties. In comparison to the previous discussed processes, a [2+2] cycloaddition allows for the rapid formation of substituted oxetanes from simple, feedstock materials (Scheme 4.2). This reaction, referred to as the Paternò–Büchi reaction, typically proceeds by the absorption of a photon by a carbonyl containing compound, generating its (n,π*) triplet excited state. This species undergoes stepwise reaction with a ground-state olefin, affording a triplet biradical intermediate that then intersystem crosses to its singlet surface, subsequently recombining to yield an oxetane product.[21] In contrast, there exist limited examples of the opposite, in which an excited-state alkene reacts with a ground-state carbonyl compound, a so-called transposed Paternò–Büchi reaction.[22] In this section we restrict our discussion to the former.

Scheme 4.2. Initial Discovery and Generalized Mechanism of the Paternò–Büchi Reaction

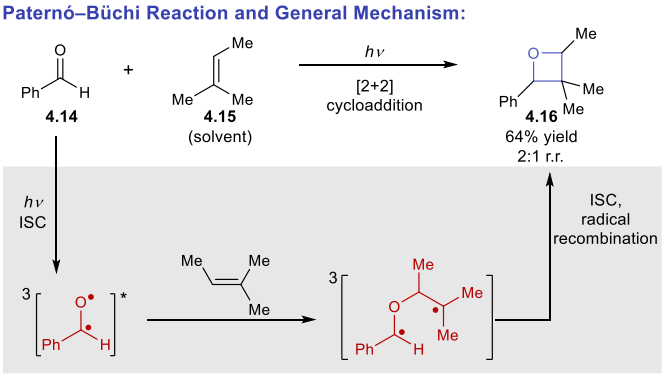

The Paternò–Büchi reaction has a slightly controversial origin. In 1909, while investigating the photoreaction between benzaldehyde **4.14** and alkene **4.15**, Paternò proposed that the

corresponding cycloadduct was formed, but without thorough characterization.[23] In the same year, Ciamician reported the same type of photoreaction of benzaldehyde with safrole and isosafrole.[24] However, Ciamician did not report the structures of the photoproducts. It wasn't until 1954 that Paternò's results were reexamined by Büchi using more modern techniques to identify the structure of the oxetane product.[25] Since then, the Paternò–Büchi reaction has gained popularity as a powerful tool to afford synthetically valuable oxetanes amenable to derivatization[26–28] and as key intermediates in the synthesis of natural products.[29–31]

4.1.3 Stereocontrol of the Paternò–Büchi Reaction

Given the utility of the Paternò–Büchi reaction, there has been considerable interest toward the control of its outcome. In most cases, the regioselectivity is affected by both the polarity matching of the electrophilic oxyl radical, which typically reacts with the most electron-rich position of an alkene.[32] For example, irradiation of benzaldehyde in the presence of 2,3-dihydrofuran (**4.17**) results in oxetane **4.18** in a regioisomeric ratio of >98:2 (Scheme 4.3A),[33] disfavoring the formation of the ketal adduct. Based upon a frontier molecular orbital approach, this selectivity can be rationalized by examining the HOMO of **4.17**, in which the β carbon bears the most electron density with an atomic coefficient of –0.36 eV.[34] These results are in accord with the first bond formation, the regiochemical-determining step, occurring as a result of nucleophilic attack on the excited state of the carbonyl oxygen. Additionally, the regiochemical behavior of the same reaction was probed by the relative stabilities of the biradical intermediates formed following C–O bond formation. Computational experiments by D'Auria and coworkers concluded that indeed structure **4.19** is thermodynamically favored over **4.20** by 2 kcal/mol (Scheme 4.3B).

Interestingly, this photocycloaddition also exhibits good diastereoselectivity, yielding a mixture of 88/12 of the *endo* and *exo* isomers. This result is justified by stereochemical models

proposed by Griesbeck and coworkers (Scheme 4.3C).[35] During the reaction, biradical intermediate **4.19** must undergo intersystem crossing prior to ring closure. Accordingly, the orbitals occupied by the radicals adopt a perpendicular orientation, maximizing angular momentum to facilitate spin-orbit coupling.[36] Thus, C–C bond rotation of **4.19** produces biradical conformers **4.21** and **4.22**, in which the conformer that yields the *exo* adduct is depopulated by unfavorable steric interactions between the aryl ring and the alpha proton. DFT investigations revealed that *endo* conformer **4.21** is favored by 2 kcal/mol, consistent with experimental observations. Furthermore, the introduction of more sterically demanding groups to the alpha position results in an erosion of this diastereoselectivity (65:35),[37] explained by the relative population of conformers **4.23** and **4.24**.[38] However, exceptions to this model exist. For example, photoexcited benzaldehyde reacts with conjugated alkenes, such as furan, to exclusively form the *exocyclic* adduct. It is hypothesized that "memory effects" which arise from fast intersystem

Scheme 4.3. Regio- and Diastereoselectivity of the Paternò–Büchi Reaction

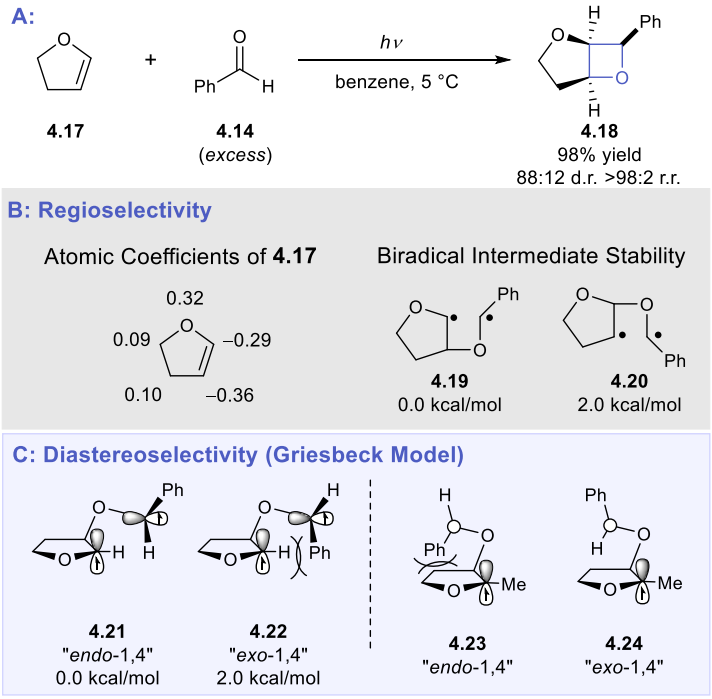

crossing to a singlet diradical intermediate, secondary orbital interactions, or conformers analogous to **4.23** and **4.24** may lead to the thermodynamic products.[39]

Beyond the intrinsic selectivity, methods to control the absolute stereochemistry of the Paternò–Büchi reaction have also been extensively studied.[4041] Early efforts by Scharf[42] and Zamojski[43,44] utilized acyclic chiral aldehydes and acyl cyanides for diastereotopic differentiation of the carbonyl faces (Scheme 4.4A). Unfortunately, in both cases the diastereomeric excess (de) did not exceed 30%. Chiral auxiliary-induced facial diastereoselectivity enables proficient stereocontrol, and the use of chiral phenylglyoxylate esters proved to be an advantageous substrate due to their ease of synthesis from widely available optically-active alcohols. Gotthardt and Lenz were the first to report this approach utilizing menthol-derived substrate **4.28a** for efficient diastereocontrol of the [2+2]-photocycloaddition with tetramethylethylene (**4.29**).[45,46] Interestingly, the selectivity of this reaction was found to have a strong temperature dependence, exhibiting a preference for the *exo* diastereomer under cryogenic conditions and yielding the oxetane product in 53% de. Following this, Scharf and coworkers investigated the chiral induction

Scheme 4.4. Chiral Induction Using Chiral Carbonyl Substrates

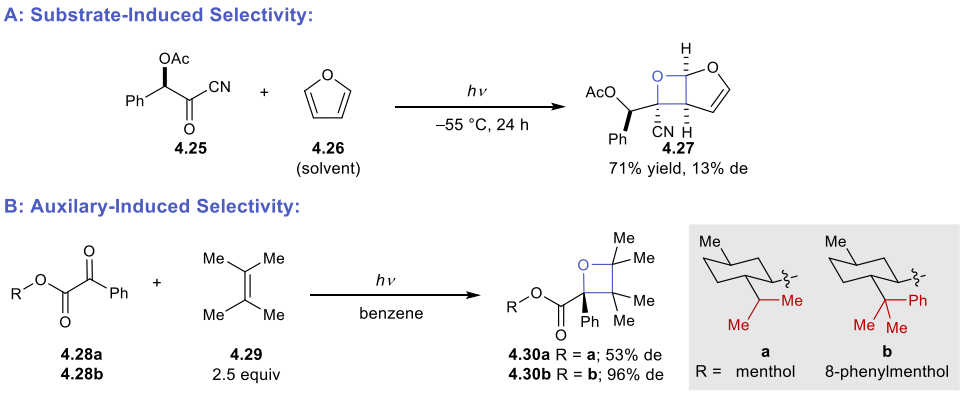

of this reaction by systematically varying the "concavity" of the alcohol auxiliary.[47,48] This work established 8-phenylmenthol as a superior auxiliary, affording 98:2 diastereoselectivity for the same reaction and other cycloadditions.[49,50]

Alternatively, the facial selectivity of the Paternò–Büchi reaction can be influenced by the stereochemistry of the alkene coupling partner. These examples can also be divided into substrate-induced and auxiliary-induced stereocontrol strategies. Given the abundance of methods for stereoselective 1,4-additions to Michael acceptors, enantiomerically pure silyl enol ethers can be readily synthesized in a few steps. In 1995 Bach demonstrated that the [2+2]-cycloaddition of chiral substrate **4.31** with benzaldehyde proceeds without racemization of the stereogenic center, obtaining oxetane **4.32** in >95% ee (Scheme 4.5A).[51] The transposition of the chiral information from the γ- to the α-carbon was less effective in controlling the facial diastereoselectivity.[52] Mechanistic investigations of this system revealed that the approach of the excited-state carbonyl occurs from the less shielded face, predicted by a 1,3-allylic-strain model.[53] Similar effects have been observed in photocycloadditions with L-Ascorbic Acid[54] and D-isosorbide derivatives.[55]

Chiral directing groups have also been demonstrated in enantiospecific Paternò–Büchi reactions. D'Auria and coworkers disclosed that enantioenriched 2-furylmethanol **4.34** reacts selectively with benzophenone to yield oxetane **4.35** without loss of ee (Scheme 4.5B). The authors proposed the hydroxyl group induces facial selectivity by participating in a hydrogen-bonding interaction with the carbonyl oxygen.[56,57]

In comparison to the optically active α-ketoesters discussed above, alkenes modified with chiral auxiliaries have been underexplored in Paternò–Büchi reactions, and these studies have been less successful. In 2001, Bach reported that *N*-Acyl enamides are suitable alkene substrates for the cycloaddition with excited-state carbonyls.[58] With this result in hand, Bach postulated that using

Evan's chiral oxazolidinone auxiliary may provide a unique mode of stereocontrol for the Paternò–Büchi reaction.[59] In practice, phenyl-substituted oxazolidinone substrate **4.36a** was found to react in overall good yield with benzaldehyde, albeit with an unsatisfactory 30% de. On the other hand, the benzyl enecarbamate **4.36b** yielded the corresponding oxetane with an improved 62% de.

Scheme 4.5. Chiral Induction Using Chiral Alkene Substrates

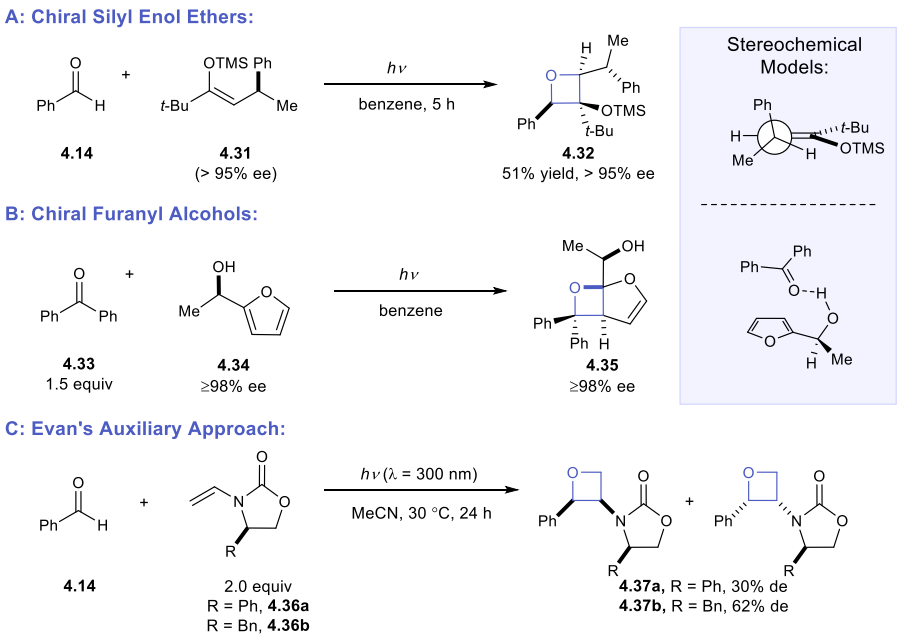

Using an approach conceptually similar to that of D'Auria outlined above, Bach questioned whether a chiral host could preorganize an alkene substrate for efficient facial discrimination of a photochemical reaction. Accordingly, host **4.39**, derived from Kemp's triacid,[60] was appended with both a benzaldehyde that can participate in a Paternò–Büchi reaction and an amide that can readily bind prochiral cyclic enamide **4.38** through hydrogen-bonding interactions. This complexation preferentially orients the *Si*-face of the alkene in close proximity to the aldehyde. Thus, photoexcitation of the hydrogen-bound host results in excellent diastereoselectivity (95:5) of the fused oxetane product (Scheme 4.6).[61]

Scheme 4.6. Diastereoselective Paternò–Büchi Reaction Using Hydrogen–Bonding Template

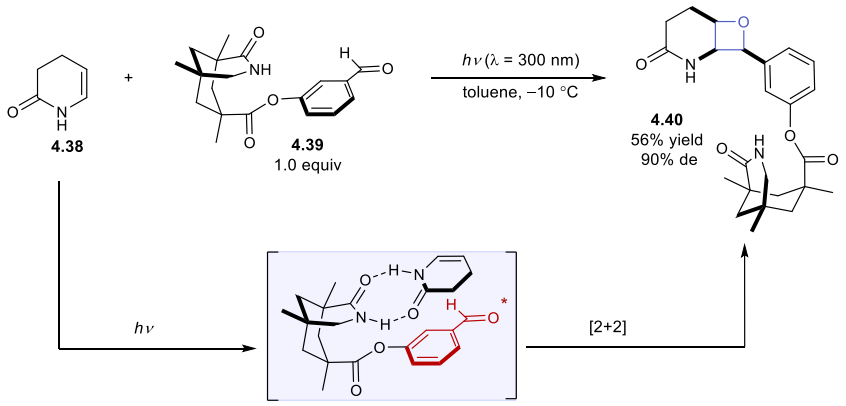

4.1.4 Limitations in Current Enantioselective Photocatalytic Reactions

Despite its importance in the history of photochemistry and the synthetic utility of this reaction, to date no examples of an enantioselective catalytic Paternò–Büchi have been reported. Indeed, highly enantioselective catalysis of excited-state photoreactions has only recently been shown to be feasible. Interestingly, although most of the existing reports involve the coordination of a chiral Lewis or Brønsted acid to the carbonyl of an enone substrate, these enantioselective reactions occur exclusively at the alkene moiety and not at the carbonyl. [62–66]

The binding of a carbonyl to an exogenous catalyst, unfortunately, can perturb the nature of its excited state and alter its photoreactivity. The common organic reactions of excited-state carbonyl compounds, including the Paternò–Büchi reaction, generally arise from a (n,π*) triplet state,[6768] which can be conceptualized as the excitation of an electron from the non-bonding oxygen-centered lone pair into the C=O π* antibonding orbital.[69] However, upon coordination to Brønsted or Lewis acids the (n,π*) state is strongly destabilized and the lowest-energy excited state is often (π,π*) in nature.[70,71] For instance, Bach recently reported the reversal in chemoselectivity of 2-napthaldehyde (**4.41**) by Lewis acid coordination (Scheme 4.7).[72] In the absence of a Lewis

Acid, the (n,π*) excited state was shown undergo smooth [2+2] photocycloaddition with **4.29** to afford the oxetane. In contrast, addition of $AlBr_3$ inhibits the Paternò–Büchi reaction and preferentially reacts to afford *ortho* photocycloaddition products.[73]

Scheme 4.7. Paternò–Büchi Reaction and *ortho*-Photocycloaddition of 2-Napthaldehyde

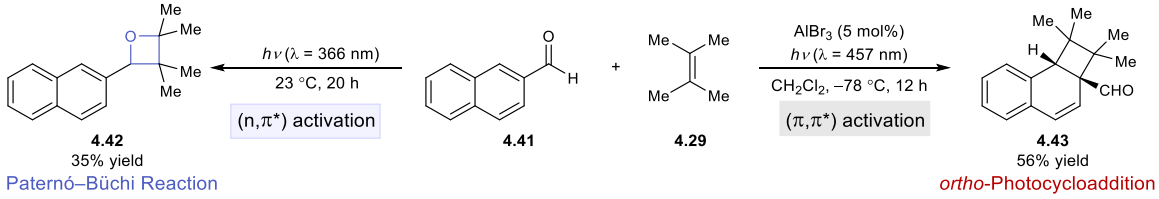

We recently reported another demonstration of divergent reactivity of carbonyl substrates in a photochemical system (Scheme 4.8).[74] Independently, the Schindler group[75] and ours uncovered the first example of a catalyzed visible-light Paternò–Büchi reaction, avoiding the use of high-energy UV light. This methodology was found to proceed by Dexter Energy Transfer (DET) from a photoexcited iridium catalyst to phenyl glyoxylate ester **4.44a**. Upon sensitization to the (n,π*) triplet, the excited-state carbonyl proceeds to react with electron-rich olefin substrates to afford oxetanes. To our surprise, in an attempt to control the stereoselectivity of this photocycloaddition through the introduction a $Y(OTf)_3$ Lewis acid, the chemoselectivity shifts to a photoredox regime, now favoring allylic functionalized products. Broadly speaking, established strategies for controlling excited-state stereochemistry are unlikely to be applicable to enantioselective Paternò–Büchi reactions because they all require pre-coordination of a carbonyl compound to a Lewis or Brønsted acidic catalyst that deactivates the necessary (n,π*) state.

Scheme 4.8. Divergent Photocatalytic Reactions of α-Ketoesters

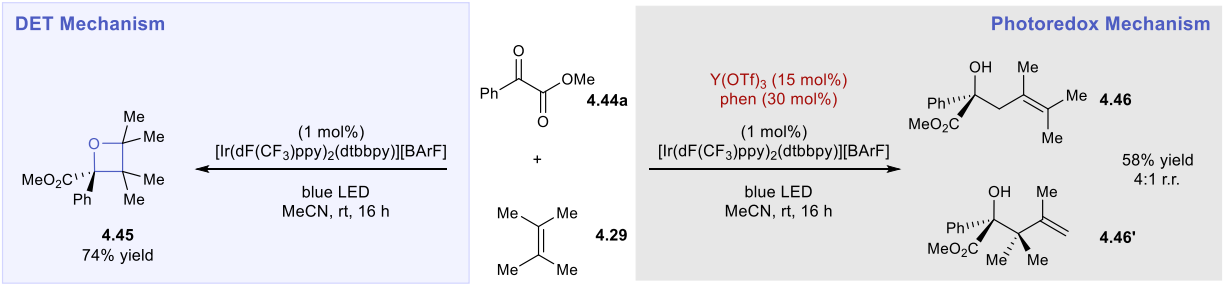

4.1.5 Prior Work and Mechanistic Hypothesis

Recently, our laboratory reported a family of hydrogen-bonding chiral Ir photosensitizers based upon a design originally developed by Meggers.[76,77] These photosensitizers are excellent, highly enantioselective catalysts for excited-state [2+2] cycloaddition reactions.[78] As discussed in Chapter 3, our investigations probing the intermolecular photocycloaddition of quinolones with maleimides demonstrated that the reaction proceeds via an unusual mechanism.[79] NMR titrations, kinetic experiments, and time-resolved luminescence measurements were consistent with a selective ground-state association between the catalyst pyrazole N–H and the quinoline substrate. Unexpectedly, after excitation of the complex, energy transfer proceeds exclusively to unassociated maleimide. Thus, the excited-state photosensitizer generates an excited-state maleimide within a solvent cage, and the reaction of the triplet-state maleimide must be faster than cage-escape to account for the high enantioselectivities obtained at low catalyst loadings. Wondering if this phenomenon might enable the discovery of other highly enantioselective bimolecular photoreactions, we sought to develop the first highly enantioselective Paternò–Büchi reaction. Mechanistically, the chiral Ir photosensitizer would selectively bind quinolone **4.47** in the ground state while controlling the reaction of an unbound excited-state carbonyl. Unlike previous attempts with chiral Lewis acids, the proposed system would allow access to the

unperturbed (n,π*) configuration of the triplet carbonyl substrate, via DET, proximal to chiral information enabling asymmetric catalysis of the Paternò–Büchi cycloaddition (Scheme 4.9).

Scheme 4.9. Mechanistic Hypothesis of an Enantioselective Catalytic Paternò–Büchi Reaction

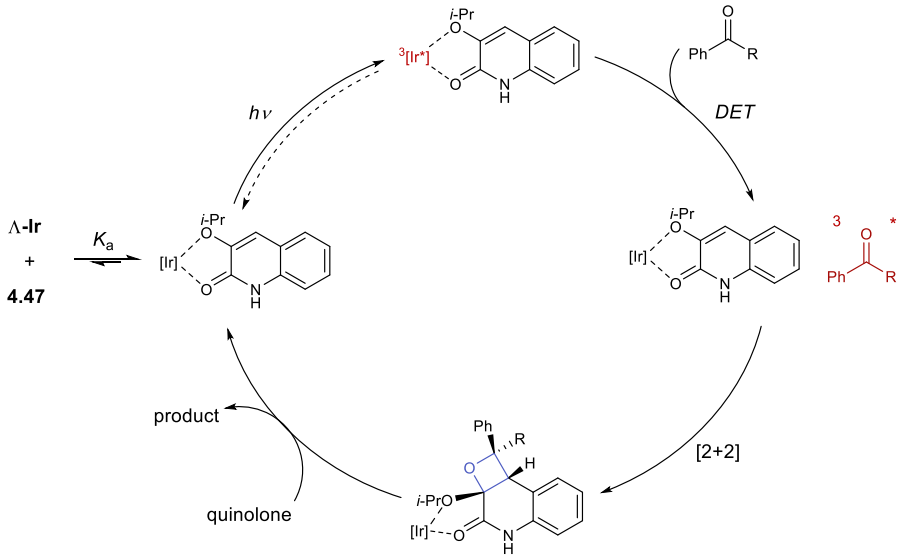

4.2 Results and Discussion

4.2.1 Optimization of Reaction Conditions

We began our investigation by examining conditions similar to those previously reported for the [2+2] photocycloaddition of maleimide with quinolone (Table 4.1). Using chiral photocatalyst Λ-**4.49a**, quinolone **4.47** and methyl α-ketoester **4.44a** successfully underwent a Paternò–Büchi reaction forming oxetane **4.48a** in appreciable yield, near perfect regioselectivity for the ketal, and a slight excess of the *endo* diastereomer (entry 1). To our delight, these conditions afforded **4.48a** in low but significant enantioselectivity. Next, we observed that the ee is dependent on the light source used, increasing with longer wavelengths (entries 1–3). These results are in accord with the absorbance of **4.44a** tailing into the visible, causing direct excitation and thus racemic background reaction. We next turned toward the variation of both the phenylpyridine

(ppy) and pyrazole ligands for further optimization. The methoxy unit of ligand **B1** has a deleterious effect on the ee of the adduct (entry 4). Cyclometalating ppy ligands of varying fluorination patterns were surveyed. Photocatalysts Λ-**4.49c** and Λ-**4.49d**, which were optimal for previous systems,[7880] displayed only minor improvements in facial selectivity for the *exo* product (entries 5 and 6). Catalyst Λ-**4.49e** bearing the common ppy ligand **A4** provided a substantial increase, albeit at only 55% ee for the major isomer (entry 7). Lastly, inspired by privileged C_2-symmetric scaffolds in asymmetric catalysis, Λ-**4.49f** was designed and tested (entry 8), outperforming the phenylpyrazole (**B2**) analogue. Unfortunately, the diastereoselectivity was still poor and with the minor *exo* oxetane providing superior selectivity in 89% ee.

Table 4.1. Optimization of the Chiral Photocatalyst Structure

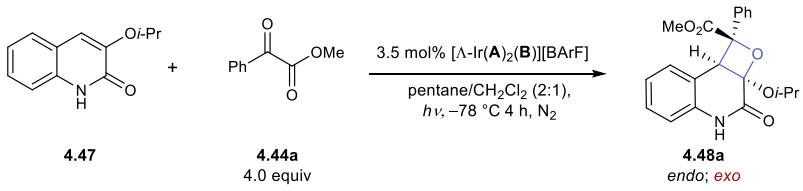

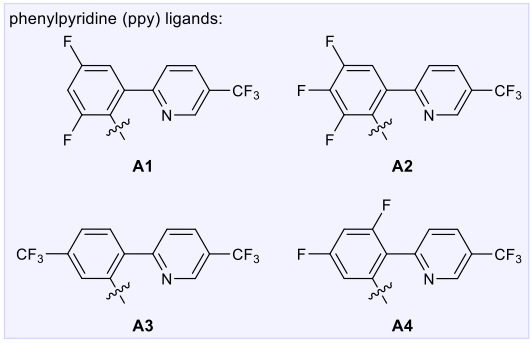

entry	photocatalyst	λ_{max} (nm)	yield (d.r.)	ee (%)
1	**4.49a** [Λ-Ir(**A1**)$_2$(**B1**)][BArF]	427	79% (2:1)	11; 23
2	**4.49a** [Λ-Ir(**A1**)$_2$(**B1**)][BArF]	440	73% (2:1)	27; 50
3	**4.49a** [Λ-Ir(**A1**)$_2$(**B1**)][BArF]	456	97% (2:1)	33; 59
4	**4.49b** [Λ-Ir(**A1**)$_2$(**B2**)][BArF]	456	99% (2:1)	31; 50
5	**4.49c** [Λ-Ir(**A2**)$_2$(**B2**)][BArF]	456	92% (2:1)	23; 64
6	**4.49d** [Λ-Ir(**A3**)$_2$(**B2**)][BArF]	456	99% (2:1)	30; 63
7	**4.49e** [Λ-Ir(**A4**)$_2$(**B2**)][BArF]	456	71% (1.5:1)	55; 78
8	**4.49f** [Λ-Ir(**A4**)$_2$(**B3**)][BArF]	456	73% (1.5:1)	74; 89

We noted that generally the minor diastereomer exhibited higher enantioselectivity compared to the major product. Thus, we questioned if the diastereoselectivity could be tuned to favor the highly enantioenriched *exo* isomer over the less selective *endo* isomer. We constructed a series of α-ketoesters of varying steric bulk on the ester unit. To our delight, the increased bulk (**4.44a**–**g**) resulted in a reversal in d.r. from 1.5:1 to 1:6 (Table 4.2), however a concurrent erosion in enantioselectivity occured. A key obersvation was that when the reaction is conducted under air rather than an inert N_2 atmosphere, the enantiomeric excess of the cycloaddition was consistently higher with a more profound effect on bulky esters (**4.44d**–**g**). Fascinated by these results, we undertook mechanistic investigations to further optimize this system.

Table 4.2. Effects of Sterics and Oxygen on Diastereoselectivity and Enantioselectivity

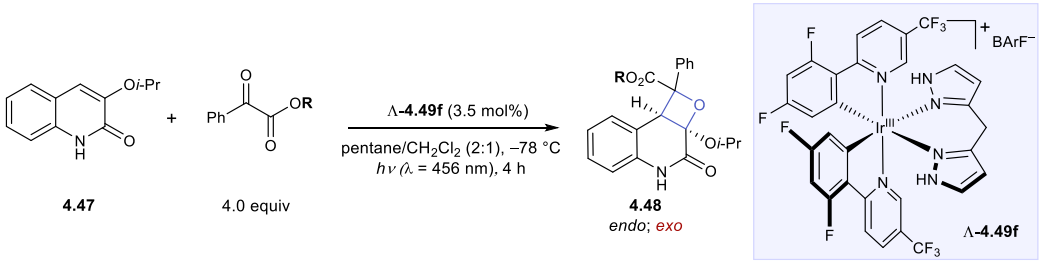

Effect of Sterics and Oxygen:

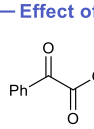

	4.44a	4.44b	4.44c	4.44d	4.44e	4.44f	4.44g
yield	99%	89%	87%	73%	73%	74%	66%
d.r. (*endo*/*exo*)	1.5:1	1:1	1:3	1:4	1:5	1:5	1:6
ee (%)	74; 89	65; 81	55; 77	55	56	27; 56	51
ee (%) under air	77; 91	67; 82	81	77	77	62; 78	78

4.2.2 Mechanistic Investigations as a Tool for Optimization

We commenced mechanistic investigations by first gaining an understanding of the ground-state interactions between the optimal photocatalyst and reactants. For ease of operation, we used the solid adamantyl α-ketoester **4.44f** for these studies. The ground-state interactions were

probed through NMR titration experiments (Figure 4.3A). Holding the concentration of Λ-**4.49f** constant with increasing amounts of quinolone **4.47** caused a dramatic downfield shift for the N–H proton resonances of both the quinolone and pyrazole. This binding isotherm was well fit by a non-cooperative 1:2 [Ir]:**4.47** model with equilibrium constants of K_{a1} = 279 ± 1 M^{-1} and K_{a2} = 183 ± 2 M^{-1},[81,82] indicating that the C_2-symmetric photocatalyst may associate two equivalents of the quinolone substrate. This 1:2 binding model was confirmed with a Job plot (Figure 4.3B).[83] An identical NMR experiment was performed with alpha-ketoester **4.44f**. However, in this case the chemical shift of the photosensitizer pyrazole proton remained almost unchanged after a 20-fold excess of ester was added. Consequently, the calculated association constant was comparatively smaller (K_a = 6.6 ± 0.6 M^{-1}). Lastly, a similar titration revealed no ground-state interaction between the quinolone and phenyl glyoxylate substrates. The stronger association constant measured for **4.47** is consistent with our initial mechanistic hypothesis.

Figure 4.3. NMR Titration Binding and Job Plot

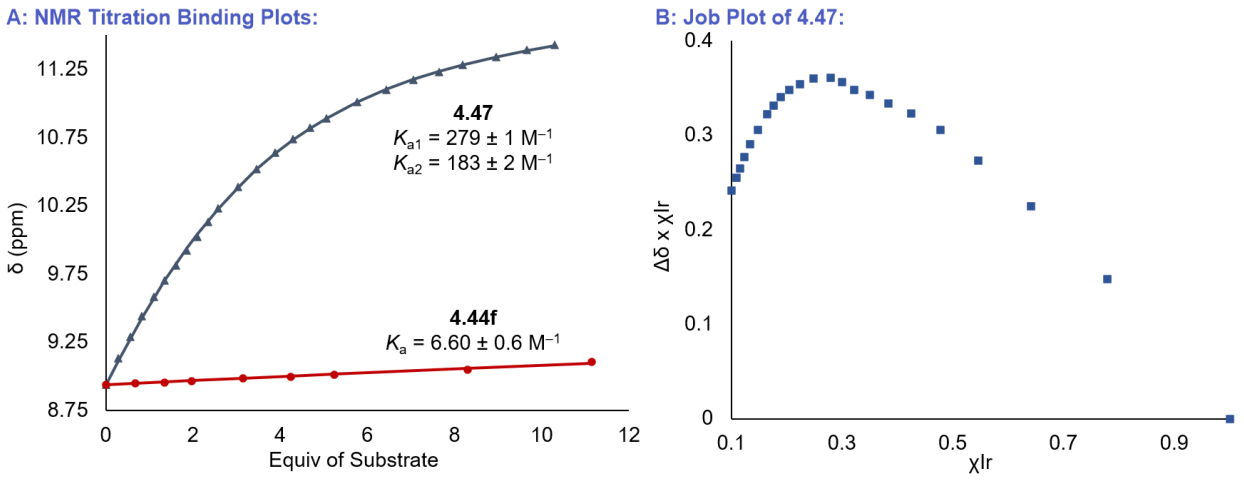

We then turned our attention to the excited-state reactivity, beginning with steady-state luminescence quenching experiments (Figure 4.4). Unexpectedly, both the quinolone and ester quench photoexcited Λ-**4.49f** with similar Stern-Volmer constants (K_{SV}**4.47** = 9,400 M^{-1} and K_{SV}**4.44f**

= 3,980 M^{-1}). Electrochemical studies in CH_2Cl_2 revealed an irreversible anodic peak potential of +1.74 V and reduction potential <–1.7 V vs. SCE for quinolone **4.47**. Likewise, the oxidation and reduction potentials of **4.44f** were measured at >+1.75 V and –1.41 V respectively. These redox potentials are well outside of those for the photoexcited catalyst (+1.23 V and –1.13 V), meaning photoinduced electron transfer is unlikely. Secondly, control experiments indicate that no reaction occurs in the absence of light, ruling out a purely thermal process. On the other hand, the triplet energy (E_T) of Λ-**4.49f** was measured to be 63 kcal/mol, sufficiently high for DET to both **4.47** (~55 kcal/mol) and **4.44f** (61 kcal/mol).[84] These findings contradict our mechanistic hypothesis outlined above in which we presumed that only the phenyl glyoxylate ester could feasibly be sensitized and not the quinolone.

Figure 4.4. Steady-State Luminescence Quenching Plots

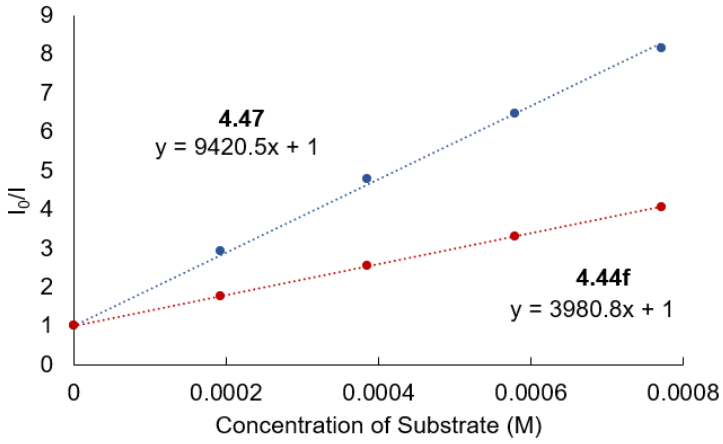

Photochemical systems in which the substrate can bind directly to a photocatalyst typically undergo an intracomplex quenching at a rate that outcompetes any diffusional processes.[85] Therefore, in these reactions the Stern-Volmer constant mirrors the binding constant. For example, the enantioselective intramolecular [2+2]-photocycloaddition discussed in Chapter 2 exhibited a K_a of 3,000 M^{-1} and K_{SV} of 3,200 M^{-1} using CH_2Cl_2 as the solvent. With this in mind, we wondered

if two energy transfer mechanisms may be possible in the current reaction: a *static* quenching mechanism that occurs via energy transfer to the bound quinolone and *dynamic* quenching which arises from a diffusional, bimolecular energy transfer with free quinolone. Furthermore, the work in Chapter 3 demonstrated that the geometry in which the 3-*iso*-propoxy quinolone binds to the chiral photocatalyst can affect orbital overlap, which is critical for energy transfer to occur. Due to the same effect, we questioned if perhaps the degree of static quenching in the current system is minimal compared to the dynamic quenching.

To distinguish between these pathways time-resolved luminescence quenching experiments were conducted in collaboration with the Wright group at the University of Wisconsin–Madison. In the absence of either substrate, the Λ-**4.49f** was found to undergo first-order decay with a lifetime of 2.4 μs, following photoexcitation by a pulsed laser. The addition of increasing amounts of **4.47** resulted in both a decrease in the emission intensity immediately after laser excitation (static) and the lifetime of the photocatalyst (dynamic) (Figure 4.5A). Owing to its near instantaneous nature, the initial decrease in emission intensity correlates with a static quenching process by bound quinolone ($k_{q,static} > 10^8$ s^{-1}). Secondly, the inverse relationship between quinolone concentration and photocatalyst lifetime is consistent with a diffusional quenching process. The data from both decay pathways was used to construct Stern-Volmer plots (Figure 4.5B). In support of our hypothesis, K_{SV} (290 M^{-1}) for static quenching was calculated to be within experimental error of the binding constant of **4.47** to Λ-**4.49f** (K_{a1} = 279 M^{-1}). Alternatively, the Stern-Volmer constant for dynamic DET was found to be K_{SV} =7,100 M^{-1}.

Figure 4.5. Time-Resolved Luminescence Quenching Plots

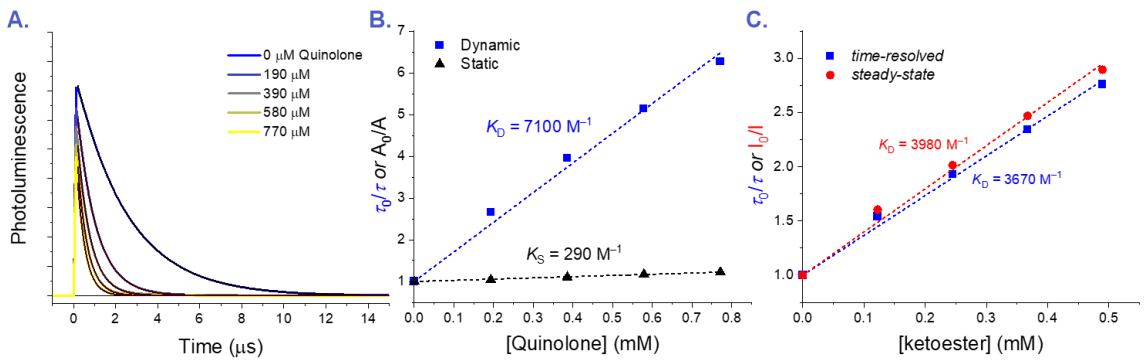

Time-resolved experiments were also performed with α-ketoester **4.44f**. As expected, with increasing concentrations of **4.44f** only the lifetime of photoexcited Λ-**4.49f** is affected, meaning that this substrate reacts only through a collisional quenching pathway. This result is consistent with the lack of binding observed during NMR titration experiments. Furthermore, the Stern-Volmer constant (K_{SV} = 3,670 M^{-1}) matches closely with the steady-state experiments, evidenced by overlaying the two datasets (Figure 4.5C). Collectively, these time-resolved studies indicate three distinct pathways in which the chiral photocatalyst is quenched. Both the quinolone and glyoxylate ester are activated via dynamic energy transfer by a diffusional encounter complex while an internal static quenching mechanism with bound substrate is possible.

These results pose a complex mechanistic picture in which *both* the quinolone or α-ketoester triplet states can lead to enantioenriched product formation. Our mechanistic hypothesis is presented below (Scheme 4.10). Photoexcitation of the catalyst–substrate complex leads to divergent pathways. A triplet rebound mechanism (left) is possible in which excited-state **4.44f** reacts with bound **4.47** to yield scalemic **4.48f**. Alternatively, the photoexcited substrate–catalyst complex can undergo *static* quenching by bound **4.47**, which could further react with ground-state **4.44f** to yield the enriched oxetane (right). The time-resolved experiments revealed this pathway

to be kinetically prominent at room temperature, quenching approximately 85% of photoexcited Λ-**4.49f** at relevant concentrations. In Chapter 3 we note a temperature dependence on the quenching of the optimal photocatalyst Λ-**4.49a**. At ambient conditions **4.47** quenches with a K_{SV} = 47 $M^{-1}s^{-1}$. However, conducting the same experiment at –78 °C shows no change in photoluminescence, consistent with a temperature-induced binding geometry change that lacks efficient orbital overlap for DET to occur. Therefore, we hypothesize the same phenomenon is possible in the current Paternò–Büchi reaction, in which at cryogenic conditions the extent of static quenching becomes negligible. These experiments are currently underway in our laboratory.

Scheme 4.10. Possible Scalemic Product Forming Pathways

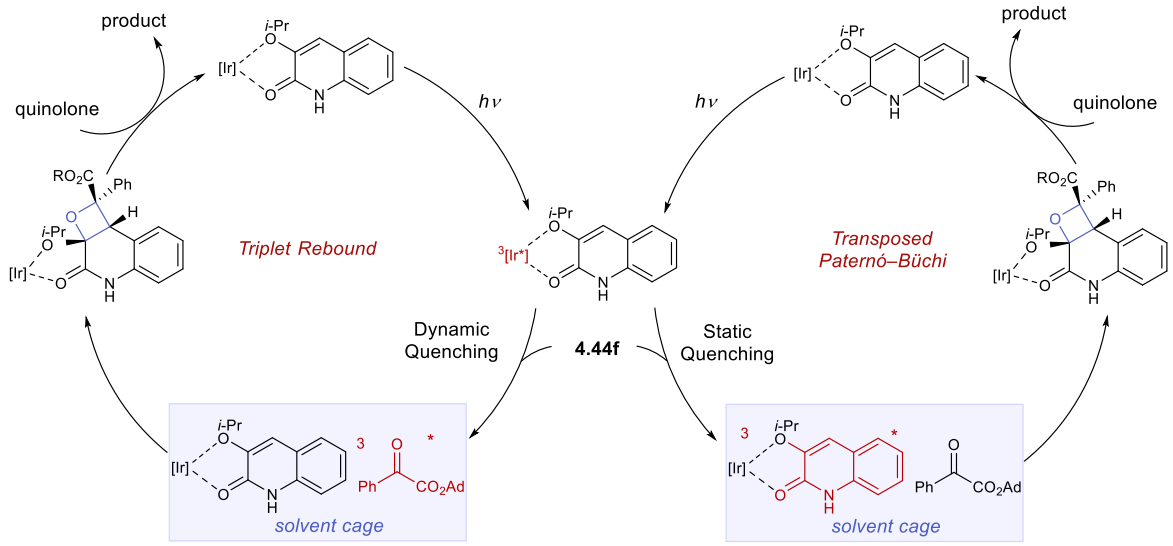

With this understanding. we postulated that non-stereoselective reaction pathways absent in the previously reported [2+2]-photocycloaddition with maleimide could be problematic in the current reaction (Scheme 4.11). The room temperature time-resolved experiments indicated that dynamic quenching of the substate–catalyst adduct by a second equivalent of unbound quinolone occurs at a similar rate compared to **4.44f** ($k_{q\mathbf{4.47}}$ = 2.96 x 10^9 $M^{-1}s^{-1}$ vs. $k_{q\mathbf{4.44f}}$ = 1.66 x 10^9 $M^{-1}s^{-1}$). This produces a triplet-excited **4.47** that can further react without the stereochemical influence

of the chiral photocatalyst via a transposed Paternò–Büchi reaction (Scheme 4.11A). Additionally, the triplet lifetime of α-ketoester **4.44a** has been reported to be exceptionally long (ca. 13 μs in benzene)[86] due to captodative stabilization of the diradical nature of the (n,π*) state. This lifetime is two orders of magnitude longer than that of maleimide (170 ns).[87] During the course of the previous intermolecular reaction, we observed the formation of maleimide dimer that presumably arises from solvent-cage escape of triplet maleimide. In this sense, ground-state maleimide acts as a scavenger, preventing the formation of racemic product. Hence, in the Paternò–Büchi reaction, we speculate that triplet **4.44a*** is persistent enough to escape the solvent cage and react with an unbound alkene partner in solution, subsequently decreasing the ee of the cyclization (Scheme 4.11B). To test this hypothesis, the excited-state lifetimes were measured for a series of phenyl glyoxylate esters. Interestingly, the more sterically-encumbered substrates (**4.44d**–**f**) bear an order of magnitude longer-lived excited state compared to **4.44a** or **4.44b**. Notably, the more persistent triplet α-ketoesters also exhibit a more dramatic increase in enantioselectivity when the reactions are conducted under air, in the presence of O_2. These results are consistent with quenching of the caged-escaped α-ketoester by molecular oxygen, effectively decreasing the lifetime of the carbonyl substrate, slowing the rate of racemic Paternò–Büchi reaction. Correspondingly, the emission of substrate **4.44f** was shown to decrease in intensity when O_2 is present in comparison to oxygen-free conditions. In a similar fashion, O_2 is reported to be an excellent quencher of (π,π*) excited states.[88] Alternatively, it is also reasonable to presume that O_2 may also inhibit racemic pathway A by deactivating triplet quinolone formed by collisional energy transfer.

Scheme 4.11. Possible Racemic Pathways

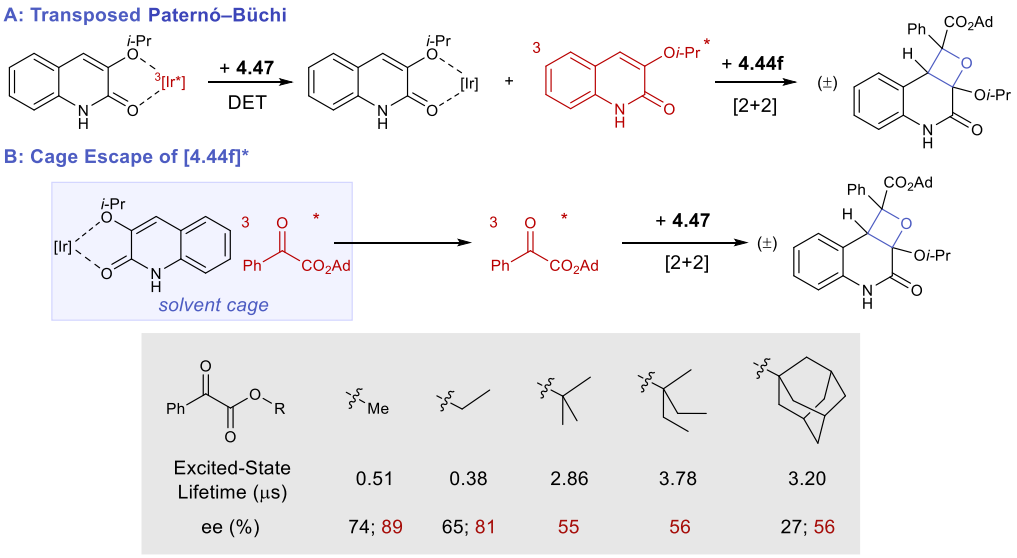

Both racemic pathways have a dependence on the concentration of unbound **4.47**, thus we questioned if fast collisional quenching processes that lead to racemic reactivity could be suppressed by limiting [**4.47**]. In support of this hypothesis, slow addition of **4.47** via syringe pump afforded oxetane **4.48f** in excellent yield, >20:1 d.r. and 86% ee (Table 4.3, entry 1). Toluene was revealed to be the optimal solvent, boosting the enantioselectivity to 96% (entry 2). Increasing the concentration, in addition to adding small amounts of dichloromethane to fully solubilize the photocatalyst, improved the ee of the cycloaddition to 98% (entries 4-7). We believe this trend is consistent with increasing the rate of reaction, holding the concentration of unreacted and unbound **4.47** as low as possible. Lastly, varying the amount of α-ketoester had a negligible impact on selectivity (entries 8 and 9). It's worth noting that with the slow addition of quinolone its overall concentration is minimal, meaning that the dynamic quenching pathway by **4.44f** becomes the prevailing mode of deactivation of **4.49f***. Therefore, under optimal reaction conditions the triplet rebound mechanism (Scheme 4.10 left) is likely the primary product forming pathway.

Table 4.3. Slow Addition Experiments and Final Optimization

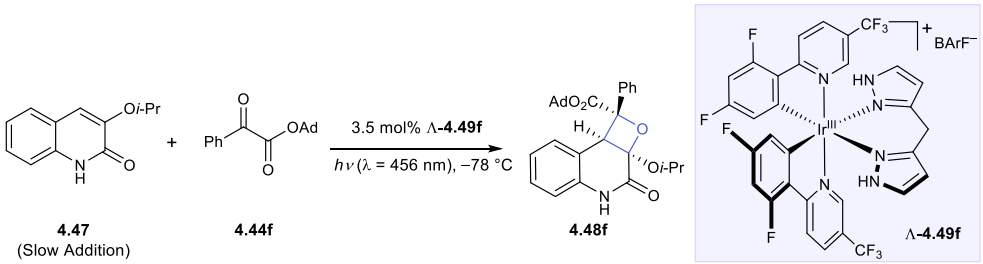

Entry	Solvent	Concentration[a]	Equiv of **4.44f**	Yield[b]	d.r.	ee (%)
1	pentane/CH_2Cl_2 (2:1)	5 mM	4.0	87 %	>20:1	86
2	$PhCH_3$	5 mM	4.0	71 %	>20:1	96
3	$PhCH_3/CH_2Cl_2$ (2:1)	5 mM	4.0	59 %	17:1	89
4[c]	$PhCH_3$	5 mM	4.0	65 %	>20:1	96
5[c]	$PhCH_3$	2.5 mM	4.0	58%	10:1	92
6[c]	$PhCH_3$	10 mM	4.0	48%	>20:1	97
7[c]	$PhCH_3$	20 mM	4.0	76%	>20:1	98
8[c]	$PhCH_3$	20 mM	2.0	68%	13:1	95
9[c]	$PhCH_3$	20 mM	5.0	84%	>20:1	97

[a] Final concentration after slow addition. [b] NMR yield. [c] Reaction conducted under batch conditions.
[e] 100 μL of CH_2Cl_2 added.

4.3 Conclusion and Outlook

Despite its discovery in the early 20th century and the utility of the Paternò–Büchi reaction, this [2+2] photocycloaddition has yet to be rendered enantioselective under catalytic conditions. This difficulty is a result of the limitations imposed by current asymmetric photochemical strategies. These methods typically require strong binding interactions to carbonyl moieties, which perturbs its photophysics disfavoring an (n,π*) excited state and thus causing divergent reactivity. The methodology discussed above utilizes a C_2-symmetric chiral iridium photocatalyst to recruit a quinolone alkene partner through hydrogen-bonding interactions and favors a triplet rebound mechanism via Dexter energy transfer to an unbound α-ketoester. This strategy ensures that the photophysics of the reacting carbonyl remain unchanged, allowing for exclusive oxetane formation. Optimization of the photocycloaddition revealed an interesting dependence on the presence of O_2 for higher enantioselectivity. Inspired by these observations, the mechanism of this

reaction was probed using NMR, steady-state, and time-resolved spectroscopic experiments that provided critical insights for optimization. These studies identified problematic racemic, collisional Dexter energy transfer pathways that can be minimized via slow addition of the quinolone substrate to afford oxetane products in enantioselectivities up to 98%. We expect the findings of this research to be highly impactful as a new method to afford enantioenriched polysubstituted oxetanes and as a novel approach for asymmetric photochemical synthesis.

4.4 Contributions

Dr. Wesley B. Swords conducted and analyzed time-resolved luminescence quenching experiments, in addition to offering insightful discussion. Dr. Kent Meyers and Prof. John C. Wright provided the ultra-fast instrumentation and aided in the design of the time-resolved experiments. Prof. Tehshik P. Yoon provided expertise, resources, and funding for researchers.

4.5 Experimental Procedures

4.5.1 General Information

4.5.1.a Reagent Preparation

Dichloromethane and toluene were dried by elution through alumina as described by Grubbs.[89] Except in the case of aqueous reactions, all reaction glassware was flame- or oven-dried prior to use. Flash column chromatography was carried out with Purasil 60 Å silica gel (230–400 mesh) and thin layer chromatography (TLC) was performed utilizing pre-coated silica gel F_{254} plates from SiliCycle Inc. containing a fluorescent indicator. Plates were visualized using either cerium ammonium molybdate (CAM), $KMnO_4$, or phosphomolybdic acid (PMA) stain. Reverse-phase chromatographic separations were performed using C18 Sfär columns and a Biotage Selekt. Reactions that require visible light irradiation used PR160-Kessil lamps of specified wavelengths as the light source. The emission spectrum of the 427nm, 440 nm, and 456 nm Kessil lamps is shown below in Figure 4.6 (reproduced from http://kessil.com/science/PR160L.php). 3-Isopropoxyquinolin-2(1H)-one (**4.47**), di(1H-pyrazol-3-yl)methane (**4.55**),[90] and chiral photocatalysts Λ-**4.49a-e** were prepared as previously described. Methyl 2-oxo-2-phenylacetate (**4.44a**), ethyl 2-oxo-2-phenylacetate (**4.44b**) were purchased from commercial vendors and purified by silica gel chromatography (5:95 MTBE/hexanes) prior to use. Racemic photocatalyst $[Ir(dF(CF_3)ppy)_2(dtbbpy)]$ $[PF_6]$ was synthesized following the published route.[91] $Pd(PPh_3)_4$ was purchased from Strem Chemical. $IrCl_3 \bullet xH_2O$ was provided by a generous gift from Sigma Aldrich. All other reagents were purchased from commercial suppliers and used without additional purification.

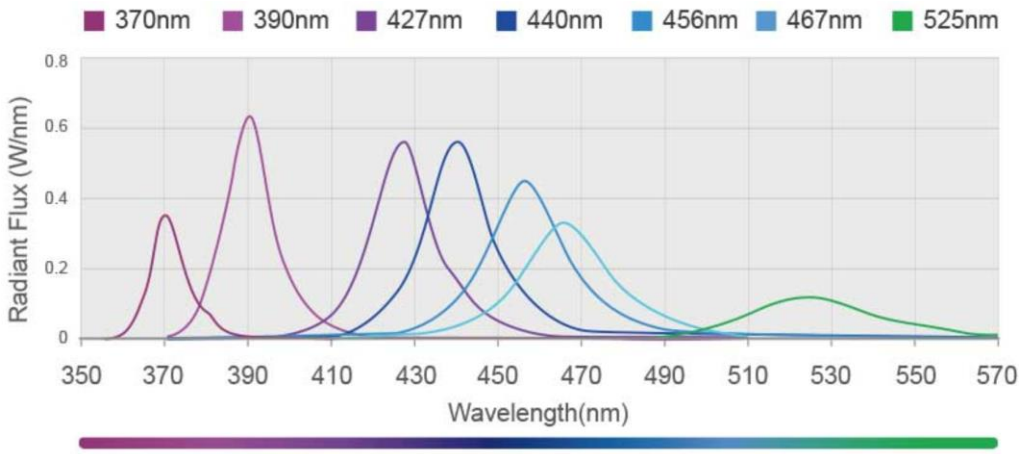

Figure 4.6. The radiance spectra of the PR150-Kessil lamps used

4.5.1.b Product Characterization

^{1}H, $^{13}C\{^{1}H\}$, and $^{19}F\{^{1}H\}$ NMR spectra were obtained using a Bruker Avance-400, Avance-500, or Avance-600 spectrometer with DCH, Prodigy, BBFO+, or TCI-F probes. ^{1}H spectra were internally referenced to tetramethyl silane (0.00 ppm) or the residual protio-solvent peak in acetone-d_6 or DMSO-d_6. $^{13}C\{^{1}H\}$ spectra were internally referenced to $CDCl_3$ (77.16 ppm) or DMSO-d_6 (39.52 ppm). $^{19}F\{^{1}H\}$ spectra were absolute referenced to the corresponding ^{1}H spectra using the method described by Harris.[92,93] Multiplicities are defined using the following abbreviations: s (singlet), d (doublet), t (triplet), q (quartet), p (pentet), sext (sextet), hept (heptet), br. (broad), app. (apparent). Diastereomeric ratios were determined from ^{1}H NMR spectra of the crude reaction mixture. The spectrometers used for this work are supported by the NSF (CHE-1048642, CHE-0342998, CHE-9208463), NIH (S10 OD012245, S10 RR13866-01), and a generous gift from Paul J. and Margaret M. Bender.

Mass spectrometry was performed with a Thermo Q Exactive™ Plus (electrospray ionization or atmospheric solids analysis probe (ASAP-MS)) equipped with an orbitrap detector. This instrumentation is supported by the NIH (1S10 OD020022-1) and the University of Wisconsin.

Cyclic voltammograms were acquired using a Pine Research WaveNow potentiostat/galvanostat.

Enantiomeric excesses were determined for isolated, purified material using chiral HPLC (Waters Alliance), Daicel CHIRALCEL® columns and Chromasolv®-grade solvents.

UV-Vis absorption spectra were acquired using a Varian Cary® 50 UV-visible spectrophotometer with a scan rate of 300 nm/min. UV-Vis emission spectra were acquired on Hitachi F-4500 fluorescence spectrophotometer.

4.5.2 Synthesis of Starting Materials

4.5.2.a Synthesis of Resolved Chiral Iridium Photocatalysts

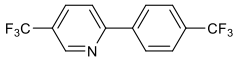

5-(Trifluoromethyl)-2-(4-(trifluoromethyl)phenyl)pyridine (4-CF_3(CF_3)ppy, **4.50**): A 50 mL round-bottomed flask was charged with 2-chloro-5-(trifluoromethyl)pyridine (907 mg, 5.00 mmol, 1.0 equiv.) and 4-(trifluoromethyl)phenylboronic acid (1.06 g, 5.58 mmol, 1.1 equiv.), followed by $Pd(PPh_3)_4$ (146 mg, 0.128 mmol, 0.025 equiv.). Benzene (6.7 mL, 0.75 M with respect to substrate) was added, followed by 2 M aq. Na_2CO_3 (10.0 mmol, 2.0 equiv.) and EtOH (1.25 mL, 4 M with respect to substrate). The solution was stirred vigorously and sparged for 5 min with N_2, resulting in a slight lightening of color. Following this, the mixture was heated at reflux (80 °C) under N_2 and maintained at this temperature for 2 d. The reaction was then cooled to room temperature and H_2O (6 mL/mmol substrate) was added. The mixture was extracted three times into an equal volume of CH_2Cl_2 and the combined organic layers were concentrated *in vacuo*. Following workup, the product was purified by flash column chromatography on silica gel (CH_2Cl_2) to afford a white solid (1.334 g, 4.58 mmol, 92% yield), which contained roughly 5% of an impurity by NMR analysis. Representative ^1H and ^{19}F data are provided below, but no additional characterization was performed. Instead, the crude material was carried on to the cyclometalation reaction without further purification.

^{1}H NMR (400 MHz, $CDCl_3$) δ 8.99 (s, 1H), 8.17 (d, *J* = 8.2 Hz, 2H), 8.04 (dd, *J* = 8.4, 2.2 Hz, 1H), 7.90 (d, *J* = 8.4 Hz, 1H), 7.77 (d, *J* = 8.2 Hz, 2H).

^{19}F NMR (377 MHz, $CDCl_3$) δ –62.36 (s, 3F), –62.78 (s, 3F).

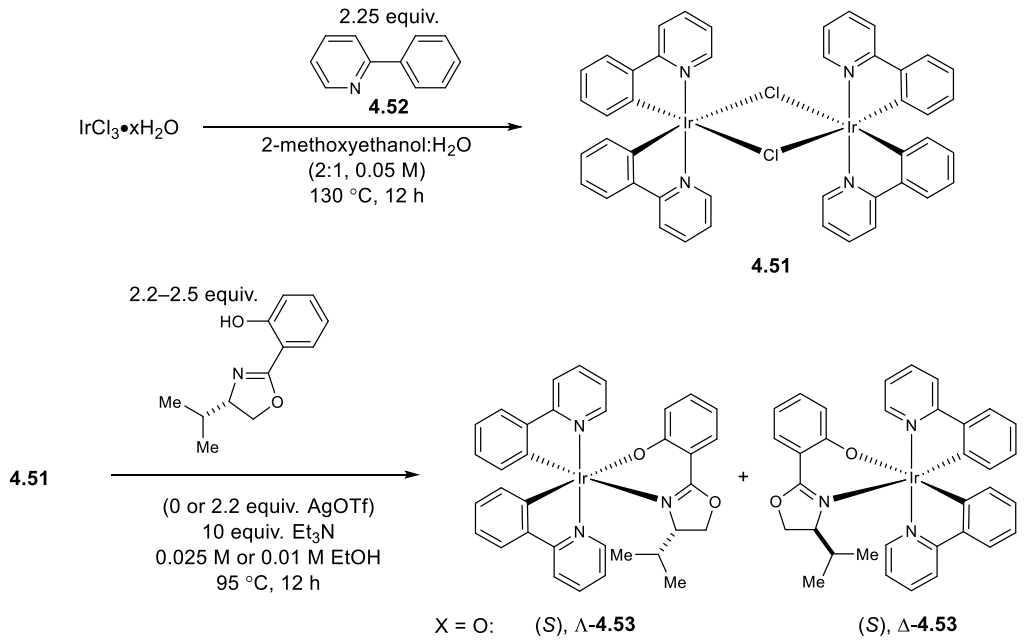

General Procedure 4.A: Resolved iridium diastereomers were prepared using a modification of the procedure reported by Meggers.**Error! Bookmark not defined.** **Error! Bookmark not defined.** A round-bottomed flask was charged with $IrCl_3$•xH_2O (1.00 mmol, 1.0 equiv.), ppy ligand (2.25 mmol, 2.25 equiv.) and a 2:1 mixture of 2-methoxyethanol:H_2O (20 mL total, 0.05 M with respect to $IrCl_3$). The solution was heated at reflux (130 °C) under N_2 overnight. After cooling to room temperature, H_2O was added, resulting in precipitation. The resulting solid was isolated by suction filtration on a frit and rinsed with H_2O and hexanes before drying under vacuum. Crude iridium dimer **4.51** (mass corrected for residual 2-methoxyethanol) was not further purified or characterized, but was directly subjected to one of the following two cleavage reactions.

Ir(4-CF_3(CF_3)ppy)$_2$(*i*-PrHBO) (**4.53**): Prepared according to General Procedure 4.A using $IrCl_3$ (607 mg, 2.03 mmol, 1.0 equiv.) and **4.50** (1.334 g, 4.57 mmol, 2.3 equiv.). Iridium dimer **4.51** was isolated as an orange powder (1.3196 g, 0.817 mmol, 81% crude yield) and carried on without further purification. The cleavage was performed using **4.53** (421 mg, 2.05 mmol, 2.5 equiv.) and Et_3N (1.2 mL, 8.6 mmol, 10.5 equiv.). Following workup, the diastereomers were separated by flash column chromatography on silica gel (gradient, 14:86 to 30:70 EtOAc:hexanes). Combined yield: 867 mg, 0.888 mmol, 54% yield from **4.53**; 44% yield from $IrCl_3$.

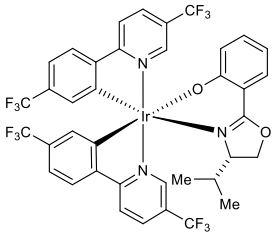

(*S*),Λ-**4.53**: Isolated as a bright orange solid (342 mg, 0.350 mmol, 22% yield from **4.51**; 17% yield from $IrCl_3$). >98:2 dr.

^{1}H NMR (500 MHz, $CDCl_3$) δ 9.29 (s, 1H), 8.57 (s, 1H), 7.97 (d, *J* = 8.6 Hz, 1H), 7.92 (dd, *J* = 8.6, 2.1 Hz, 1H), 7.78 (d, *J* = 8.6 Hz, 1H), 7.73 (dd, *J* = 8.6, 2.0 Hz, 1H), 7.60 (d, *J* = 8.2 Hz, 1H), 7.51 – 7.46 (m, 2H), 7.01 – 6.96 (m, 3H), 6.48 (dd, *J* = 8.7, 1.1 Hz, 1H), 6.45 (s, 1H), 6.27 (ddd, *J* = 8.1, 6.9, 1.2 Hz, 1H), 6.04 (s, 1H), 4.18 (dd, *J* = 9.3, 4.1 Hz, 1H), 4.13 (t, *J* = 9.3 Hz, 1H), 3.65 (ddd, *J* = 9.1, 4.0, 2.9 Hz, 1H), 0.27 (septd, *J* = 6.8, 2.8 Hz, 1H), 0.14 (d, *J* = 7.0 Hz, 3H), –0.01 (d, *J* = 6.9 Hz, 3H).

^{19}F NMR (377 MHz, $CDCl_3$) δ –62.42 (s, 3F), –62.76 (s, 3F), –63.02 (s, 3F), –63.03 (s, 3F).

HRMS (ESI^+) calculated for $[C_{38}H_{27}F_{12}IrN_3O_2]^+$ ($[M+H]^+$). Requires *m/z* 976.1512; found *m/z* 976.1521.

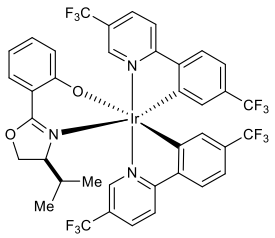

(*S*),Δ-**4.53**: Isolated as an orange powder (525 mg, 0.537 mmol, 33% yield from **4.51**; 26% yield from $IrCl_3$). >98:2 dr, but considerable amounts of an unknown impurity are present.

^{1}H NMR (500 MHz, $CDCl_3$) δ 9.26 (s, 1H), 8.85 (s, 1H), 8.11 – 8.06 (m, 2H), 8.02 (d, *J* = 8.6 Hz, 1H), 7.95 (dd, *J* = 8.6, 2.0 Hz, 1H), 7.77 (d, *J* = 8.2 Hz, 1H), 7.72 (d, *J* =

8.2 Hz, 1H), 7.53 (dd, *J* = 8.0, 1.9 Hz, 1H), 7.18 – 7.12 (m, 2H*), 7.09 (ddd, *J* = 8.8, 6.9, 1.9 Hz, 1H), 6.68 (s, 1H), 6.51 (dd, *J* = 8.7, 1.1 Hz, 1H), 6.44 (ddd, *J* = 8.1, 6.9, 1.1 Hz, 1H), 6.25 (s, 1H), 4.32 – 4.26 (m, 1H), 3.78 (t, *J* = 9.2 Hz, 1H), 2.91 (ddd, *J* = 9.4, 3.7, 1.9 Hz, 1H), 1.54 – 1.50 (m, 1H), 0.85 (d, *J* = 6.8 Hz, 3H), 0.22 (d, *J* = 7.0 Hz, 3H). * = overlapped with impurity.

^{19}F NMR (377 MHz, $CDCl_3$) δ –62.19 (s, 3F), –62.23 (s, 3F), –63.05 (s, 3F), –63.15 (s, 3F).

HRMS (ESI^+) calculated for $[C_{38}H_{27}F_{12}IrN_3O_2]^+$ ($[M+H]^+$). Requires *m/z* 976.1512; found *m/z* 976.1518.

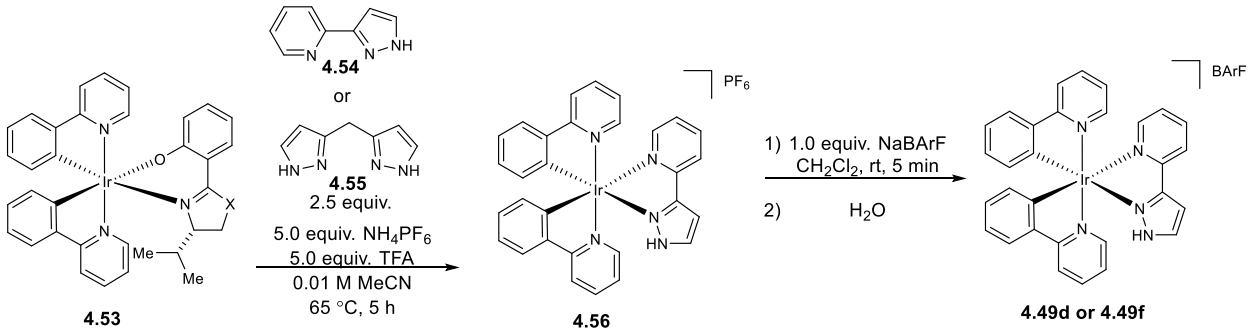

General Procedure 4.B: A round-bottomed flask was charged with **4.53** (0.080 mmol, 1.0 equiv.), NH_4PF_6 (0.40 mmol, 5.0 equiv.), pyrazole ligand **4.54** or **4.55** (0.20 mmol, 2.5 equiv.) and dry MeCN (8 mL, 0.01 M with respect to Ir), then placed under a nitrogen atmosphere. Trifluoroacetic acid (0.40 mmol, 5.0 equiv.) was added by syringe, and the solution was heated to 65 °C in the dark. After 5 h, the mixture was cooled and directly concentrated *in vacuo*. The crude residue was purified by flash column chromatography on silica gel to afford the iridium complex **4.56** which was carried on without further characterization.

The cationic (**4.56**) iridium complex (1.0 equiv.) was dissolved in a minimal amount of CH_2Cl_2 and NaBArF (1.0 equiv.) was added. After stirring for 5 min at room temperature, the mixture was washed with two large portions of H_2O (roughly 5 times the volume of organic solvent). A significant emulsion often formed during this process, which necessitated removal of

the aqueous layer by pipette. The organic phase was then dried by repeatedly passing it through small plugs of Celite® until homogeneous. This filtrate was then concentrated *in vacuo* and reconcentrated from CH_2Cl_2/pentane to afford cationic iridium complexes **5.56** as crystalline powders.

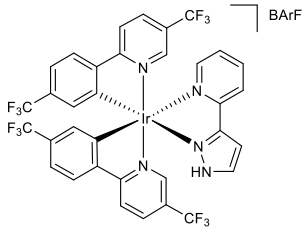

Λ-[Ir(4-CF_3(CF_3)ppy)$_2$(pypz)][BArF] (**Λ-4.49d**): Prepared according to General Procedure 4.B using (*S*),Λ-**4.53d** (78.6 mg, 0.0805 mmol, 1.0 equiv.), NH_4PF_6 (67.5 mg, 0.414 mmol, 5.1 equiv.), **4.54** (30.5 mg, 0.210 mmol, 2.6 equiv.) and trifluoroacetic acid (31 µL, 0.40 mmol, 5.0 equiv.) Following workup, the crude residue was purified by flash column chromatography on silica gel (gradient, 40:60 to 60:40 acetone:hexanes) to afford the iridium complex **4.56d** as a yellow powder, which was carried on without further purification or characterization. This material was treated with NaBArF (72.5 mg, 0.0818 mmol, 1.0 equiv.) according to General Procedure 4.B, providing the final iridium catalyst **Λ-4.49d** as a yellow powder (109 mg, 0.612 mmol, 76% yield over two steps).

^{1}H NMR (500 MHz, $CDCl_3$) δ 10.58 (s, 1H), 8.16 – 8.07 (m, 4H), 7.88 – 7.83 (m, 3H), 7.78 – 7.74 (m, 2H), 7.69 (s, 8H), 7.65 (s, 1H), 7.55 (s, 1H), 7.45 (s, 4H), 7.44 (dd, *J* = 2.9, 1.3 Hz, 1H), 7.40 (app. ddd, *J* = 9.3, 7.9, 1.0 Hz, 2H), 7.35 (ddd, *J* = 7.7, 5.6, 1.3 Hz, 1H), 6.70 (dd, *J* = 3.0, 1.6 Hz, 1H), 6.39 (d, *J* = 1.1 Hz, 1H), 6.34 (d, *J* = 1.1 Hz, 1H).

^{19}F NMR (377 MHz, $CDCl_3$) δ –62.54 (s, 24F), –63.23 (s, 3F), –63.26 (s, 3F), –63.43 (s, 3F), –63.44 (s, 3F).

HRMS (ESI^+) calculated for $[C_{34}H_{19}F_{12}IrN_5]^+$ ($[M]^+$). Requires *m/z* 916.1049; found *m/z* 916.1049.

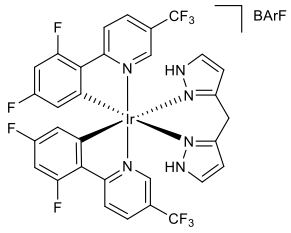

Λ-[Ir(dF(CF$_3$)ppy)$_2$(dpzm)][BArF] (**Λ-4.49f**): Prepared according to General Procedure 4.B using (*S*),Λ-**4.53f** (75.2 mg, 0.0824 mmol, 1.0 equiv.), NH_4PF_6 (69.6 mg, 0.427 mmol, 5.2 equiv.), **4.55** (31.0 mg, 0.209 mmol, 2.5 equiv.) and trifluoroacetic acid (31 µL, 0.40 mmol, 4.9 equiv.) Following workup, the crude residue was purified by flash column chromatography on silica gel (gradient, 40:60 to 50:50 acetone:hexanes) to afford cationic iridium complex **4.56f** as a yellow powder, which was carried on without further purification or characterization. This material was treated with NaBArF (70.7 mg, 0.0798 mmol, 1.0 equiv.) according to General Procedure 4.B, providing the final iridium catalyst **Λ-4.49f** as a yellow solid (50.6 mg, 0.0294 mmol, 36% yield over two steps).

^{1}H NMR (500 MHz, $CDCl_3$) δ 9.36 (s, 2H), 8.47 (dd, *J* = 8.8, 3.1 Hz, 2H), 8.09 (dd, *J* = 8.8, 2.0 Hz, 2H), 7.68 (s, 8H), 7.62 (s, 2H), 7.50 (dd, *J* = 2.8, 1.7 Hz, 2H), 7.47 (s, 4H), 6.68 (ddd, *J* = 12.3, 8.8, 2.3 Hz, 2H), 6.35 (t, *J* = 2.5 Hz, 2H), 5.69 (dd, *J* = 7.7, 2.3 Hz, 2H), 4.38 (s, 2H).

^{19}F NMR (377 MHz, $CDCl_3$) δ –62.52 (s, 24F*), –63.11 (s, 6F), –99.36 (d, *J* = 13.2 Hz, 2F), –104.09 (d, *J* = 13.5 Hz, 2F). * = Actual integration is significantly higher than expected. However, this is not the case for the ^{1}H signals corresponding to BArF.

HRMS (ESI$^+$) calculated for $[C_{31}H_{18}F_{10}IrN_6]^+$ ([M]$^+$). Requires *m/z* 855.1034; found *m/z* 855.1036.

5.5.2.b Synthesis of α-Keto esters

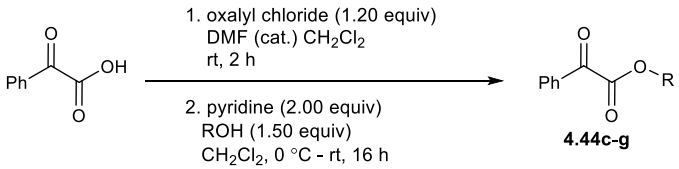

General Procedure 4.C: Oxalyl Chloride (1.20 equiv) was added to a solution of 2-oxo-2-phenylacetic acid in dry CH_2Cl_2 (1.0 M), followed by the addition of a catalytic amount of DMF. After stirring at ambient temperature for 2 h, the solvent and oxalyl chloride were removed by reduced pressure. The slurry was redissolved in dry CH_2Cl_2 (1.0 M) and cooled to 0 °C using an ice bath. To this solution was added pyridine (2.00 equiv) and the appropriate alcohol (2.00 equiv). The reaction mixture was allowed to stir overnight (16 h) at room temperature. Following this, the reaction was quenched with $NaHCO_3$ (aq. sat. 50 mL) and the organic and aqueous layers were separated. The organic layer was washed with 1.0 M HCl (aq. 50 mL), H_2O (50 mL), and brine (50 mL). The organic layer was dried over Na_2SO_4, filtered, and concentrated *in vacuo*. The crude mixture was purified by silica gel flash chromatography (gradient from 0-10% MTBE/hexanes) to yield the corresponding α-ketoester.

isopropyl 2-oxo-2-phenylacetate (4.44c): Prepared according to General Procedure 4.C using 2-oxo-2-phenylacetic (1.00 g, 6.66 mmol, 1.00 equiv), oxalyl chloride (0.70 mL, 7.99 mmol, 1.20 equiv), *iso*-propanol (0.80 mL, 13.3 mmol, 2.00 equiv), and pyridine (0.60 mL, 9.99 mmol, 1.00 equiv). Following purification, a slight yellow oil was afforded in 83% yield (1.0686 g, 5.53 mmol).

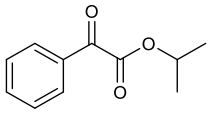

^{1}H NMR: (500 MHz, $CDCl_3$) δ 8.03 – 7.97 (m, 2H), 7.69 – 7.62 (m, 1H), 7.51 (t, J = 7.8 Hz, 2H), 5.33 (hept, J = 6.3 Hz, 1H), 1.42 (s, 3H), 1.41 (s, 3H).

^{13}C NMR: (126 MHz, $CDCl_3$) δ 186.7, 163.6, 134.8, 132.6, 130.0, 128.9, 70.7, 21.7.

HRMS (ASAP) m/z: [M + H]+ Calcd for C11H13O3 193.0859; Found 193.0858.

tert-butyl 2-oxo-2-phenylacetate (4.44d): Prepared according to General Procedure 4.C using

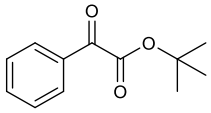

2-oxo-2-phenylacetic (1.50 g, 9.99 mmol, 1.00 equiv), oxalyl chloride (1.05 mL, 12.0 mmol, 1.20 equiv), *tert*-butanol (1.91 mL, 19.99 mmol, 2.00 equiv), and pyridine (1.62 mL, 19.99 mmol, 2.00 equiv). Following purification, a slight yellow oil was afforded in 88% yield (1.8116 g, 8.80 mmol).

^{1}H NMR: (500 MHz, $CDCl_3$) δ 7.97 (dd, *J* = 8.4, 1.4 Hz, 2H), 7.69 – 7.60 (m, 1H), 7.51 (t, *J* = 7.8 Hz, 2H), 1.64 (s, 9H).

^{13}C NMR: (126 MHz, $CDCl_3$) δ 186.8, 163.7, 134.6, 132.6, 129.9, 128.8, 84.8, 28.1.

HRMS (ESI) m/z: [M + Na]+ Calcd for C12H14O3Na 229.0835; Found 229.0832.

3-methylpentan-3-yl 2-oxo-2-phenylacetate (4.44e): Prepared with slight modification of

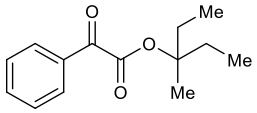

General Procedure 4.C using 2-oxo-2-phenylacetic (2.00 g, 13.32 mmol, 1.00 equiv), oxalyl chloride (1.35 mL, 16.0 mmol, 1.20 equiv), 3-methylpentan-3-ol (1.633 g, 16.00 mmol, 1.20 equiv), and pyridine (1.34 mL, 16.65 mmol, 1.25 equiv). Following purification, a colorless oil was afforded in 54% yield (2.7251 g, 7.18 mmol).

^{1}H NMR: (500 MHz, $CDCl_3$) δ 7.99 (dd, *J* = 8.3, 1.4 Hz, 2H), 7.69 – 7.61 (m, 1H), 7.55 – 7.47 (m, 2H), 2.04 (dq, *J* = 15.0, 7.5 Hz, 2H), 1.91 (dq, *J* = 14.7, 7.5 Hz, 2H), 1.57 (s, 3H), 0.95 (t, *J* = 7.5 Hz, 6H).

^{13}C NMR: (126 MHz, $CDCl_3$) δ 186.8, 163.7, 134.6, 132.6, 129.9, 128.8, 90.4, 30.5, 22.9, 8.0.

HRMS (ASAP) m/z: [M + NH4]+ Calcd for C14H21NO3 252.1594; Found 252.1591.

(1s,3s)-adamantan-1-yl 2-oxo-2-phenylacetate (4.44f): Prepared with slight modification of

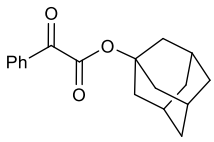

General Procedure 4.C using 2-oxo-2-phenylacetic (2.00 g, 13.32 mmol, 1.00 equiv), oxalyl chloride (1.35 mL, 16.0 mmol, 1.20 equiv), 1-adamantol (2.434

g, 16.00 mmol, 1.20 equiv), and pyridine (1.34 mL, 16.65 mmol, 1.25 equiv). Following purification, a colorless solid was afforded in 72% yield (2.7251 g, 9.58 mmol).

^{1}H NMR: (500 MHz, $CDCl_3$) δ 8.02 – 7.95 (m, 2H), 7.67 – 7.61 (m, 1H), 7.54 – 7.48 (m, 2H), 2.29 (d, *J* = 2.9 Hz, 6H), 2.28 – 2.23 (m, 3H), 1.78 – 1.67 (m, 6H).

^{13}C NMR: (126 MHz, $CDCl_3$) δ 186.7, 163.4, 134.6, 132.6, 129.9, 128.8, 85.0, 41.4, 36.0, 31.1.

HRMS (ESI) m/z: [M + Na]+ Calcd for C18H20O3Na 307.1305; Found 307.1301.

3-ethylpentan-3-yl 2-oxo-2-phenylacetate (4.44g): Prepared with slight modification of

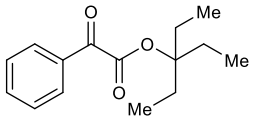

General Procedure 4.C using 2-oxo-2-phenylacetic (1.50 g, 9.99 mmol, 1.00 equiv), oxalyl chloride (1.05 mL, 12.0 mmol, 1.20 equiv), 3-ethylpentan-3-ol (2.10 mL, 15.00 mmol, 1.50 equiv), and pyridine (1.62 mL, 19.99 mmol, 2.00 equiv). Following purification, a colorless oil was afforded in 51% yield (1.2601 g, 5.01 mmol).

^{1}H NMR: (500 MHz, $CDCl_3$) δ 8.02 – 7.97 (m, 2H), 7.66 – 7.61 (m, 1H), 7.54 – 7.48 (m, 2H), 1.99 (q, *J* = 7.5 Hz, 6H), 0.93 (t, *J* = 7.5 Hz, 9H).

^{13}C NMR: (126 MHz, $CDCl_3$) δ 186.8, 163.6, 134.6, 132.6, 129.9, 128.8, 93.3, 27.1, 7.7.

HRMS (ESI) m/z: [M + Na]+ Calcd for C15H20O3Na 271.1305; Found 271.1303.

4.5.3 Photosensitized Cycloadditions

4.5.3.a Reaction Optimization

Table 4.4. Evaluation of Chiral Photocatalyst Structure

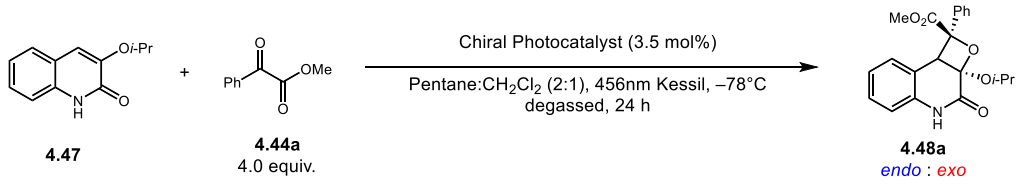

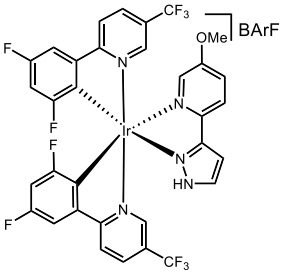	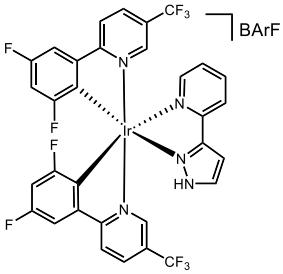	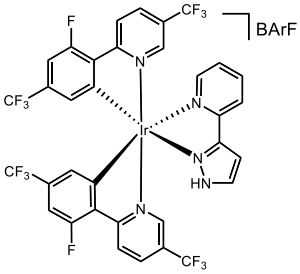	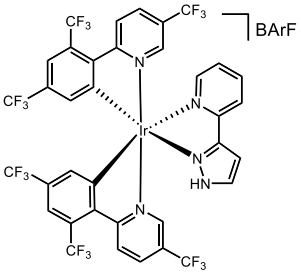
97% yield (2:1 d.r.) 33% ee, 59% ee	>99% yield (2:1 d.r.) 31% ee, 50% ee	74% yield (2:1 d.r.) 43% ee, 71% ee	30% yield (3:1 d.r.) 11% ee,
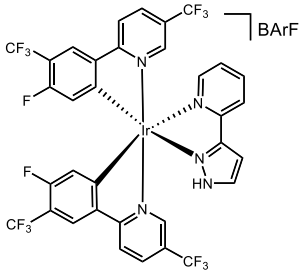	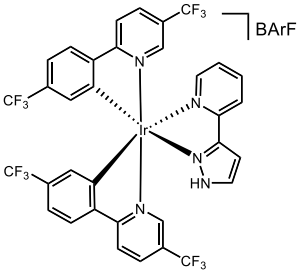	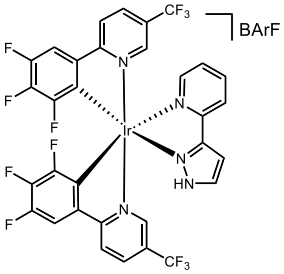	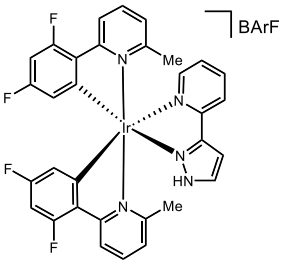
>99% yield (1.5:1 d.r.) 34% *ee*, 63% ee	>99% yield (2:1 d.r.) 30% *ee*, 63% ee	92% yield (2:1 d.r.) 23% *ee*, *64% ee*	80% yield (3:1 d.r.) 22% ee, 8% ee
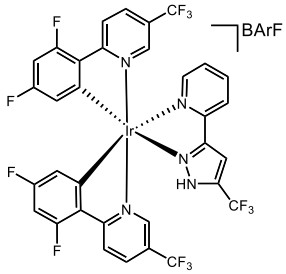	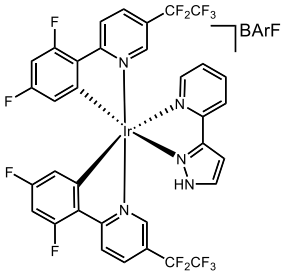	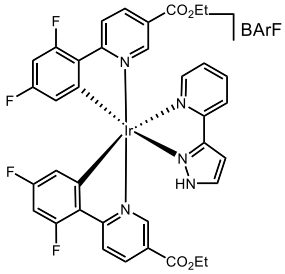	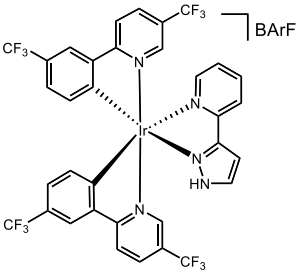
92% yield (2:1 d.r.) 20% *ee*, *33% ee*	74% yield (2:1 d.r.) 61% ee, 72% ee	76% yield (3:1 d.r.) 71% *ee*, 76% ee	>99% yield (2:1 d.r.) 40% ee, 73% ee

Table 4.5. Evaluation of C_2-symmetric Photocatalysts

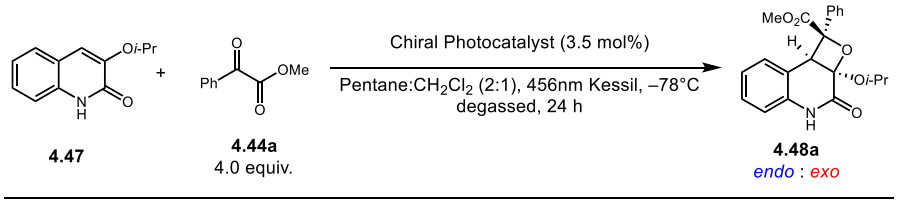

4.47 + **4.44a** 4.0 equiv. → **4.48a** *endo* : *exo*

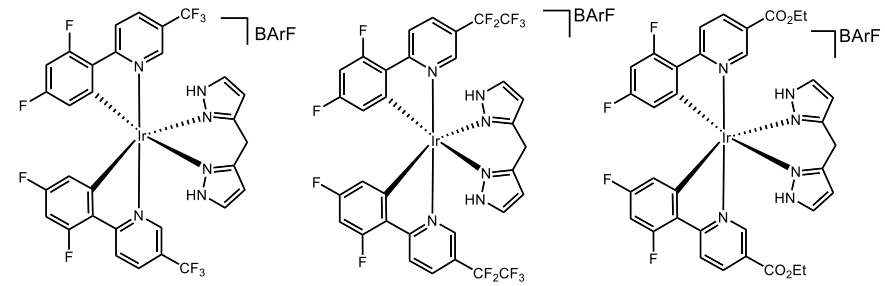

73% yield (2:1 d.r.)
75% *ee*, 89% *ee*

>99% yield (1.5:1 d.r.)
59% *ee*, 72% *ee*

85% yield (1.5:1 d.r.)
74% *ee*, 86% *ee*

Table 4.6. Evaluation of Cyclometalating Ligand on pypz catalyst using **4.44g**

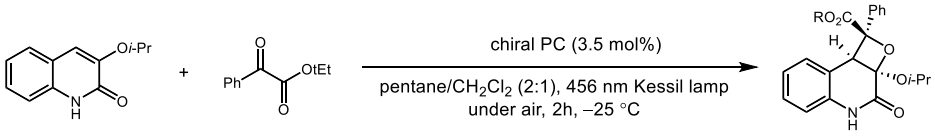

4.47 + **4.44g** 4.0 equiv. → **4.48g** *exo*

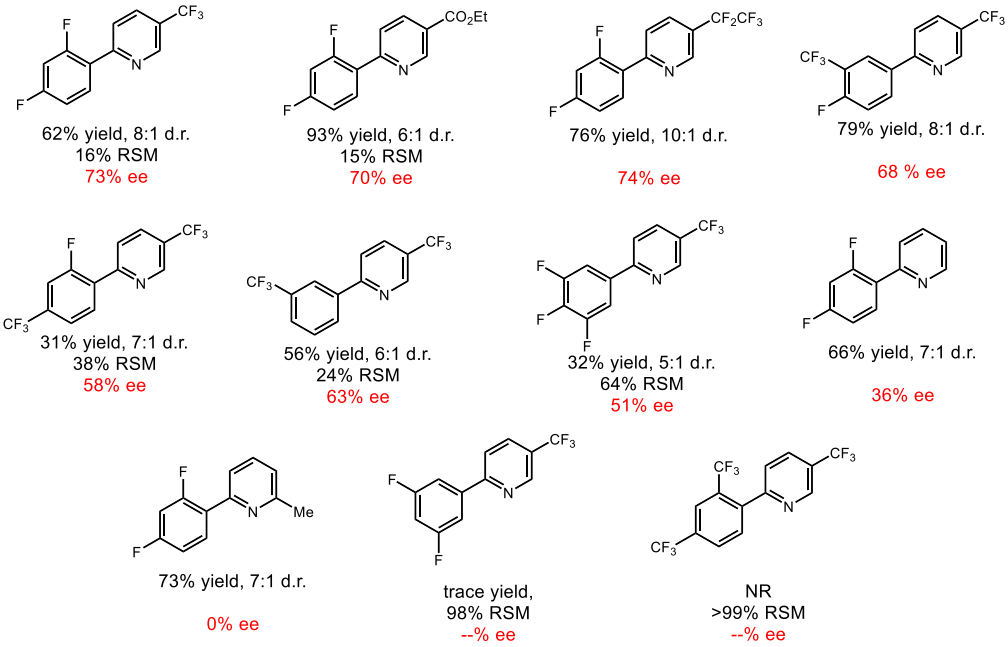

62% yield, 8:1 d.r.
16% RSM
73% ee

93% yield, 6:1 d.r.
15% RSM
70% ee

76% yield, 10:1 d.r.
74% ee

79% yield, 8:1 d.r.
68 % ee

31% yield, 7:1 d.r.
38% RSM
58% ee

56% yield, 6:1 d.r.
24% RSM
63% ee

32% yield, 5:1 d.r.
64% RSM
51% ee

66% yield, 7:1 d.r.
36% ee

73% yield, 7:1 d.r.
0% ee

trace yield,
98% RSM
--% ee

NR
>99% RSM
--% ee

Table 4.7. Solvent Screen using **4.44g** and Λ-**4.49f** at –25 °C. HFX = 1,3-hexafluoroxylene

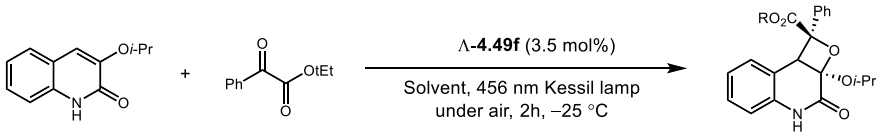

4.47 | **4.44g** 4.0 equiv. | **4.48g** *exo*

Entry	Solvent	Yield	d.r.	ee	RSM
1	Toluene	79%	3:1	60%	16%
2	CH_2Cl_2	72%	2:1	37%	16%
3	Pentane/CH_2Cl_2 (2:1)	74%	2.5:1	60%	21%
4	$PhCF_3$	73%	4:1	48%	
5	HFX/$PhCF_3$ (2:1)	87%	6:1	64%	
6	HFX/$PhCF_3$ (1:1)	39%	4:1	61%	59%
7	HFX	35%	4:1	67%	58%
8	HFX/Toluene (2:1)	31%	4:1	55%	45%
9	HFX/CH_2Cl_2 (2:1)	39%	3:1	52%	49%
10	Toluene/HFX (2:1)	68%	3:1	52%	63%
11	CH_2Cl_2/HFX (2:1)	72%	3:1	45%	33%
12	HFX/$PhCF_3$/Toluene (2:1:1)	38%	4:1	56%	48%
13	HFX/$PhCF_3$/CH_2Cl_2 (2:1:1)	41%	4:1	56%	54%
14	HFX/$PhCF_3$/Pentane (2:1:1)	49%	4:1	55%	42%

Table 4.8. Effect of Solvent and Temperature. HFX = 1,3-hexafluoroxylene

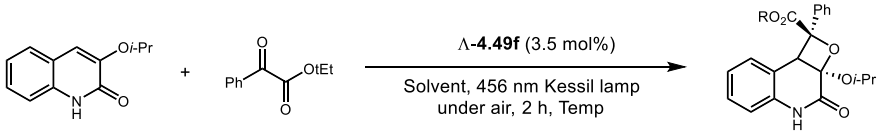

4.47 | **4.44g** 4.0 equiv. | **4.48g** *exo*

Entry	Solvent	Temp	Yield	d.r.	ee	RSM
1*	HFX/$PhCF_3$ (2:1)	–55 °C	76%	10:1	76%	--
2	HFX/$PhCF_3$/CH_2Cl_2 (2:1:1)	–65 °C			85%	
3	HFX/$PhCF_3$/Toluene (2:1:1)	–65 °C	56%	10:1	86%	48%
4*	HFX/$PhCF_3$/Toluene (2:1:1)	–75 °C	82%	14:1	91%	--

* Rxn frozen when stopped

4.5.3.c Racemic [2+2] Photocycloadditions

General Procedure 4.D: A Schlenk tube was charged with quinolone (1.0 equiv.), α-ketoester (5.0 equiv), (±)-[Ir(dF(CF_3)ppy)$_2$(dtbbpy)][PF_6] (0.01 equiv.), and dry CH_2Cl_2 (0.05 M with respect to quinolone). The solution was irradiated by a 456 nm Kessil lamp for 4 hours at –78 °C, then concentrated *in vacuo*. Purification by silica gel chromatography provided racemic product which was used to develop and calibrate chiral HPLC methods. All characterization and spectroscopic data are reported for the enantioenriched species.

4.5.3.d Isolation Scale Enantioselective [2+2] Photocycloadditions

General Procedure 4.E: A Schlenk tube was charged with Λ-**4.49f** (3 mol%) and α-ketoester (5.00 equiv). 100 μL of CH_2Cl_2 was added to solubilize the photocatalyst, followed by dilution with 1.55 mL of toluene. This vessel was capped with a septum and cooled to –78 °C while irradiated with a 456 nm Kessil lamp. In a separate vessel, the quinolone substrate (1.00 equiv) was dissolved in 4.0 mL of toluene. 3.50 mL of this solution was added to the former via syringe (16 gauge needle, glass, gas-tight syringe) at a rate of 0.35 mL/h using a syringe pump. After 16 h, the crude reaction mixture was concentrated *in vacuo*. An internal standard was added for quantitative NMR analysis. The sample was purified by silica gel chromatography (EtOAc/hexanes gradient). *Note: The oxetane products were found to decompose on normal-phase silica gel.* Following this, the product was further purified by reverse-phase column chromatography using a H_2O/MeOH gradient to yield the corresponding oxetane.

methyl (1R,2aR,8bS)-2a-isopropoxy-3-oxo-1-phenyl-2a,3,4,8b-tetrahydro-1H-oxeto[2,3-c]quinoline-1-carboxylate (4.48a): Prepared according to General Procedure 4.E using Λ-**4.49f**

(6.32 mg, 3.68 μmol, 3 mol%), methyl 2-oxo-2-phenylacetate (101 mg, 0.613 mmol, 5.00 equiv) and 3-isopropoxyquinolin-2(1H)-one (25.0 mg. 0.123 mmol, 1.00 equiv.) to afford **4.48a** as a 2:1 mixture of *exo* and *endo* diastereomers (favoring the *exo*) in 87% NMR yield.

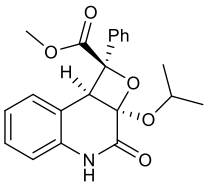

(4.48a *endo*):

^{1}H NMR: (500 MHz, $CDCl_3$) δ 8.16 (d, *J* = 11.4 Hz, 1H), 7.68 – 7.62 (m, 2H), 7.46 (dd, *J* = 8.4, 6.9 Hz, 2H), 7.42 – 7.35 (m, 1H), 7.28 (ddd, *J* = 7.2, 4.2, 2.6 Hz, 2H), 7.10 (td, *J* = 7.5, 1.1 Hz, 1H), 6.84 (d, *J* = 8.2 Hz, 1H), 4.57 (s, 1H), 4.56 (hept, *J* = 6.3 Hz, 1H), 3.34 (s, 3H), 1.26 (d, *J* = 6.1 Hz, 3H), 1.19 (d, *J* = 6.2 Hz, 3H).

^{13}C NMR: (126 MHz, $CDCl_3$) δ 169.7, 164.7, 139.8, 136.2, 129.7, 129.6, 128.4, 128.3, 125.1, 123.6, 116.9, 115.9, 96.1, 83.8, 68.6, 55.2, 52.4, 24.1, 23.8.

HRMS (ESI) m/z: [M – H]– Calcd for C21H20NO5 366.1347; Found 366.1348.

HPLC: Daicel CHIRALCEL® AS-H, 10% EtOH, 90% hexanes, 1 mL/min, 258.1 nm; t_1 = 8.0 min, t_2 = 12.7 min; Area% = 12.84 : 87.16 (74% ee).

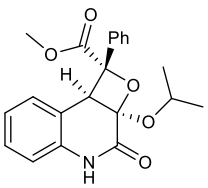

(4.48a *exo*):

^{1}H NMR: (500 MHz, $CDCl_3$) δ 7.87 (s, 1H), 7.29 – 7.23 (m, 2H), 7.23 (dd, *J* = 7.6, 1.4 Hz, 1H), 7.15 – 7.09 (m, 3H), 7.05 (td, *J* = 7.7, 1.5 Hz, 1H), 6.96 (td, *J* = 7.5, 1.2 Hz, 1H), 6.45 (dd, *J* = 8.0, 1.1 Hz, 1H), 4.91 (s, 1H), 4.74 (hept, *J* = 6.2 Hz, 1H), 3.83 (s, 3H), 1.33 (d, *J* = 6.2 Hz, 6H).

^{13}C NMR: (126 MHz, $CDCl_3$) δ 171.9, 164.6, 136.1, 134.5, 129.7, 129.1, 128.2, 127.8, 125.3, 123.4, 117.0, 115.3, 95.5, 82.7, 68.7, 53.0, 52.3, 24.3, 23.8.

HRMS (ESI) m/z: [M – H]– Calcd for C21H20NO5 366.1347; Found 366.1347.

HPLC: Daicel CHIRALCEL® AD–H, 30% *i*-PrOH, 70% hexanes, 1 mL/min, 287.2 nm; t_1 = 8.9 min, t_2 = 10.6 min; Area% = 97.69 : 2.31 (95% ee).

ethyl (1S,2aR,8bS)-2a-isopropoxy-3-oxo-1-phenyl-2a,3,4,8b-tetrahydro-1H-oxeto[2,3-c]quinoline-1-carboxylate (4.48b): Prepared according to General Procedure 4.E using Λ-**4.49f** (6.32 mg, 3.68 μmol, 3 mol%), ethyl 2-oxo-2-phenylacetate (109 mg, 0.613 mmol, 5.00 equiv) and 3-isopropoxyquinolin-2(1H)-one (25.0 mg. 0.123 mmol, 1.00 equiv.) to afford **4.48b** as a 2:1 mixture of *exo* and *endo* diastereomers (favoring the *exo*) in 87% NMR yield.

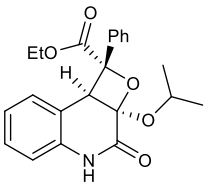

(4.48b *exo*):

^{1}H NMR: (500 MHz, $CDCl_3$) δ 7.44 (s, 1H), 7.30 – 7.24 (m, 2H), 7.23 (d, *J* = 7.5 Hz, 1H), 7.14 – 7.06 (m, 3H), 7.05 (td, *J* = 7.7, 1.5 Hz, 1H), 6.99 – 6.92 (m, 1H), 6.40 (d, *J* = 7.9 Hz, 1H), 4.90 (s, 1H), 4.76 (hept, *J* = 6.2 Hz, 1H), 4.36 (dq, *J* = 10.7, 7.1 Hz, 1H), 4.23 (dq, *J* = 10.8, 7.1 Hz, 1H), 1.35 (dd, *J* = 6.2, 3.8 Hz, 6H), 1.29 (t, *J* = 7.1 Hz, 3H).

^{13}C NMR: (126 MHz, $CDCl_3$) δ 171.5, 164.4, 136.1, 134.5, 129.7, 129.1, 128.1, 127.8, 125.3, 123.4, 117.1, 115.1, 95.5, 82.5, 68.6, 62.1, 52.2, 24.3, 23.8, 14.1.

HRMS (ESI) m/z: [M – H]– Calcd for $C_{22}H_{22}NO_5$ 380.1504; Found 380.1506.

HPLC: Daicel CHIRALCEL® IC, 30% *i*-PrOH, 70% hexanes, 1 mL/min, 250 nm; t_1 = 4.26 min, t_2 = 5.15 min; Area% = 92.39 : 7.61 (85% ee).

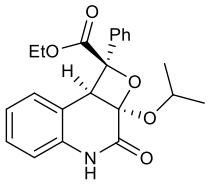

(4.48b *endo*):

^{1}H NMR: (500 MHz, $CDCl_3$) δ 8.16 (s, 1H), 7.71 – 7.60 (m, 2H), 7.49 – 7.41 (m, 2H), 7.41 – 7.34 (m, 1H), 7.32 – 7.27 (m, 2H), 7.09 (td, *J* = 7.5, 1.1 Hz, 1H), 6.83 (dd, *J* = 8.0, 1.1 Hz, 1H), 4.57 (s, 1H), 4.55 (hept, *J* = 6.3 Hz, 1H), 3.81 (qt, *J* = 7.2, 4.3 Hz, 2H), 1.25 (d, *J* = 6.1 Hz, 3H), 1.19 (d, *J* = 6.2 Hz, 3H), 0.89 (t, *J* = 7.1 Hz, 3H).

^{13}C NMR: (126 MHz, $CDCl_3$) δ 169.2, 164.8, 140.1, 136.4, 129.8, 129.6, 128.3, 128.2, 125.1, 123.6, 117.0, 115.9, 96.0, 83.5, 68.5, 61.9, 55.1, 24.1, 23.8, 13.6.

HRMS (ESI) m/z: [M – H]– Calcd for C22H22NO5 380.1504; Found 380.1506.

HPLC: Daicel CHIRALCEL® AS–H, 10% EtOH, 90% hexanes, 1 mL/min, 250 nm; t_1 = 6.4 min, t_2 = 8.5 min; Area% = 80.88 : 19.12 (62% ee).

isopropyl (1R,2aR,8bS)-2a-isopropoxy-3-oxo-1-phenyl-2a,3,4,8b-tetrahydro-1H-oxeto[2,3-c]quinoline-1-carboxylate (4.48c): Prepared according to General Procedure 4.E using Λ-**4.49f** (6.32 mg, 3.68 μmol, 3 mol%), **4.44c** (118 mg, 0.613 mmol, 5.00 equiv) and 3-isopropoxyquinolin-2(1H)-one (25.0 mg. 0.123 mmol, 1.00 equiv.) to afford **4.48c** as a 4:1 mixture of *exo* and *endo* diastereomers (favoring the *exo*) in 92% isolated yield.

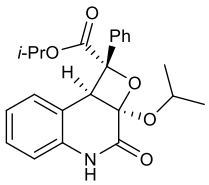

(4.48c *exo*):

^{1}H NMR: (500 MHz, $CDCl_3$) δ 7.30 – 7.22 (m, 1H), 7.21 (dd, *J* = 7.6, 1.4 Hz, 1H), 7.14 – 7.01 (m, 4H), 6.99 – 6.92 (m, 1H), 6.47 (d, *J* = 7.9 Hz, 1H), 5.15 (hept, *J* = 6.3 Hz, 1H), 4.89 (s, 1H), 4.76 (hept, *J* = 6.2 Hz, 1H), 1.36 (d, *J* = 6.0 Hz, 3H), 1.34 (d, *J* = 6.5 Hz, 3H), 1.32 (d, *J* = 6.3 Hz, 3H), 1.20 (d, *J* = 6.2 Hz, 3H).

^{13}C NMR: (126 MHz, $CDCl_3$) δ 171.0, 164.8, 136.1, 134.6, 129.6, 129.1, 128.0, 127.7, 125.3, 123.4, 117.1, 115.5, 95.4, 82.6, 69.9, 68.4, 52.1, 24.3, 23.9, 21.6, 21.5.

HRMS (ESI) m/z: [M – H]– Calcd for C23H24NO5 394.1660; Found 394.1661.

HPLC: Daicel CHIRALCEL® IC, 30% *i*-PrOH, 70% hexanes, 1 mL/min, 250 nm; t_1 = 4.14 min, t_2 = 4.82 min; Area% = 11.15 : 88.85 (78% ee).

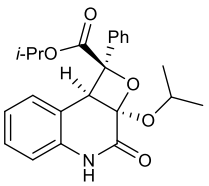

(4.48c *endo*):

^{1}H NMR: (500 MHz, $CDCl_3$) δ 8.41 (s, 1H), 7.67 – 7.63 (m, 2H), 7.48 – 7.41 (m, 2H), 7.41 – 7.34 (m, 1H), 7.33 – 7.24 (m, 2H), 7.09 (td, *J* = 7.5, 1.2 Hz, 1H), 6.85 (d, *J* = 7.9 Hz, 1H), 4.66 (hept, *J* = 6.2 Hz, 1H), 4.56 (s, 1H), 4.54 (hept. *J* = 6.2 Hz,

1H), 1.25 (d, *J* = 6.1 Hz, 3H), 1.18 (d, *J* = 6.2 Hz, 3H), 0.92 (dd, *J* = 6.3, 2.4 Hz, 3H), 0.82 (d, *J* = 6.3 Hz, 3H).

^{13}C NMR: (126 MHz, $CDCl_3$) δ 168.7, 165.0, 140.4, 136.5, 129.8, 129.6, 128.3, 128.1, 125.1, 123.6, 117.1, 116.1, 96.0, 83.2, 70.0, 68.3, 55.0, 24.1, 23.8, 21.1, 21.1, 21.0.

HRMS (ESI) m/z: [M – H]– Calcd for C23H24NO5 394.1660; Found 394.1664.

HPLC: Daicel CHIRALCEL® AS–H, 10% EtOH, 90% hexanes, 1 mL/min, 250 nm; t_1 = 7.0 min, t_2 = 8.54 min; Area% = 58.0 : 42.0 (16% ee).

tert-butyl (1S,2aR,8bS)-2a-isopropoxy-3-oxo-1-phenyl-2a,3,4,8b-tetrahydro-1H-oxeto[2,3-c]quinoline-1-carboxylate (4.48d): Prepared according to General Procedure 4.E using Λ-**4.49f** (6.32 mg, 3.68 μmol, 3 mol%), **4.44d** (126 mg, 0.613 mmol, 5.00 equiv) and 3-isopropoxyquinolin-2(1H)-one (25.0 mg. 0.123 mmol, 1.00 equiv.) to afford **4.48d** in 76% NMR yield (>20:1 d.r.) and 79% isolated yield.

^{1}H NMR: (500 MHz, $CDCl_3$) δ 7.25 (s, 3H), 7.20 (dd, *J* = 7.6, 1.4 Hz, 1H), 7.10 (p, *J* = 3.4, 2.9 Hz, 3H), 7.03 (td, *J* = 7.7, 1.5 Hz, 1H), 6.94 (td, *J* = 7.5, 1.2 Hz, 1H), 6.42 (dd, *J* = 7.9, 1.2 Hz, 1H), 4.90 (s, 1H), 4.76 (hept, *J* = 6.2 Hz, 1H), 1.48 (s, 9H), 1.38 (d, *J* = 6.1 Hz, 3H), 1.35 (d, *J* = 6.2 Hz, 3H).

^{13}C NMR: (126 MHz, $CDCl_3$) δ 170.5, 164.7, 136.1, 135.0, 129.6, 129.0, 127.9, 127.7, 127.7, 125.2, 123.3, 117.3, 115.2, 95.2, 83.0, 82.8, 68.3, 51.8, 27.9, 24.3, 24.0.

HRMS (ESI) m/z: [M – H]– Calcd for C24H26NO5 408.1816; Found 408.1819.

HPLC: Daicel CHIRALCEL® IC, 30% *i*-PrOH, 70% hexanes, 1 mL/min, 250 nm; t_1 = 4.42 min, t_2 = 5.21 min; Area% = 2.23 : 97.77 (96% ee).

3-methylpentan-3-yl (1R,2aR,8bS)-2a-isopropoxy-3-oxo-1-phenyl-2a,3,4,8b-tetrahydro-1H-oxeto[2,3-c]quinoline-1-carboxylate (4.48e): Prepared according to General Procedure 4.E using Λ-**4.49f** (6.32 mg, 3.68 μmol, 3 mol%), **4.44e** (144 mg, 0.613 mmol, 5.00 equiv) and 3-isopropoxyquinolin-2(1H)-one (25.0 mg. 0.123 mmol, 1.00 equiv.) to afford **4.48e** as a white solid (95% isolated yield, 51 mg, >20:1 d.r.).

^{1}H NMR: (500 MHz, $CDCl_3$) δ 7.95 (s, 1H), 7.28 – 7.19 (m, 3H), 7.14 – 7.01 (m, 4H), 6.97 (t, *J* = 7.4 Hz, 1H), 6.46 (d, *J* = 7.8 Hz, 1H), 4.94 (s, 1H), 4.74 (hept, *J* = 6.2 Hz, 1H), 1.89 (dqd, *J* = 14.9, 7.4, 3.1 Hz, 2H), 1.75 (dqd, *J* = 14.8, 7.5, 3.6 Hz, 2H), 1.38 (s, 3H), 1.35 (dd, *J* = 17.4, 6.3 Hz, 6H), 0.78 (t, *J* = 7.5 Hz, 3H), 0.73 (t, *J* = 7.5 Hz, 3H).

^{13}C NMR: (126 MHz, $CDCl_3$) δ 170.3, 165.0, 136.2, 135.1, 129.6, 129.0, 127.8, 127.6, 125.3, 123.3, 117.4, 115.5, 95.2, 88.2, 82.5, 68.1, 51.5, 30.5, 30.4, 24.2, 24.0, 22.6, 7.8, 7.7.

HRMS (ESI) m/z: [M – H]– Calcd for C26H30NO5 436.2130; Found 436.2134.

HPLC: Daicel CHIRALCEL® IC, 20% *i*-PrOH, 80% hexanes, 1 mL/min, 250 nm; t_1 = 4.24 min, t_2 = 4.94 min; Area% = 2.09 : 97.91 (96% ee).

(1s,3R)-adamantan-1-yl (1S,2aR,8bS)-2a-isopropoxy-3-oxo-1-phenyl-2a,3,4,8b-tetrahydro-1H-oxeto[2,3-c]quinoline-1-carboxylate (4.48f): Prepared according to General Procedure 4.E using Λ-**4.49f** (6.32 mg, 3.68 μmol, 3 mol%), **4.44f** (171 mg, 0.613 mmol, 5.00 equiv) and 3-isopropoxyquinolin-2(1H)-one (25.0 mg. 0.123 mmol, 1.00 equiv.) to afford **4.48f** in 84% NMR yield (>20:1 d.r.) and 77% isolated yield.

^{1}H NMR: (500 MHz, $CDCl_3$) δ 8.32 (s, 1H), 7.29 – 7.24 (m, 2H), 7.18 (dd, *J* = 7.6, 1.4 Hz, 1H), 7.13 – 7.07 (m, 3H), 7.03 (td, *J* = 7.7, 1.5 Hz, 1H), 6.94 (td, *J* = 7.5, 1.1 Hz, 1H), 6.50 (dd, *J* =

7.9, 1.1 Hz, 1H), 4.88 (s, 1H), 4.75 (hept, *J* = 6.2 Hz, 1H), 2.21 – 2.16 (m, 3H), 2.15 – 2.11 (m, 6H), 1.67 – 1.62 (m, 6H), 1.39 (d, *J* = 6.1 Hz, 3H), 1.35 (d, *J* = 6.2 Hz, 3H).

^{13}C NMR: (126 MHz, $CDCl_3$) δ 170.2, 165.1, 136.1, 135.0, 129.5, 128.9, 127.9, 127.6, 125.2, 123.3, 117.3, 115.6, 95.2, 83.0, 82.7, 68.2, 51.8, 41.1, 36.0, 30.9, 24.3, 24.0.

HRMS (ESI) m/z: [M – H]– Calcd for C30H32NO5 486.2286; Found 486.2287.

HPLC: Daicel CHIRALCEL® IC, 20% *i*-PrOH, 80% hexanes, 1 mL/min, 250 nm; t_1 = 4.79 min, t_2 = 6.25 min; Area% = 1.56 : 98.44 (97% ee).

3-ethylpentan-3-yl (1R,2aR,8bS)-2a-isopropoxy-3-oxo-1-phenyl-2a,3,4,8b-tetrahydro-1H-oxeto[2,3-c]quinoline-1-carboxylate (4.48g): Prepared according to General Procedure 4.E using Λ-**4.49f** (6.32 mg, 3.68 μmol, 3 mol%), **4.44g** (152 mg, 0.613 mmol, 5.00 equiv) and 3-isopropoxyquinolin-2(1H)-one (25.0 mg. 0.123 mmol, 1.00 equiv.) to afford **4.48g** as a white solid (77% isolated yield, 44 mg, >20:1 d.r.).

^{1}H NMR: (500 MHz, $CDCl_3$) δ 8.29 (s, 1H), 7.29 – 7.20 (m, 3H), 7.14 – 7.02 (m, 4H), 6.98 (td, *J* = 7.5, 1.2 Hz, 1H), 6.50 (dd, *J* = 7.9, 1.1 Hz, 1H), 4.95 (s, 1H), 4.74 (hept, *J* = 6.2 Hz, 1H), 1.82 (q, *J* = 7.5 Hz, 6H), 1.34 (dd, *J* = 16.4, 6.2 Hz, 6H), 0.71 (t, *J* = 7.5 Hz, 9H).

^{13}C NMR: (126 MHz, $CDCl_3$) δ 170.1, 165.3, 136.3, 135.1, 129.5, 129.0, 127.8, 127.5, 125.4, 123.3, 117.3, 115.7, 95.1, 91.0, 82.3, 68.0, 51.4, 26.8, 24.2, 24.0, 7.4.

HRMS (ESI) m/z: [M – H]– Calcd for C27H32NO5 450.2286; Found 450.2291.

HPLC: Daicel CHIRALCEL® IC, 20% *i*-PrOH, 80% hexanes, 1 mL/min, 250 nm; t_1 = 4.28 min, t_2 = 4.75 min; Area% = 2.26 : 97.74 (95% ee).

(1s,3S)-adamantan-1-yl (1R,2aR,8bS)-5-fluoro-2a-isopropoxy-3-oxo-1-phenyl-2a,3,4,8b-tetrahydro-1H-oxeto[2,3-c]quinoline-1-carboxylate (4.48h): Prepared with slight modification of General Procedure 4.E using Λ-**4.49f** (6.32 mg, 3.68 μmol, 3 mol%), **4.44f** (105 mg, 0.369 mmol, 3.00 equiv) and 8-fluoro-3-isopropoxyquinolin-2(1H)-one (27.2 mg. 0.123 mmol, 1.00 equiv.) to afford **4.48h** in 86% NMR yield (12.5:1 d.r.) and 65% isolated yield.

^{1}H NMR: (500 MHz, $CDCl_3$) δ 7.28 – 7.23 (m, 3H), 7.18 (s, 1H), 7.15 – 7.07 (m, 3H), 6.98 (d, *J* = 7.2 Hz, 1H), 6.87 (td, *J* = 8.0, 5.4 Hz, 1H), 6.82 (ddd, *J* = 9.8, 8.2, 1.4 Hz, 1H), 4.90 (s, 1H), 4.79 (hept, *J* = 6.3 Hz, 1H), 2.18 (s, 3H), 2.12 (d, *J* = 3.5 Hz, 5H), 1.66 (t, *J* = 3.1 Hz, 6H), 1.38 (d, *J* = 6.4 Hz, 3H), 1.36 (d, *J* = 6.6 Hz, 3H).

^{13}C NMR: (126 MHz, $CDCl_3$) δ 170.0, 163.6, 148.8 (d, *J* = 242 Hz), 134.8, 128.1, 127.8, 125.1, 124.8, 123.1 (d, *J* = 7.5 Hz), 123.0, 114.9 (d, *J* = 18.0 Hz), 94.8, 83.3, 82.7, 68.7, 52.0, 41.1, 36.0, 30.9, 24.4, 24.0.

^{19}F NMR: (377 MHz, $CDCl_3$) δ -135.3.

HRMS (ESI) m/z: [M + Na]+ Calcd for C30H32FNO5Na 528.2157; Found 528.2154.

HPLC: Daicel CHIRALCEL® IC, 20% *i*-PrOH, 80% hexanes, 1 mL/min, 250 nm; t_1 = 5.4 min, t_2 = 8.0 min; Area% = 77.84 : 22.16 (56% ee).

(1s,3S)-adamantan-1-yl (1R,2aR,8bS)-6-bromo-2a-isopropoxy-3-oxo-1-phenyl-2a,3,4,8b-tetrahydro-1H-oxeto[2,3-c]quinoline-1-carboxylate (4.48i): Prepared with slight modification of General Procedure 4.E using Λ-**4.49f** (6.32 mg, 3.68 μmol, 3 mol%), **4.44f** (105 mg, 0.369 mmol, 3.00 equiv) and 7-bromo-3-isopropoxyquinolin-2(1H)-one (34.7 mg. 0.123 mmol, 1.00 equiv.) to afford **4.48i** in 77% NMR yield (11:1 d.r.) and 71% isolated yield.

^{1}H NMR: (500 MHz, $CDCl_3$) δ 7.25 – 7.21 (m, 3H), 7.18 – 7.10 (m, 3H), 7.10 – 7.03 (m, 2H), 6.56 (d, *J* = 1.6 Hz, 1H), 4.82 (s, 1H), 4.75 (hept, *J* = 6.1 Hz, 1H), 2.18 (s, 3H), 2.11 (d, *J* = 3.0 Hz, 6H), 1.66 (t, *J* = 3.1 Hz, 6H), 1.38 (d, *J* = 6.1 Hz, 3H), 1.35 (d, *J* = 6.2 Hz, 3H).

^{13}C NMR: (126 MHz, $CDCl_3$) δ 170.0, 164.4, 137.3, 134.8, 131.0, 128.2, 127.9, 126.3, 125.2, 122.3, 118.0, 116.5, 94.8, 83.3, 82.4, 68.6, 51.5, 41.1, 36.0, 30.9, 24.3, 24.0.

HRMS (ESI) m/z: [M + Na]+ Calcd for C30H32BrNO5Na 588.1356; Found 588.1354.

HPLC: Daicel CHIRALCEL® IC, 20% *i*-PrOH, 80% hexanes, 1 mL/min, 250 nm; t_1 = 3.99 min, t_2 = 5.67 min; Area% = 92.62 : 7.68 (85% ee).

4.5.4 NMR Binding Experiments

Association constants for the binding of quinolone **4.47** and **4.44f** to the Λ-**4.49f** were determined through NMR titration studies.

Titration Study of (±)-**4.49f with 4.47.** A stock 1.50 mM solution of (±)-**4.49f** was prepared in a toluene-*d*8/CD_2Cl_2 (2:1) cosolvent. 450 µL of this solution was transferred to an NMR tube. Next, a stock solution of 4.47 (3.8 mM) was created by dissolving 5.9 mg in 0.750 mL of the former solution. The NMR titration was conducted by adding increasing amounts of second solution to the first, acquiring ^{1}H NMR spectra between each titration (Figure 4.7). The titration was quantified by monitoring the chemical shift of multiple protons on the catalyst, which varied with increasing [**4.47**]. These data were fit to a 1:2 [Ir]:**4.47** binding model following the method developed by Thordarson.[94] This provided the K_a values shown in Figure 4.7. Similarly, the same NMR titration data was used to construct the Job plot in Figure 4.3B.

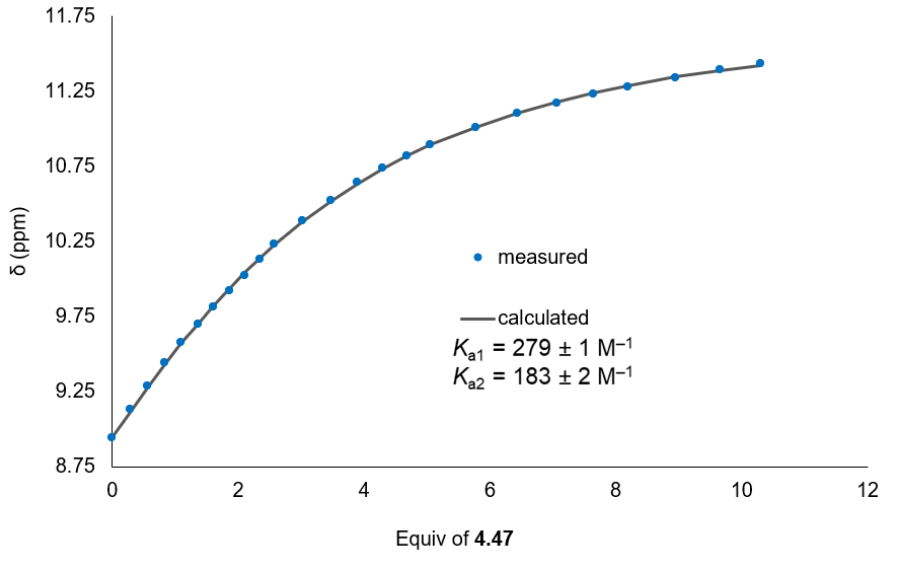

Figure 4.7. Measured and calculated association constants for **4.49f** and **4.47** in toluene-*d*8/CD_2Cl_2 (2:1)

Titration Study of (±)**-4.49f with 4.44f.** An analogous titration was performed to assess the binding of **4.44f** to the photocatalyst, using the same stock solution of **4.49f** and a 1.36 mM stock solution of adamantly α-ketoester. The experiment was repeated with fresh stock solutions to further probe a lower-concentration region. The titration data is shown below in Figure 4.8.

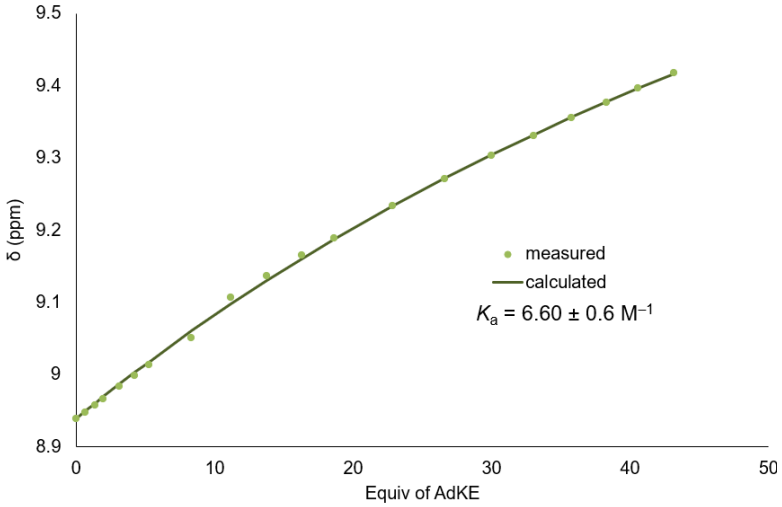

Figure 4.8. Measured and calculated association constants for **4.49f** and **4.44f** in toluene-*d*8/CD_2Cl_2 (2:1)

A control experiment was performed to rule out any ground-state interactions between the quinolone substrate and methyl phenyl glyoxylate. ^{1}H NMR spectra were acquired of solutions containing the same concentration of **4.47** but with increasing equivalents of ester **4.44a**. The stacked spectra demonstrate that the chemical shifts remain unchanged up to an excess of 8 equiv of **4.44a**, Figure 4.9. These results indicate that neither species associate to the other.

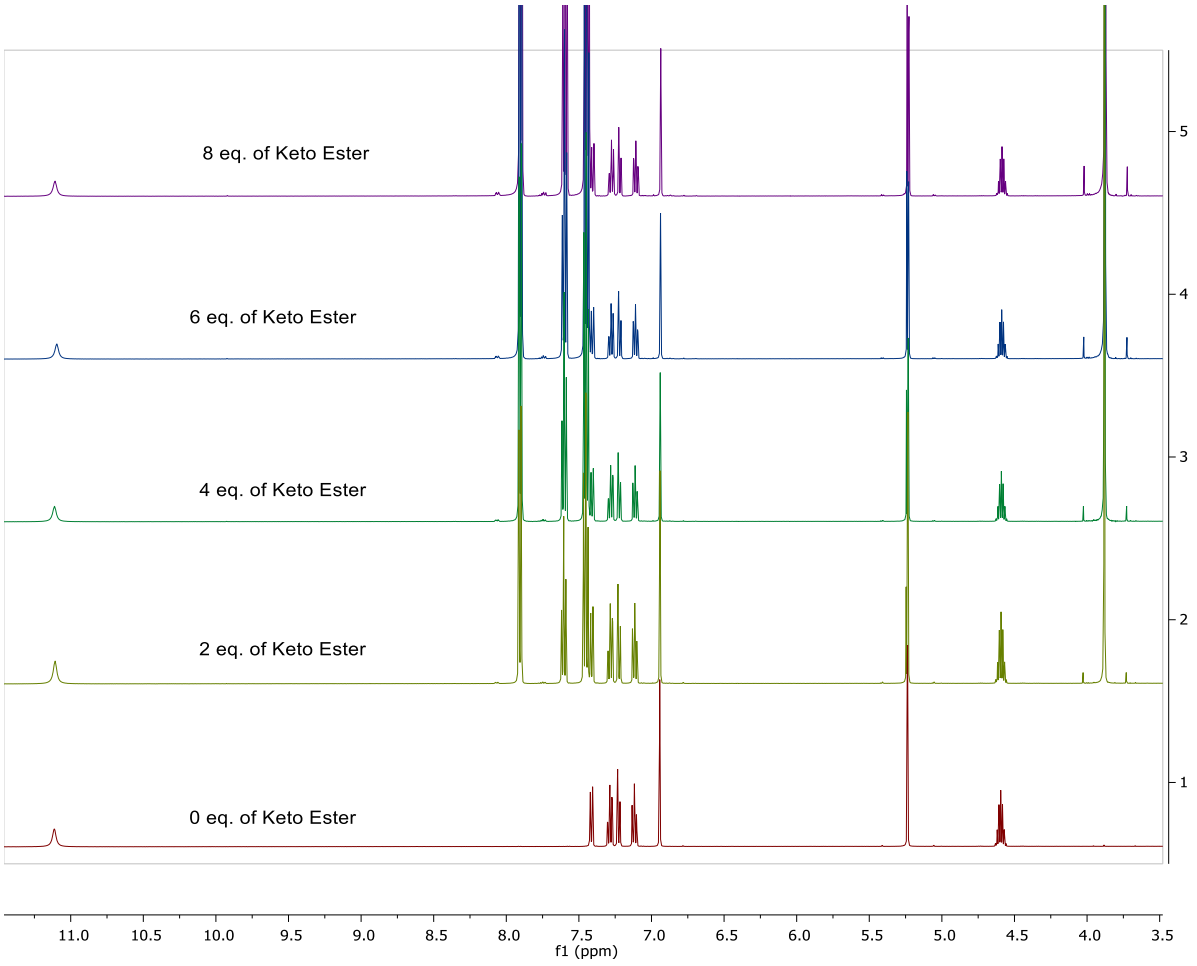

Figure 4.9. NMR titration of **4.47** with **4.44a**, probing for ground-state interactions

4.5.5 Photophysical Measurements

4.5.5.a Absorption and Emission Spectra

The absorbance and emission spectra of photocatalyst **4.49f** was measured in a comixture of toluene/dichloromethane (5:1) at a concentration of 8.0×10^{-5} M, shown in Figure 4.10. The triplet energy of **4.49f** was calculated as the wavelength at which emission is 10% of its maximum (λ_{max}).[95–97] E_T = 63 kcal/mol.

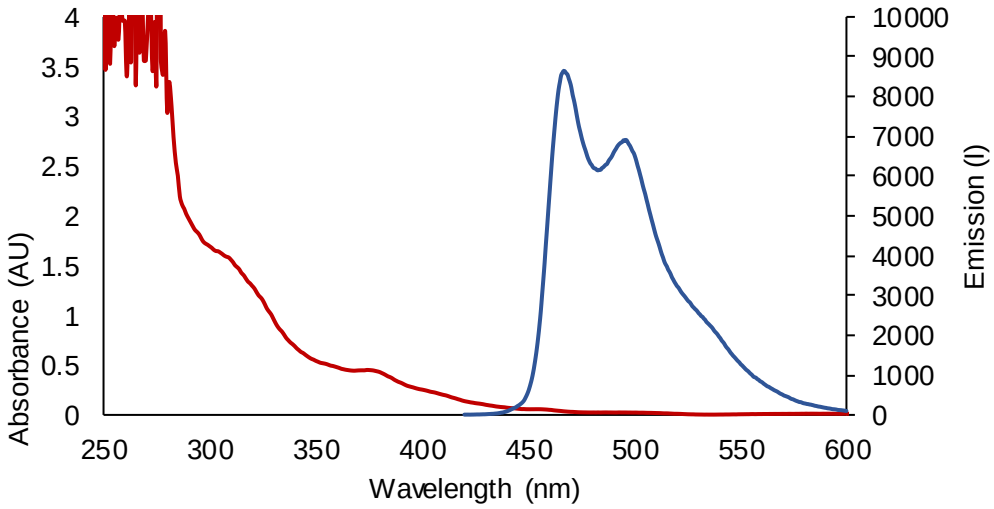

Figure 4.10. The absorbance and emission spectra of photocatalyst **4.49f**.

After sparging with argon gas for 5 minutes, the absorbance and emission spectra of a 10mM solution of **4.44f** in a comixture of toluene/dichloromethane (2:1) was measured at a concentration of 0.010 M, shown in Figure 4.11. The experiment was repeated at the same concentration, however w/o sparging. Note that this sample exhibits much lower photoluminescence intensity in comparison to the previous sample. This result indicates that O_2 quenches **4.44f***, in accord with our mechanistic hypothesis. The E_T of this sample was estimated to be 61 kcal/mol.

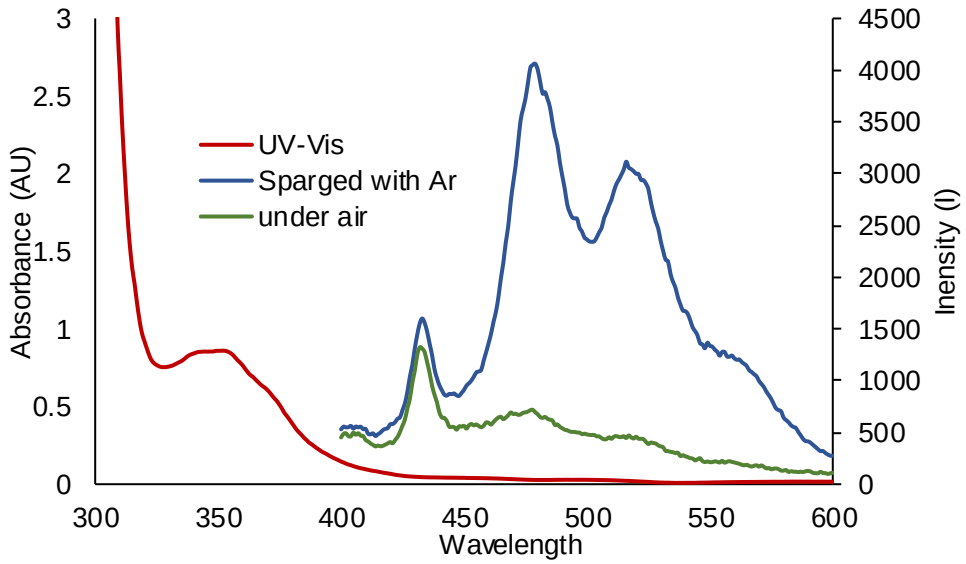

Figure 4.11. Absorbance and emission of **4.44f** sparged and under air.

The absorbance spectra of the title quinolone **4.47** (top) and adamantly ester **4.44f** (middle) were measured at varying concentrations in toluene/dichloromethane (5:1) cosolvent. The results are shown below in Figure 4.12. Note that the absorbance of **4.44f** extends into the visible range, causing background reactions at lower wavelengths. The absorbance of the individual reaction components and their mixtures were measures at relevant concentrations (batch) in a toluene/dichloromethane (5:1) cosolvent mixture, Figure 4.12 (bottom)

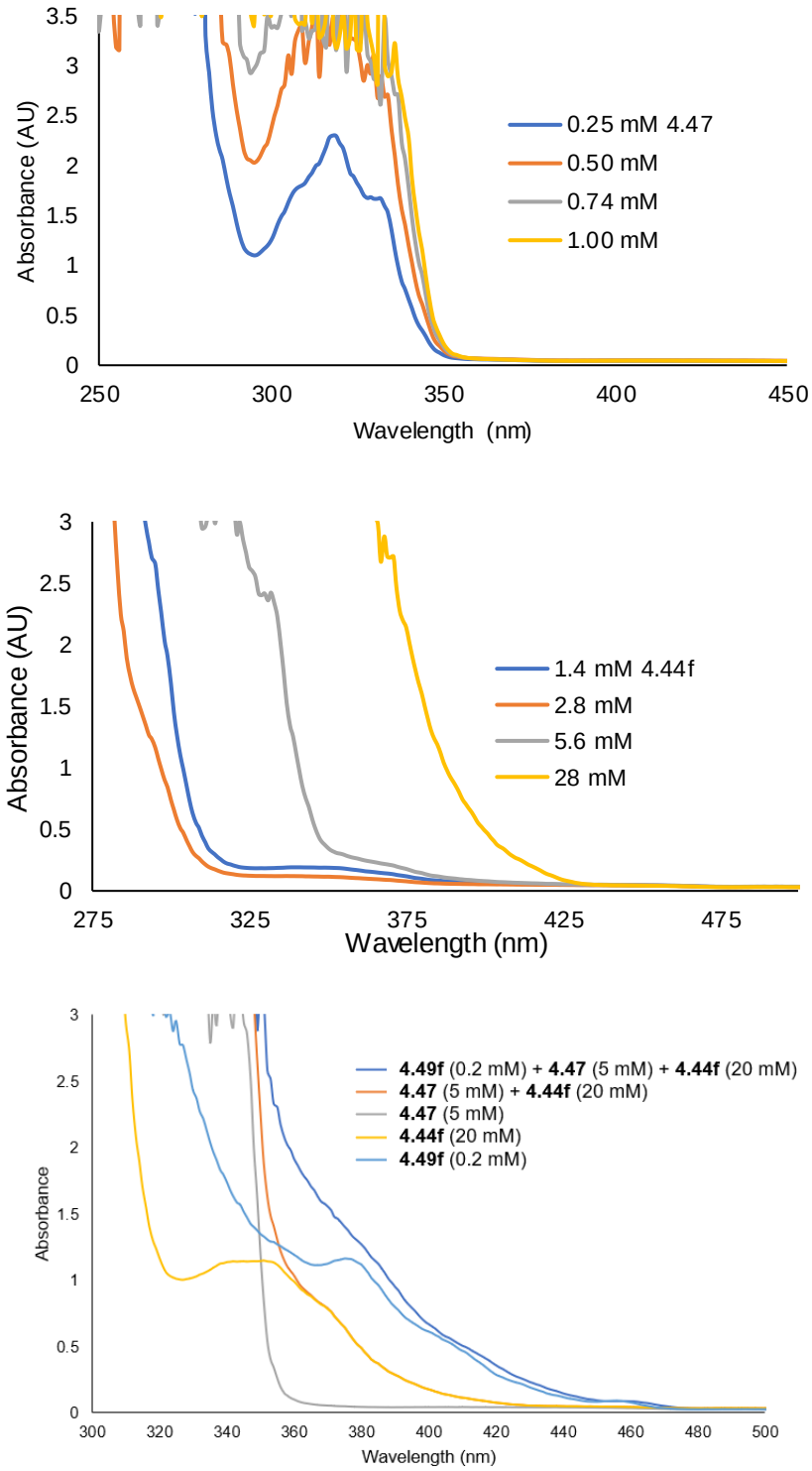

Figure 4.12. Absorbance spectra of **4.47** (top) and **4.44f** (middle) at varying concentrations. Absorbance spectra of the individual and combined reaction components at batch concentrations bottom)

4.5.5.b Steady-State Stern-Volver Quenching Experiments

Stern–Volmer experiments were conducted as previously described.[98] Five separate solutions were prepared containing (±)-**4.49f** (1.3×10^{-4} M) and **4.47** (ranging from 0 to 7.7×10^{-4} M) in toluene/CH_2Cl_2 (2:1), and each was sparged with Argon for 5 min. The solutions were irradiated at 450 nm, and the emission intensity (I) at 480 nm was compared to the initial emission intensity (I_0) at the same wavelength. These data result in a linear Stern–Volmer relationship, shown below (Figure 4.13, left). The same experiment was conducted with substrate 4.44f ranging in concentrations of 0 to 5.0×10^{-4} M). The data for this experiment is shown in Figure 4.13 (right)

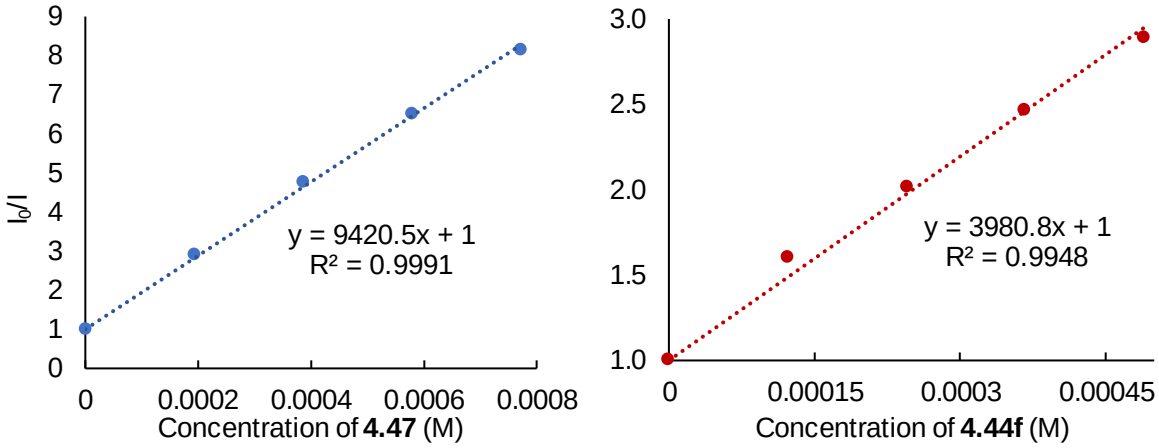

Figure 4.13. Steady-State Stern–Volmer experiment for the quenching of photoexcited catalyst **4.49f** by quinolone **4.47** (left) and **4.44f** (right)

4.5.5.c Time-Resolved Stern-Volmer Quenching Experiments

Time-resolved emission decays were collected on a home-built set-up (Figure 4.14). Visible light excitation was provided by a colinear optical parametric amplifier (OPA, Light Conversion ORPHEUS-HP) optically coupled to a Yb:KGW amplifier (Light Conversion CARBIDE), which emits 0.4 mJ, 250 femtosecond pulses centered at 1025 nm. During data collection the OPA was tuned to 360 nm (ketoester lifetimes) or 450 nm (emission quenching studies). The output laser pulse was 400 femtoseconds, and the native 100 kHz pulse rate was reduced to 1 kHz. This allowed the use of an electronically triggered PC oscilloscope. Under these conditions the power of the laser averaged 0.7 μJ/pulse (360 nm) and 1.1 mJ/pulse (450 nm). From the OPA, the visible laser pulses were directed to the sample with UV-enhanced aluminum mirrors and the laser was *not* refocused onto the sample to reduce localized heating and non-linear effects due to two-photon absorption. At the sample, the unfocused laser had a ~5 mm diameter. The samples were prepared in toluene and enclosed within a 1 cm^2 cuvette. The solutions were sparged with argon for 2–3 minutes before measurement. Emission was collected at 90° to the incident laser pulse. The emission was collimated and refocused onto the photomultiplier tube detector (PMT, RCA 1P28A) with a voltage bias applied (typically 800 mV, Keithley Instruments 244 High Voltage Supply). A longpass filter (Corning 3-71) was placed between the lenses to filter out any scattered excitation beam. The entire wavelength range of emission (~500–800 nm) was collected and provided ample signal. The PMT output was passed through a pre-amplifier (Thorlabs AMP 140) and monitored with a Picoscope 2205A PC oscilloscope (Pico Technology) and provided a 40 ns resolution. The data was digitized using homebuilt LabVIEW code (National Instruments) and analyzed in Origin 2020 (OriginLab).

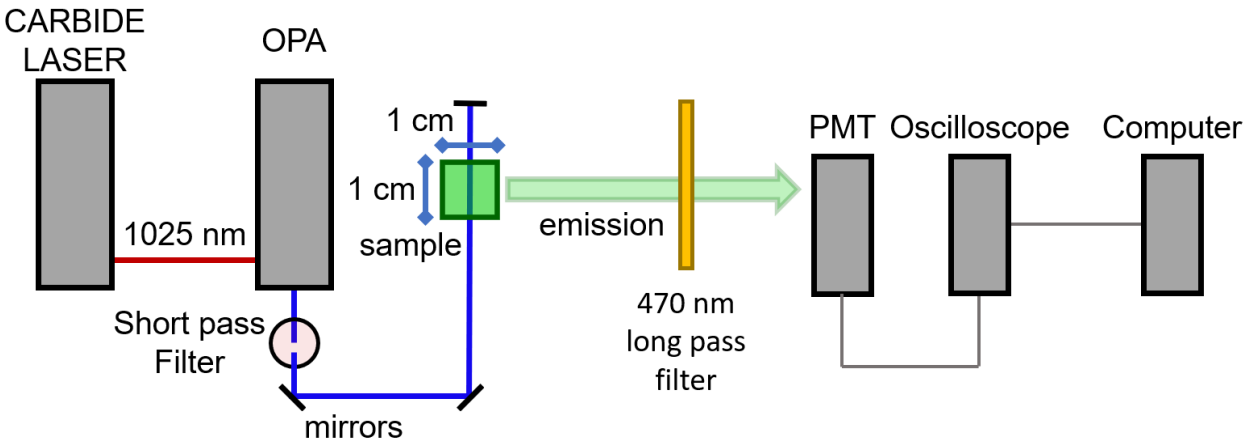

Figure 4.14. Box diagram of the experimental setup for time-resolved emission studies

The time-resolved Stern-Volmer quenching studies were conducted with the same samples used for the steady-state quenching experiments. The resulting data is shown above in Figure 4.5.

The excited state lifetimes of α-ketoesters **4.44a**, **b**, **d**, **e**, and **f** were conducted using 10 mM solutions of each sample in toluene/CH_2Cl_2 (2:1). The samples were sparged with argon for 5 minutes prior to their use. The excited-states were found to undergo first-order decay (Figure 4.15).

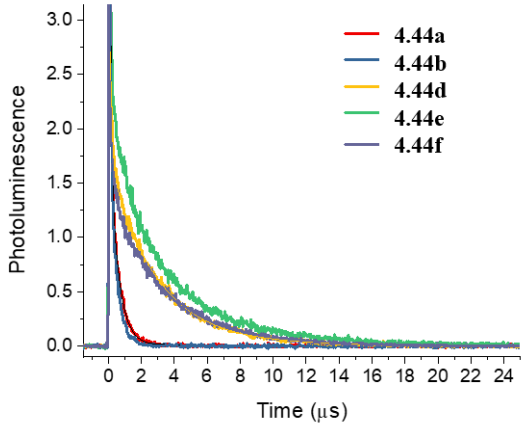

Ketoester	Lifetime (μs)
4.44a	0.51
4.44b	0.38
4.44d	2.86
4.44e	3.78
4.44f	3.20

Figure 4.15. First-order decay of excited state α-ketoester substrates (left) and measured lifetimes (right)

4.5.6 Cyclic Voltammetry Data

Cyclic voltammetry experiments were performed in CH_2Cl_2 with analyte (1 mM) and [(*n*-Bu)$_4$N]$^+$[PF$_6$]$^-$ (100 mM) using a glassy carbon working electrode, platinum wire counter electrode, a Ag/AgNO$_3$ MeCN reference electrode, and a scan rate of 50 mV/s. Ferrocene was added as an internal reference to SCE. When the redox events were irreversible, half-peak potentials were estimated from the voltammograms (Figure 4.16).

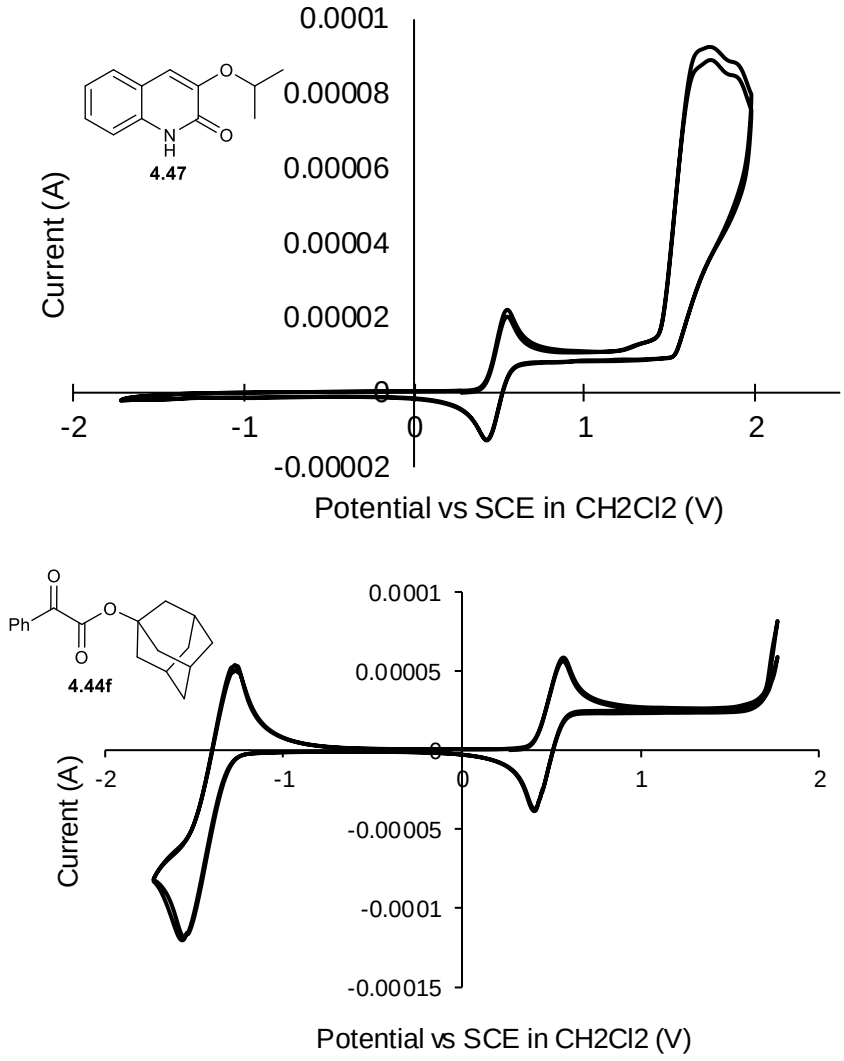

Figure 4.16. Cyclic voltammograms of quinolone substrate **4.47** and α-ketoester **4.44f** with ferrocene added

Quinolone **4.47**: **4.47**/**4.47**$^{\bullet-}$ $E_{p/2} < -1.7$ V vs. SCE in CH_2Cl_2
4.47$^{\bullet+}$/**4.47** $E_{p/2} = +1.74$ V vs. SCE in CH_2Cl_2

α-ketoester **4.44f**: **4.44f**/**4.44f**$^{\bullet-}$ $E_{p/2} = -1.27$ V vs. SCE in CH_2Cl_2
4.44f$^{\bullet+}$/**4.44f** $E_{p/2} > +1.75$ V vs. SCE in CH_2Cl_2

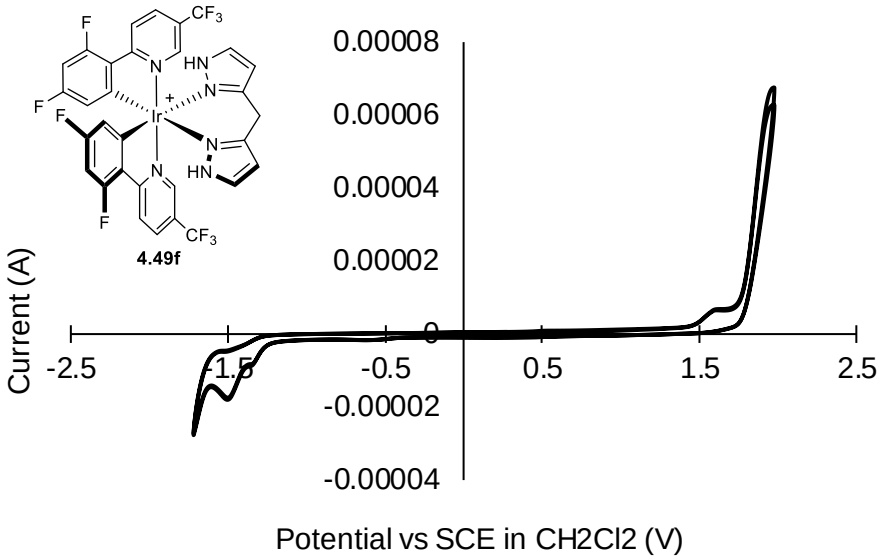

Figure 4.17. Cyclic voltammograms of photocatalyst **4.49f**

Iridium Catalyst **4.49f**: Ir^{III}/Ir^{II} $E_{p/2} = -1.50$ V vs. SCE in CH_2Cl_2
Ir^{IV}/Ir^{III} $E_{p/2} = +1.60$ V vs. SCE in CH_2Cl_2

The excited state redox potentials of iridium catalyst **4.49f** and α-ketoester **4.44f** were computed from the appropriate equations[99,100] using the ground state potentials obtained above and the energy gap between zero vibrational levels of the ground and excited states ($E_{0,0}$). The latter value was approximated as the wavelength at which emission is 10% of its maximum.[95–97] This provides a generous estimate for the excited state redox potentials, demonstrating that photoinduced electron transfer is endergonic even under limiting conditions.

$E(Ir^{III*}/Ir^{II}) = E(Ir^{III}/Ir^{II}) + E_{0,0}$
$= -1.50\ V + 2.73\ V$
$= +1.23\ V$ vs. SCE in CH_2Cl_2

$E(Ir^{IV}/Ir^{III*}) = E(Ir^{IV}/Ir^{III}) - E_{0,0}$
$= 1.60\ V - 2.73\ V$
$= -1.13\ V$ vs. SCE in CH_2Cl_2

$E(\mathbf{4.44f}^*/\mathbf{4.44f}^{\bullet-}) = E(\mathbf{4.44f}/\mathbf{4.44f}^{\bullet-}) + E_{0,0}$
$= -1.27\ V + 2.65\ V$
$= +1.24\ V$ vs. SCE in CH_2Cl_2

4.6 References and Notes

[1] Wuitschik, G.; Carreira, E. M.; Wagner, B.; Fischer, H.; Parilla, I.; Schuler, F.; Roger-Evans, M.; Müller, K. Oxetanes in Drug Discovery: Structural and Synthetic Insights. *J. Med. Chem*. **2010**, *53*, 3327–3246.

[2] Talele, T. T.; Natural-Products-Inspired Use of the *gem*-Dimethyl Group in Medicinal Chemistry. *J. Med. Chem.* **2018**, *61*, 2166–2210.

[3] Burkhard, J. A.; Wuitschik, G.; Rogers-Evans, M.; Möller, K.; Carreira, E. Oxetanes as Versatile Elements in Drug Discovery and Synthesis. *Angew. Chem. Int. Ed*. **2010**, *49*, 9052–9067.

[4] Galanis, A.; Ma, H.; Rajkhowa, T.; Ramachandran, A.; Small, D.; Cortes, J.; Levis, M. Crenolanib is a potent inhibitor of FLT3 with activity against resistance-conferring point mutants. *Biood*. **2014**, *123*, 94–100.

[5] Kung, P. -P.; Bingham, P.; Brooun, A.; Collins, M.; Deng, Y. -L.; Dinh, D.; Fan, C.; Gajiwala, K. S.; Grantner, R.; Gukasyan, H. J.; Hu, W.; Huang, B.; Kania, R.; Kephart, S. E.; Krivacic, C.; Kumpf, R. A.; Khamphavong, P.; Kraus, M.; Liu, W.; Maegley, K. A.; Nguyen, L.; Ren, S. Richter, D.; Rollins, R. A.; Sach, N.; Sharma, S.; Sherrill, J.; Spangler, J.; Stewart, A. E.; Sutton, S.; Uryu, S.; Verhelle, D.; Wang, H.; Wang, S.; Wythes, M.; Xin, S.; Yamazaki, S.; Zhu, H.; Zhu, J, Zehnder, L.; Edwards, M. Optimization of Orally Bioavailable Enhancer of Zeste Homolog 2 (EZH2) Inhibitors Using Ligand and Property-Based Design Strategies: Identification of Development Candidate ®-5,8-Dichloro-7-(methoxy(oxetan-3-yl)methyl)-2-((4-methoxy-6-methyl-2-oxo-1,2-dihydropyridin-3-yl)methyl)-3,4-dihydroisoquinolin-1(2*H*)-one (PF-06821497). *J. Med. Chem.* **2018**, *61*, 650–665.

[6] Crawford, J. J.; Johnson, A. R.; Misner, D. L.; Belmont, L. D.; Castanedo, G.; Choy, R.; Melis, C.; Dong, L.; Eigenbrot, C.; Erickson, R.; Ghilardi, N.; Hau, J.; Katewa, A.; Kohli, P. B.; Lee, W.; Lubach, J. W.; McKenzie, B. S.; Ortwine, D. F.; Schutt, L.; Tay, S.; Wei, B.; Reif, K.; Liu, L.; Wong, H.; Young, W. B. Discovery of GDC-0853: A Potent, Selective, and Noncovalent Bruton's Tyrosine Kinase Inhibitor in Early Clinical Development. *J. Med. Chem.* **2018**, *61*, 2227–2245.

[7] Zheng, X.; Gao, L.; Wang, L.; Liang, C.; Wang, B.; Liu, Y.; Feng, S.; Zhang, B.; Zhou, M.; Yu, X.; Xiang, K.; Chen, L.; Guo, T.; Shen, H. C.; Zou, G.; Wu, J. Z.; Yun, H. Discovery of Ziresovir as a Potent, Selective, and Orally Bioavailable Respiratory Syncytial Virus Fusion Protein Inhibitor. *J. Med. Chem*. **2019**, *62*, 6003–6014.

[8] Yang, H.; Zhao, L.; Zhou, L.; Duan, Y.; Li, G. GDC-0349 inhibits non-small cell lung cancer cell growth. *Cell Death and Disease*. **2020**, *11*, 1–13.

[9] Blomgren, P.; Chandrasekhar, J.; Di Paulo, J. A.; Fung, W.; Geng, G.; Ip, C.; Jones, R.; Kropf, J. E.; Landson, E. B.; Lee, S.; Lo, J. LR.; Mitchell, S. A.; Murray, B.; Pohlmeyer, C.; Schmitt,

A.; Saukawa-Pirrone, K.; Wise, S.; Xiong, J. -M.; Xu, J.; Yu, H.; Zhao, Z.; Currie, K. S. Discovery of Lanraplenib (GS-9876): A Once-Daily Spleen Tyrosine Kinase Inhibitor for Autoimmune Diseases. *ACS Med. Chem. Lett.* **2020**, *11*, 506–513.

[10] Saxena, A. R.; Gorman, D. N.; Esquejo, R. M.; Bergman, A.; Chidsey, K.; Buckeridge C.; Griffith, D. A.; Kim, A. M. Danuglipron (PF-06882961) intype 2 diabetes: a randomized, placebo-controlled, multiple ascending-dose phase trial 1. *Nat. Med.* **2021**, *27*, 1079–1087.

[11] Pell, A. S.; Pilcher, G. Measurements of Heats of Combustion by Flame Calorimetry. Part 3. - Ethylene Oxide, Trimethylene Oxide, Tetrahydrofuran and Tetrahydropy. *Trans. Faraday Soc.* **1965**, *61*, 71 −77.

[12] Eigenmann, H. K.; Golden, D. M.; Benson, S. W. Revised Group Additivity Parameters for the Enthalpies of Formation of Oxygen-Containing Organic Compounds. *J. Phys. Chem.* **1973**, *77*, 1687−1691.

[13] Di Martino, A.; Galli, C.; Gargano, P.; Mandolini, L. Ring-Closure Reactions. Part 23. Kinetics of Formation of Three- to Seven-Membered-Ring N-Tosylazacycloalkanes. The Role of Ring Strain in Small- and Common-Sized-Ring Formation. *J. Chem. Soc., Perkin Trans. 2* **1985**, 1345−1349.

[14] Picard, P.; Leclercq, D.; Bats, J.-P.; Moulines, J. An Efficient One-Pot Synthesis of Oxetanes from 1,3-Diols. *Synthesis* **1981**, 550−551.

[15] Servrin, M.; Krief, A. Regioselective and [C,C] Connective Routes to Oxetane and Tetrahydrofuranes. *Tetrahedron Lett.* **1980**, *21*, 585−586.

[16] Ehlinger, E.; Magnus, P. Silicon in Synthesis. 10. The (Trimethylsilyl)allyl Anion: A β-Acyl Anion Equivalent for the Conversion of Aldehydes and Ketones into γ-Lactones. *J. Am. Chem. Soc.* **1980**, *102*, 5004−5011.

[17] Manabe, S.; Nishino, C. Stereochemistry of cis-Clerodane Diterpenes. *Tetrahedron* **1986**, *42*, 3461−3470.

[18] Jenkinson, S. F.; Fleet, G. W. J. Oxetanes from the Ring Contraction of α-Triflates from γ-Lactones: Oxetane Nucleosides and Oxetane Amino Acids. *Chimia* **2011**, *65*, 71 −75.

[19] Austin, G. N.; Fleet, G. W. J.; Peach, J. M.; Prout, K.; Son, J. C. Chiral Oxetanes from Sugar Lactones: Synthesis of Derivatives of 3,5-Anhydro-1,2-O-Isopropylidine-α-D-Glucuronic Acid and of 3,5-Anhydro-1,2-O-Isopropylidine-β-L-Iduronic Acid. *Tetrahedron Lett.* **1987**, *28*, 4741−4744.

[20] Okuma, K.; Tanaka, Y.; Kaji, S.; Ohta, H. Reaction of Dimethyloxosulfonium Methylide with Epoxides. Preparation of Oxetanes. *J. Org. Chem.* **1983**, *48*, 5133−5134.

[21] Arnold, D. R.; Hinman, R. L.; Glick, A. H. Chemical properties of a carbonyl n,π* state. The photochemical preparation of oxetanes. *Tetrahedron Lett.* **1964**, 1425–1430.

[22] Kumarasamy, E.; Raghunathan, R.; Kandappa, S. K.; Sreenithya, A.; Jockusch, S.; Sunoj, R. B.; Sivaguru, J. Transposed Paternò-Büchi reaction. *J. Am. Chem. Soc*. **2017**, *139*, 655–662.

[23] Paternò, E.; Chieffi, G. Sintesi in chimica organica per mezzo della luce. Nota II. Composti degli idrocarburi non saturi con aldeidi e chetoni. *Gazz. Chim. Ital.* **1909**, *39*, 341–361.

[24] Ciamician, G.; Silber, P. Chemische Lichtwirkungen. *Ber. Dtsch. Chem. Ges.* ***1909***, *42*, 1386–1391.

[25] Büchi, G.; Inman, C. G.; Lipinsky, E. S. Light-catalyzed organic reactions. I. The reaction of carbonyl compounds with 2-methyl-2-butene in the presence of ultraviolet light. *J. Am. Chem. Soc.*, **1954**, *76*, 4327–4331.

[26] Bach, T.; Kather, K. Intramolecular Nucleophilic Substitution at the C-4 Position of Functionalized Oxetanes: A Ring Expansion for the Construction of Various Heterocycles. *J. Org. Chem*. **1996**, *61*, 7642−7643.

[27] Bach, T.; Kather, K.; Kramer, O. Synthesis of Five-, Six-, and Seven-Membered Heterocycles by Intramolecular Ring Opening Reactions of 3-Oxetanol Derivatives. *J. Org. Chem*. **1998**, *63*, 1910−1918.

[28] Boxall, R. J.; Grainger, R. S.; Aricò, C. S.; Ferris, L. Intramolecular Ring-Opening Reactions of 1-(2-Methoxyphenyl)-6-oxabicyclo[3.2.0]heptanes: Spirocyclic Dihydrobenzofurans from Fused Bicyclic Oxetanes. *Synlett* **2008**, *2008*, 25 −28.

[29] Schreiber, S. L.; Satake, K. Application of the furan carbonyl photocycloaddition reaction to the synthesis of the bis(tetrahydrofuran) moiety of asteltoxin. *J. Am. Chem. Soc.* **1983**, *105*, 6723–6724.

[30] Schreiber, S. L.; Satake, K. Studies of the furan-carbonyl photocycloaddition reaction: The determination of the absolute stereostructure of asteltoxin. *Tetrahedron Lett.* **1986**, *27*, 2575–2578.

[31] Bach, T.; Hehn, J. P. Photochemical Reactions as Key Steps in Natural Product Synthesis. *Angew. Chem. Int. Ed*. **2011**, *50*, 1000–1045.

[32] Kong, F. -F.; Zhai, B. -C.; Song, Q. -H. Substituent effects on the regioselectivity of the Paternò–Büchi reaction of 5- or/and 6-methyl substituted uracils with 4,4’-disubstituted benzophenones. *Photochem. Photobiol. Sci.* **2008**, *7*, 1332–1336.

[33] Griesbeck, A. G.; Stadtmüller, S. Electronic Control of Stereoselectivity in Photocycloaddition Reactions. 4. Effects of Methyl Substituents at the Donor Olefin. *J. Am. Chem. Soc.* **1991**, *113*, 6923–6928.

[34] D'Auria, M.; Emmanuele, L.; Racioppi, R. Regio- and stereoselectivity in the Paternò–Büchi reaction on furan derivatives. *J. Photochem. Photobio. A: Chem.* **2004**, *163*, 103–111.
[35] Griesbeck, A. G.; Stadtmüller, S. Photocycloaddition of Benzaldehyde to Cyclic Olefins: Electronic Control of Endo Stereoselectivity. *J. Am. Chem. Soc.* **1990**, *112*, 1281–1283.

[36] Salem, L.; Rowland, C. The Electronic Properties of Diradicals. *Angew. Chem. Int. Ed.* **1972**, *11*, 92–111.

[37] Another comparison of the how the Griesbeck model can explain diastereoselectivity can be found within reference 34. Please see Table 1, entries 1 and 2.

[38] D'Auria, M.; Emanuele. L.; Racioppi, R. Regio- and stereoselectivity in the Paternò–Büchi reaction between 2,3-dihydrofuran and furan with benzaldehyde. *Lett. Org. Chem.* **2006**, *3*, 244–246.

[39] Griesback, A. G.; Mauder, H.; Stadtmüller, S. Intersystem Crossing in Triplet 1,4-Biradicals: Conformational Memory Effects on the Stereoselectivity of Photocycloaddition Reactions. *Acc. Chem. Res.* **1994**, *27*, 70–75.

[40] Bach, T. Stereoselective Intermolecular [2+2]-Photocycloaddition Reactions and Their Application in Synthesis. *Synthesis* **1998**, *5*, 683–703.

[41] D'Auria, M. The Paternò–Büchi Reaction — a Comprehensive Review. *Photochem. Photobiol. Sci.* **2019**, *18*, 2297–2362.

[42] Zagar, C.; Scharf, H. -D. Chiral Induction in Photochemical Reactions, XIII. The Paternò–Büchi Reaction of Achiral and Chiral Acyl Cyanides with Furan. *Chem. Ber.* **1991**, *124*, 967.

[43] Schreiber, S. L. [2+2] Photocycloadditions in the Synthesis of Chiral Molecules. *Science* **1985**, *227*, 857–863.

[44] Jarosz, S.; Zamojski, A. Asymmetric photocycloaddition between furan and optically active ketones. *Tetrahedron* **1982**, *38*, 1453–1456.

[45] Gotthardt, H.; Lenz, W. Unusually High Asymmetric Induction in the Photochemical Formation of Oxetanes. *Angew. Chem. Int. Ed.* **1979**, *18*, 868.

[46] Kock, H.; Scharf, H. -D.; Runsink, J.; Leismann, H. Regio- and Diastereoselektivität bei der Oxetanbildung chiraler Phenylglyoxalate mit elektronenreichen Olefinen. *Chem Ber.* **1985**, *118*, 1485–1503.

[47] Kock, H.; Runsink, J.; Scharf, H. -D. Investigation of chiral induction in photochemical oxetane formation. *Tetrahedron Lett.* **1983**, *24*, 3217–3220.

[48] Buschmann, H.; Scharf, H. -D.; Hoffman, N.; Esser, P. The Isoinversion Principle — a General Model of Chemical Selectivity. *Angew. Chem. Int. Ed. Engl.* **1991**, *30*, 477–515.
[49] Nehrings, A.; Scharf, H. -D.; Runsink, J. Photochemical Synthesis of an L-Erythose Building Block and Its use in the Preparation of Methyl 2,3,*O*-Isopropylidene-β-L-apio-furanoside. *Angew. Chem. Int. Ed.* **4985**, *24*, 877–878.

[50] D'Auria, M. Emanuele, L.; Racioppi, R. On the Paternò–Büchi Reaction of chiral phenylglyoxalate esters with furan derivatives. *Photochem. Photobiol. Sci.* **2003**, *2*, 904–913.

[51] Bach, T.; Jödicke, K.; Kather, K.; Hecht, J. Facial Diastereoselectivity in the Paternò–Büchi Reaction of Chiral Silyl Enol Ethers. *Angew. Chem. Int. Ed. Engl.* **1995**, *34*, 2271–2273.

[52] Bach, T.; Jödicke, K.; Wibbeling, B. Reversal of the Facial Diastereoselectivity in the Paternò–Büchi Reaction of Silyl Enol Ethers Carrying a Chiral Substituent in α-Position. *Tetrahedron* **1996**, *52*, 10861–10878.

[53] Bach, T.; Jödicke, K.; Kather, K.; Fröhlich, R. 1,3-Allylic Strain as a Control Element in the Paternò–Büchi Reaction of Chiral Silyl Enol Ethers: Synthesis of Diastereomerically Pure Oxetanes Containing Four Contiguous Stereogenic Centers. *J. Am. Chem. Soc.* **1997**, *119*, 2437–2445.

[54] Thopate, S. R.; Kulkarni, M. G.; Puranik, V. G. The Paternò–Büchi Reaction of L-Ascorbic Acid. *Angew. Chem. Int. Ed.* **1998**, *37*, 1110–1112.

[55] Ralph, M. Ng, S.; Booker-Milburn, K. I. Short Flow-Photochemistry Enabled Synthesis of the Cytotoxic Lactone (+)-Goniofufurone. *Org. Lett.* **2016**, *18*, 968–971.

[56] D'Auria, M.; Racioppi, R.; Romaniello, G. The Paternò–Büchi Reaction of 2-Furylmethanols. *Eur. J. Org. Chem.* **2000**, 3265–3272.

[57] D'Auria, M.; Emmanuele, L.; Racioppi, R.; Valente, A. Paternò–Büchi reaction between aromatic carbonyl compounds and 1-(3-furyl)alkanols. *Photochem. Photobiol. Sci.* **2008**, *7*, 98–103.

[58] Bach, T.; Schröder, J. The Paternò–Büchi Reaction of α-Alkyl-Substituted Enecarbamates and Benzaldeyhde. *Synthesis* **2001**, *8*, 1117–1124.

[59] Bach, T.; Schröder, J.; Brandl, T.; Hecht, J.; Harms. K. Facial Diastereoselectivity in the Photocycloaddition of Chiral *N*-Acyl Enamines to Benzaldeyhde. *Tetrahedron* **1998**, *54*, 4507–4520.

[60] Kemp, D. S.; Petrakis, K. S. Synthesis and Conformational Analysis of cis,cis-1,3,5-trimethylcyclohexane-1,3,5-tricarboxylic acid. *J. Org. Chem.* **1981**, *46*, 5140–5143.

[61] Bach, T.; Bergmann, H.; Harms, K. High Facial Diastereoselectivity in the Photocycloaddition of a Chiral Aromatic Aldehyde and an Enamide Induced by Intermolecular Hydrogen Bonding. *J. Am. Chem. Soc.* **1999**, *121*, 10650–10651.

[62] Sherbrook, E. M.; Genzink, M. J.; Park, B.; Guzei, I. A.; Baik, M. -H.; Yoon, T. P. Chiral Brønsted acid-controlled intermolecular asymmetric [2+2] photocycloadditions. *Nat. Commun.* **2021**, *12*, 1–7.

[63] Brenninger, C.; Jolliffe, J. D.; Bach, T. Chromophore Activation of α,β-Unsaturated Carbonyl Compounds and Its Application to Enantioselective Photochemical Reactions. *Angew. Chem. Int. Ed.* **2018**, *57*, 14338 – 14349.

[64] Schwinger, D. P.; Bach, T. Chiral 1,3,2-Oxazaborolidine Catalysts for Enantioselective Photochemical Reactions. *Acc. Chem. Res.* **2020**, *53*, 1933−1943.

[65] Brimioulle, R.; Lenhart, D.; Maturi, M. M.; Bach, T. Enantioselective Catalysis of Photochemical Reactions. *Angew. Chem. Int. Ed.* **2015**, *54*, 3872–3890.

[66] Yoon, T. P. Photochemical Stereocontrol Using Tandem Photoredox-Chiral Lewis Acid Catalysis. *Acc. Chem. Res.* **2016**, *49*, 2307–2315.

[67] Turro, N. J. *Modern Molecular Photochemistry;* Benjamin/Cummings: Menlo Park, CA, 1978; pp 432 ff.

[68] Cowan, D. O.; Drisko, R. L. *Elements of Organic Photochemistry*; Plenum Press: New York, 1976; pp181 ff.

[69] Swenton, J. S. Photochemistry of organic compounds. II, Carbonyl compounds. *J. Chem. Educ.* **1969**, *46*, 217–226.

[70] Schuster, D. I.; Lem, G.; Kaprindidis, N. A. New Insights inti an Old Mechanism: [2+2] Photocycloaddition of Enones to Alkenes. *Chem. Rev.* **1993**, *93*, 3–22.

[71] Brimioulle, R.; Bauer, A.; Bach, T. Enantioselective Lewis Acid Catalysis in Intramolecular [2 + 2] Photocycloaddition Reactions: A Mechanistic Comparison between Representative Coumarin and Enone Substrates. *J. Am. Chem. Soc.* **2015**, *137*, 5170–5176.

[72] Stegbauer, S.; Jeremias, N.; Jandl, C.; Bach, T. Reversal of reaction type selectivity by Lewis acid coordination: the *ortho* photocycloaddition of 1- and 2-napthaldehyde. *Chem. Sci.* **2019**, *10*, 8566–8570.

[73] A noteworthy enantioselective variant of this reaction has been reported: Stegbauer, S.; Jandl, C.; Bach, T. Enantioselective Lewis Acid Catalyzed *ortho* Photocycloaddition of Olefins to Phenanthrene-9-carboxaldehydes. *Angew. Chem. Int. Ed.* **2018**, *57*, 14593−14596.

[74] Zheng, J.; Dong, X.; Yoon, T. P. Divergent Photocatalytic Reactions of α-Ketoesters under Triplet Sensitization and Photoredox Conditions. *Org. Lett.* **2020**, *22*, 6520–6525.

[75] Rykaczewski, K. A. Schindler, C. S. Visible-Light-Enabled Paternò–Büchi Reaction via Triplet Energy Transfer for the Synthesis of Oxetanes. *Org. Lett.* **2020**, *22*, 6516–65119.

[76] Chen, L.-A.; Xu, W.; Huang, B.; Ma, J.; Wang, L.; Xi, J.; Harms,K.; Gong, L.; Meggers, E. Asymmetric Catalysis with an Inert Chiral-at-Metal Iridium Complex. *J. Am. Chem. Soc.* **2013**, *135*, 10598−10601.

[77] Huo, H.; Shen, X.; Wang, C.; Zhang, L.; Röse, P.; Chen, L. A.; Harms, K.; Marsch, M.; Hilt, G.; Meggers, E. Asymmetric Photoredox Transition-Metal Catalysis Activated by Visible Light. *Nature* **2014**, *515*, 100–103.

[78] Skubi, K. L.; Kidd, J. B.; Jung, H.; Guzei, I. A.; Baik, M. H.; Yoon, T. P. Enantioselective Excited-State Photoreactions Controlled by a Chiral Hydrogen-Bonding Iridium Sensitizer. *J. Am. Chem. Soc.* **2017**, *139*, 17186–17192.

[79] Zheng, J.; Swords, W. B.; Jung, H.; Skubi, K. L.; Kidd, J. B.; Meyer, G. J.; Baik, M. H.; Yoon, T. P. Enantioselective Intermolecular Excited-State Photoreactions Using a Chiral Ir Triplet Sensitizer: Separating Association from Energy Transfer in Asymmetric Photocatalysis. *J. Am. Chem. Soc.* **2019**, *141*, 13625–13634.

[80] Swords, W. B.; Yoon, T. P. Chiral-at-Ir Photosensitized Asymmetric 6π-Elecrocyclization. *Manuscript in Preparation*.

[81] The 1:1 vs 1:2 fit, and binding constants were evaluated using the online resource developed by Thordarson: http://supramolecular.org/

[82] Thordarson, P. Determining association constants from titration experiments in supramolecular chemistry. *Chem. Soc. Rev.* **2011**, *40*, 1305–1323.

[83] Renny, J. S.; Tomasevich, L. L; Tallmadge E. H.; Collum, D. B. Method of Continuous Variations: Applications of Job Plots to the Study of Molecular Associations in Organometallic Chemistry. *Angew. Chem. Int. Ed.* **2013**, *52*, 11998–12013.

[84] The triplet energies of photocatalyst Λ-**4.49f** and α-ketoester **4.44f** were found using 10% luminescence intensity of the λ_{max}. The triplet energy for quinolone **4.47** was computationally derived in chapter 3.

[85] Lakowicz, J. R. *Principles of Fluorescence Spectroscopy, Third Edition*; Springer: New York, NY, 2006; pp 278 ff.

[86] Fedorov, A. V.; Danilov, E. O.; Rodgers, M. A. J.; Neckers, D. C. Time-Resolved Step-Scan Fourier Transform Infrared Spectroscopy of Alkyl Phenylglyoxylates. *J. Am. Chem. Soc.* **2001**, *123*, 5136–5137.

[87] von Sonntag, J.; Beckert, D.; Knolle, W.; Mehnert, R. Electron Transfer as the Initiation Mechanism of Photocurable Maleimide–Vinyl Ether Based Resins. *Radiat. Phys. Chem.* **1999**, *55*, 609–613.

[88] Turro, N. J.; Ramaurthy, V.; Scaiano, J. C. *Modern Molecular Photochemistry of Organic Molecules;* University Science Books: Sausalito, CA, 2010; pp 1015 ff.

[89] Pangborn, A. B.; Giardello, M. A.; Grubbs, R. H.; Rosen, R. K.; Timmers, F. T. Safe and Convenient Procedure for Solvent Purification. *Organometallics* **1996**, *15*, 1518.

[90] Kravtsov, I. V.; Baranin, S. V.; Belyakov, P. A.; Dorokhov, V. A. Boron-chelate assisted synthesis of di[pyrazol-3(5)-yl]methane and 1,1',2,2'-tetra[pyrazol-3(5)-yl]ethane. *Mend. Commun.* **2009**, *19*, 27–29.

[91] Lowry, M. S.; Goldsmith, J. I.; Slinker, J. D.; Rohl, R.; Pascal, R. A., Jr.; Malliaras, G. G.; Bernhard, S. Single-Layer Electroluminescent Devices and Photoinduced Hydrogen Production from an Ionic Iridium(III) Complex. *Chem. Mater.* **17**, 5712–5719 (2005).

[92] Harris, R. K.; Becker, E. D.; de Menezes, S. M. C.; Goodfellow, R.; Granger, P. NMR Nomenclature. Nuclear Spin Properties and Conventions for Chemical Shifts. *Pure Appl. Chem.* **73**, 1795–1818 (2001).

[93] Harris, R. K.; Becker, E. D.; de Menezes, S. M. C.; Granger, P.; Hoffman, R. E.; Zilm, K. W. Further Conventions for NMR Shielding and Chemical Shifts. *Pure Appl. Chem.* **80**, 59–84 (2008).

[94] Thordarson, P. Determining association constants from titration experiments in supramolecular chemistry. *Chem. Soc. Rev.* **40**, 1305–1323 (2011).

[95] McClure, L. J.; Ford, P. C. Ligand Macrocycle Effects on the Photophysical Properties of Rhodium(III) Complexes. A Detailed Investigation of cis- and trans-Dicyano(l14,8,11-tetraazacyclotetradecane)rhodium(III) and Related Species. *J. Phys. Chem.* **96**, 6640–6650 (1992).

[96] Døssing, A.; Ryu, C. K.; Kudo, S.; Ford, P. C. Competitive Bimolecular Electron- and Energy-Transfer Quenching of the Excited State(s) of the Tetranuclear Copper(I) Cluster $Cu_4I_4py_4$. Evidence for Large Reorganization Energies in an Excited-State Electron Transfer. *J. Am. Chem. Soc.* **115**, 5132–5137 (1993).

[97] Zhu, Q.; Gentry, E. C.; Knowles, R. R. Catalytic Carbocation Generation Enabled by the Mesolytic Cleavage of Alkoxyamine Radical Cations. *Angew. Chem. Int. Ed.* **55**, 9969–9973 (2013).

[98] Cismesia, M. A.; Yoon, T. P. Characterizing chain processes in visible light photoredox catalysis. *Chem. Sci.* **6**, 5426–5434 (2015).

[99] Rehm, D.; Weller, A. Kinetics of Fluorescence Quenching by Electron and H–Atom Transfer. *Isr. J. Chem.* **8**, 259–271 (1970).

[100] Ballardini, R.; Varani, G.; Indelli, M. T.; Scandola, F.; Balzani, V. Free Energy Correlation of Rate Constants for Electron Transfer Quenching of Excited Transition Metal Complexes. *J. Am. Chem. Soc.* **100**, 7219–7223 (1978).

Chapter 5. Construction of Complex Cyclobutane Building Blocks by Photosensitized [2+2] Cycloaddition of Vinyl Boronate Esters

Portions of this work have been published previously:

Scholz, S. O.; Kidd, J. B.; Capaldo, L.; Flikweert, N. E.; Littlefield, R. M.; Yoon, T. P. Construction of Complex Cyclobutane Building Blocks by Photosensitized [2+2] Cycloaddition of Vinyl Boronate Esters. *Org. Lett.* **2021**, *23*, 3496–3501.

A provisional patent containing portions of this work has been filed:

Yoon, T. P.; Scholz, S. O.; Flikweet, N. E.; Littlefield, R. M., Photochemical Methods of Making Cyclobutane Boronates and Related Compounds. U.S. Patent 62,540682, Aug 3, 2017.

5.1 Introduction

Cyclobutane rings feature prominently in thousands of natural products, many of which are known to exhibit interesting biological activity (Figure 5.1).[1,2] The structures of these naturally occurring cyclobutanes can be complex: they are often embedded in polycyclic ring systems and can feature multiple stereogenic centers. In contrast, synthetic pharmaceutical agents rarely contain cyclobutanes; only nine cyclobutane-containing drug molecules have been approved by the FDA, and the structures of the cyclobutane scaffolds are generally simple, non-stereogenic, and minimally substituted.[3] One reason for this disparity is the challenge of synthesizing structurally complex cyclobutane rings, especially in a manner that is highly tolerant of diverse functional groups.[4–10] The development of methods to produce complex cyclobutane building blocks amenable to rapid diversification and elaboration, therefore, is a highly desirable goal that has the potential to spur innovations in medicinal chemistry.

Figure 5.1. Cyclobutane Containing Natural Products and Medicines

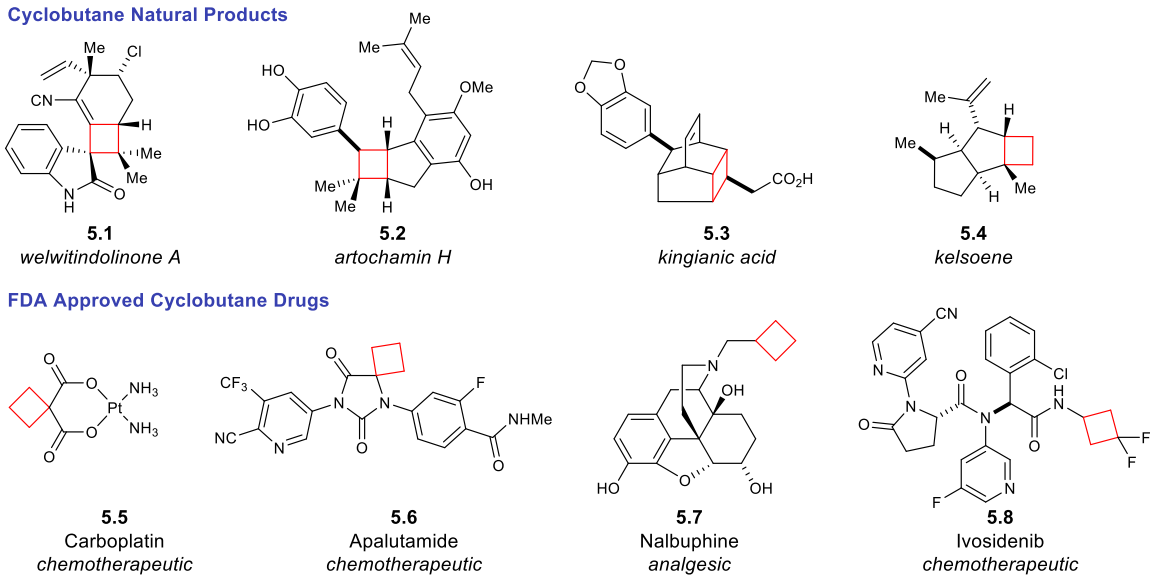

5.1.1 Strategies to Synthesize Cyclobutyl-Boronic Acid Derivatives

Functionalized organoboron reagents are among the most versatile building blocks for medicinal chemistry.[11–14] Boronate esters can be transformed into a variety of different functionalities, often in a stereospecific manner. The ability to prepare structurally complex cyclobutane cores bearing a carbon–boron bond could therefore provide a powerful tool for the discovery of new biologically active compounds with novel ring scaffolds. Relatively few strategies for the preparation of cyclobutyl boronate esters have been reported, however (Scheme 5.1). These have included annulations strategies,[15–19] strain-releasing ring expansion, and ring contraction reactions by 1,2-metalate shift.[20–24] Protocols have also been disclosed that derivatize preformed cyclobutenes,[25–31] functionalized cyclobutanes[32–37] or by C–H activation of cyclobutanes.[38–40] Additionally, these valuable scaffolds can be afforded by thermal cumulene cycloadditions[41,42] and the photoisomerization of 1,2–azaborines.[43] Despite these recent advances, however, many rely upon prefunctionalized starting materials and rarely grant access to complex, polycyclic cyclobutane scaffolds.

Scheme 5.1. Synthesis of Cyclobutyl Boronic Acid Derivatives

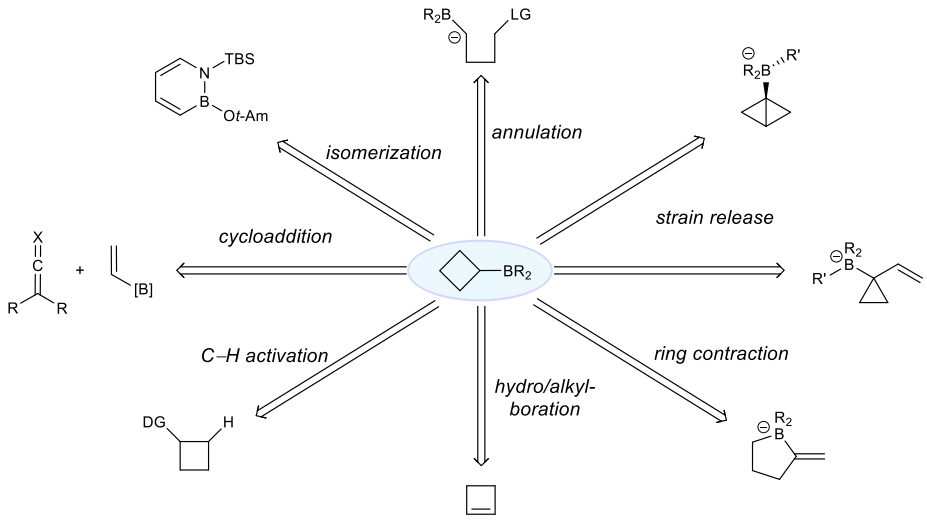

5.1.2 Photocycloadditions of Vinyl Boronate Esters and Prior Work

We wondered whether visible light triplet sensitization might offer a direct, alternative method for the preparation of structurally diverse cyclobutane boronate esters. There are limited examples of direct UV-initiated photocycloadditions involving vinyl boronate esters (Scheme 5.2A),[44,45] including a single example of an enantioselective photocycloaddition reported recently by Bach (Scheme 5.2B).[46,47] More recently, during the course of our investigations, Grygorenko reported a benzophenone-accelerated [2+2] cycloaddition involving vinyl boronic acid derivatives (Scheme 5.2C).[48] This study describes UV-initiated [2+2] photocycloadditions of triplet-state maleimide, which enables access to complex cyclobutane boronate ester building blocks but is limited to the

Scheme 5.2. Photochemical [2+2] Cycloadditions of Vinyl Boronate Ester Derivatives

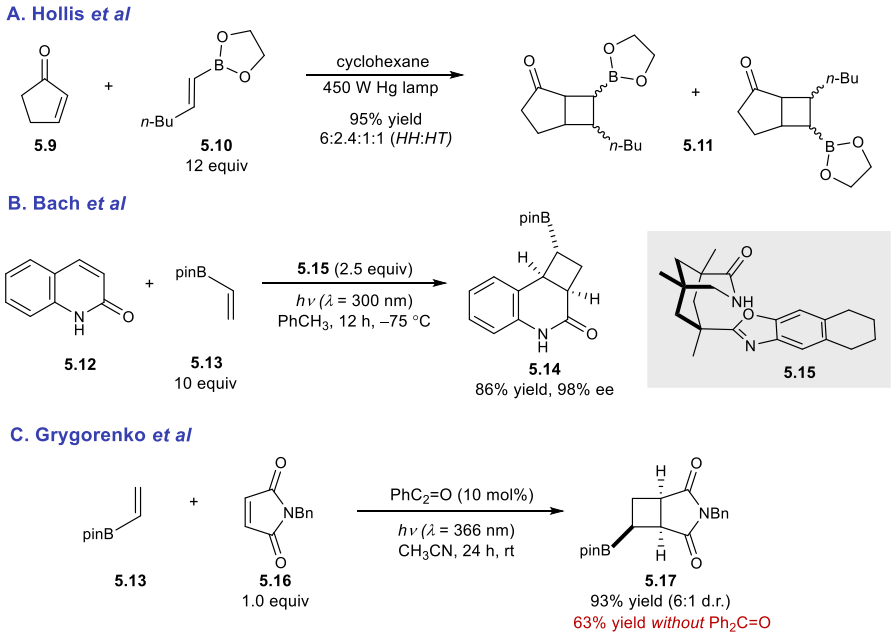

production of the 3-azabicyclo[3.2.0]heptane skeleton. The results also left unanswered the question of whether visible light sensitization might enable [2+2] cycloadditions of structurally

varied electron-rich triplet olefins, which have very different electronic properties and reactivities than electron-deficient triplet maleimide, with vinyl boronate esters.

For the past several years, our laboratory and others have been studying the use of visible-light-activated transition metal photocatalysts in triplet sensitization reactions.[49–51] Several important benefits have motivated the use of these photocatalysts.[52,53] Ru and Ir polypyridyl complexes generally exhibit near-perfect intersystem crossing efficiencies and long excited-state triplet lifetimes. Their structures can be tuned to span a wide range of excited-state triplet energies and redox potentials. Finally, these complexes can be activated using relatively long wavelengths of visible light that are lower in energy and substantially more tolerant of structural complexity than the short-wavelength UV light required for direct photoexcitation of simple organic compounds. We have demonstrated the utility of this strategy for the intramolecular [2+2] cycloaddition of styrene and 1,3-diene substrates and have applied these methods to the synthesis of natural products including cannabiocicyclolic acid and epiraikovenal (Scheme 5.3).[54,55]

Scheme 5.3. Photosensitized [2+2] Cycloadditions of Styrenes and 1,3-Dienes

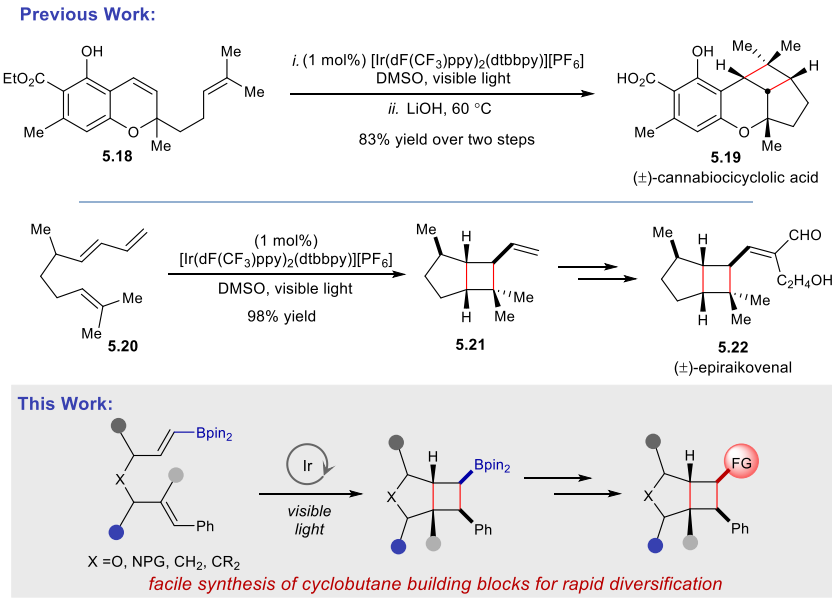

5.2 Results and Discussion

5.2.1 Compatibility of Boron Moieties

At the outset, one initial concern was the stability of carbon–boron bonds under photocatalytic conditions. Organoboron reagents are frequently utilized as radical precursors in a wide range of photochemical transformations,[56,57] including photoredox reactions utilizing the same class of transition metal complexes we found to be optimal for sensitization of styrenes and 1,3-dienes. Thus, it was not obvious at the outset of our investigations that boron-containing functionalities of the products would survive the conditions of photocatalytic triplet sensitization. We therefore began our investigation by testing the compatibility of several common boronic acid derivatives with the conditions previously developed for triplet sensitization and [2+2] cycloaddition of simple unfunctionalized styrenes. Gratifyingly, these vinyl boronates generally reacted smoothly to afford the corresponding boron-substituted cyclobutane products in good yield (Table 5.1) The highest yields were observed using the B(pin) group (**5.25a**), which is advantageous considering the wealth of methods available for direct synthesis and modification of

Table 5.1. Examining Boron Moiety Compatibility for Triplet Sensitization with **5.23**

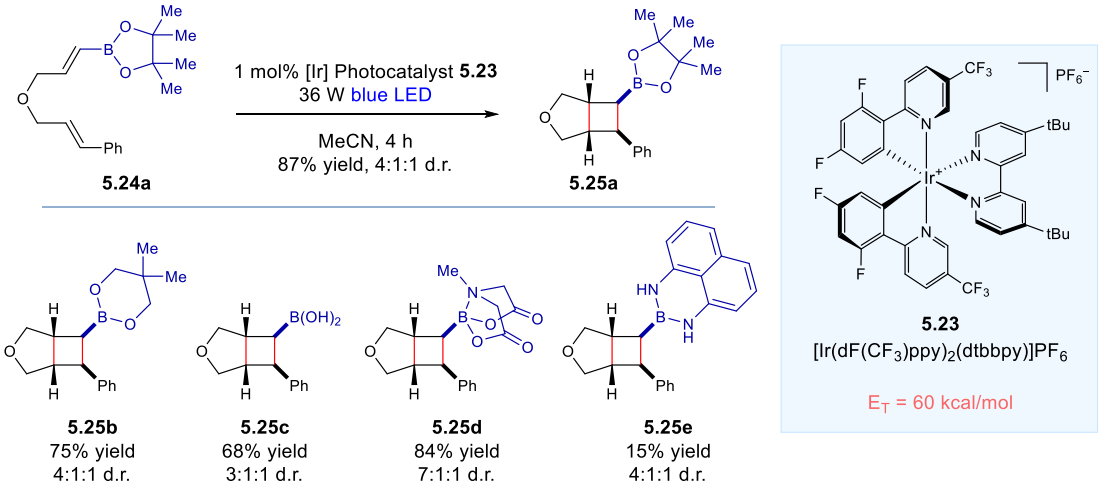

this common boronate ester. The diastereomers of the cycloadduct were also readily separated by chromatography using boric acid doped silica.58 However, an alternate boronate ester **(5.25b)** and the free boronic acid group (**5.25c**) were also well tolerated. Interestingly, a MIDA boronate also underwent [2+2] cycloaddition in good yields (**5.25d**) despite the fact that alkyl boronates are often easily oxidized and can be efficient radical precursors in a range of photoredox methods.[59,60] Of the boronate derivatives screened, only a vinyl B(dan)-containing substrate provided an unsatisfactory yield (**5.25e**). We attribute the slow rate of conversion to competitive quenching of the photocatalyst by the electron-rich naphthalene moiety.

5.2.2 Reaction Scope

Studies probing the scope of this reaction are summarized in Table 5.2. While we were unable to develop effective conditions for high-yielding intermolecular cycloadditions, intramolecular reactions occurred smoothly with a variety of ether, amine, and all-carbon tethers (**5.25a**–**5.25j**). This includes tethers that introduce steric bulk proximal to the reacting vinyl boronate ester and styrene (**5.25k** and **5.25l**), which did not significantly decrease the reactivity of the system. Structurally varied styrene units were tolerated well under the reaction conditions, consistent with the relative insensitivity of styrene triplet energies to perturbation. These include both substitutions on the arene (**5.25m**–**5.25p**) and alkene (**5.25q**) moieties. Similarly, dienes, which possess triplet energies similar to those of styrenes, also react smoothly to provide vinylcyclobutanes in good yields (**5.25r** and **5.25s**). Importantly, this provides access to cyclobutanes featuring two orthogonal synthetic handles amenable to further elaboration. Finally, the relocation of the B(pin) moiety to the bridgehead position did not significant decrease the yield of the reaction (**5.25t**), although the diastereoselectivity was diminished.

Table 5.2. Scope Studies for the Sensitized [2+2] Cycloaddition of Vinyl Boronate Esters

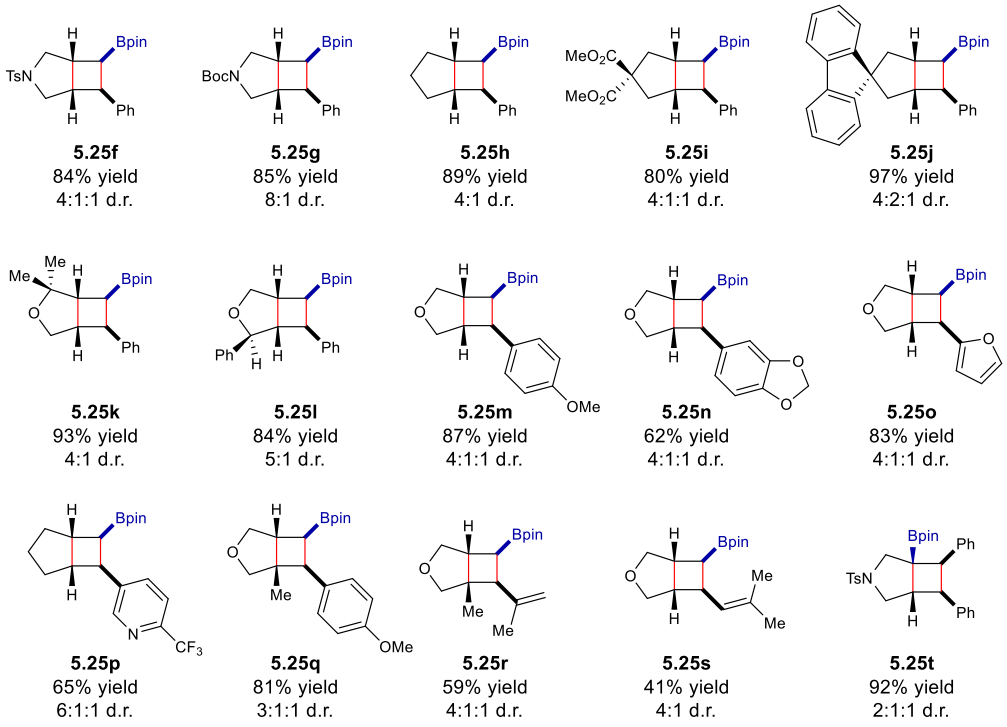

5.2.3 Diversification Reactions

One central motivation for this investigation was the potential utility of cyclobutane boronate esters as rapidly diversifiable building blocks. As a demonstration of the versatility of the boronic ester group in this context, we explored conditions for the further conversion of compound **5.25a** into functionalized derivatives (Scheme 5.4). First, we examined the scalability of this transformation and obtained an excellent yield (94%) of cycloadduct on gram scale using reduced loadings of photocatalyst **5.23**. Protodeboronation61 of **5.25a** yields product **5.26**, which is similar to the fused cyclobutane core of the antipsychotic pharmaceutical candidate belaperidone.[62] Arylation[63] by treatment of the boronate ester with lithiated furan affords **5.27**. Fluorination[64] (**5.28**), oxygenation (**5.29**), and bromination[65] (**5.30**) can be accomplished in good yields using known methods. Similarly, Zweifel olefination[66] (**5.31**) and Matteson homologation[67]

(**5.32**) proceed in good yields and afford products bearing versatile functional group handles that enable further diversification of the cyclobutane scaffold. Likewise, the potassium trifluoroborate salt[68] **5.33** was obtained in good yield and was a suitable reactant for metallophotoredox cross-coupling to afford **5.34** as a single diastereomer.59

Scheme 5.4. C–B Derivatization of **5.25a** into Highly Functionalized Cyclobutane Scaffolds

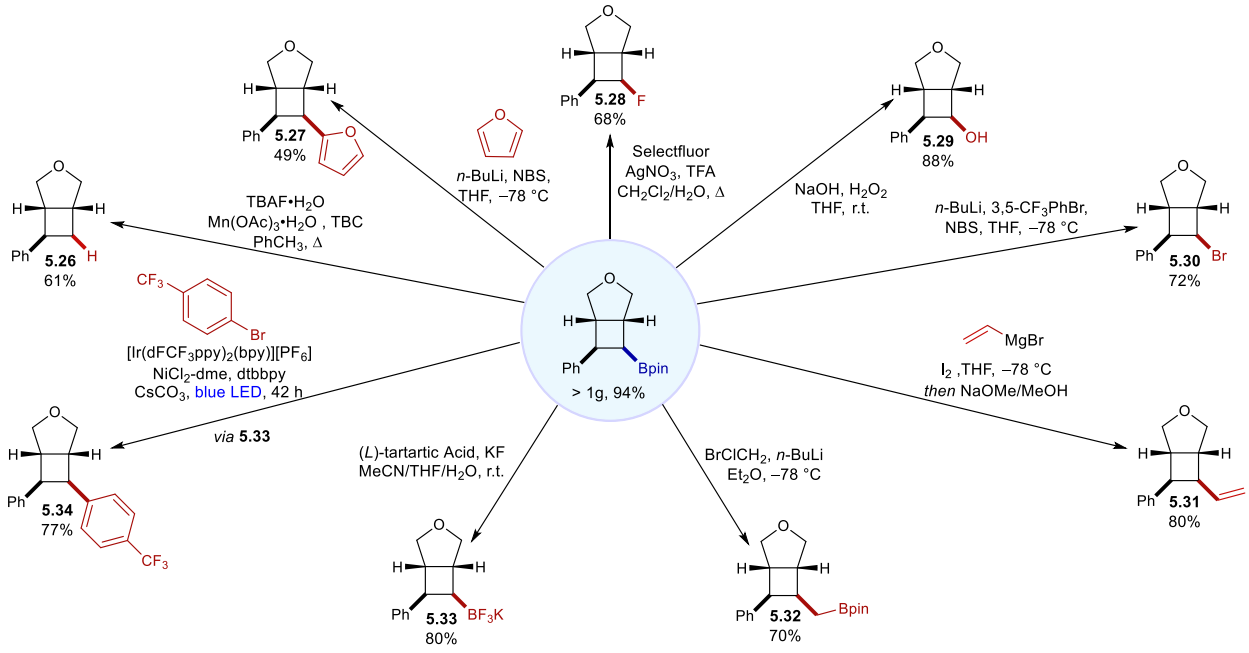

5.2.4 Mechanistic Investigation

Our design plan for this reaction was premised on the assumption that the iridium photocatalyst would sensitize the styrene moiety of the substrate, the excited state of which would initiate a typical stepwise triplet-state [2+2] photocycloaddition reaction. Gilmour and co-workers have recently disclosed the sensitization of vinyl pinacol boronate esters to enable a selective contra-thermodynamic *E*→*Z* isomerization.[69,70] With these findings in mind, we wondered whether competitive sensitization of the vinyl boronate ester might also be responsible for the formation of the observed cycloadduct. To test this possibility, we prepared vinyl boronate **5.35**

lacking a styrene moiety. Irradiation of **5.35** in the presence of photosensitizer **5.23** or thioxanthone (64 kcal/mol)[71] yields no observable change to the starting material (Figure 5.2A). Interestingly, irradiation at 350 nm in the presence of xanthone as a higher-energy triplet sensitizer (74 kcal/mol)71 resulted in geometrical isomerization of the vinyl boronate, indicative of triplet energy transfer, without formation of the [2+2] cycloadduct.

Figure 5.2. Probing the Participation of the Vinyl Boronate Ester Triplet State

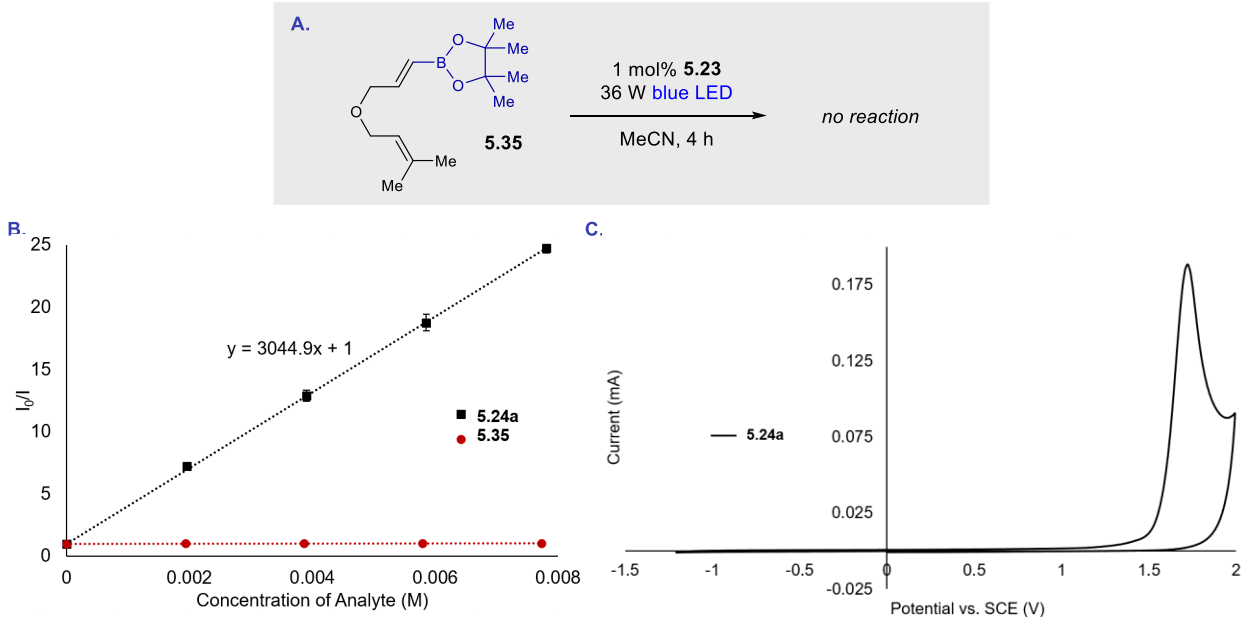

Steady-state Stern–Volmer luminescence quenching experiments show that the emission of photocatalyst **5.23** is not impacted by the addition of vinyl boronate **28** (Figure 5.2B). On the other hand, the phosphorescence of the photocatalyst was quenched by **5.24a** in a concentration-dependent fashion, from which a bimolecular quenching rate constant of k_q = 1.3 x 10^9 M^{-1} s^{-1} could be determined. These studies suggest that the cycloaddition is initiated by sensitization of the styrene moiety and not the vinyl boronate. Moreover, the cyclic voltammogram of **5.24a** features a reduction and oxidation of < –1.2 V vs. SCE and 1.73 vs. SCE, well outside of the range

of photocatalyst **5.23** (–0.89 V vs. SCE and +1.21 V vs. SCE)[72] (Figure 5.2C). Collectively, these data establish that the key photocatalytic step involves energy transfer to the styrenyl alkene and not the vinyl boronate ester.

5.3 Conclusion

In summary, we have developed a highly efficient photosensitized [2+2] cycloaddition of vinyl boronate esters. Despite the variety of photoredox methods that utilize organoboron compounds as radical precursors, we found that simple vinyl boronates readily reacted with excited-state triplet alkenes that are generated by visible light triplet sensitization. The scope of this cycloaddition proved to be broad, easily tolerating the same wide variety of functional groups as other methods for visible light triplet sensitization. More importantly, the ability to access a range of structurally complex cyclobutane boronate esters by photocatalysis coupled with the synthetic versatility of boronate ester chemistry suggests a flexible strategy to prepare novel compounds in an underexplored region of chemical space.

5.4 Contributions

Dr. Spencer O. Scholz performed the optimization of this system. In addition to this, Dr. Luca Capaldo and Rowan M. Littlefield assisted in the scope investigation. Niecia E. Flikweert conducted early studies into the synthetic elaboration of the cyclobutane products. Prof. Tehshik P. Yoon provided expertise, resources, and funding for researchers.

5.5 Experimental Procedures

5.5.1 General Information

5.5.1.a Reagent Preparation

Dichloromethane, tetrahydrofuran, diethyl ether, toluene, and acetonitrile were dried by elution through alumina as described by Grubbs.[73] Where specified, either a 23W CFL or 36W H150 Blue from Kessil Lights was used. Flash chromatography was performed with Sigma Aldrich 60 Å silica gel (230–400 mesh) and thin layer chromatography (TLC) was performed utilizing pre-coated silica gel F_{254} plates from SiliCycle Inc. containing a fluorescent indicator. Plates were visualized using either cerium ammonium molybdate (CAM), $KMnO_4$, or phosphomolybdic acid (PMA) stain. For reactions that require heating an oil bath was used. Reactions that require visible light irradiation used a H150 Blue Kessil lamp as the light source. The emission spectrum is shown below in Figure 5.3. UV irradiation was conducted using a Rayonet RP-200 Photoreactor with 3500 Å bulbs. The photocatalyst $[Ir(dF(CF_3)ppy)_2(dtbbpy)](PF_6)$ utilized in this study was synthesized as previously reported.[74] Boric-acid doped silica was prepared according to Hitosugi *et* al.[75] *N*-Cinnamyl-4-methyl-N-(prop-2-yn-1-yl)benzenesulfonamide,[76] *t*-butyl cinnamyl(prop-2-yn-1-yl)carbamate,[77] dimethyl 2-cinnamyl-2-(prop-2-yn-1-yl)malonate,[78] and *N*-cinnamyl-4-methyl-N-(3-phenylprop-2-yn-1-yl)benzenesulfonamide[79] were prepared as previously reported.

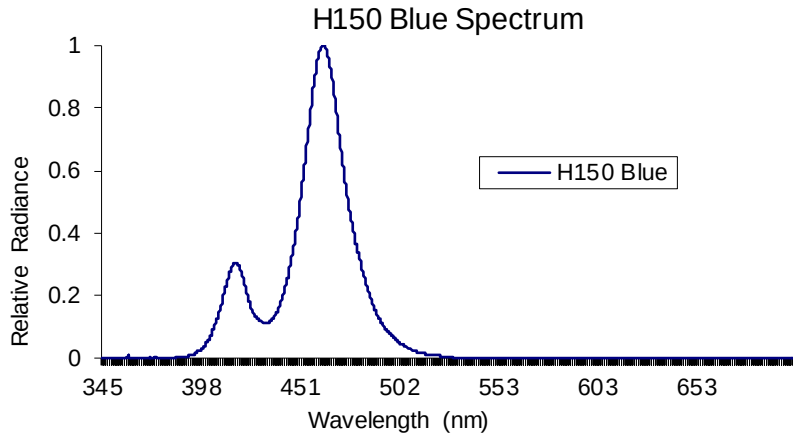

Figure 5.3. The emission spectrum of a H150 Blue Kessil lamp used for visible-light photoreactions.

5.5.1.b Product Characterization

^{1}H, $^{13}C\{^{1}H\}$, and $^{19}F\{^{1}H\}$ NMR spectra were obtained using a Bruker Avance-400, Avance-500, or Avance-600spectrometer with DCH, Prodigy, BBFO+, or TCI-F probes. ^{1}H spectra were internally referenced to tetramethyl silane (0.00 ppm) or the residual protio-solvent peak in acetone-d6 or DMSO-d6. $^{13}C\{^{1}H\}$ spectra were internally referenced to CDCl3 (77.16 ppm) or DMSO-d6(39.52 ppm). $^{19}F\{^{1}H\}$ spectra were absolute referenced to the corresponding ^{1}H spectra using the method described by Harris.[80] Multiplicities are defined using the following abbreviations: s (singlet), d (doublet), t (triplet), q (quartet), p (pentet), sext (sextet), sept (septet), br. (broad), app. (apparent). The spectrometers used for this work are supported by the NSF (CHE-1048642, CHE-0342998, CHE-9208463), NIH (S10 OD012245, S10 RR13866-01), and a generous gift from Paul J. and Margaret M. Bender. Mass spectrometry was performed with a Thermo Q Exactive™ Plus (electrospray ionization or atmospheric solids analysis probe (ASAP-MS)) equipped with an orbitrap detector. This instrumentation is supported by the NIH (1S10

OD020022-1) and the University of Wisconsin. Cyclic voltammograms were acquired using a Pine Research WaveNow potentiostat/galvanostat.

5.5.2 Synthesis of Starting Materials

5.5.2.a Synthesis of alkyne precursors.

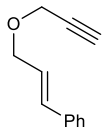

(*E*)-(3-(Prop-2-yn-1-yloxy)prop-1-en-1-yl)benzene (5.36): A 200 mL round bottom flask was charged with cinnamyl alcohol (6.71 g, 50.0 mmol, 1.0 equiv.) and hexanes (40 mL, 1.25 M) before the addition of NaOH (50 wt% in water, 10 equiv.), resulting in a dark orange heterogeneous solution. The suspension was vigorously stirred for an additional 10 min before addition of tetrabutylammonium chloride (0.888 g, 3.00 mmol, 0.06 equiv.) followed by dropwise addition of propargyl bromide (80 wt% in toluene, 57.5 mmol, 1.15 equiv.) After 3 h, the reaction was diluted with 200 mL of water and extracted with hexanes (2 x 100 mL). The combined organic layers were washed with brine, dried over $MgSO_4$ and concentrated *in vacuo*. The resulting oil was purified by vacuum distillation (0.02 Torr, 65–85 °C) to yield a clear oil (6.07 g, 75% yield). Spectral data were in complete accordance with previously reported values.[81]

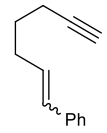

Hept-1-en-6-yn-1-ylbenzene (5.37): A flame dried 100 mL round bottom flask was charged with NaHMDS (1.83 mg, 10.0 mmol, 1.00 equiv.) and THF (30 mL) under N_2. To the stirred suspension at 0 °C was added benzyltriphenylphosphonium chloride (3.88 g, 10.0 mmol, 1.00 equiv.) portionwise. After stirring 1 h at 0 ˚C, 5-hexyn-1-al (961 mg, 10.0 mmol, 1.00 equiv.) as a solution in THF (20 mL). The resulting solution was allowed to warm to room temperature and stirred for 16 h. The reaction was quenched by addition NH_4Cl (sat. aq. solution) and extracted twice with Et_2O. The combined organic layers were washed with brine, dried over $MgSO_4$, and concentrated *in vacuo* to yield the crude product, which was passed through a short silica plug

purified in 99:1 hex/Et_2O to yield 861 mg (51% yield) of the product as a clear oil and inseparable mixture of *trans* and *cis* isomers in a 3:1 ratio that was used without further purification.

9-Cinnamyl-9-(prop-2-yn-1-yl)-9H-fluorene (5.38). In a 250 mL 3-neck round bottom flask 1.5 g of 9-cinnamyl-9H-fluorene (5.0 mmol, 1.0 equiv.) was dissolved in 100 mL of dry THF (0.05 M) under nitrogen atmosphere. The solution was cooled to –78°C and 2.6 mL of n-BuLi (2.5 M in hexanes, 6.4 mmol, 1.2 equiv.) was added slowly to afford a dark red solution. The solution was allowed to warm to room temperature for and stirred for 15 mins. Subsequently, propargyl bromide (80% solution in toluene, 768 µL, 6.9 mmol, 1.3 equiv.) was added dropwise. After 4 h the reaction was quenched with 20 mL of water at 0°C. The reaction was extracted with Et_2O (3 x 50 mL) and the combined organic phases were dried over $MgSO_4$ and concentrated *in vacuo* to yield the product as a colorless oil (1.50 g, 94% yield) that was carried on without further purification.

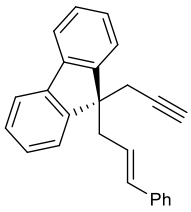

^{1}H NMR (500 MHz, $CDCl_3$) δ 7.72 (dt, *J* = 7.6, 0.9 Hz, 2H), 7.65 – 7.61 (m, 2H), 7.37 (td, *J* = 7.5, 1.2 Hz, 2H), 7.32 (td, *J* = 7.5, 1.3 Hz, 2H), 7.21 (dd, *J* = 8.3, 6.4 Hz, 2H), 7.17 – 7.13 (m, 3H), 6.31 (d, *J* = 15.7 Hz, 1H), 5.89 – 5.77 (m, 1H), 2.98 (dd, *J* = 7.5, 1.4 Hz, 2H), 2.71 (d, *J* = 2.6 Hz, 2H), 2.07 (t, *J* = 2.6 Hz, 1H).

^{13}C NMR (126 MHz, $CDCl_3$) δ 149.0, 140.2, 137.4, 133.2, 128.4, 127.6, 127.1, 127.0, 126.1, 125.5, 123.8, 119.9, 81.4, 70.8, 52.2, 40.7, 28.7.

HRMS (ASAP-orbitrap) m/z: [M + H]+ Calcd for C25H201 321.1638; Found 321.1636.

(*E*)-(3-((2-Methylbut-3-yn-2-yl)oxy)prop-1-en-1-yl)benzene (5.39): A flame-dried 100 mL round bottom flask was charged with NaH (400 mg, 10.0 mmol, 1.2 equiv.) and THF (40 mL, 0.2 M) before adding 2-methyl-3-butyn-2-ol (0.8 mL, 8.3 mmol, 1.0 equiv.) dropwise at 0 °C. After stirring for 30 min at 0 °C, tetrabutylammonium iodide (150 mg,

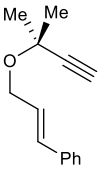

0.332 mmol, 0.04 equiv.) was added followed by dropwise addition of cinnamyl bromide (1.97g, 10.0 mmol, 1.2 equiv.). The solution was allowed to warm to room temperature and stirred for 16 h, before the addition of NH_4Cl (sat. aq. solution). The solution was extracted with EtOAc, dried over $MgSO_4$, and concentrated *in vacuo* to give the crude product, which was further purified by flash column chromatography using a gradient of hexanes to 9:1 hexanes:Et_2O, yielding the product as a clear oil (1.67 g, 100% yield).

^{1}H NMR: (500 MHz, $CDCl_3$) δ 7.38 (d, *J* = 7.3 Hz, 2H), 7.30 (t, *J* = 7.3 Hz, 2H), 7.22 (t, *J* = 7.3 Hz, 1H), 6.62 (dt, *J* = 15.9, 1.6 Hz, 1H), 6.32 (dt, *J* = 15.9, 6.0 Hz, 1H), 4.28 (dd, *J* = 6.0, 1.5 Hz, 2H), 2.46 (s, 1H), 1.53 (s, 6H).

^{13}C NMR: (126 MHz, $CDCl_3$) δ 137.1, 132.0, 128.6, 127.6, 126.8, 126.6, 86.2, 72.3, 70.4, 65.3 29.0.

HRMS (ASAP-orbitrap) m/z: [M + H]+ Calcd for C14H17O 201.1274; Found 201.1273.

(*E*)-(3-(Prop-2-yn-1-yloxy)prop-1-ene-1,3-diyl)dibenzene (5.40): A 25 mL round bottom flask

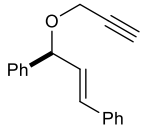

was charged with trans-1,3-diphenyl-2-propene-1-ol (2.10 g, 10.0 mmol, 1.0 equiv.) and CH_2Cl_2 (3 mL, 3.33 M) before the addition of NaOH (50 wt% in water, 10 equiv). The resulting solution was vigorously stirred for 10 min before addition of tetrabutylammonium chloride (0.166 g, 0.600 mmol, 0.06 equiv.) followed by dropwise addition of propargyl bromide (80 wt% in toluene, 1.28 mL, 11.5 mmol, 1.15 equiv.) After vigorously stirring for 16 h, the reaction was diluted with water and extracted with CH_2Cl_2. The combined organic layers were washed with brine, dried over $MgSO_4$ and concentrated *in vacuo*. The resulting oil was purified by flash column chromatography using a gradient elution of 98:2 to 95:5 Hex:Et_2O to yield the product as clear oil (2.24 g, 90% yield).

^{1}H NMR: (500 MHz, $CDCl_3$) δ 7.42–7.35 (m, 6H), 7.31–7.27 (m, 3H), 7.24–7.21 (m, 1H), 6.66 (d, *J* = 15.8 Hz, 1H), 6.29 (dd, *J* = 16.0, 7.3 Hz, 1H), 5.20, (d, *J* = 7.1 Hz, 1H), 4.22 (dd, *J* = 15.8, 2.5 Hz, 1H), 4.15 (dd, *J* = 15.8, 2.5 Hz, 1H), 2.45–2.44 (m, 1H).

^{13}C NMR: (126 MHz, $CDCl_3$) δ 140.2, 136.4, 132.4, 129.2, 128.7, 128.7, 128.0, 127.9, 127.1, 126.7, 81.0, 79.9, 74.5, 55.4.

HRMS (ASAP-orbitrap) m/z: [M + H]+ Calcd for C18H17O 249.1274; Found 249.1272.

(*E*)-1-Methoxy-4-(3-(prop-2-yn-1-yloxy)prop-1-en-1-yl)benzene (5.41): A 10 mL round

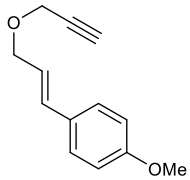

bottom flask was charged with NaH (38 mg, 0.872 mmol. 1.5 equiv.) and THF (1.2 mL) and cooled to 0 °C. A solution of (*E*)-3-(4-methoxyphenyl)prop-2-en-1-ol (0.0955 g, 0.582 mmol, 1.0 equiv.) in THF (1.5 mL) was added dropwise and allowed to stir at 0 °C for 30 min before adding propargyl bromide (80 wt% in toluene, 0.097 mL, 1.5 equiv.). The solution was allowed to warm to room temperature and stirred for 16 h before adding NH_4Cl (sat. aq. solution) and extracting the solution with EtOAc. The organic layer was washed with brine, dried over $MgSO_4$, and concentrated *in vacuo* to give the crude product, which was purified by flash column chromatography using 10:1 hexanes:EtOAc to yield the desired product as a clear oil (96 mg, 81% yield). Spectral data were in complete accordance with previously reported values.[82]

(*E*)-5-(3-(Prop-2-yn-1-yloxy)prop-1-en-1-yl)benzo[*d*][1,3]dioxole (5.42): A 10 mL round

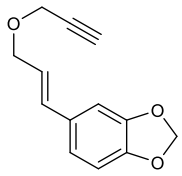

bottom flask was charged with (*E*)-3-(benzo[d][1,3]dioxol-5-yl)prop-2-en-1-ol83 (0.220 g, 1.23 mmol, 1.0 equiv.) and CH_2Cl_2 (0.6 mL, 3.33 M) before the addition of NaOH (50 wt% in water, 10 equiv). The resulting solution was vigorously stirred for 10 min before addition of tetrabutylammonium chloride (0.020 g, 0.0738 mmol, 0.06 equiv.) followed by dropwise addition of propargyl bromide (80 wt% in toluene, 0.158 mL, 1.41

mmol, 1.15 equiv.) After vigorously stirring for 16 h, the reaction was diluted with water and extracted with CH_2Cl_2. The combined organic layers were washed with brine, dried over $MgSO_4$ and concentrated *in vacuo*. The resulting oil was purified by flash column chromatography with 10% EtOAc in hexanes to yield the product as clear oil (0.230 g, 87% yield).

^{1}H NMR: (500 MHz, $CDCl_3$) δ 6.93 (d, *J* = 1.7 Hz, 1H), 6.82 (dd, *J* = 8.0, 1.7 Hz, 1H), 6.75 (d, *J* = 8.0 Hz, 1H), 6.55 (d, *J* = 15.9 Hz, 1H), 6.10 (dt, *J* = 15.8, 6.3 Hz, 1H), 5.95 (s, 2H), 4.21 (dd, *J* = 6.4, 1.4 Hz, 2H), 4.19 (d, *J* = 2.4 Hz, 2H), 2.45 (t, *J* = 2.4 Hz, 1H).

^{13}C NMR: (126 MHz, $CDCl_3$) δ 148.2, 147.6, 133.4, 132.1, 123.3, 121.5, 108.4, 106.0, 101.2, 79.9, 74.6, 70.4, 57.1.

HRMS (ASAP-orbitrap) m/z: [M + H]+ Calcd for C13H13O3 216.0781; Found 216.0782.

(*E*)-2-(3-(Prop-2-yn-1-yloxy)prop-1-en-1-yl)furan (5.43): A 50 mL round bottom was charged

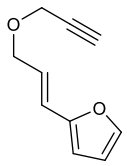

with NaH (277 mg, 6.92 mmol. 1.5 equiv.) and THF (10 mL) and cooled to 0 °C. A solution of (*E*)-3-(furan-2-yl)prop-2-en-1-ol (573 g, 4.62 mmol, 1.0 equiv.) in THF (12 mL) was added dropwise and allowed to stir at 0 °C for 30 min before adding propargyl bromide (80 wt% in toluene, 0.70 mL, 6.92 mmol, 1.5 equiv.). The solution was allowed to warm to room temperature and stirred for 16 h before adding an additional portion of propargyl bromide (80 wt% in toluene, 0.40 mL, 3.95 mmol, 0.85 equiv.) and allowing to stir for 12 h. The reaction was quenched by addition of NH_4Cl (sat. aq. solution) and extracted with EtOAc. The organic layer was washed with brine, dried over $MgSO_4$, and concentrated *in vacuo* to give the crude product, which was purified by flash column chromatography using 10:1 hexanes:EtOAc, to yield the product as a clear oil (575 mg, 77% yield). Spectral data were in complete accordance with previously reported values.[81]

5-(Hept-1-en-6-yn-1-yl)-2-(trifluoromethyl)pyridine (5.44): A flame dried 25 mL round bottom

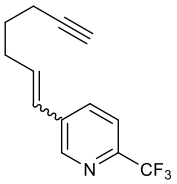

flask was charged with hex-5-yn-1-yltriphenylphosphonium hexafluorophosphate84 (0.732 mg, 1.5 mmol, 1.00 equiv.) and THF (4 mL) under N_2 and cooled to –78 °C before adding a solution of nBuLi (0.732 mL, 2.05 M in hexanes, 1.00 equiv.). The solution was allowed to warm to 0 °C and stirred for 30 min before the addition of 5-formyl-2-(trifluoromethyl)pyridine (0.288 mg, 1.65 mmol, 1.10 equiv.) dropwise as a solution in THF (4 mL). The resulting solution was allowed to warm to room temperature and stirred for 16 h. The reaction was quenched by addition NH_4Cl (sat. aq. solution) and extracted twice with Et_2O. The combined organic layers were washed with brine, dried over $MgSO_4$, and concentrated *in vacuo* to yield the crude product, which was further purified by flash column chromatography in 9:1 hexanes:EtOAc, yielding the product as a clear oil and mixture of *cis* and *trans* isomers (4:1, 270 mg, 75%) that was carried on without further purification.

(*E*)-1-Methoxy-4-(2-methyl-3-(prop-2-yn-1-yloxy)prop-1-en-1-yl)benzene (5.45): A 50 mL

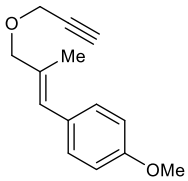

round-bottomed flask was charged with NaH (60% w/w, 127 mg, 3.31 mmol, 1.56 equiv.) and THF (10 mL) and cooled to 0 °C. A solution of (*E*)-3-(4-methoxyphenyl)prop-2-en-1-ol (377 mg, 2.12 mmol, 1 equiv.)) in THF (12 mL) was added dropwise and allowed to stir at 0 °C for 30 min before adding propargyl bromide (80 wt% in toluene, 353 µL, 3.16 mmol, 1.5 equiv.). The solution was allowed to warm to room temperature and stirred for 16 h before adding an additional portion of propargyl bromide (80% solution in toluene, 353 µL, 3.16 mmol, 1.5 equiv.) and stirring for 12 h. The reaction was quenched by addition of NH_4Cl (sat. aq. solution) and extracted with EtOAc. The organic layer was washed with brine, dried over $MgSO_4$, and concentrated *in vacuo* to give the crude product,

which was purified by flash column chromatography using silica gel with 20% EtOAc in hexanes to yield the product (306 mg, 67% yield) as an oil.

^{1}H NMR: (500 MHz, $CDCl_3$) δ 7.24 (d, J = 8.7 Hz, 2H), 6.88 (d, J = 8.7 Hz, 2H), 6.47 (s, 1H), 4.17 (d, J = 2.3 Hz, 2H), 4.11 (d, J = 1.2 Hz, 2H), 3.82 (s, 3H), 2.45 (t, J = 2.4 Hz, 1H), 1.91 (d, J = 1.3 Hz, 3H).

^{13}C NMR: (126 MHz, $CDCl_3$) δ 158.4, 132.7, 130.3, 130.06, 127.9, 113.8, 80.0, 76.4, 74.5, 56.9, 55.4, 15.7.

HRMS (ASAP-orbitrap) m/z: [M + H]+ Calcd for C14H17O2 217.1223; Found 217.1221.

(E)-2,4-dimethyl-5-(prop-2-yn-1-yloxy)penta-1,3-diene (5.46): A 50 mL round-bottomed flask

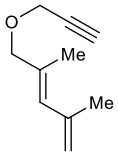

was charged with NaH (60% w/w, 161.0 mg, 6.70 mmol, 1.50 equiv) and THF (10 mL) and cooled to 0 °C. A solution of (*E*)-2,4-dimethylpenta-2,4-dien-1-ol (0.50 g, 4.4 mmol, 1.0 equiv.) in THF (12 mL) was added dropwise and allowed to stir at 0 °C for 30 min before adding propargyl bromide (80 wt% in toluene, 746 μL, 6.92 mmol, 1.5 equiv.). The solution was allowed to warm to room temperature and stir for 16 h, before adding an additional portion of propargyl bromide (80% solution in toluene, 373 μL, 3.2 mmol, 0.75 equiv.) and stirring for 12 h. The reaction was quenched by addition of NH_4Cl (sat. aq. solution) and extracted with EtOAc. The organic layer was washed with brine, dried over $MgSO_4$, and concentrated *in vacuo* to give the crude product, which was purified by flash column chromatography using silica gel with 10% EtOAc in hexanes to yield the product (383 mg, 58% yield) as a slightly yellow oil.

^{1}H NMR: (500 MHz, $CDCl_3$) δ 6.01 – 5.82 (m, 1H), 5.01 (t, *J* = 1.8 Hz, 1H), 4.93 – 4.80 (m, 1H), 4.13 (d, *J* = 2.3 Hz, 2H), 3.99 (d, *J* = 1.1 Hz, 2H), 2.43 (t, *J* = 2.4 Hz, 1H), 1.87 (s, 3H), 1.84 (d, *J* = 1.3 Hz, 3H).

^{13}C NMR: (126 MHz, $CDCl_3$) δ 149.3, 141.4, 133.7, 128.8, 115.2, 83.2, 71.3, 24.8, 23.5, 15.5.

HRMS (ASAP-orbitrap) m/z: [M + H]+ Calcd for C10H15O 151.1117; Found 151.1117.

(*E)*-5-Methyl-1-(prop-2-yn-1-yl)oxy)hexa-2,4-diene (5.47): A 25 mL round bottom flask was

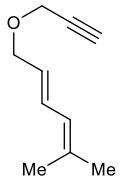

charged with (*E*)-5-methylhexa-2,4-diene-1-ol85 (1.72 g, 15.3 mmol, 1.0 equiv.) and CH_2Cl_2 (5 mL, 3.33 M) before the addition of NaOH (50 wt% in water, 10 equiv). The resulting solution was vigorously stirred for 10 min before addition of tetrabutylammonium chloride (0.256 g, 0.92 mmol, 0.06 equiv.) followed by dropwise addition of propargyl bromide (80 wt% in toluene, 1.96 mL, 17.6 mmol, 1.15 equiv.) After vigorously stirring for 16 h, the reaction was diluted with water and extracted with CH_2Cl_2. The combined organic layers were washed with brine, dried over $MgSO_4$ and concentrated *in vacuo*. The resulting oil was purified by flash column chromatography 2% EtOAc in hexanes to yield the product as clear oil (2.01 g, 87% yield). Spectral data were in complete accordance with previously reported values.[86]

5.5.2.b Synthesis of vinyl pinacolato boronate esters

General procedure 5.1: An oven-dried 25 mL Schlenk tube was charged with alkyne (1.0 equiv.) and bis(cyclopentadienyl)zirconium chloride hydride (0.05 equiv.) and purged with N_2. To the flask was added 1,2-DCE (3.0 M) followed by dropwise addition of 4,4,5,5-tetramethyl-1,3,2-dioxaborolane at 0 °C under a positive N_2 flow, resulting in vigorous gas evolution. The reaction vessel was sealed and heated at 60 °C for 20 h. The reaction was allowed to cool to room temperature before quenching by careful dropwise addition of MeOH (0.15 equiv.), concentrating *in vacuo*, and purifying by flash column chromatography on boric-acid doped silica gel.

2-((*E*)-3-(Cinnamyloxy)prop-1-en-1-yl)-4,4,5,5-tetramethyl-1,3,2-dioxaborolane (5.24a):

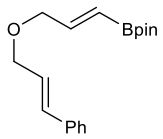

Prepared according to general procedure 5.1 using 2.50 g *(E)*-(3-prop-2-yn-1-yloxy)prop-1-en-1-yl)benzene (13.4 mmol, 1.00 equiv.), 2.12 mL 4,4,5,5-

tetramethyl-1,3,2-dioxaborolane (14.7 mmol, 1.1 equiv.) and 172 mg bis(cyclopentadienyl)zirconium chloride hydride (0.670 mmol, 0.05 equiv.). Purified using 95:5 hex:EtOAc to yield 3.38g (81% yield) of the desired product as a clear oil.

^{1}H NMR: (500 MHz, $CDCl_3$) δ 7.38 (d, *J* = 7.4 Hz, 2H), 7.31 (t, *J* = 7.6 Hz, 2H), 7.24 (tt, 7.3, 1.4 Hz, 1H), 6.67 (dt, *J* = 18.1, 4.7 Hz, 1H), 6.61 (d, *J* = 16.0 Hz, 1H), 6.28 (dt, *J* = 15.9, 5.9 Hz, 1H), 5.74 (dt, *J* = 18.2, 1.8 Hz, 1H), 4.16 (dd, *J* = 5.9, 1.5 Hz, 2H), 4.12 (dd, *J* = 4.7, 1.8 Hz, 2H), 1.27 (s, 12H).

^{13}C NMR: (126 MHz, $CDCl_3$) δ 149.3, 136.9, 132.4, 128.7, 127.8, 126.6, 126.2, 83.4, 71.8, 71.1, 24.9. The signal for the carbon attached to boron was not observed due to quadrupolar relaxation of the boron nucleus.

^{11}B NMR: (128 MHz, $CDCl_3$) δ 29.7.

HRMS (ESI-orbitrap) m/z: [M + NH4]+ Calcd for C19H27BO4NH4 347.2377; Found 347.2371.

***N*-Cinnamyl-4-methyl-*N*-((*E*)-3-(4,4,5,5-tetramethyl-1,3,2-dioxaborolan-2-yl)allyl)benzenesulfonamide (5.24f):** Prepared according to general procedure 5.1 using 0.325 g *N*-cinnamyl-4-methyl-*N*-(prop-2-yn-1-yl)benzenesulfonamide (1.00 mmol, 1.00 equiv.), 0.158 mL 4,4,5,5-tetramethyl-1,3,2-dioxaborolane (1.10 mmol, 1.1 equiv.) and 13 mg bis(cyclopentadienyl)zirconium chloride hydride (0.0500 mmol, 0.05 equiv.). Purified using a gradient of 95:5 to 7:3 hex:EtOAc to yield 330 mg (74% yield) of the desired product as an off-white solid.

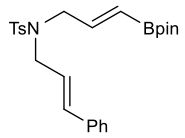

^{1}H NMR: (500 MHz, $CDCl_3$) δ 7.72 (d, *J* = 8.2 Hz, 2H) 7.29–2.26 (m, 4H), 7.24–7.22 (m, 3H), 6.42 (*J* = 18.1, 5.6 Hz, 1H), 6.38 (d, *J* = 16.0 Hz, 1H), 5.91 (dt, *J* = 15.9, 6.8 Hz, 1H), 5.56 (dt, *J* = 18.0, 1.7 Hz, 1H), 3.95 (d, *J* = 7.0 Hz, 2H), 3.90 (dd, *J* = 5.6, 1.6 Hz, 2H), 2.42 (s, 3H), 1.24 (s, 12H).

^{13}C NMR: (126 MHz, $CDCl_3$) δ; 147.3, 143.4, 137.6, 136.4, 134.3, 129.8, 128.7, 128.0, 127.5, 126.6, 123.9, 83.5, 50.7, 49.6, 24.9, 21.6. The signal for the carbon attached to boron was not observed due to quadrupolar relaxation of the boron nucleus.

HRMS (ESI-orbitrap) m/z: [M + H]+ Calcd for C25H33BNO4S 453.2254; Found 453.2249.

***tert*-Butyl cinnamyl((E)-3-(4,4,5,5-tetramethyl-1,3,2-dioxaborolan-2-yl)allyl)carbamate**

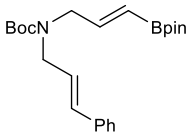

(5.24g): Synthesized according to general procedure 5.1 using 543 mg dimethyl 2-cinnamyl-2-(prop-2-yn-1-yl)malonate (2.00 mmol, 1.00 equiv.), 290 μL 4,4,5,5-tetramethyl-1,3,2-dioxaborolane (2.0 mmol, 1.0 equiv.) and 26 mg bis(cyclopentadienyl)zirconium chloride hydride (0.1 mmol, 0.05 equiv.). Purified using boric acid-doped silica gel and a gradient 90:10 hex/EtOAc to yield 535 mg (67% yield) of the desired product as a viscous oil.

^{1}H NMR: (400 MHz, DMSO-d_6 at 80°C) δ 7.38 (d, J = 6.9 Hz, 2H), 7.32 (t, J = 7.5 Hz, 2H), 7.27 – 7.20 (m, 1H), 6.48 (d, J = 16.4 Hz, 1H), 6.43 (dt, J = 5.1 Hz, 1H), 6.17 (dt, J = 15.9, 6.1 Hz, 1H), 5.43 (d, J = 18 Hz, 1H), 3.93 (d, J = 6.2 Hz, 2H), 3.91 – 3.88 (m, 2H), 1.42 (s, 9H), 1.21 (s, 12H).

^{13}C NMR: (101 MHz, DMSO-d_6 at 80°C) δ 155.1, 149.3, 137.2, 132.0, 129.0, 127.9, 126.6, 126.4, 83.4, 79.4, 55.2, 50.6, 49.2, 28.6, 25.0.

^{11}B NMR: (128.4 MHz, $CDCl_3$) δ 29.9.

HRMS (ESI-orbitrap) m/z: [M + H]+ Calcd for C23H35BNO4 2399.2690; Found 399.2686.

4,4,5,5-Tetramethyl-2-((1*E*)-7-phenylhepta-1,6-dien-1-yl)-1,3,2-dioxaborolane (5.24h):

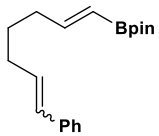

Prepared according to general procedure 5.1 using 0.340 g hept-1-en-6-yn-1-ylbenzene (2.00 mmol, 1.00 equiv.), 0.316 mL 4,4,5,5-tetramethyl-1,3,2-dioxaborolane (2.20 mmol, 1.1 equiv.) and 26 mg bis(cyclopentadienyl)zirconium chloride hydride (0.100 mmol). Purified using a gradient of 98:2 to 9:1 hex:Et_2O to yield 313 mg (53%

yield) of the desired product as a clear oil and inseparable mixture of *trans* and *cis* isomers in a 3:1 ratio that was used without further purification.

Dimethyl-2-cinnamyl-2-((*E*)-3-(4,4,5,5-tetramethyl-1,3,2-dioxaborolan-2-yl)allyl)

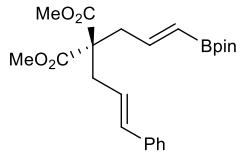

malonatedioxaborolane (5.24i): Synthesized according to general procedure 5.1 using 1.00 g dimethyl 2-cinnamyl-2-(prop-2-yn-1-yl)malonate (3.50 mmol, 1.00 equiv.), 1.12 mL 4,4,5,5-tetramethyl-1,3,2-dioxaborolane (7.7 mmol, 2.2 equiv.) and 45 mg bis(cyclopentadienyl)zirconium chloride hydride (0.175 mmol, 0.05 equiv.). Purified using boric-acid doped silica gel and a gradient 80:20 hex/EtOAc to yield 1.1 g (76% yield) of the desired product as a viscous oil.

^{1}H NMR: (500 MHz, $CDCl_3$) δ 7.33 – 7.18 (m, 5H), 6.49 – 6.38 (m, 2H), 6.03 (dt, *J* = 15.4, 7.6 Hz, 1H), 5.55 (dt, *J* = 17.6, 1.3 Hz, 1H), 3.72 (s, 6H), 2.80 (m, 4H), 1.26 (s, 12H).

^{13}C NMR: (126 MHz, $CDCl_3$) δ 171.2, 147.0, 137.2, 134.3, 128.6, 127.5, 126.4, 123.9, 83.4, 58.0, 52.7, 39.4, 36.5, 24.9. The signal for the carbon attached to boron was not observed due to quadrupolar relaxation of the boron nucleus.

^{11}B NMR: (128 MHz, $CDCl_3$) δ 29.40.

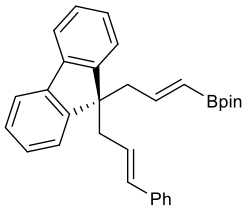

2-((*E*)-3-(9-Cinnamyl-9H-fluoren-9-yl)prop-1-en-1-yl)-4,4,5,5-tetramethyl-1,3,2-dioxaborolane (5.24j): Prepared according to general procedure 5.1 using 1.00 g 9-cinnamyl-9-(prop-2-yn-1-yl)-9H- fluorene (**5.38**) (3.10 mmol, 1.00 equiv.), 0.540 mL 4,4,5,5-tetramethyl-1,3,2-dioxaborolane (3.72 mmol, 1.2 equiv.) and 40 mg bis(cyclopentadienyl)zirconium chloride hydride (0.155 mmol). Purified by recrystallization in 94:6 hex/EtOAc to yield 819 mg (56% yield) of the desired product as a white solid.

^{1}H NMR: (500 MHz, $CDCl_3$) δ 7.70 – 7.67 (m, 2H), 7.43 – 7.40 (m, 2H), 7.35 – 7.24 (m, 4H), 7.21 – 7.15 (m, 2H), 7.14 – 7.10 (m, 1H), 7.10 – 7.06 (m, 2H), 6.31 (dt, *J* = 17.7, 7.1 Hz, 1H), 6.19 (d, *J* = 15.7 Hz, 1H), 5.73 (dt, *J* = 15.3, 7.4 Hz, 1H), 5.36 (d, *J* = 17.8 Hz, 1H), 2.85 – 2.76 (m, 4H), 1.19 (s, 12H).

^{13}C NMR: (126 MHz, $CDCl_3$) δ 149.5, 149.3, 140.6, 137.7, 132.9, 128.4, 127.3, 127.1, 127.0, 126.1, 125.9, 124.0, 120.0, 83.1, 54.3, 45.6, 42.6, 24.8. The signal for the carbon attached to boron was not observed due to quadrupolar relaxation of the boron nucleus.

^{11}B NMR: (128 MHz, $CDCl_3$) δ 29.4

HRMS (ESI-orbitrap) m/z: [M + NH4]+ Calcd for C31H33BO2NH4 466.2912; Found 466.2919.

HRMS (ESI-orbitrap) m/z: [M + NH4]+ Calcd for C23H31BO6NH4 431.2588; Found 431.2590.

2-((*E*)-3-(Cinnamyloxy)-3-methylbut-1-en-1-yl)-4,4,5,5-tetramethyl-1,3,2-dioxaborolane

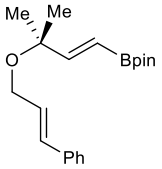

(5.24k): Prepared according to general procedure 5.1 using 0.341 g (*E*)-(3-((2-methylbut-3-yn-2-yl)oxy)prop-1-en-1-yl)benzene (1.71 mmol, 1.00 equiv.), 0.316 mL 4,4,5,5-tetramethyl-1,3,2-dioxaborolane (2.40 mmol, 1.29 equiv.) and 26 mg bis(cyclopentadienyl)zirconium chloride hydride (0.050 mmol). Purified using a gradient of 95:5 to 9:1 hex/EtOAc to yield 304 mg (79% yield) of the desired product as a clear oil.

^{1}H NMR: (500 MHz, $CDCl_3$) δ 7.37 (d, *J* = 6.8 Hz, 2H), 7.29 (t, *J* = 7.6 Hz, 2H), 7.21 (t, *J* = 7.3 Hz, 1H), 6.62 (d, 16.2 Hz, 1H), 6.59 (d, 14.9, 1H), 6.28 (dt, *J* = 15.9, 5.8, 1H), 5.60 (d, *J* = 18.5 Hz, 1H), 4.01 (dd, *J* = 5.8, 1.6 Hz, 2H), 1.34 (s, 6H), 1.28 (s, 12H).

^{13}C NMR: (126 MHz, $CDCl_3$) δ 157.9, 137.2, 131.3, 128.6, 127.6, 127.5, 126.6, 83.5, 76.5, 64.1, 26.1, 25.0. The signal for the carbon attached to boron was not observed due to quadrupolar relaxation of the boron nucleus.

HRMS (ESI-orbitrap) m/z: [M + Na]+ Calcd for C20H29BO3Na 350.2138; Found 350.2134.

2-((*E*)-3-(((*E*)-1,3-Diphenylallyl)oxy)prop-1-en-1-yl)-4,4,5,5-tetramethyl-1,3,2-dioxaborolane (5.24l): Prepared according to general procedure 5.1 using 0.497 g (*E*)-3-(prop-2-yn-1-yloxy)prop-1-ene-1,3-diyl)dibenzene (2.00 mmol, 1.00 equiv.), 0.316 mL 4,4,5,5-tetramethyl-1,3,2-dioxaborolane (2.40 mmol, 1.2 equiv.) and 26 mg bis(cyclopentadienyl)zirconium chloride hydride (0.050 mmol). Purified using a gradient of 95:5 to 9:1 hex/EtOAc to yield 350 mg (48% yield) of the desired product as a clear oil.

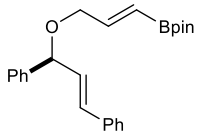

^{1}H NMR: (500 MHz, $CDCl_3$) δ 7.41–7.32 (m, 6H), 7.30–7.27 (m, 3H), 7.23 (t, 7.2 Hz, 1H), 6.70 (dt, *J* = 18.2, 4.5 Hz, 1H), 6.63 (d, *J* = 15.8 Hz, 1H), 6.27 (dd, *J* = 15.9, 6.9 Hz, 1H), 5.79 (dt, *J* = 18.1, 1.8 Hz, 1H), 4.97 (d, *J* = 6.9 Hz, 1H), 4.14 (ddd, *J* = 14.6, 4.6, 1.8 Hz, 1H), 4.09 (ddd, *J* = 14.7, 4.5, 1.8 Hz), 1.27 (s, 12H).

^{13}C NMR: (126 MHz, $CDCl_3$) δ 149.4, 141.2, 136.7, 131.5, 130.4, 128.7, 128.6, 127.8, 127.8, 127.0, 126.8, 83.4, 82.0, 69.8, 24.9. The signal for the carbon attached to boron was not observed due to quadrupolar relaxation of the boron nucleus.

HRMS (ESI-orbitrap) m/z: [M + Na]+ Calcd for C24H29BO3Na 398.2138; Found 398.2135.

2-((E)-3-(((E)-3-(4-Methoxyphenyl)allyl)oxy)prop-1-en-1-yl)-4,4,5,5-tetramethyl-1,3,2-dioxaborolane (5.24m): Prepared according to a modification of general procedure 5.1 using 0.746 g (*E*)-1- methoxy-4-(3-(prop-2-yn-1-yloxy)prop-1-en-1-yl)benzene (3.58 mmol, 1.00 equiv.), 0.571 mL 4,4,5,5-tetramethyl-1,3,2-dioxaborolane (3.94 mmol, 1.1 equiv.) and 63.2 mg bis(cyclopentadienyl)zirconium chloride hydride (0.179 mmol, 0.05 equiv.). Purified using 10:1.5 hex/EtOAc to yield 532 mg (45% yield) of the desired product as a clear oil.

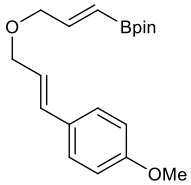

^{1}H NMR: (500 MHz, $CDCl_3$) δ 7.32 (d, *J* = 8.7 Hz, 2H), 6.85 (d, *J* = 8.7 Hz, 2H), 6.67 (dt, *J* = 18.2, 4.7 Hz, 1H), 6.55 (dd, *J* = 15.9, 1.5 Hz, 1H), 6.15 (dt, *J* = 15.9, 6.1 Hz, 1H) 5.74 (dt, *J* =

18.2, 1.8 Hz, 1H), 4.14 (dd, *J* = 6.1, 1.5 Hz, 2H), 4.11 (dd, *J* = 4.8, 1.8 Hz, 2H), 3.81 (s, 3H), 1.27 (s, 12H).

^{13}C NMR: (126 MHz, $CDCl_3$) δ 159.4, 149.4, 132.2, 129.7, 127.8, 123.9, 114.1, 83.4, 71.7, 71.2, 55.4, 24.9. The signal for the carbon attached to boron was not observed due to quadrupolar relaxation of the boron nucleus.

^{11}B NMR: (128 MHz, $CDCl_3$) δ 29.89.

HRMS (ESI-orbitrap) m/z: [M + NH4]+ Calcd for C19H27BO4NH4 347.2377; Found 347.2371.

2-((*E*)-3-(((*E*)-3-(Benzo[*d*][1,3]dioxol-5-yl)allyl)oxy)prop-1-en-1-yl)-4,4,5,5-tetramethyl-

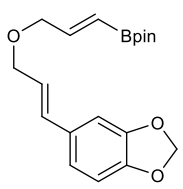

1,3,2-dioxaborolane (5.24n): Prepared according to general procedure 5.1 using 0.225 g (*E*)-5-(3-(prop-2-yn-1- yloxy)prop-1-en-1-yl)benzo[*d*][1,3]dioxole (1.04 mmol, 1.00 equiv.), 0.184 mL 4,4,5,5-tetramethyl-1,3,2-dioxaborolane (1.28 mmol, 1.2 equiv.) and 33 mg bis(cyclopentadienyl)zirconium chloride hydride (0.0104 mmol). Purified using a gradient of 95:5 to 9:1 hex/EtOAc to yield 289 mg (81% yield) of the desired product as a clear oil.

^{1}H NMR: (500 MHz, $CDCl_3$) δ 6.92 (d, *J* = 1.6 Hz, 1H), 6.81 (dd, *J* = 8.0, 1.7 Hz, 1H), 6.75 (d, *J* = 8.0 Hz, 1H), 6.67 (dt, *J* = 18.1, 4.7 Hz, 1H), 6.52 (d, *J* = 15.9 Hz, 1H), 6.11 (dt, *J* = 15.9, 6.0 Hz, 1H), 5.73 (dt, *J* = 18.2, 1.7 Hz, 1H), 5.30 (s, 2H), 4.13 (dd, *J* = 6.1, 1.5 Hz, 2H), 4.10 (dd, *J* = 4.7, 1.8 Hz, 2H), 1.27 (s, 12H).

^{13}C NMR: (126 MHz, $CDCl_3$) δ 149.3, 148.1, 147.4, 132.2, 131.4, 124.3, 121.3, 108.4, 106.0, 101.2, 83.4, 71.8, 71.1, 24.9. The signal for the carbon attached to boron was not observed due to quadrupolar relaxation of the boron nucleus.

HRMS (ESI-orbitrap) m/z: [M + Na]+ Calcd for C19H25BO5Na 366.1724; Found 366.1723.

2-((*E*)-3-(((*E*)-3-(Furan-2-yl)allyl)oxy)prop-1-en-1-yl)-4,4,5,5-tetramethyl-1,3,2-dioxaborolane (5.24o): 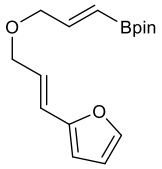

Prepared according to a modification of general procedure 5.1 using 0.195 g (*E*)-2-(3-(prop-2-yn-1-yloxy)prop-1-en-1-yl)furan (1.20 mmol, 1.00 equiv.), 0.261 mL 4,4,5,5-tetramethyl-1,3,2-dioxaborolane (1.80 mmol, 1.5 equiv.) and 22 mg bis(cyclopentadienyl)zirconium chloride hydride (0.0600 mmol, 0.05 equiv.). Purified using 10:1 hex/EtOAc to yield 189 mg (54% yield) of the desired product as a clear oil.

^{1}H NMR: (500 MHz, $CDCl_3$) δ 7.34 (d, *J* = 1.7 Hz, 1H), 6.66 (dt, *J* = 18.2, 4.7 Hz, 1H), 6.44 (dt, *J* = 16.0, 1.6 Hz, 1H), 6.36 (dd, *J* = 3.3, 1.8 Hz, 1H), 6.23 (d, *J* = 3.3 Hz, 1H), 6.20 (dt, *J* = 18.4, 5.6 Hz, 1H), 5.74 (dt, *J* = 18.2, 1.8 Hz; 1H), 4.13 (dd, *J* = 5.7, 1.6 Hz, 2H), 4.11 (dd, 4.7, 1.8 Hz, 2H), 1.27 (s, 12H).

^{13}C NMR: (126 MHz, $CDCl_3$) δ 152.6, 149.2, 142.1, 124.8, 120.4, 111.4, 108.0, 83.4, 71.8, 70.5, 24.9. The signal for the carbon attached to boron was not observed due to quadrupolar relaxation of the boron nucleus.

^{11}B NMR: (128 MHz, $CDCl_3$) δ 29.9.

HRMS (ESI-orbitrap) m/z: [M + Na]+ Calcd for C16H23BO4Na 312.1618; Found 312.1616.

5-((6*E*)-7-(4,4,5,5-Tetramethyl-1,3,2-dioxaborolan-2-yl)hepta-1,6-dien-1-yl)-2-(trifluoromethyl)pyridine (5.24p): 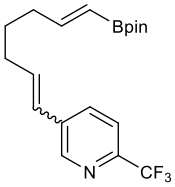

Prepared according to general procedure 5.1 using 0.240 g 5-(hept-1-en-6-yn-1-yl)-2-(trifluoromethyl)pyridine (1.00 mmol, 1.00 equiv.), 0.172 mL 4,4,5,5-tetramethyl-1,3,2-dioxaborolane (1.20 mmol, 1.2 equiv.) and 13 mg bis(cyclopentadienyl)zirconium chloride hydride (0.050 mmol). Purified using a gradient of 95:5 to 9:1 hex/EtOAc to yield 251 mg (68% yield) of the desired product as a clear oil and inseparable mixture of *E*:*Z* isomers in a ratio of 2:1 that was used without further purification.

2-((*E*)-3-(((*E*)-3-(4-Methoxyphenyl)-2-methylallyl)oxy)prop-1-en-1-yl)-4,4,5,5-tetramethyl-1,3,2-dioxaborolane (5.24q). Synthesized according to general procedure 5.1 using 285 mg (*E*)-1-methoxy-4-(2-methyl-3-(prop-2-yn-1-yloxy)prop-1-en-1-yl)benzene (**2.45**) (1.41 mmol, 1.00 equiv.), 0.241 mL 4,4,5,5-tetramethyl-1,3,2-dioxaborolane (1.69 mmol, 1.2 equiv.) and 18 mg bis(cyclopentadienyl)zirconium chloride hydride (0.07 mmol, 0.05 equiv.). Purified using boric acid-doped silica gel and a gradient 85:15 hex/EtOAc to yield 318 mg (100% yield) of the desired product as a slightly yellow oil.

^{1}H NMR: (500 MHz, $CDCl_3$) δ 7.22 (d, J = 8.7 Hz, 2H), 6.87 (d, J = 8.7 Hz, 2H), 6.68 (dt, J = 18.1, 4.7 Hz, 1H), 6.44 (s, 1H), 5.75 (dt, J = 18.2, 1.8 Hz, 1H), 4.08 (dd, J = 4.7, 1.8 Hz, 2H), 4.02 (d, J = 1.2 Hz, 2H), 3.81 (s, 3H), 1.88 (d, J = 1.3 Hz, 3H), 1.27 (s, 12H).

^{13}C NMR: (126 MHz, $CDCl_3$) δ 158.2, 149.5, 133.6, 130.3, 130.2, 126.6, 113.6, 83.4, 76.8, 71.4, 55.4, 24.9, 15.6. The signal for the carbon attached to boron was not observed due to quadrupolar relaxation of the boron nucleus.

^{11}B NMR (128 MHz, $CDCl_3$) δ 29.8.

HRMS (ESI-orbitrap) m/z: [M + Na]+ Calcd for C20H29BO4Na 366.2087; Found 366.2086.

2-((*E*)-3-(((*E*)-2,4-Dimethylpenta-2,4-dien-1-yl)oxy)prop-1-en-1-yl)-4,4,5,5-tetramethyl-1,3,2-dioxaborolane (5.24r): Prepared according to general procedure 5.1 with slight modification using 0.162 g (*E*)- 2,4-dimethyl-5-(prop-2-yn-1-yloxy)penta-1,3-diene (1.07 mmol, 1.00 equiv.), 0.171 mL 4,4,5,5-tetramethyl-1,3,2-dioxaborolane (1.18 mmol, 1.2 equiv.) and 14 mg bis(cyclopentadienyl)zirconium chloride hydride (0.0535 mmol, 0.05 equiv.). Purified using of 20:1 pentanes/EtO_2 to yield 81 mg (28% yield) of the desired product as a clear oil.

^{1}H NMR: (500 MHz, $CDCl_3$) δ 6.66 (dt, *J* = 18.2, 6.7 Hz, 1 H), 5.90 (t, *J* = 1.4 Hz, 1H), 5.72 (dt, *J* = 18.1, 1.8 Hz, 1H), 4.99 (d, 1H), 4.84 (s, 1H), 4.04 (dd, *J* = 4.7, 1.8 Hz, 2H), 3.91 (s, 2H), 1.86 (s, 3H), 1.82 (s, 3H), 1.27 (s, 12H).

^{13}C NMR: (126 MHz, $CDCl_3$) δ 149.5, 141.6, 133.9, 129.0, 115.3, 83.4, 76.8, 71.5, 24.9, 23.7, 15.6. The signal for the carbon attached to boron was not observed due to quadrupolar relaxation of the boron nucleus.

^{11}B NMR: (128 MHz, $CDCl_3$) δ 29.87.

HRMS (ESI-orbitrap) m/z: [M + H]+ Calcd for C16H28BO3 279.2126; Found 279.2125.

4,4,5,5-Tetramethyl-2-((*E*)-3-(((*E*)-5-methylhexa-2,4-dien-1-yl)oxy)prop-1-en-1-yl)-1,3,2-dioxaborolane (5.24s): Prepared according to general procedure 5.1 using 0.300 g (*E)*-5-methyl-1-(prop-2-yn-1-yl)oxy)hexa-2,4-diene (2.00 mmol, 1.00 equiv.), 0.316 mL 4,4,5,5-tetramethyl-1,3,2-dioxaborolane (2.60 mmol, 1.2 equiv.) and 26 mg bis(cyclopentadienyl)zirconium chloride hydride (0.100 mmol). Purified using a gradient of 95:5 to 9:1 hex/EtOAc to yield 132 mg (24% yield) of the desired product as a clear oil.

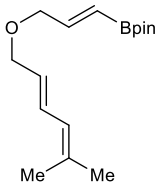

^{1}H NMR: (500 MHz, $CDCl_3$) δ 6.65 (dt, *J* = 18.1, 4.7 Hz, 1H), 6.44 (ddt, *J* = 15.1, 11.1 1.4, 1H), 5.83 (d, *J* = 10.8, 1H), 5.70 (dt, *J* = 18.2, 1.8 Hz, 1H), 5.62 (dt, *J* = 15.1, 6.3 Hz, 1H), 4.06 (dd, *J* = 4.7, 1.8 Hz, 2H), 4.03 (d, *J* = 6.3 Hz, 2H), 1.78 (s, 3H), 1.76 (s, 3H), 1.27 (s, 12H).

^{13}C NMR: (126 MHz, $CDCl_3$) δ 149.5, 136.2, 129.8, 126.5, 124.5, 83.4, 71.6, 71.2, 26.1, 24.9, 18.5. The signal for the carbon attached to boron was not observed due to quadrupolar relaxation of the boron nucleus.

^{11}B NMR: (128 MHz, $CDCl_3$) δ 29.9.

HRMS (ESI-orbitrap) m/z: [M + Na]+ Calcd for C16H27BO3Na 300.1982; Found 300.1978.

***N*-Cinnamyl-4-methyl-N-((*E*)-3-phenyl-2-(4,4,5,5-tetramethyl-1,3,2-dioxaborolan-2-yl)allyl)benzenesulfonamide (5.24t).** 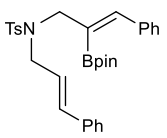

Synthesized in an analogous procedure reported by Moure.[87] A flame-dried 10 mL round-bottomed flask was charged with 240 mg of N-cinnamyl-4-methyl-N-(3-phenylprop-2-yn-1-yl)benzenesulfonamide (1 equiv., 0.6 mmol), 6 mg of CuCl (0.1 equiv., 0.06 mmol), 167 mg of bis(pinacolato)diboron (1.1 equiv., 0.66 mmol) and 8.6 mg of NaOtBu (0.15 equiv., 0.9 mmol). The flask was sealed and purged with nitrogen for 5 minutes. A degassed solution of 24.2 mg of tri-*tert*-butylphosphine (0.12 equiv., 0.072 mmol) in dry toluene (1.6 mL) was added to the reaction vessel. Finally, 48.5 μL of MeOH was added and the mixture was stirred at room temperature for 2 h. The reaction was quenched with MeOH, filtered through a silica plug, flushing with CH_2Cl_2. The crude material was purified *via* column chromatography using hexane/EtOAc 8:2 as the eluent mixture to yield301 mg (95%) of a white solid

^{1}H NMR: (500 MHz, $CDCl_3$) δ 7.62 (d, *J* = 8.2 Hz, 2H), 7.39 (s, 1H), 7.31 – 7.15 (m, 10H), 7.08 – 7.01 (m, 2H), 6.18 (d, *J* = 15.8 Hz, 1H), 5.81 (dt, *J* = 15.9, 6.8 Hz, 1H), 4.13 (d, *J* = 1.5 Hz, 2H), 3.85 (dd, *J* = 6.8, 1.4 Hz, 2H), 2.36 (s, 3H), 1.28 (s, 12H).

^{13}C NMR: (126 MHz, $CDCl_3$) δ 145.2, 143.0, 137.0, 136.8, 136.6, 133.6, 129.5, 129.4, 128.4, 128.3, 127.8, 127.8, 127.6, 126.5, 124.4, 83.9, 50.1, 45.6, 24.9, 21.6. The signal for the carbon attached to boron was not observed due to quadrupolar relaxation of the boron nucleus.

HRMS (ESI-orbitrap) m/z: [M + H]+ Calcd for C31H37BNO4S 529.2567; Found 529.2566.

(*E*)-4,4,5,5-Tetramethyl-2-(3-((3-methylbut-2-en-1-yl)oxy)prop-1-en-1-yl)-1,3,2-dioxaborolane (5.35): 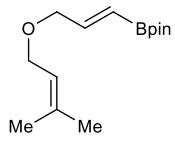

Synthesized according to general procedure 5.1 using 3-methyl-1-(prop-2-yn-1-yloxy)but-2-ene (1.07 g, 8.62 mmol, 1.0 equiv), 4,4,5,5-tetramethyl-1,3,2-dioxaborolane (1.75 mL, 12.1 mmol, 1.4 equiv.), and

bis(cyclopentadienyl)zirconium chloride hydride (222.0 mg, 0.862 mmol, 0.10 equiv). Purified by flash chromatography using boric-acid doped silica gel with an elution gradient of 95:5 to 9:1 hexanes/EtOAc to yield 1.23 g (57% yield) of the desired product as a clear oil.

^{1}H NMR: (500 MHz, $CDCl_3$) δ 6.65 (dt, *J* = 18.1, 4.9 Hz, 1H), 5.69 (dt, *J* = 18.2, 1.8 Hz, 1H), 5.35 (ddt, *J* = 8.3, 5.4, 1.5 Hz, 1H), 4.04 (dd, *J* = 4.9, 1.8 Hz, 2H), 3.97 (d, *J* = 6.9 Hz, 2H), 1.74 (d, *J* = 1.3 Hz, 3H), 1.66 (d, *J* = 1.4 Hz, 3H), 1.26 (s, 12H).

^{13}C NMR: (126 MHz, $CDCl_3$) δ 149.6, 137.0, 121.1, 83.2, 71.6, 66.9, 25.8, 24.8, 18.1. The signal for the carbon attached to boron was not observed due to quadrupolar relaxation of the boron nucleus.

^{11}B NMR: (128.4 MHz, $CDCl_3$) δ 29.8.

HRMS (ESI-orbitrap) m/z: [M + F]– Calcd for C14H25BO3F 271.1886; Found 271.1888.

5.5.2.c Synthesis of other vinyl boronate ester derivatives

2-((*E*)-3-(Cinnamyloxy)prop-1-en-1-yl)-5,5-dimethyl-1,3,2-dioxaborinane (5.24b): A 10 mL round bottom flask was charged with $MgSO_4$ (250 mg, 500 wt%) and flame activated under vacuum. After cooling to room temperature, the vessel was charged with ((*E*)-3-(cinnamyloxy)prop-1-en-1-yl)boronic acid (50.0 mg, 0.230 mmol, 1.0 equiv.), 2,2-dimethyl-1,3-propanediol (26.3 mg, 0.230 mmol, 1.0 equiv.) and $CHCl_3$ (4.5 mL, 0.05 M). The vessel was fitted with an oven-dried reflux condenser and brought to a reflux under an N_2 atmosphere for 2 h, before cooling to room temperature. The reaction was passed through a plug of Celite® to remove the desiccant and washed with CH_2Cl_2. The solution was concentrated to yield 65 mg (100% yield) of the desired product sufficiently clean to use in the next step.

^{1}H NMR: (500 MHz, $CDCl_3$) δ 7.38 (d, *J* = 7.40 Hz, 2H), 7.21 (t, *J* = 7.4 Hz, 2H), 7.23 (tt, *J* = 7.4, 1.4 Hz, 1H), 6.61 (d, *J* = 16.0 Hz, 1H), 6.59 (dt, *J* = 18.0 5.0 Hz, 1H), 6.29 (dt, *J* = 15.9, 5.9 Hz, 1H), 5.65 (dt, *J* = 18.0, 1.7 Hz, 1H), 4.16 (dd, *J* = 5.9, 1.6 Hz, 1H), 4.11 (dd, *J* = 5.0, 1.7 Hz, 1H), 3.65 (dd, *J* = 5.9, 1.6 Hz, 4H), 0.97 (s, 6H).

^{13}C NMR: (126 MHz, $CDCl_3$) δ 146.6, 137.0, 132.4, 128.7, 127.7, 126.6, 126.3, 72.3, 72.1, 72.0, 31.9, 22.0. The signal for the carbon attached to boron was not observed due to quadrupolar relaxation of the boron nucleus.

^{11}B NMR: (128 MHz, $CDCl_3$) δ 25.5.

HRMS (ESI-orbitrap) m/z: [M + H]+ Calcd for C17H24BO3 286.1849; Found 256.1850.

((*E*)-3-(Cinnamyloxy)prop-1-en-1-yl)boronic acid (5.24c): A 100 mL round bottom flask was

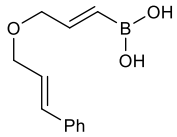

charged with ammonium acetate (964 mg, 12.5 mmol, 3 equiv.), sodium periodate (2.67 g, 12.5 mmol, 3 equiv.), 2-((*E*)-3-(cinnamyloxy)prop-1-en-1-yl)-4,4,5,5-tetramethyl-1,3,2-dioxaborolane (1.24 g, 4.15 mmol, 1 equiv.) and a 1:1 mixture of acetone and water (50 mL, 0.083 M). The vessel was fitted with a septum and stirred for 24 h at room temperature under N_2. The solution was filtered through a pad of Celite© with multiple washes of acetone and concentrated *in vacuo* to remove the organic solvent. The remaining aqueous layer was extracted with EtOAc (3x) and the combined organic layers were washed with water (3x), brine, dried over Na_2SO_4, and concentrated *in vacuo* to give the crude product as a white solid and 1:1 mixture of dehydrated species, which was used without further purification (767 mg, 85%). The mixture of products was found to be stable indefinitely if stored at –40 ˚C under inert atmosphere.

^{1}H NMR: (500 MHz, $CDCl_3$) δ 7.40–7.38 (m, 4H), 7.33–7.30 (m, 4H), 7.26–7.27 (m, 2H), 7.01 (dt, *J* = 17.9, 4.5 Hz, 1H), 6.65 (d, *J* = 6.3 Hz, 1H), 6.61 (d, *J* = 6.1 Hz, 1H), 6.57 (dt, *J* = 18.1, 4.6

Hz, 1H), 6.33–6.27 (m, 2H), 5.85 (dt, *J* = 17.9, 1.8 Hz, 1H), 5.73 (dt, *J* = 18.1, 1.8 Hz, 1H), 4.30 (bs, 2H), 4.20–4.17 (m, 6H), 4.14 (dd, *J* = 4.6, 1.8 Hz, 2H).

2-((*E*)-3-(Cinnamyloxy)prop-1-en-1-yl)-6-methyl-1,3,6,2-dioxazaborocane-4,8-dione

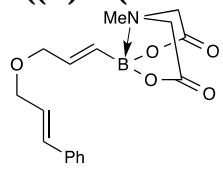

(5.24d): A dry 25 mL round bottom flask was charged with ((*E*)-3-(cinnamyloxy)prop-1-en-1-yl)boronic acid (54.5 mg, 0.25 mmol, 1.0 equiv.), methyiminodiacetic acid (38.5 mg, 0.260 mmol, 1.05 equiv.), toluene (10 mL) and DMSO (1 mL), and fitted with a Dean–Stark apparatus. The reaction was heated to reflux for 2 h. The reaction was allowed to cool completely before concentrating the reaction to remove the toluene. The residue was diluted with Et_2O and loaded onto a silica plug. The silica plug was washed several times with Et_2O before eluting the product with THF, yielding 48 mg (59% yield) of the desired product as a clear oil.

^{1}H NMR: (500 MHz, $CDCl_3$) δ 7.39 (d, *J* = 7.4 Hz, 2H), 7.32 (d, *J* = 7.4 Hz, 2H), 7.24 (t, 7.4 Hz, 1H), 6.61 (d, *J* = 16.0 Hz, 1H), 6.36–6.24 (m, 1H), 5.73 (dt, *J* = 17.8, 1.8 Hz, 1H), 4.18 (dd, *J* = 6.1, 1.5 Hz, 1H), 4.11 (dd, *J* = 4.6, 1.8 Hz, 1H), 3.84 (d, *J* = 16.3 Hz, 1H), 3.68 (d, *J* = 16.3 Hz, 1H) 2.84 (s, 3H).

^{13}C NMR: (126 MHz, $CDCl_3$) δ167.1, 143.6, 136.8, 132.8, 128.7, 127.9, 126.6, 126.0, 71.8, 71.4, 61.6, 46.8. The signal for the carbon attached to boron was not observed due to quadrupolar relaxation of the boron nucleus.

^{11}B NMR: (128 MHz, $CDCl_3$) δ 11.6.

HRMS (ESI-orbitrap) m/z: [M + Na]+ Calcd for C17H20BNO5Na 351.1363; Found 351.1363.

2-((*E*)-3-(Cinnamyloxy)prop-1-en-1-yl)-2,3-dihydro-1H-naphtho[1,8-de][1,3,2]diazaborinine (5.24e): A 10 mL round bottom flask was charged with $MgSO_4$ (250 mg, 500 wt%) and flame activated under vacuum. After

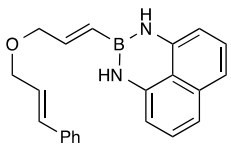

cooling to room temperature, the vessel was charged with ((*E*)-3-(cinnamyloxy)prop-1-en-1-yl)boronic acid (50 mg, 0.230 mmol, 1.0 equiv.), 1,8-diaminonaphthalene (36 mg, 0.230 mmol, 1.0 equiv.) and $CHCl_3$ (4.5 mL, 0.05 M). The vessel was fitted with an oven-dried reflux condenser and brought to a reflux under an N_2 atmosphere for 16 h, before cooling to room temperature. The reaction was passed through a plug of Celite® to remove the desiccant and washed with CH_2Cl_2. After concentrating the solution *in vacuo*, the crude reaction mixture was purified by flash column chromatography to yield 72 mg (92% yield) of the product as a dark purple oil.

^{1}H NMR: (500 MHz, $CDCl_3$) δ 7.40 (d, *J* = 7.8 Hz, 2H), 7.32 (dd, *J* = 8.4 Hz, 7.0 Hz, 2H), 7.27–7.23 (m, 1H), 7.09 (t, *J* = 7.7 Hz, 2H), 7.01 (d, *J* = 8.2 Hz, 2H), 6.64 (d, *J* = 15.9 Hz, 1H), 6.42 (dt, *J* = 18.2, 4.9 Hz, 1H), 6.36–6.27 (m, 3H), 5.88 (dt, *J* = 18.3, 1.8 Hz, 1H), 5.74 (s, 2H), 4.20 (d, *J* = 6.0 Hz, 2H), 4.16 (d, *J* = 5.0 Hz, 2H).

^{13}C NMR: (126 MHz, $CDCl_3$) δ 142.8, 141.2, 136.8, 136.5, 132.8, 128.7, 127.9, 127.7, 126.7, 126.0, 120.0, 117.8, 105.9, 72.2, 71.3. The signal for the carbon attached to boron was not observed due to quadrupolar relaxation of the boron nucleus.

^{11}B NMR: (128 MHz, $CDCl_3$) δ 28.4.

HRMS (ESI-orbitrap) m/z: [M + Na]+ Calcd for C22H21BN2ONa 362.1675; Found 362.1673.

5.5.3 Photosensitized [2+2] Cycloadditions

5.5.3.a [2+2] Photocycloadditions of vinyl boronate esters

General procedure 5.2: An oven-dried Schlenk tube was charged with vinyl boronate ester (1.0 equiv.), $Ir(dF(CF_3)ppy)_2(dtbbpy)(PF)_6$ (0.01 equiv.), and CH_3CN (0.05 M). The homogenous solution was degassed by three freeze-pump-thaw cycles before irradiating with a 36W H150 Kessil lamp at a distance of 5 cm for the 4 hours. The reaction was concentrated and purified by

flash column chromatography on boron-doped silica gel (see general experimental section) using the conditions specified.

4,4,5,5-Tetramethyl-2-(-7-phenyl-3-oxabicyclo[3.2.0]heptan-6-yl)-1,3,2-dioxaborolane

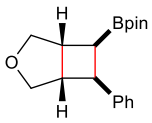

(5.25a): Synthesized according to general procedure 5.2 using 90.0 mg 2-((*E*)-3-(cinnamyloxy)prop-1-en-1-yl)-4,4,5,5-tetramethyl-1,3,2-dioxaborolane (0.300 mmol, 1.0 equiv.), 3.3 mg $Ir(dF(CF_3)ppy)_2(dtbbpy)(PF)_6$ (1 mol%) and 6 mL CH_3CN (0.05 M) yielding 78.2 mg (87% yield) of the desired product in 4:1:1 d.r. as a colorless oil, after flash column chromatography with boric-acid doped silica gel using 85:15 hexanes:EtOAc. The diastereomers could be further separated using a gradient elution in 98:2 to 88:12 hexanes:EtOAc on boric-acid doped silica gel.

^{1}H NMR: (500 MHz, $CDCl_3$) δ 7.32–7.25 (m, 4H), 7.16 (tt, *J* = 7.1, 1.3 Hz, 1H), 3.96 (d, *J* = 9.3 Hz, 1H), 3.92 (d, *J* = 9.2 Hz, 1H), 3.62 (d, *J* = 9.2, 5.5 Hz, 1H), 3.57 (dd, *J* = 9.3, 5.3, Hz, 1H), 3.46 (dd, *J* = 11.3, 5.3 Hz, 1H), 3.24 (dt, *J* = 7.7, 5.6 Hz, 1H), 3.09 (dt, *J* = 7.9, 5.7 Hz, 1H), 2.12 (ddd, *J* = 11.3, 5.6, 1.2 Hz, 1H), 1.00 (s, 6H), 0.87 (s, 6H).

^{13}C NMR: (126 MHz, $CDCl_3$) δ 144.6, 128.3, 127.6, 126.1, 83.2, 75.2, 74.3, 44.4, 43.6, 37.0, 25.1, 24.8. The signal for the carbon attached to boron was not observed due to quadrupolar relaxation of the boron nucleus.

^{11}B NMR: (128 MHz, $CDCl_3$) δ 33.3.

HRMS (ESI-orbitrap) m/z: [M + H]+ Calcd for C18H26BO3 301.1973; Found 301.1971.

NOE:

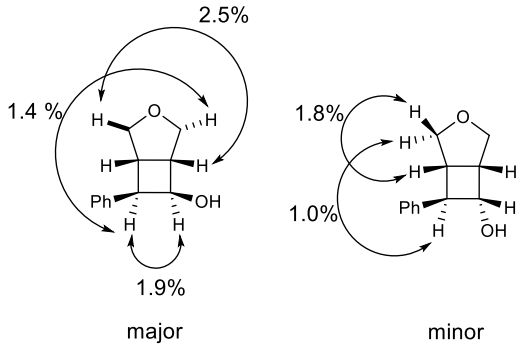

5,5-Dimethyl-2-(-7-phenyl-3-oxabicyclo[3.2.0]heptan-6-yl)-1,3,2-dioxaborinane (5.25b):

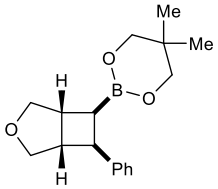

Synthesized according to general procedure 5.2 using **5.24b** (94.1 mg, 0.300 mmol, 1.0 equiv.), $Ir(dF(CF_3)ppy)_2(dtbbpy)(PF)_6$ (3.7 mg, 3.3 μmol, 1 mol%) and 6 mL CH_3CN (0.05 M) yielding 70.6 mg (75% yield) of the desired product in 4:1:1 d.r. as a colorless oil, after flash column chromatography with boric-acid doped silica gel using 85:15 hexanes:EtOAc. The diastereomers could be further separated using a gradient elution in 98:2 to 88:12 hexanes:EtOAc on boric-acid doped silica gel.

^{1}H NMR: (600 MHz, $CDCl_3$) δ 7.33 – 7.29 (m, 4H), 7.17 (tt, *J* = 5.7, 2.6 Hz, 1H), 3.99 (d, *J* = 9.3 Hz, 1H), 3.93 (d, *J* = 9.1 Hz, 1H), 3.63 (dd, *J* = 9.2, 5.5 Hz, 1H), 3.59 (dd, *J* = 9.3, 5.3 Hz, 1H), 3.44 (dd, *J* = 11.3, 5.1 Hz, 1H), 3.34 (dd, *J* = 10.8, 1.3 Hz, 2H), 3.25 (dd, *J* = 10.7, 1.4 Hz, 2H), 3.22 – 3.17 (m, 1H), 3.10 (dt, *J* = 7.9, 5.6 Hz, 1H), 2.05 (dd, *J* = 11.2, 5.6 Hz, 1H), 0.70 (s, 6H).

^{13}C NMR: (151 MHz, $CDCl_3$) δ 145.1, 128.1, 127.3, 125.7, 75.1, 74.2, 71.7, 44.4, 44.0, 36.4, 31.3, 21.7. The signal for the carbon attached to boron was not observed due to quadrupolar relaxation of the boron nucleus.

^{11}B NMR: (128.4 MHz, $CDCl_3$) δ 29.3.

HRMS (ASAP-orbitrap) m/z: [M + H]+ Calcd for C17H24BO3 287.1813; Found 287.1808.

(7-Phenyl-3-oxabicyclo[3.2.0]heptan-6-yl)boronic acid (5.25c): Synthesized according to

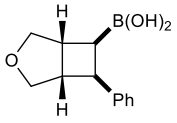

general procedure 5.2 using **5.24c** (56.8 mg, 0.300 mmol, 1.0 equiv.), $Ir(dF(CF_3)ppy)_2(dtbbpy)(PF)_6$ (3.4 mg, 3.0 μmol, 1 mol%) and 6 mL CH_3CN (0.05 M). Immediately following the reaction, $NaBO_3H_2O$ (138.0 mg, 0.896 mmol, 3.0 equiv) in 1.0 mL of THF/H_2O was added and the resulting mixture was allowed to react for 2 h to afford the corresponding alcohol. The crude reaction was then concentrated via reduced pressure yielding 38.5 mg (68% yield) of the desired product in 3:1:1 d.r. as a colorless oil, after flash column chromatography with boric-acid doped silica gel using 85:15 hexanes:EtOAc. For characterization data of the alcohol see compound **5.29**.

4-Methyl-8-(-7-phenyl-3-oxabicyclo[3.2.0]heptan-6-yl)dihydro-4l4,8l4-

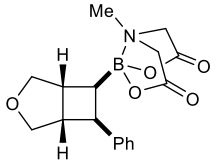

[1,3,2]oxazaborolo[2,3-b][1,3,2]oxazaborole-2,6(3H,5H)-dione (5.25d): Synthesized according to general procedure 5.2 using **5.24d** (75.3 mg, 0.230 mmol, 1.0 equiv.), $Ir(dF(CF_3)ppy)_2(dtbbpy)(PF)_6$ (2.6 mg, 2.3 μmol, 1 mol%) and 5 mL CH_3CN (0.05 M) yielding 63.2 mg (84% yield) of the desired product in 7:1:1 d.r. as a colorless oil, after flash column chromatography with boric-acid doped silica gel using an elution gradient of 80:20 to 70:30 Et_2O:MeCN.

^{1}H NMR: (500 MHz, $CDCl_3$) δ 7.35 (d, *J* = 7.1 Hz, 2H), 7.30 (t, *J* = 7.5 Hz, 2H), 7.22 (t, *J* = 7.3 Hz, 1H), 3.97 (d, *J* = 9.4 Hz, 1H), 3.91 (d, *J* = 9.4 Hz, 1H), 3.66 (d, *J* = 17.2 Hz, 1H), 3.66 (dd, *J* = 9.6, 5.7 Hz, 1H), 3.57 (d, *J* = 17.4 Hz, 1H), 3.54 (dd, *J* = 9.4, 5.6 Hz, 1H), 3.43 (dd, *J* = 10.9, 5.8 Hz, 1H), 3.34 – 3.29 (m, 1H), 3.29 (d, *J* = 15.7 Hz, 1H), 3.09 (dt, *J* = 8.0, 5.7 Hz, 1H), 2.61 (s, 3H), 1.90 (dd, *J* = 10.9, 5.8 Hz, 1H), 1.82 (d, *J* = 15.8 Hz, 1H).

^{13}C NMR: (126 MHz, $CDCl_3$) δ 167.7, 166.9, 143.3, 128.9, 128.8, 126.8, 75.3, 74.1, 63.2, 61.7, 46.0, 43.6, 43.4, 37.7.

^{11}B NMR: (128.4 MHz, $CDCl_3$) δ 13.2.

HRMS (ESI-orbitrap) m/z: [M + Na]+ Calcd for C17H20BO5Na 352.1327; Found 352.1325.

2-(-7-Phenyl-3-oxabicyclo[3.2.0]heptan-6-yl)-2,3-dihydro-1H-naphtho[1,8-de][1,3,2]diazaborinine (5.25e): Synthesized according to general procedure 5.2 using **5.24e** (62.3 mg, 0.183 mmol, 1.0 equiv.), $Ir(dF(CF_3)ppy)_2(dtbbpy)(PF)_6$ (2.0 mg, 1.8 μmol, 1 mol%) and 4 mL CH_3CN (0.05 M) yielding 9.2 mg (15% yield) of the desired product in 4:1:1 d.r. as a purple oil, after flash column chromatography with boric-acid doped silica gel using an elution gradient of 95:5 to 90:10 hexanes:EtOAc.

^{1}H NMR: (500 MHz, $CDCl_3$) δ 7.36 (t, *J* = 7.6 Hz, 2H), 7.26 (m, 3H), 7.08 (t, *J* = 7.8 Hz, 2H), 7.01 (d, *J* = 8.3 Hz, 2H), 6.29 (d, *J* = 7.3 Hz, 2H), 5.55 (s, 2H), 3.88 (d, *J* = 9.1 Hz, 1H), 3.78 (d, *J* = 10.1 Hz, 1H), 3.67 (dd, *J* = 10.7, 8.8 Hz, 1H), 3.53 (dd, *J* = 9.1, 4.2 Hz, 1H), 3.43 (dd, *J* = 10.0, 6.8 Hz, 1H), 3.24 (q, *J* = 7.5 Hz, 1H), 2.99 (td, *J* = 7.2, 4.2 Hz, 1H), 2.20 – 2.14 (m, 1H).

^{13}C NMR: (126 MHz, $CDCl_3$) δ 141.0, 140.8, 136.3, 128.6, 127.8, 127.5, 126.4, 119.6, 117.7, 105.8, 73.8, 68.8, 43.5, 40.1, 38.1, 29.7.

^{11}B NMR: (128.4 MHz, $CDCl_3$) δ 31.5.

HRMS (ESI-orbitrap) m/z: [M + H]+ Calcd for C22H22BNO 341.1820; Found 341.1818.

6-Phenyl-7-(4,4,5,5-tetramethyl-1,3,2-dioxaborolan-2-yl)-3-tosyl-3-azabicyclo[3.2.0]heptane (5.25f): Synthesized according to general procedure 5.2 using 136 mg *N*-cinnamyl-4-methyl-*N*-((*E*)-3-(4,4,5,5-tetramethyl-1,3,2-dioxaborolan-2-yl)allyl)benzenesulfonamide (0.300 mmol, 1.0 equiv.), 3.3 mg $Ir(dF(CF_3)ppy)_2(dtbbpy)(PF)_6$ (1 mol%) and 6 mL CH_3CN (0.05 M) yielding 98.4 mg (84% yield) of the desired product in 4:1:1

d.r. after chromatography on boric acid-doped silica gel using a gradient of 98:2 hexanes:EtOAc to 88:12 hexanes:EtOAc.

^{1}H NMR: (500 MHz, $CDCl_3$) δ 7.66 (d, *J* = 8.3 Hz, 2H), 7.26 (d, *J* = 7.9 Hz, 2H), 7.18 (m, 4H), 7.08 (tt, *J* = 6.9, 1.8 Hz, 1H), 3.49–3.45 (m, 2H), 3.41 (d, *J* = 9.8 Hz, 1H), 3.04 (dt, *J* =6.9, 6.4 Hz, 1H), 2.93 (dt, *J* = 6.9, 6.4 Hz, 1H), 2.72 (dd, *J* = 9.5, 6.3 Hz, 1H), 2.69 (dd, *J* = 9.6, 6.2 Hz, 1H), 2.37 (s, 3H), 2.19 (dd, *J* = 11.3, 5.5 Hz, 1H), 0.90 (s, 6H), 0.77 (s, 6H).

^{13}C NMR: (126 MHz, $CDCl_3$) δ 144.1, 143.7, 132.5, 129.7, 128.4, 128.2, 127.5, 126.3, 83.3, 55.2, 54.6, 43.7, 43.1, 35.8, 25.1, 24.7, 21.7; The signal for the carbon attached to boron was not observed due to quadrupolar relaxation of the boron nucleus.

^{11}B NMR: (128.4 MHz, $CDCl_3$) δ 33.3.

HRMS (ASAP-orbitrap) m/z: [M + H]+ Calcd for C25H33BO4S 453.2222; Found 454.2227.

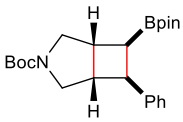

***tert*-Butyl 6-phenyl-7-(4,4,5,5-tetramethyl-1,3,2-dioxaborolan-2-yl)-3-azabicyclo[3.2.0]heptane-3-carboxylate (5.25g):** Synthesized according to general procedure 5.2 using 128 mg *tert*-butyl cinnamyl((*E*)-3-(4,4,5,5-tetramethyl-1,3,2-dioxaborolan-2-yl)allyl)carbamate (**5.24g**) (0.3 mmol, 1.00 equiv.), 3.3 mg $Ir(dF(CF_3)ppy)_2(dtbbpy)(PF)_6$ and 6 mL CH_3CN (0.05 M) yielding 109 mg (85% yield) of the desired product in 8:1 d.r.

^{1}H NMR: (500 MHz, $CDCl_3$ at room temperature) δ 7.28 – 7.25 (m, 4H), 7.17 – 7.12 (m, 1H), 3.76 – 3.19 (m, 6H), 3.12 – 2.97 (m, 1H), 2.19 – 2.09 (m, 1H), 1.49 (s, 9H), 0.97 (s, 6H), 0.89 (s, 6H).

^{13}C NMR: (126 MHz, $CDCl_3$) δ 155.3, 143.9, 128.1, 127.1, 126.0, 83.1, 79.2, 53.7 – 52.3 (m), 44.4 – 42.4 (m), 36.2, 35.2, 28.6, 24.8, 24.6. The signal for the carbon attached to boron was not observed due to quadrupolar relaxation of the boron nucleus.

^{11}B NMR: (128.4 MHz, $CDCl_3$) δ 32.83.

HRMS (ASAP-orbitrap) m/z: [M + Na]+ Calcd for C23H34BNO4Na 422.2473; Found 422.2460.

4,4,5,5-Tetramethyl-2-(-7-phenylbicyclo[3.2.0]heptan-6-yl)-1,3,2-dioxaborolane (5.25h):

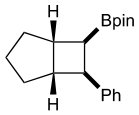

Synthesized according to general procedure 2 using 89.4 mg 4,4,5,5-tetramethyl-2-((1*E*)-7-phenylhepta-1,6-dien-1-yl)-1,3,2-dioxaborolane (0.300 mmol, 1.0 equiv.), 3.3 mg $Ir(dF(CF_3)ppy)_2(dtbbpy)(PF)_6$ (1 mol%) and 6 mL CH_3CN (0.05 M) yielding 80 mg (89% yield) of the desired product as an inseparable mixture of diastereomers in 4:1 d.r. after flash column chromatography on boric-acid doped silica gel, using a gradient of 99:1 to 95:5 hexanes:EtOAc.

^{1}H NMR: (500 MHz, $CDCl_3$) δ 7.31 (d, *J* = 7.1 Hz, 2H), 7.28 – 7.23 (m, 2H), 7.16 – 7.08 (m, 1H), 3.14 (dd, *J* = 11.4, 5.0 Hz, 1H), 3.01 (dt, 7.1, 5.51 Hz, 1H), 2.94 – 2.88 (m, 1H), 2.05 – 1.96 (m, 1H), 1.87 – 1.81 (m, 2H), 1.65 – 1.57 (m, 4H), 0.99 (s, 6H), 0.86 (s, 6H).

^{13}C NMR: (126 MHz, $CDCl_3$) δ 146.0, 128.1, 127.8, 125.7, 83.0, 44.4, 44.0, 36.1, 34.0, 33.5, 25.3, 25.1. The signal for the carbon attached to boron was not observed due to quadrupolar relaxation of the boron nucleus.

^{11}B NMR: (128 MHz, $CDCl_3$) δ 32.9.

HRMS (ESI-orbitrap) m/z: [M + NH4]+ Calcd for C19H27BO2NH4 316.2442; Found 316.2439.

Dimethyl-6-phenyl-7-(4,4,5,5-tetramethyl-1,3,2-dioxaborolan-2-yl)-bicyclo[3.2.0]heptane-

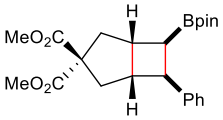

3,3-dicarboxylate (5.25i). Synthesized according to general procedure 2 using 128 mg dimethyl 2-cinnamyl-2-((E)-3-(4,4,5,5-tetramethyl-1,3,2-dioxaborolan-2-yl)allyl)malonatedioxaborolane **5.24i** (0.3 mmol, 1.00 equiv.), 3.3 mg $Ir(dF(CF_3)ppy)_2(dtbbpy)(PF)_6$ and 6 mL CH_3CN (0.05 M) yielding 102 mg (80% yield) of the

desired product in 4:1:1 d.r.. The crude reaction mixture was purified by flash chromatography using boric-acid doped silica gel with 1% MeOH in CH_2Cl_2 as a colorless oil.

^{1}H NMR: (500 MHz, $CDCl_3$) δ 7.25 (t, *J* = 3.5 Hz, 4H), 7.13 (ddd, *J* = 8.6, 5.0, 3.8 Hz, 1H), 3.78 (s, 3H), 3.72 (s, 3H), 3.42 (dd, *J* = 10.9, 5.8 Hz, 1H), 3.23 – 3.14 (m, 1H), 3.00 – 2.92 (m, 1H), 2.59 (dddd, *J* = 20.1, 13.9, 8.3, 1.2 Hz, 2H), 2.41 (ddd, *J* = 13.7, 4.5, 2.2 Hz, 2H), 2.03 (ddd, *J* = 10.9, 5.3, 1.2 Hz, 1H), 0.96 (s, 6H), 0.86 (s, 6H).

^{13}C NMR: ^{13}C NMR (126 MHz, $CDCl_3$) δ 172.9, 172.8, 144.5, 128.1, 127.4, 125.9, 83.0, 64.1, 52.8, 52.7, 45.3, 44.0, 42.4, 41.5, 36.7, 24.9, 24.6. The signal for the carbon attached to boron was not observed due to quadrupolar relaxation of the boron nucleus.

HRMS (ESI-orbitrap) m/z: [M + Na]+ Calcd for C23H31BO6Na 436.2142; Found 436.2136.

4,4,5,5-Tetramethyl-2-(-6-phenylspiro[bicyclo[3.2.0] heptane-3,9'-fluoren]-7-yl)-1,3,2-dioxaborolane (5.25j) Synthesized according to general procedure 5.2 using 134 mg 4,4,5,5-tetramethyl-2-((*E*)-3-(((*E*)-5-methylhexa-2,4-dien-1-yl)oxy)prop-1-en-1-yl)-1,3,2-dioxaborolane **5.24j** (0.3 mmol, 1.00 equiv.), 3.3 mg $Ir(dF(CF_3)ppy)_2(dtbbpy)(PF)_6$ and 6 mL CH_3CN (0.05 M). The crude reaction mixture was purified via flash chromatography on boric acid-doped silica gel using 6% EtOAc in hexanes to yield 129 mg (97% yield) of the desired product in 4:2:1 d.r. In order to isolate the major diastereomer, the mixture was oxidized to afford the correspondent alcohol mixture and purified via flash chromatography on silica gel, using hexanes:MTBE 80:20 as the eluent mixture. The boronate ester was converted to the corresponding alcohol for characterization purposes. The following characterization is reported for the corresponding alcohol.

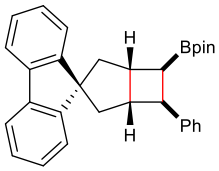

^{1}H NMR: (500 MHz, $CDCl_3$) δ 7.75 – 7.70 (m, 2H), 7.64 – 7.53 (m, 1H), 7.47 – 7.39 (m, 4H), 7.39 – 7.27 (m, 6H), 4.58 (td, *J* = 6.7, 3.4 Hz, 1H), 3.75 (dd, *J* = 7.0, 5.2 Hz, 1H), 3.52 (qd, *J* =

8.3, 4.8 Hz, 1H), 3.29 – 3.17 (m, 1H), 2.49 (dd, *J* = 13.8, 7.2 Hz, 1H), 2.38 (dd, *J* = 13.6, 7.6 Hz, 1H), 2.32 – 2.24 (m, 2H).

^{13}C NMR: (126 MHz, $CDCl_3$) δ 153.9, 149.9, 140.3, 139.0, 138.5, 129.0, 128.9, 127.6, 127.6, 127.4, 127.1, 127.1, 123.1, 122.8, 120.0, 119.9, 74.6, 63.7, 51.3, 50.0, 46.9, 44.3, 41.6.

HRMS (ASAP-orbitrap) m/z: [M + Na]+ Calcd for C25H22ONa 339.1743; Found 339.1742.

2-(4,4-Dimethyl-7-phenyl-3-oxabicyclo[3.2.0]heptan-6-yl)-4,4,5,5-tetramethyl-1,3,2-dioxaborolane (5.25k): Synthesized according to general procedure 5.2 using 98.4 mg 2-((*E*)-3-(cinnamyloxy)-3-methylbut-1-en-1-yl)-4,4,5,5-tetramethyl-1,3,2-dioxaborolane (0.300 mmol, 1.0 equiv.), 3.3 mg $Ir(dF(CF_3)ppy)_2(dtbbpy)(PF)_6$ (1 mol%) and 6 mL CH_3CN (0.05 M) yielding 91 mg (93% yield) of the desired product in 4:1 d.r. after flash column chromatography on boric acid-doped silica gel, eluting with 8:2 hexanes/EtOAc. Further separation of the diastereomers could be achieved by flash column chromatography on boric-acid doped silica in 96:4 hexanes:EtOAc.

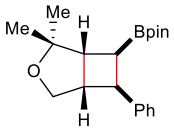

^{1}H NMR: (500 MHz, $CDCl_3$) δ 7.32 (d, *J* = 7.3 Hz, 2H), 7.27 (t, *J* = 7.4 Hz, 2H), 7.15 (tt, *J* = 7.3, 1.5 Hz, 1H), 3.94 (dd, *J* = 9.7, 6.0 Hz, 1H), 3.90 (dd, *J* = 9.6, 1.6, 1H), 3.33 (dd, *J* = 11.0, 4.0 Hz, 1H), 3.19 – 3.15 (m, 1H), 2.83 (t, *J* = *7.2* Hz, 1H), 2.37 (dd, *J* = 10.4, 7.2 Hz, 1H), 1.28 (s, 3H), 1.14 (s, 3H), 0.99 (s, 6H), 0.84 (s, 6H).

^{13}C NMR: (126 MHz, $CDCl_3$) δ 145.3, 128.3, 127.6, 126.1, 83.1, 82.1, 71.9, 46.2, 45.6, 43.7, 25.1, 24.5, 22.6; The signal for the carbon attached to boron was not observed due to quadrupolar relaxation of the boron nucleus.

^{11}B NMR: (128.4 MHz, $CDCl_3$) δ 33.4.

HRMS (ESI-orbitrap) m/z: [M + H]+ Calcd for C20H30BO3 346.2552; Found 346.2555.

2-(4,7-Diphenyl-3-oxabicyclo[3.2.0]heptan-6-yl)-4,4,5,5-tetramethyl-1,3,2-dioxaborolane

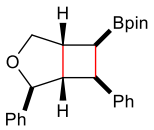

(5.25l): Synthesized according to general procedure 5.2 using 113 mg 2-((*E*)-3-(((*E*)-1,3-diphenylallyl)oxy)prop-1-en-1-yl)-4,4,5,5-tetramethyl-1,3,2-dioxaborolane (0.300 mmol, 1.0 equiv.), 3.3 mg $Ir(dF(CF_3)ppy)_2(dtbbpy)(PF)_6$ (1 mol%) and 6 mL CH_3CN (0.05 M) yielding 95 mg (84% yield) of the desired product in 5:1 d.r. after flash column chromatography on boric acid-doped silica gel, using a gradient of 98:2 hexanes:EtOAc to 88:12 hexanes:EtOAc.

^{1}H NMR: (500 MHz, $CDCl_3$) δ 7.36 – 7.27 (m, 8H), 7.25–7.21 (m, 1H), 7.19 – 7.15 (m, 1H), 5.10 (s, 1H), 4.09 (dd, *J* = 9.3, 6.3 Hz, 1H), 3.99 (dd, *J* = 9.3, 2.1 Hz, 1H), 3.78 (dd, *J* = 11.2, 6.0 Hz, 1H), 3.55 (dd, *J* = 7.7, 6.2 Hz, 1H), 3.14 (dd, *J* = 7.9, 4.7 Hz, 1H), 3.16–3.12 (m, 1H), 2.24 (ddd, *J* = 11.2, 4.9, 1.2 Hz, 1H), 0.98 (s, 6H), 0.89 (s, 6H).

^{13}C NMR: (126 MHz, $CDCl_3$) δ 144.1, 143.2, 128.5, 127.5, 127.2, 126.5, 126.0, 86.4, 83.3, 74.5, 50.4, 43.7, 37.4, 25.1, 24.8; The signal for the carbon attached to boron was not observed due to quadrupolar relaxation of the boron nucleus.

^{11}B NMR: (128 MHz, $CDCl_3$) δ 33.4.

HRMS (ESI-orbitrap) m/z: [M + NH4]+ Calcd for C24H29BO3NH4 394.2552; Found 394.2559.

4,4,5,5-Tetramethyl-2-(-7-phenyl-3-oxabicyclo[3.2.0]heptan-6-yl)-1,3,2-dioxaborolane

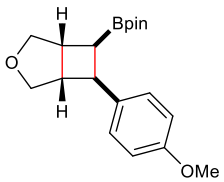

(5.25m): Synthesized according to general procedure 5.2 with slight modification using 91 mg (0.300 mmol, 1.0 equiv.) (E)-1-methoxy-4-(3-(prop-2-yn-1-yloxy)prop-1-en-1-yl)benzene, 3.3 mg $Ir(dF(CF_3)ppy)_2(dtbbpy)(PF)_6$ (1 mol%) and 6 mL CH_3CN (0.05 M). The reaction was irradiated for 17 h using a 23 W CFL, yielding 79 mg (87% yield of white solid in 4:1:1 d.r. after chromatography on silica gel in 5:1 hexanes:EtOAc.

^{1}H NMR: (500 MHz, $CDCl_3$) δ 7.24 (d, *J* = 8.5 Hz, 2H), 6.83 (d, *J* = 8.7 Hz, 2H), 3.93 (d, *J* = 9.6 Hz, 1H), 3.60 (d, *J* = 9.2 Hz, 1H), 3.55 (s, 3H), 3.42 – 3.38 (m, 1H), 3.19 (dd, *J* = 8.8, 5.4 Hz, 1H), 3.17 (m, 1H), 2.08 (t, *J* = 9.3 Hz, 1H), 1.02 (s, 6H), 0.89 (s, 6H).

^{13}C NMR: (126 MHz, $CDCl_3$) δ 158.1, 137.0, 128.6, 113.7, 83.2, 75.2, 74.3, 55.6, 44.8, 42.8, 36.8, 25.2, 24.8. The signal for the carbon attached to boron was not observed due to quadrupolar relaxation of the boron nucleus.

^{11}B NMR: (128 MHz, $CDCl_3$) δ 32.9.

HRMS (ASAP-orbitrap) m/z: [M + H]+ Calcd for C19H28BO4 330.2111; Found 330.2106.

2-(-7-(Benzo[*d*][1,3]dioxol-5-yl)-3-oxabicyclo[3.2.0]heptan-6-yl)-4,4,5,5-tetramethyl-1,3,2-dioxaborolane (5.25n): Synthesized according to general procedure 5.2 using 103 mg 2-((*E*)-3-(((*E*)-3-(benzo[*d*][1,3]dioxol-5-yl)allyl)oxy)prop-1-en-1-yl)-4,4,5,5-tetramethyl-1,3,2-dioxaborolane (0.300 mmol, 1.0 equiv.), 3.3 mg $Ir(dF(CF_3)ppy)_2(dtbbpy)(PF)_6$ (1 mol%) and 6 mL CH_3CN (0.05 M) yielding 64 mg (62% yield) of the desired product in 4:1:1 d.r. after flash column chromatography on boric acid-doped silica gel, using 96:4 hexanes:EtOAc.

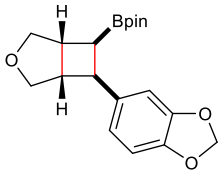

^{1}H NMR: (500 MHz, $CDCl_3$) δ 6.85 (d, *J* = 1.5 Hz, 1H), 6.74 (dd, *J* = 8.1, 1.6 Hz, 1H), 6.72 (d, *J* = 7.9, Hz, 1H), 5.89 (s, 2H), 3.94 (d, 9.3 Hz, 1H), 3.90 (d, *J* = 9.2 Hz, 1H), 3.60 (dd, *J* = 9.3, 5.4 Hz, 1H), 3.54 (dd, *J* = 9.3, 5.2 Hz, 1H), 3.37 (dd, *J* = 11.2, 5.2 Hz, 1H), 3.13 (dt, 7.8, 5.3 Hz, 1H), 3.06 (dt, *J* = 7.7, 5.3 Hz, 1H), 2.07 (dd, *J* = 11.2, 5.5 Hz, 1H), 1.06 (s, 6H), 0.95 (s, 6H).

^{13}C NMR: (126 MHz, $CDCl_3$): δ 174.4, 145.7, 138.7, 120.3, 108.2, 107.9, 100.7, 83.1, 75.0, 74.1, 45.0, 43.3, 37.0, 25.0, 24.7; The signal for the carbon attached to boron was not observed due to quadrupolar relaxation of the boron nucleus.

^{11}B NMR: (128 MHz, $CDCl_3$) δ 33.1.

HRMS (ESI-orbitrap) m/z: [M + H]+ Calcd for C19H26BO5 345.1871; Found 345.1866.

2-(7-(Furan-2-yl)-3-oxabicyclo[3.2.0]heptan-6-yl)-4,4,5,5-tetramethyl-1,3,2-dioxaborolane

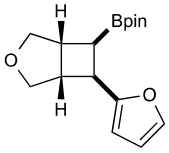

(5.25o): Synthesized according to a modification of general procedure 5.2 using 87 mg (0.300 mmol, 1.0 equiv.), 2-((*E*)-3-(((*E*)-3-(furan-2-yl)allyl)oxy)prop-1-en-1-yl)-4,4,5,5-tetramethyl-1,3,2-dioxaborolane**,** 3.3 mg $Ir(dF(CF_3)ppy)_2(dtbbpy)(PF)_6$ (1 mol%) and 6 mL CH_3CN (0.05 M). The reaction was irradiated for 13 h using a 23 W CFL, yielding 72 mg (83% yield of white solid in 4:1:1 d.r. after chromatography on silica gel in 5:1 hexanes:EtOAc.

^{1}H NMR: (500 MHz, $CDCl_3$) δ 7.34–7.33 (m, 1H), 6.29 (dd, *J* = 3.2, 1.9 Hz, 1H), 6.03 (d, *J* = 3.2 Hz, 1H), 4.19 (d, *J* = 9.6 Hz, 1H), 3.97 (d, *J* = 9.4 Hz, 1H), 3.45 (dd, *J* = 9.4, 5.2 Hz, 1H), 3.41 (dd, *J* = 9.6, 5.3 Hz, 1H), 3.29, (dd, *J* = 8.2, 5.0 Hz, 1H), 3.15–3.10 (m, 2H), 2.22 (dd, *J* = 9.9, 8.3 Hz, H), 1.27 (s, 6H), 1.26 (s, 6H).

^{13}C NMR: (126 MHz, $CDCl_3$): δ 159.3, 141.2, 110.2, 103.9, 83.6, 73.5, 71.9, 45.2, 37.7, 37.0, 25.1, 25.0; The signal for the carbon attached to boron was not observed due to quadrupolar relaxation of the boron nucleus.

^{11}B NMR: (128 MHz, $CDCl_3$) δ 33.5.

HRMS (ESI-orbitrap) m/z: [M + H]+ Calcd for C16H24BO4 291.1762; Found 291.1761.

5-(7-(4,4,5,5-Tetramethyl-1,3,2-dioxaborolan-2-yl)bicyclo[3.2.0]heptan-6-yl)-2-(trifluoromethyl)pyridine (5.25p): Synthesized according to general procedure 5.2 using 110 mg

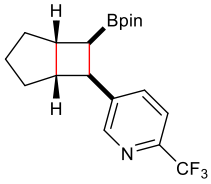

5-((6*E*)-7- (4,4,5,5-tetramethyl-1,3,2-dioxaborolan-2-yl)hepta-1,6-dien-1-yl)-2-(trifluoromethyl)pyridine (0.300 mmol, 1.0 equiv.), 3.3 mg $Ir(dF(CF_3)ppy)_2(dtbbpy)(PF)_6$ (1 mol%) and 6 mL CH_3CN (0.05 M) yielding

71.3 mg (65% yield) of the desired product in 6:1:1 d.r. after flash column chromatography on boric acid-doped silica gel, using a gradient of 98:2 to 95:5 hexanes:EtOAc.

^{1}H NMR: (500 MHz, $CDCl_3$) δ 8.65 (d, *J* = 2.1 Hz, 1H), 7.81 (dd, *J* = 8.1, 2.1 Hz, 1H), 7.59 (d, *J* = 8.1 Hz, 1H), 3.22 (dd, *J* = 11.3, 4.7 Hz, 1H), 3.05–2.97 (m, 1H), 2.98–2.93 (m, 1H), 2.09–1.99 (m, 1H), 1.92 (dd, *J* = 10.8, 6.0 Hz, 1H), 1.90–1.86 (m, 1H), 1.71–1.59 (m, 4H), 0.98 (s, 6H), 0.87 (s, 6H).

^{13}C NMR: (126 MHz, $CDCl_3$) δ 149.9, 145.7 (q, *J* = 34.5 Hz), 144.8, 136.1, 121.2 (q, *J* = 273.6 Hz), 119.9 (q, *J* = 2.8 Hz), 83.3, 43.5, 41.6, 36.5, 33.9, 33.4, 25.2, 25.0, 25.0; The signal for the carbon attached to boron was not observed due to quadrupolar relaxation of the boron nucleus.

^{11}B NMR: (128 MHz, $CDCl_3$) δ 33.3

^{19}F NMR: (376.5 MHz, $CDCl_3$) δ 67.7.

HRMS (ESI-orbitrap) m/z: [M + H]+ Calcd for C19H26BF3NO2 368.2007; Found 368.2015.

2-(7-(4-Methoxyphenyl)-1-methyl-3-oxabicyclo[3.2.0]heptan-6-yl)-4,4,5,5-tetramethyl-1,3,2-dioxaborolane (5.25q). Synthesized according to general procedure 5.2 using 103 mg 2-((*E*)-3-(((*E*)-3-(4-methoxyphenyl)-2-methylallyl)oxy)prop-1-en-1-yl)-4,4,5,5-tetramethyl-1,3,2-dioxaborolane **5.24q** (0.3 mmol, 1.00 equiv.), 3.3 mg $Ir(dF(CF_3)ppy)_2(dtbbpy)(PF)_6$ and 6 mL CH_3CN (0.05 M). The crude reaction mixture was purified via flash chromatography on boric acid-doped silica gel using 20% MTBE in hexanes to yield 83 mg (81% yield) of the desired product in 3:1:1 d.r. In order to isolate the major and the prevalent minor diastereomer, the mixture was oxidized to afford the corresponding alcohol mixture and purified via a preparative TLC (hexanes/EtOAC 6:4). The boronate ester was converted to the corresponding alcohol for characterization purposes. The following characterization is reported for the corresponding alcohol.

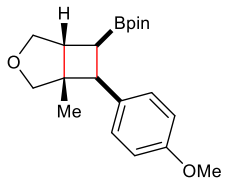

Major: ^{1}H NMR: ^{1}H NMR (500 MHz, $CDCl_3$) δ 7.30 (d, *J* = 8.6 Hz, 2H), 6.88 (d, *J* = 8.6 Hz, 2H), 4.38 – 4.30 (m, 1H), 4.05 (d, *J* = 9.6 Hz, 1H), 3.87 (d, *J* = 9.0 Hz, 1H), 3.80 (s, 3H), 3.69 (dd, *J* = 9.6, 5.8 Hz, 1H), 3.43 (d, *J* = 7.3 Hz, 1H), 3.25 (d, *J* = 9.0 Hz, 1H), 2.44 – 2.39 (m, 1H), 1.73 (s, 1H), 1.13 (s, 3H).

^{13}C NMR: (126 MHz, $CDCl_3$) δ 158.6, 132.0, 128.7, 113.7, 80.6, 72.3, 71.7, 55.4, 53.7, 51.8, 48.1, 18.3.

HRMS (ASAP-orbitrap) m/z: [M + H]+ Calcd for C14H19O3 253.1329; Found 253.1326.

Prevalent minor: ^{1}H NMR: (500 MHz, $CDCl_3$) δ 7.13 (d, *J* = 8.6 Hz, 2H), 6.88 (d, *J* = 8.7 Hz, 2H), 4.31 (q, *J* = 5.0 Hz, 1H), 4.02 (d, *J* = 9.2 Hz, 1H), 3.80 (s, 3H), 3.60 (d, *J* = 9.8 Hz, 1H), 3.57 (dd, *J* = 9.3, 4.2 Hz, 1H), 3.17 (d, *J* = 7.1 Hz, 1H), 2.98 (d, *J* = 9.7 Hz, 1H), 2.42 (t, *J* = 4.3 Hz, 1H), 1.93 – 1.87 (m, 1H), 1.41 (s, 3H);

^{13}C NMR: (126 MHz, $CDCl_3$) δ 158.5, 130.8, 129.0, 114.1, 73.6, 71.8, 71.7, 57.3, 55.4, 53.5, 44.3, 29.9.

4,4,5,5-tetramethyl-2-(-7-(prop-1-en-2-yl)-3-oxabicyclo[3.2.0]heptan-6-yl)-1,3,2-dioxaborolane (5.25r): Synthesized according to general procedure 5.2 using 83.4 mg (*E*)-2,4-dimethyl-5-(prop-2-yn-1-yloxy)penta-1,3-diene (0.300 mmol, 1.0 equiv.), 3.3 mg $Ir(dF(CF_3)ppy)_2(dtbbpy)(PF)_6$ (1 mol%) and 6 mL CH_3CN (0.05 M) yielding 49 mg (59% yield) of the desired product in 4:1:1 d.r. after flash column chromatography on boric acid-doped silica gel, using 10:1 hexanes:EtOAc.

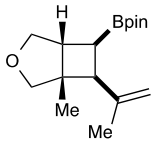

Major: ^{1}H NMR: (500 MHz, $CDCl_3$) δ 4.85 (q, J = 1.3 Hz, 1H), 4.82 – 4.79 (m, 1H), 3.84 (dd, J = 9.4, 1.2 Hz, 1H), 3.80 (d, J = 8.9 Hz, 1H), 3.73 (dd, J = 9.4, 5.9 Hz, 1H), 3.23 (d, J = 8.9 Hz, 1H), 3.07 (d, J = 10.6 Hz, 1H), 2.37 (t, J = 5.5 Hz, 1H), 1.74 (dd, J = 10.7, 5.0 Hz, 1H), 1.66 (s, 3H), 1.25 (s, 6H), 1.25 (s, 6H), 1.19 (s, 3H).

^{13}C NMR: (126 MHz, $CDCl_3$) δ 145.9, 110.8, 83.4, 80.6, 75.4, 49.8, 47.4, 43.9, 25.1, 23.5, 16.8. The signal for the carbon attached to boron was not observed due to quadrupolar relaxation of the boron nucleus.

^{11}B NMR: (128 MHz, $CDCl_3$) δ 33.8.

HRMS (ESI$^+$) calculated for $[C_{16}H_{27}BO_3+H]^+$ requires 278.2162 *m/z*, found 278.2163 *m/z*.

Prevalent minor: ^{1}H NMR: (500 MHz, CDCl3) δ 4.90 (q, J = 1.6 Hz, 1H), 4.68 (s, 1H), 3.85 (d, J = 9.3 Hz, 1H), 3.65 (d, J = 9.1 Hz, 1H), 3.55 (dd, J = 9.0, 4.3 Hz, 1H), 3.19 (d, J = 9.3 Hz, 1H), 2.64 (d, J = 10.2 Hz, 1H), 2.37 (dd, J = 7.5, 4.3 Hz, 1H), 1.62 (s, 3H), 1.60 (m, 1H), 1.28 (s, 3H),1.24 (s, 12H).

^{13}C NMR: (126 MHz, $CDCl_3$) δ 144.3, 110.7, 83.2, 75.2, 73.2, 49.2, 48.0, 44.4, 25.3, 25.1, 24.9, 24.8, 22.2. The signal for the carbon attached to boron was not observed due to quadrupolar relaxation of the boron nucleus.

^{11}B NMR: (128 MHz, $CDCl_3$) δ 33.6.

4,4,5,5-Tetramethyl-2-(-7-(2-methylprop-1-en-1-yl)-3-oxabicyclo[3.2.0]heptan-6-yl)-1,3,2-dioxaborolane (5.25s): Synthesized according to general procedure 5.2 using 84 mg 4,4,5,5-tetramethyl-2-((*E*)-3-(((*E*)-5-methylhexa-2,4-dien-1-yl)oxy)prop-1-en-1-yl)-1,3,2-dioxaborolane **5.24s** (0.3 mmol, 1.00 equiv.), 3.3 mg $Ir(dF(CF_3)ppy)_2(dtbbpy)(PF)_6$ and 6 mL CH_3CN (0.05 M).

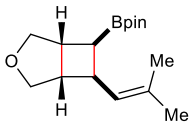

The crude reaction mixture was purified via flash chromatography on boric acid-doped silica gel using 35% diethyl ether in hexanes to yield 34.5 mg (41% yield) of the desired product in 4:1 d.r. In order to isolate the major diastereomer, the mixture was oxidized to afford the correspondent alcohol mixture and purified via flash chromatography on silica gel, using CH_2Cl_2:MeOH (94:6) as the eluent mixture. The following characterization is reported for the corresponding alcohol.

^{1}H NMR: (500 MHz, CDCl3) δ 5.26 (d, J = 8.4, 1.2 Hz, 1H), 4.06 (m, 1H), 4.02 (d, J = 9.5 Hz, 1H), 3.89 (d, J = 9.3 Hz, 1H), 3.50 (dd, J = 9.4, 5.6 Hz, 1H), 3.45 (dd, J = 9.4, 5.5 Hz, 1H), 2.99 - 2.95 (m, 1H), 2.78-2.75 (m, 1H), 2.70-2.66 (m, 1H), 1.80 (s, 3H=, 1.59 (s, 3H).

^{13}C NMR: (126 MHz, $CDCl_3$) δ 137.8, 121.7, 73.3, 72.3, 71.4, 48.3, 42.8, 42.4, 25.9, 18.9.

HRMS (ASAP-orbitrap) m/z: [M + H]+ Calcd for C10H17O2 169.1223; Found 169.1221.

6,7-Diphenyl-1-(4,4,5,5-tetramethyl-1,3,2-dioxaborolan-2-yl)-3-tosyl-3-

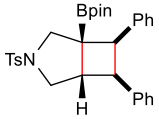

azabicyclo[3.2.0]heptane (5.25t): Synthesized according to general procedure 5.2 using 159 mg *N*-cinnamyl-4-methyl-*N*-((*Z*)-3-phenyl-2-(4,4,5,5-tetramethyl-1,3,2-dioxaborolan-2-yl)allyl)benzenesulfonamide (**5.24t**) (0.3 mmol, 1.00 equiv.), 3.3 mg $Ir(dF(CF_3)ppy)_2(dtbbpy)(PF)_6$ and 6 mL CH_3CN (0.05 M) yielding 146 mg (92% yield) of the desired product in 2:1:1 d.r.

^{1}H NMR: (500 MHz, $CDCl_3$) δ 7.77 (d, *J* = 8.3 Hz, 2H), 7.34 (d, *J* = 8.0 Hz, 2H), 7.10 (t, *J* = 7.6 Hz, 2H), 7.07 – 6.93 (m, 4H), 6.93 – 6.87 (m, 4H), 4.13 (dd, *J* = 10.1, 7.5 Hz, 1H), 3.84 (d, J = 10.7 Hz, 1H), 3.80 (d, *J* = 10.2 Hz, 1H), 3.63 (d, *J* = 9.6 Hz, 1H), 3.57 (dd, *J* = 7.4, 5.4 Hz, 1H), 2.98 (d, *J* = 10.6 Hz, 1H), 2.93 (dd, *J* = 9.6, 5.4 Hz, 1H), 2.43 (s, 3H), 0.97 (s, 6H), 0.78 (s, 6H).

^{13}C NMR: (126 MHz, $CDCl_3$) δ 143.5, 140.4, 140.0, 132.6, 129.5, 129.3, 128.0, 127.7, 127.5, 127.5, 125.9, 125.4, 83.5, 57.0, 54.7, 51.4, 44.8, 42.6, 24.6, 24.4, 21.5.

^{11}B NMR: (128 MHz, $CDCl_3$) δ 32.7.

HRMS (ESI-orbitrap) m/z: [M + H]+ Calcd for C31H37BNO4S 529.2567; Found 529.2564.

5.5.3.b Gram-Scale Reaction

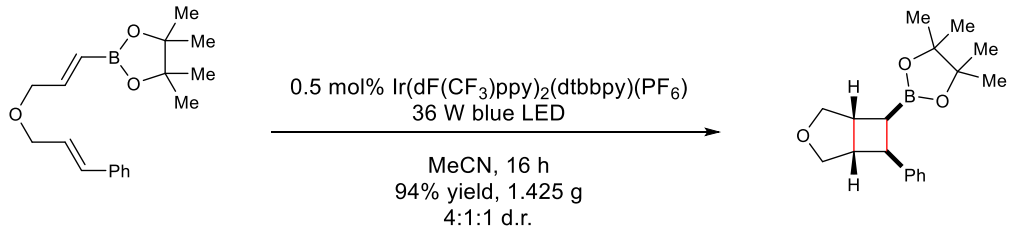

Synthesized according to general procedure 5.2 using 2-((*E*)-3- (cinnamyloxy)prop-1-en-1-yl)-4,4,5,5-tetramethyl-1,3,2-dioxaborolane (1.5156 g, 5.05 mol, 1.0 equiv.), $Ir(dF(CF_3)ppy)_2(dtbbpy)(PF)_6$ (28.3 mg, 25.2 μmol, 0.5 mol%) and 10 mL CH_3CN (0.50 M) yielding 1.425 g of **5.25a** (94% yield) of the desired product in 4:1:1 d.r. as a colorless oil, after flash column chromatography with boric-acid doped silica gel using 85:15 hexanes:EtOAc.

5.5.4 Boronic Ester Functionalization

5.5.4.a Protodeboronation

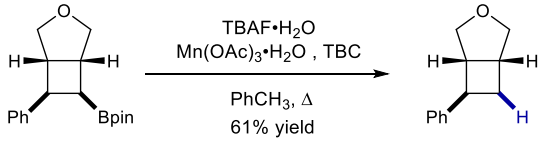

6-Phenyl-3-oxabicyclo[3.2.0]heptane (5.26): A Schlenk tube was charged with **5.25a** (65.1 mg, 0.217mmol, 1.0 equiv), $Mn(OAc)_3 \cdot 2H_2O$ (71.4 mg, 0.260 mmol, 1.20 equiv), 4-*tert*-butylcatechol (189.5 mg, 1.08 mmol, 5.0 equiv), and $TBAF \cdot H_2O$ (84.0 mg, 0.260 mmol, 1.2 equiv). The reaction vessel was purged with N_2 for 10 min. followed by the addition of toluene (3.0 mL, 0.075 M). The mixture was heated to 80 °C for 18 h before cooling to ambient temperature. The heterogenous reaction was filtered through a pad of celite with excess EtOAc, then concentrated via reduced pressure. The crude reaction mixture was purified by flash chromatography with silica gel using 10% EtOAc in hexanes as the eluent to afford 22.9 mg (61%) of the product as a clear oil.

^{1}H NMR: (500 MHz, $CDCl_3$) δ 7.32 (t, *J* = 7.6 Hz, 2H), 7.28 – 7.23 (m, 2H), 7.23 – 7.17 (m, 1H), 3.99 (t, *J* = 9.0 Hz, 2H), 3.62 (dd, *J* = 9.2, 5.8 Hz, 1H), 3.52 (dd, *J* = 9.3, 4.7 Hz, 1H), 3.29 – 3.21 (m, 1H), 3.04 – 2.93 (m, 2H), 2.31 (dt, *J* = 12.5, 8.2 Hz, 1H), 2.21 – 2.14 (m, 1H).

^{13}C NMR: (126 MHz, $CDCl_3$) δ 146.1, 128.4, 126.4, 125.9, 74.5, 74.0, 47.2, 42.0, 35.3, 31.8.

HRMS (ASAP-orbitrap) m/z: [M + H]+ Calcd for C12H15O 175.1117; Found 175.1116.

5.5.4.b Furanylation

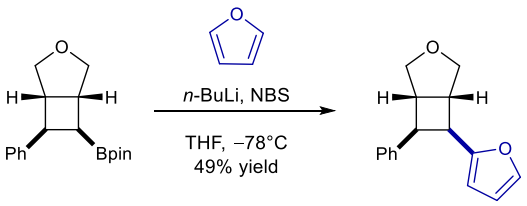

6-(Furan-2-yl)-7-phenyl-3-oxabicyclo[3.2.0]heptane (2.27): A flame-dried 50 mL round-bottomed flask was charged with furan (21.7 µL, 0.298 mmol, 1.20 equiv) and 1.2 mL THF and cooled to –78°C (dry-ice/acetone). A solution of *n*-BuLi (2.5 M in hexanes,0.12 mL, 0.298 mmol, 1.20 equiv) was added dropwise, and the solution was allowed to warm to ambient temperature and stir for 1 h, before cooling to –78 °C. In a separate flask, compound **5.25a** (74.6 mg, 0.248 mmol, 1.0 equiv) was dissolved in 1 mL of THF, followed by dropwise addition to the former solution. After stirring for 1 h, a solution of NBS (53.1 mg, 0.298 mmol, 1.2 equiv) in 1.2 mL of THF was added dropwise and allowed to react for 1 h. The reaction was quenched with $Na_2S_2SO_3$ (saturated aqueous solution, 10 mL) followed by slowly warming to ambient temperature. The reaction mixture was then extracted with Et_2O (10 mL × 3). The combined organics were dried over $MgSO_4$, filtered, then concentrated *via* reduced pressure. The product was purified by flash column chromatography on silica using an elution gradient of 15-20% EtOAc in hexanes to yield 29.3 mg (49%) of the product as a clear oil.

^{1}H NMR: (500 MHz, $CDCl_3$) δ 7.15 (dd, *J* = 7.9, 6.7 Hz, 2H), 7.11 – 7.03 (m, 4H), 6.09 (dd, *J* = 3.2, 1.8 Hz, 1H), 5.88 (d, *J* = 3.2 Hz, 1H), 4.09 (d, *J* = 9.5 Hz, 1H), 4.04 (d, *J* = 9.4 Hz, 1H), 3.68 (dd, *J* = 9.6, 5.3 Hz, 2H), 3.62 (td, *J* = 9.3, 5.0 Hz, 2H), 3.29 (tdd, *J* = 13.3, 8.5, 5.0 Hz, 2H).

^{13}C NMR: (126 MHz, $CDCl_3$) δ 154.8, 141.3, 140.8, 127.7, 127.7, 126.0, 109.8, 106.5, 73.8, 73.7, 46.6, 42.6, 41.2, 40.9.

HRMS (ASAP-orbitrap) m/z: [M + H]+ Calcd for C16H17O2 241.1223; Found 241.1220.

5.5.4.c Fluorination

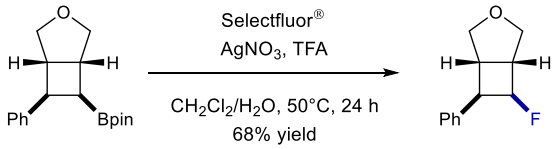

6-Fluoro-7-phenyl-3-oxabicyclo[3.2.0]heptane (5.28): A 24 mL vial was charged with **5.25a** (79.0 mg, 0.263 mmol 1.0 mmol), $AgNO_3$ (134 mg , 0.789 mmol, 3.0 equiv), and Selectfluor (280 mg, 0.789 mmol, 3.0 equiv). This mixture was dissolved in a biphasic combination of CH_2Cl_2 (0.70mL) and water (0.70 mL) followed by addition of trifluoroacetic acid (122.0 µL, 1.58 mmol 6.0 equiv). The reaction mixture was allowed to stir at 50 °C for 24 hours under N_2. At the conclusion of the reaction, the resulting mixture was extracted with EtOAc (10 mL × 3). The combined organic phases were dried over anhydrous $MgSO_4$ and concentrated under reduced pressure. The product was purified by flash column chromatography with silica gel using a gradient of 5–10% EtOAc in hexanes as the eluent to afford 34.2 mg (68%) of the product as a clear oil.

^{1}H NMR: (500 MHz,$CDCl_3$) δ 7.37 – 7.32 (m, 2H), 7.26 – 7.20 (m, 3H), 5.00 (dt, *J* = 54.3, 7.1 Hz, 1H), 4.44 (dd, *J* = 9.9, 1.8 Hz, 1H), 3.97 (d, *J* = 9.1 Hz, 1H), 3.70 (ddd, *J* = 10.1, 7.6, 2.9 Hz, 1H), 3.57 (dd, *J* = 9.1, 3.9 Hz, 1H), 3.43 (dt, *J* = 22.2, 6.7 Hz, 1H), 3.22 (p, *J* = 6.9 Hz, 1H), 2.69 (tt, *J* = 6.8, 3.2 Hz, 1H).

^{13}C NMR: (126 MHz, $CDCl_3$) δ 141.00, 128.64, 126.79, 126.51, 88.66 (d, *J* = 225.0 Hz), 72.45, 66.51 (d, *J* = 6.6 Hz), 50.40 (d, *J* = 22.3 Hz), 42.17 (d, *J* = 22.6 Hz), 38.81 (d, *J* = 13.2 Hz).

^{19}F NMR: (376.5 MHz, $CDCl_3$) δ –176.5.

HRMS (ASAP-orbitrap) m/z: [M + H]+ Calcd for C12H14FO 193.1023; Found 193.1023.

5.5.4.d Oxygenation

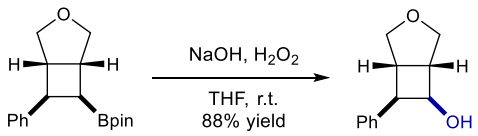

7-Phenyl-3-oxabicyclo[3.2.0]heptan-6-ol (5.29): A 25 mL round-bottomed flask was charged with **5.25a** (51.4 mg), dissolved in THF (3.0 mL), and cooled to 0 °C (ice/water). A 2:1 v/v mixture of 3.0 M NaOH(aq) and 30% H_2O_2 was prepared and degassed by gently sparging with N_2 over 1 min. This solution was added dropwise to the former while vigorously stirring, followed by warming to ambient temperature and allowing to react for 1 h. The reaction was quenched by the careful addition of NH_4Cl (saturated aqueous solution, 5 mL). The resulting mixture was extracted with EtOAc (15 mL × 3). The combined organics was dried over anhydrous $MgSO_4$, filtered, then concentrated by reduced pressure. The crude reaction was purified by flash chromatography with silica gel using a 15 – 20% EtOAc in hexanes elution gradient to afford 28.6 mg (88%) of the product as a colorless oil.

^{1}H NMR: (500 MHz, $CDCl_3$) δ 7.38 (t, *J* = 7.6 Hz, 2H), 7.32 – 7.26 (m, 3H), 4.25 (ddd, *J* = 7.7, 4.8, 3.0 Hz, 1H), 4.10 (d, *J* = 9.5 Hz, 1H), 3.96 (d, *J* = 9.4 Hz, 1H), 3.56 (ddd, *J* = 9.6, 5.6, 1.7 Hz, 2H), 3.43 (ddd, *J* = 7.0, 5.4, 1.2 Hz, 1H), 3.20 (dt, *J* = 8.4, 5.4 Hz, 1H), 2.87 (ddt, *J* = 8.5, 4.4, 2.9 Hz, 1H), 1.42 (d, *J* = 5.4 Hz, 1H).

^{13}C NMR: (126 MHz, $CDCl_3$) δ 137.6, 128.8, 128.7, 127.0, 73.3, 72.0, 71.6, 49.3, 48.1, 41.0.

HRMS (ASAP-orbitrap) m/z: [M + H]+ Calcd for C12H15O2 191.1067; Found 191.1065.

5.5.4.e Bromination

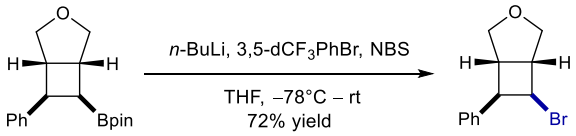

6-Bromo-7-phenyl-3-oxabicyclo[3.2.0]heptane (5.30): A flame-dried 50 mL round-bottomed flask was charged with the 1-bromo-3,5-bis(trifluoromethyl)benzene (150 mg, 0.50 mmol, 2.0 equiv) and dissolved in anhydrous THF (1.20 mL). The flask was cooled to –78 ºC (dry ice/acetone) followed by dropwise addition of *n*-BuLi (2.5 M in hexanes, 0.20 mL, 0.50 mmol, 2.0 equiv) and allowed to react for 1 h. A separate flame-dried, pear-shaped flask was charged with **5.25a** and dissolved in anhydrous THF (1.25 mL). This solution was added dropwise to the former ArLi mixture. and allowed to stir for 30 min at –78 ºC. The reaction was warmed to ambient temperature followed by stirring for 30 min. A second flame-dried, pear-shaped flask was charged with NBS (89.0 mg, 0.50 mmol, 2.0 equiv) and THF (1.25 mL) that was subsequently added dropwise to the reaction mixture. After stirring for 1 h, the reaction was quenched with NaS_2O_3 (20 wt% in H_2O, 5 mL) slowly –78 ºC and allowed to warm to rt. The mixture was extracted with EtOAc (15 mL × 3), dried over Na_2SO_4, and concentrated. The product was purified by flash column chromatography on silica gel using 5% EtOAc in hexanes as the eluent to afford 45.8 mg (72%) of the desired product as a colorless oil.

^{1}H NMR: (500 MHz, $CDCl_3$) δ 7.38 – 7.33 (m, 2H), 7.27 (dt, *J* = 7.1, 2.0 Hz, 3H), 4.68 (t, *J* = 8.3 Hz, 1H), 4.52 (dd, *J* = 10.1, 1.2 Hz, 1H), 3.96 (d, *J* = 9.2 Hz, 1H), 3.79 (dd, *J* = 10.1, 6.9 Hz, 1H),

3.57 (t, *J* = 7.46 Hz, 1H), 3.53 (dd, *J* = 9.2, 3.9 Hz, 1H), 3.22 (qt, *J* = 7.00, 1.50 Hz, 1H), 3.11 (td, *J* = 6.8, 3.9 Hz, 1H).

^{13}C NMR: (126 MHz, $CDCl_3$) δ 141.1, 128.7, 127.1, 126.2, 73.0, 71.0, 53.9, 50.7, 45.0, 43.0.

HRMS (ASAP-orbitrap) m/z: [M + H]+ Calcd for C12H14BrO 253.0223; Found 253.0220.

5.5.4.f Zweifel Olefination

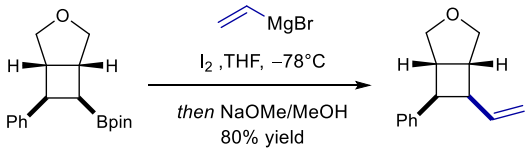

6-Phenyl-7-vinyl-3-oxabicyclo[3.2.0]heptane (5.31): Vinyl magnesium bromide (2.0 M in THF, 1.0 mL 1.00 mmol, 4.0 equiv) was added dropwise to a solution of **5.25a** (75 mg, 0.25 mmol, 1.0 equiv) in anhydrous THF (1.50 mL) at 0 °C (ice/water) and the resulting solution was stirred at ambient temperature for 30 min. The solution was cooled to –78 °C (dry ice/acetone) and then a solution of iodine (250 mg, 1.00 mmol, 4.0 equiv) in anhydrous THF (2.40 mL) was added dropwise before stirring for 20 min. A freshly prepared suspension of NaOMe (110 mg, 2.00 mmol, 8.0 equiv) in methanol (1.50 mL) was added in a single portion before warming to 0 °C and stirring for a further 30 min. $Na_2S_2O_3$ (saturated aqueous solution, 10 mL) was added, followed by DCM (15 mL). The phases were separated, and the aqueous phase was extracted with CH_2Cl_2 (2 × 10 mL). The combined organic phases were dried using anhydrous $MgSO_4$ and concentrated under reduced pressure. The product was purified by flash column chromatography on silica using a gradient of 5% EtOAc in hexanes as the eluent to afford 40.0 mg (80%) of a clear oil.

^{1}H NMR: (400 MHz, $CDCl_3$) δ 7.30 (dd, *J* = 8.5, 6.6 Hz, 2H), 7.22 – 7.15 (m, 3H), 5.49 (ddd, *J* = 17.6, 10.3, 7.8 Hz, 1H), 4.92 (dt, *J* = 17.2, 1.6 Hz, 1H), 4.85 (dt, *J* = 10.3, 1.5 Hz, 1H), 4.01 (t, *J* =

8.8 Hz, 2H), 3.62 (ddd, *J* = 11.4, 9.3, 5.5 Hz, 2H), 3.47 (dd, *J* = 9.9, 5.3 Hz, 1H), 3.22 – 3.14 (m, 1H), 3.09 – 3.01 (m, 1H), 2.90 (dt, *J* = 9.4, 5.3 Hz, 1H).

^{13}C NMR: (101 MHz, $CDCl_3$) δ 141.1, 138.9, 128.2, 128.1, 126.0, 114.4, 73.9, 73.7, 46.2, 45.5, 42.0.

HRMS (ASAP-orbitrap) m/z: [M + H]+ Calcd for C14H17O 201.1274; Found 201.1273.

5.5.4.g Matteson Homologation

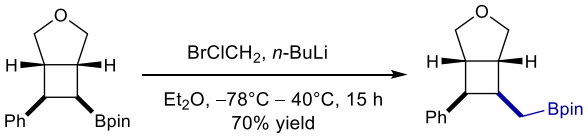

4,4,5,5-Tetramethyl-2-((-7-phenyl-3-oxabicyclo[3.2.0]heptan-6-yl)methyl)-1,3,2-dioxaborolane (5.32): A 25 mL flame-dried, round-bottomed flask was charged with **5.25a** (75.0 mg, 0.25 mmol, 1.0 equiv), bromochloromethane (41 µL, 0.62 mmol, 2.50 equiv), and dissolved in anhydrous Et_2O (2.50 mL) before cooling to –78 °C (dry ice/acetone). Next, *n*-BuLi (2.5 M in hexanes, 0.26 mL, 0.65 mmol, 2.60 equiv) was added dropwise before heating to reflux overnight. Following this, the mixture was cooled to ambient temperature, filtered through a silica plug with excess EtOAc, and concentrated. The product was purified by flash column chromatography on silica gel using an elution gradient of 5-10% EtOAc in hexanes to afford 54.6 mg (70%) of the product as a clear oil.

^{1}H NMR: (500 MHz, $CDCl_3$) δ 7.28 (t, *J* = 7.6 Hz, 2H), 7.22 – 7.14 (m, 3H), 4.02 (d, *J* = 9.1 Hz, 1H), 3.96 (d, *J* = 9.2 Hz, 1H), 3.57 (dt, *J* = 9.4, 4.9 Hz, 2H), 3.37 (dd, *J* = 9.1, 5.2 Hz, 1H), 3.13 (dt, *J* = 7.3, 5.4 Hz, 1H), 2.61 – 2.50 (m, 2H), 1.14 (s, 6H), 1.11 (s, 6H), 0.61 (dd, *J* = 16.0, 10.3 Hz, 1H), 0.49 (dd, *J* = 15.9, 6.2 Hz, 1H).

^{13}C NMR: (126 MHz, $CDCl_3$) δ 141.5, 128.6, 128.0, 125.9, 82.8, 74.0, 46.3, 45.2, 41.3, 37.7, 24.9, 24.6. The signal for the carbon attached to boron was not observed due to quadrupolar relaxation of the boron nucleus.

^{11}B NMR: (128.4 MHz, $CDCl_3$) δ 33.1.

HRMS (ASAP-orbitrap) m/z: [M + Na]+ Calcd for C19H17BO3Na 333.2232; Found 333.2224.

5.5.4.h Trifluoroborate Salt

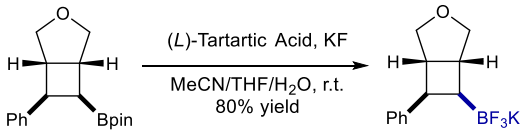

Trifluoro(-7-phenyl-3-oxabicyclo[3.2.0]heptan-6-yl)-l4-borane, potassium salt (5.33): A 24 mL vial was charged with **5.25a** (815.6 mg, 2.72 mmol, 1.0 equiv) and dissolved in a 1:1 mixture of MeOH/MeCN (20.0 mL). To this solution was added KF (631.5mg, 10.87 mmol, 4.0 equiv) in H_2O (2.40 mL) before stirring for 10 min. Following this, a solution of (*L*)-tartaric acid (857.0 mg, 5.71 mmol, 2.1 equiv) in THF (11.50 mL) was added to the reaction and stirred for 30 min. producing a white precipitate. (Note: Sonication was required to fully solubilize (*L*)-Tartaric Acid in THF.) The white solid was collected on a glass frit and washed with MeCN (3 × 10 mL). The solid was collected and dried under vacuum overnight to yield 605.6 mg (80%) of the desired product.

^{1}H NMR: (500 MHz, DMSO-d_6) δ 7.31 – 7.24 (m, 2H), 7.11 (t, *J* = 7.6 Hz, 2H), 7.02 – 6.94 (m, 1H), 3.70 (dd, *J* = 8.6, 1.7 Hz, 1H), 3.64 (d, *J* = 8.8 Hz, 1H), 3.56 (dd, *J* = 8.5, 6.4 Hz, 1H), 3.35 (dd, *J* = 8.9, 4.9 Hz, 1H), 3.12 (dd, *J* = 10.9, 6.7 Hz, 1H), 2.99 – 2.90 (m, 1H), 2.61 (q, *J* = 6.4 Hz, 1H), 1.22 (dq, *J* = 11.0, 5.5 Hz, 1H).

^{13}C NMR: (126 MHz, DMSO-d_6) δ 147.0, 128.6, 127.2, 124.5, 76.1, 73.5, 45.4, 44.0, 38.0. The signal for the carbon attached to boron was not observed due to quadrupolar relaxation of the boron nucleus.

^{19}F NMR: (376.5 MHz, $CDCl_3$) δ –137.6.

HRMS (ESI-orbitrap) m/z: [M – K]– Calcd for C12H13BF3O 241.1017; Found 241.1019.

5.5.4.i Metallophotoredox Cross-Coupling

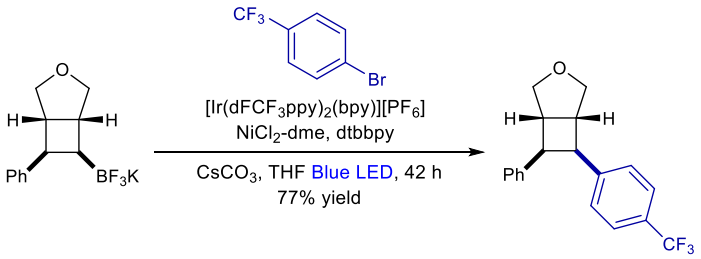

6-Phenyl-7-(4-(trifluoromethyl)phenyl)-3-oxabicyclo[3.2.0]heptane (5.34): A flame-dried Schlenk tube was charged with $NiCl_2$·dme (3.9 mg, 0.018 mmol, 0.10 equiv), 4,4'-di-*t*-butyl-2,2'-bipyridine (4.8 mg, 0.018 mmol, 0.10 equiv), and anhydrous THF (1.0 mL). The mixture was heated until completely homogenous, then concentrated to a pale evergreen solid by rotary evaporation. Compound **5.33** (74.9 mg, 0.267 mmol, 1.50 equiv), Ir(dF(CF_3)ppy)$_2$(bpy)(PF_6) (4.5 mg, 0.005 mmol, 0.025 equiv), and $CsCO_3$ (87.1 mg, 0.267 mmol, 1.50 equiv) were added to the Schlenk tube followed by the addition of dry dioxane (3.50 mL) and 1-bromo-4-(trifluoromethyl)benzene (40.1 mg, 0.178 mmol, 1.0 equiv) by syringe. The mixture was degassed by sparging with N_2 for 15 min. before being placed in a water bath and irradiated with a 427 nm P150 Kessil lamp with a fan blowing from above for 42 h. (*Note: This reaction was found to perform poorly at warm temperatures*.) Following this the crude reaction was filtered through a celite plug with excess EtOAc and concentrated by reduced pressure. The product was purified by

flash column chromatography on silica gel using an elution gradient of 10–20% EtOAc in hexanes to afford 43.9 mg (77%) of the desired product as a clear oil.

^{1}H NMR: (500 MHz, $CDCl_3$) δ 7.58 (d, *J* = 8.1 Hz, 2H), 7.37 (d, *J* = 8.0 Hz, 2H), 7.34 – 7.29 (m, 2H), 7.26 – 7.19 (m, 3H), 4.05 (d, *J* = 9.2 Hz, 1H), 3.85 (t, *J* = 9.4 Hz, 1H), 3.77 (dd, *J* = 10.1, 1.4 Hz, 1H), 3.66 (dd, *J* = 9.7, 6.6 Hz, 1H), 3.54 (dd, *J* = 9.2, 4.2 Hz, 1H), 3.49 (dd, *J* = 10.2, 6.8 Hz, 1H), 3.29 (dt, *J* = 9.1, 7.3 Hz, 1H), 3.15 (td, *J* = 7.0, 4.1 Hz, 1H).

^{13}C NMR: (126 MHz, $CDCL_3$) δ 144.5 (q *J* = 1.5 Hz), 143.9, 128.7 (q, *J* = 32.4 Hz), 128.6, 128.1, 126.5, 126.4, 125.4 (q, *J* = 3.8 Hz), 124.3 (q, *J* = 271.5 Hz), 73.0, 68.3, 46.1, 45.5, 44.1, 40.6.

^{19}F NMR: (376.5 MHz, $CDCl_3$) δ –62.4.

HRMS (ASAP-orbitrap) m/z: [M + H]+ Calcd for C19H18F3O 319.1304; Found 319.1301.

5.5.5 Mechanistic Studies

5.5.5.a Isomerization Experiments

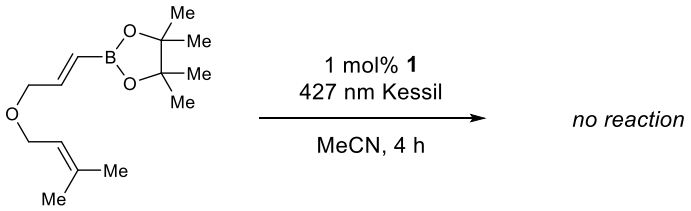

An oven-dried Schlenk tube was charged with **5.35** (49.3 mg, 0.198 mmol, 1.0 equiv.), **5.23** (1.7 mg, 1.0 mol%), and CH_3CN (4.0 mL, 0.05 M). The homogenous solution was degassed by sparging with N_2 for 15 min. before irradiating with a 427 nm Kessil lamp at a distance of 5 cm for 4 h. Next, 1,3,5-trimethoxybenzene (4.1 mg) was added as an internal standard and the crude mixture was concentrated by reduced pressure. The reaction was analyzed by quantitative ^{1}H NMR. This experiment resulted in no isomerization of the vinyl boronate ester (Figure 5.4).

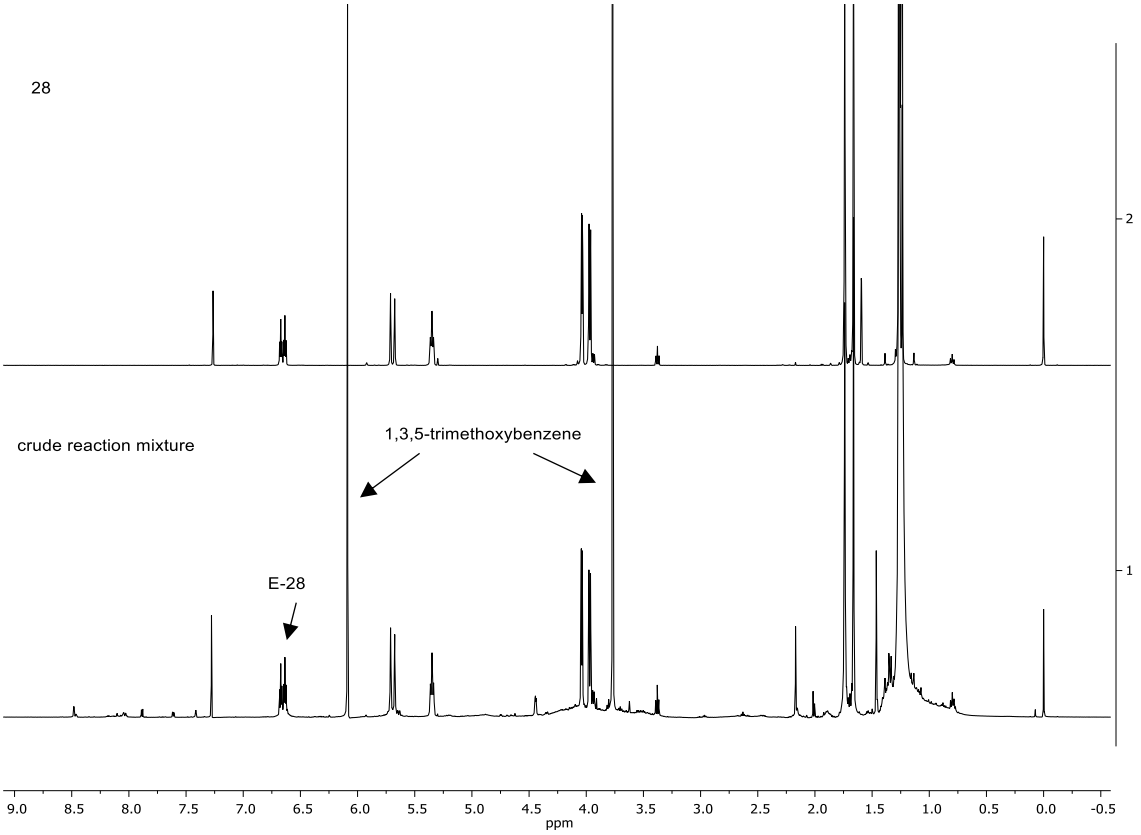

Figure 5.4. Isomerization experiment of **5.35** (**28**) using photocatalyst **5.23** as a photosensitizer.

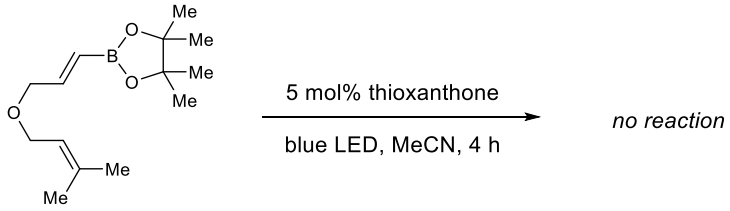

An oven-dried Schlenk tube was charged with **5.35** (74.1 mg, 0.294 mmol, 1.0 equiv.), thioxanthone (3.1 mg, 5.0 mol%), and CH_3CN (6 mL, 0.05 M). The homogenous solution was degassed by sparging with N_2 for 15 min. before irradiating with a 36W H150 Kessil lamp at a distance of 5 cm for 4 hours. Next, 1,3,5-trimethoxybenzene (6.5 mg) was added as an internal standard and the crude mixture was concentrated by reduced pressure. The reaction was analyzed

by quantitative ^{1}H NMR. This experiment resulted in no isomerization of the vinyl boronate ester (Figure 5.5).

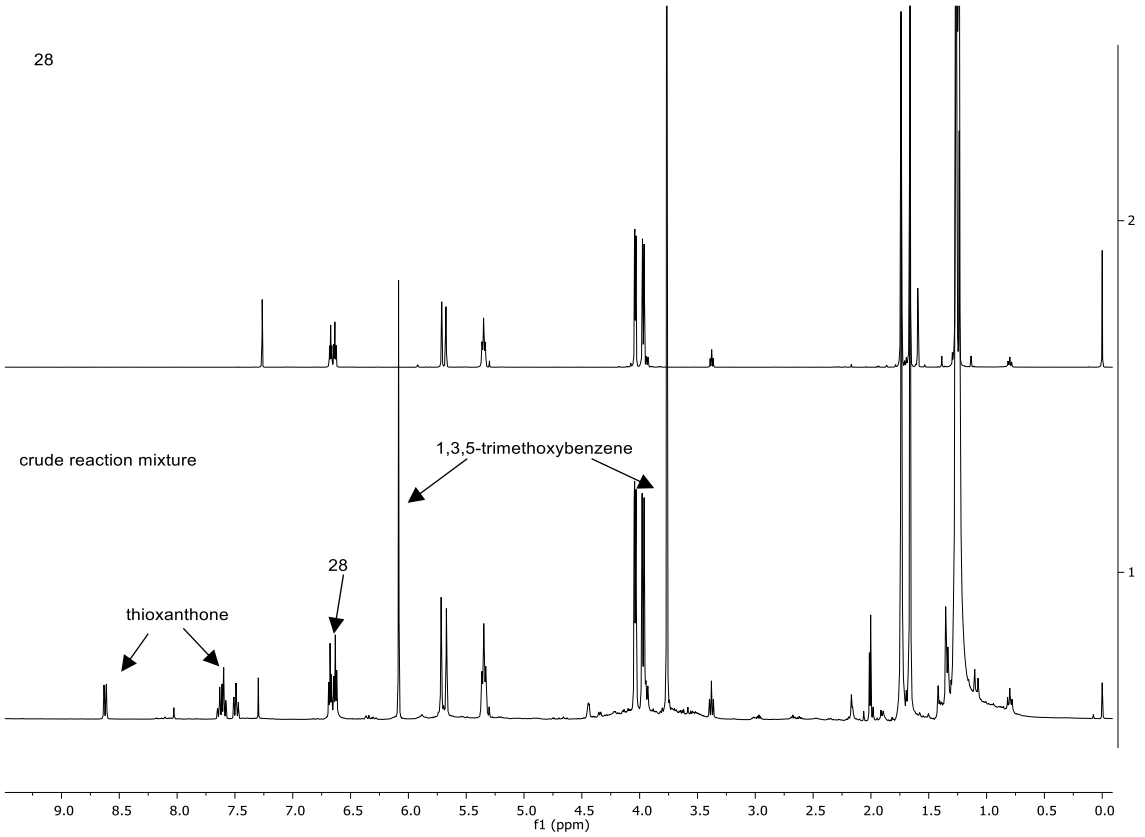

Figure 5.5. Isomerization experiment of **5.35** (**28**) using thioxanthone as a photosensitizer.

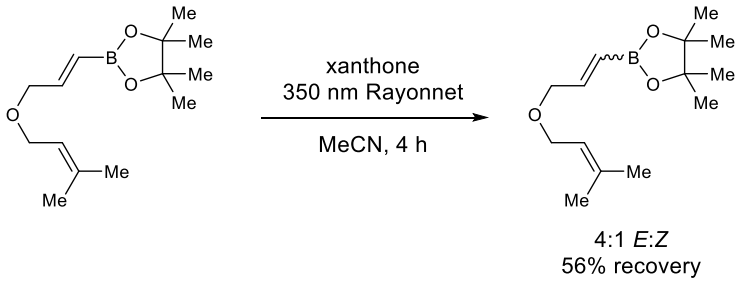

An oven-dried quartz tube was charged with **5.35** (16.8 mg, 0.0667 mmol, 1.0 equiv.), xanthone (13.1 mg, 0.0667 mmol, 1 equiv), and CH_3CN (1.33 mL, 0.05 M). The homogenous solution was

degassed by sparging with N_2 for 15 min. before irradiating with 350 nm light using a Rayonet reactor for 4 h. Next, phenanthrene (7.2 mg) was added as an internal standard and the crude mixture was concentrated by reduced pressure. The reaction was analyzed by quantitative ^1H NMR. This experiment resulted in an isomerization of **5.35** in a ratio of 4:1 *E*:*Z*., shown in Figure 5.6.

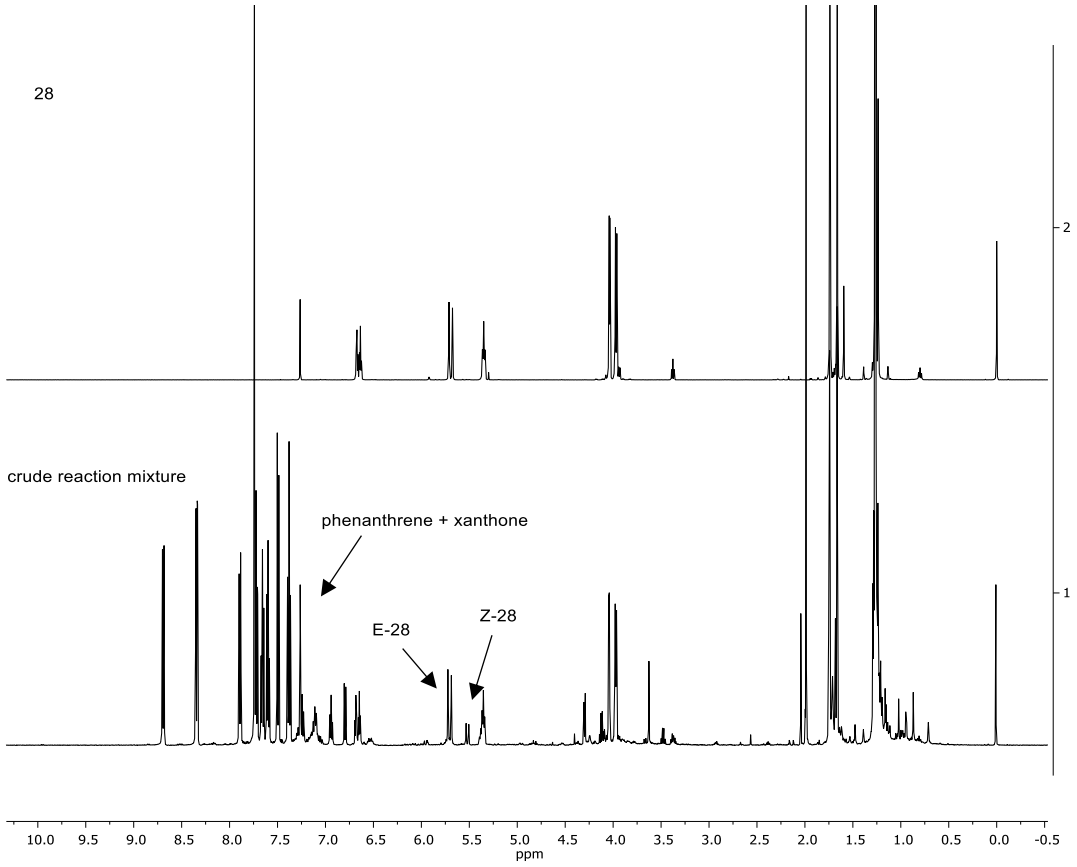

Figure 5.6. Isomerization experiment of **5.35** (**28**) using xanthone as a photosensitizer at 350 nm.

5.5.5.b Stern–Volmer Quenching Experiments

Stern–Volmer experiments were conducted as previously described.[88] Five separate solutions were prepared containing photocatalyst **5.23** (1.7 x 10^{-6} M) and **5.24a** (ranging from 0 to 7.8 x 10^{-3} M) in MeCN, and each was sparged with N_2 for 15 min. The solutions were irradiated at 410 nm, and the emission intensity (I) at 480 nm was compared to the initial emission intensity (I_0) at the same wavelength. This experiment was repeated in triplicate. The data points for the three experiments were averaged and the standard deviation is represented by error bars. These data result in a linear Stern–Volmer relationship (Figure 5.7), consistent with the proposed mechanism in which the photoexcited catalyst is quenched by substrate. Stern–Volmer luminescence quenching experiments for vinyl pinacol boronate ester **5.35** were conducted using the same procedure as outlined above. These data result in no correlation in luminescence intensity and concentration of **5.35** (Figure 5.8). The rate of quenching of was determined using the excited-state lifetime of photocatalyst **5.23** (2.3 μs) found by Bernhard and coworkers.[89]

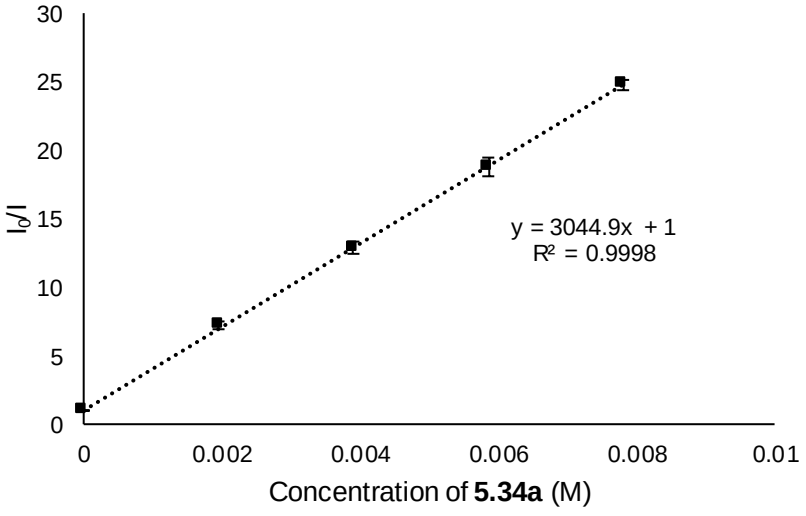

Figure 5.7. Stern–Volmer experiment for the quenching of photoexcited catalyst **5.23** by title substrate **5.24a**.

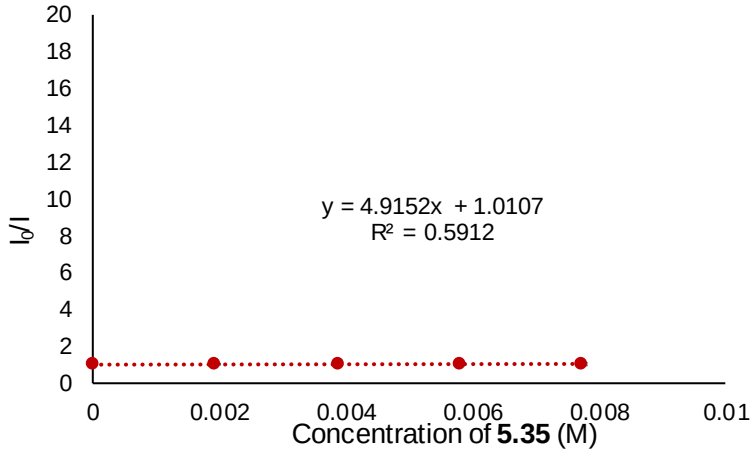

Figure 5.8. Stern–Volmer experiment for the quenching of photoexcited catalyst **5.23** by compound **5.35**.

5.5.5.c Cyclic Voltammetry Data

Cyclic voltammetry experiments were performed in MeCN with analyte (1 mM) and [(*n*-Bu)$_4$N]$^+$[PF$_6$]$^-$ (100 mM) using a glassy carbon working electrode, platinum wire counter electrode, a Ag/AgNO$_3$ MeCN reference electrode, and a scan rate of 50 mV/s. Ferrocene was added as an internal reference to SCE. As the redox event for substrate **5.24a** was irreversible, the peak potentials were used from the voltammogram (Figure 5.9). The decrease in current for the second cycle was shown to be consistent with electrode passivation.

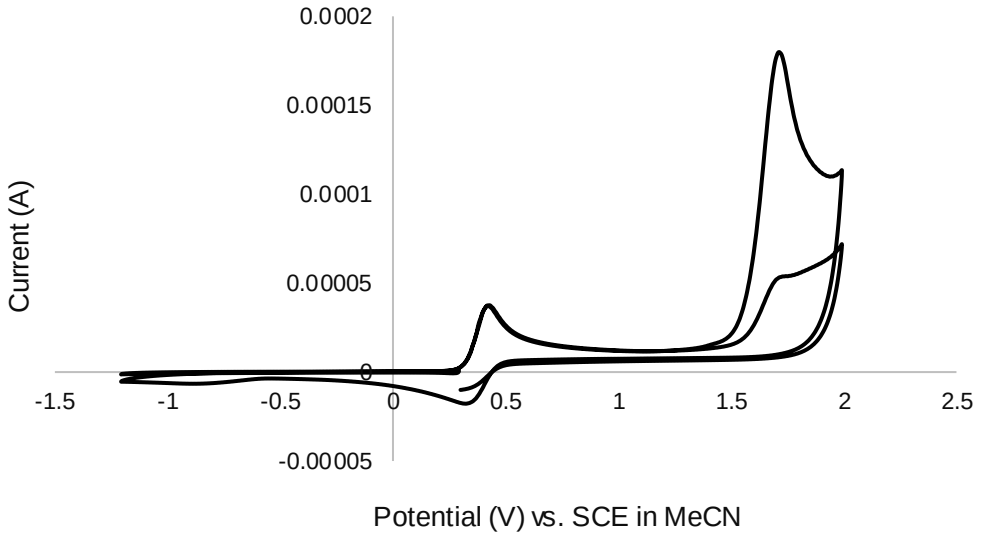

Figure 5.9. Cyclic voltammogram of title substrate **5.24a** and with ferrocene added.

Substrate **5.24a**: **5.24a /5.24a**$^{\bullet-}$ $E_{p/2} < -1.2$ V vs. SCE in MeCN
5.24a$^{\bullet+}$**/5.24a** $E_{p/2} = +1.73$ V vs. SCE in MeCN

5.6 References and Notes

[1] 2,738 Hits on Reaxys. https://www.reaxys.com (accessed March 6, 2021).

[2] Sergeiko, A.; Poroikov, V. V.; Hanus, L. O.; Dembitsky, V. M. Cyclobutane-Containing Alkaloids: Origin, Synthesis, and Biological Activites. *Open. Med. Chem. J.* **2008**, *2*, 26–37.

[3] 8 of 9 FDA approved drugs feature achiral or racemic cyclobutane. https://www.drugbank.ca (accessed March 6, 2021).

[4] Antonsen, S.; Østby, R. B.; Stenstrøm, Y. Naturally Occurring Cyclobutanes: Their Biological Significance and Synthesis. *Studies in Nat. Prod. Chem.* **2018**, *57*, 1–40.

[5] Li, J.; Gao, K.; Bian, M.; Ding, H. Recent advances in the total synthesis of cyclobutane-containing natural products. *Org. Chem. Front.*, **2020**, *7*, 136–154. *Angew. Chem. Int. Ed.* **2011**, *50*, 1000–1045.

[6] Hoffman, N. Photochemical Reactions as Key Steps in Organic Synthesis. *Chem. Rev.* **2008**, *108*, 1052–1103.

[7] Bach, T.; Hehn, J. P.; Photochemical Reactions as Key Steps in Natural Product Synthesis. *Angew. Chem. Int. Ed.* **2011**, *50*, 1000–1045.

[8] Poplata, S.; Tröster, A.; Zou, Y.; Bach, T.; Tröster, A.; Zou, Y.; Bach, T. Recent Advances in the Synthesis of Cyclobutanes by Olefin [2 + 2] Photocycloaddition Reactions. *Chem. Rev.* **2016**, *116*, 9748–9815.

[9] Xu, Y.; Conner, M. L.; Brown, M. K. Cyclobutane and Cyclobutene Synthesis: Catalytic Enantioselective [2+2] Cycloadditions. *Angew. Chem. Int. Ed.* **2015**, *54*, 11918–11928.

[10] Genzink, M. J.; Kidd, J. B.; Swords, W. B.; Yoon, T. P. Chiral Photocatalyst Structures in Asymmetric Photochemical Synthesis. *Chem. Rev.* **2021**

[11] Srebnik, M.; Ramachandran, V. P. The Utility of Chiral Organoboranes in the Preparation of Optically Active Compounds. *Aldrichimica Acta* **1987**, *20*, 9–24.

[12] Lennox, A. J. J.; Lloyd-Jones, G. C. Selection of Boron Reagents for Suzuki–Miyaura Coupling. *Chem. Soc. Rev.* **2014**, *43*, 412–443.

[13] Sandford, C.; Aggarwal, V. K. Stereospecific Functionalizations and Transformations of Secondary and Tertiary Boronic Esters. *Chem. Commun.* **2017**, *53*, 5481–5494.

[14] Fyfe, J. W. B.; Watson, A. J. B. Recent Developments in Organoboron Chemistry: Old Dogs, New Tricks. *Chem* **2017**, *3*, 31–55.

[15] Man, H. -W.; Hiscox, W. C.; Matteson, D. S. A highly enantioselective and diastereoselective synthesis of cyclobutanes via boronic esters. *Org. Lett.* **1999**, *1*, 379–381.

[16] Ito, H.; Toyoda, T.; Sawamura, M. Stereospecific Synthesis of Cyclobutylboronates through Copper(I)-Catalyzed Reaction of Homoallylic Sulfonates and a Diboron Derivative. *J. Am. Chem. Soc.* **2010**, *132*, 5990–5992.

[17] Hong, K.; Liu, X.; Morken, J. P. Simple Access to Elusive α-Boryl Carbanions and Their Alkylation: An Umpolung Construction for Organic Synthesis. *J. Am. Chem. Soc.*, **2014**, *136*, 10581–10584.

[18] Whyte, A.; Mirabi, B.; Torelli, A.; Prieto, L.; Bajohr, J.; Lautens, M. Asymmetric Synthesis of Boryl-Functionalized Cyclobutanols. *ACS Catal.* **2019**, *9*, 9253–9258

[19] Shu, C.; Noble, A.; Aggarwal, V. K. Photoredox-Catalyzed Cyclobutane Synthesis by a Deboronative Radical Addition–Polar Cyclization Cascade. *Angew. Chem. Int. Ed.* **2019**, *58*, 3870–3874

[20] Fawcett, A.; Biberger, T.; Aggarwal, V. K. Carbopalladation of C–C σ-bonds enabled by strained boronate complexes. *Nat. Chem.* **2019**, *11*, 117–122.

[21] Silvi, M.; Aggarwal, V. K. Radical Addition to Strained σ-Bonds Enables the Stereocontrolled Synthesis of Cyclobutyl Boronic Esters. *J. Am. Chem. Soc.* **2019**, *141*, 9511–9515.

[22] Kondo, M.; Kanazawa, J.; Ichikawa, T.; Shimokawa, T.; Nahashima, Y.; Miyamoto, K.; Uchiyama, M. Silaboration of [1.1.1] Propellane: A Storable Feedstock for Bicyclo-[1.1.1] pentane Derivatives. *Angew. Chem. Int. Ed.* **2020**, *59*, 1970–1974.

[23] Hari, D. P.; Abell, J. C.; Fasano, V.; Aggarwal, V. K. Ring-Expansion Induced 1,2-Metalate Rearrangements: Highly Diastereoselective Synthesis of Cyclobutyl Boronic Esters. *J. Am. Chem. Soc.* **2020**, *142*, 5515–5520.

[24] Davenport, R.; Silvi, M.; Noble, A.; Hosni, Z.; Fey, N.; Aggarwal, V. K. Visible-Light-Driven Strain-Increase Ring Contraction Allows the Synthesis of Cyclobutyl Boronic Esters. *Angew. Chem. Int. Ed.* **2020**, *59*, 6525–6528.

[25] Brener, L.; Brown, H. C. Hydroboration. 47. Unique stereospecificity of the hydroboration of 1,3-dimethylcycloalkenes with 9-borabicyclo[3.3.1]nonane. *J. Org Chem.* **1977**, *42*, 2702–2704.

[26] Guisán-Ceinos, M.; Parra, A.;Martín-Heras, V.; Tortosa, M. Enantioselective Synthesis of Cyclobutylboronates via a Copper-Catalyzed Desymmetrization Approach. *Angew. Chem. Int. Ed*. **2016**, *55*, 6969 –6972.

[27] Mercer, J. A. M.; Cohen, C. M., Shuken, S. R.; Wagner, A. M.; Smith, M. W., Moss, F. R.; Smith, M. D., Vuhala, R.; Gonzalez-Martinez, A.; Boxer, S. G.; Burns, N. Z. Chemical Synthesis and Self-Assembly of a Ladderane Phospholipid. *J. Am. Chem. Soc.* **2016**, *138*, 15845–15848.

[28] Logan, K. M.; Brown, M. K. Catalytic Enantioselective Arylboration of Alkenylarenes. *Angew. Chem. Int. Ed*. **2017**, *56*, 851–855.

[29] Clement, H. A.; Boghi, M.; McDonald, R. M.; Bernier, L.; Coe, J. W.; Farrell, W.; Helal, C. J.; Reese, M. R.; Sach, N. W.; Lee, J. C.; Hall, D. G. High-Throughput Ligand Screening Enables the Enantioselective Conjugate Borylation of Cyclobutenones to Access Synthetically Versatile Tertiary Cyclobutylboronates. *Angew. Chem. Int. Ed*. **2019**, *58*, 18405–18409.

[30] Parsutkar, M. M.; Pagar, V. V.; RajanBabu, T. V. Catalytic Enantioselective Synthesis of Cyclobutenes from Alkynes and Alkenyl Derivatives. *J. Am. Chem. Soc*. **2019**, *141*, 15367–15377.

[31] Hancock, E. N.; Kuker, E. L.; Tantillo, D. J.; Brown, M. K. Lessons in Strain and Stability: Enantioselective Synthesis of (+)-[5]-Ladderanoic Acid. *Angew. Chem. Int. Ed*. **2020**, *59*, 436–441.

[32] Atack, T. C.; Lecker, R. M.; Cook, S. P. Iron-Catalyzed Borylation of Alkyl Electrophiles. *J. Am. Chem. Soc*. **2014**, *136*, 9521–9523.

[33] Zhou, X. -F.; Wu, Y. -D.; Dai, J. -J.; Li, Y. -J.; Huang, Y.; Xu, H. -J. Borylation of primary and secondary alkyl bromides catalyzed by Cu2O nanoparticles. *RSC Adv*. **2015**, *5*, 46672–46676.

[34] Hu, D.; Wang, L.; Li, P. Decarboxylative Borylation of Aliphatic Esters under Visible-Light Photoredox Conditions. *Org. Lett.* **2017**, *19*, 2770–2773.

[35] Melnykov, K. P.; Granat, D. S.; Volochnyuk, D. M.; Ryabukhim, S. V.; Grygorenko, O. O. Multigram Synthesis of C4/C5 3,3-Difluorocyclobutyl-Substituted Building Blocks. *Synthesis* **2018**, *50*, 4949–4957.

[36] Beck, J. C.; Lacker, C. R.; Chapman, L. M.; Reisman, S. E. A modular approach to prepare enantioenriched cyclobutanes: synthesis of (+)-rumphellaone A. *Chem. Sci.* **2019**, *10*, 2315–2319.

[37] Chernykh, A. V.; Melnykov, K. P.; Tolmacheva, N. A.; Kondratov, I. S.; Radchenko, D. S.; Daniliuc, C. G.; Volochnyuk, D. M.; Ryabukhin, S. V.; Kuchkovska, Y. O.; Grygorenko, O. O. Last of the *gem*-Difluorocycloalkanes: Synthesis and Characterization of 2,2-Difluorocyclobutyl-Substituted Building Blocks. *J. Org. Chem.* **2019**, *13*, 8487–8496.

[38] Murakami, R.; Tsunoda, K.; Iwai, T.; Sawamura, M. Stereoselective C–H Borylations of Cyclopropanes and Cyclobutanes with Silica-Supported Monophosphane–Ir Catalysts. *Chem. Eur. J.* **2014**, *20*, 13127–13131.

[39] He, J.; Shao, Q.; Wu, Q.; Yu, J. -Q. Pd(II)-Catalyzed Enantioselective C(sp3)–H Borylation. *J. Am. Chem. Soc.* **2017**, *139*, 3344–3347.

[40] Oeschger, R.; Su, B.; Yu, I.; Ehinger, C.; Romero, E.; He, S.; Hartwig, J. Diverse Functionalization of Strong Alkyl C – H Bonds by Undirected Borylation. *Science* **2020**, *3*, 736–741.

[41] Fish, R. H. The Cycloaddition of Diphenylketene to 2-Vinyl-4,6,6-trimethyl-1,3,2-dioxaborinane. *J. Org. Chem.* **1969**, *34*, 1127–1128.

[42] Conner, M. L.; Brown, M. K. Synthesis of 1,3-Substituted Cyclobutanes by Allenoate-Alkene [2+2] Cycloaddition. *J. Org. Chem.* **2016**, *81*, 8050–8060.

[43] Giustra, Z. X.; Yang, X.; Chen, M.; Bettinger, H. F.; Liu, S. -Y. Accessing 1,2-Substituted Cyclobutanes through 1,2-Azaborine Photoisomerization. *Angew. Chem. Int. Ed.* **2019**, *58*, 18918–18922.

[44] Hollis, W. G.; Lappenbisch, W. C.; Everberg, K. A.; Woleben, C. M. The Use of Alkenylboronate Esters in [2+2] Enone-Olefin Photocycloadditions. *Tetrahedron Lett.* **1993**, *34*, 7517–7520.

[45] Kleinnijenhuis, R. A.; Timmer, B. J. J.; Lutteke, G.; Smits, J. M. M.; de Gelder, R.; van Maarseveen, J. H.; Hiemstra, H. Formal Synthesis of Solanoeclepin A: Enantioselective Allene Diboration and Intramolecular [2+2] Photocycloaddition for the Construction of the Tricyclic Core. *Chem. Eur. J.* **2016**, *22*, 1266–1269.

[46] Coote, S. C.; Bach, T. Enantioselective Intermolecular [2+2] Photocycloadditions of Isoquinolone Mediated by a Chiral Hydrogen-Bonding Template. *J. Am. Chem. Soc.* **2013**, *135*, 14948–14951.

[47] Coote, S. C.; Pöthig, A.; Bach, T. Enantioselective Template Directed [2+2] Photocycloadditions of Isoquinolones: Scope, Mechanism and Synthetic Applications. *Chem. Eur. J.* **2015**, *21*, 6906.

[48] Demchuk, O. P.; Hryshchuk, O. V.; Vashchenko, B. V.; Kozytskiy, A. V.; Tymtsunik, A. V.; Komarov, I. V.; Grygorenko, O. O. Photochemical [2+2] Cycloaddition of Alkenyl Boronic Acid Derivatives: An Entry into 3-Azabicyclo[3.2.0]heptane Scaffold. *J. Org. Chem.* **2020**, *85*, 5927−5940.

[49] Strieth-Kalthoff, F.; James, M. J.; Teders, M.; Pitzer, L.; Glorius, F. Energy Transfer Catalysis Mediated by Visible Light: Principles, Applications, Directions. *Chem. Soc. Rev.* **2018**, *47*, 7190–7202.

[50] Zhou, Q.-Q.; Zou, Y.-Q.; Lu, L.-Q.; Xiao, W.-J. Visible-Light-Induced Organic Photochemical Reactions through Energy-Transfer Pathways. *Angew. Chem. Int. Ed.* **2019**, *58*, 1586–1604.

51 Großkopf, J.; Kratz, T.; Rigotti, T.; Bach, T. Enantioselective Photochemical Reactions Enabled by Triplet Energy Transfer. *Chem. Rev.* **2021** https://doi.org/10.1021/acs.chemrev.1c00272

[52] Kalyanasundaram, K. Photophysics, Photochemistry and Solar Energy Conversion with Tris(bipyridyl)ruthenium(II) and Its Analogues. *Coord. Chem. Rev.* **1982**, *46*, 159–244.

[53] You, Y.; Nam, W. Photofunctional Triplet Excited States of Cyclometalated Ir(III) Complexes: Beyond Electroluminescence. *Chem. Soc. Rev.* **2012**, *41*, 7061–7084.

[54] Lu, Z.; Yoon, T. P. Visible Light Photocatalysis of [2+2] Styrene Cycloadditions by Energy Transfer. *Angew. Chem. Int. Ed.* **2012**, *51*, 10329–10332.

[55] Hurtley, A. E.; Lu, Z.; Yoon, T. P. Cycloaddition of 1,3-Dienes by Visible Light Photocatalysis. *Angew. Chem. Int. Ed.* **2014**, *53*, 8991–8994.

[56] Duret, G.; Quinlan, R.; Bisseret, P.; Blanchard, N. Boron Chemistry in a New Light. *Chem. Sci.* **2015**, *6*, 5366–5382.

[57] Koike, T.; Akita, M. Combination of Organotrifluoroborates with Photoredox Catalysis Marking a New Phase in Organic Radical Chemistry. *Org. Biomol. Chem.* **2016**, *14*, 6886–6890.

[58] Hitosugi, S.; Tanimoto, D; Nakamishi, W.; Isobe, H. A Facile Chromatographic Method for the Purification of Pinacol Boronic Esters. *Chem. Lett.* **2012**, *41*, 972–973.

[59] Tellis, J. C.; Primer, D. N.; Molander, G. A. Single-Electron Transmetalation in Organoboron Cross-Coupling by Photoredox/Nickel Dual Catalysis. *Science* **2014**, *345*, 433–436.

[60] Tellis, J. C.; Kelly, C. B.; Primer, D. N.; Jouffroy, M.; Patel, N. R.; Molander, G. A. Single-Electron Transmetalation via Photoredox/Nickel Dual Catalysis: Unlocking a New Paradigm for sp3–sp2 Cross-Coupling. *Acc. Chem. Res*. **2016**, *49*, 1429–1439.

[61] Rasappan, R.; Aggarwal. V. L.; Synthesis of hydroxyphthioceranic acid using a traceless lithiation-borylation-protodeboronation strategy. *Nat. Chem*. **2014**, *6*, 810–814.

[62] NIH. U.S. National Library of Medicine. National Center for Biotechnology Information. Belaperidone. https://pubchem.ncbi.nlm.nih.gov/compound/Belaperidone (accessed March 20, 2020).

[63] Bonet, A.; Odachowski, M.; Leonori, D.; Essafi, D.; Aggarwal, V. K. Enantiospecific sp2–sp3 coupling of secondary and tertiary boronic esters. *Nat. Chem.* **2014**, *6*, 584–589.

[64] Li, Z.; Wang, Z.; Zhu, L.; Tan, X.; Li, C. Silver-Catalyzed Radical Fluorination of Alkylboronates in Aqueous Solution. *J. Am. Chem. Soc.* **2014**, *136*, 16439–16443.

[65] Larouche-Gauthier, R.; Elford, T. G.; Aggarwal, V. K. Ate Complexes of Secondary Boronic Esters as Chiral Organometallic-Type Nucleophiles for Asymmetric Synthesis. *J. Am. Chem. Soc*. **2011**, *133*, 16794–16797.

[66] Zweifel, G.; Arzoumanian, H.; Whitney, C. C. A Convenient Stereoselective Synthesis of Substituted Alkenes via Hydroboration-Iodination of Alkynes. *J. Am. Chem. Soc.* **1967**, *89*, 3652–3653.

[67] Matteson, D. S.; Mah, R. W. H. Neighboring Boron in Nucleophilic Displacement. *J. Am. Chem. Soc*. **1963**, *85*, 2599–2603.

[68] Bagutski, V.; Ros, A.; Aggarwal, V. K. Improved method for the conversion of pinacolboronic esters into trifluoroborate salts. Facile synthesis of chiral and tertiary trifluoroborates. *Tetrahedron* **2009**, *65*, 9956–9960.

[69] Molloy, J. J.; Metternich, J. B.; Daniliuc, C. G.; Watson, A. J. B.; Gilmour, R. Contra-Thermodynamic, Photocatalytic *E*→*Z* Isomerization of Styrenyl Boron Species: Vectors to Facilitate Exploration of Two-Dimensional Chemical Space. *Angew. Chem. Int. Ed*. **2018**, *57*, 3168–3172.

[70] Molloy, J. J.; Schäfer, M.; Wienhold, M.; Morack, T.; Daniliuc, C. G.; Gilmour, R. Boron-enabled geometric isomerization of alkenes via selective energy-transfer catalysis. *Science* **2020**, *369*, 302–306.

[71] Romero, N. A.; Nicewicz, D. A. Organic Photoredox Catalysis. *Chem. Rev.* **2016**, *116*, 10075–10166.

[72] Lowry, M. S.; Goldsmith, J. I.; Slinker, J. D.; Rohl, R.; Pascal, R. A.; Malliaras, G. G.; Bernhard, S. Single-Layer Electroluminescent Devices and Photoinduced Hydrogen Production from an Ionic Iridium(III) Complex. *Chem. Mater.* **2005**, *17*, 5712–5719.

[73] Pangborn, A. B.; Giardello, M. A.; Grubbs, R. H.; Rosen, R. K.; Timmers, F. T. Safe and Convenient Procedure for Solvent Purification. *Organometallics* **1996**, *15*, 1518.

[74] Lowry, M. S.; Goldsmith, J. I.; Slinker, J. D.; Rohl, R.; Pascal, R. A.; Malliaras, G. G.; Bernhard, S. Single-Layer Electroluminescent Devices and Photoinduced Hydrogen Production from an Ionic Iridium(III) Complex. *Chem. Mater.* **2005**, *17*, 5712.

[75] Hitosugi, S.; Tanimoto, D; Nakamishi, W.; Isobe, H. A Facile Chromatographic Method for the Purification of Pinacol Boronic Esters. *Chem. Lett.* **2012**, *41*, 972–973.

[76] Cecchini, C.; Lanzi, M.; Cera, G.; Malacria, M.; Maestri, G. Complementary Reactivity of 1,6-Enynes with All-Metal Aromatic Trinuclear Complexes and Carboxylic Acids. *Synth.* **2019**, *51*, 1216–1224.

[77] Nishimura, T.; Takiguchi, Y.; Maeda, Y.; Hayashi, T. *Adv. Synth. Catal.* **2013**, *355* (7), 1374–1382.

[78] Vaghi, L.; Benincori, T.; Cirilli, R.; Alberico, E.; Mussini, P. R.; Pierini, M.; Pilati, T.; Rizzo, S.; Sannicolò, F. *European J. Org. Chem.* **2013**, *2013* (36), 8174–8184.

[79] Hatial, I.; Das, J.; Ghosh, A. K.; Basak, A. Base-Induced Cyclization of Propargyl Alkenylsulfones: A High-Yielding Synthesis of 4,5-Disubstituted 2*H*-Thiopyran 1,1-Dioxides. *Eur. J. Org. Chem.* **2015**, 6017–6024.

[80] Harris, R. K.; Becker, E. D.; Cabral de Menezes, S. M.; Goodfellow, R.; Granger, P. NMR Nomenclature. Nuclear Spin Properties and Conventions for Chemical Shifts (IUPAC Recommendations 2001. *Pure Appl. Chem.* **2001**, *73*, 1795–1818; Harris, R. K; Becker, E. D.; Cabral de Menezes, S. M.; Granger, P.; Hoffman, R. E.; Zilm, K. W. Further Conventions for NMR Shielding and Chemical Shifts (IUPAC Recommendations 2008. *Pure Appl. Chem*, **2008**, *80*, 59–84.

[81] Huple, D. B.; Mokar, B. D.; Liu, R. S. Alkene-Directed N-Attack Chemoselectivity in the Gold-Catalyzed [2+2+1]-Annulations of 1,6-Enynes with N-Hydroxyanilines. *Angew. Chem. Int. Ed.* **2015**, *54*, 14924.

[82] Hayashi, N.; Hirokawa, Y.; Shibata, I.; Yasuda, M.; Baba, A. Hydroindation of Allenes and Its Application to Radical Cyclization. *Org. Biomol. Chem.* **2008**, *6*, 1949.

[83] Reichl, K. D.; Dunn, N. L.; Fastuca, N. J.; Radosevich, A. T. Biphilic Organophosphorus Catalysis: Regioselective Reductive Transposition of Allylic Bromides via PIII/PV Redox Cycling. *J. Am. Chem. Soc.* **2015**, *137*, 5292.

[84] Luo, J.; Theron, R.; Sewell, L. J.; Hooper, T. N.; Weller, A. S.; Oliver, A. G.; McIndoe, J. S. Rhodium-Catalyzed Selective Partial Hydrogenation of Alkynes. *Organometallics* **2015**, *34*, 3021

[85] Curti, C.; Sartori, A.; Battistini, L.; Brindani, N.; Rassu, G.; Pelosi, G.; Lodola, A.; Mor, M.; Casiraghi, G.; Zanardi, F. Pushing the Boundaries of Vinylogous Reactivity: Catalytic Enantioselective Mukaiyama Aldol Reactions of Highly Unsaturated 2-Silyloxyindoles. *Chem. Eur. J.* **2015**, *21*, 6433

[86] Deboef, B.; Counts, W. R.; Gilbertson, S. R. Rhodium-Catalyzed Synthesis of Eight-Membered Rings. *J. Org. Chem.* **2007**, *72*, 799.

[87] Moure, A. L.; Mauleón, P.; Arrayás, R. G.; Carretero, J. C. Formal Regiocontrolled Hydroboration of Unbiased Internal Alkynes via Borylation/Allylic Alkylation of Terminal Alkynes. *Org. Lett.* **2013**, *15*, 2054–2057.

[88] Cismesia, M. A.; Yoon, T. P. Characterizing chain processes in visible light photoredox catalysis. *Chem. Sci.* ***2015***, *6*, 5426–5434.

[89] Lowry, M. S.; Goldsmith, J. I.; Slinker, J. D.; Rohl, R.; Pascal, R. A.; Malliaras, G. G.; Bernhard, S. Single-Layer Electroluminescent Devices and Photoinduced Hydrogen Production from an Ionic Iridium(III) Complex. *Chem. Mater.* 2005, *17*, 5712–5719.

Appendix A. Investigation of Photosensitized Transposed Paternò–Büchi Reactions

A.1 Introduction

Our mechanistic investigations in Chapter 4 suggest that scalemic oxetane formation may arise by static energy transfer to the hydrogen bound quinolone and subsequent cycloaddition with ground state α-ketoester. The feasibility of this alternative transposed Paternò–Büchi reaction (Scheme A.1) in which the cycloaddition is initiated by the triplet (π,π*) of **A.11** was investigated.

Scheme A.1. Proposed of Transposed Paternò–Büchi Reaction

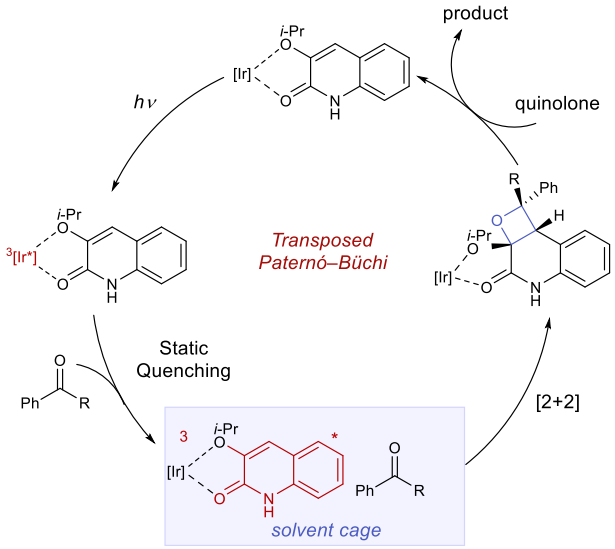

Few examples of such reactivity have been reported. In 2017, Sivaguru and coworkers demonstrated an atropospecific transposed Paternò–Büchi reaction of **A.1** (Scheme A.2A).[1] The authors provided mechanistic rationale that this reaction proceeds by sensitization of the enamide followed by its subsequent intramolecular [2+2] photocycloaddition with the proximal carbonyl, affording oxetane **A.2** in appreciable yield. Notably, hydrazones and oximes were shown to be proficient reaction partners for the analogous aza Paternò–Büchi to form azetidines.[2] The Schindler group disclosed a comparable visible-light intramolecular cycloaddition of oxime-tethered styrenes activated by DET from an iridium photocatalyst.[3] In addition to these strategies,

tripyrazole (Tp) ligated Cu(I)–Norbornene complexes, reported by Flores and Schmidt, have been shown to undergo intermolecular carbonyl–olefin [2+2] photocycloadditions (Scheme A.2B).[4,5] However, this chemistry is exclusive to aliphatic ketones and norbornene. Despite these recent advances, a generalizable intermolecular transposed Paternò–Büchi reaction has yet to be reported.

Scheme A.2. Examples of Transposed Paternò–Büchi Reactions

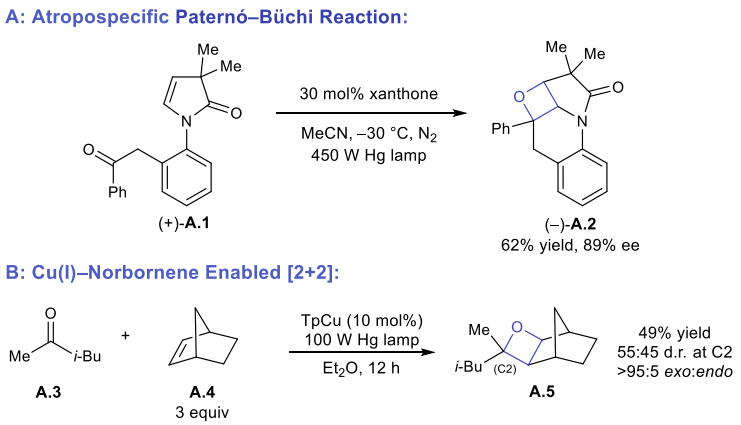

A.2 Results and Discussion

Thus, we commenced our investigation of this alternate mechanistic cycle by replacing the sensitizable α-ketoester with benzophenone, a substrate with a triplet energy (69 kcal/mol)[6] in which energy transfer from the photoexcited catalyst is thermodynamically uphill (Figure A.1). To our surprise, at room temperature, quinolone **A.11** was found to react smoothly to afford oxetane **A.6** in 42%. Next, a preliminary screen was performed to determine the breadth of carbonyls amenable to this mode of reactivity (Scheme A.3). Benzaldeyhde (**A.7**), furfural (**A.8**), and 1,2-cyclohexadione (**A.9**) all reacted with good yield, demonstrating the potential of this transposed Paternò–Büchi reaction as a broadly applicable disconnection for the formation of diverse oxetanes. Furthermore, an electron-rich pyridyl styene was found to be a competent alkene

coupling partner, reacting with benzaldehyde producing **A.10** in an appreciable yield. Unsuccessful carbonyl substrates include acetophenone, cyclohexanone, and valeraldehyde.

Figure A.1. Steady-State Stern–Volmer experiment for the quenching of photoexcited catalyst **4.49f** by benzophenone

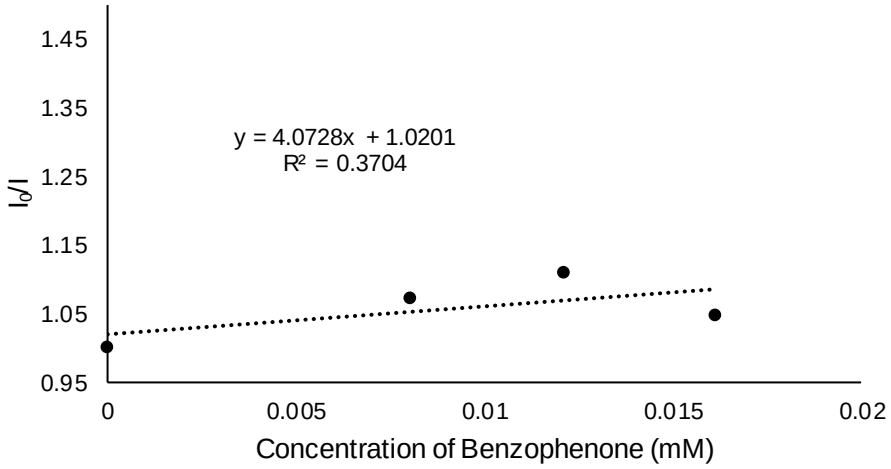

Scheme A.3. Proof-of-Concept Transposed Paternò–Büchi Reactions

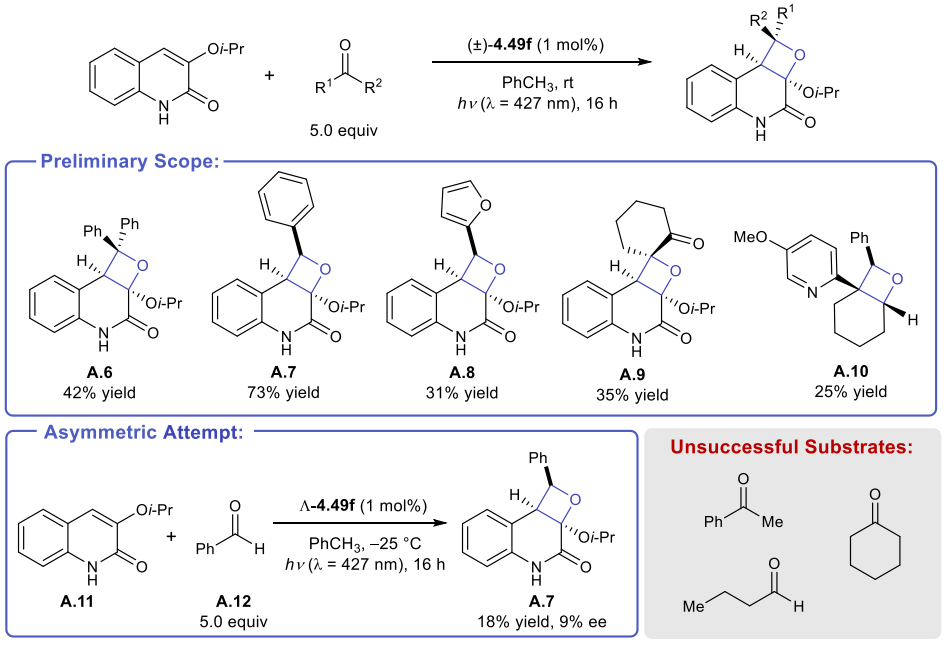

After demonstrating this proof-of-principle, we attempted to render this reaction enantioselective. Unfortunately, conducting the cycloaddition at room temperature resulted in racemic product, and the reaction rate is significantly slowed at cryogenic temperatures. Nonetheless, using the optimal chiral photocatalyst used in Chapter 4 (Λ-**4.49f**), With 5 equivalents of benzaldehyde the cycloaddition progressed sluggishly with **A.11** in 9% ee at –25 °C. Mechanistically, this implies that an enantioselective transposed Paternò–Büchi is possible for the title reaction in Chapter 4, although further research would be required to optimize this lead result.

A.3 References

[1] Kumarasamy, E.; Raghunathan, R.; Kandappa, S. K.; Sreenithya, A.; Jockusch, S.; Sunoj, R. B.; Sivaguru, J. Transposed Paternò-Büchi reaction. *J. Am. Chem. Soc*. **2017**, *139*, 655–662.

[2] Kumarasamy, E.; Kandappa, S. K.; Raghunathan, R.; Jockusch, S.; Sivaguru, J. Realizing an Aza Paternò–Büchi Reaction. *Angew. Chem Int. Ed*. **2017**, *56*, 7056–7061.

[3] Becker, M. R.; Richardson, A. D.; Schindler, C. S. Functionalized Azetidines Via Visible-Light Enabled Aza Paternò–Büchi Reactions. *Nat. Commun*. **2019**, *10*, 1–8.

[4] Flores, D. M.; Schmidt, V. A. Intermolecular 2+2 Carbonyl–Olefin Photocycloadditions Enabled by Cu(I)–Norbornene MLCT. *J. Am. Chem. Soc*. **2019**, *141*, 8741–8745.

[5] Flores, D. M.; Neville, M. L.; Schmidt, V. A. Intermolecular 2+2 Imine-Olefin Photocycloadditions Enabled by Cu(I)-Alkene MLCT. *ChemRxix* **2021**. DOI: 10.33774/chemrxiv-2021-t45sg.

[6] Turro, N. J.; Ramaurthy, V.; Scaiano, J. C. *Modern Molecular Photochemistry of Organic Molecules;* University Science Books: Sausalito, CA, 2010; pp 621.

Appendix B. ^{1}H, ^{13}C, ^{19}F, and ^{11}B NMR Spectra of New Compounds

B.1 List of New Compounds for Chapter 2

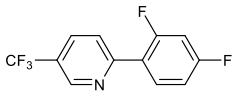

2.33

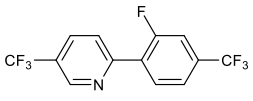

2.34

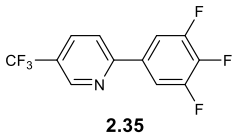

2.35

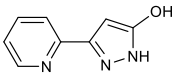

2.42

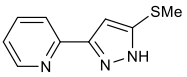

2.43

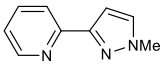

2.46

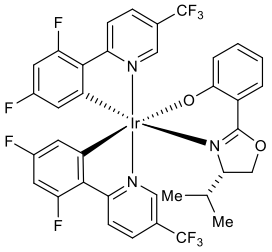

(*S*),Λ-**2.50**

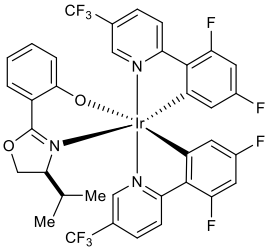

(*S*),Δ-**2.50**

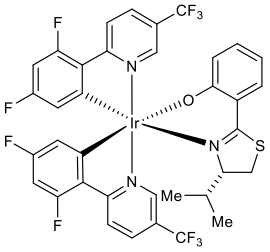

(*S*),Λ-**2.51**

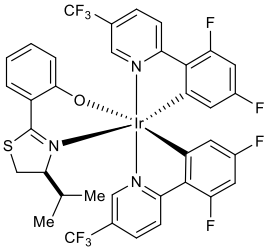

(*S*),Δ-**2.51**

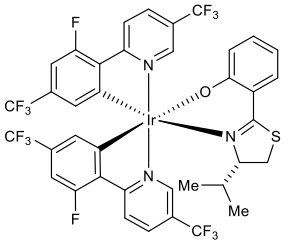

(*S*),Λ-**2.52**

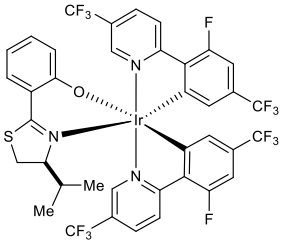

(*S*),Δ-**2.52**

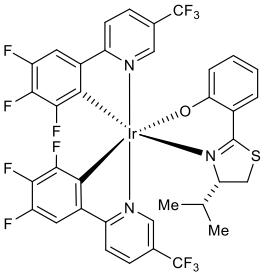

(*S*),Λ-**2.53**

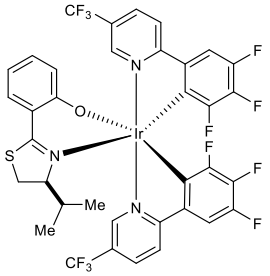

(*S*),Δ-**2.53**

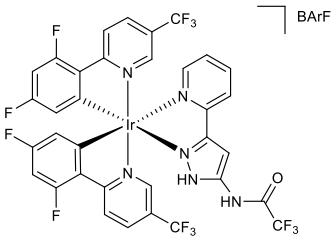

Λ-**2.30a**

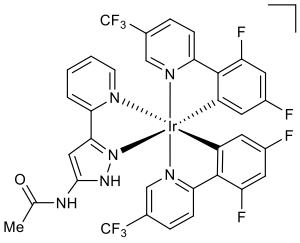

Δ-**2.30b**

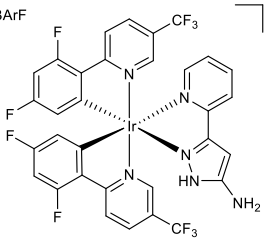

Λ-**2.30c**

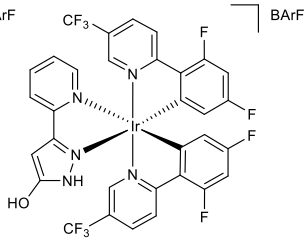

Δ-**2.30d**

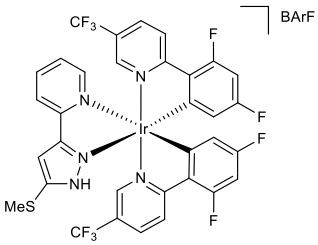

Δ-**2.30e**

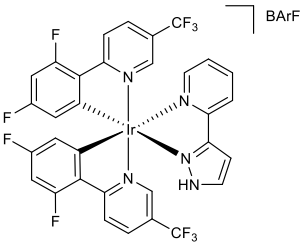

Λ-**2.30f**

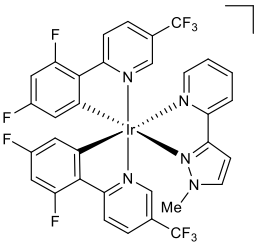

Λ-**2.30g**

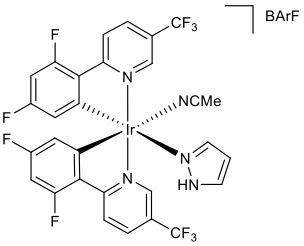

Λ-**2.30h**

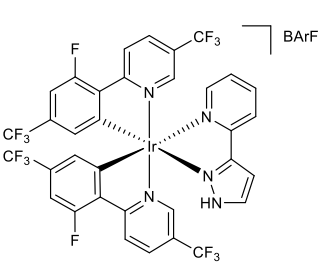

Λ-**2.31**

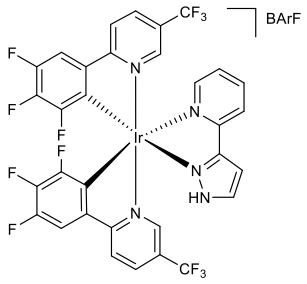

Λ-**2.32**

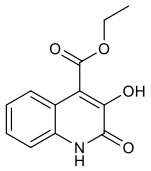

2.55a

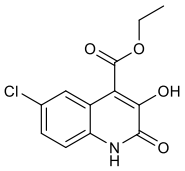

2.55b

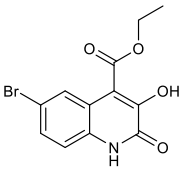

2.55c

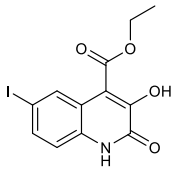

2.55d

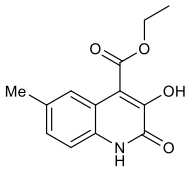

2.55f

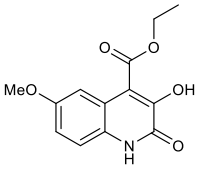

2.55g

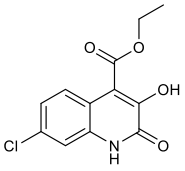

2.55h

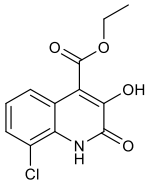

2.55i

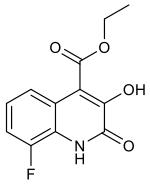

2.55j

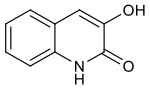

2.56a

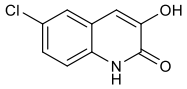

2.56b

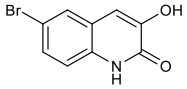

2.56c

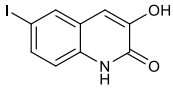

2.56d

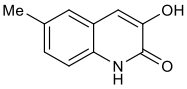

2.56f

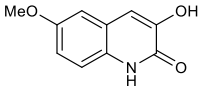

2.56g

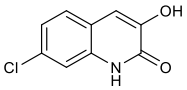

2.56h

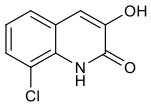

2.56i

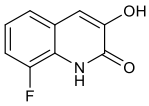

2.56j

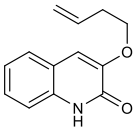

2.28a

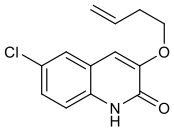

2.28b

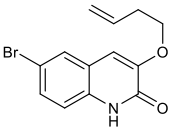

2.28c

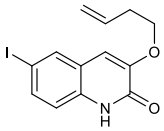

2.28d

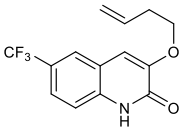

2.28e

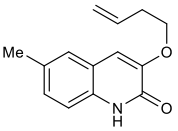

2.28f

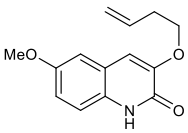

2.28g

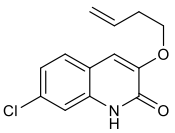

2.28h

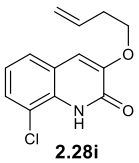

2.28i

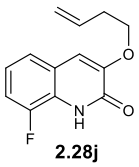

2.28j

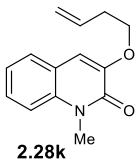

2.28k

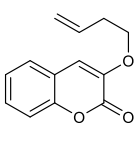

2.28l

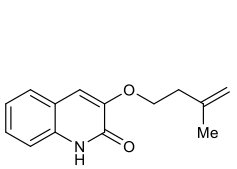

2.28m

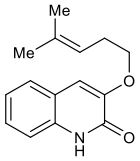

2.28n

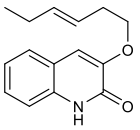

(*E*)-**2.28o**

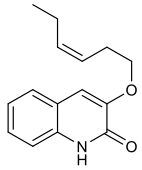

(*Z*)-**2.28o**

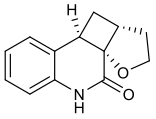

2.29a

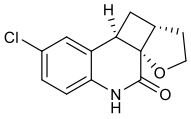

2.29b

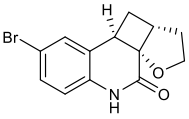

2.29c

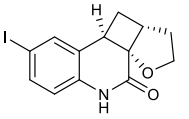

2.29d

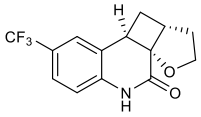

2.29e

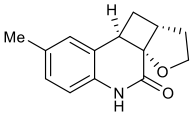

2.29f

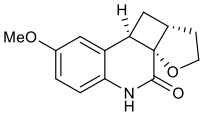

2.29g

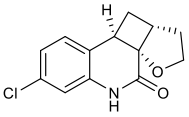

2.29h

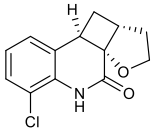

2.29i

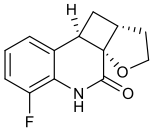

2.29j

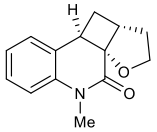

2.29k

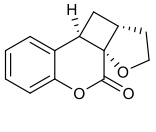

2.29l

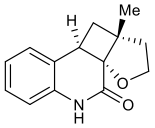

2.29m

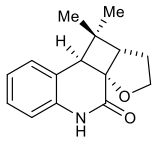

2.29n

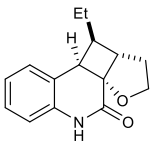

2.29o

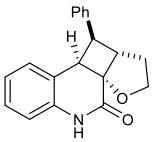

2.29p

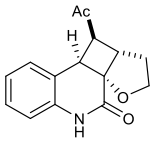

2.29q

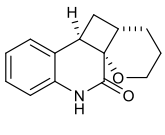

2.29r

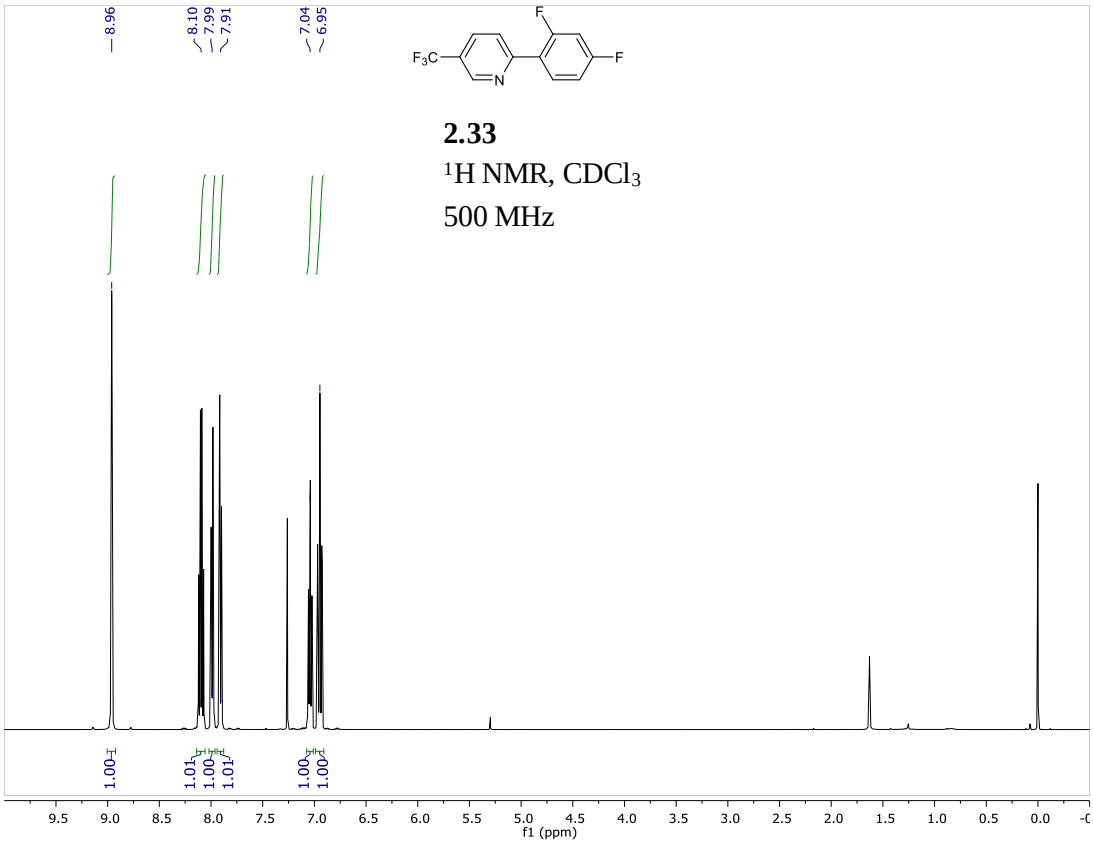
8.96
8.10
7.99
7.91
7.04
6.95
F
F3C
N
F
2.33
1H NMR, CDCl3
500 MHz
1.00
1.01
1.00
1.01
1.00
1.00
f1 (ppm)

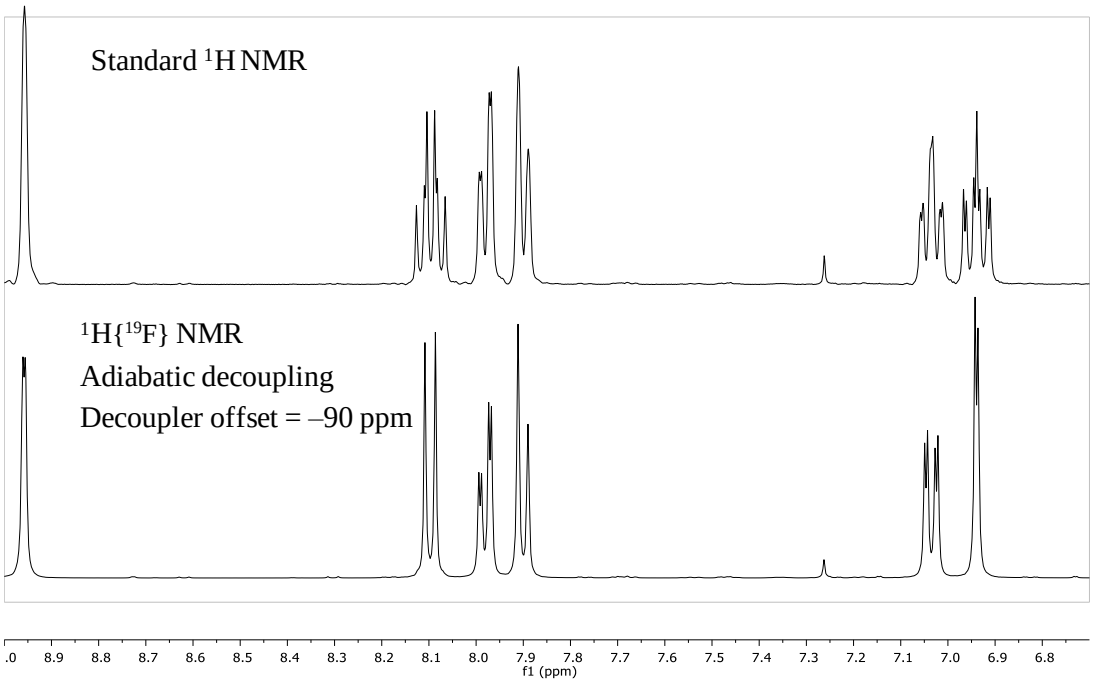
Standard 1H NMR
1H{19F} NMR
Adiabatic decoupling
Decoupler offset = –90 ppm
f1 (ppm)

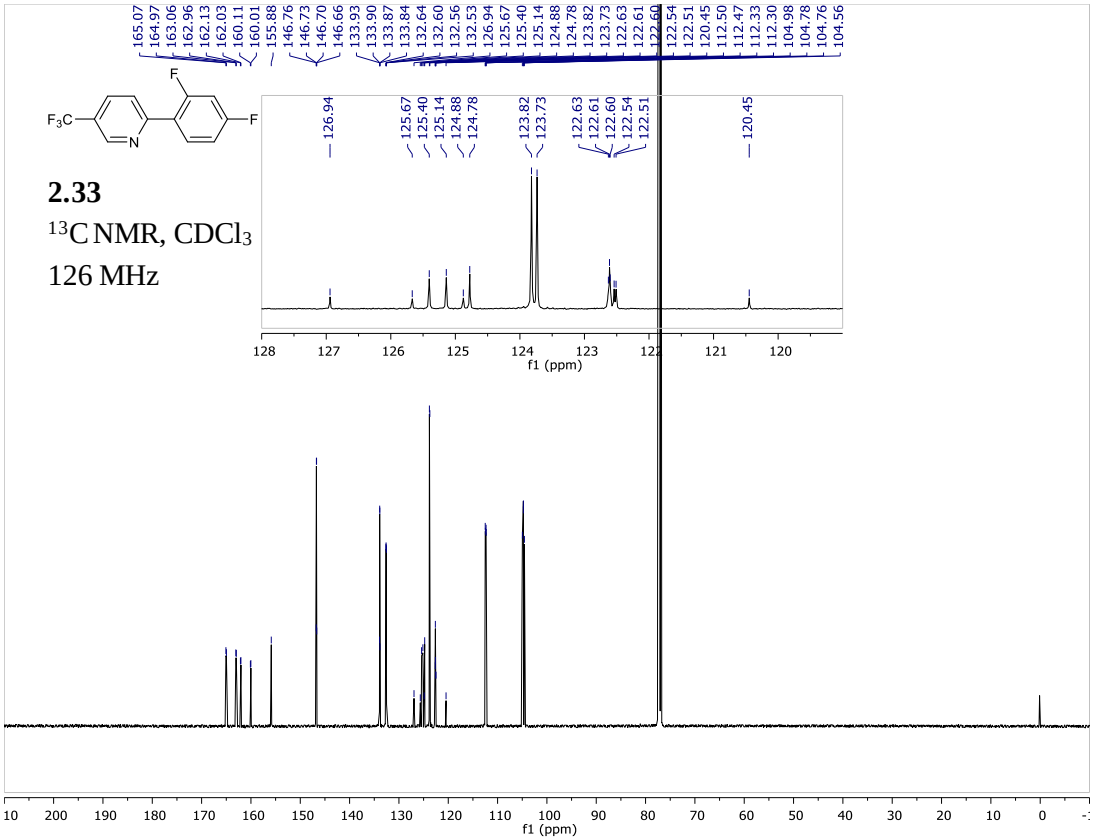
F
F3C
N
F
2.33
13C NMR, CDCl3
126 MHz
f1 (ppm)

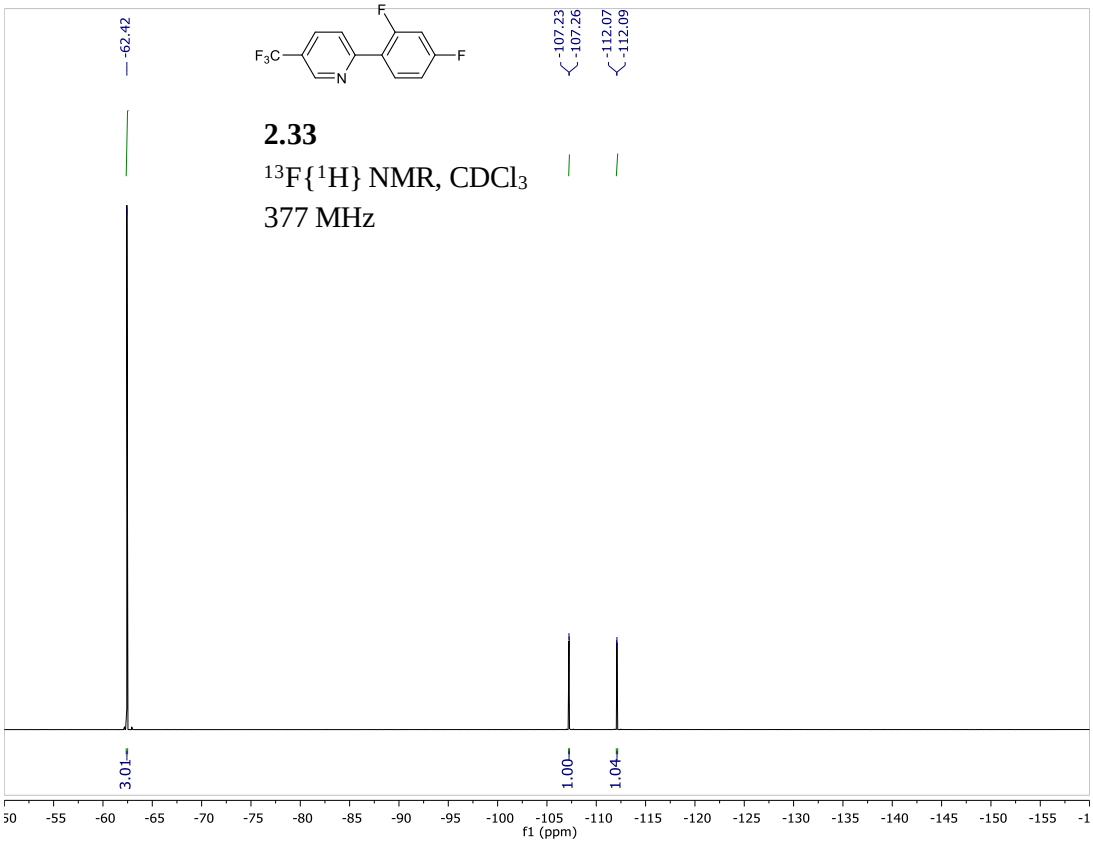
F
F3C
N
F
2.33
13F{1H} NMR, CDCl3
377 MHz
3.01
1.00
1.04
f1 (ppm)

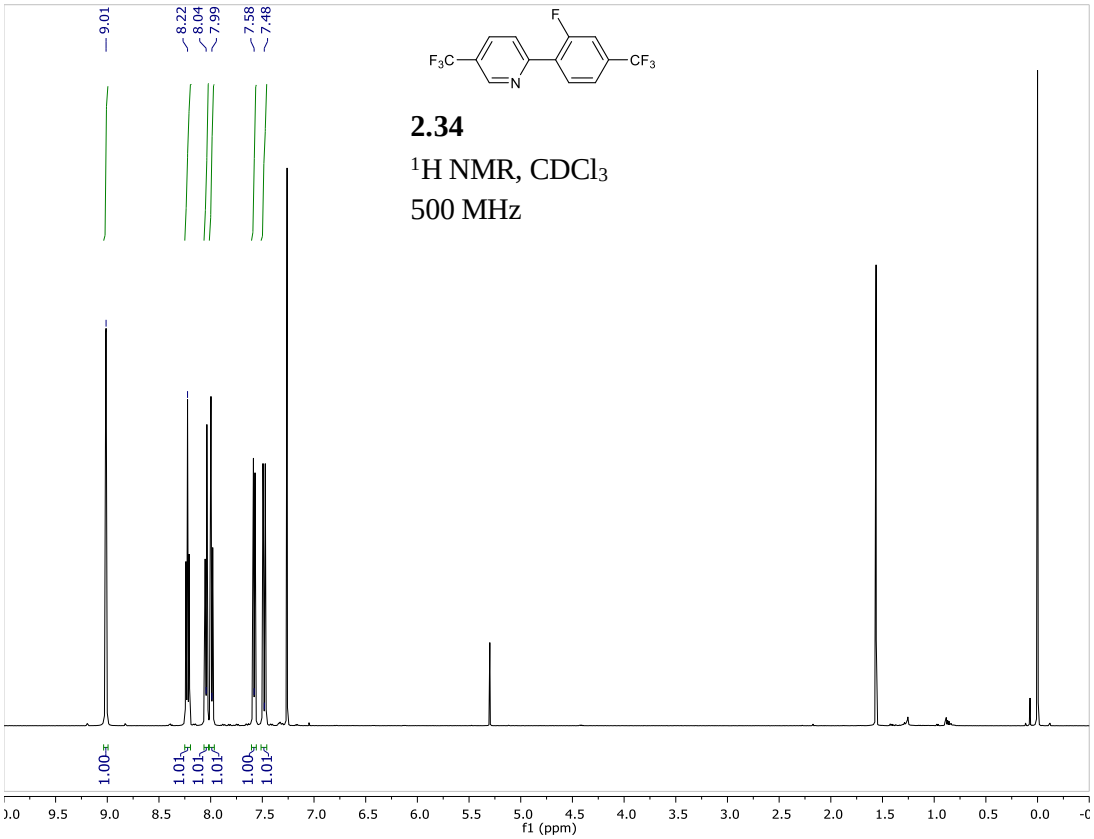
9.01
8.22
8.04
7.99
7.58
7.48
F
F3C
CF3
N
2.34
1H NMR, CDCl3
500 MHz
1.00
1.01
1.01
1.01
1.00
1.01
f1 (ppm)

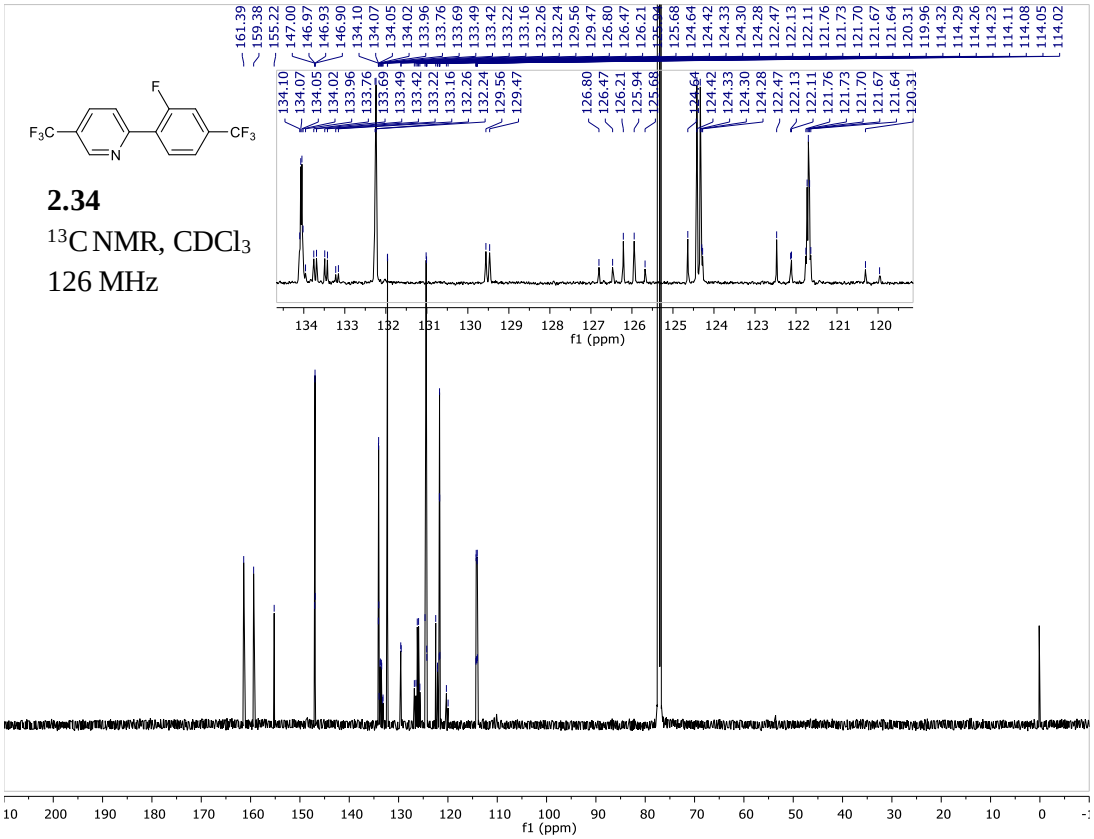
F
F3C
CF3
N
2.34
13C NMR, CDCl3
126 MHz
f1 (ppm)

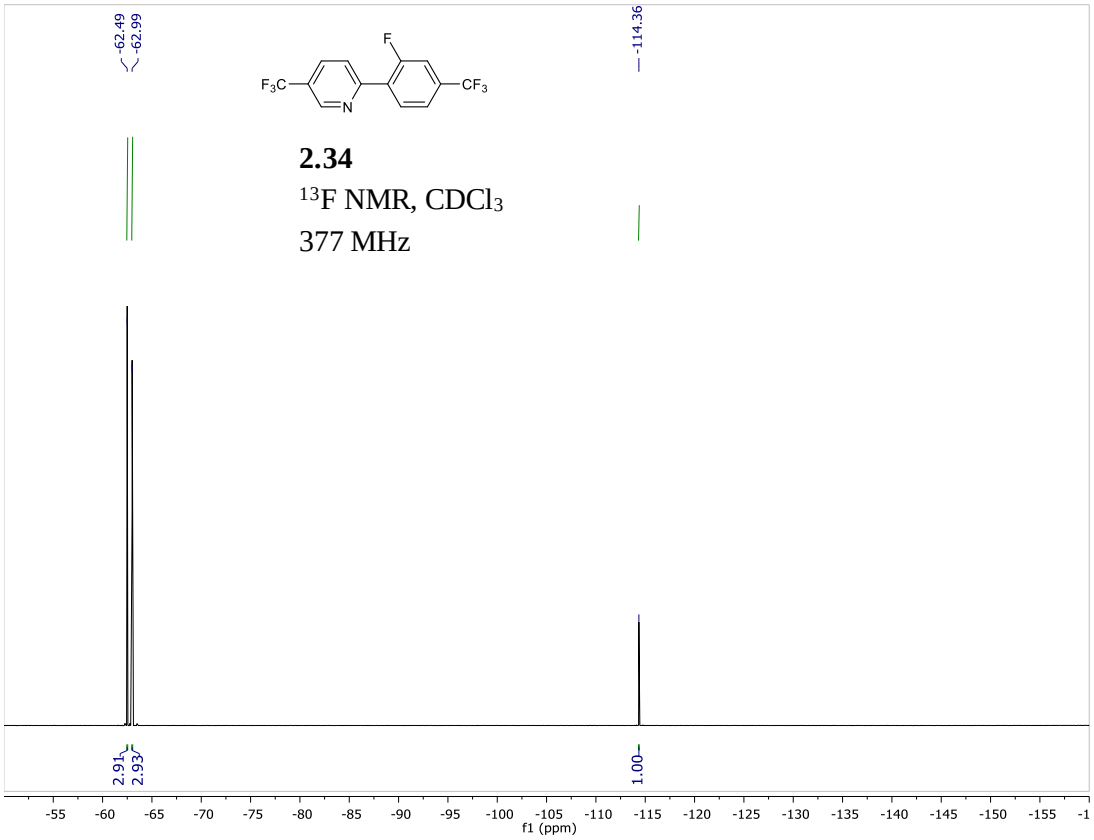

2.34

^{13}F NMR, $CDCl_3$

377 MHz

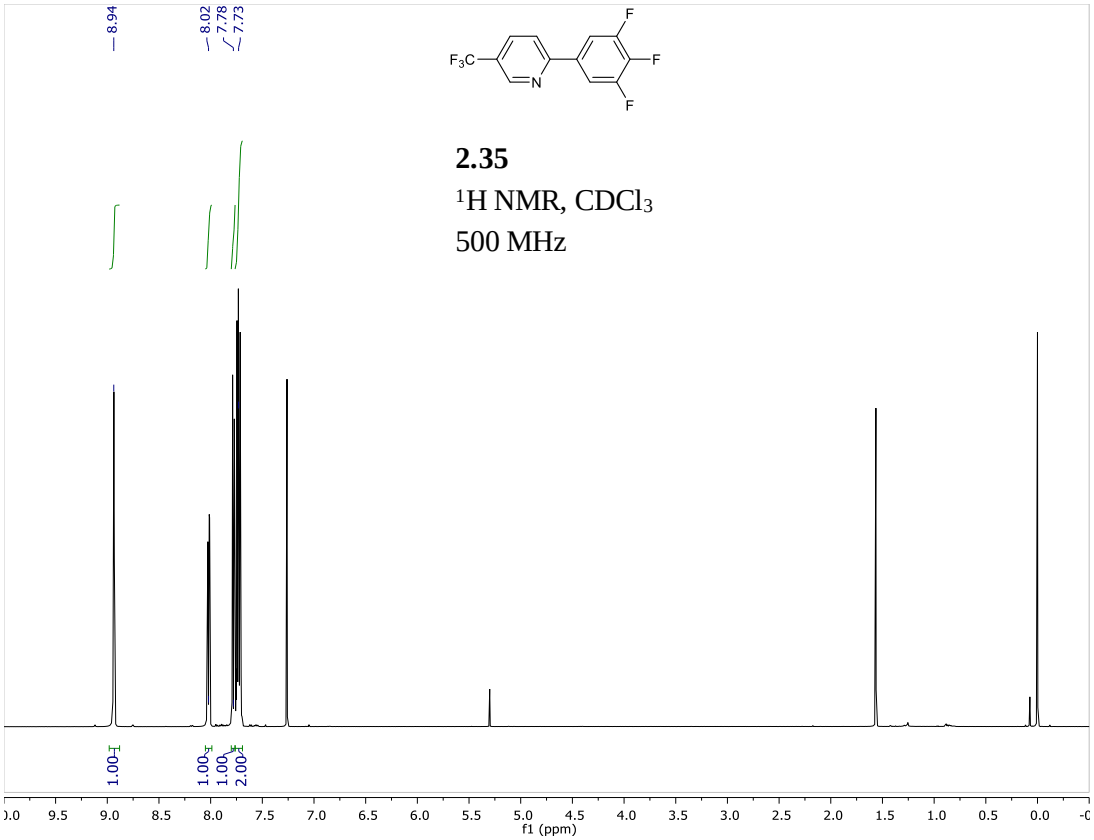

2.35

^{1}H NMR, $CDCl_3$

500 MHz

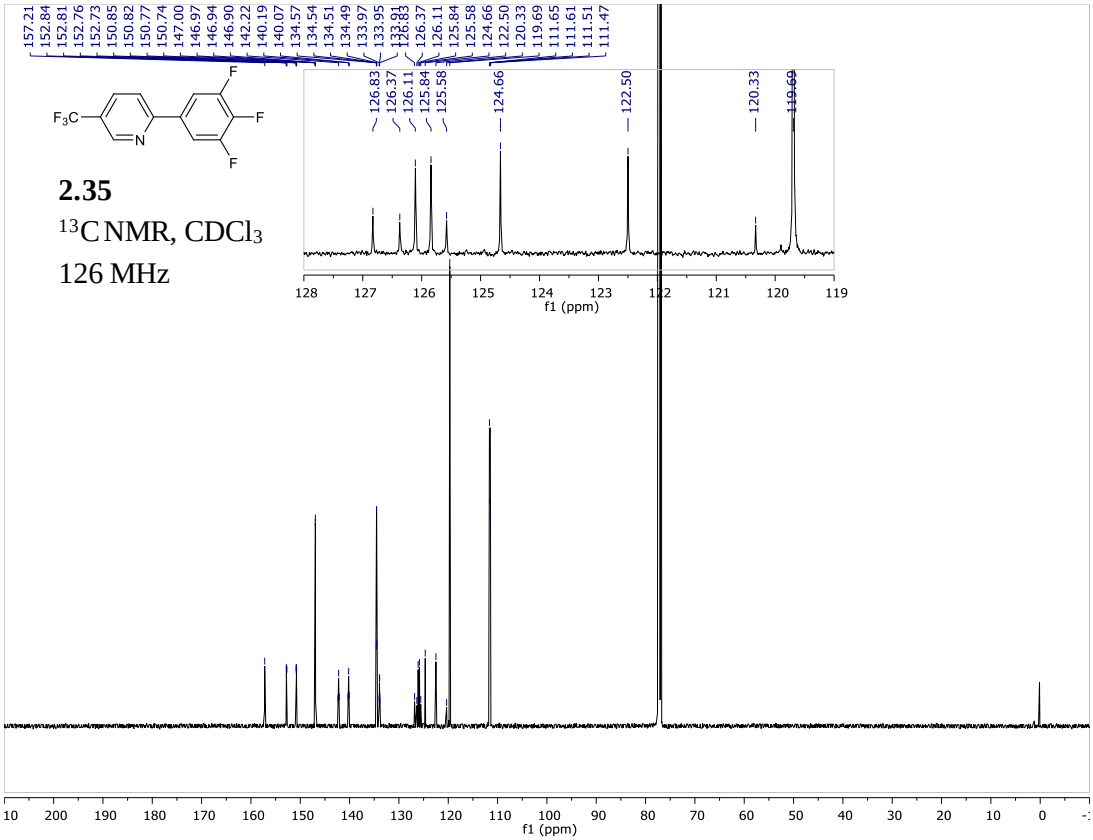
157.21
152.84
152.81
152.76
152.73
150.85
150.82
150.77
150.74
147.00
146.97
146.94
146.90
142.22
140.19
140.07
134.57
134.54
134.51
134.49
133.97
133.95
133.91
126.83
126.37
126.11
125.84
125.58
125.84
125.58
124.66
122.50
120.33
119.69
111.65
111.61
111.51
111.47
F3C
N
F
F
F
2.35
13C NMR, CDCl3
126 MHz
f1 (ppm)
f1 (ppm)

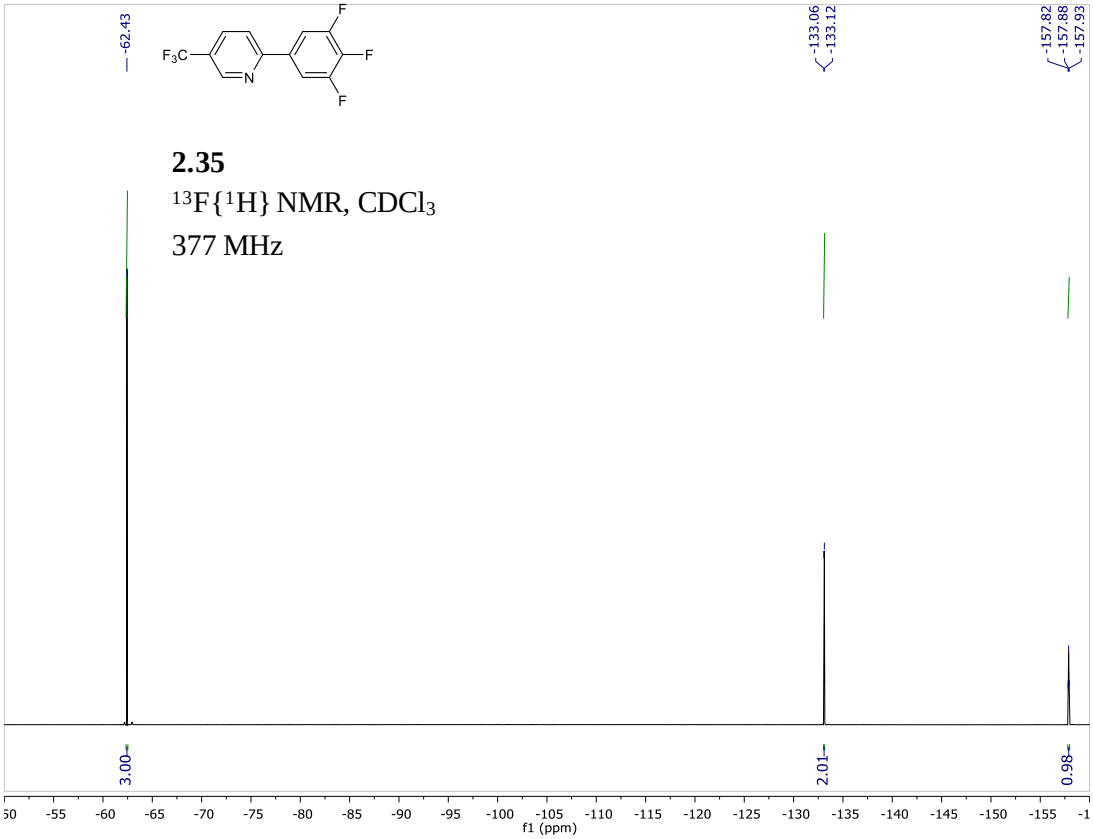
-62.43
-133.06
-133.12
-157.82
-157.88
-157.93
F3C
N
F
F
F
2.35
19F{1H} NMR, CDCl3
377 MHz
3.00
2.01
0.98
f1 (ppm)

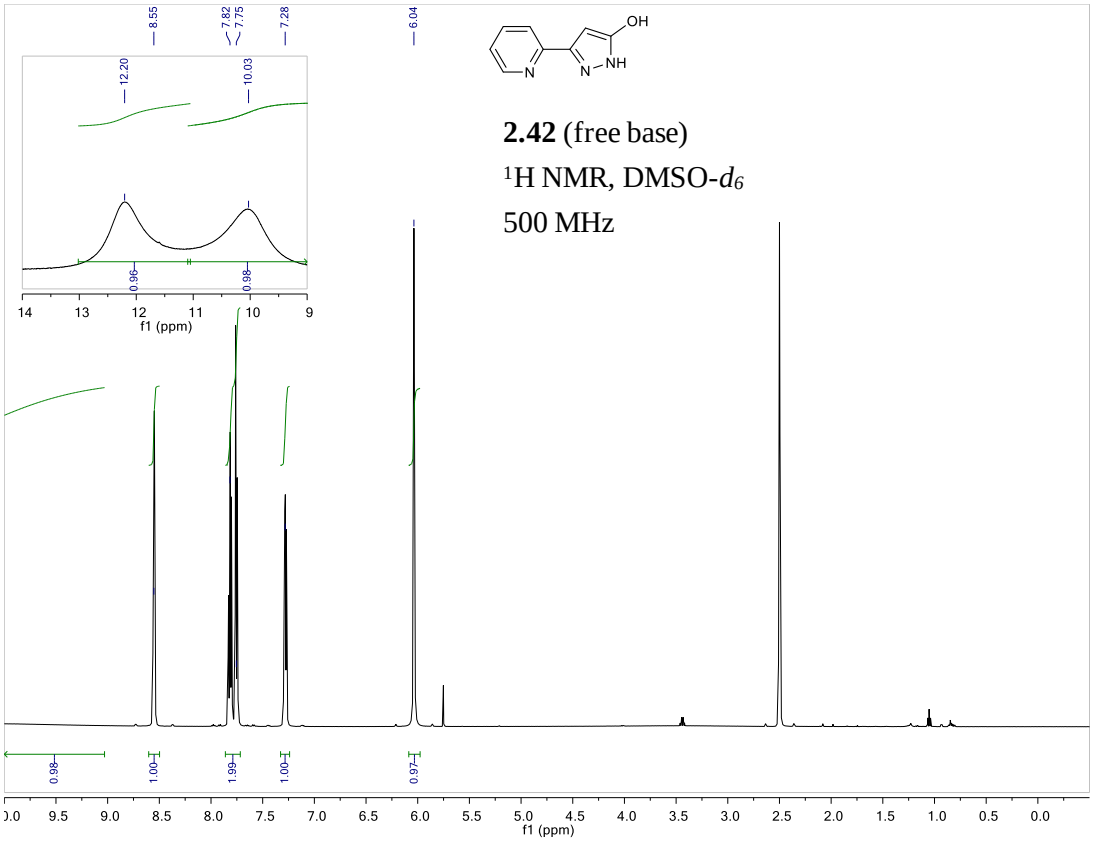

2.42 (free base)

^{1}H NMR, DMSO-d_6

500 MHz

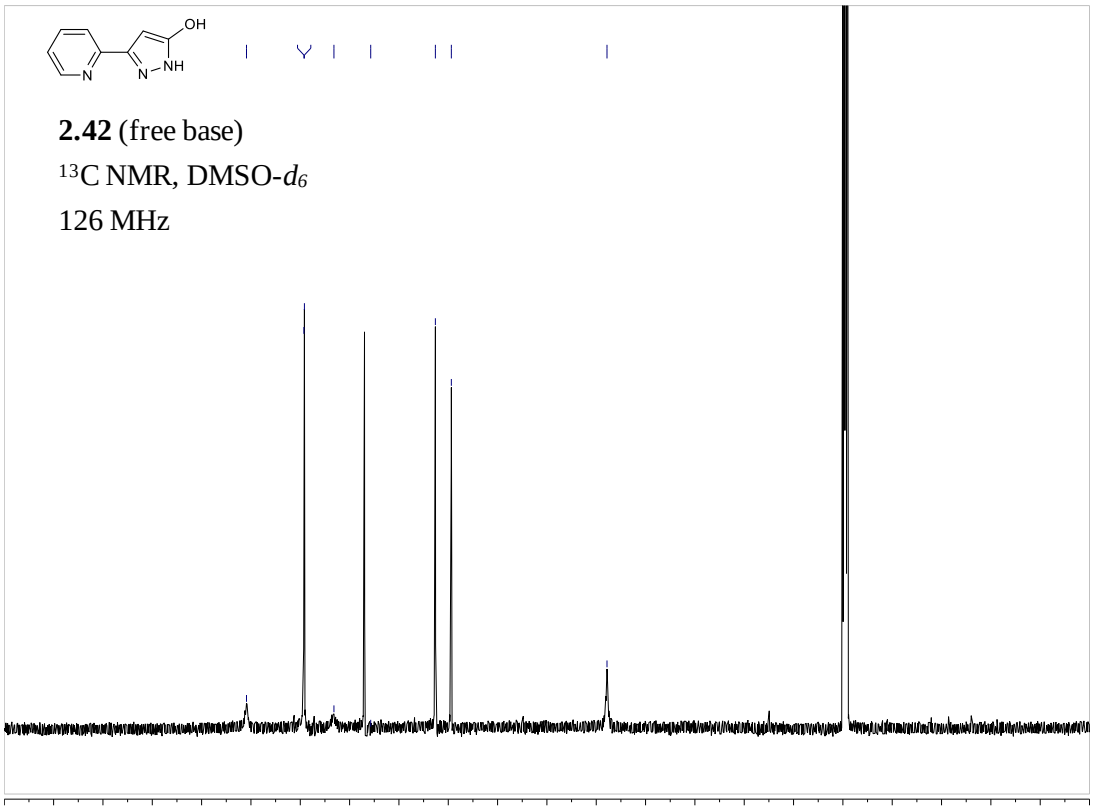

2.42 (free base)

^{13}C NMR, DMSO-d_6

126 MHz

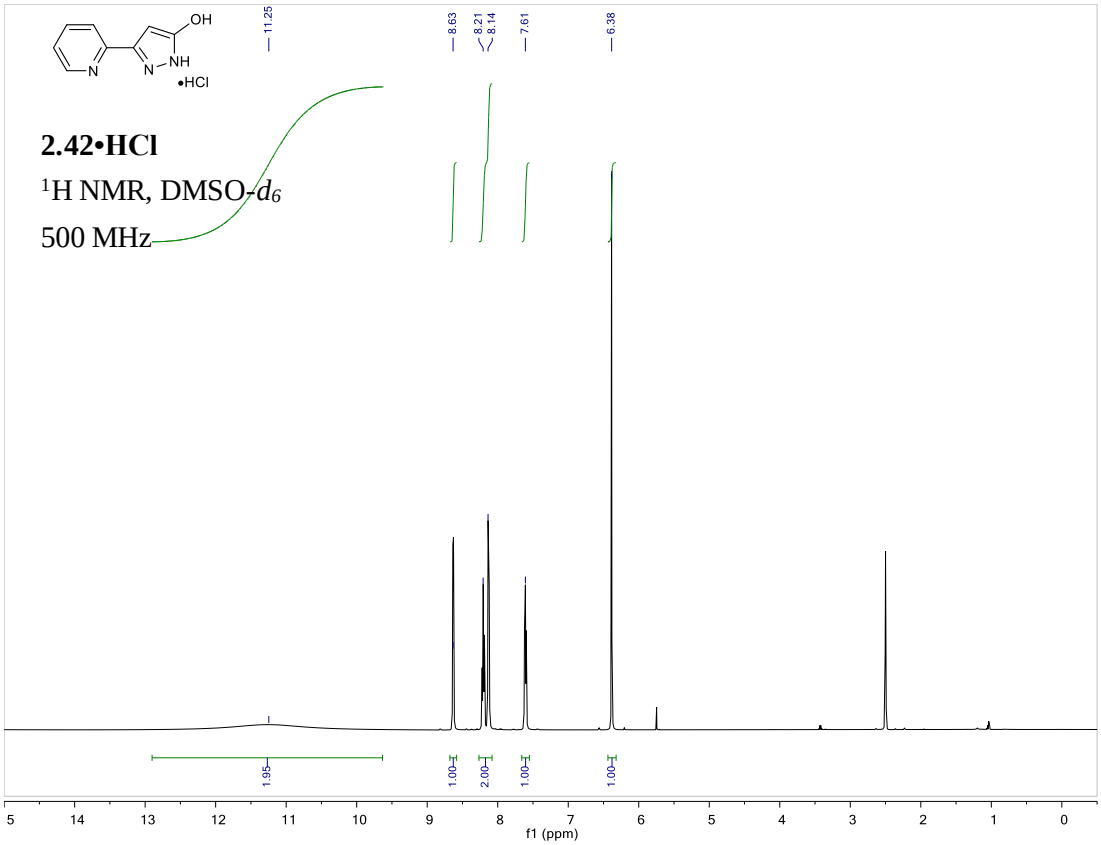
OH
NH
N
•HCl
11.25
8.63
8.21
8.14
7.61
6.38
2.42•HCl
1H NMR, DMSO-d6
500 MHz
1.95
1.00
2.00
1.00
1.00
f1 (ppm)

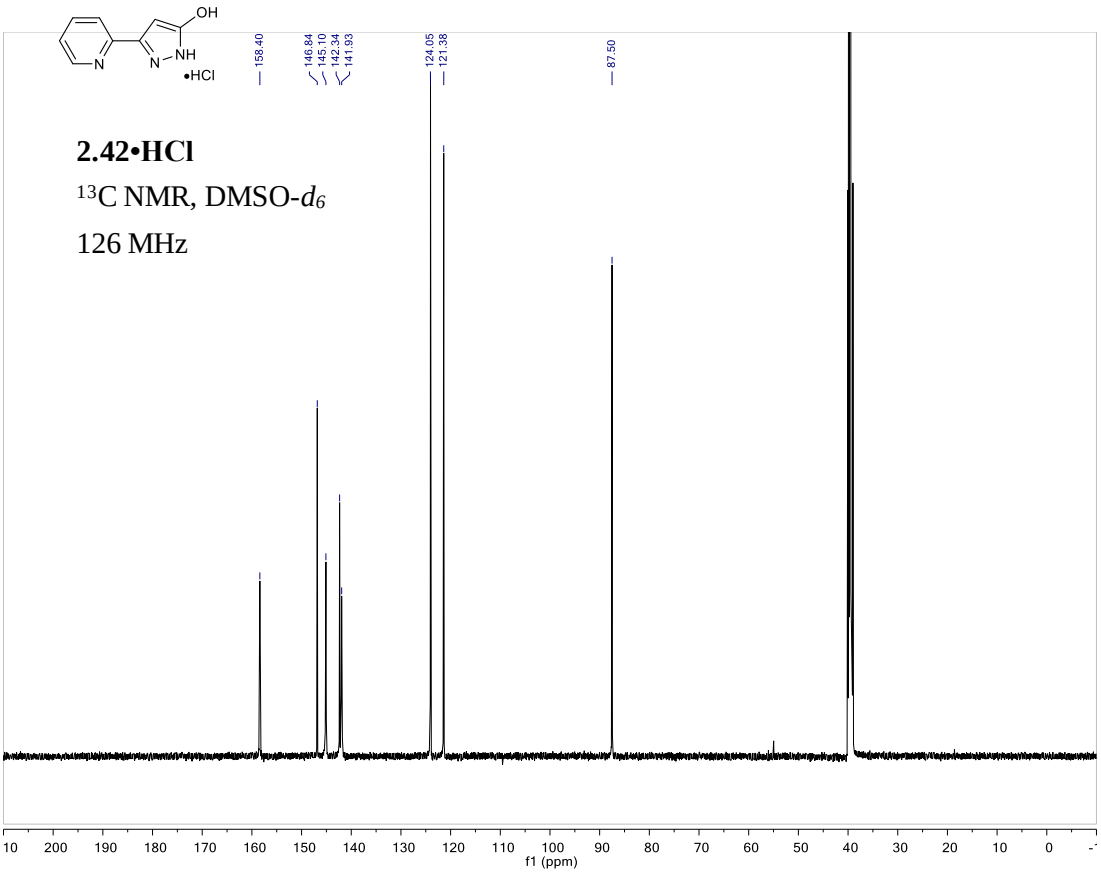
OH
NH
N
•HCl
158.40
146.84
145.10
142.34
141.93
124.05
121.38
87.50
2.42•HCl
13C NMR, DMSO-d6
126 MHz
f1 (ppm)

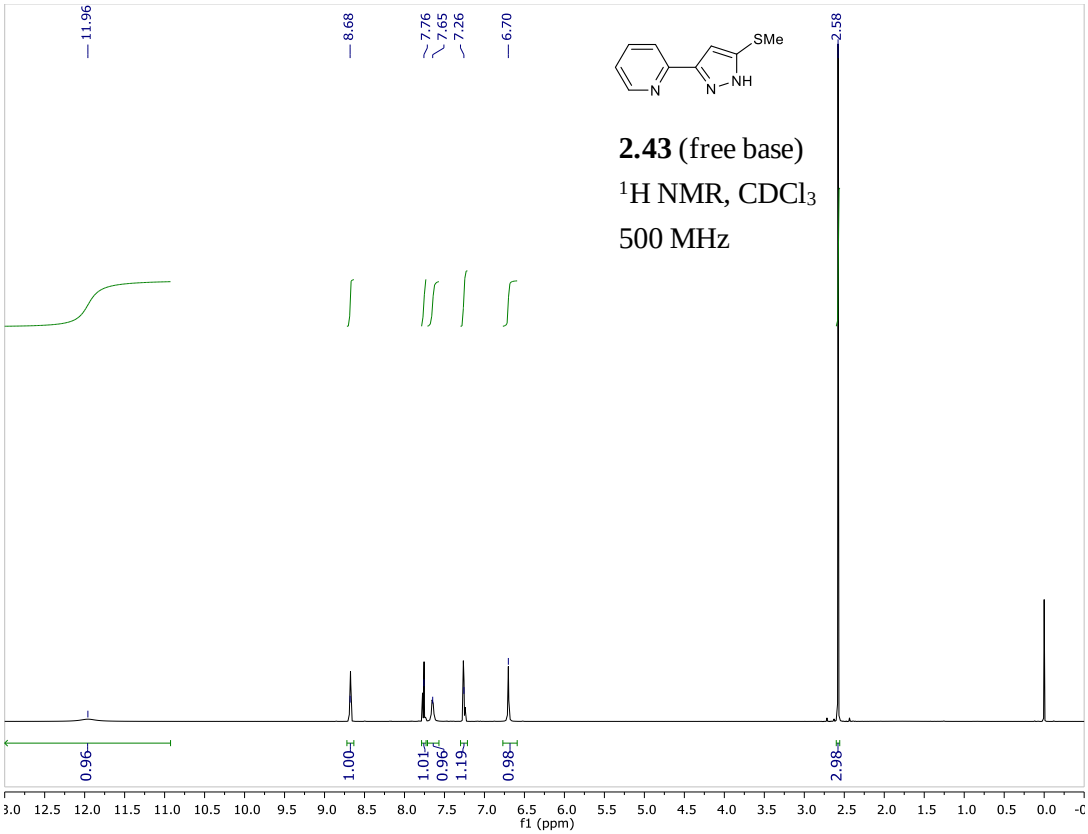

2.43 (free base)

^{1}H NMR, $CDCl_3$

500 MHz

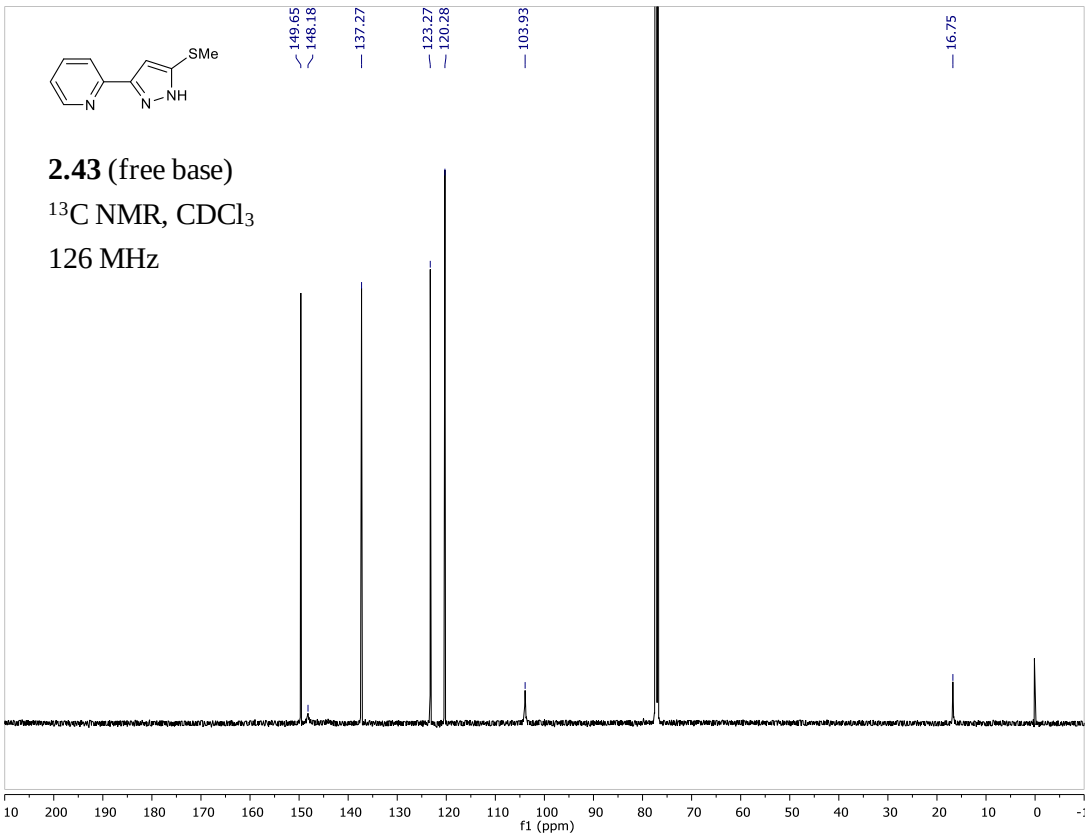

2.43 (free base)

^{13}C NMR, $CDCl_3$

126 MHz

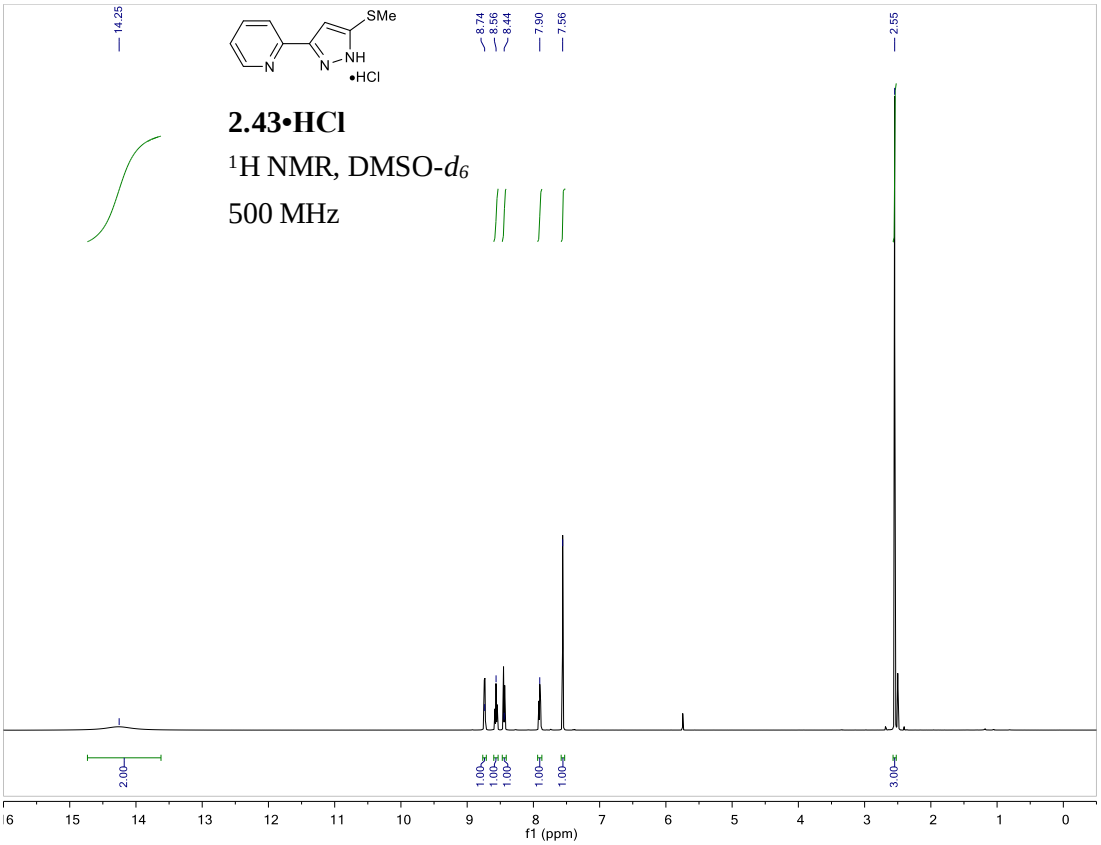

2.43•HCl

^{1}H NMR, DMSO-d_6

500 MHz

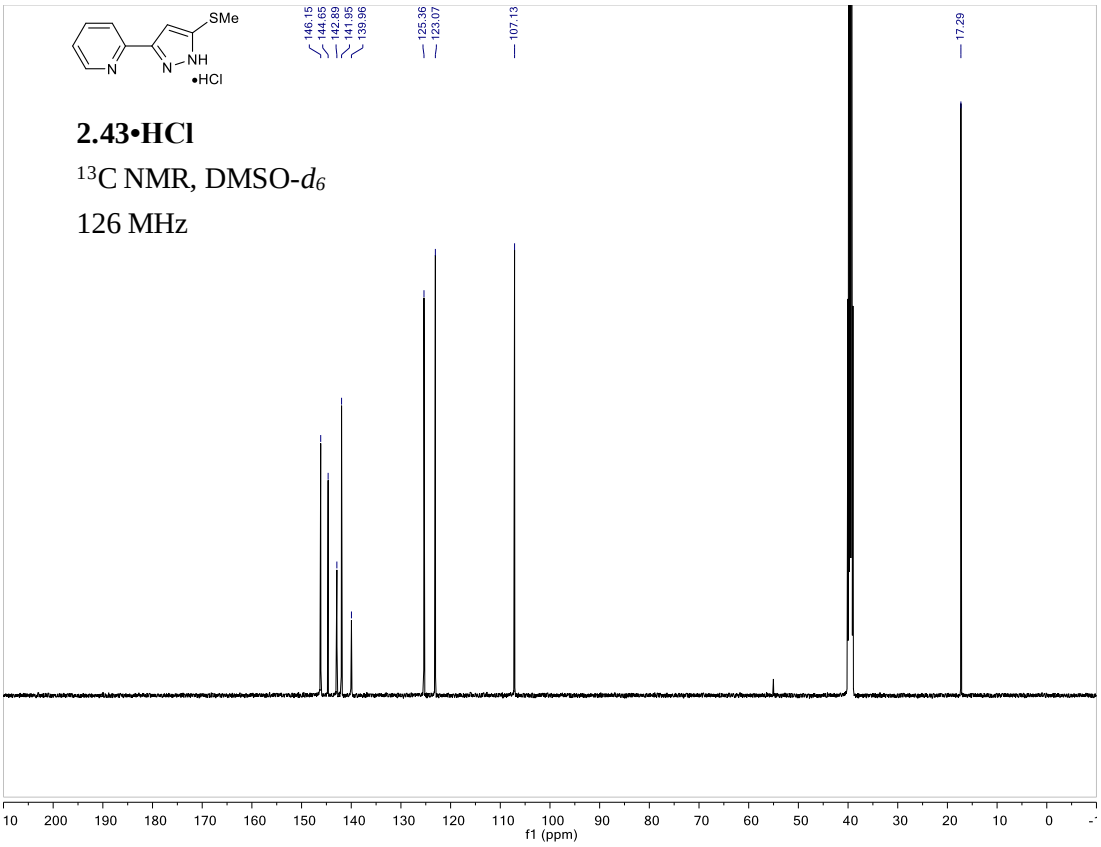

2.43•HCl

^{13}C NMR, DMSO-d_6

126 MHz

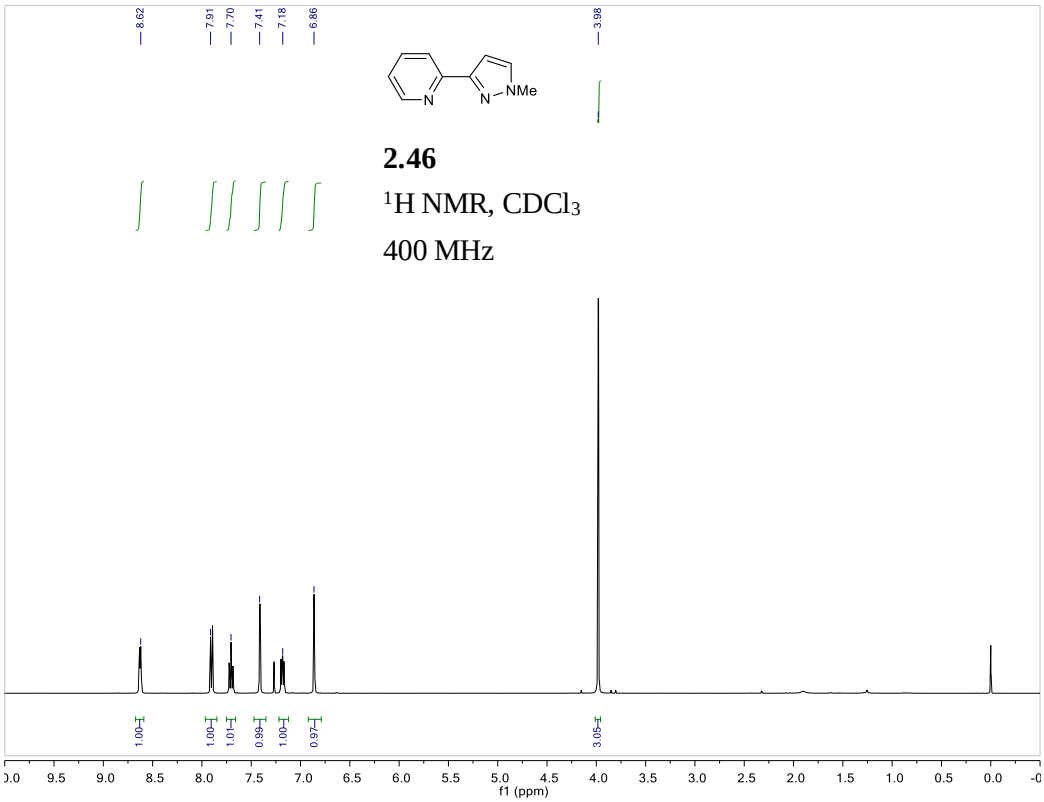
8.62
7.91
7.70
7.41
7.18
6.86
3.98
NMe
2.46
1H NMR, CDCl3
400 MHz
1.00
1.00
1.01
0.99
1.00
0.97
3.05
f1 (ppm)

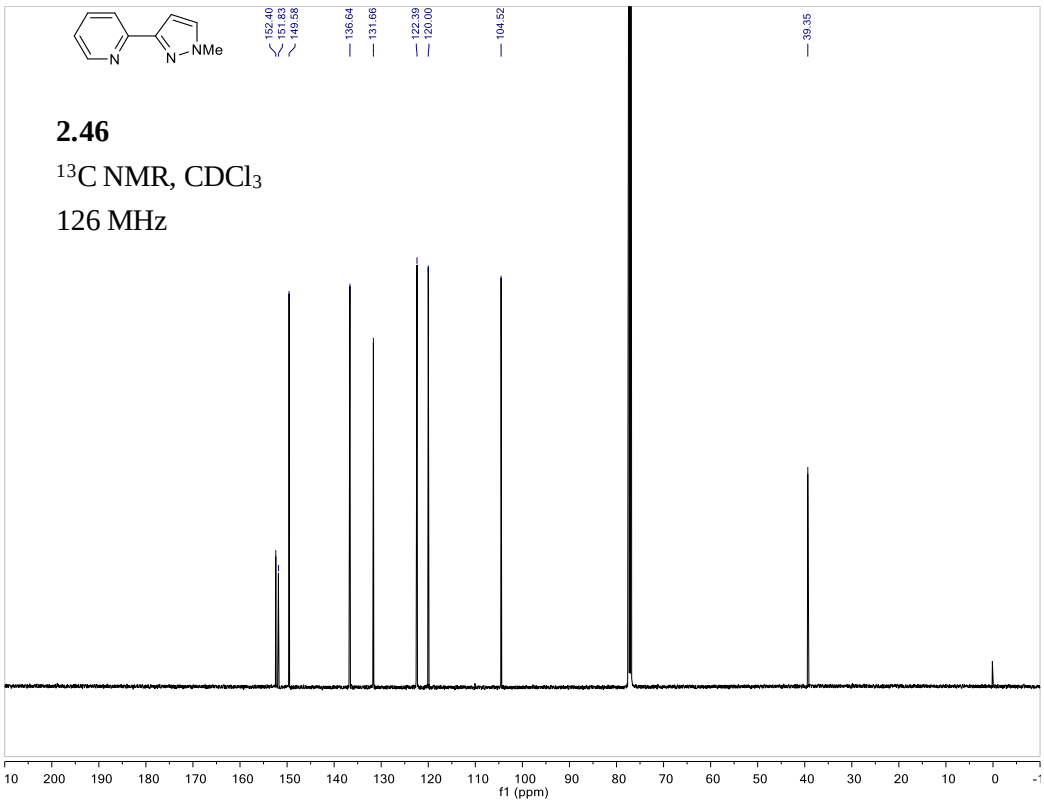
NMe
152.40
151.83
149.58
136.64
131.66
122.39
120.00
104.52
39.35
2.46
13C NMR, CDCl3
126 MHz
f1 (ppm)

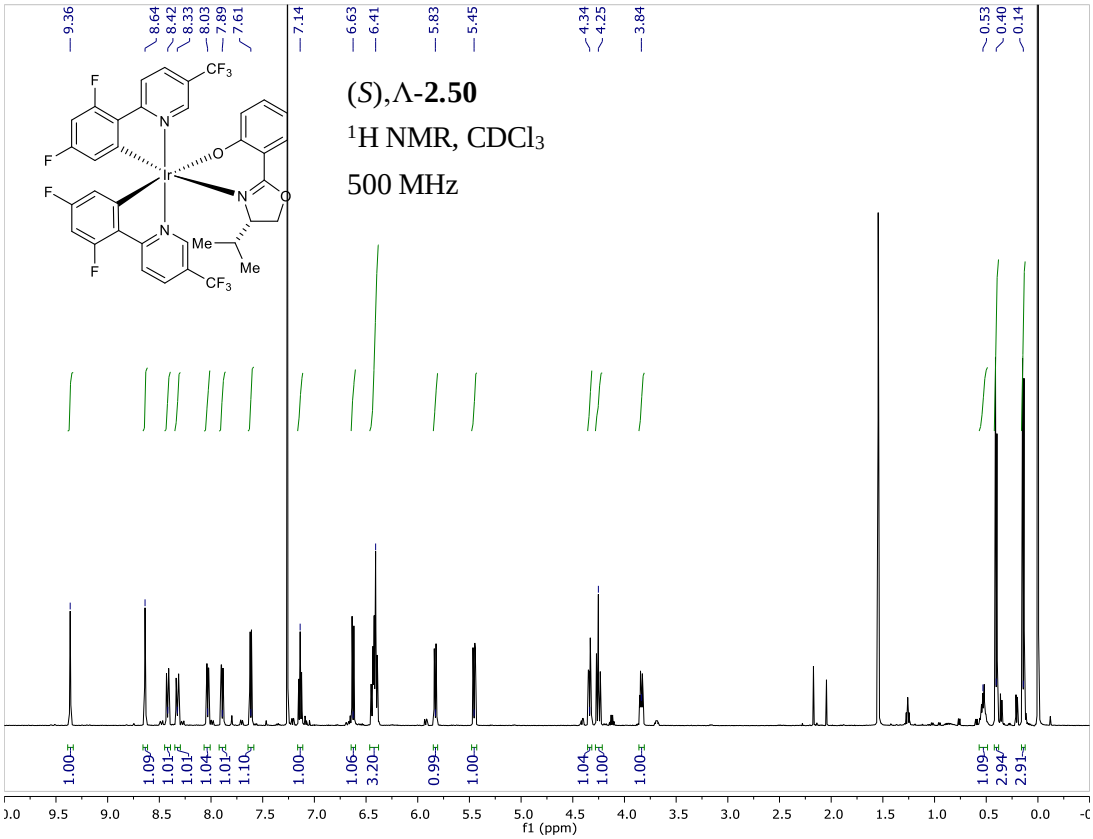
(S),Λ-2.50
1H NMR, CDCl3
500 MHz
f1 (ppm)

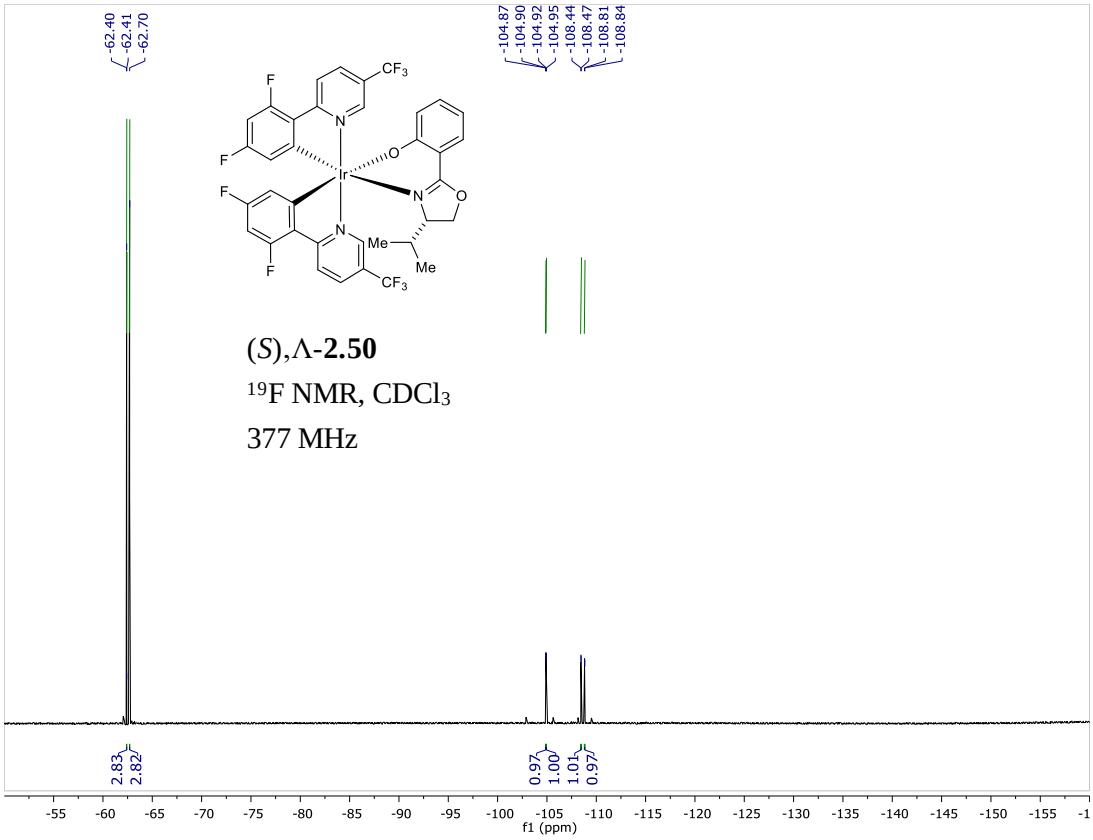
(S),Λ-2.50
19F NMR, CDCl3
377 MHz
f1 (ppm)

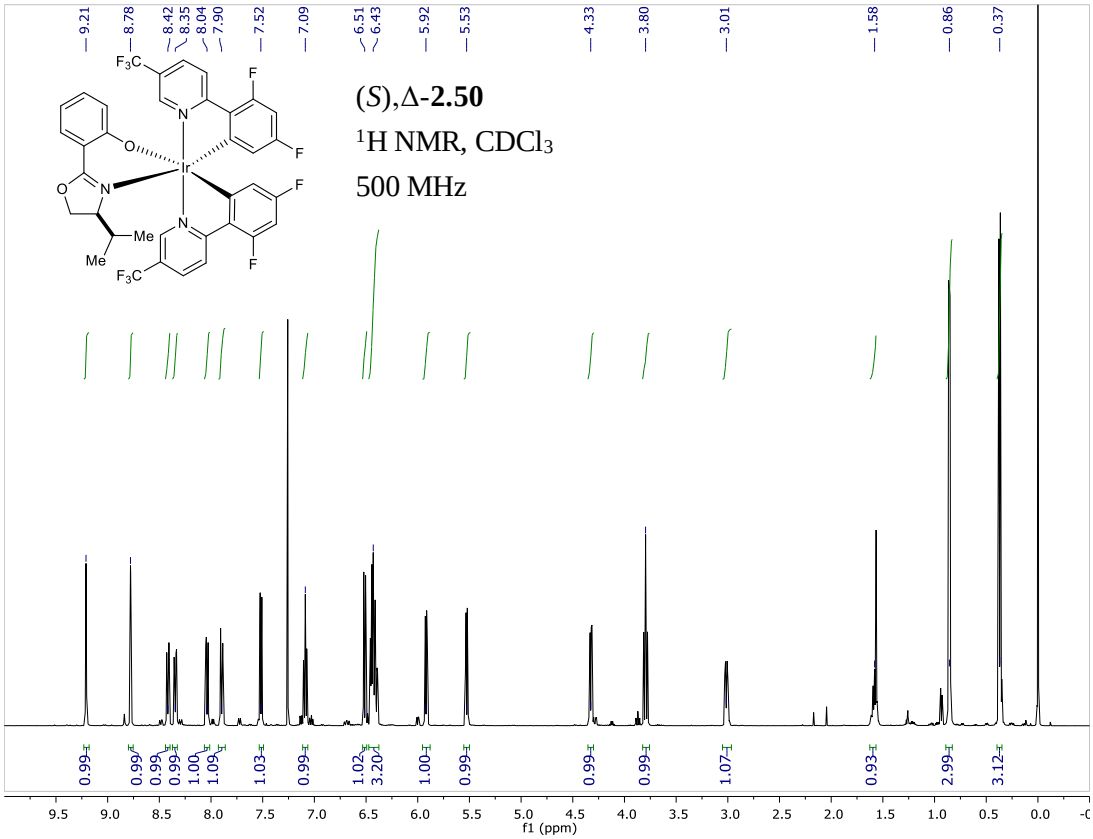
(S),Δ-2.50
1H NMR, CDCl3
500 MHz
f1 (ppm)

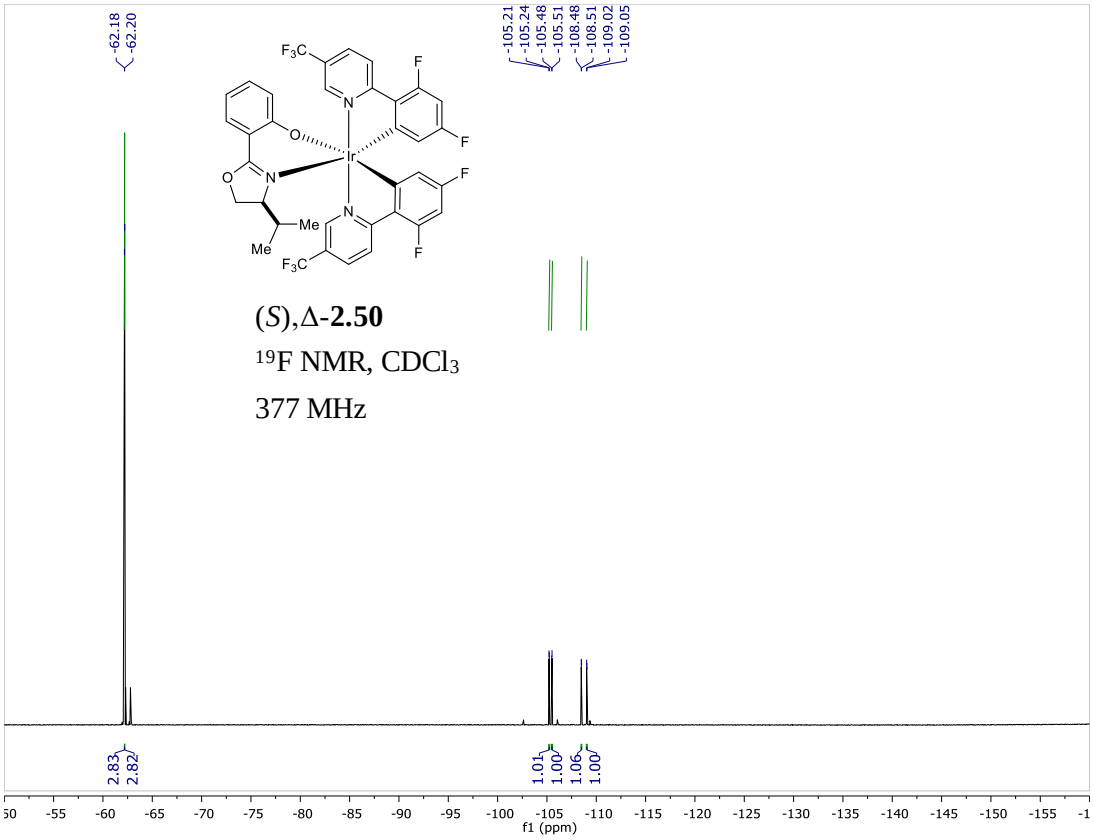
(S),Δ-2.50
19F NMR, CDCl3
377 MHz
f1 (ppm)

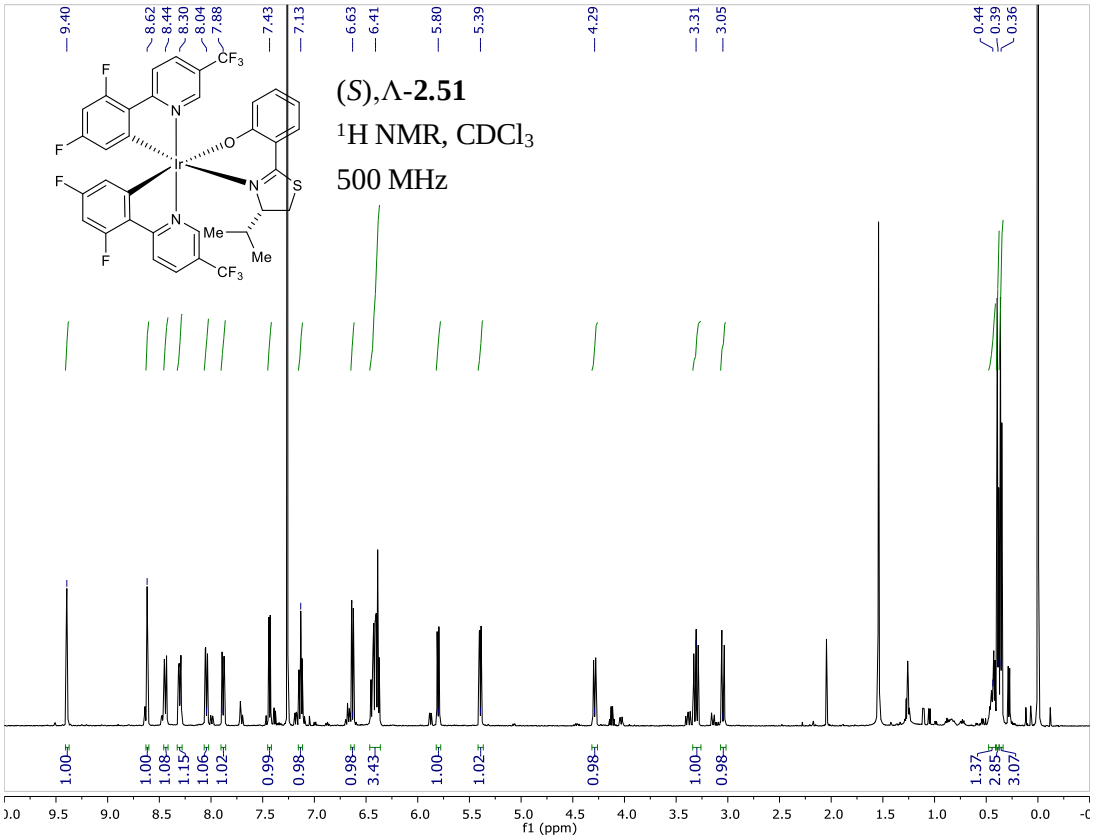
(S),Λ-2.51
1H NMR, CDCl3
500 MHz
f1 (ppm)

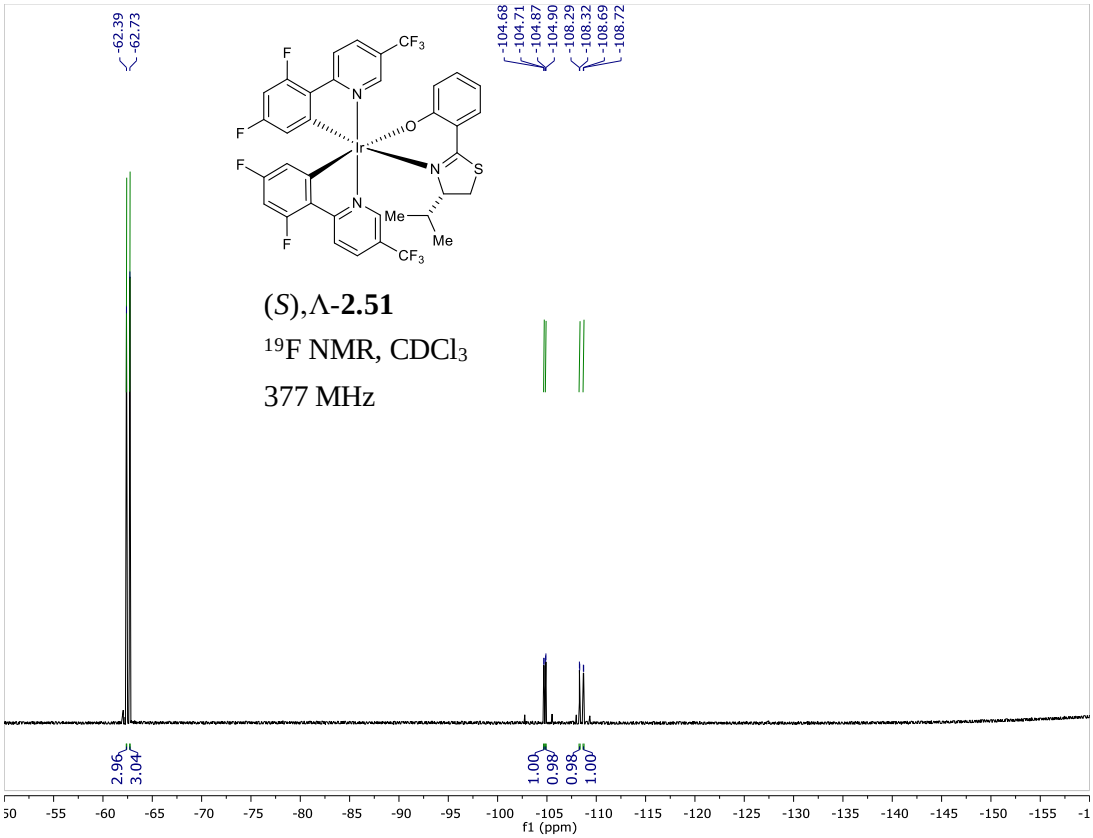
(S),Λ-2.51
19F NMR, CDCl3
377 MHz
f1 (ppm)

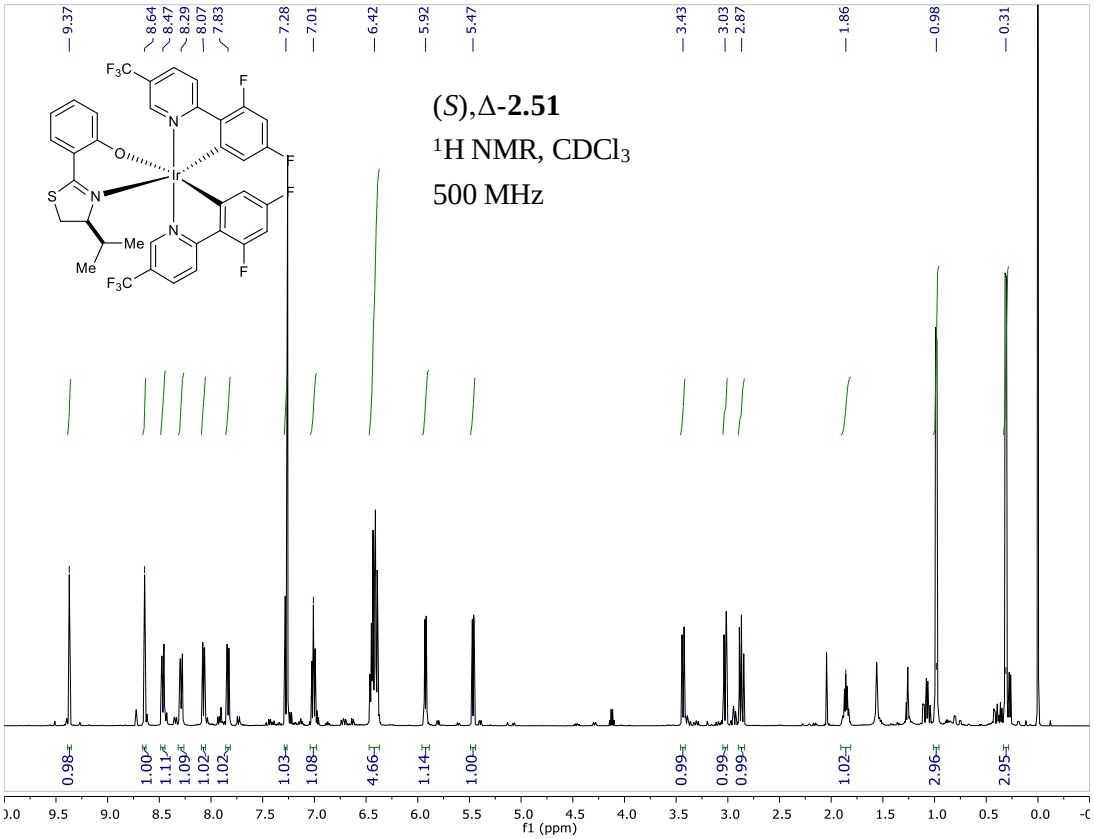
(S),Δ-2.51
1H NMR, CDCl3
500 MHz
f1 (ppm)

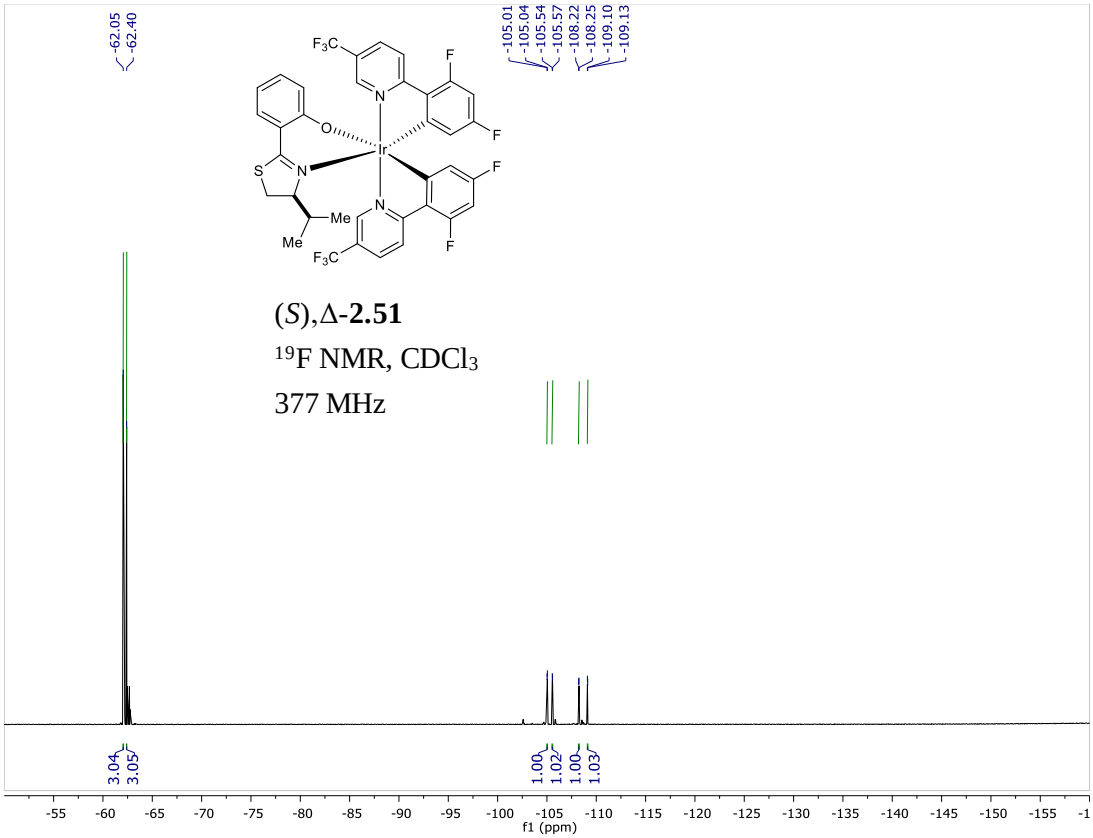
(S),Δ-2.51
19F NMR, CDCl3
377 MHz
f1 (ppm)

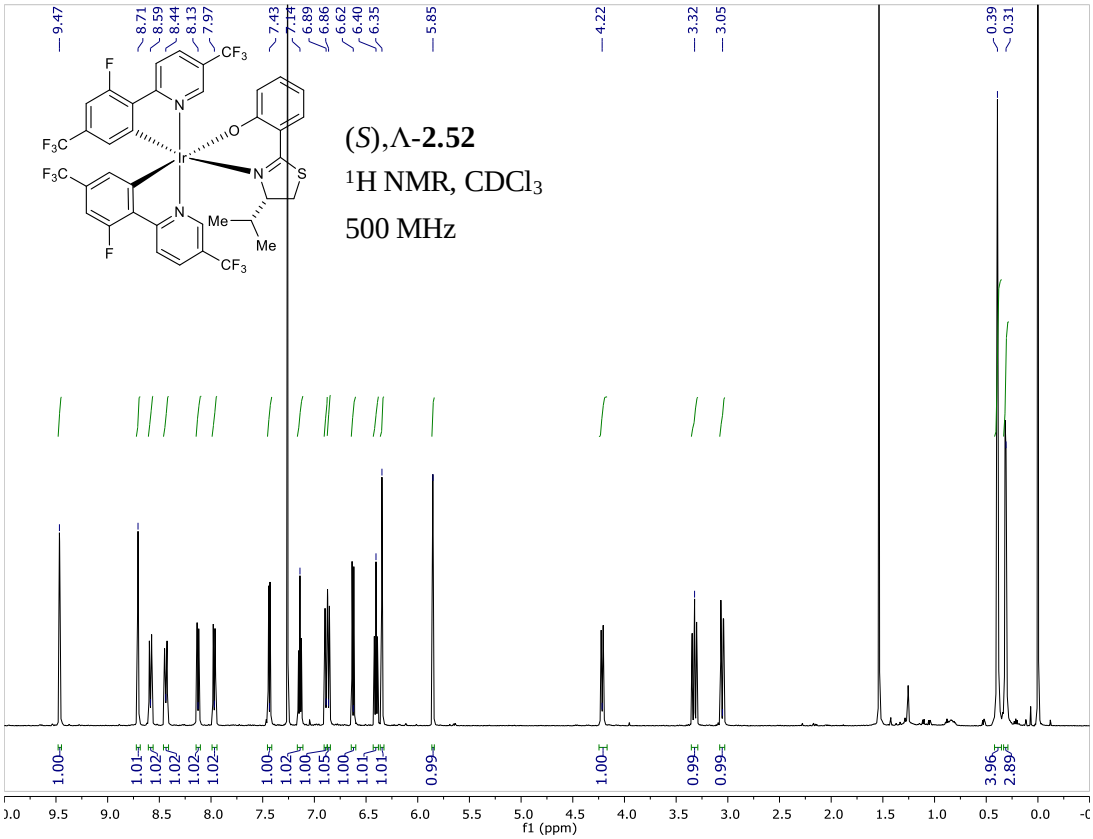
(S),Λ-2.52
1H NMR, CDCl3
500 MHz
f1 (ppm)

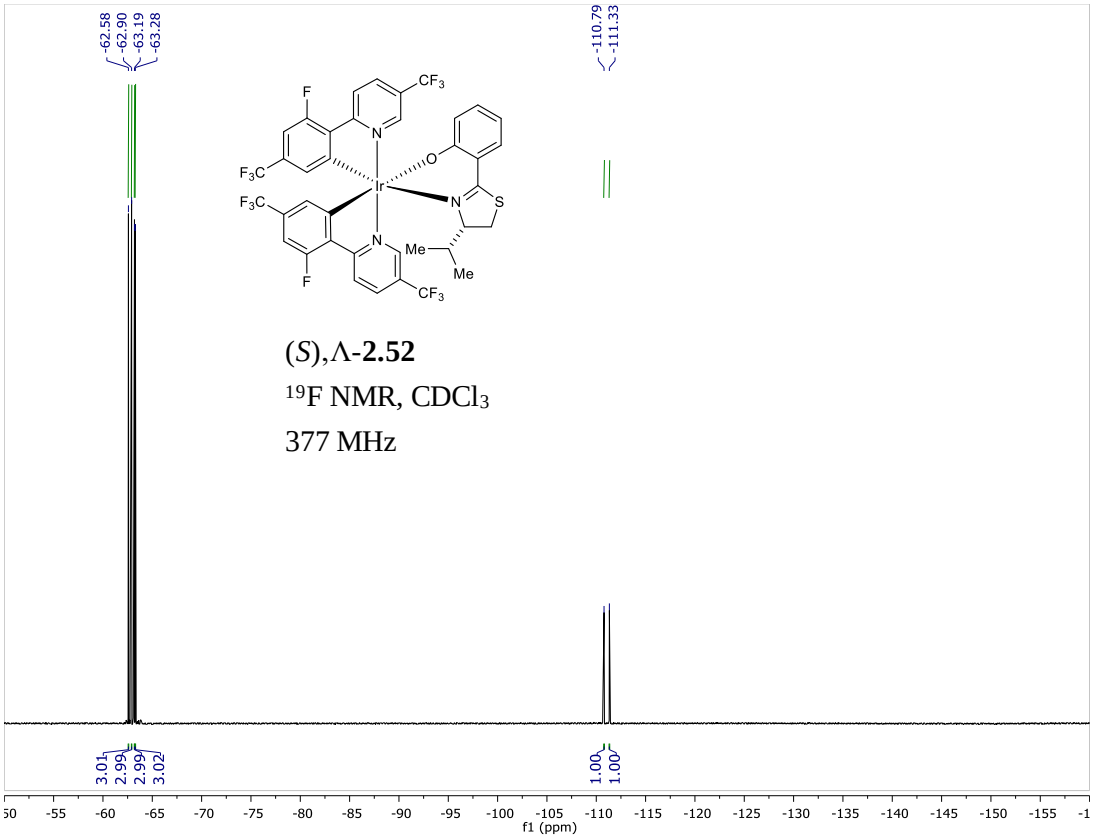
(S),Λ-2.52
19F NMR, CDCl3
377 MHz
f1 (ppm)

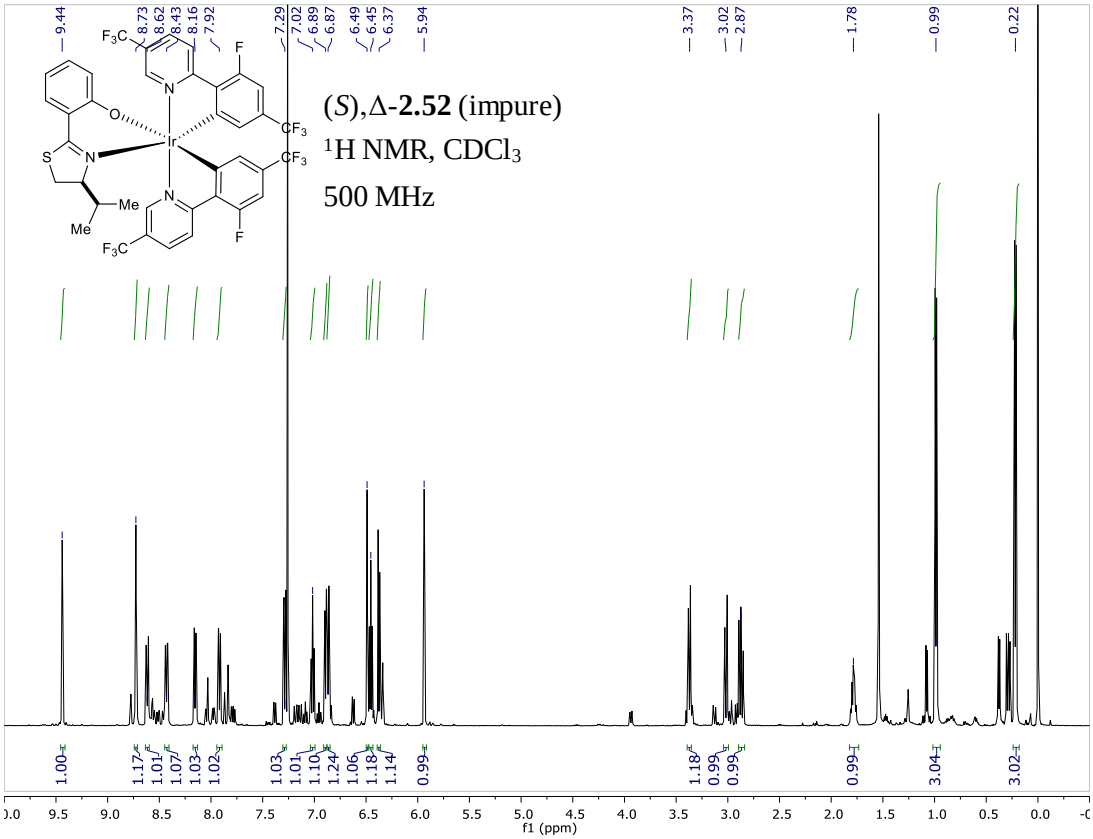
(S),Δ-2.52 (impure)
1H NMR, CDCl3
500 MHz
f1 (ppm)

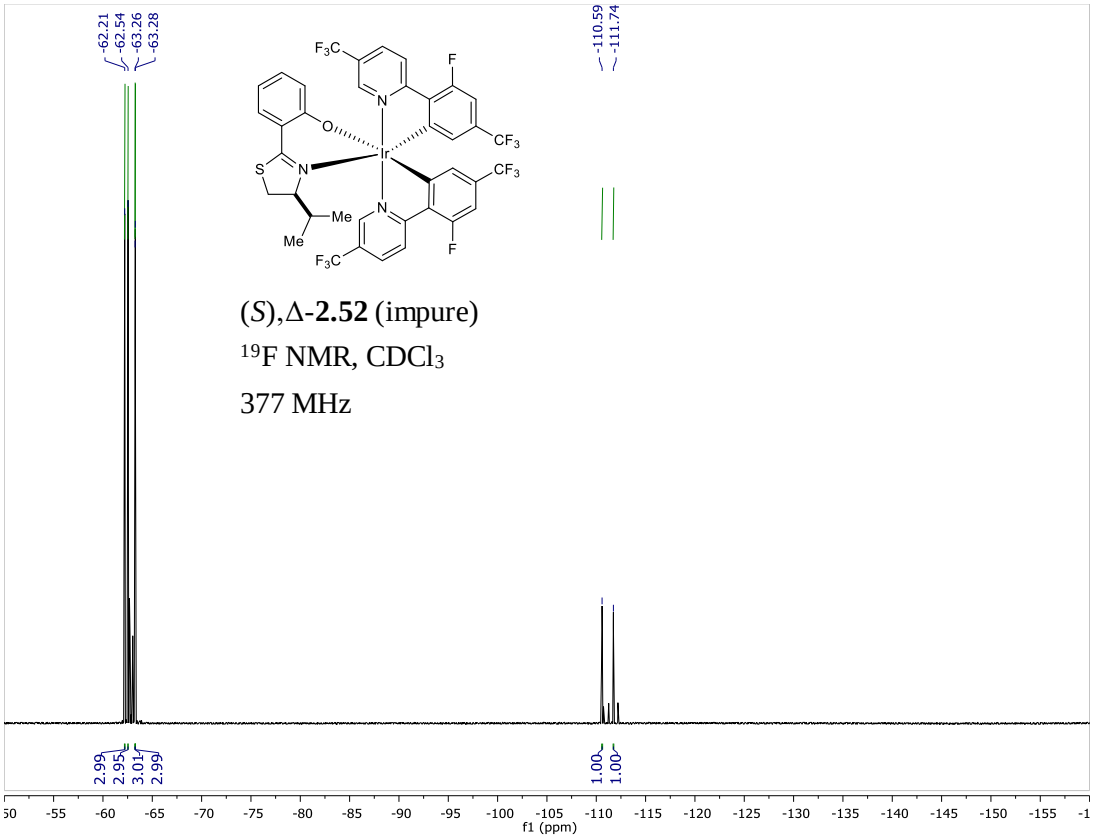
(S),Δ-2.52 (impure)
19F NMR, CDCl3
377 MHz
f1 (ppm)

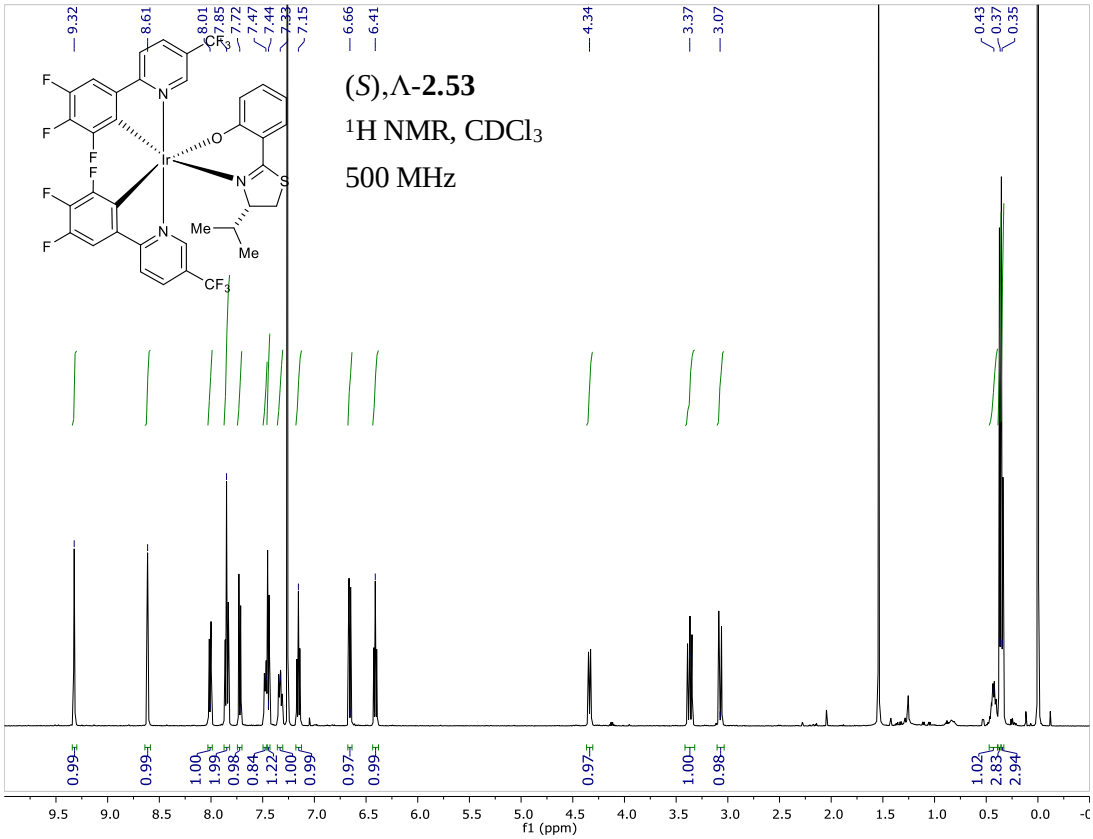
(S),Λ-2.53
1H NMR, CDCl3
500 MHz
f1 (ppm)

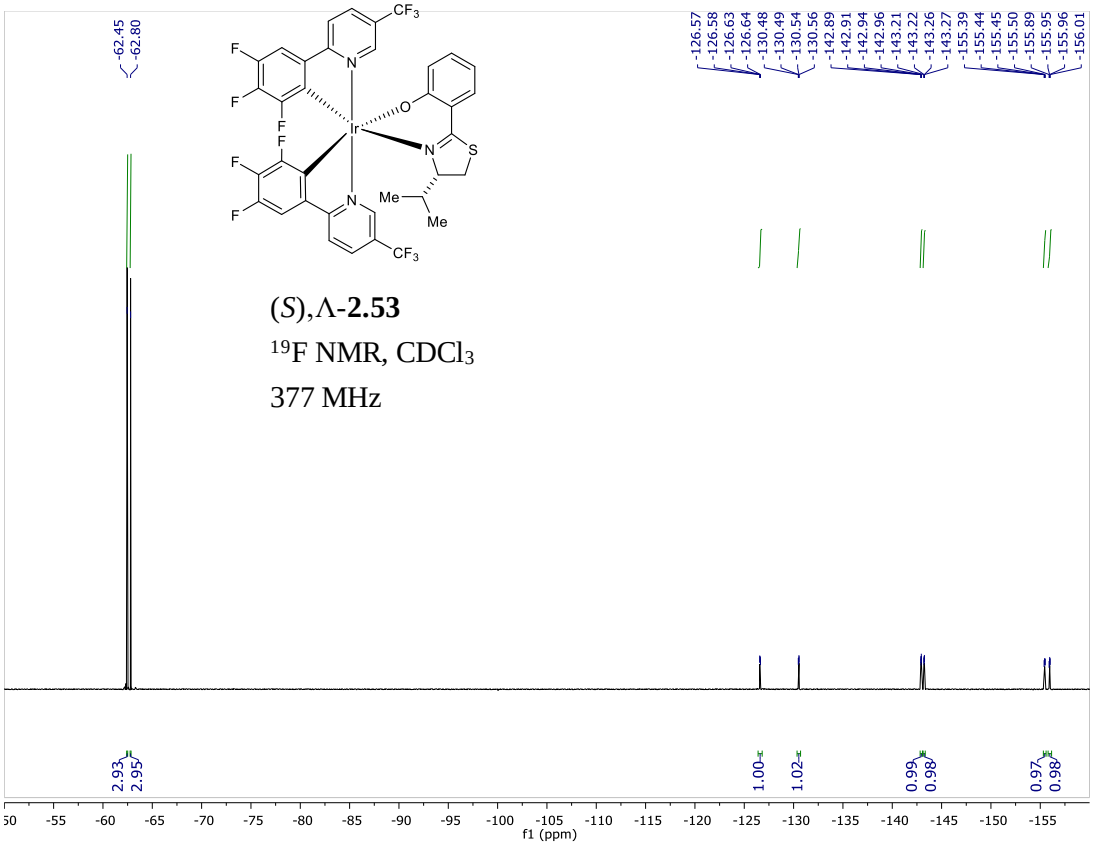
(S),Λ-2.53
19F NMR, CDCl3
377 MHz
f1 (ppm)

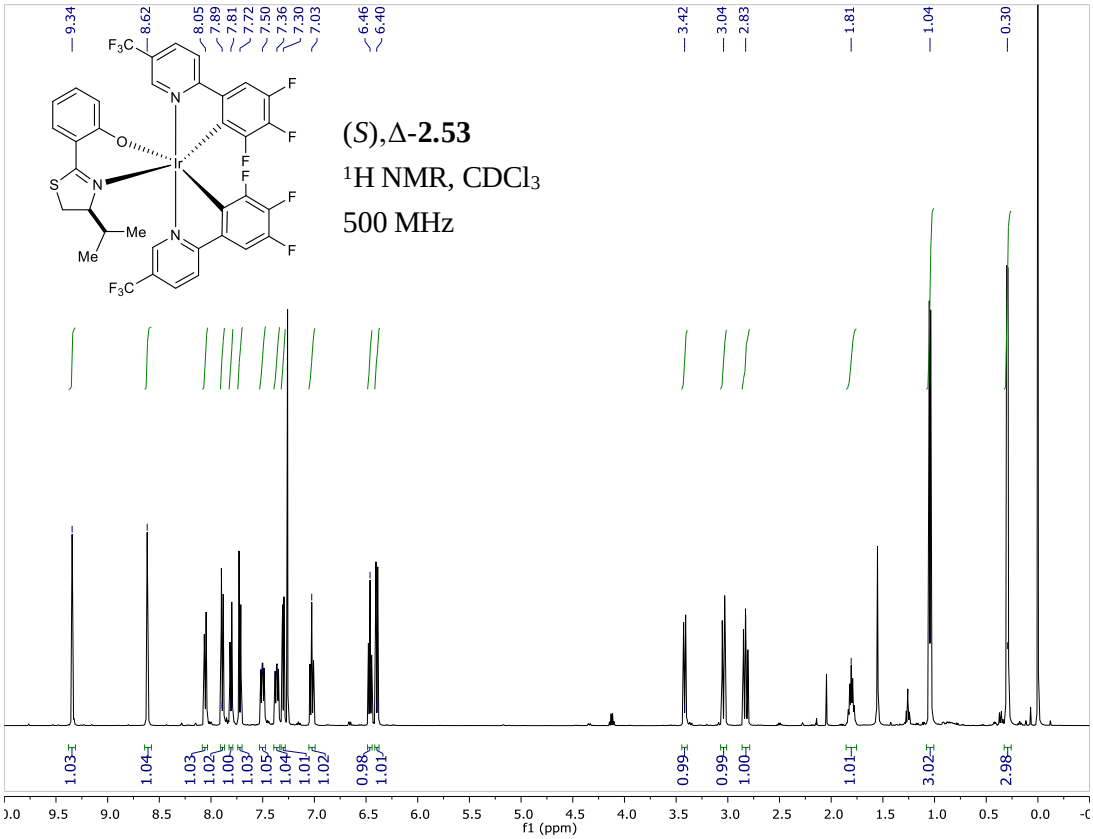
(S),Δ-2.53
1H NMR, CDCl3
500 MHz
f1 (ppm)

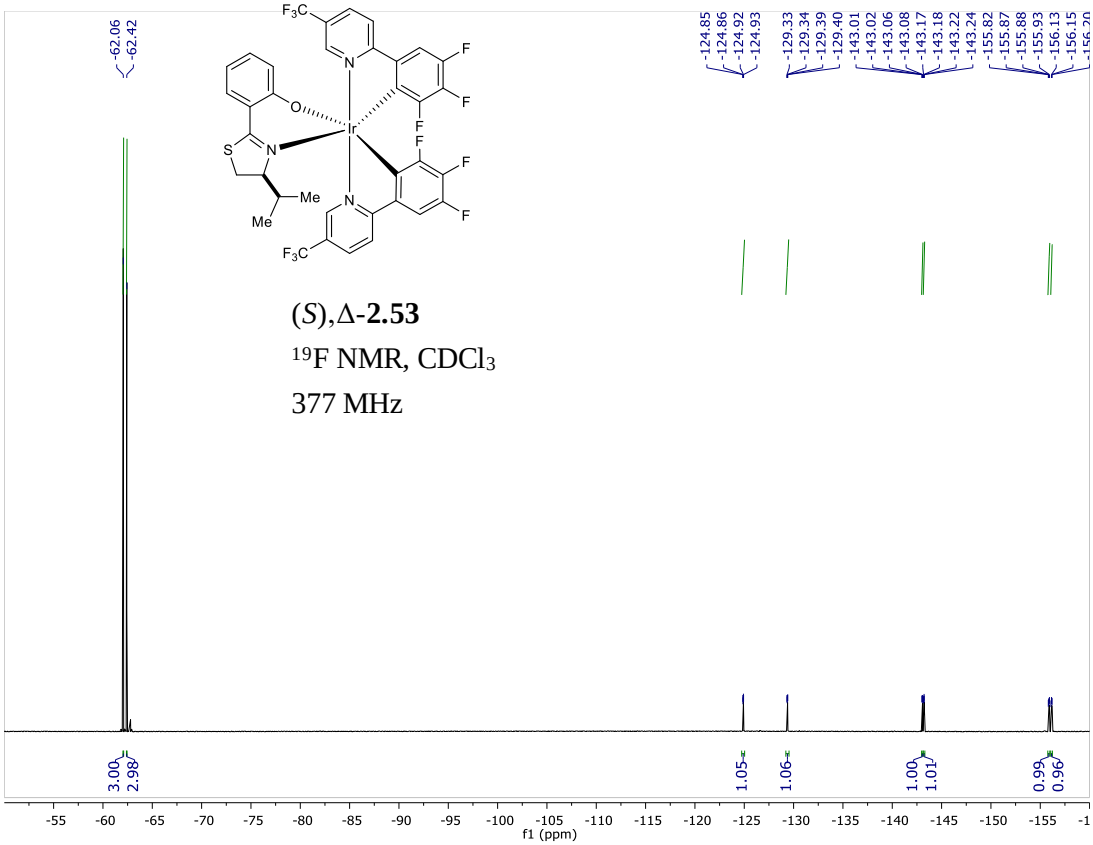
(S),Δ-2.53
19F NMR, CDCl3
377 MHz
f1 (ppm)

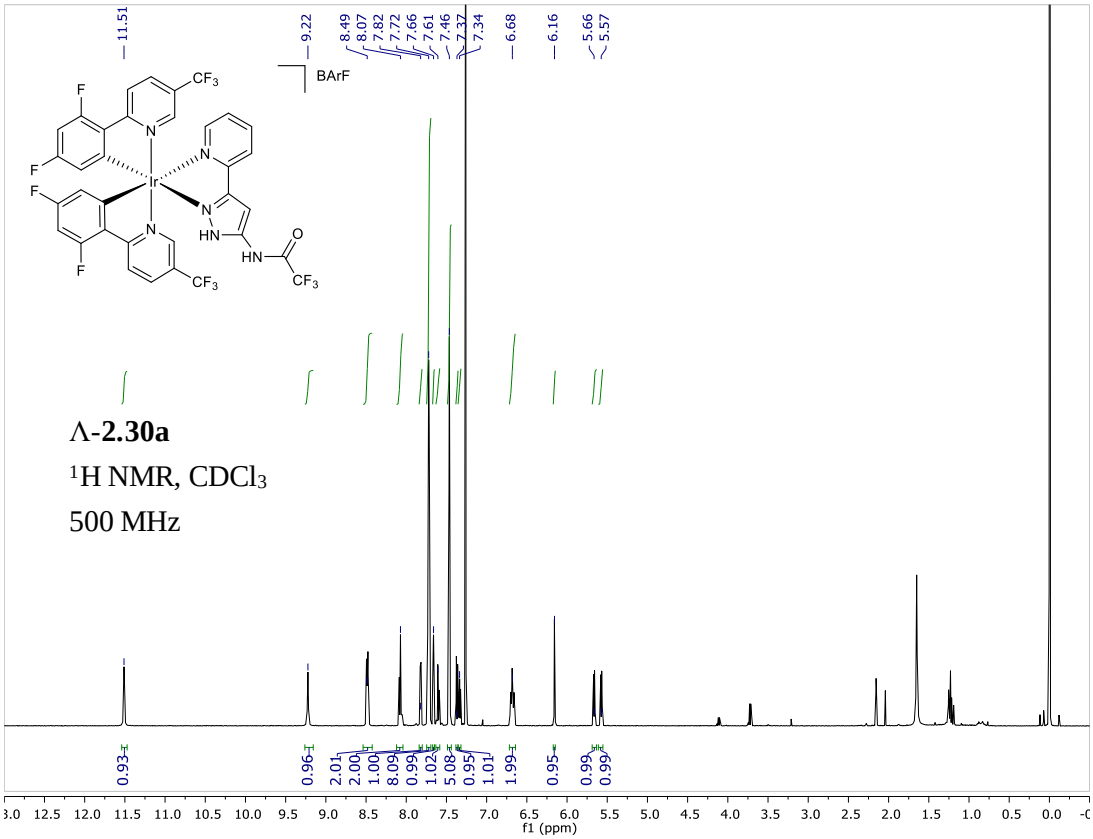

Λ-2.30a

^{1}H NMR, $CDCl_3$

500 MHz

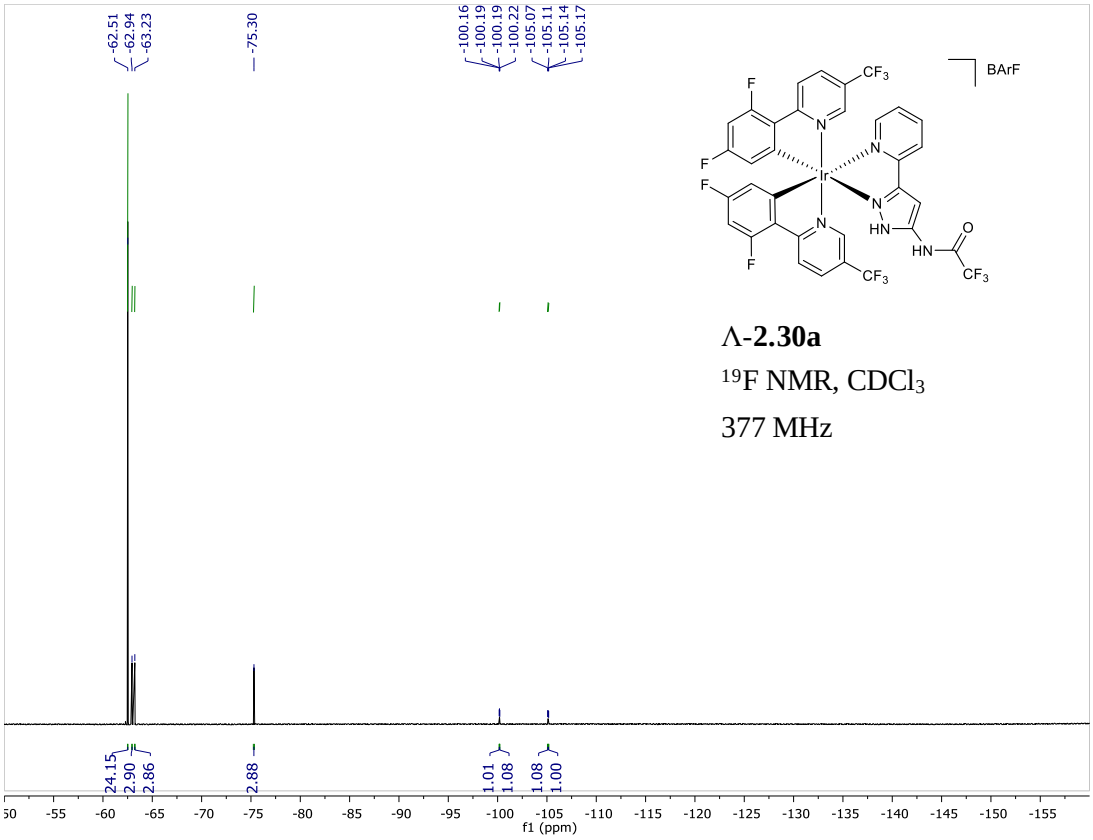

Λ-2.30a

^{19}F NMR, $CDCl_3$

377 MHz

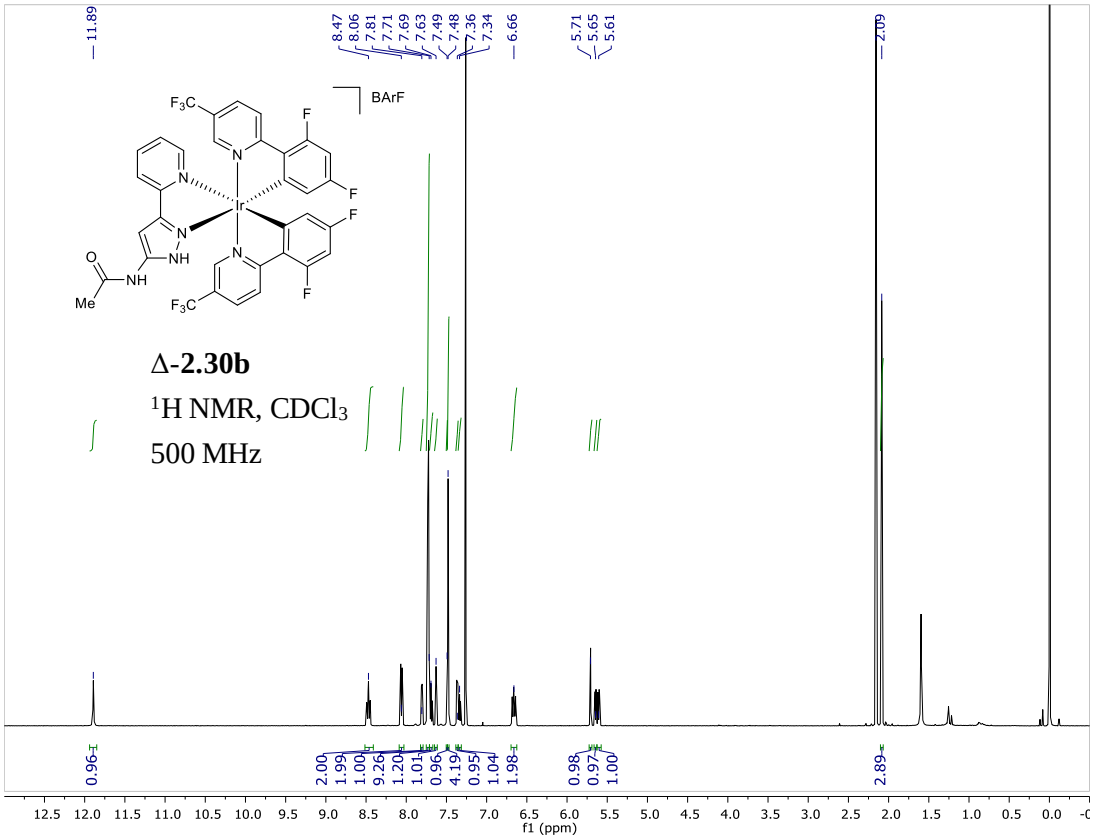
11.89
8.47
8.06
7.81
7.71
7.69
7.63
7.49
7.48
7.36
7.34
6.66
5.71
5.65
5.61
2.09
BArF
F3C
F
N
Ir
NH
O
NH
Me
Δ-2.30b
1H NMR, CDCl3
500 MHz
0.96
2.00
1.99
1.00
9.26
1.20
1.01
0.96
4.19
0.95
1.04
1.98
0.98
0.97
1.00
2.89
f1 (ppm)

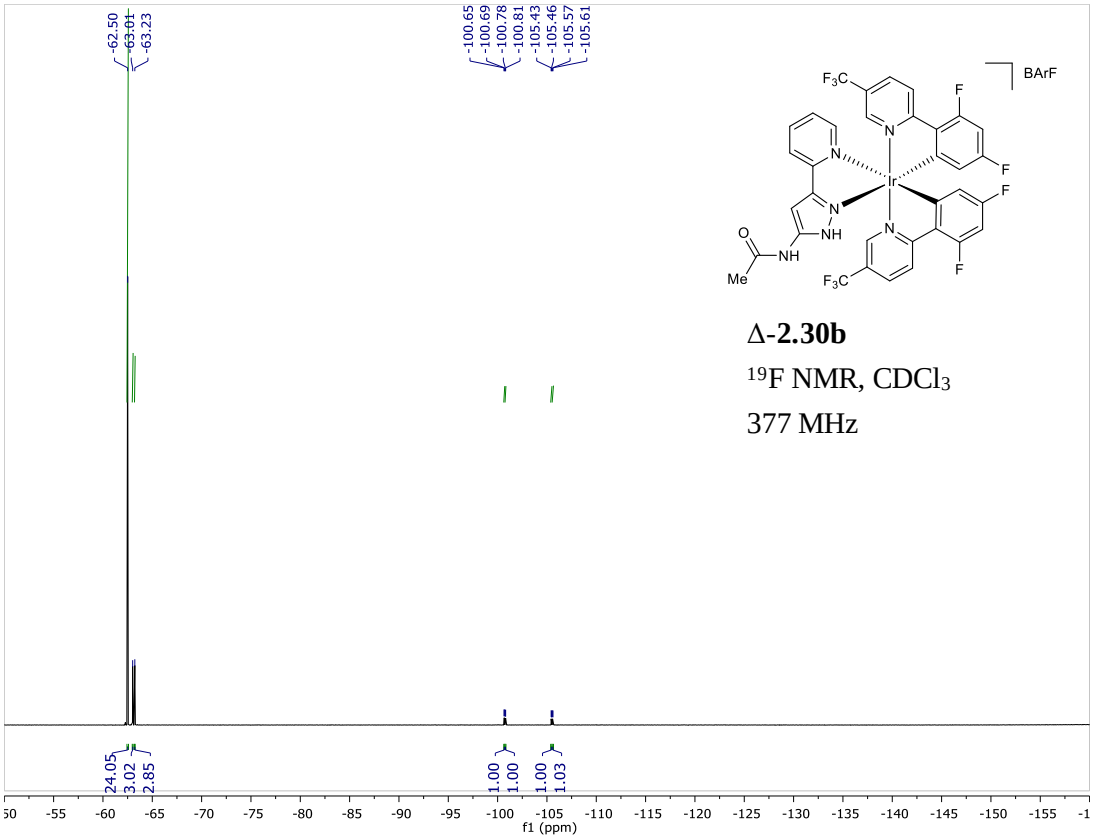
-62.50
-63.01
-63.23
-100.65
-100.69
-100.78
-100.81
-105.43
-105.46
-105.57
-105.61
BArF
F3C
F
N
Ir
NH
O
NH
Me
Δ-2.30b
19F NMR, CDCl3
377 MHz
24.05
3.02
2.85
1.00
1.00
1.00
1.03
f1 (ppm)

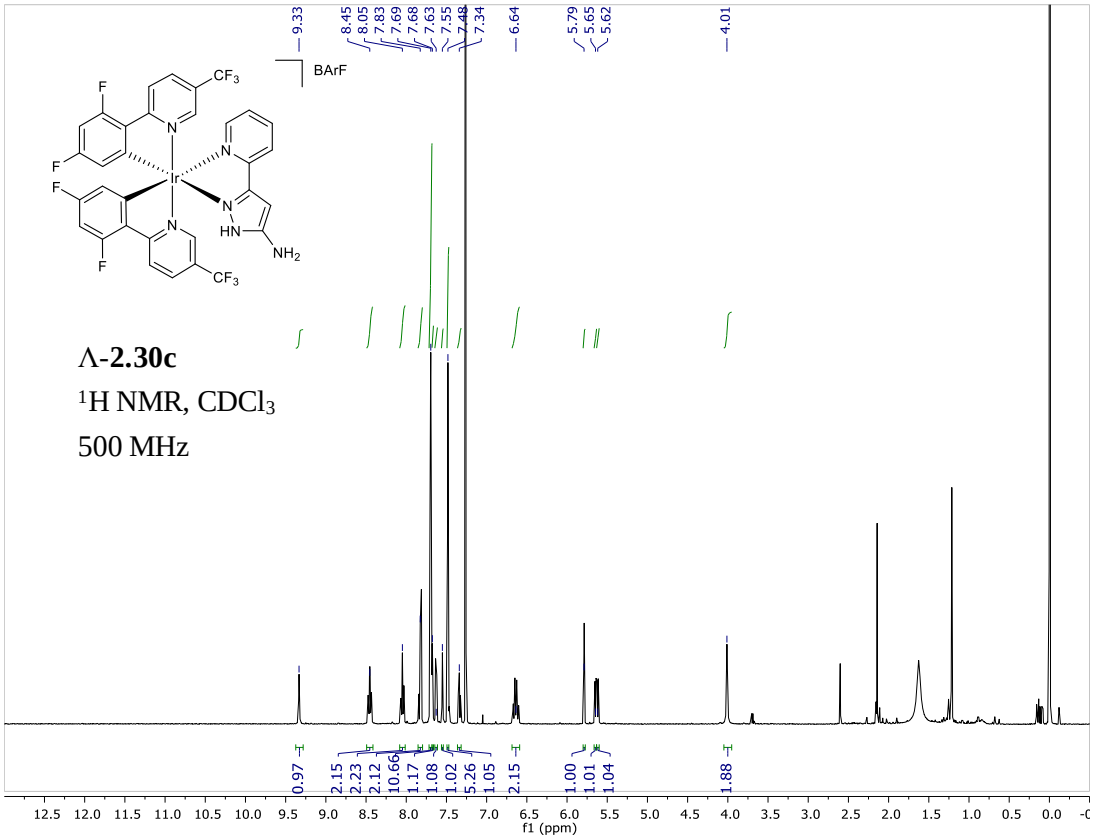
BArF
Λ-2.30c
1H NMR, CDCl3
500 MHz
f1 (ppm)

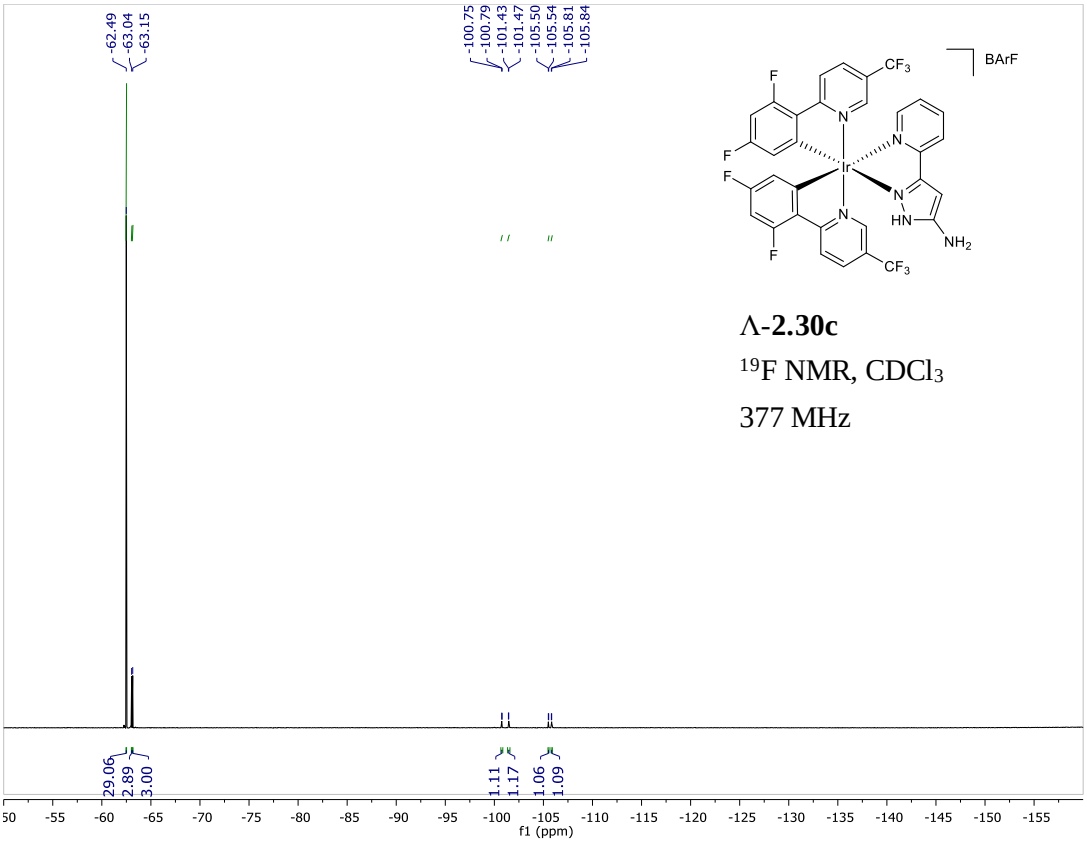
BArF
Λ-2.30c
19F NMR, CDCl3
377 MHz
f1 (ppm)

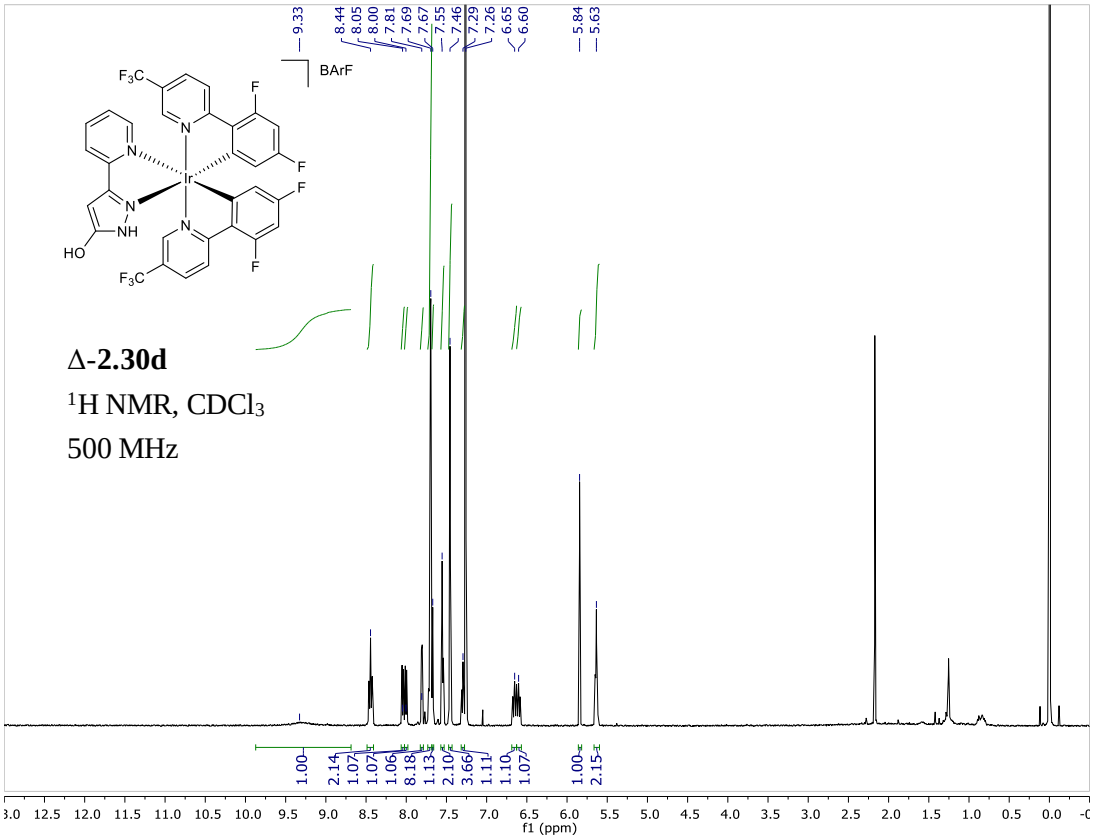

Δ-2.30d

^{1}H NMR, $CDCl_3$

500 MHz

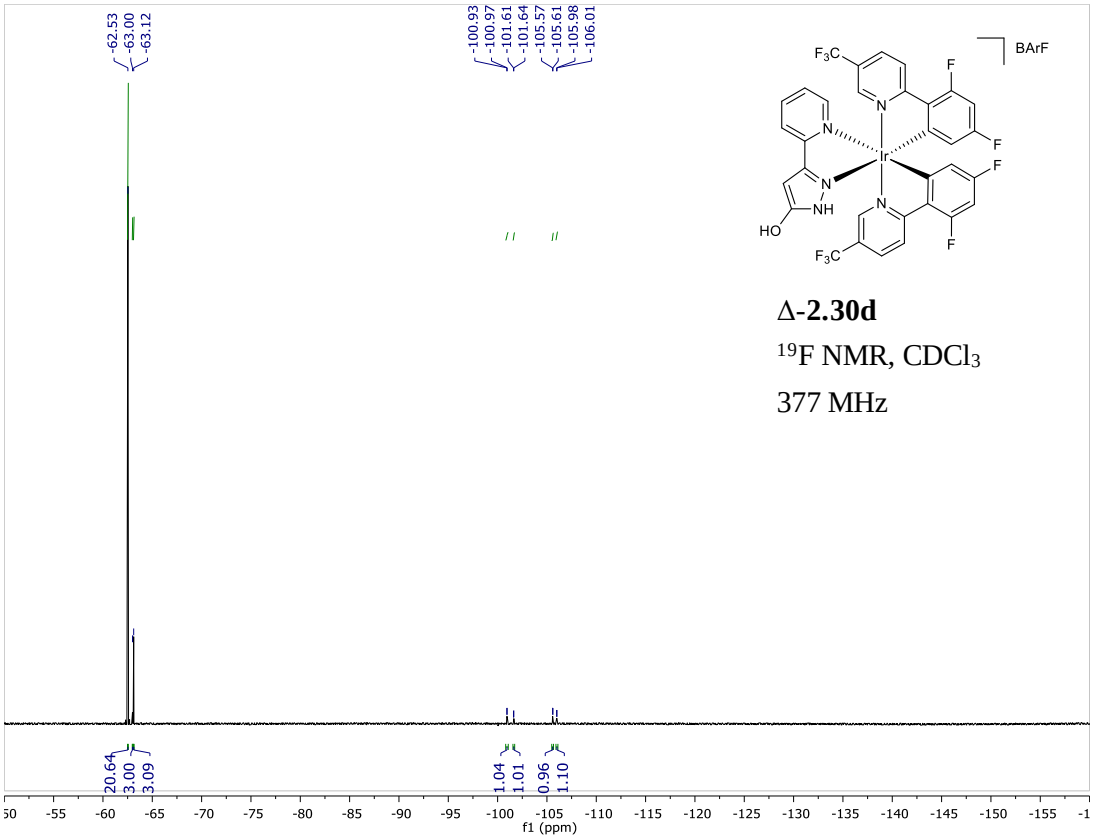

Δ-2.30d

^{19}F NMR, $CDCl_3$

377 MHz

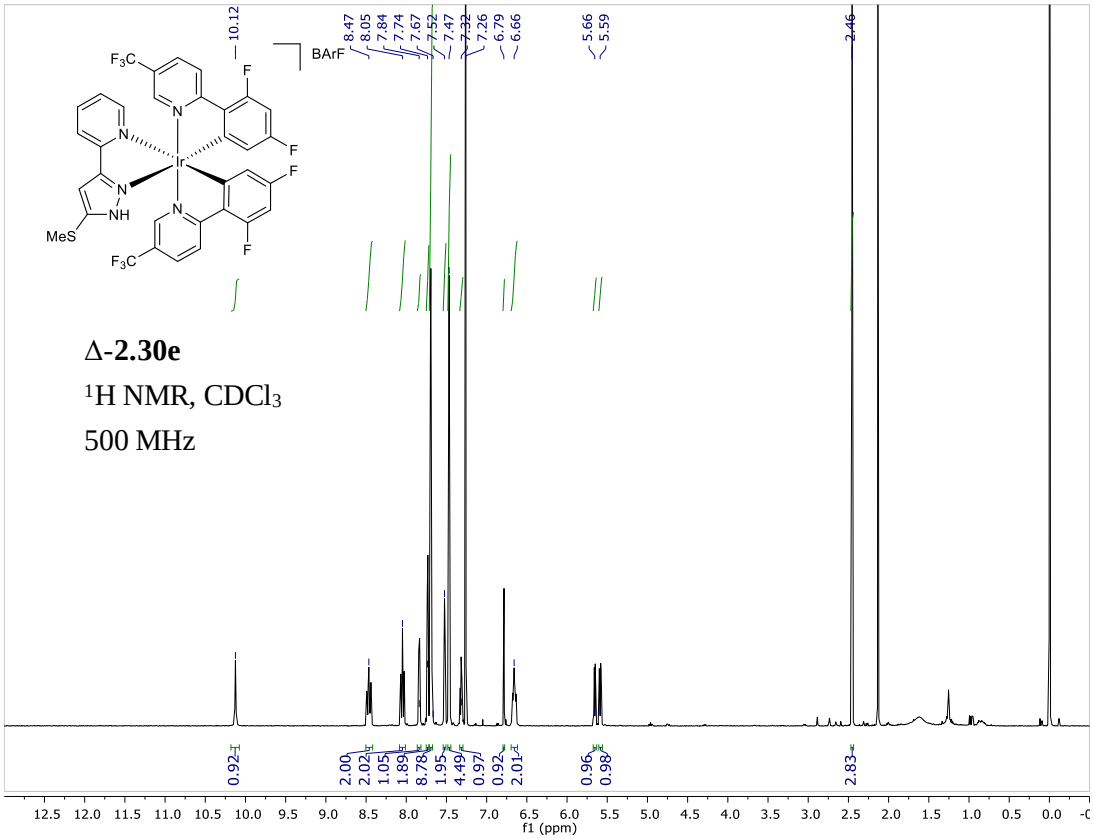

Δ-**2.30e**

^{1}H NMR, $CDCl_3$

500 MHz

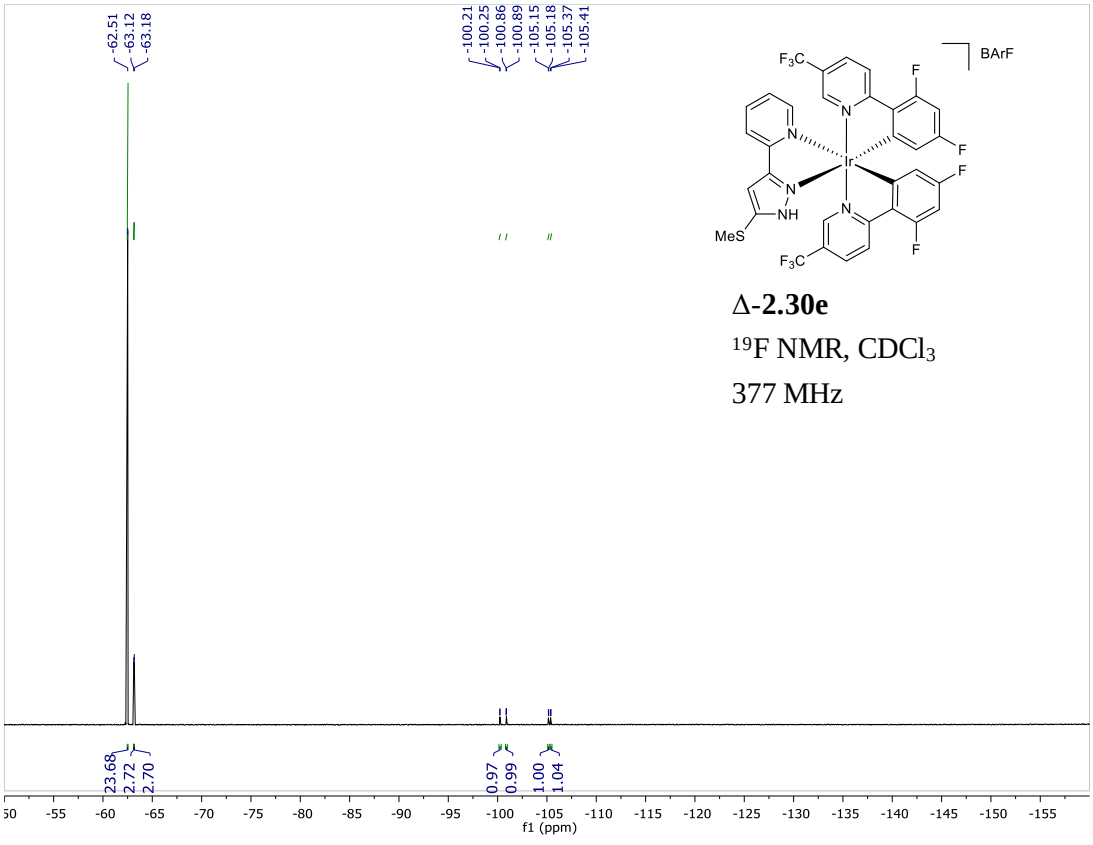

Δ-**2.30e**

^{19}F NMR, $CDCl_3$

377 MHz

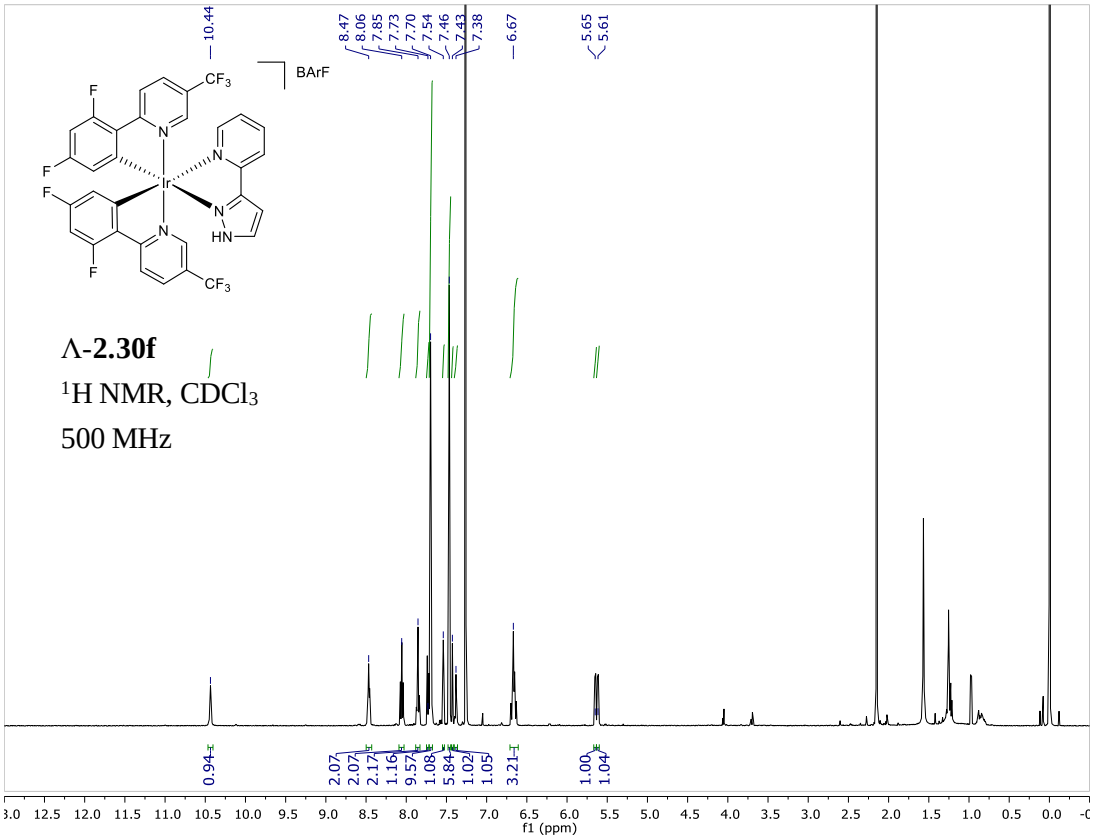

Λ-2.30f

^{1}H NMR, $CDCl_3$

500 MHz

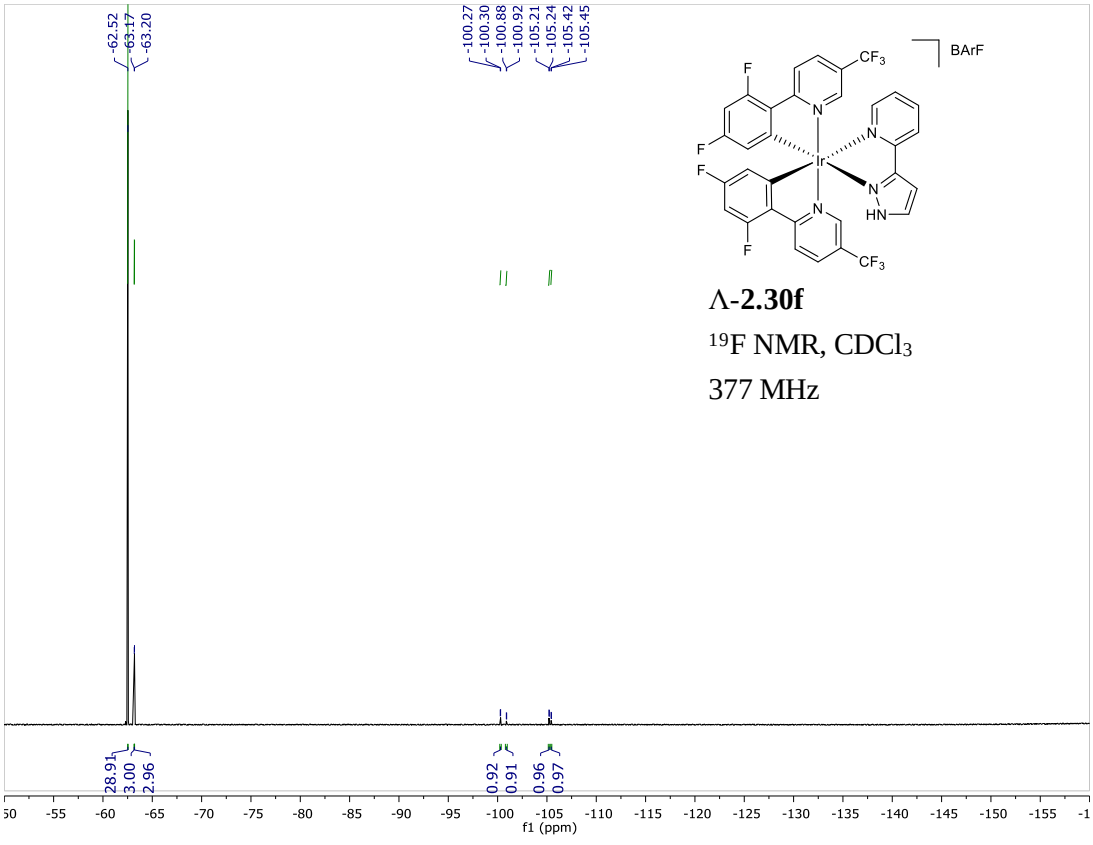

Λ-2.30f

^{19}F NMR, $CDCl_3$

377 MHz

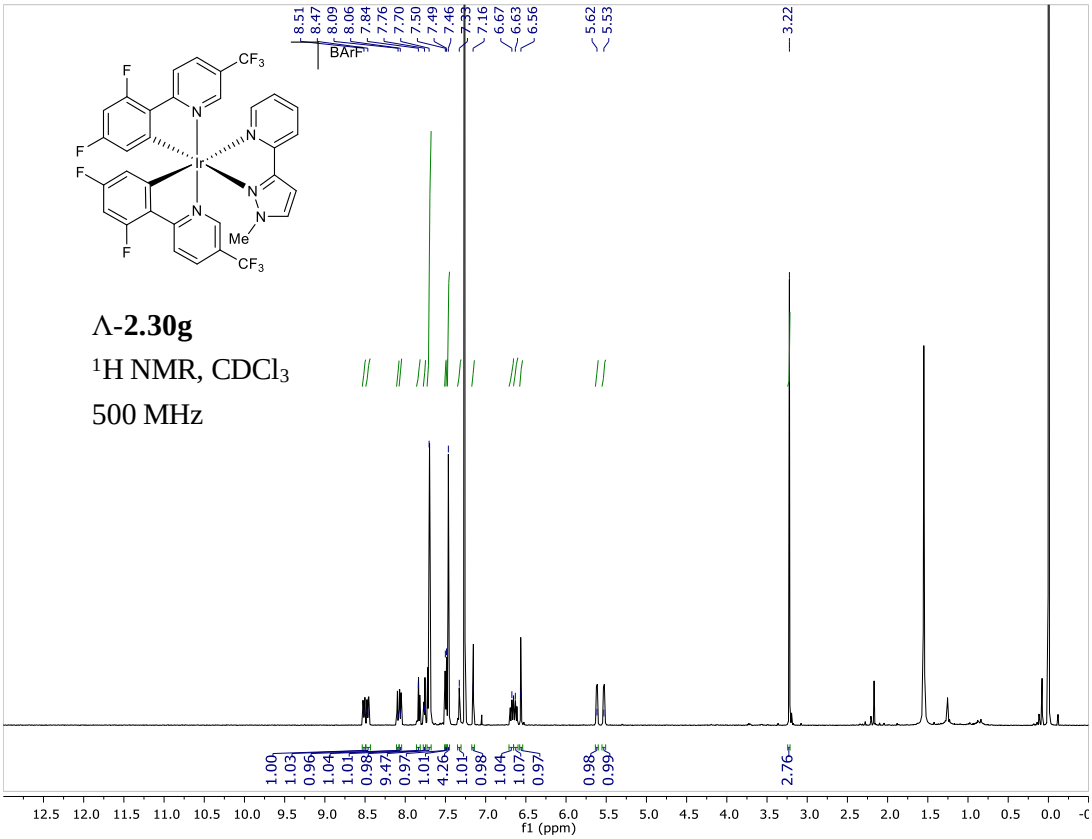

Λ-**2.30g**

^{1}H NMR, $CDCl_3$

500 MHz

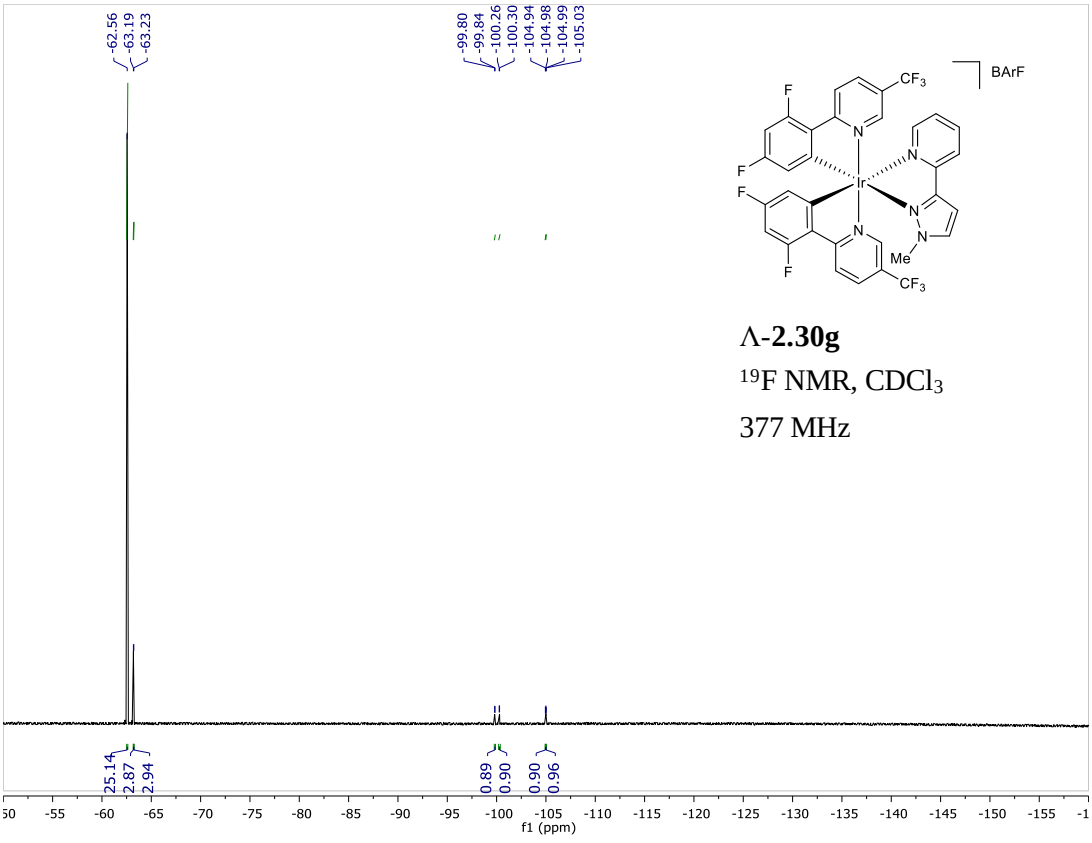

Λ-**2.30g**

^{19}F NMR, $CDCl_3$

377 MHz

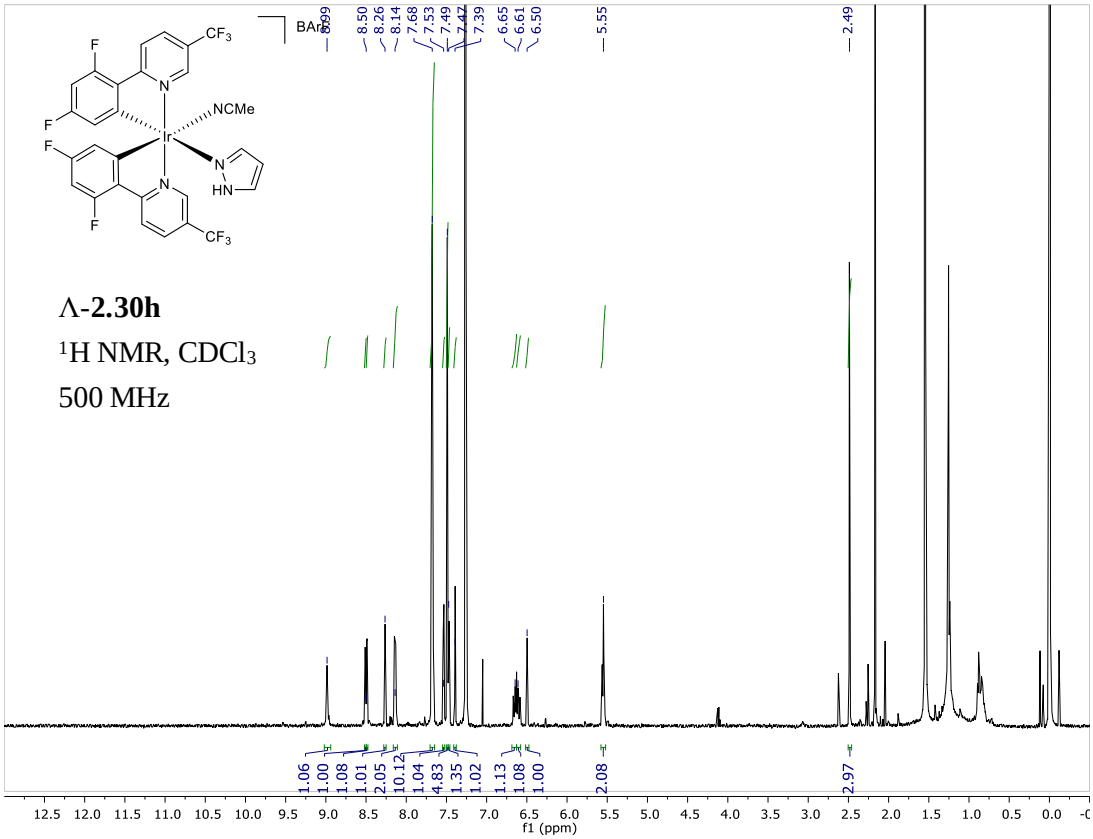

Λ-2.30h

^{1}H NMR, $CDCl_3$

500 MHz

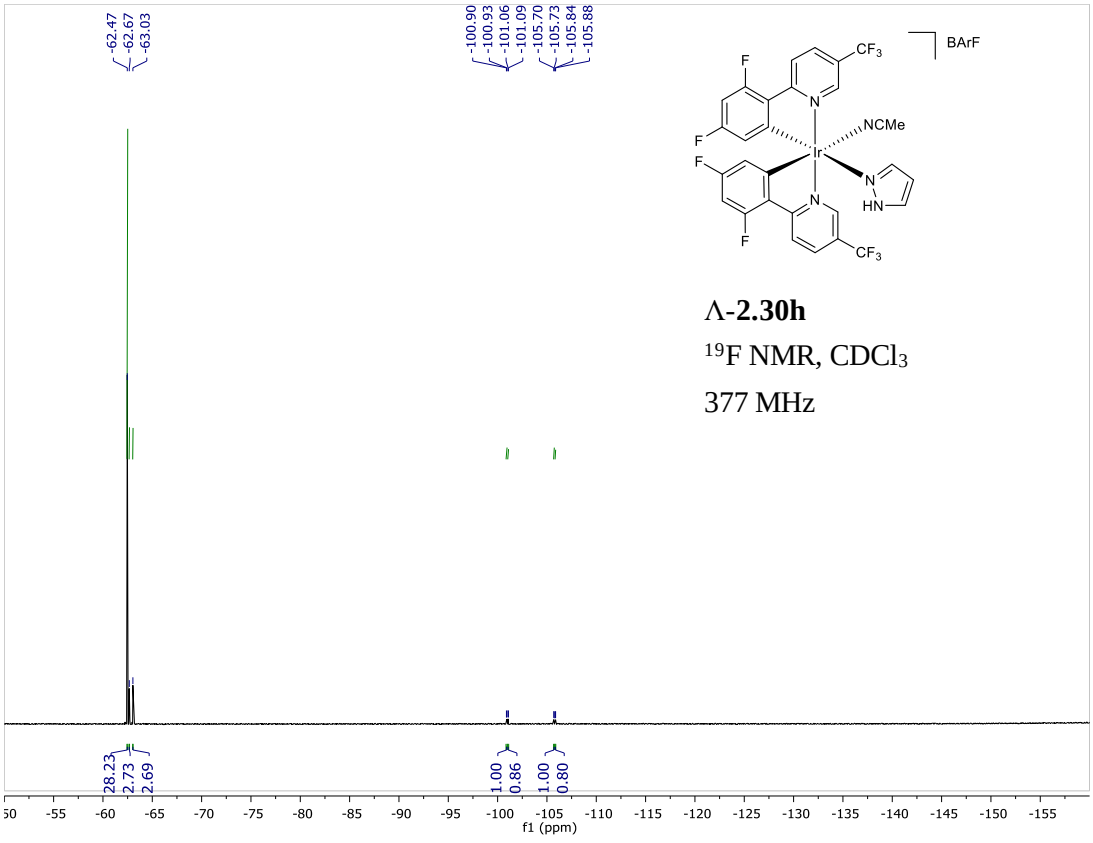

Λ-2.30h

^{19}F NMR, $CDCl_3$

377 MHz

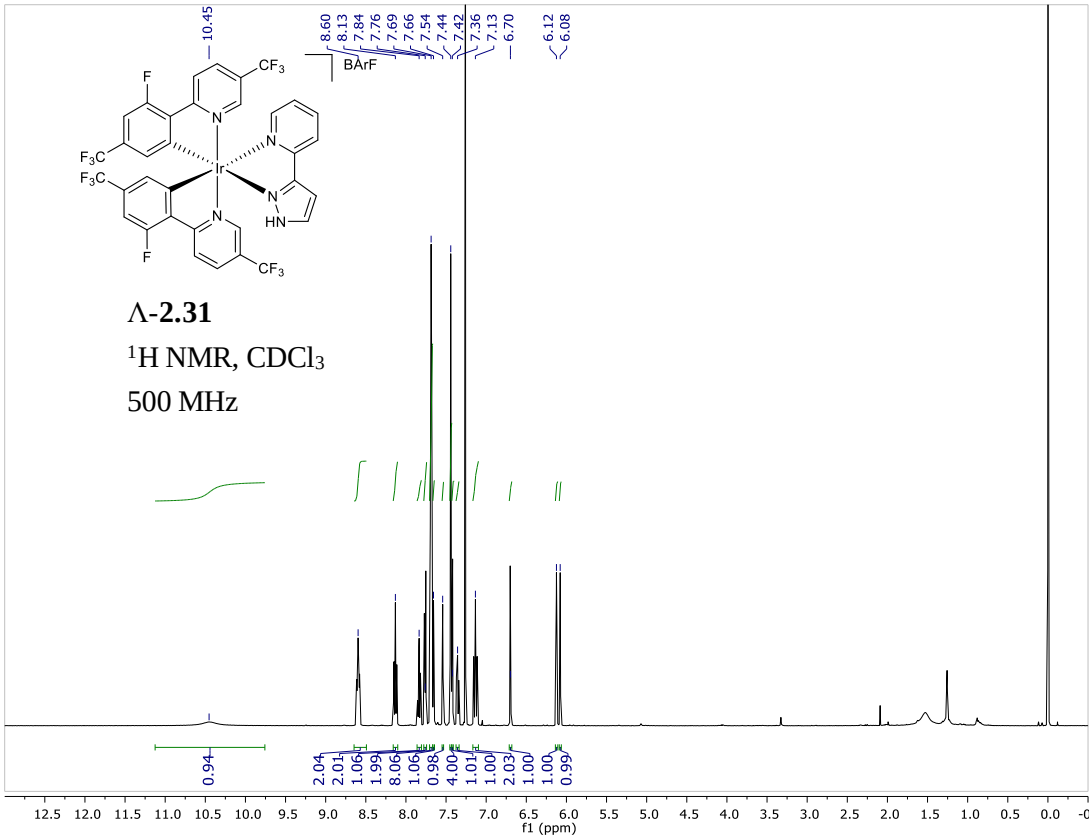

Λ-2.31

^{1}H NMR, $CDCl_3$

500 MHz

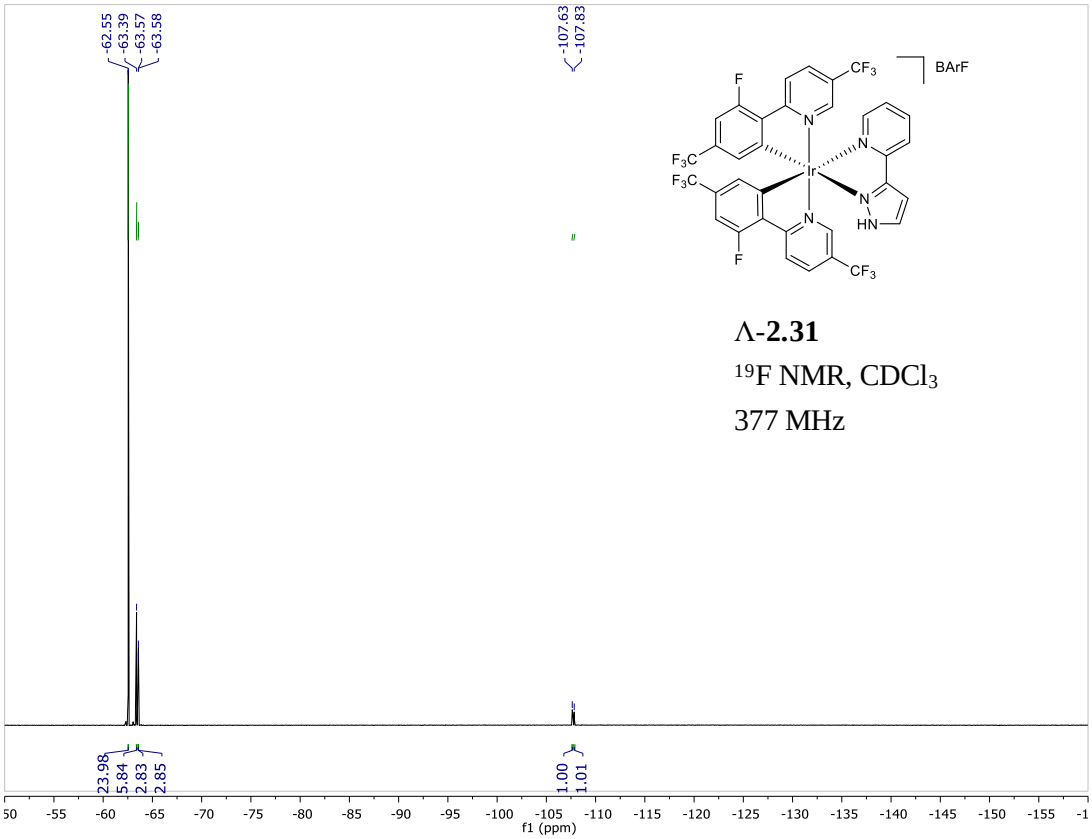

Λ-2.31

^{19}F NMR, $CDCl_3$

377 MHz

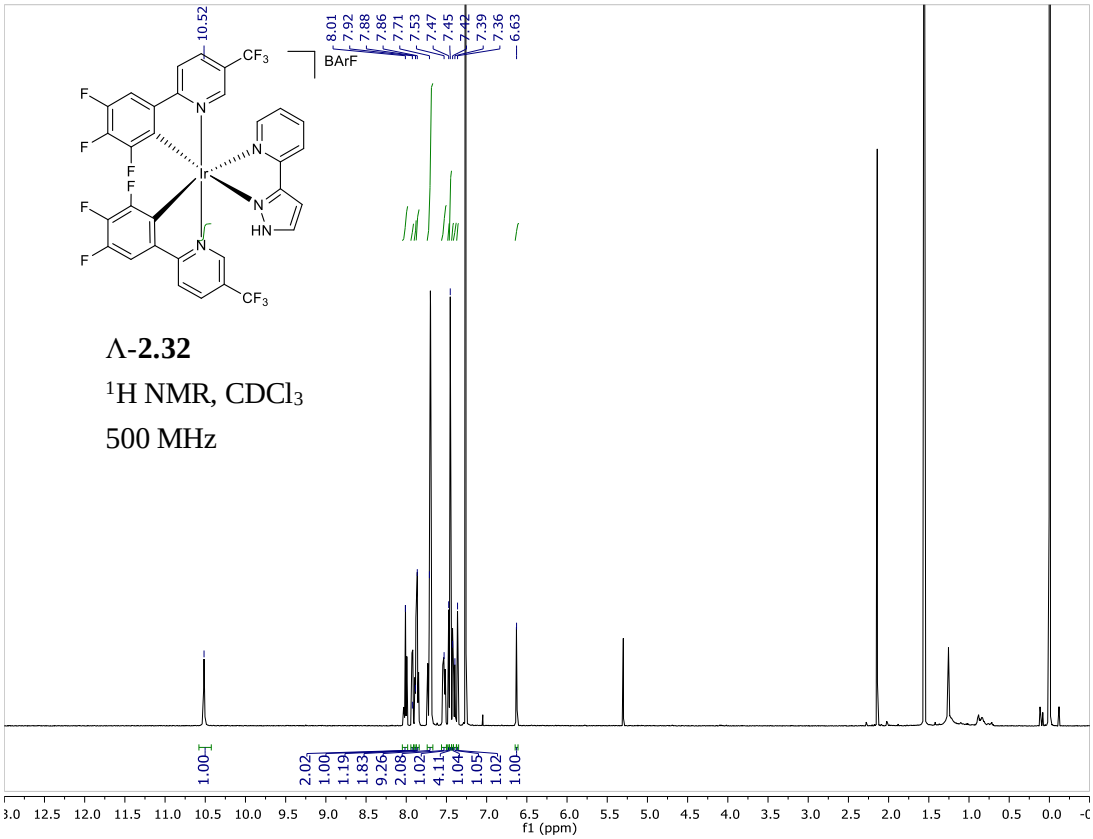

Λ-**2.32**

^{1}H NMR, $CDCl_3$

500 MHz

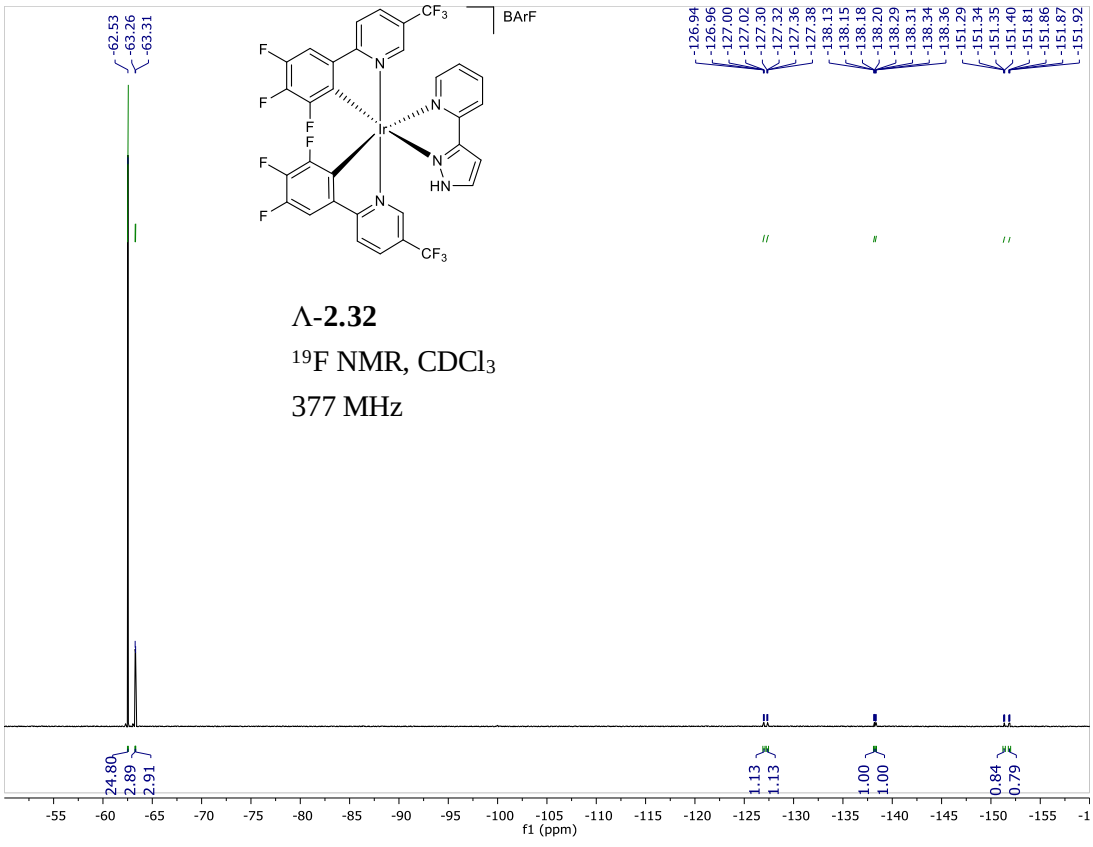

Λ-**2.32**

^{19}F NMR, $CDCl_3$

377 MHz

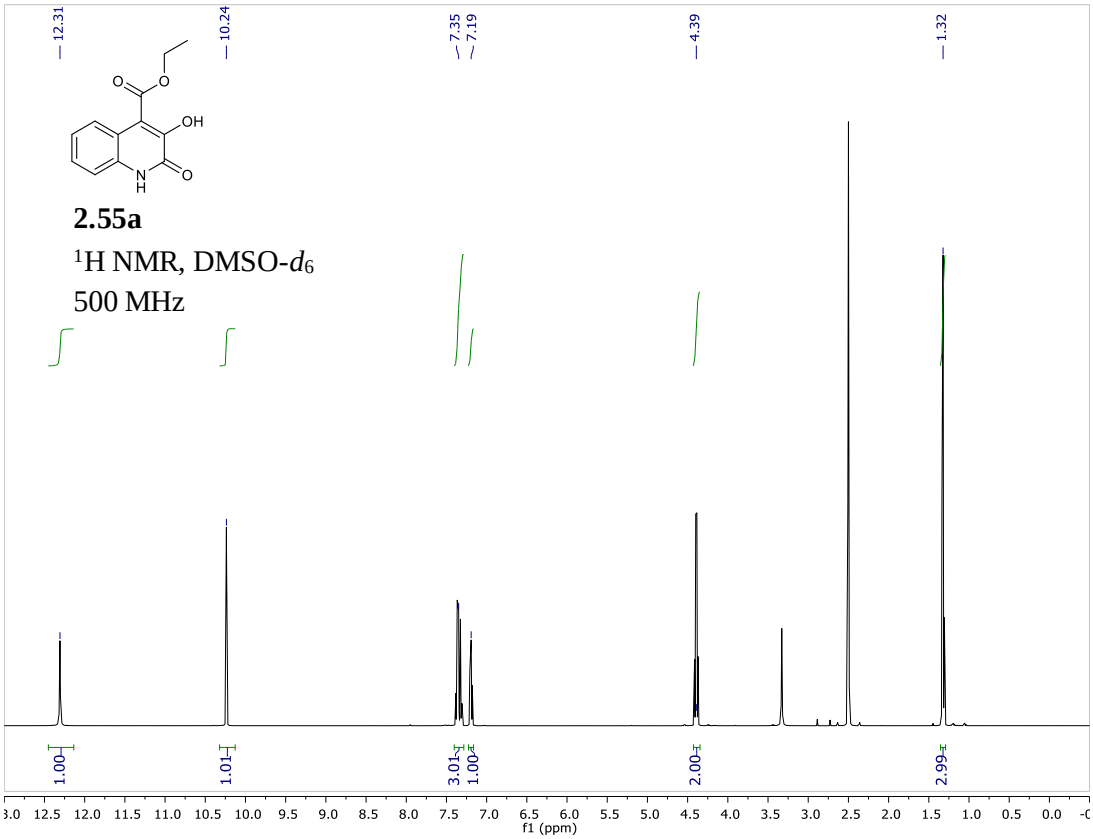

2.55a

^{1}H NMR, DMSO-d_6

500 MHz

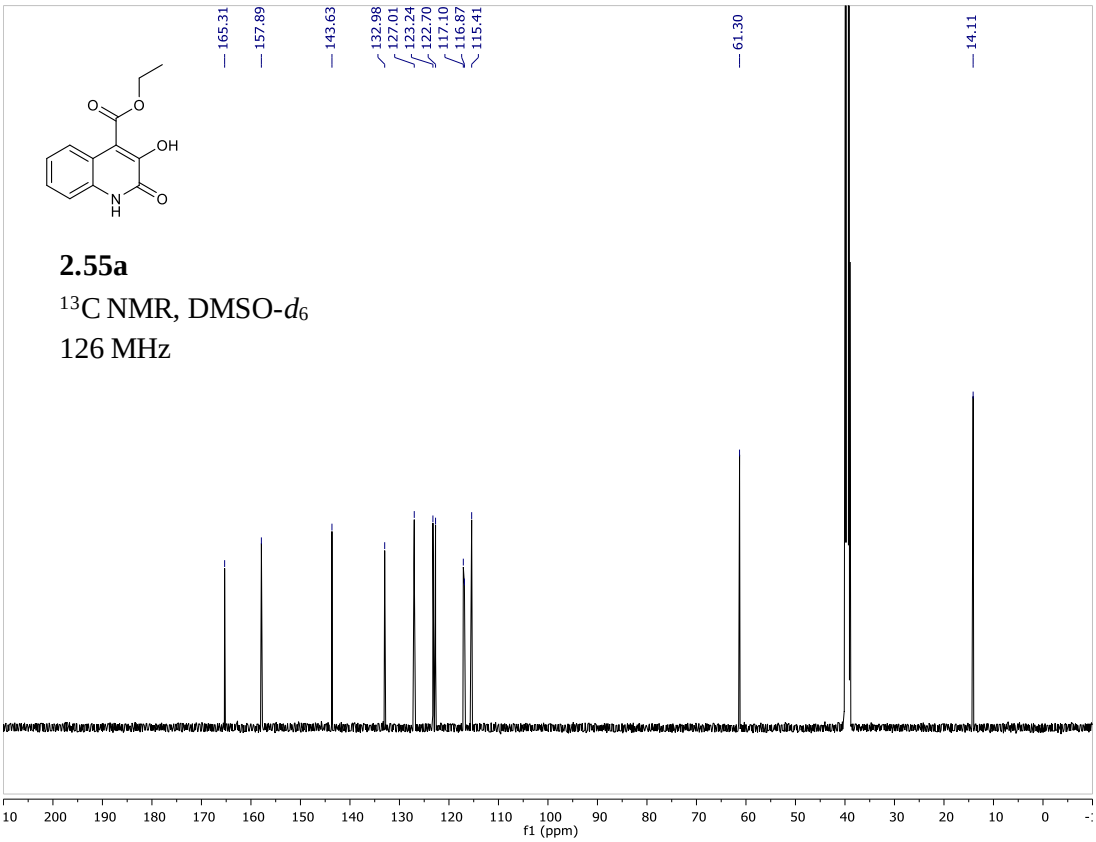

2.55a

^{13}C NMR, DMSO-d_6

126 MHz

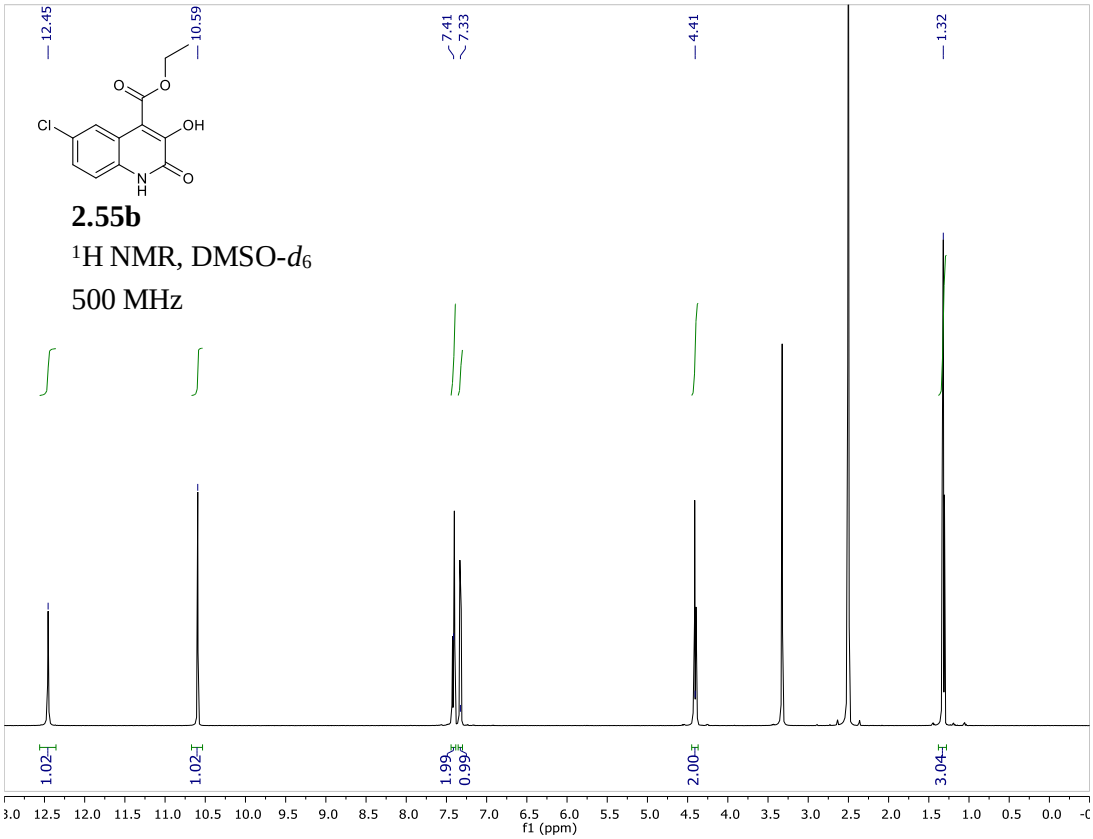

2.55b

^{1}H NMR, DMSO-d_6

500 MHz

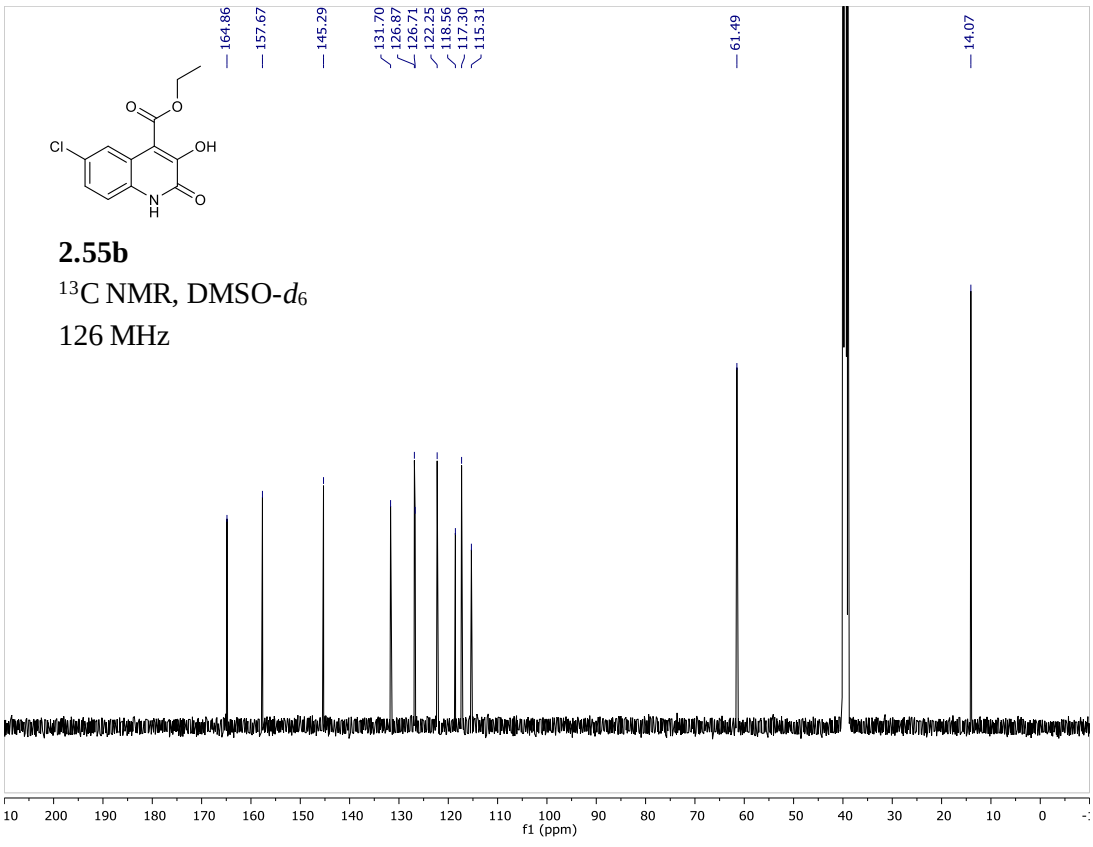

2.55b

^{13}C NMR, DMSO-d_6

126 MHz

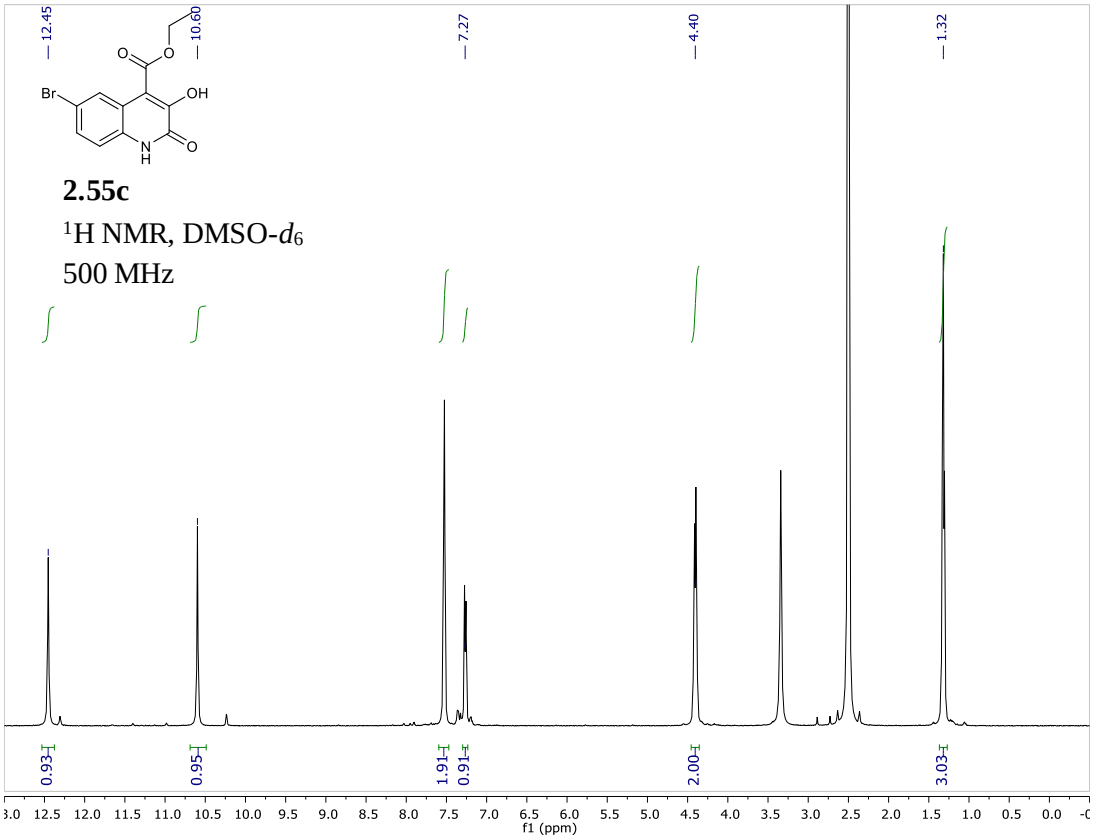

2.55c

^{1}H NMR, DMSO-d_6

500 MHz

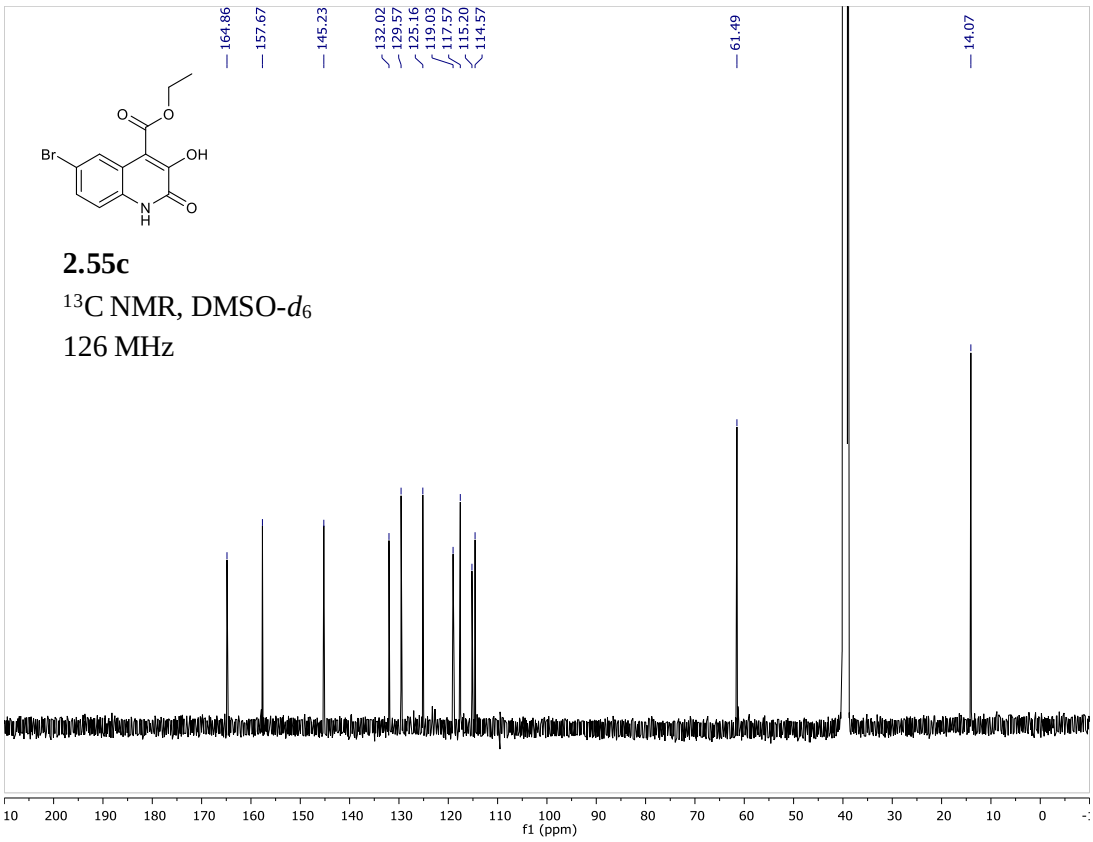

2.55c

^{13}C NMR, DMSO-d_6

126 MHz

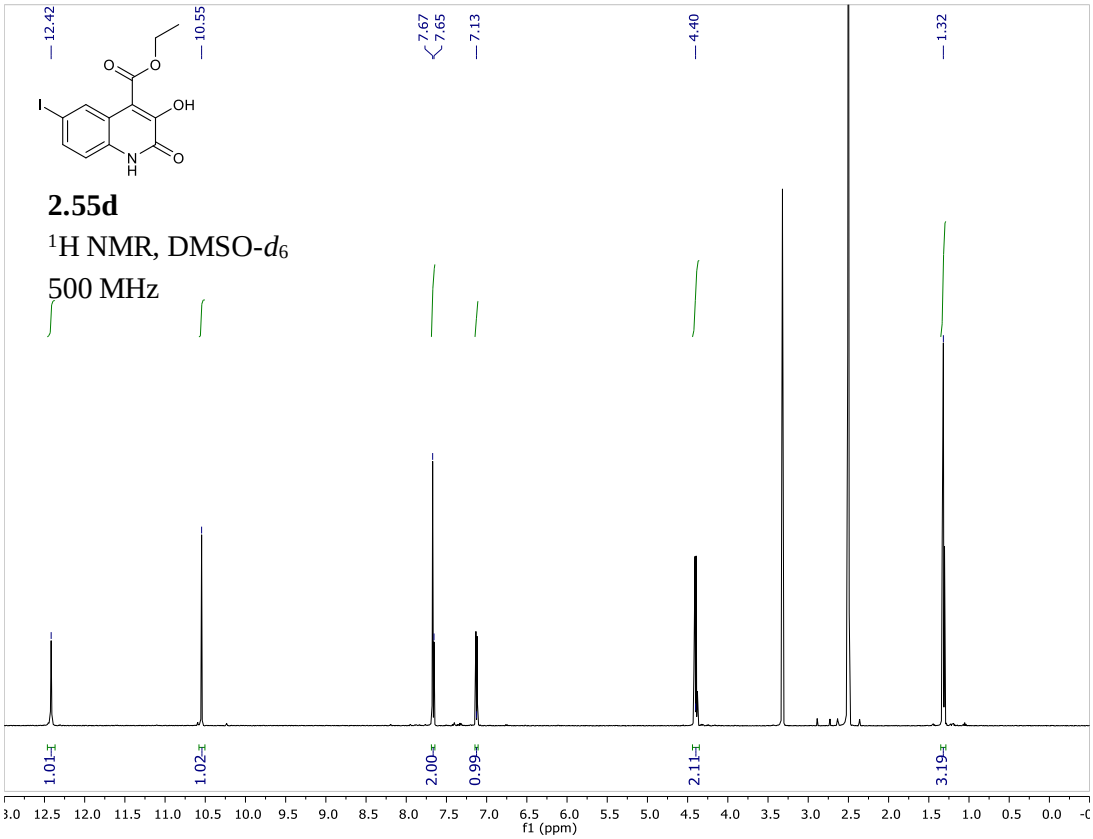

2.55d

^{1}H NMR, DMSO-d_6

500 MHz

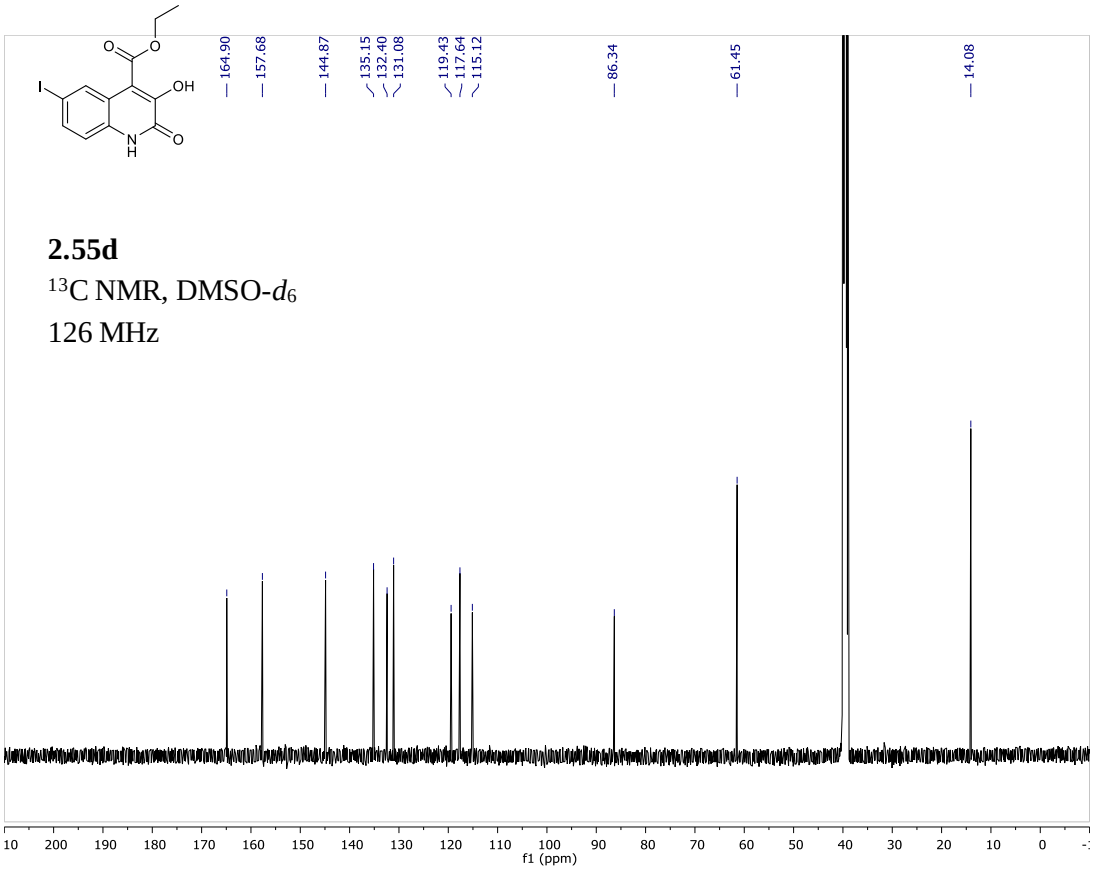

2.55d

^{13}C NMR, DMSO-d_6

126 MHz

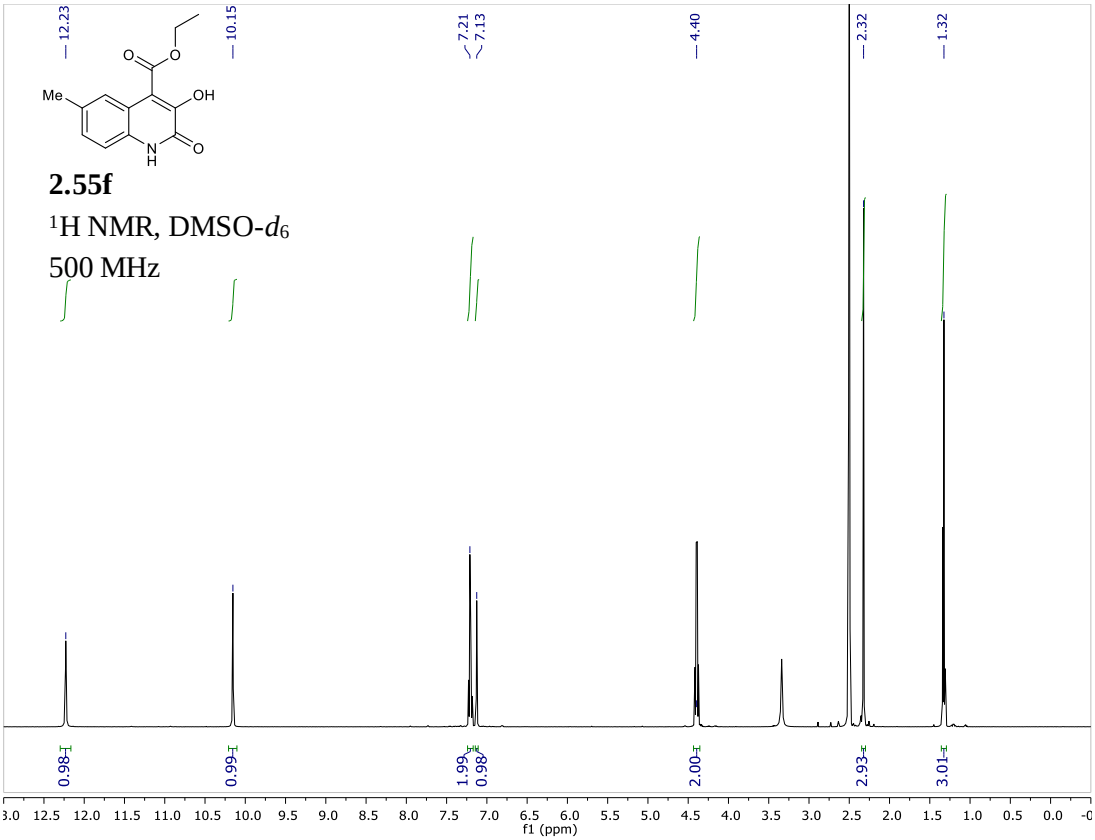

2.55f

^{1}H NMR, DMSO-d_6

500 MHz

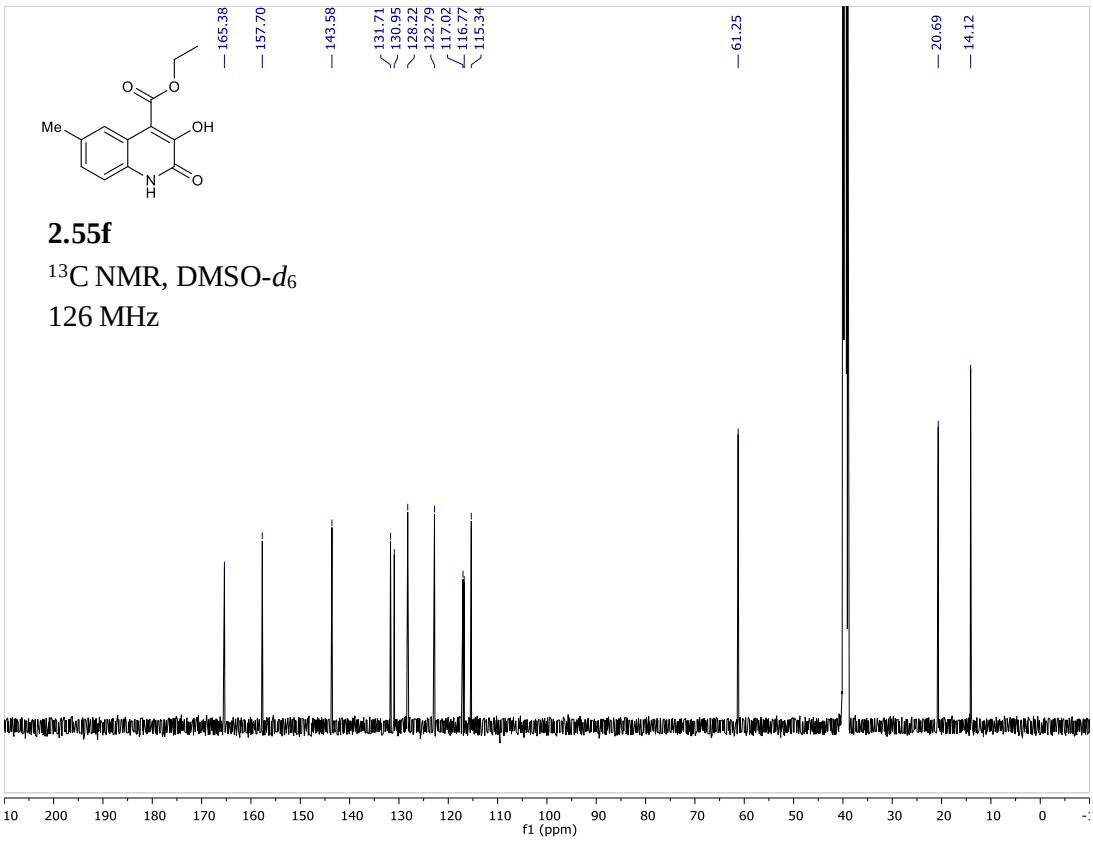

2.55f

^{13}C NMR, DMSO-d_6

126 MHz

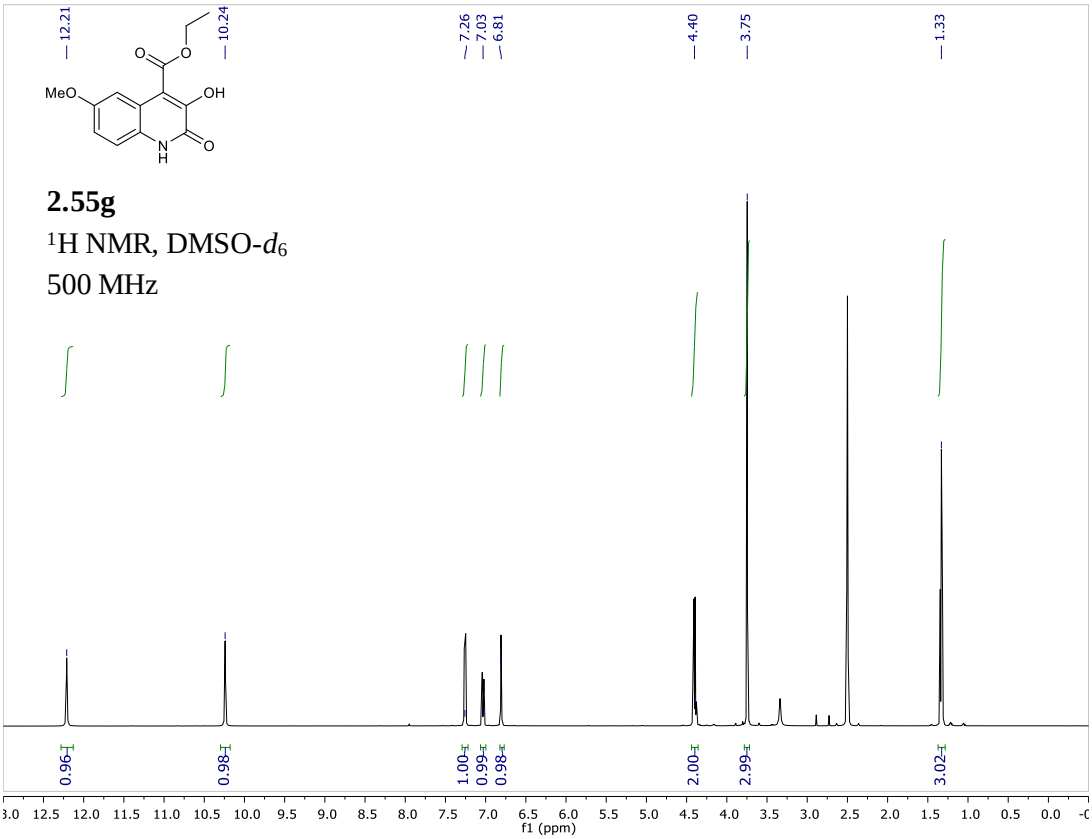

2.55g

^{1}H NMR, DMSO-d_6

500 MHz

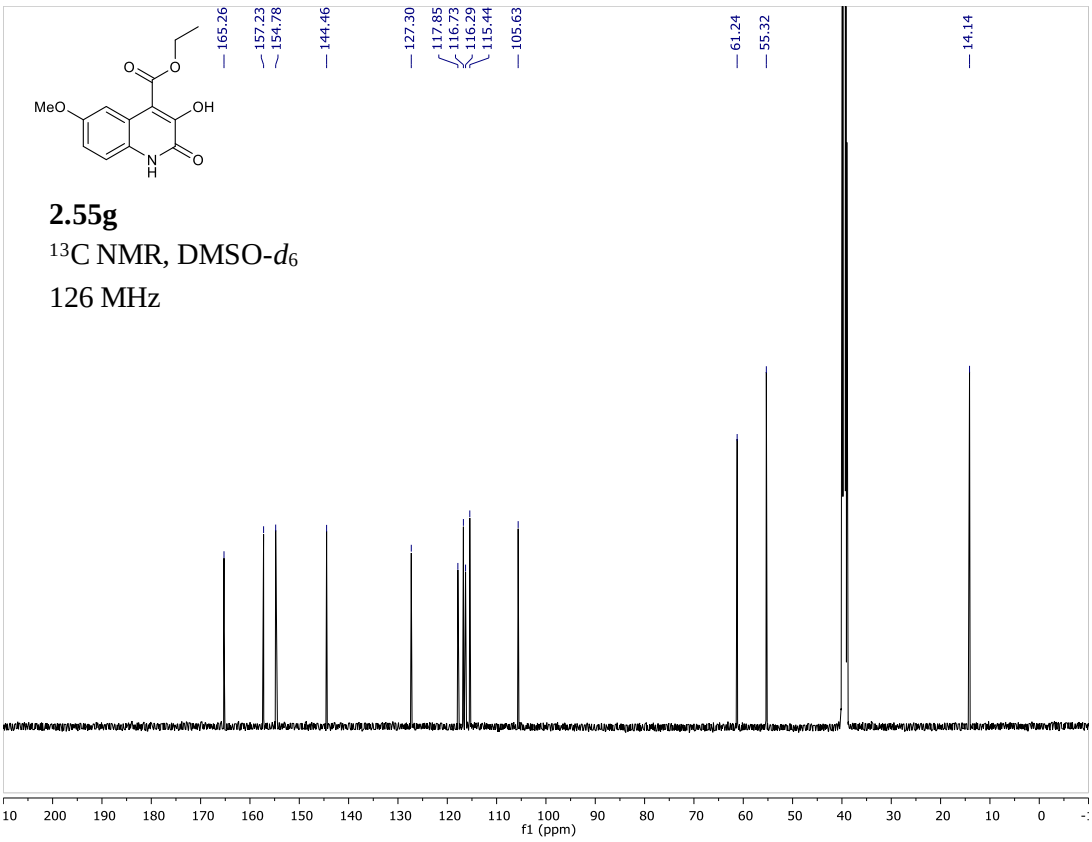

2.55g

^{13}C NMR, DMSO-d_6

126 MHz

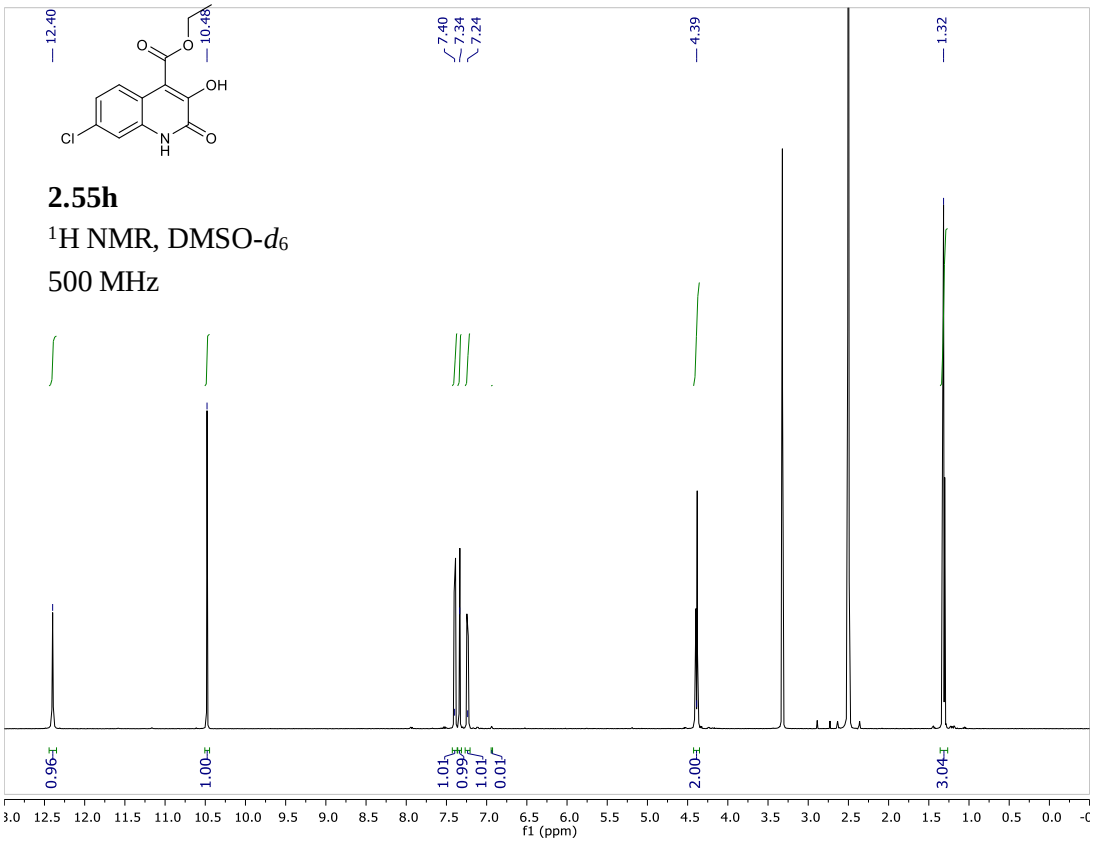

2.55h

^{1}H NMR, DMSO-d_6

500 MHz

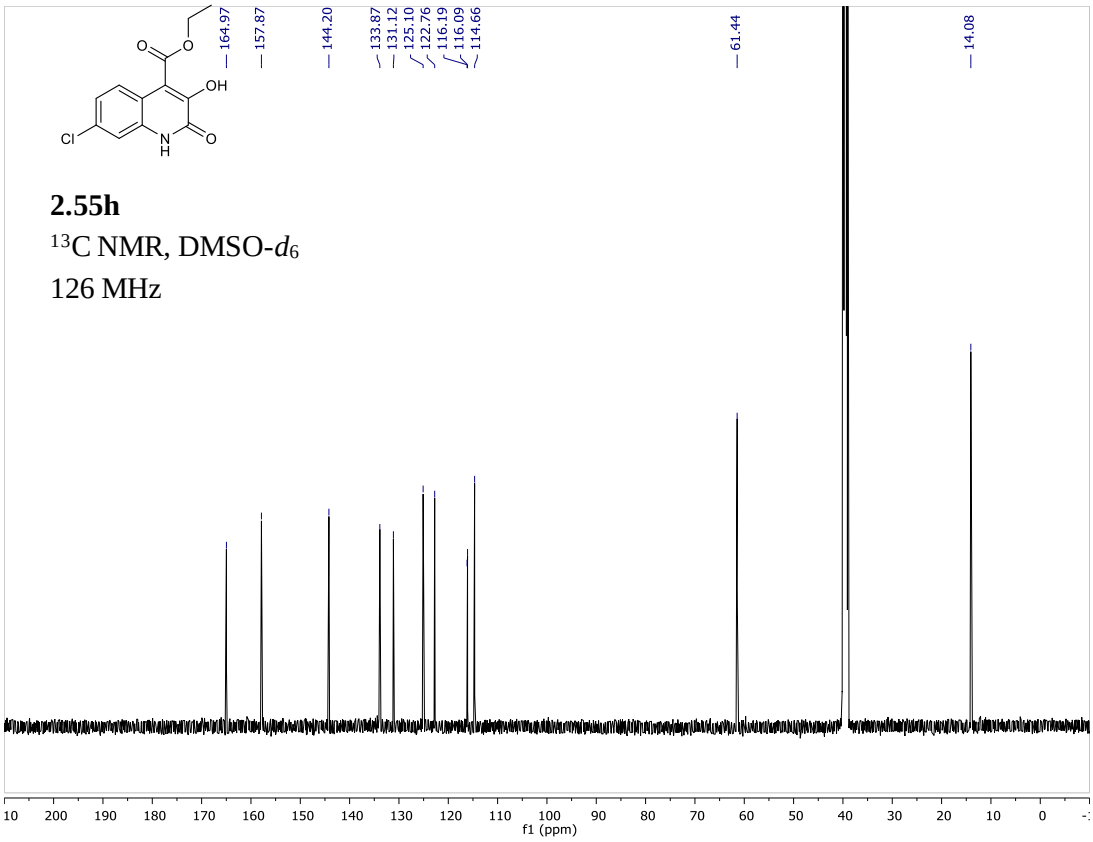

2.55h

^{13}C NMR, DMSO-d_6

126 MHz

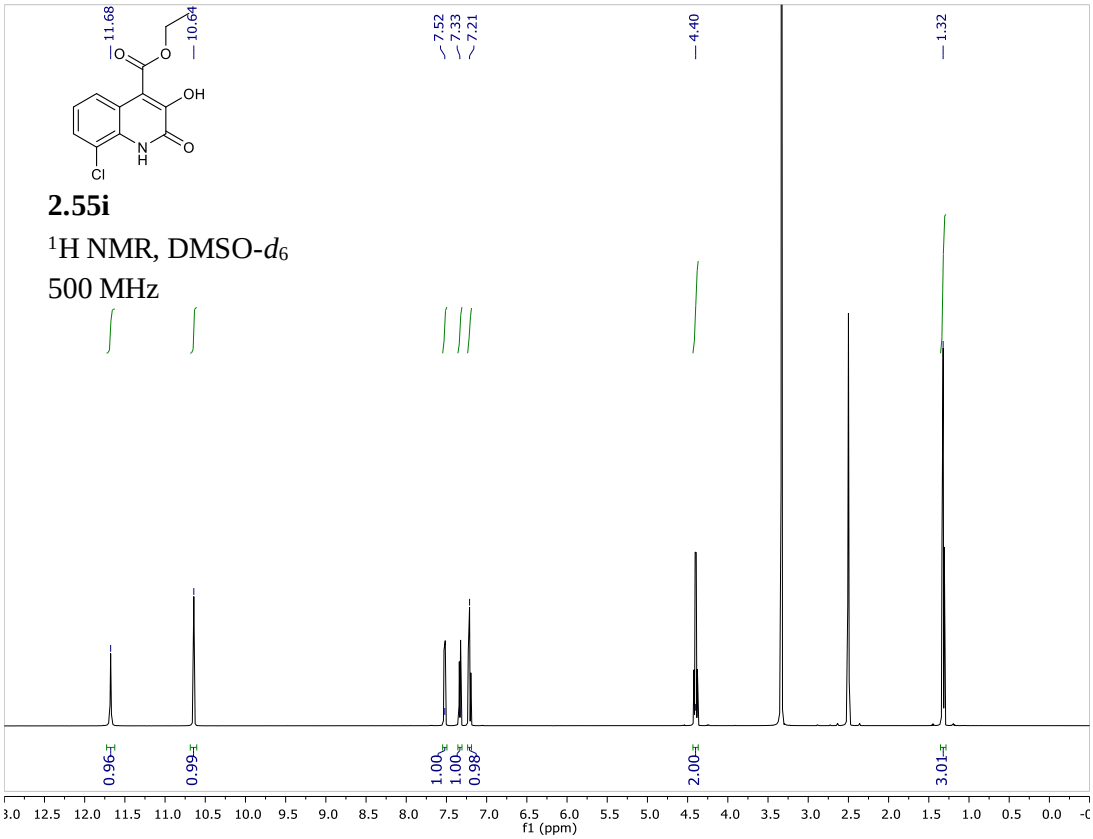

2.55i

^{1}H NMR, DMSO-d_6

500 MHz

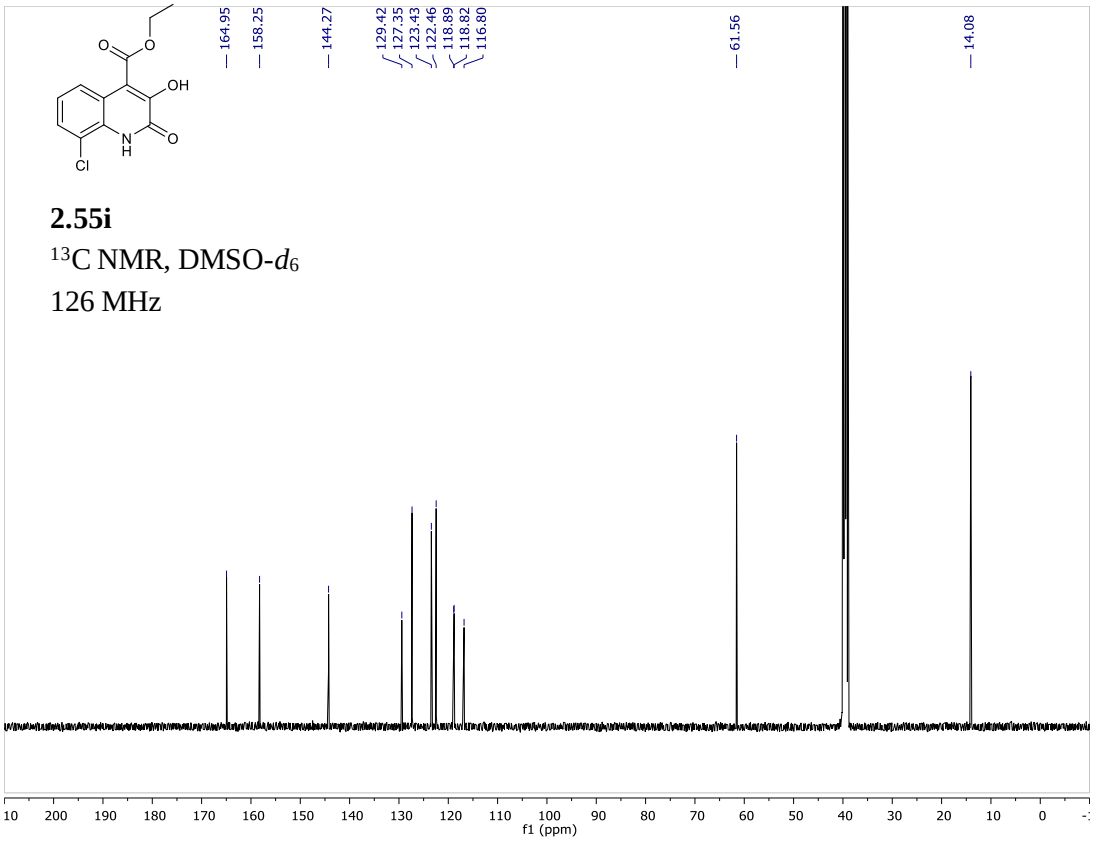

2.55i

^{13}C NMR, DMSO-d_6

126 MHz

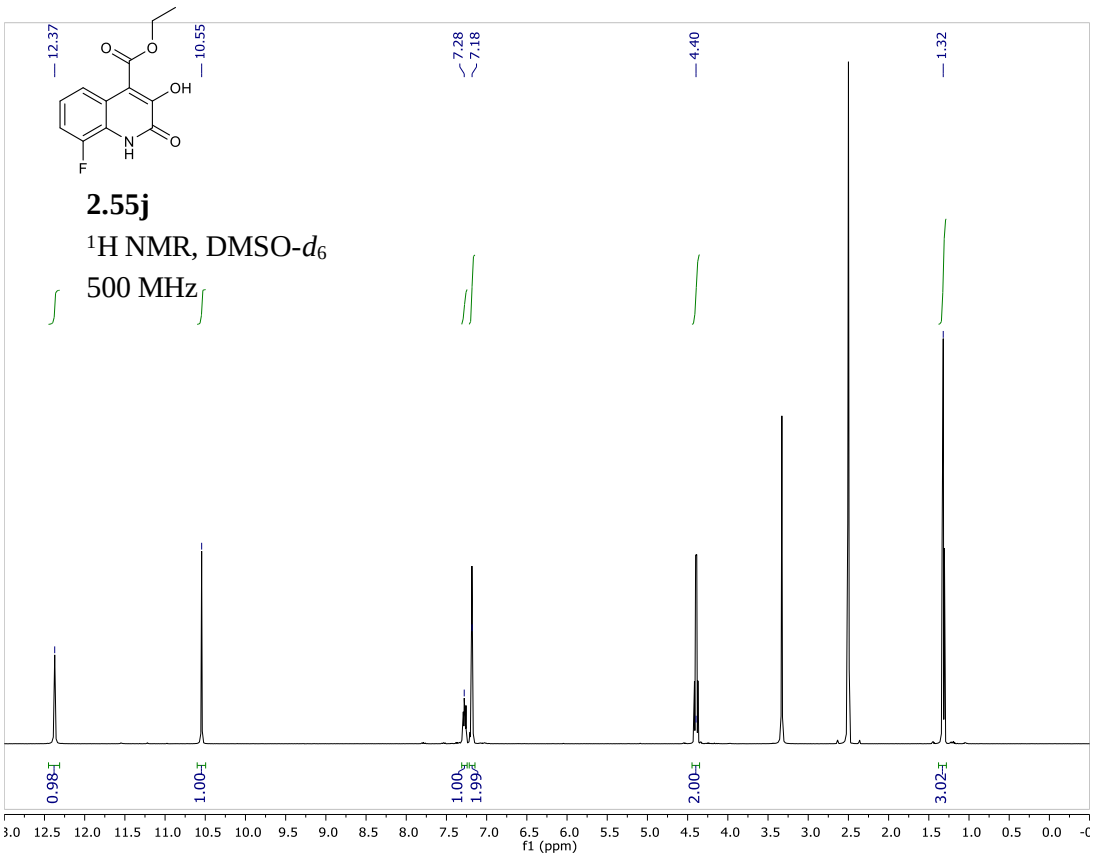

2.55j

^{1}H NMR, DMSO-d_6

500 MHz

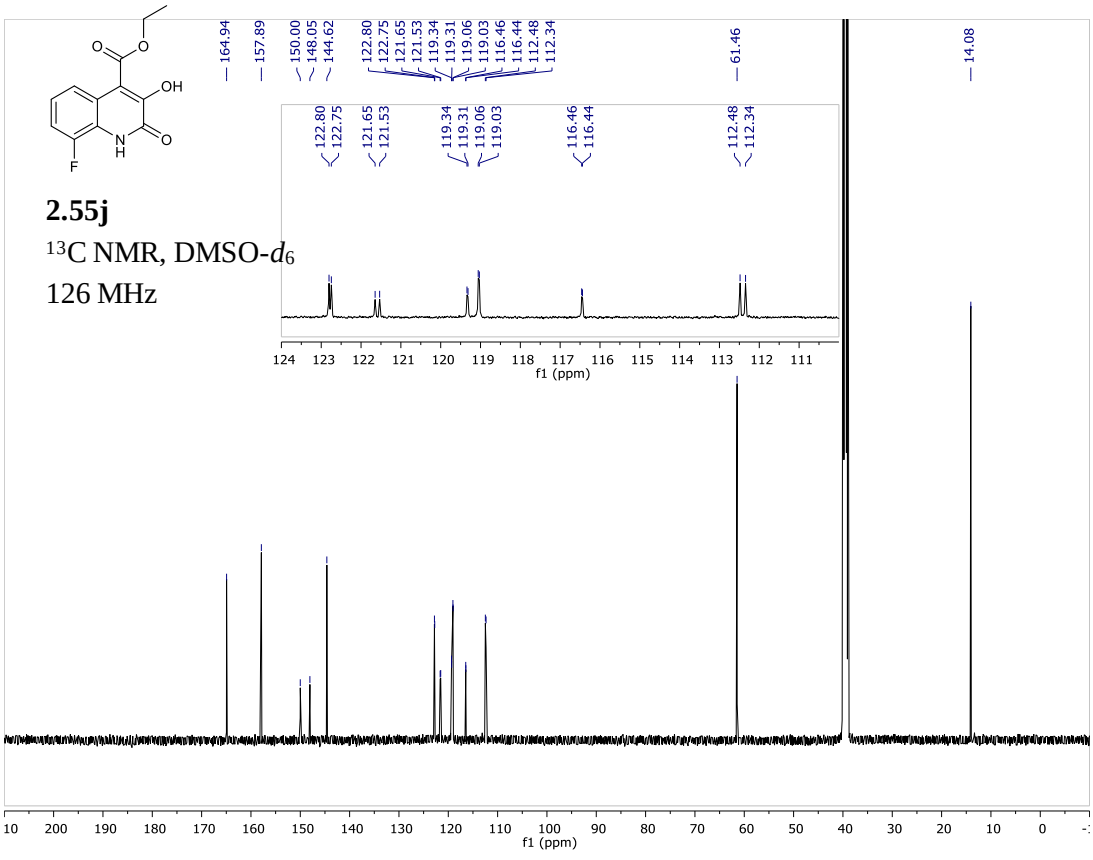

2.55j

^{13}C NMR, DMSO-d_6

126 MHz

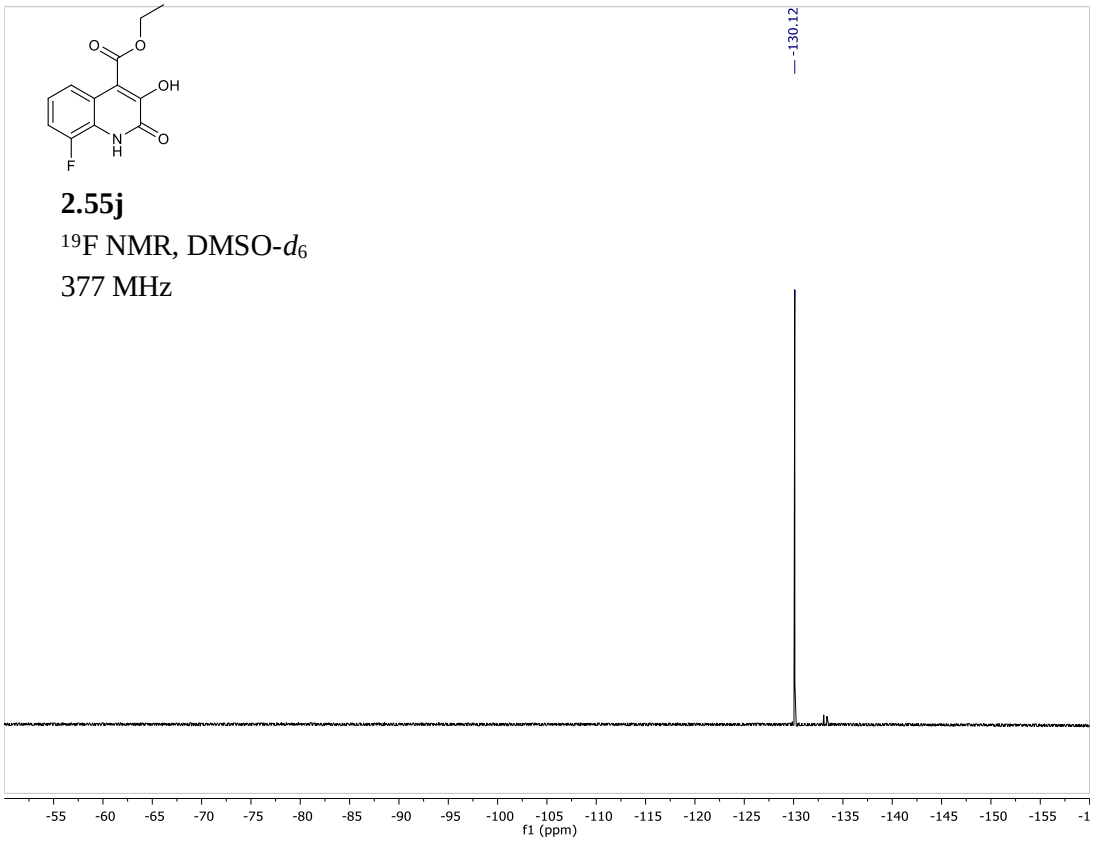

2.55j

^{19}F NMR, DMSO-d_6

377 MHz

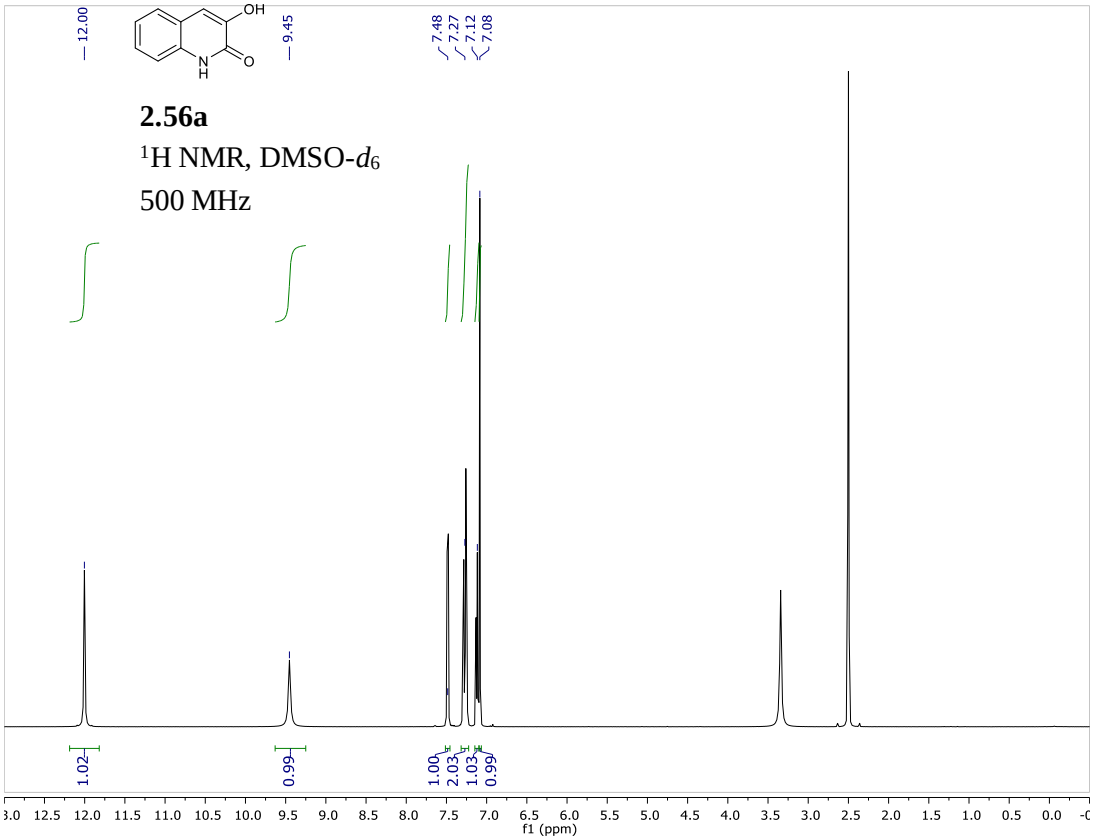

2.56a

^{1}H NMR, DMSO-d_6

500 MHz

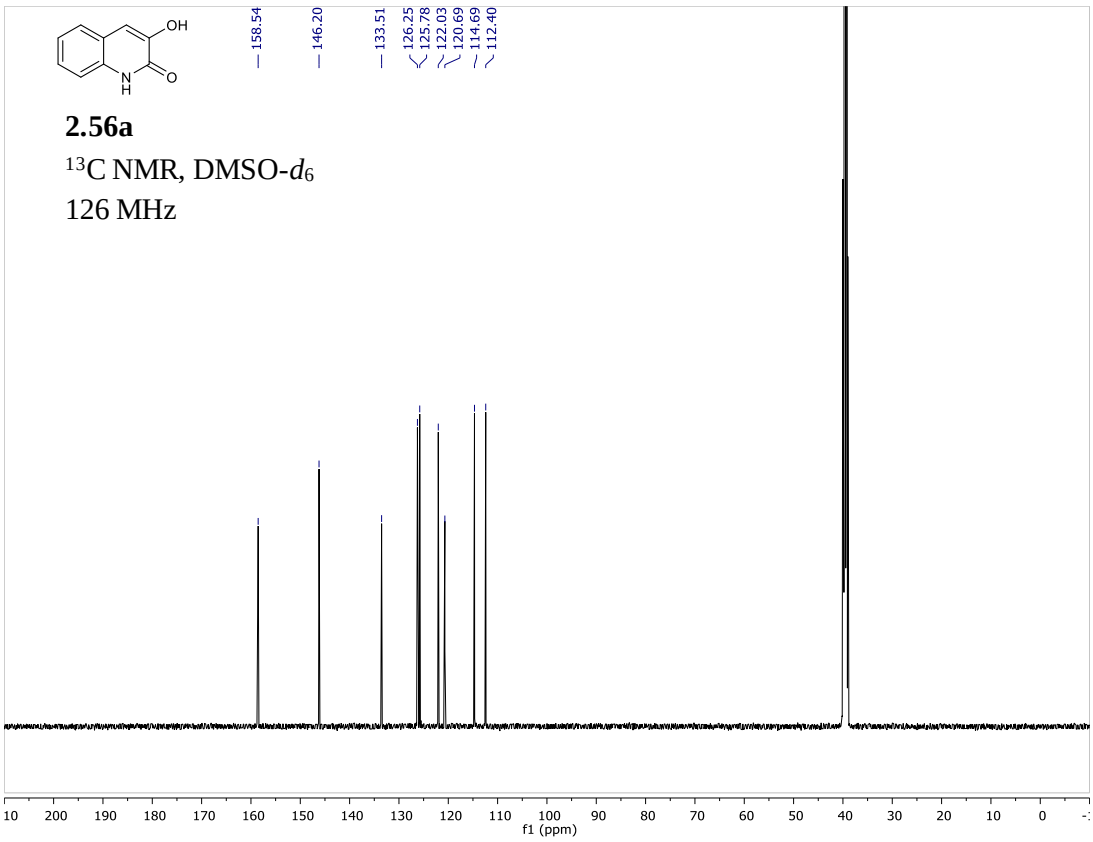

2.56a

^{13}C NMR, DMSO-d_6

126 MHz

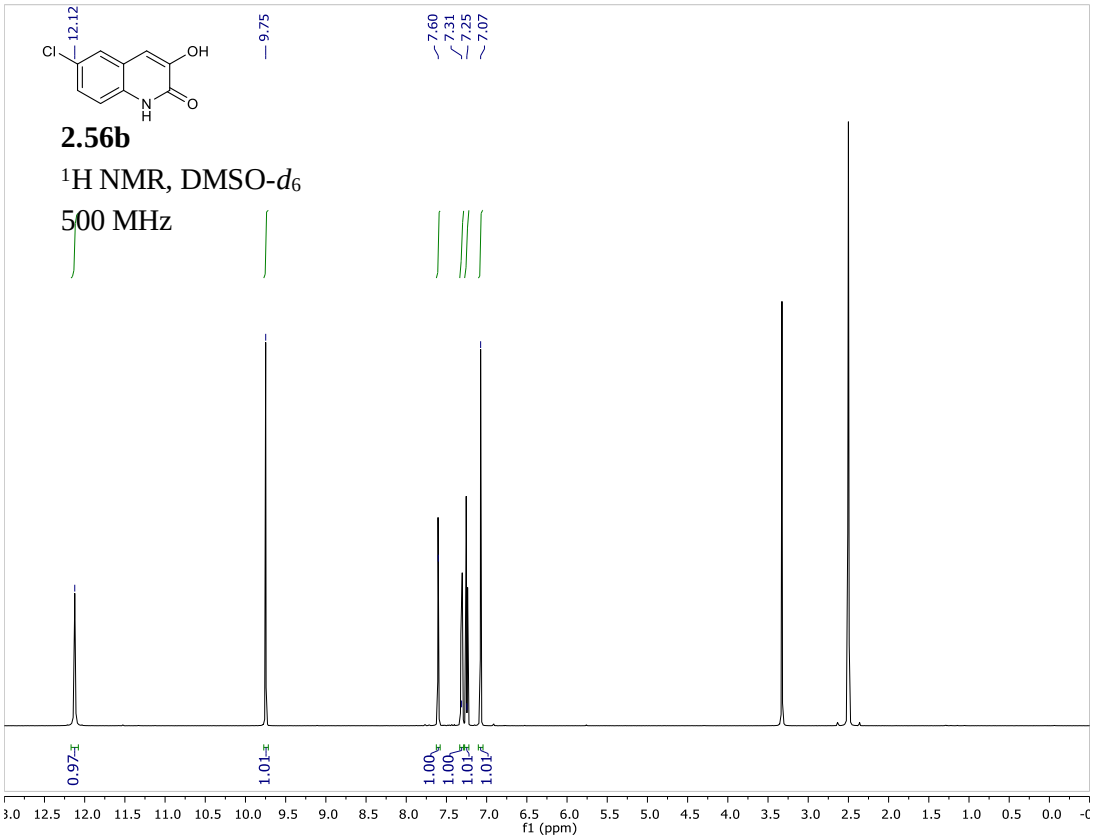

2.56b

^{1}H NMR, DMSO-d_6

500 MHz

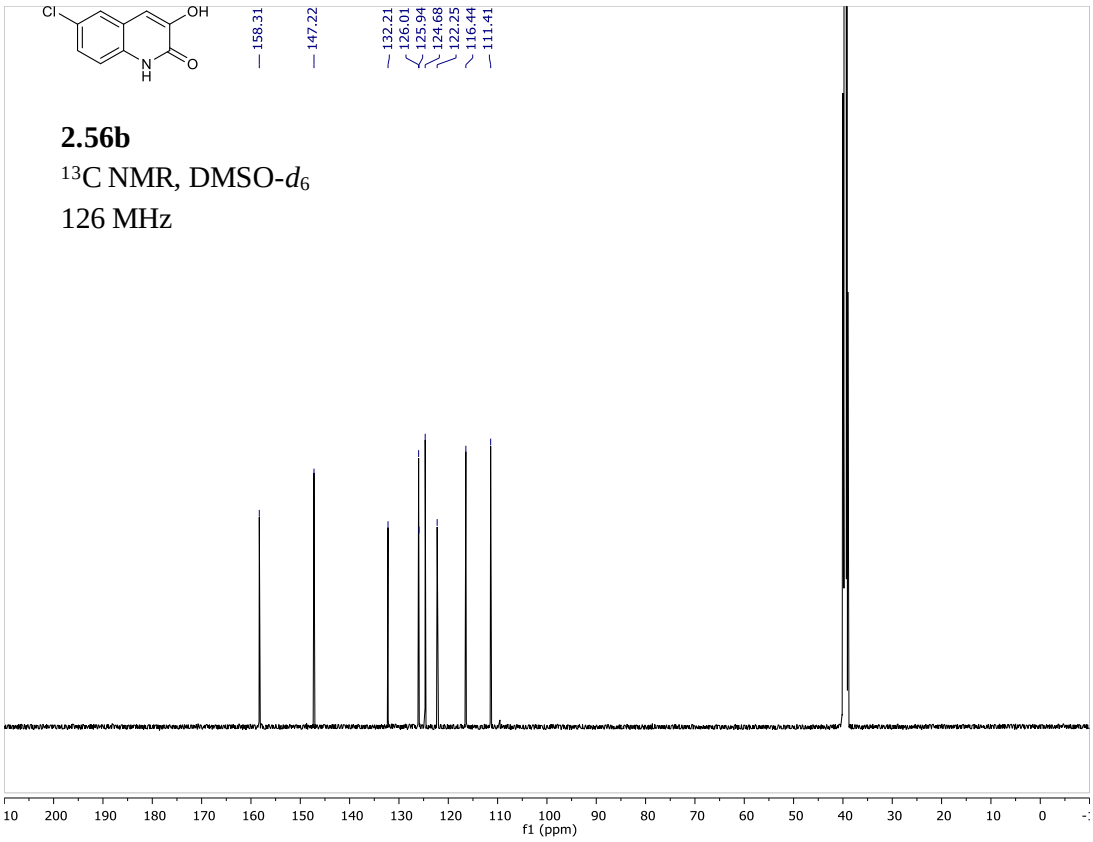

2.56b

^{13}C NMR, DMSO-d_6

126 MHz

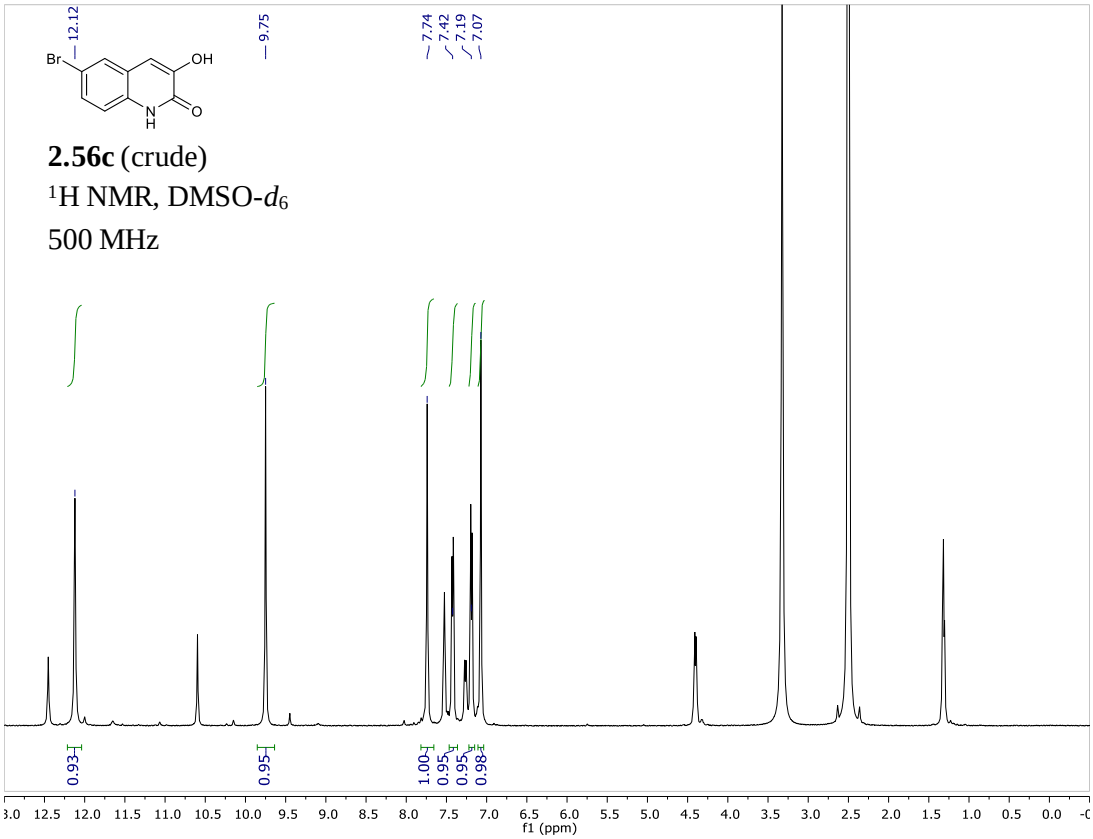

2.56c (crude)
^{1}H NMR, DMSO-d_6
500 MHz

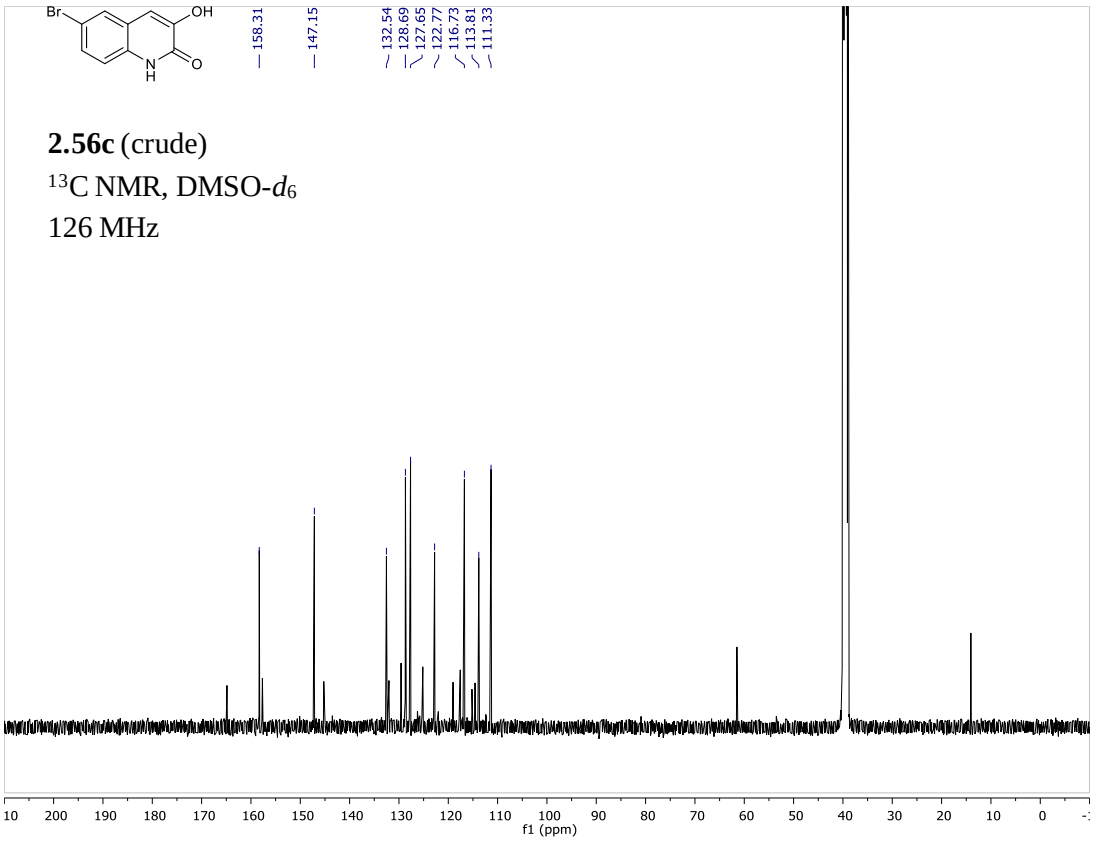

2.56c (crude)
^{13}C NMR, DMSO-d_6
126 MHz

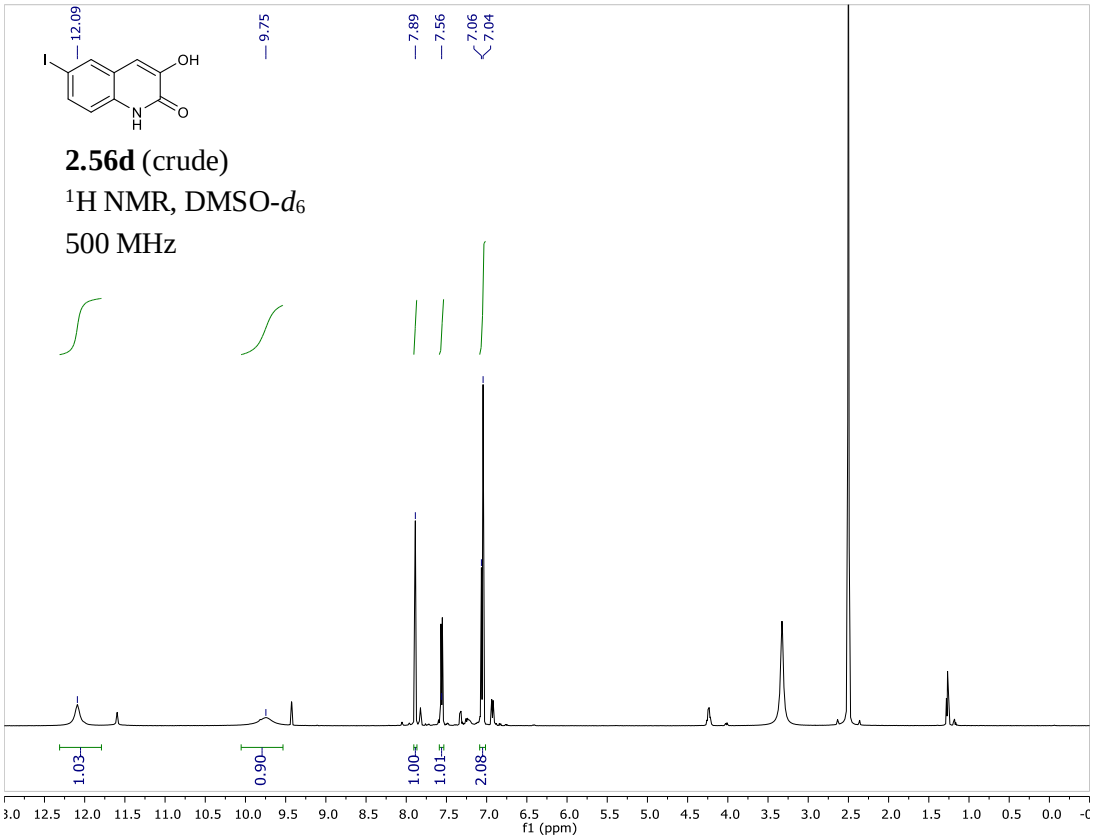

2.56d (crude)
^{1}H NMR, DMSO-d_6
500 MHz

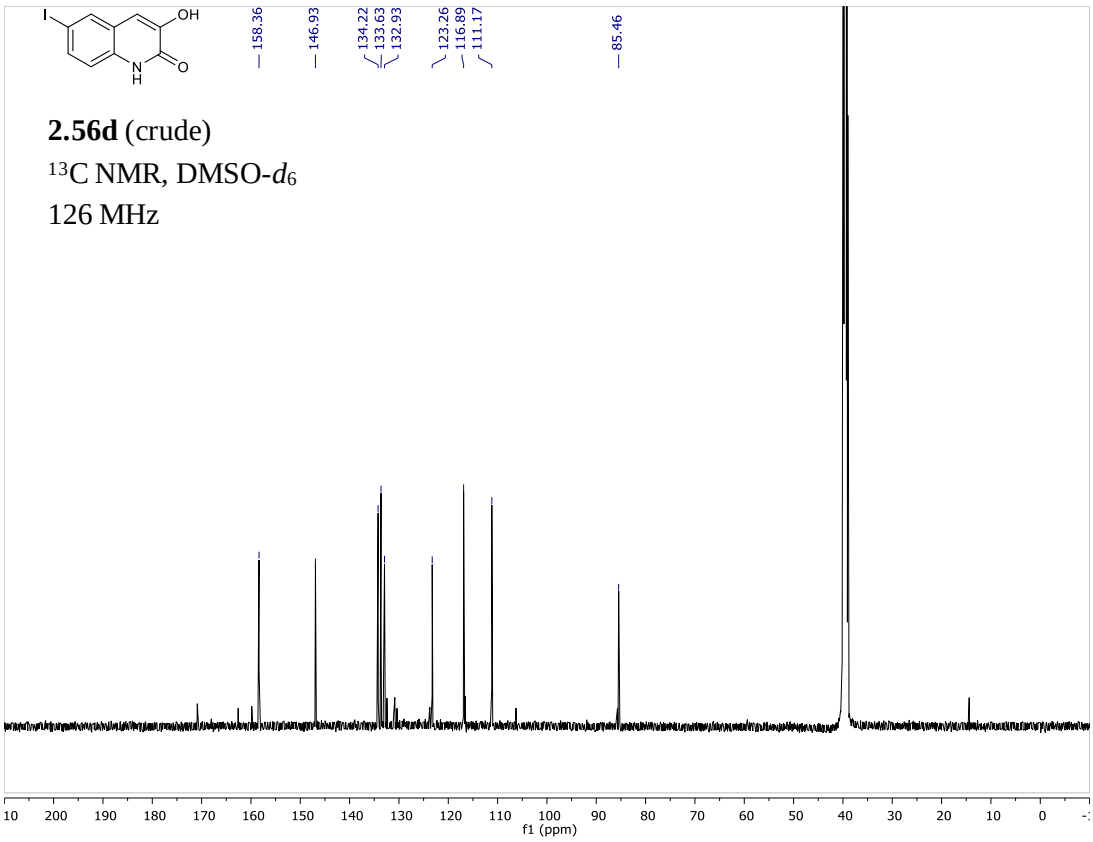

2.56d (crude)
^{13}C NMR, DMSO-d_6
126 MHz

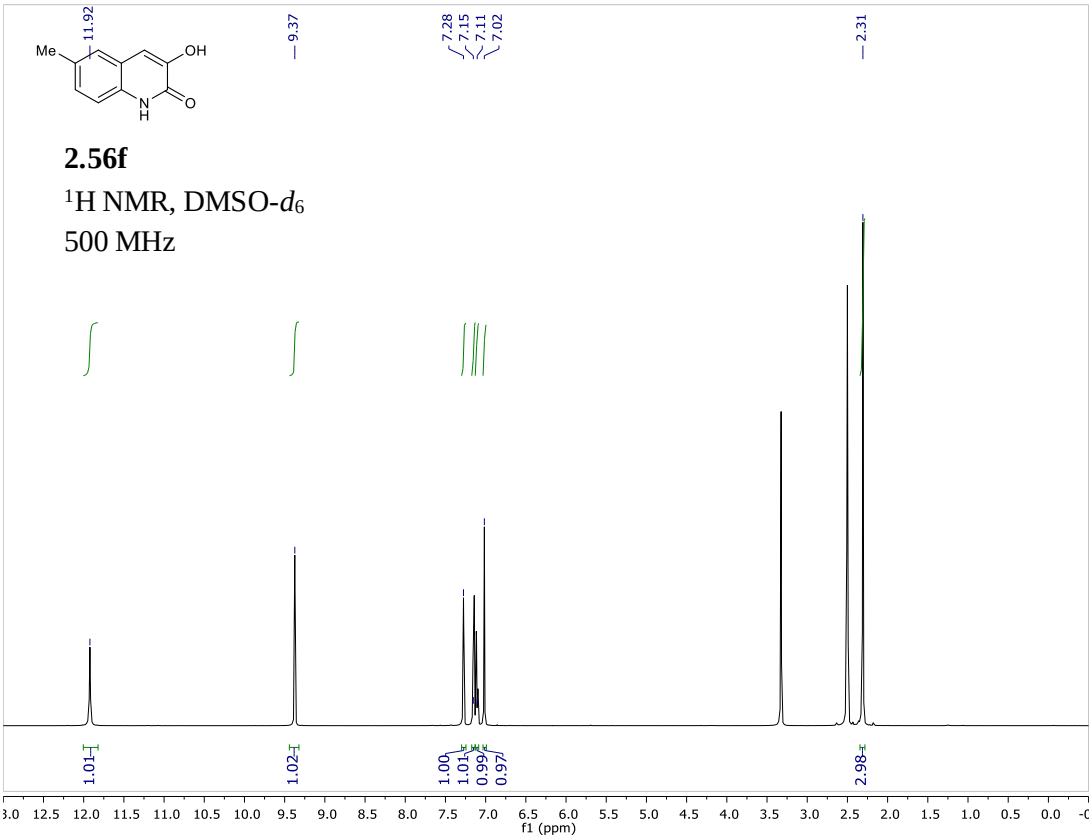

2.56f

^{1}H NMR, DMSO-d_6

500 MHz

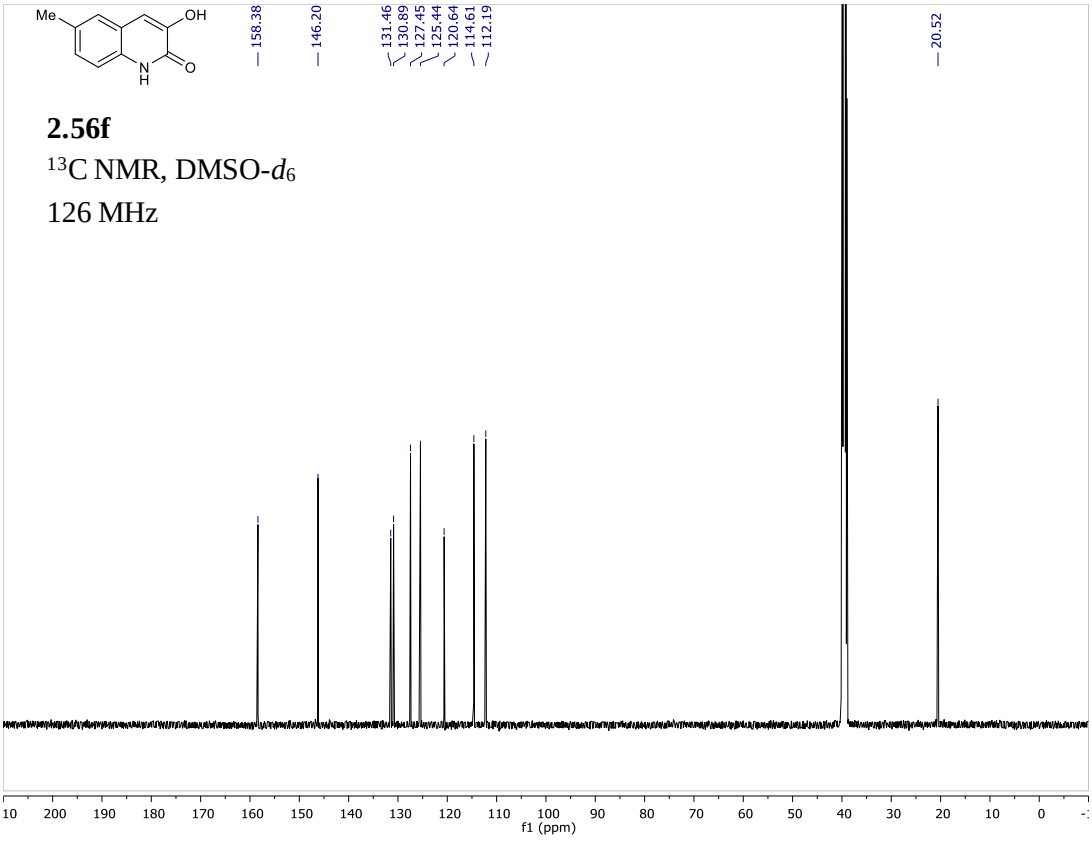

2.56f

^{13}C NMR, DMSO-d_6

126 MHz

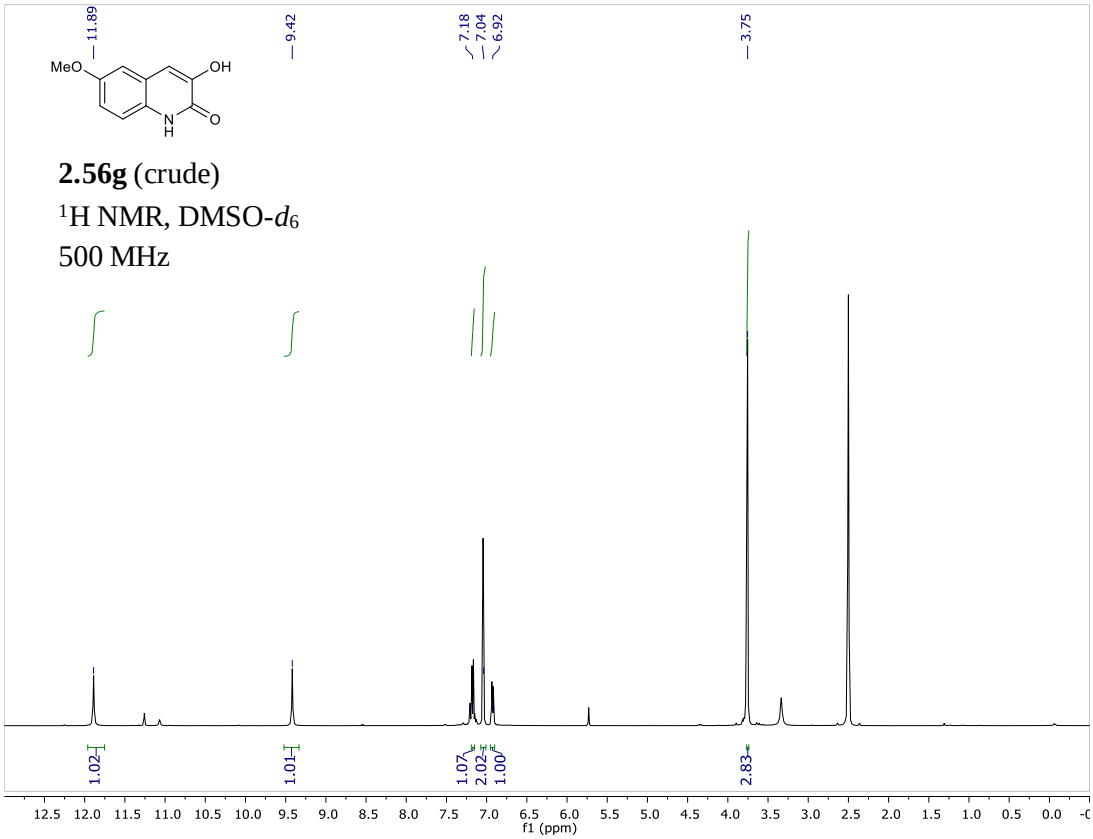

2.56g (crude)
^{1}H NMR, DMSO-d_6
500 MHz

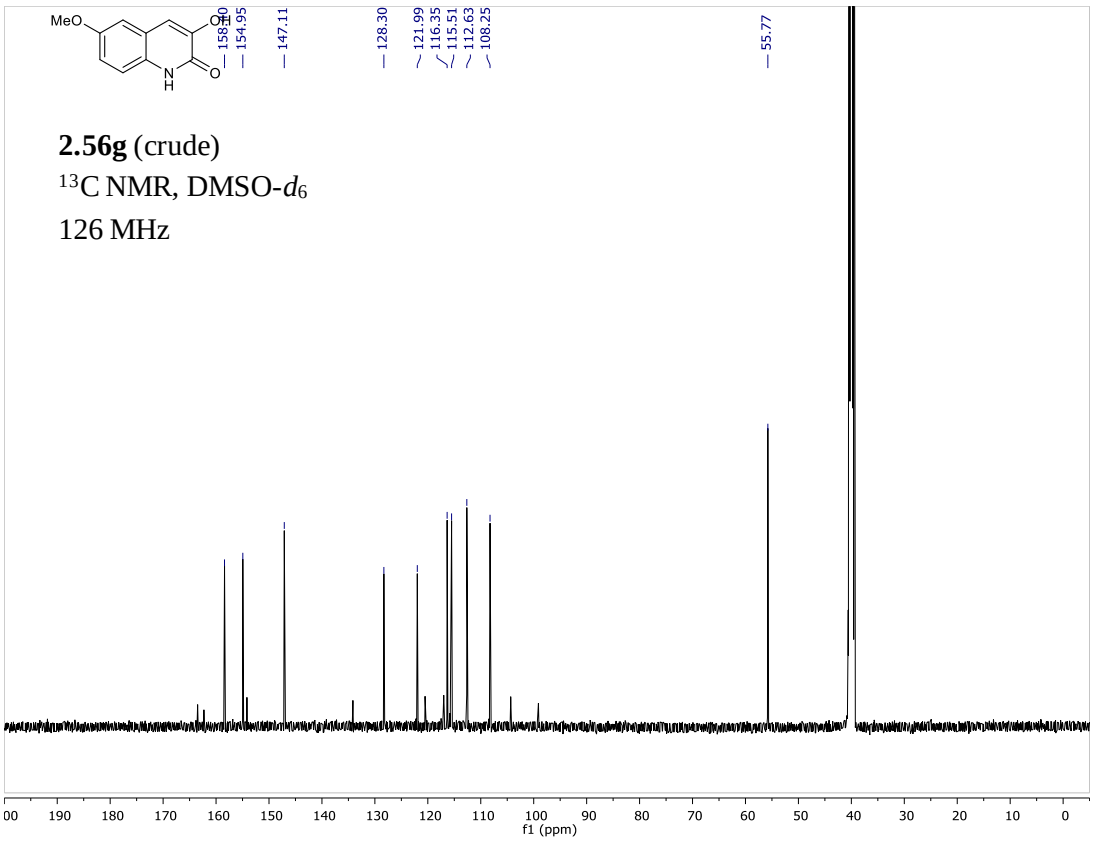

2.56g (crude)
^{13}C NMR, DMSO-d_6
126 MHz

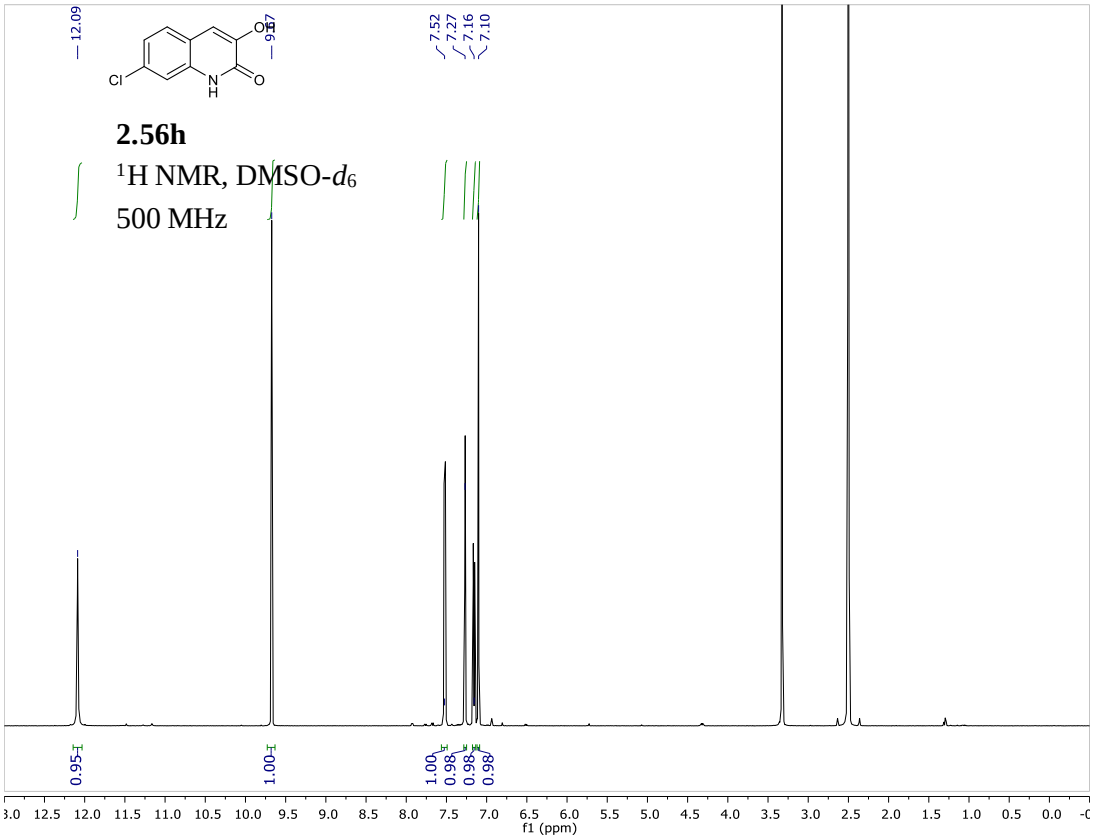
12.09
9.37
7.52
7.27
7.16
7.10
Cl
OH
N
H
O
2.56h
1H NMR, DMSO-d6
500 MHz
0.95
1.00
1.00
0.98
0.98
0.98
f1 (ppm)

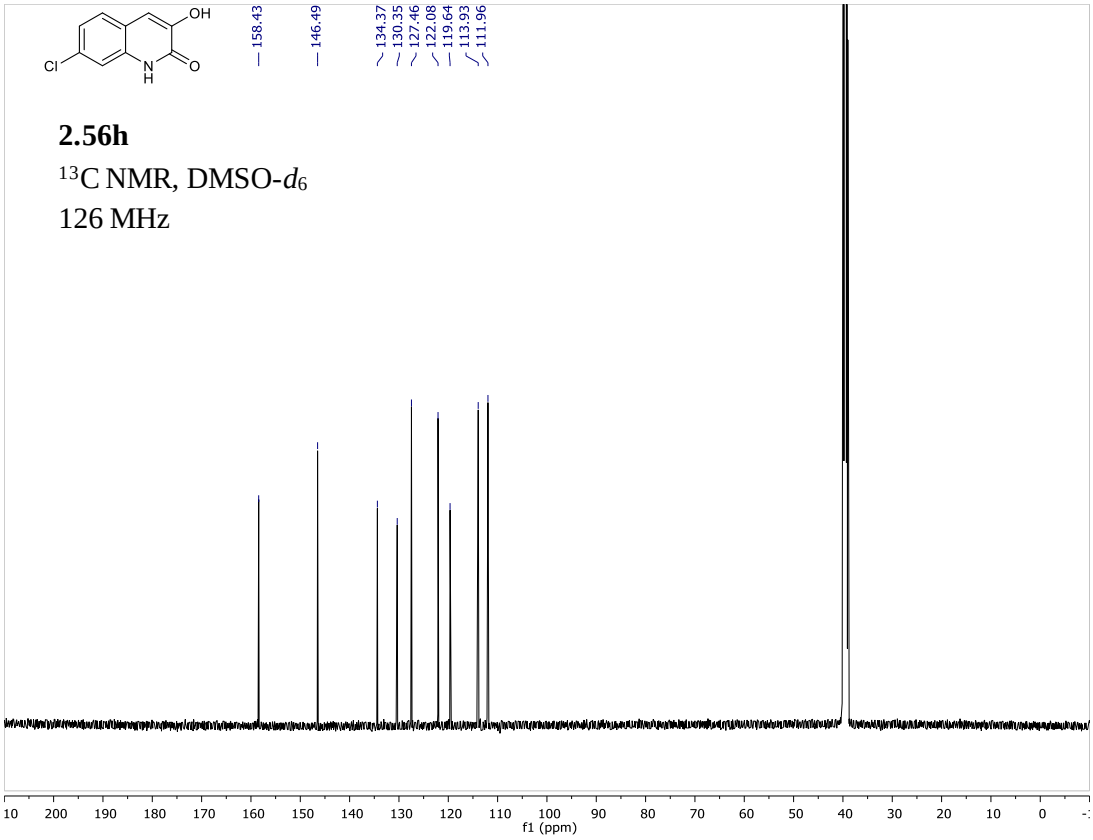
158.43
146.49
134.37
130.35
127.46
122.08
119.64
113.93
111.96
Cl
OH
N
H
O
2.56h
13C NMR, DMSO-d6
126 MHz
f1 (ppm)

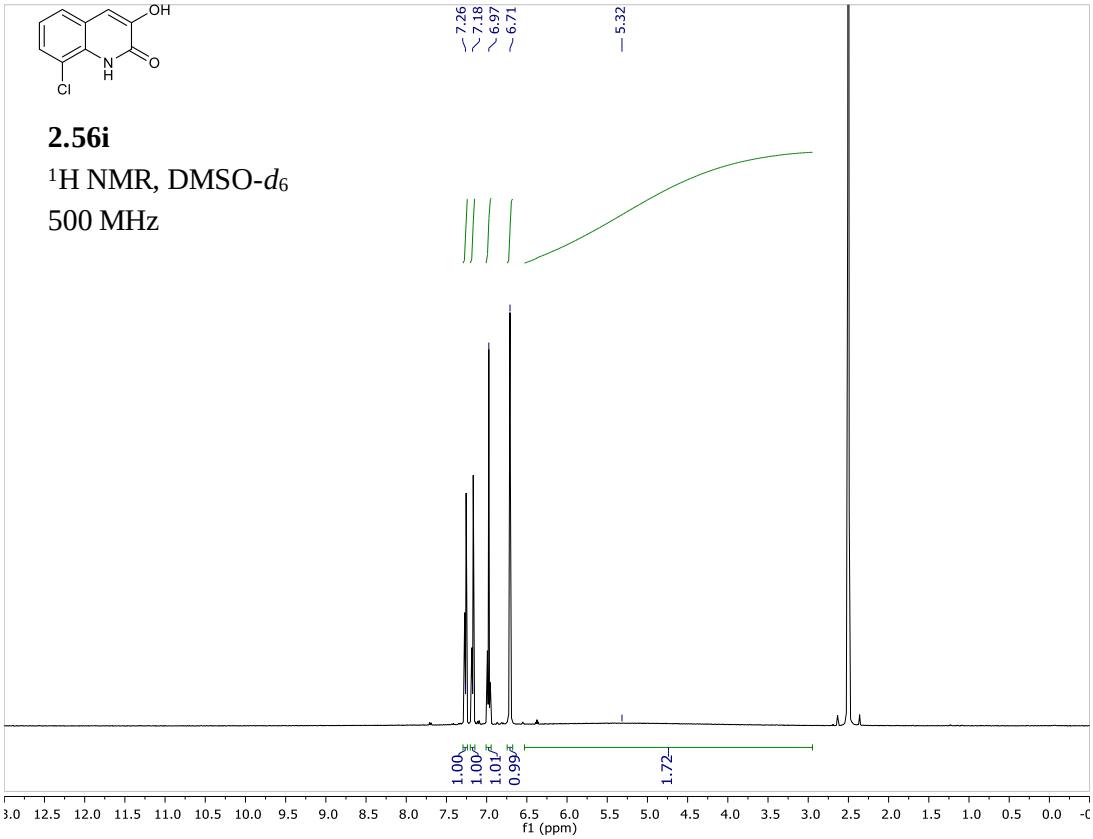

2.56i

^{1}H NMR, DMSO-d_6

500 MHz

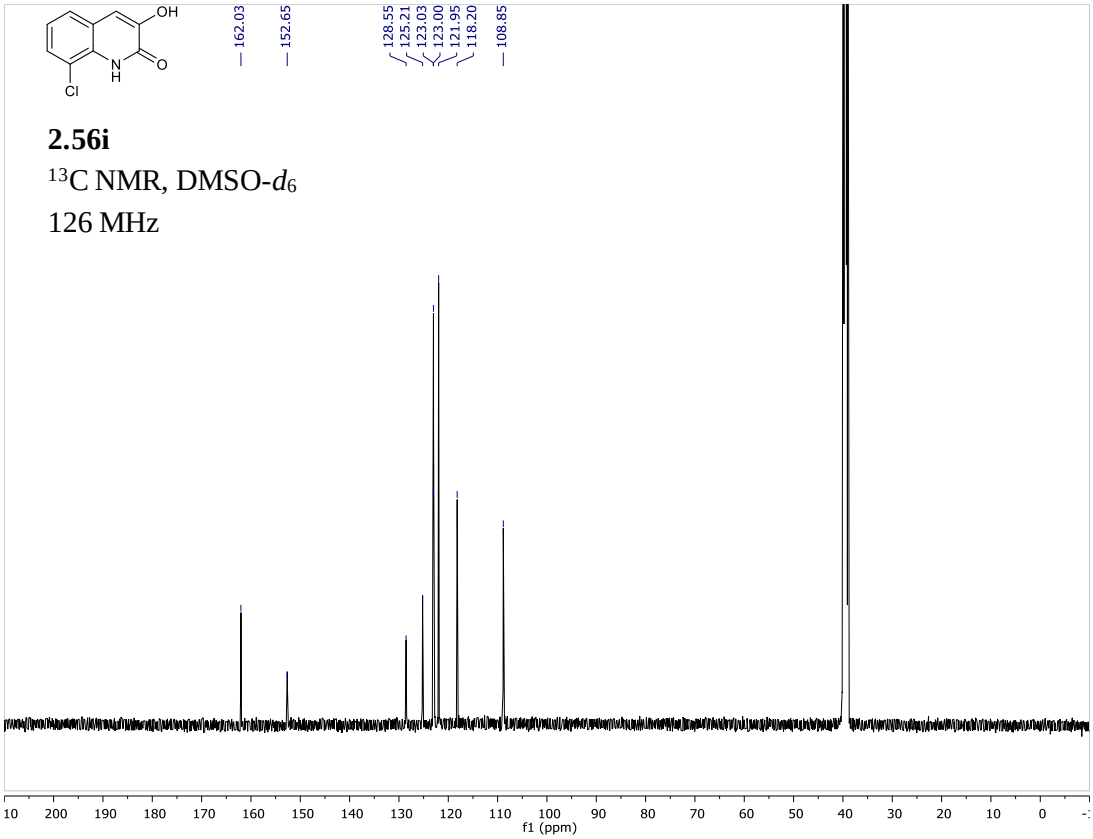

2.56i

^{13}C NMR, DMSO-d_6

126 MHz

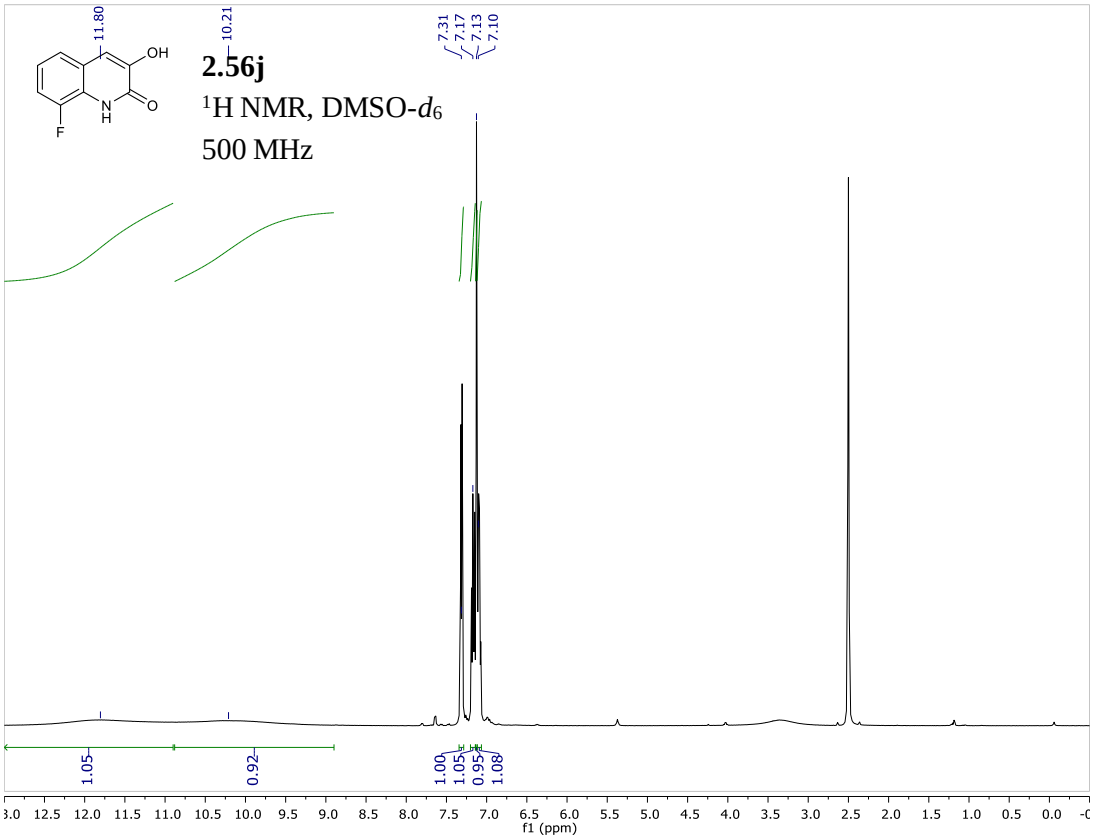
11.80
10.21
7.31
7.17
7.13
7.10
OH
N
H
O
F
2.56j
1H NMR, DMSO-d6
500 MHz
1.05
0.92
1.00
1.05
0.95
1.08
f1 (ppm)

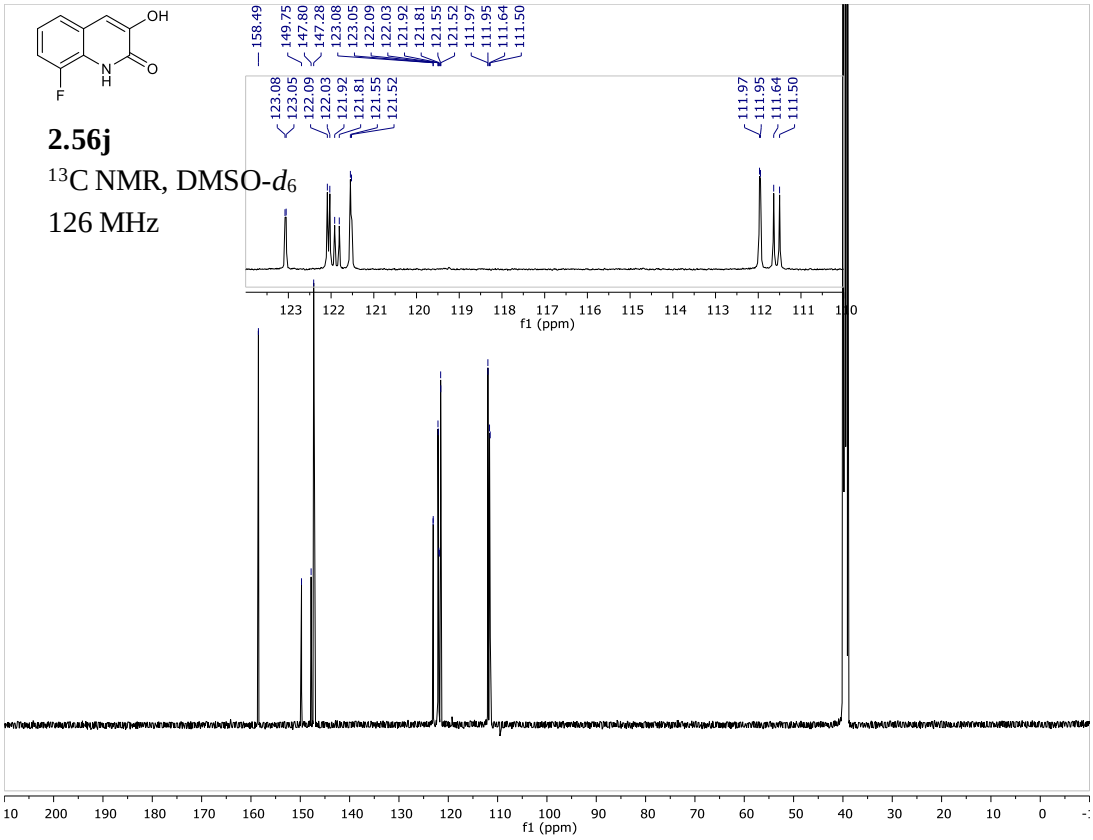
158.49
149.75
147.80
147.28
123.08
123.05
122.09
122.03
121.92
121.81
121.55
121.52
111.97
111.95
111.64
111.50
OH
N
H
O
F
2.56j
13C NMR, DMSO-d6
126 MHz
f1 (ppm)

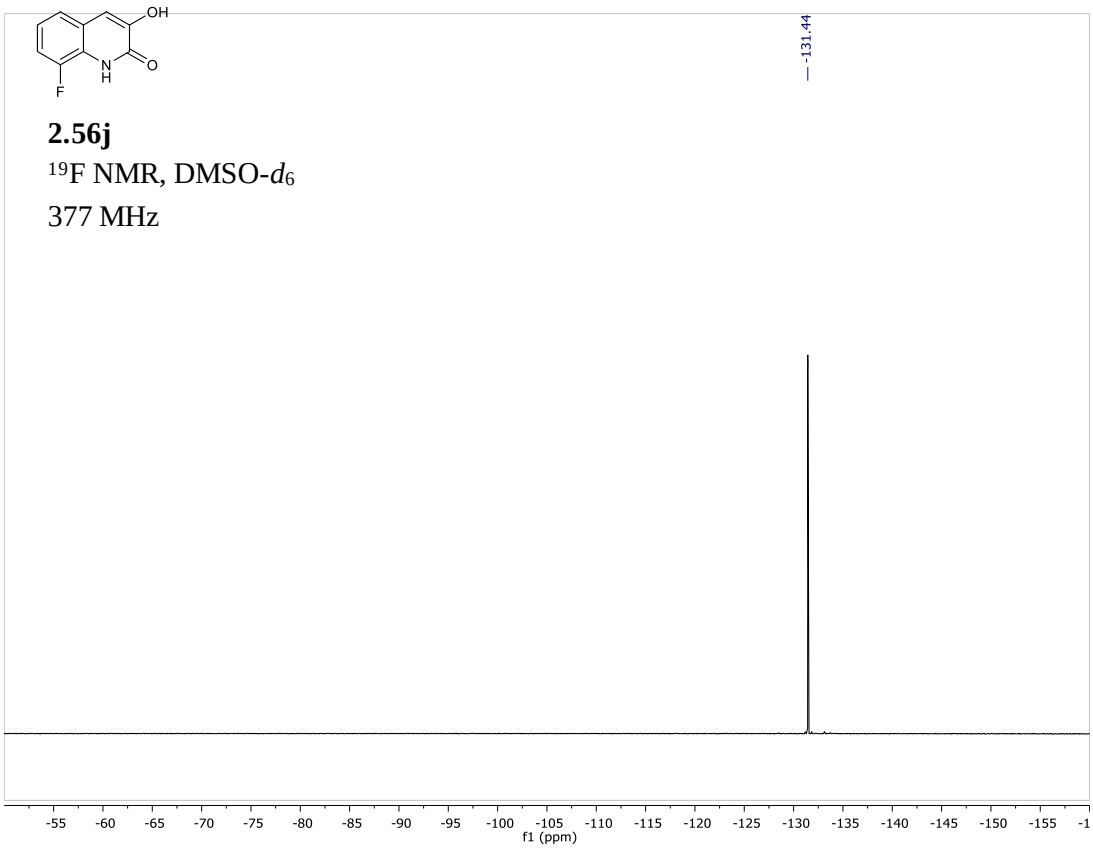

2.56j

^{19}F NMR, DMSO-d_6

377 MHz

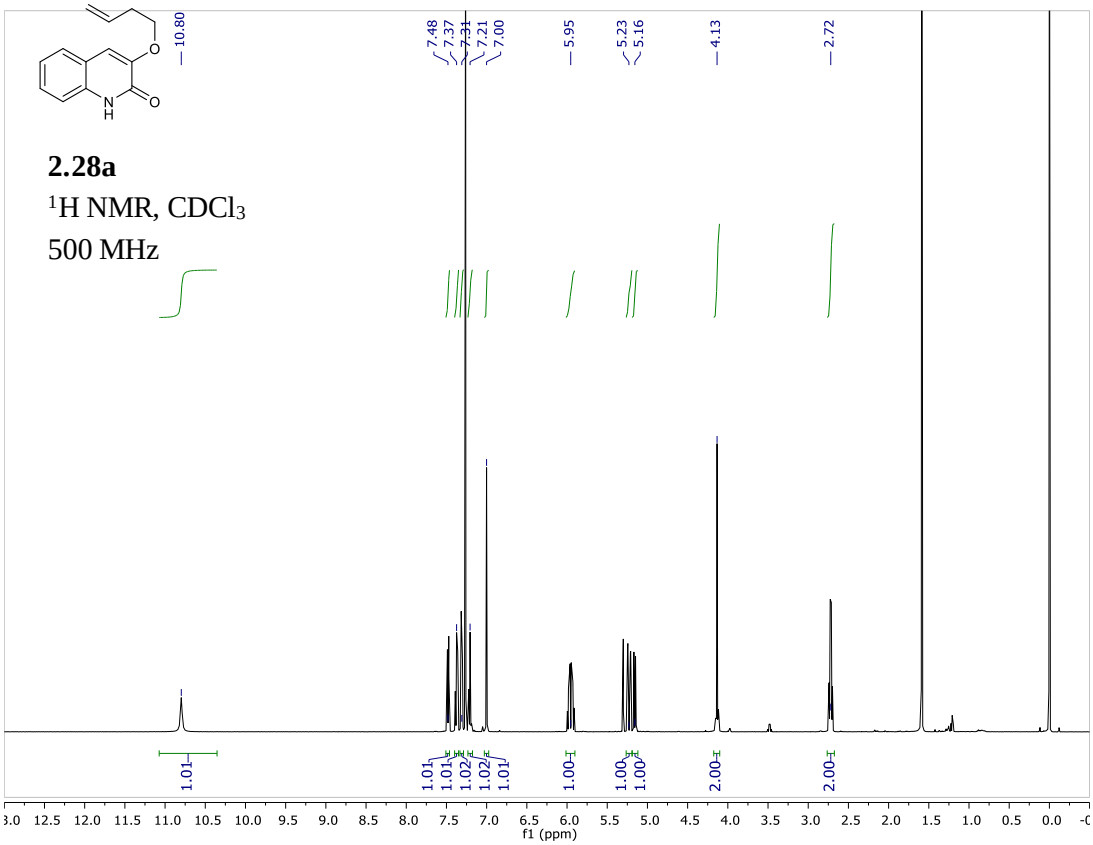

2.28a

^{1}H NMR, $CDCl_3$

500 MHz

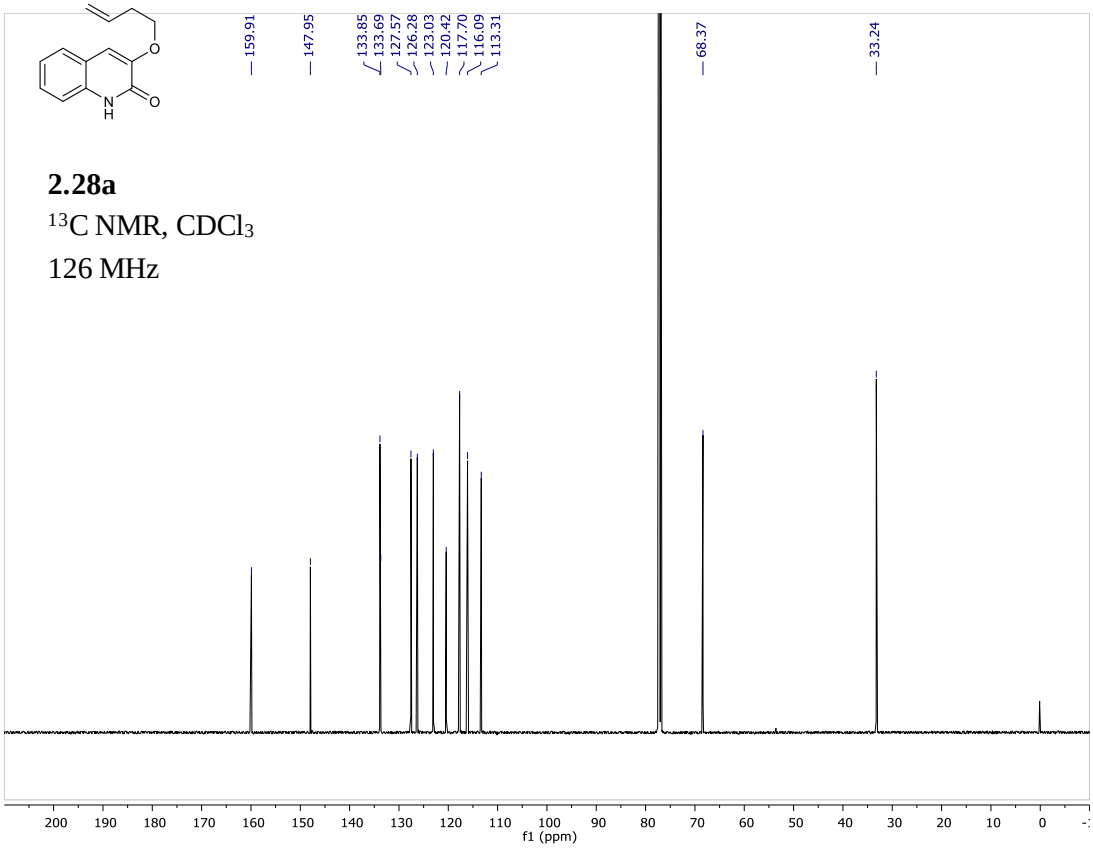

2.28a

^{13}C NMR, $CDCl_3$

126 MHz

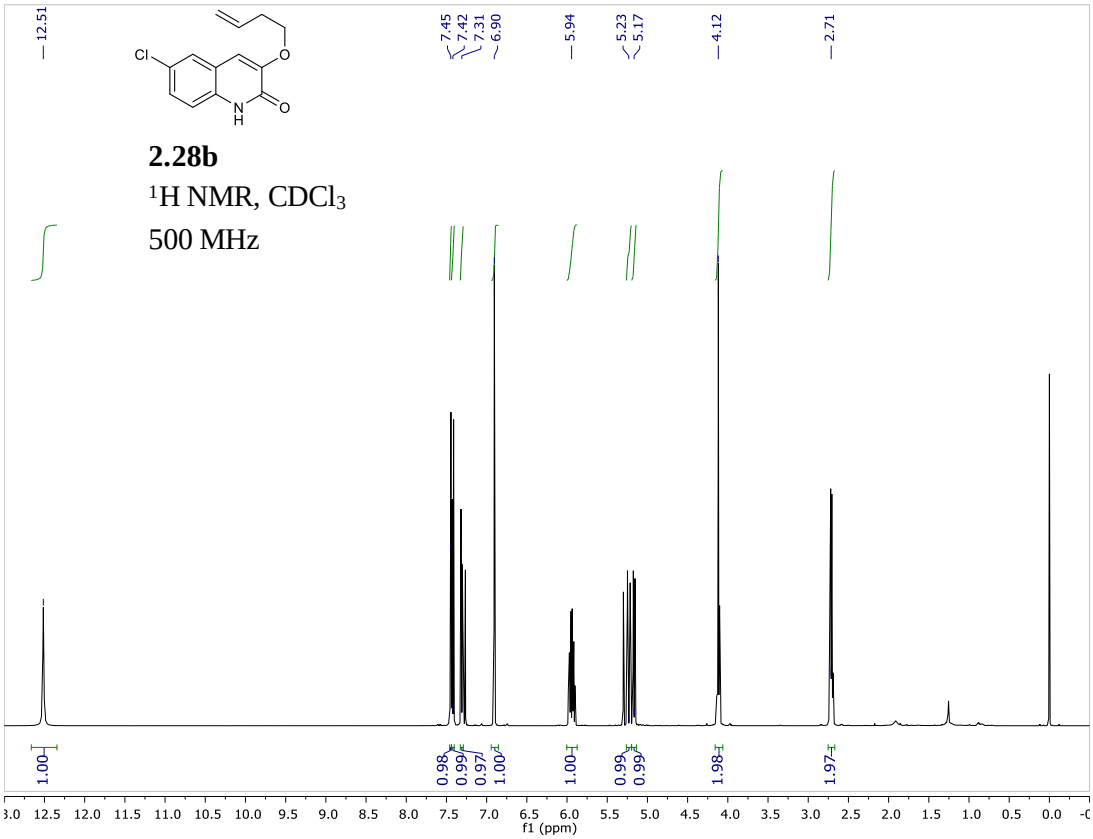

2.28b

^{1}H NMR, $CDCl_3$

500 MHz

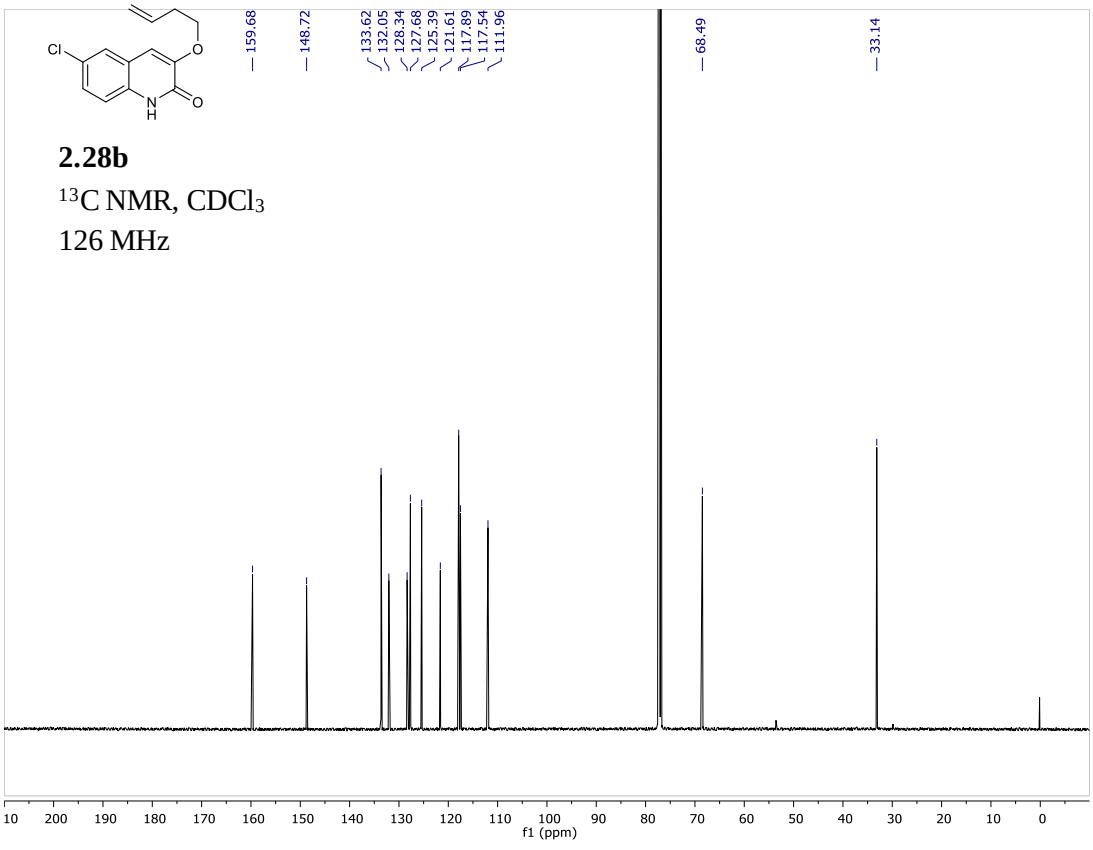

2.28b

^{13}C NMR, $CDCl_3$

126 MHz

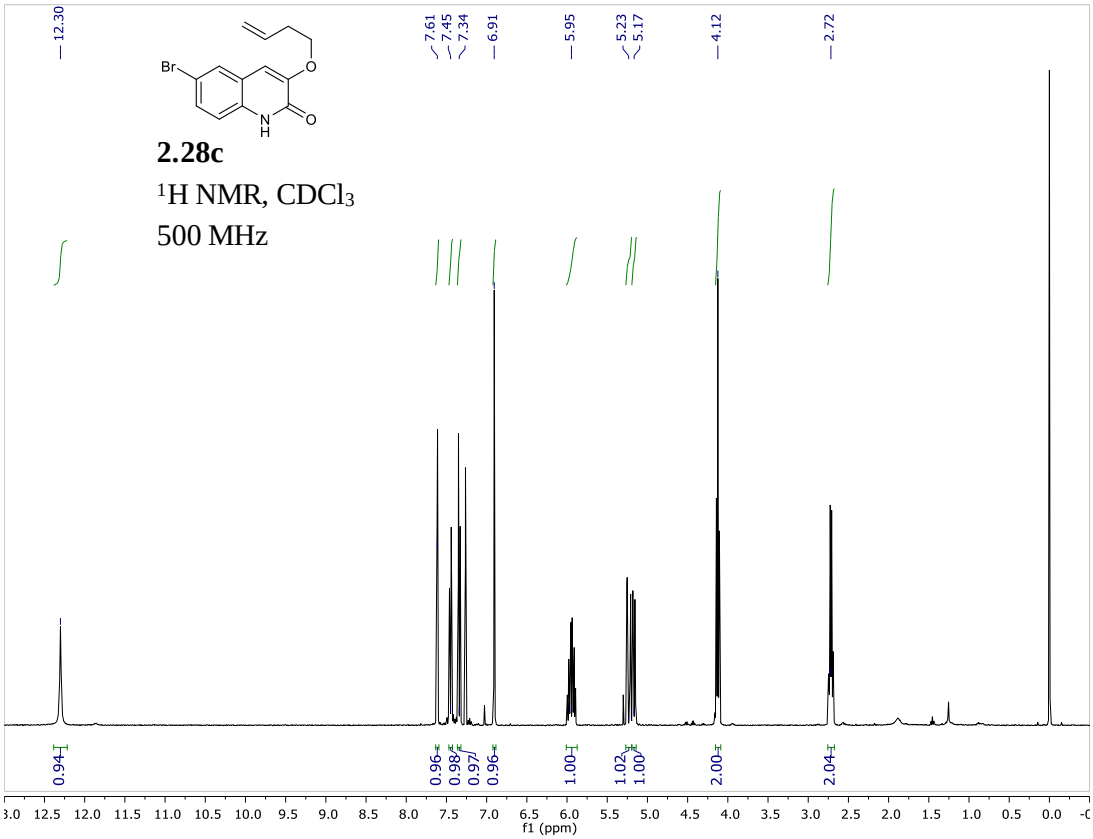
12.30
7.61
7.45
7.34
6.91
5.95
5.23
5.17
4.12
2.72
Br
O
N
H
O
2.28c
1H NMR, CDCl3
500 MHz
0.94
0.96
0.98
0.97
0.96
1.00
1.02
1.00
2.00
2.04
f1 (ppm)

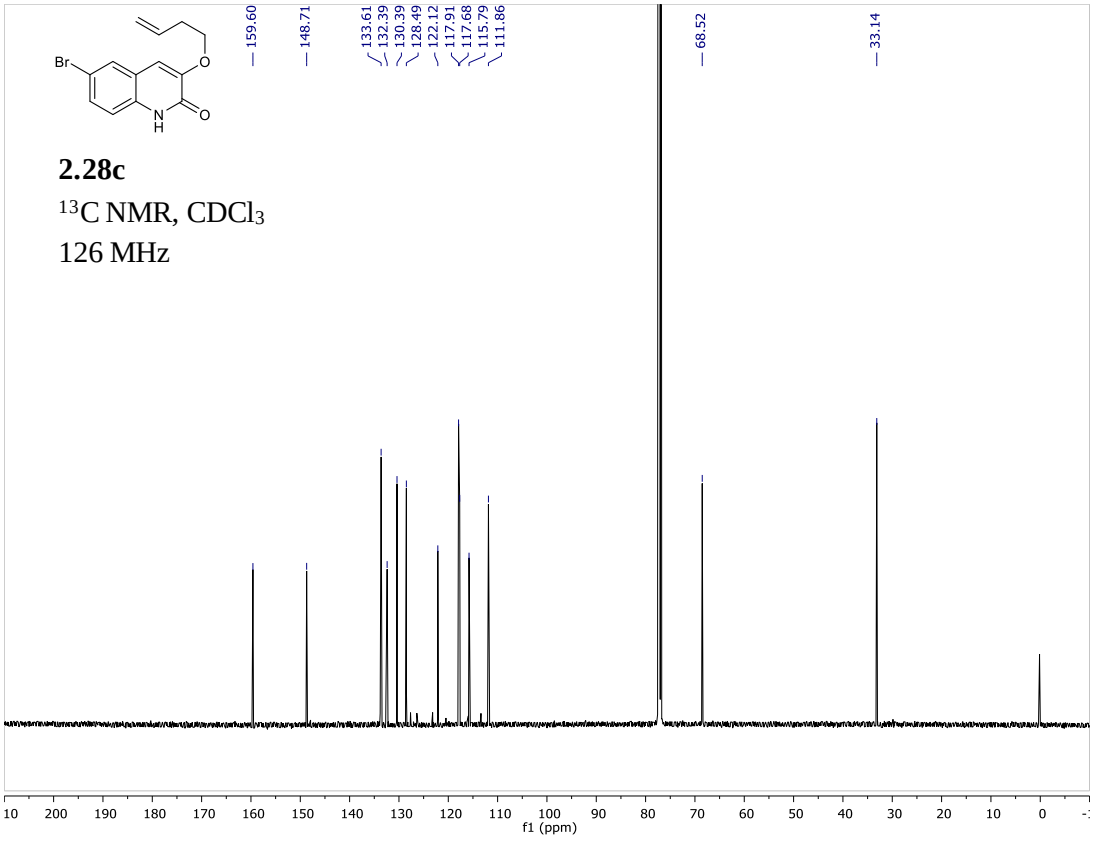
159.60
148.71
133.61
132.39
130.39
128.49
122.12
117.91
117.68
115.79
111.86
68.52
33.14
Br
O
N
H
O
2.28c
13C NMR, CDCl3
126 MHz
f1 (ppm)

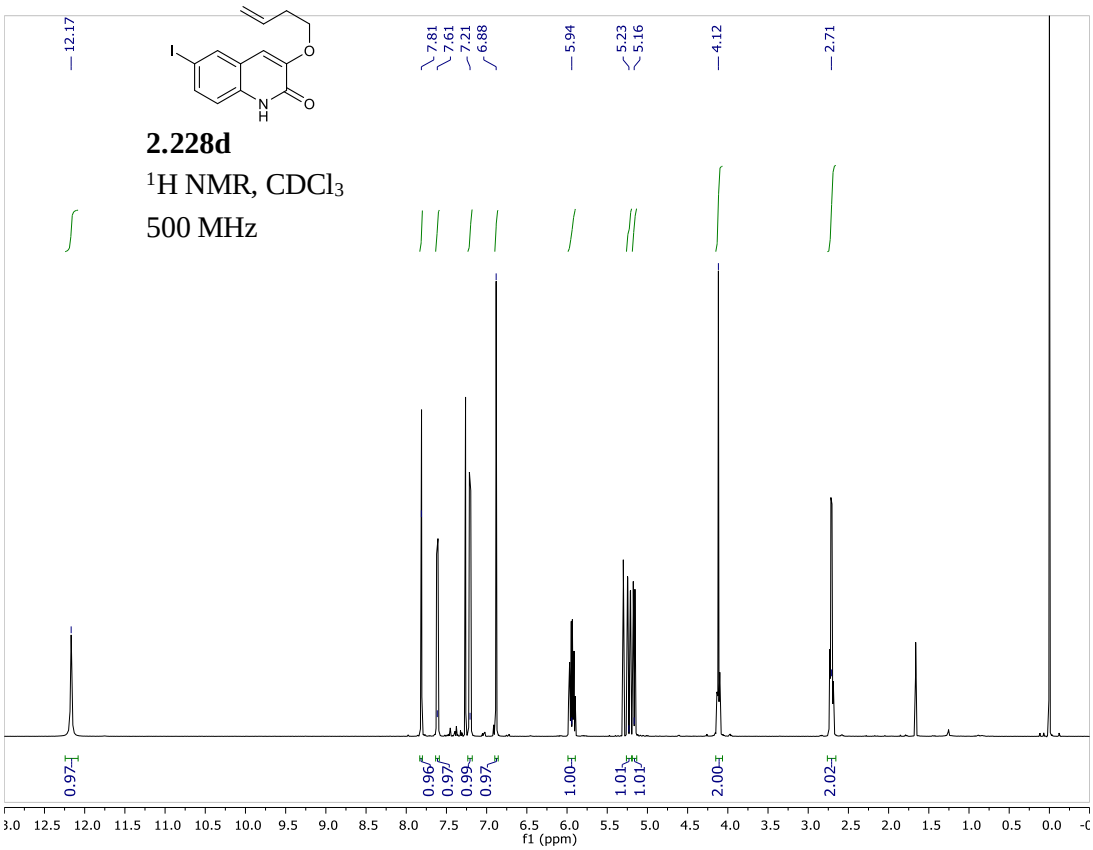
12.17
7.81
7.61
7.21
6.88
5.94
5.23
5.16
4.12
2.71
2.28d
1H NMR, CDCl3
500 MHz
0.97
0.96
0.97
0.99
0.97
1.00
1.01
1.01
2.00
2.02
f1 (ppm)

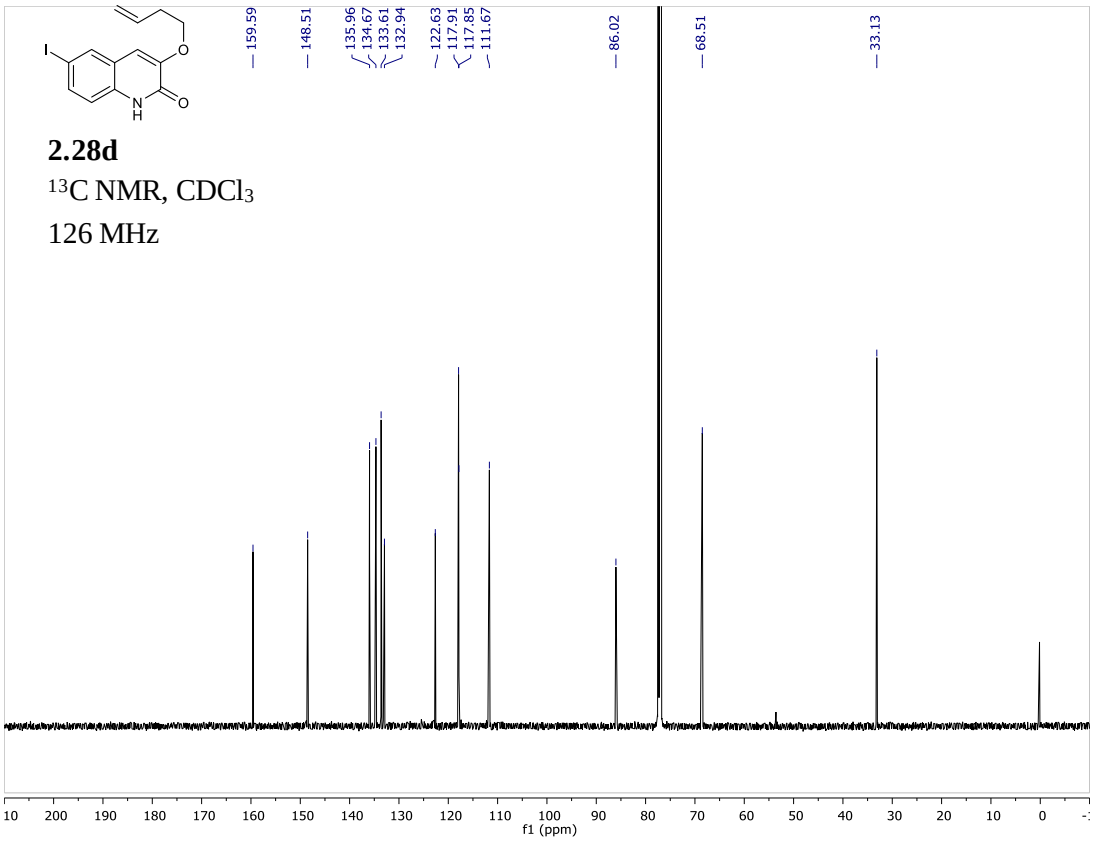
159.59
148.51
135.96
134.67
133.61
132.94
122.63
117.91
117.85
111.67
86.02
68.51
33.13
2.28d
13C NMR, CDCl3
126 MHz
f1 (ppm)

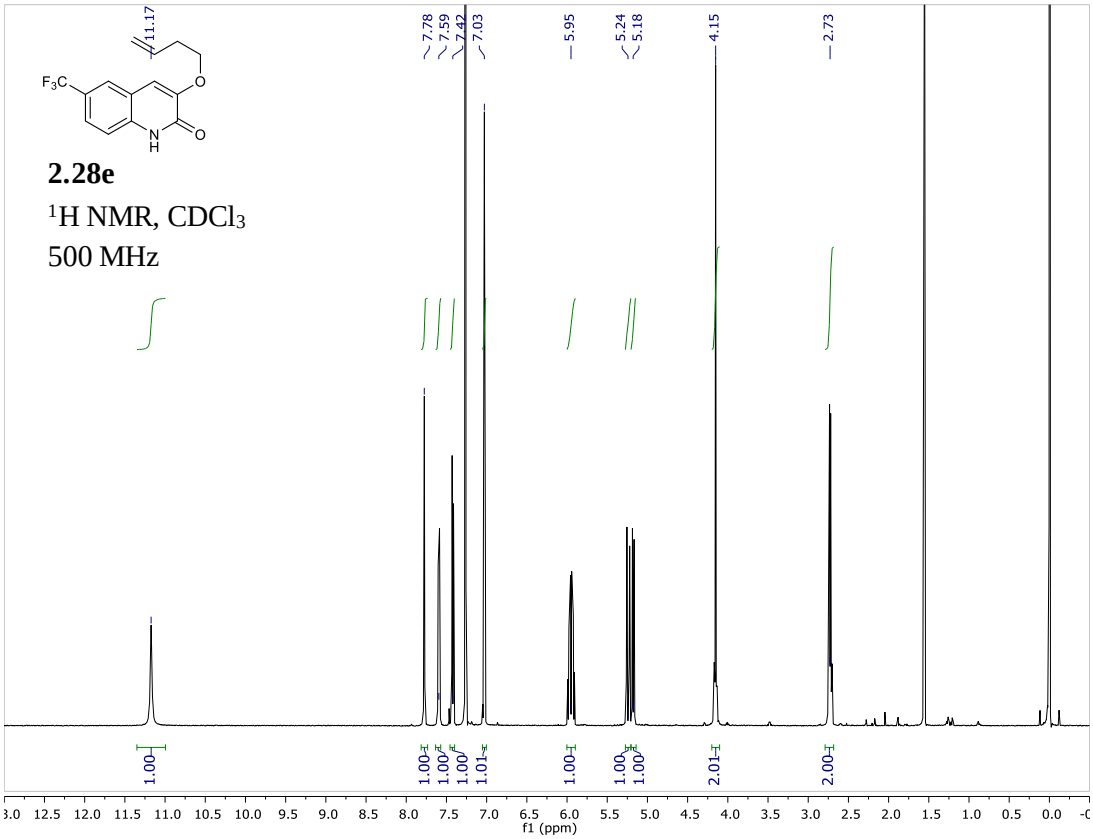
11.17
7.78
7.59
7.42
7.03
5.95
5.24
5.18
4.15
2.73
F3C
O
N
H
O
2.28e
1H NMR, CDCl3
500 MHz
1.00
1.00
1.00
1.01
1.00
1.00
1.00
2.01
2.00
f1 (ppm)

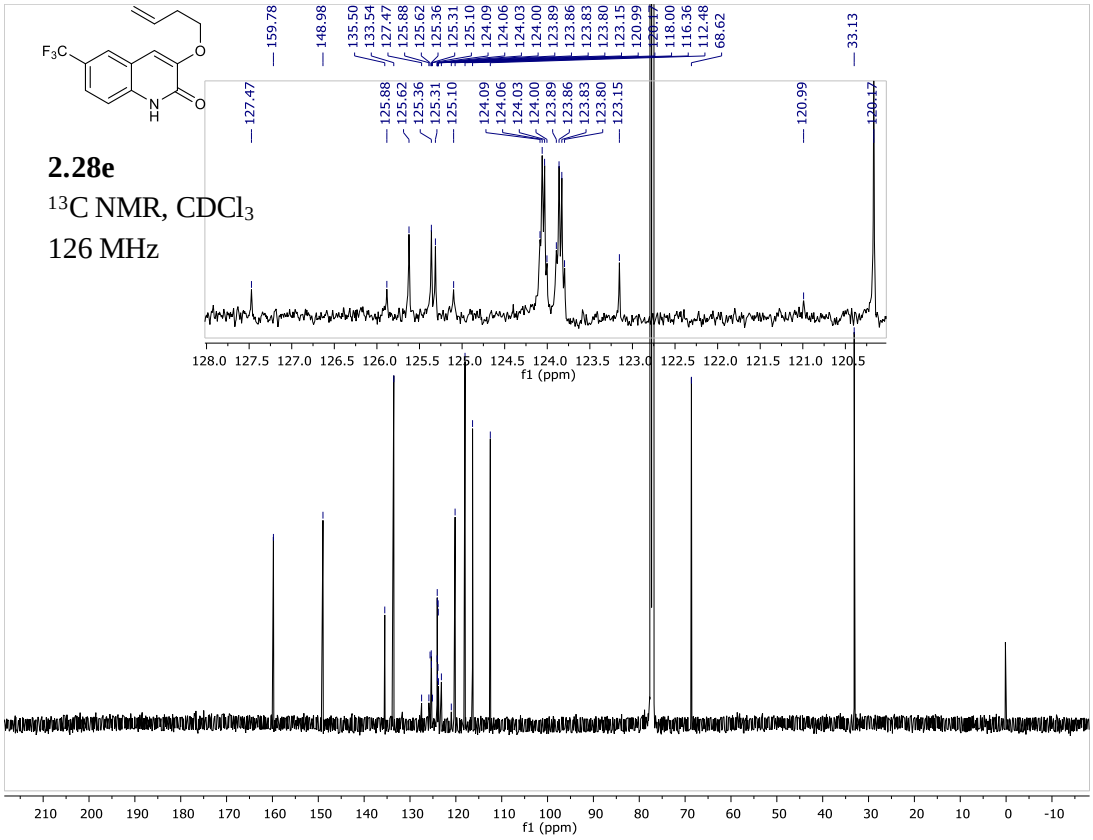
159.78
148.98
135.50
133.54
127.47
125.88
125.62
125.36
125.31
125.10
124.09
124.06
124.03
124.00
123.89
123.86
123.83
123.80
123.15
120.99
120.17
118.00
116.36
112.48
68.62
33.13
F3C
O
N
H
O
2.28e
13C NMR, CDCl3
126 MHz
f1 (ppm)

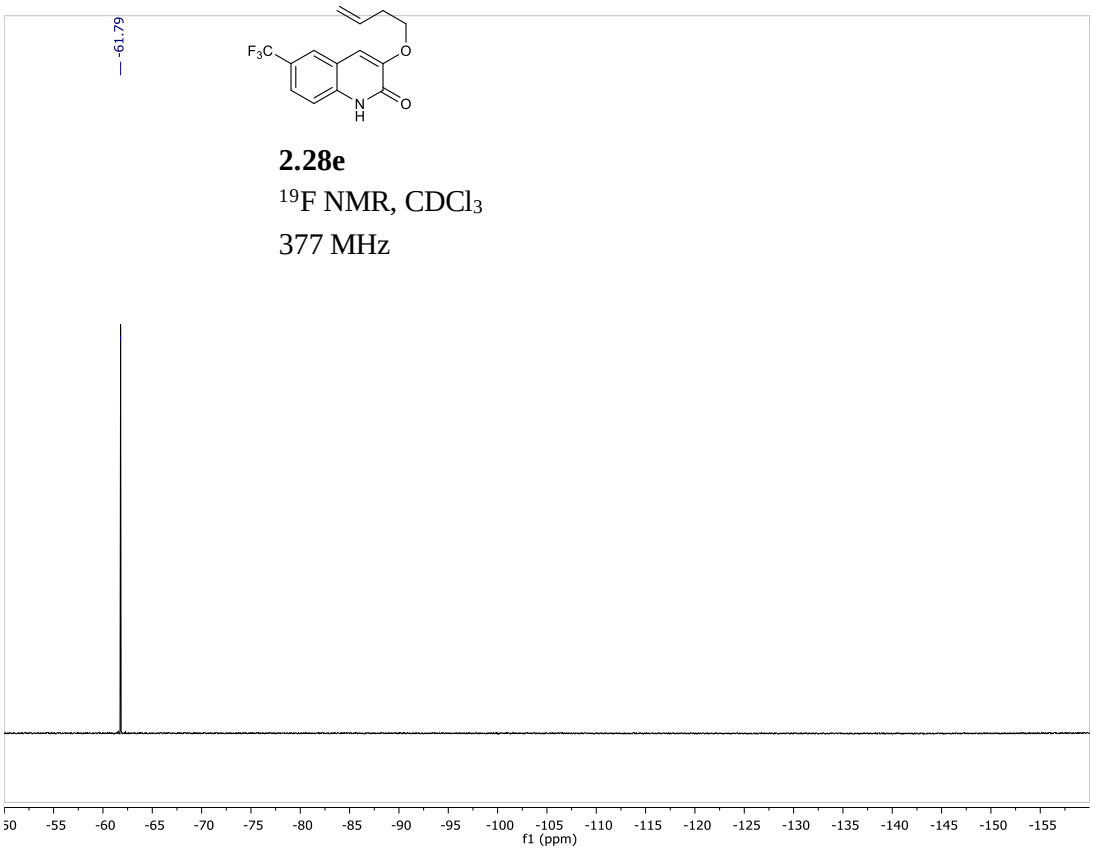

2.28e

^{19}F NMR, $CDCl_3$

377 MHz

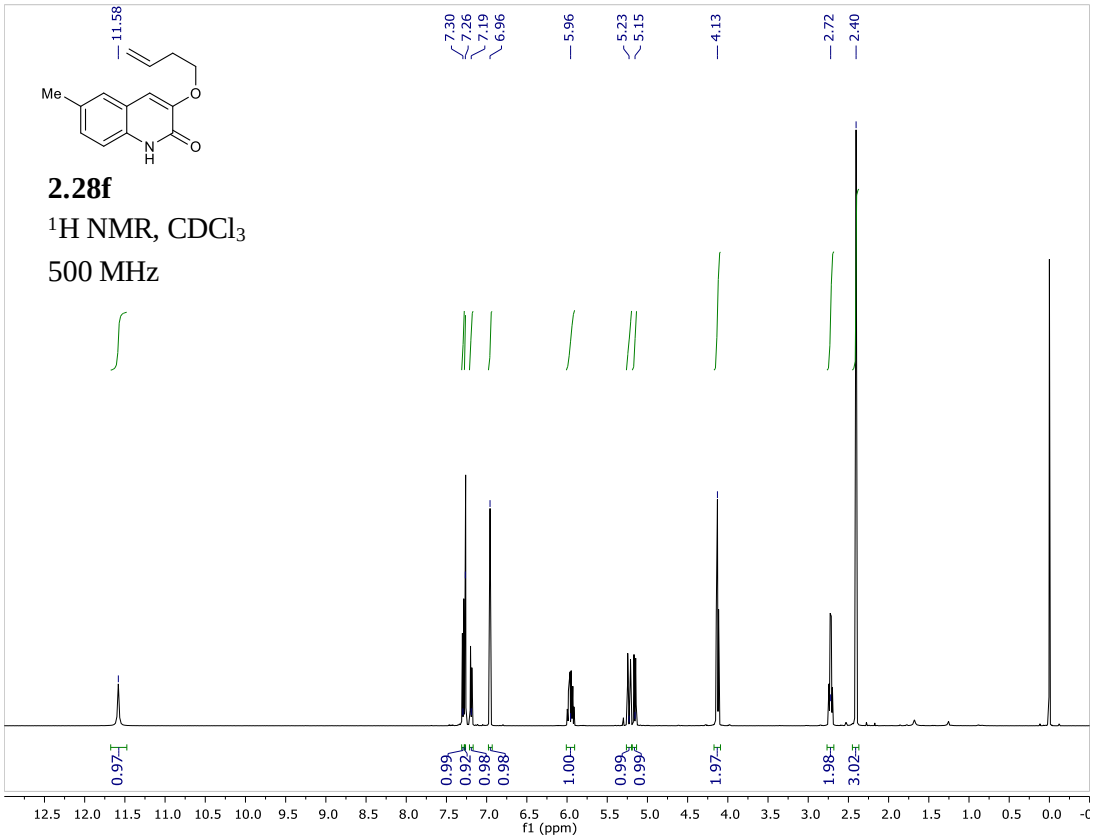

2.28f

^{1}H NMR, $CDCl_3$

500 MHz

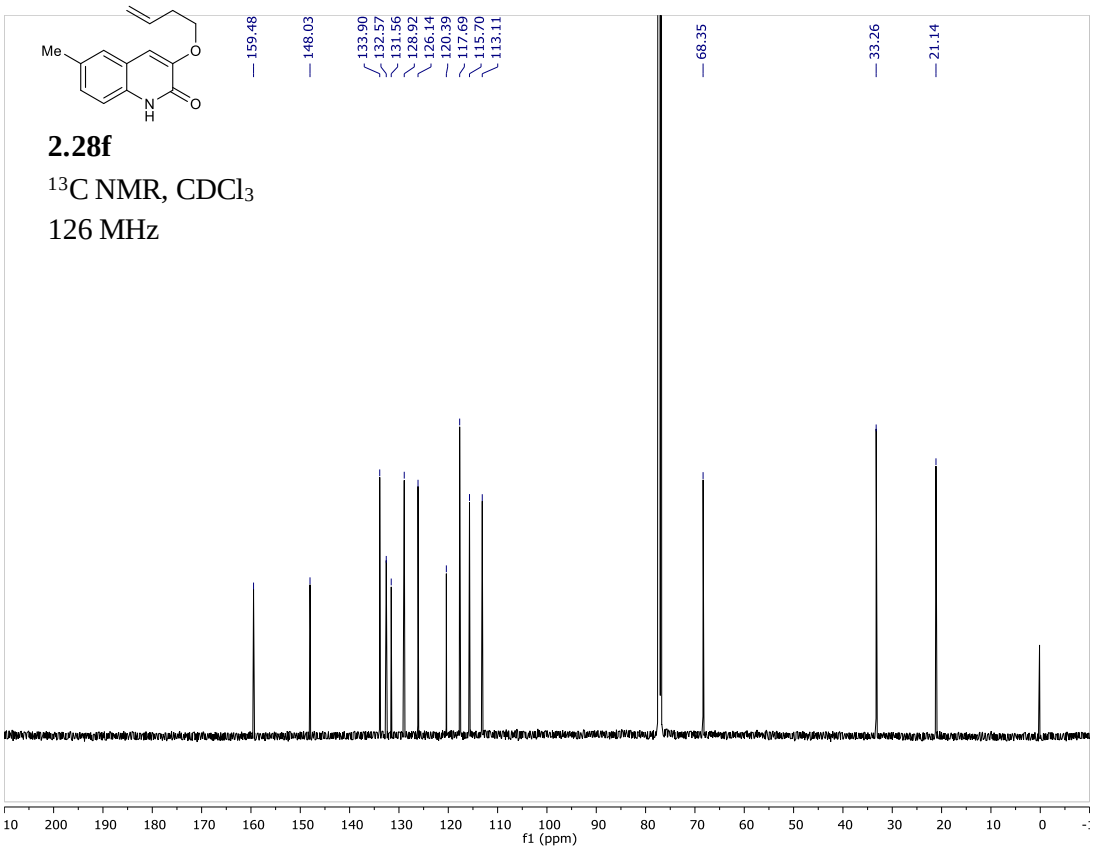

2.28f

^{13}C NMR, $CDCl_3$

126 MHz

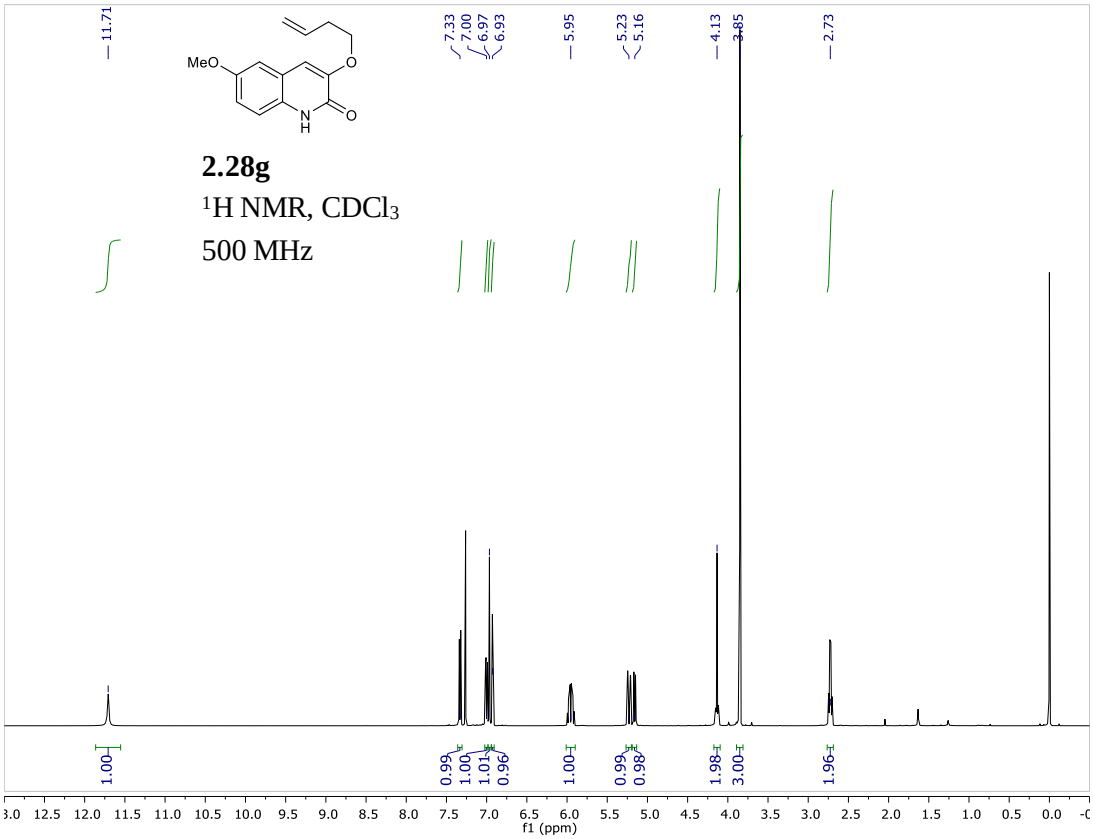
11.71
7.33
7.00
6.97
6.93
5.95
5.23
5.16
4.13
3.85
2.73
MeO
O
N
H
O
2.28g
1H NMR, CDCl3
500 MHz
1.00
0.99
1.00
1.01
0.96
1.00
0.99
0.98
1.98
3.00
1.96
f1 (ppm)

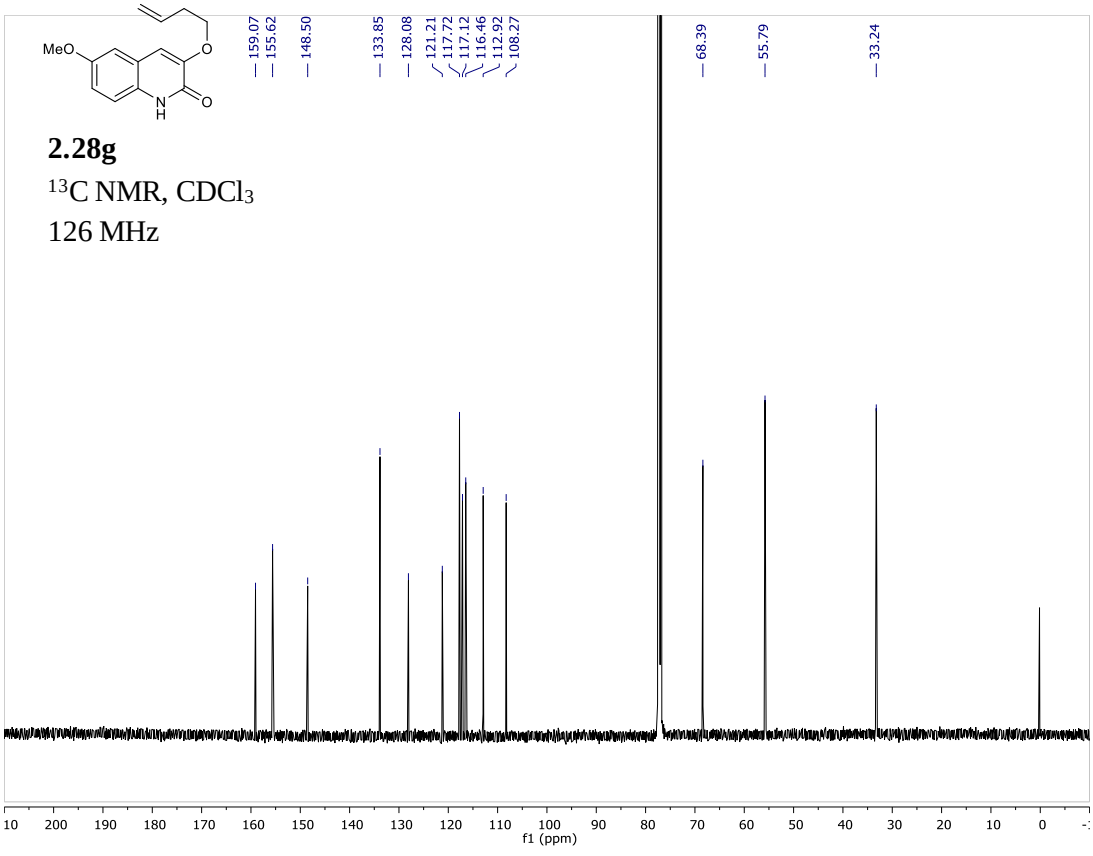
159.07
155.62
148.50
133.85
128.08
121.21
117.72
117.12
116.46
112.92
108.27
68.39
55.79
33.24
MeO
O
N
H
O
2.28g
13C NMR, CDCl3
126 MHz
f1 (ppm)

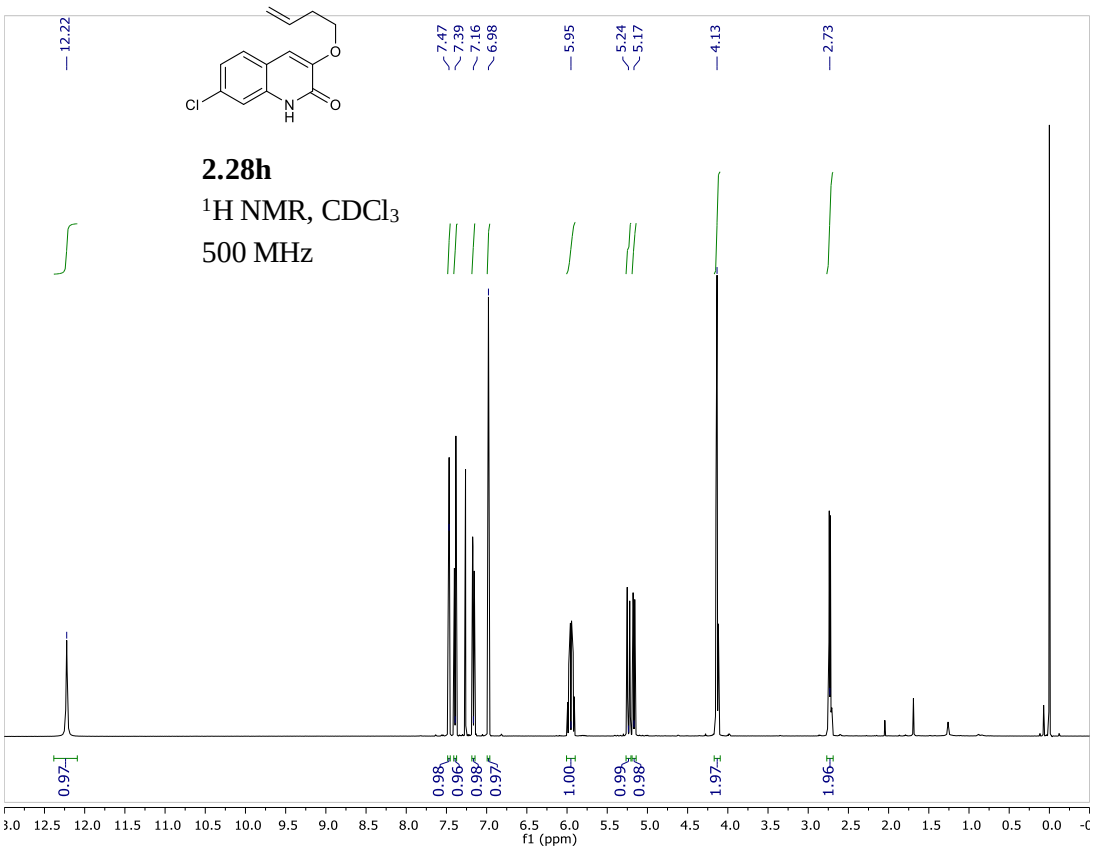
12.22
7.47
7.39
7.16
6.98
5.95
5.24
5.17
4.13
2.73
Cl
O
N
H
O
2.28h
1H NMR, CDCl3
500 MHz
0.97
0.98
0.96
0.98
0.97
1.00
0.99
0.98
1.97
1.96
f1 (ppm)

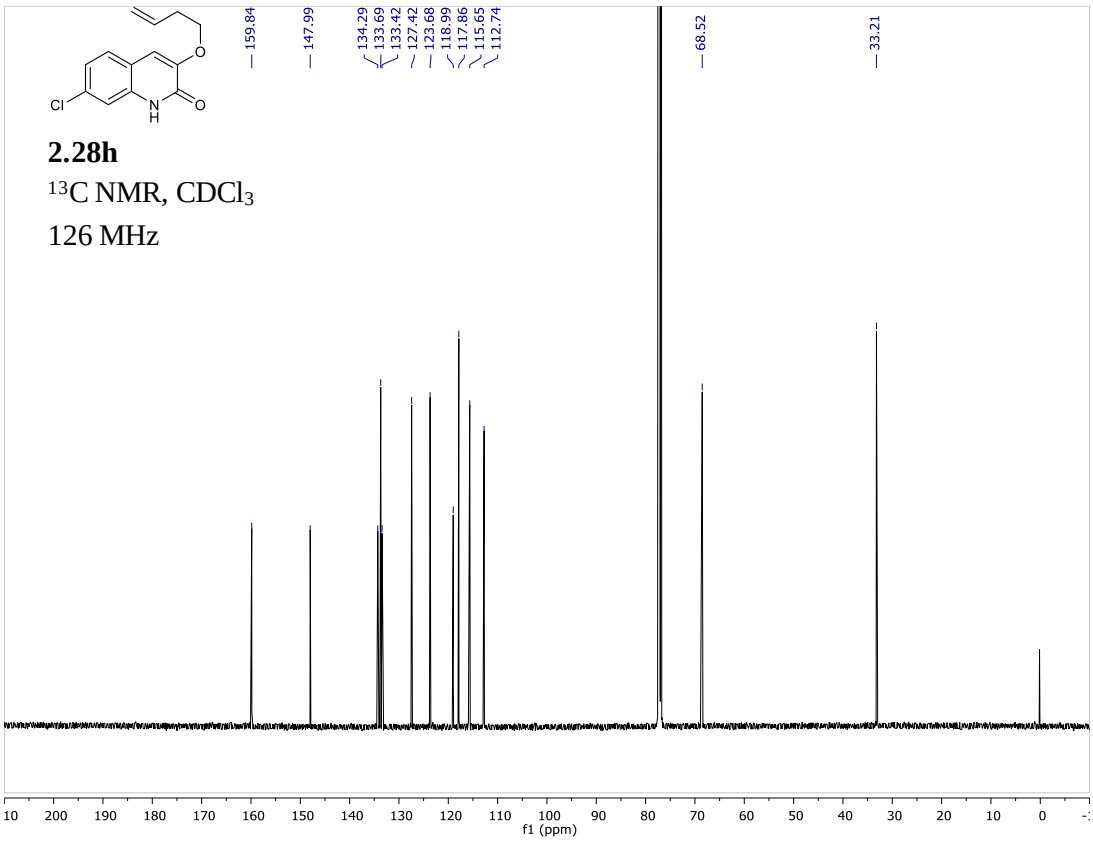
159.84
147.99
134.29
133.69
133.42
127.42
123.68
118.99
117.86
115.65
112.74
68.52
33.21
Cl
O
N
H
O
2.28h
13C NMR, CDCl3
126 MHz
f1 (ppm)

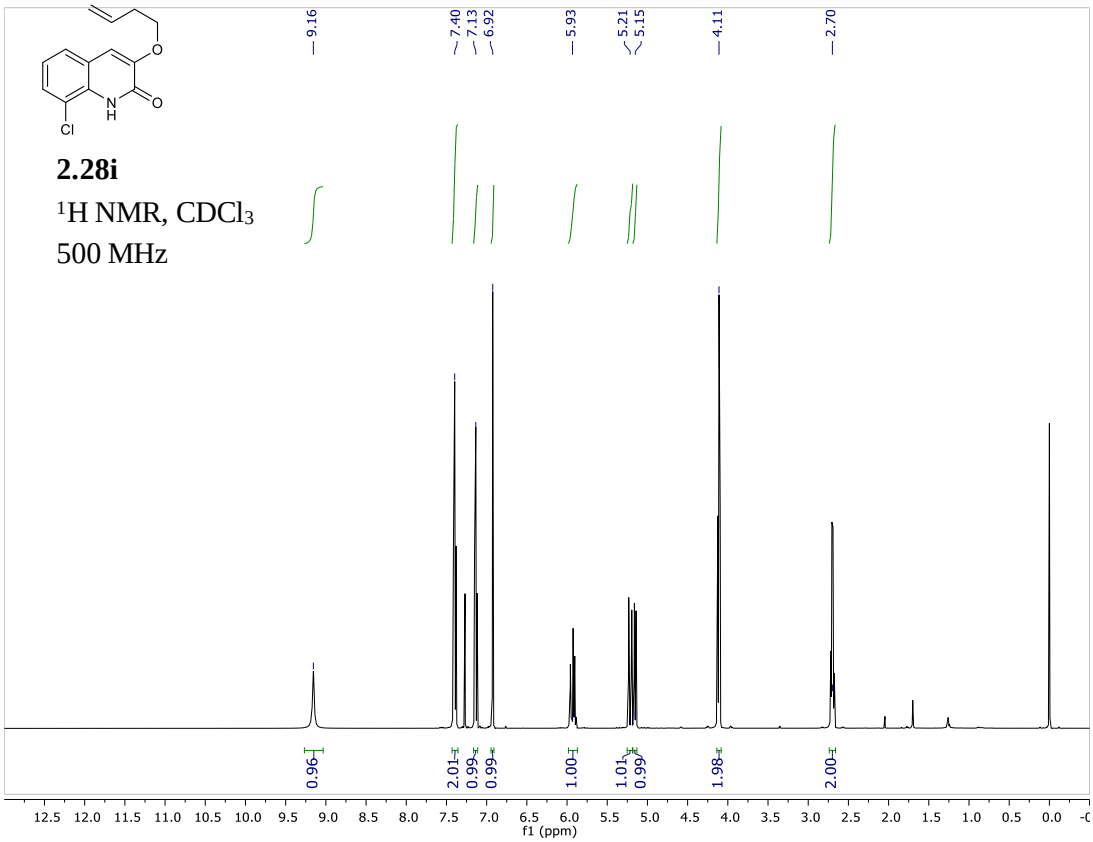

2.28i

^{1}H NMR, $CDCl_3$

500 MHz

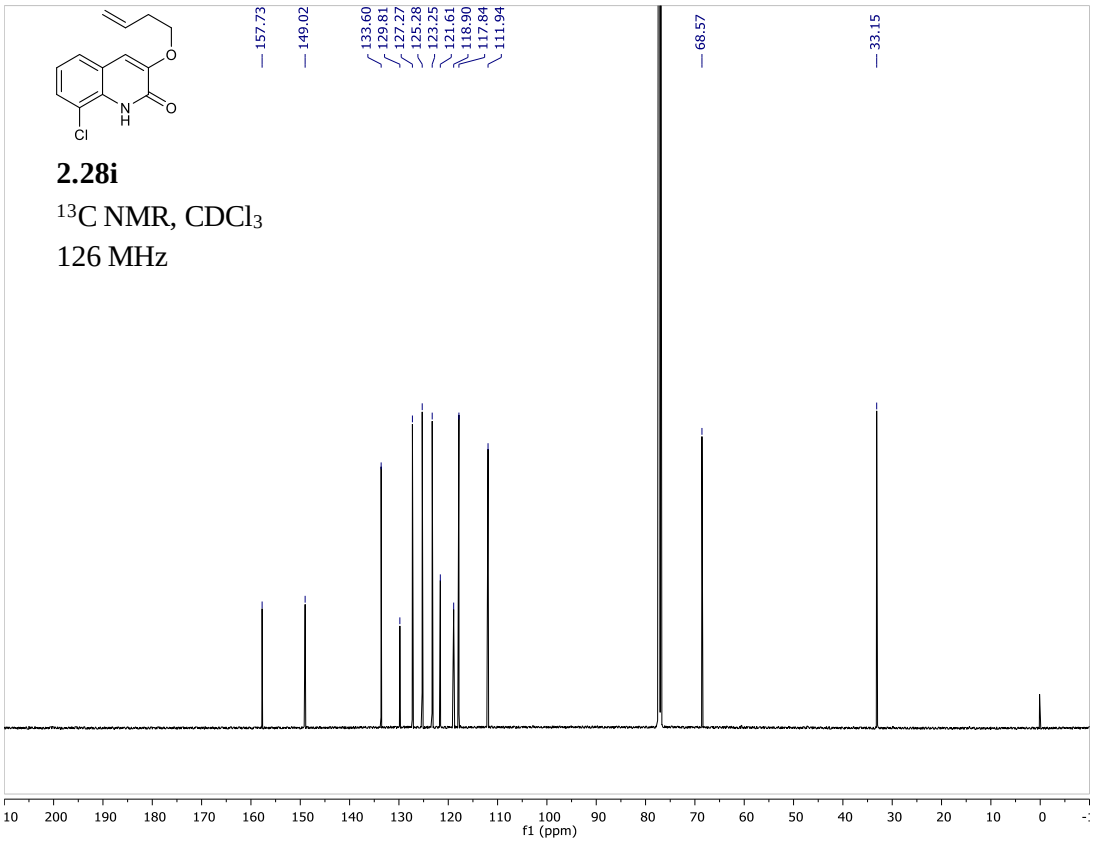

2.28i

^{13}C NMR, $CDCl_3$

126 MHz

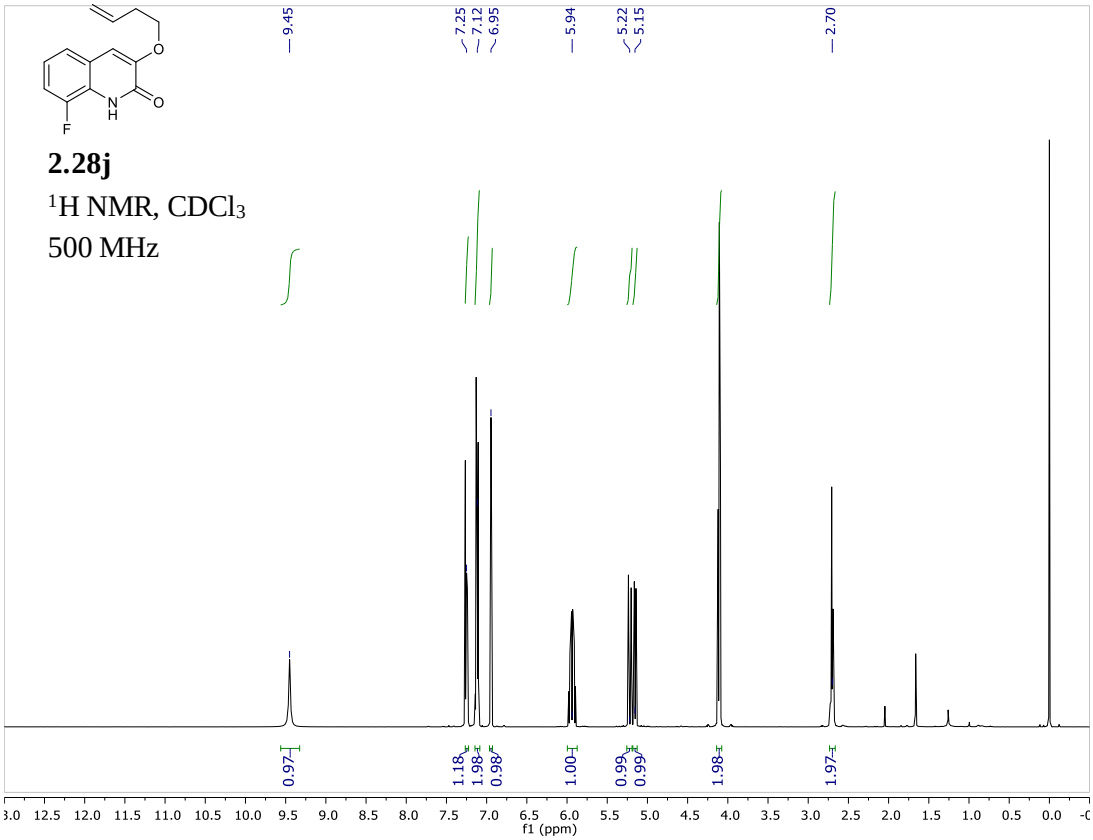

2.28j

^{1}H NMR, $CDCl_3$

500 MHz

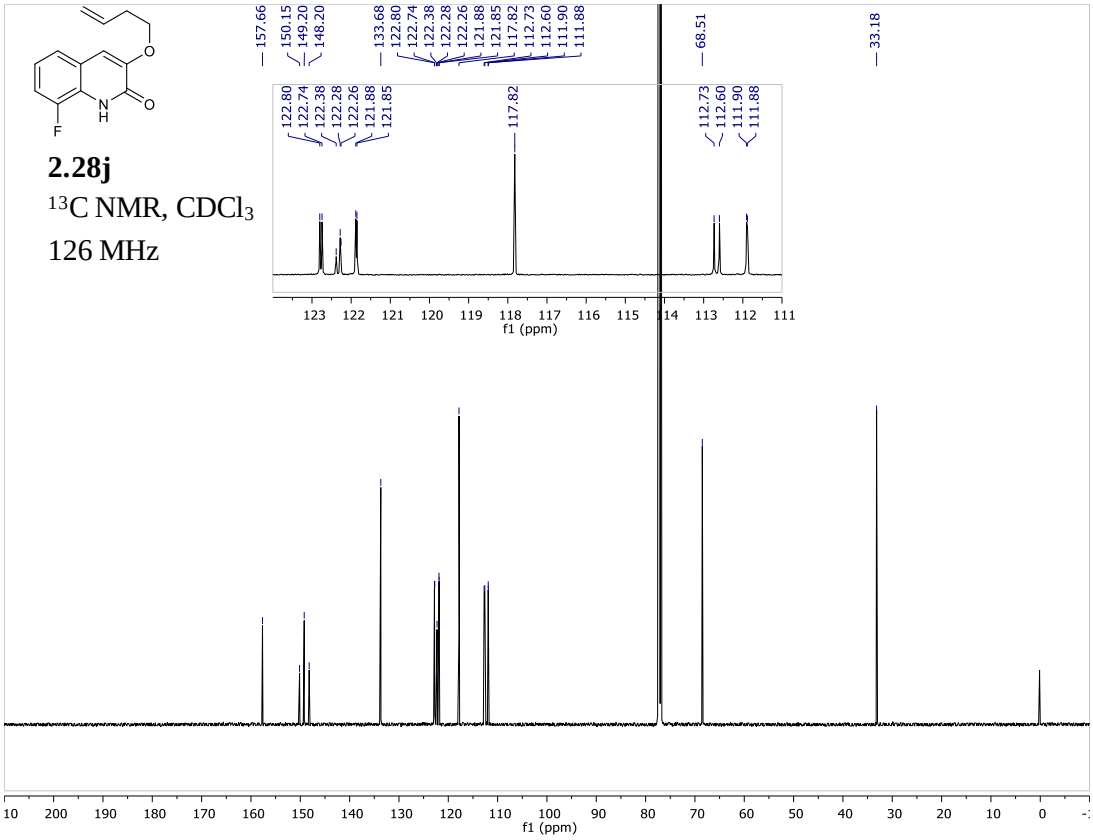

2.28j

^{13}C NMR, $CDCl_3$

126 MHz

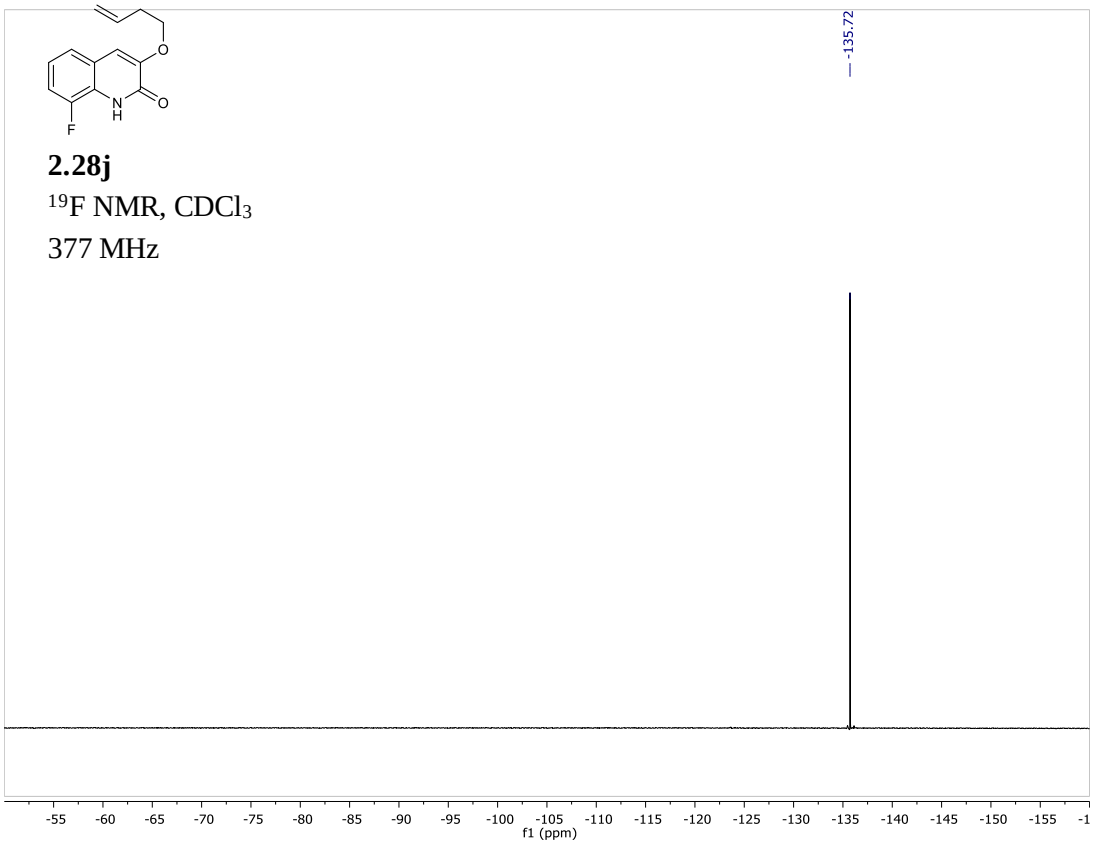

2.28j

^{19}F NMR, $CDCl_3$

377 MHz

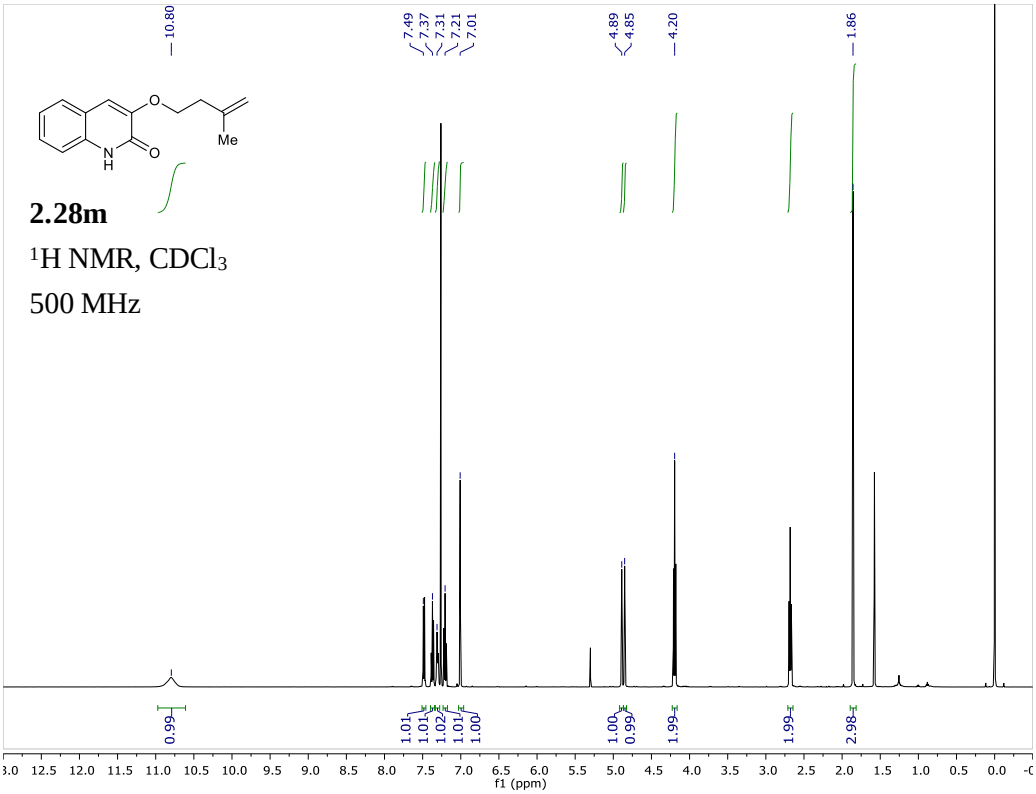
10.80
7.49
7.37
7.31
7.21
7.01
4.89
4.85
4.20
1.86
O
Me
N
H
O
2.28m
1H NMR, CDCl3
500 MHz
0.99
1.01
1.01
1.02
1.01
1.00
1.00
0.99
1.99
1.99
2.98
f1 (ppm)

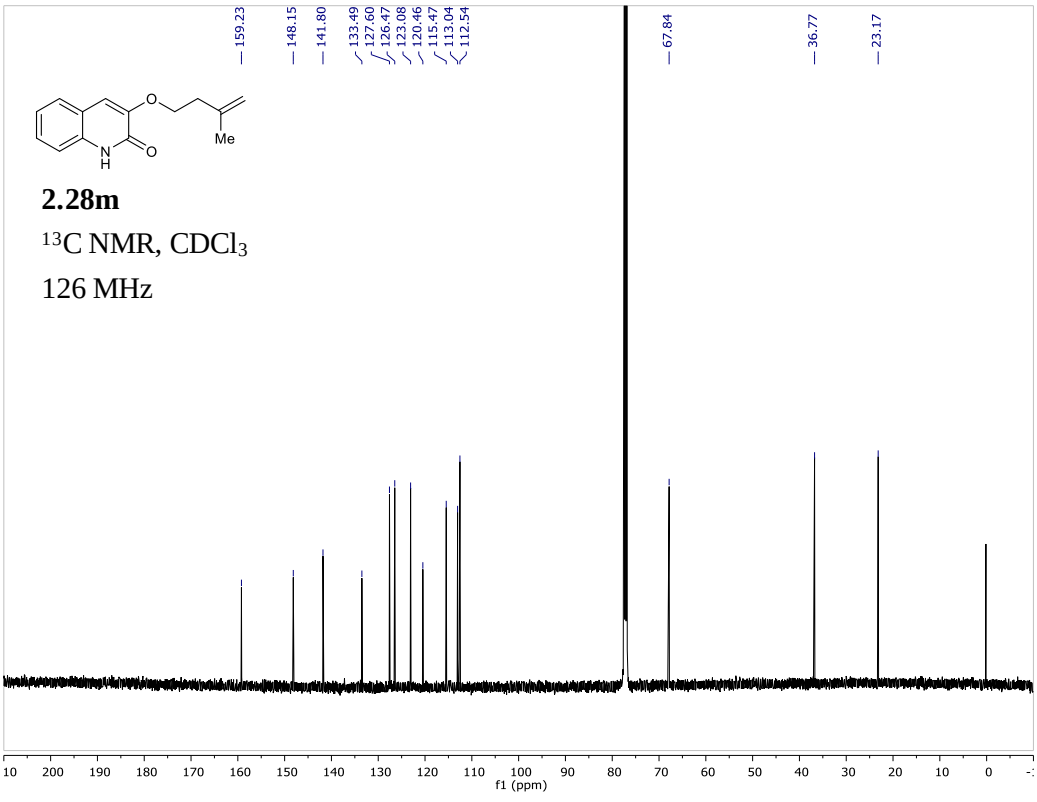
159.23
148.15
141.80
133.49
127.60
126.47
123.08
120.46
115.47
113.04
112.54
67.84
36.77
23.17
O
Me
N
H
O
2.28m
13C NMR, CDCl3
126 MHz
f1 (ppm)

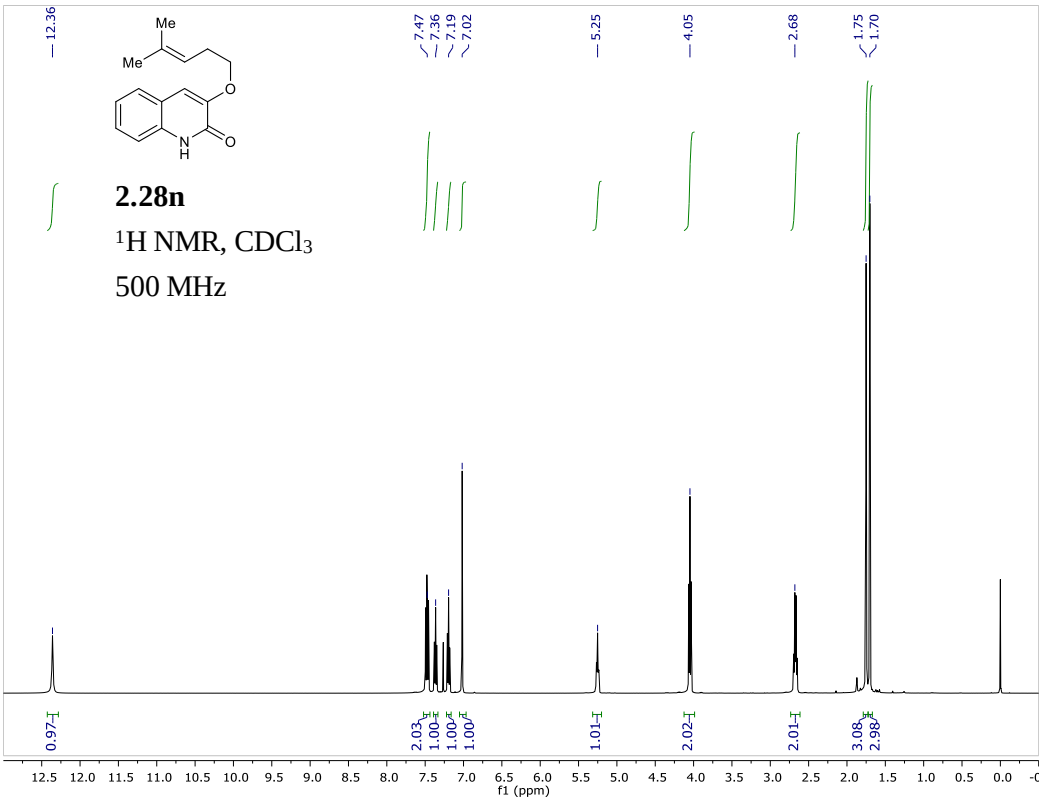

2.28n

^{1}H NMR, $CDCl_3$

500 MHz

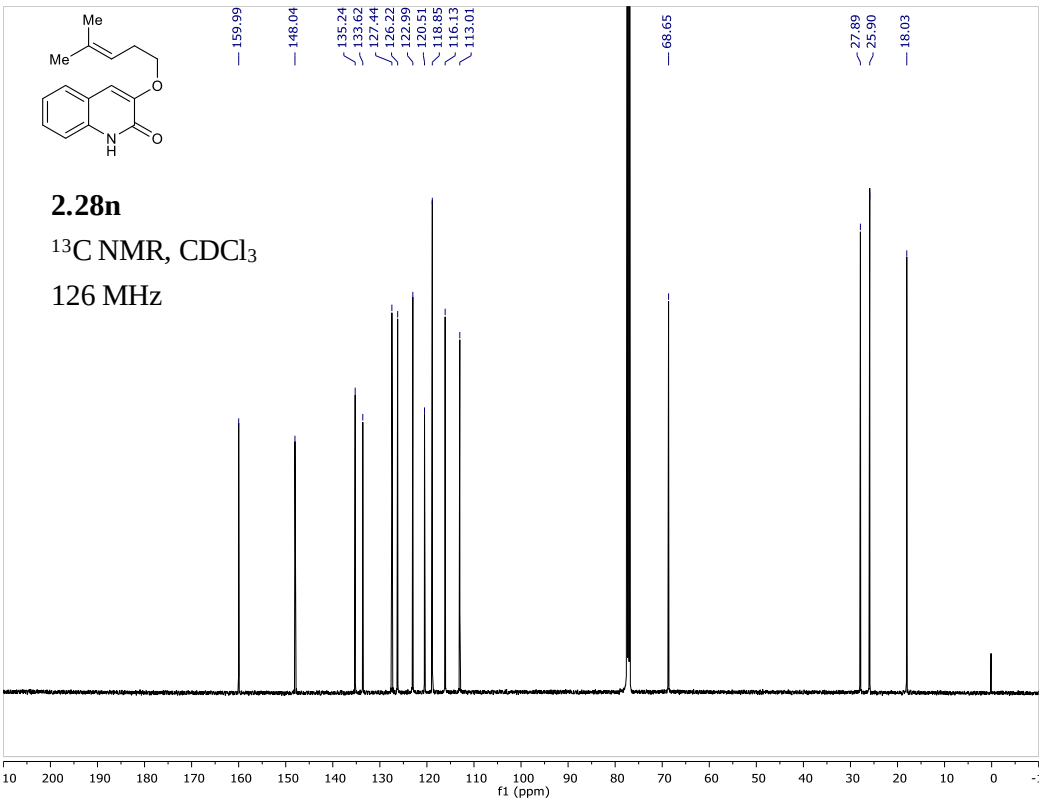

2.28n

^{13}C NMR, $CDCl_3$

126 MHz

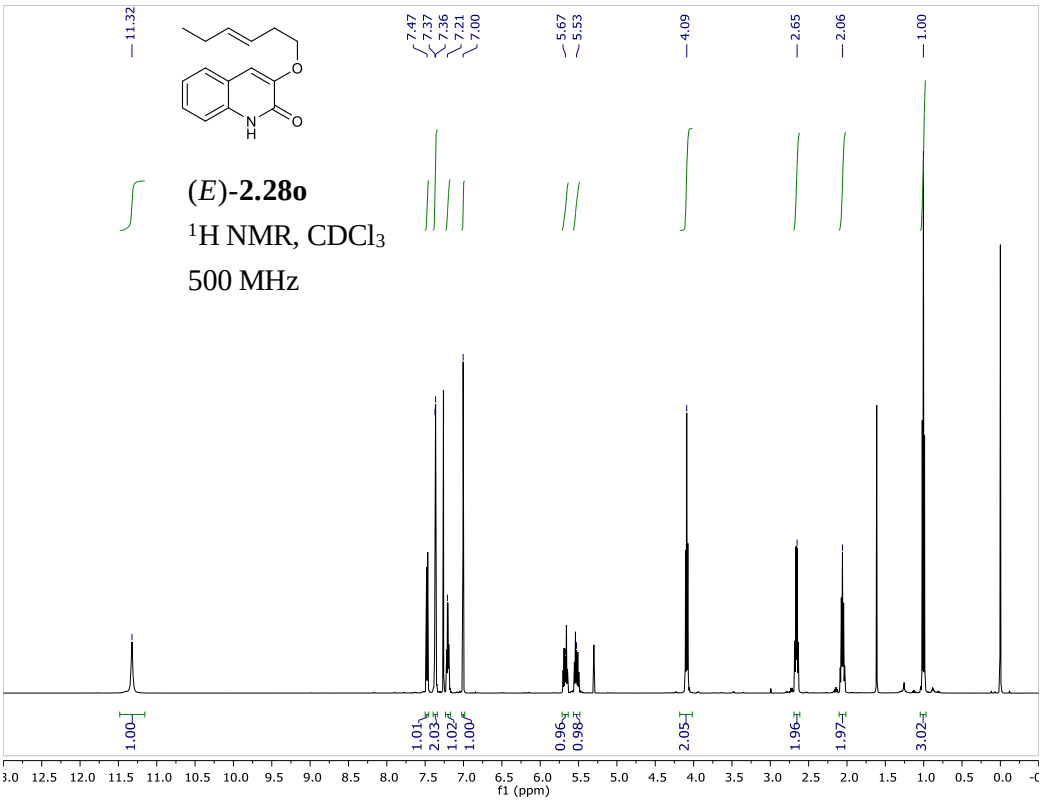
11.32
7.47
7.37
7.36
7.21
7.00
5.67
5.53
4.09
2.65
2.06
1.00
(E)-2.28o
1H NMR, CDCl3
500 MHz
1.00
1.01
2.03
1.02
1.00
0.96
0.98
2.05
1.96
1.97
3.02
f1 (ppm)

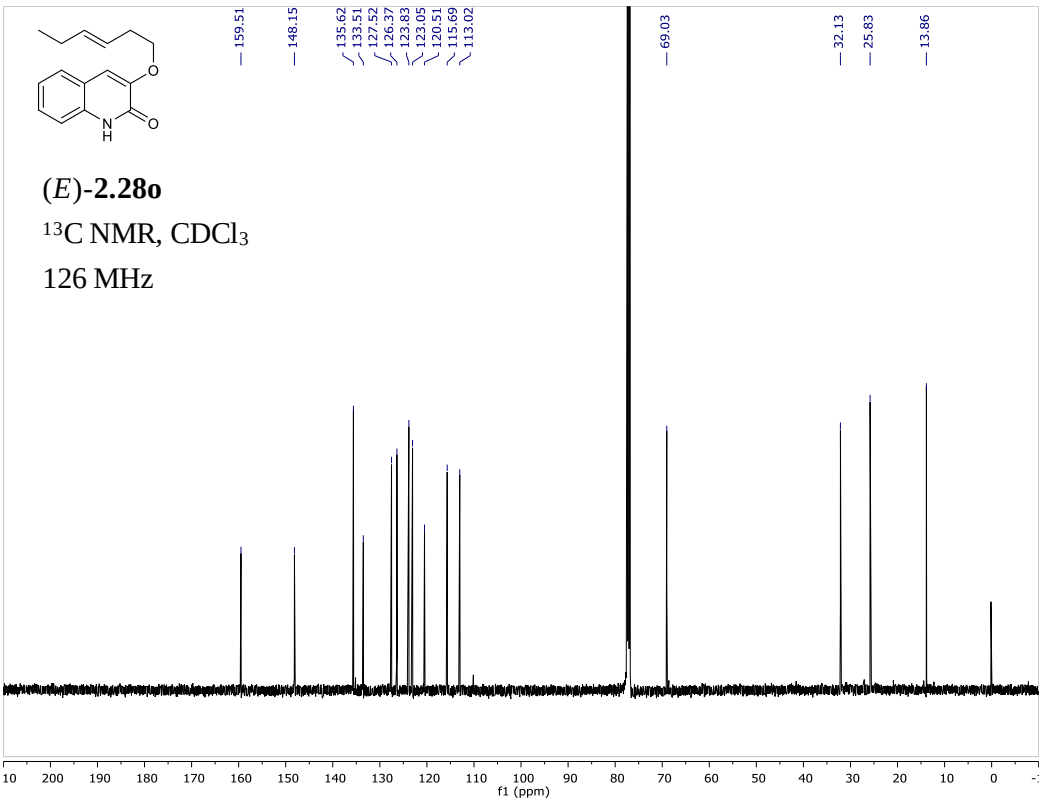
159.51
148.15
135.62
133.51
127.52
126.37
123.83
123.05
120.51
115.69
113.02
69.03
32.13
25.83
13.86
(E)-2.28o
13C NMR, CDCl3
126 MHz
f1 (ppm)

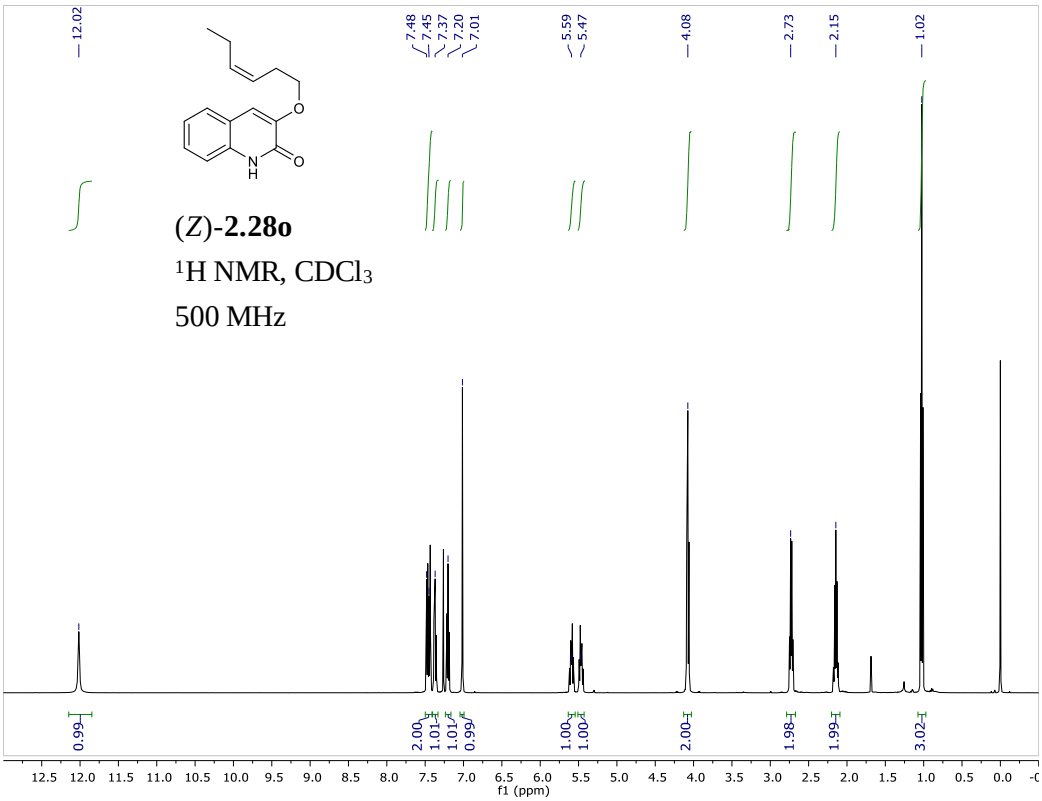
12.02
7.48
7.45
7.37
7.20
7.01
5.59
5.47
4.08
2.73
2.15
1.02
(Z)-2.28o
1H NMR, CDCl3
500 MHz
0.99
2.00
1.01
1.01
0.99
1.00
1.00
2.00
1.98
1.99
3.02
f1 (ppm)

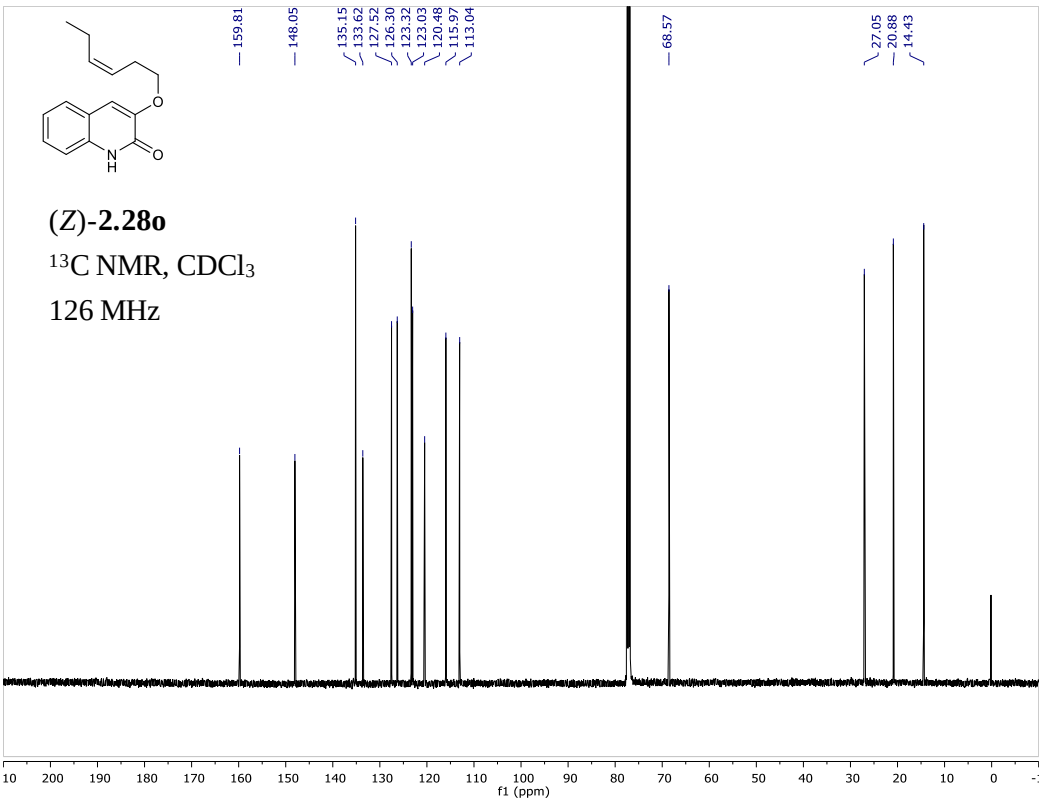
159.81
148.05
135.15
133.62
127.52
126.30
123.32
123.03
120.48
115.97
113.04
68.57
27.05
20.88
14.43
(Z)-2.28o
13C NMR, CDCl3
126 MHz
f1 (ppm)

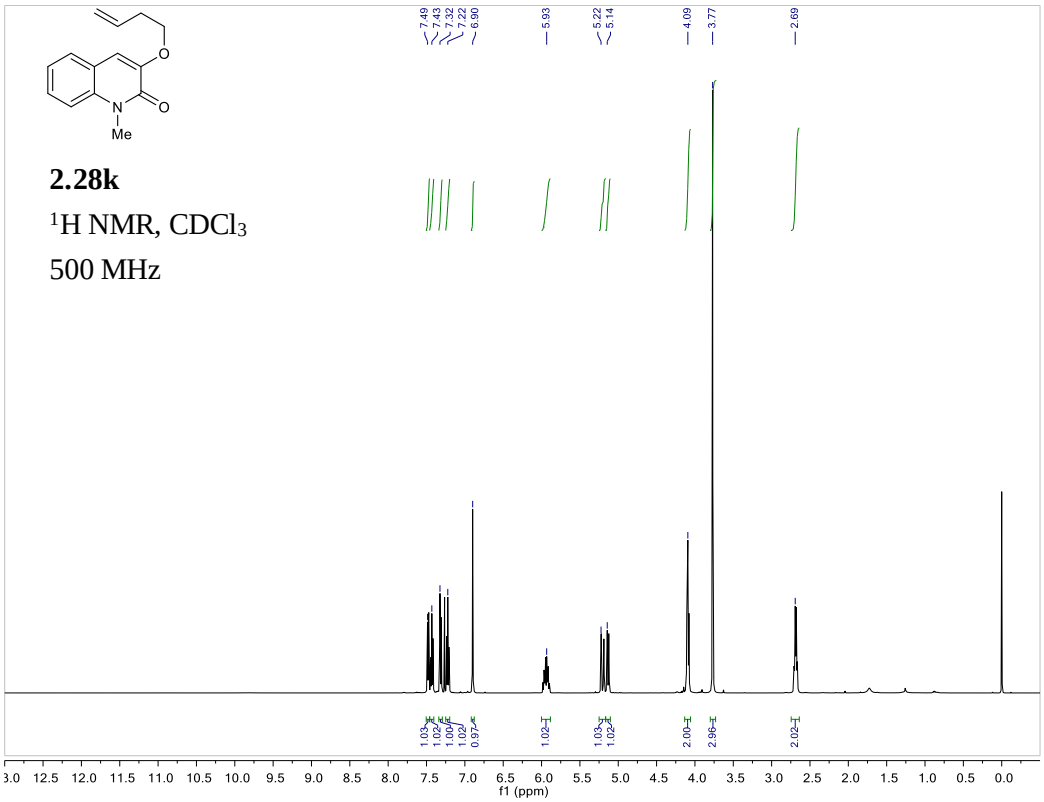
7.49
7.43
7.32
7.22
6.90
5.93
5.22
5.14
4.09
3.77
2.69
Me
2.28k
1H NMR, CDCl3
500 MHz
f1 (ppm)

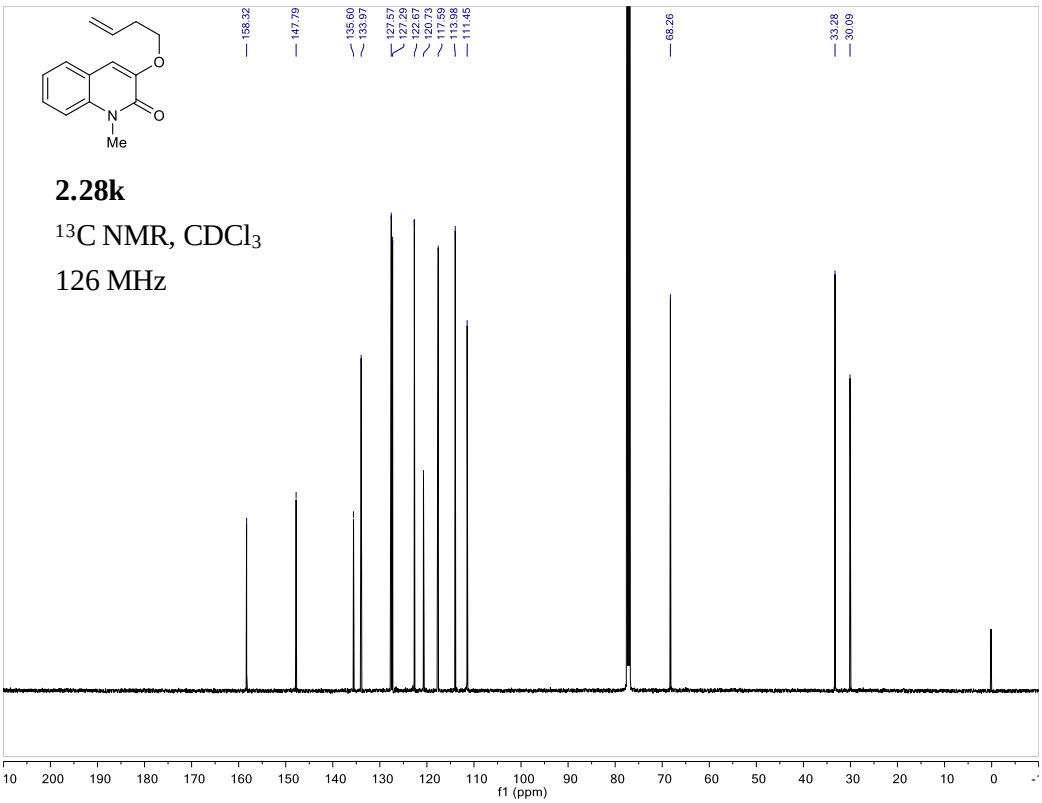
158.32
147.79
135.60
133.97
127.57
127.29
122.67
120.73
117.59
113.98
111.45
68.26
33.28
30.09
Me
2.28k
13C NMR, CDCl3
126 MHz
f1 (ppm)

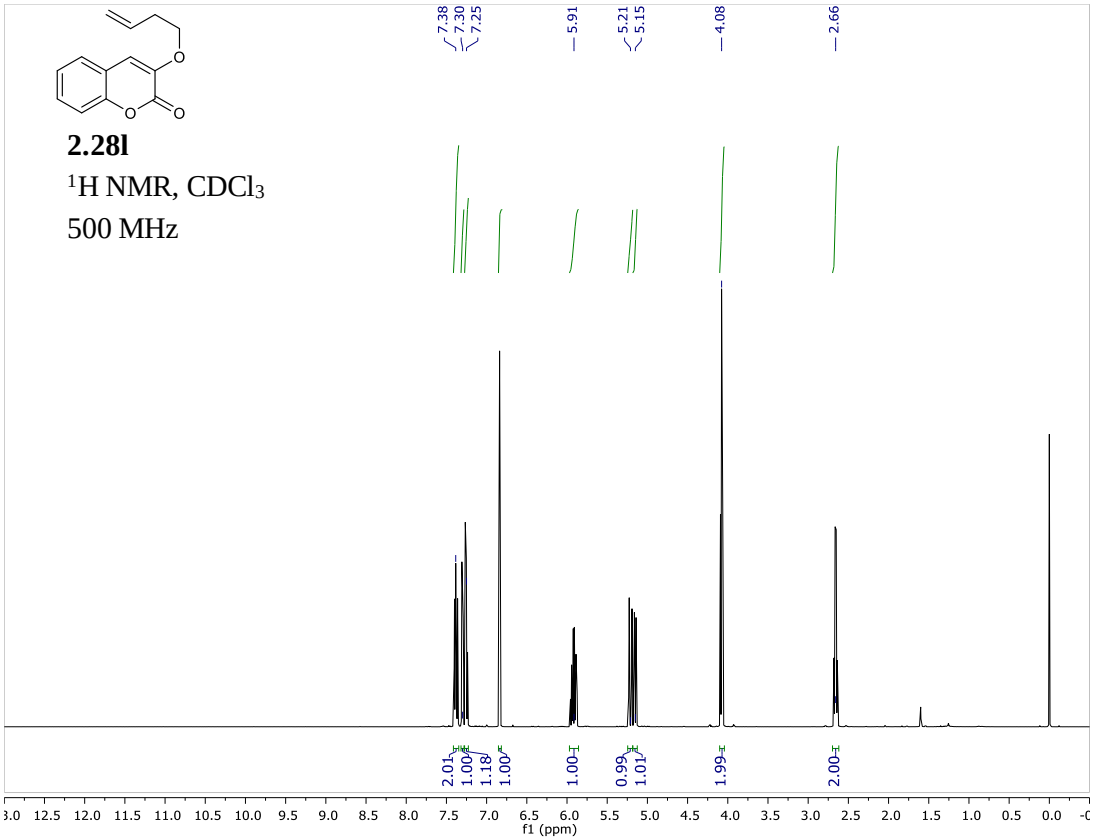

2.28l

^{1}H NMR, $CDCl_3$

500 MHz

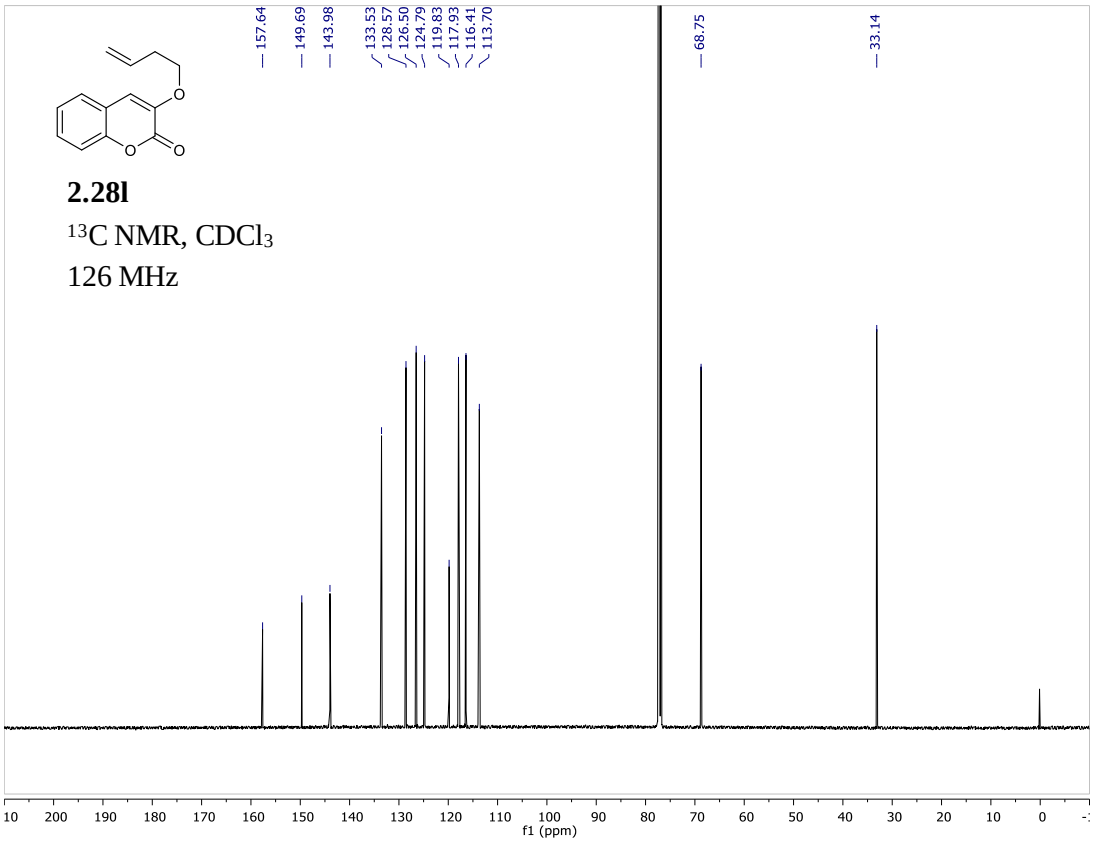

2.28l

^{13}C NMR, $CDCl_3$

126 MHz

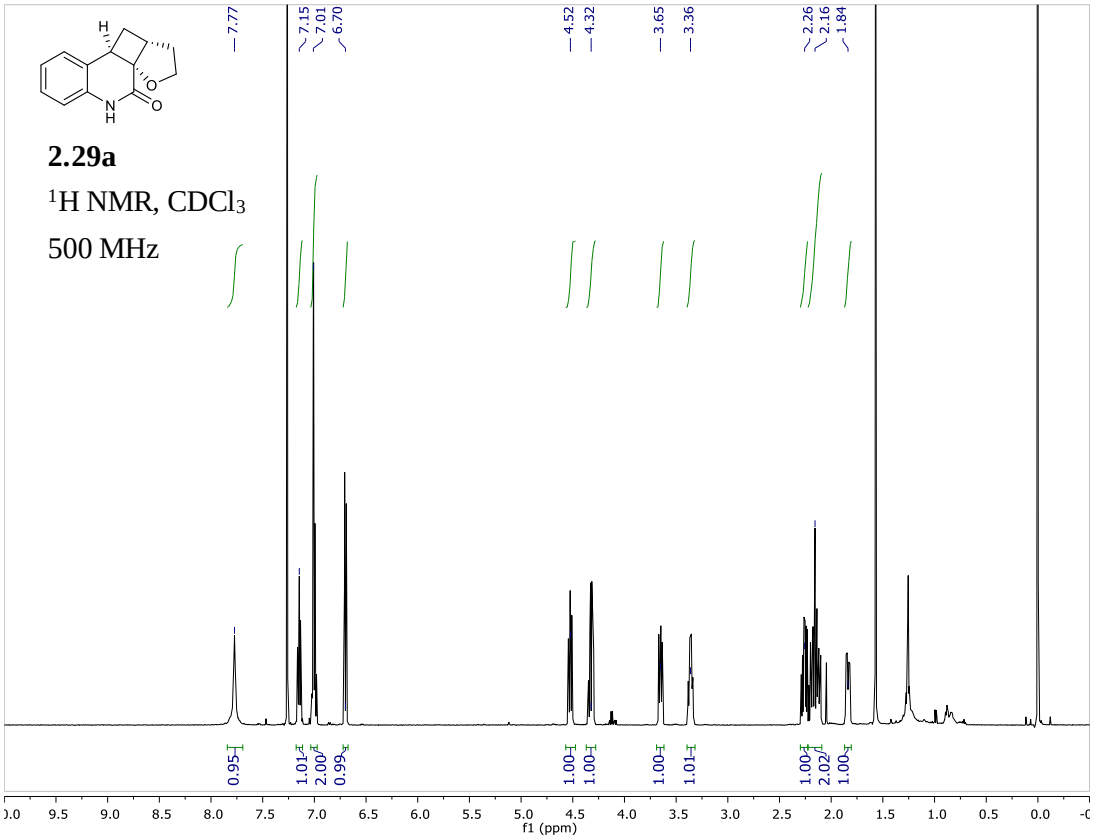

2.29a

^{1}H NMR, $CDCl_3$

500 MHz

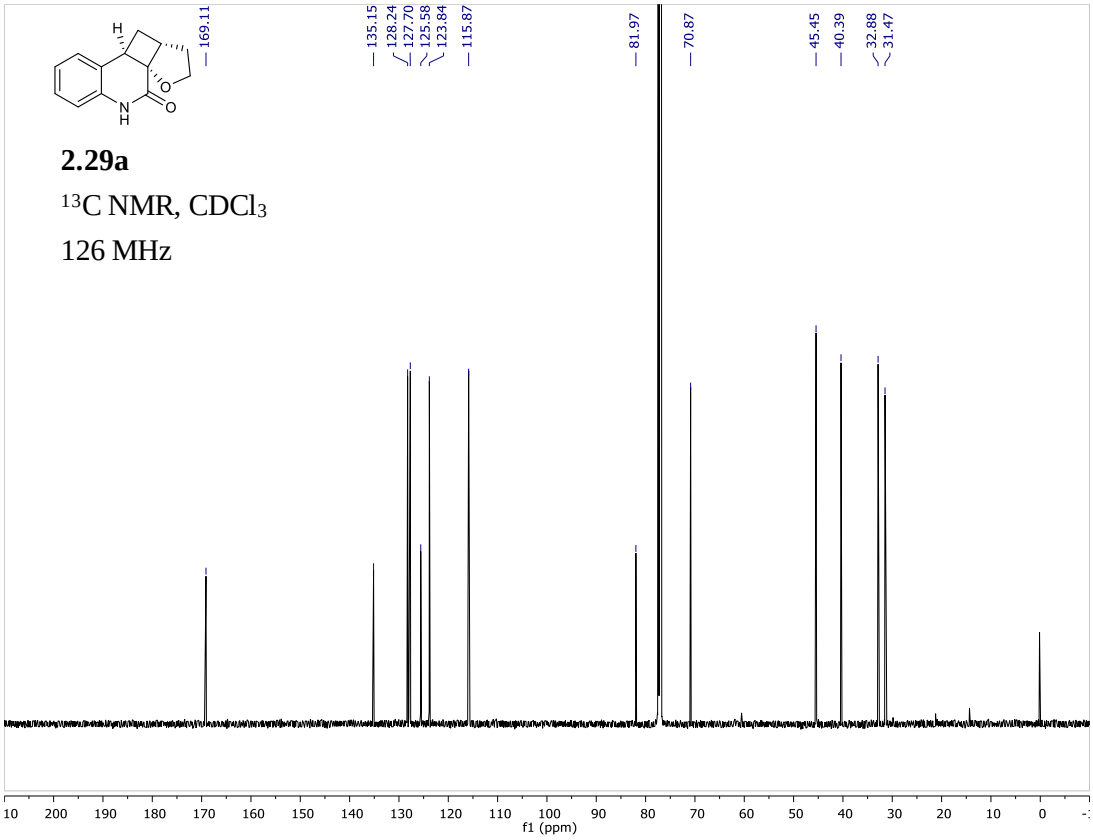

2.29a

^{13}C NMR, $CDCl_3$

126 MHz

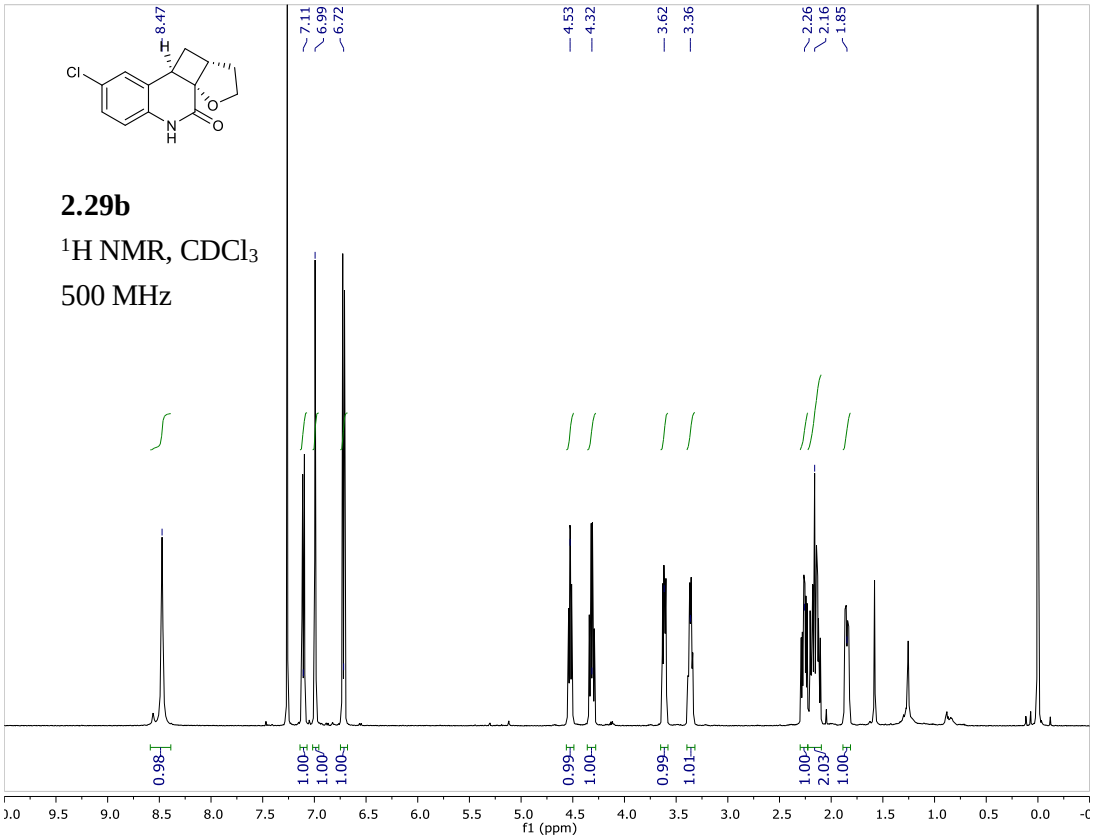

2.29b

^{1}H NMR, $CDCl_3$

500 MHz

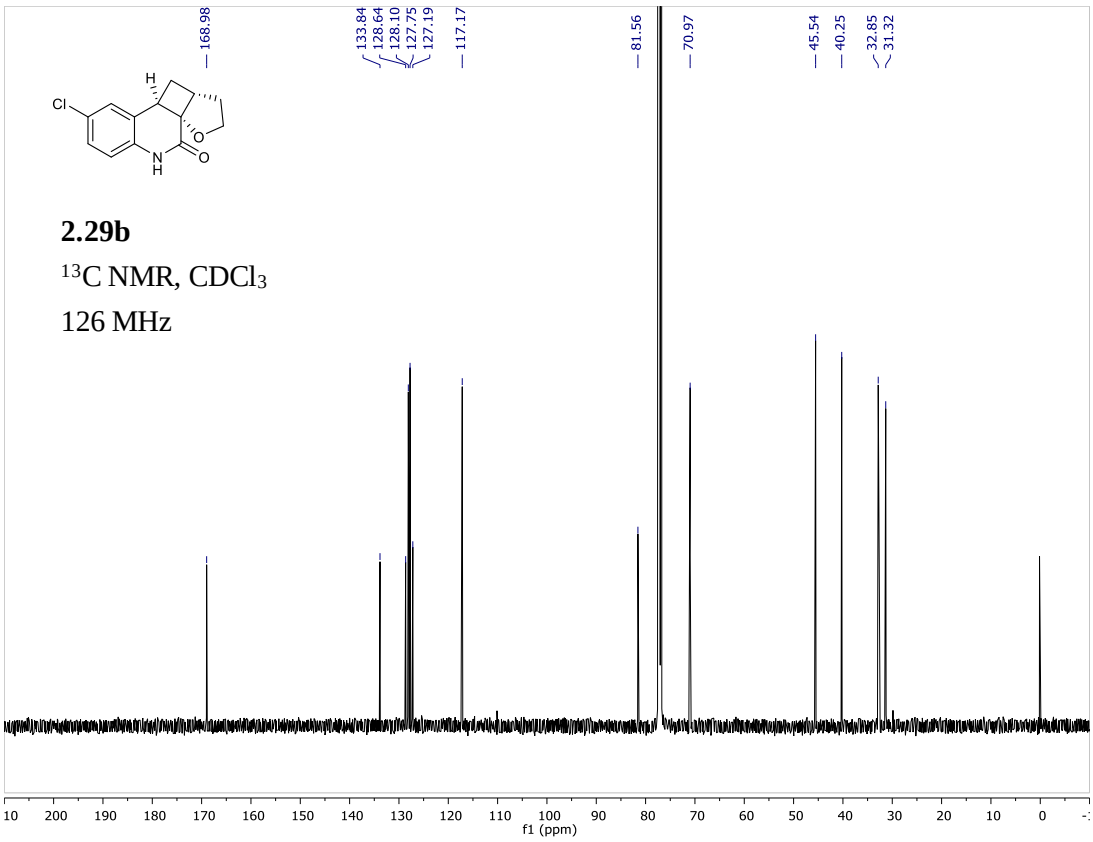

2.29b

^{13}C NMR, $CDCl_3$

126 MHz

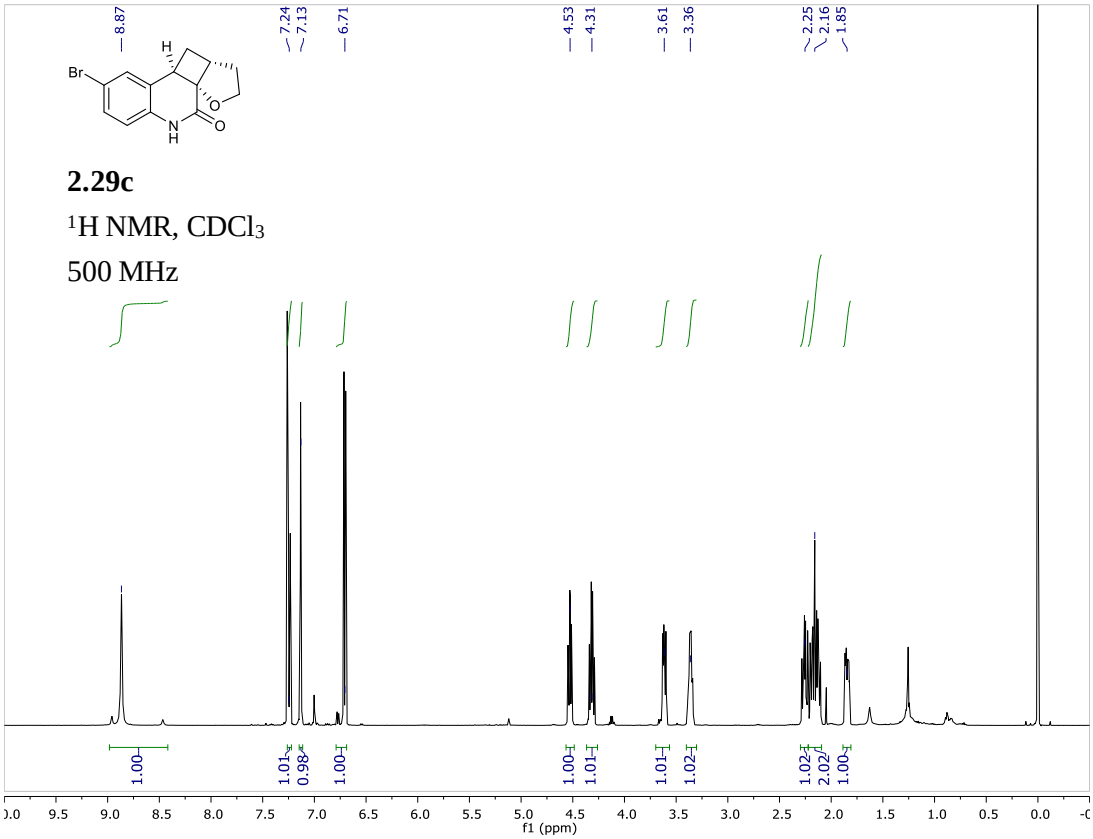

2.29c

^{1}H NMR, $CDCl_3$

500 MHz

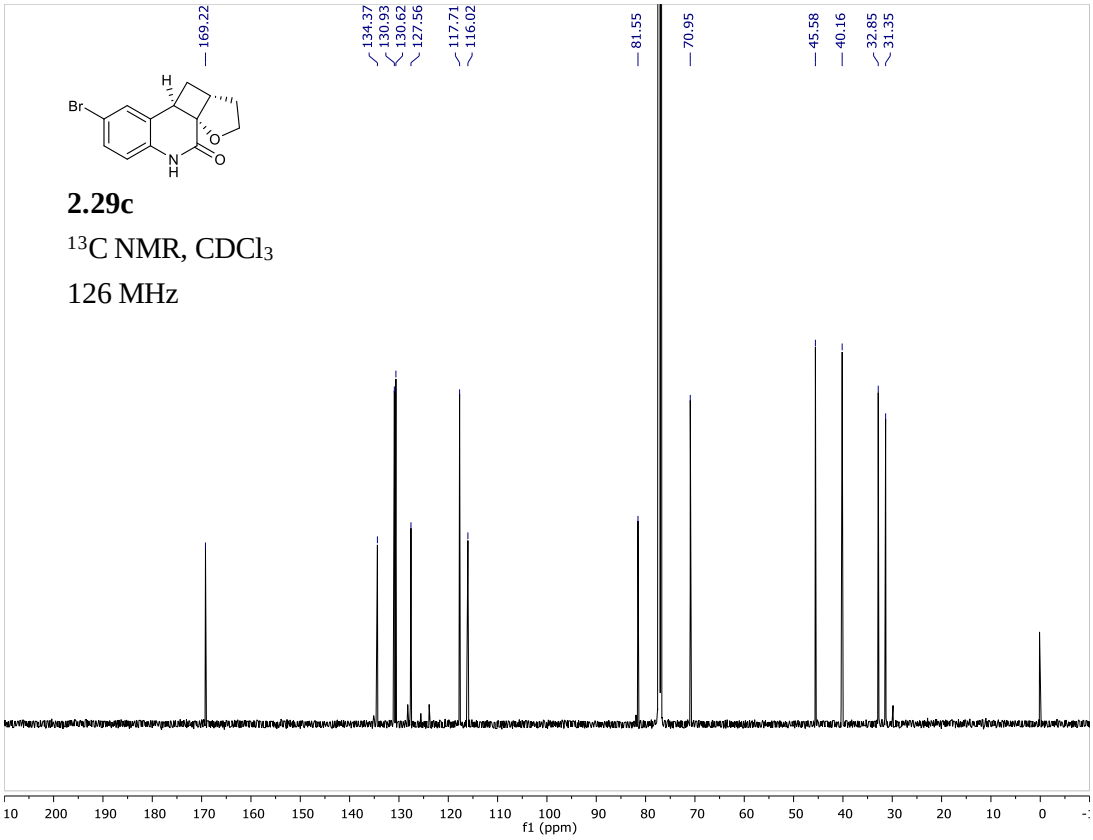

2.29c

^{13}C NMR, $CDCl_3$

126 MHz

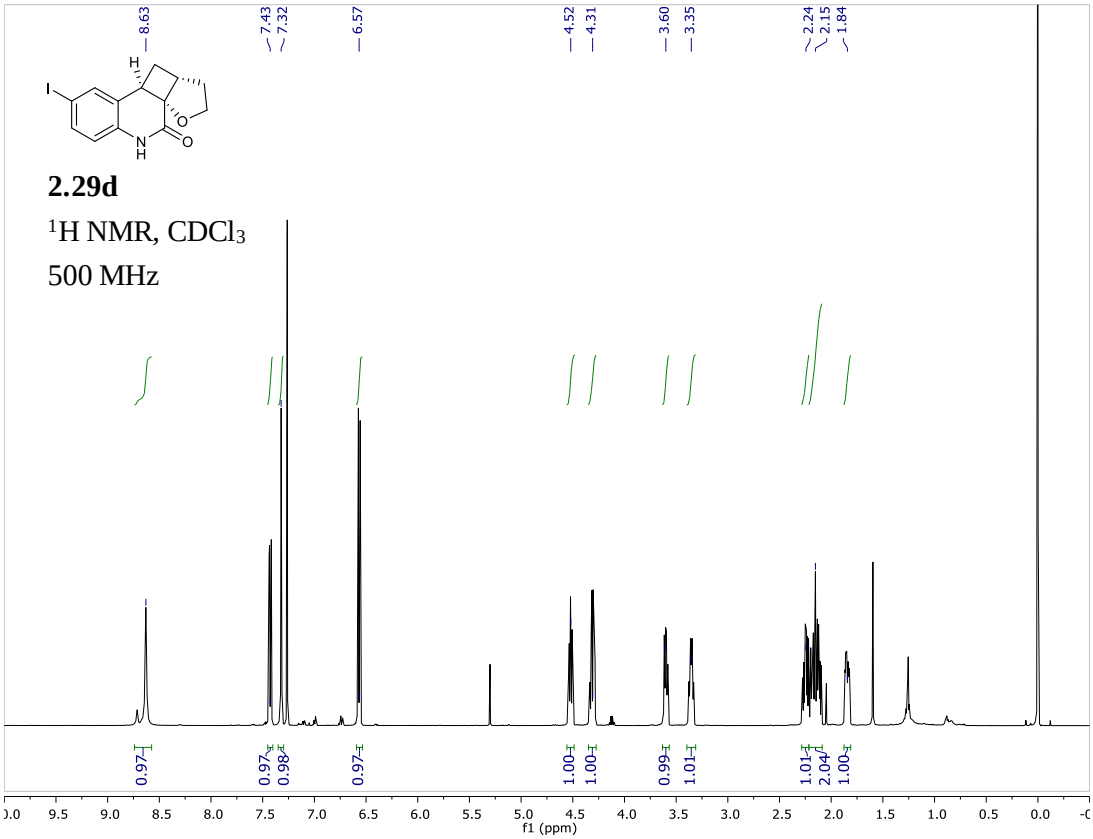

2.29d

^{1}H NMR, $CDCl_3$

500 MHz

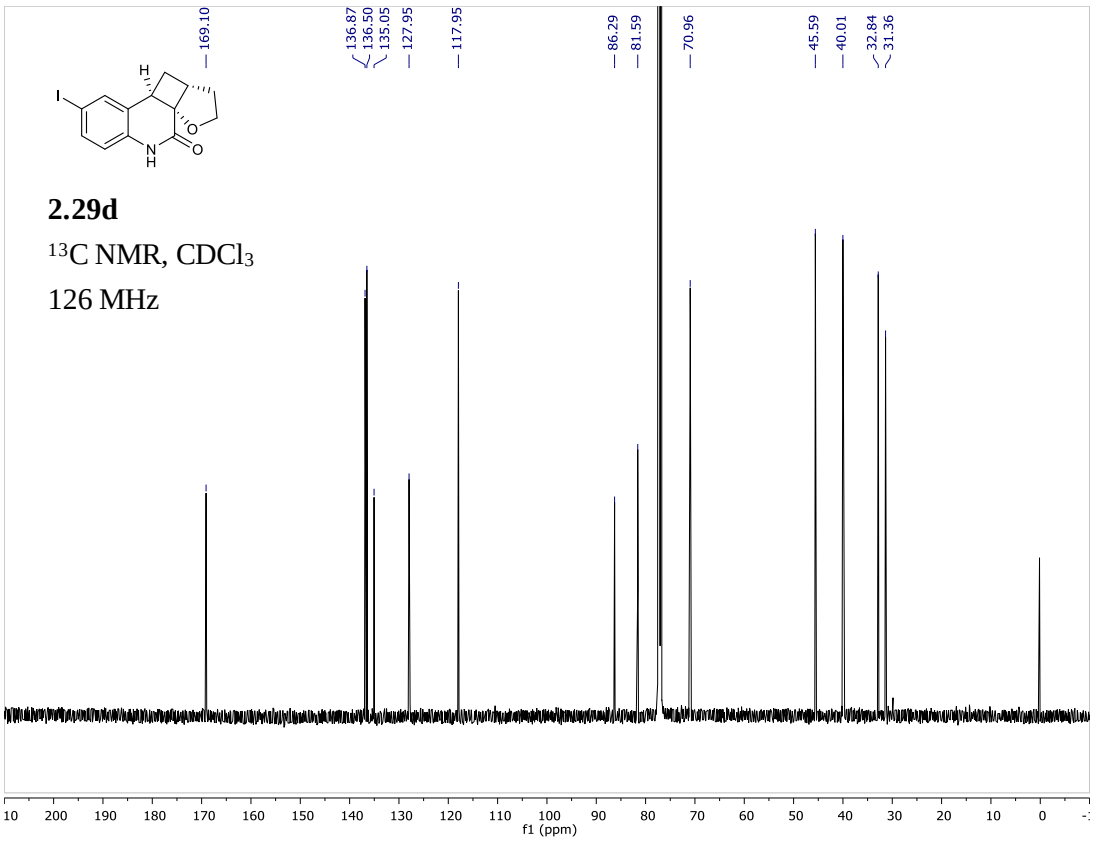

2.29d

^{13}C NMR, $CDCl_3$

126 MHz

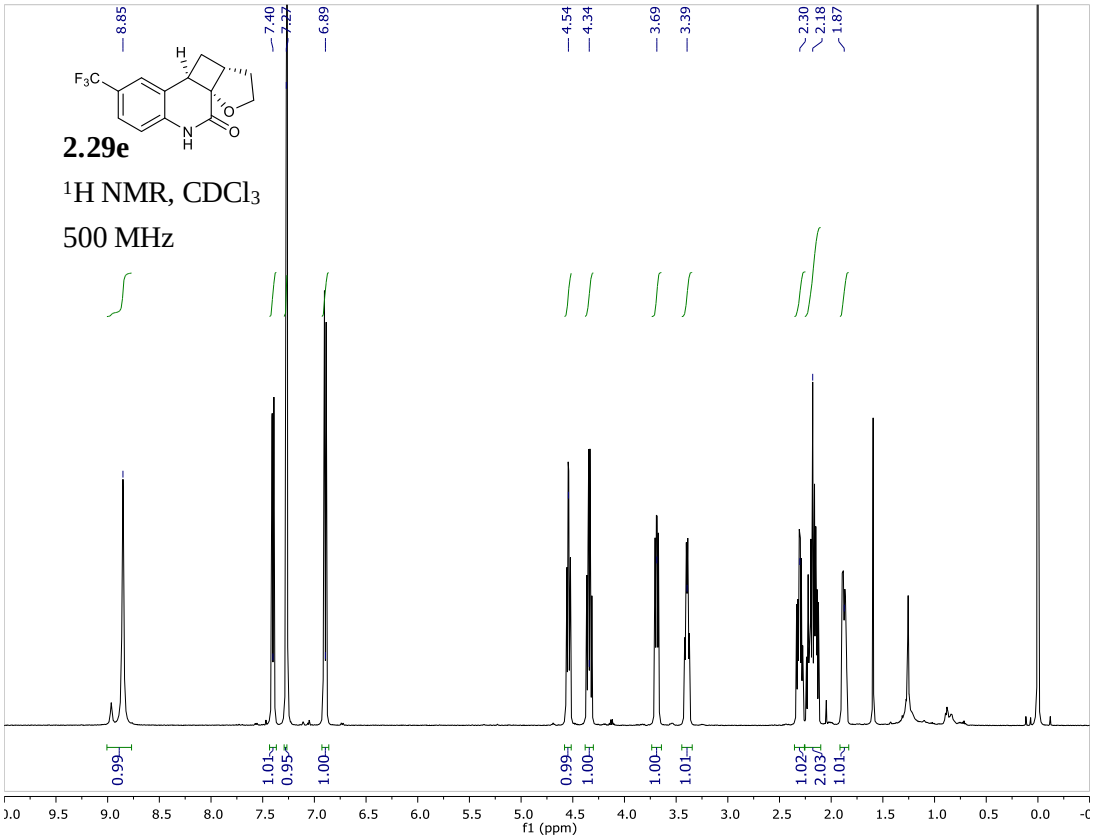
8.85
7.40
7.37
6.89
4.54
4.34
3.69
3.39
2.30
2.18
1.87
F3C
H
O
N
H
O
2.29e
1H NMR, CDCl3
500 MHz
0.99
1.01
0.95
1.00
0.99
1.00
1.00
1.01
1.02
2.03
1.01
f1 (ppm)

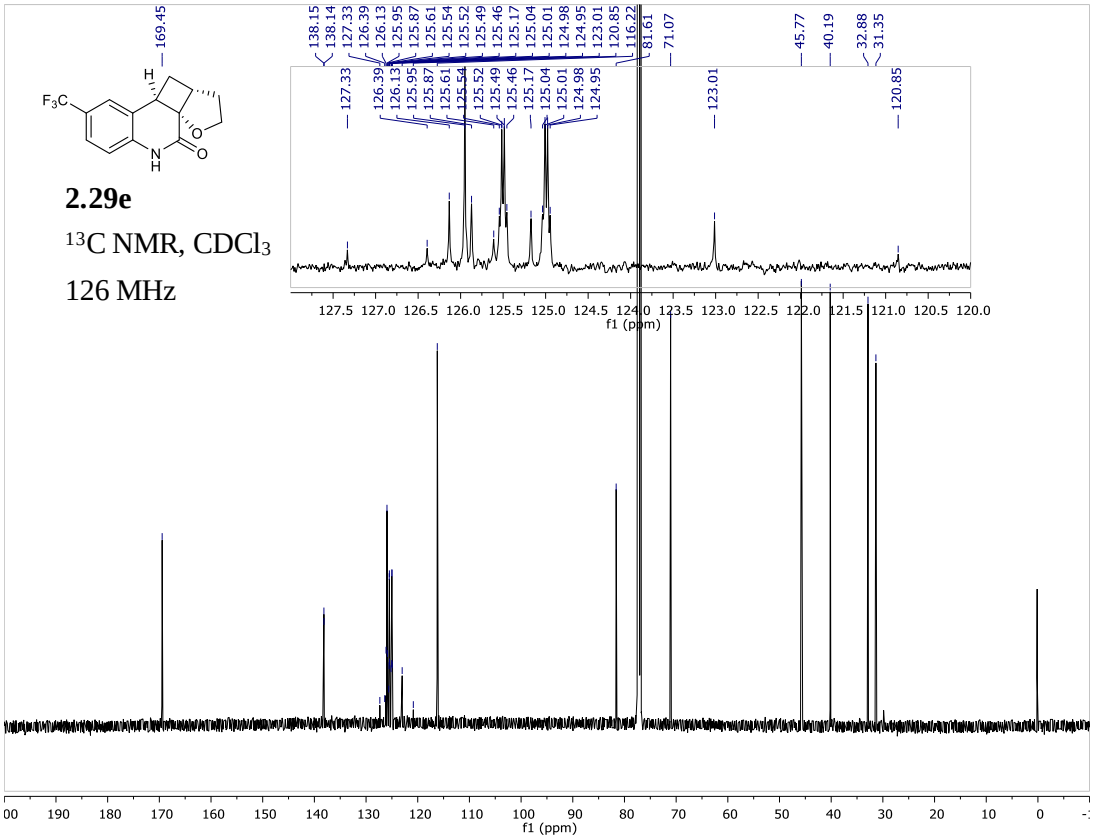
169.45
138.15
138.14
127.33
127.33
126.39
126.13
125.95
125.87
125.61
125.54
125.52
125.49
125.46
125.17
125.04
125.01
124.98
124.95
123.01
120.85
116.22
81.61
71.07
45.77
40.19
32.88
31.35
F3C
H
O
N
H
O
2.29e
13C NMR, CDCl3
126 MHz
f1 (ppm)
f1 (ppm)

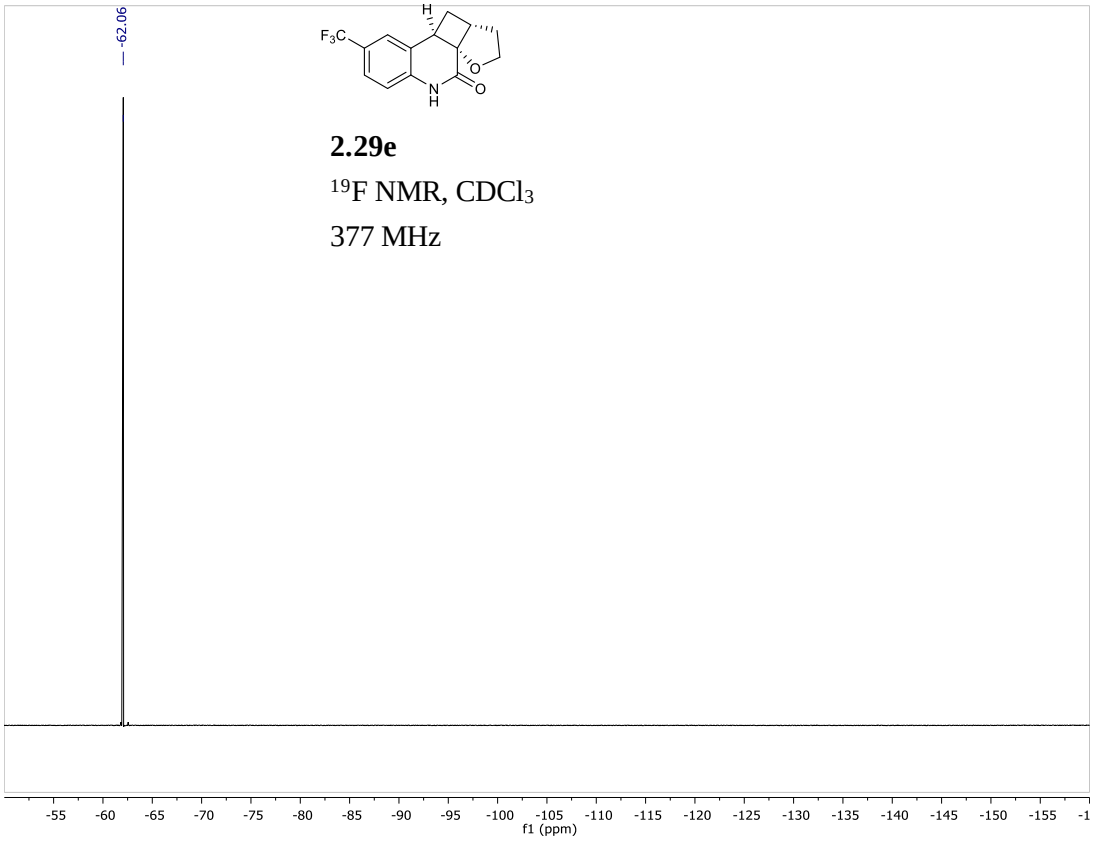

2.29e

^{19}F NMR, $CDCl_3$

377 MHz

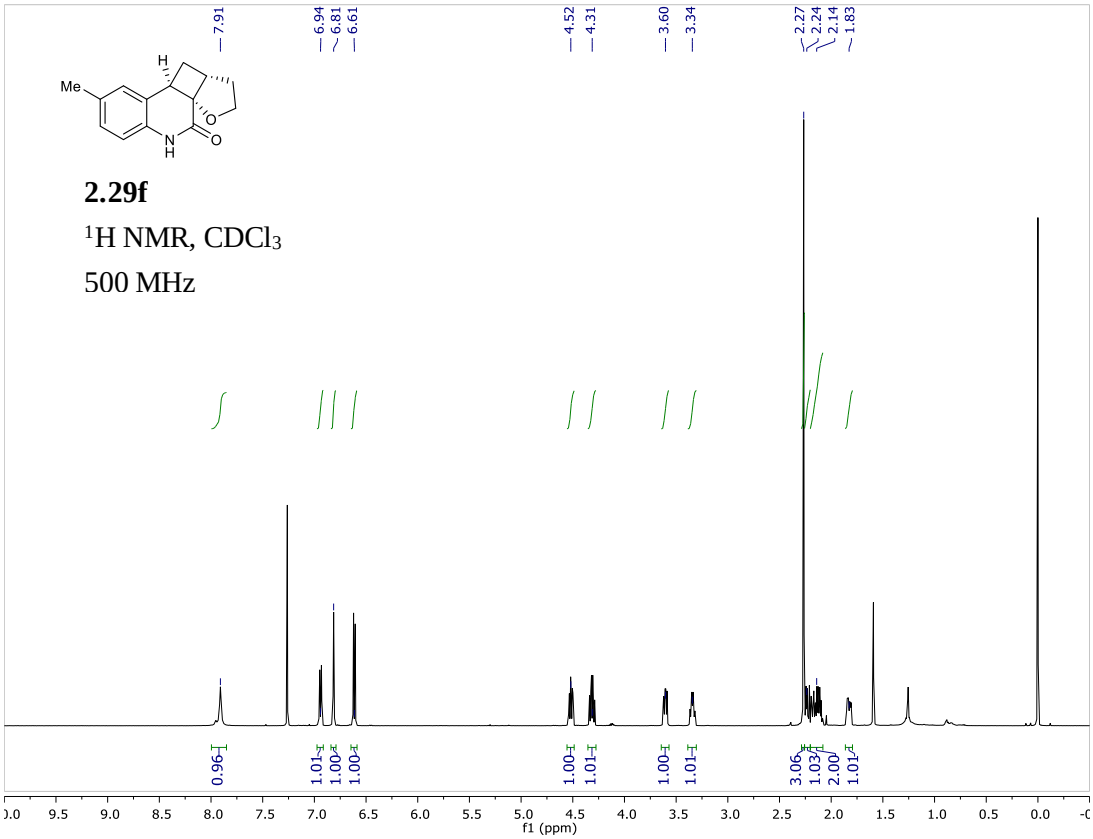

2.29f

^{1}H NMR, $CDCl_3$

500 MHz

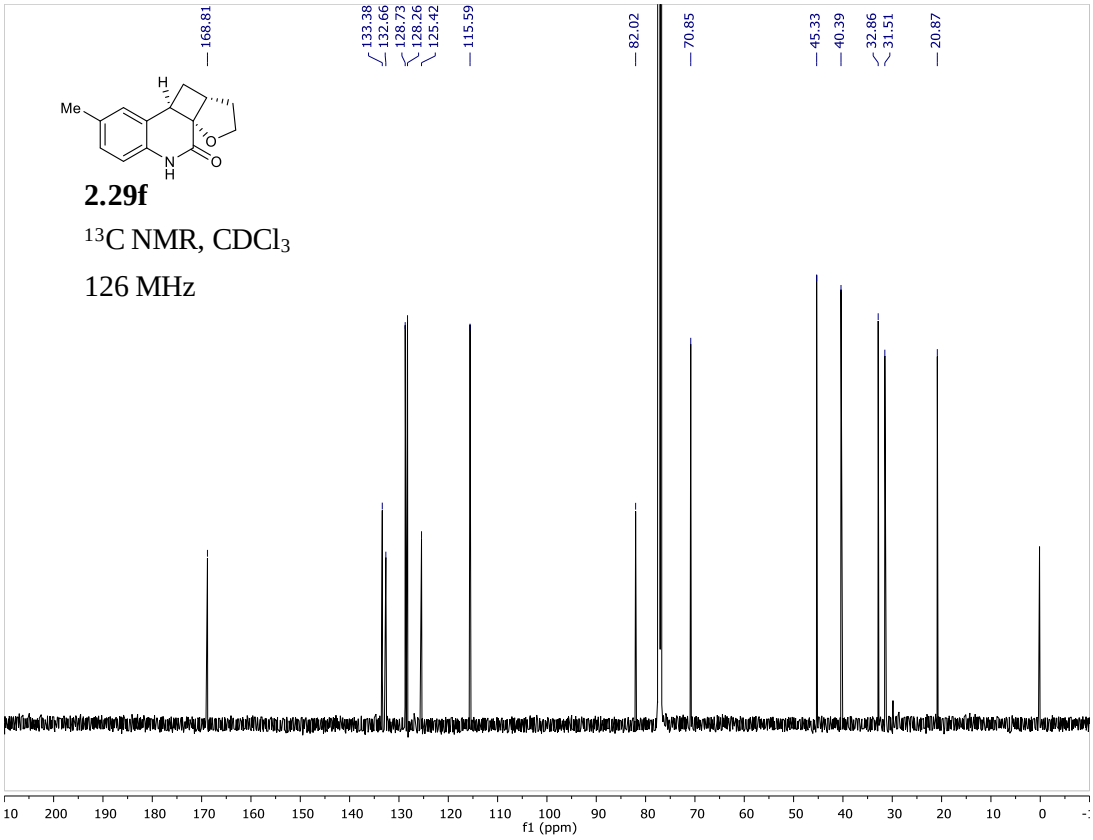

2.29f

^{13}C NMR, $CDCl_3$

126 MHz

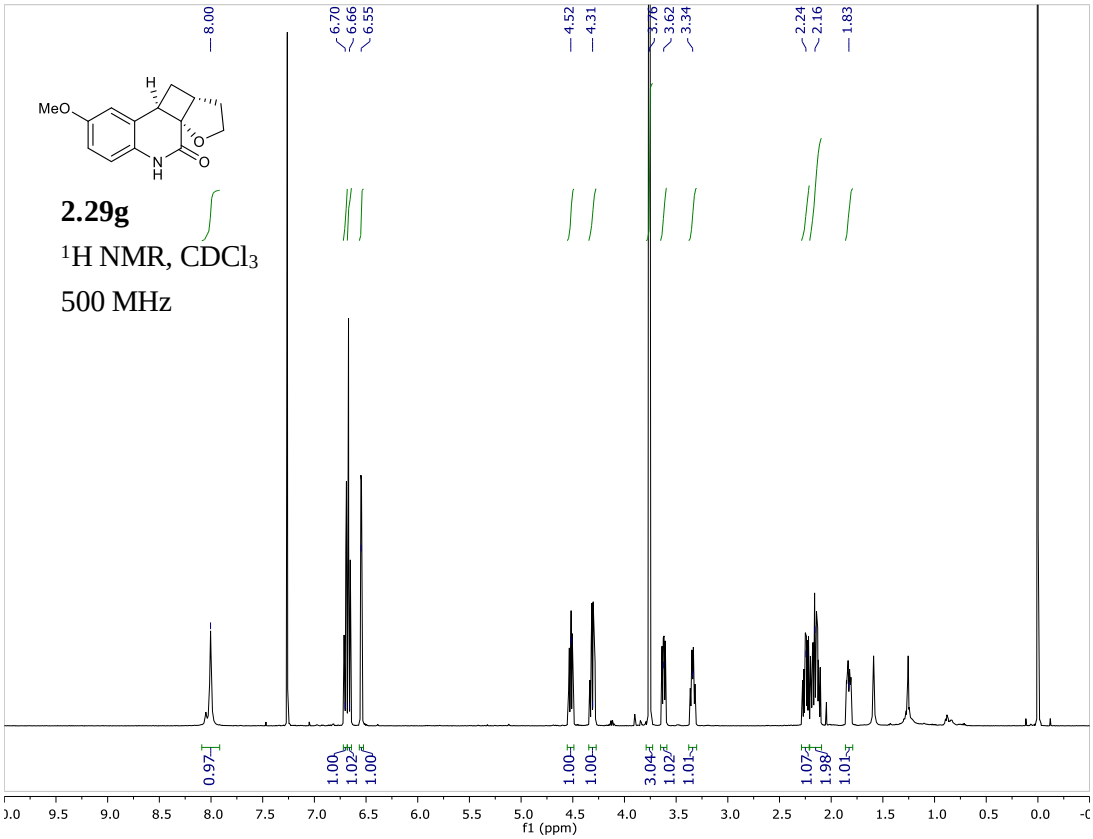
8.00
6.70
6.66
6.55
4.52
4.31
3.76
3.62
3.34
2.24
2.16
1.83
MeO
H
O
N
H
O
2.29g
1H NMR, CDCl3
500 MHz
0.97
1.00
1.02
1.00
1.00
1.00
3.04
1.02
1.01
1.07
1.98
1.01
f1 (ppm)

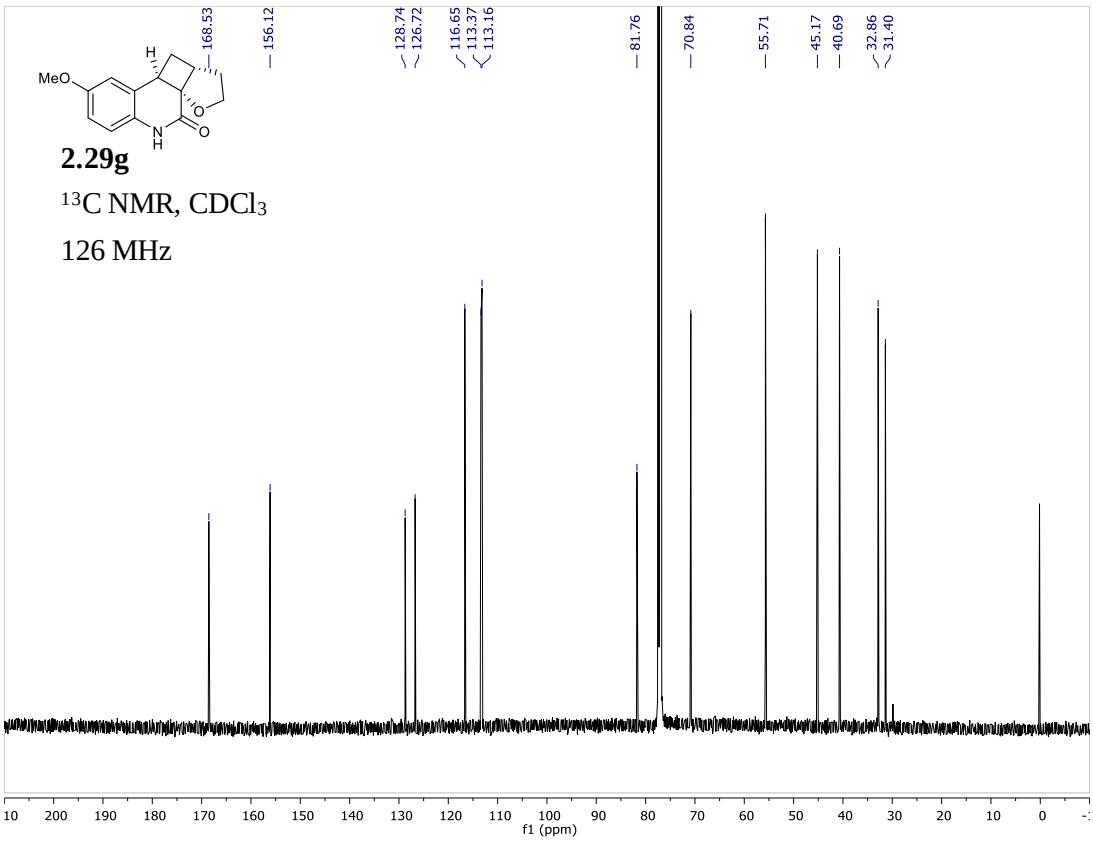
168.53
156.12
128.74
126.72
116.65
113.37
113.16
81.76
70.84
55.71
45.17
40.69
32.86
31.40
MeO
H
O
N
H
O
2.29g
13C NMR, CDCl3
126 MHz
f1 (ppm)

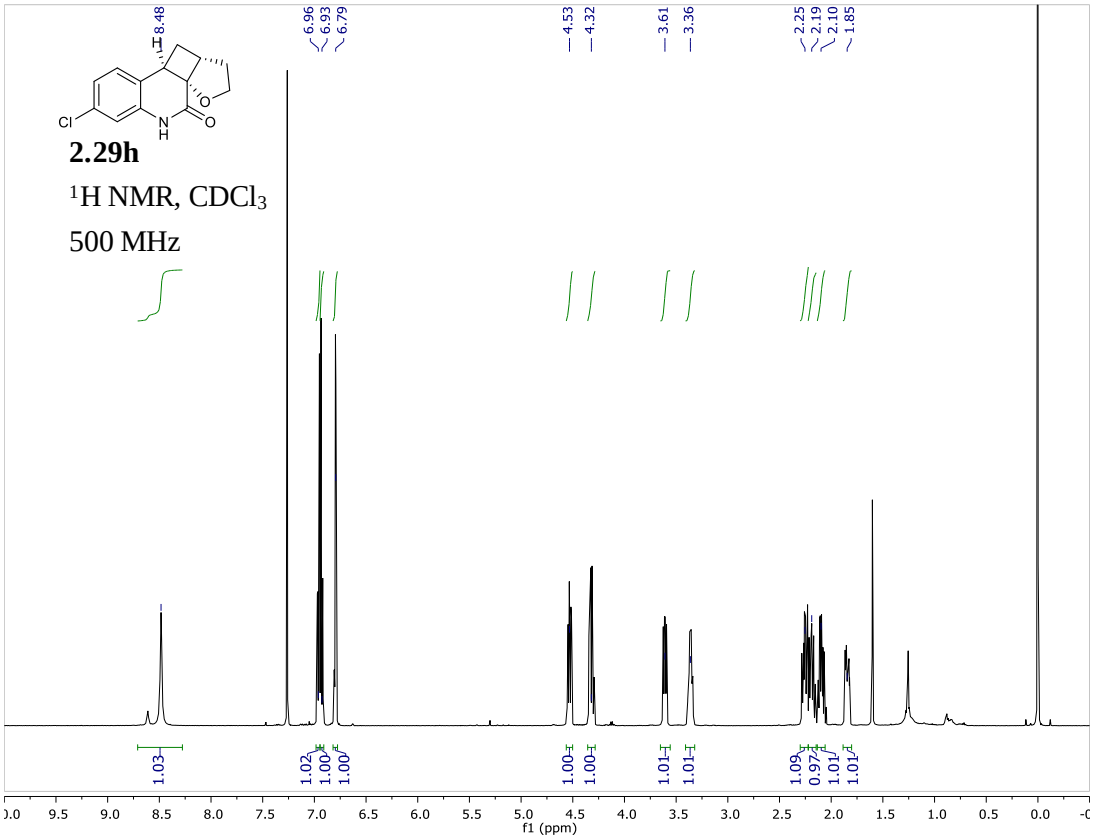
8.48
6.96
6.93
6.79
4.53
4.32
3.61
3.36
2.25
2.19
2.10
1.85
Cl
H
N
O
O
2.29h
1H NMR, CDCl3
500 MHz
1.03
1.02
1.00
1.00
1.00
1.00
1.01
1.01
1.09
0.97
1.01
1.01
f1 (ppm)

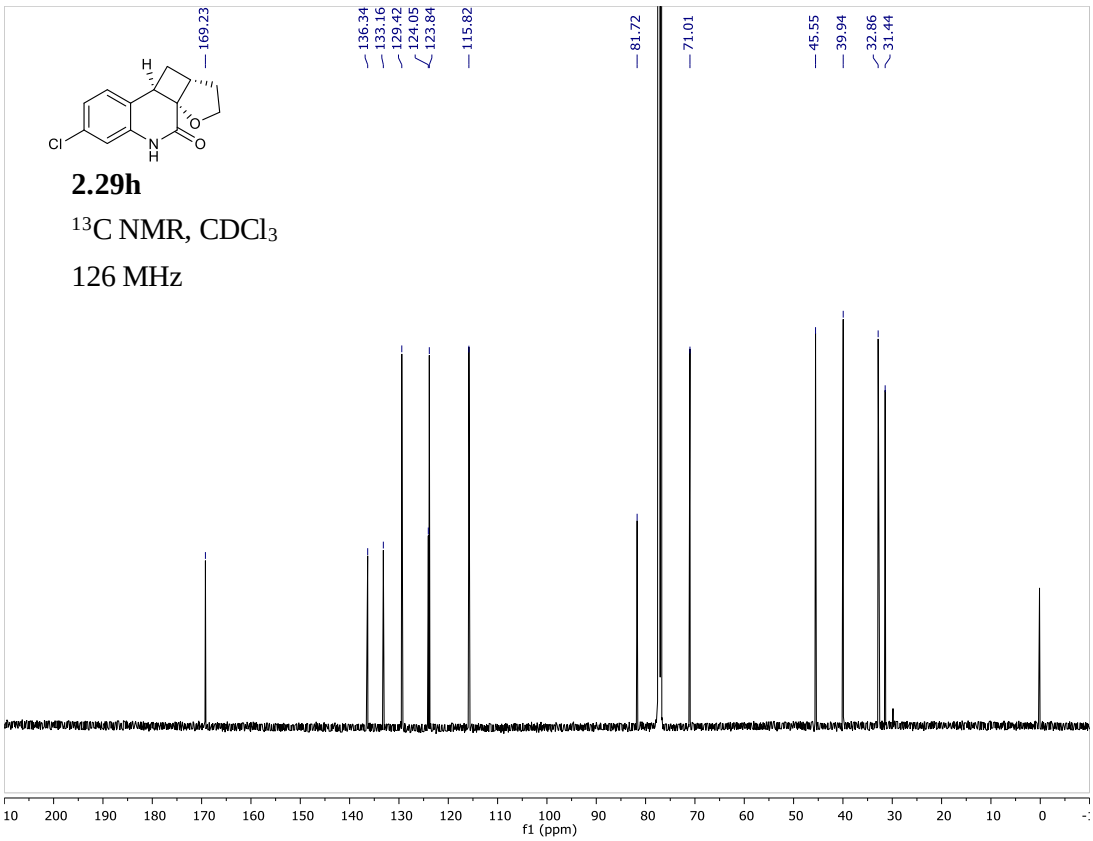
169.23
136.34
133.16
129.42
124.05
123.84
115.82
81.72
71.01
45.55
39.94
32.86
31.44
Cl
H
N
O
O
2.29h
13C NMR, CDCl3
126 MHz
f1 (ppm)

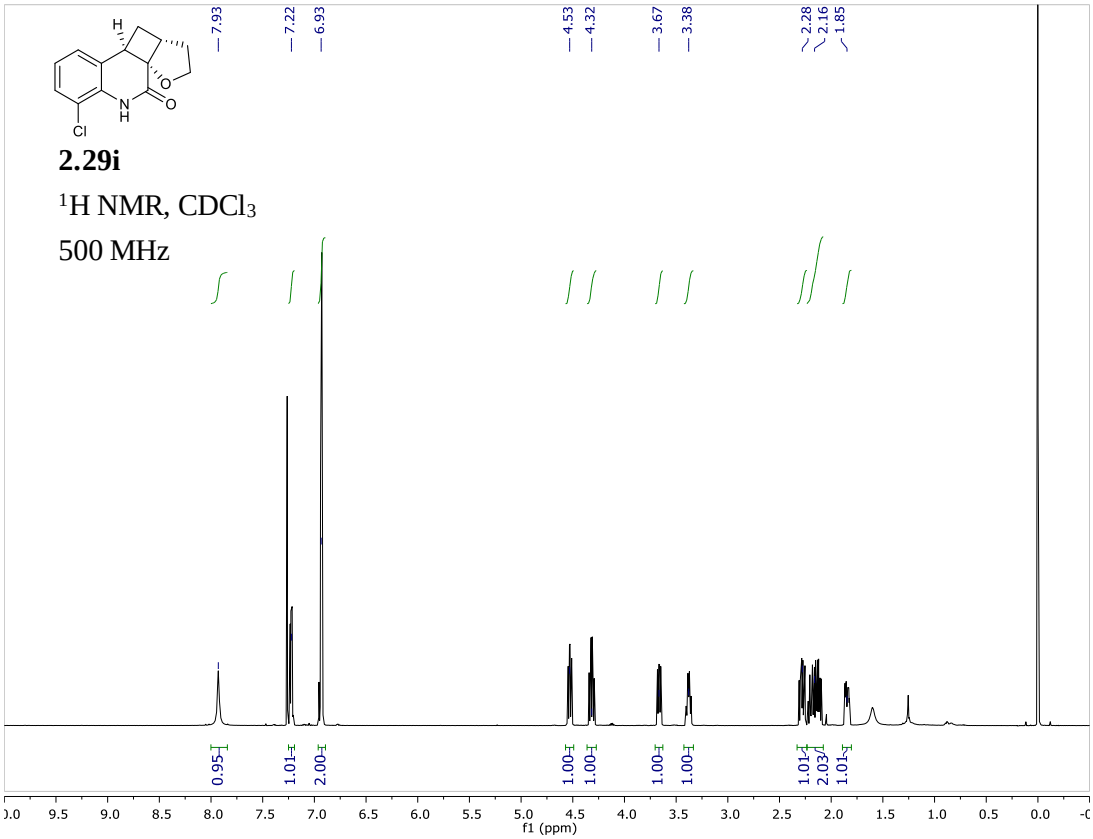

2.29i

^{1}H NMR, $CDCl_3$

500 MHz

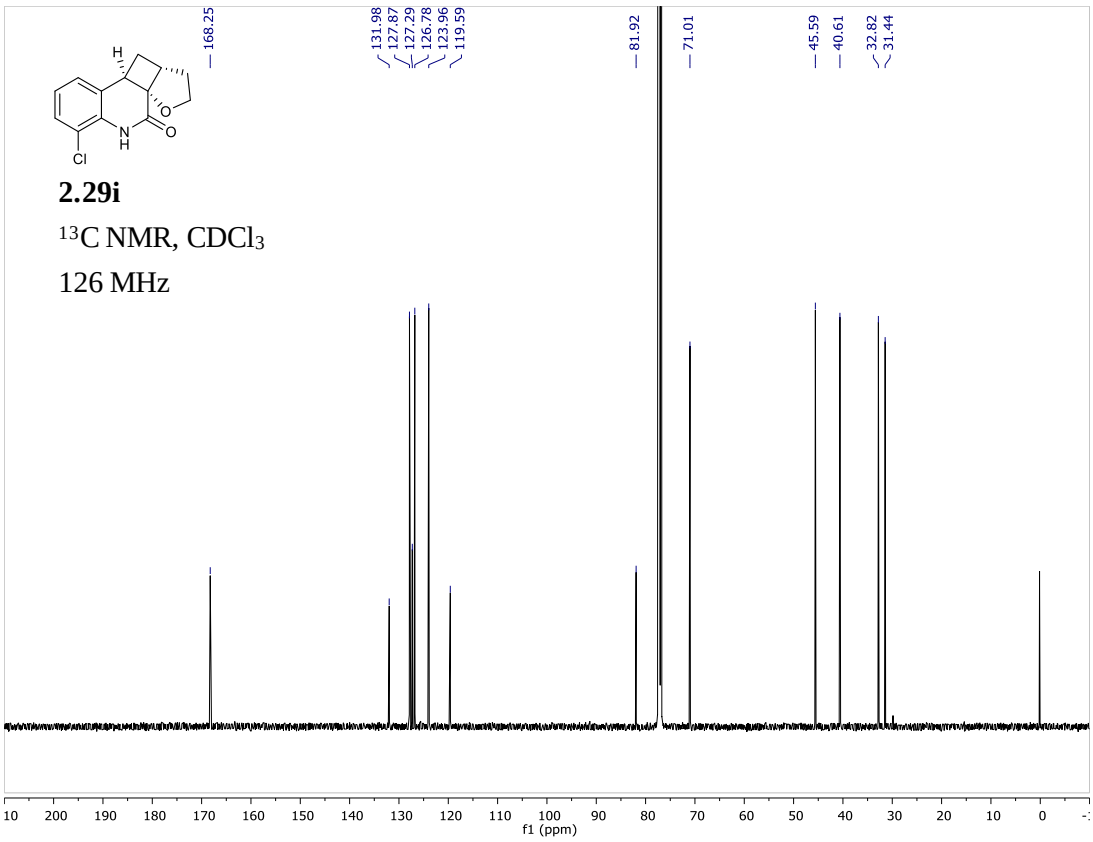

2.29i

^{13}C NMR, $CDCl_3$

126 MHz

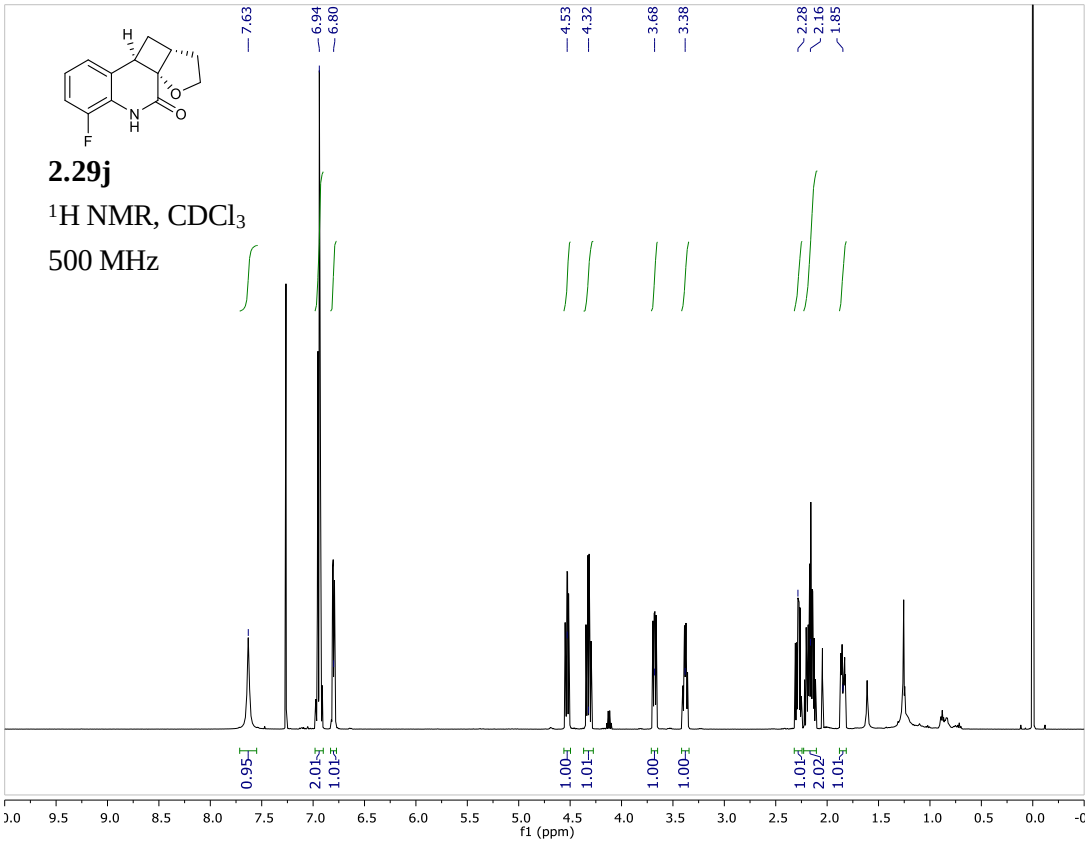

2.29j

^{1}H NMR, $CDCl_3$

500 MHz

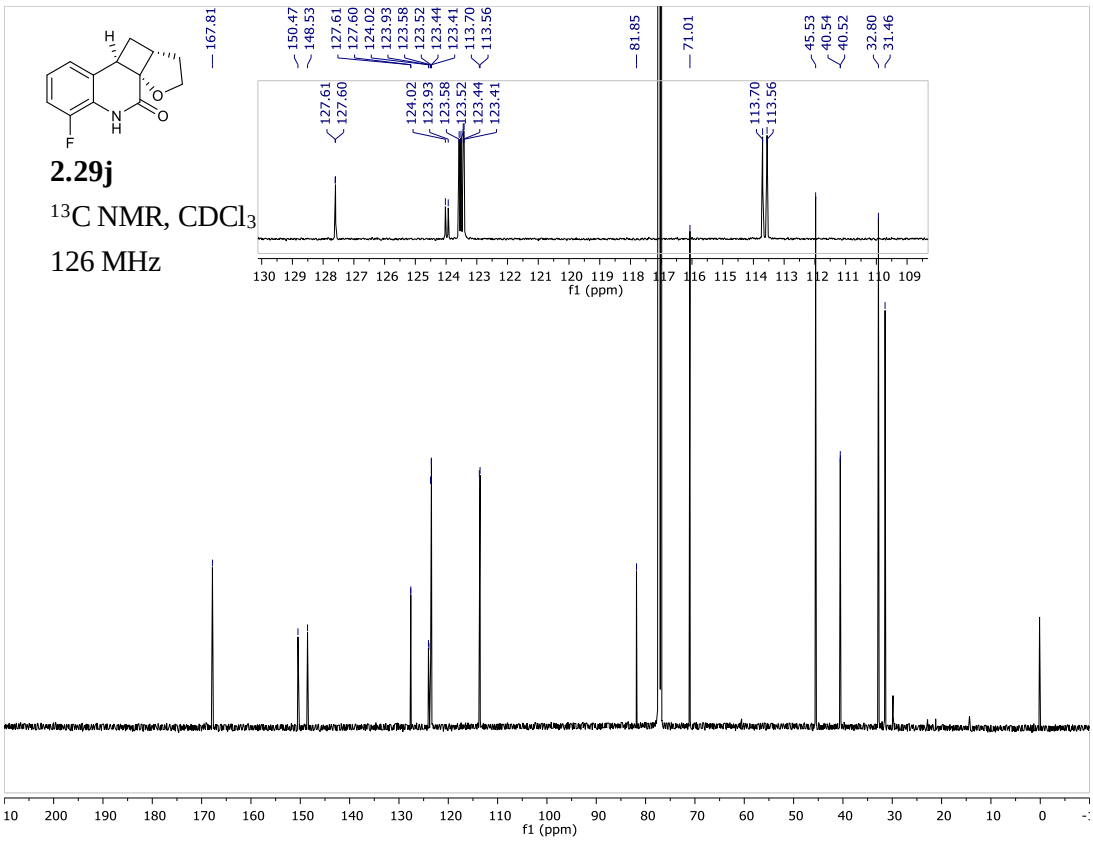

2.29j

^{13}C NMR, $CDCl_3$

126 MHz

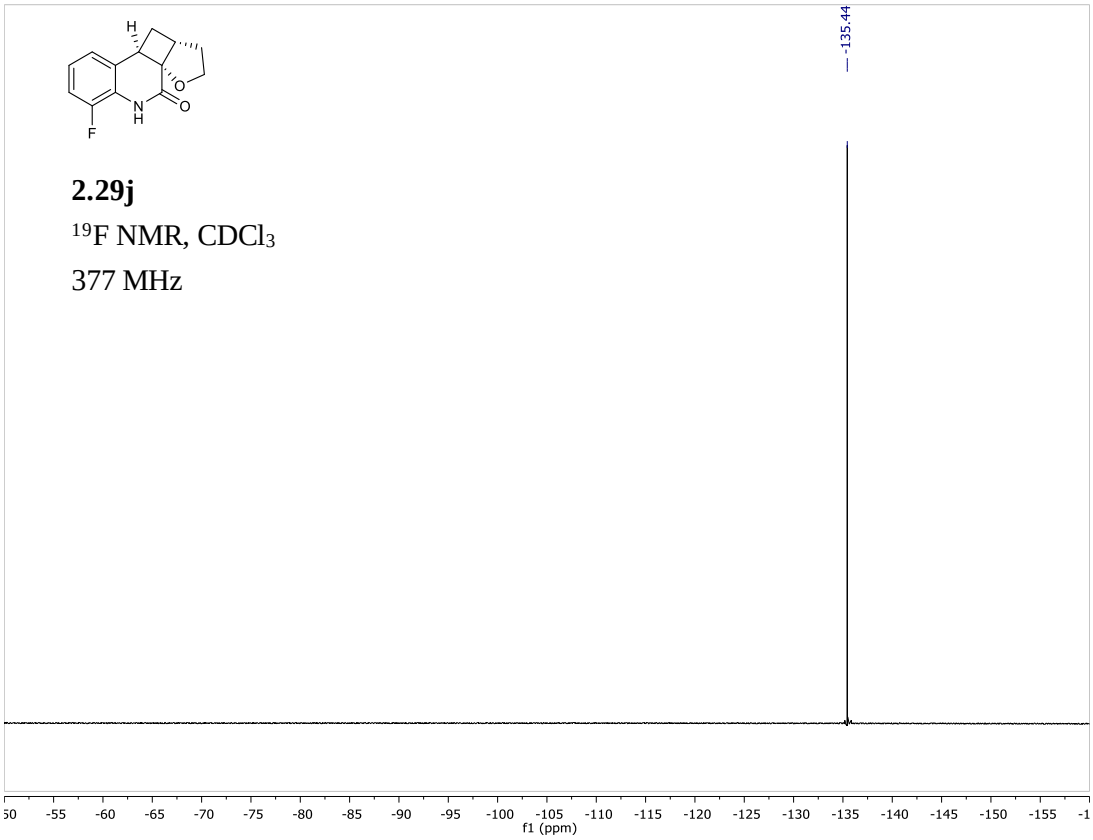

2.29j

^{19}F NMR, $CDCl_3$

377 MHz

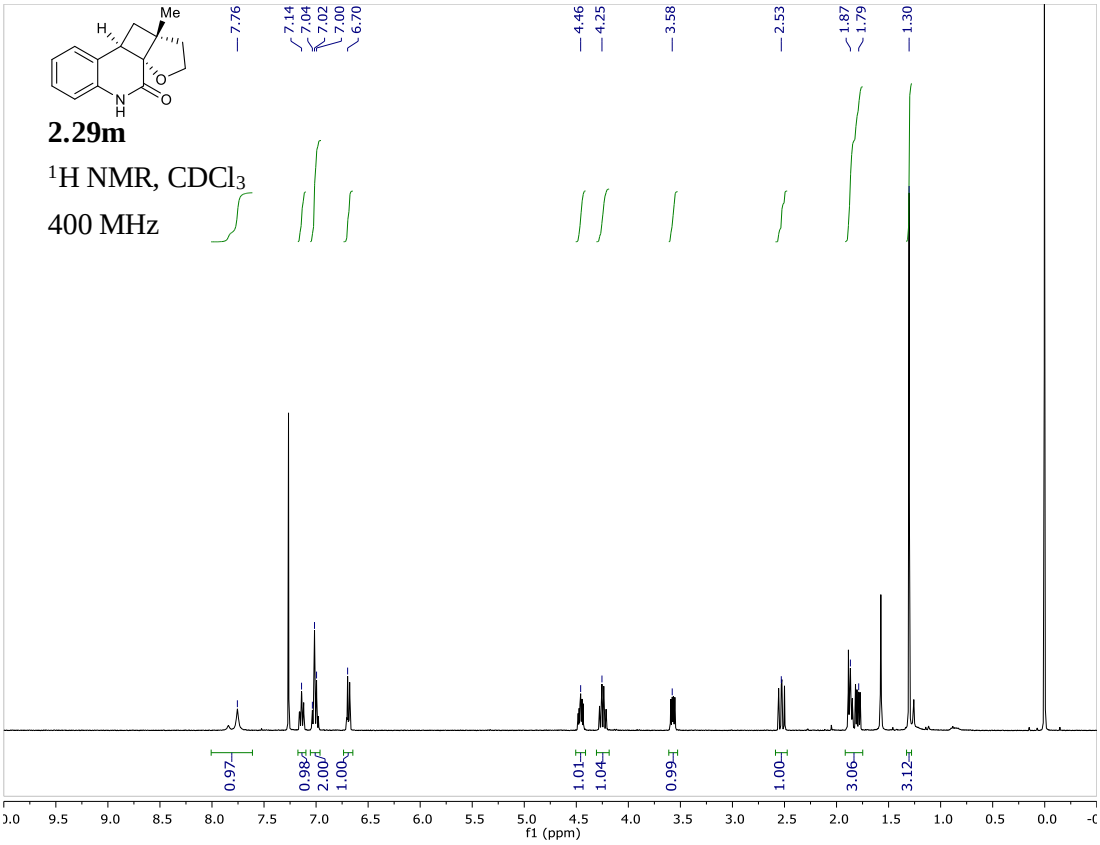

2.29m

^{1}H NMR, $CDCl_3$

400 MHz

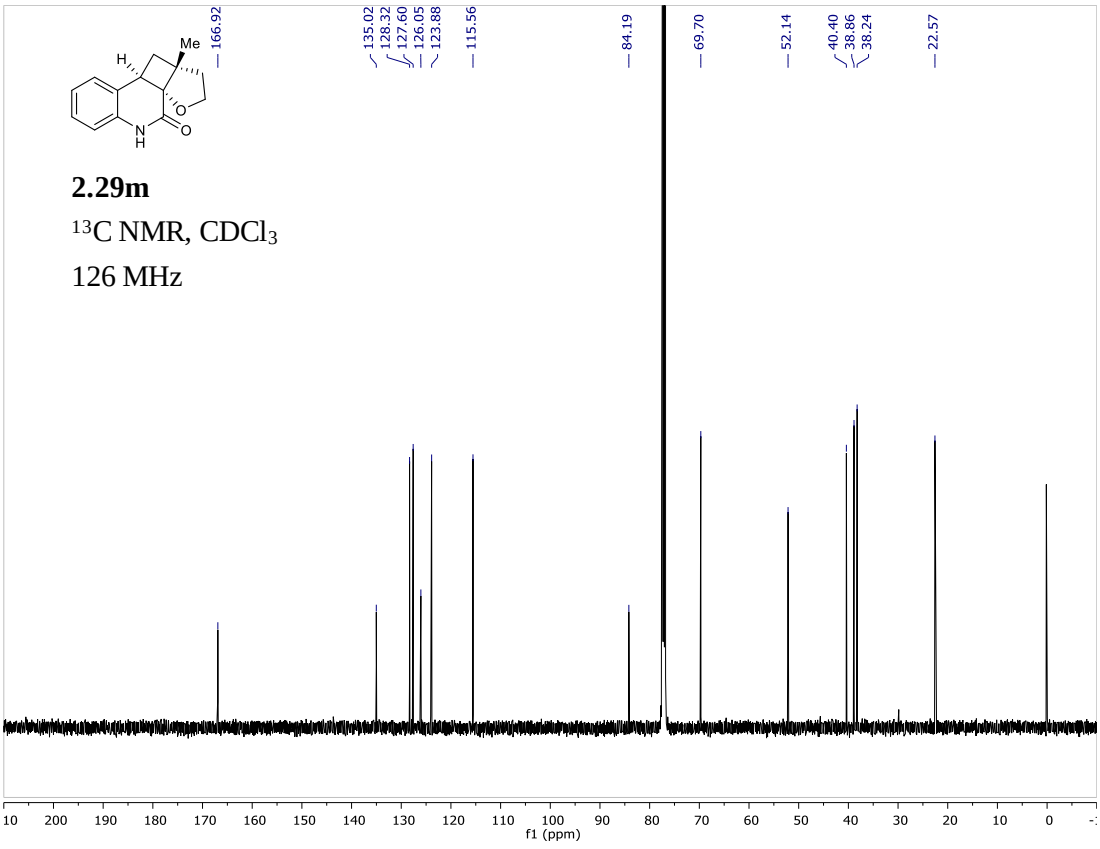

2.29m

^{13}C NMR, $CDCl_3$

126 MHz

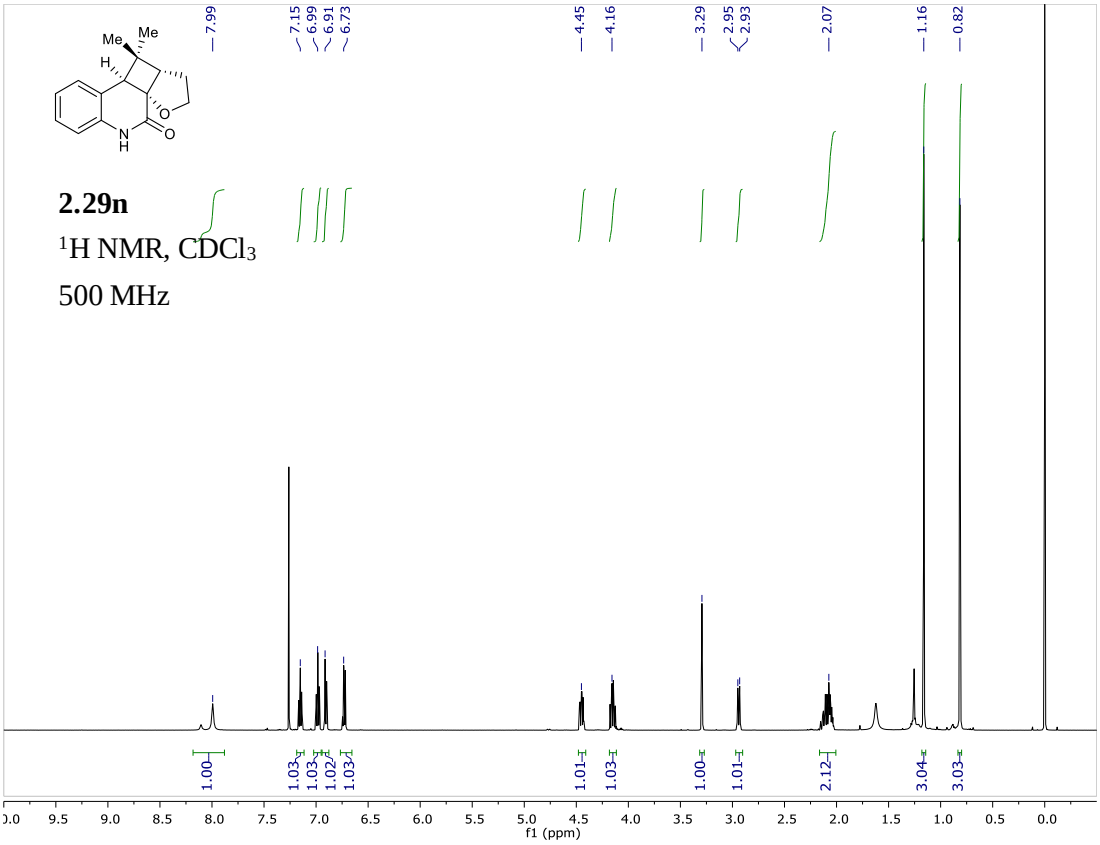

2.29n

^{1}H NMR, $CDCl_3$

500 MHz

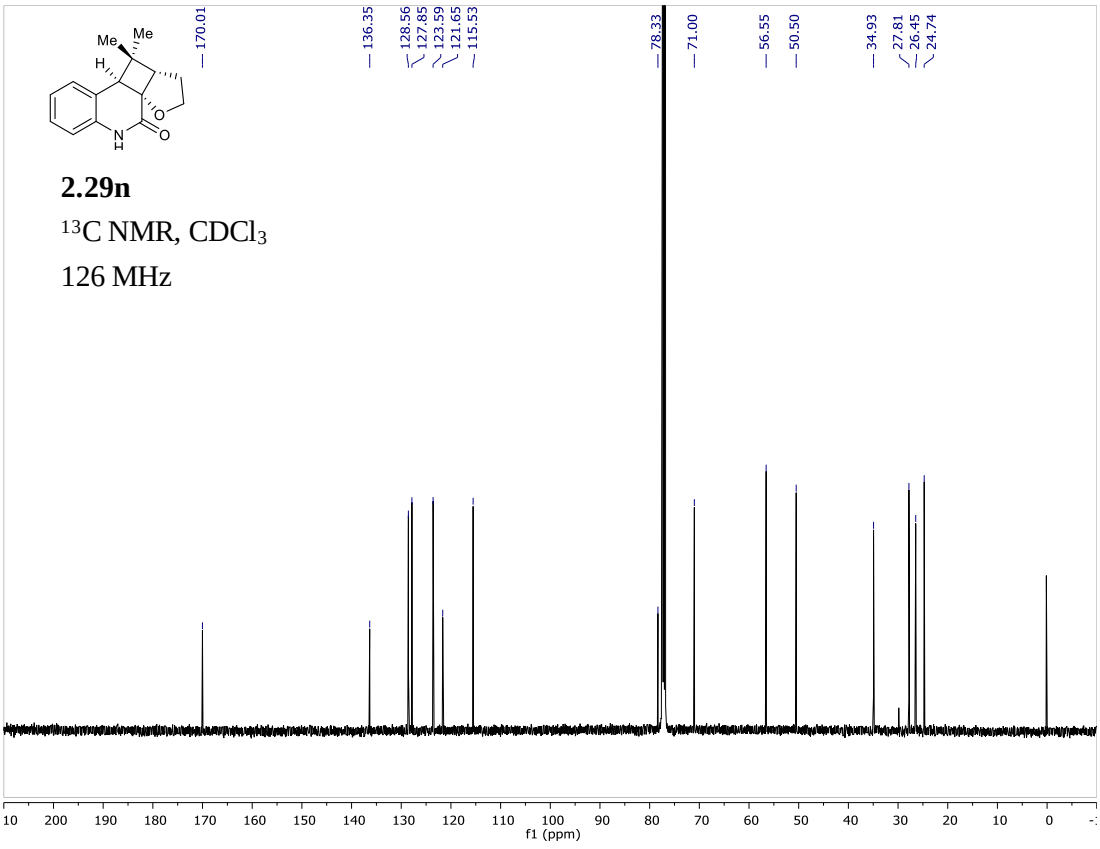

2.29n

^{13}C NMR, $CDCl_3$

126 MHz

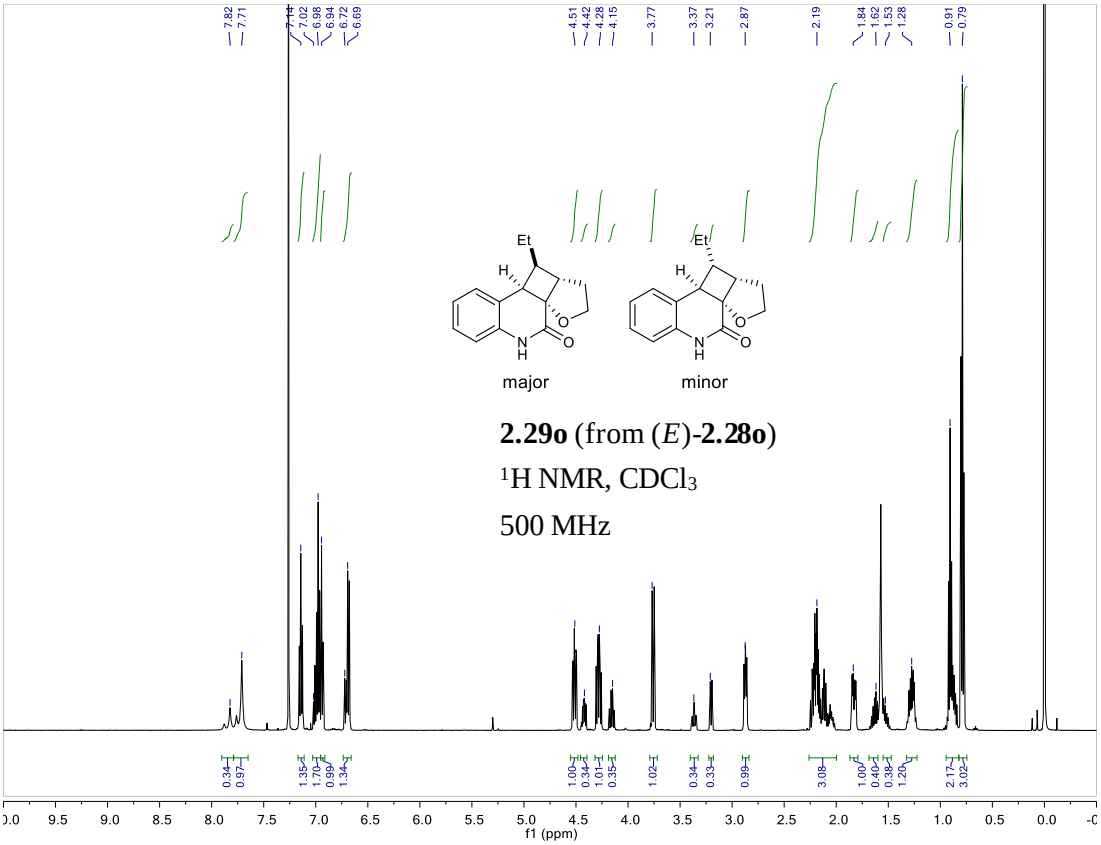
major
minor
2.29o (from (E)-2.28o)
1H NMR, CDCl3
500 MHz
f1 (ppm)

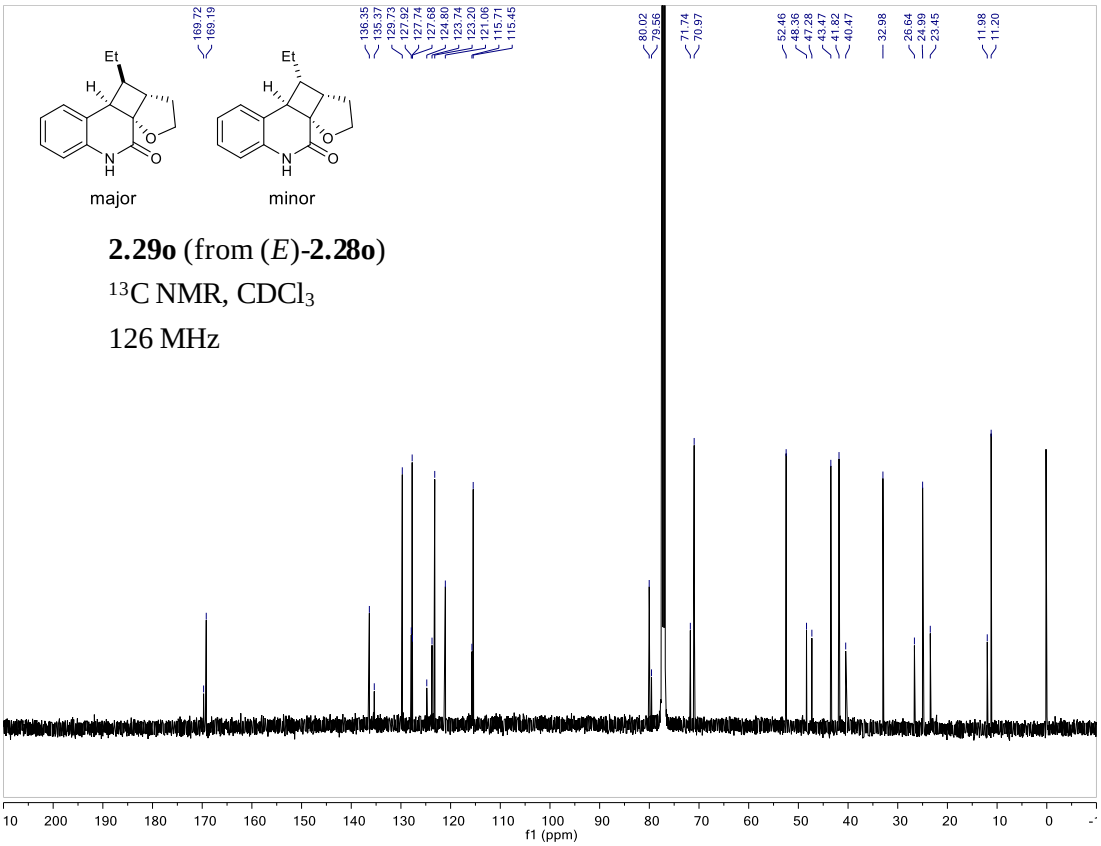
major
minor
2.29o (from (E)-2.28o)
13C NMR, CDCl3
126 MHz
f1 (ppm)

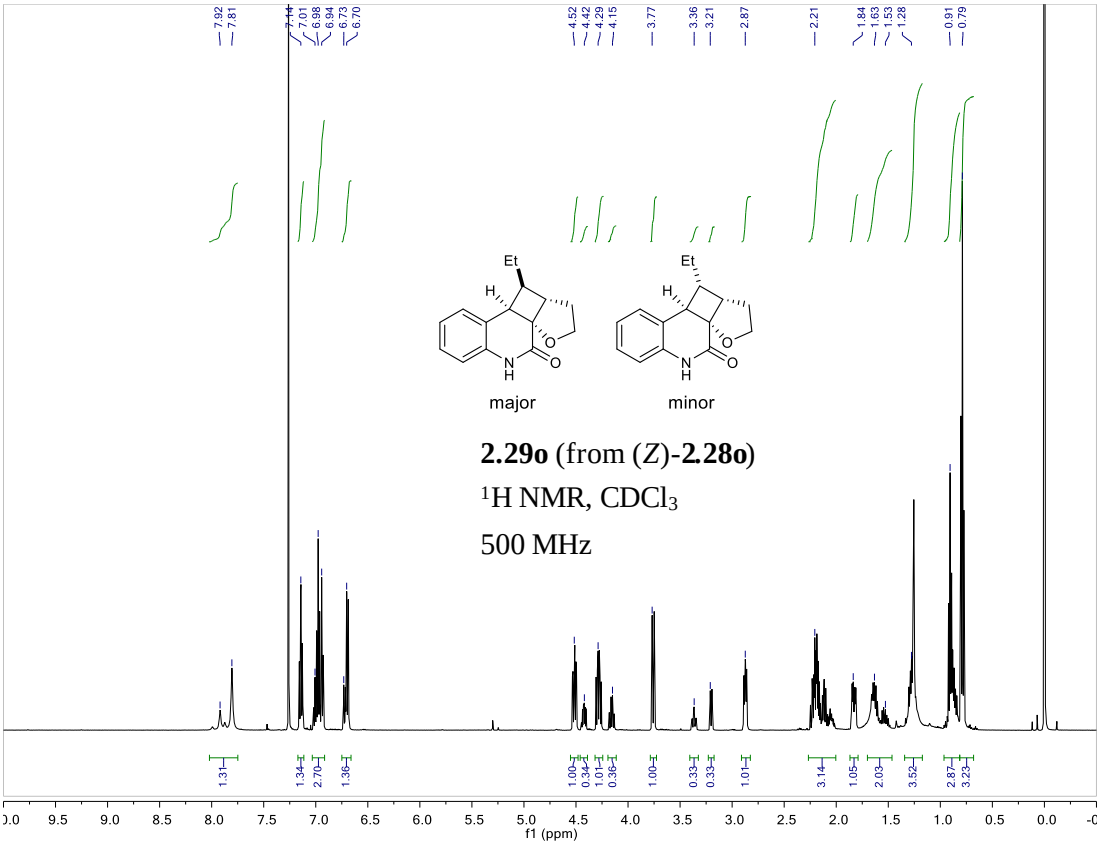
major
minor
2.29o (from (*Z*)-**2.28o**)
^{1}H NMR, $CDCl_3$
500 MHz
f1 (ppm)

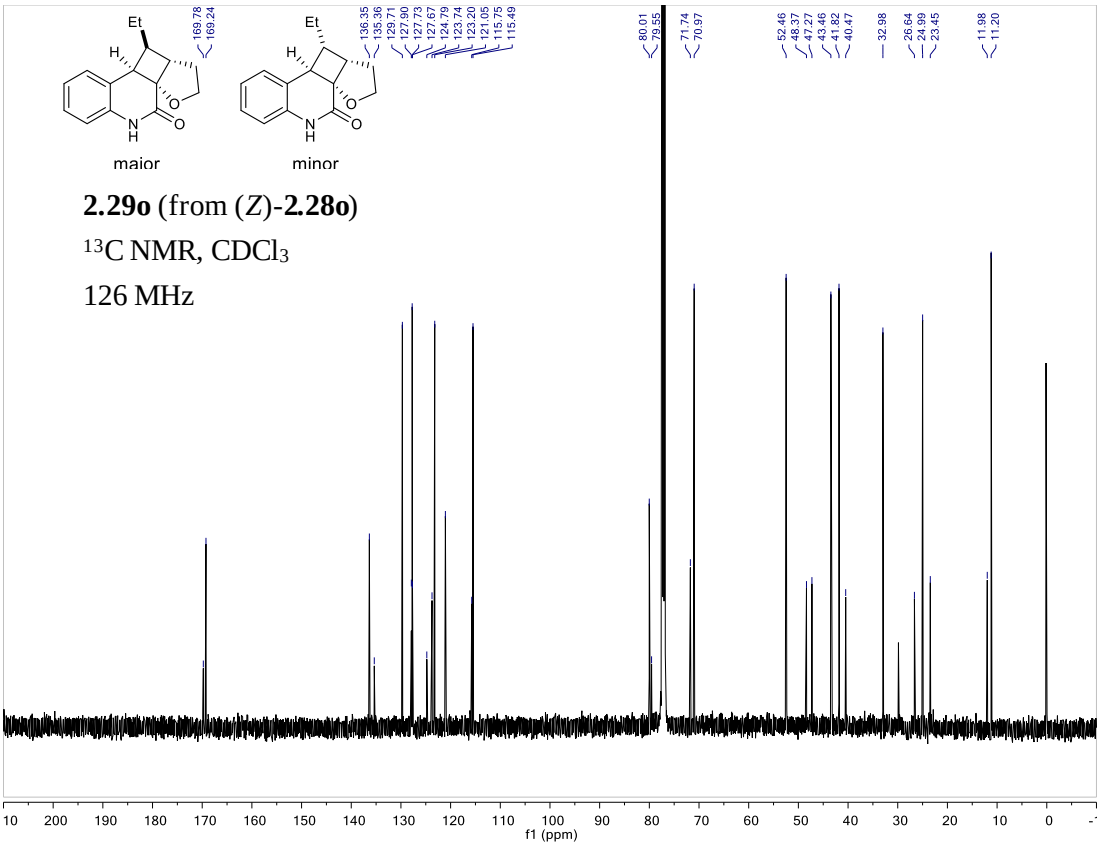
major
minor
2.29o (from (*Z*)-**2.28o**)
^{13}C NMR, $CDCl_3$
126 MHz
f1 (ppm)

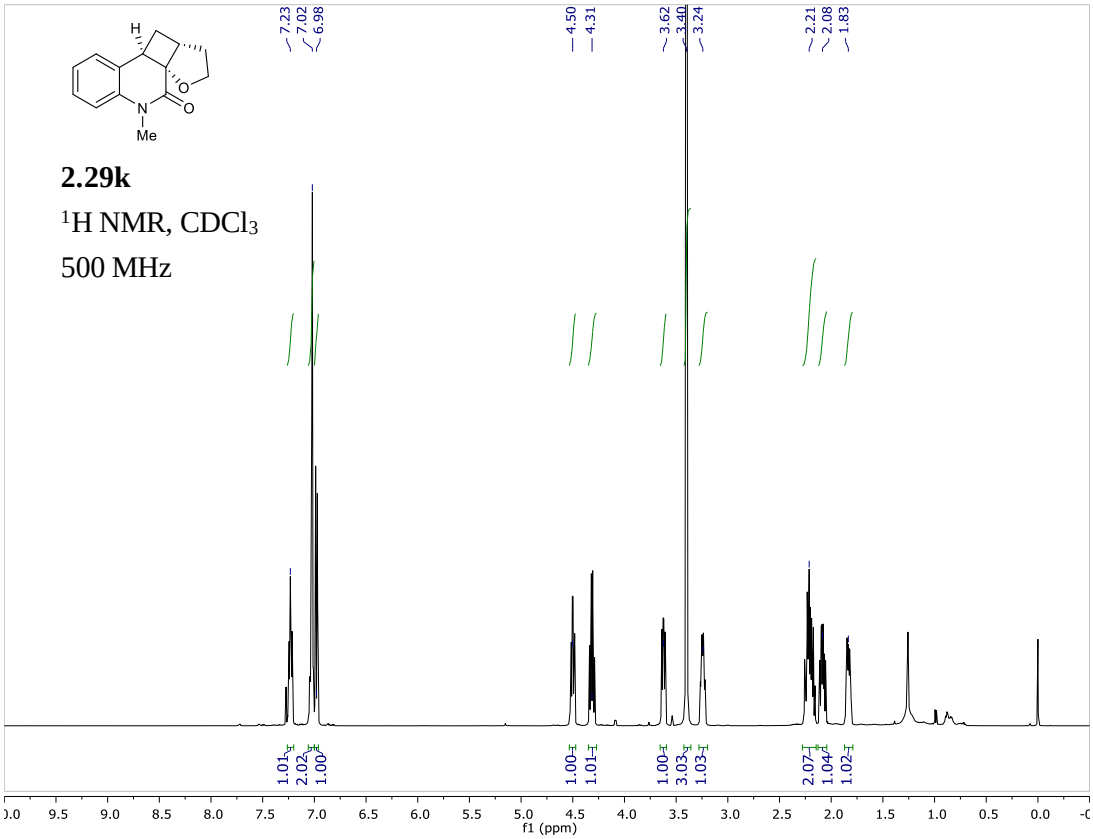

2.29k

^{1}H NMR, $CDCl_3$

500 MHz

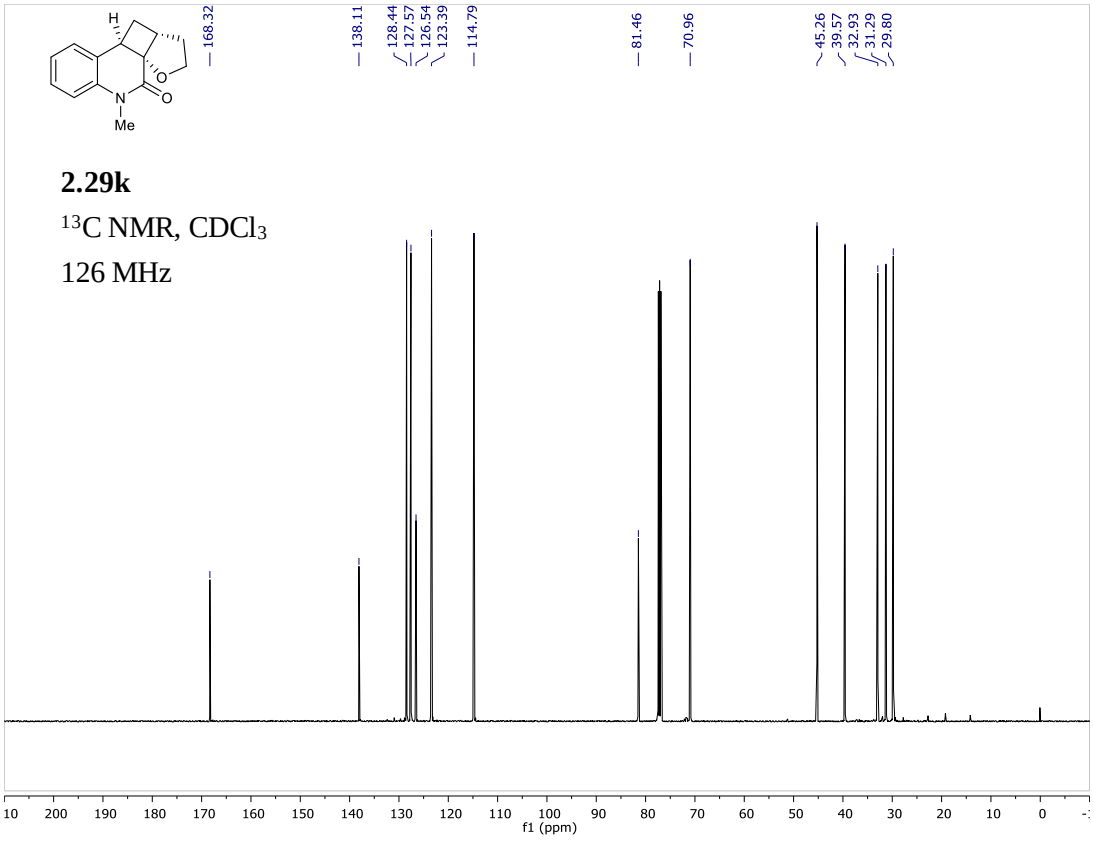

2.29k

^{13}C NMR, $CDCl_3$

126 MHz

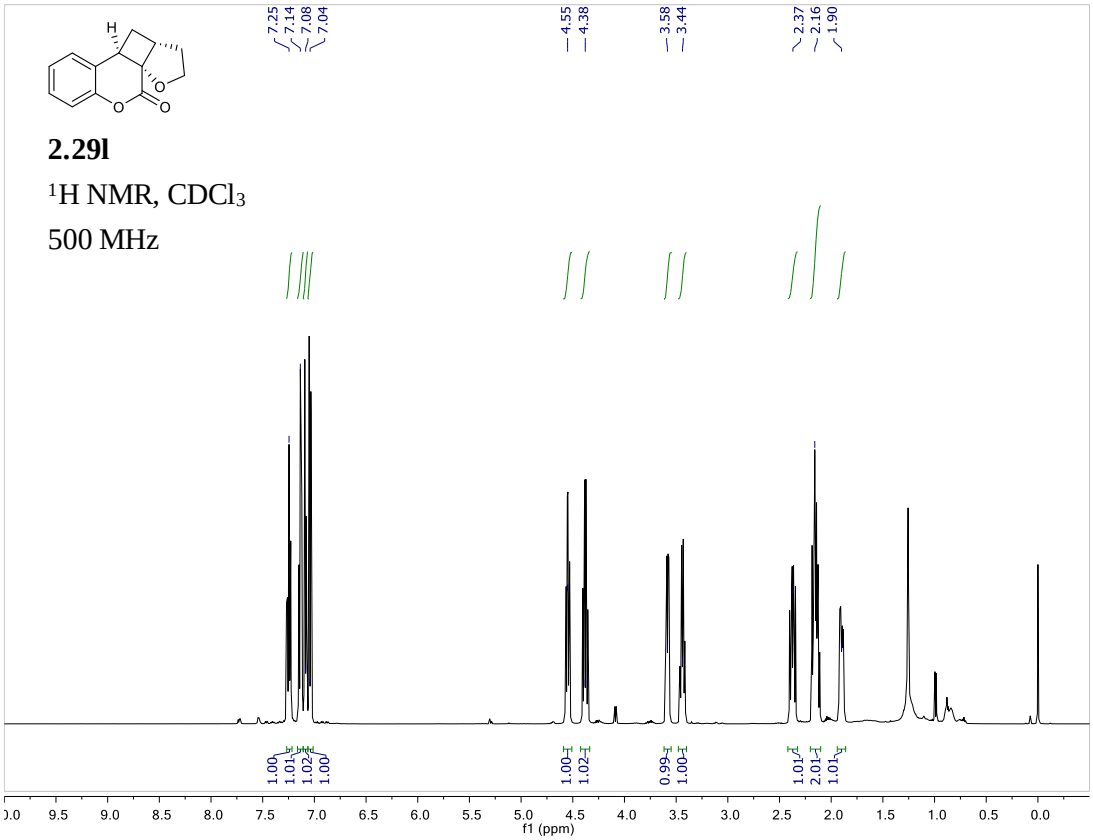

2.29l

^{1}H NMR, $CDCl_3$

500 MHz

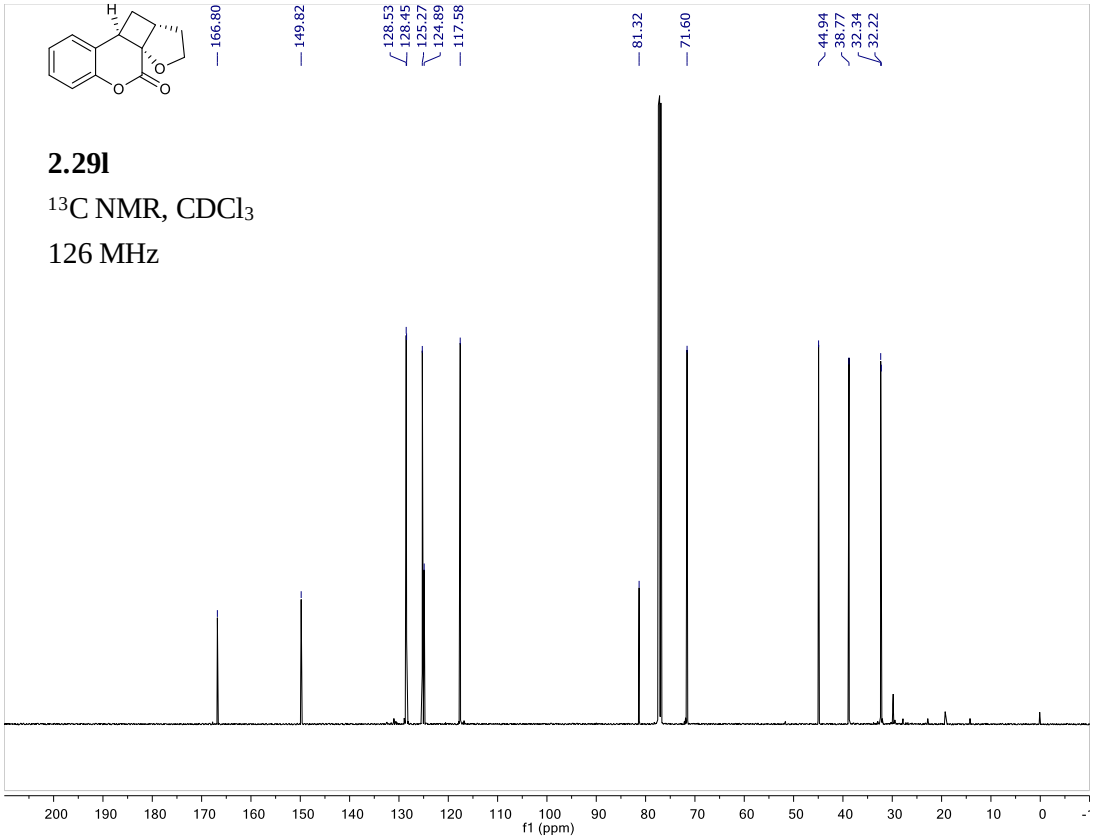

2.29l

^{13}C NMR, $CDCl_3$

126 MHz

B.2. List of New Compounds for Chapter 3

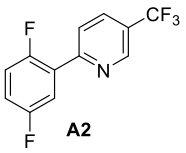

A2

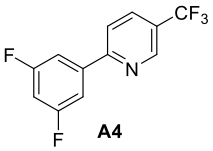

A4

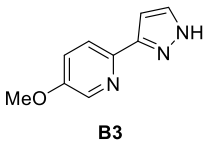

B3

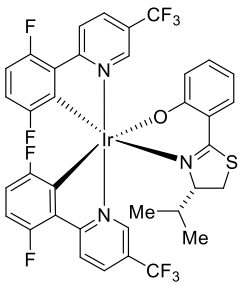

(*S*),Λ-[Ir(**A$_2$**)$_2$(*i*-PrHBT)]

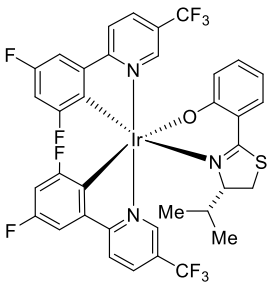

(*S*),Λ-[Ir(**A$_4$**)$_2$(*i*-PrHBT)]

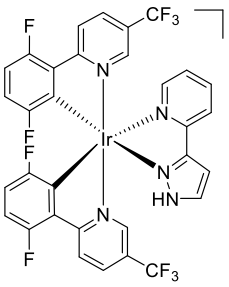

Λ-**3.28b**

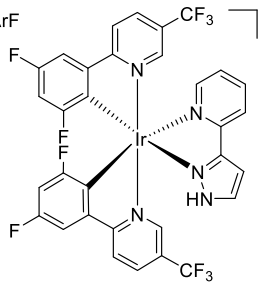

Λ-**3.28d**

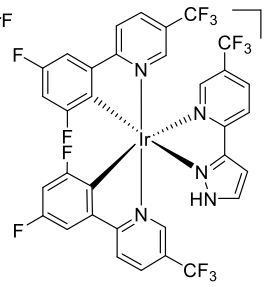

Λ-**3.28e**

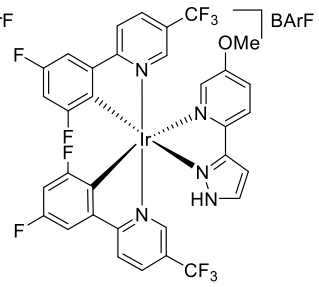

Λ-**3.28f**

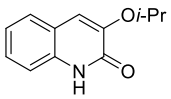

3.25c

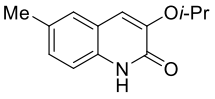

3.25e

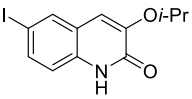

3.25f

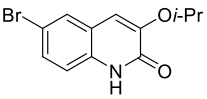

3.25g

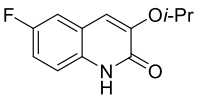

3.25h

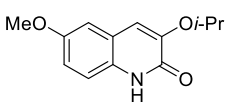

3.25i

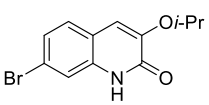

3.25j

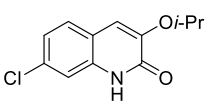

3.25k

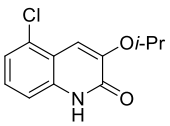

3.25l

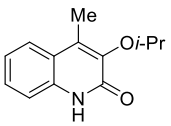

3.25m

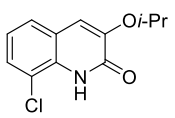
3.25n

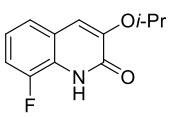
3.25o

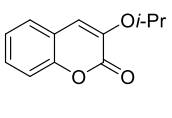
3.25p

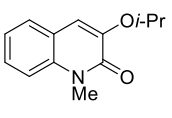
3.25q

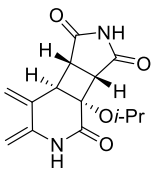
3.27c

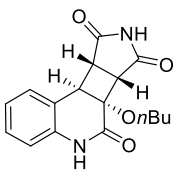
3.27a

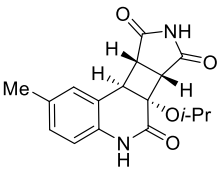
3.27e

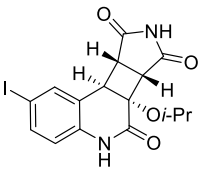
3.27f

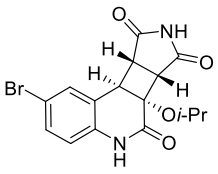
3.27g

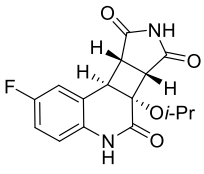
3.27h

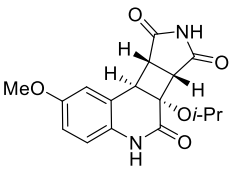
3.27i

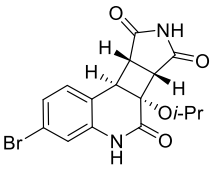
3.27j

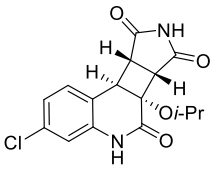
3.27k

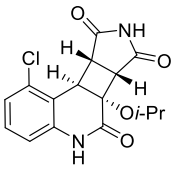
3.27l

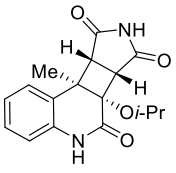
3.27m

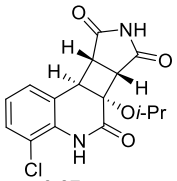
3.27n

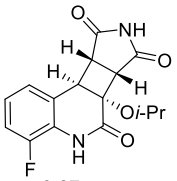
3.27o

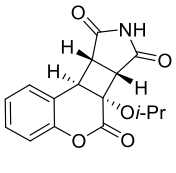
3.27p

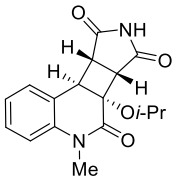
3.27q

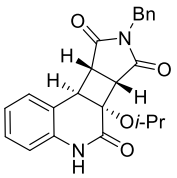
3.27r

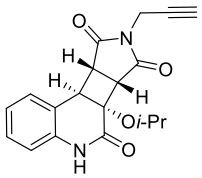
3.27s

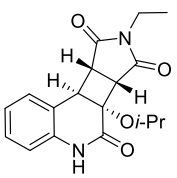
3.27t

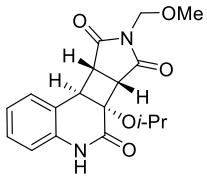
3.27u

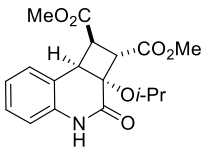
3.27v

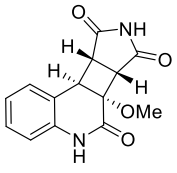
3.27b

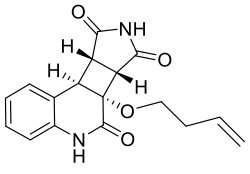
3.27w

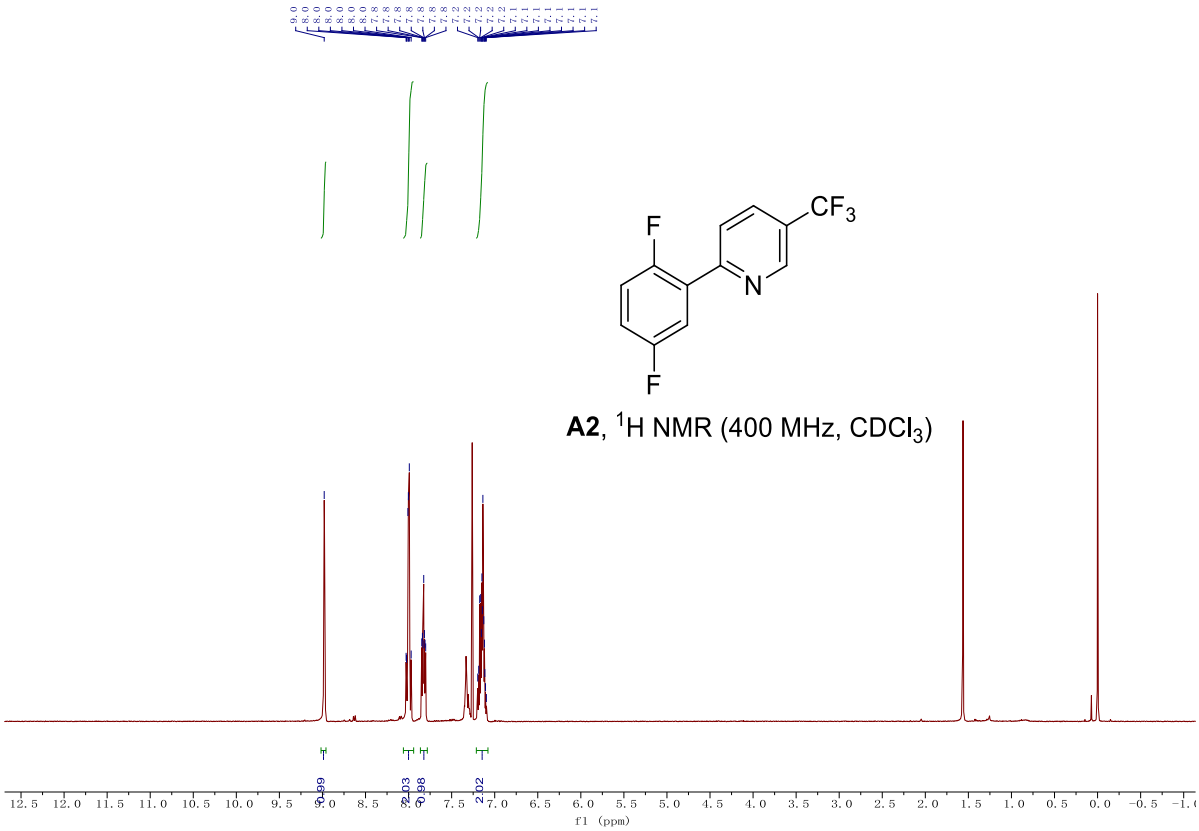

A2, ^{1}H NMR (400 MHz, $CDCl_3$)

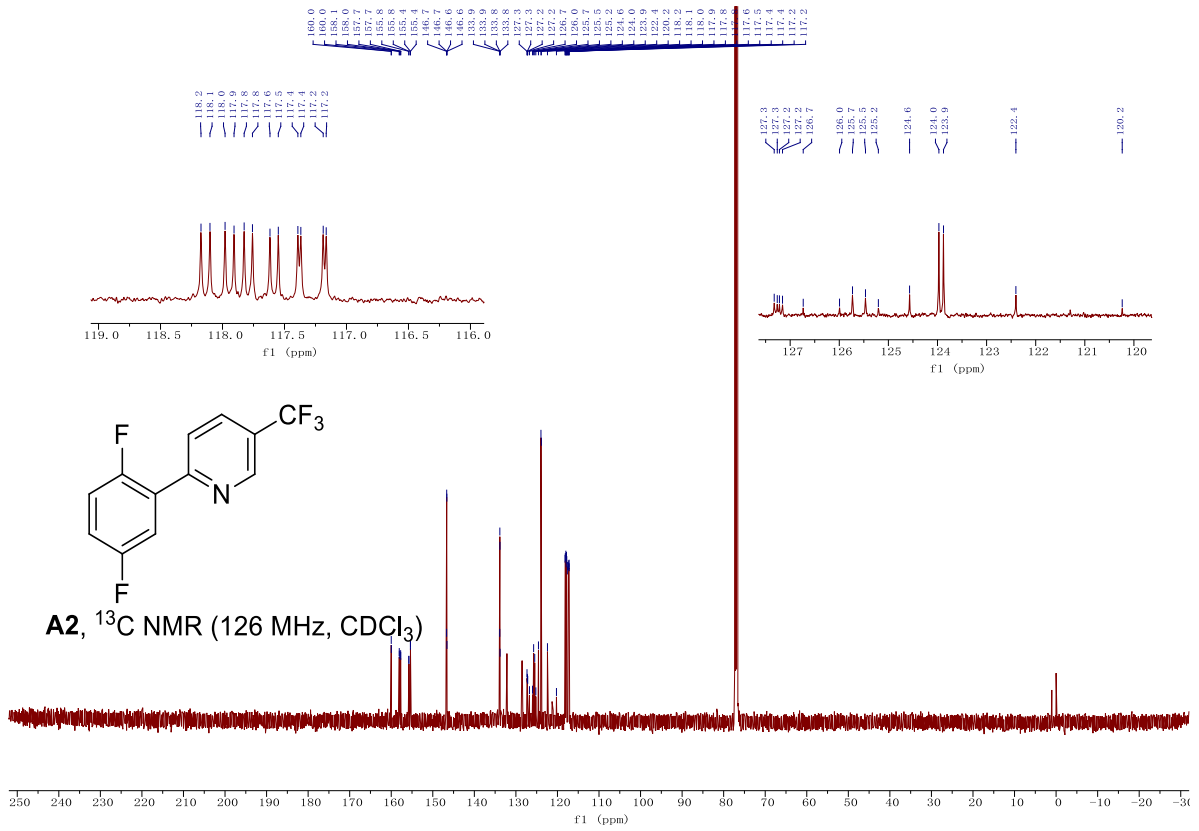

A2, ^{13}C NMR (126 MHz, $CDCl_3$)

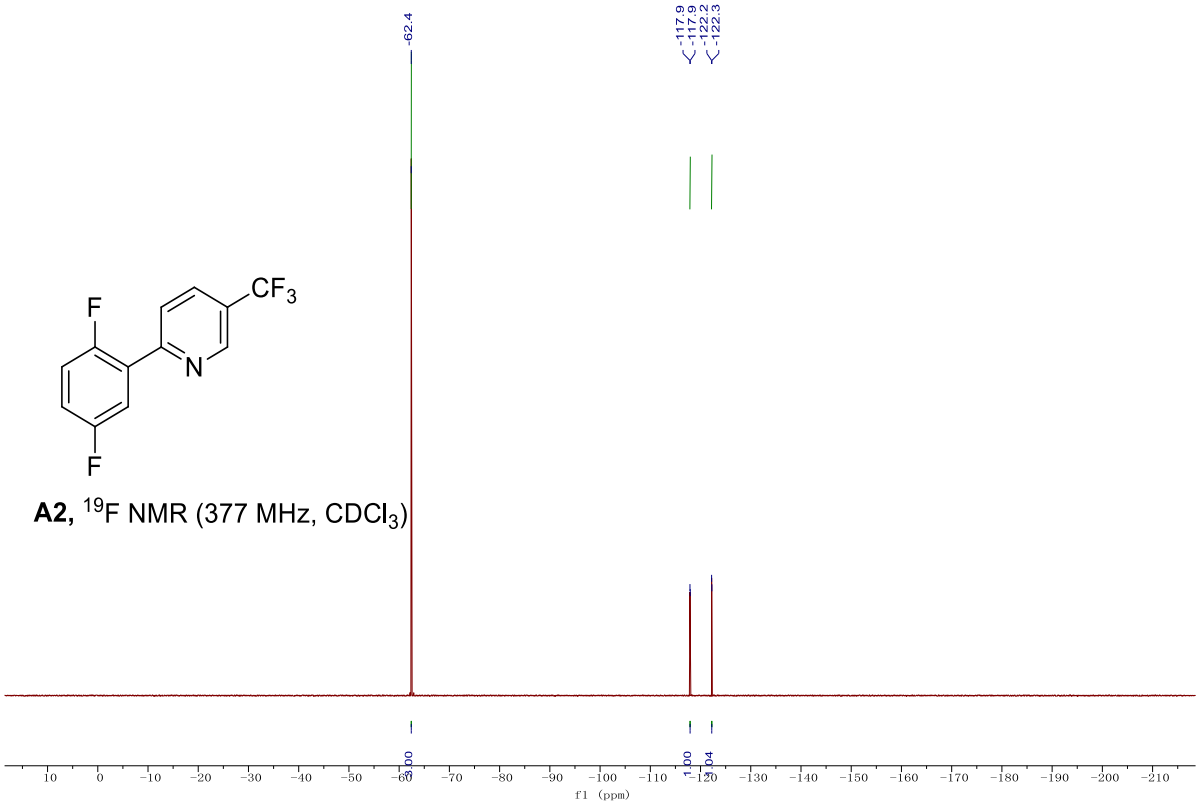

A2, ^{19}F NMR (377 MHz, $CDCl_3$)

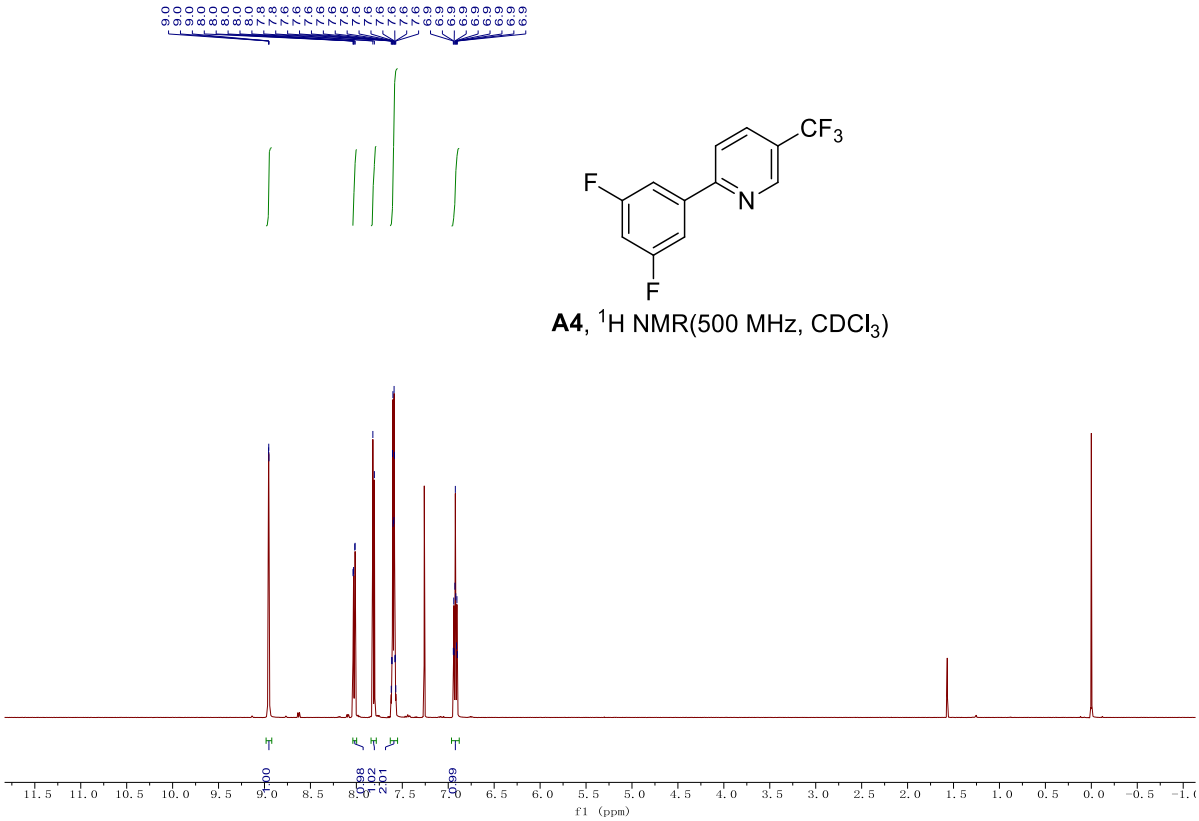

A4, ^{1}H NMR(500 MHz, $CDCl_3$)

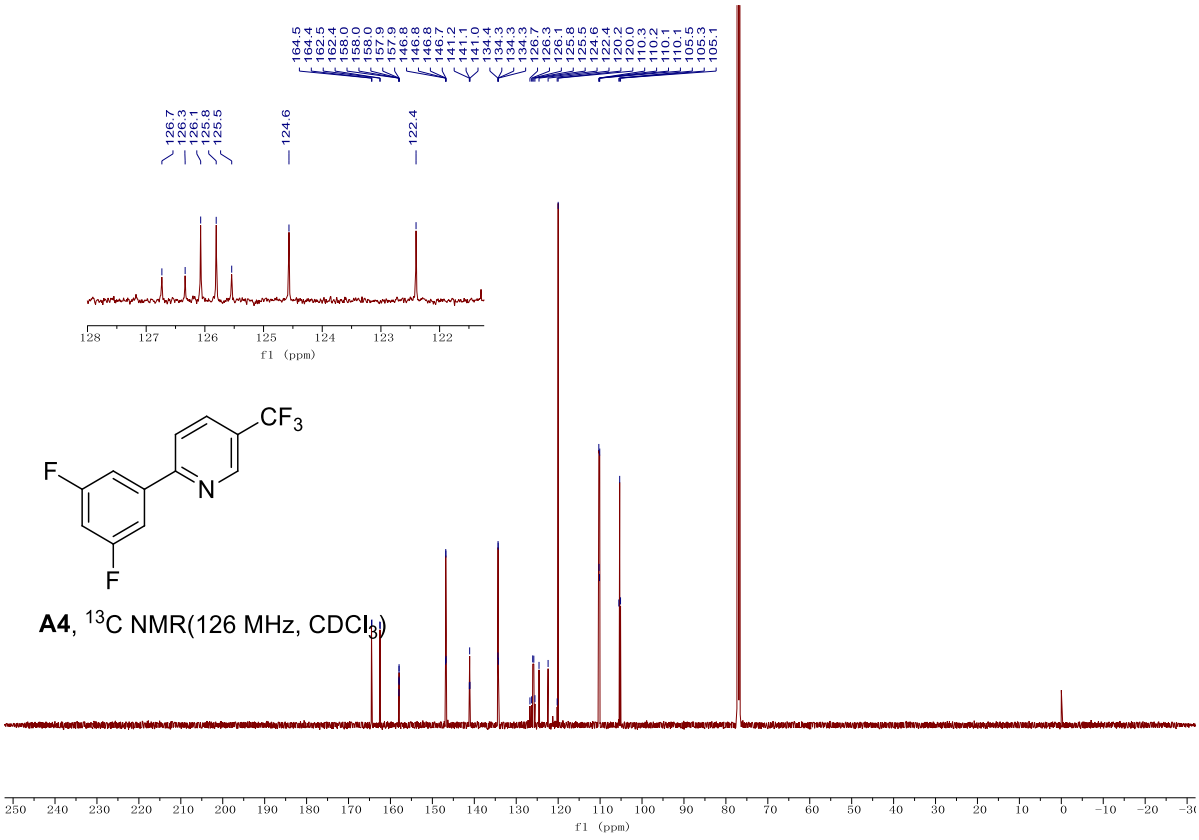

A4, ^{13}C NMR(126 MHz, $CDCl_3$)

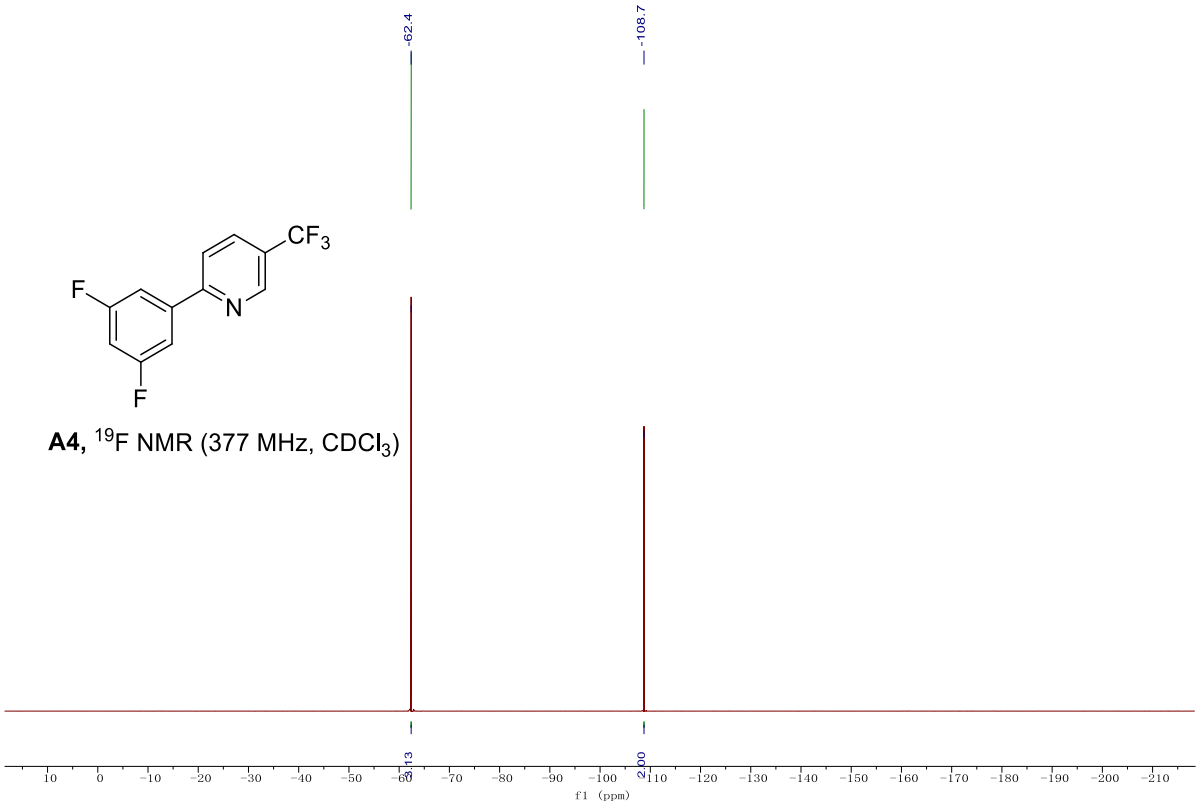

A4, ^{19}F NMR (377 MHz, $CDCl_3$)

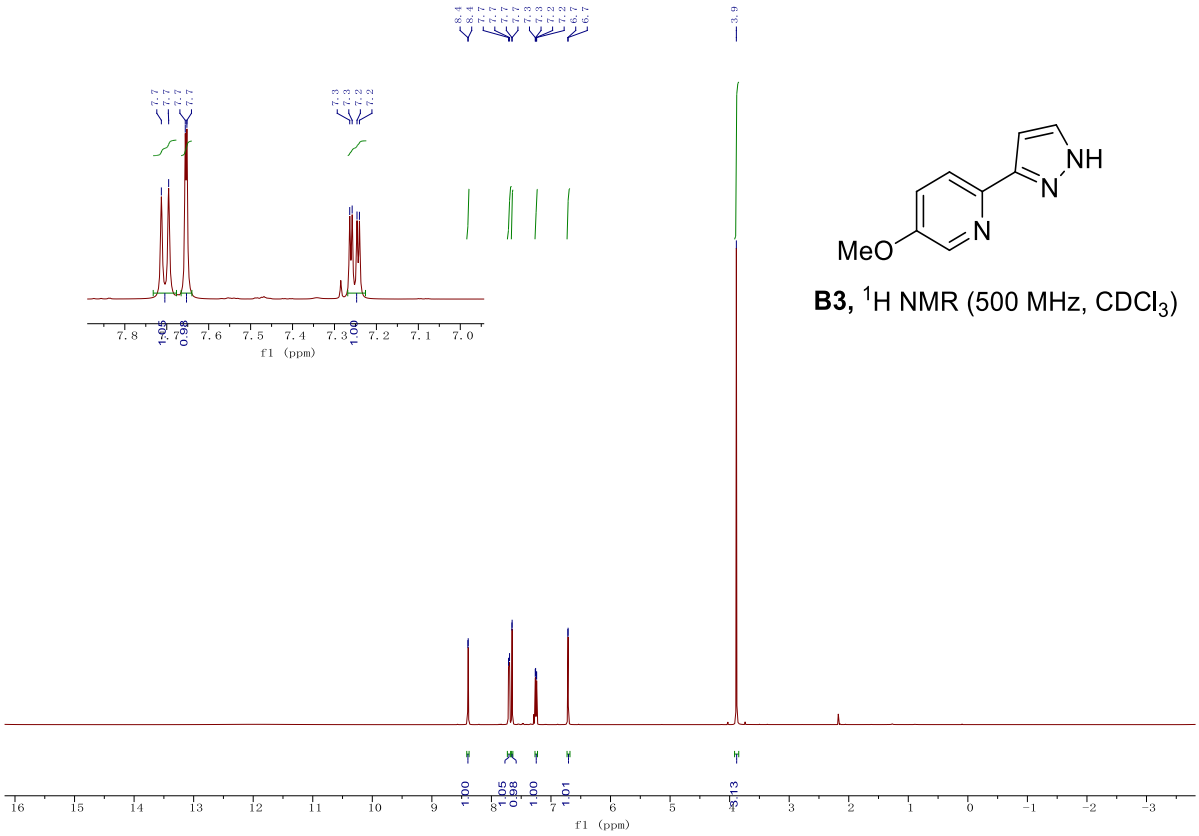

B3, ^{1}H NMR (500 MHz, $CDCl_3$)

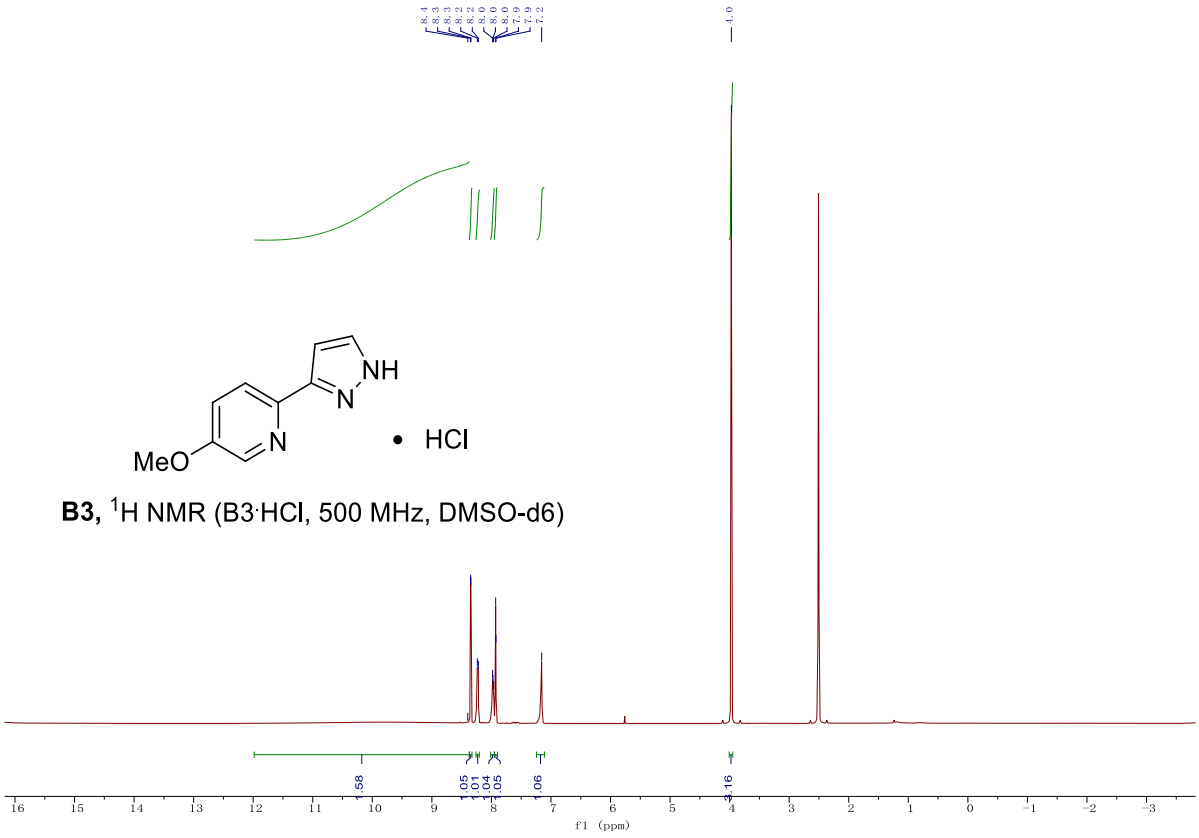

B3, ^{1}H NMR (B3·HCl, 500 MHz, DMSO-d6)

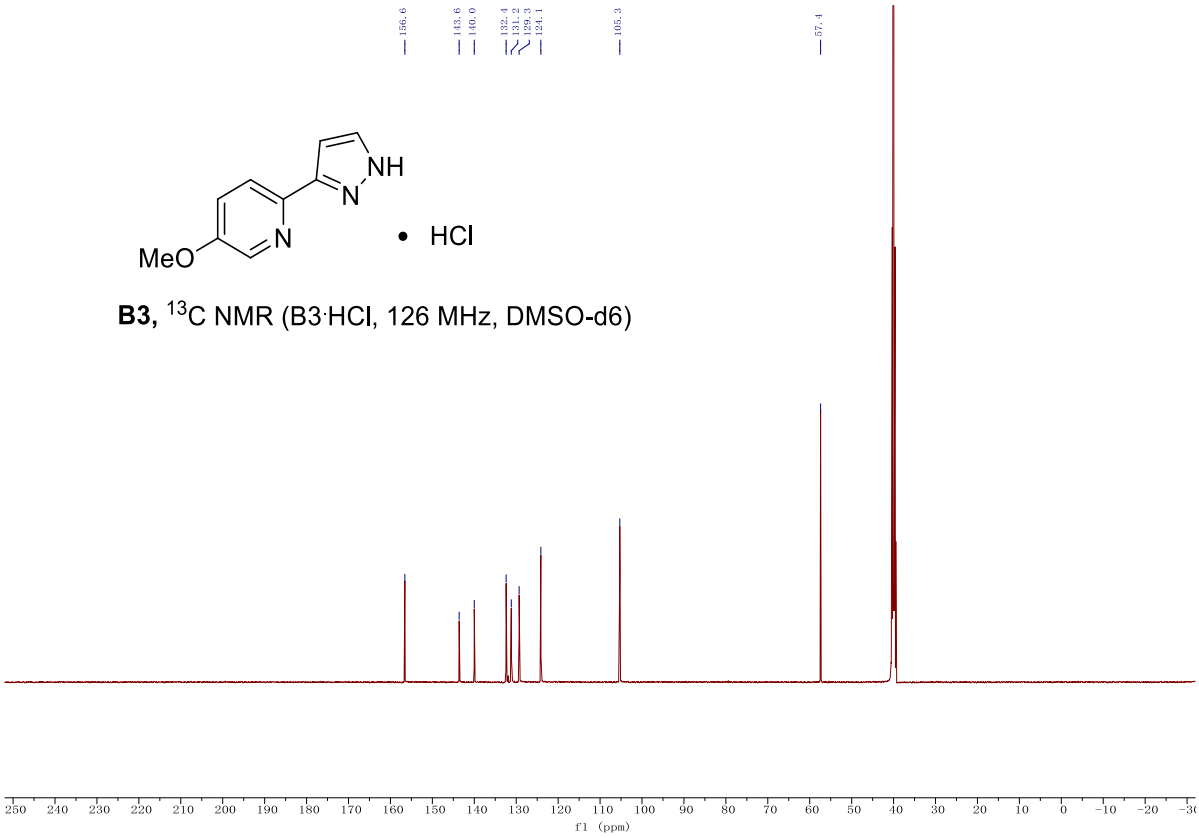

B3, ^{13}C NMR (B3·HCl, 126 MHz, DMSO-d6)

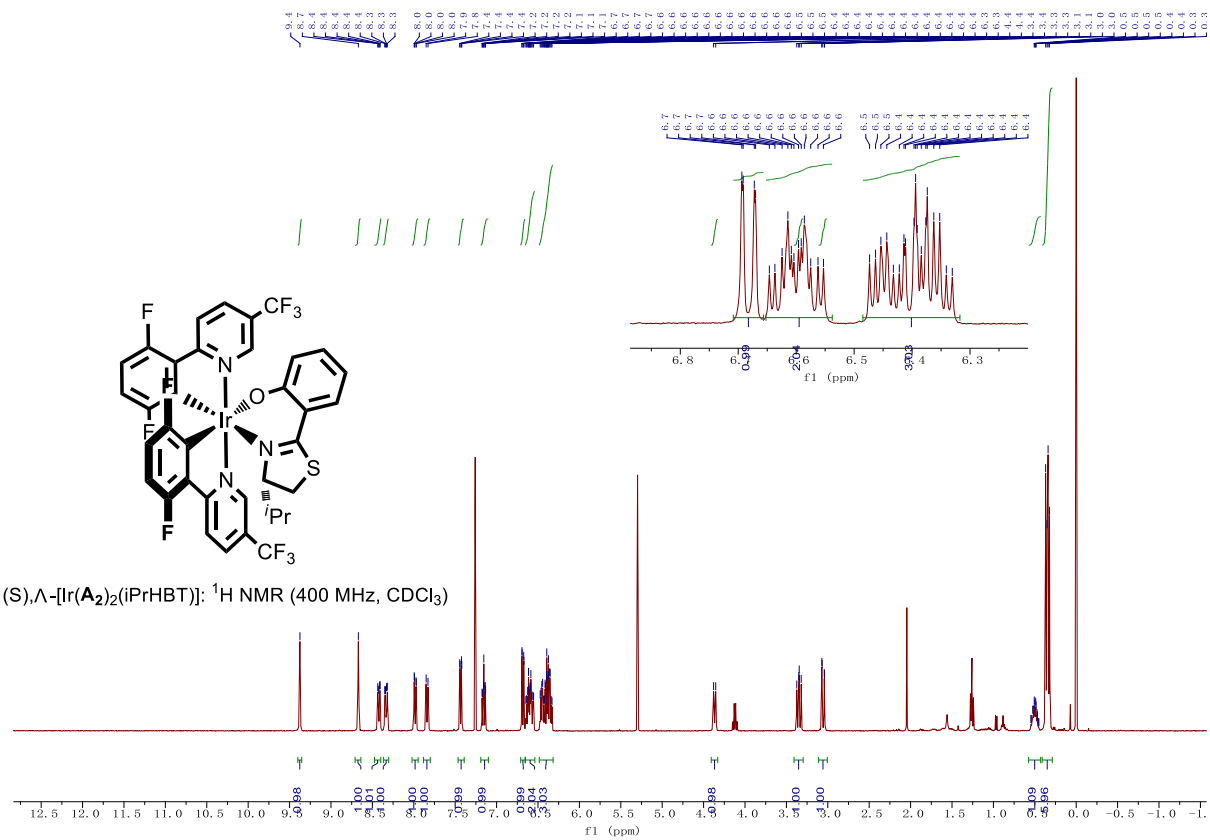

(S),Λ-[Ir(**A$_2$**)$_2$(iPrHBT)]: ^{1}H NMR (400 MHz, $CDCl_3$)

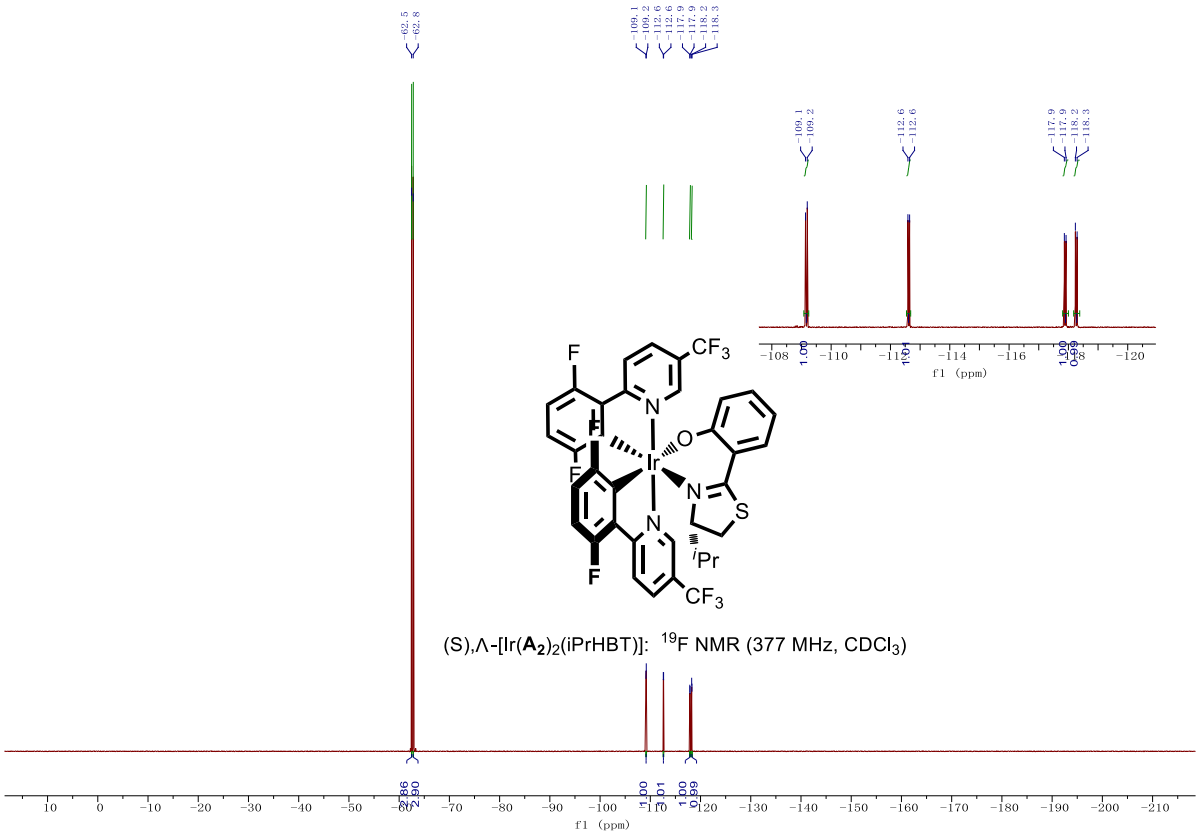

(S),Λ-[Ir(**A**$_2$)$_2$(iPrHBT)]: ^{19}F NMR (377 MHz, $CDCl_3$)

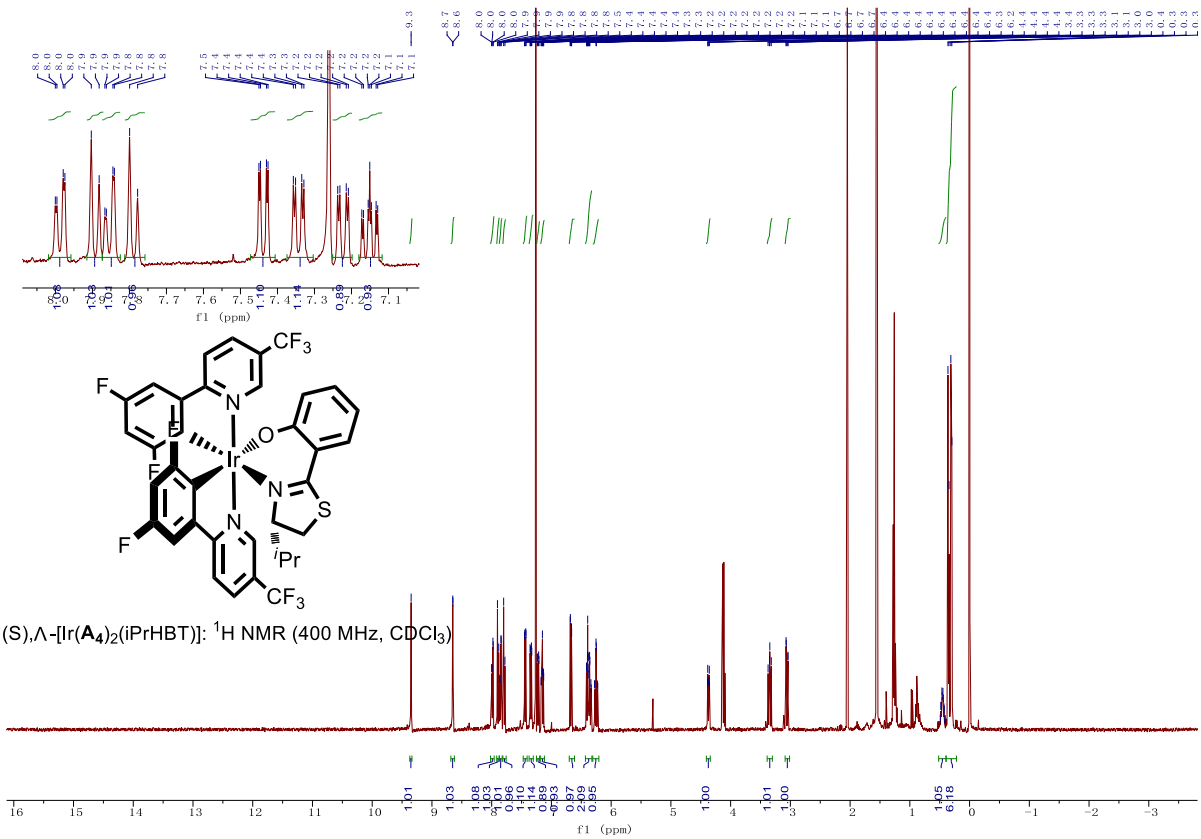

(S),Λ-[Ir(**A**$_4$)$_2$(iPrHBT)]: ^{1}H NMR (400 MHz, $CDCl_3$)

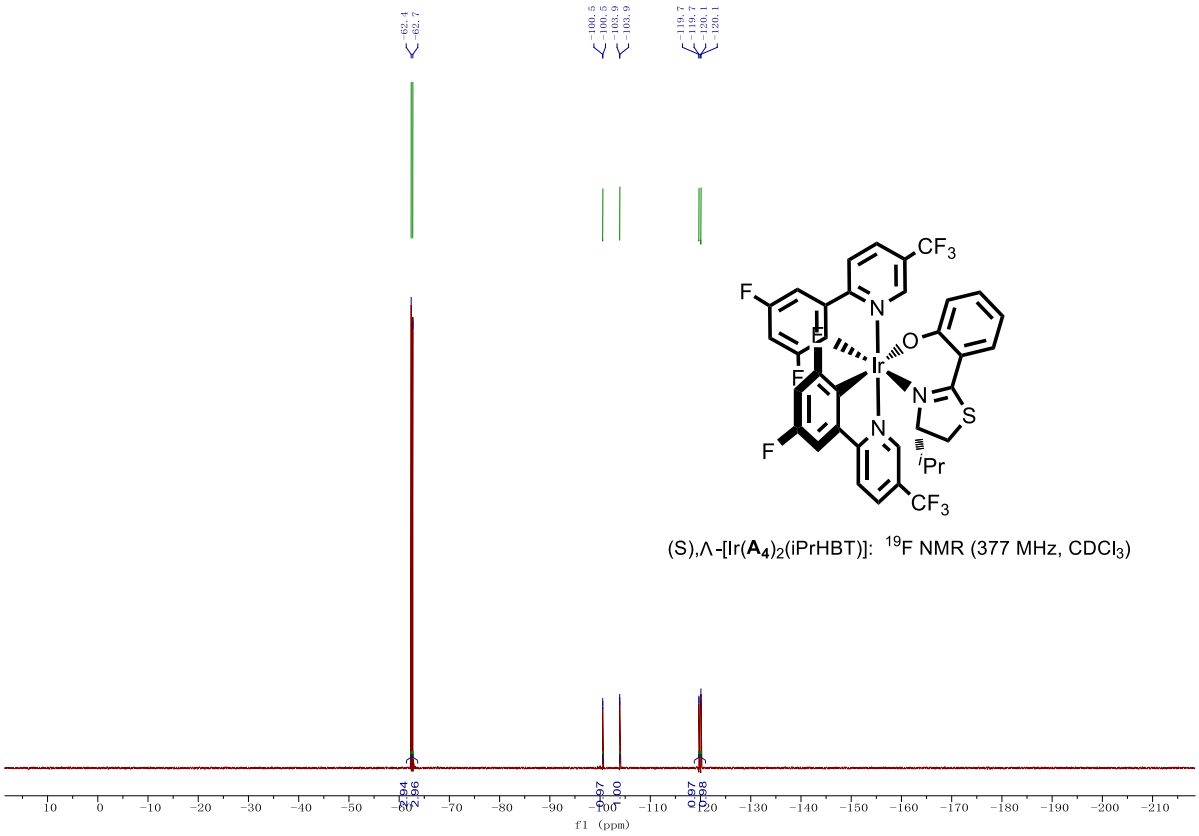
CF3
F
N
O
Ir
S
iPr
(S),Λ-[Ir(A4)2(iPrHBT)]: 19F NMR (377 MHz, CDCl3)
f1 (ppm)

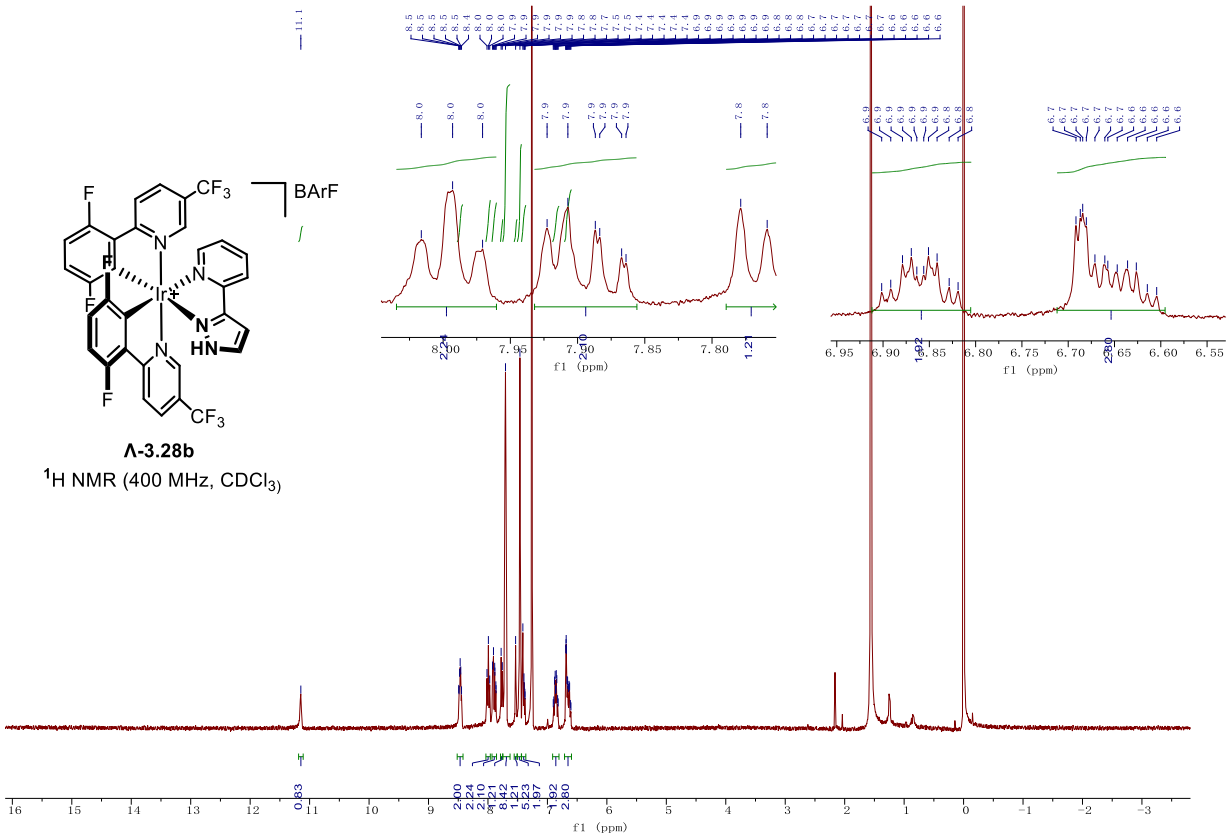
BArF
HN
Λ-3.28b
1H NMR (400 MHz, CDCl3)
f1 (ppm)

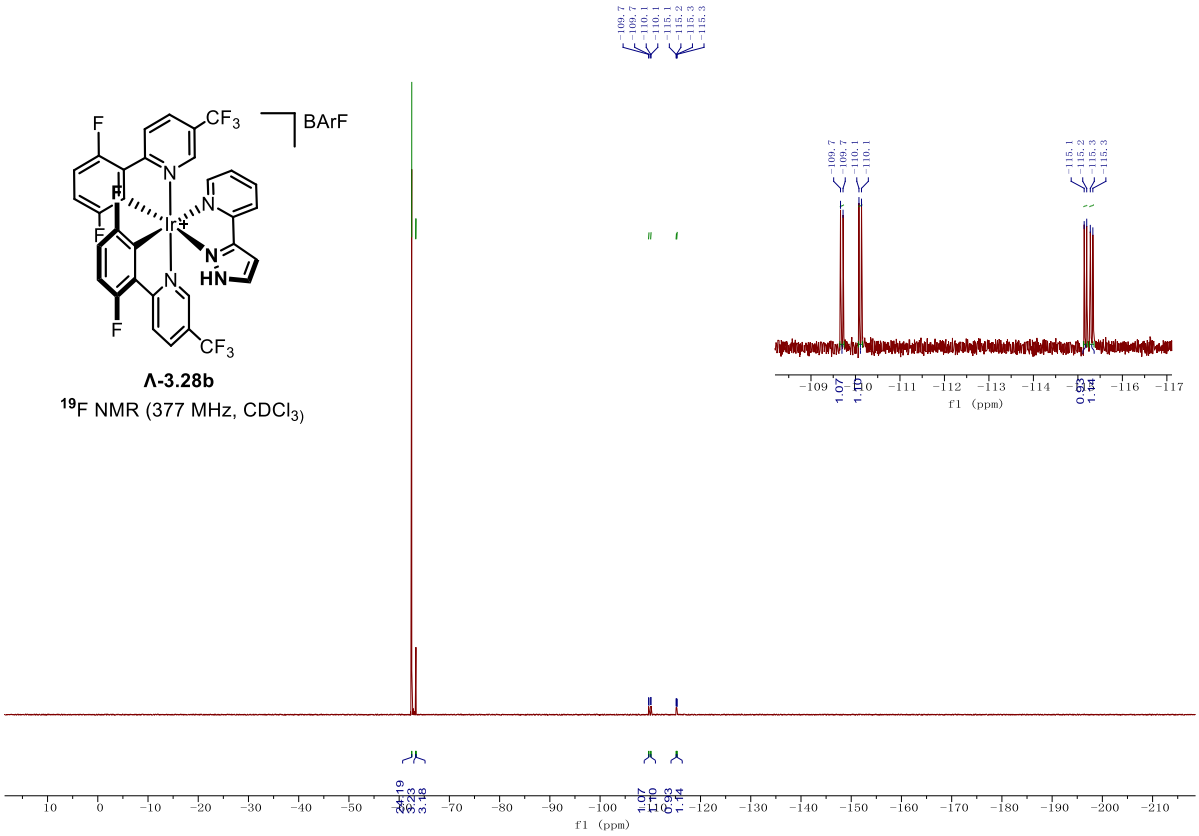
BArF
Λ-3.28b
19F NMR (377 MHz, CDCl3)
f1 (ppm)

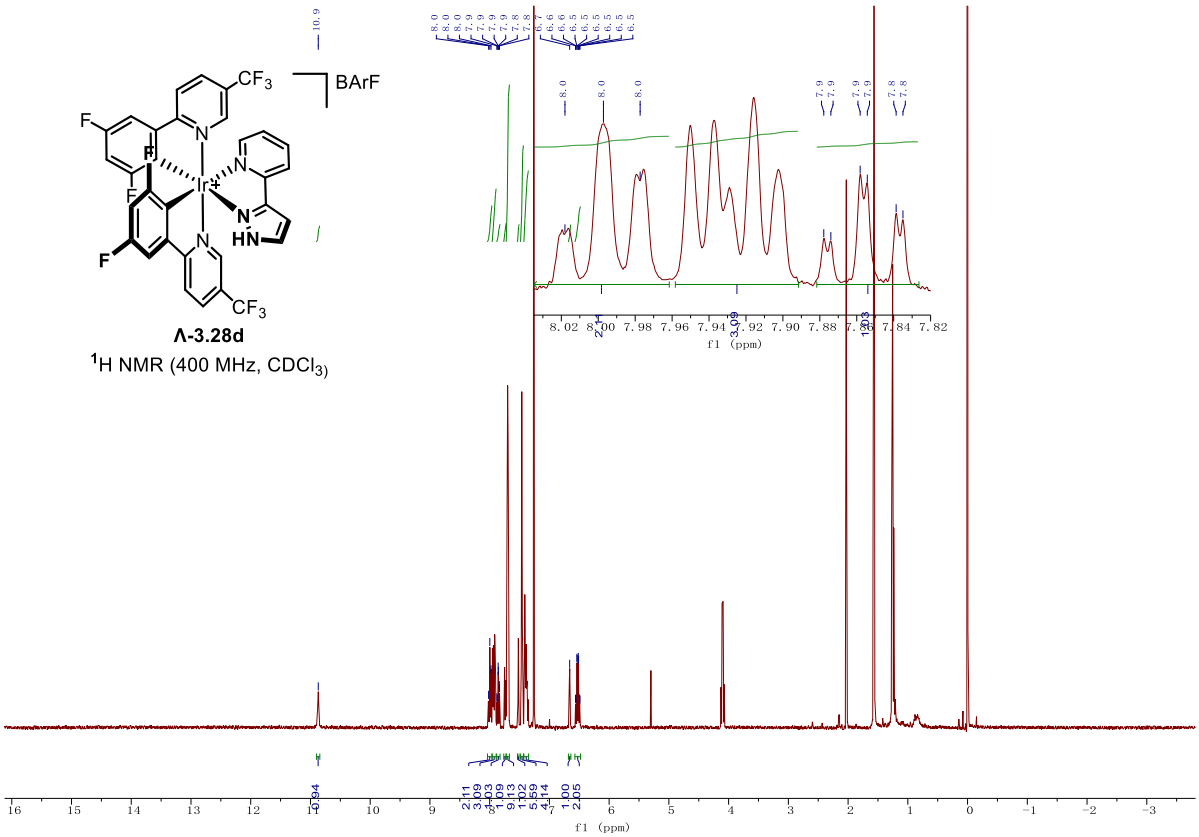
BArF
Λ-3.28d
1H NMR (400 MHz, CDCl3)
f1 (ppm)

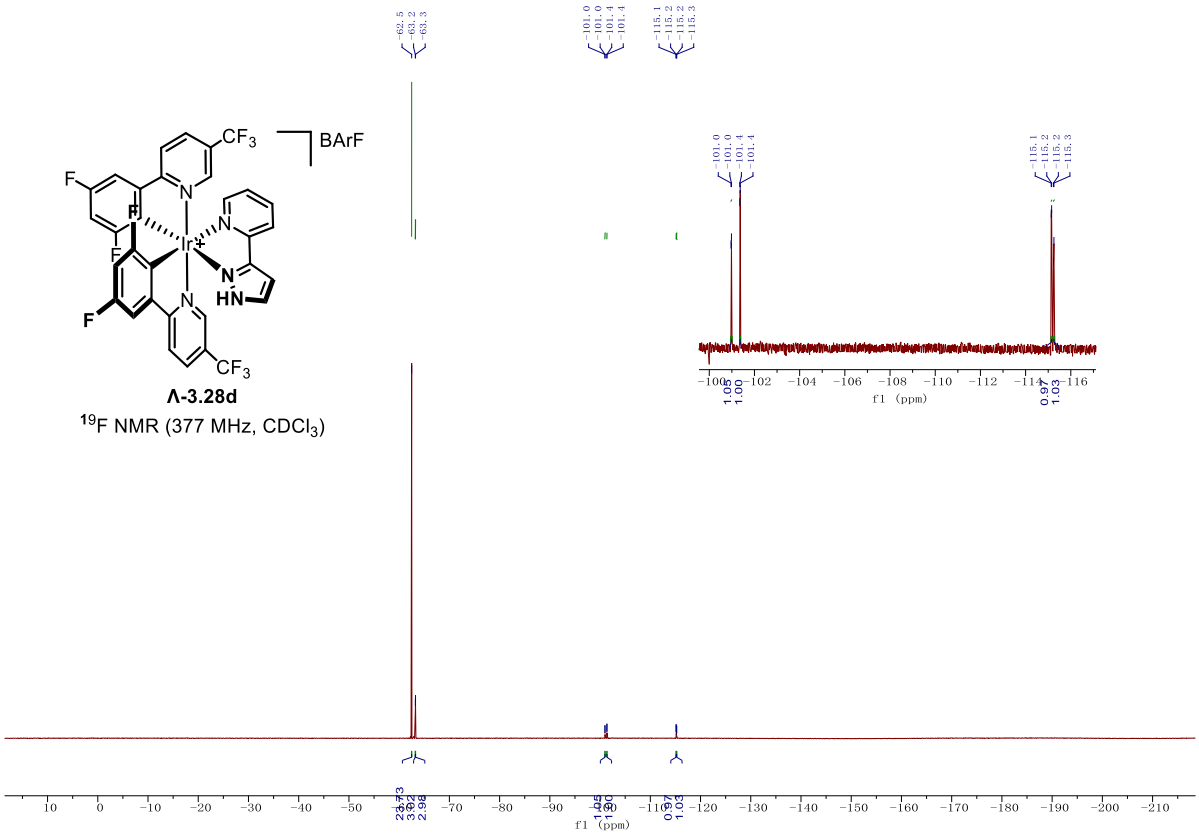
BArF
Λ-3.28d
19F NMR (377 MHz, CDCl3)
f1 (ppm)

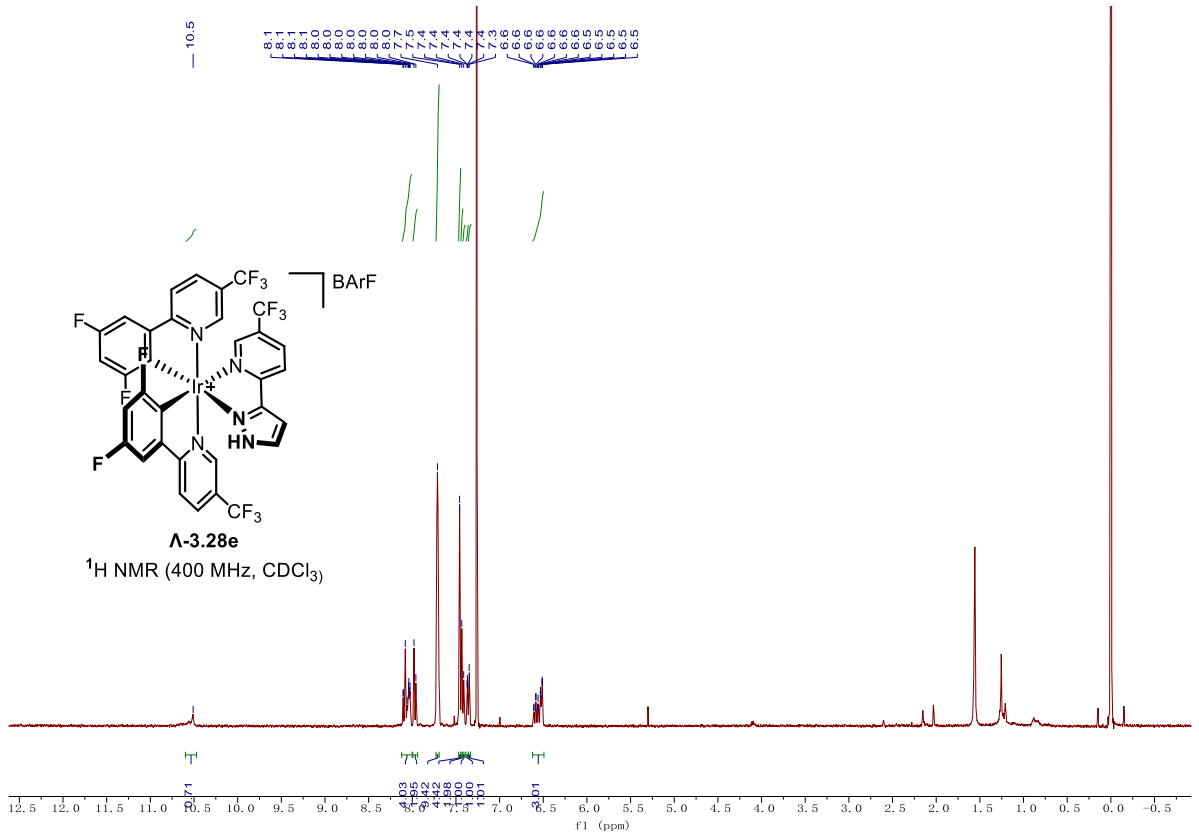
BArF
Λ-3.28e
1H NMR (400 MHz, CDCl3)
f1 (ppm)

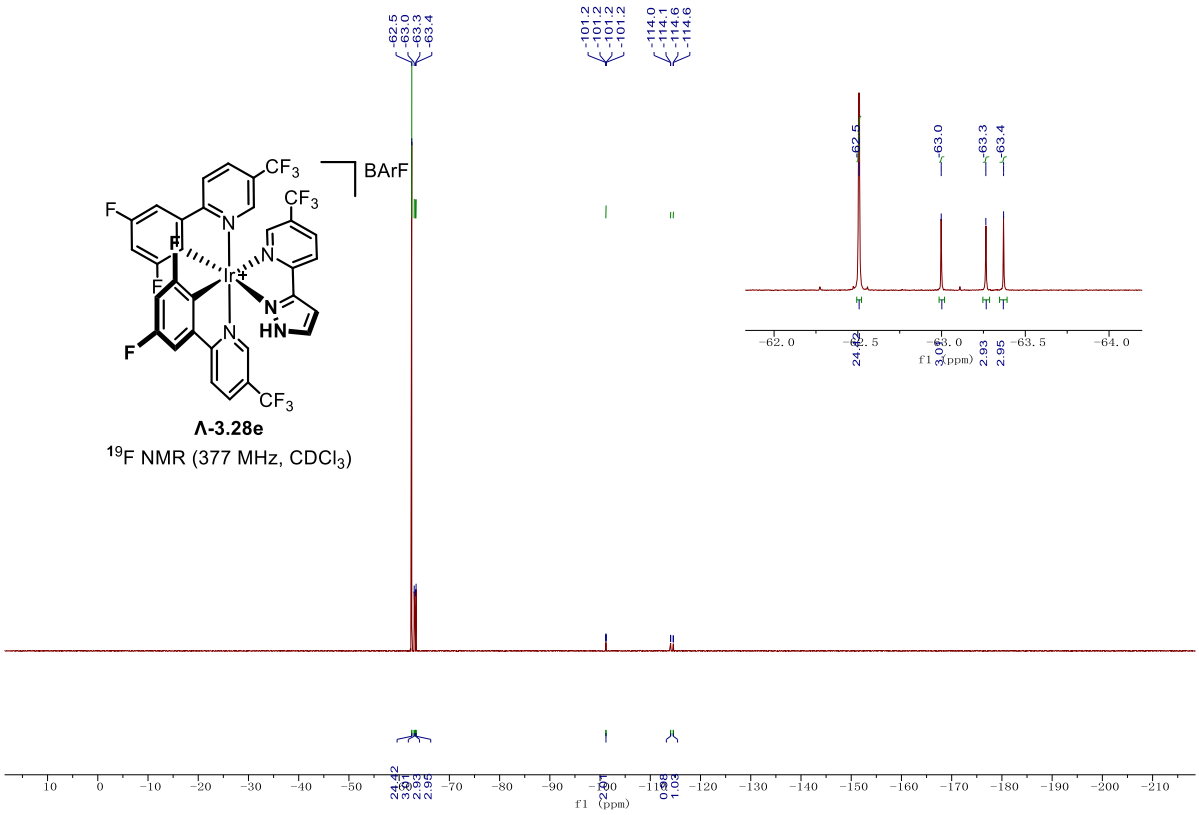
BArF
Λ-3.28e
^{19}F NMR (377 MHz, $CDCl_3$)
f1 (ppm)

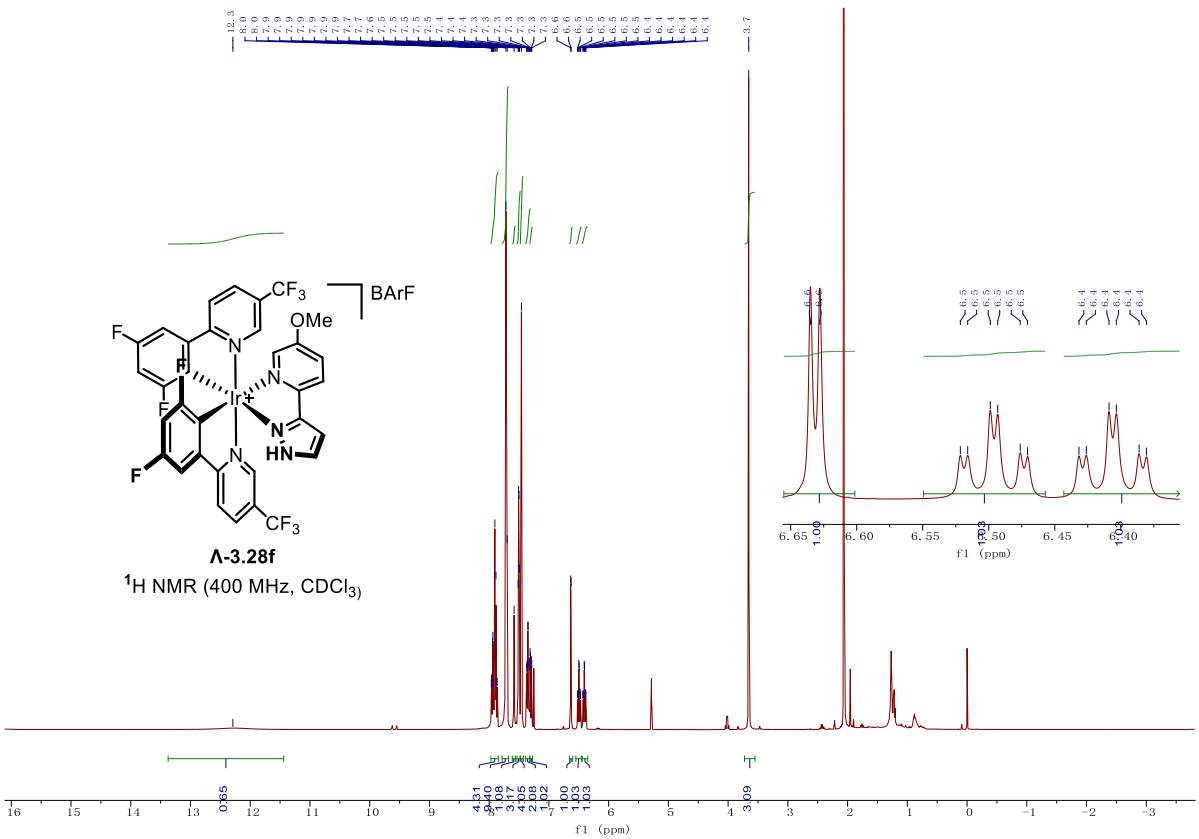
BArF
Λ-3.28f
^{1}H NMR (400 MHz, $CDCl_3$)
f1 (ppm)

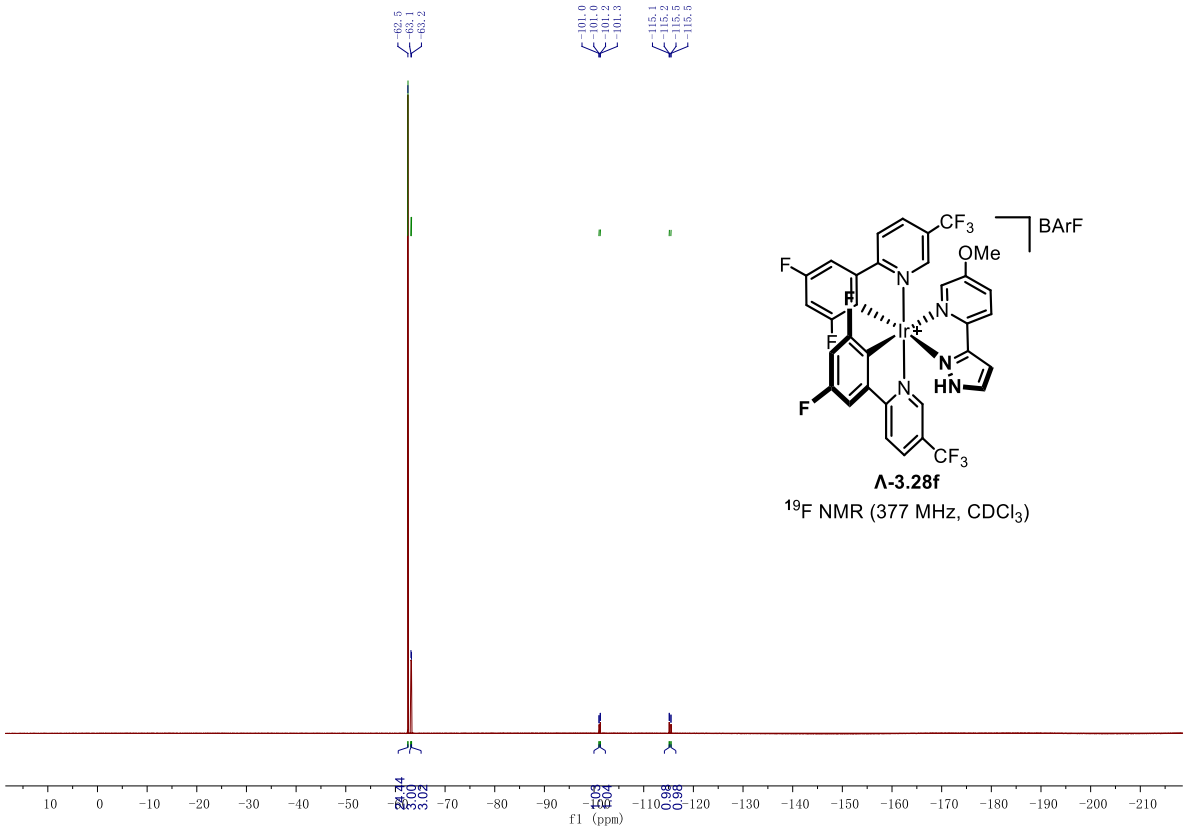

Λ-3.28f

^{19}F NMR (377 MHz, $CDCl_3$)

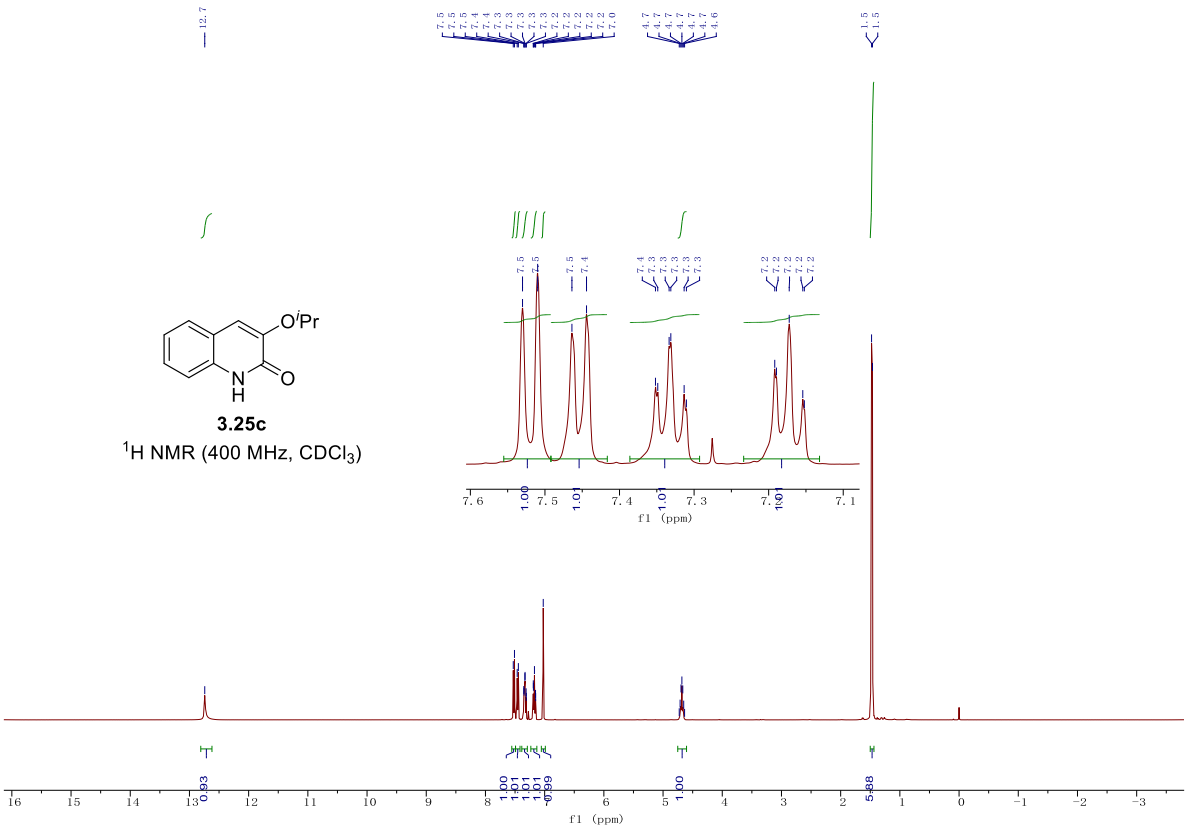

3.25c

^{1}H NMR (400 MHz, $CDCl_3$)

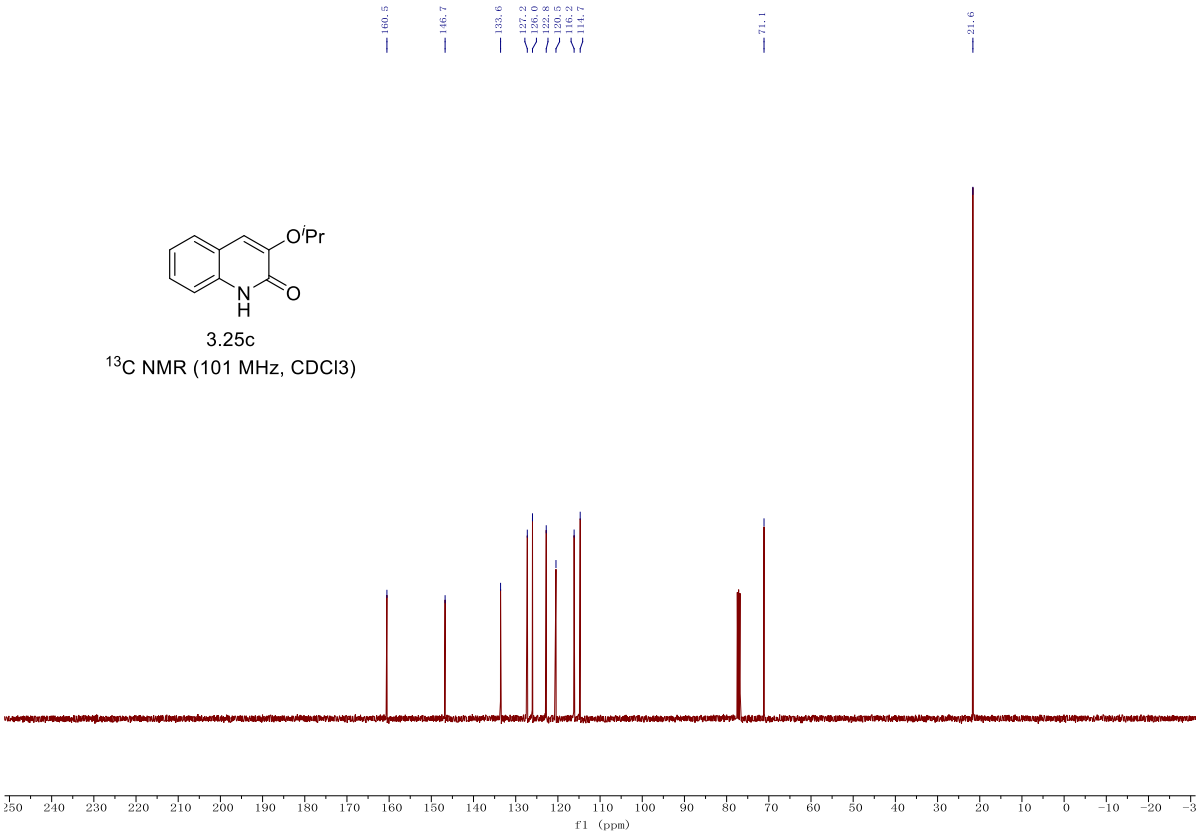

3.25c

^{13}C NMR (101 MHz, CDCl3)

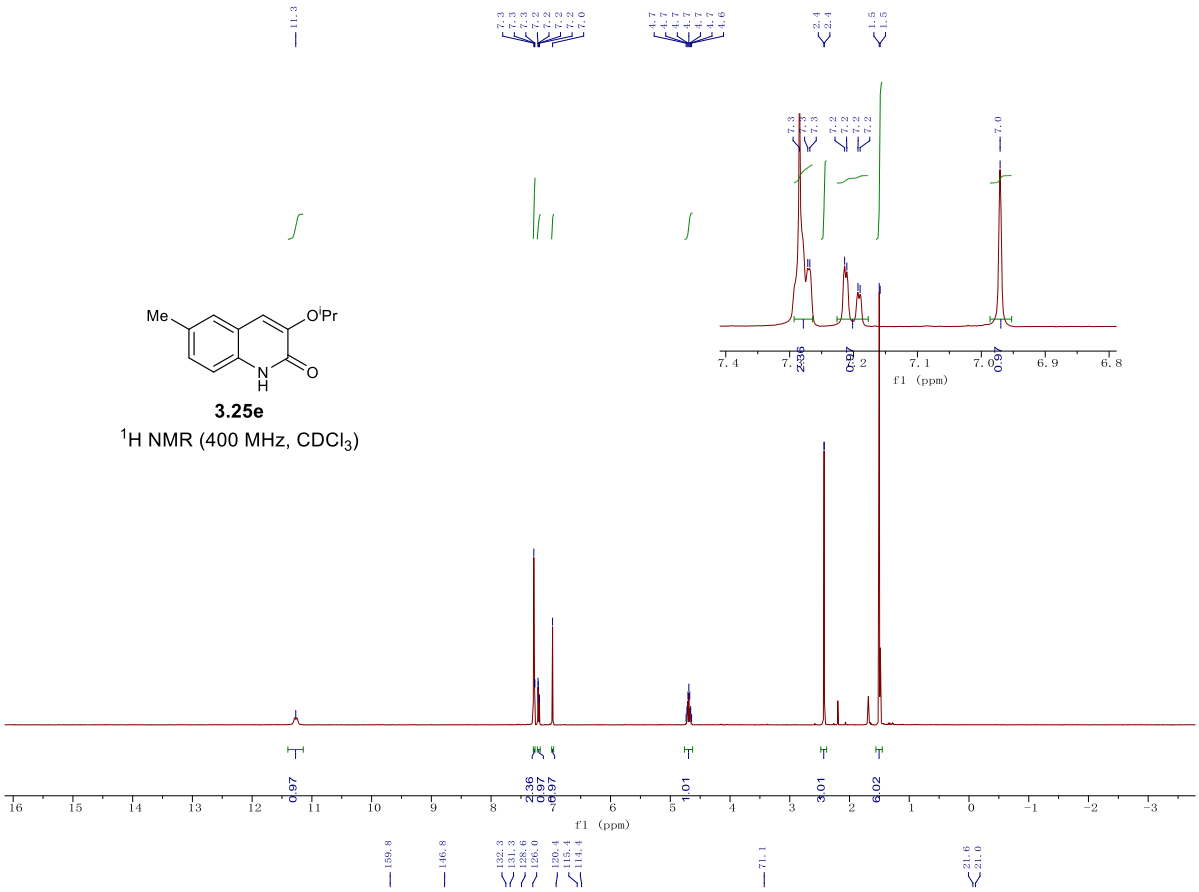

3.25e

^{1}H NMR (400 MHz, $CDCl_3$)

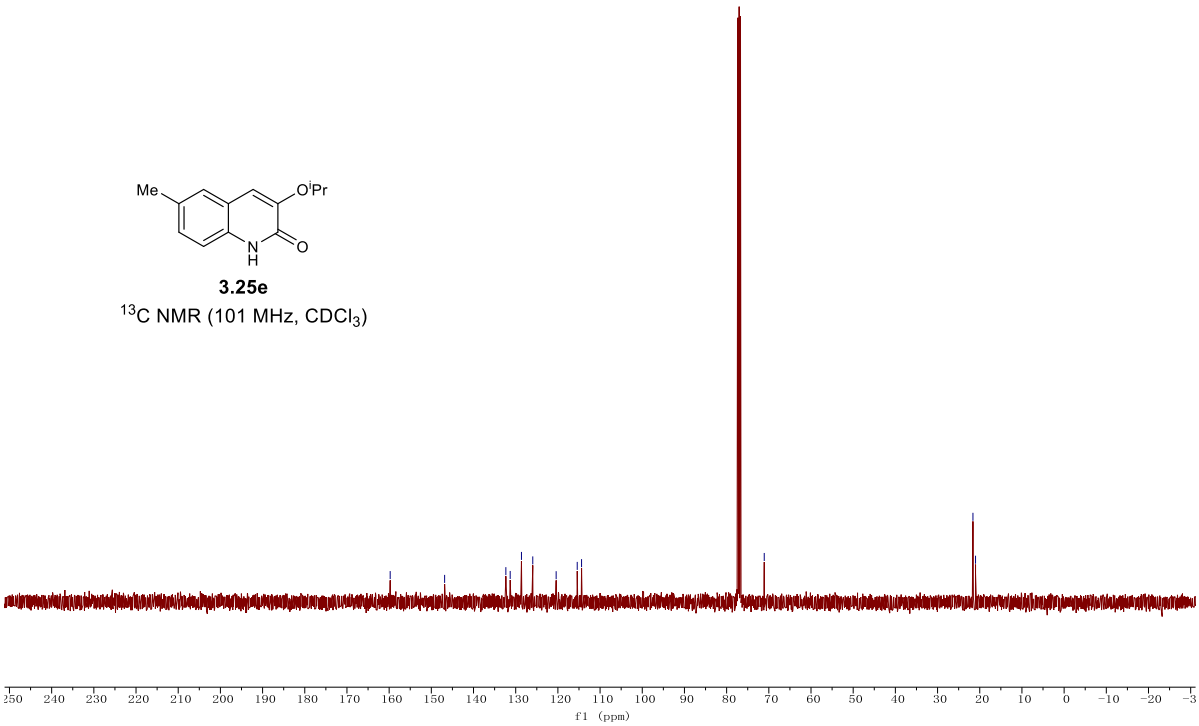

3.25e

^{13}C NMR (101 MHz, $CDCl_3$)

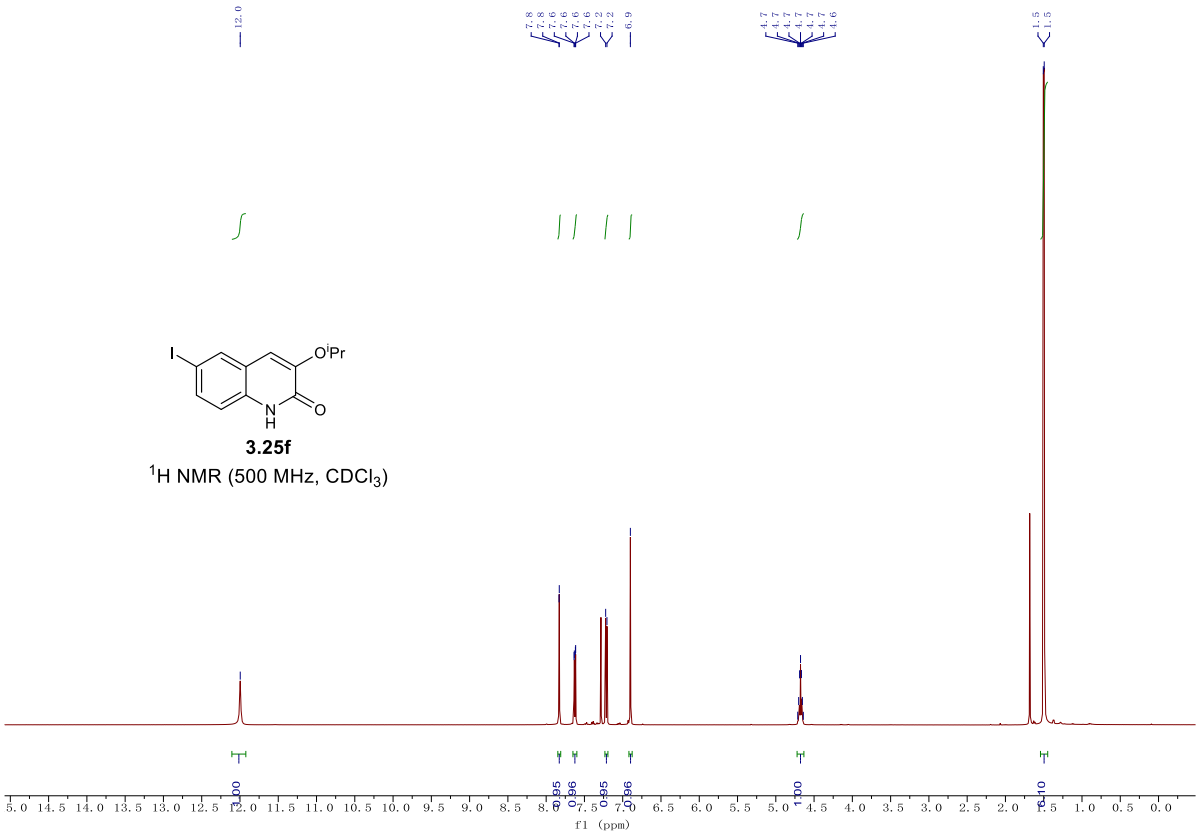
12.0
7.8
7.8
7.6
7.6
7.6
7.6
7.2
7.2
6.9
4.7
4.7
4.7
4.7
4.7
4.7
4.6
1.5
1.5
I
OiPr
N
H
O
3.25f
1H NMR (500 MHz, CDCl3)
1.00
0.95
0.96
0.95
0.96
1.00
6.10
f1 (ppm)

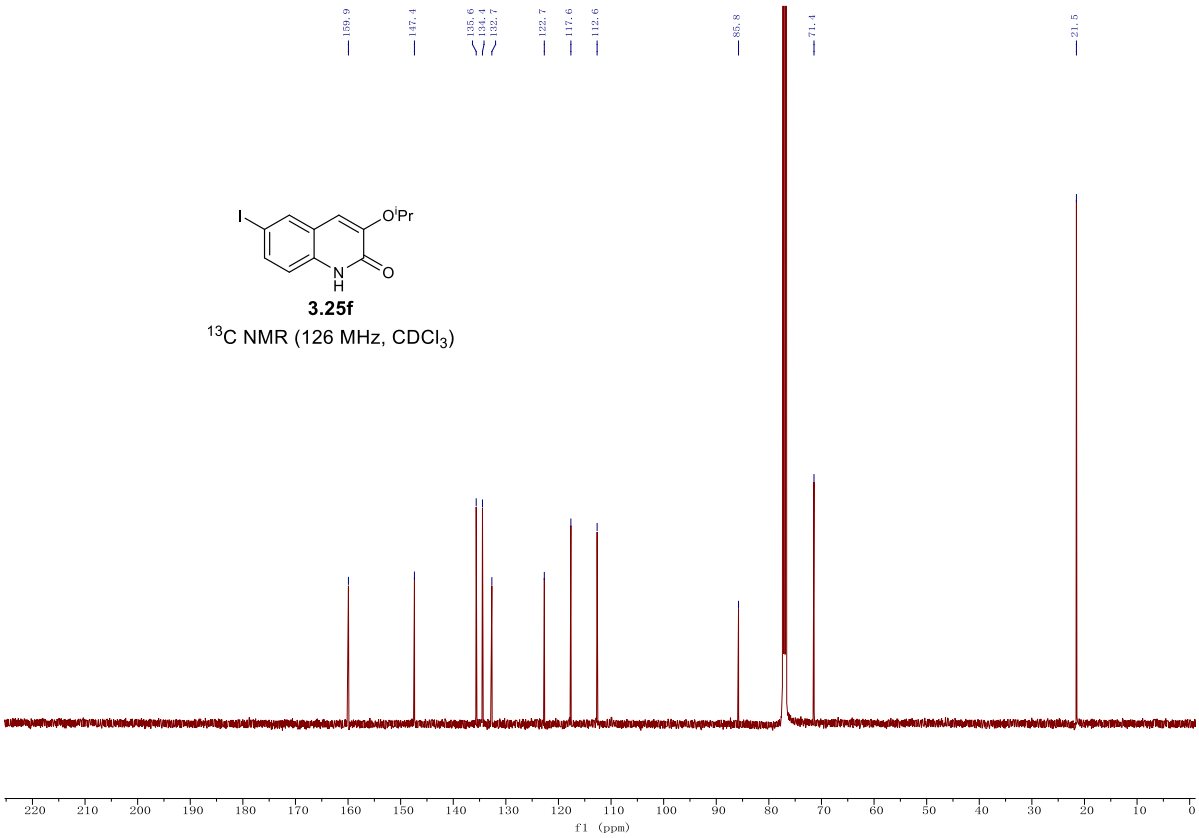
159.9
147.4
135.6
134.4
132.7
122.7
117.6
112.6
85.8
71.4
21.5
I
OiPr
N
H
O
3.25f
13C NMR (126 MHz, CDCl3)
f1 (ppm)

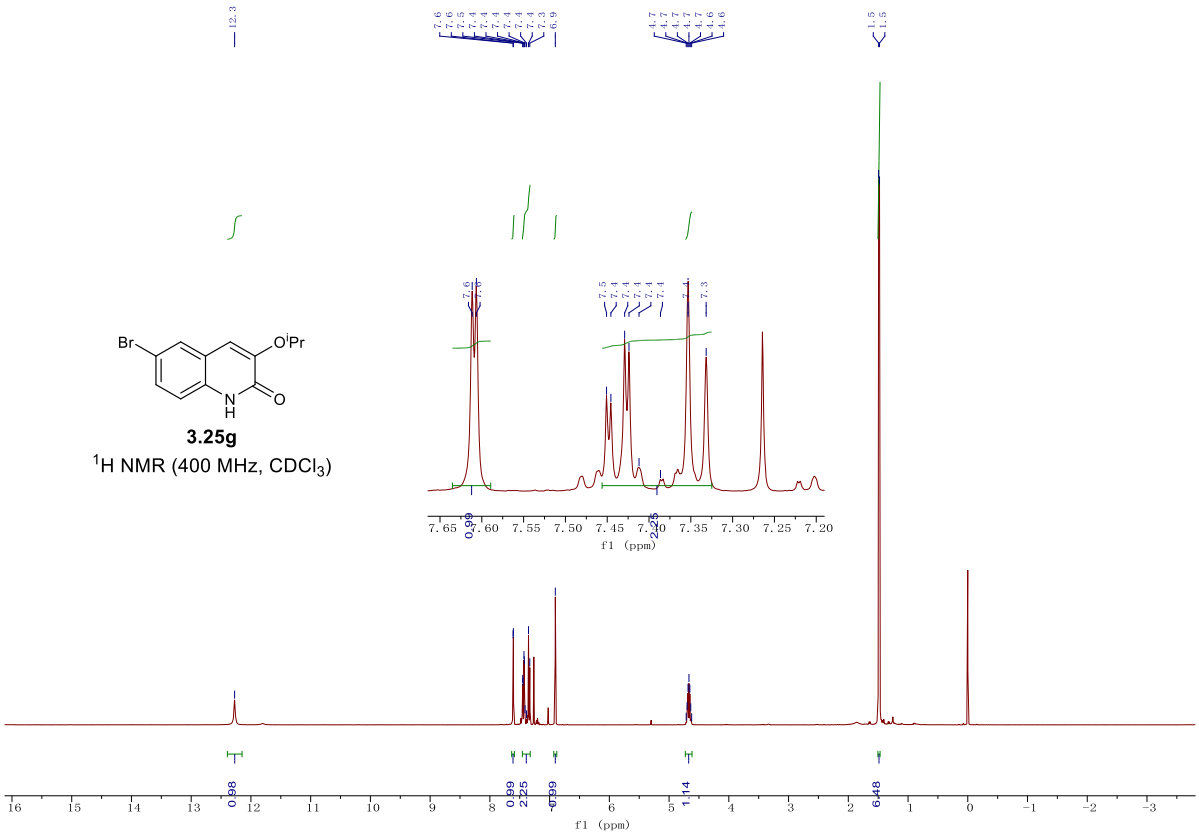

3.25g

^{1}H NMR (400 MHz, $CDCl_3$)

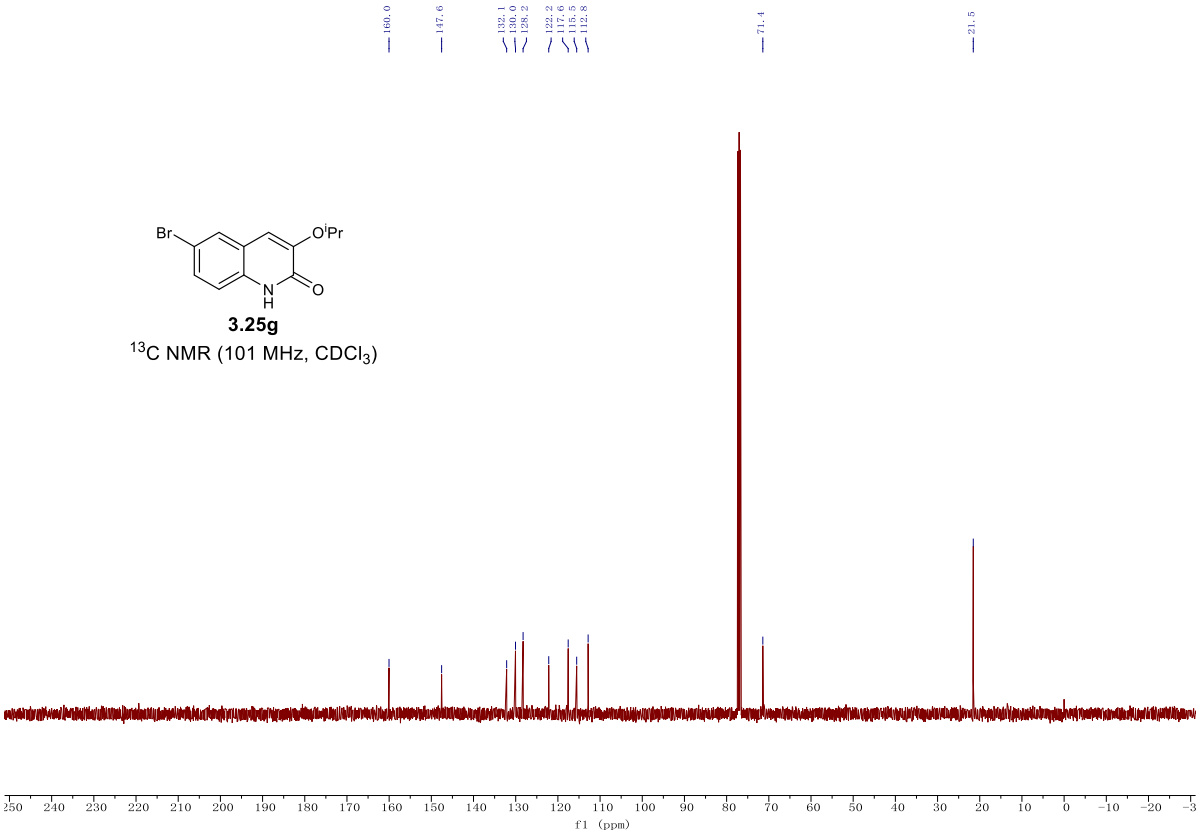

3.25g

^{13}C NMR (101 MHz, $CDCl_3$)

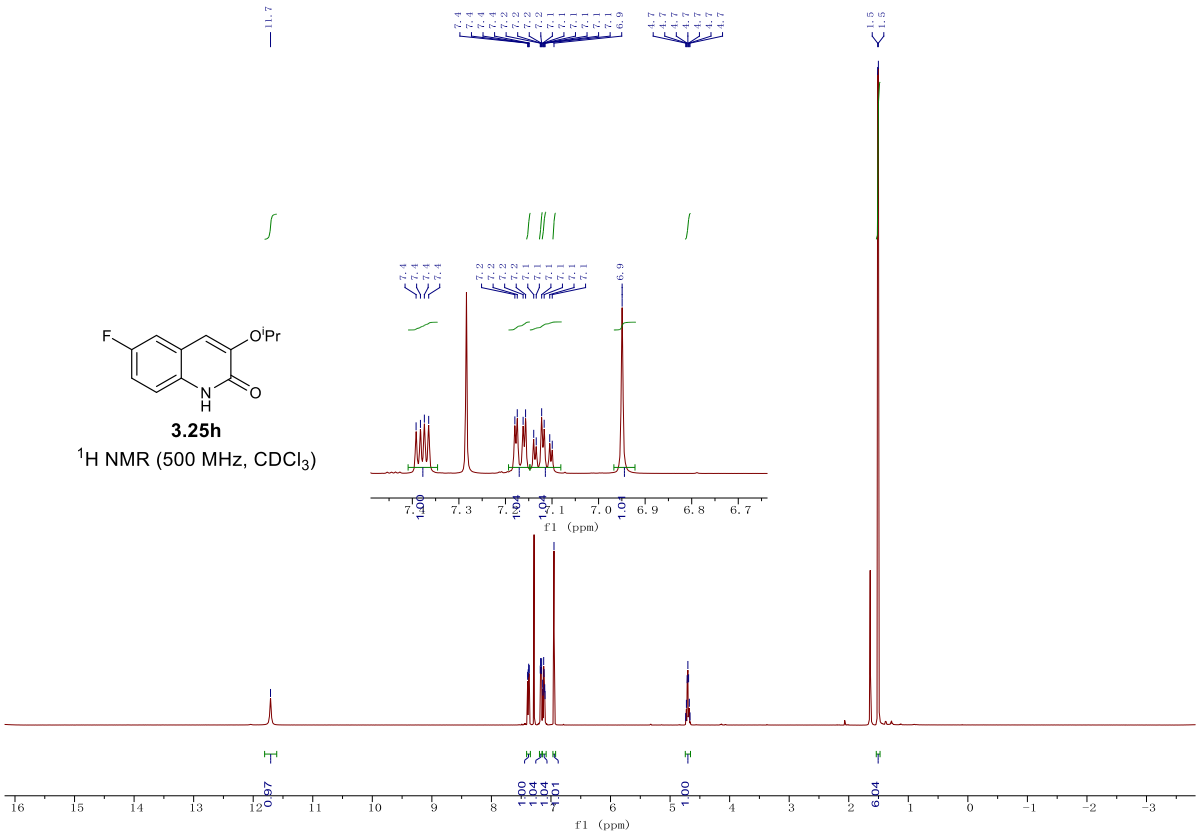
F
O^{i}Pr
N
H
O
3.25h
^{1}H NMR (500 MHz, CDCl$_3$)
f1 (ppm)

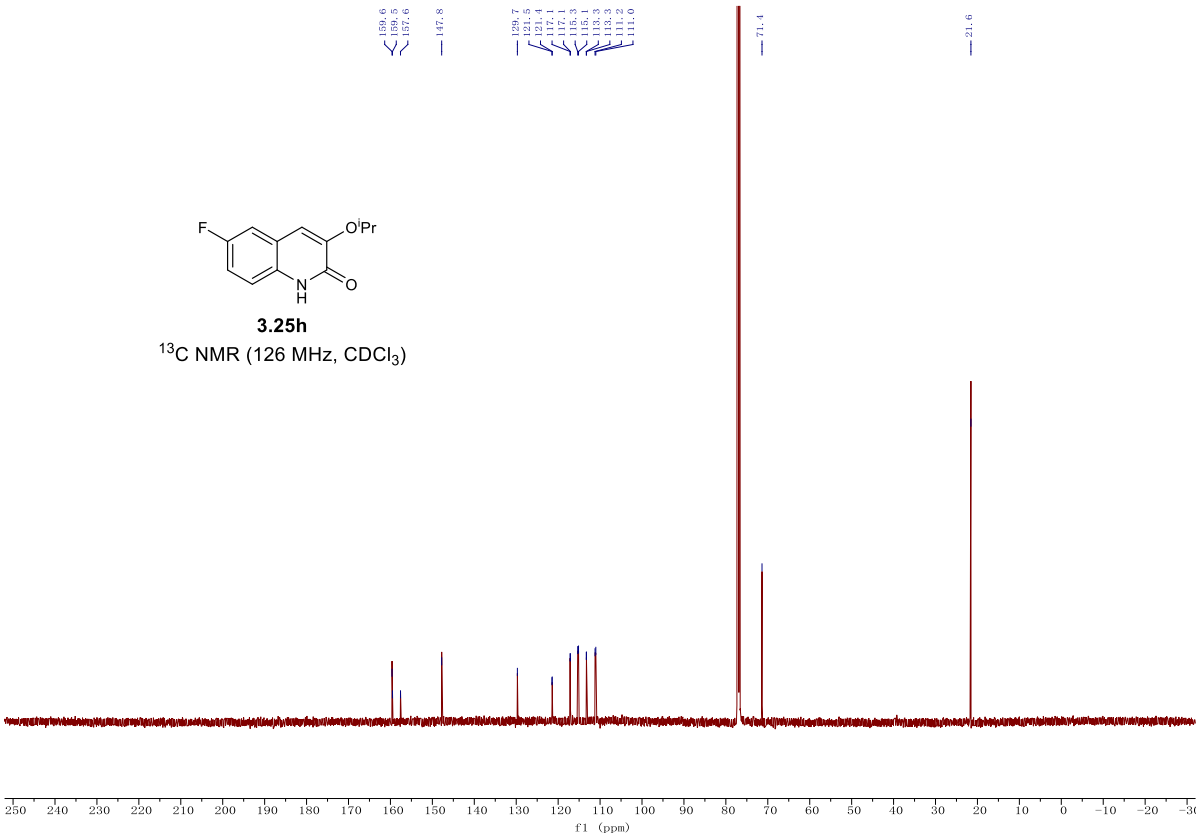
F
O^{i}Pr
N
H
O
3.25h
^{13}C NMR (126 MHz, CDCl$_3$)
f1 (ppm)

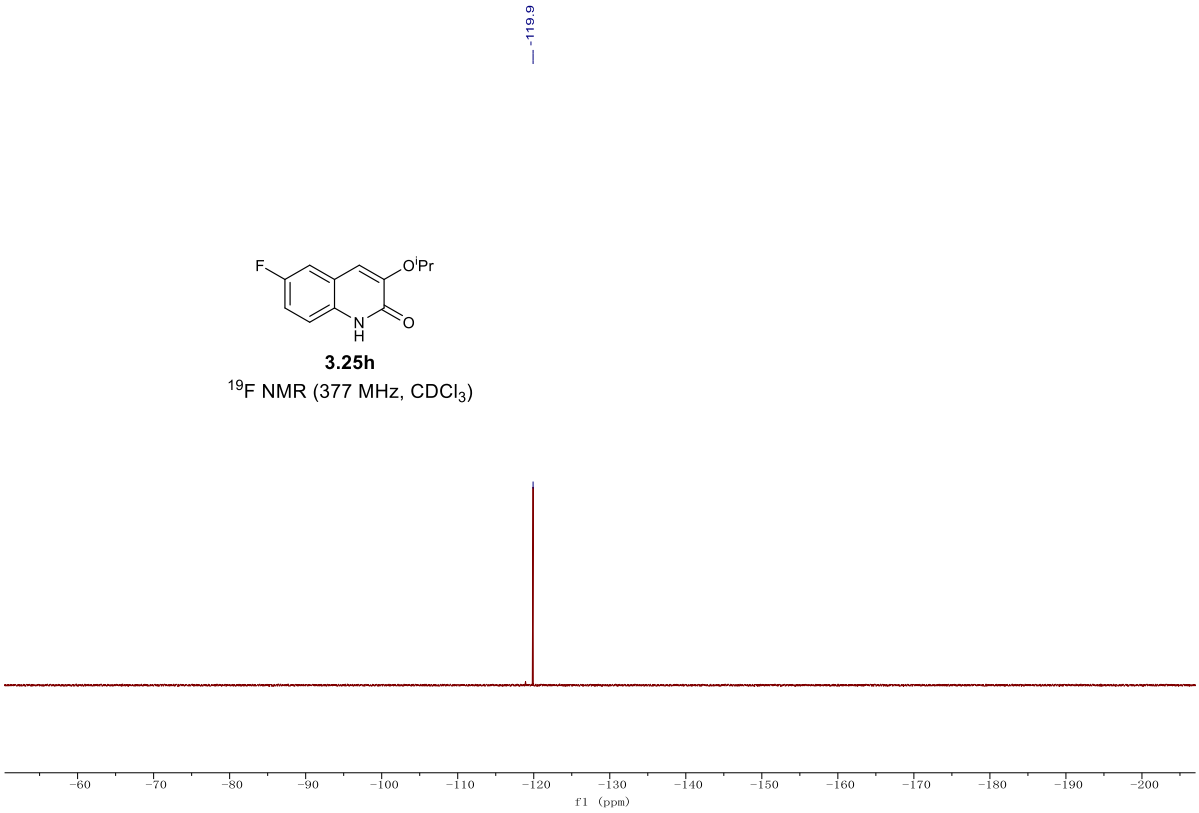

3.25h

^{19}F NMR (377 MHz, $CDCl_3$)

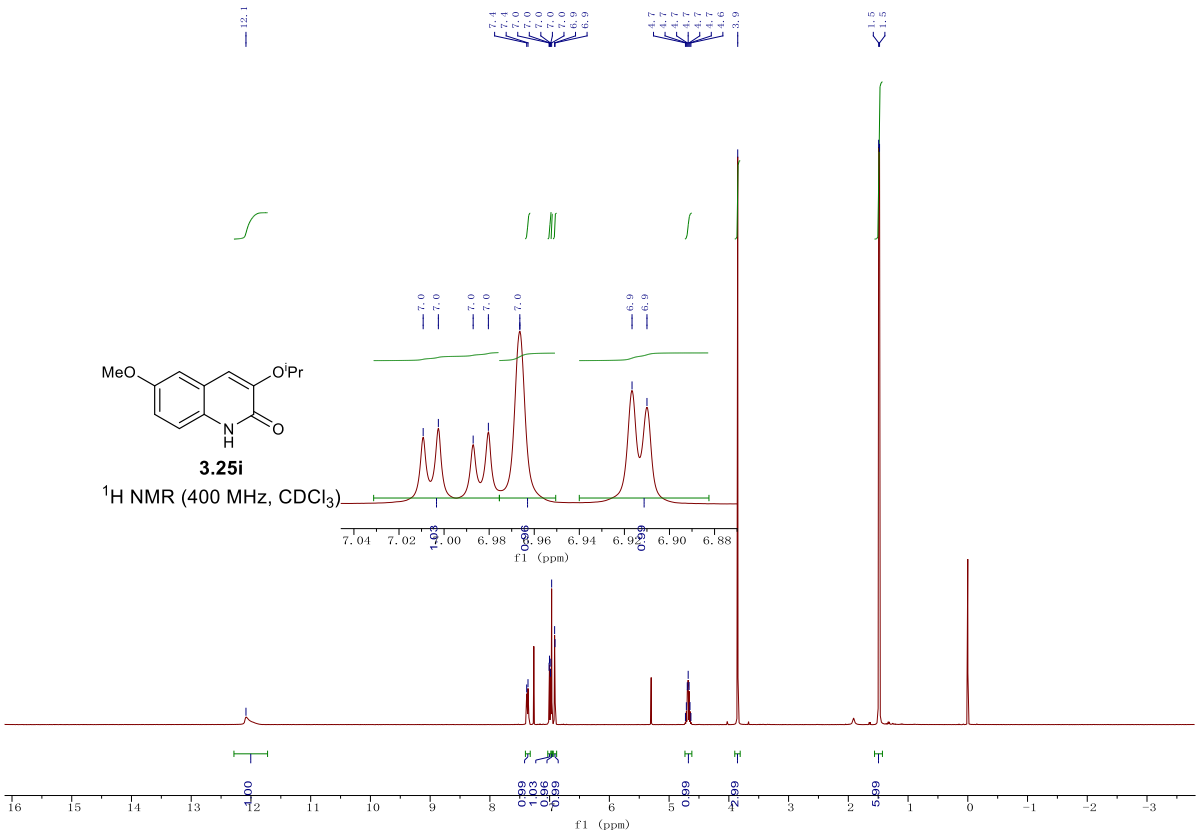

3.25i

^{1}H NMR (400 MHz, $CDCl_3$)

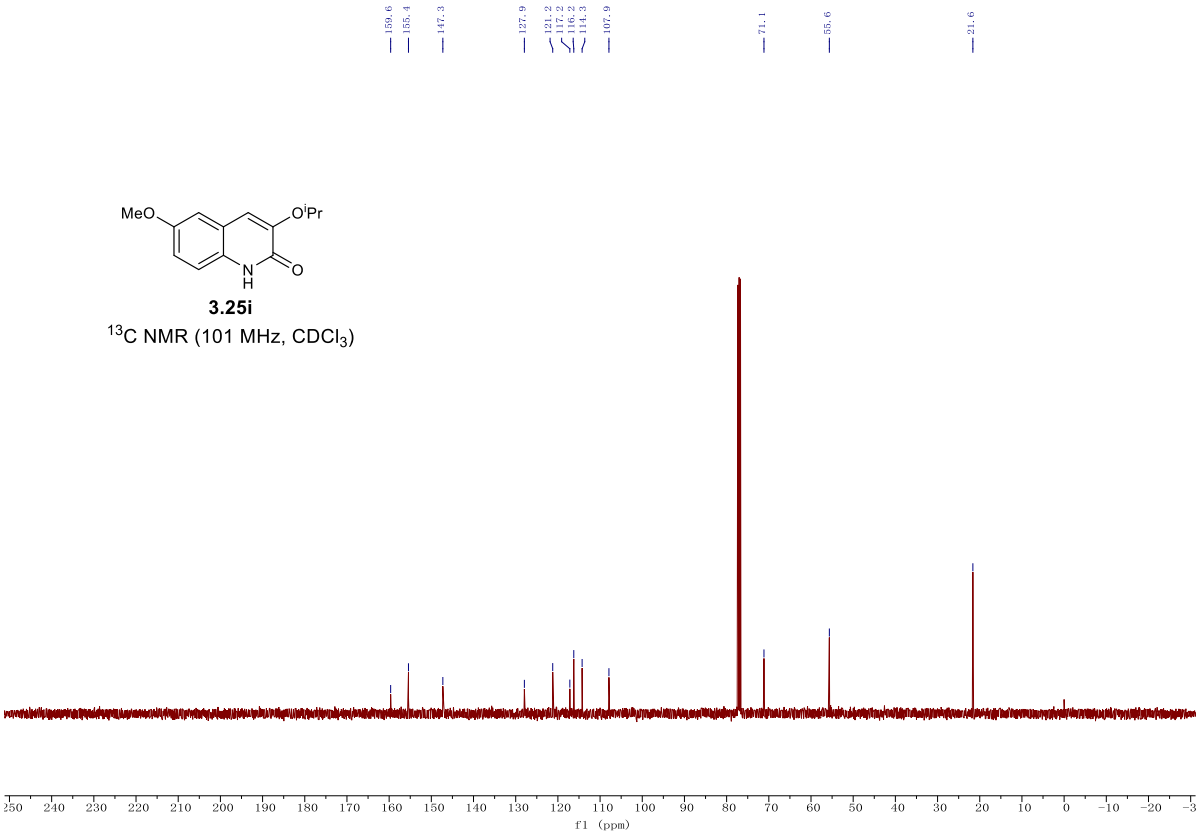

3.25i

^{13}C NMR (101 MHz, $CDCl_3$)

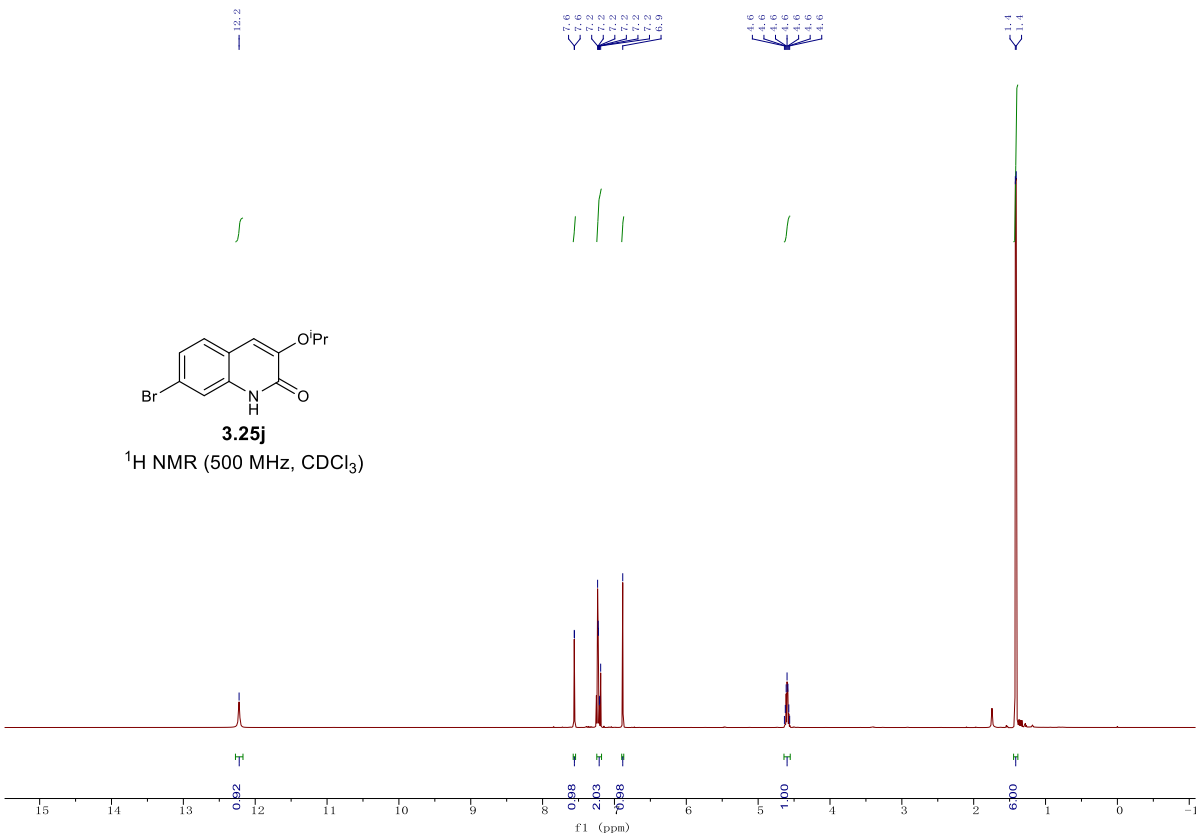

3.25j

^{1}H NMR (500 MHz, $CDCl_3$)

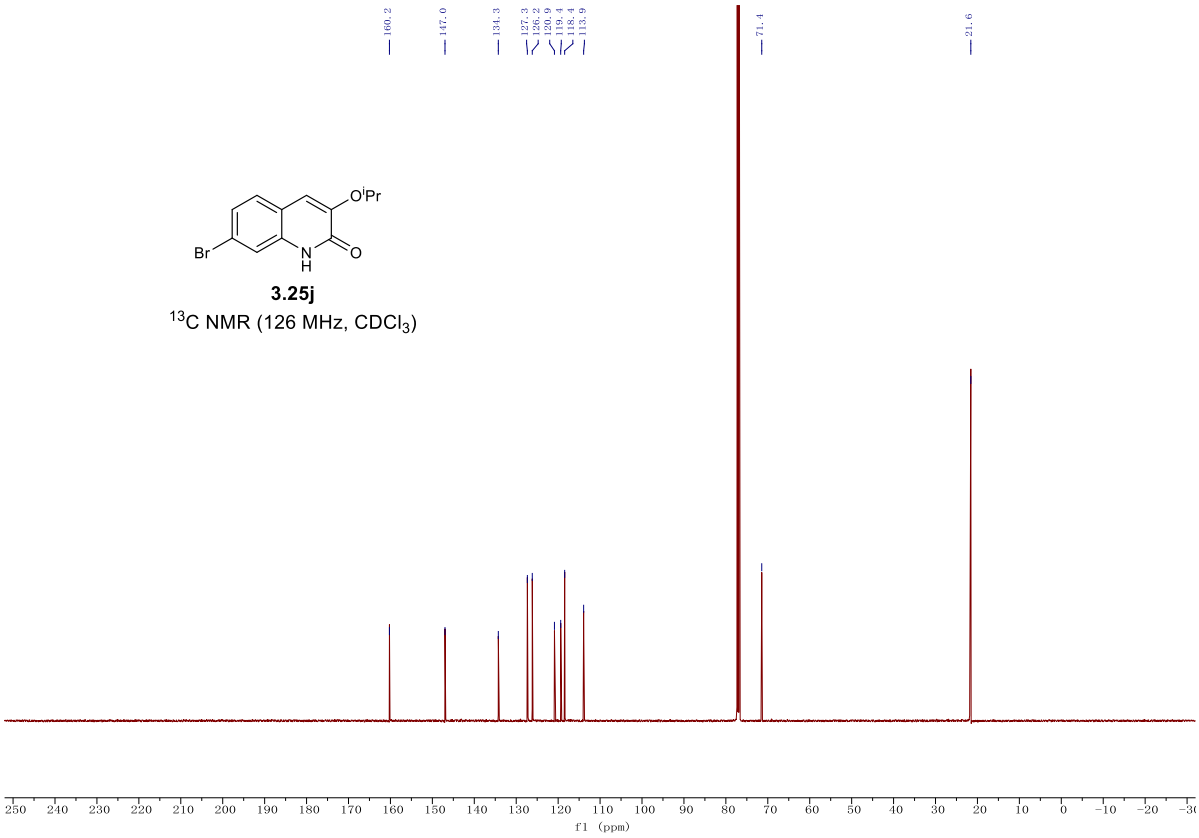

3.25j

^{13}C NMR (126 MHz, $CDCl_3$)

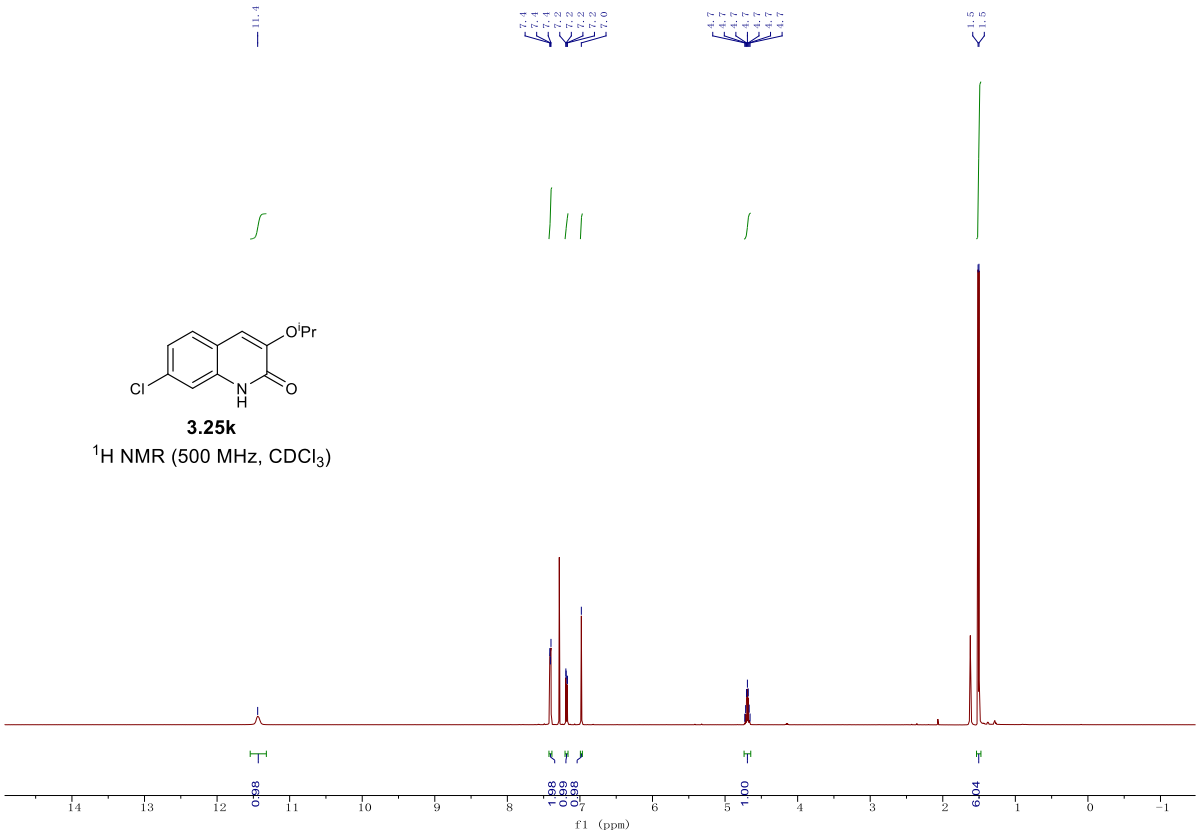

3.25k

^{1}H NMR (500 MHz, $CDCl_3$)

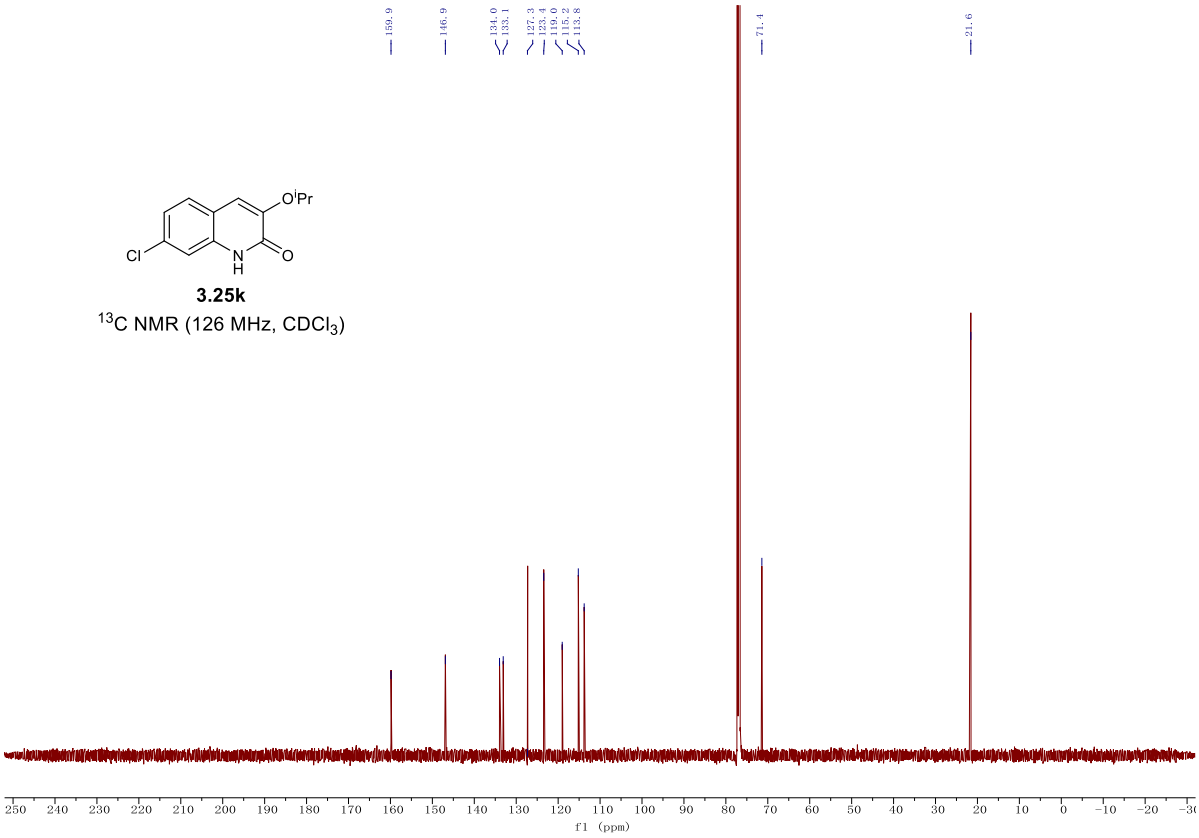

3.25k

^{13}C NMR (126 MHz, $CDCl_3$)

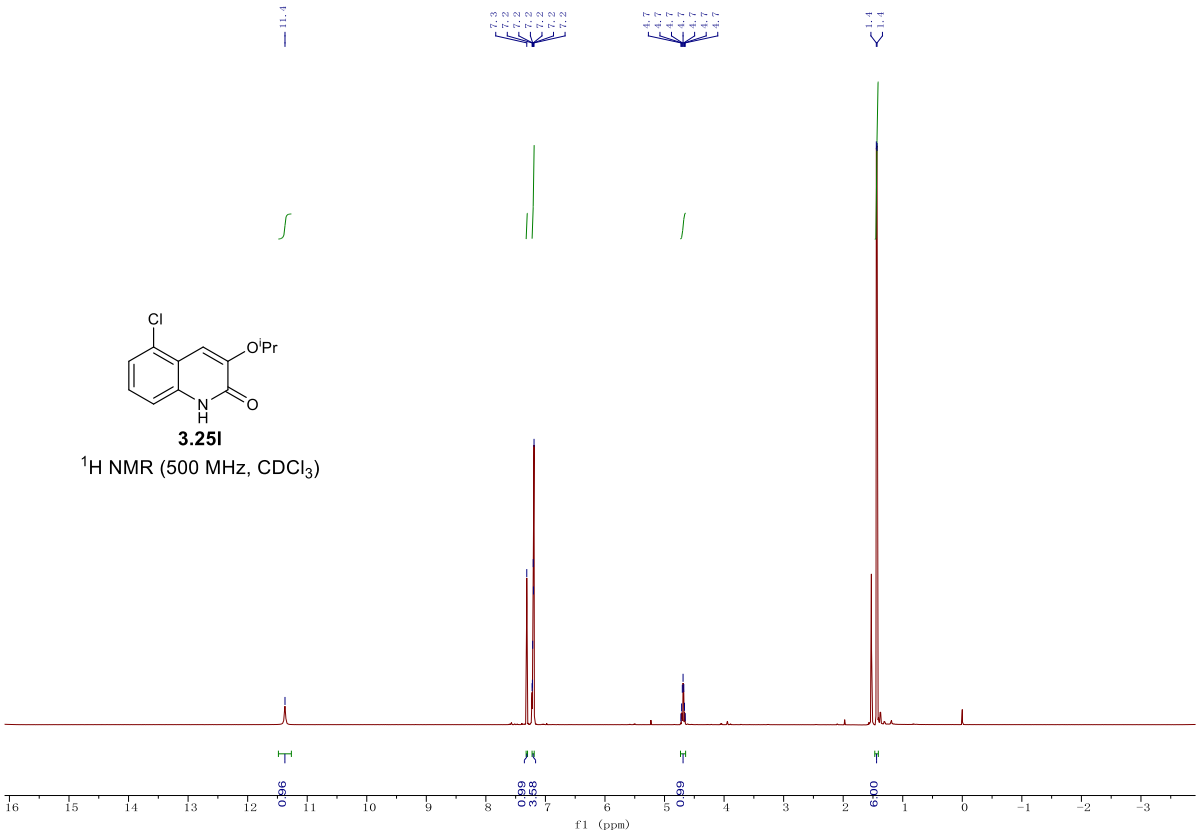

3.25l

^{1}H NMR (500 MHz, $CDCl_3$)

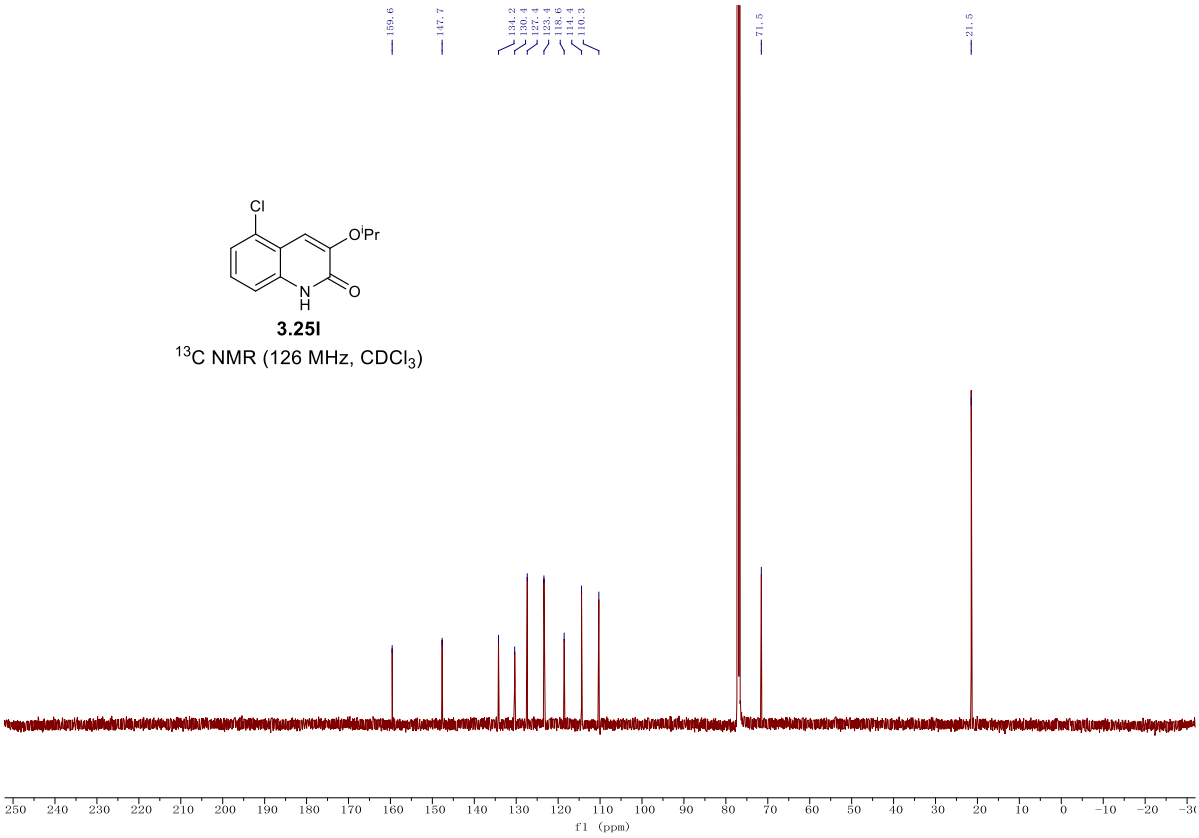

3.25l

^{13}C NMR (126 MHz, $CDCl_3$)

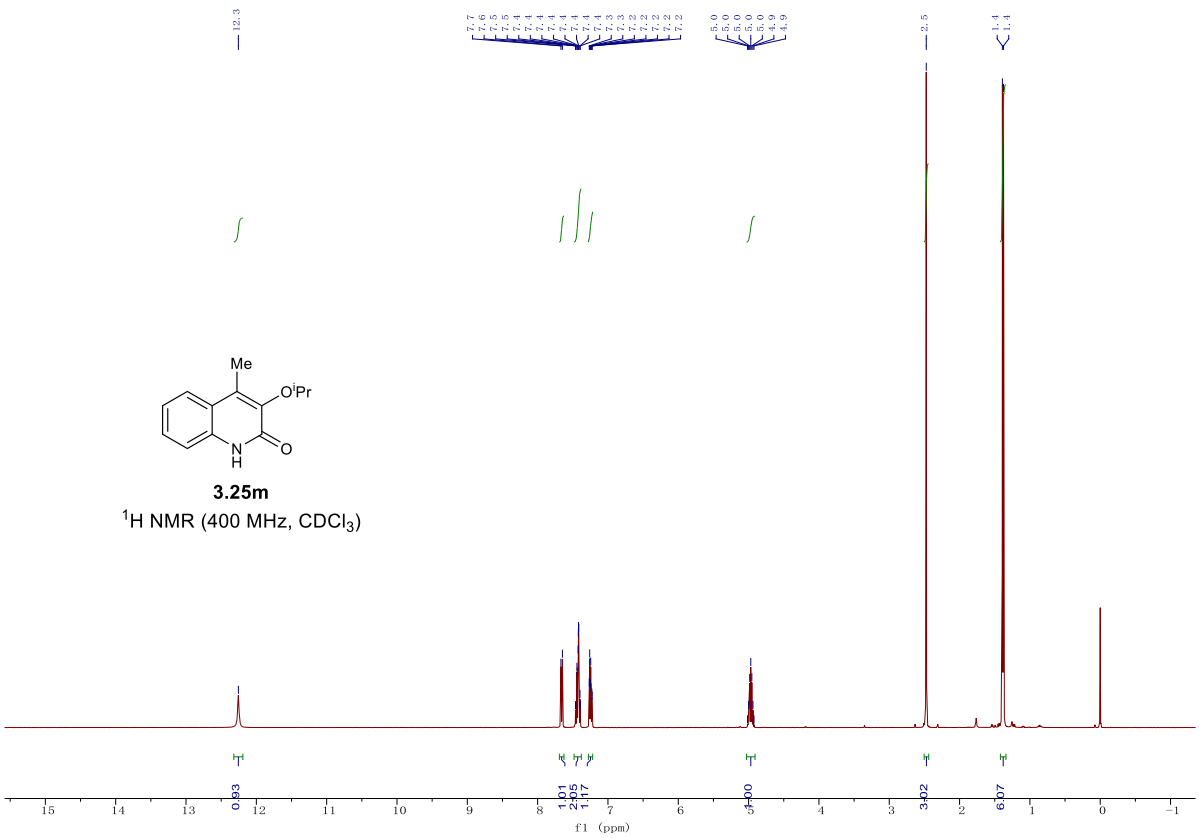

3.25m

^{1}H NMR (400 MHz, $CDCl_3$)

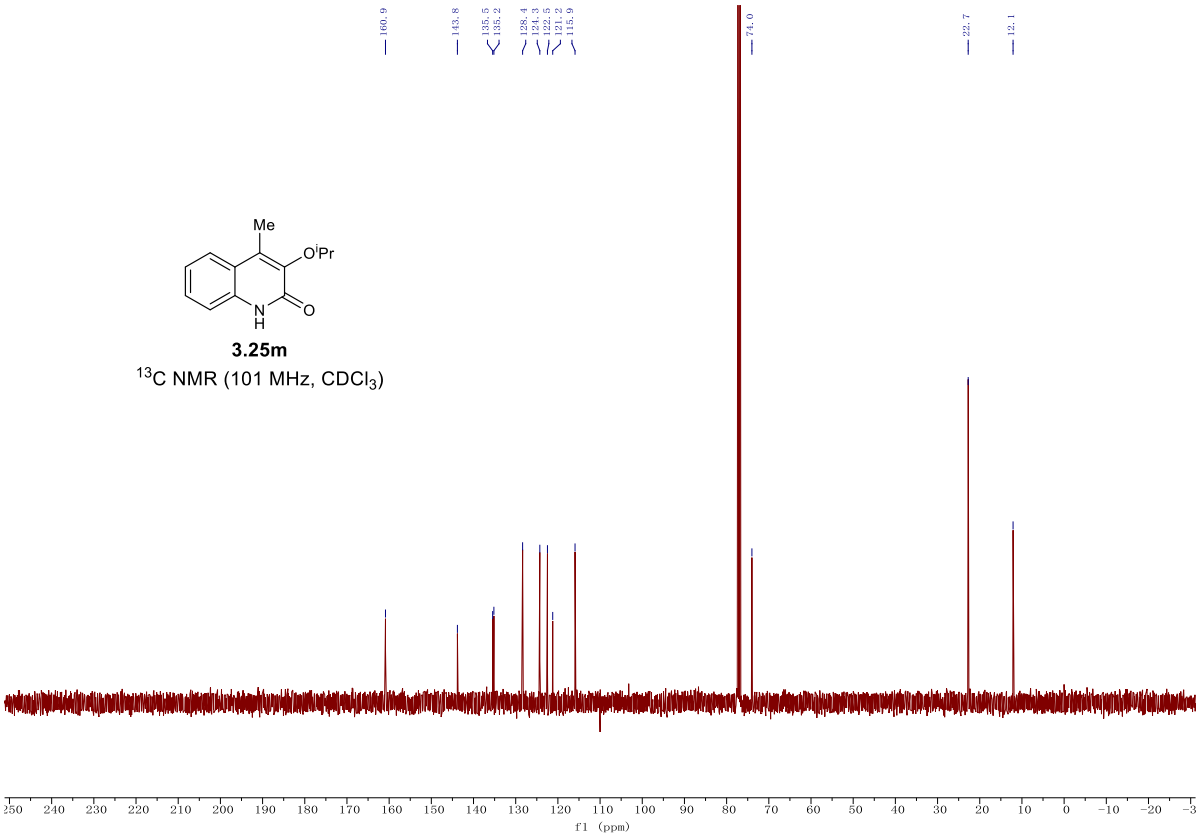

3.25m

^{13}C NMR (101 MHz, $CDCl_3$)

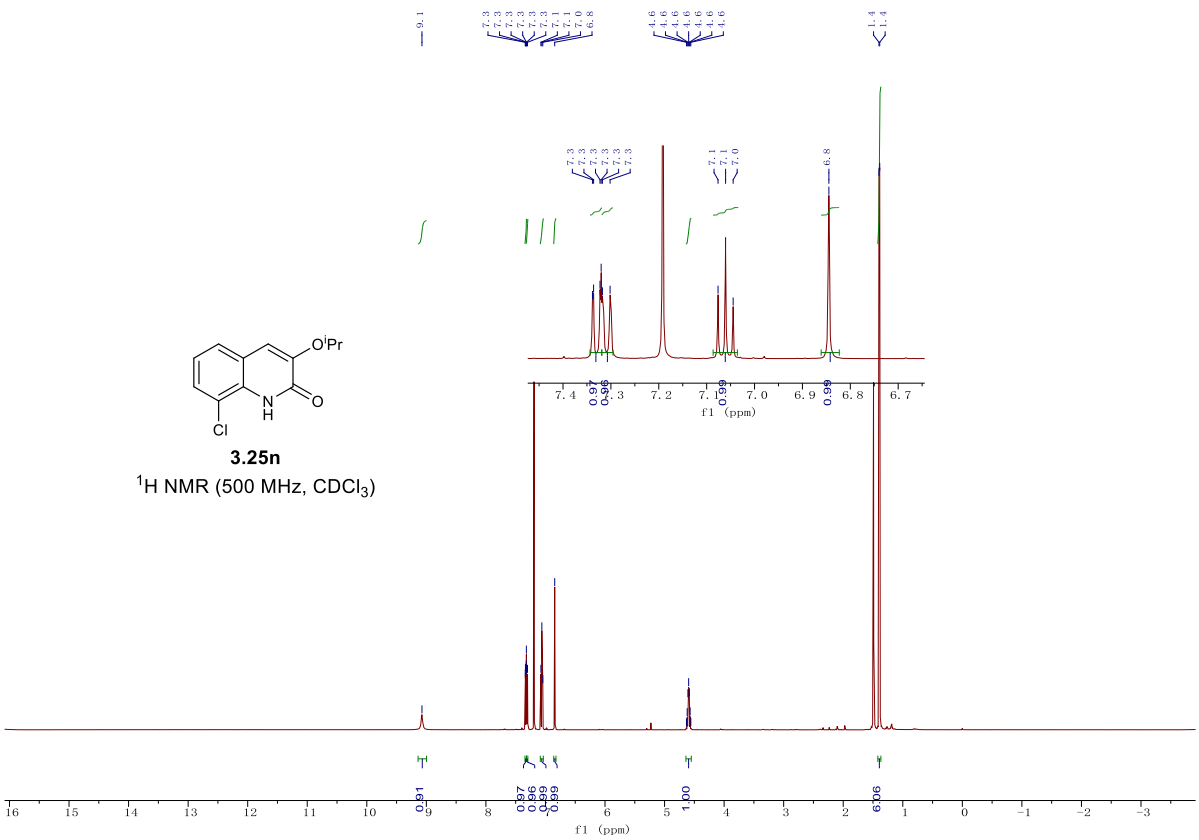

3.25n

^{1}H NMR (500 MHz, $CDCl_3$)

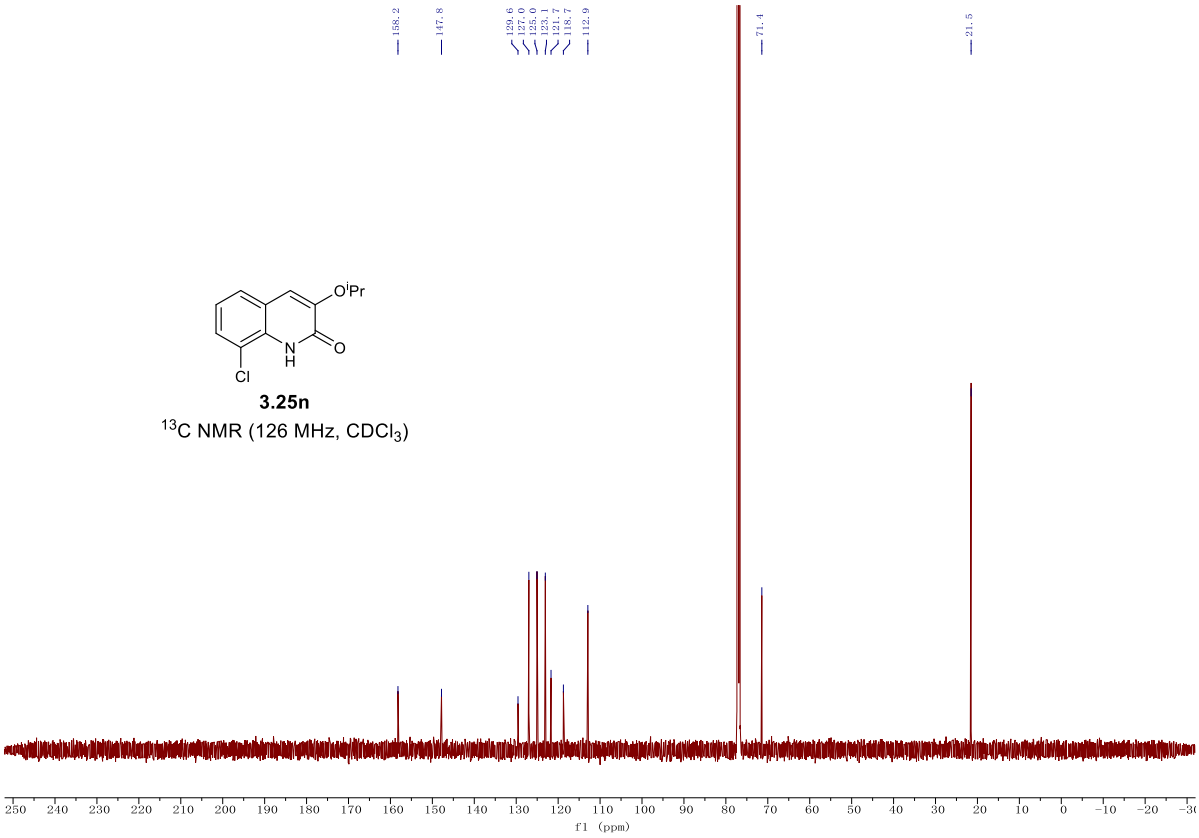

3.25n

^{13}C NMR (126 MHz, $CDCl_3$)

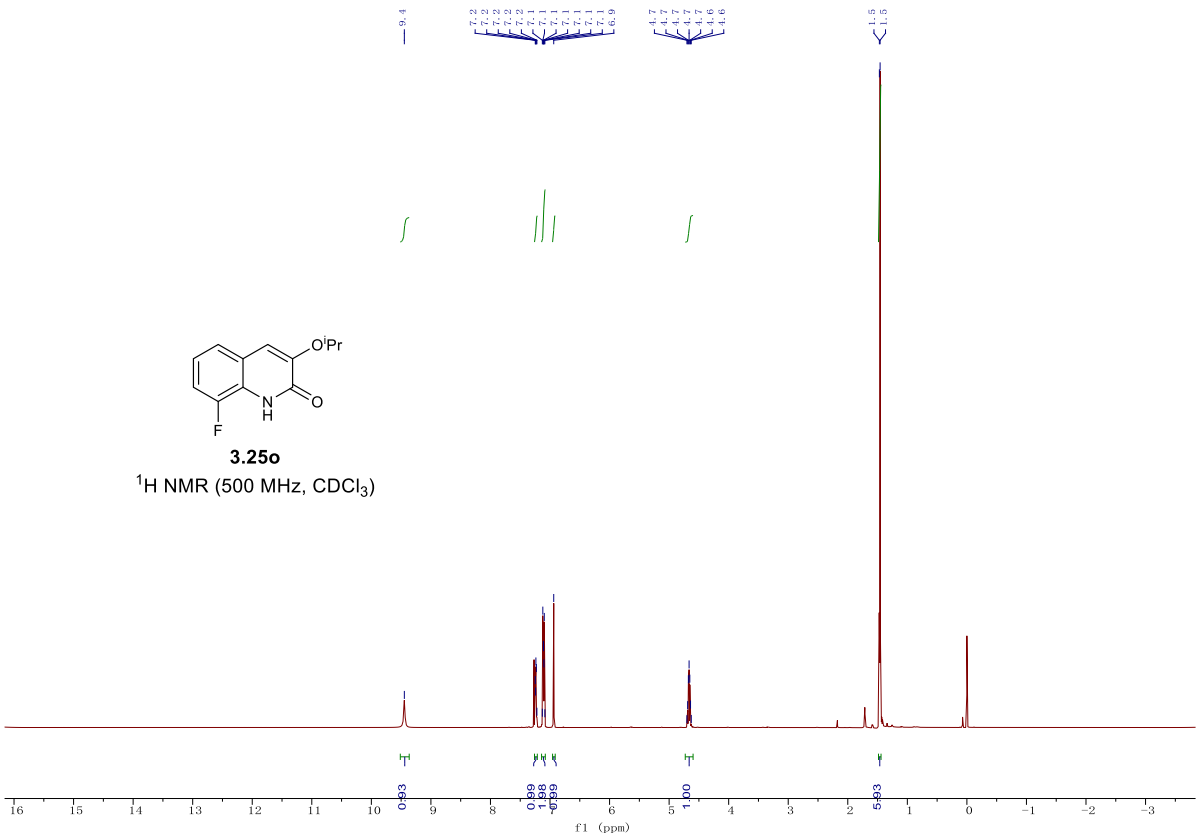

3.25o

^{1}H NMR (500 MHz, $CDCl_3$)

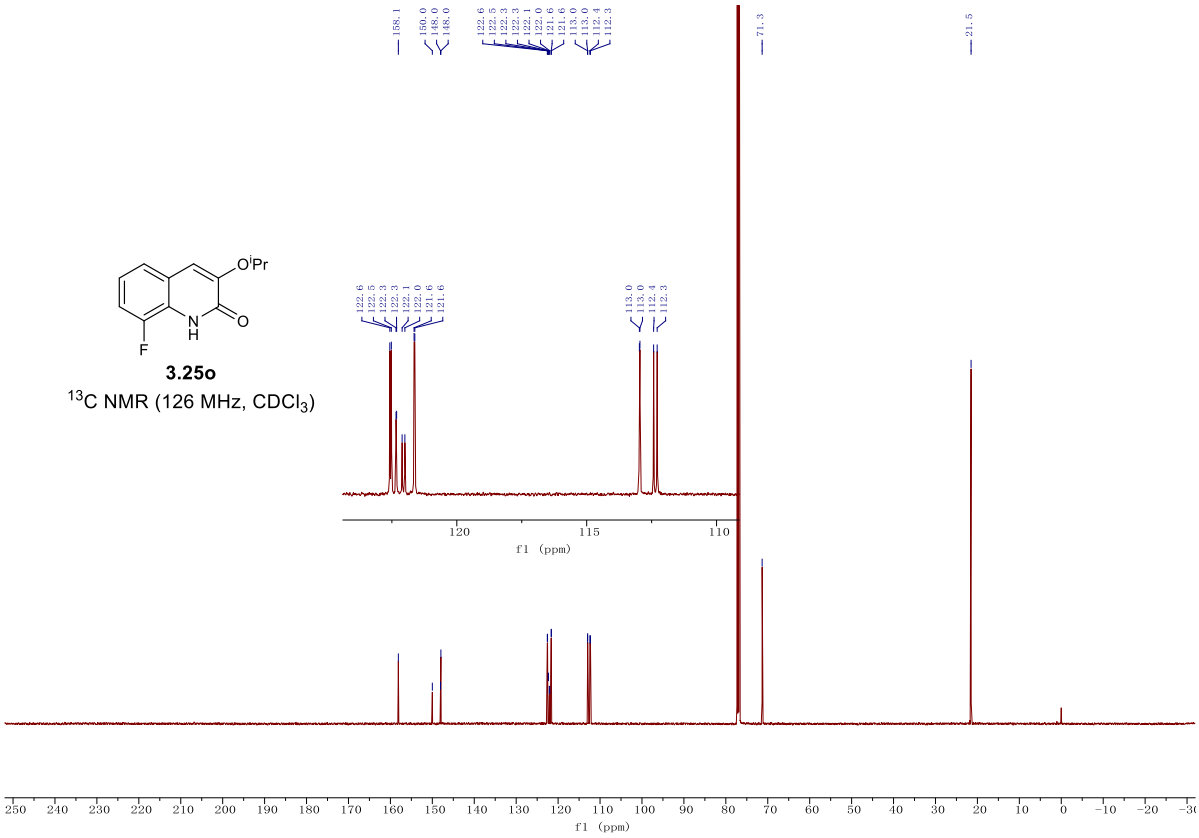
158.1
150.0
148.0
148.0
122.6
122.5
122.3
122.3
122.3
122.1
122.0
121.6
121.6
121.6
113.0
113.0
112.4
112.3
71.3
21.5
O^{i}Pr
N
H
O
F
3.25o
^{13}C NMR (126 MHz, CDCl$_3$)
f1 (ppm)

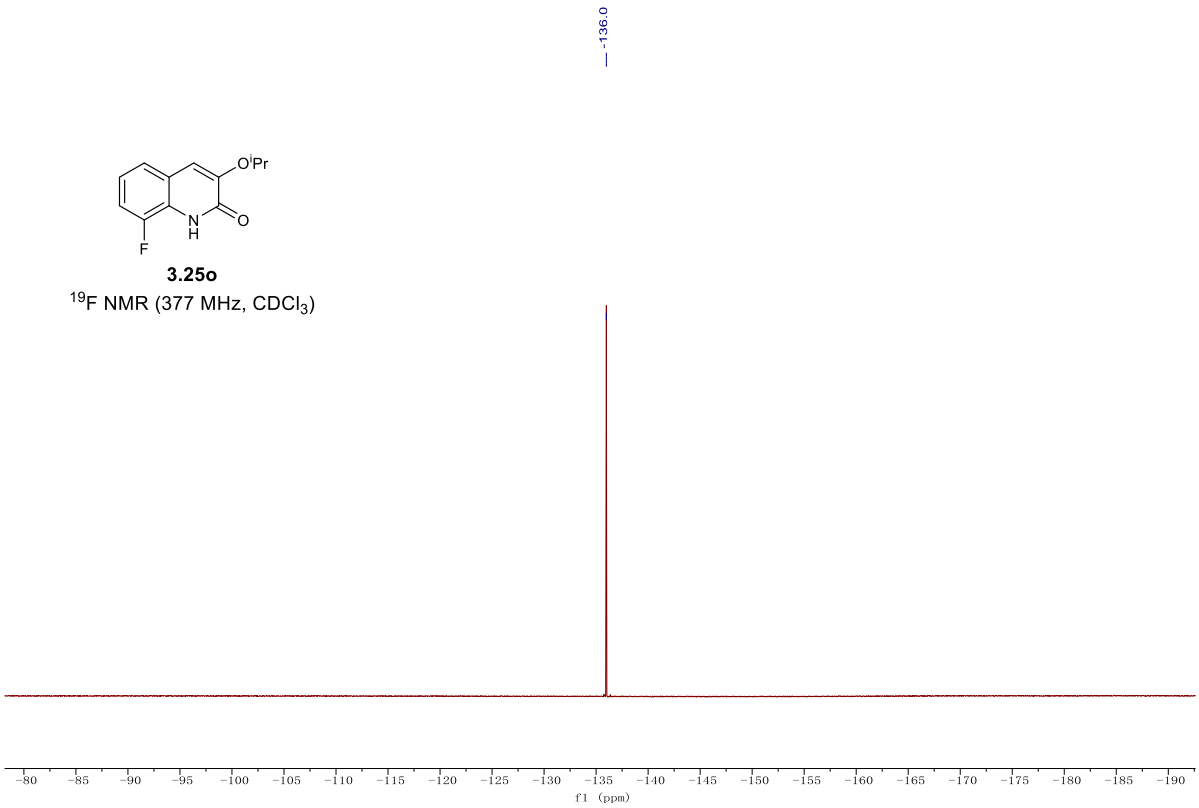
-136.0
O^{i}Pr
N
H
O
F
3.25o
^{19}F NMR (377 MHz, CDCl$_3$)
f1 (ppm)

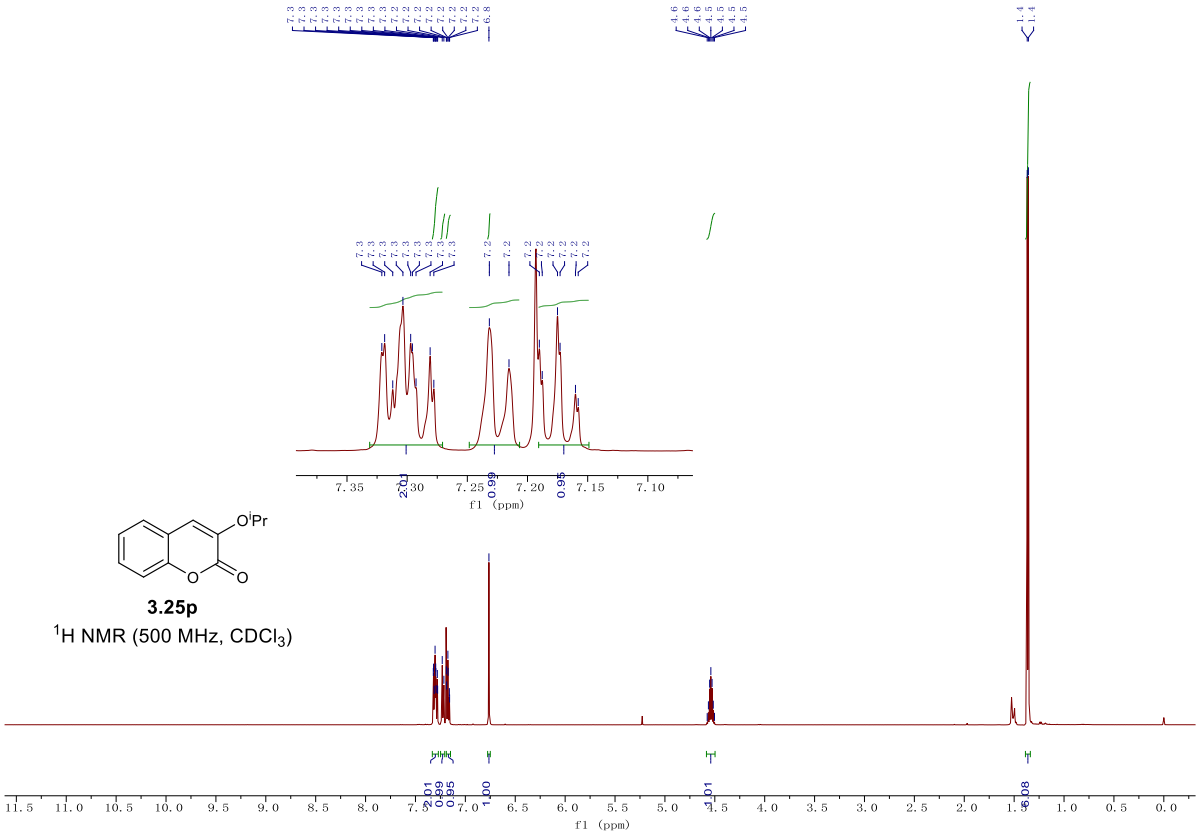
O^{i}Pr
O
O
3.25p
^{1}H NMR (500 MHz, $CDCl_3$)
f1 (ppm)

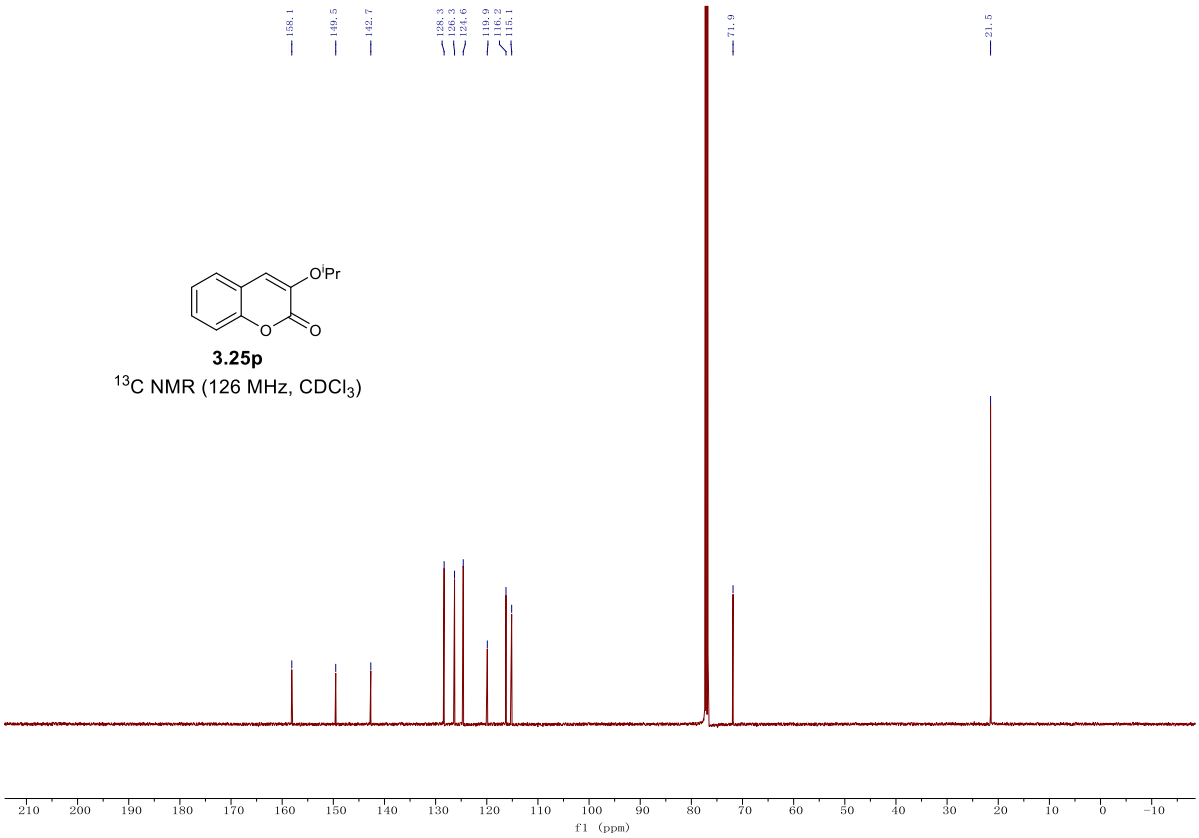
O^{i}Pr
O
O
3.25p
^{13}C NMR (126 MHz, $CDCl_3$)
f1 (ppm)

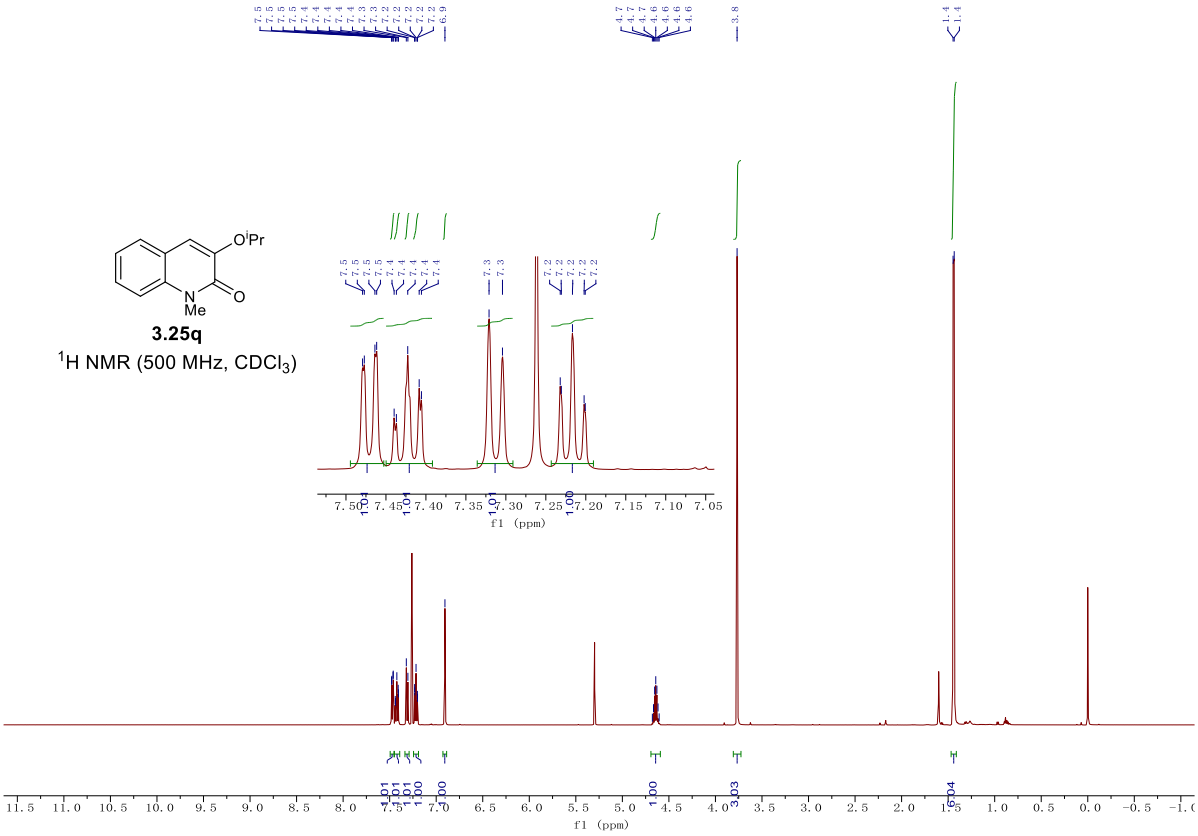
O^{i}Pr
N
Me
O
3.25q
^{1}H NMR (500 MHz, CDCl$_3$)
f1 (ppm)

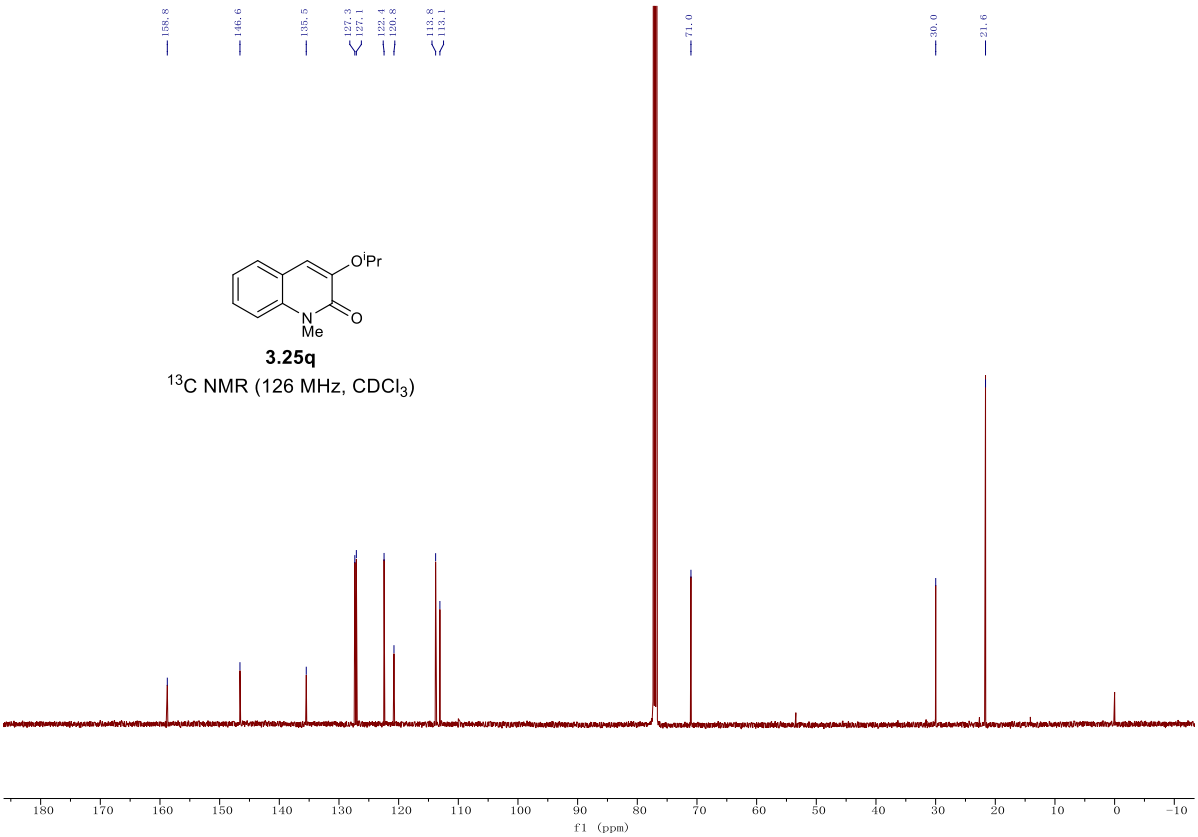
O^{i}Pr
N
Me
O
3.25q
^{13}C NMR (126 MHz, CDCl$_3$)
f1 (ppm)

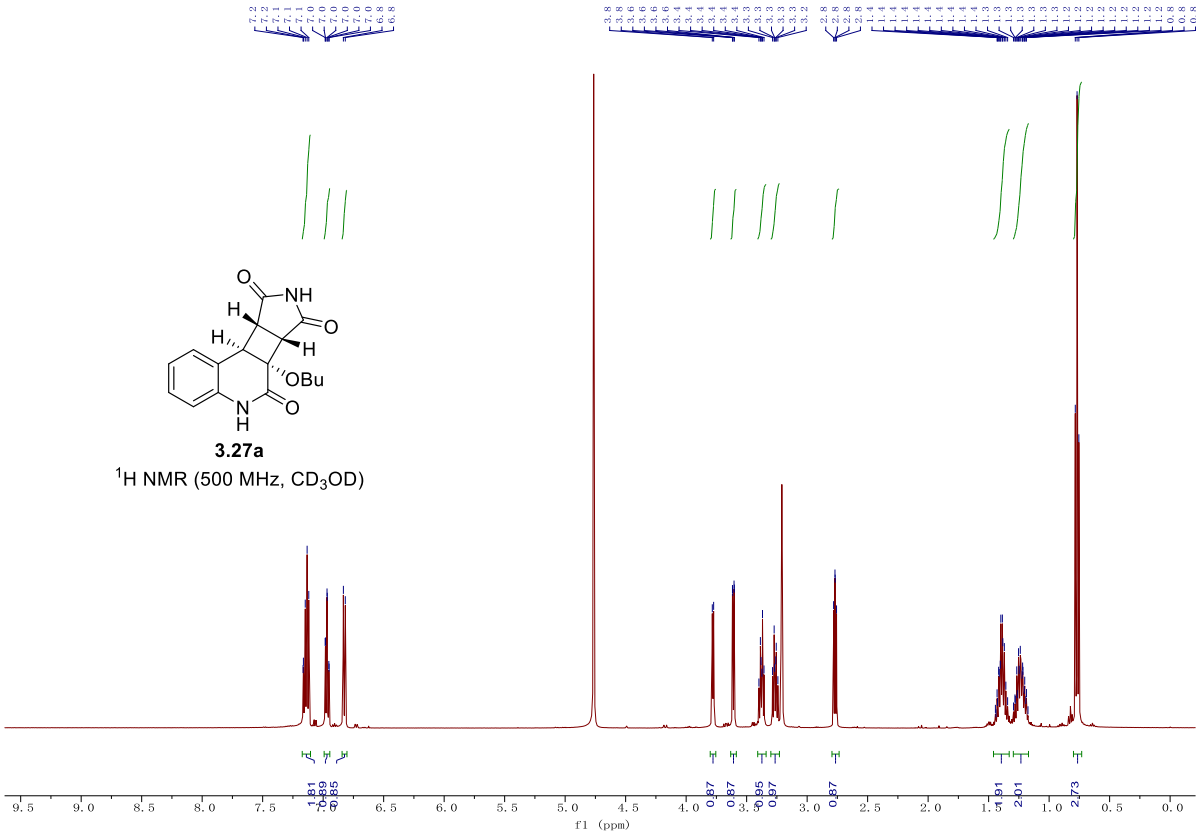

3.27a

^{1}H NMR (500 MHz, CD_3OD)

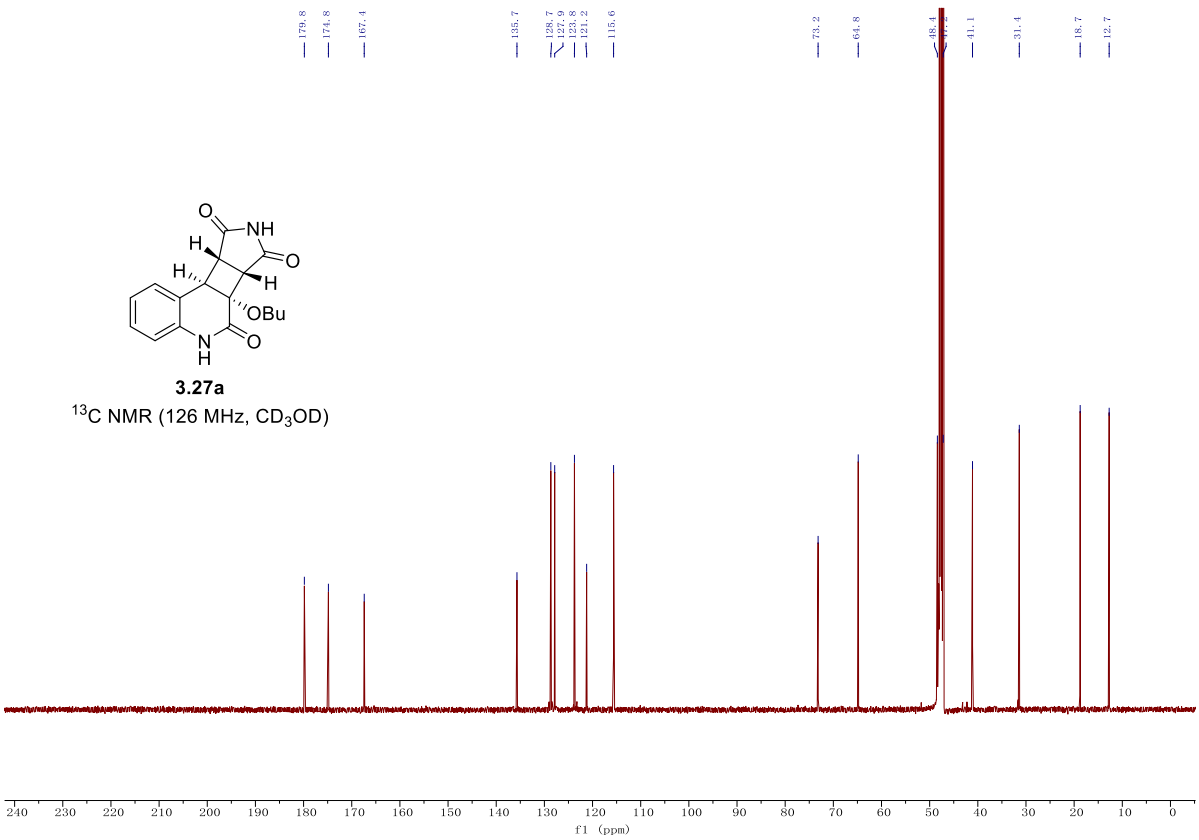

3.27a

^{13}C NMR (126 MHz, CD_3OD)

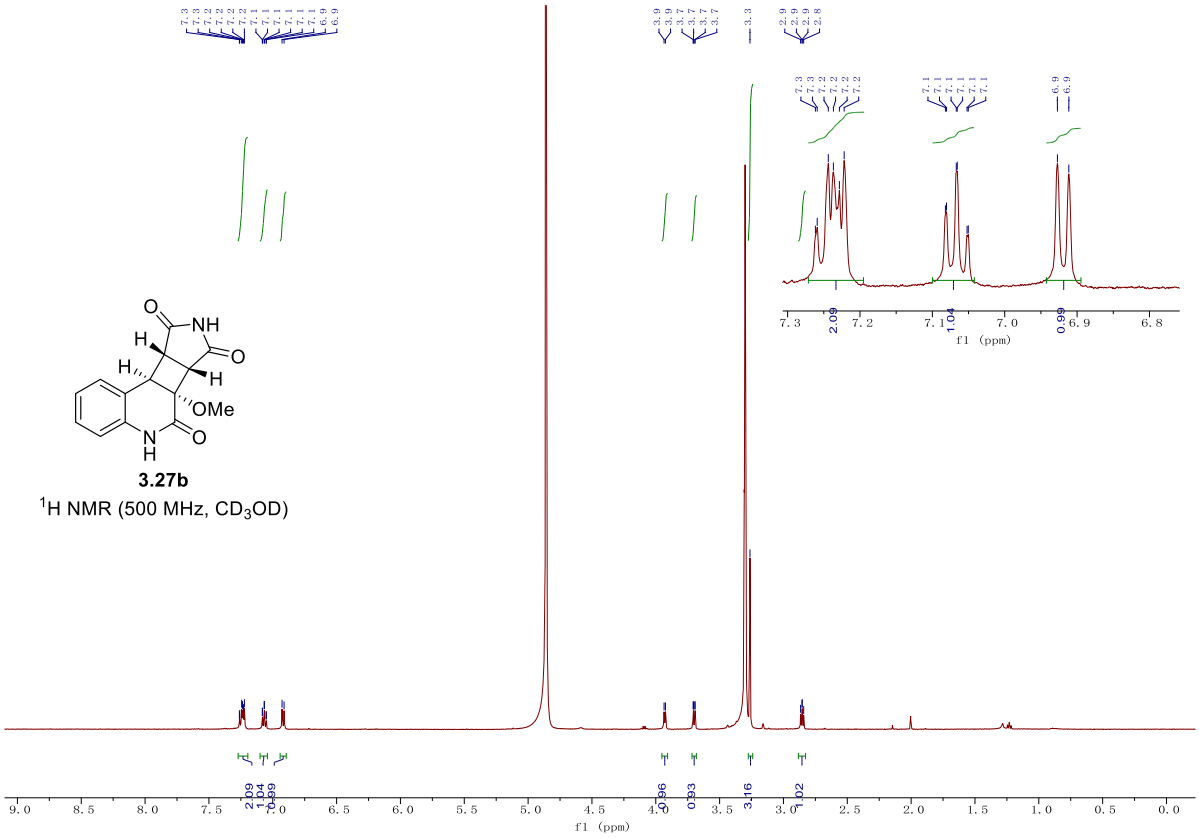

3.27b

^{1}H NMR (500 MHz, CD_3OD)

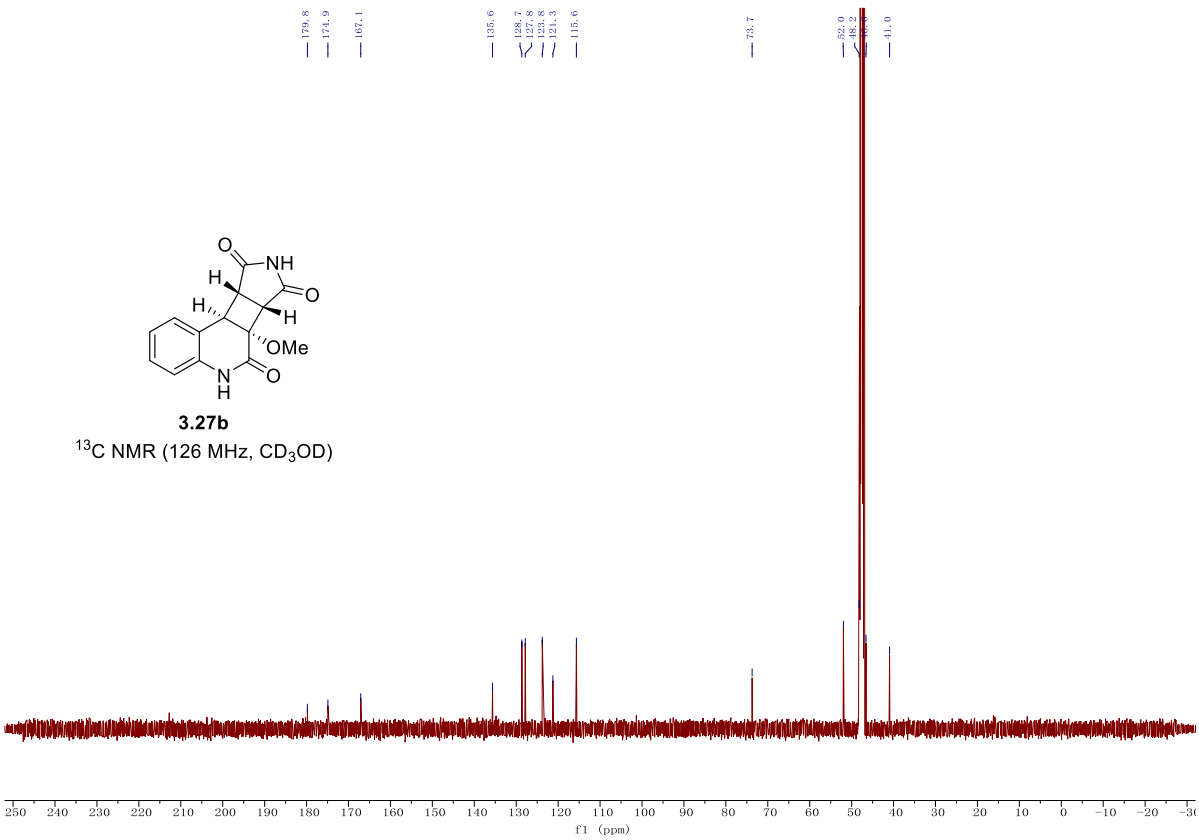

3.27b

^{13}C NMR (126 MHz, CD_3OD)

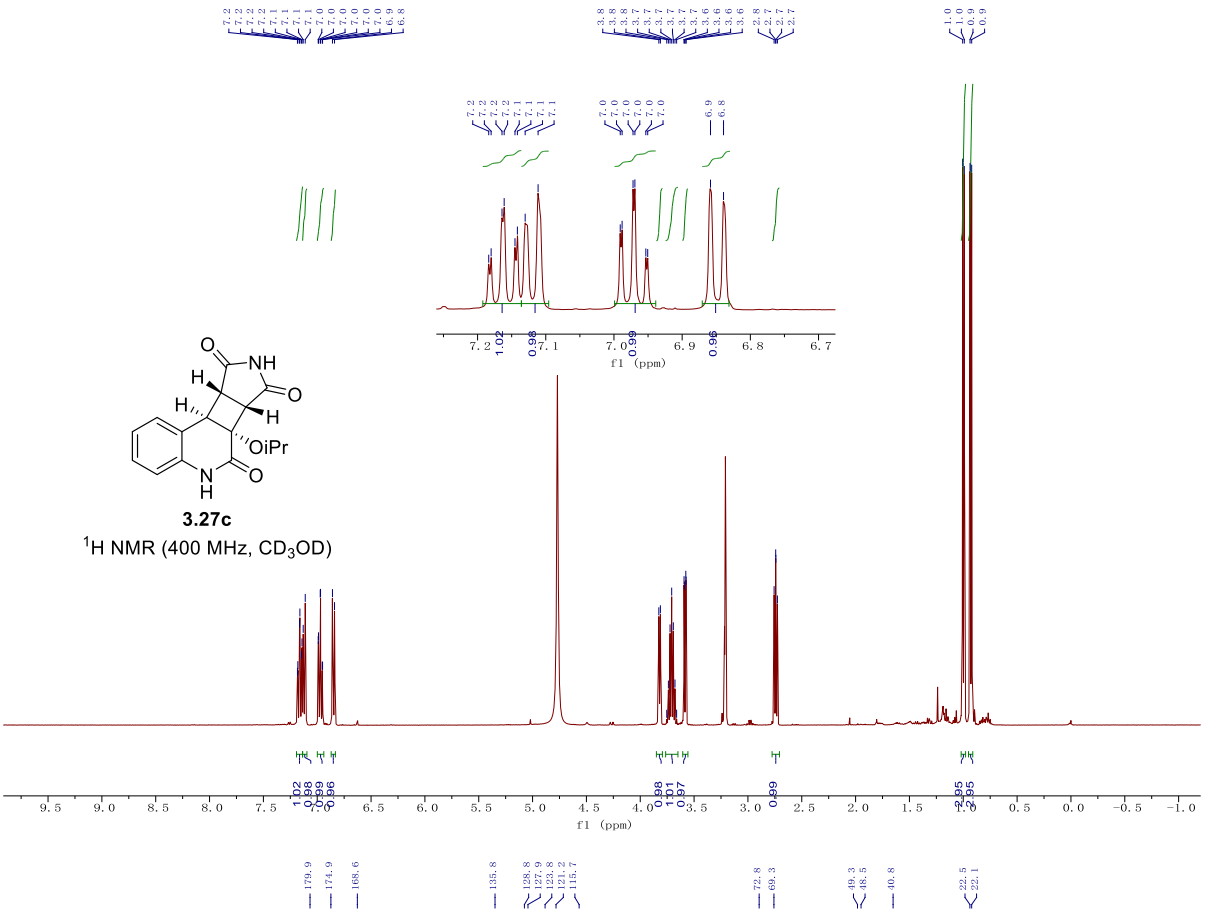

3.27c

^{1}H NMR (400 MHz, CD_3OD)

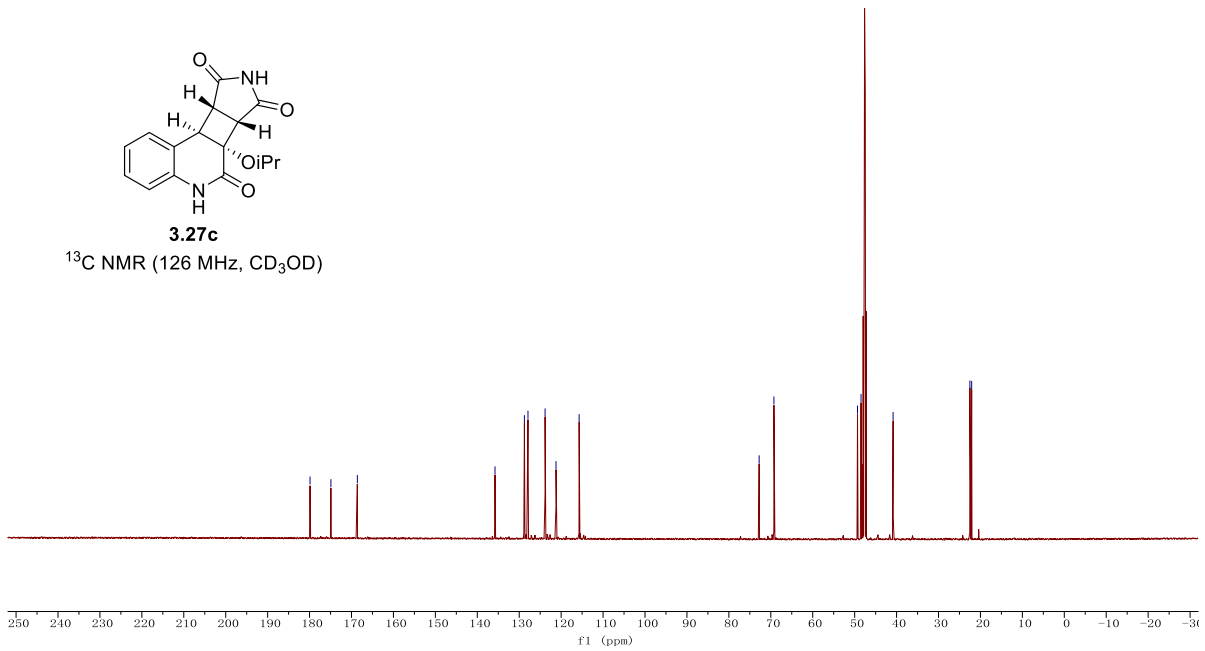

3.27c

^{13}C NMR (126 MHz, CD_3OD)

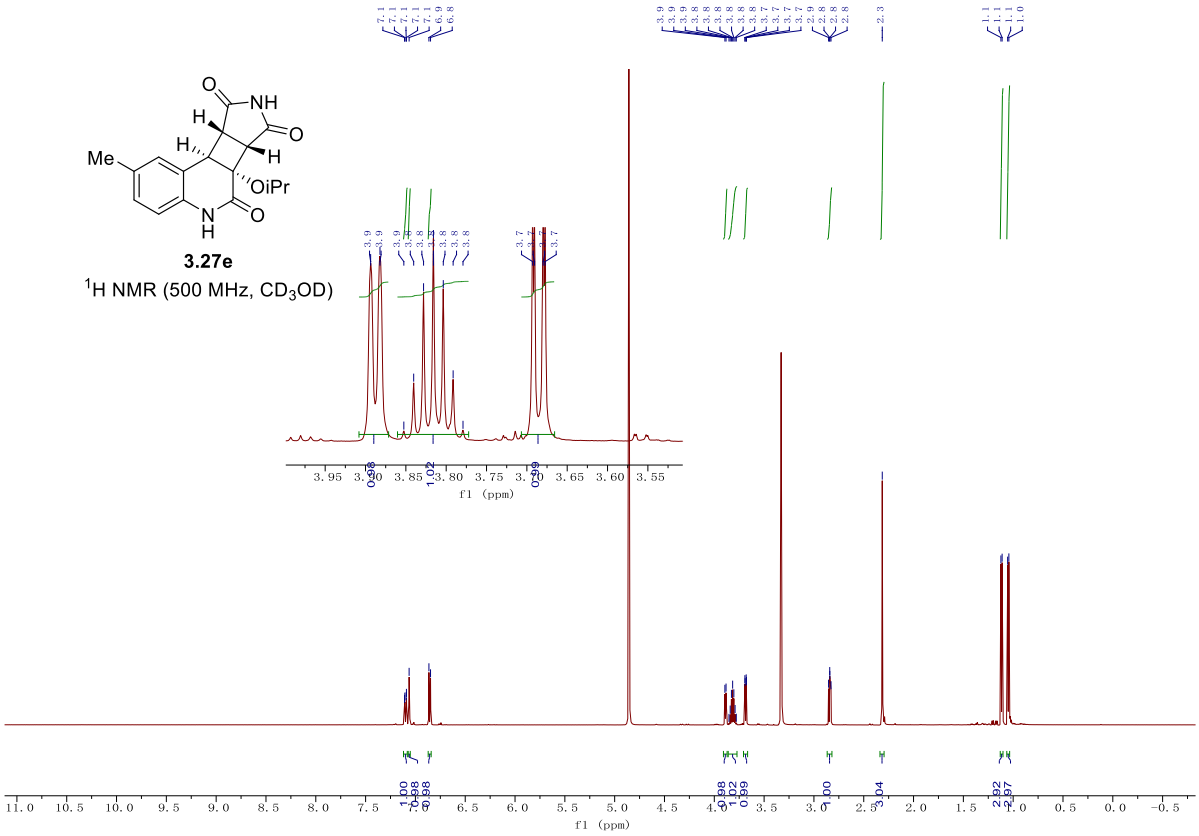
Me
O
NH
H
O
H
H
OiPr
N
H
O
3.27e
1H NMR (500 MHz, CD3OD)
f1 (ppm)

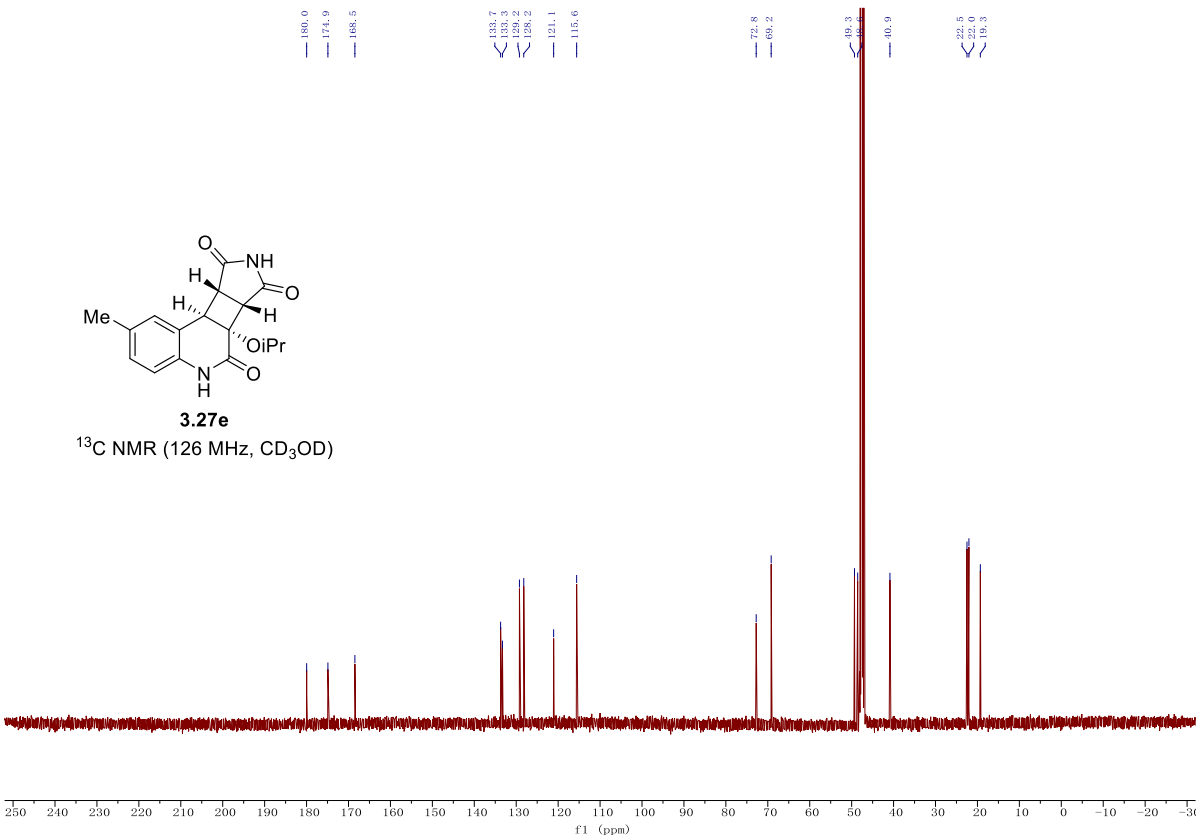
Me
O
NH
H
O
H
H
OiPr
N
H
O
3.27e
13C NMR (126 MHz, CD3OD)
f1 (ppm)

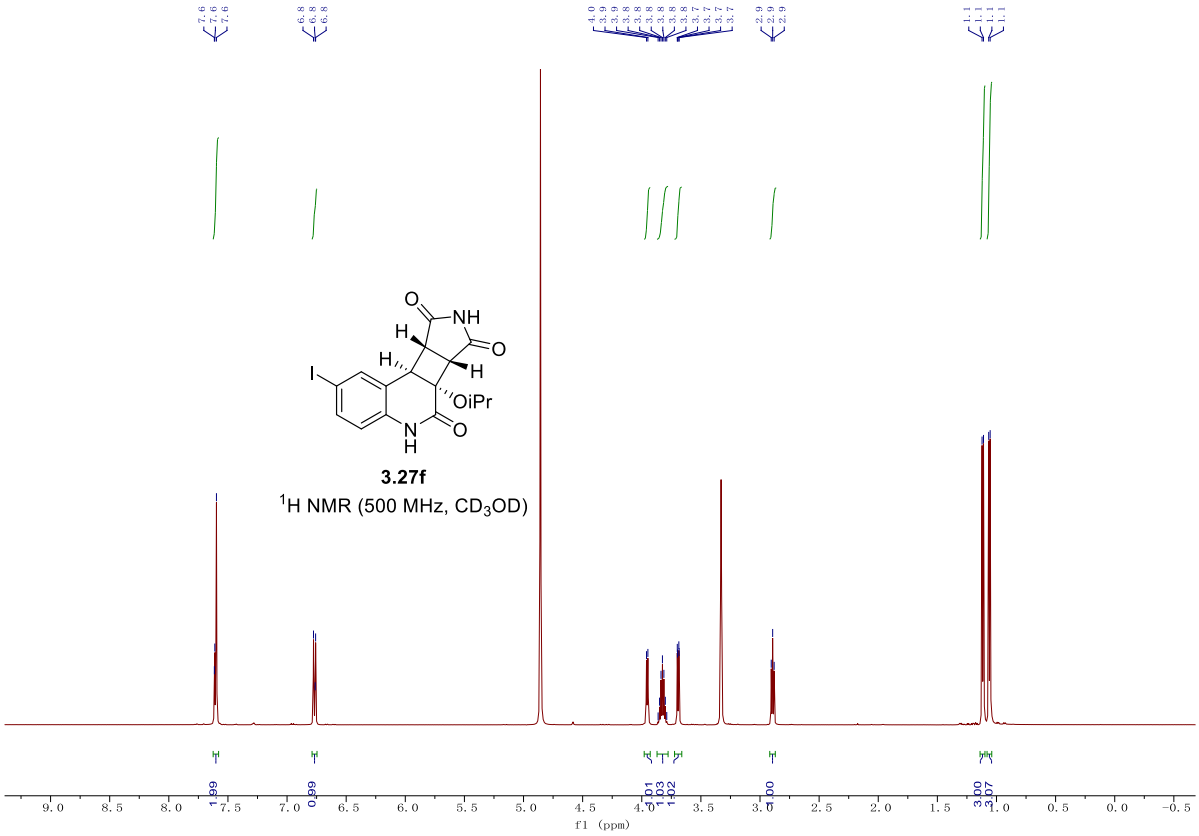

3.27f

^{1}H NMR (500 MHz, CD_3OD)

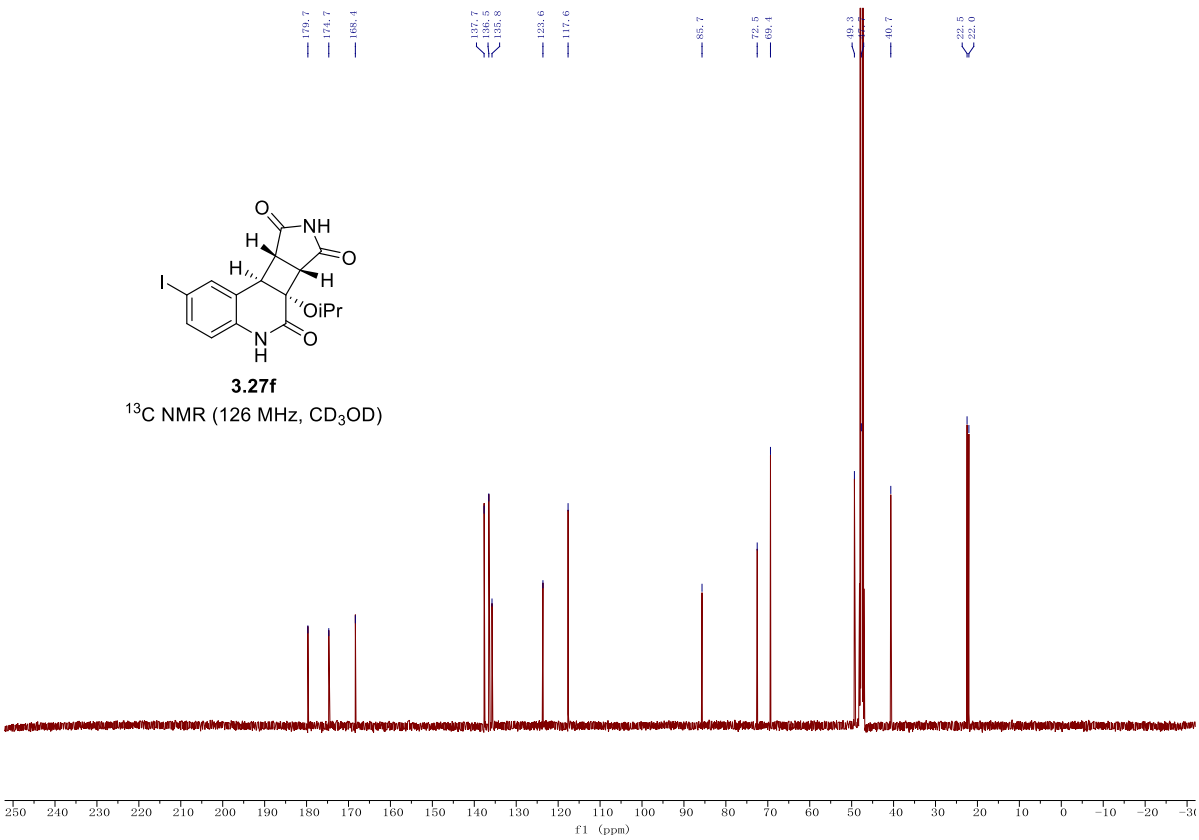

3.27f

^{13}C NMR (126 MHz, CD_3OD)

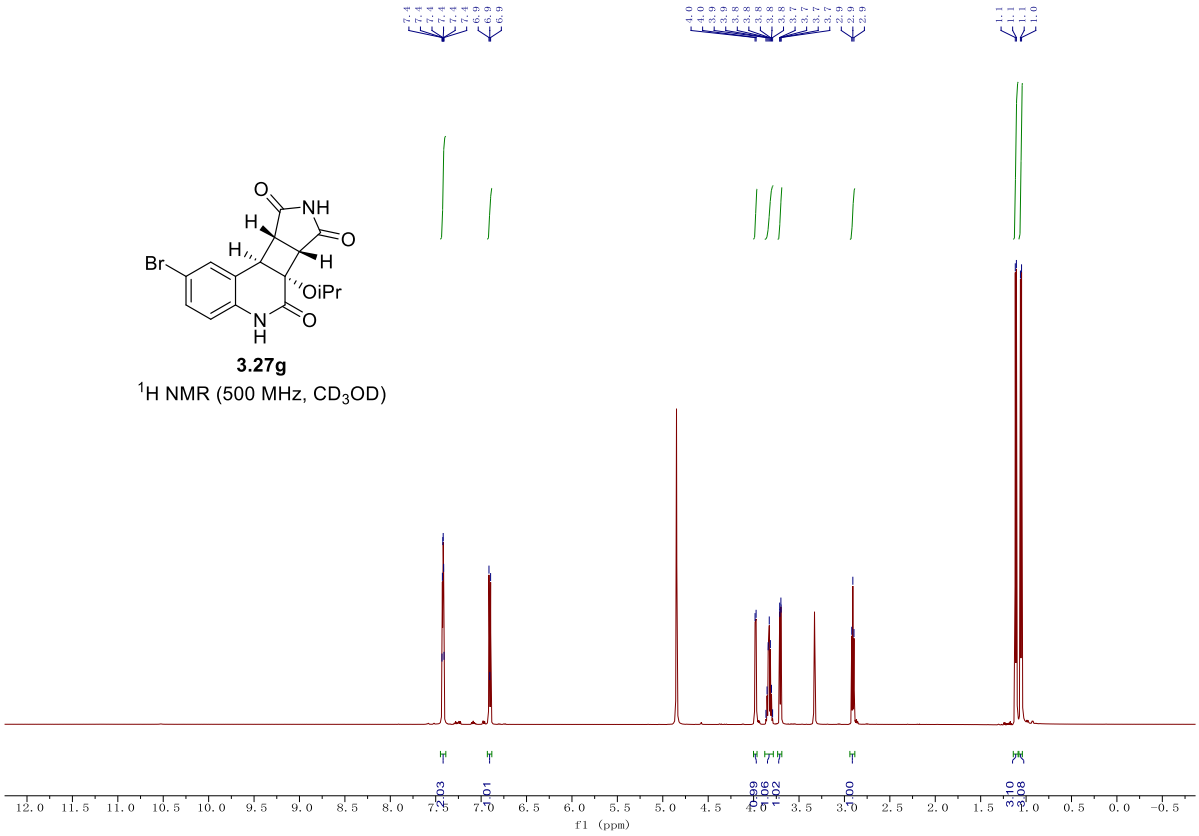

3.27g

^{1}H NMR (500 MHz, CD_3OD)

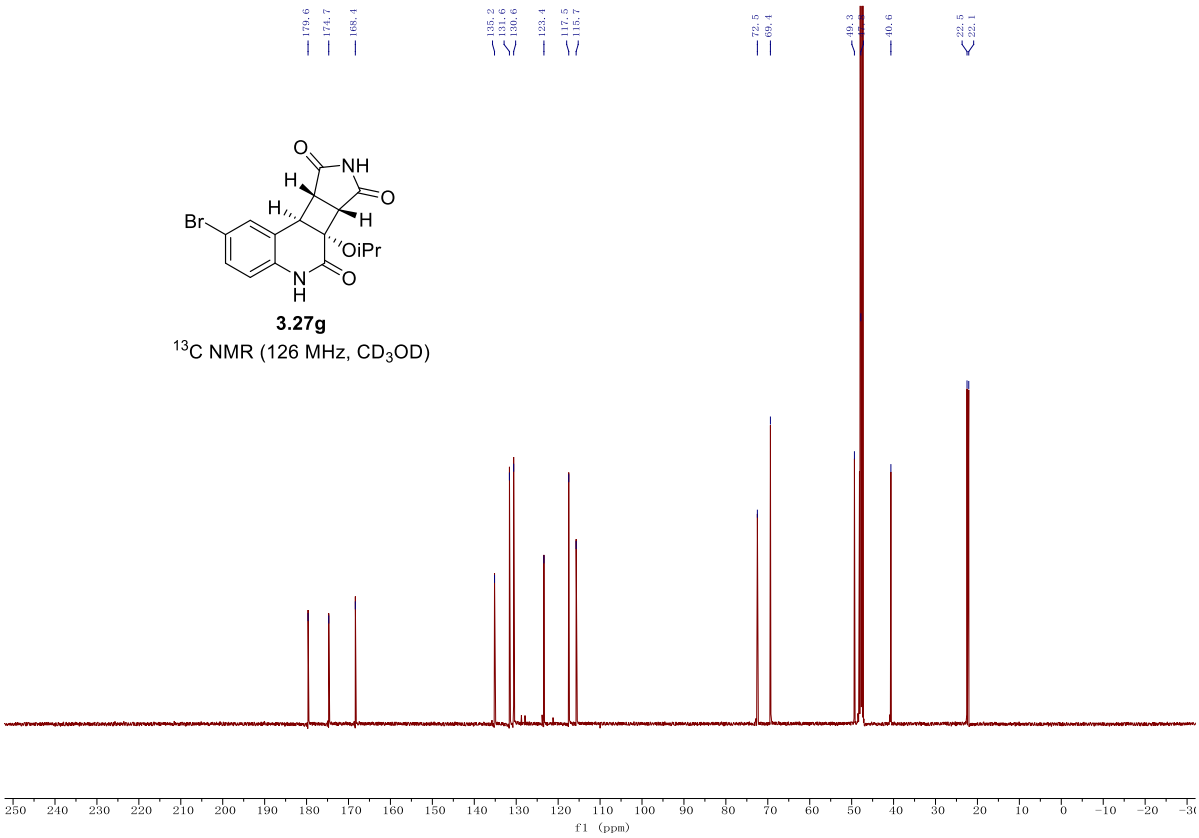

3.27g

^{13}C NMR (126 MHz, CD_3OD)

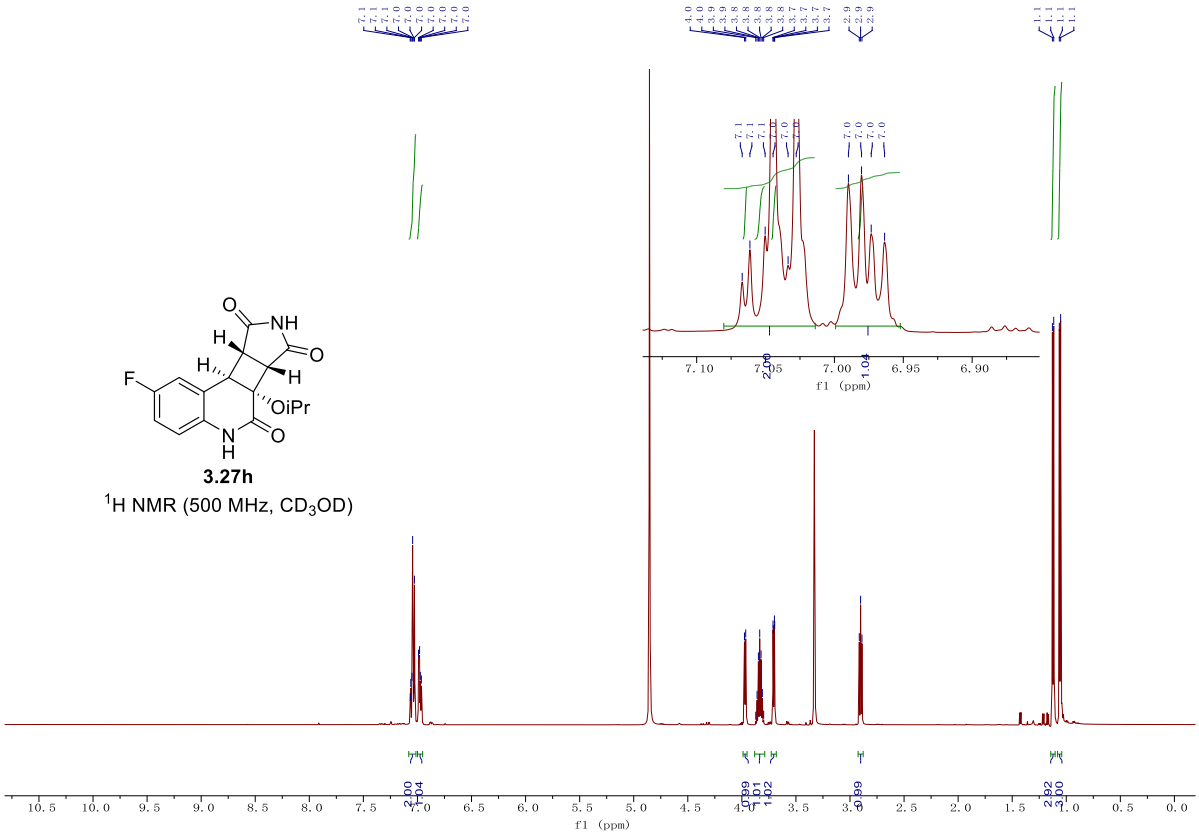
3.27h
1H NMR (500 MHz, CD3OD)
f1 (ppm)

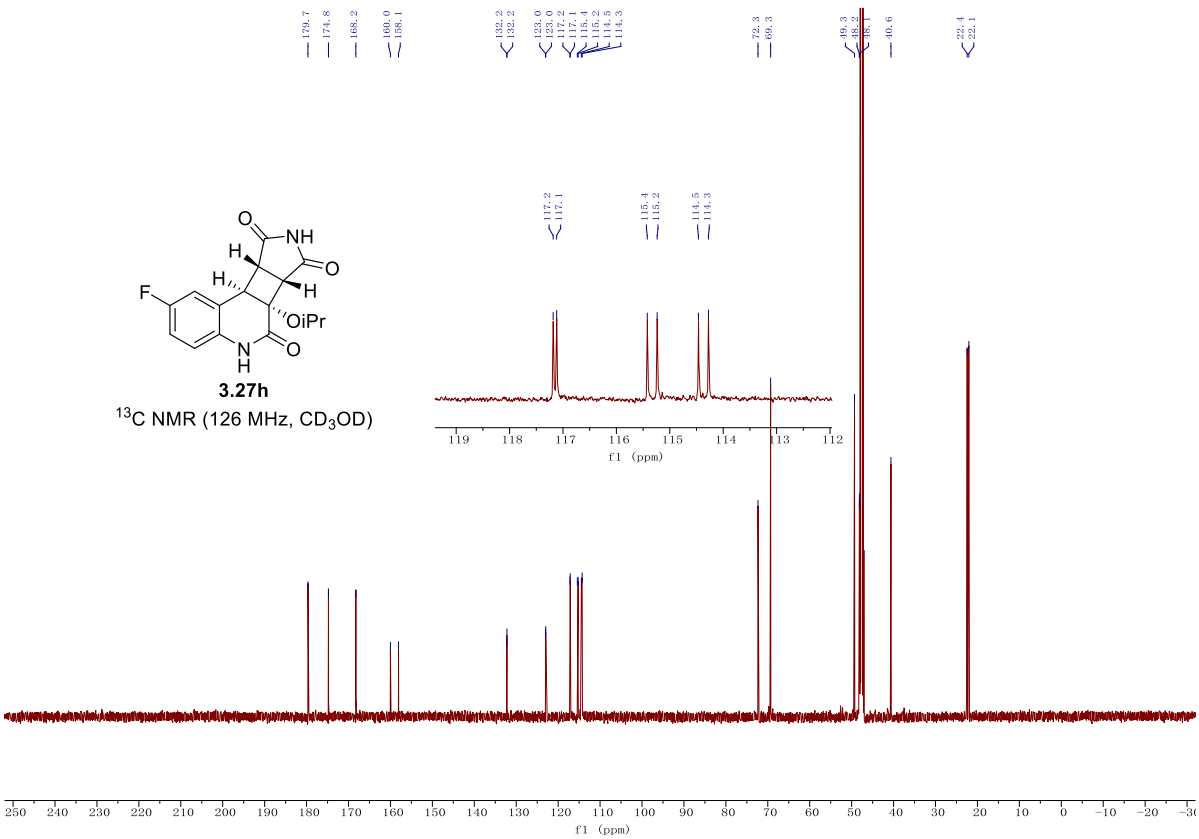
3.27h
13C NMR (126 MHz, CD3OD)
f1 (ppm)

3.27h

^{19}F NMR (377 MHz, CD_3OD)

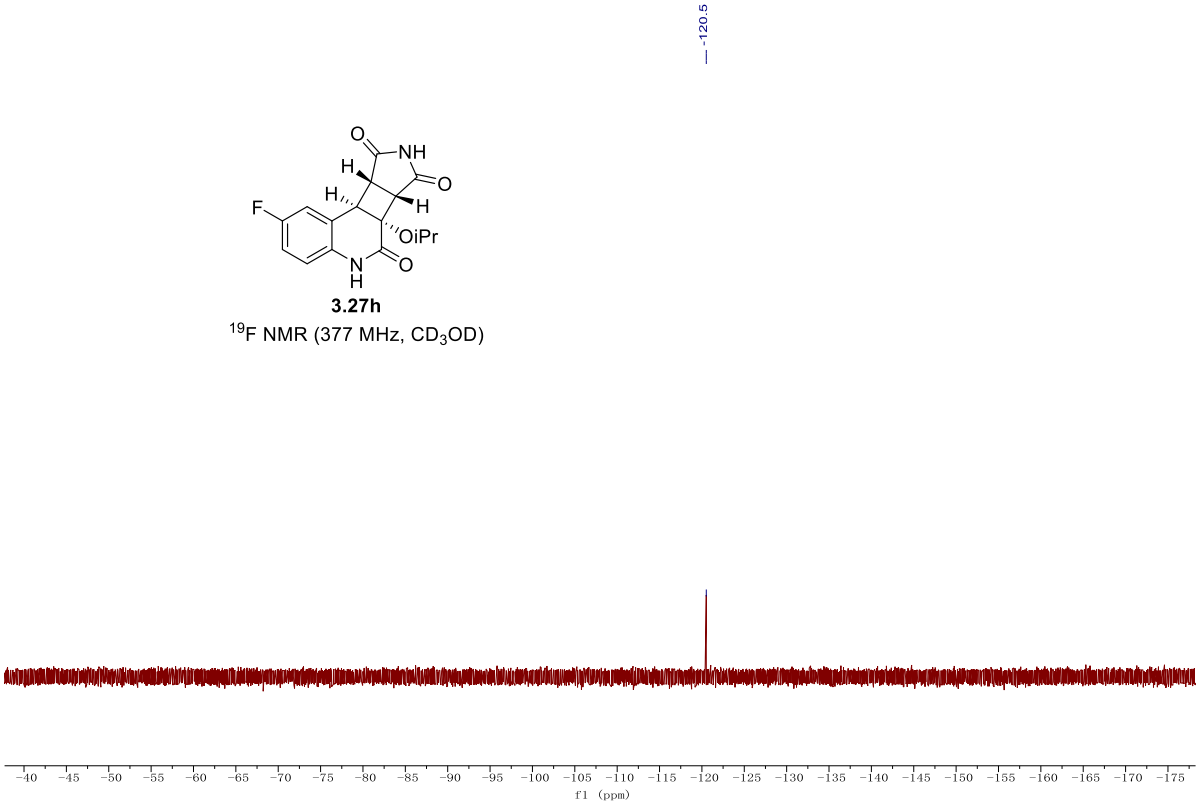

3.27i

^{1}H NMR (500 MHz, CD_3OD)

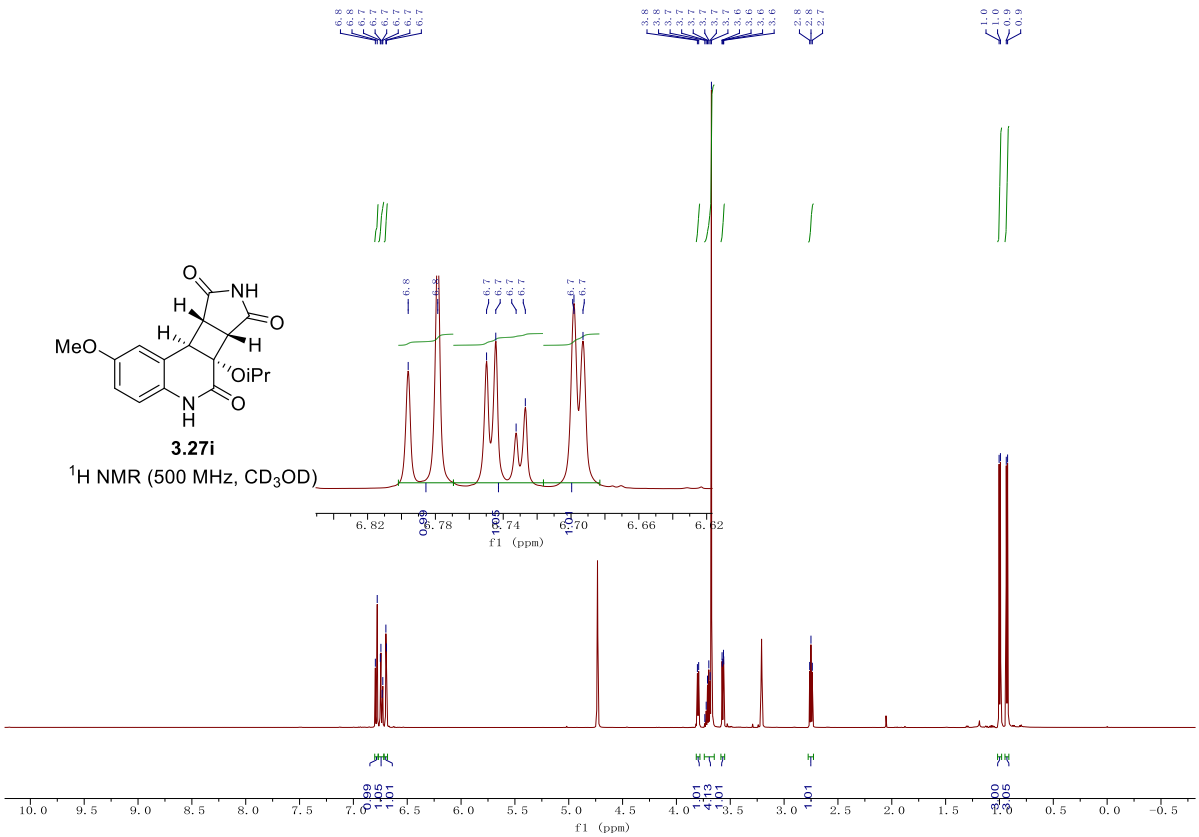

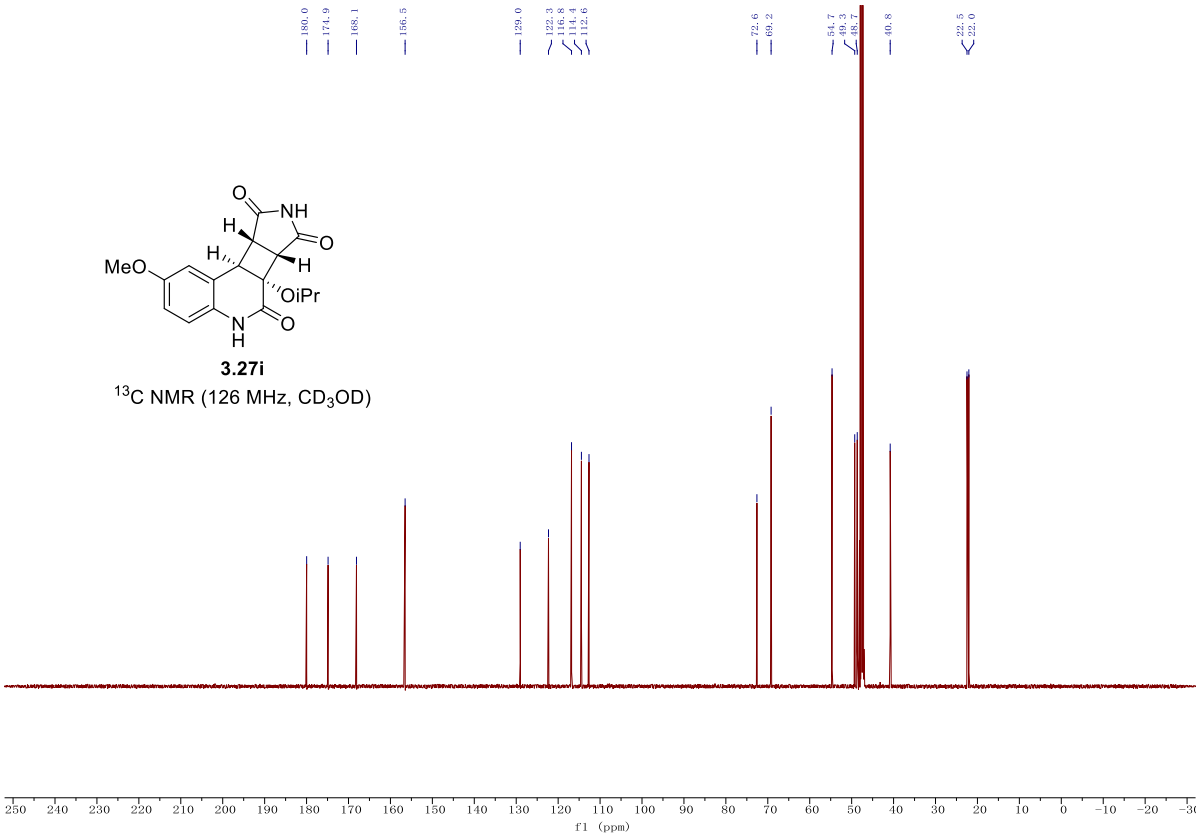

3.27i

^{13}C NMR (126 MHz, CD_3OD)

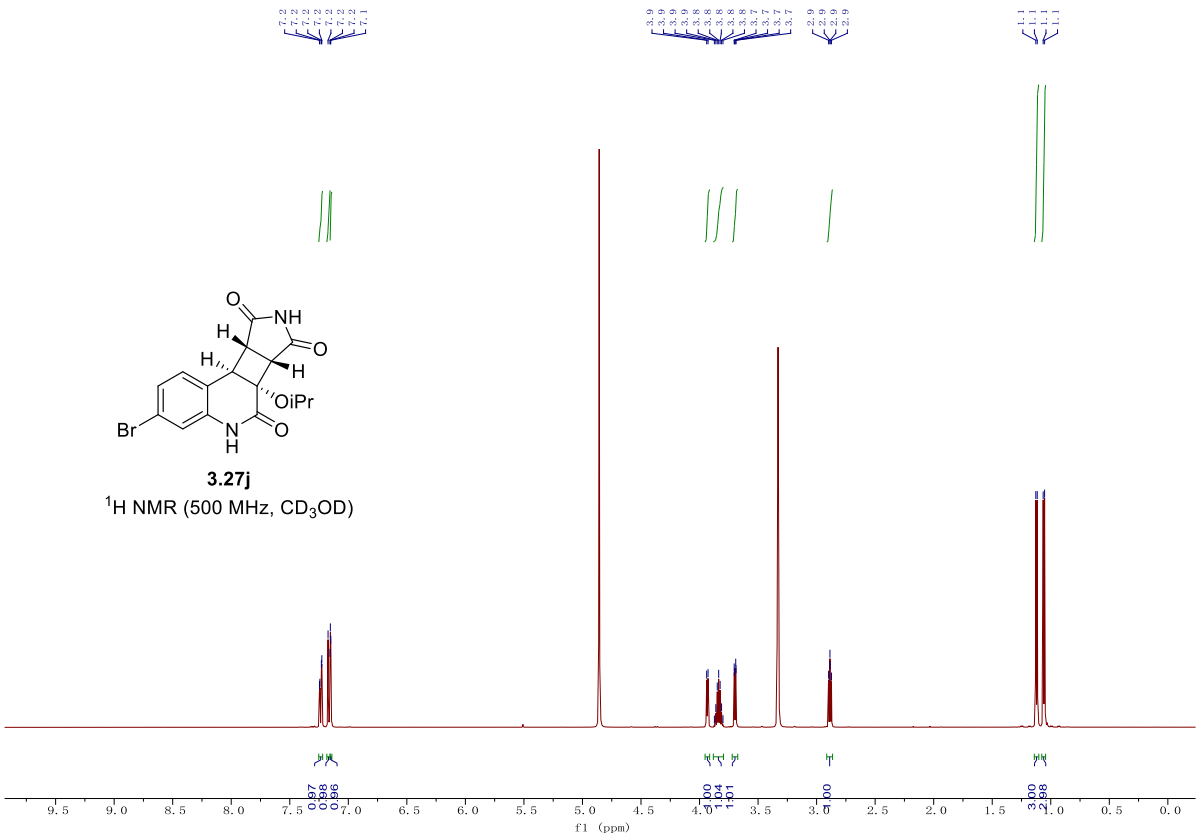

3.27j

^{1}H NMR (500 MHz, CD_3OD)

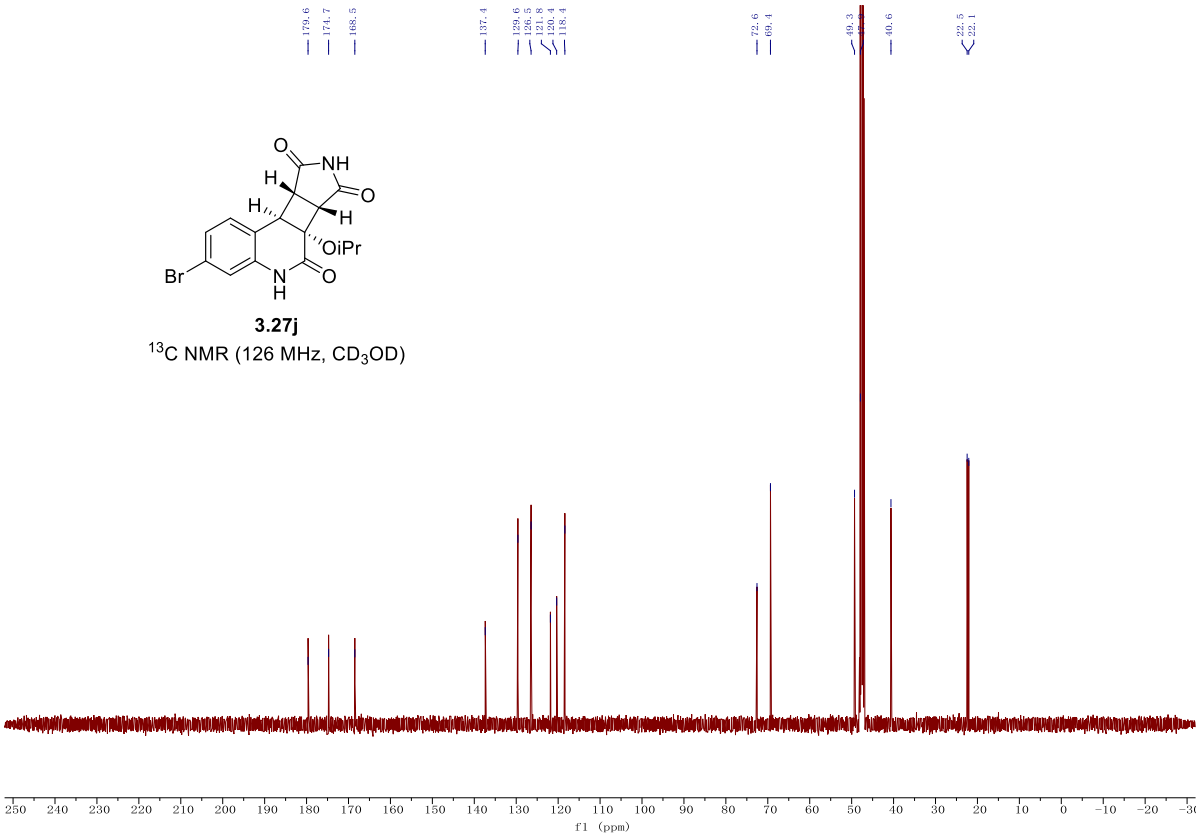

3.27j

^{13}C NMR (126 MHz, CD_3OD)

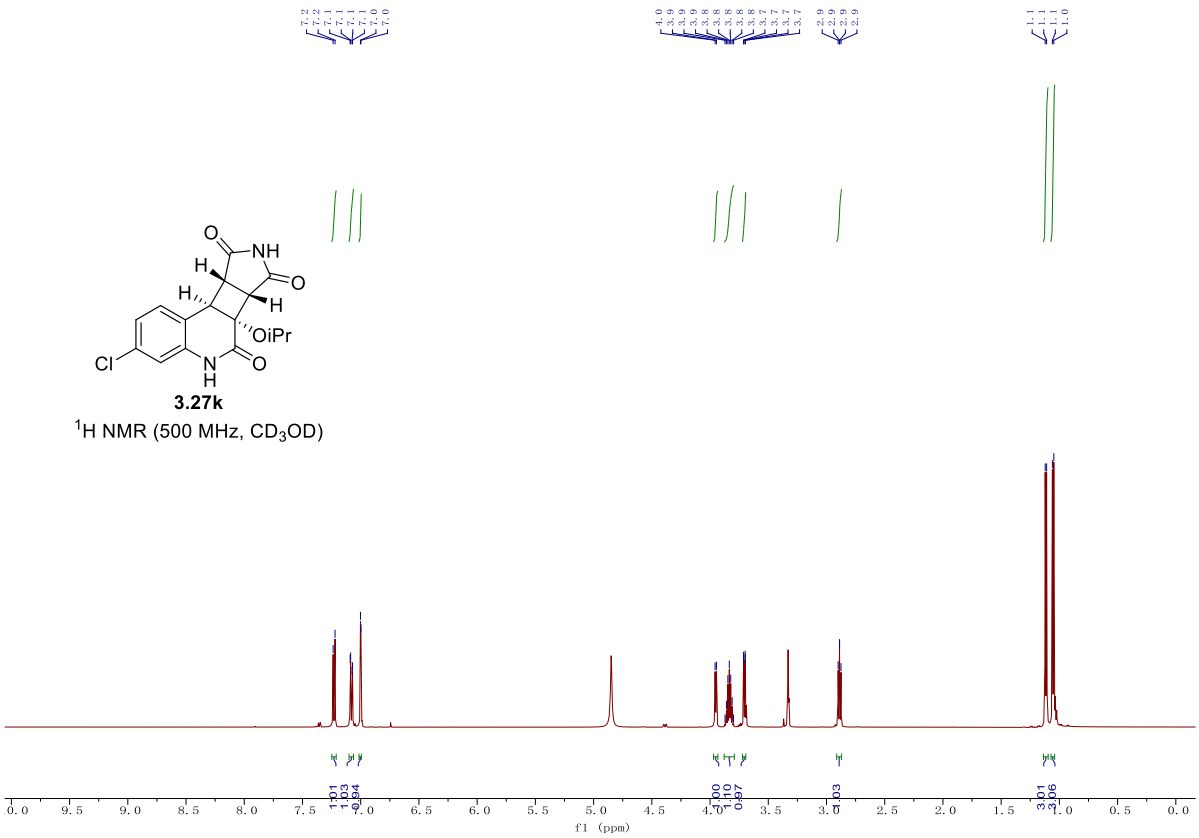

3.27k

^{1}H NMR (500 MHz, CD_3OD)

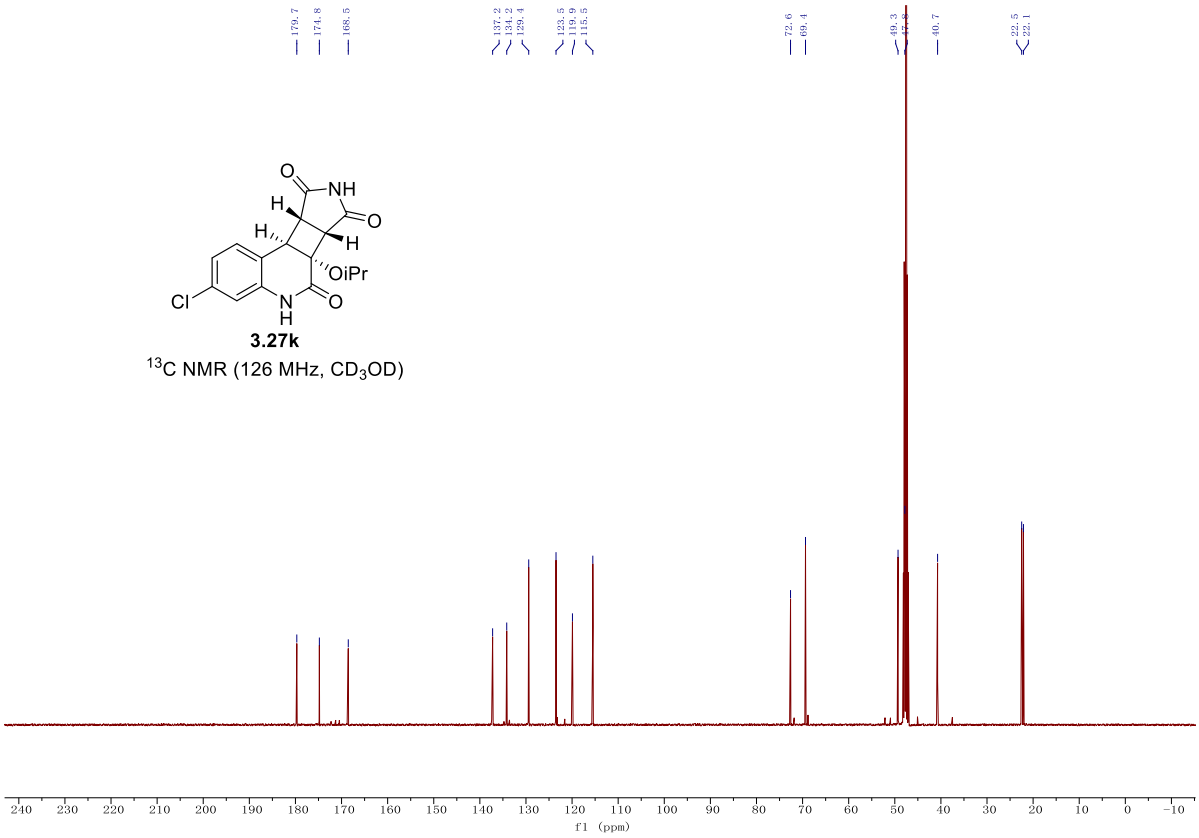

3.27k

^{13}C NMR (126 MHz, CD_3OD)

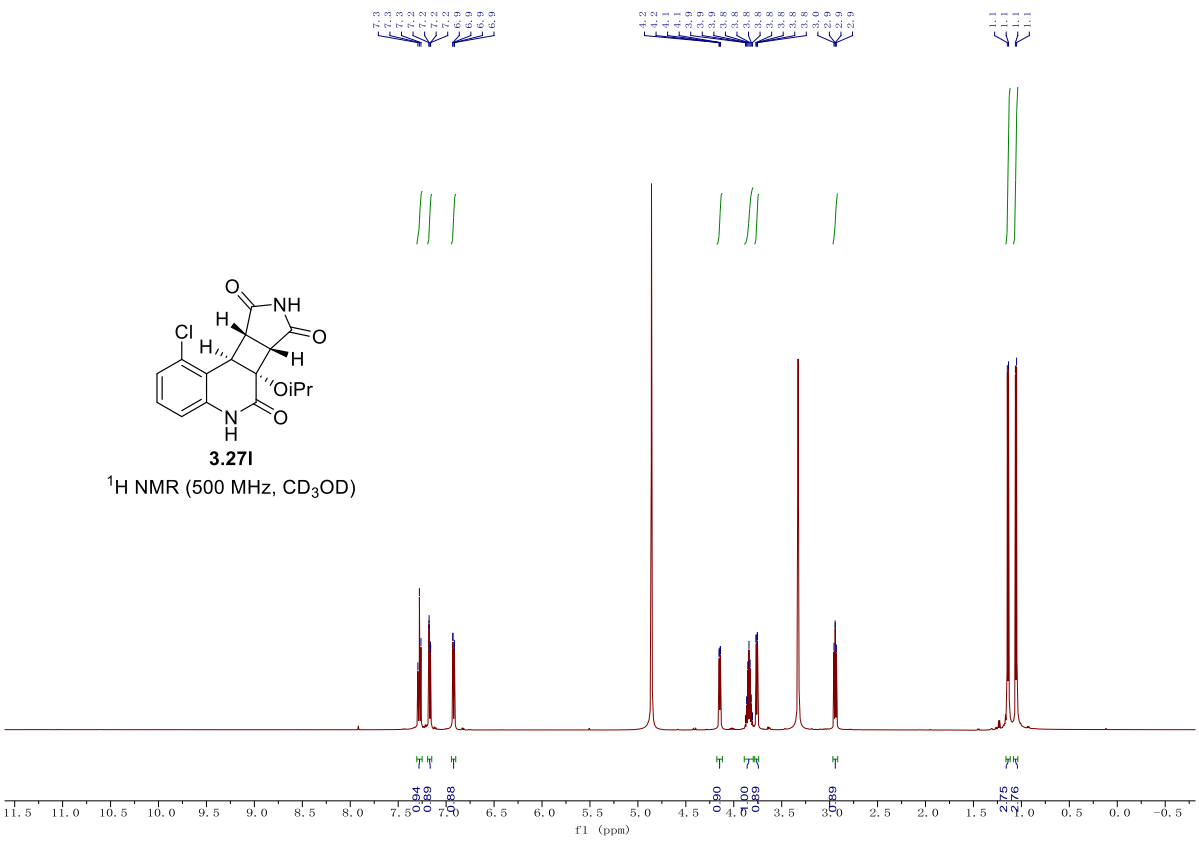

3.27l

^{1}H NMR (500 MHz, CD_3OD)

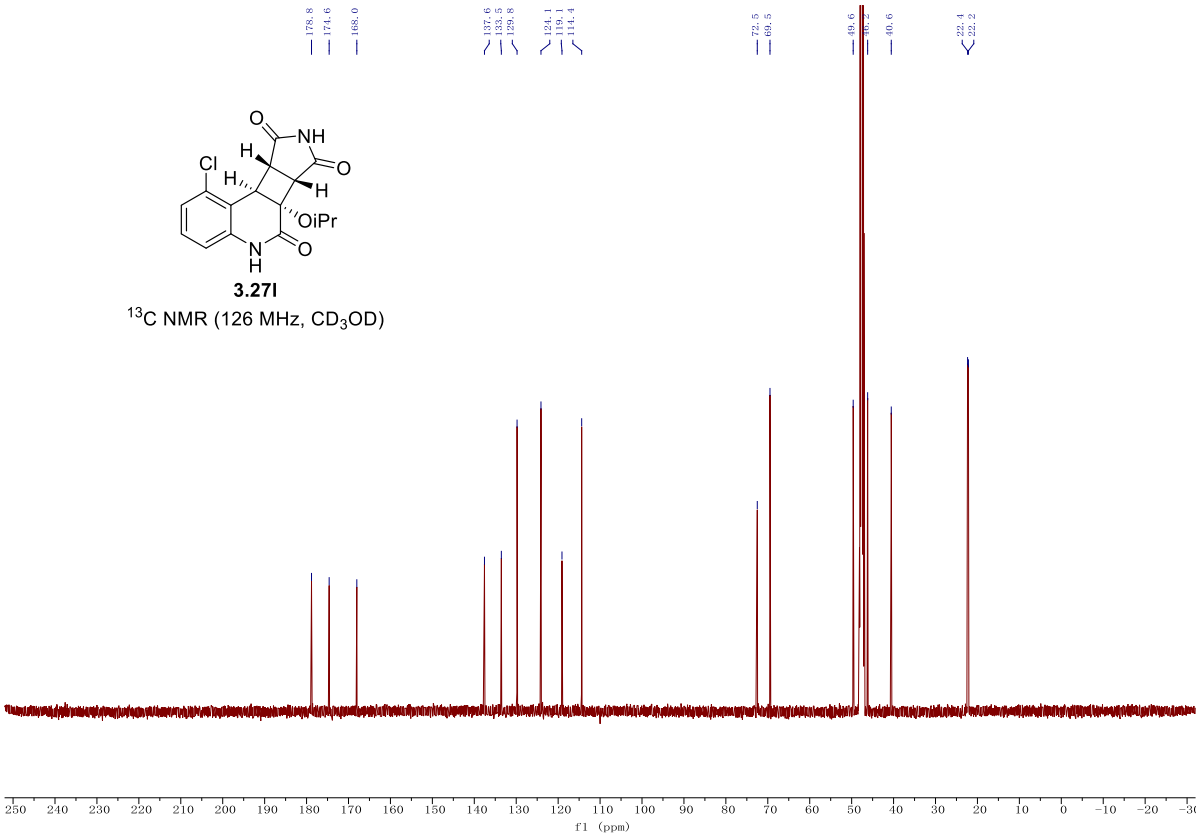

3.27l

^{13}C NMR (126 MHz, CD_3OD)

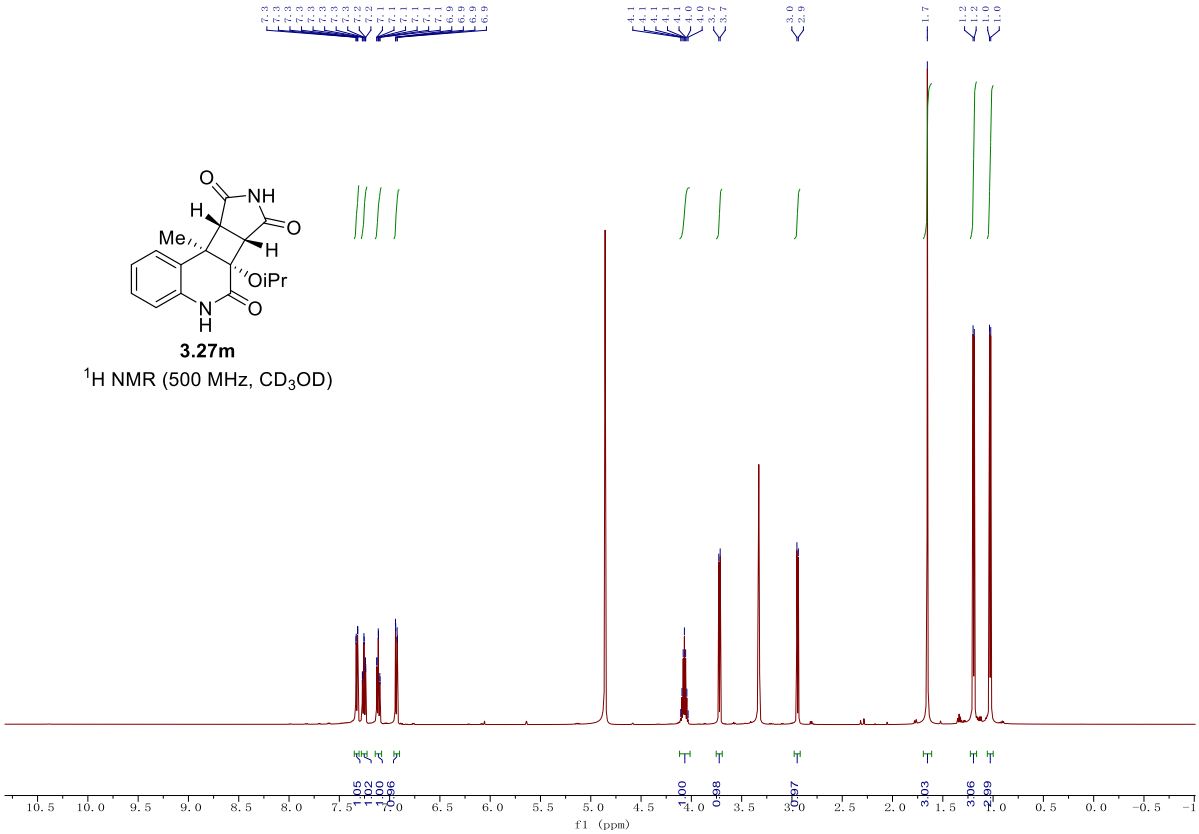

3.27m

^{1}H NMR (500 MHz, CD_3OD)

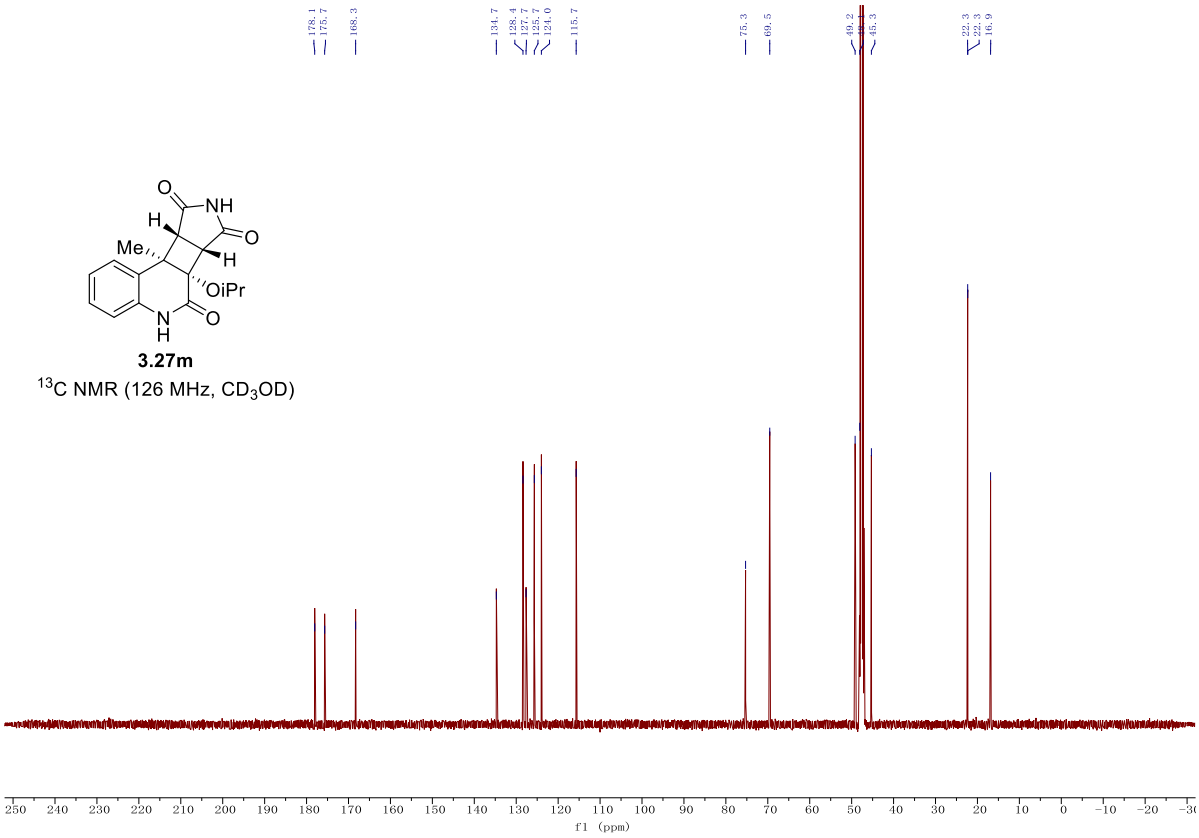

3.27m

^{13}C NMR (126 MHz, CD_3OD)

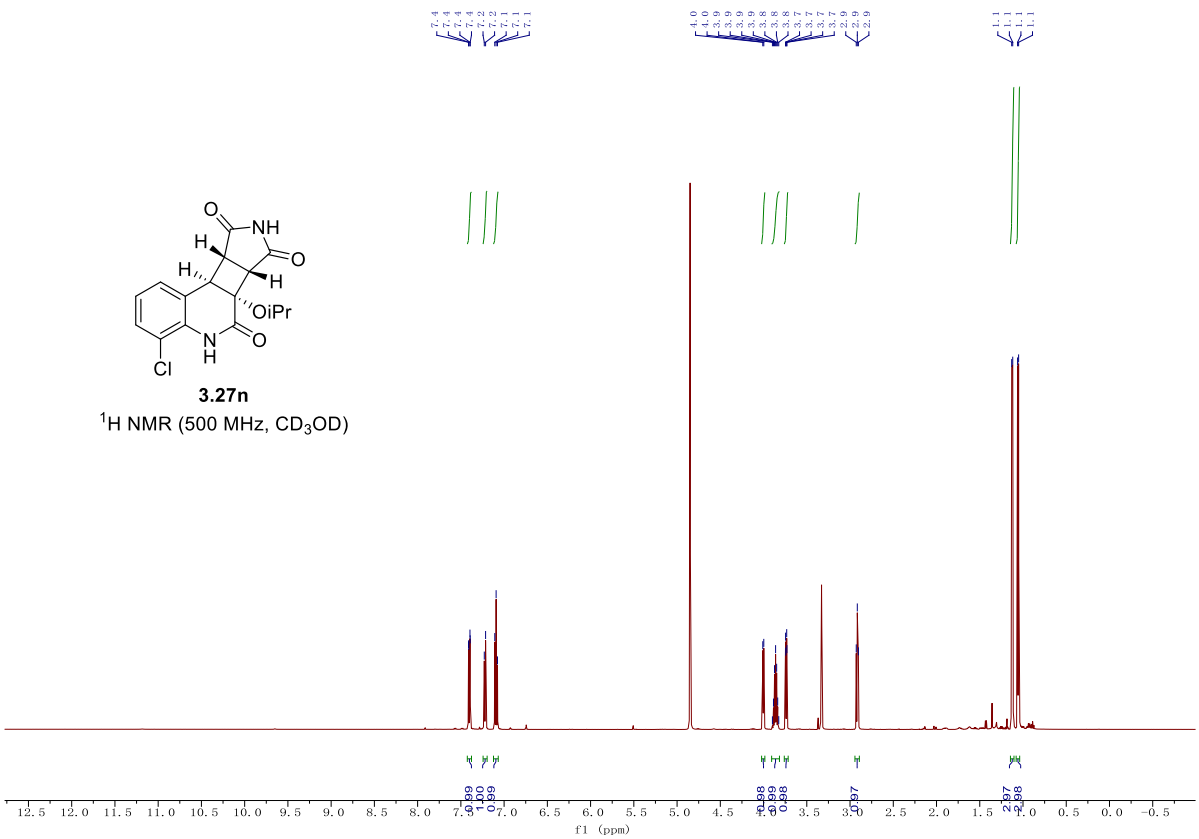

3.27n

^{1}H NMR (500 MHz, CD_3OD)

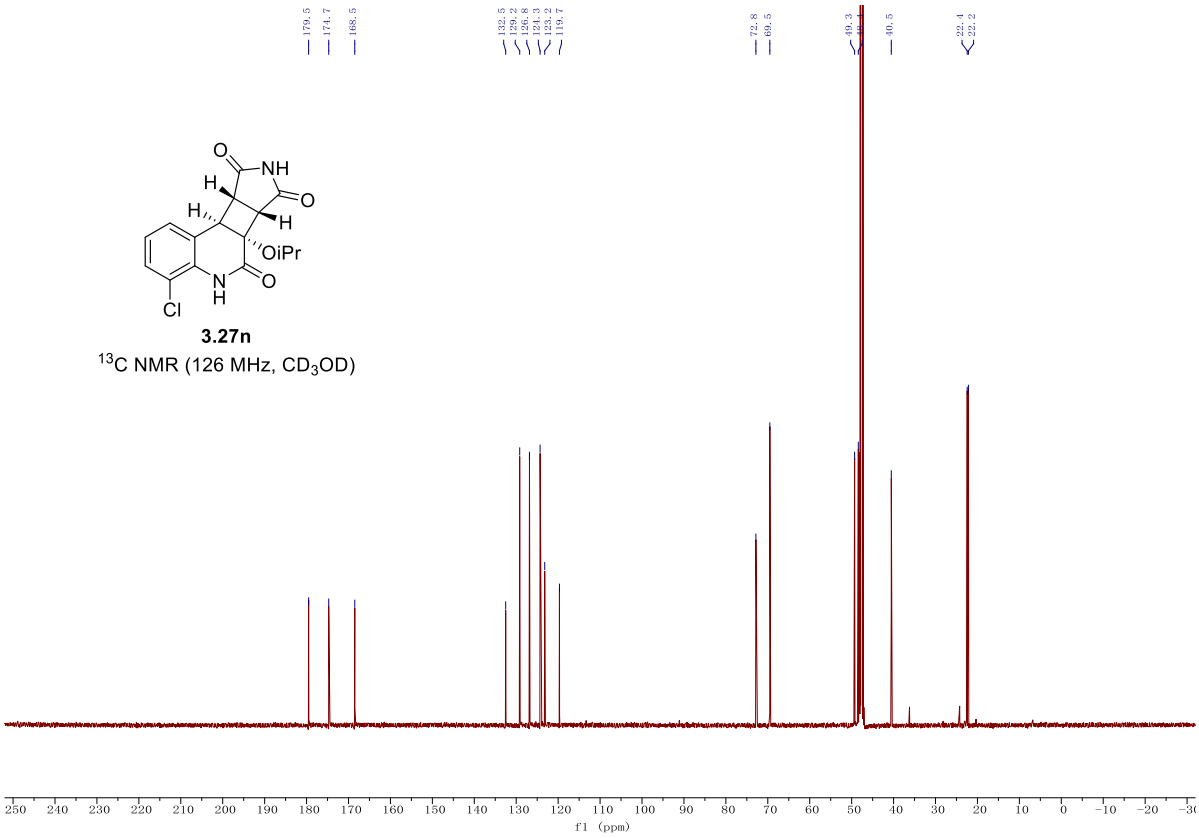

3.27n

^{13}C NMR (126 MHz, CD_3OD)

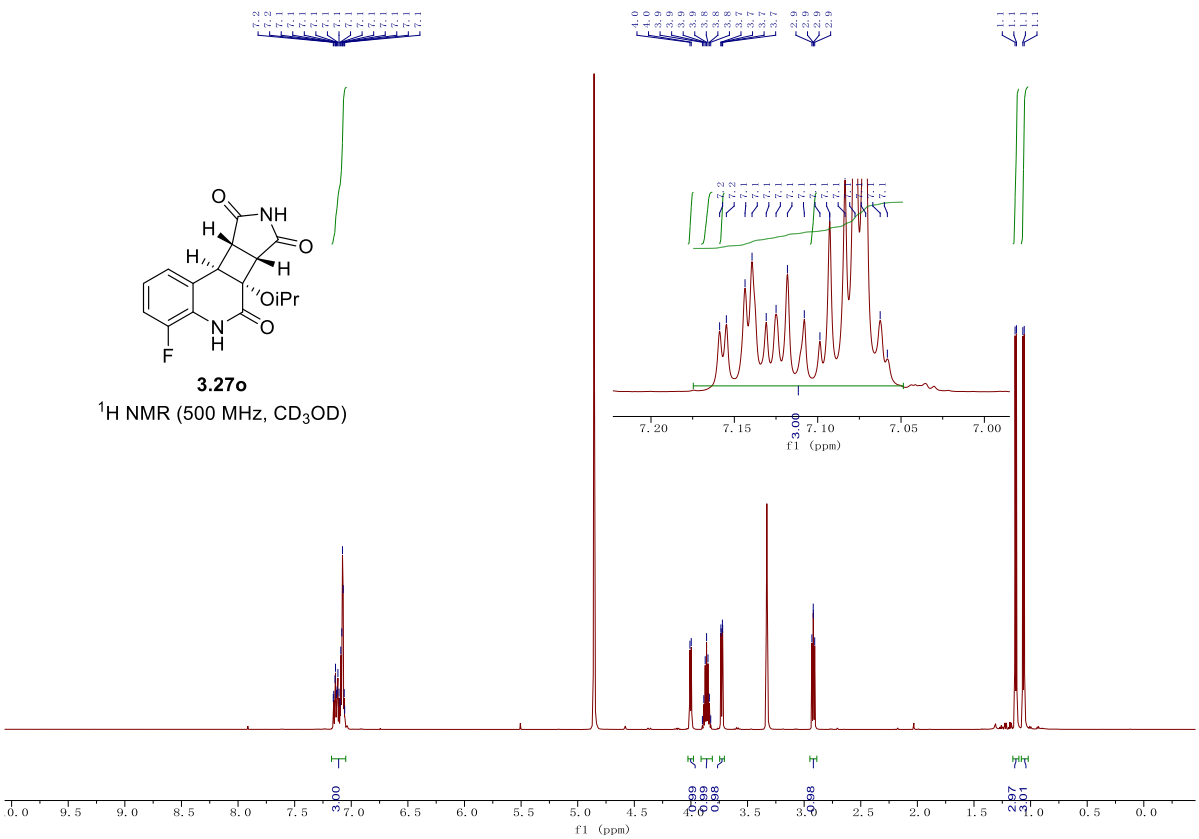

3.27o

^{1}H NMR (500 MHz, CD_3OD)

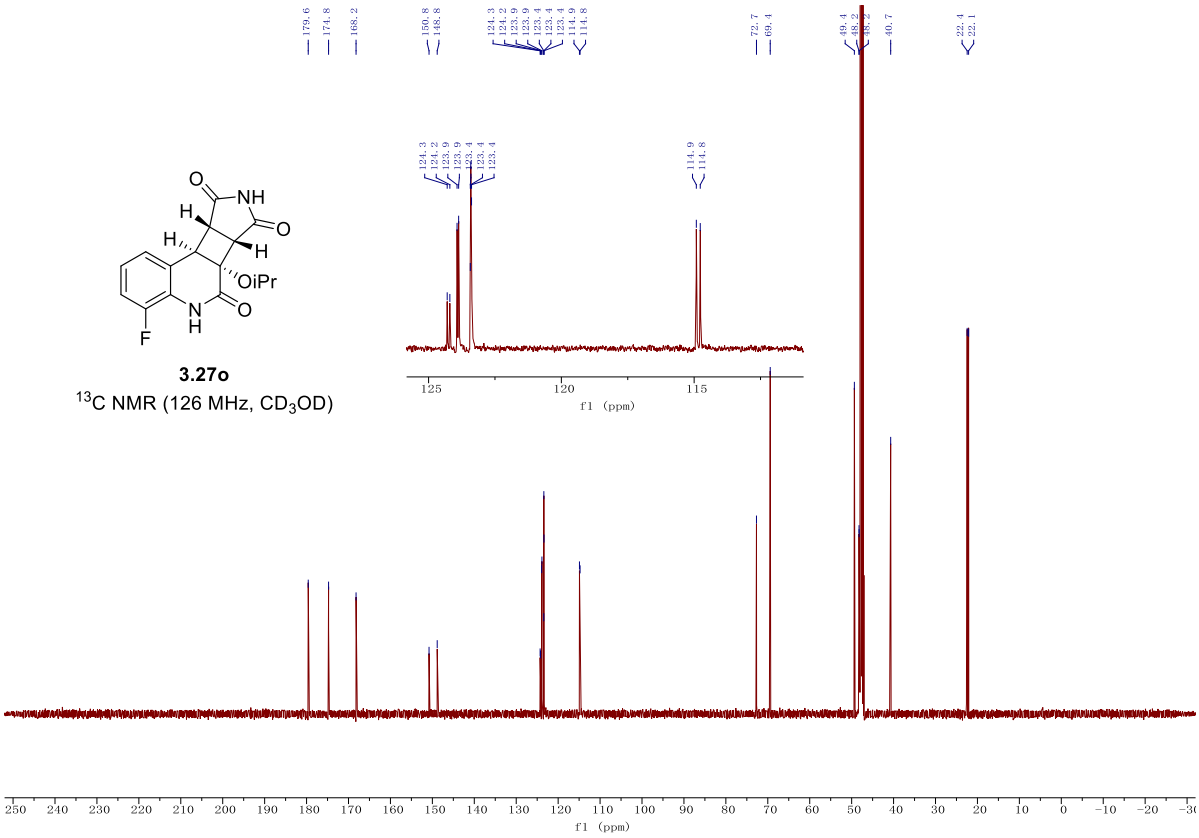

3.27o

^{13}C NMR (126 MHz, CD_3OD)

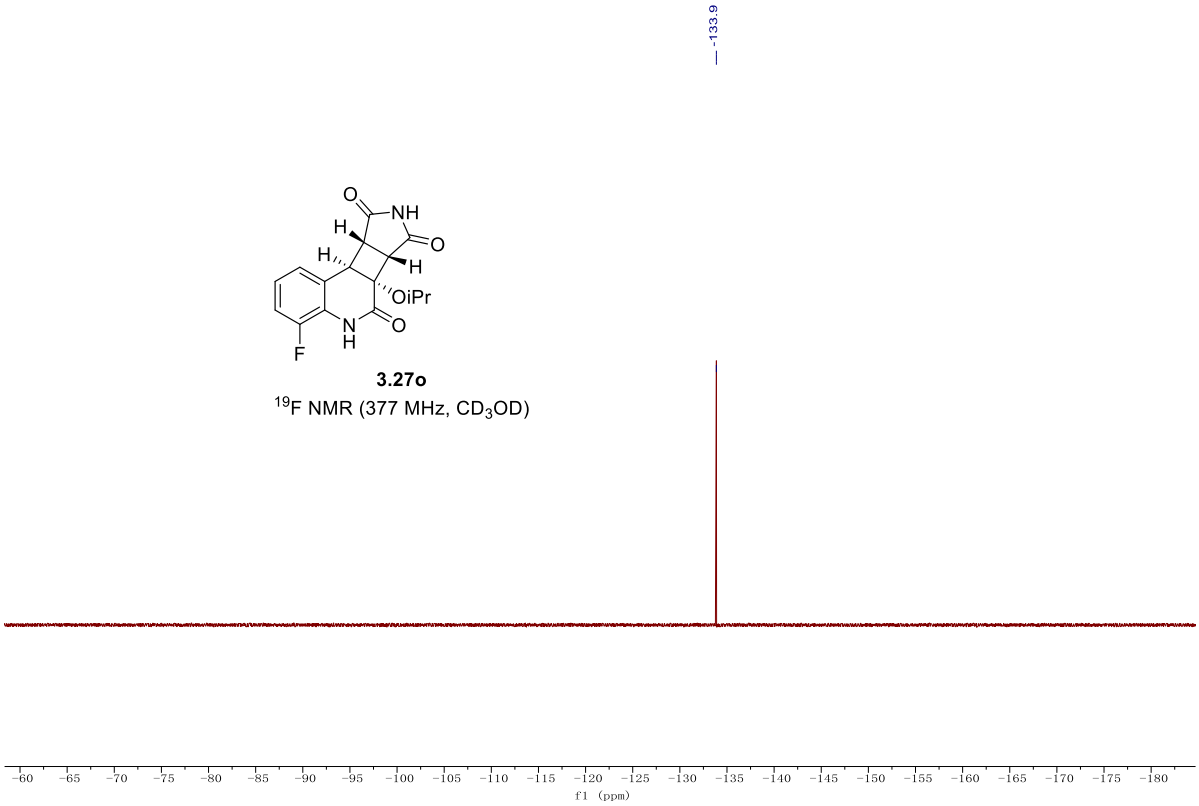

3.27o

^{19}F NMR (377 MHz, CD_3OD)

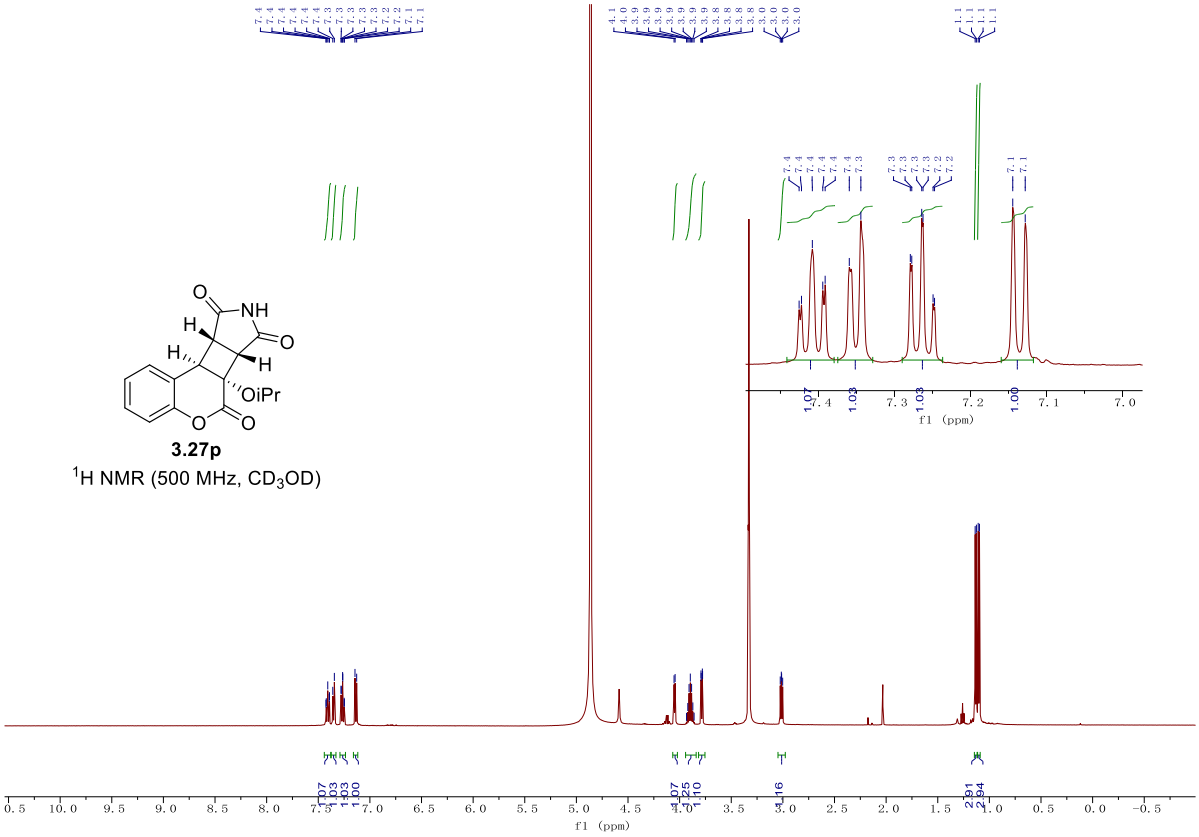

3.27p

^{1}H NMR (500 MHz, CD_3OD)

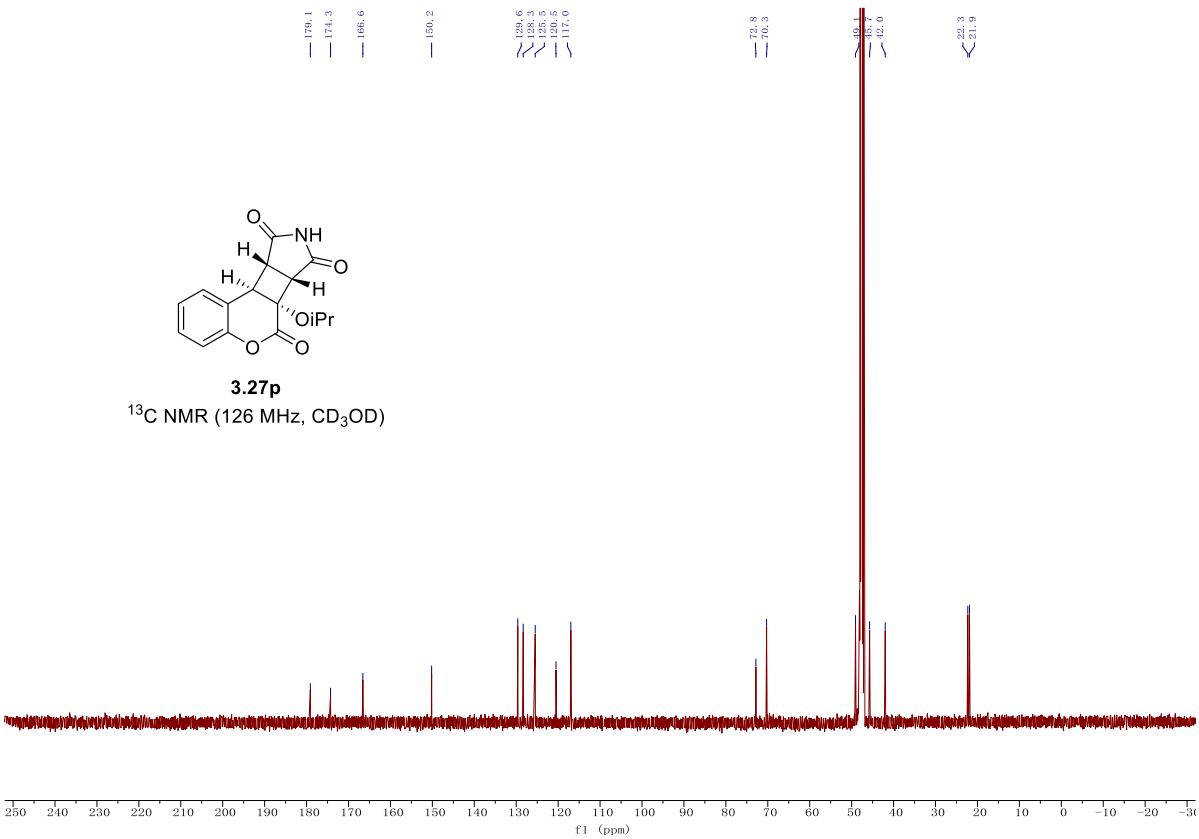

3.27p

^{13}C NMR (126 MHz, CD_3OD)

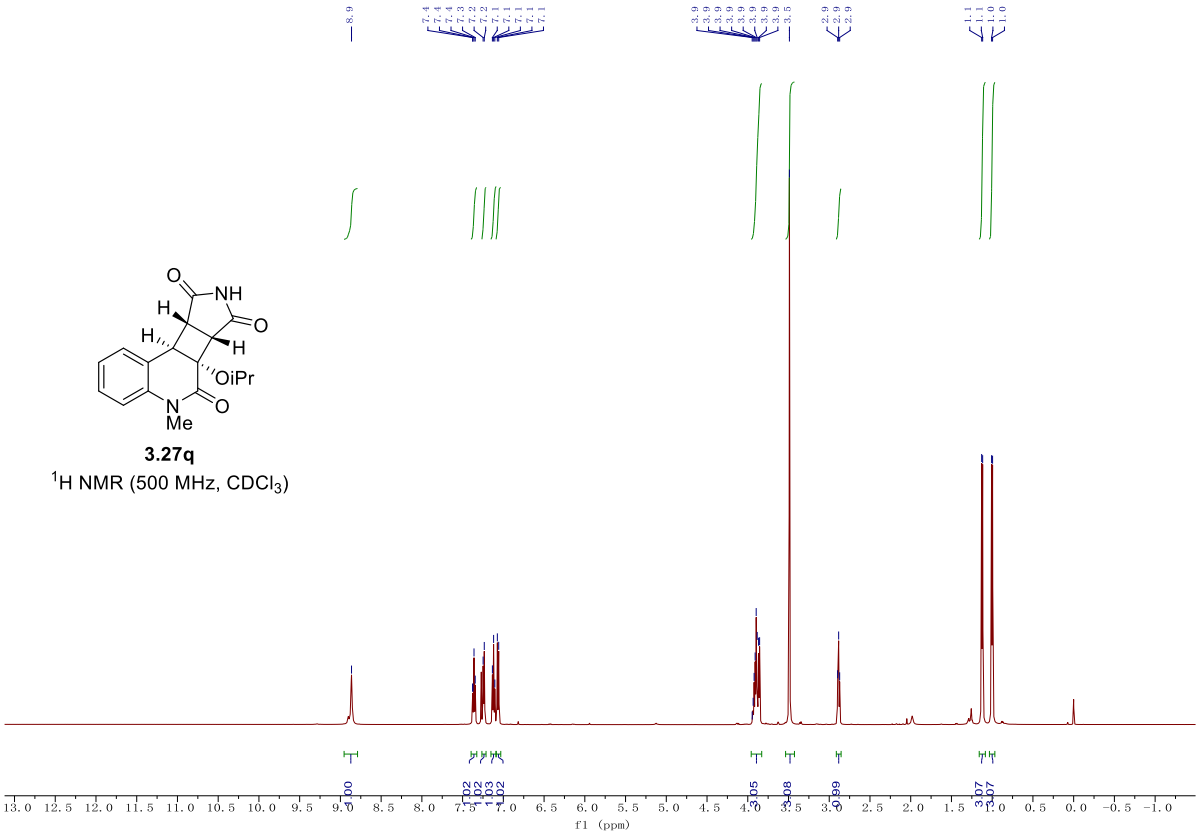

3.27q

^{1}H NMR (500 MHz, $CDCl_3$)

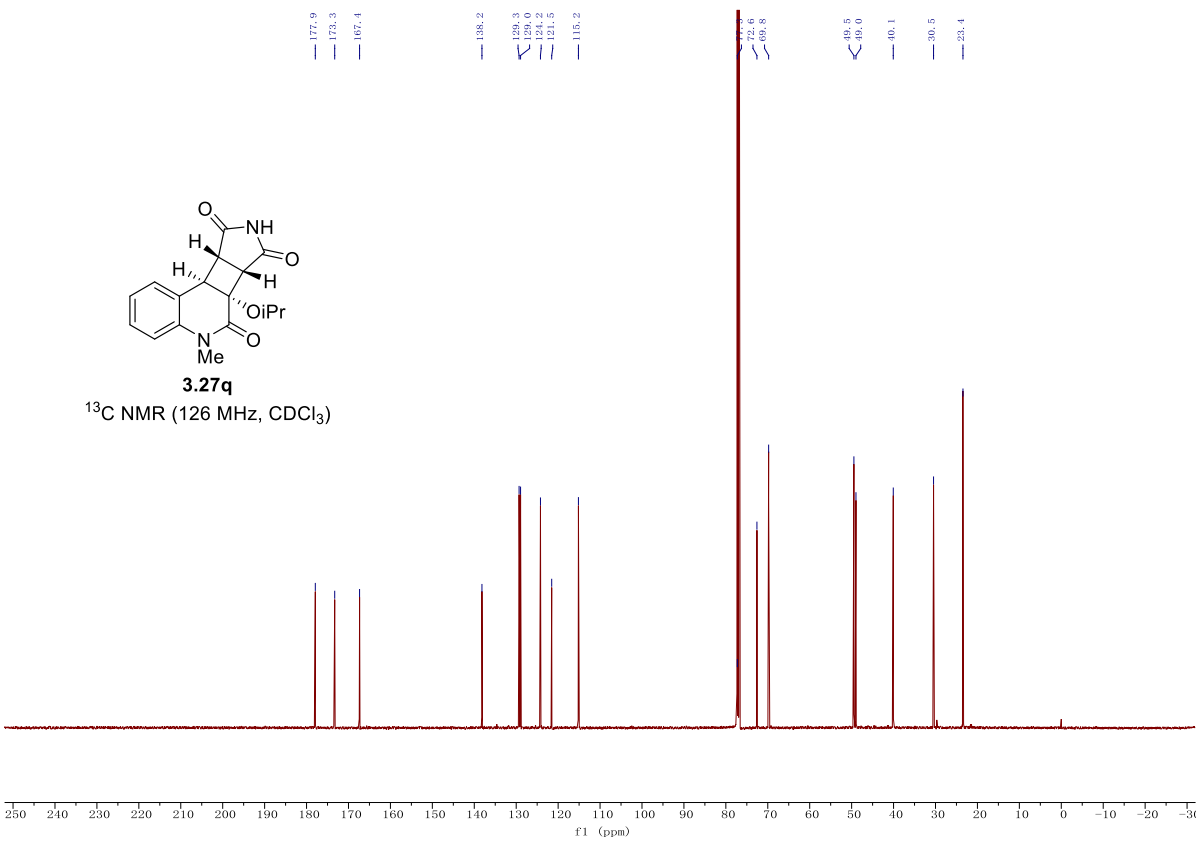

3.27q

^{13}C NMR (126 MHz, $CDCl_3$)

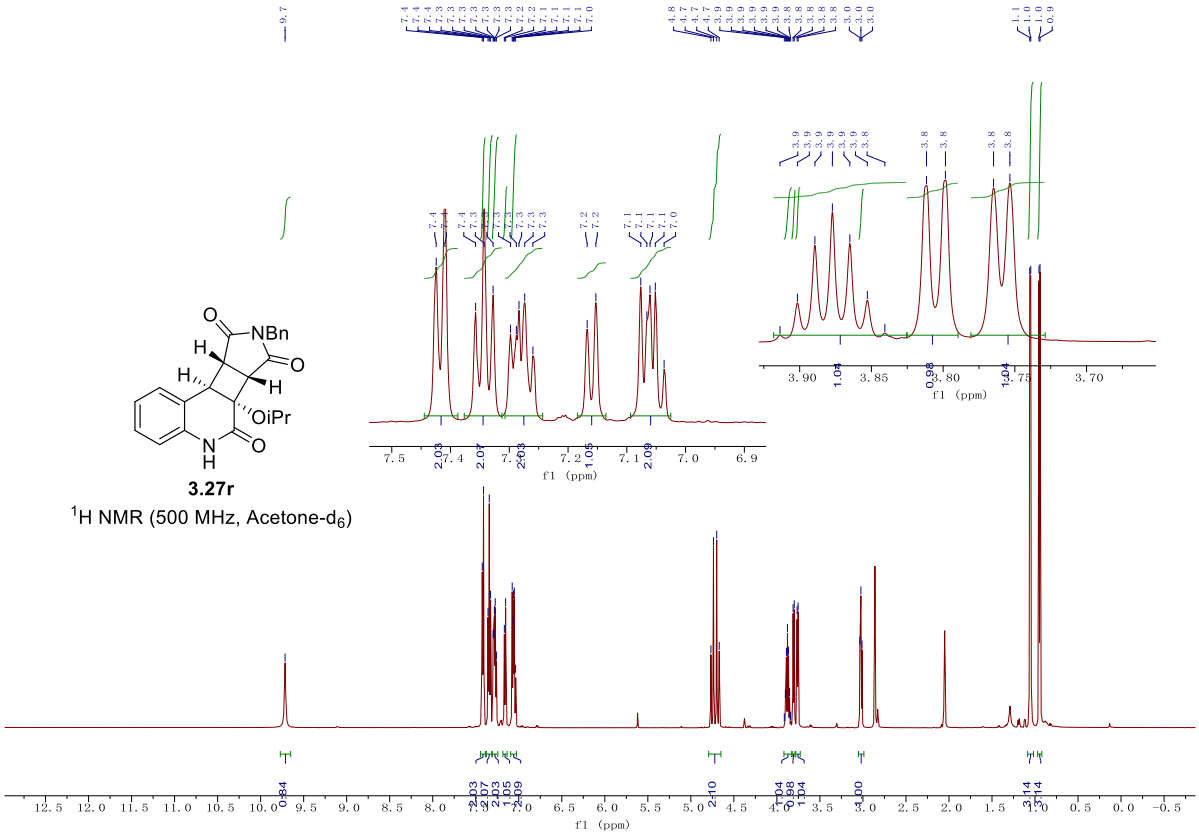

3.27r

^{1}H NMR (500 MHz, Acetone-d_6)

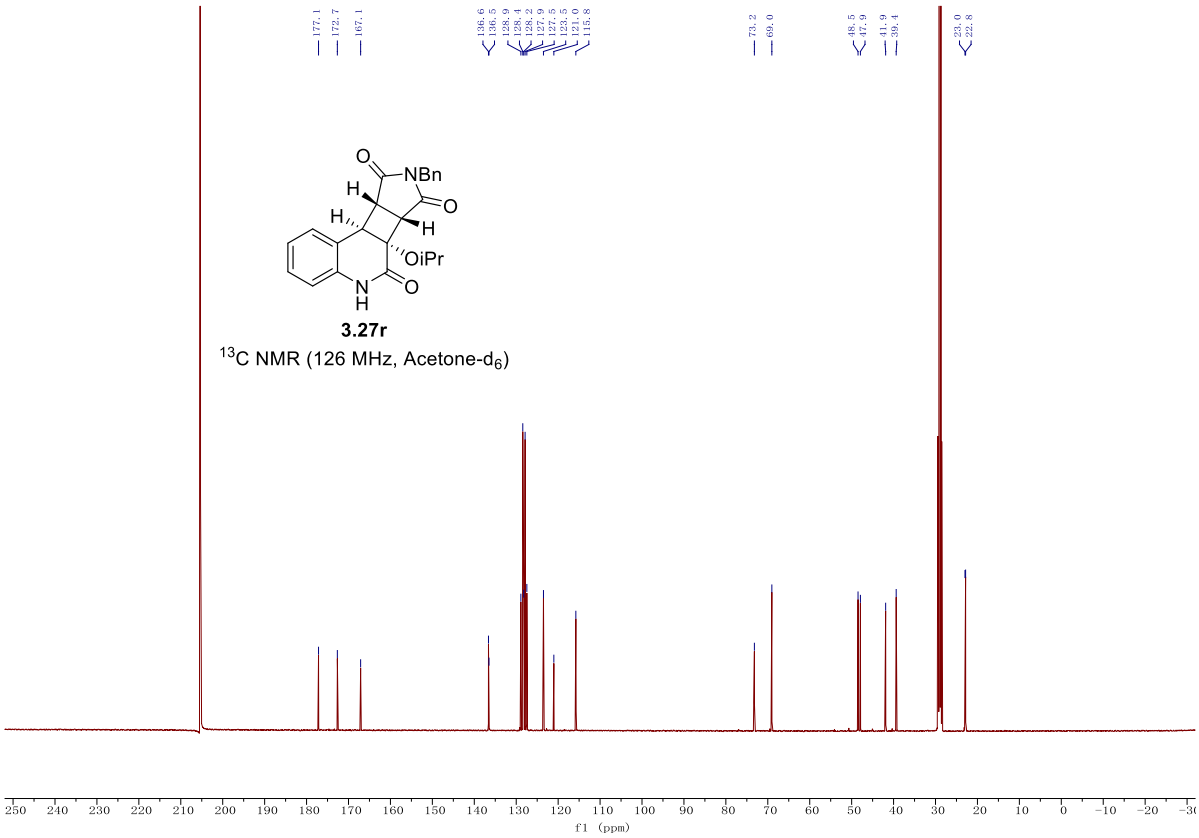

3.27r

^{13}C NMR (126 MHz, Acetone-d_6)

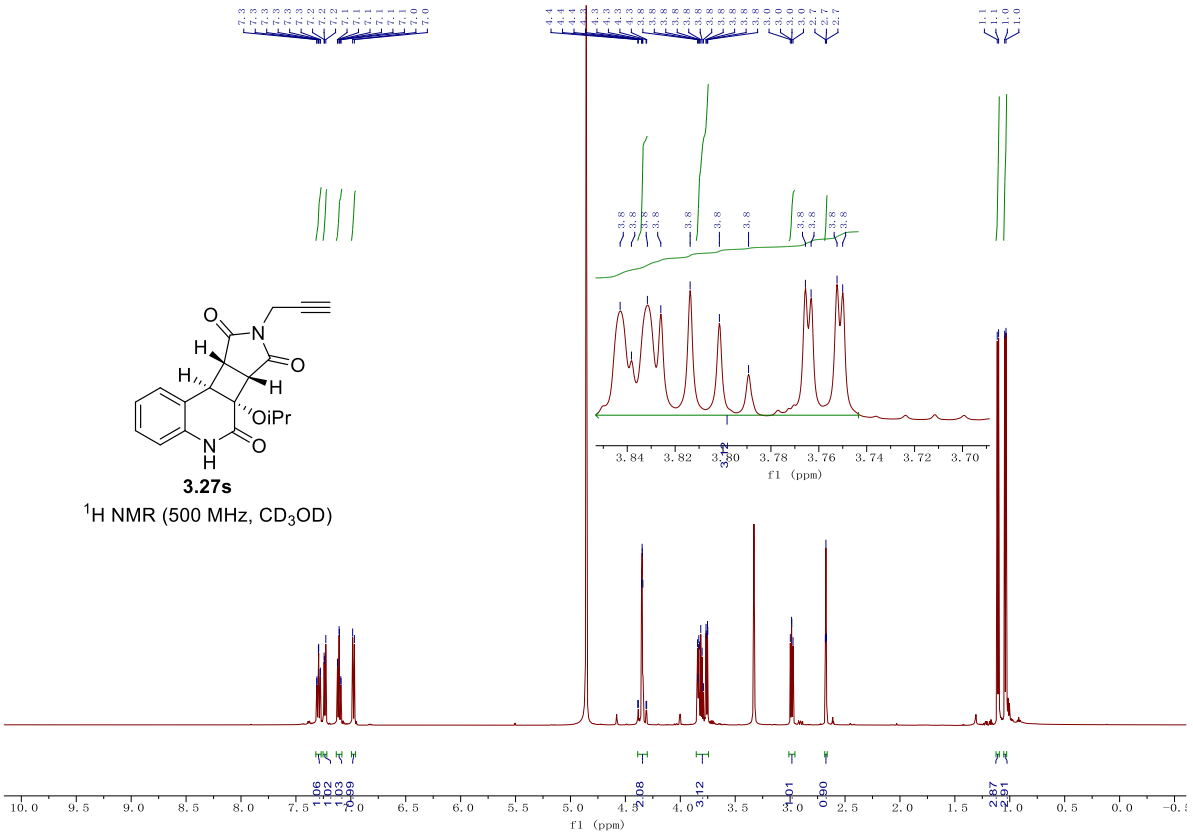

3.27s

^{1}H NMR (500 MHz, CD_3OD)

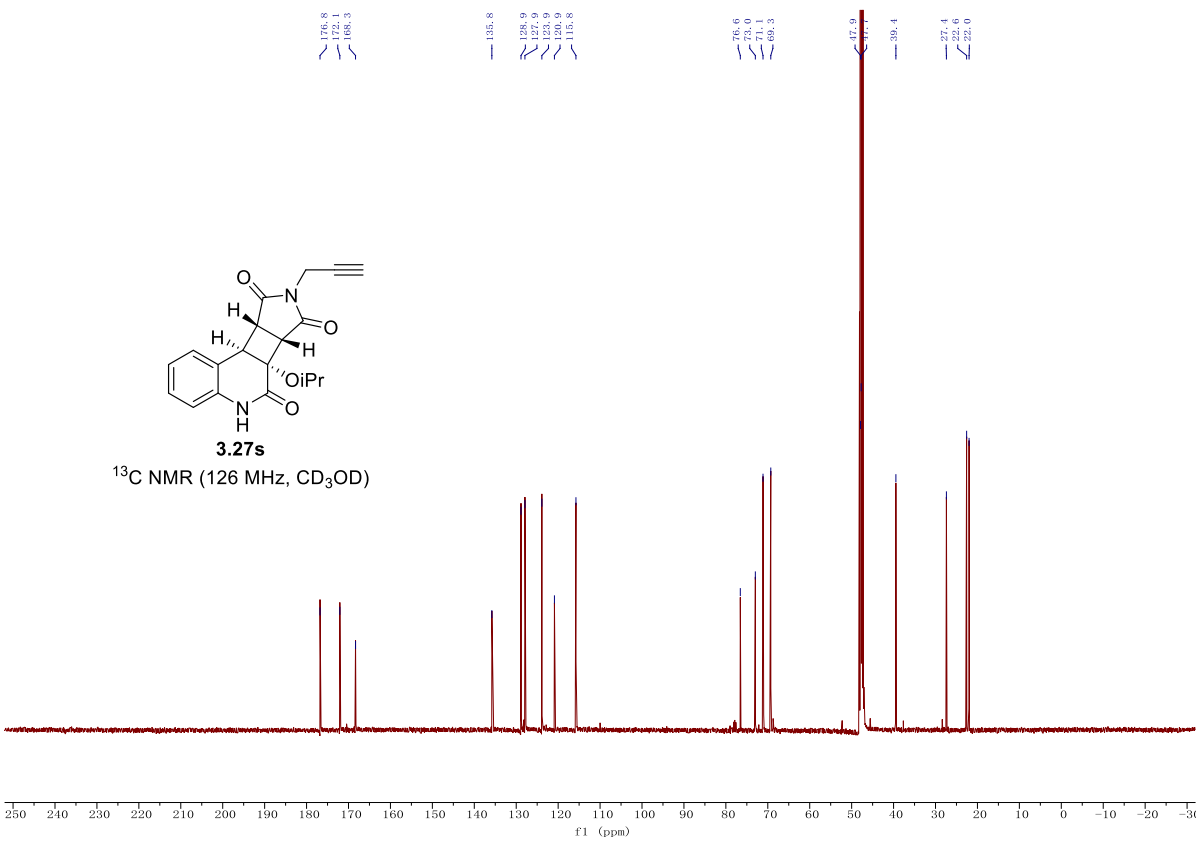

3.27s

^{13}C NMR (126 MHz, CD_3OD)

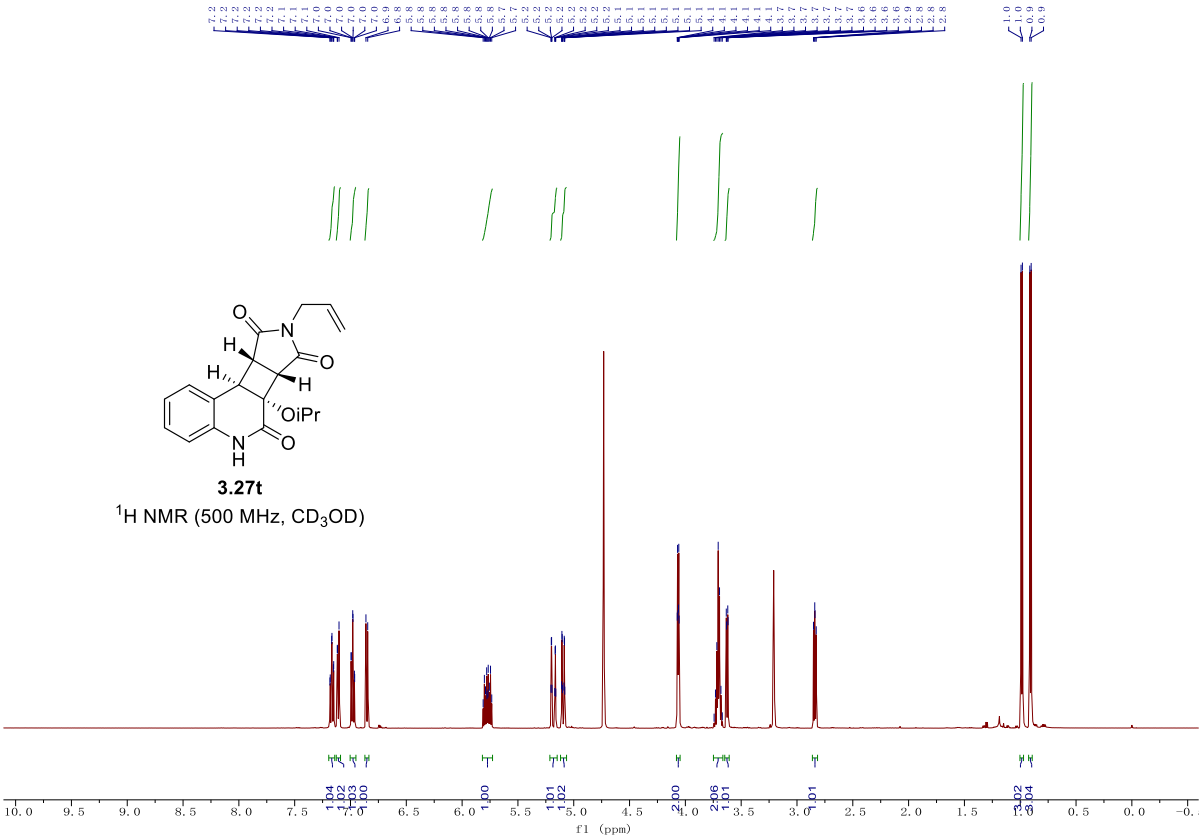

3.27t

^{1}H NMR (500 MHz, CD_3OD)

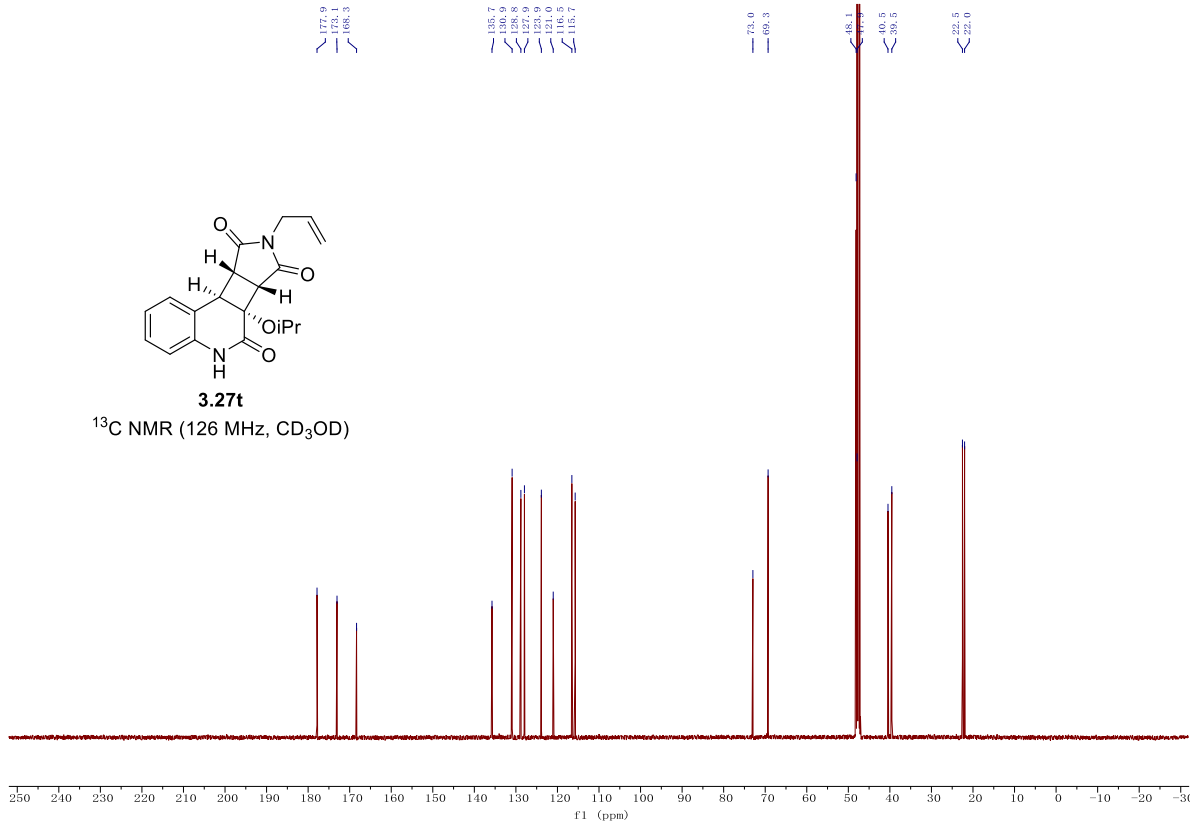

3.27t

^{13}C NMR (126 MHz, CD_3OD)

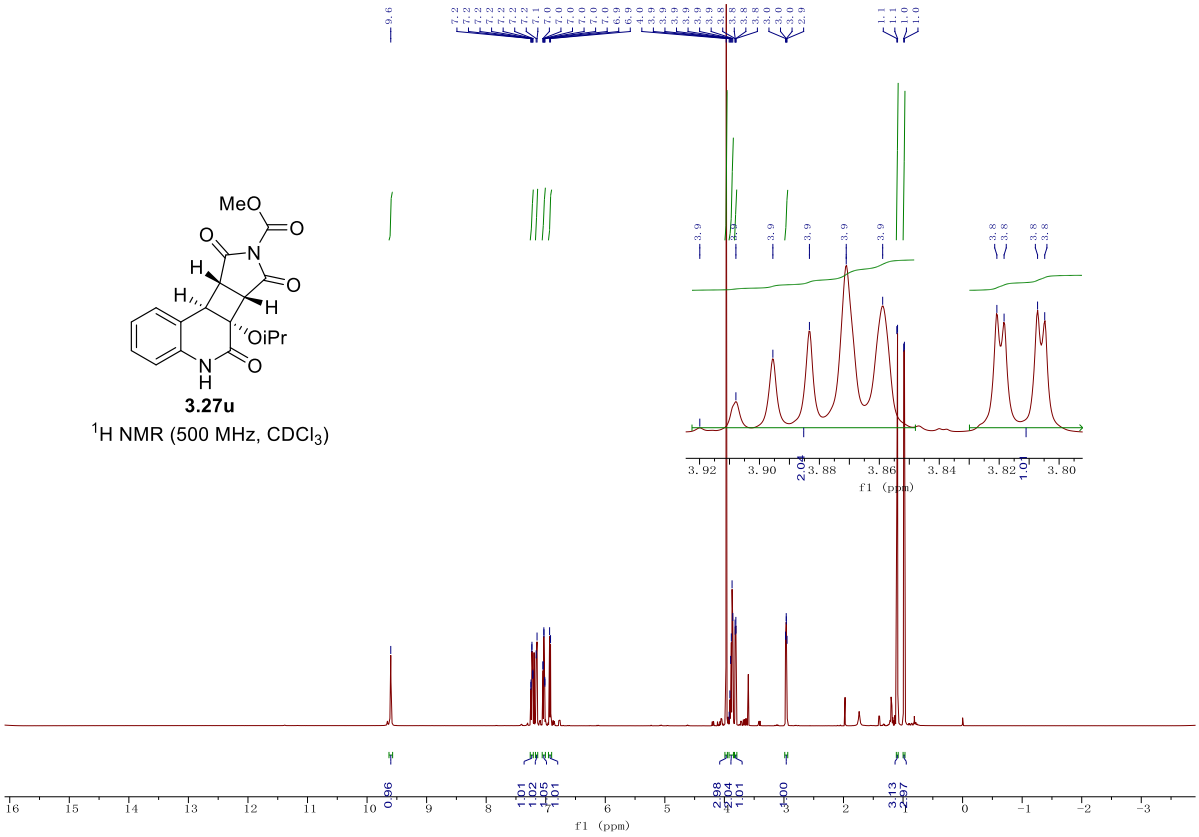

3.27u

^{1}H NMR (500 MHz, $CDCl_3$)

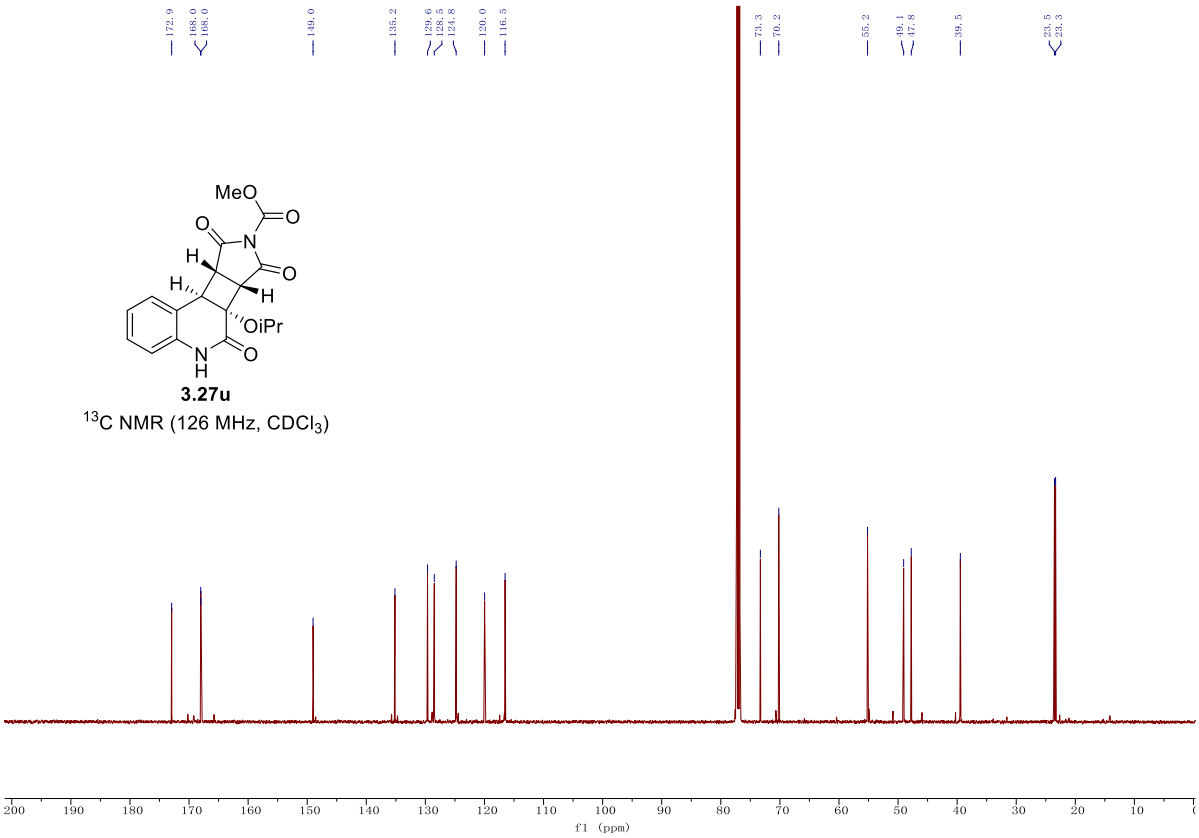

3.27u

^{13}C NMR (126 MHz, $CDCl_3$)

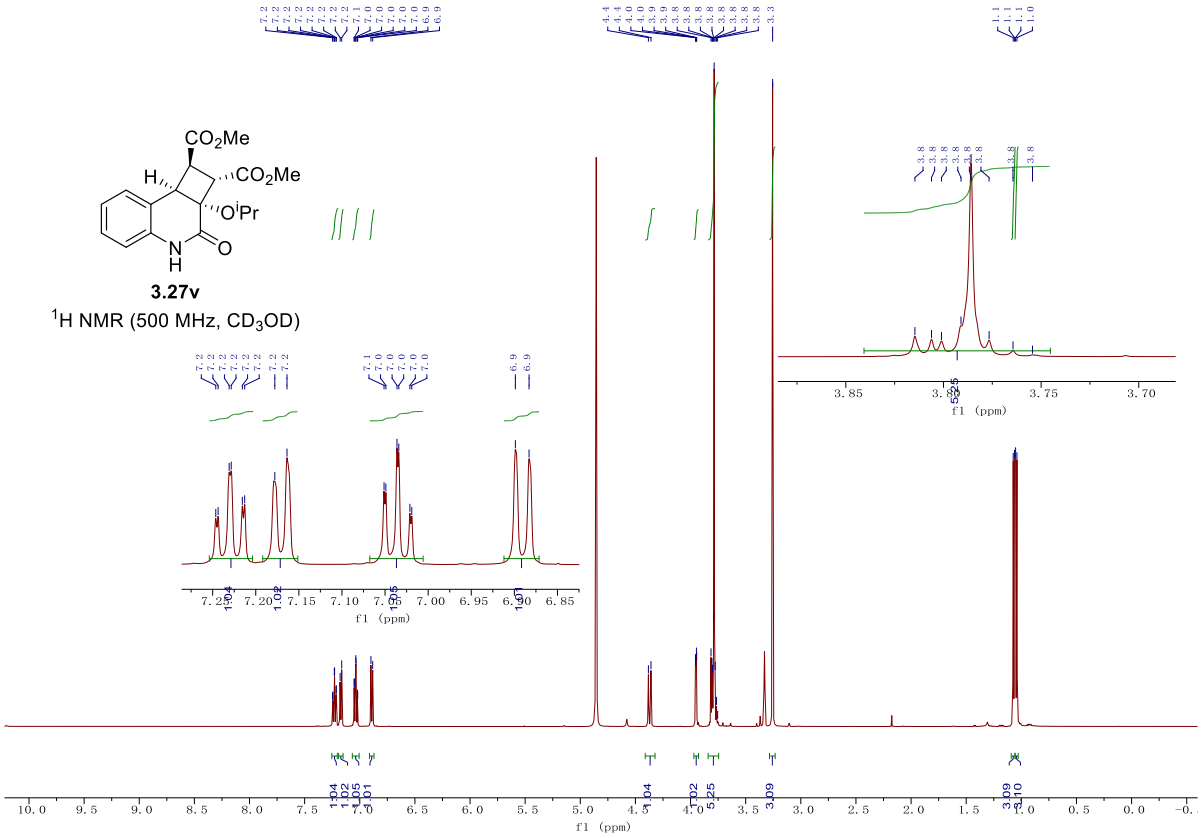

3.27v

^{1}H NMR (500 MHz, CD_3OD)

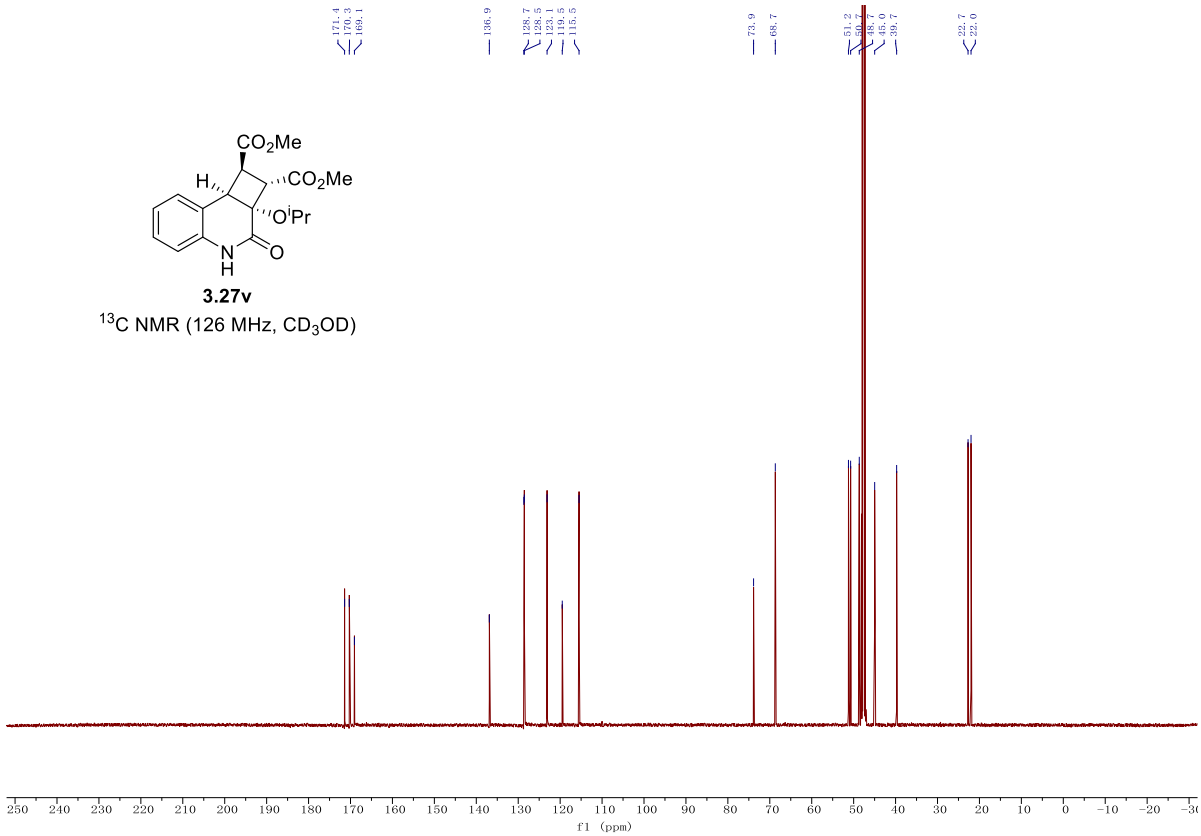

3.27v

^{13}C NMR (126 MHz, CD_3OD)

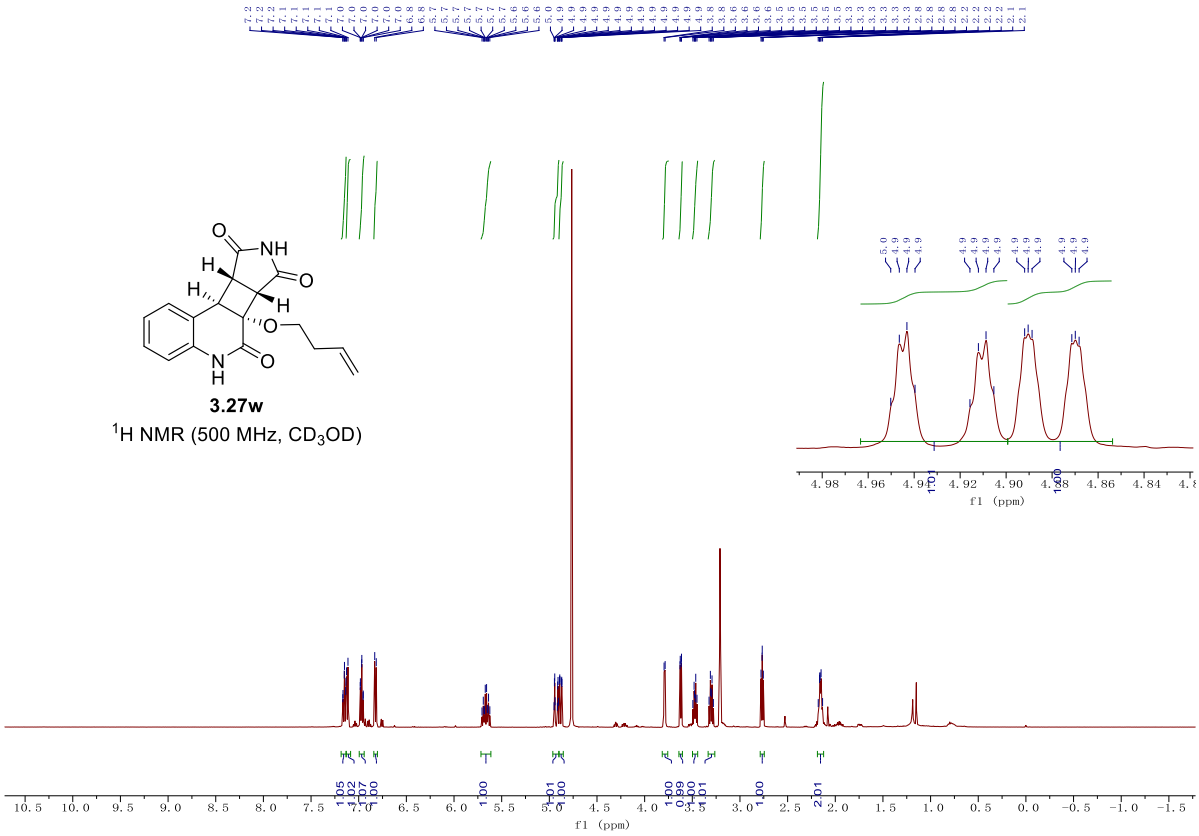

3.27w

^{1}H NMR (500 MHz, CD_3OD)

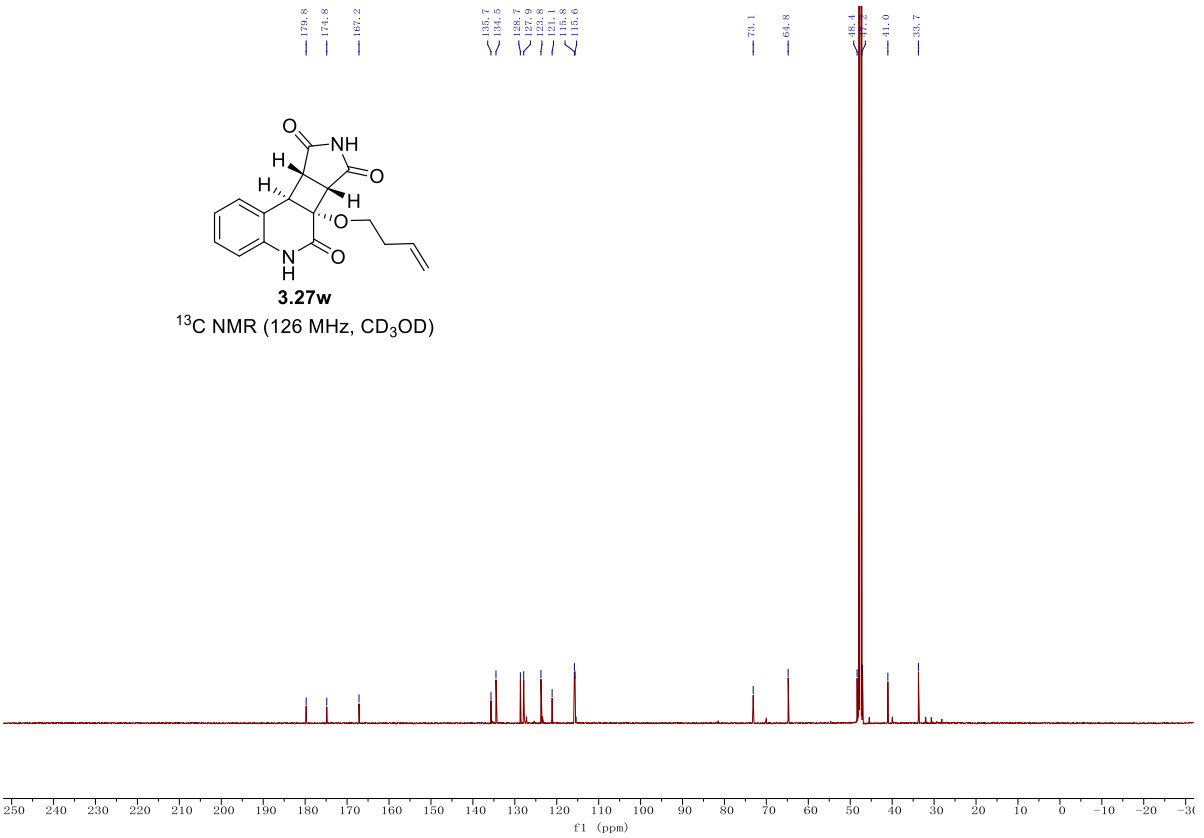

3.27w

^{13}C NMR (126 MHz, CD_3OD)

B.3. List of New Compounds for Chapter 4

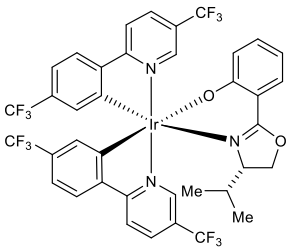

(S),Λ-**4.53d**

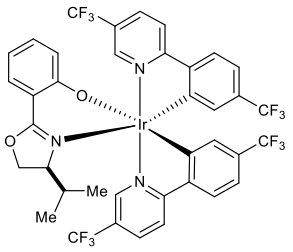

(S),Δ-**4.53d**

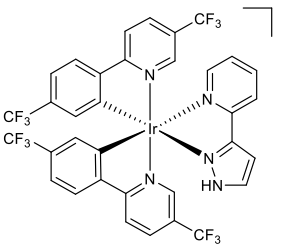

Λ-**4.49d**

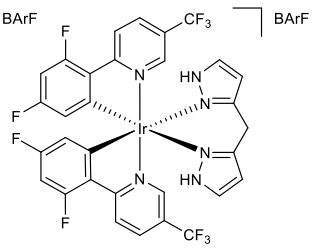

Λ-**4.49f**

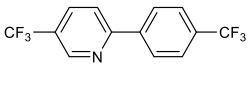

4.50

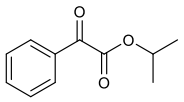

4.44c

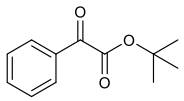

4.44d

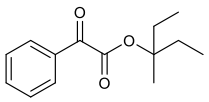

4.44e

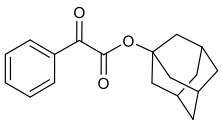

4.44f

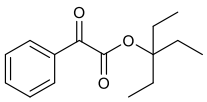

4.44g

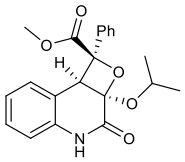

4.48a *endo*

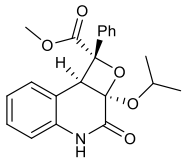

4.48a *exo*

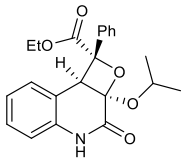

4.48b *exo*

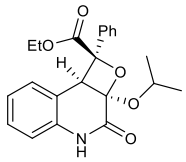

4.48b *endo*

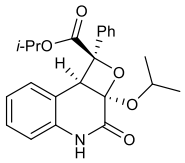

4.48c *endo*

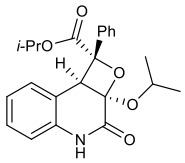

4.48c *exo*

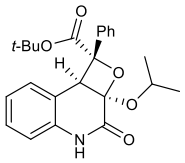

4.48d

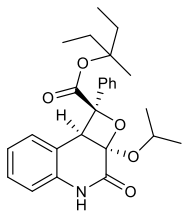

4.48e

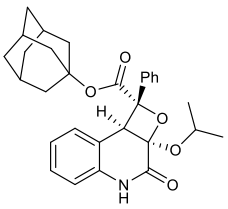

4.48f

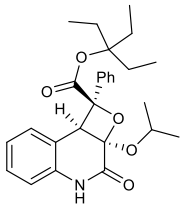

4.48g

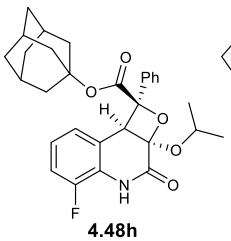

4.48h

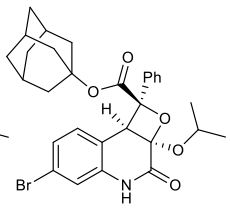

4.48i

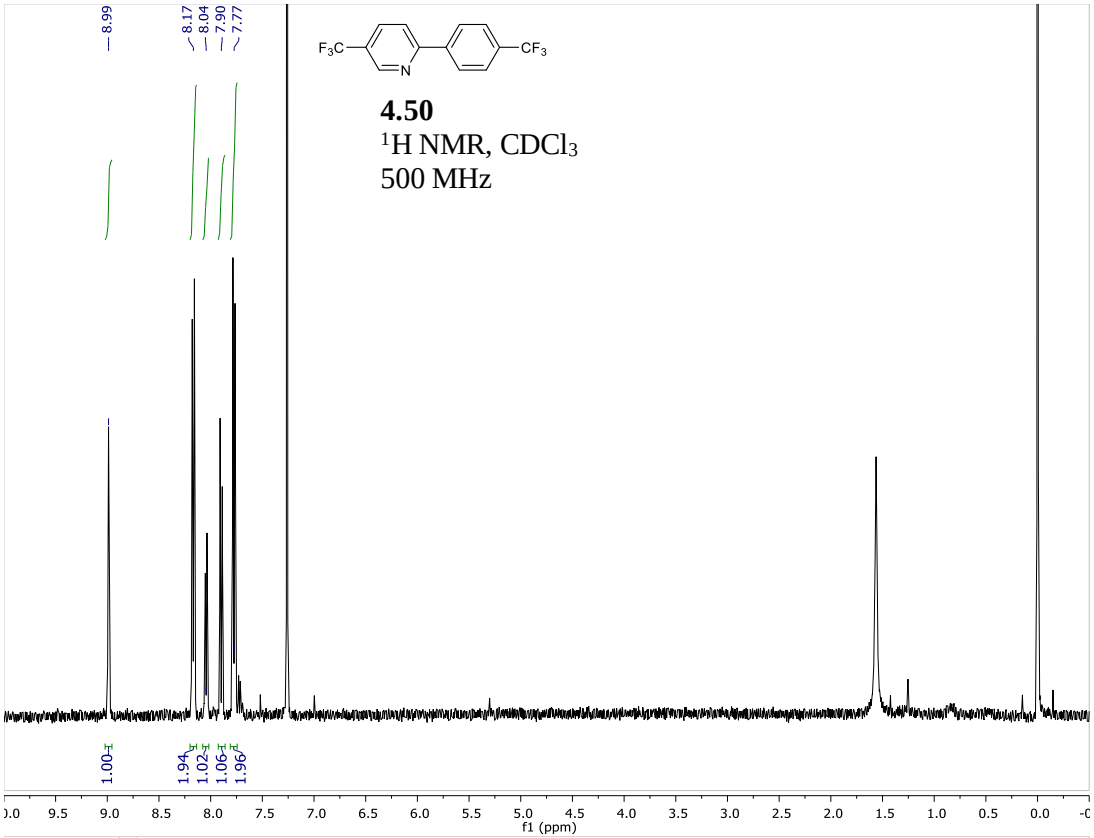
8.99
8.17
8.04
7.90
7.77
F3C
CF3
N
4.50
1H NMR, CDCl3
500 MHz
1.00
1.94
1.02
1.06
1.96
f1 (ppm)

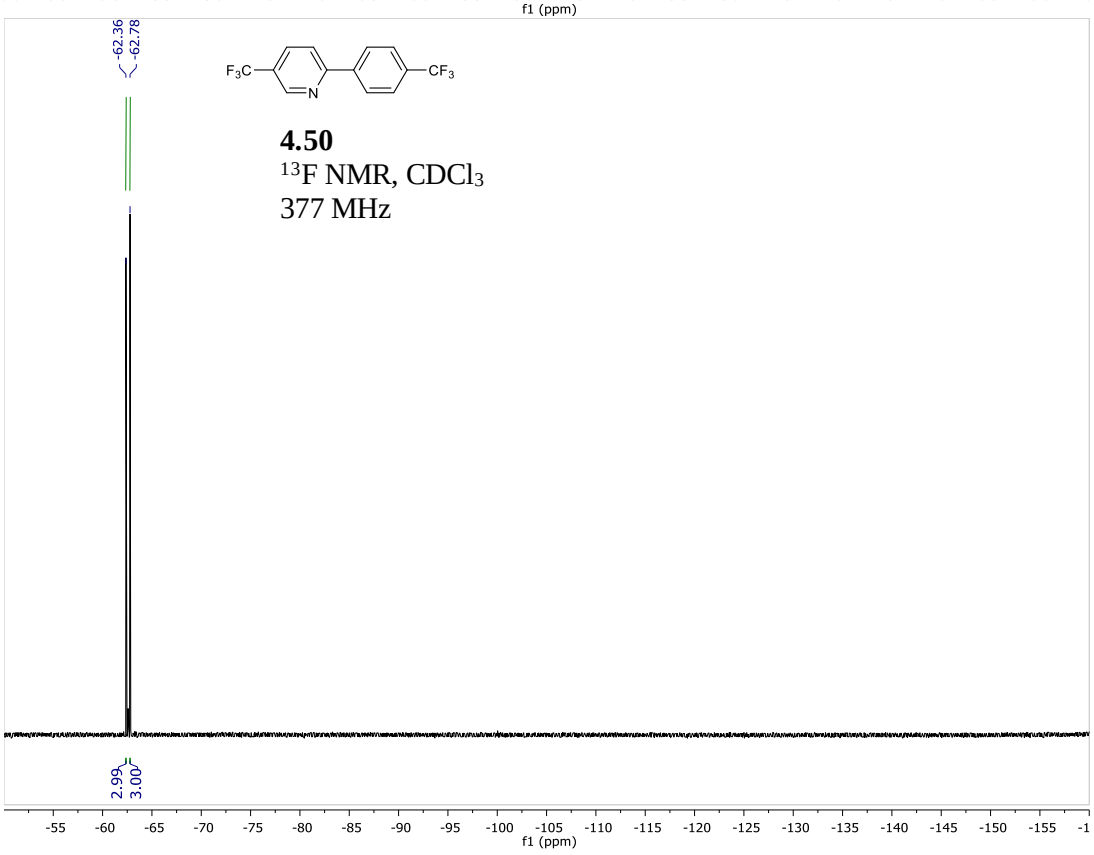
-62.36
-62.78
F3C
CF3
N
4.50
19F NMR, CDCl3
377 MHz
2.99
3.00
f1 (ppm)

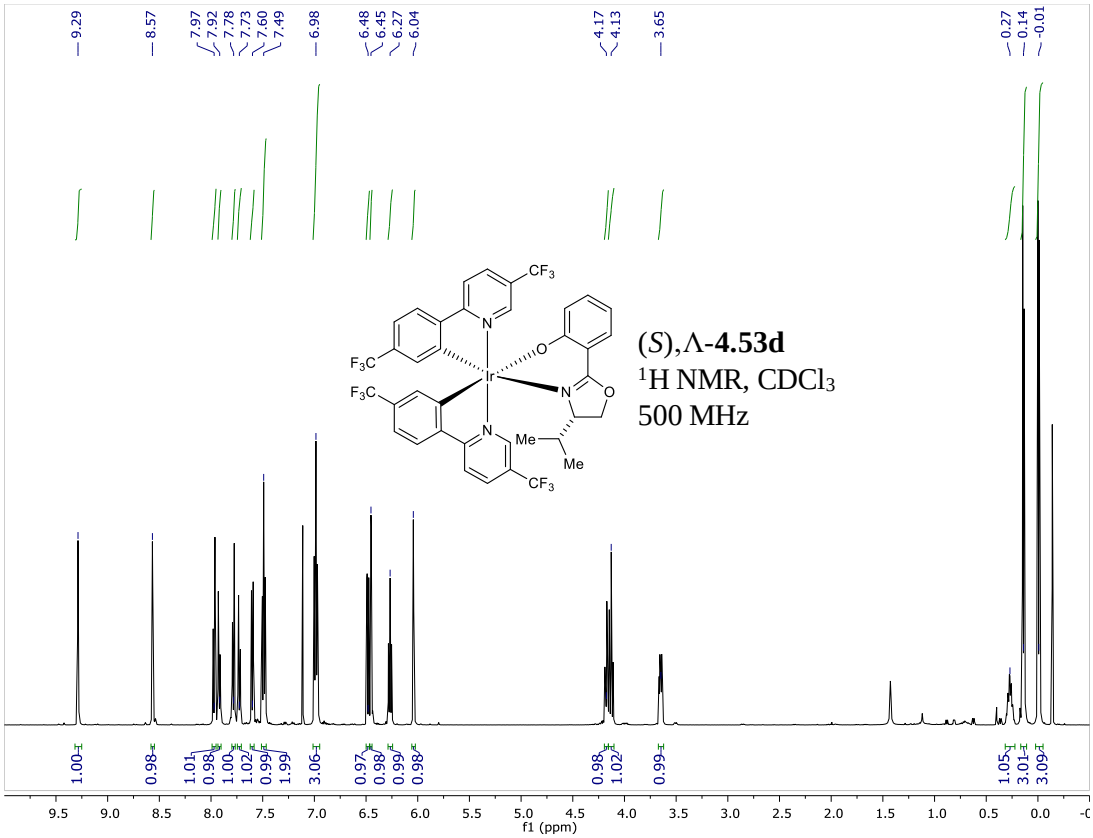

(*S*),Λ-**4.53d**
^{1}H NMR, $CDCl_3$
500 MHz

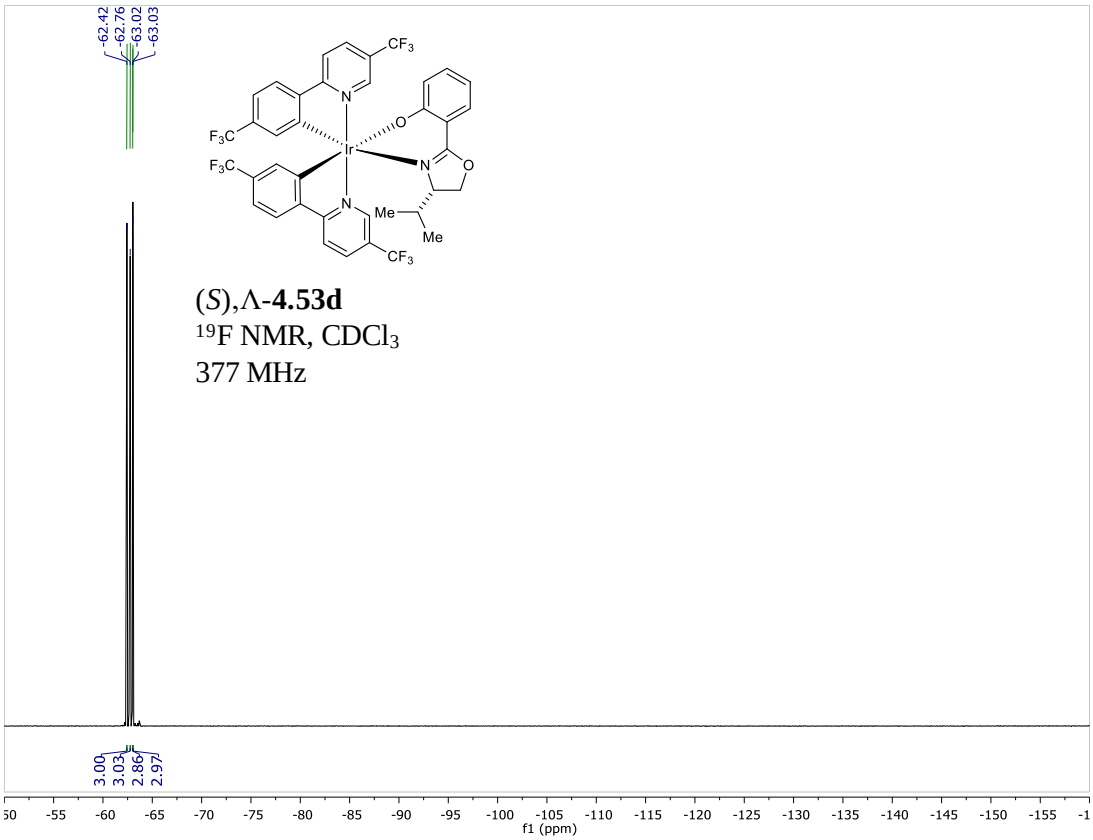

(*S*),Λ-**4.53d**
^{19}F NMR, $CDCl_3$
377 MHz

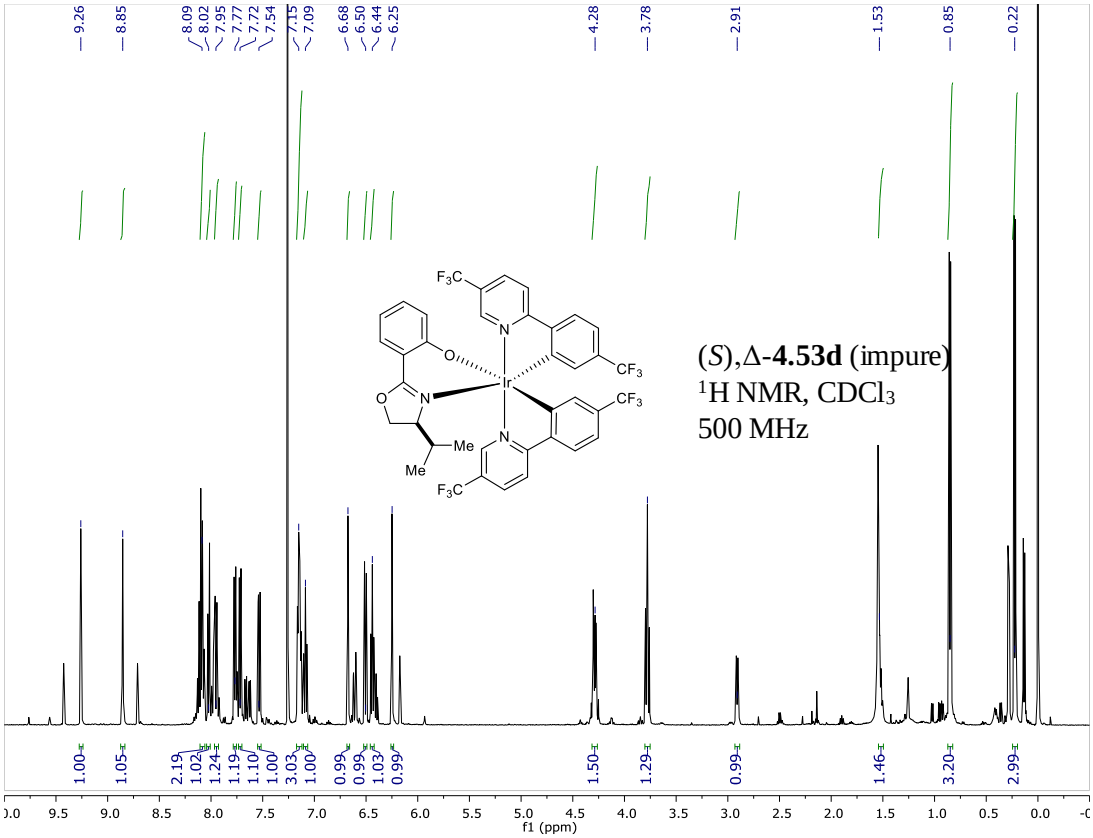
9.26
8.85
8.09
8.02
7.95
7.77
7.72
7.54
7.15
7.09
6.68
6.50
6.44
6.25
4.28
3.78
2.91
1.53
0.85
0.22
1.00
1.05
2.19
1.02
1.24
1.19
1.10
1.00
3.03
1.00
0.99
0.99
1.03
0.99
1.50
1.29
0.99
1.46
3.20
2.99
f1 (ppm)
(S),Δ-4.53d (impure)
1H NMR, CDCl3
500 MHz

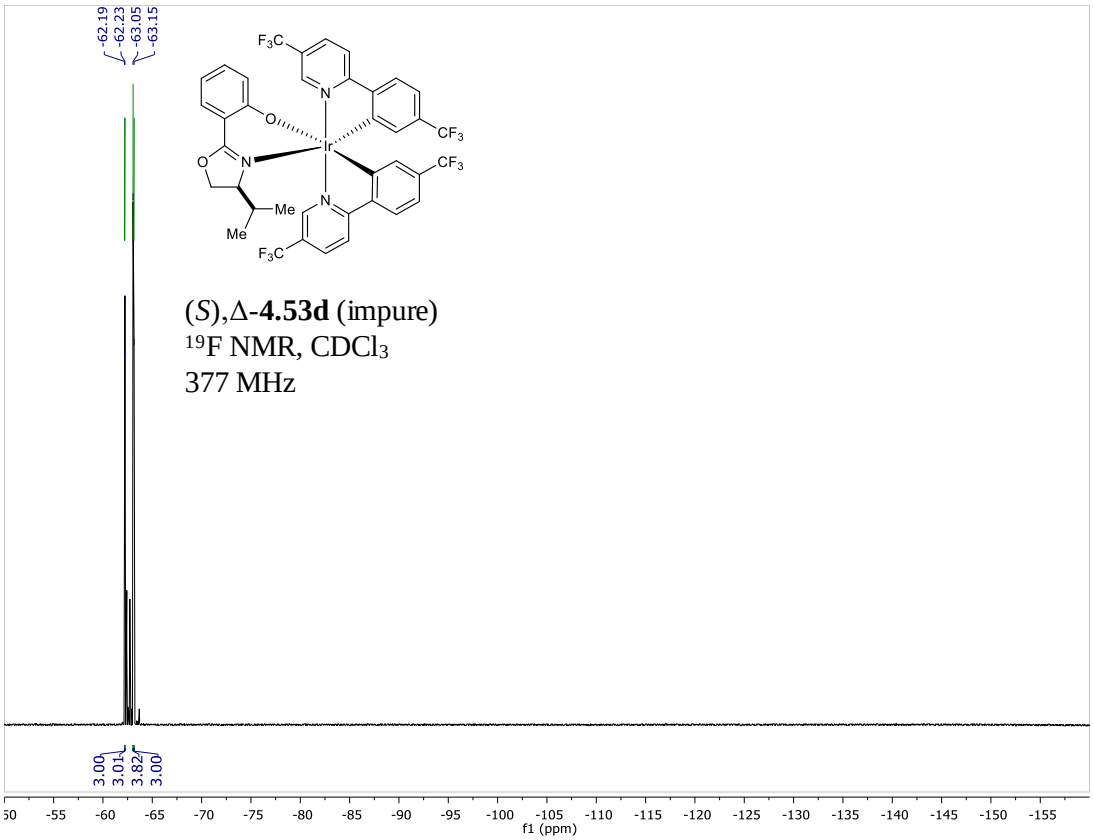
-62.19
-62.23
-63.05
-63.15
3.00
3.01
3.82
3.00
f1 (ppm)
(S),Δ-4.53d (impure)
19F NMR, CDCl3
377 MHz

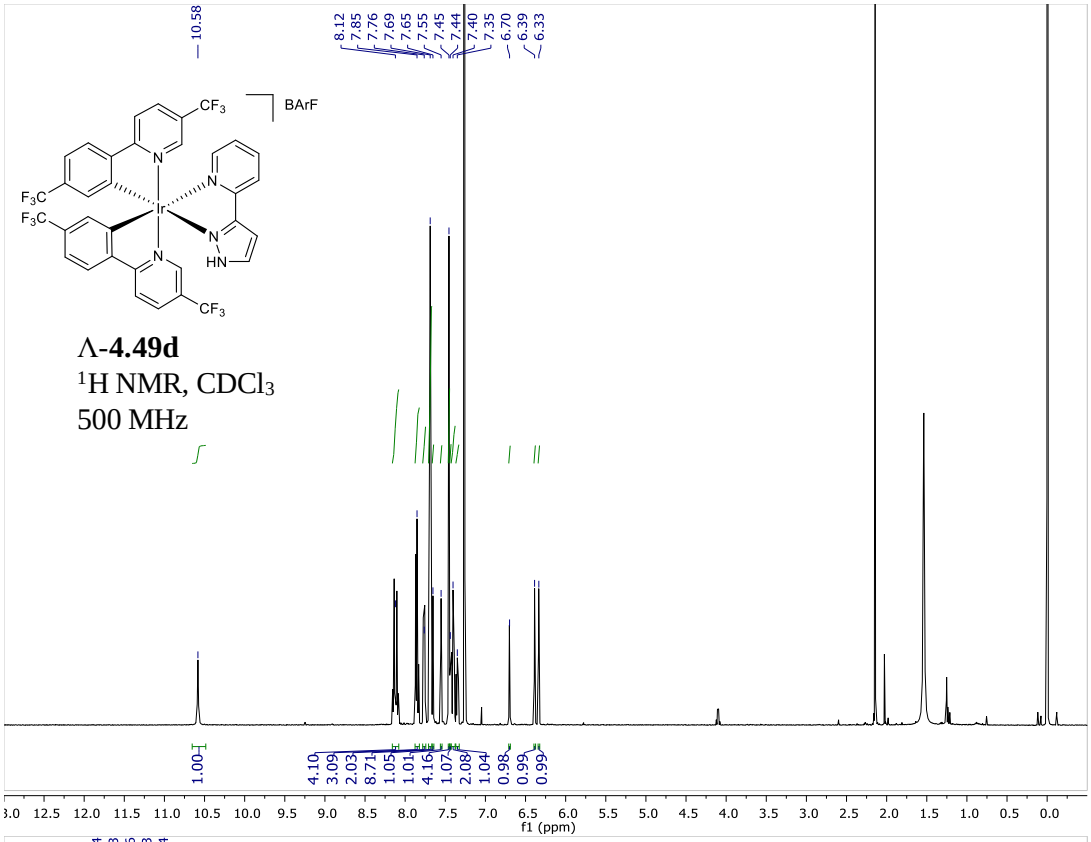

Λ-**4.49d**
^{1}H NMR, $CDCl_3$
500 MHz

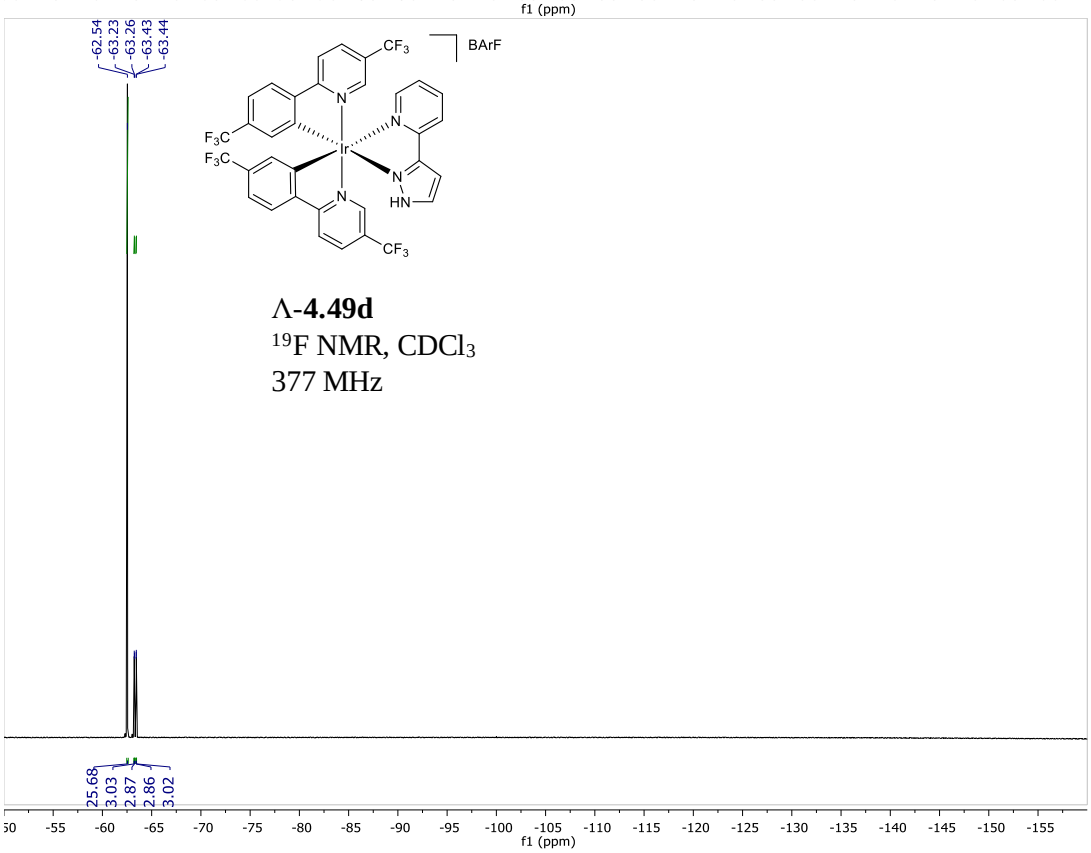

Λ-**4.49d**
^{19}F NMR, $CDCl_3$
377 MHz

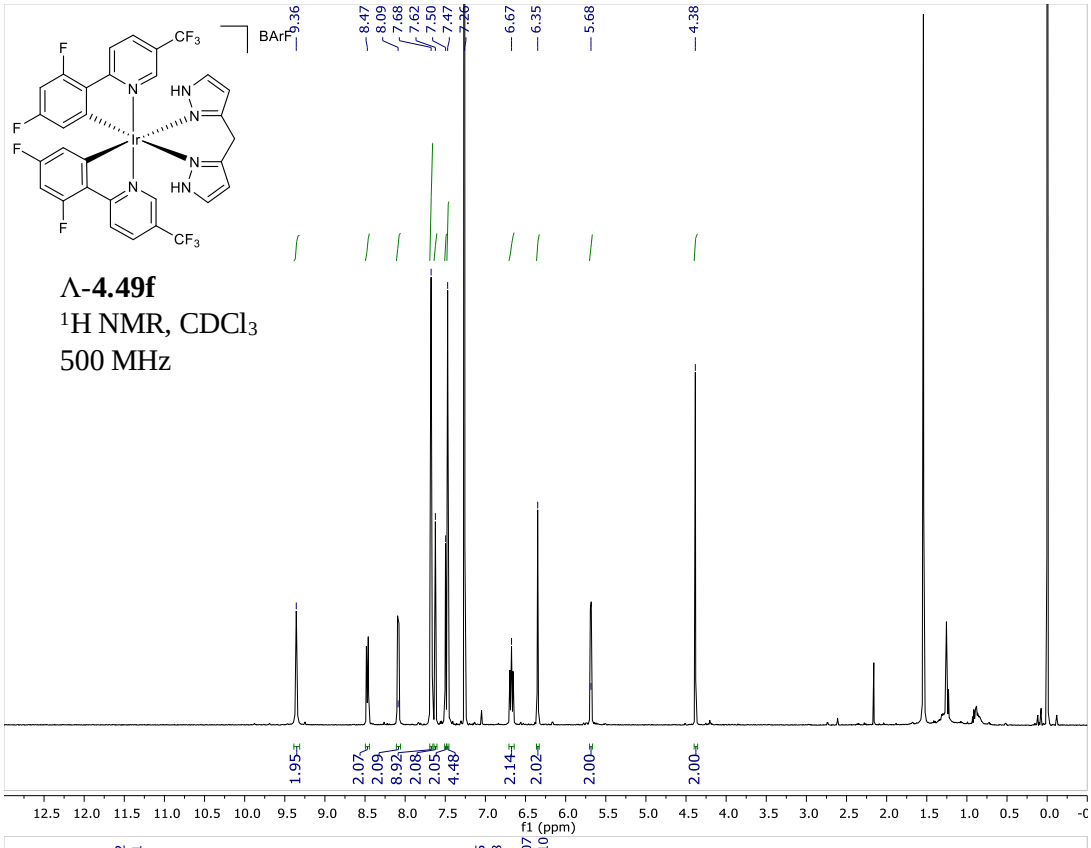

Λ-**4.49f**
^{1}H NMR, $CDCl_3$
500 MHz

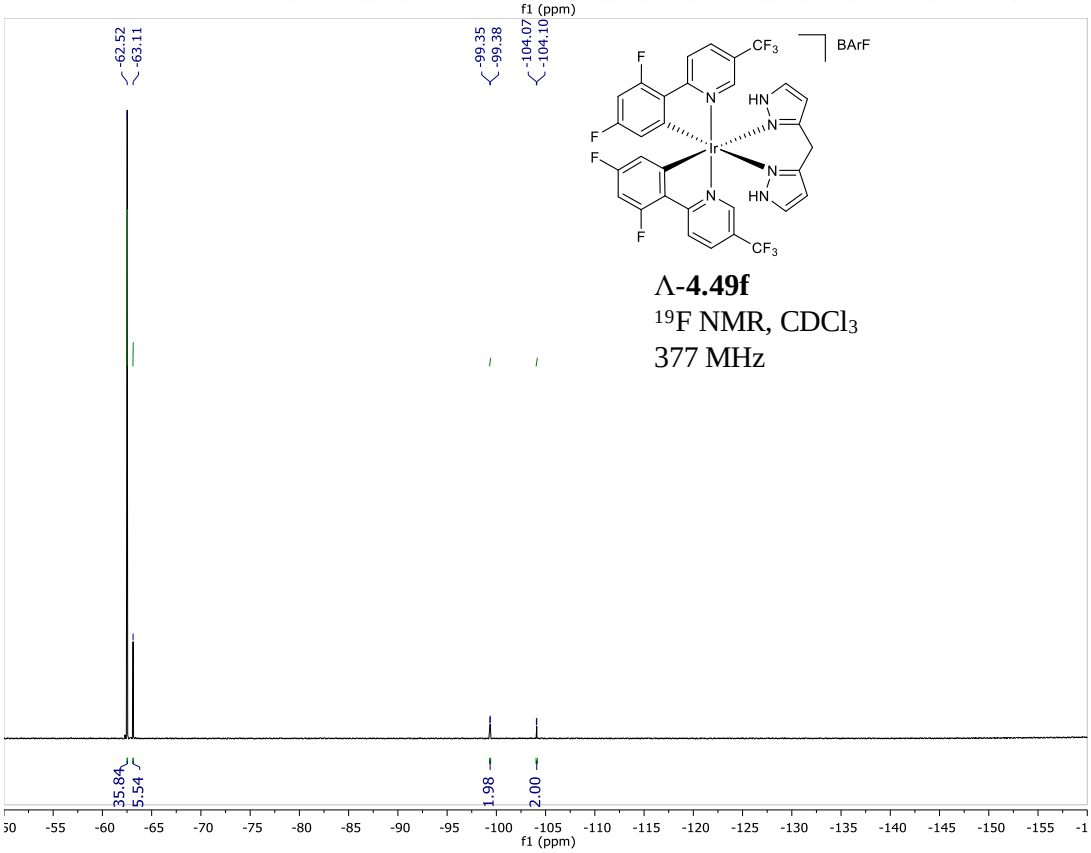

Λ-**4.49f**
^{19}F NMR, $CDCl_3$
377 MHz

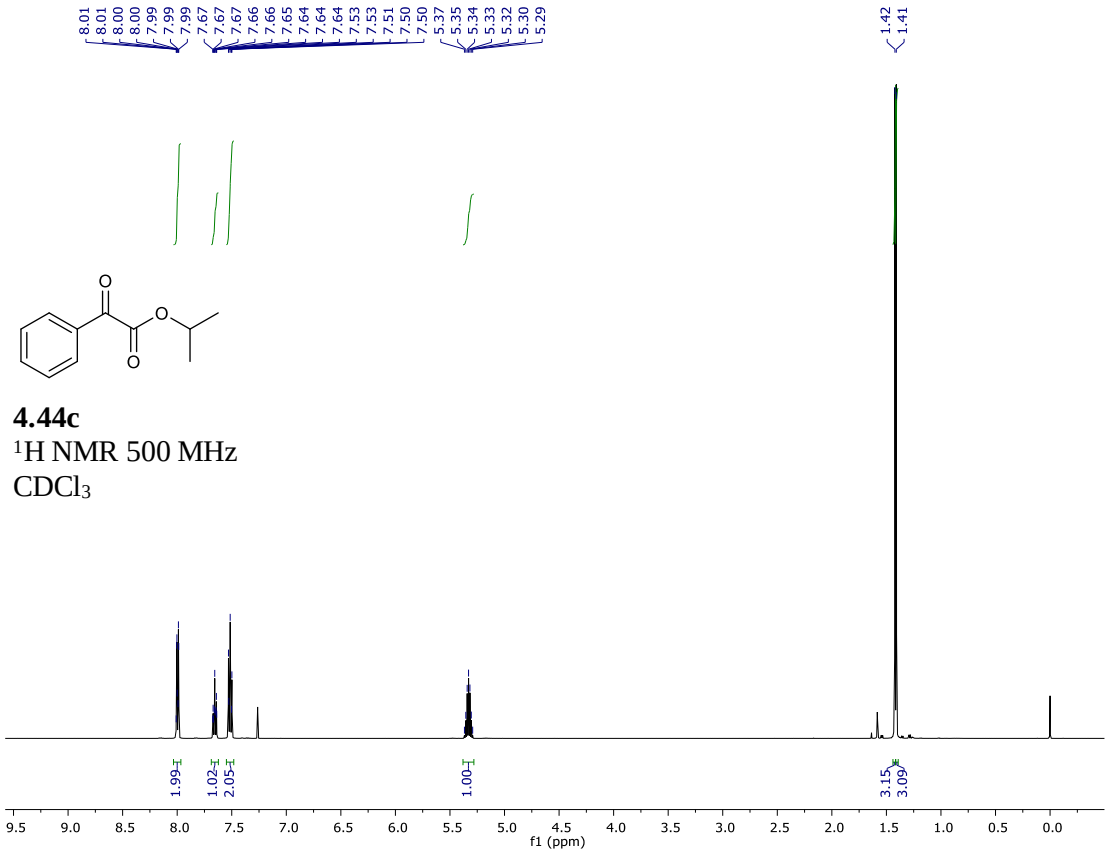

4.44c
^{1}H NMR 500 MHz
$CDCl_3$

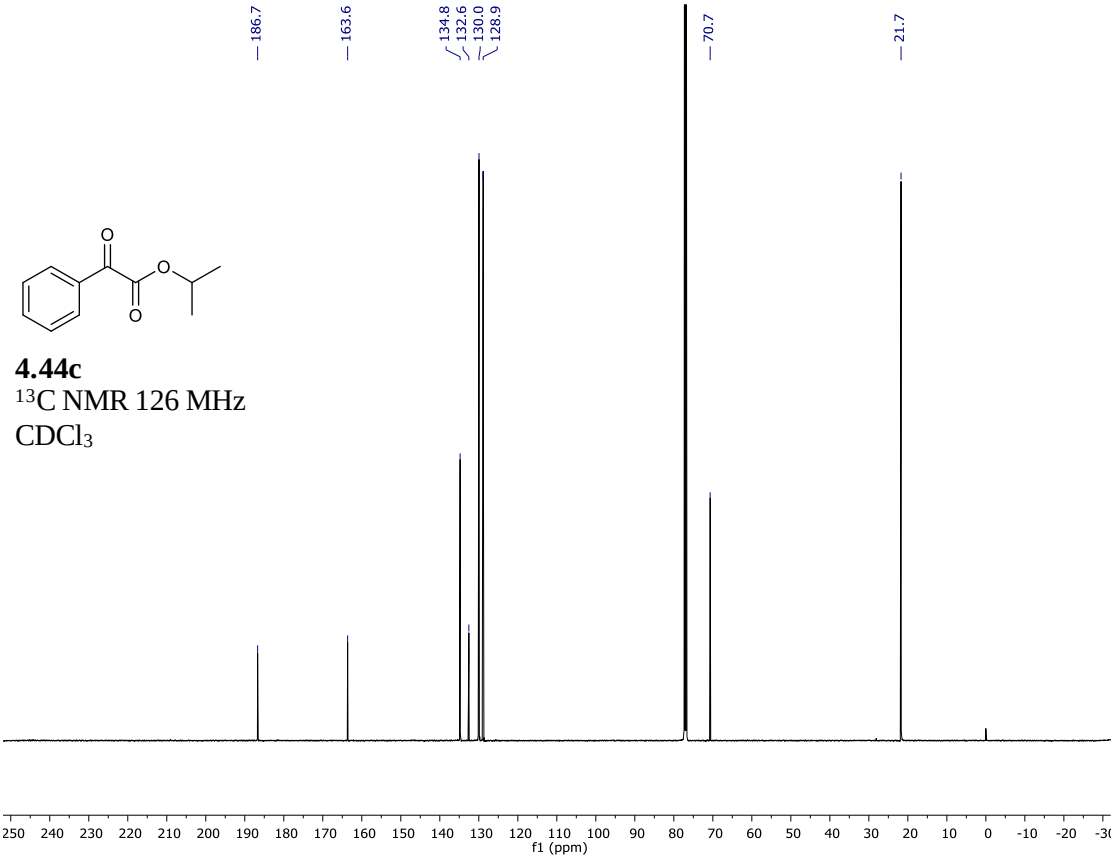

4.44c
^{13}C NMR 126 MHz
$CDCl_3$

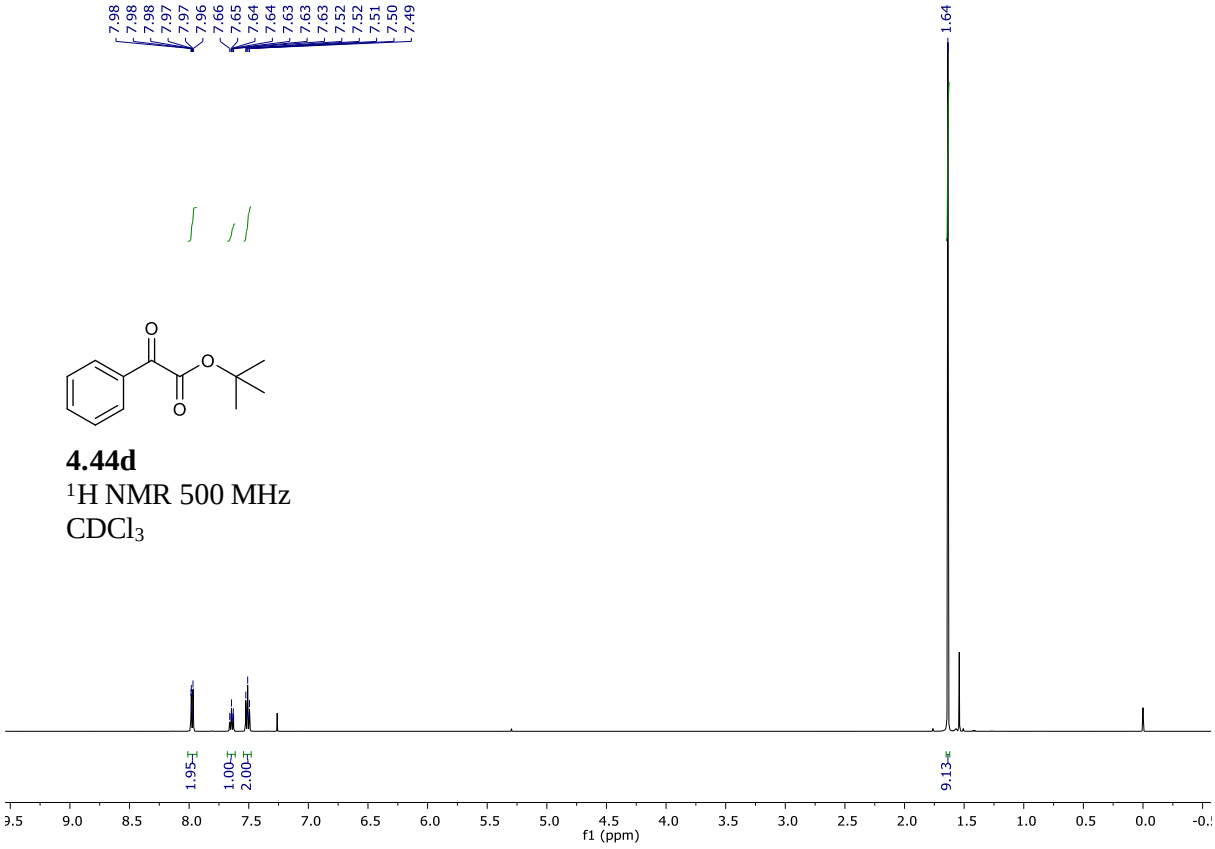

4.44d
^{1}H NMR 500 MHz
$CDCl_3$

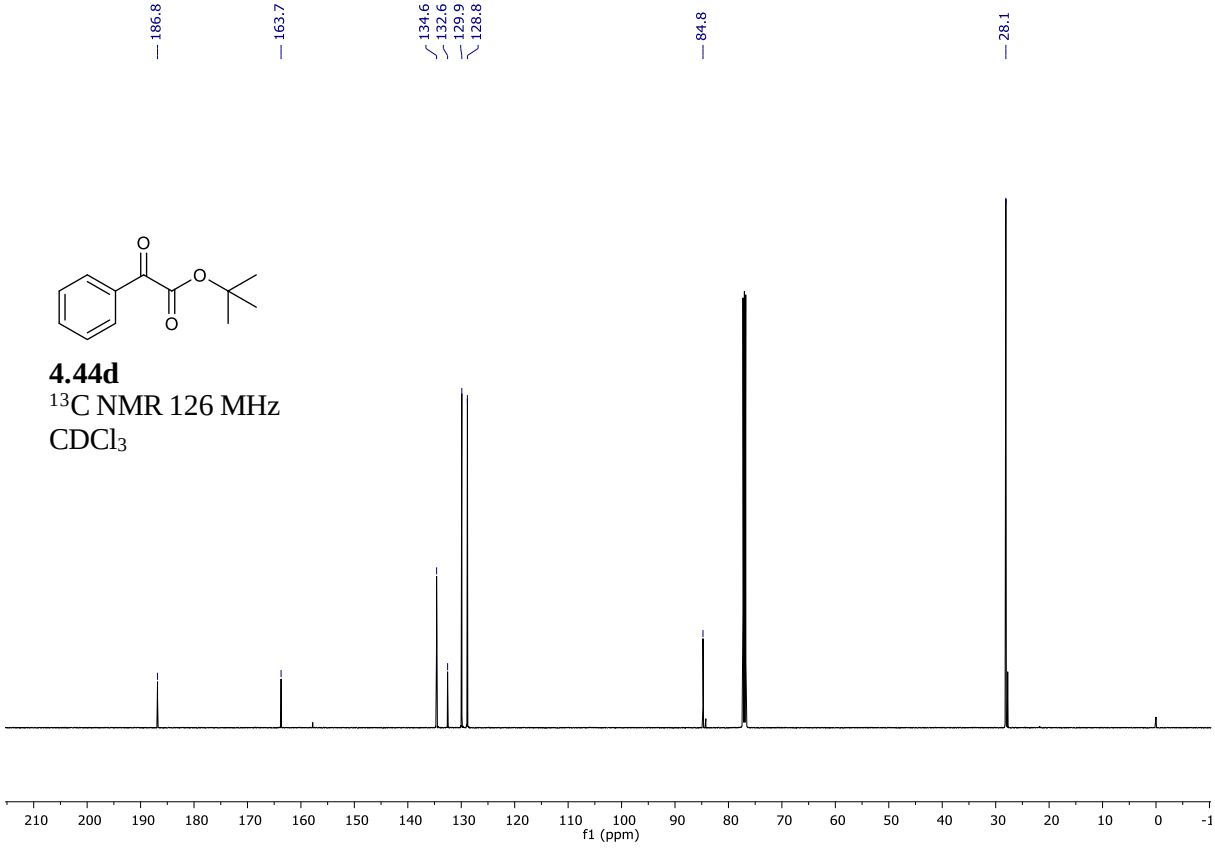

4.44d
^{13}C NMR 126 MHz
$CDCl_3$

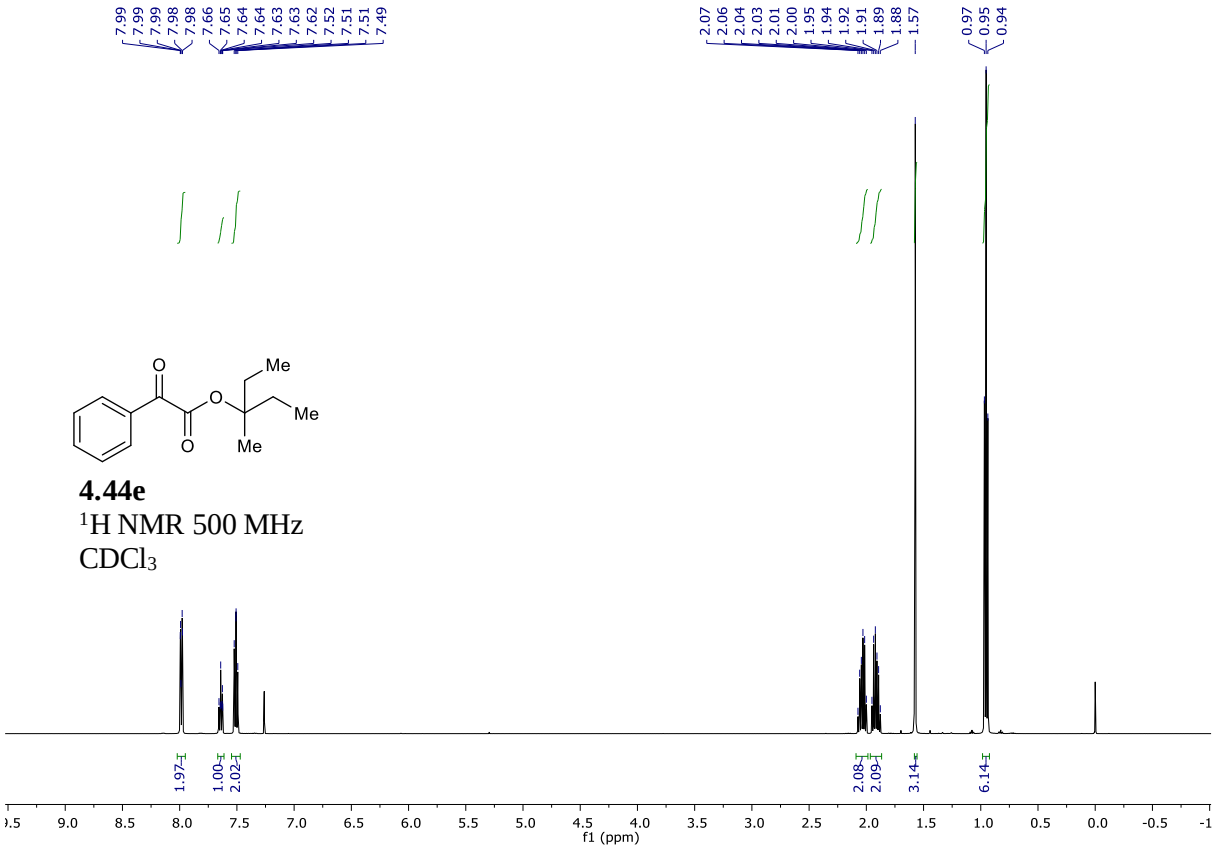

4.44e
^{1}H NMR 500 MHz
$CDCl_3$

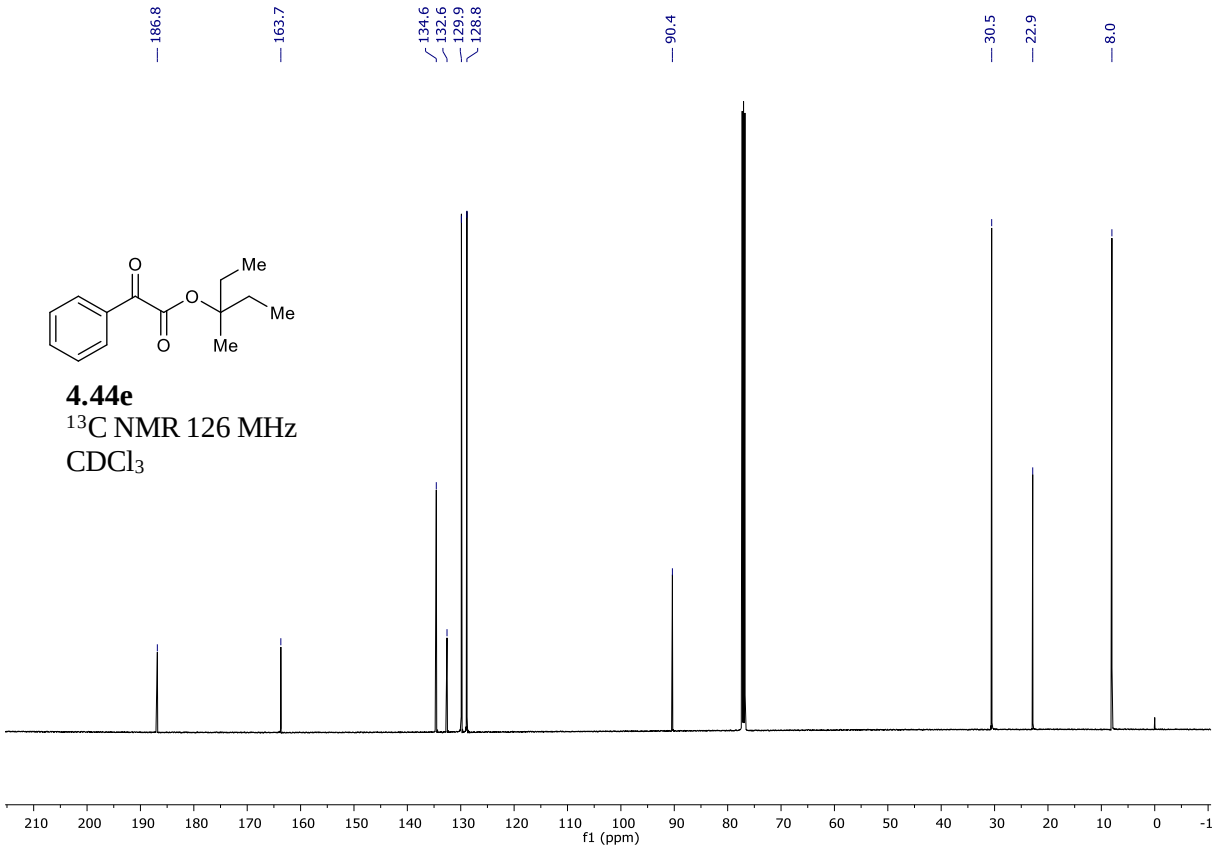

4.44e
^{13}C NMR 126 MHz
$CDCl_3$

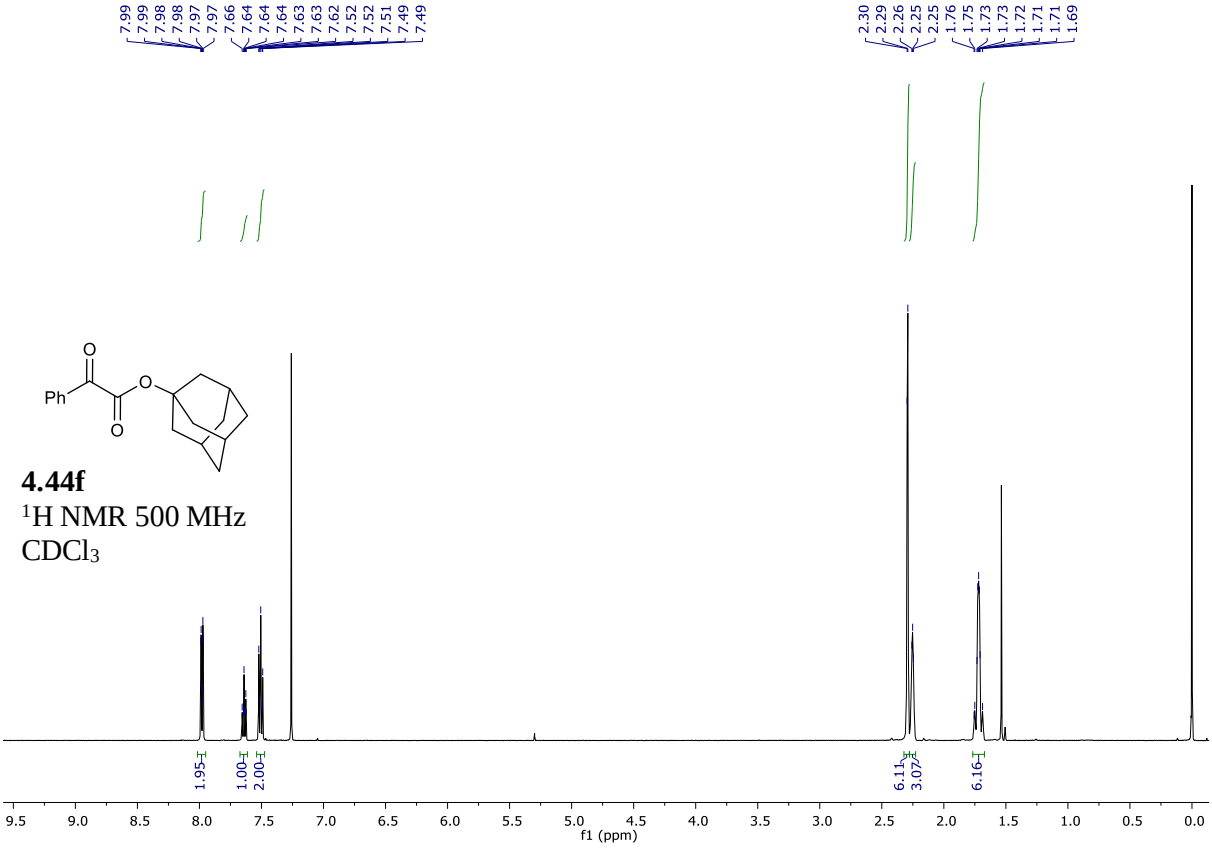

4.44f

^{1}H NMR 500 MHz

$CDCl_3$

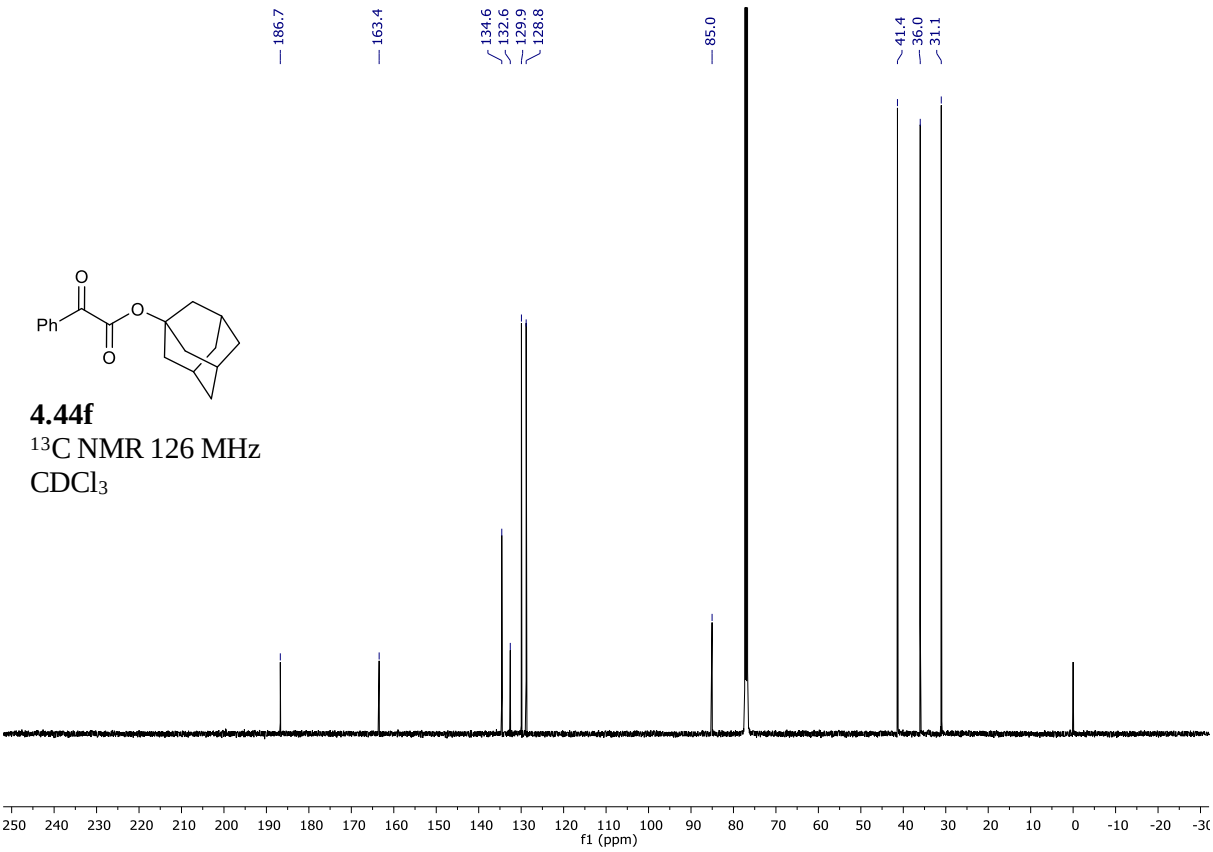

4.44f

^{13}C NMR 126 MHz

$CDCl_3$

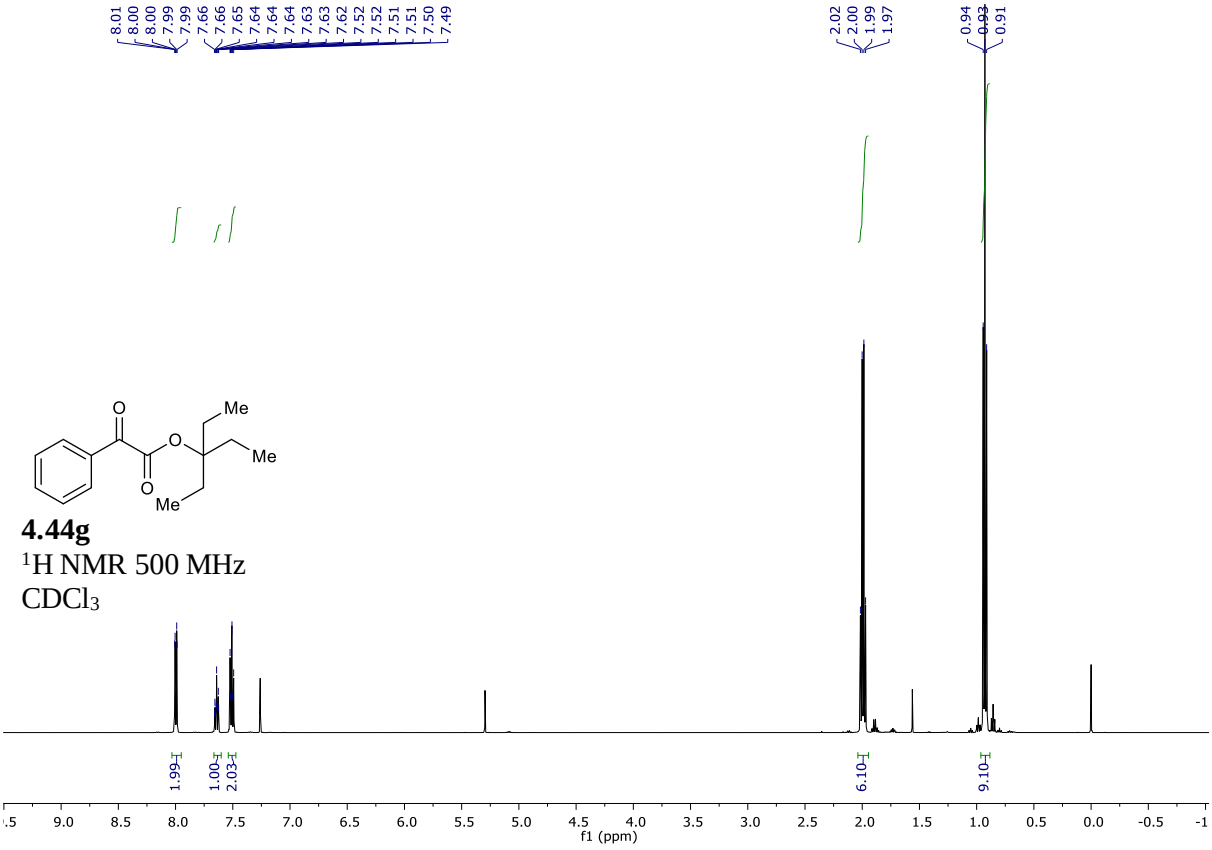

4.44g

^{1}H NMR 500 MHz

$CDCl_3$

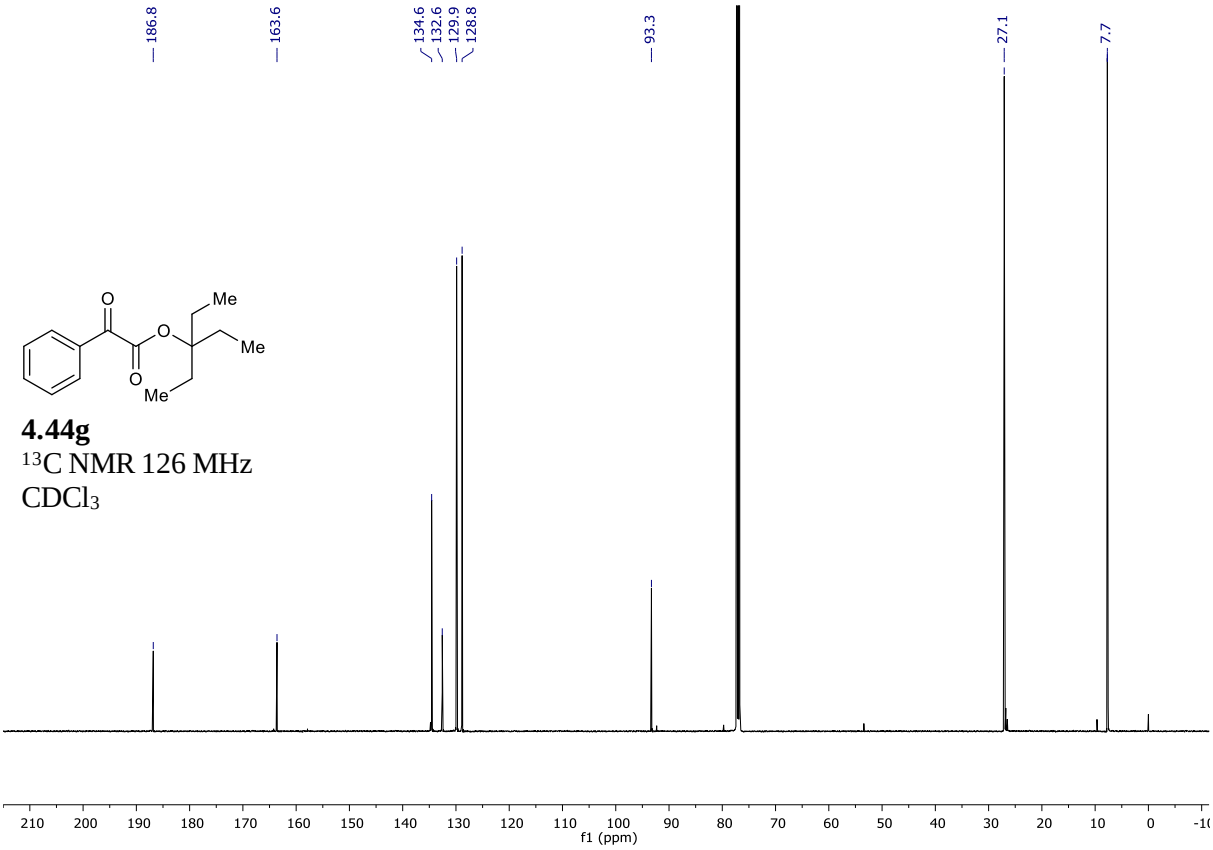

4.44g

^{13}C NMR 126 MHz

$CDCl_3$

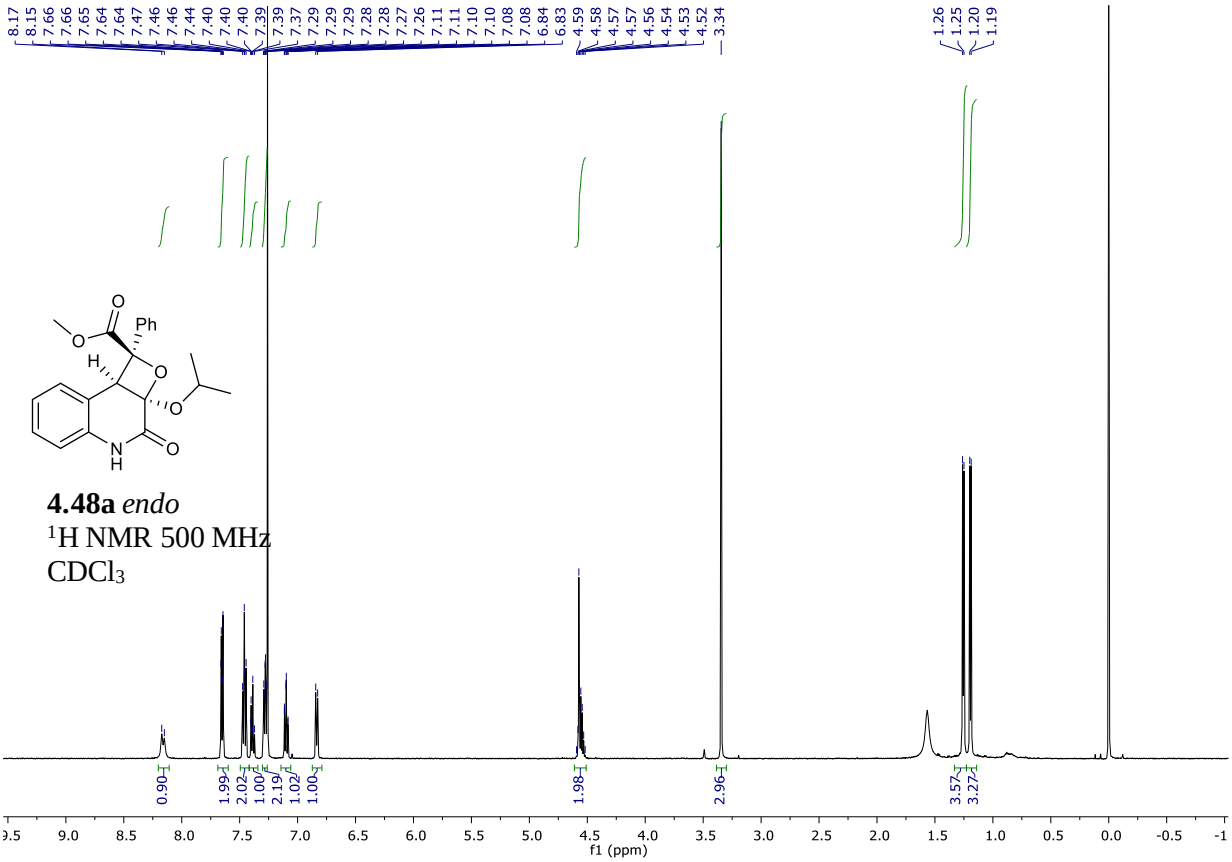

4.48a *endo*
^{1}H NMR 500 MHz
$CDCl_3$

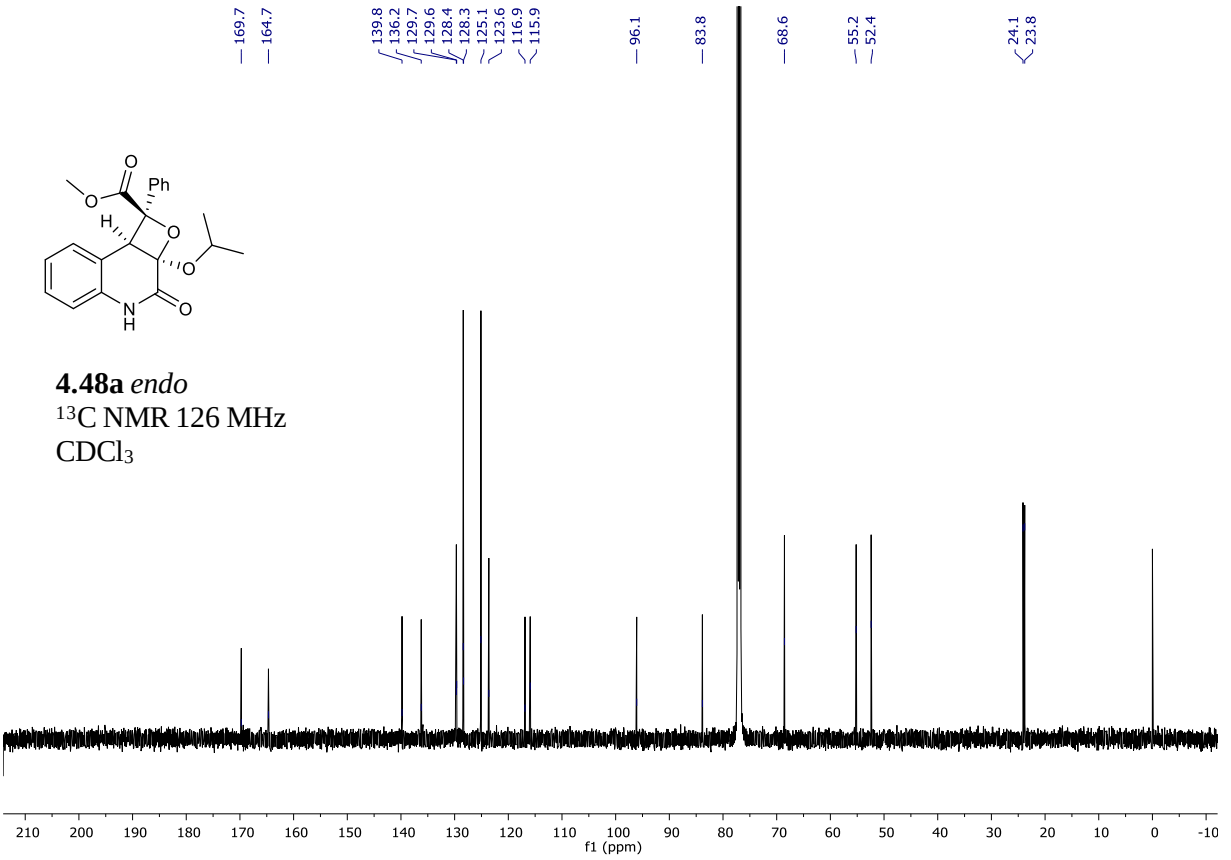

4.48a *endo*
^{13}C NMR 126 MHz
$CDCl_3$

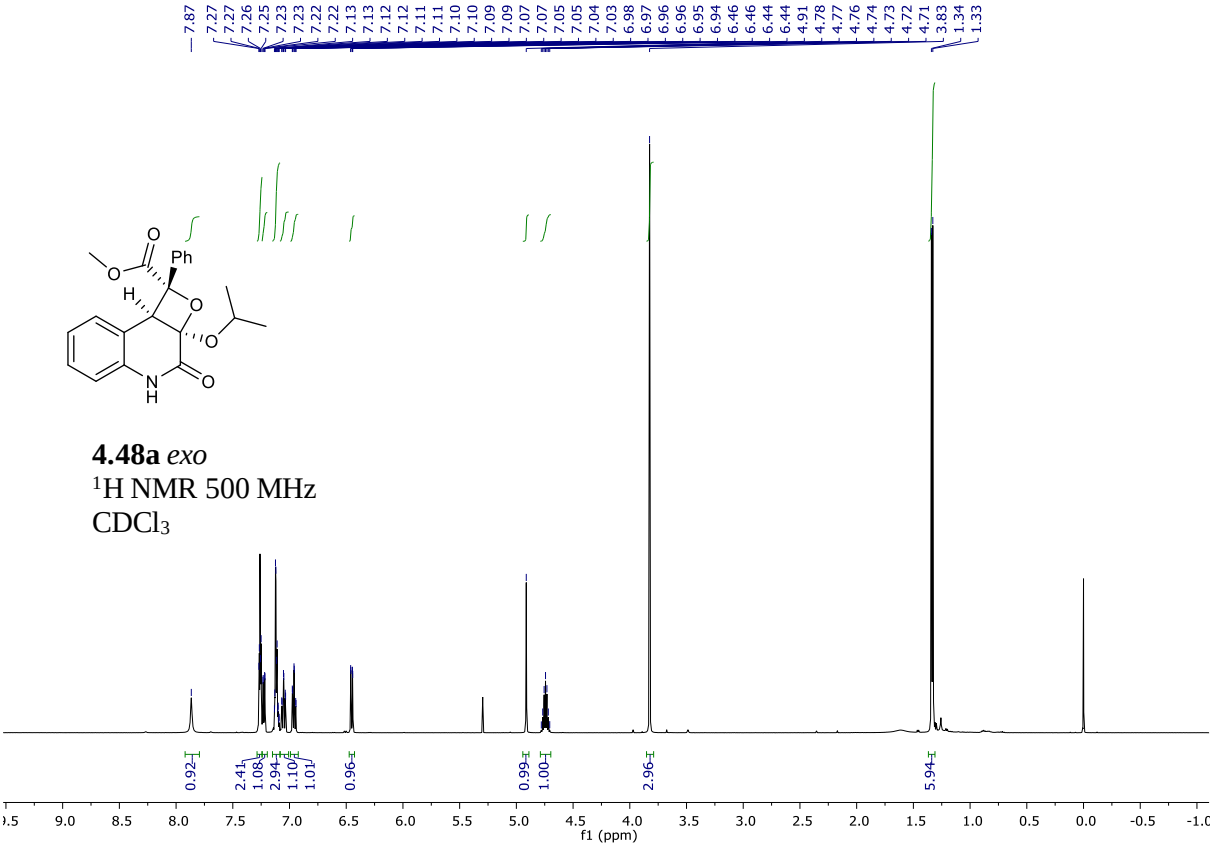

4.48a *exo*
^{1}H NMR 500 MHz
$CDCl_3$

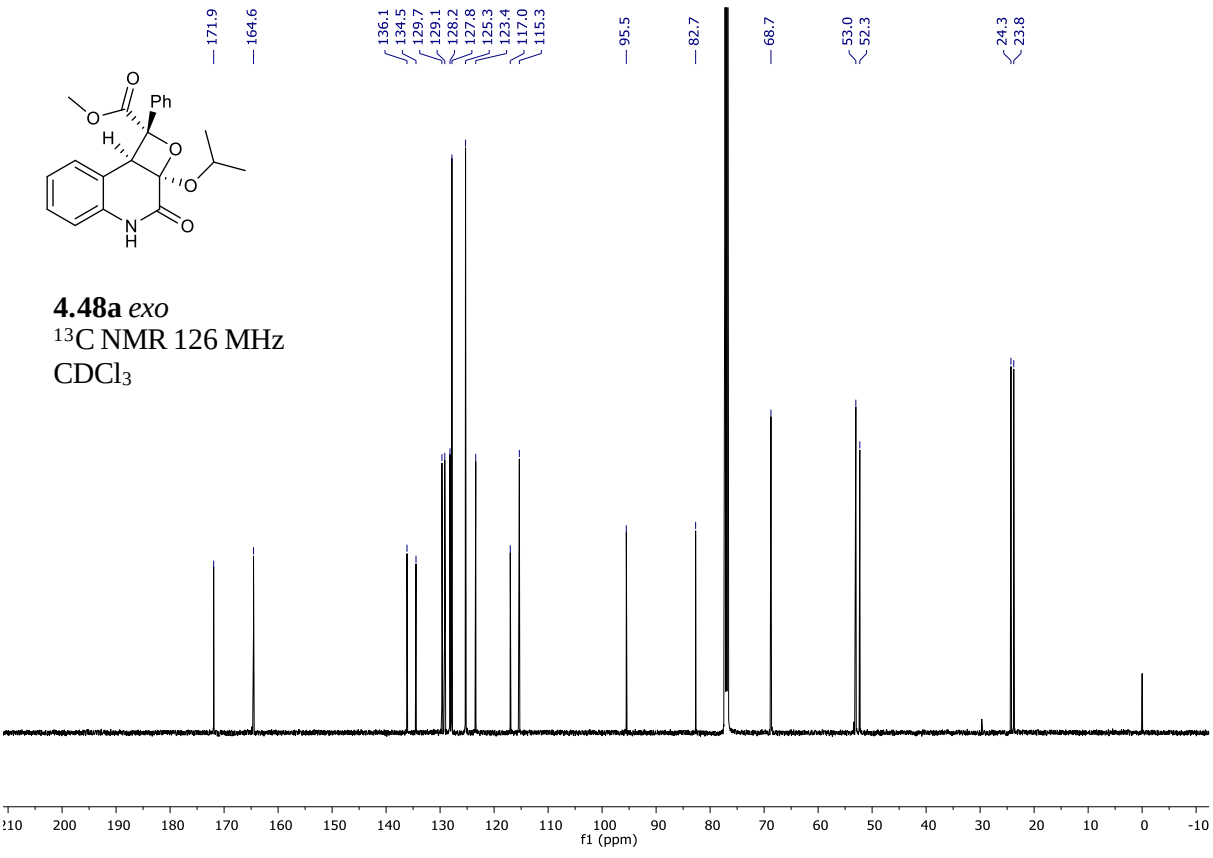

4.48a *exo*
^{13}C NMR 126 MHz
$CDCl_3$

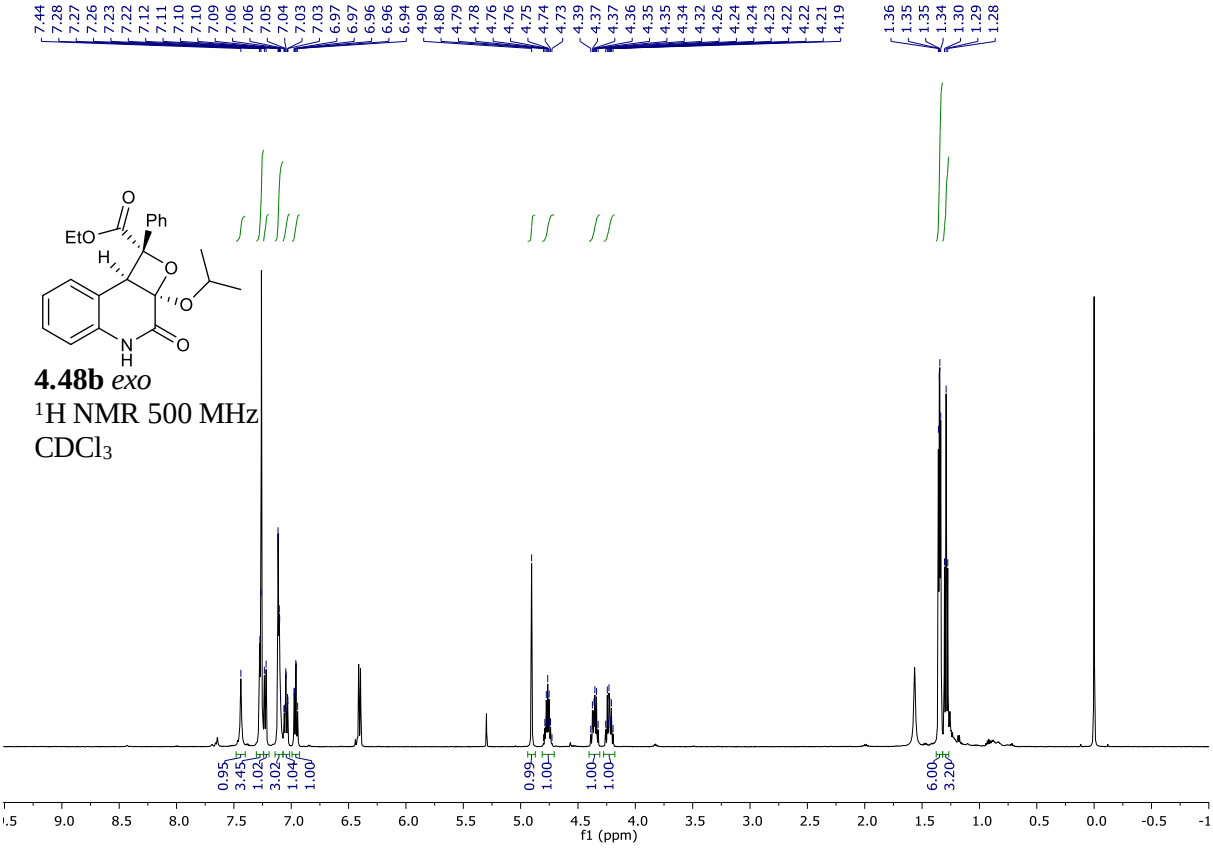

4.48b *exo*
^{1}H NMR 500 MHz
$CDCl_3$

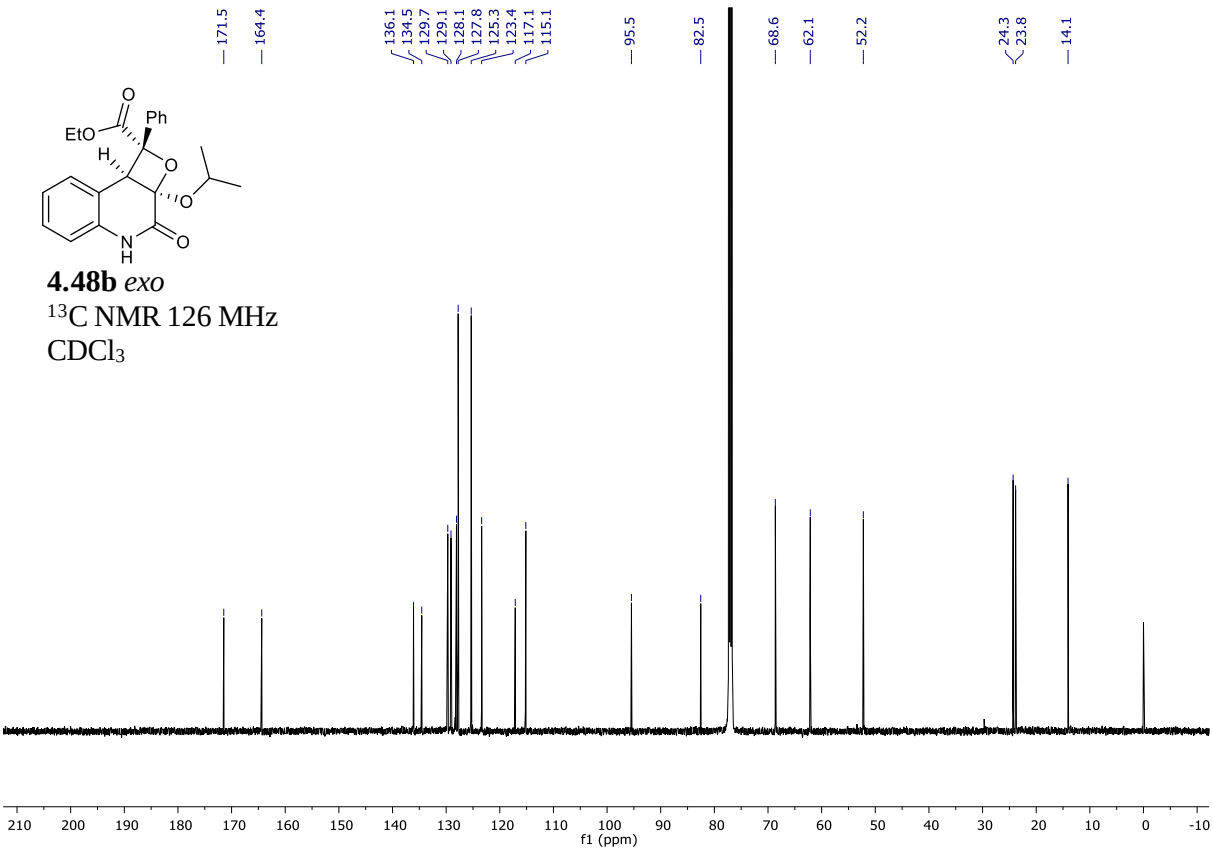

4.48b *exo*
^{13}C NMR 126 MHz
$CDCl_3$

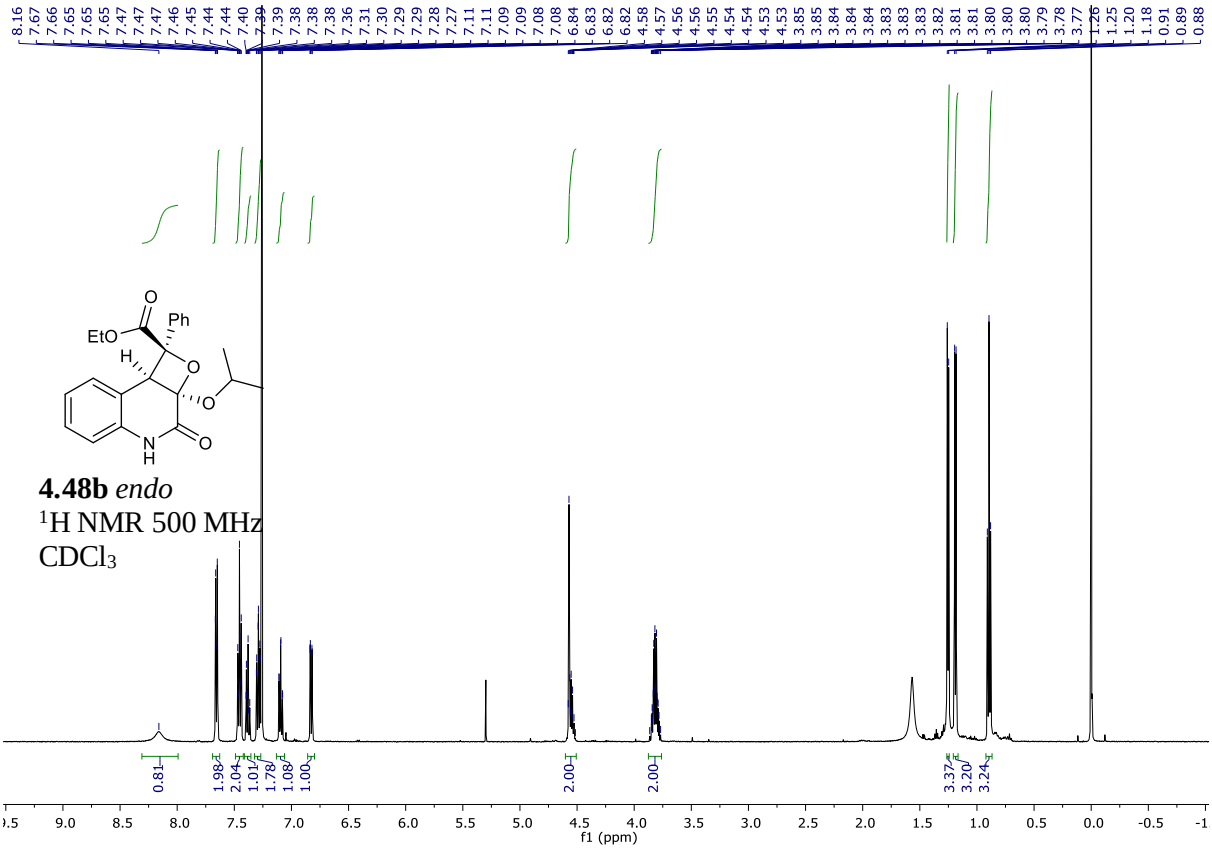
EtO
Ph
H
O
O
N
H
O
4.48b endo
1H NMR 500 MHz
CDCl3
f1 (ppm)

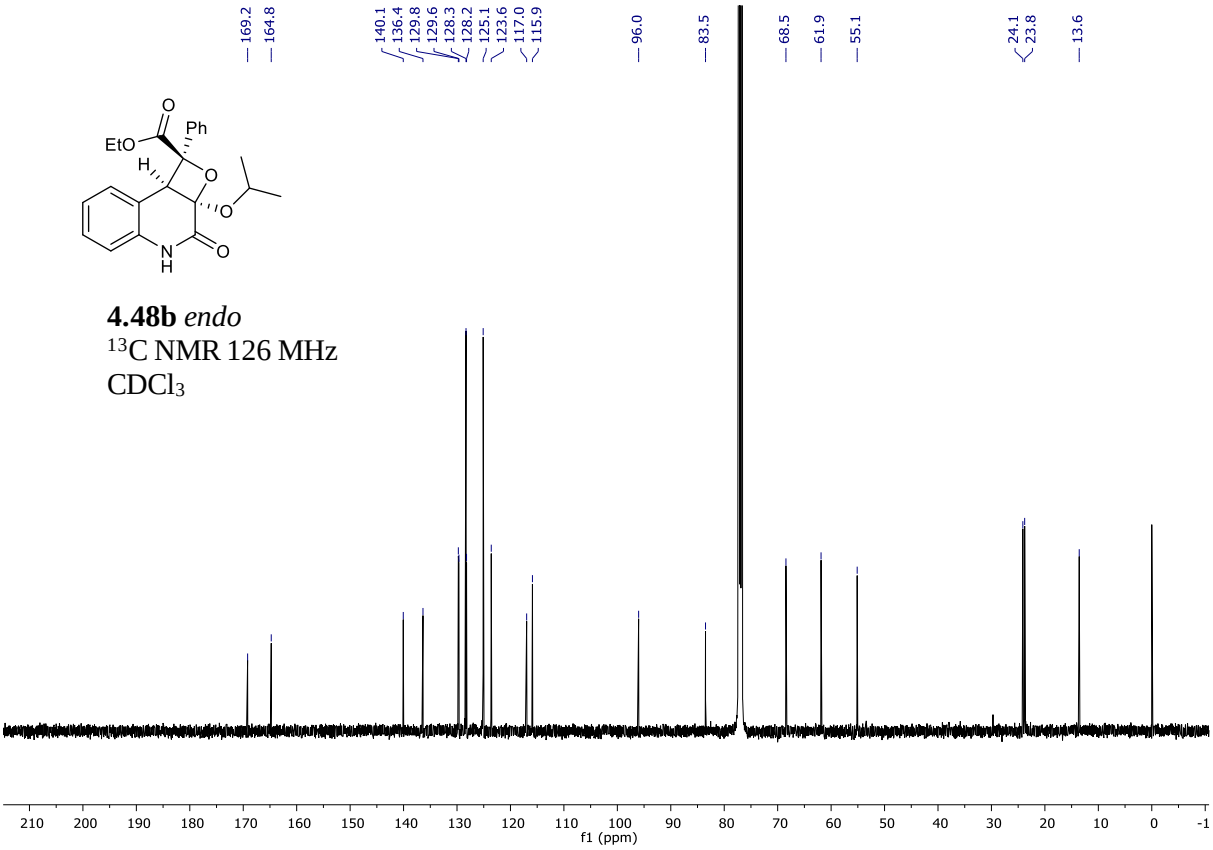
EtO
Ph
H
O
O
N
H
O
4.48b endo
13C NMR 126 MHz
CDCl3
f1 (ppm)

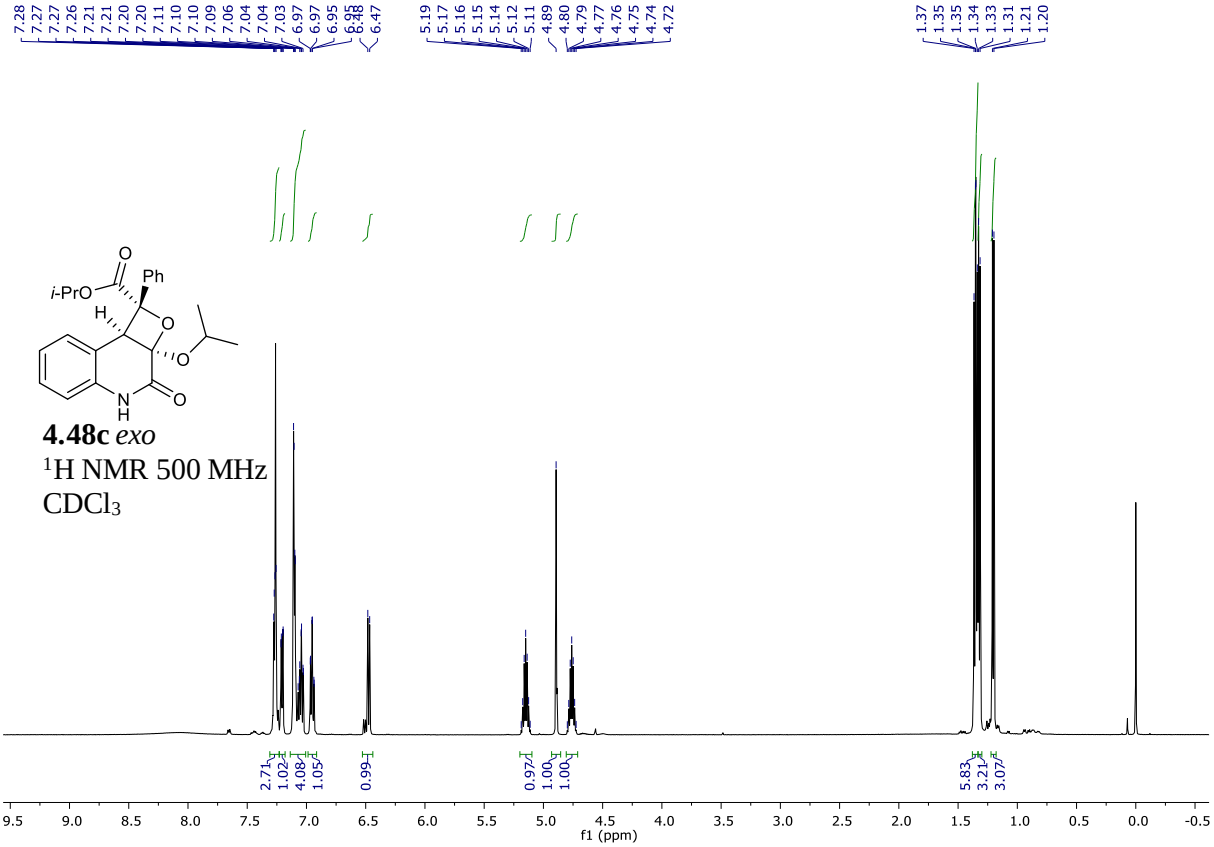

4.48c *exo*
^{1}H NMR 500 MHz
$CDCl_3$

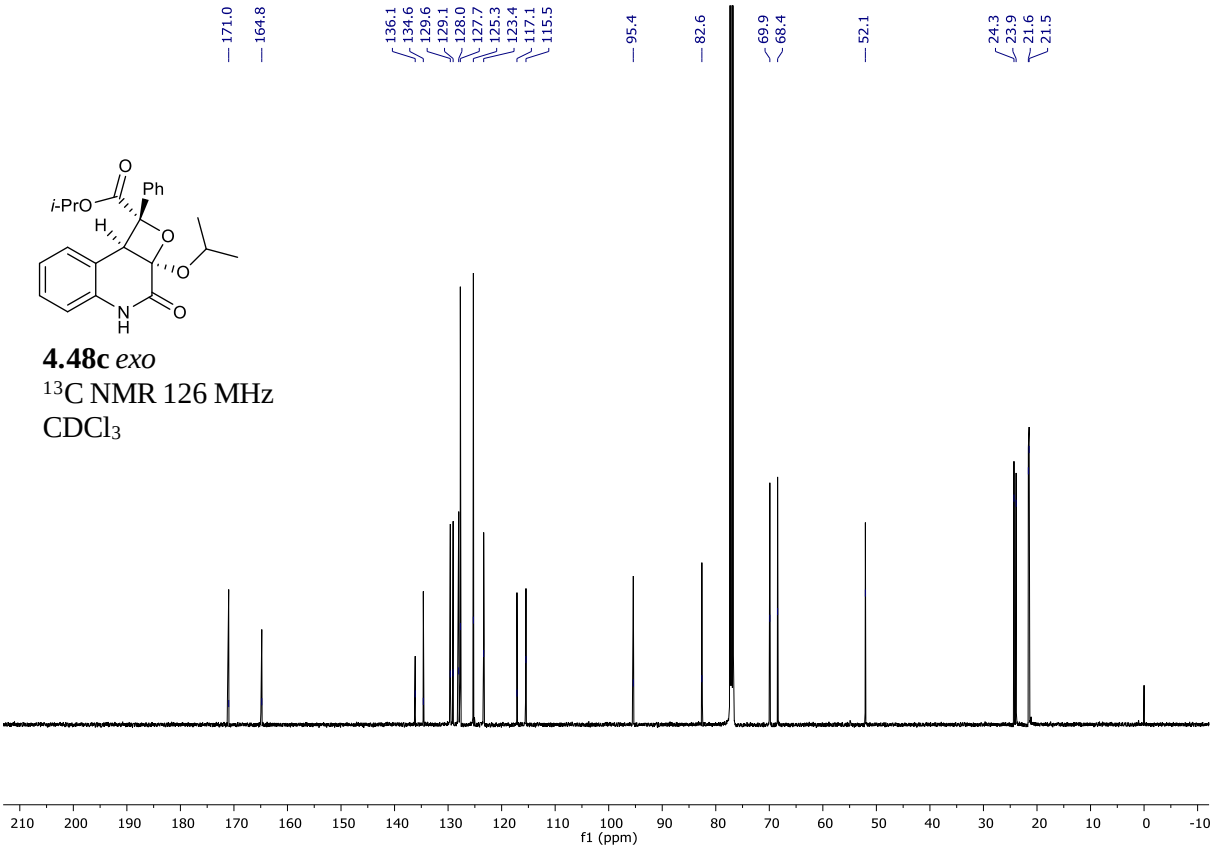

4.48c *exo*
^{13}C NMR 126 MHz
$CDCl_3$

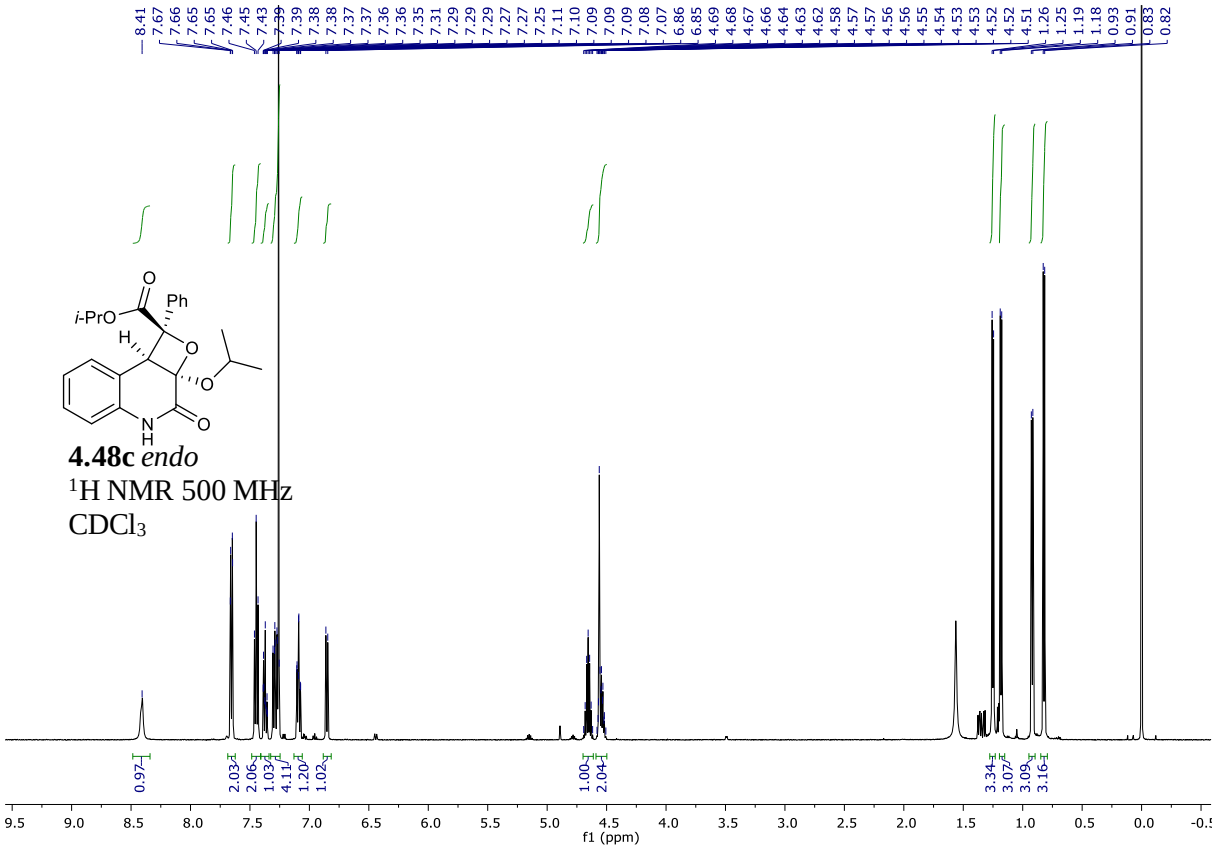

4.48c *endo*
^{1}H NMR 500 MHz
$CDCl_3$

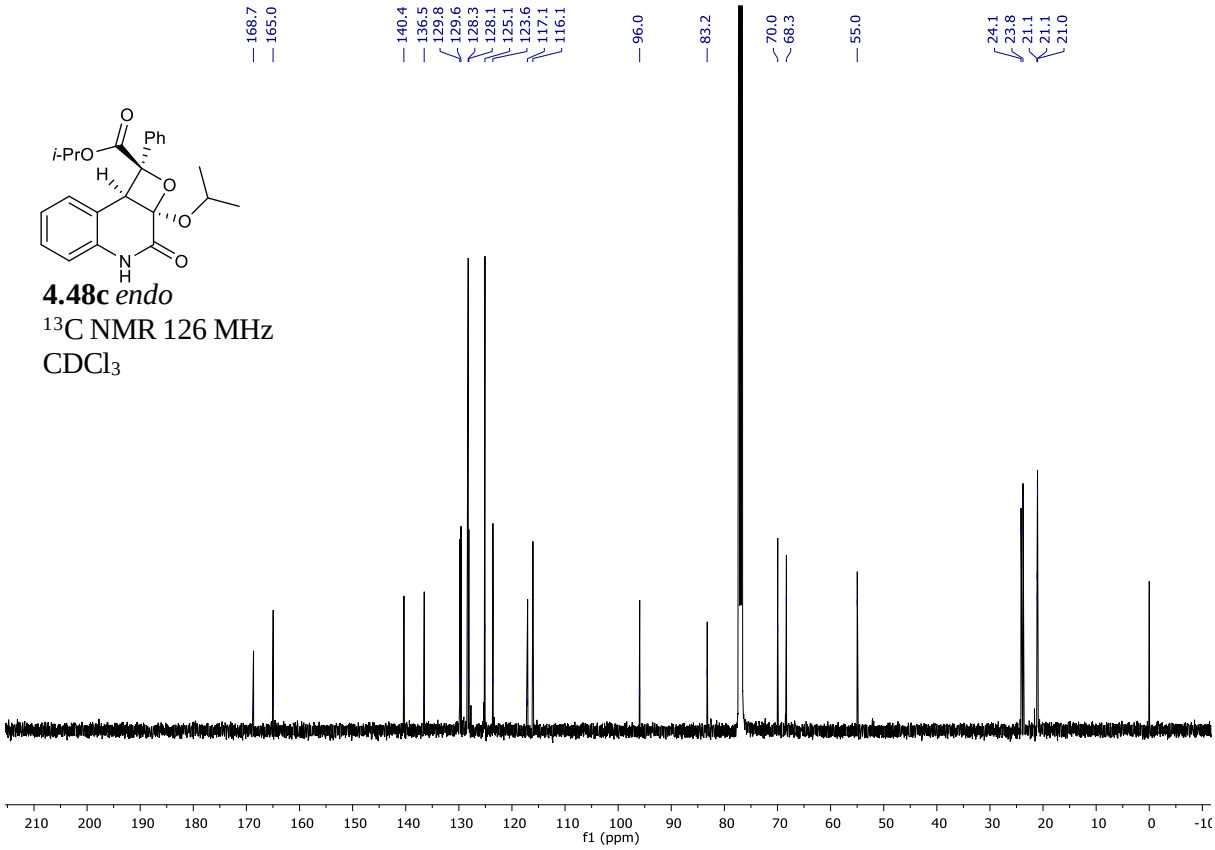

4.48c *endo*
^{13}C NMR 126 MHz
$CDCl_3$

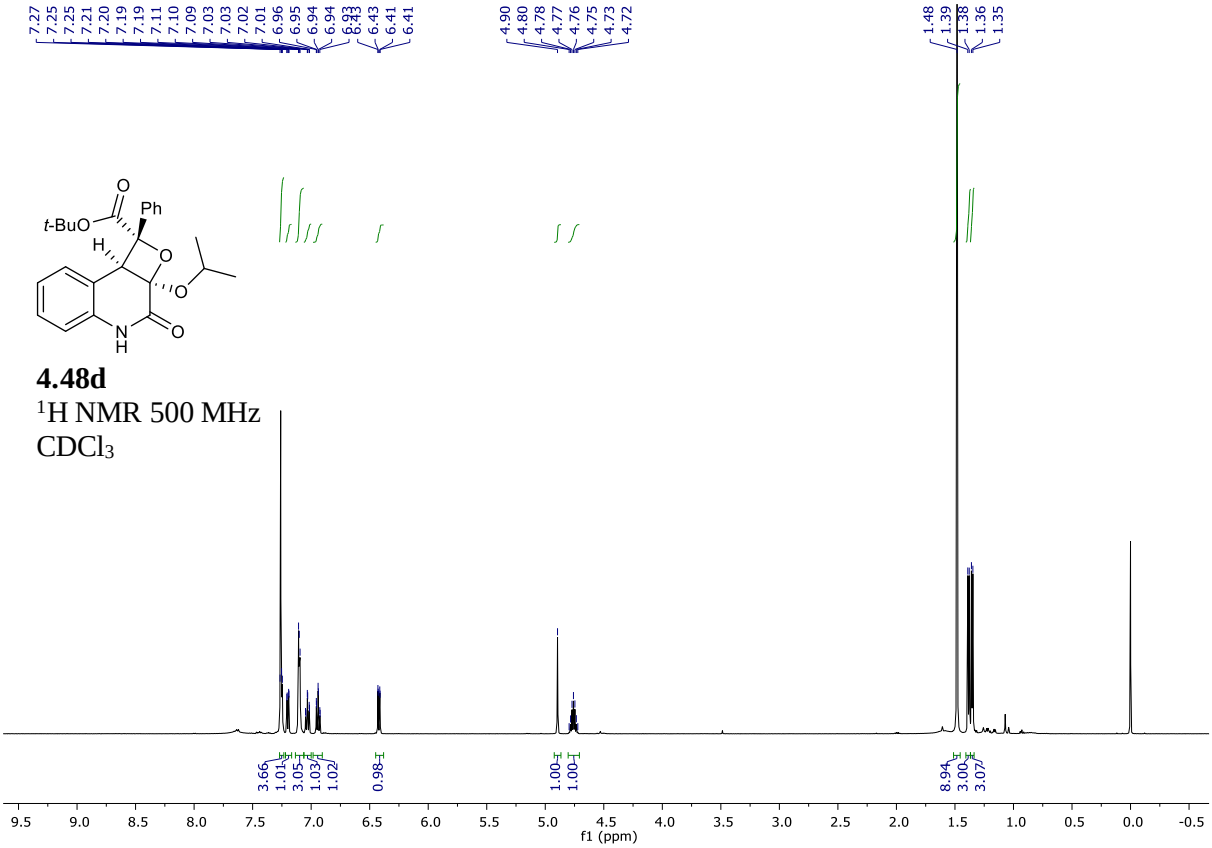

4.48d
^{1}H NMR 500 MHz
$CDCl_3$

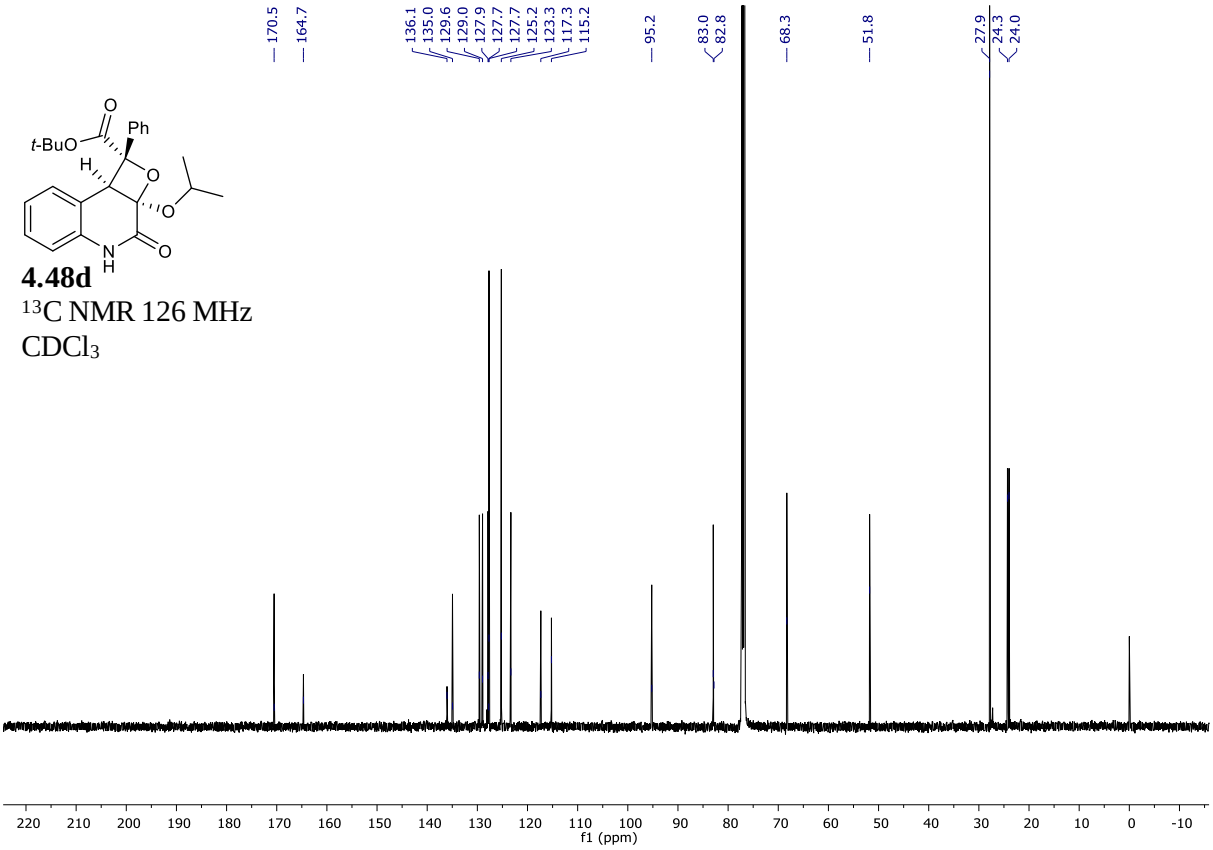

4.48d
^{13}C NMR 126 MHz
$CDCl_3$

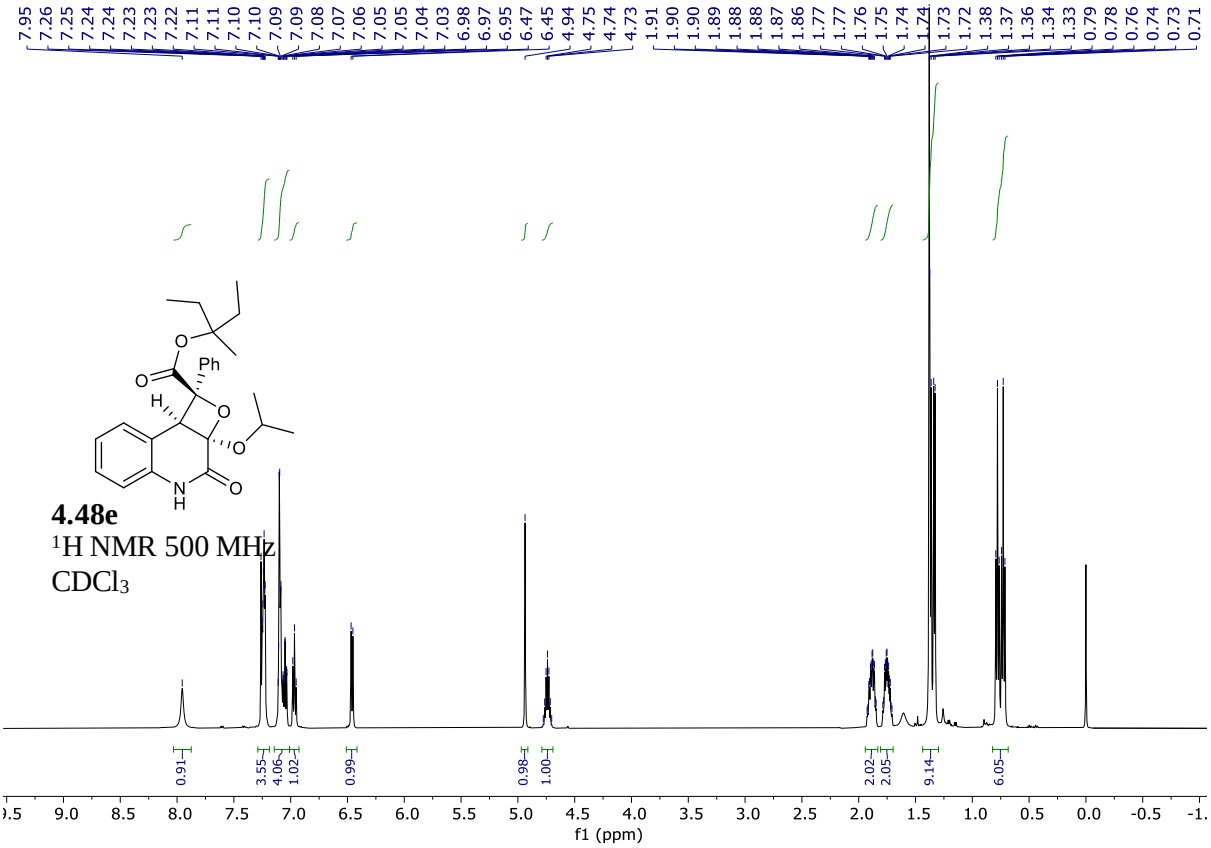

4.48e
^{1}H NMR 500 MHz
$CDCl_3$

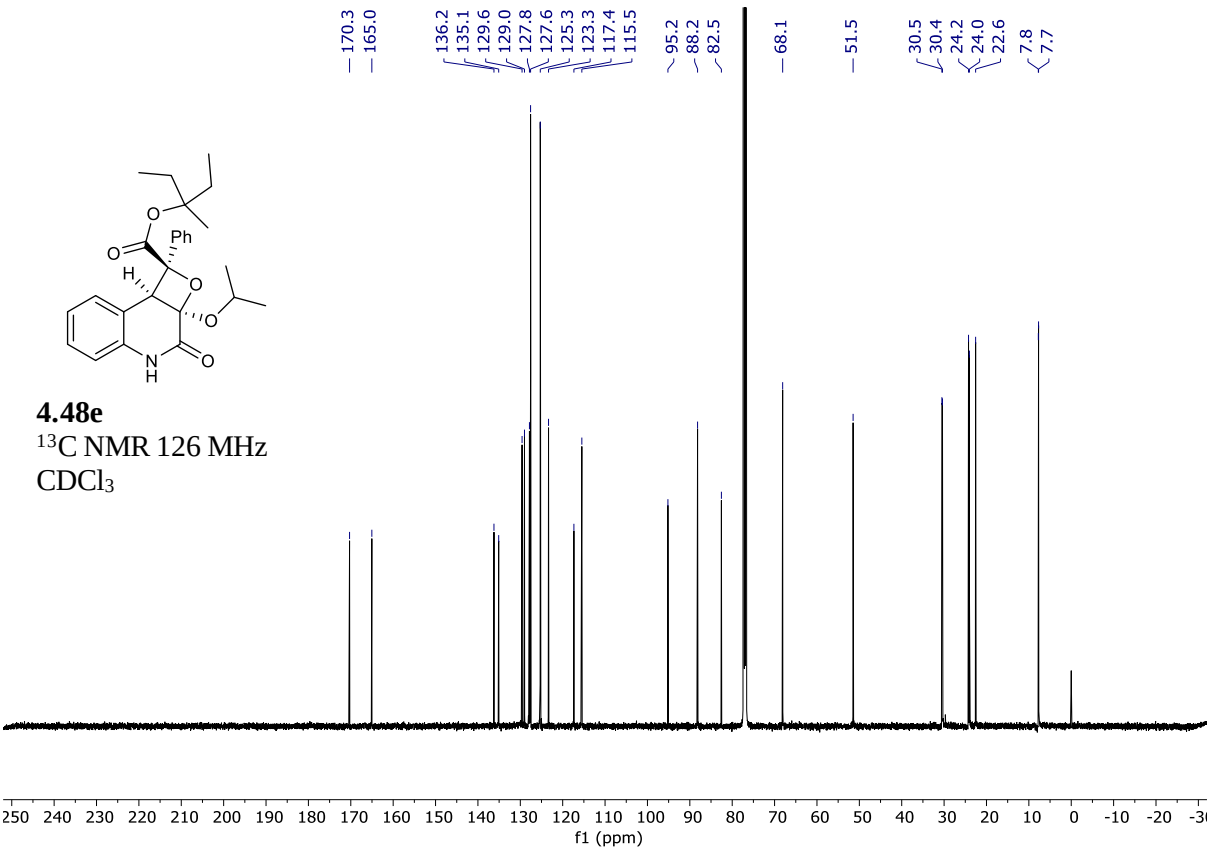

4.48e
^{13}C NMR 126 MHz
$CDCl_3$

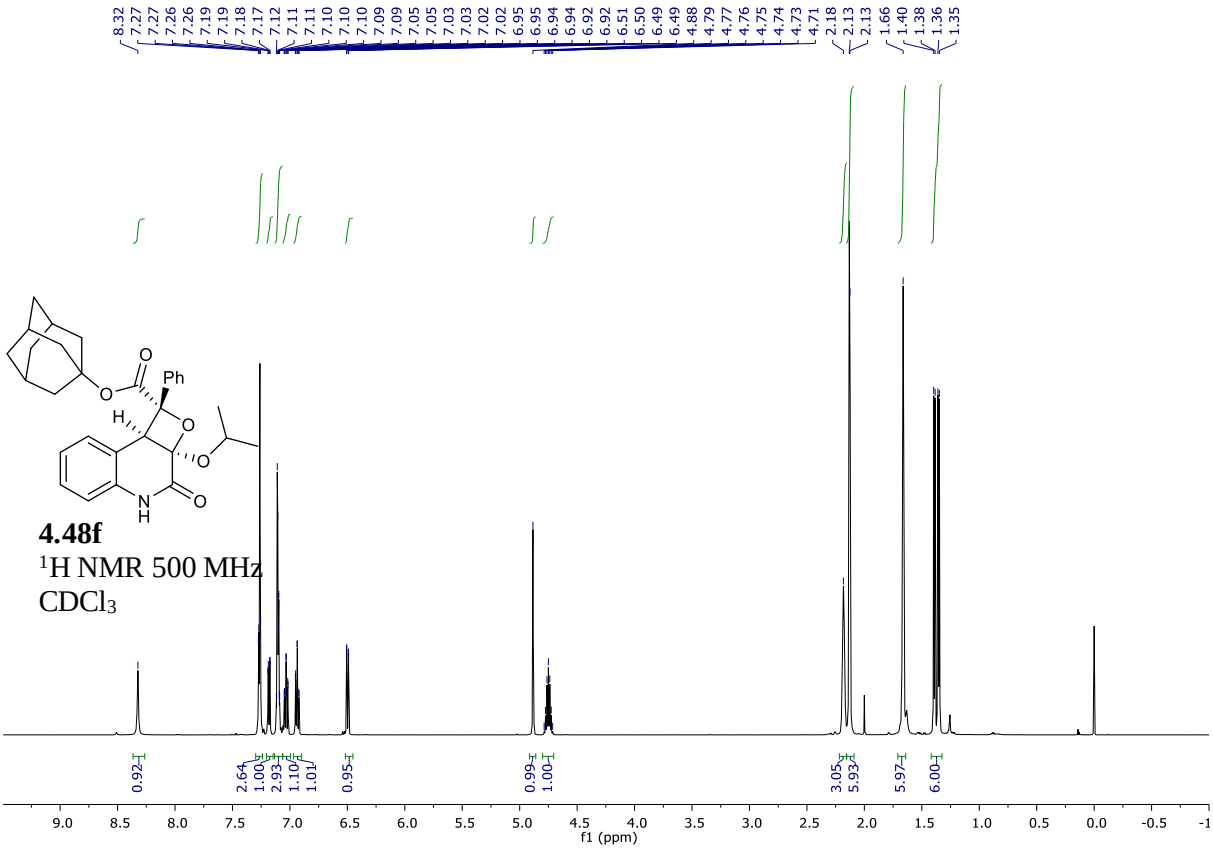

4.48f

^{1}H NMR 500 MHz

$CDCl_3$

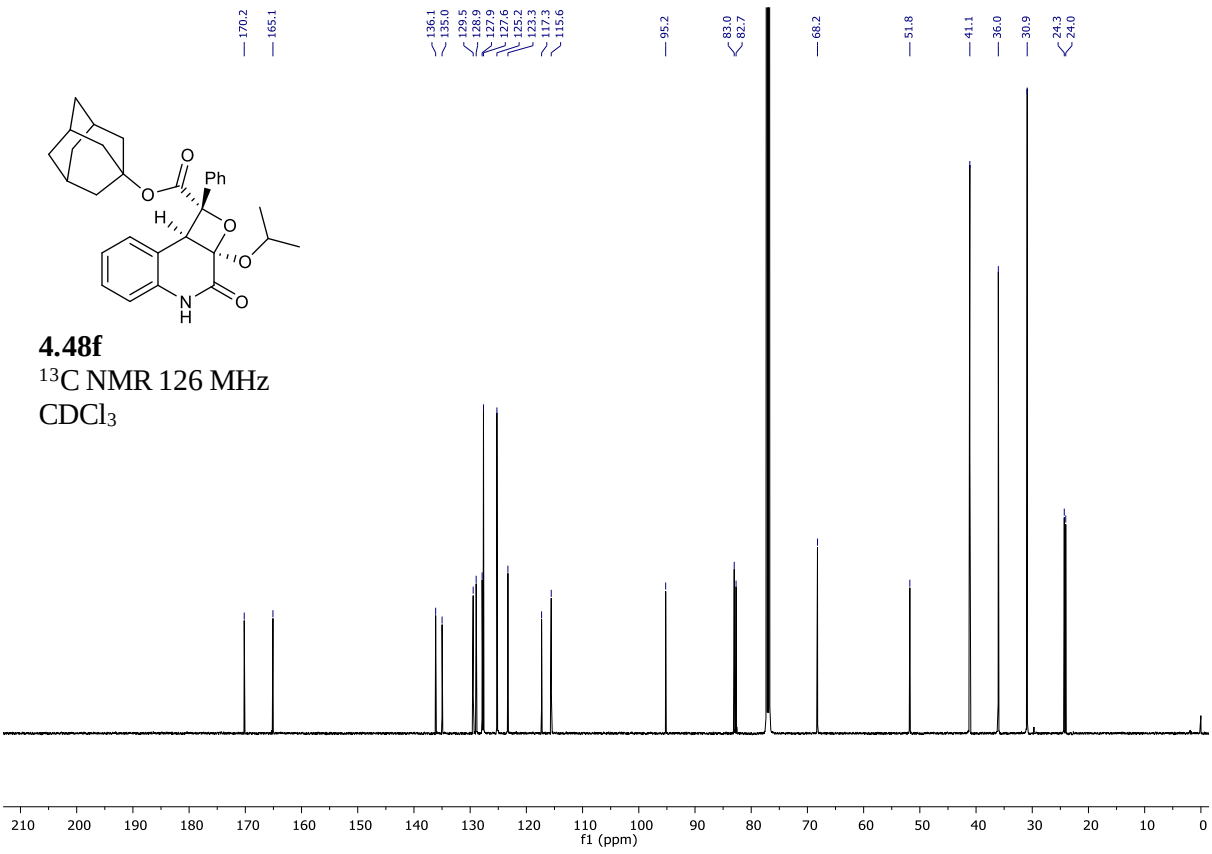

4.48f

^{13}C NMR 126 MHz

$CDCl_3$

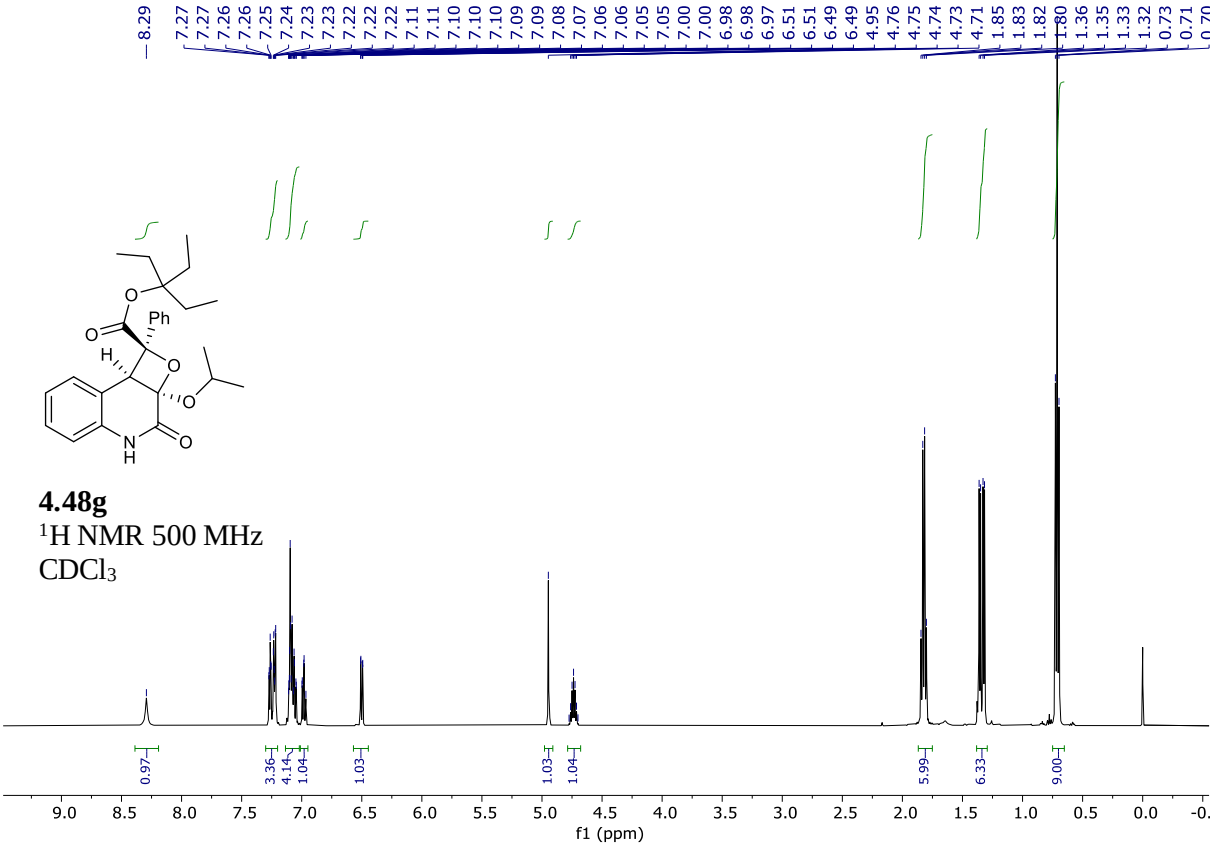

4.48g
^{1}H NMR 500 MHz
$CDCl_3$

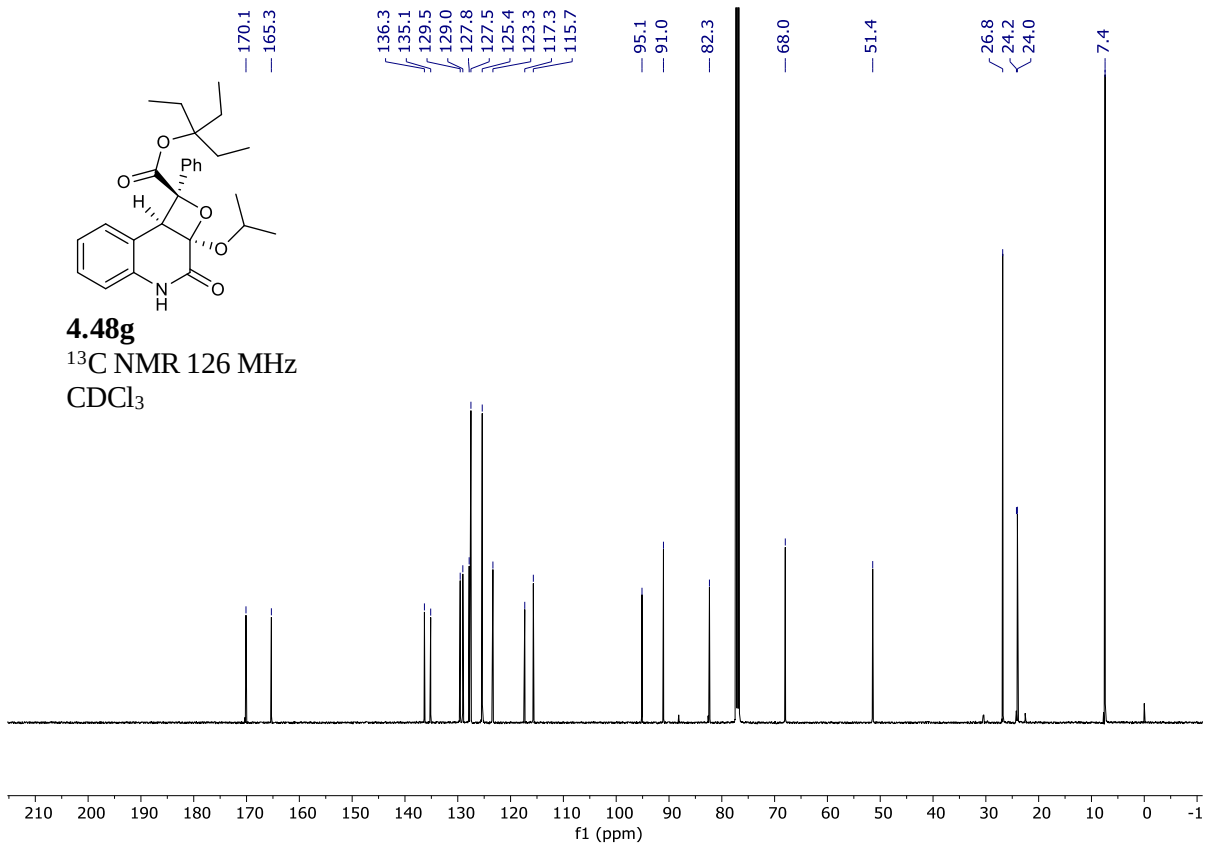

4.48g
^{13}C NMR 126 MHz
$CDCl_3$

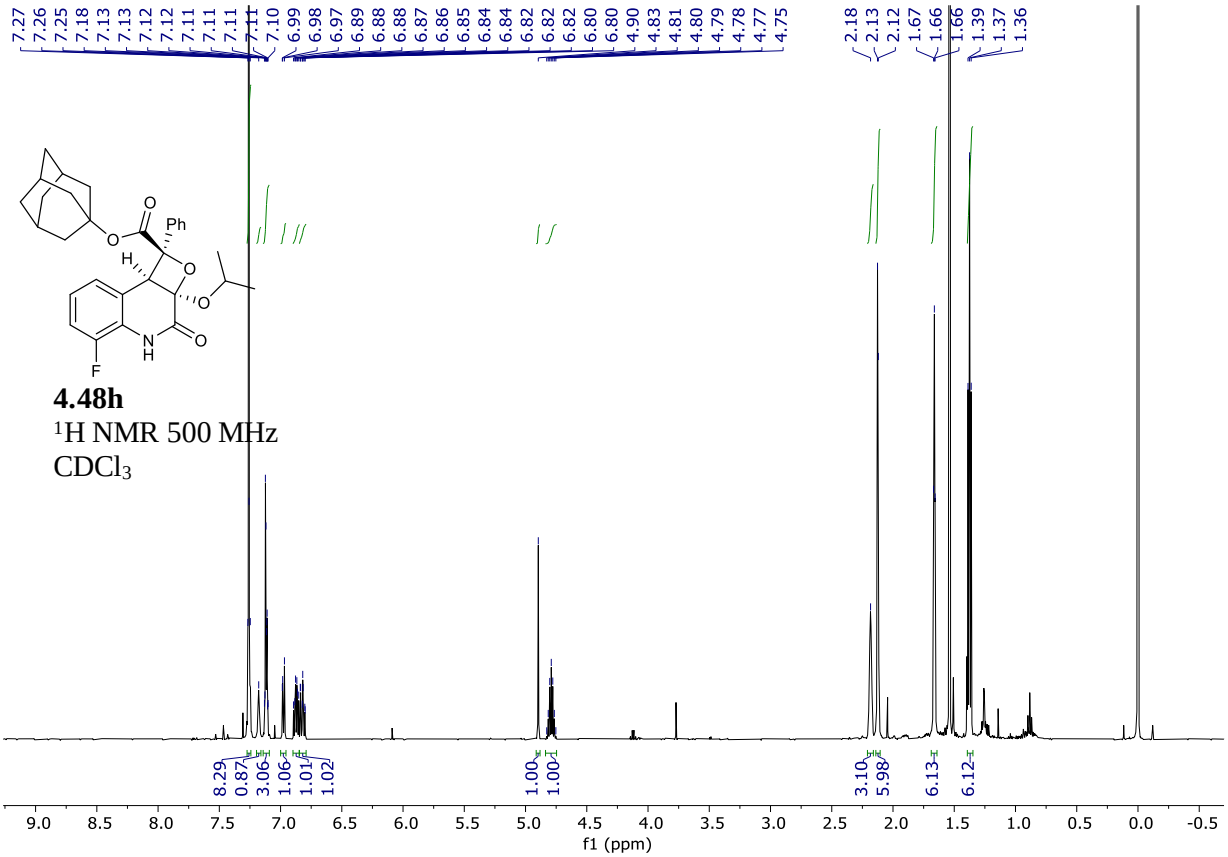

4.48h
^{1}H NMR 500 MHz
$CDCl_3$

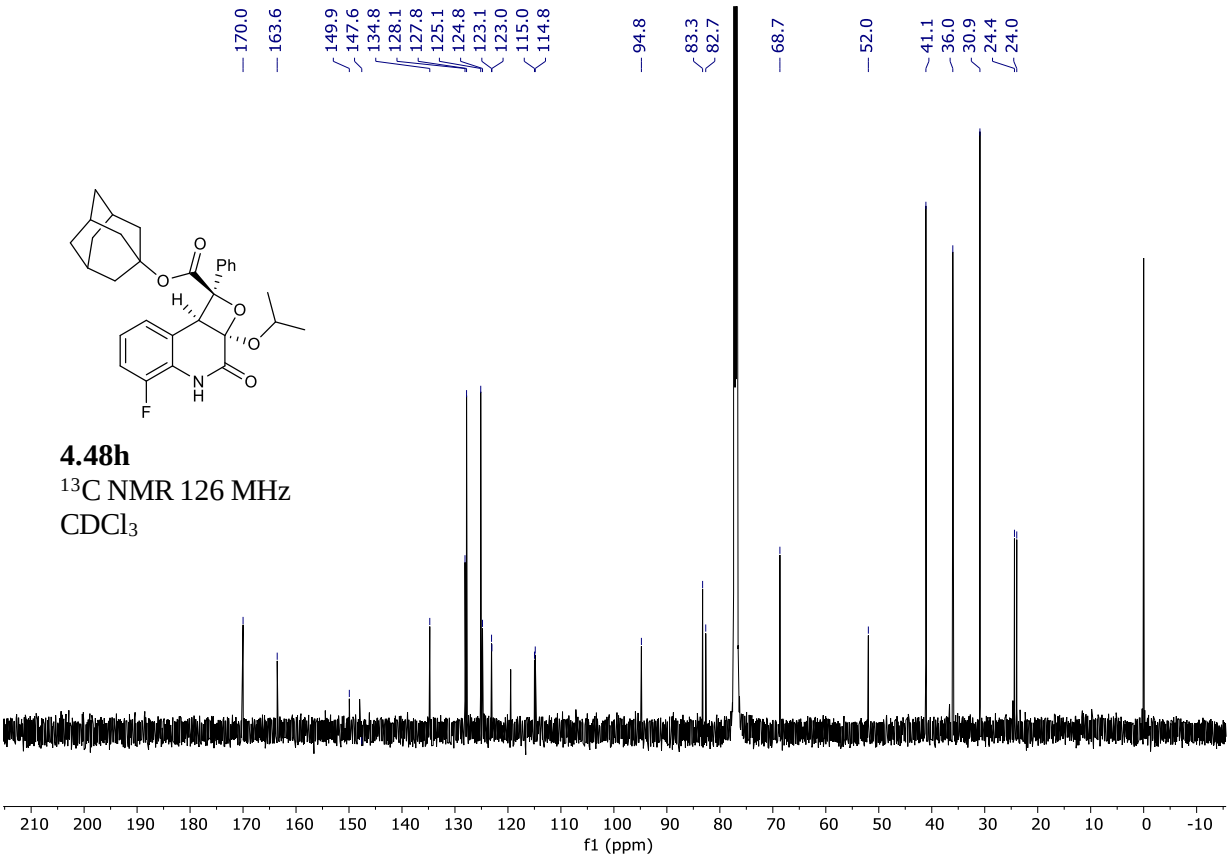

4.48h
^{13}C NMR 126 MHz
$CDCl_3$

4.48h
^{19}F NMR 377 MHz
$CDCl_3$

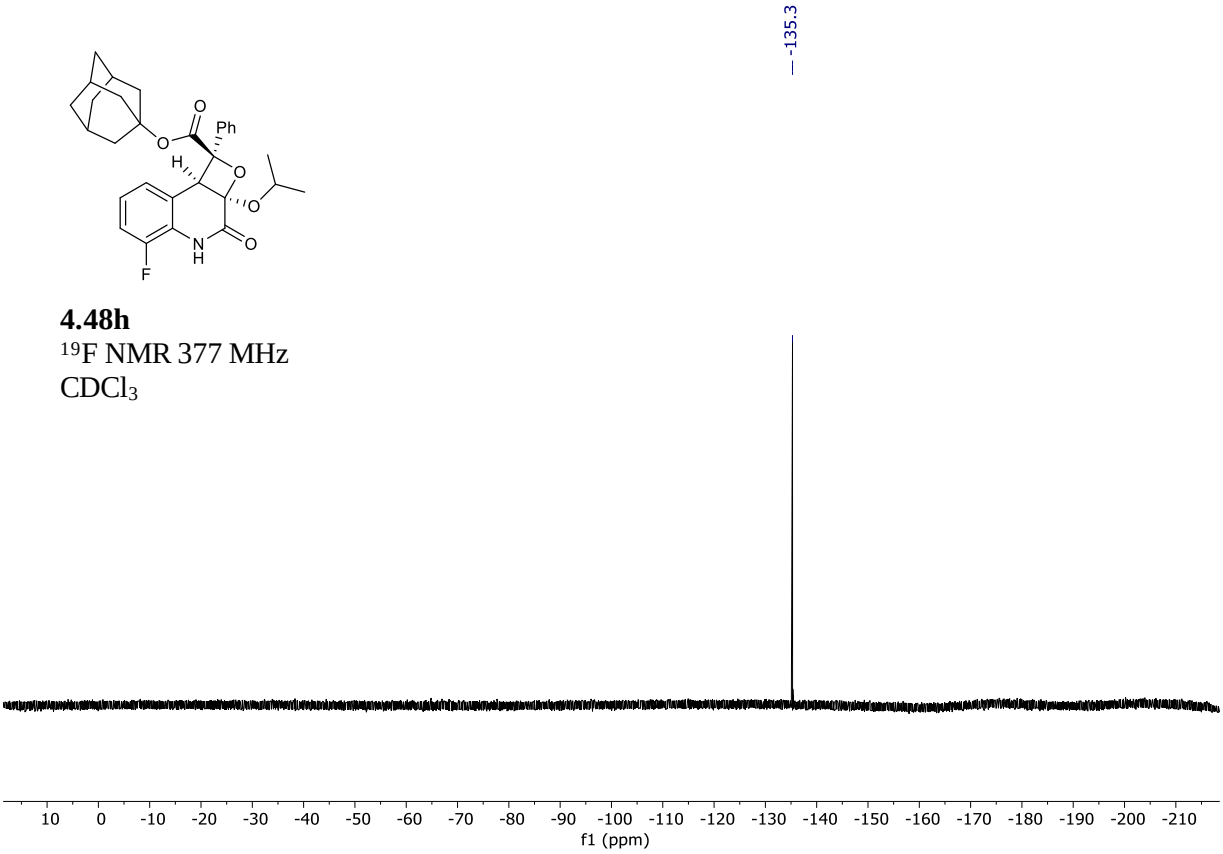

4.48i
^{1}H NMR 500 MHz
$CDCl_3$

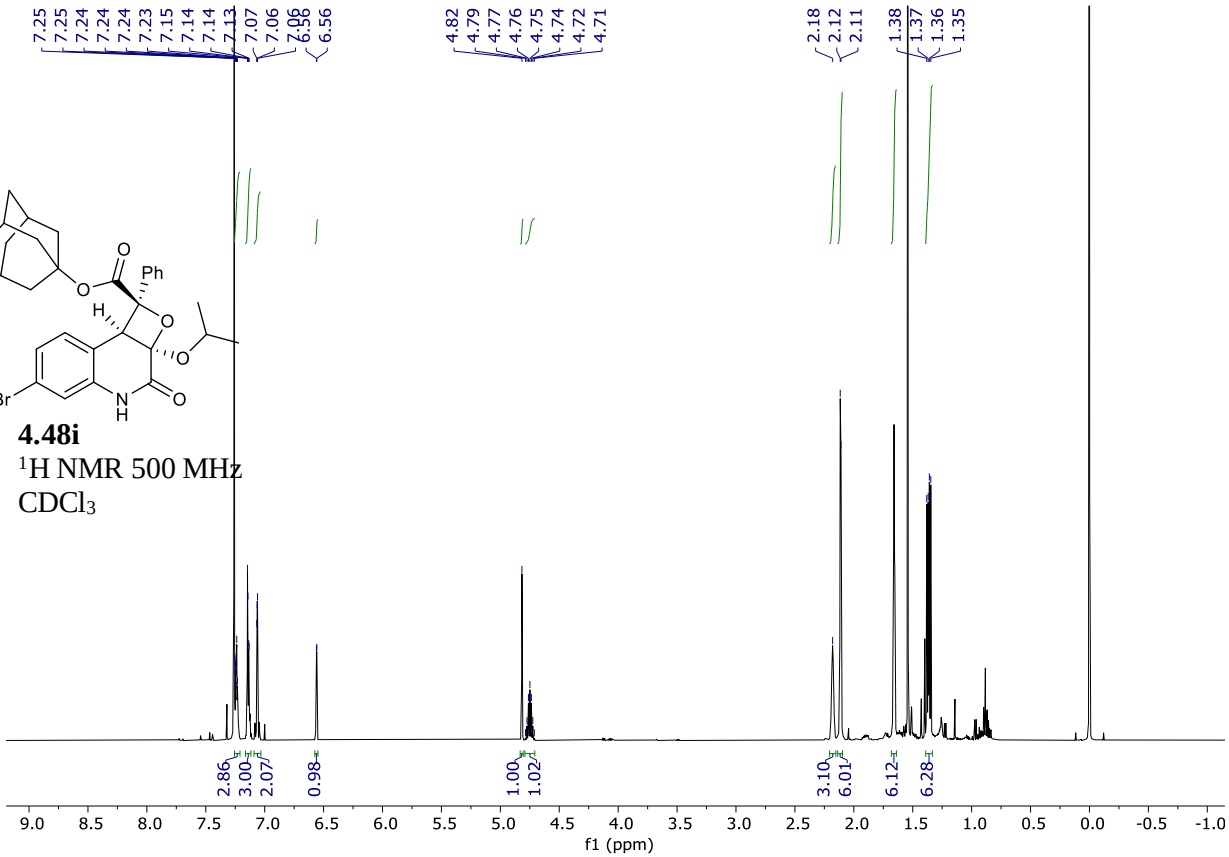

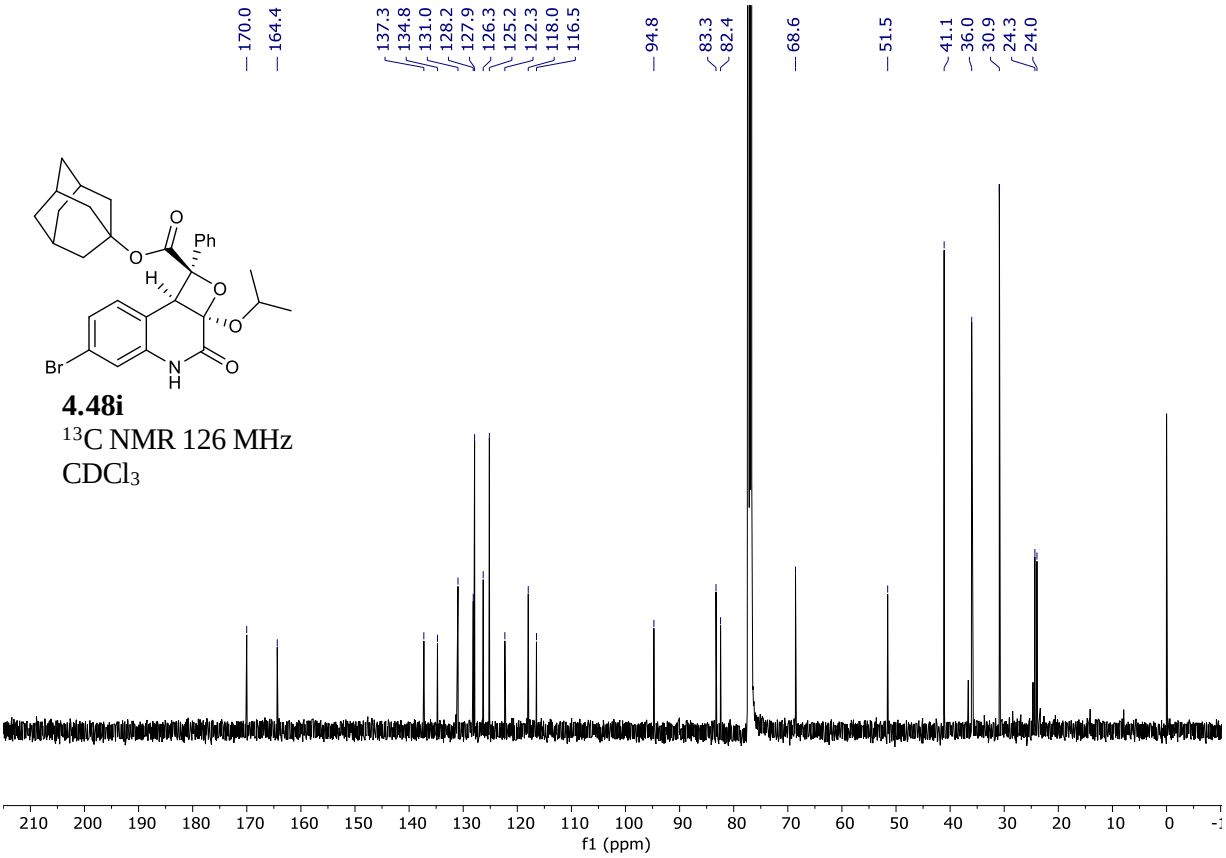

4.48i

^{13}C NMR 126 MHz

$CDCl_3$

B.4. List of New Compounds for Chapter 5

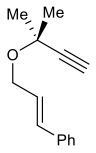

5.39

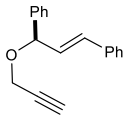

5.40

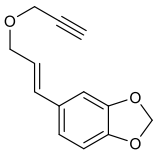

5.42

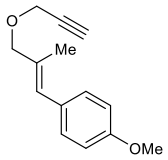

5.43

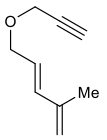

5.46

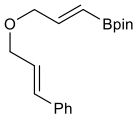

5.24a

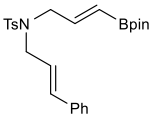

5.24f

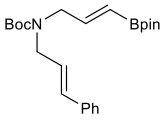

5.24g

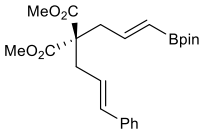

5.24i

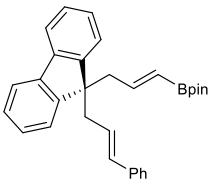

5.24j

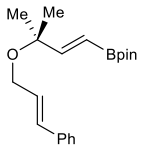

5.24k

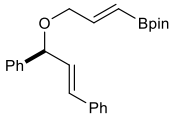

5.24l

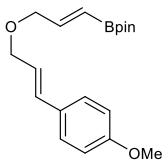

5.24m

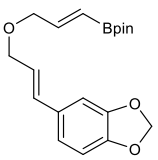

5.24n

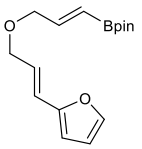

5.24o

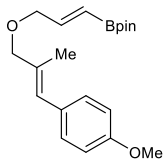

5.24q

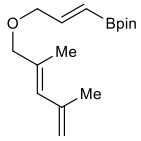

5.24r

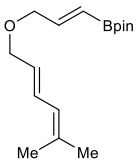

5.24s

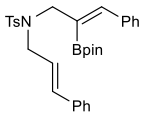

5.24t

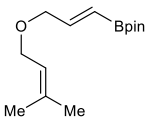

5.35

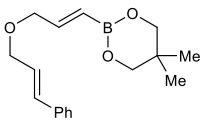

5.24b

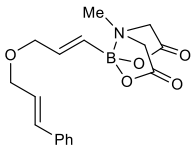

5.24d

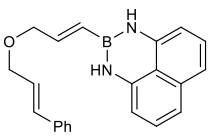

5.24e

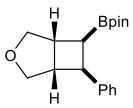

5.25a

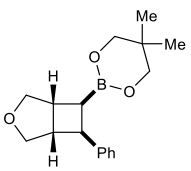

5.25b

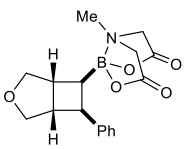

5.25e

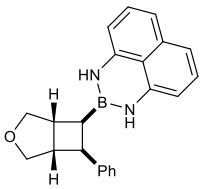

5.25e

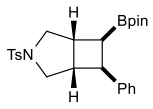

5.25f

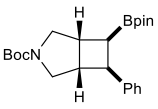

5.25g

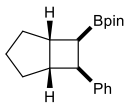

5.25h

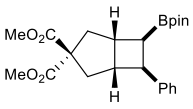

5.25i

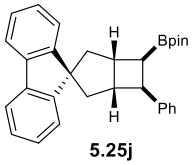

5.25j

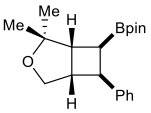

5.25k

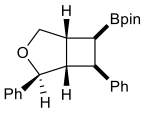

5.25l

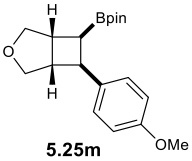

5.25m

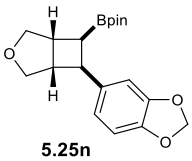

5.25n

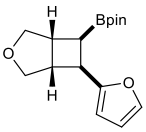

5.25o

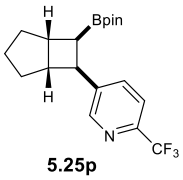

5.25p

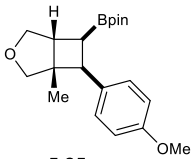

5.25q

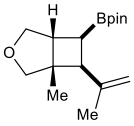

5.25r

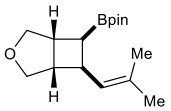

5.25s

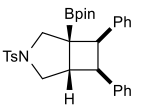

5.25t

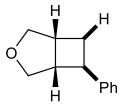

5.26

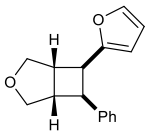

5.27

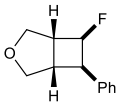

5.28

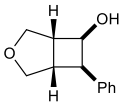

5.29

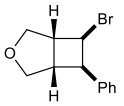

5.30

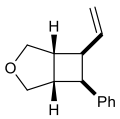

5.31

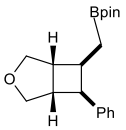

5.32

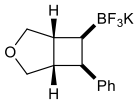

5.33

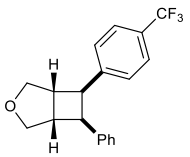

5.34

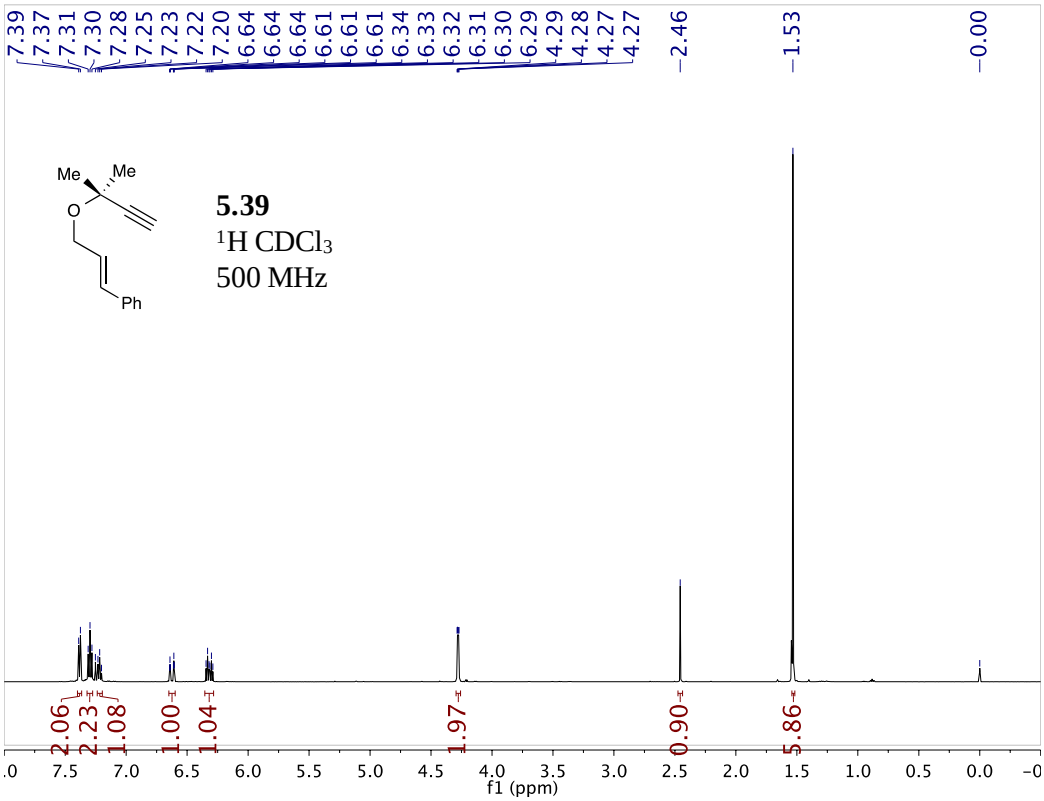
7.39
7.37
7.31
7.30
7.28
7.25
7.23
7.22
7.20
6.64
6.64
6.64
6.61
6.61
6.61
6.34
6.33
6.32
6.31
6.30
6.29
4.29
4.28
4.27
4.27
2.46
1.53
0.00
Me
Me
O
Ph
5.39
1H CDCl3
500 MHz
2.06
2.23
1.08
1.00
1.04
1.97
0.90
5.86
f1 (ppm)

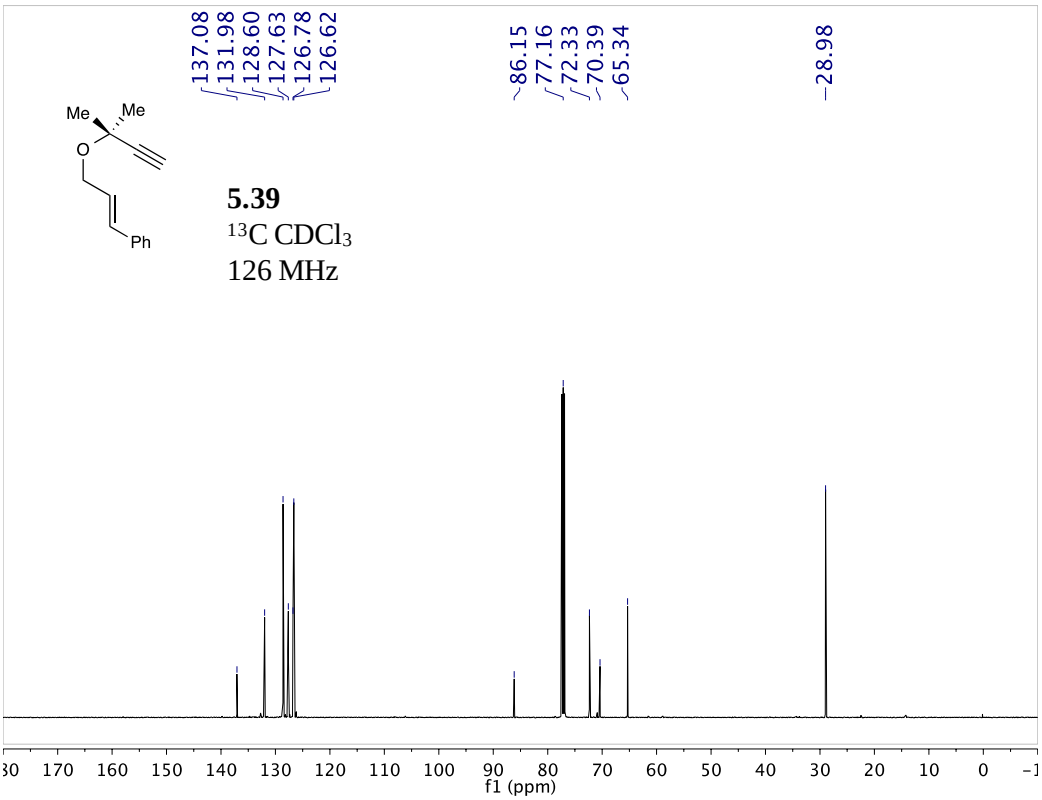
137.08
131.98
128.60
127.63
126.78
126.62
86.15
77.16
72.33
70.39
65.34
28.98
Me
Me
O
Ph
5.39
13C CDCl3
126 MHz
f1 (ppm)

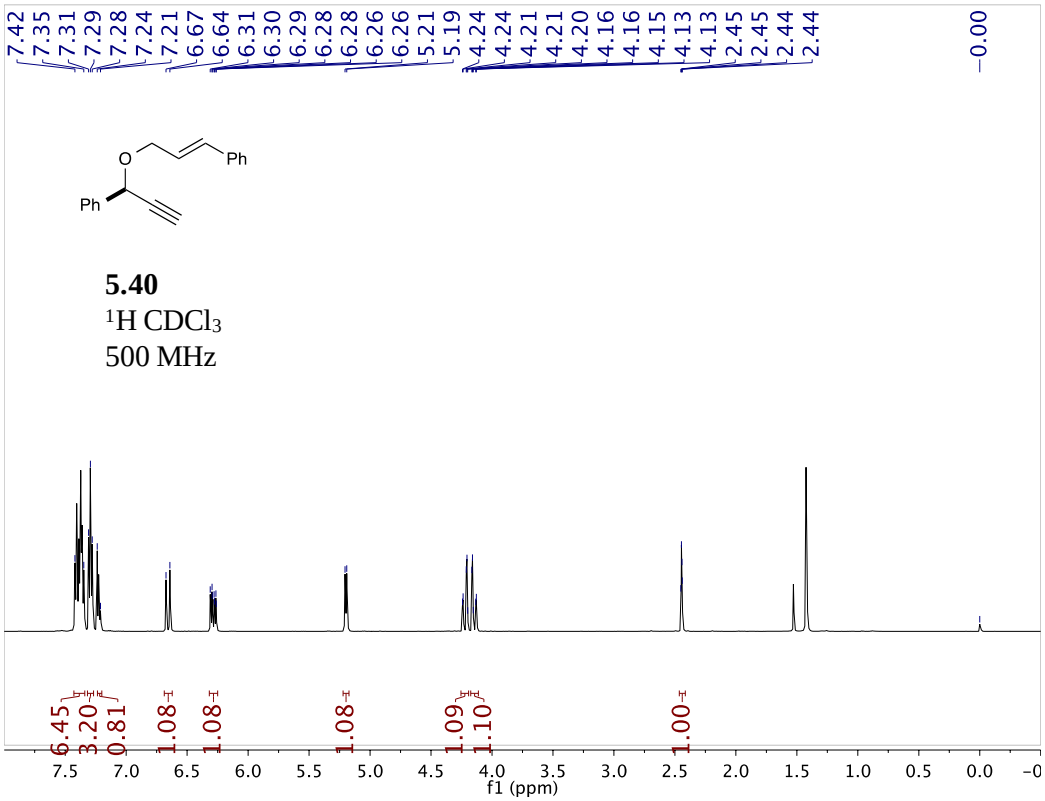

5.40
^{1}H $CDCl_3$
500 MHz

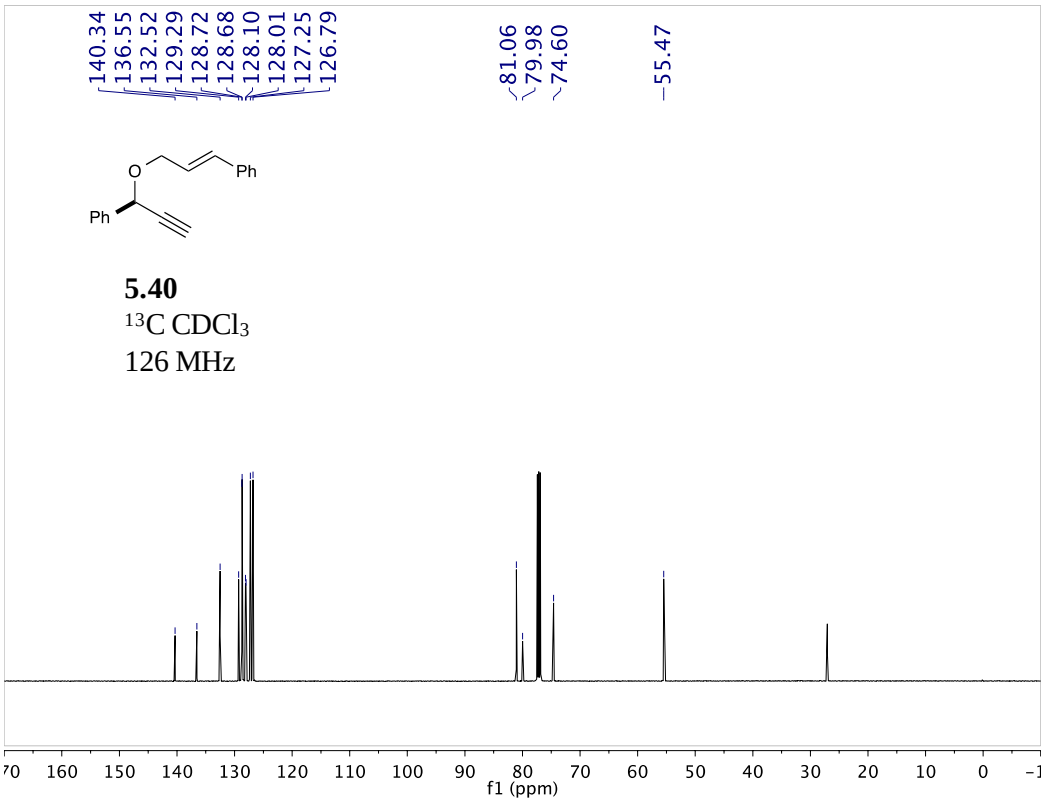

5.40
^{13}C $CDCl_3$
126 MHz

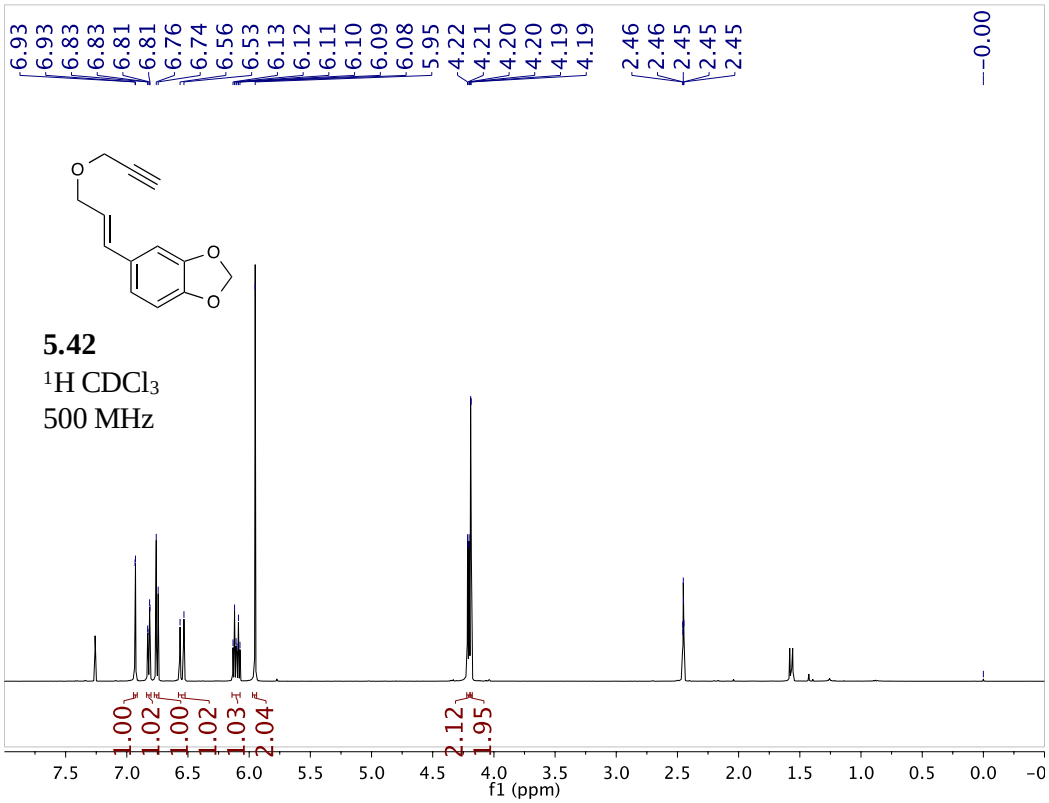
6.93
6.93
6.83
6.83
6.81
6.81
6.76
6.74
6.56
6.53
6.13
6.12
6.11
6.10
6.09
6.08
5.95
4.22
4.21
4.20
4.20
4.19
4.19
2.46
2.46
2.45
2.45
2.45
0.00
5.42
1H CDCl3
500 MHz
1.00
1.02
1.00
1.02
1.03
2.04
2.12
1.95
f1 (ppm)

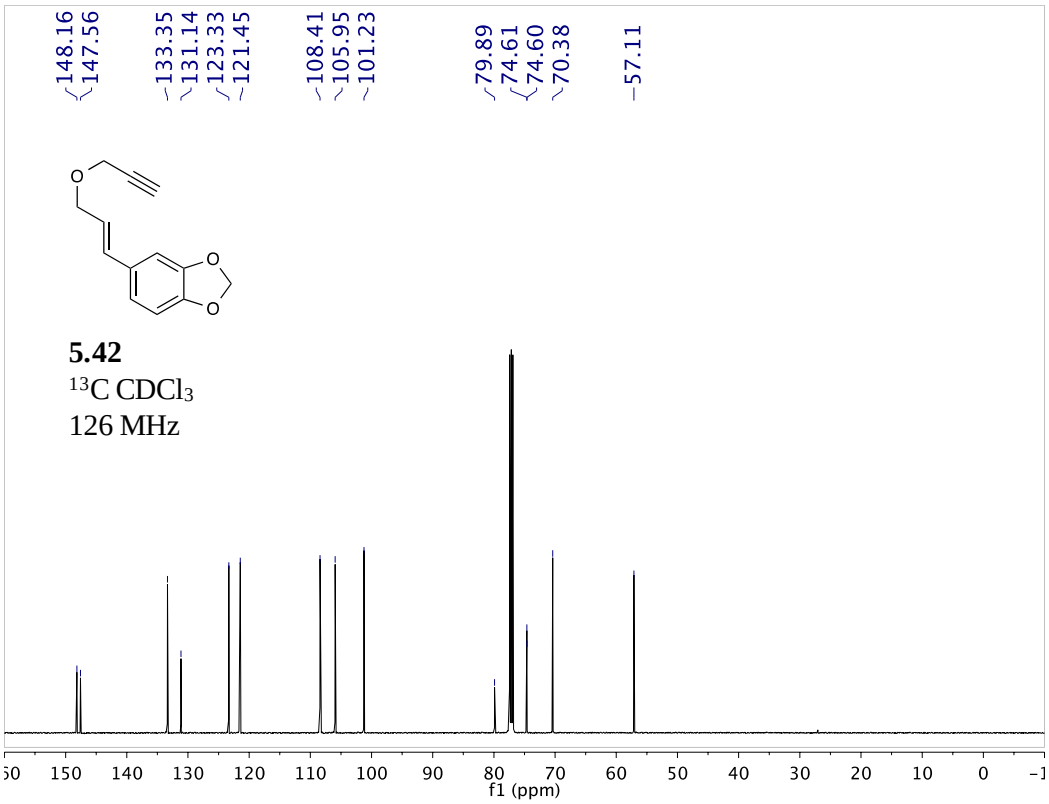
148.16
147.56
133.35
131.14
123.33
121.45
108.41
105.95
101.23
79.89
74.61
74.60
70.38
57.11
5.42
13C CDCl3
126 MHz
f1 (ppm)

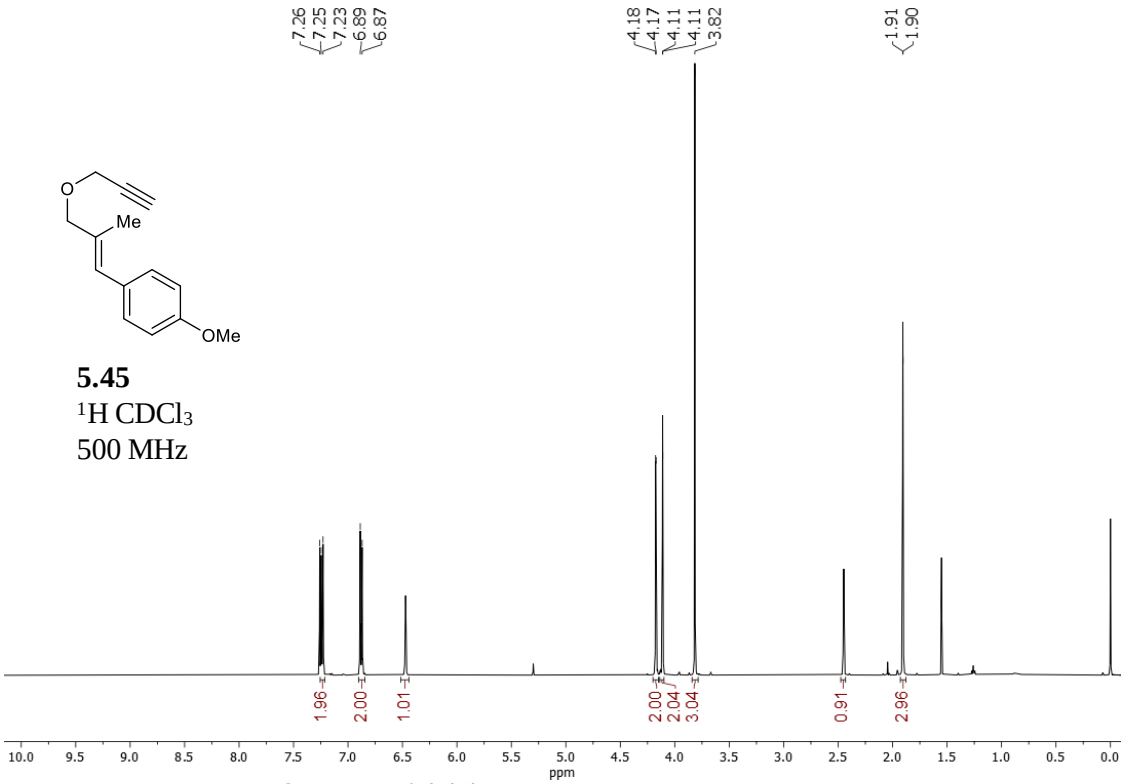

5.45
^{1}H $CDCl_3$
500 MHz

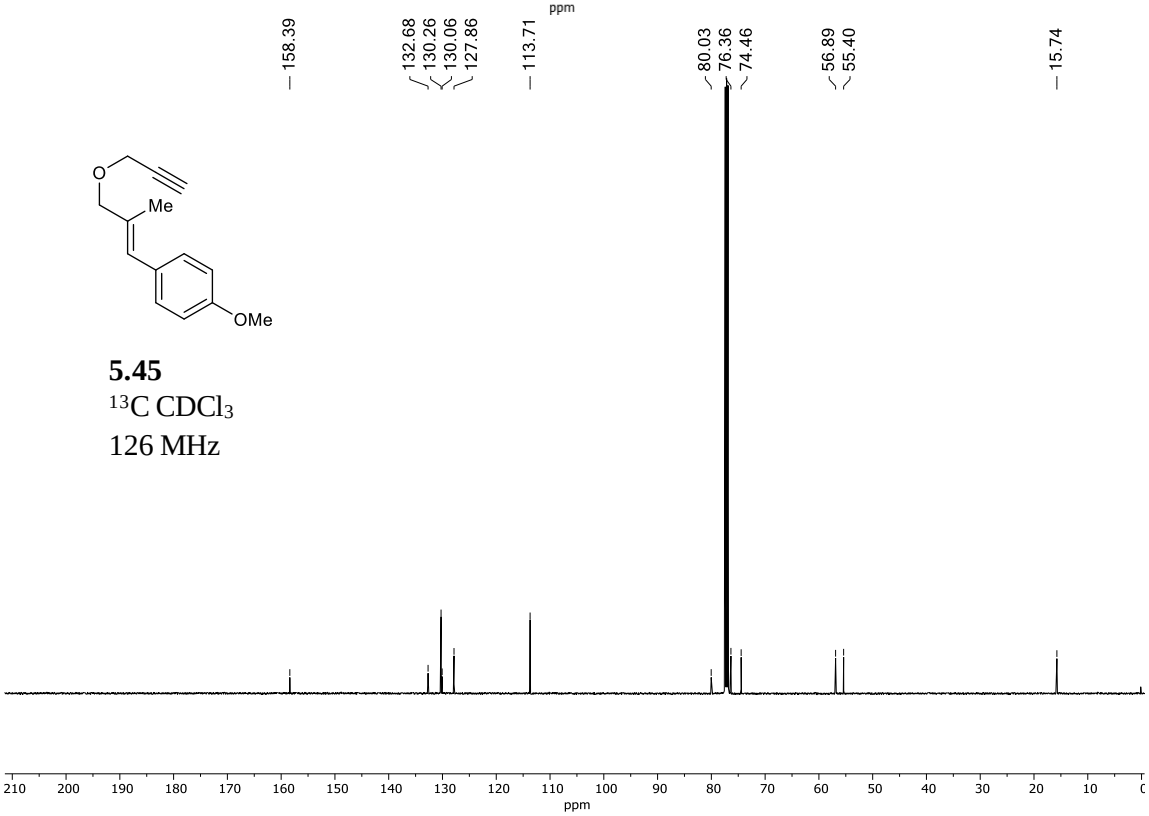

5.45
^{13}C $CDCl_3$
126 MHz

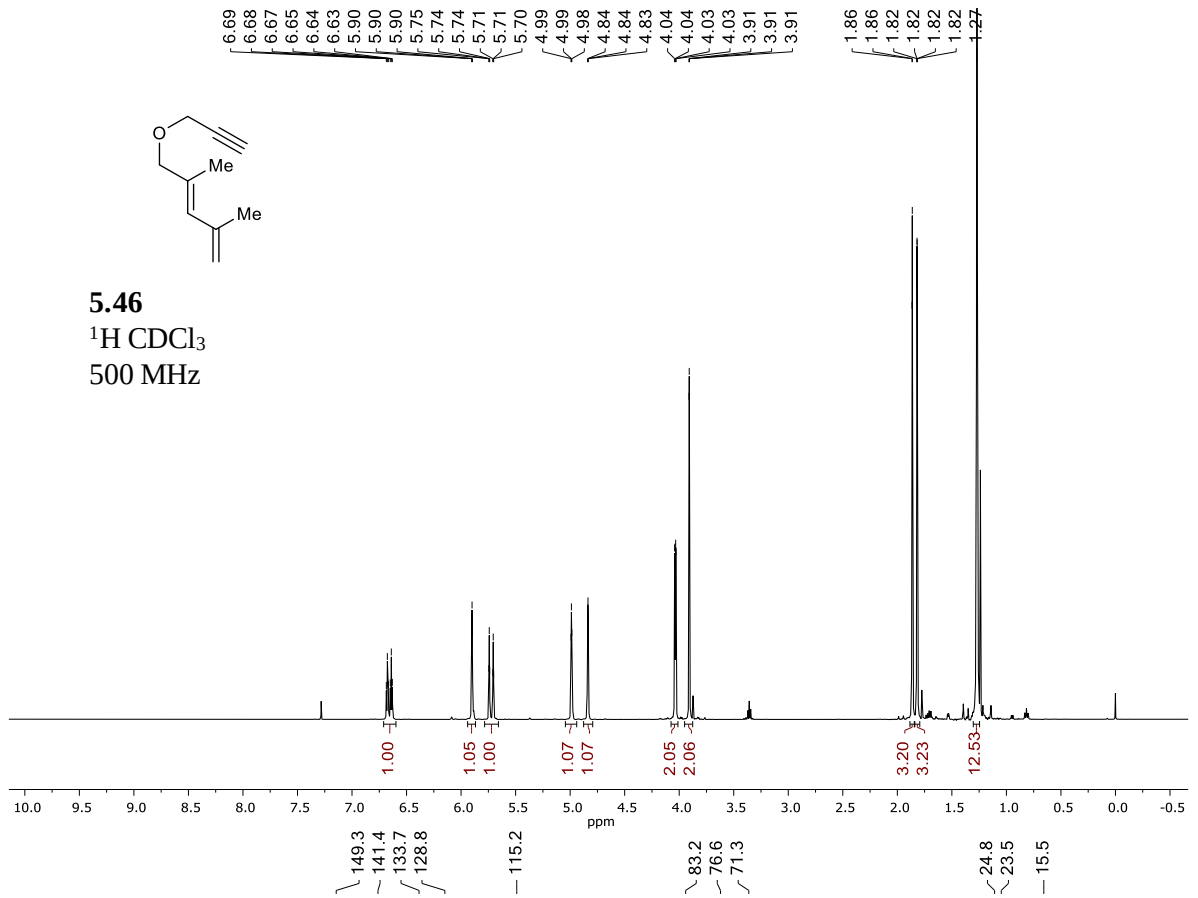

5.46
^{1}H $CDCl_3$
500 MHz

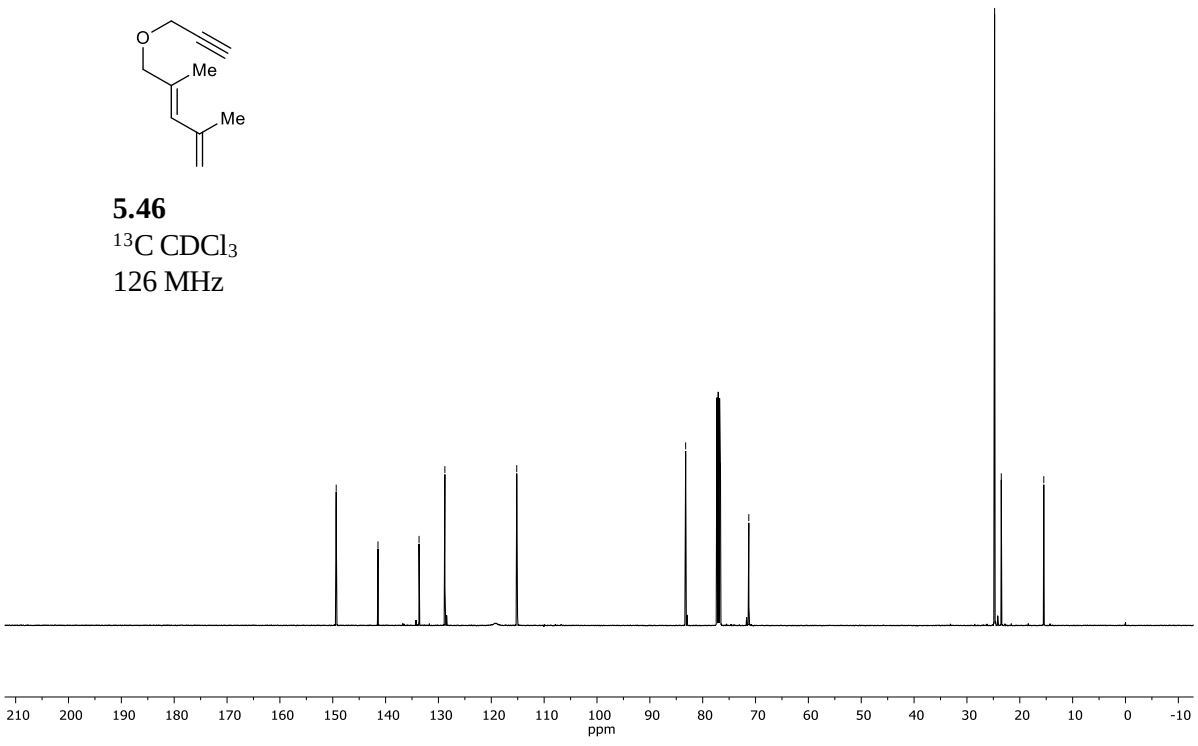

5.46
^{13}C $CDCl_3$
126 MHz

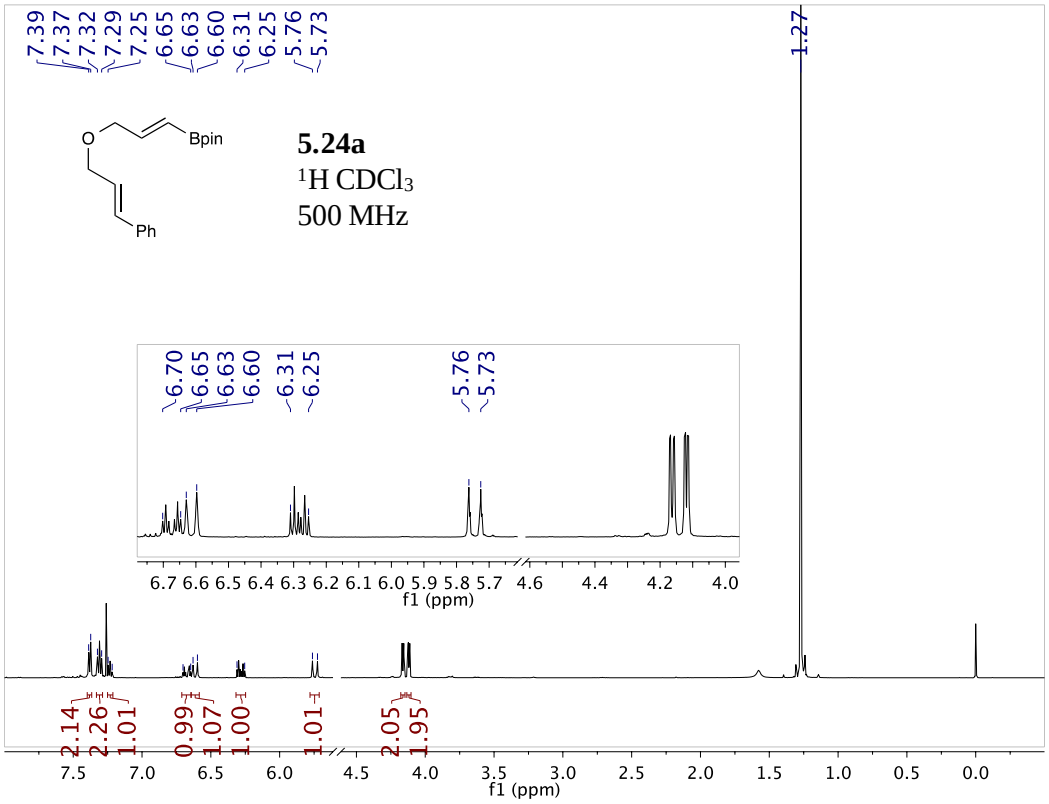
7.39
7.37
7.32
7.29
7.25
6.65
6.63
6.60
6.31
6.25
5.76
5.73
1.27
Bpin
O
Ph
5.24a
1H CDCl3
500 MHz
6.70
6.65
6.63
6.60
6.31
6.25
5.76
5.73
f1 (ppm)
2.14
2.26
1.01
0.99
1.07
1.00
1.01
2.05
1.95
f1 (ppm)

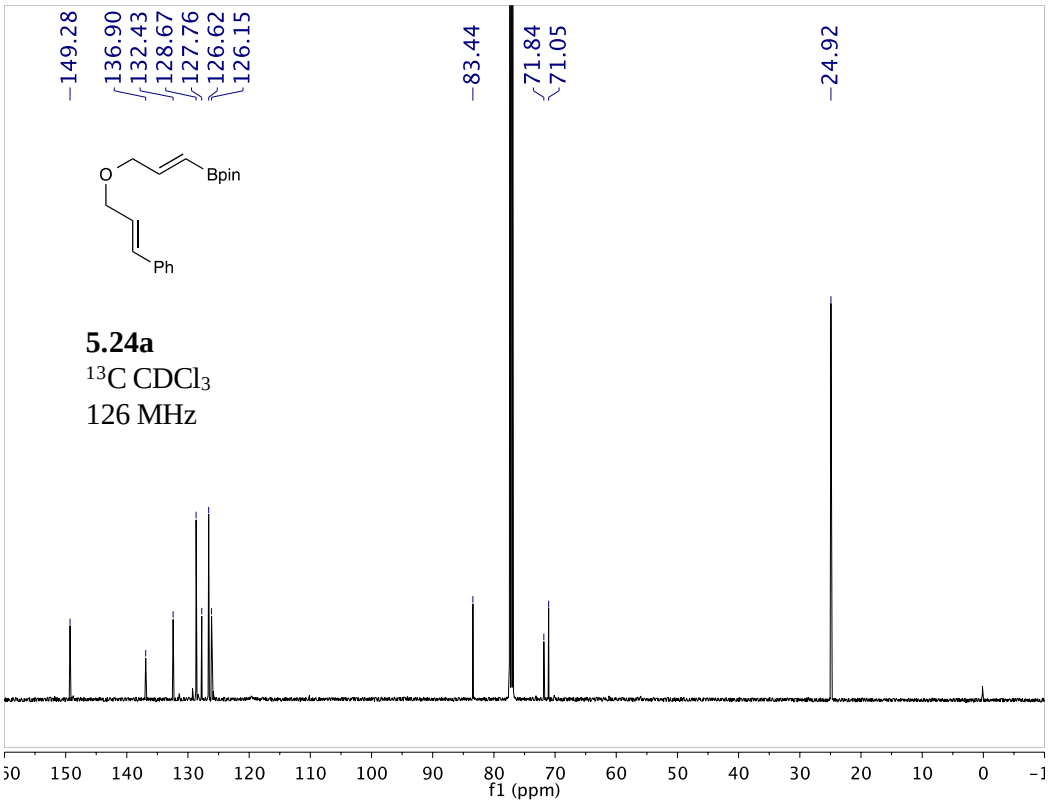
149.28
136.90
132.43
128.67
127.76
126.62
126.15
83.44
71.84
71.05
24.92
Bpin
O
Ph
5.24a
13C CDCl3
126 MHz
f1 (ppm)

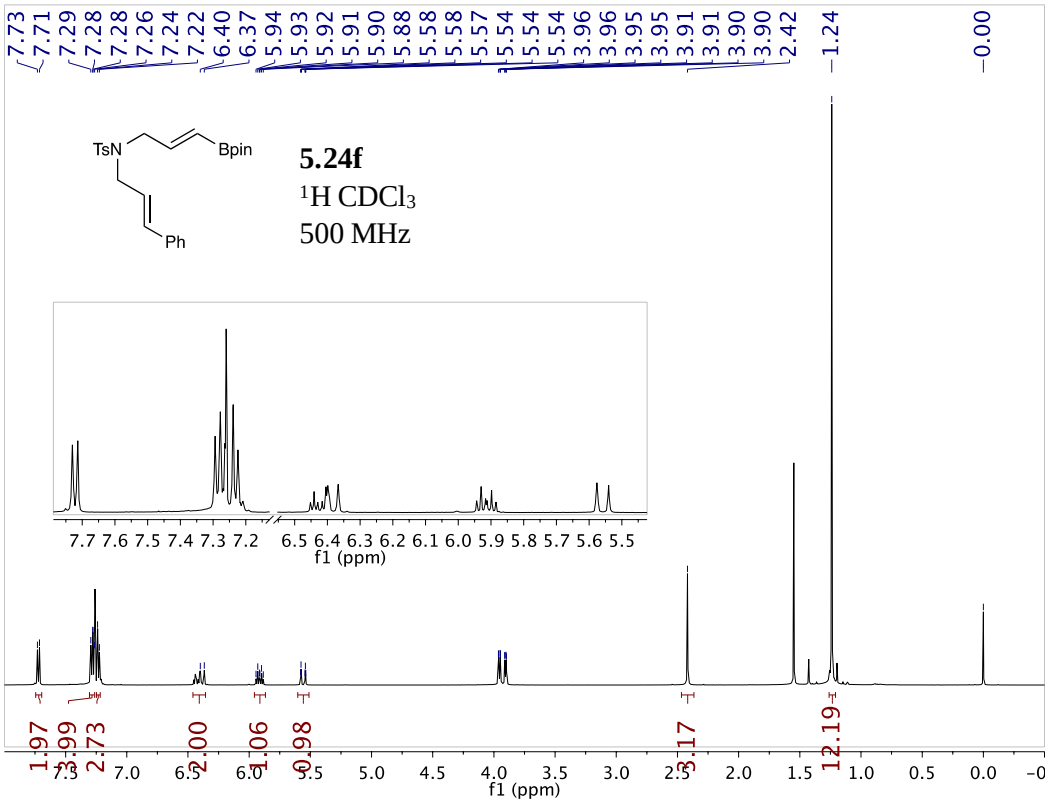
7.73
7.71
7.29
7.28
7.28
7.26
7.24
7.22
6.40
6.37
5.94
5.93
5.92
5.91
5.90
5.88
5.58
5.58
5.57
5.54
5.54
5.54
3.96
3.96
3.95
3.95
3.91
3.91
3.90
3.90
2.42
1.24
0.00
TsN
Bpin
Ph
5.24f
1H CDCl3
500 MHz
7.7 7.6 7.5 7.4 7.3 7.2
6.5 6.4 6.3 6.2 6.1 6.0 5.9 5.8 5.7 5.6 5.5
f1 (ppm)
1.97
3.99
2.73
2.00
1.06
0.98
3.17
12.19
f1 (ppm)

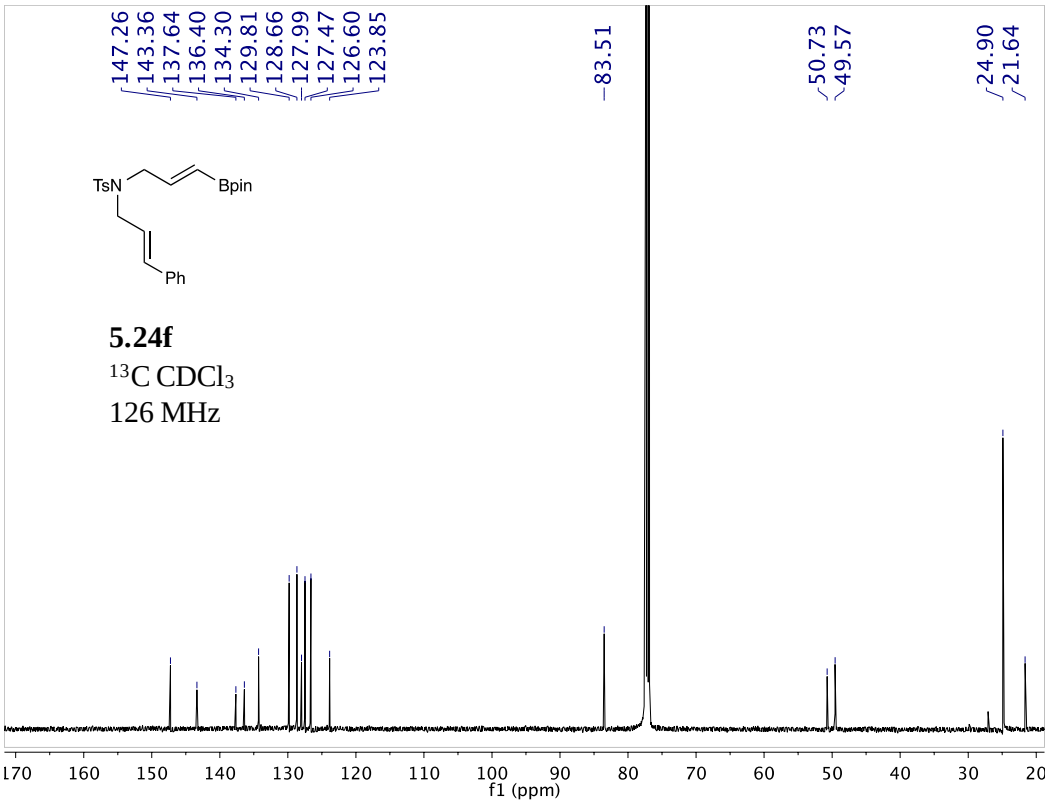
147.26
143.36
137.64
136.40
134.30
129.81
128.66
127.99
127.47
126.60
123.85
83.51
50.73
49.57
24.90
21.64
TsN
Bpin
Ph
5.24f
13C CDCl3
126 MHz
f1 (ppm)

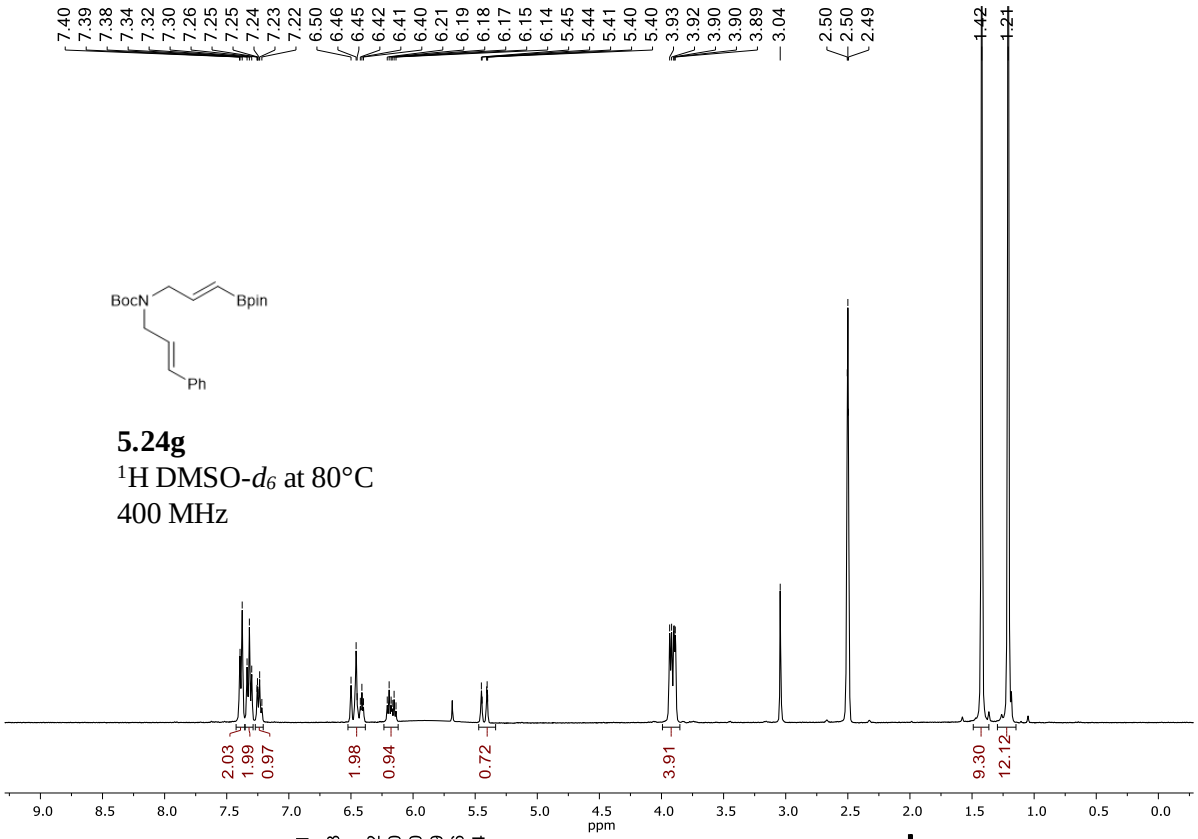

5.24g
^{1}H DMSO-d_6 at 80°C
400 MHz

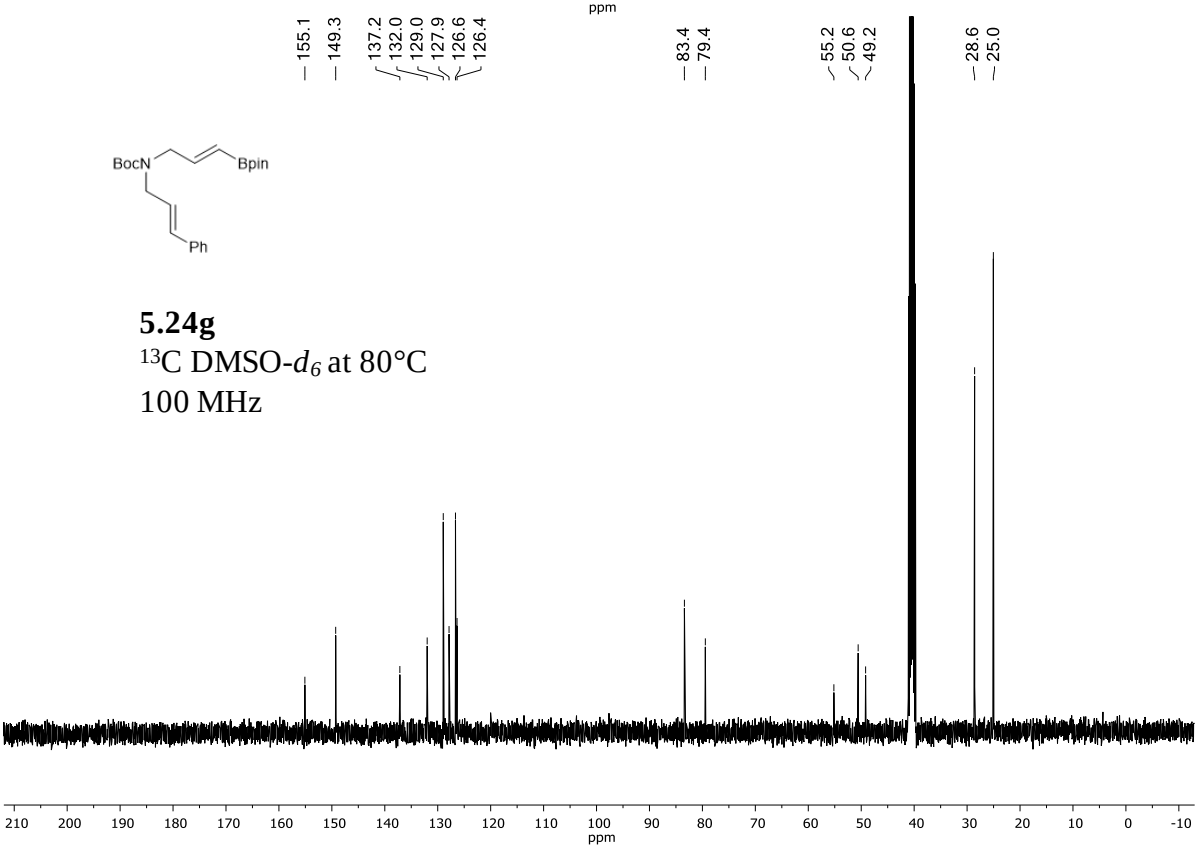

5.24g
^{13}C DMSO-d_6 at 80°C
100 MHz

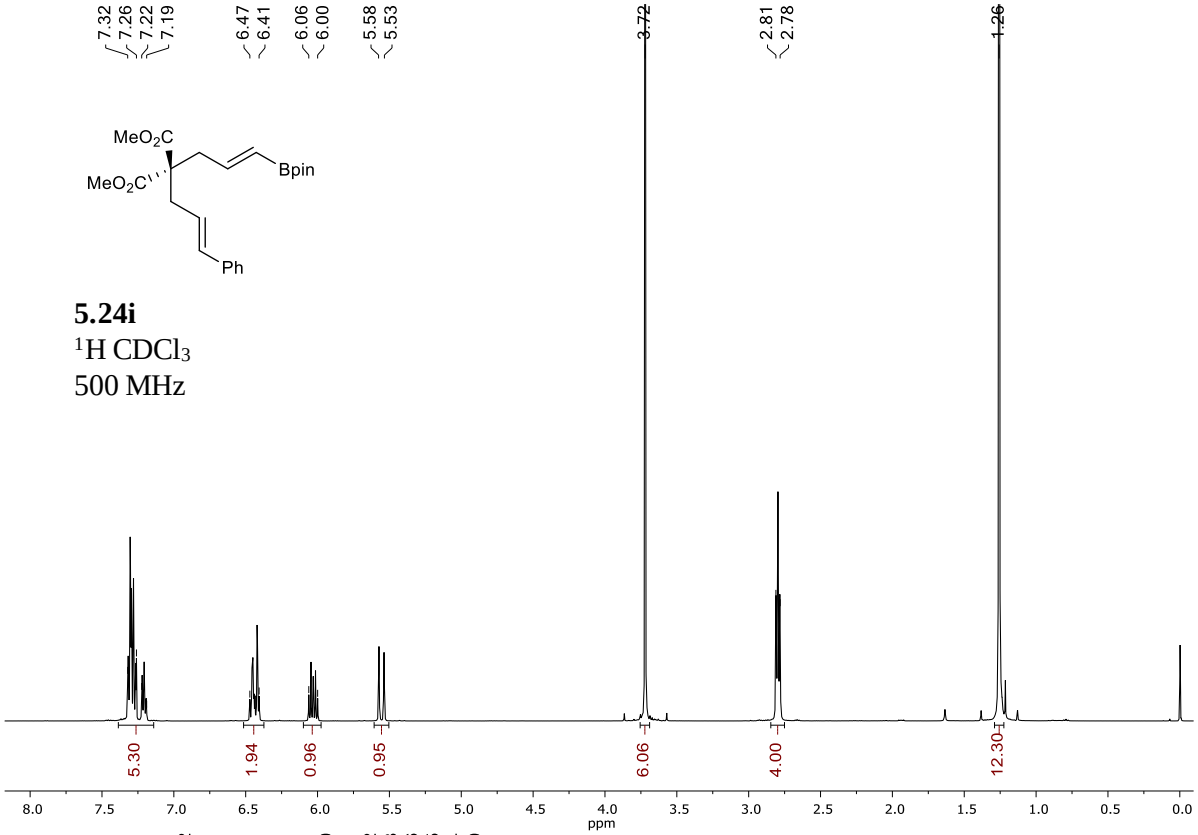

5.24i
^{1}H $CDCl_3$
500 MHz

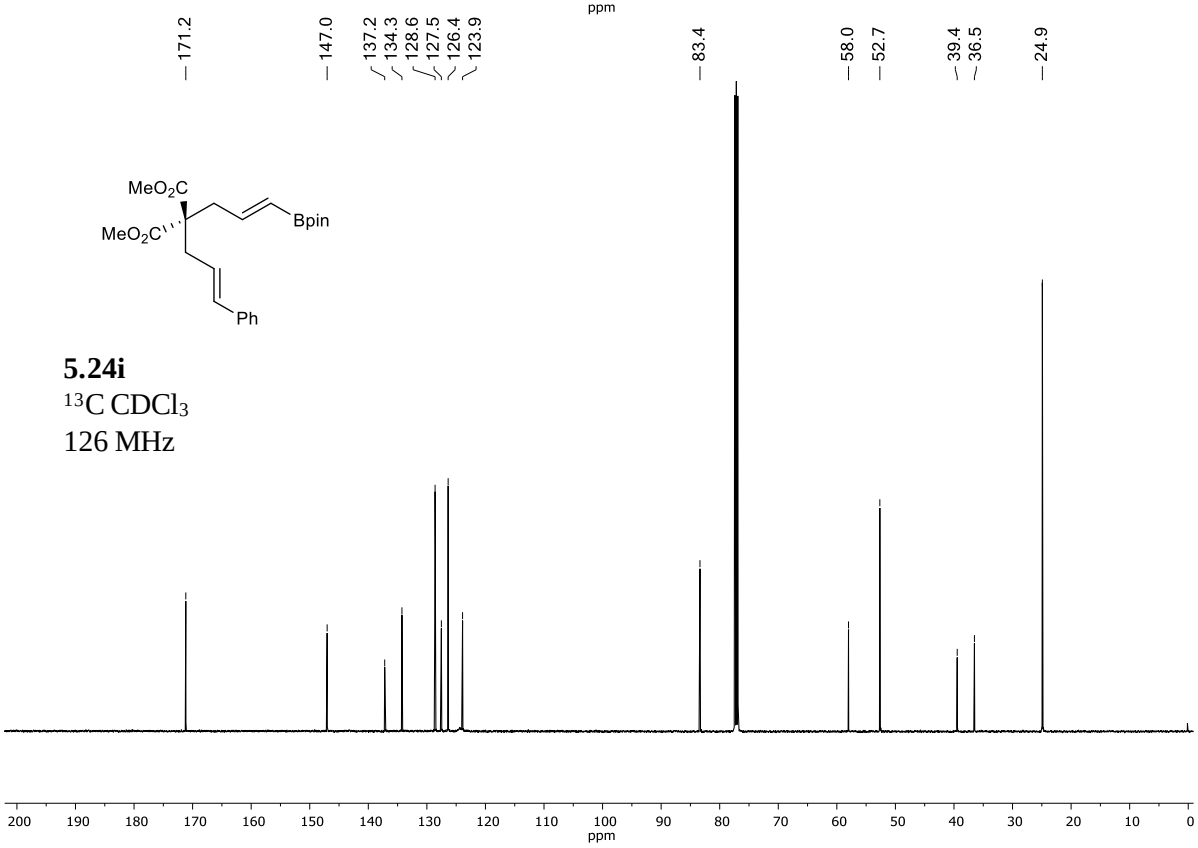

5.24i
^{13}C $CDCl_3$
126 MHz

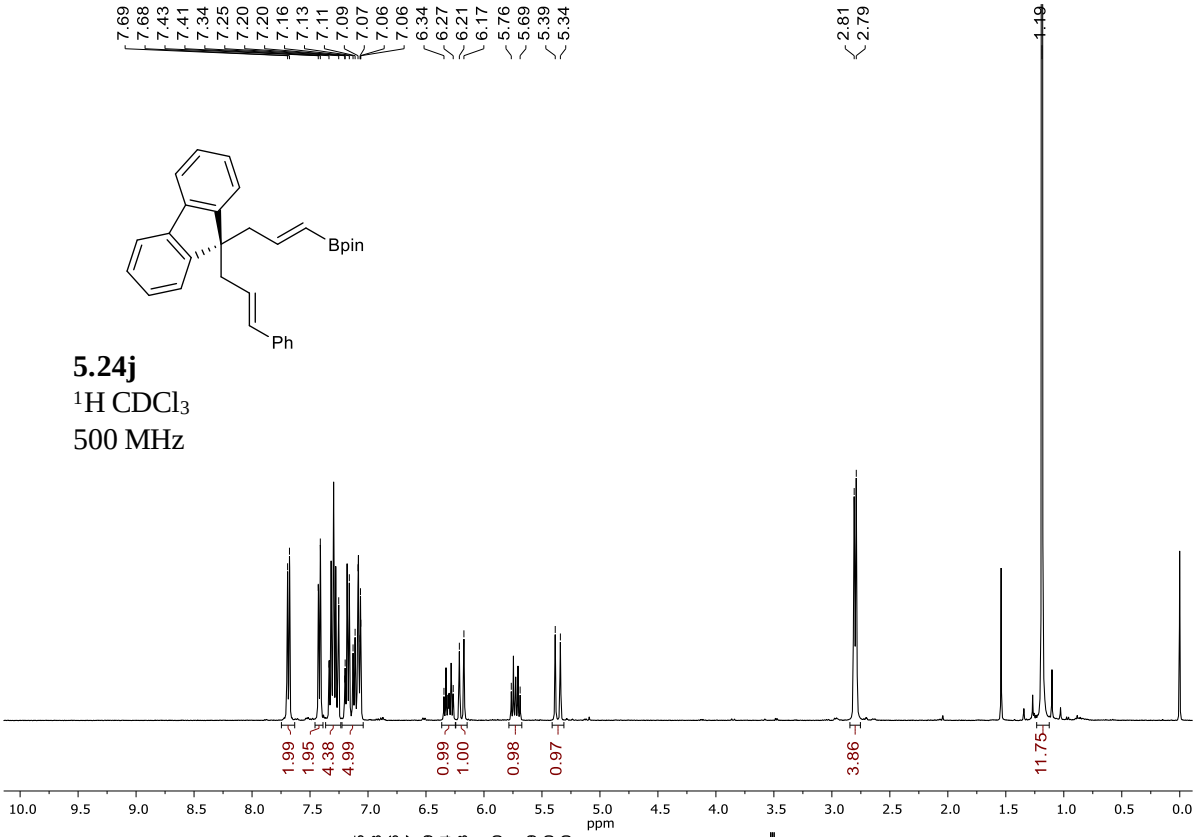

5.24j
^{1}H $CDCl_3$
500 MHz

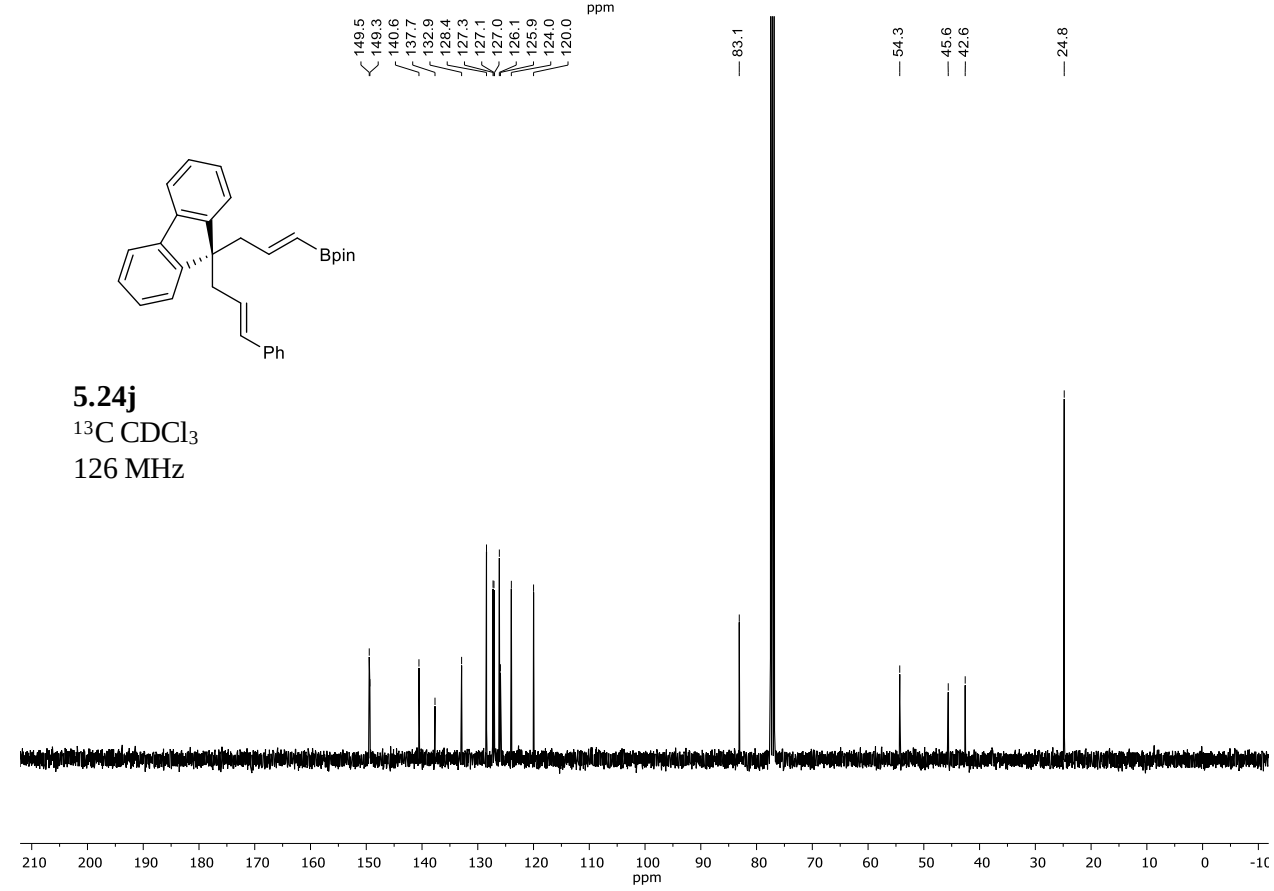

5.24j
^{13}C $CDCl_3$
126 MHz

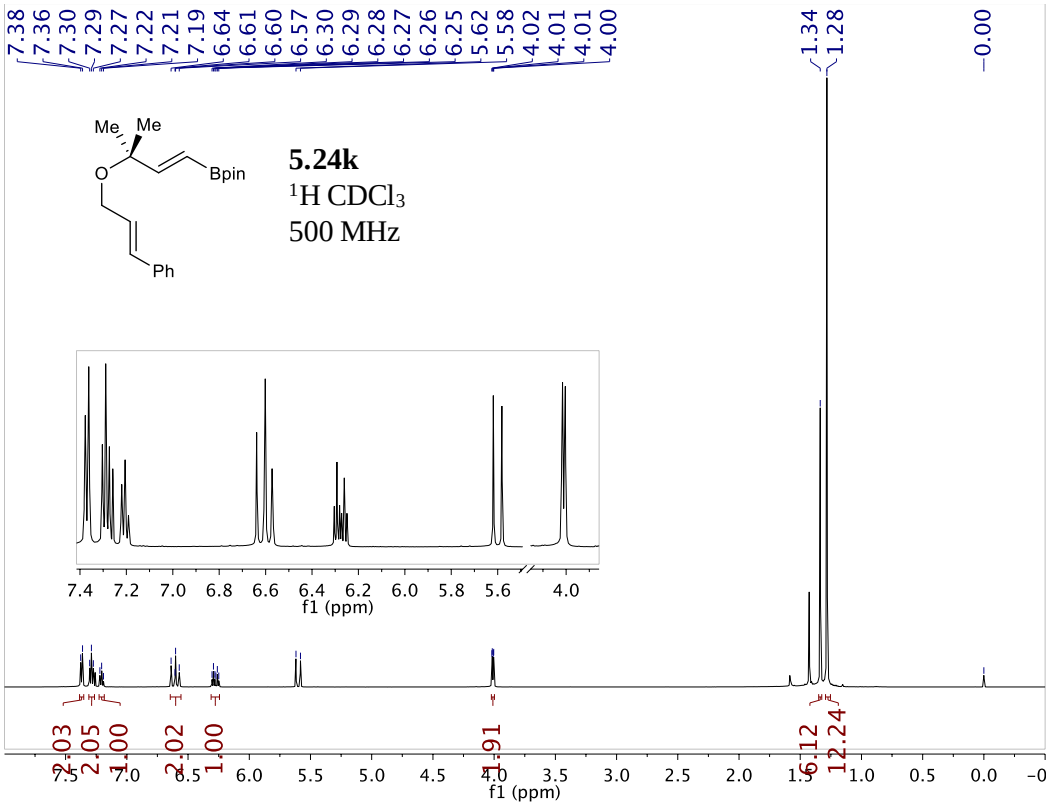
7.38
7.36
7.30
7.29
7.27
7.22
7.21
7.19
6.64
6.61
6.60
6.57
6.30
6.29
6.28
6.27
6.26
6.25
5.62
5.58
4.02
4.01
4.01
4.00
1.34
1.28
0.00
Me
Me
O
Bpin
Ph
5.24k
1H CDCl3
500 MHz
f1 (ppm)
2.03
2.05
1.00
2.02
1.00
1.91
6.12
12.24
f1 (ppm)

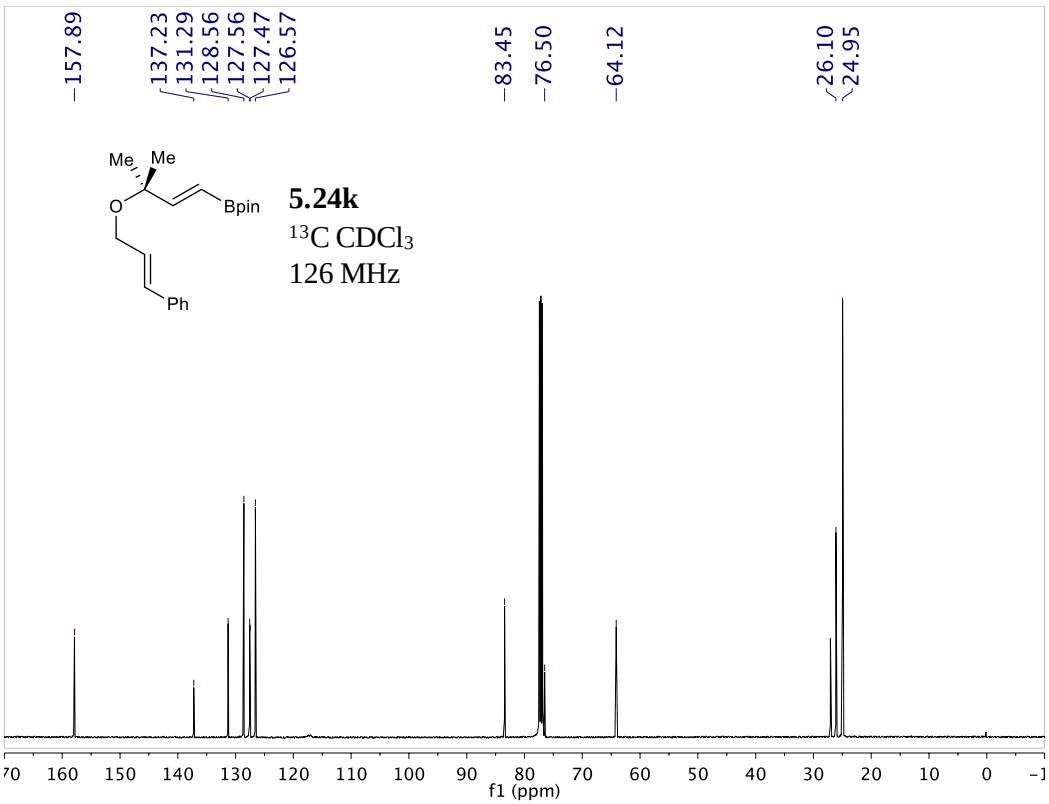
157.89
137.23
131.29
128.56
127.56
127.47
126.57
83.45
76.50
64.12
26.10
24.95
Me
Me
O
Bpin
Ph
5.24k
13C CDCl3
126 MHz
f1 (ppm)

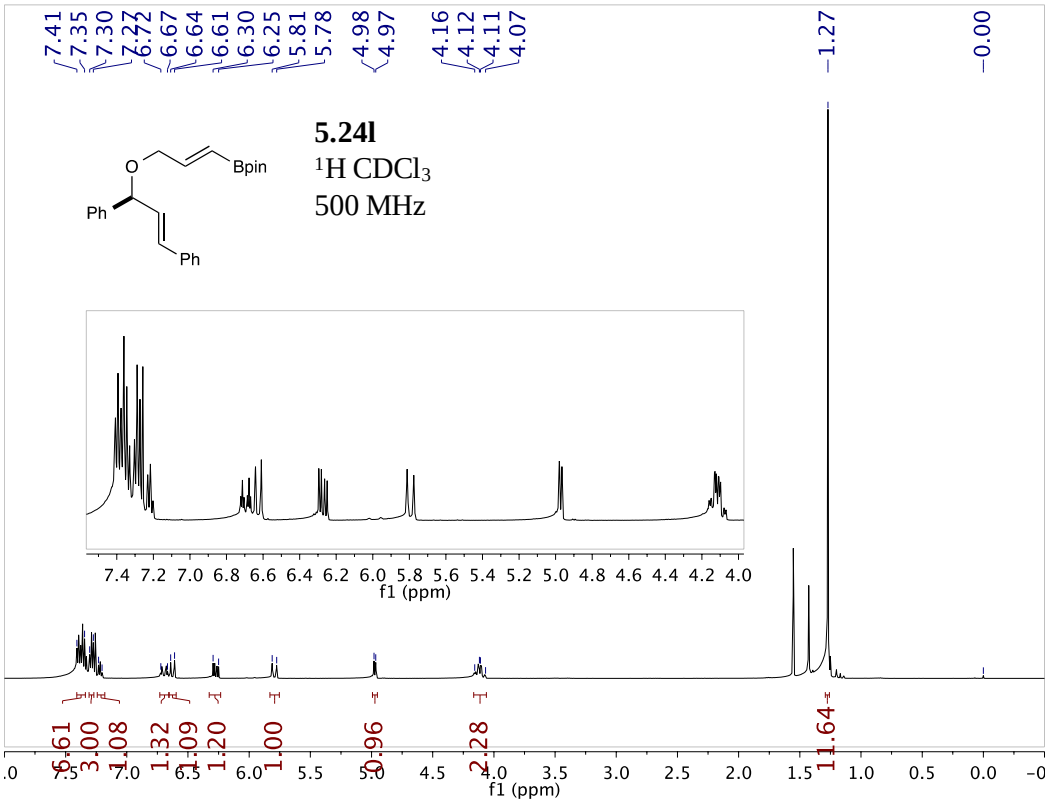
7.41
7.35
7.30
7.27
6.72
6.67
6.64
6.61
6.30
6.25
5.81
5.78
4.98
4.97
4.16
4.12
4.11
4.07
1.27
0.00
O
Bpin
Ph
Ph
5.24l
1H CDCl3
500 MHz
7.4 7.2 7.0 6.8 6.6 6.4 6.2 6.0 5.8 5.6 5.4 5.2 5.0 4.8 4.6 4.4 4.2 4.0
f1 (ppm)
5.61
3.00
1.08
1.32
1.09
1.20
1.00
0.96
2.28
11.64
f1 (ppm)

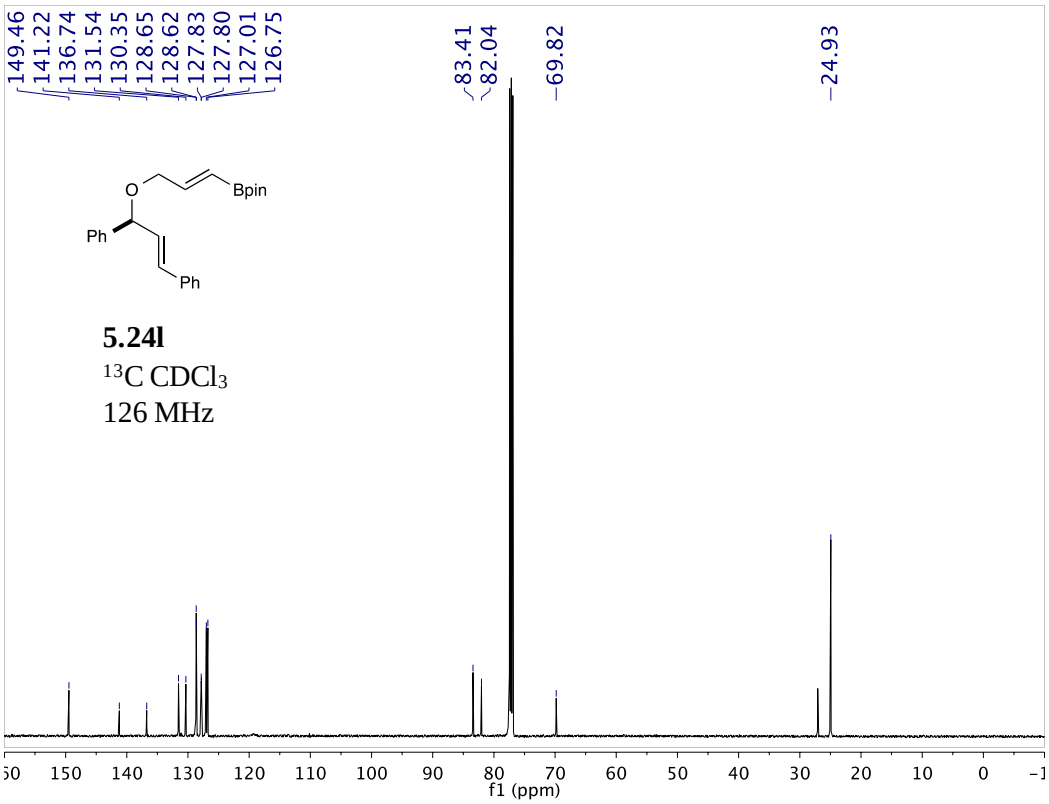
149.46
141.22
136.74
131.54
130.35
128.65
128.62
127.83
127.80
127.01
126.75
83.41
82.04
69.82
24.93
O
Bpin
Ph
Ph
5.24l
13C CDCl3
126 MHz
f1 (ppm)

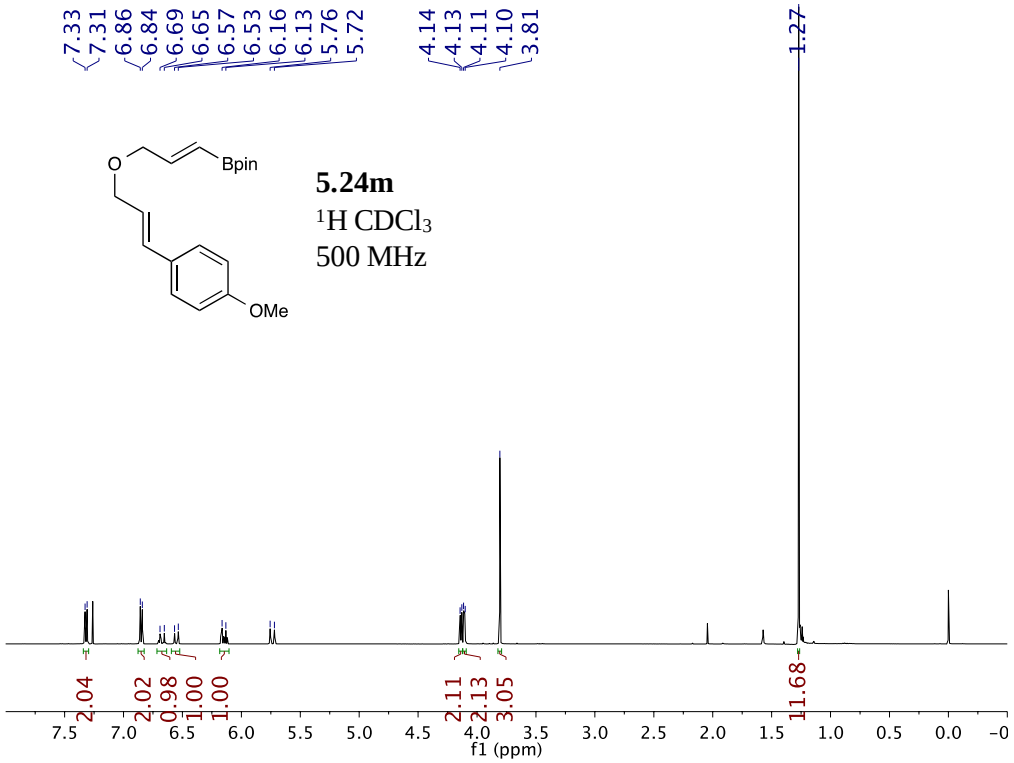
7.33
7.31
6.86
6.84
6.69
6.65
6.57
6.53
6.16
6.13
5.76
5.72
4.14
4.13
4.11
4.10
3.81
1.27
O
Bpin
OMe
5.24m
1H CDCl3
500 MHz
2.04
2.02
0.98
1.00
1.00
2.11
2.13
3.05
11.68
f1 (ppm)

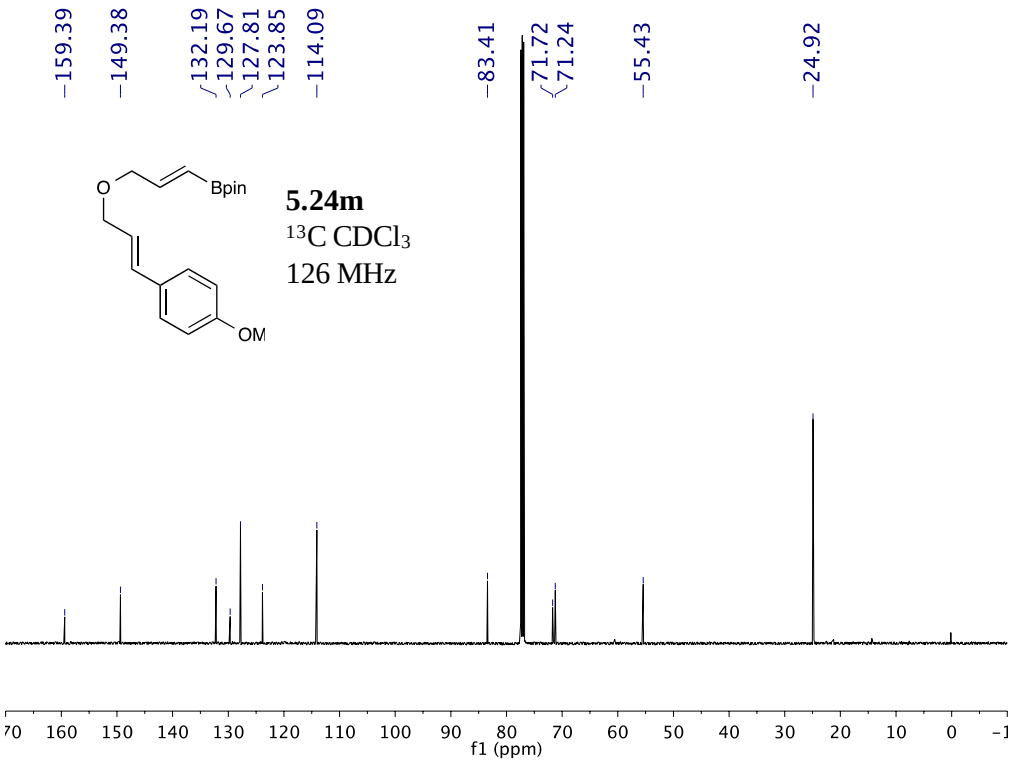
159.39
149.38
132.19
129.67
127.81
123.85
114.09
83.41
71.72
71.24
55.43
24.92
O
Bpin
OM
5.24m
13C CDCl3
126 MHz
f1 (ppm)

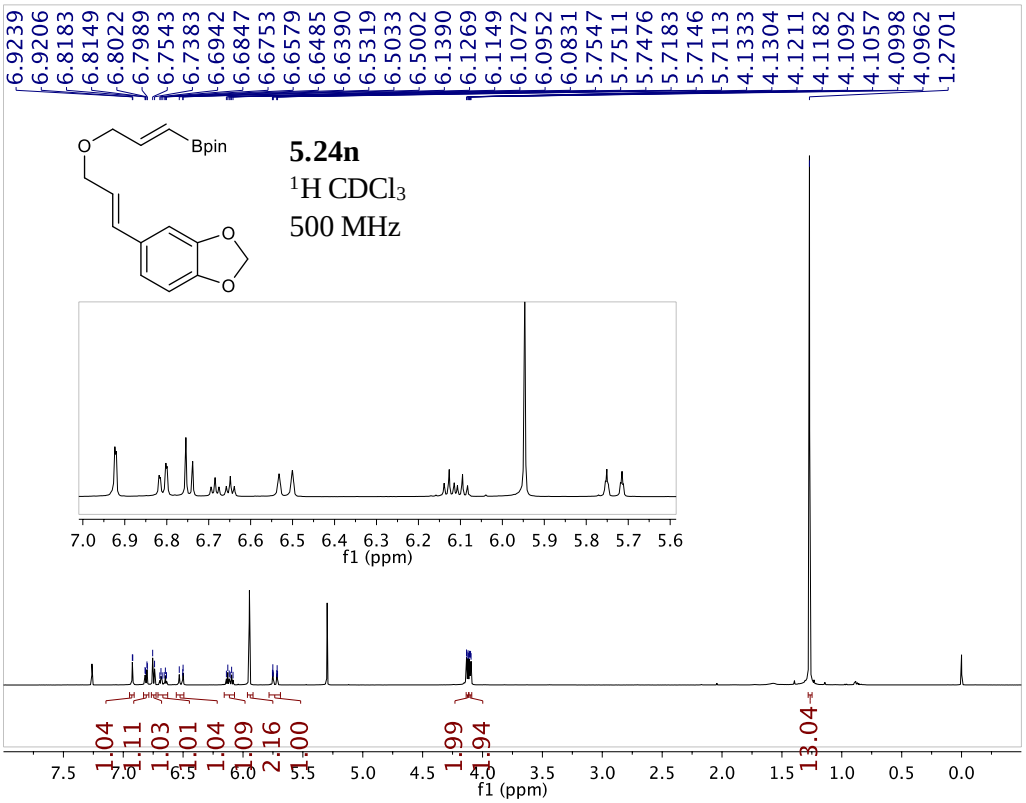
6.9239
6.9206
6.8183
6.8149
6.8022
6.7989
6.7543
6.7383
6.6942
6.6847
6.6753
6.6579
6.6485
6.6390
6.5319
6.5033
6.5002
6.1390
6.1269
6.1149
6.1072
6.0952
6.0831
5.7547
5.7511
5.7476
5.7183
5.7146
5.7113
4.1333
4.1304
4.1211
4.1182
4.1092
4.1057
4.0998
4.0962
1.2701
Bpin
5.24n
1H CDCl3
500 MHz
f1 (ppm)
1.04
1.11
1.03
1.01
1.04
1.09
2.16
1.00
1.99
1.94
13.04
f1 (ppm)

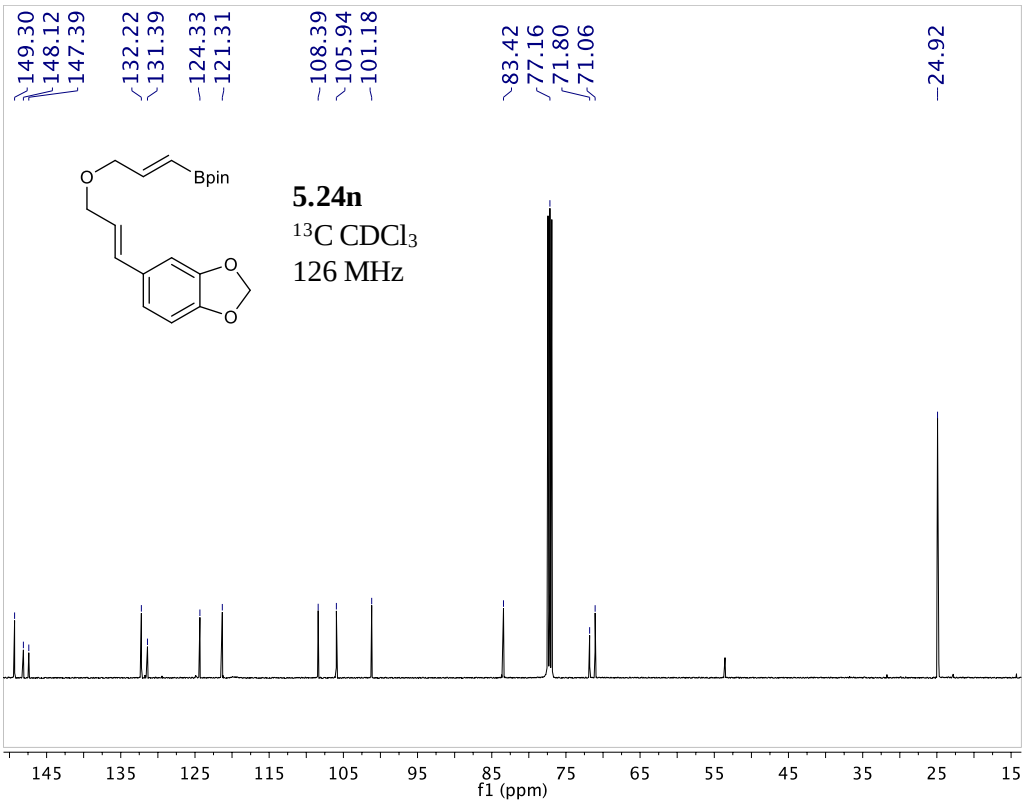
149.30
148.12
147.39
132.22
131.39
124.33
121.31
108.39
105.94
101.18
83.42
77.16
71.80
71.06
24.92
Bpin
5.24n
13C CDCl3
126 MHz
f1 (ppm)

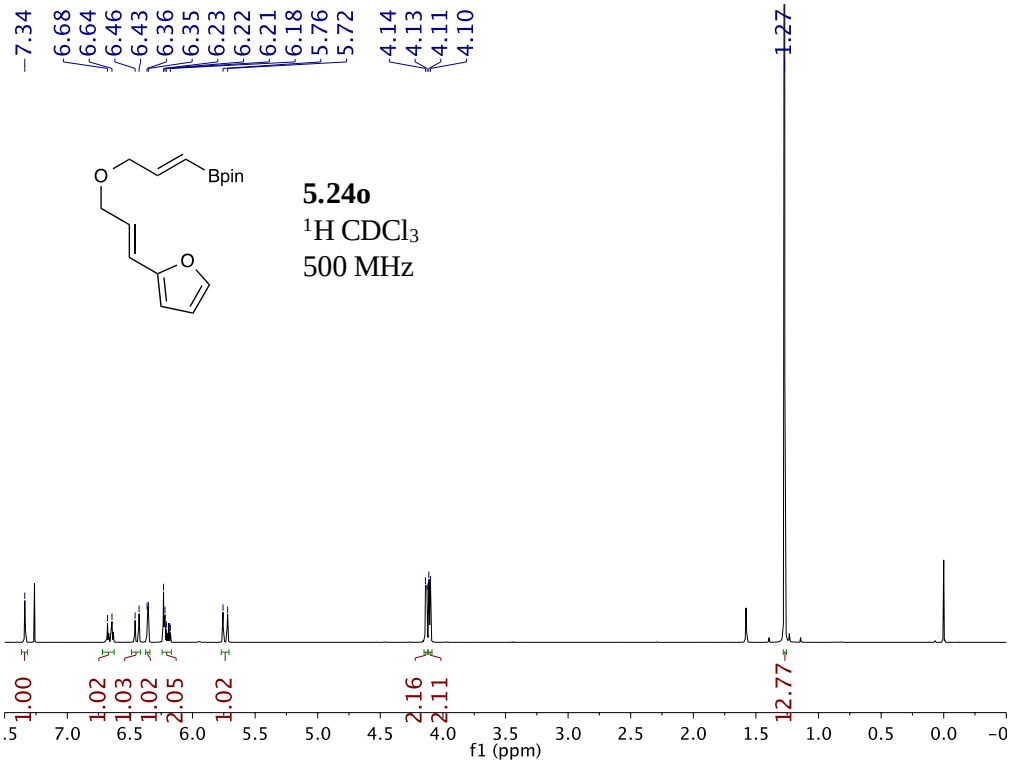
7.34
6.68
6.64
6.46
6.43
6.36
6.35
6.23
6.22
6.21
6.18
5.76
5.72
4.14
4.13
4.11
4.10
1.27
Bpin
O
O
5.24o
1H CDCl3
500 MHz
1.00
1.02
1.03
1.02
2.05
1.02
2.16
2.11
12.77
f1 (ppm)

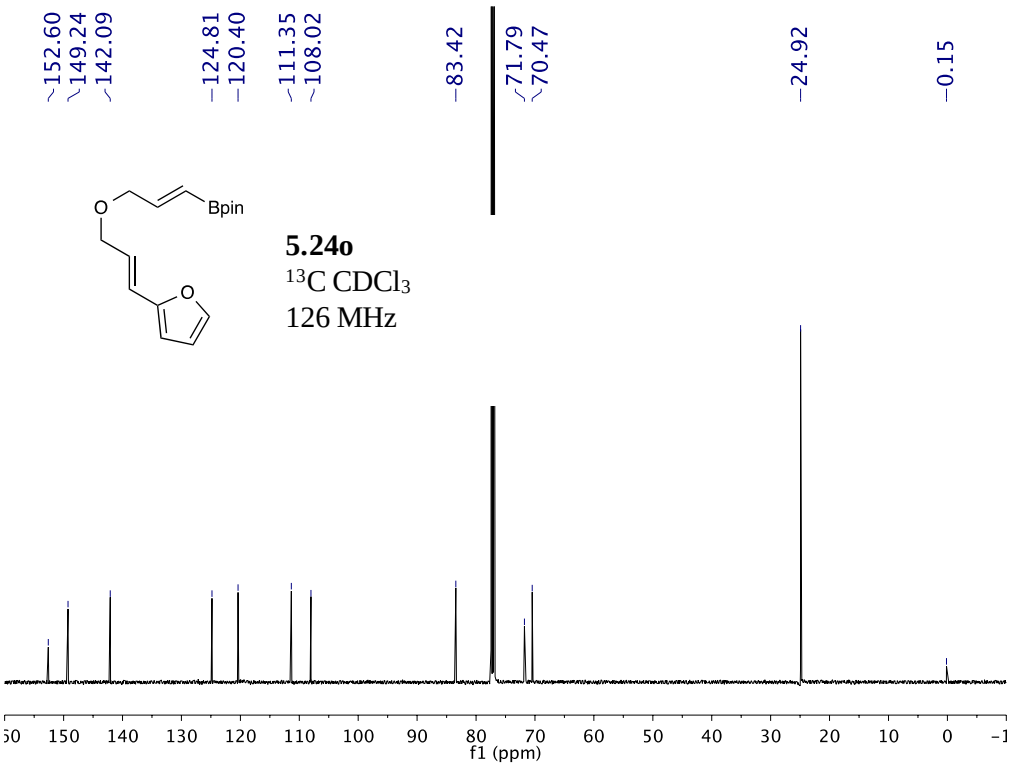
152.60
149.24
142.09
124.81
120.40
111.35
108.02
83.42
71.79
70.47
24.92
0.15
Bpin
O
O
5.24o
13C CDCl3
126 MHz
f1 (ppm)

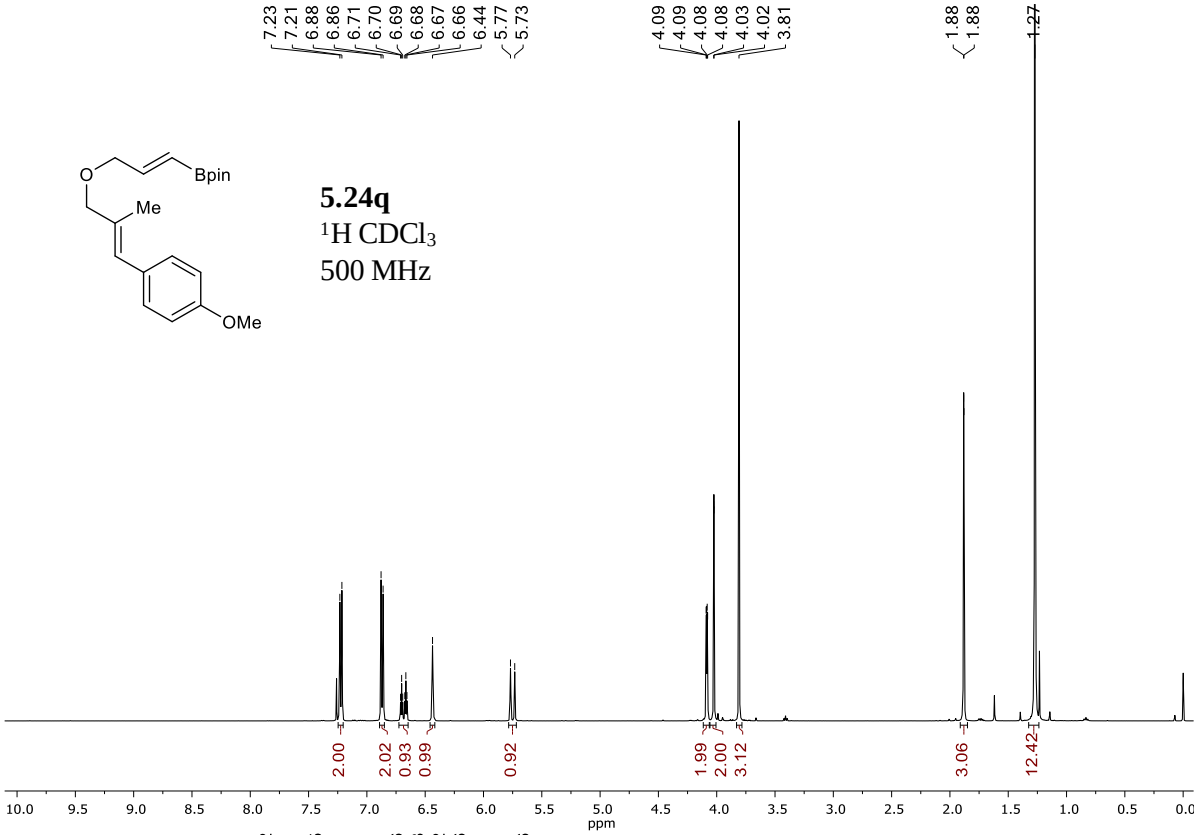
7.23
7.21
6.88
6.86
6.71
6.70
6.69
6.68
6.67
6.66
6.44
5.77
5.73
4.09
4.09
4.08
4.08
4.03
4.02
3.81
1.88
1.88
1.27
O
Bpin
Me
OMe
5.24q
1H CDCl3
500 MHz
2.00
2.02
0.93
0.99
0.92
1.99
2.00
3.12
3.06
12.42
ppm

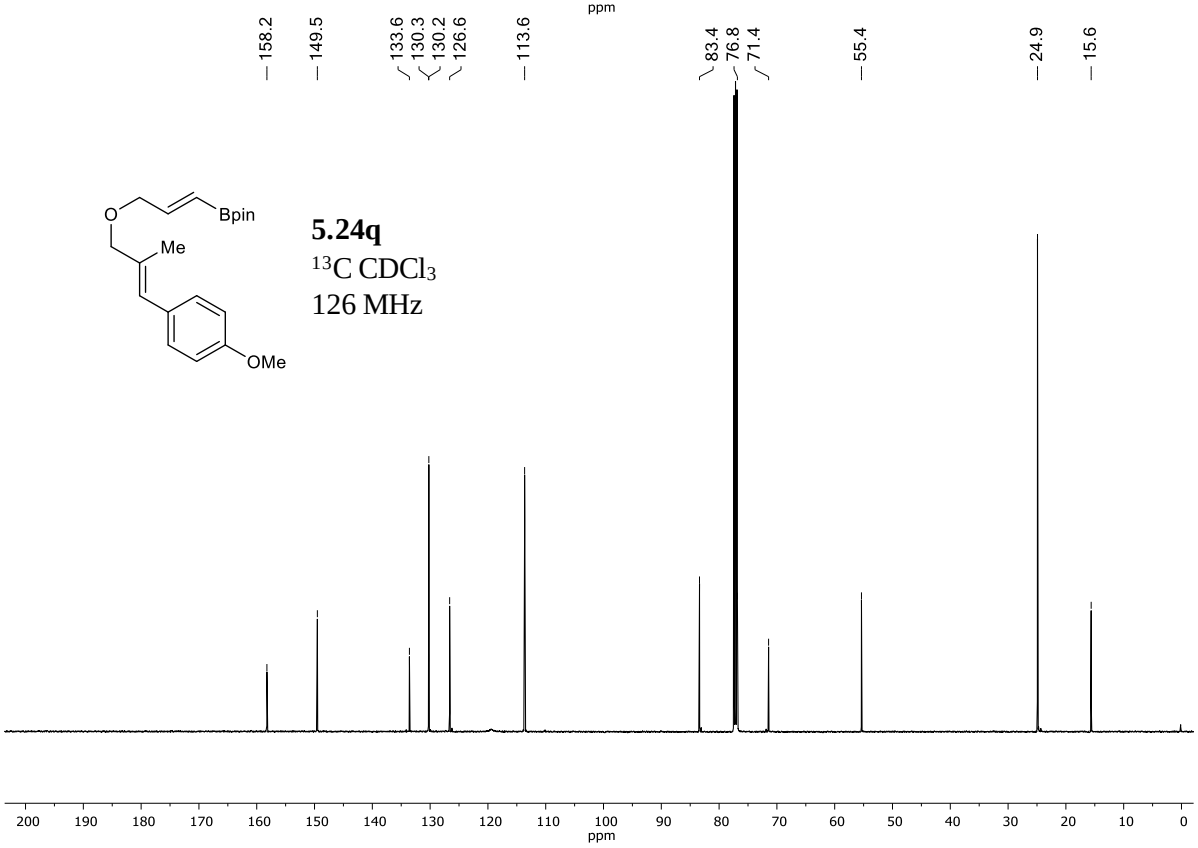
158.2
149.5
133.6
130.3
130.2
126.6
113.6
83.4
76.8
71.4
55.4
24.9
15.6
O
Bpin
Me
OMe
5.24q
13C CDCl3
126 MHz
ppm

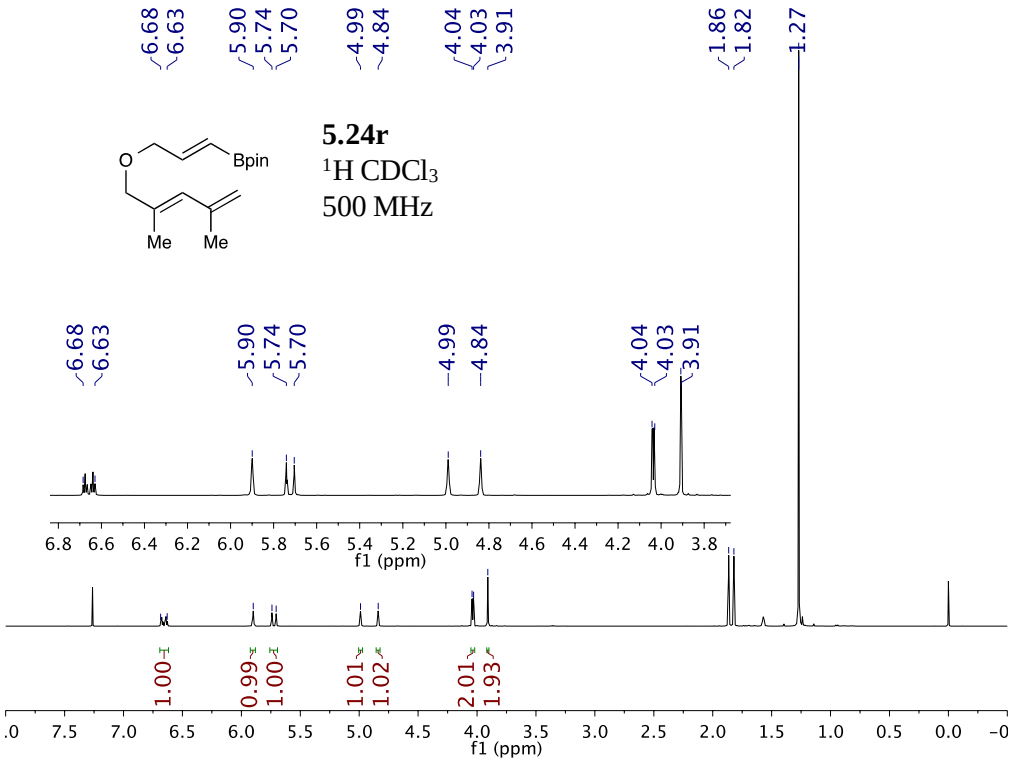
6.68
6.63
5.90
5.74
5.70
4.99
4.84
4.04
4.03
3.91
1.86
1.82
1.27
O
Bpin
Me
Me
5.24r
1H CDCl3
500 MHz
f1 (ppm)
1.00
0.99
1.00
1.01
1.02
2.01
1.93

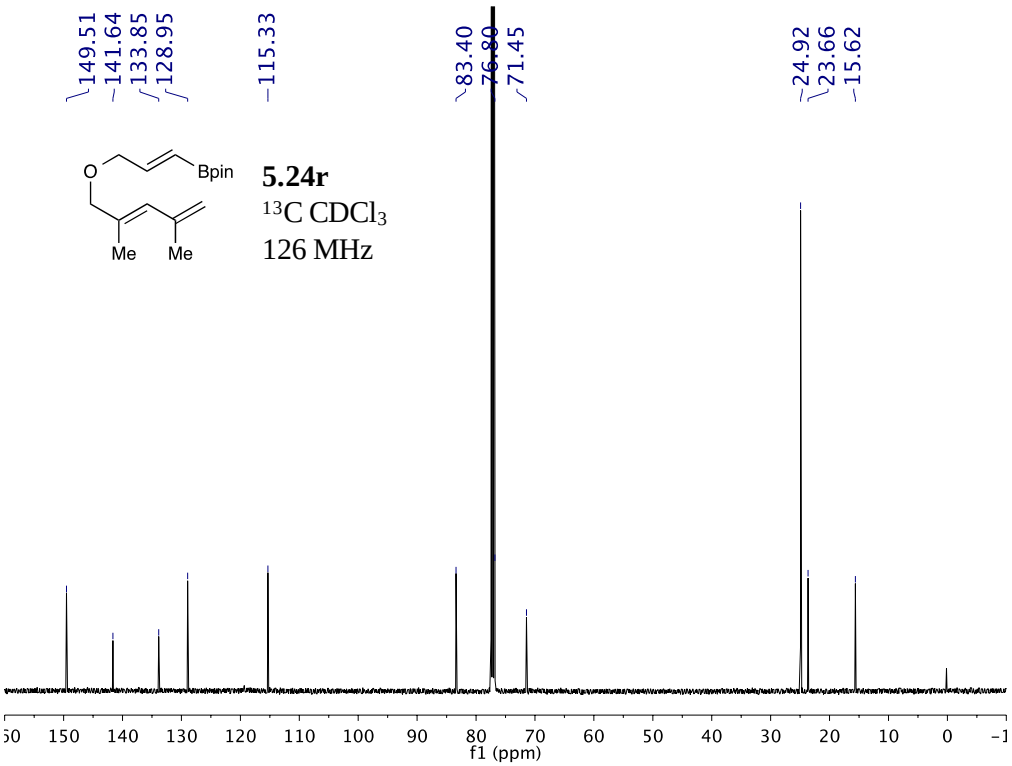
149.51
141.64
133.85
128.95
115.33
83.40
76.80
71.45
24.92
23.66
15.62
O
Bpin
Me
Me
5.24r
13C CDCl3
126 MHz
f1 (ppm)

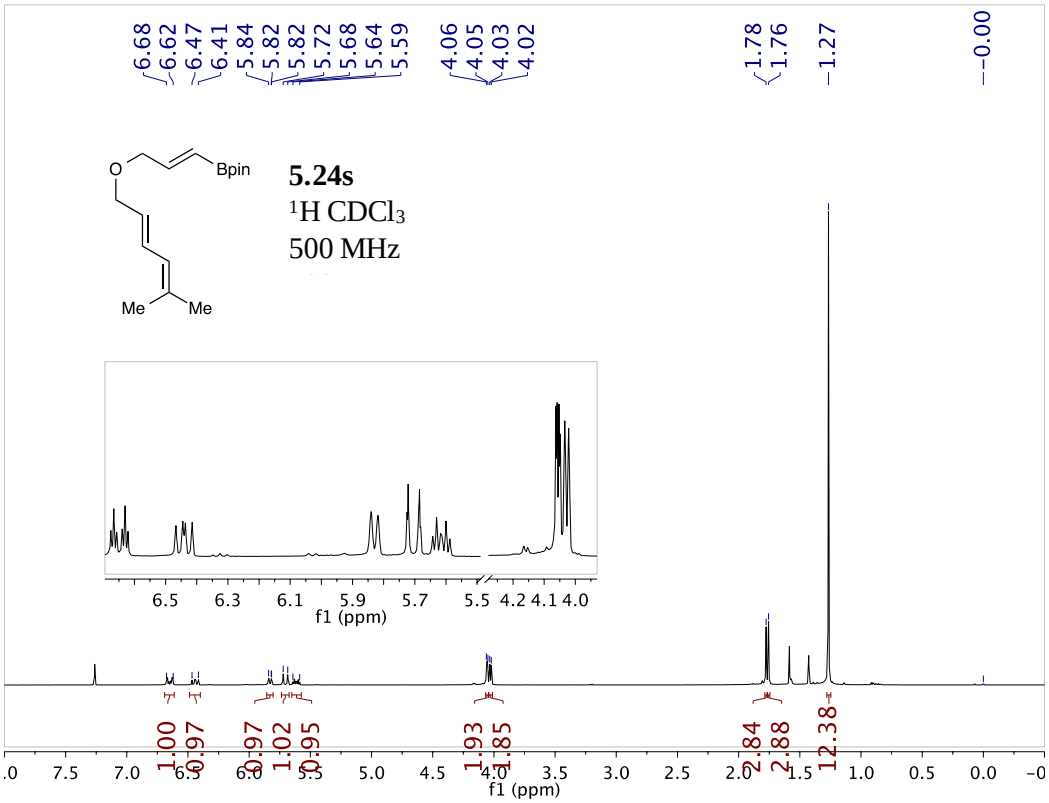
6.68
6.62
6.47
6.41
5.84
5.82
5.82
5.72
5.68
5.64
5.59
4.06
4.05
4.03
4.02
1.78
1.76
1.27
0.00
Bpin
O
Me
Me
5.24s
1H CDCl3
500 MHz
6.5 6.3 6.1 5.9 5.7 5.5 4.2 4.1 4.0
f1 (ppm)
1.00
0.97
0.97
1.02
0.95
1.93
1.85
2.84
2.88
12.38
f1 (ppm)

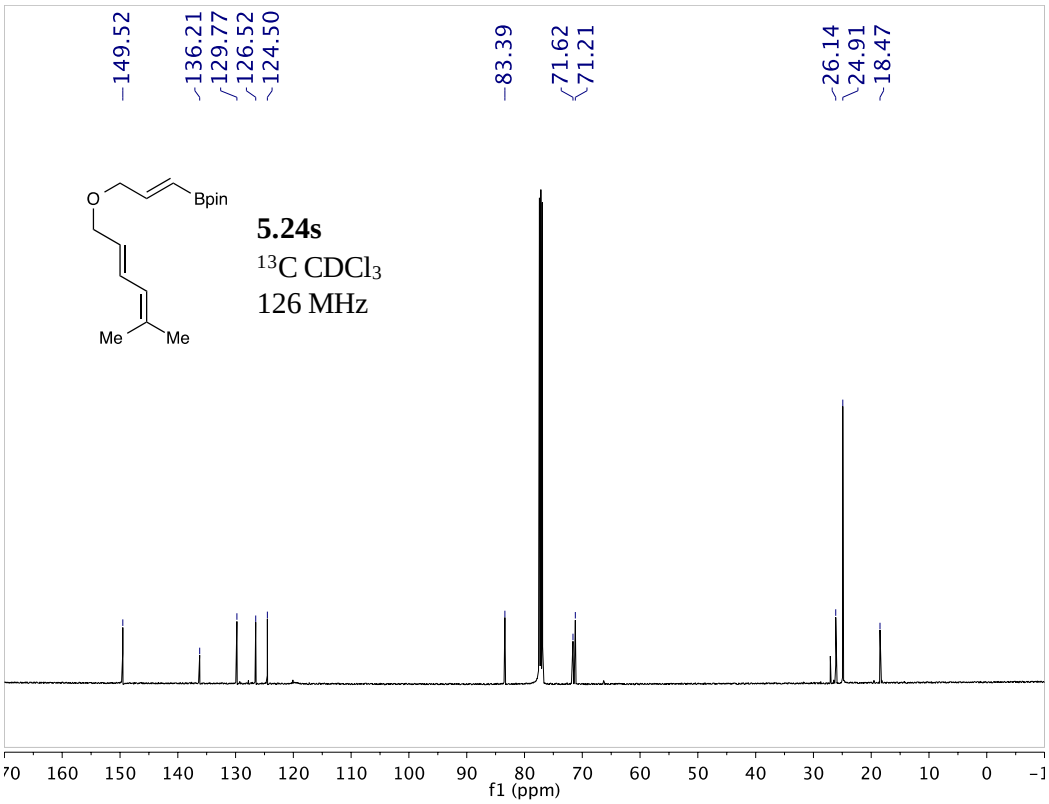
149.52
136.21
129.77
126.52
124.50
83.39
71.62
71.21
26.14
24.91
18.47
Bpin
O
Me
Me
5.24s
13C CDCl3
126 MHz
f1 (ppm)

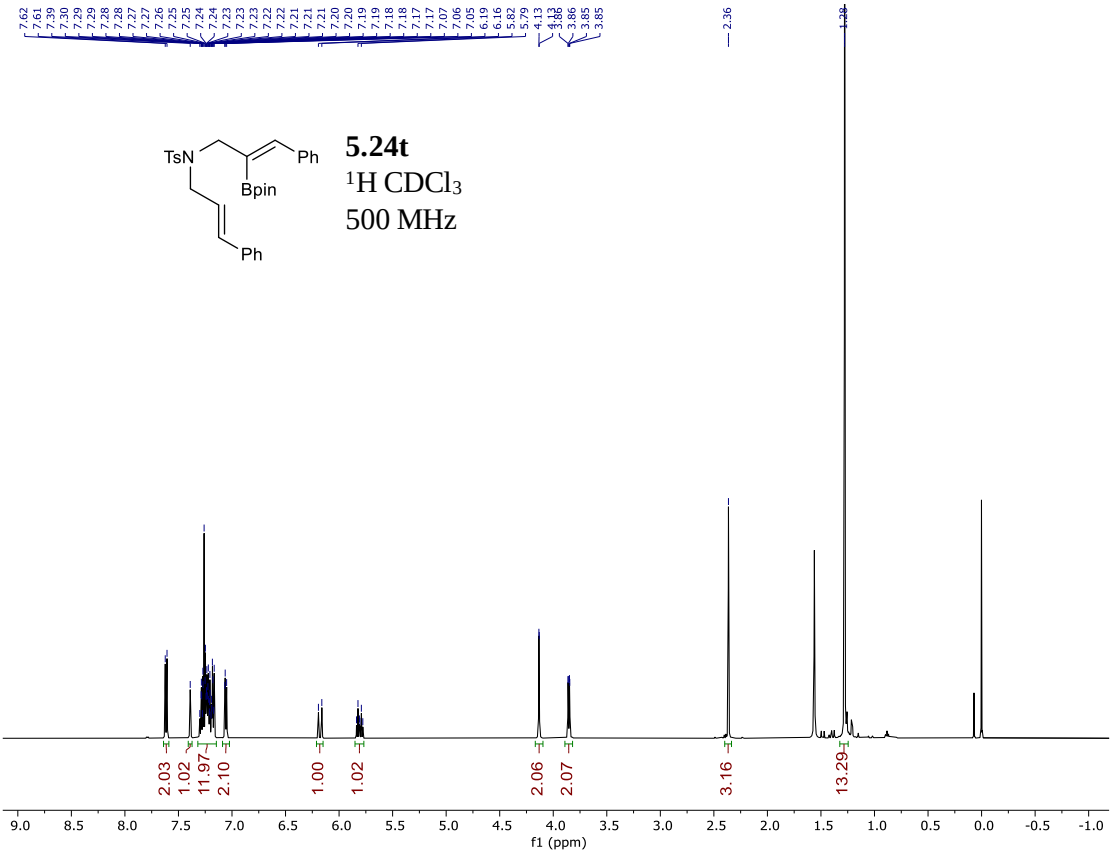
7.62 7.61 7.39 7.30 7.29 7.29 7.28 7.28 7.27 7.27 7.26 7.25 7.25 7.24 7.24 7.23 7.23 7.23 7.22 7.22 7.21 7.21 7.21 7.20 7.20 7.19 7.19 7.18 7.18 7.17 7.17 7.07 7.06 7.05 6.19 6.16 5.82 5.79 4.13 3.88 3.86 3.85 3.85
2.36
1.28
TsN
Ph
Bpin
Ph
5.24t
1H CDCl3
500 MHz
2.03 1.02 11.97 2.10 1.00 1.02 2.06 2.07 3.16 13.29
9.0 8.5 8.0 7.5 7.0 6.5 6.0 5.5 5.0 4.5 4.0 3.5 3.0 2.5 2.0 1.5 1.0 0.5 0.0 -0.5 -1.0
f1 (ppm)

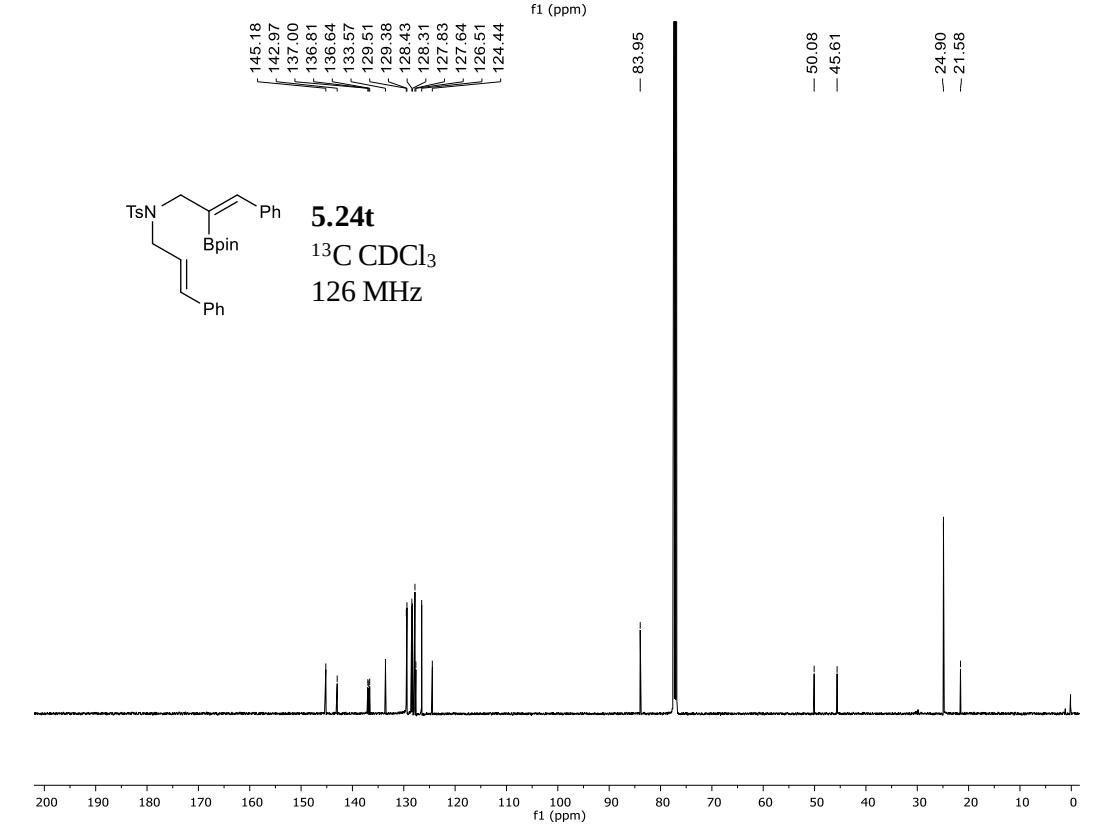
145.18 142.97 137.00 136.81 136.64 133.57 129.51 129.38 128.43 128.31 127.83 127.64 126.51 124.44
83.95
50.08 45.61
24.90 21.58
TsN
Ph
Bpin
Ph
5.24t
13C CDCl3
126 MHz
200 190 180 170 160 150 140 130 120 110 100 90 80 70 60 50 40 30 20 10 0
f1 (ppm)

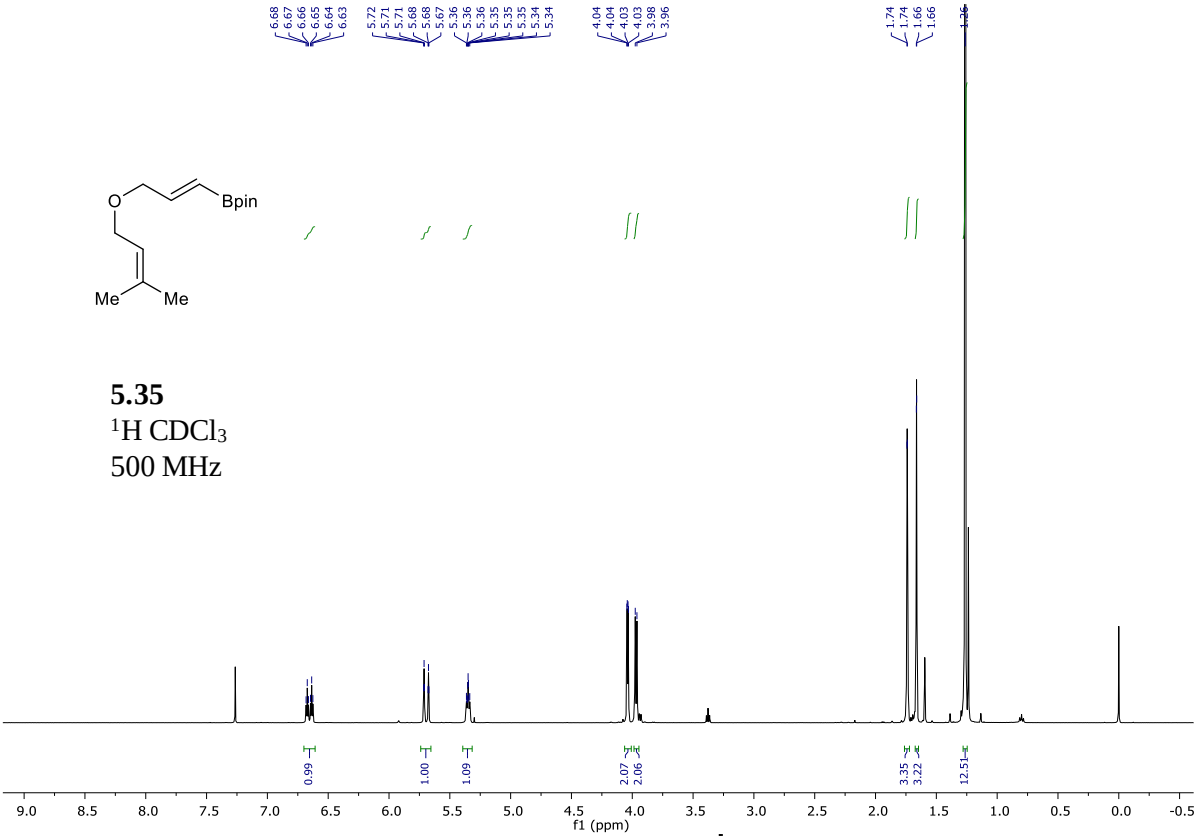

5.35
^{1}H $CDCl_3$
500 MHz

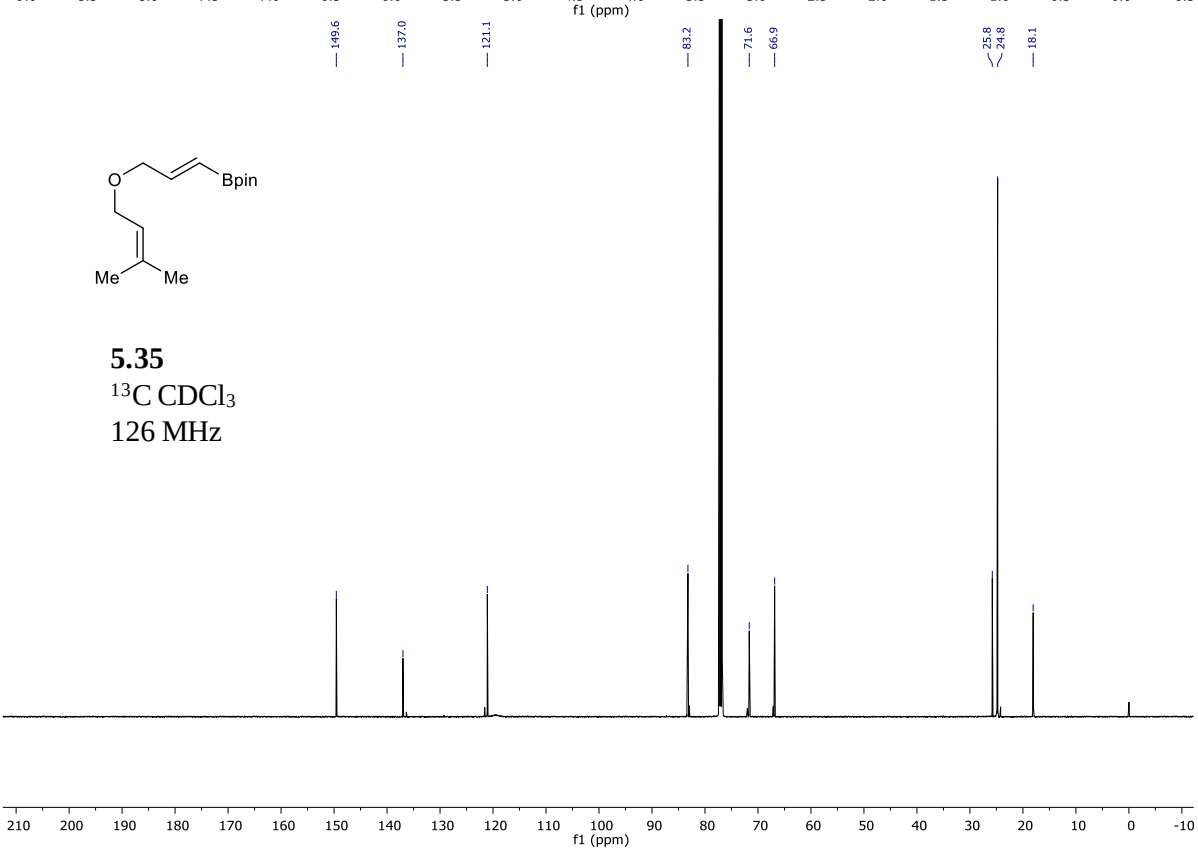

5.35
^{13}C $CDCl_3$
126 MHz

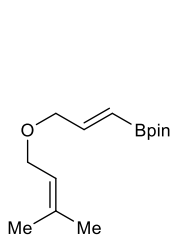

5.35
^{11}B $CDCl_3$
128 MHz

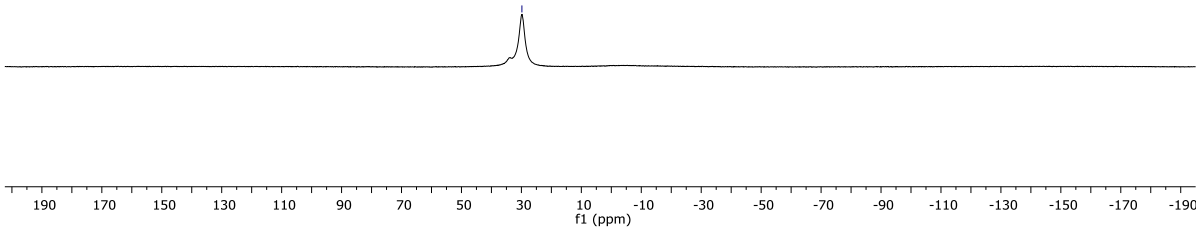

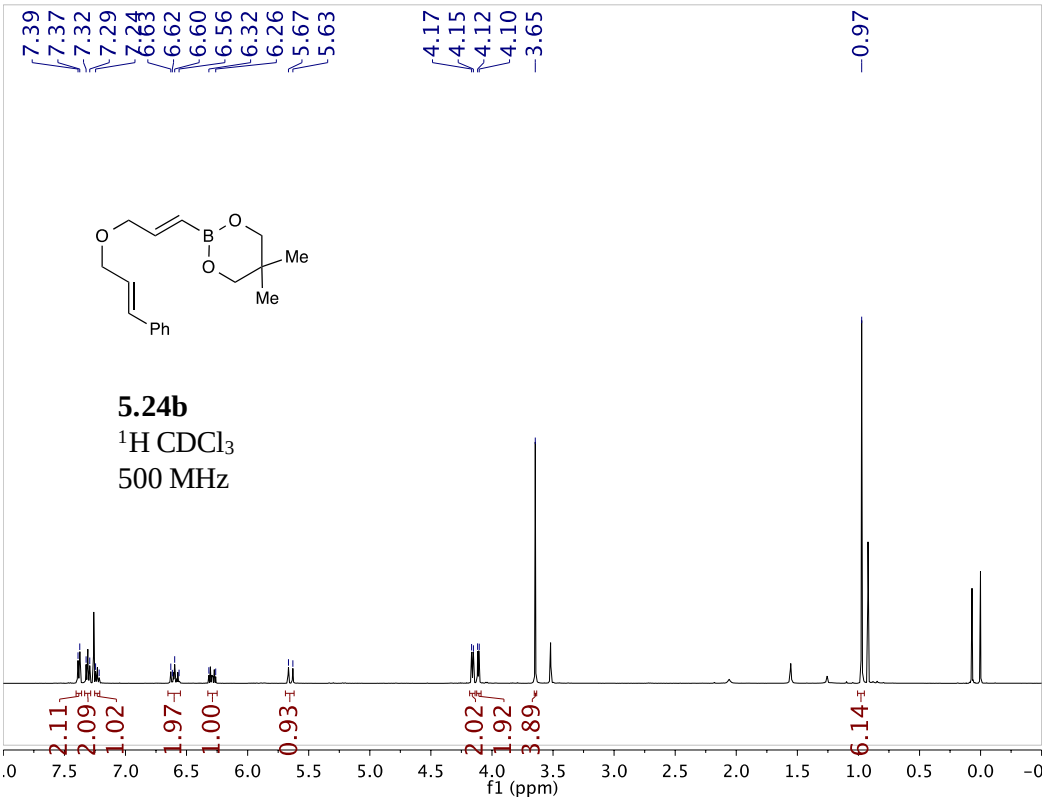
7.39
7.37
7.32
7.29
7.24
6.63
6.62
6.60
6.56
6.32
6.26
5.67
5.63
4.17
4.15
4.12
4.10
3.65
0.97
O
B
O
O
Me
Me
Ph
5.24b
1H CDCl3
500 MHz
2.11
2.09
1.02
1.97
1.00
0.93
2.02
1.92
3.89
6.14
f1 (ppm)

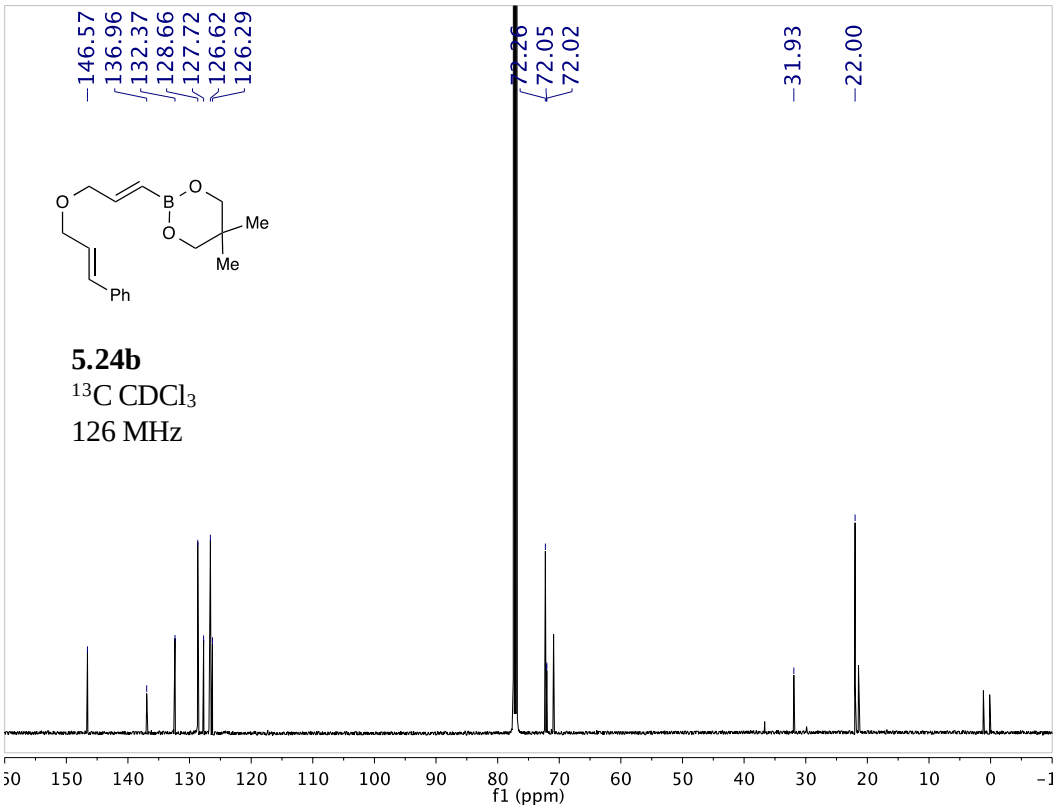
146.57
136.96
132.37
128.66
127.72
126.62
126.29
72.26
72.05
72.02
31.93
22.00
O
B
O
O
Me
Me
Ph
5.24b
13C CDCl3
126 MHz
f1 (ppm)

5.24b

^{11}B $CDCl_3$

128 MHz

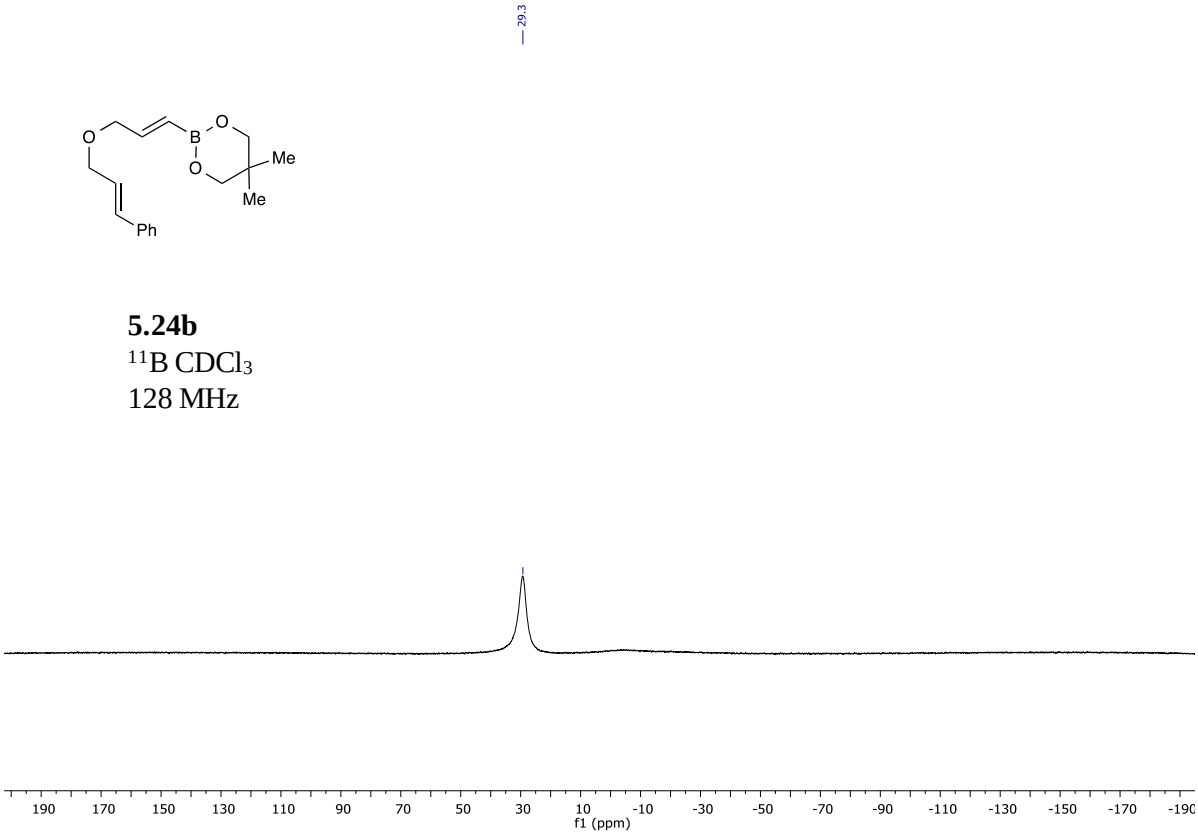

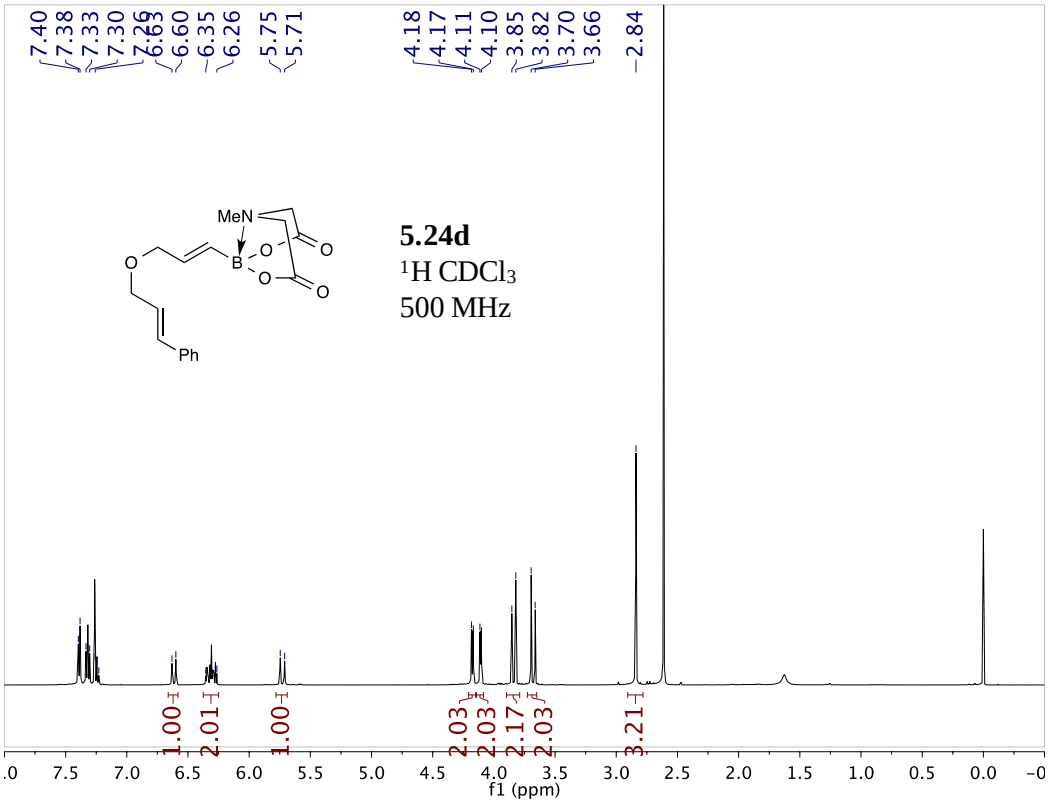
7.40
7.38
7.33
7.30
7.26
6.63
6.60
6.35
6.26
5.75
5.71
4.18
4.17
4.11
4.10
3.85
3.82
3.70
3.66
2.84
MeN
B
O
Ph
5.24d
1H CDCl3
500 MHz
1.00
2.01
1.00
2.03
2.03
2.17
2.03
3.21
f1 (ppm)

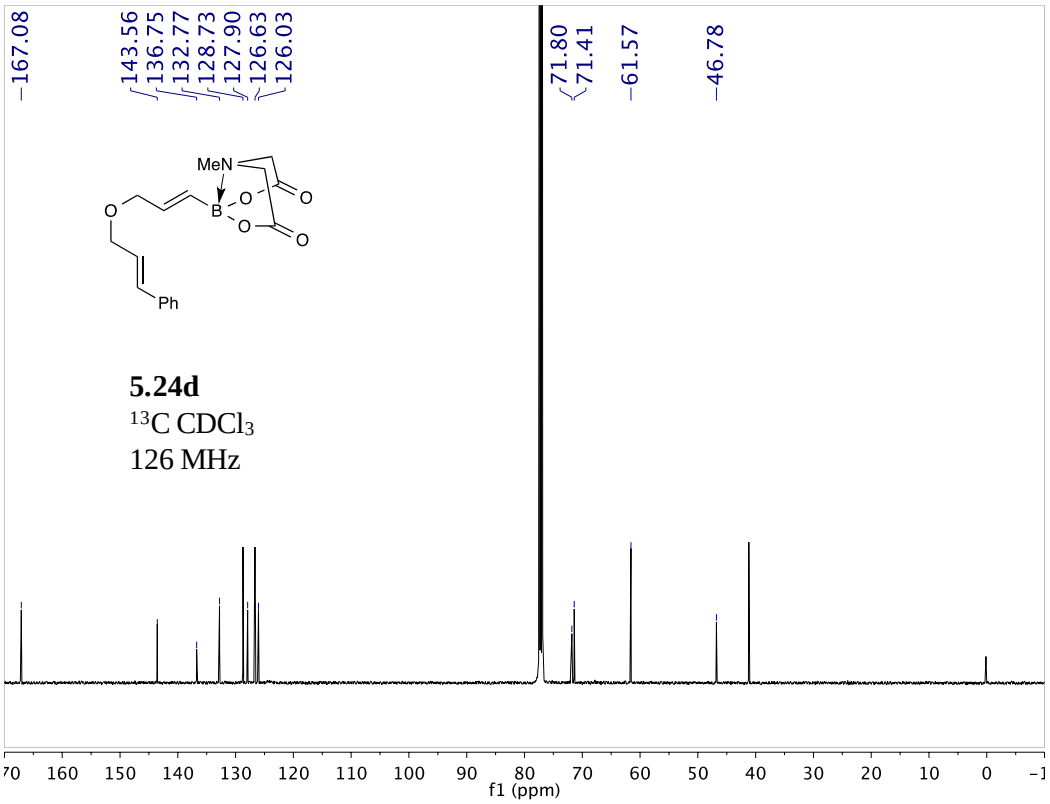
167.08
143.56
136.75
132.77
128.73
127.90
126.63
126.03
71.80
71.41
61.57
46.78
MeN
B
O
Ph
5.24d
13C CDCl3
126 MHz
f1 (ppm)

5.24d
^{11}B $CDCl_3$
128 MHz

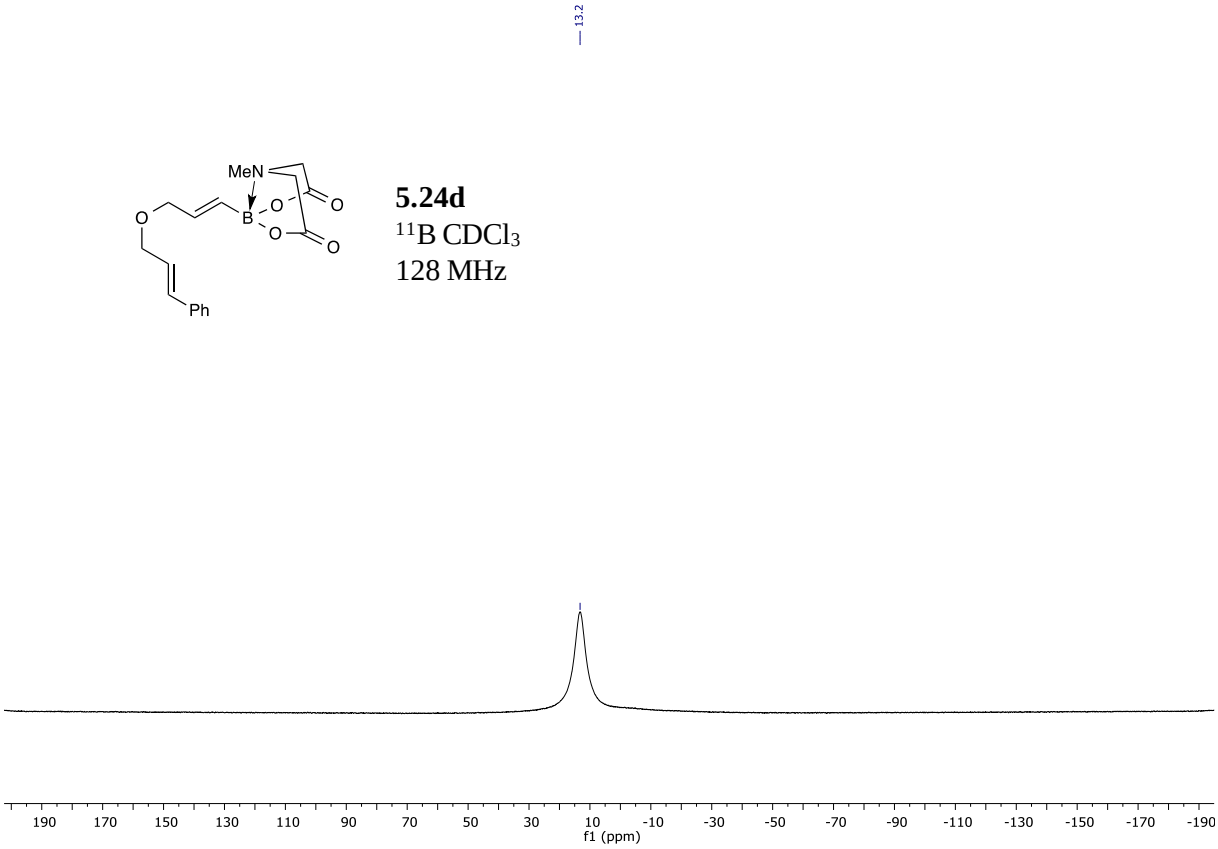

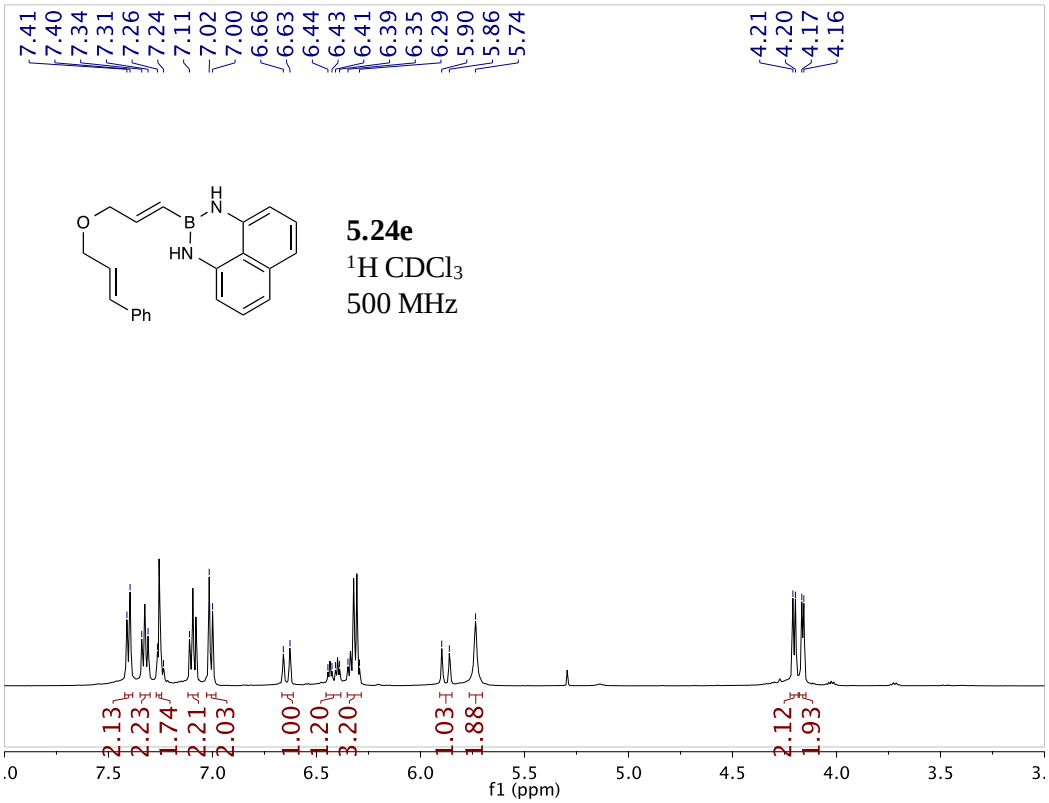
7.41
7.40
7.34
7.31
7.26
7.24
7.11
7.02
7.00
6.66
6.63
6.44
6.43
6.41
6.39
6.35
6.29
5.90
5.86
5.74
4.21
4.20
4.17
4.16
O
B
HN
H
N
Ph
5.24e
1H CDCl3
500 MHz
2.13
2.23
1.74
2.21
2.03
1.00
1.20
3.20
1.03
1.88
2.12
1.93
f1 (ppm)

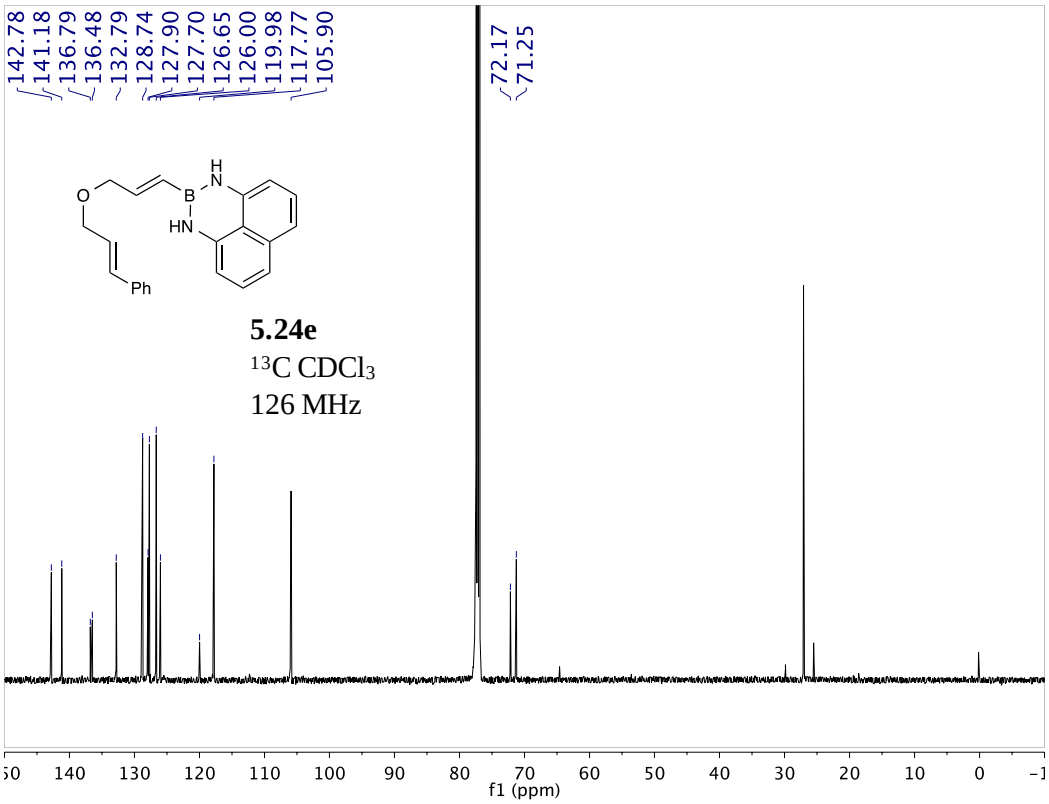
142.78
141.18
136.79
136.48
132.79
128.74
127.90
127.70
126.65
126.00
119.98
117.77
105.90
72.17
71.25
O
B
HN
H
N
Ph
5.24e
13C CDCl3
126 MHz
f1 (ppm)

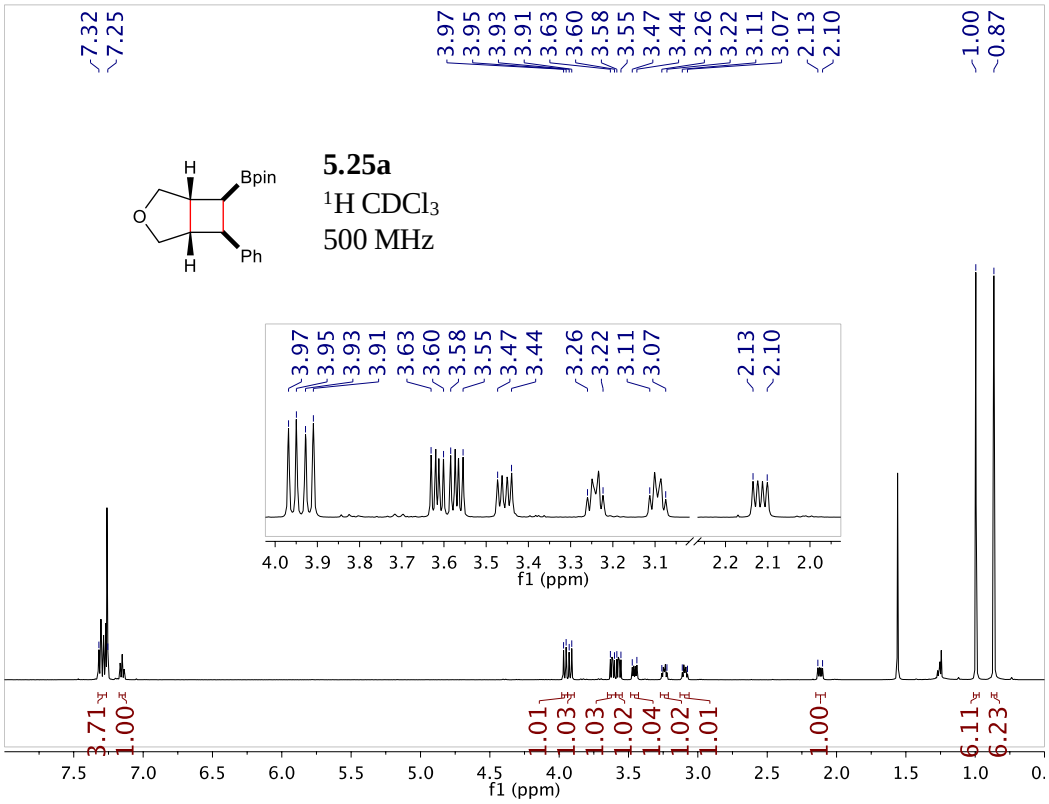
7.32
7.25
3.97
3.95
3.93
3.91
3.63
3.60
3.58
3.55
3.47
3.44
3.26
3.22
3.11
3.07
2.13
2.10
1.00
0.87
H
Bpin
O
H
Ph
5.25a
1H CDCl3
500 MHz
f1 (ppm)
3.71
1.00
1.01
1.03
1.03
1.02
1.04
1.02
1.01
1.00
6.11
6.23

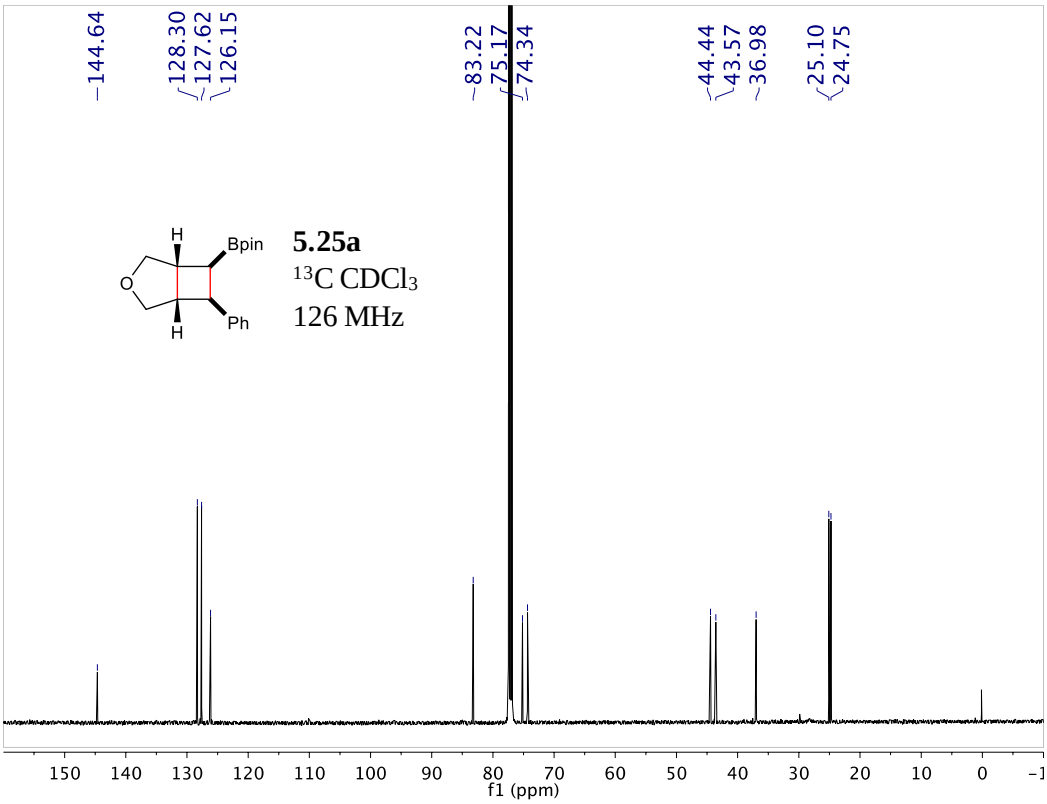
144.64
128.30
127.62
126.15
83.22
75.17
74.34
44.44
43.57
36.98
25.10
24.75
H
Bpin
O
H
Ph
5.25a
13C CDCl3
126 MHz
f1 (ppm)

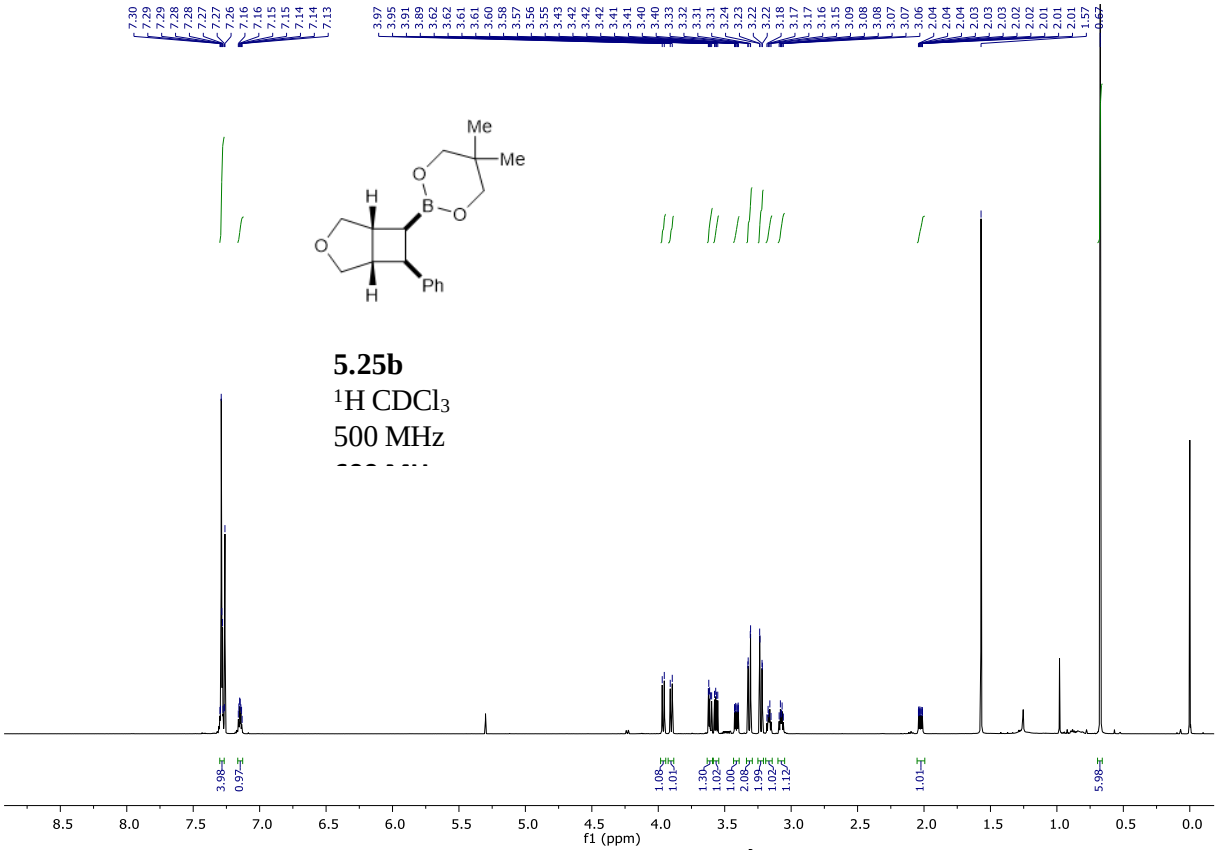
Me
Me
O
B
O
H
O
H
Ph
5.25b
1H CDCl3
500 MHz
f1 (ppm)

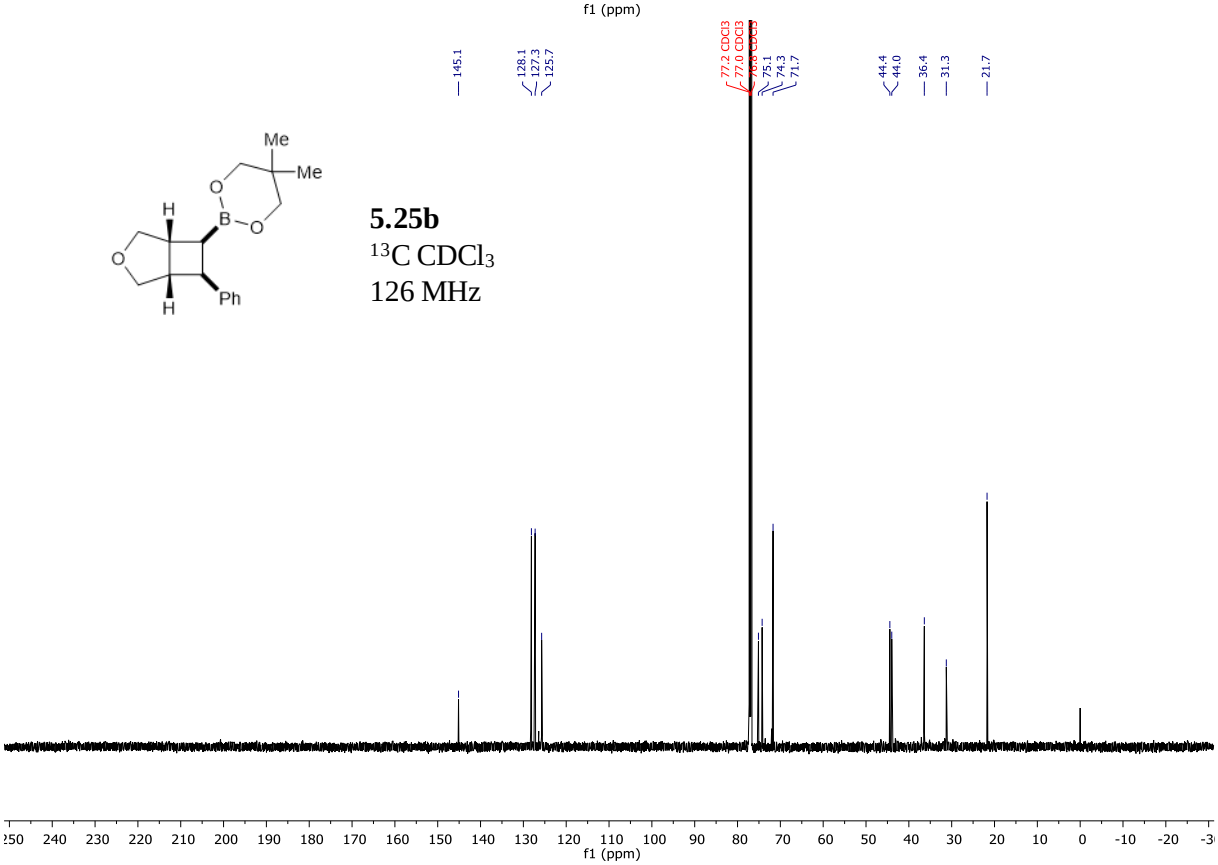
Me
Me
O
B
O
H
O
H
Ph
5.25b
13C CDCl3
126 MHz
f1 (ppm)

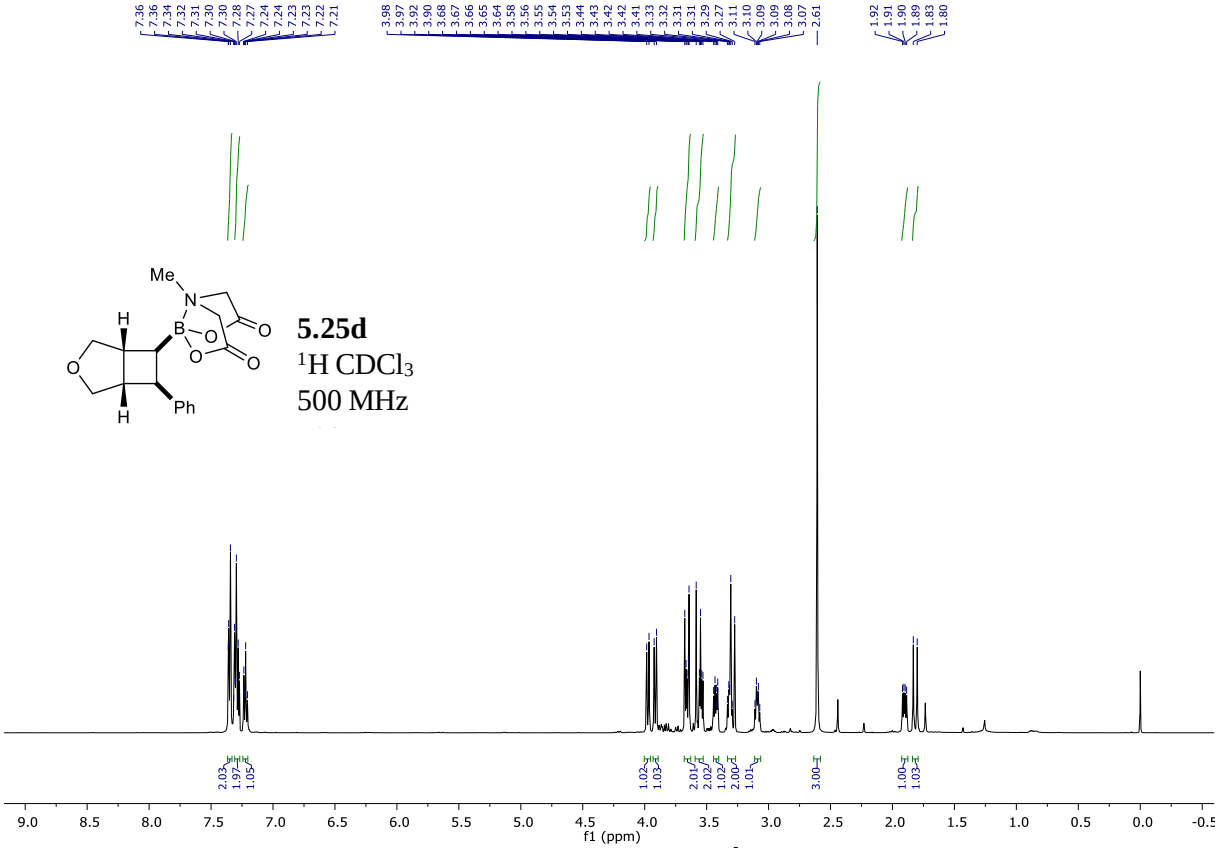
7.36 7.36 7.34 7.32 7.31 7.30 7.30 7.28 7.27 7.24 7.24 7.23 7.23 7.22 7.21
3.98 3.97 3.92 3.90 3.68 3.67 3.66 3.65 3.64 3.58 3.56 3.55 3.54 3.53 3.44 3.43 3.42 3.41 3.33 3.32 3.31 3.31 3.29 3.27 3.11 3.10 3.09 3.09 3.08 3.07 2.61
1.92 1.91 1.90 1.89 1.83 1.80
Me
N
B
O
O
O
O
H
H
O
Ph
5.25d
1H CDCl3
500 MHz
2.03 1.97 1.05 1.02 1.03 2.01 2.02 1.02 2.00 1.01 3.00 1.00 1.03
9.0 8.5 8.0 7.5 7.0 6.5 6.0 5.5 5.0 4.5 4.0 3.5 3.0 2.5 2.0 1.5 1.0 0.5 0.0 -0.5
f1 (ppm)

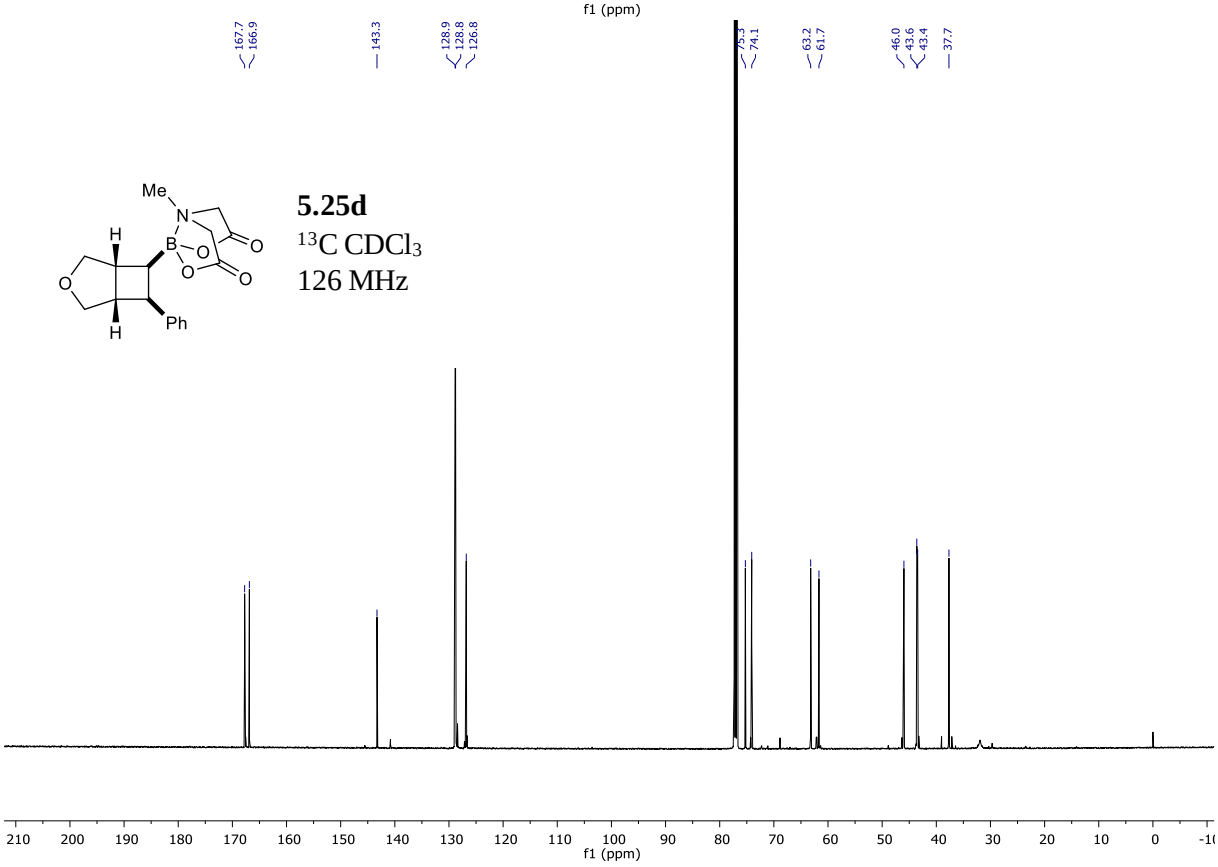
167.7 166.9 143.3 128.9 128.8 126.8 75.3 74.1 63.2 61.7 46.0 43.6 43.4 37.7
Me
N
B
O
O
O
O
H
H
O
Ph
5.25d
13C CDCl3
126 MHz
210 200 190 180 170 160 150 140 130 120 110 100 90 80 70 60 50 40 30 20 10 0 -10
f1 (ppm)

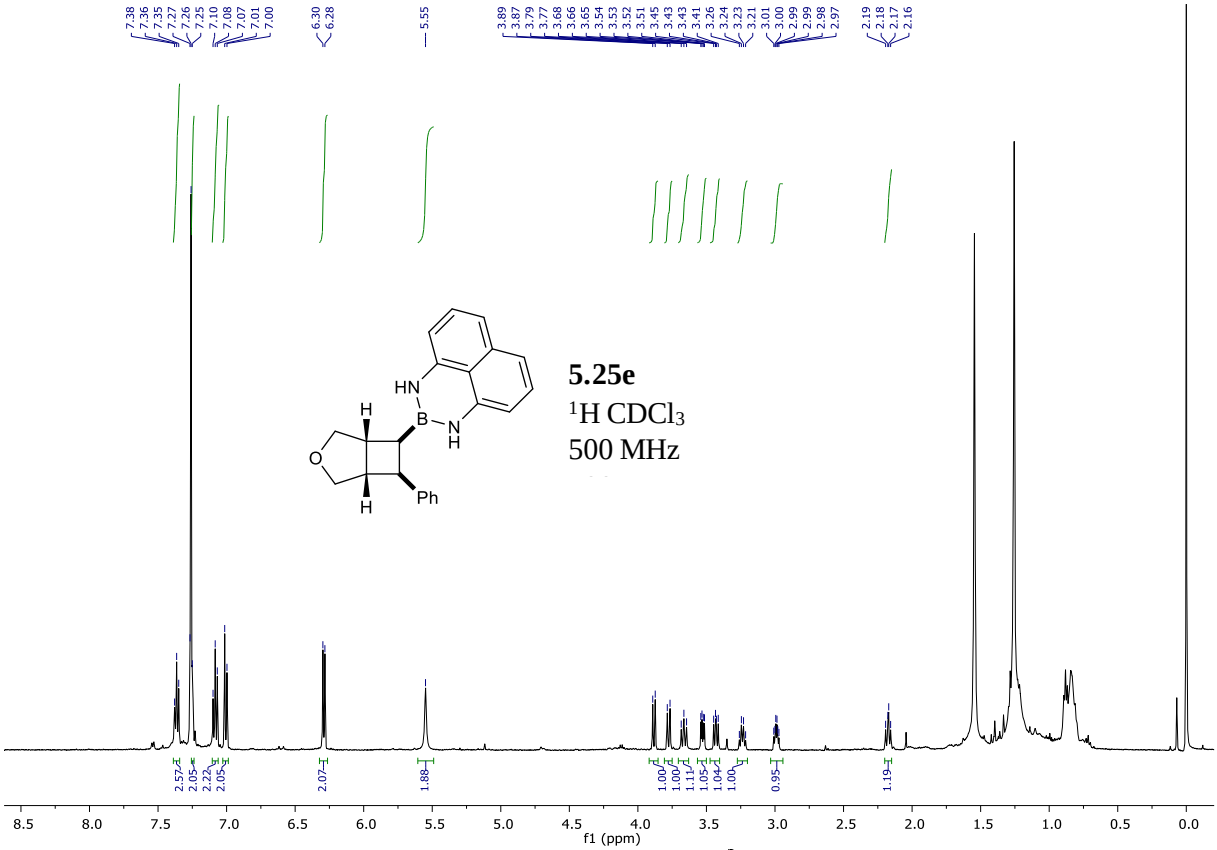
7.38
7.36
7.35
7.27
7.26
7.25
7.10
7.08
7.07
7.01
7.00
6.30
6.28
5.55
3.89
3.87
3.79
3.77
3.68
3.66
3.65
3.54
3.53
3.52
3.51
3.45
3.43
3.41
3.26
3.24
3.23
3.21
3.01
3.00
2.99
2.99
2.98
2.97
2.19
2.18
2.17
2.16
HN
B
N
H
O
H
H
Ph
5.25e
1H CDCl3
500 MHz
2.57
2.05
2.22
2.05
2.07
1.88
1.00
1.00
1.11
1.05
1.04
1.00
0.95
1.19
8.5
8.0
7.5
7.0
6.5
6.0
5.5
5.0
4.5
4.0
3.5
3.0
2.5
2.0
1.5
1.0
0.5
0.0
f1 (ppm)

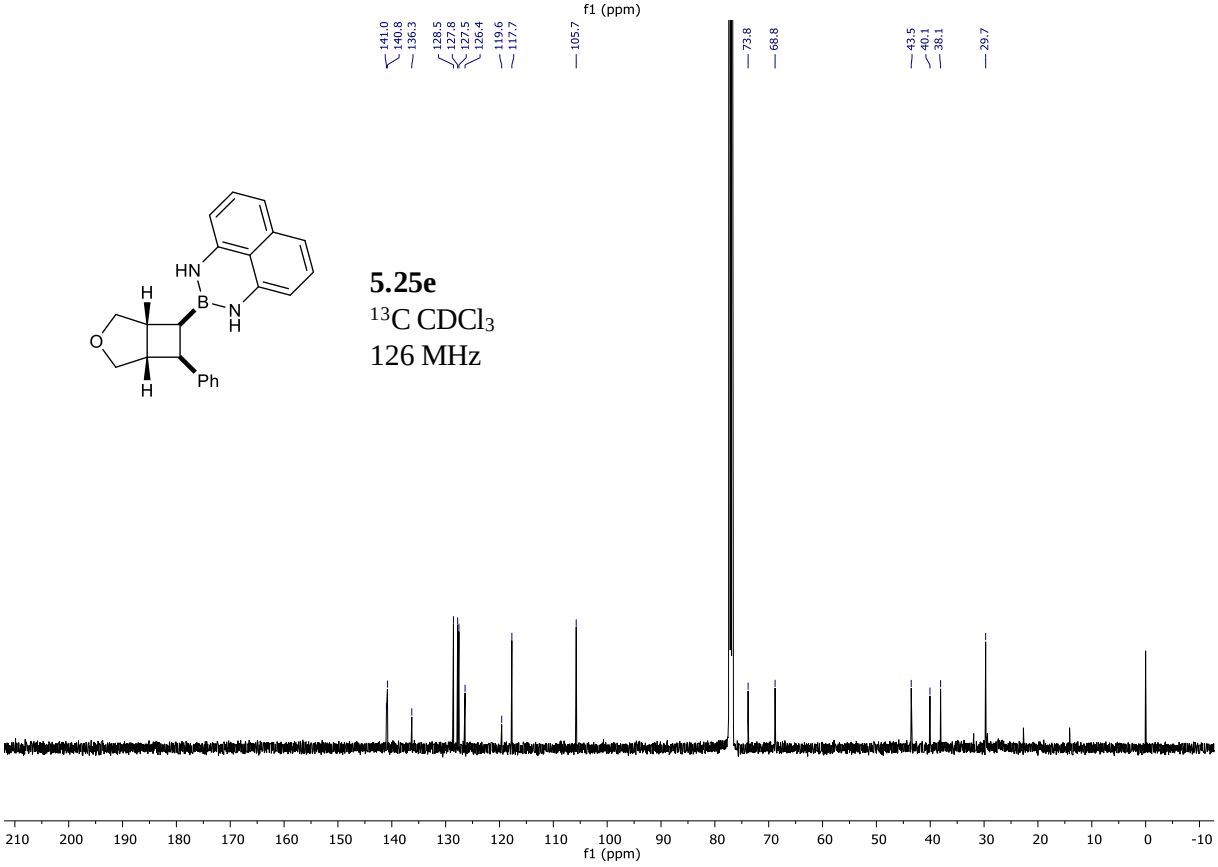
141.0
140.8
136.3
128.5
127.8
127.5
126.4
119.6
117.7
105.7
73.8
68.8
43.5
40.1
38.1
29.7
HN
B
N
H
O
H
H
Ph
5.25e
13C CDCl3
126 MHz
210
200
190
180
170
160
150
140
130
120
110
100
90
80
70
60
50
40
30
20
10
0
-10
f1 (ppm)

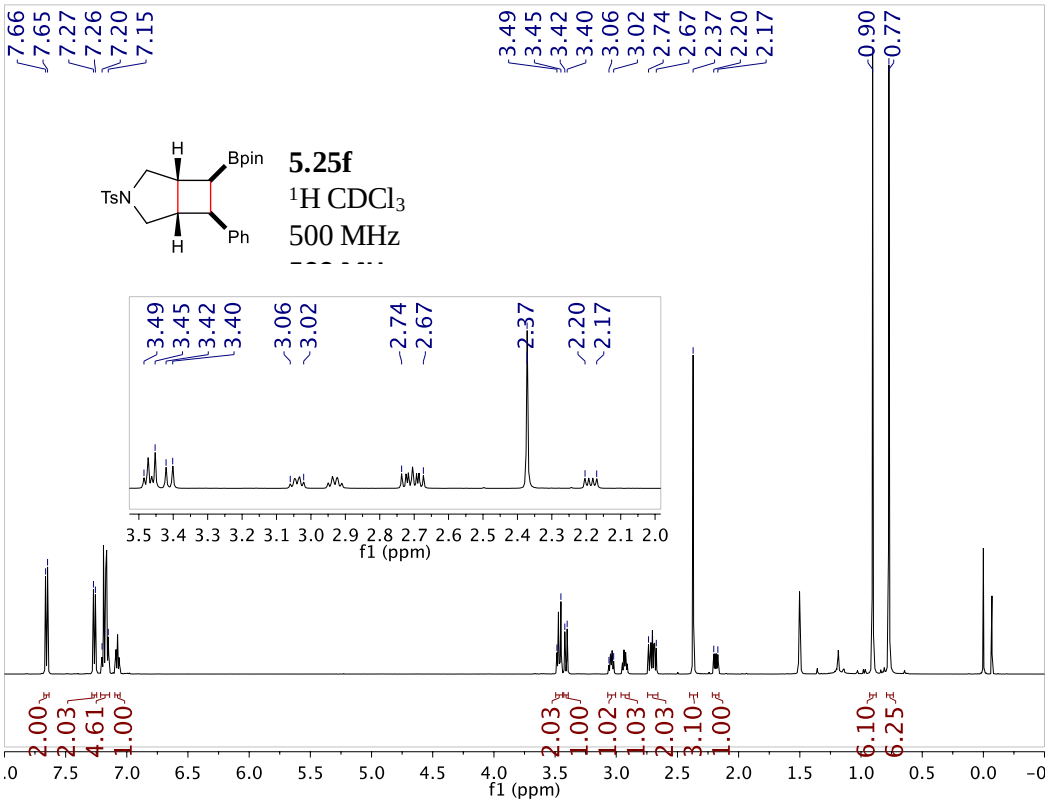
7.66
7.65
7.27
7.26
7.20
7.15
3.49
3.45
3.42
3.40
3.06
3.02
2.74
2.67
2.37
2.20
2.17
0.90
0.77
H
Bpin
TsN
Ph
H
5.25f
1H CDCl3
500 MHz
f1 (ppm)
2.00
2.03
4.61
1.00
2.03
1.00
1.02
1.03
2.03
3.10
1.00
6.10
6.25

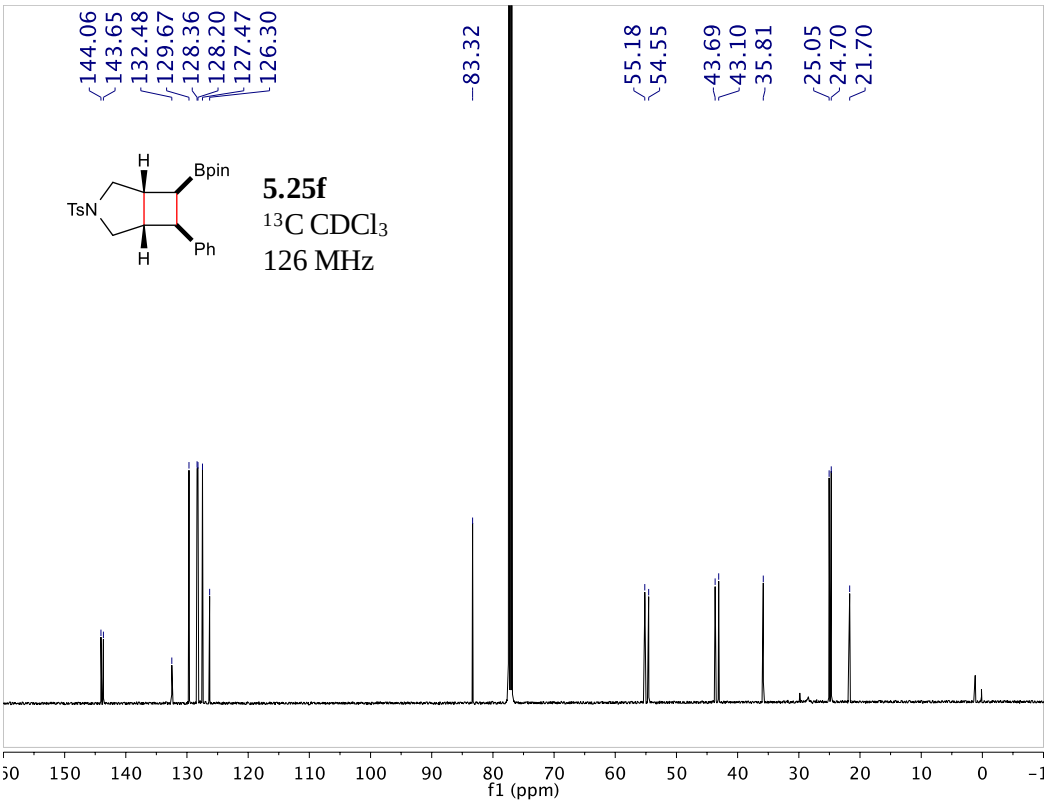
144.06
143.65
132.48
129.67
128.36
128.20
127.47
126.30
83.32
55.18
54.55
43.69
43.10
35.81
25.05
24.70
21.70
H
Bpin
TsN
Ph
H
5.25f
13C CDCl3
126 MHz
f1 (ppm)

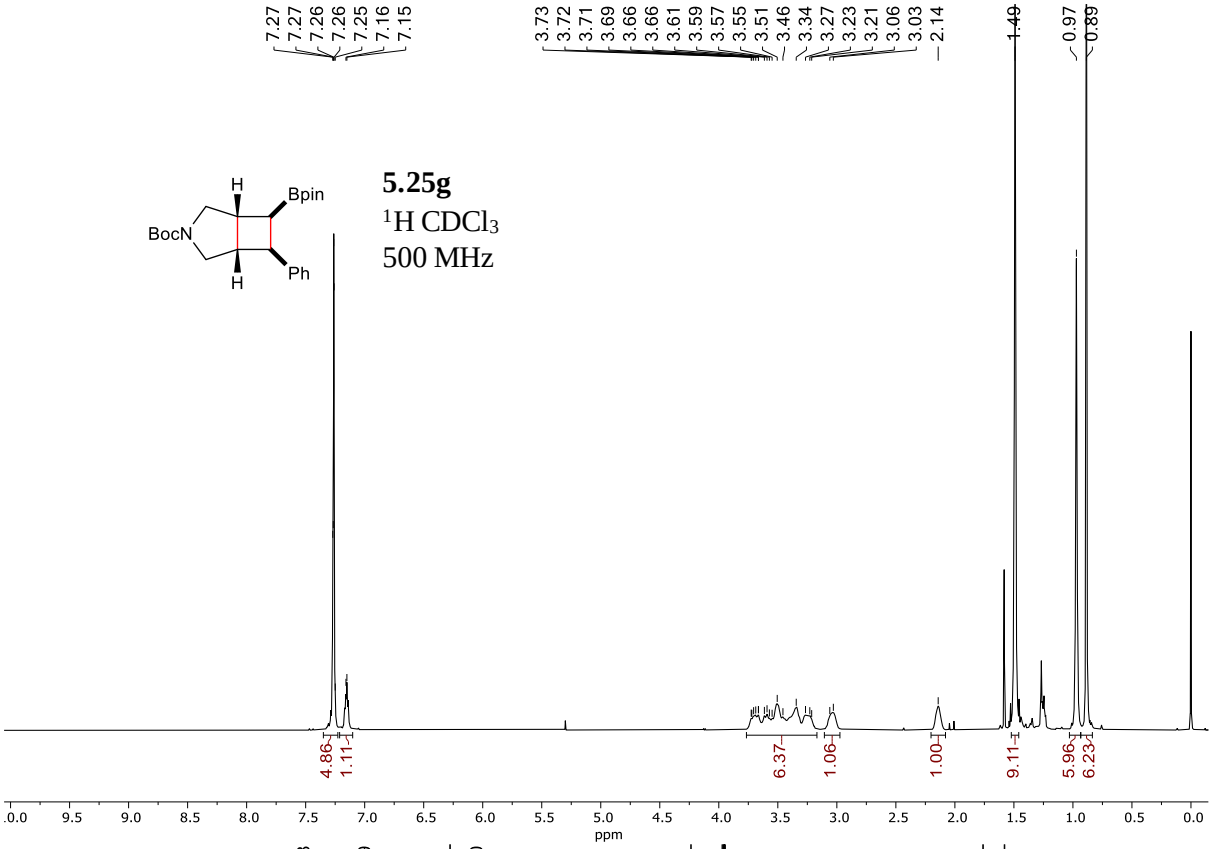
7.27
7.27
7.26
7.26
7.25
7.16
7.15
3.73
3.72
3.71
3.69
3.66
3.61
3.59
3.57
3.55
3.51
3.46
3.34
3.27
3.23
3.21
3.06
3.03
2.14
1.49
0.97
0.89
H
Bpin
BocN
Ph
H
5.25g
1H CDCl3
500 MHz
4.86
1.11
6.37
1.06
1.00
9.11
5.96
6.23
ppm

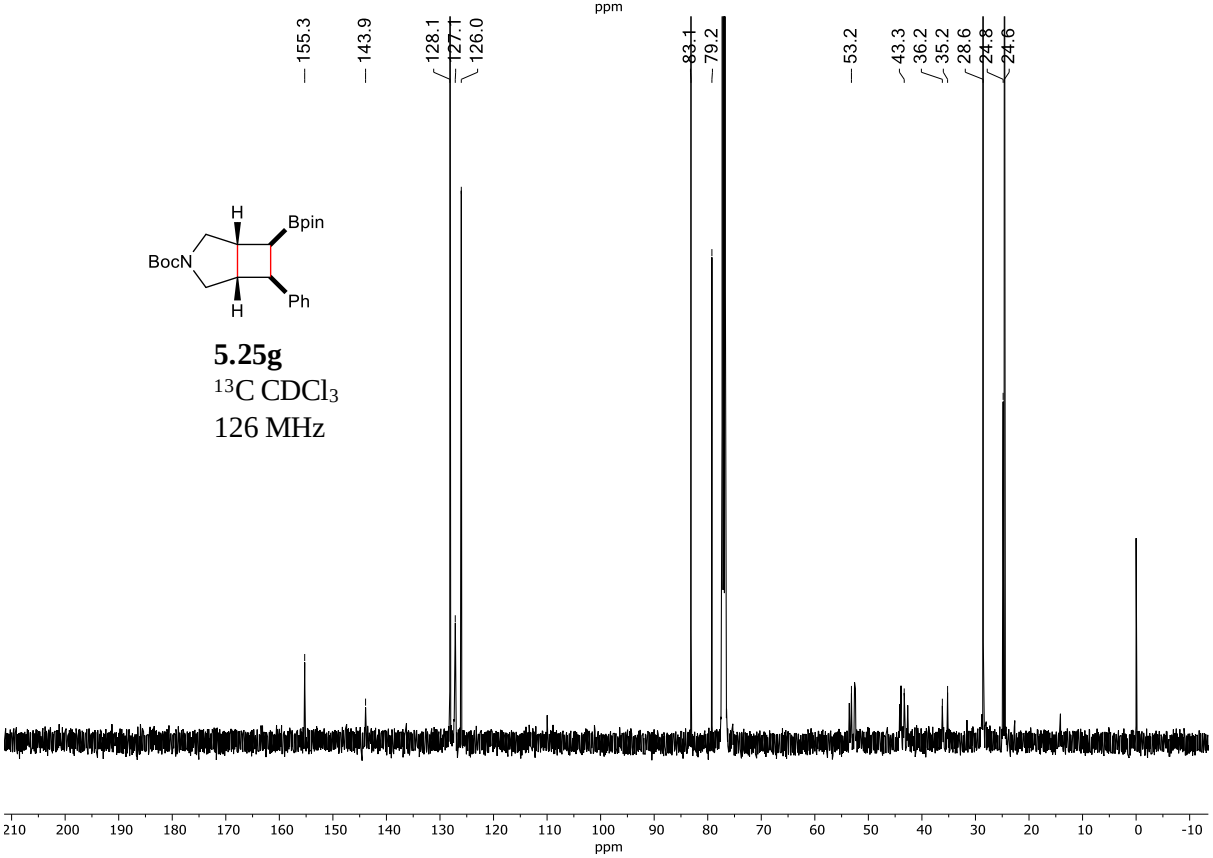
155.3
143.9
128.1
127.1
126.0
83.1
79.2
53.2
43.3
36.2
35.2
28.6
24.8
24.6
H
Bpin
BocN
Ph
H
5.25g
13C CDCl3
126 MHz
ppm

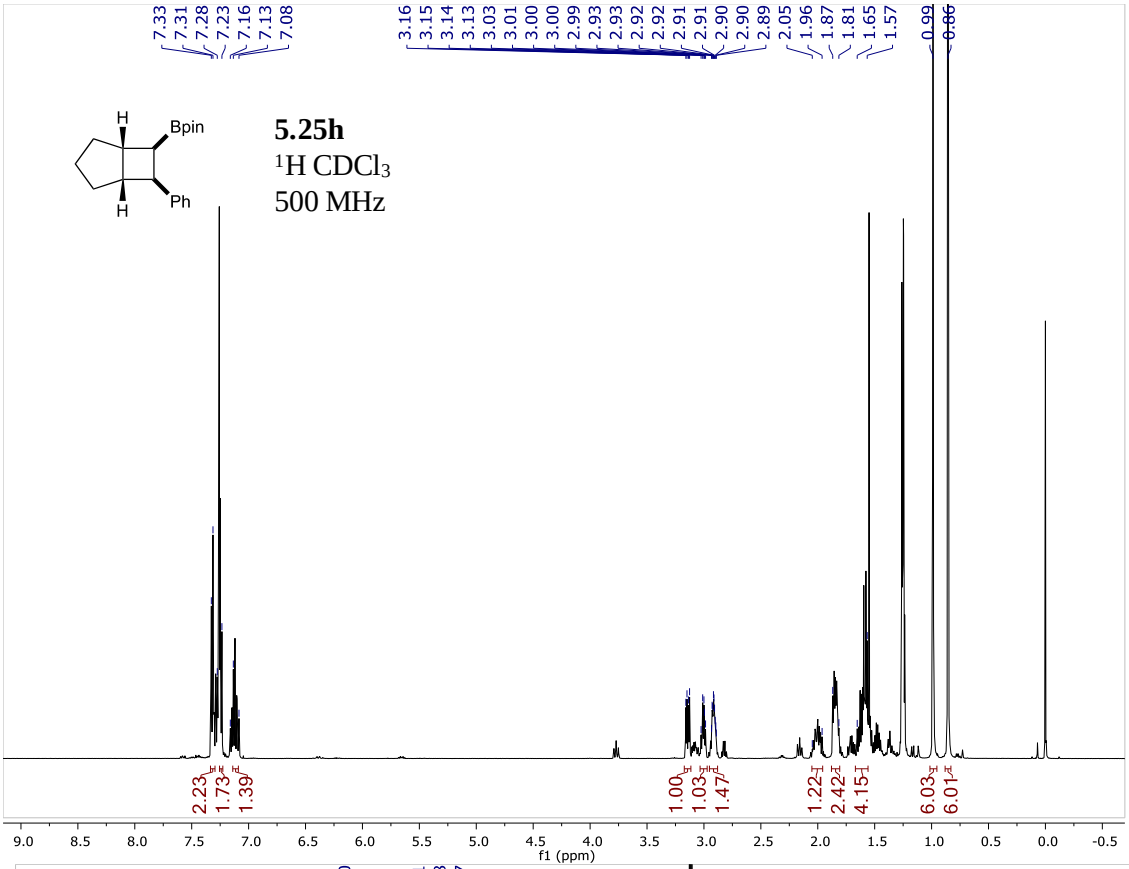
7.33
7.31
7.28
7.23
7.16
7.13
7.08
3.16
3.15
3.14
3.13
3.03
3.01
3.00
3.00
2.99
2.93
2.93
2.92
2.92
2.91
2.91
2.90
2.90
2.89
2.05
1.96
1.87
1.81
1.65
1.57
0.99
0.86
H
Bpin
H
Ph
5.25h
1H CDCl3
500 MHz
2.23
1.73
1.39
1.00
1.03
1.47
1.22
2.42
4.15
6.03
6.01
9.0
8.5
8.0
7.5
7.0
6.5
6.0
5.5
5.0
4.5
4.0
3.5
3.0
2.5
2.0
1.5
1.0
0.5
0.0
-0.5
f1 (ppm)

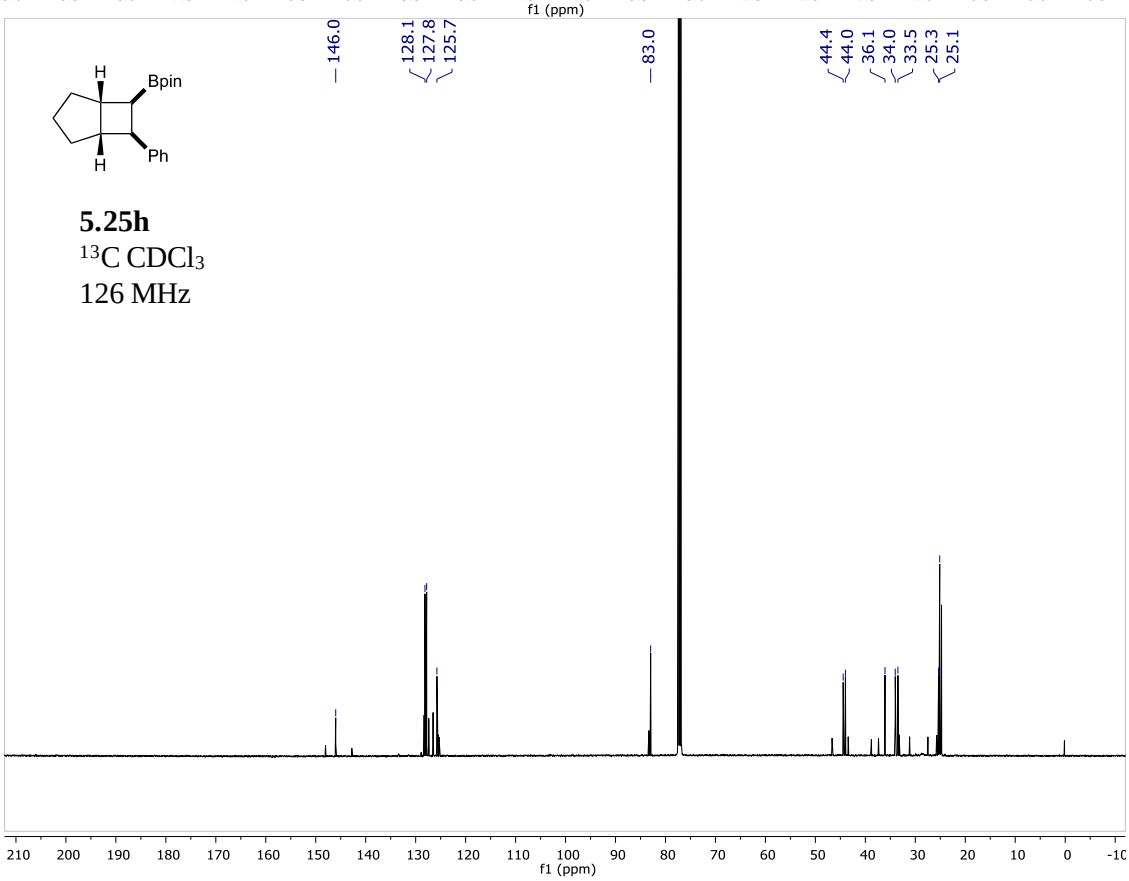
146.0
128.1
127.8
125.7
83.0
44.4
44.0
36.1
34.0
33.5
25.3
25.1
H
Bpin
H
Ph
5.25h
13C CDCl3
126 MHz
210
200
190
180
170
160
150
140
130
120
110
100
90
80
70
60
50
40
30
20
10
0
-10
f1 (ppm)

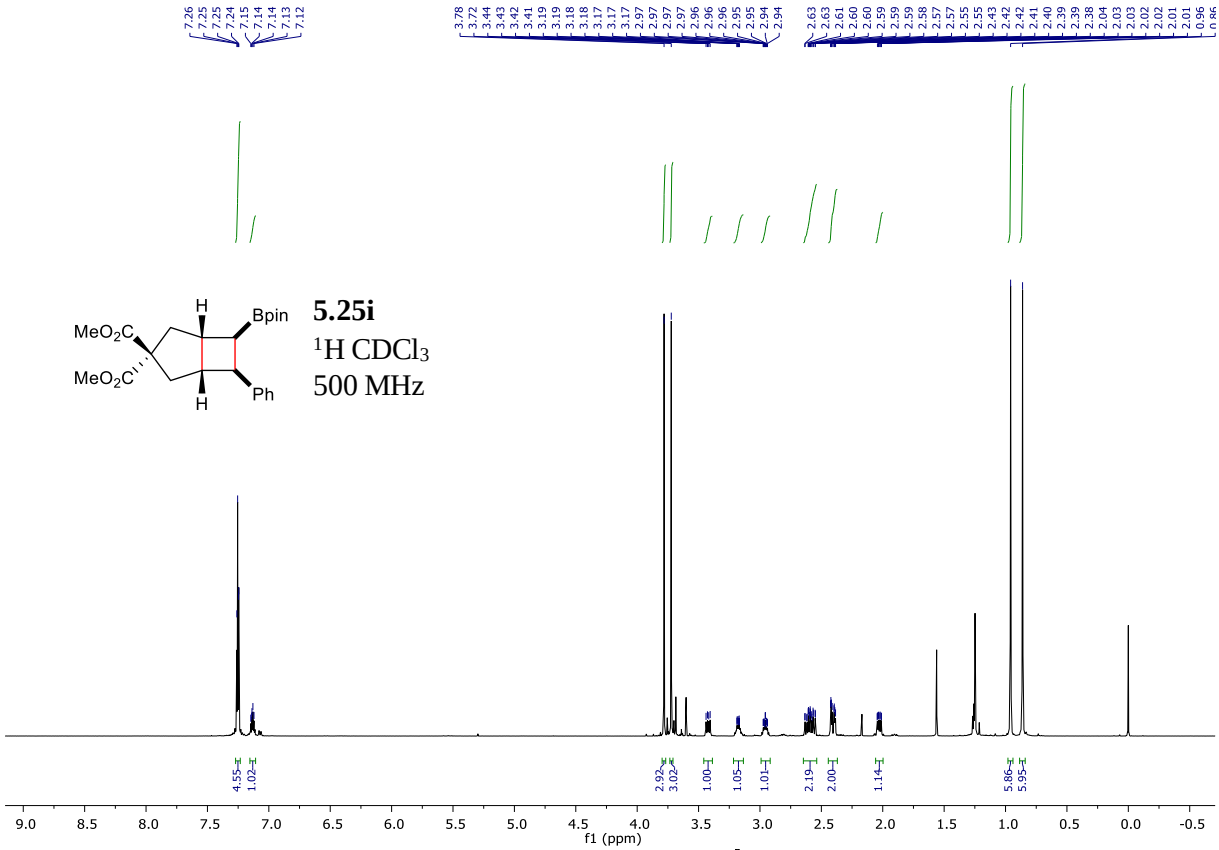
MeO2C
MeO2C
H
Bpin
Ph
H
5.25i
1H CDCl3
500 MHz
f1 (ppm)

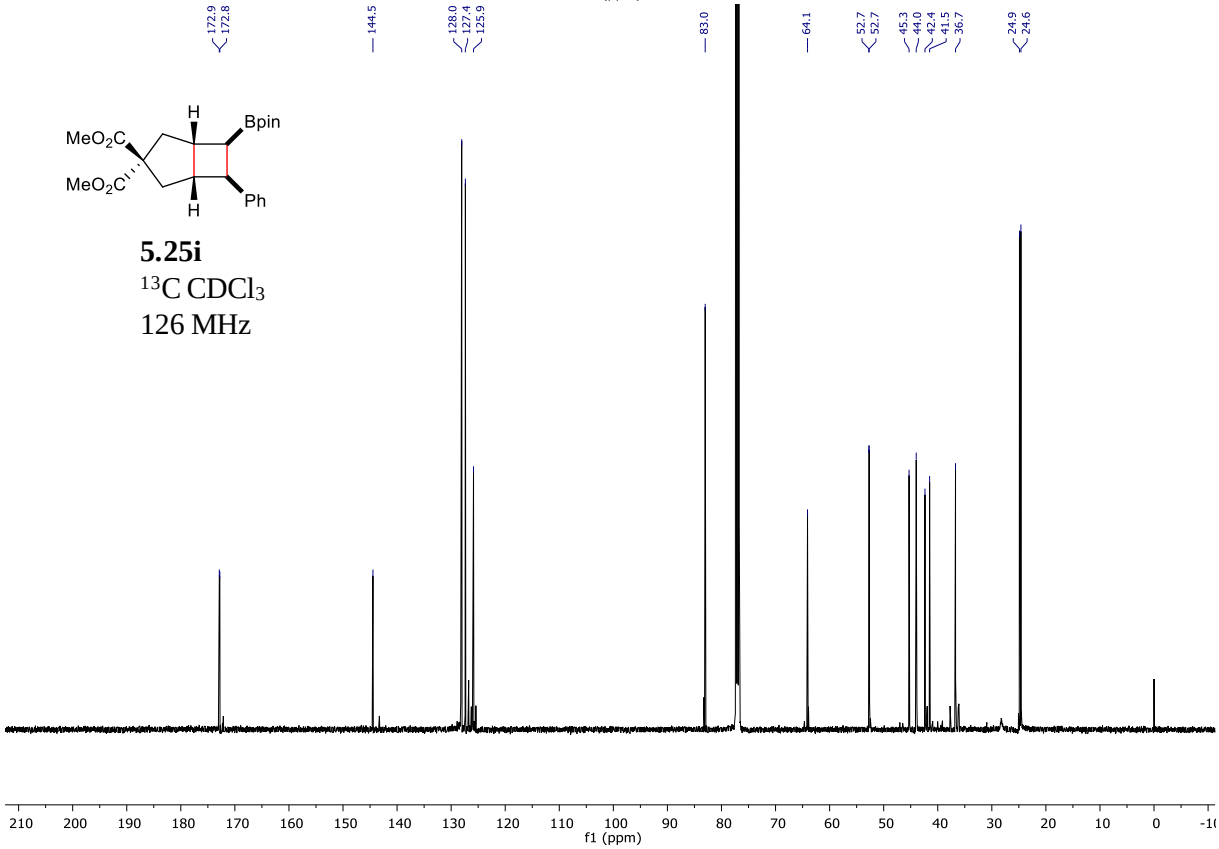
MeO2C
MeO2C
H
Bpin
Ph
H
5.25i
13C CDCl3
126 MHz
f1 (ppm)

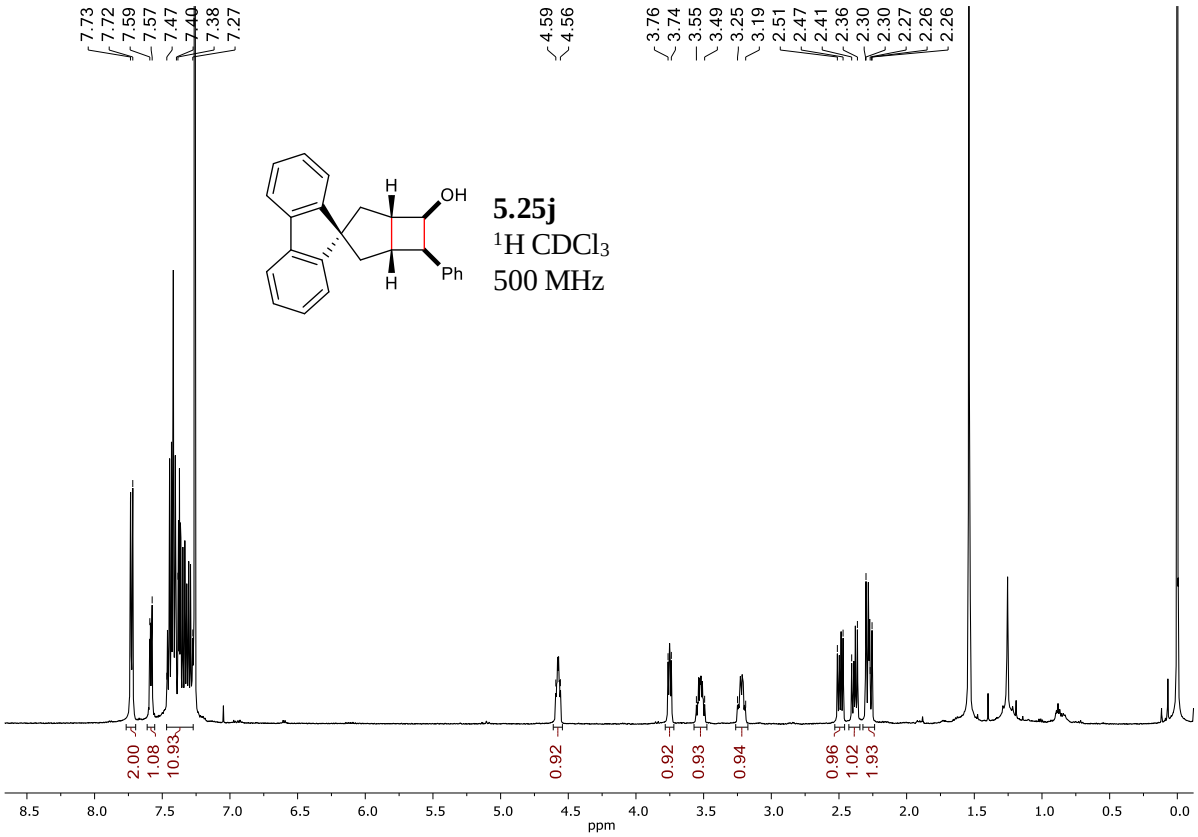
7.73
7.72
7.59
7.57
7.47
7.40
7.38
7.27
4.59
4.56
3.76
3.74
3.55
3.49
3.25
3.19
2.51
2.47
2.41
2.36
2.30
2.30
2.27
2.26
2.26
H
OH
H
Ph
5.25j
1H CDCl3
500 MHz
2.00
1.08
10.93
0.92
0.92
0.93
0.94
0.96
1.02
1.93
ppm

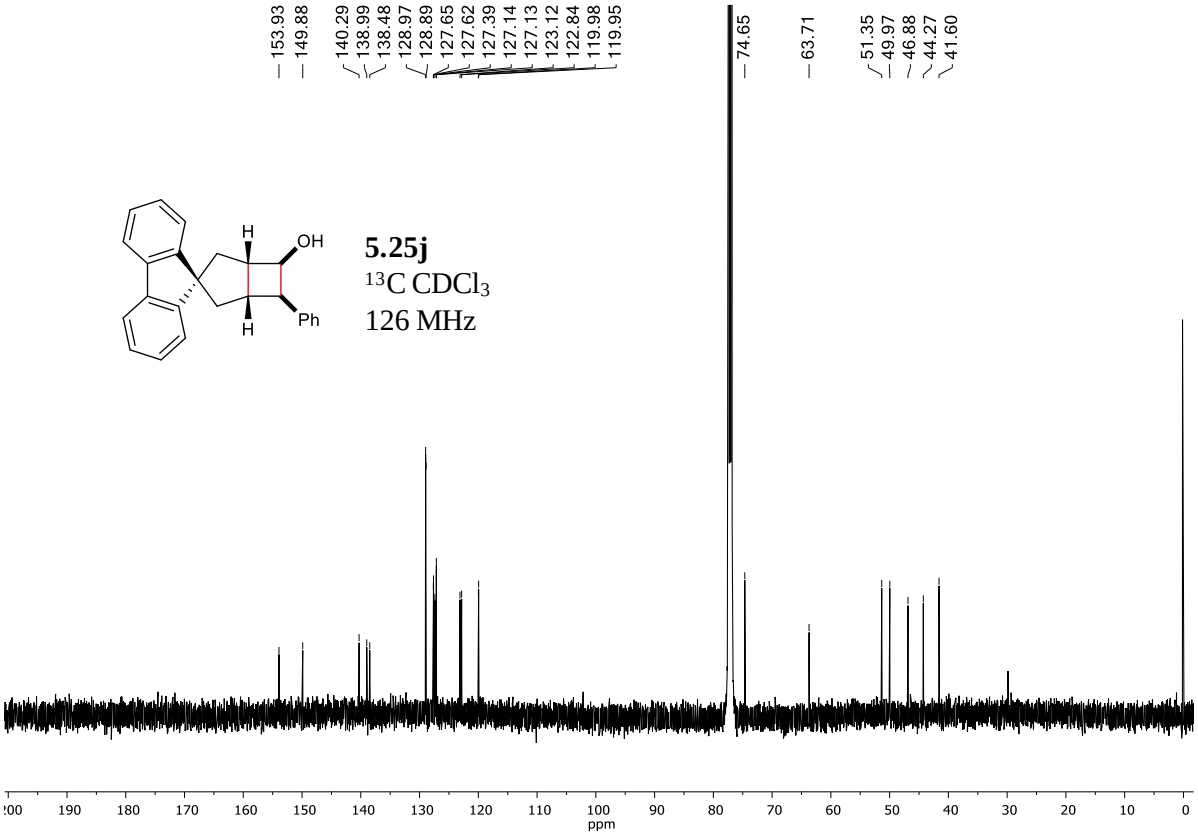
153.93
149.88
140.29
138.99
138.48
128.97
128.89
127.65
127.62
127.39
127.14
127.13
123.12
122.84
119.98
119.95
74.65
63.71
51.35
49.97
46.88
44.27
41.60
H
OH
H
Ph
5.25j
13C CDCl3
126 MHz
ppm

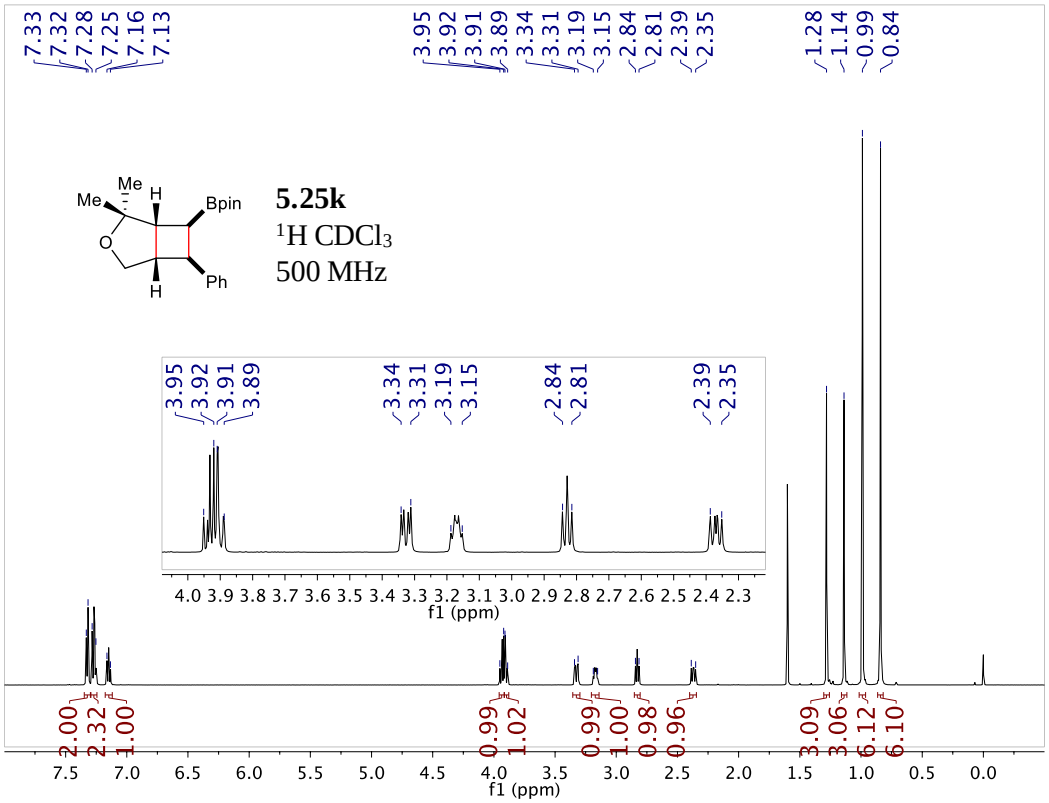
7.33
7.32
7.28
7.25
7.16
7.13
3.95
3.92
3.91
3.89
3.34
3.31
3.19
3.15
2.84
2.81
2.39
2.35
1.28
1.14
0.99
0.84
Me
H
Bpin
O
Ph
H
5.25k
1H CDCl3
500 MHz
f1 (ppm)
2.00
2.32
1.00
0.99
1.02
0.99
1.00
0.98
0.96
3.09
3.06
6.12
6.10

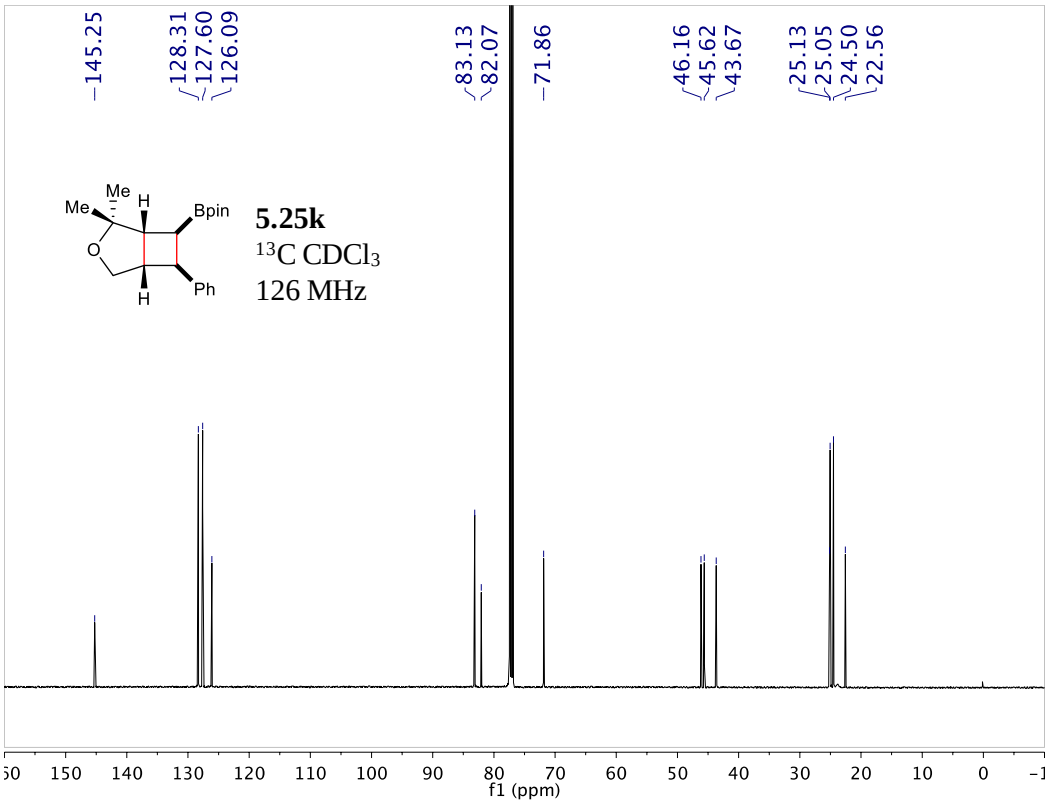
145.25
128.31
127.60
126.09
83.13
82.07
71.86
46.16
45.62
43.67
25.13
25.05
24.50
22.56
Me
H
Bpin
O
Ph
H
5.25k
13C CDCl3
126 MHz
f1 (ppm)

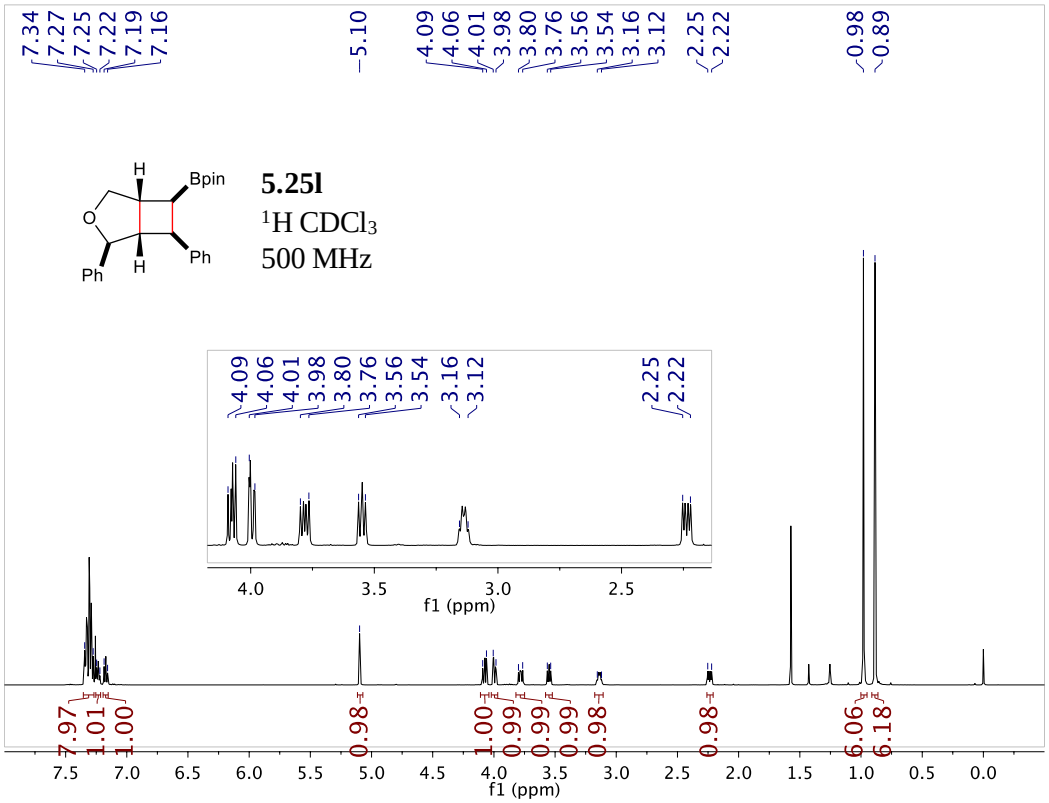
7.34
7.27
7.25
7.22
7.19
7.16
5.10
4.09
4.06
4.01
3.98
3.80
3.76
3.56
3.54
3.16
3.12
2.25
2.22
0.98
0.89
H
Bpin
O
Ph
H
Ph
5.25l
1H CDCl3
500 MHz
f1 (ppm)
7.97
1.01
1.00
0.98
1.00
0.99
0.99
0.99
0.98
0.98
6.06
6.18

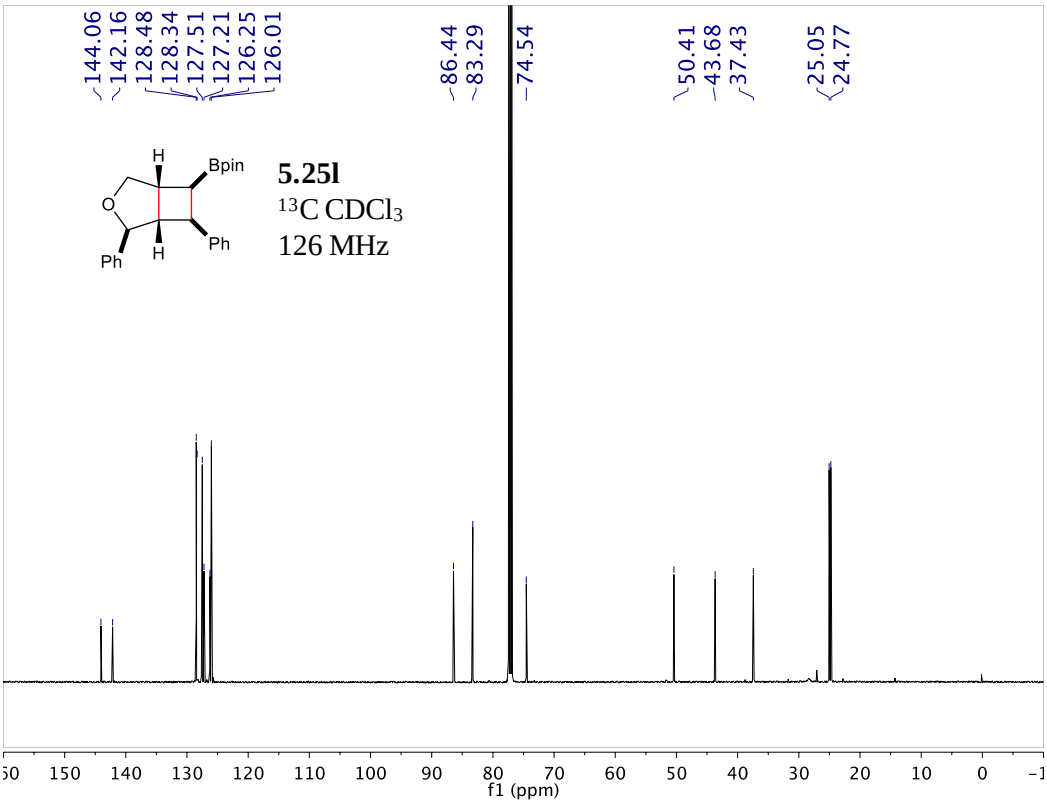
144.06
142.16
128.48
128.34
127.51
127.21
126.25
126.01
86.44
83.29
74.54
50.41
43.68
37.43
25.05
24.77
H
Bpin
O
Ph
H
Ph
5.25l
13C CDCl3
126 MHz
f1 (ppm)

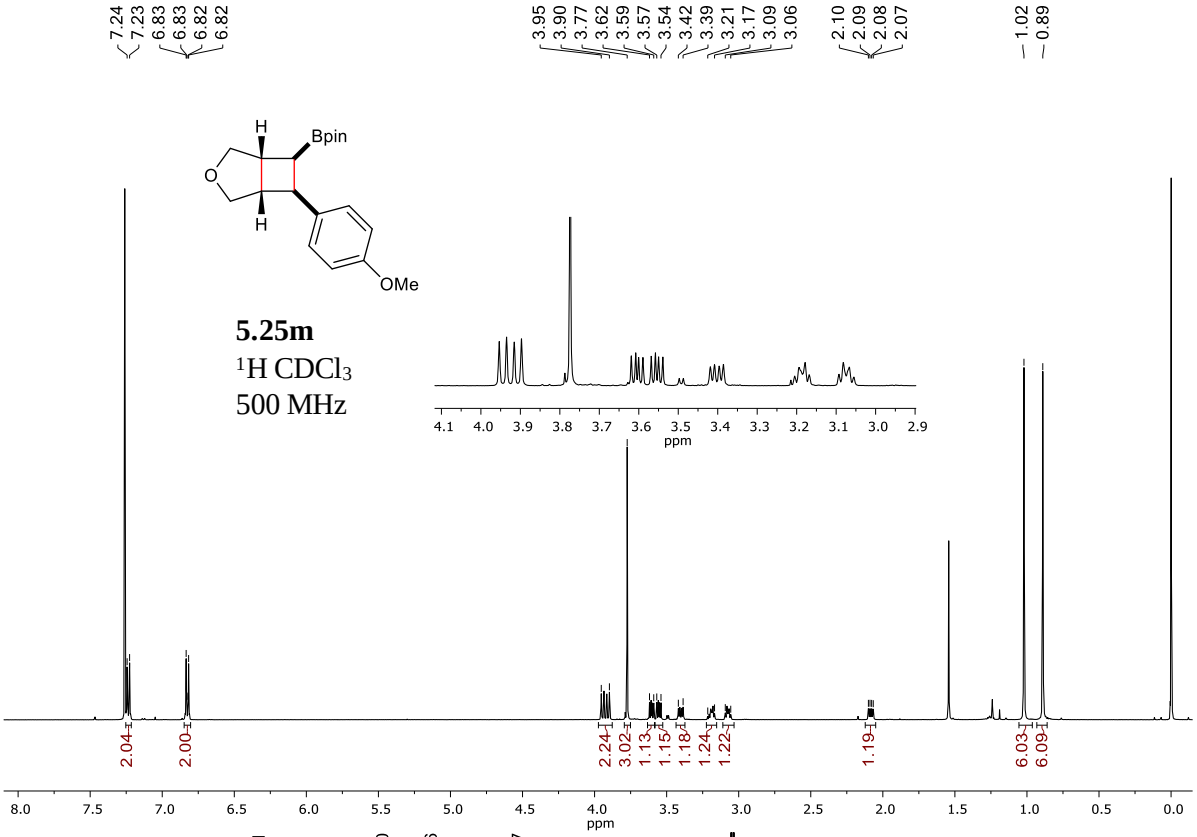
7.24
7.23
6.83
6.83
6.82
6.82
3.95
3.90
3.77
3.62
3.59
3.57
3.54
3.42
3.39
3.21
3.17
3.09
3.06
2.10
2.09
2.08
2.07
1.02
0.89
H
Bpin
O
H
OMe
5.25m
1H CDCl3
500 MHz
ppm
2.04
2.00
2.24
3.02
1.13
1.15
1.18
1.24
1.22
1.19
6.03
6.09

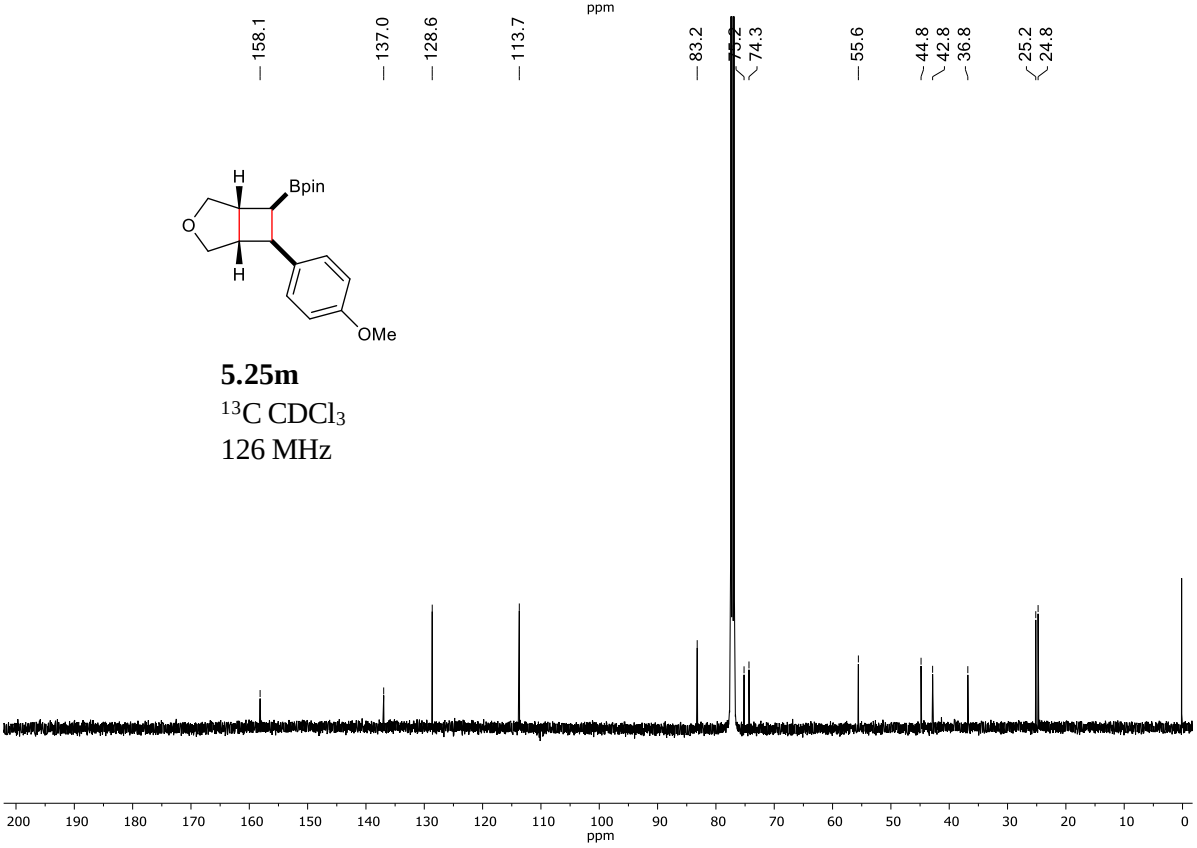
158.1
137.0
128.6
113.7
83.2
74.3
55.6
44.8
42.8
36.8
25.2
24.8
H
Bpin
O
H
OMe
5.25m
13C CDCl3
126 MHz
ppm

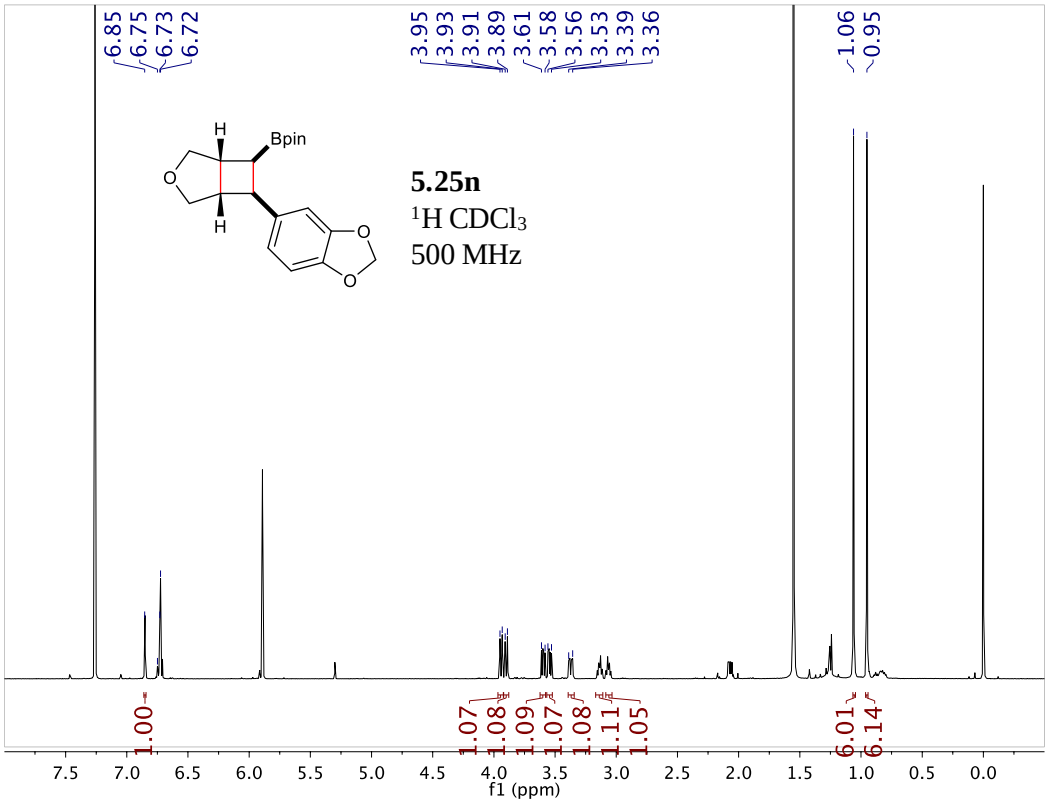
6.85
6.75
6.73
6.72
3.95
3.93
3.91
3.89
3.61
3.58
3.56
3.53
3.39
3.36
1.06
0.95
H
Bpin
O
H
O
O
5.25n
1H CDCl3
500 MHz
1.00
1.07
1.08
1.09
1.07
1.08
1.11
1.05
6.01
6.14
7.5
7.0
6.5
6.0
5.5
5.0
4.5
4.0
3.5
3.0
2.5
2.0
1.5
1.0
0.5
0.0
f1 (ppm)

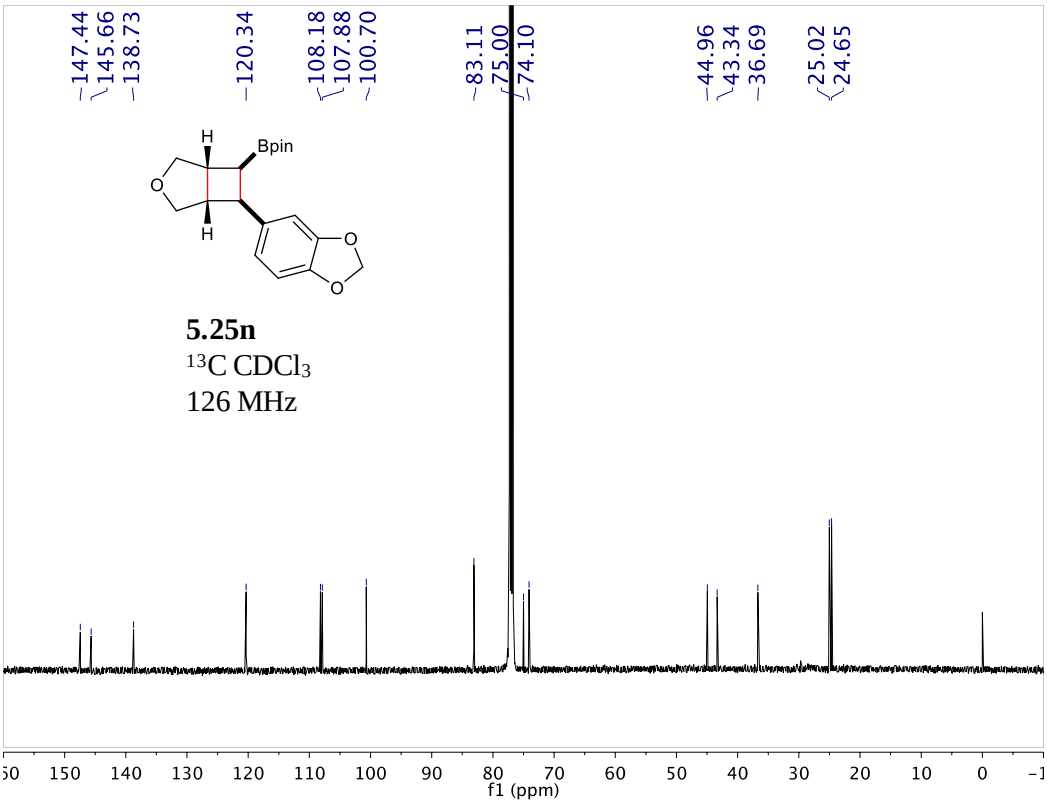
147.44
145.66
138.73
120.34
108.18
107.88
100.70
83.11
75.00
74.10
44.96
43.34
36.69
25.02
24.65
H
Bpin
O
H
O
O
5.25n
13C CDCl3
126 MHz
150
140
130
120
110
100
90
80
70
60
50
40
30
20
10
0
f1 (ppm)

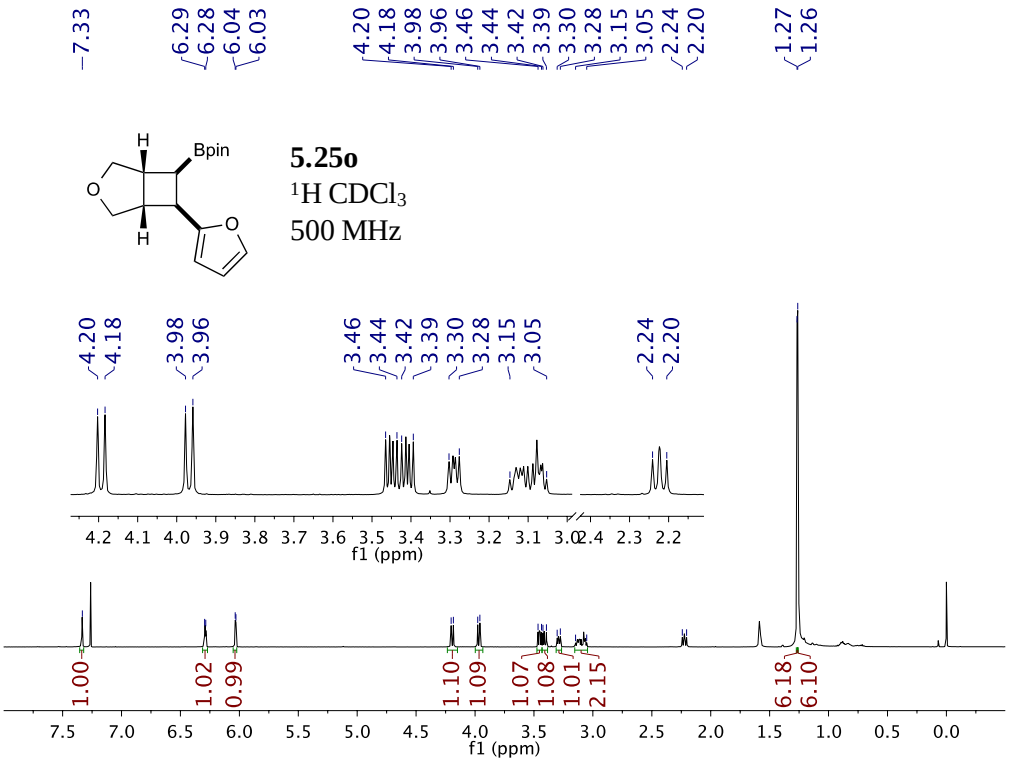
7.33
6.29
6.28
6.04
6.03
4.20
4.18
3.98
3.96
3.46
3.44
3.42
3.39
3.30
3.28
3.15
3.05
2.24
2.20
1.27
1.26
Bpin
O
H
H
O
5.25o
1H CDCl3
500 MHz
f1 (ppm)
1.00
1.02
0.99
1.10
1.09
1.07
1.08
1.01
2.15
6.18
6.10

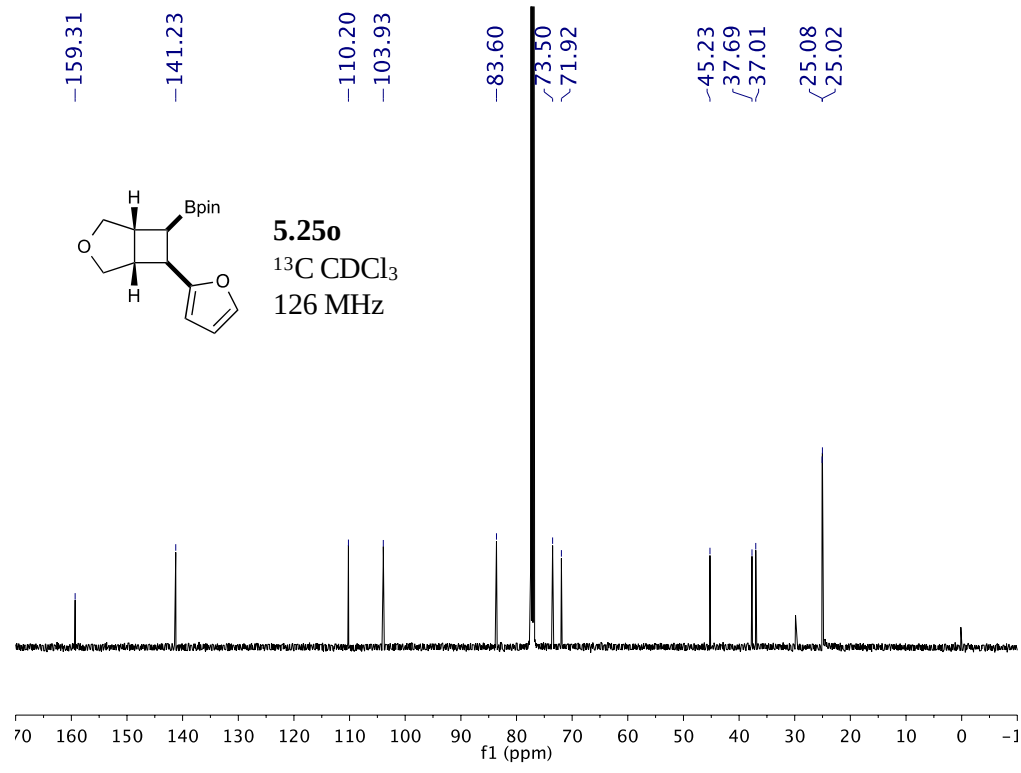
159.31
141.23
110.20
103.93
83.60
73.50
71.92
45.23
37.69
37.01
25.08
25.02
Bpin
O
H
H
O
5.25o
13C CDCl3
126 MHz
f1 (ppm)

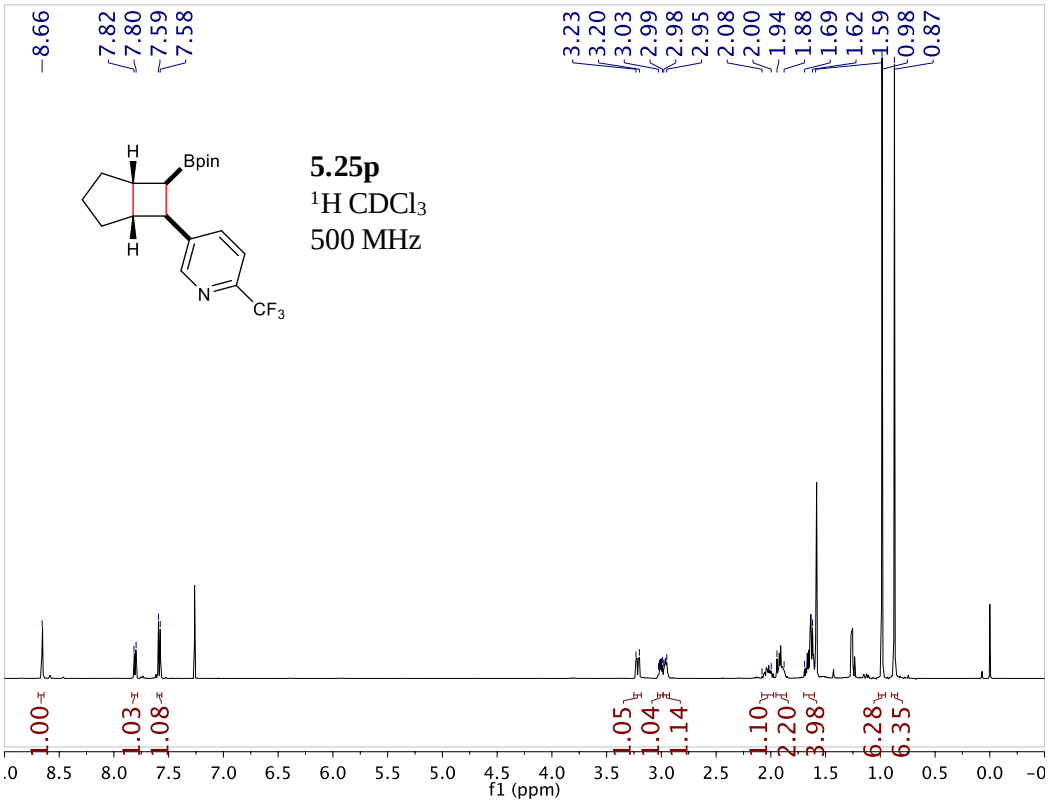
8.66
7.82
7.80
7.59
7.58
3.23
3.20
3.03
2.99
2.98
2.95
2.08
2.00
1.94
1.88
1.69
1.62
1.59
0.98
0.87
H
Bpin
H
N
CF3
5.25p
1H CDCl3
500 MHz
1.00
1.03
1.08
1.05
1.04
1.14
1.10
2.20
3.98
6.28
6.35
f1 (ppm)

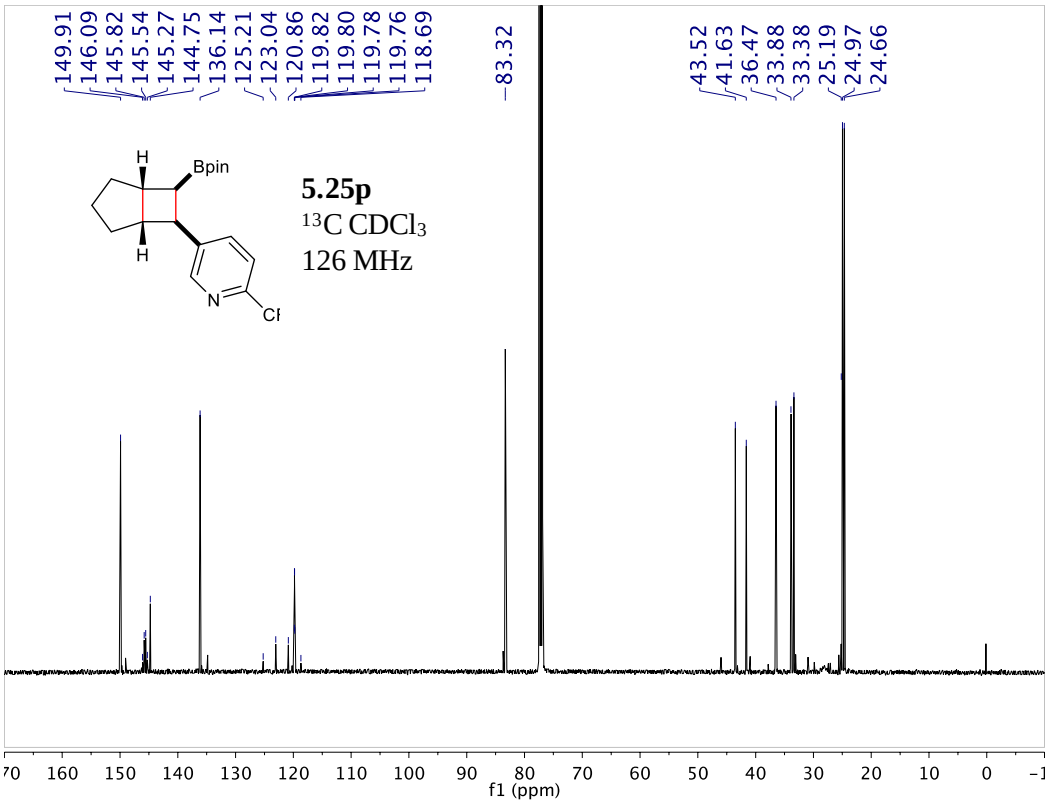
149.91
146.09
145.82
145.54
145.27
144.75
136.14
125.21
123.04
120.86
119.82
119.80
119.78
119.76
118.69
83.32
43.52
41.63
36.47
33.88
33.38
25.19
24.97
24.66
H
Bpin
H
N
Cl
5.25p
13C CDCl3
126 MHz
f1 (ppm)

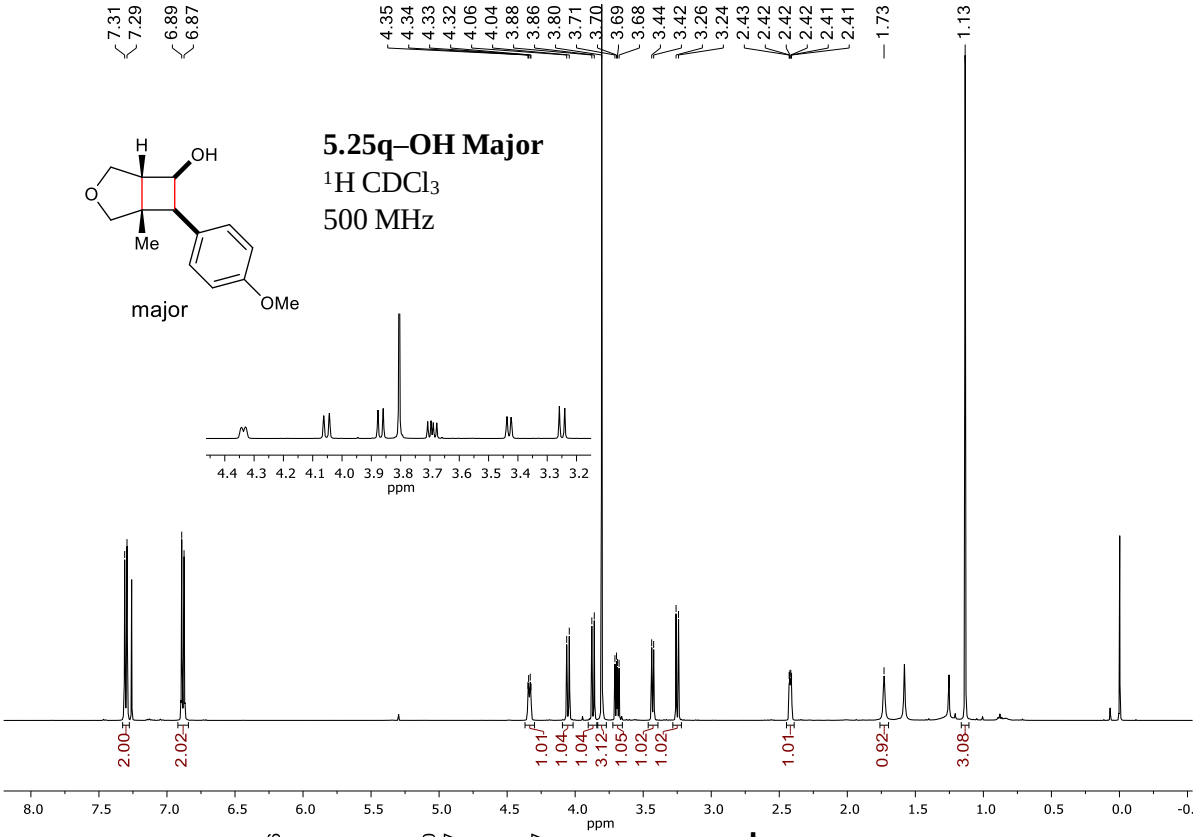
7.31
7.29
6.89
6.87
4.35
4.34
4.33
4.32
4.06
4.04
3.88
3.86
3.80
3.71
3.70
3.69
3.68
3.44
3.42
3.26
3.24
2.43
2.42
2.42
2.42
2.41
2.41
1.73
1.13
H
OH
O
Me
major
OMe
5.25q–OH Major
1H CDCl3
500 MHz
4.4 4.3 4.2 4.1 4.0 3.9 3.8 3.7 3.6 3.5 3.4 3.3 3.2
ppm
2.00
2.02
1.01
1.04
1.04
3.12
1.05
1.02
1.02
1.01
0.92
3.08
8.0 7.5 7.0 6.5 6.0 5.5 5.0 4.5 4.0 3.5 3.0 2.5 2.0 1.5 1.0 0.5 0.0
ppm

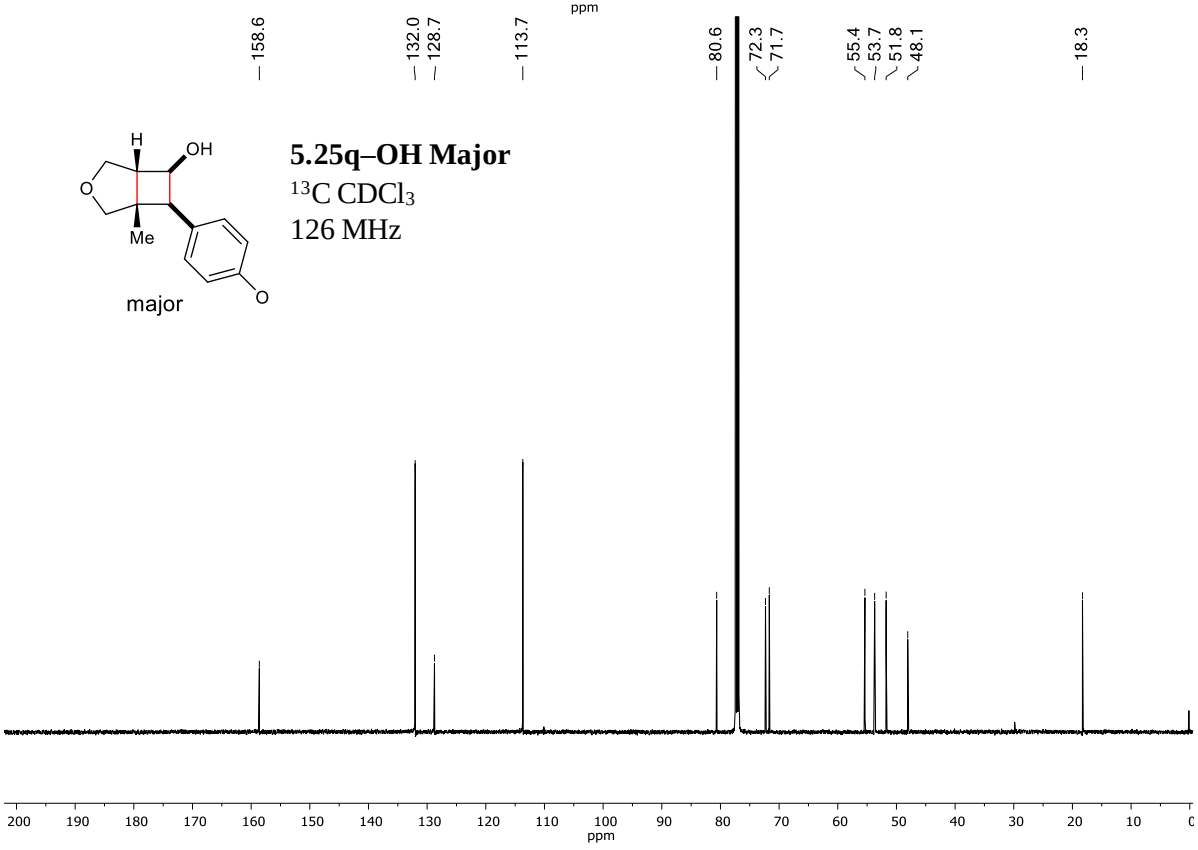
158.6
132.0
128.7
113.7
80.6
72.3
71.7
55.4
53.7
51.8
48.1
18.3
H
OH
O
Me
major
O
5.25q–OH Major
13C CDCl3
126 MHz
200 190 180 170 160 150 140 130 120 110 100 90 80 70 60 50 40 30 20 10
ppm

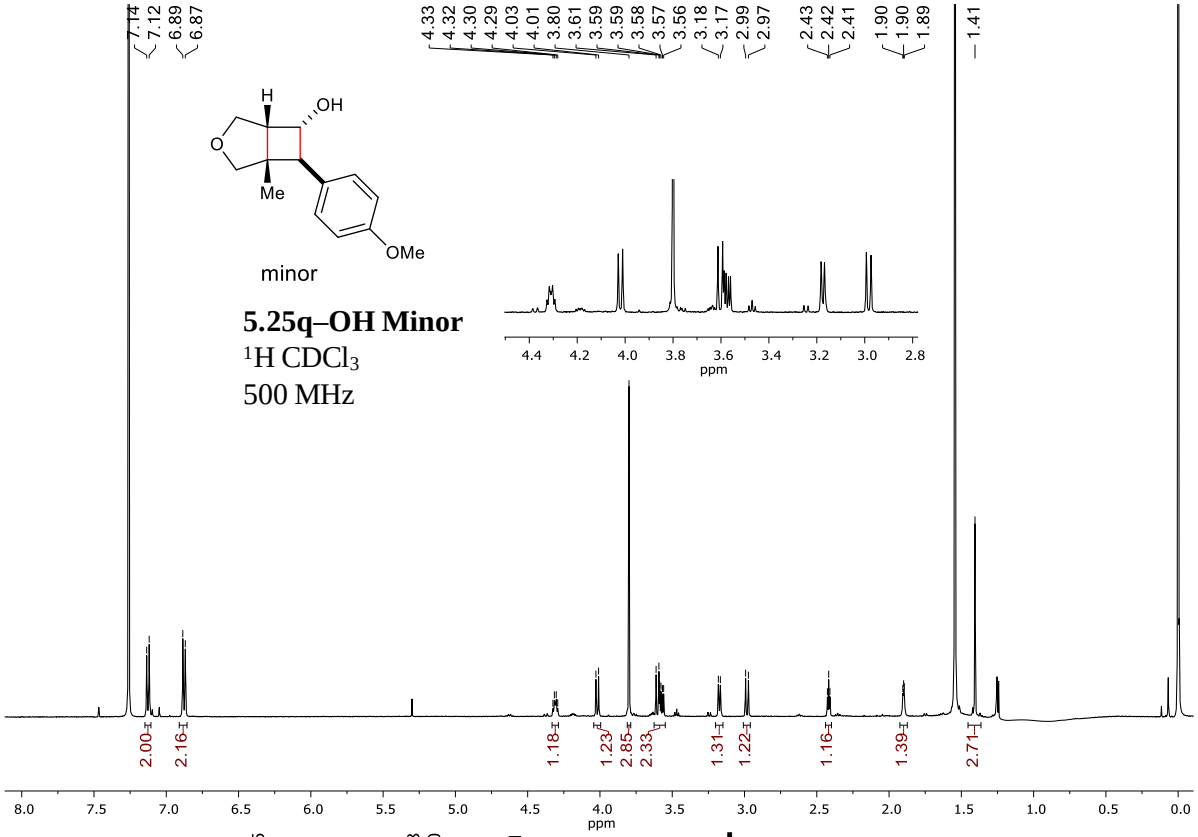
7.14
7.12
6.89
6.87
4.33
4.32
4.30
4.29
4.03
4.01
3.80
3.61
3.59
3.59
3.58
3.57
3.56
3.18
3.17
2.99
2.97
2.43
2.42
2.41
1.90
1.90
1.89
1.41
H
OH
O
Me
OMe
minor
5.25q–OH Minor
1H CDCl3
500 MHz
ppm
2.00
2.16
1.18
1.23
2.85
2.33
1.31
1.22
1.16
1.39
2.71

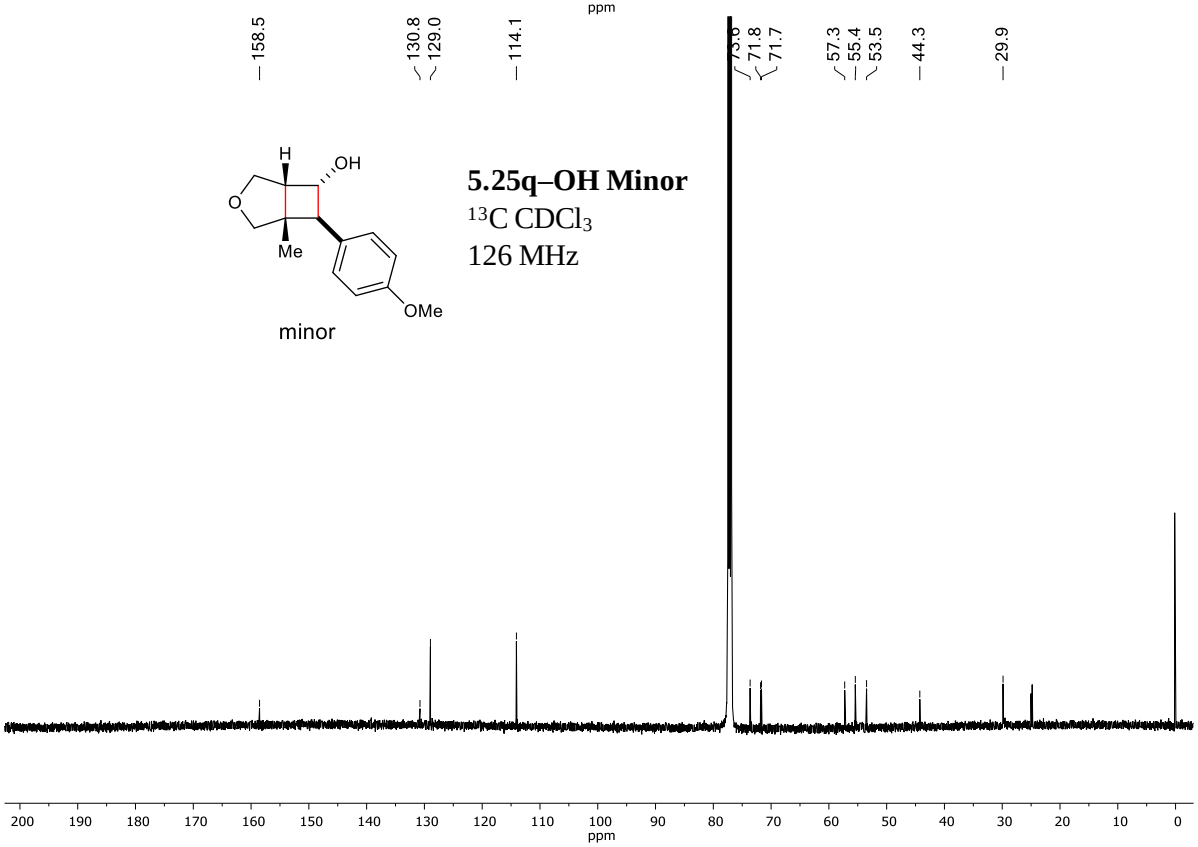
158.5
130.8
129.0
114.1
79.6
71.8
71.7
57.3
55.4
53.5
44.3
29.9
H
OH
O
Me
OMe
minor
5.25q–OH Minor
13C CDCl3
126 MHz
ppm

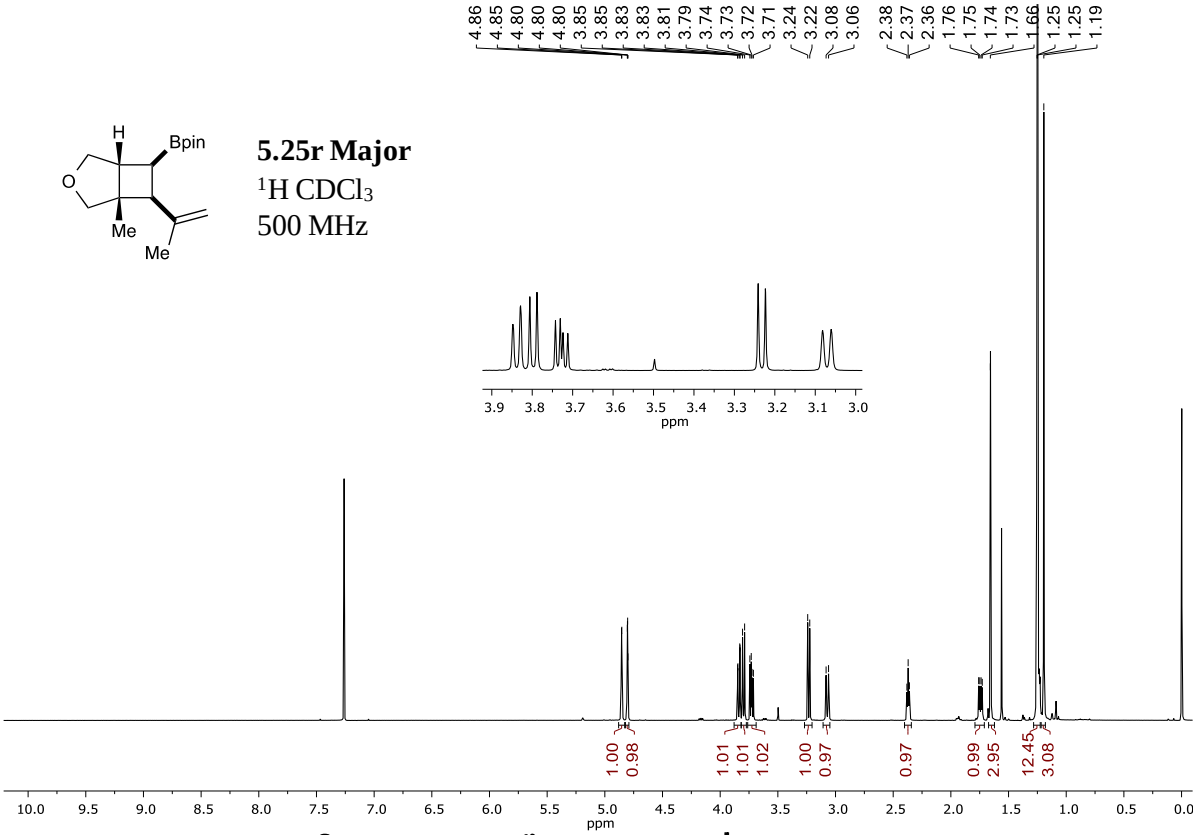
4.86
4.85
4.80
4.80
4.80
3.85
3.85
3.83
3.83
3.81
3.79
3.74
3.73
3.72
3.71
3.24
3.22
3.08
3.06
2.38
2.37
2.36
1.76
1.75
1.74
1.73
1.66
1.25
1.25
1.19
H
Bpin
O
Me
Me
5.25r Major
1H CDCl3
500 MHz
3.9 3.8 3.7 3.6 3.5 3.4 3.3 3.2 3.1 3.0
ppm
1.00
0.98
1.01
1.01
1.02
1.00
0.97
0.97
0.99
2.95
12.45
3.08
10.0 9.5 9.0 8.5 8.0 7.5 7.0 6.5 6.0 5.5 5.0 4.5 4.0 3.5 3.0 2.5 2.0 1.5 1.0 0.5 0.0
ppm

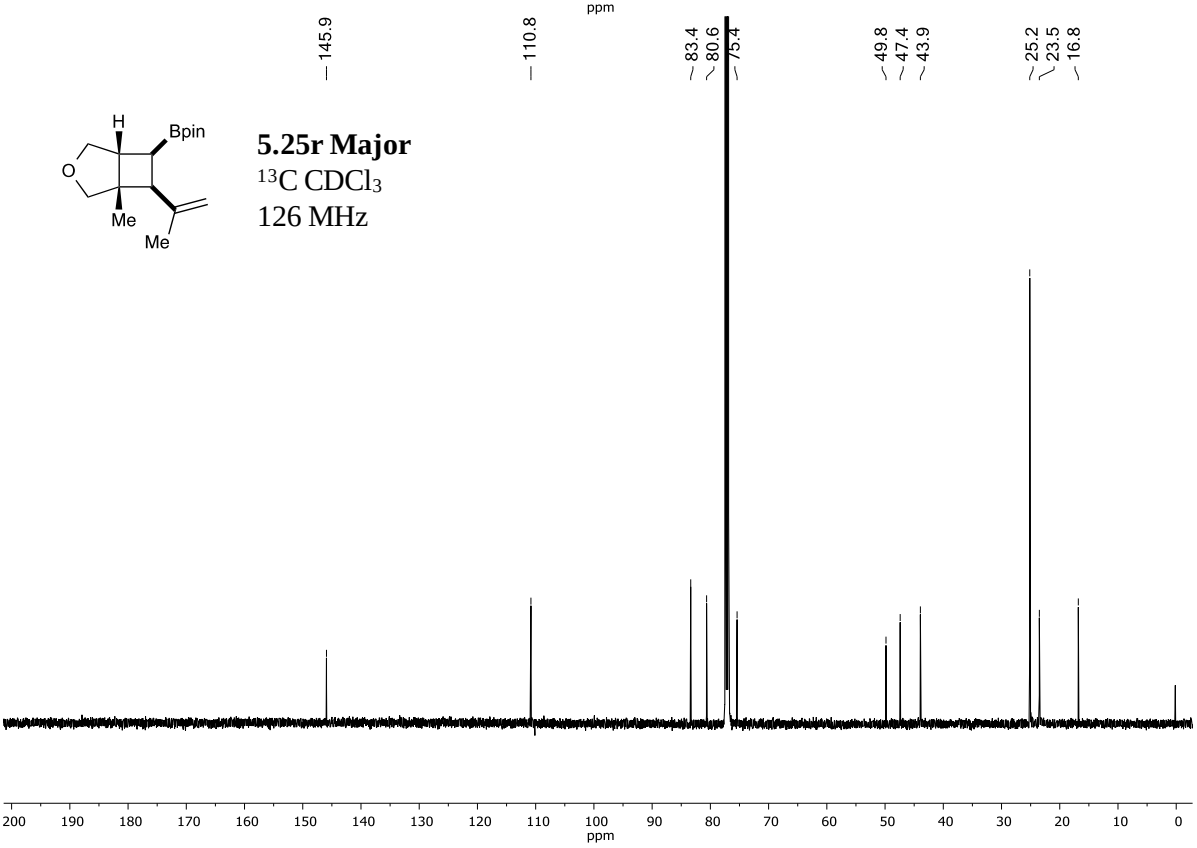
145.9
110.8
83.4
80.6
75.4
49.8
47.4
43.9
25.2
23.5
16.8
H
Bpin
O
Me
Me
5.25r Major
13C CDCl3
126 MHz
200 190 180 170 160 150 140 130 120 110 100 90 80 70 60 50 40 30 20 10 0
ppm

5.25r Minor
^{1}H $CDCl_3$
500 MHz

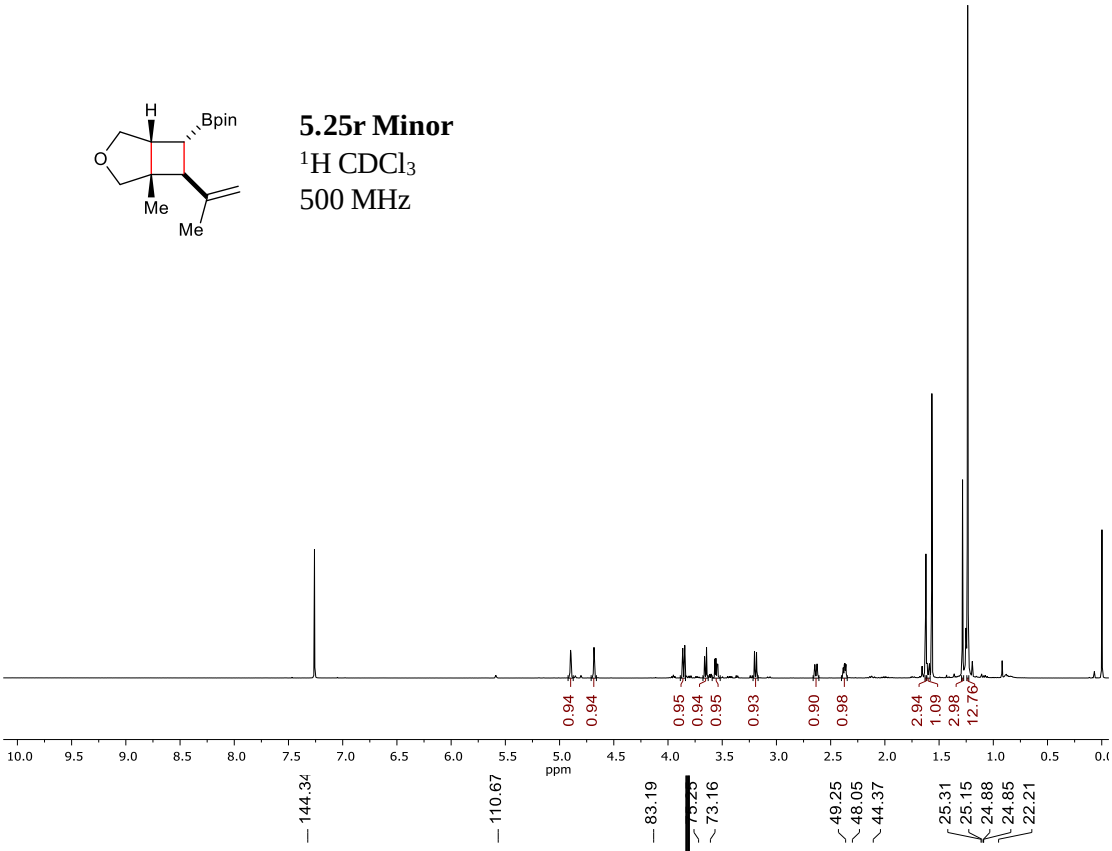

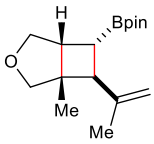

5.25r Minor
^{13}C $CDCl_3$
126 MHz

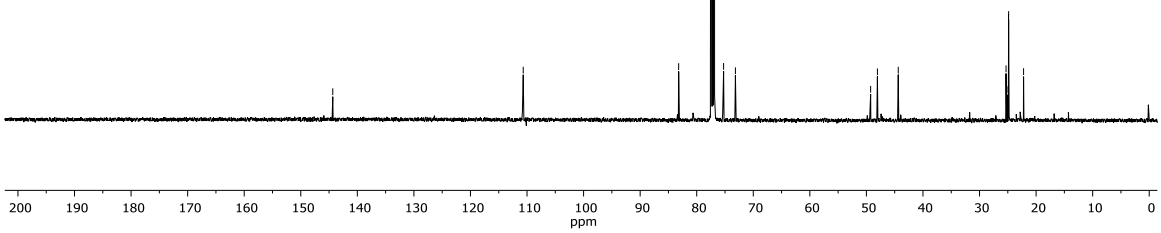

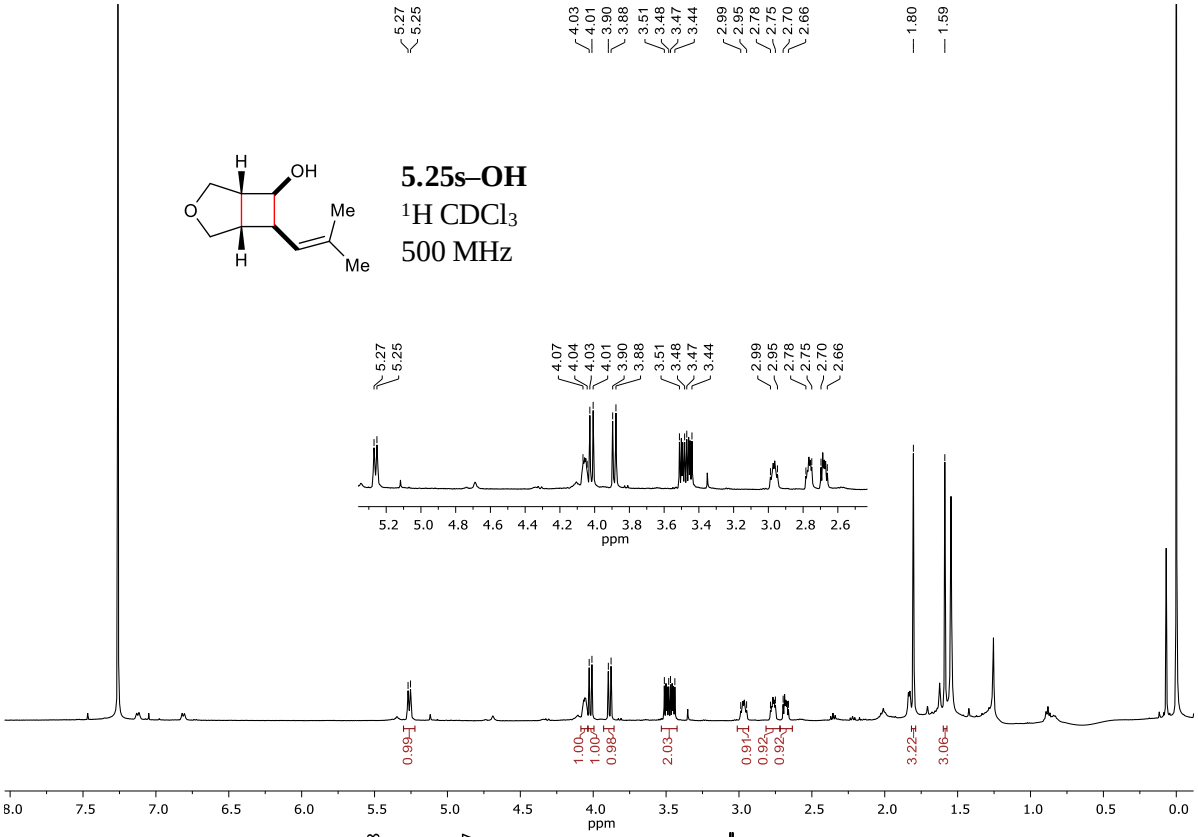
5.27
5.25
4.03
4.01
3.90
3.88
3.51
3.48
3.47
3.44
2.99
2.95
2.78
2.75
2.70
2.66
1.80
1.59
OH
H
O
H
Me
Me
5.25s–OH
1H CDCl3
500 MHz
ppm
0.99
1.00
1.00
0.98
2.03
0.91
0.92
0.92
3.22
3.06

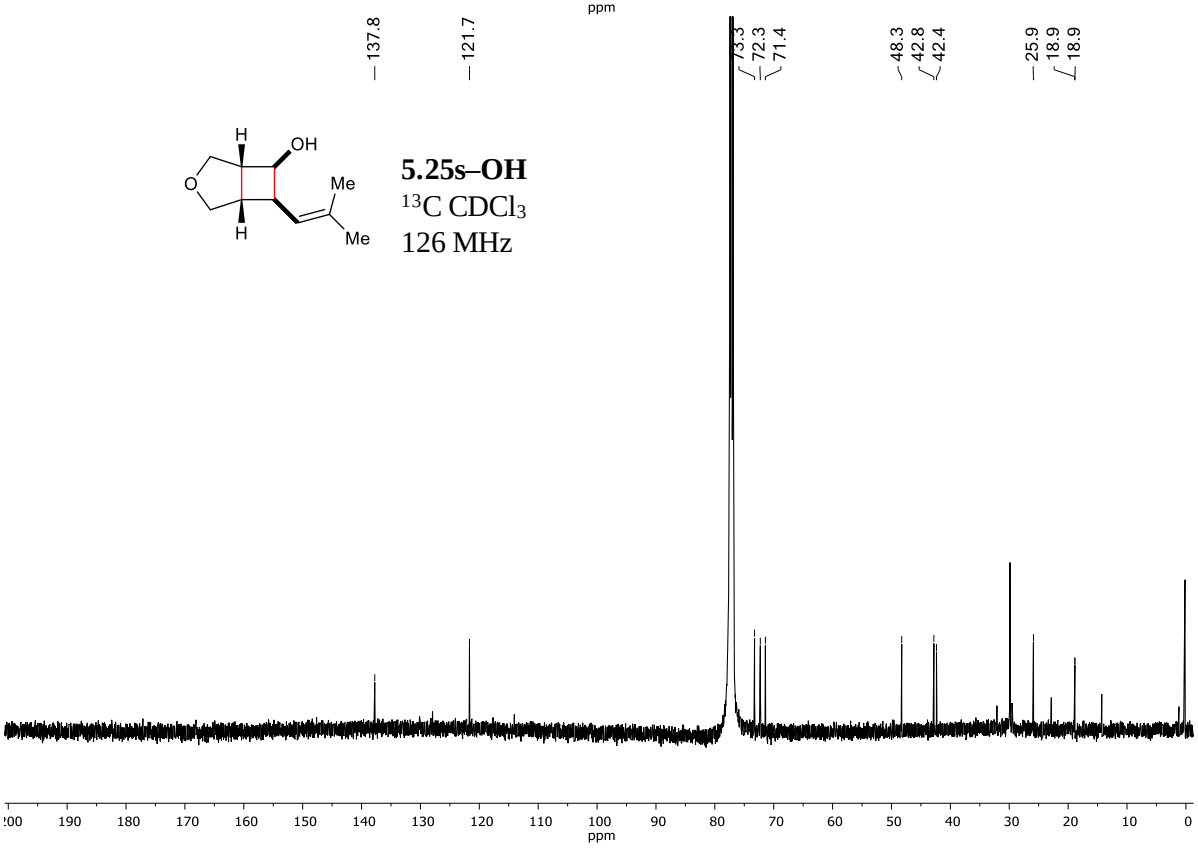
137.8
121.7
73.3
72.3
71.4
48.3
42.8
42.4
25.9
18.9
18.9
OH
H
O
H
Me
Me
5.25s–OH
13C CDCl3
126 MHz
ppm

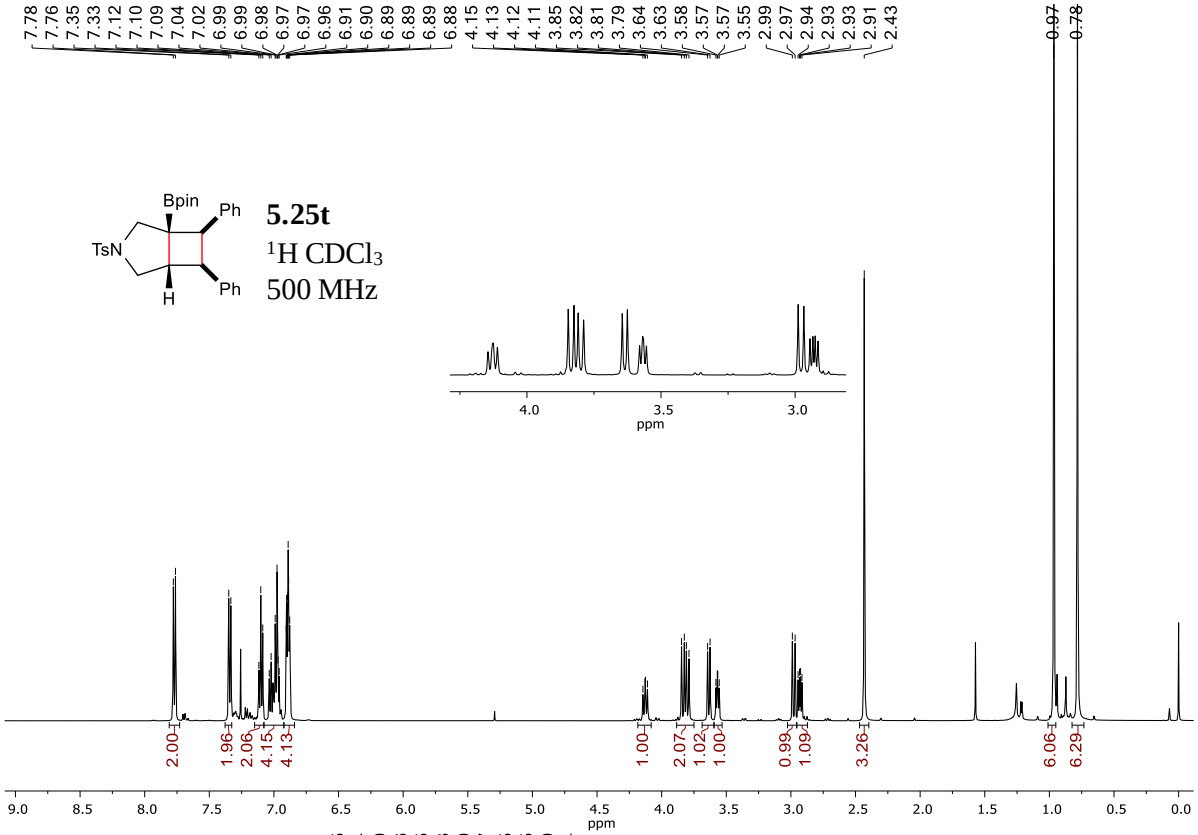
7.78 7.76 7.35 7.33 7.12 7.10 7.09 7.04 7.02 6.99 6.99 6.98 6.97 6.97 6.96 6.91 6.90 6.89 6.89 6.89 6.88
4.15 4.13 4.12 4.11 3.85 3.82 3.81 3.79 3.64 3.63 3.58 3.57 3.57 3.55 2.99 2.97 2.94 2.93 2.93 2.91 2.43
0.97 0.78
Bpin
Ph
TsN
H
Ph
5.25t
1H CDCl3
500 MHz
4.0 3.5 3.0
ppm
2.00 1.96 2.06 4.15 4.13 1.00 2.07 1.02 1.00 0.99 1.09 3.26 6.06 6.29
9.0 8.5 8.0 7.5 7.0 6.5 6.0 5.5 5.0 4.5 4.0 3.5 3.0 2.5 2.0 1.5 1.0 0.5 0.0
ppm

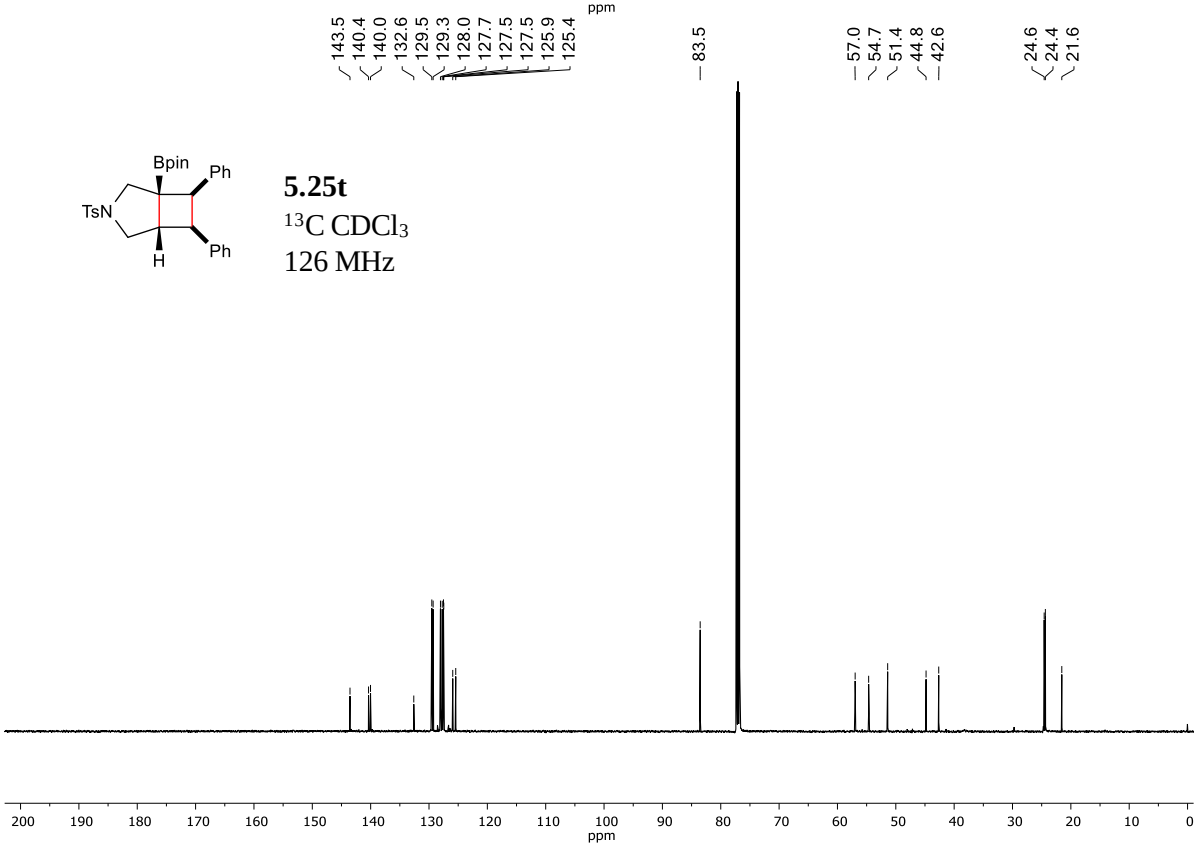
143.5 140.4 140.0 132.6 129.5 129.3 128.0 127.7 127.5 127.5 125.9 125.4
83.5
57.0 54.7 51.4 44.8 42.6
24.6 24.4 21.6
Bpin
Ph
TsN
H
Ph
5.25t
13C CDCl3
126 MHz
200 190 180 170 160 150 140 130 120 110 100 90 80 70 60 50 40 30 20 10 0
ppm

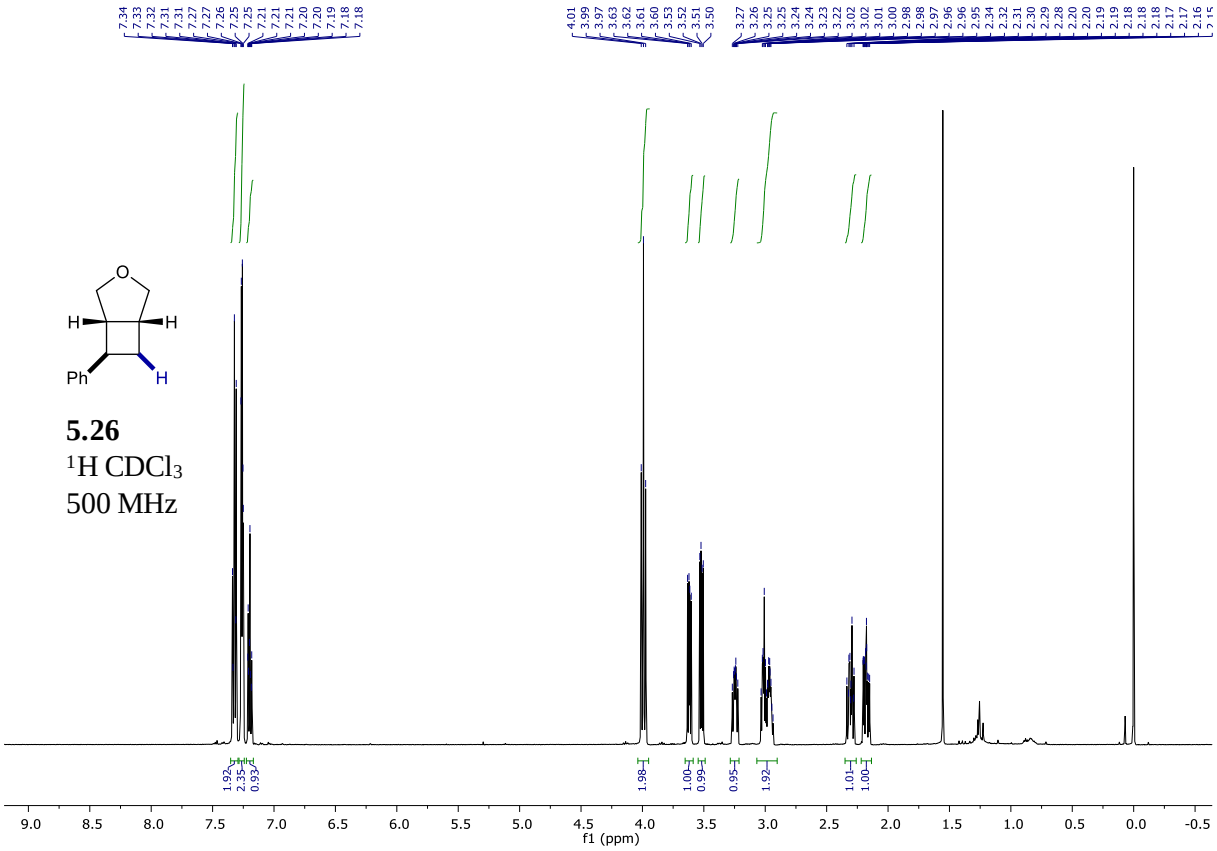
7.34 7.33 7.32 7.31 7.31 7.27 7.27 7.26 7.25 7.25 7.21 7.21 7.20 7.20 7.19 7.18 7.18
4.01 3.99 3.97 3.63 3.62 3.61 3.60 3.53 3.52 3.51 3.50
3.27 3.26 3.25 3.25 3.24 3.24 3.23 3.22 3.02 3.02 3.01 3.00 2.98 2.98 2.97 2.96 2.96 2.95 2.34 2.32 2.31 2.30 2.29 2.28 2.20 2.20 2.19 2.19 2.18 2.18 2.17 2.17 2.16
O
H
H
Ph
H
5.26
1H CDCl3
500 MHz
1.92
2.35
0.93
1.98
1.00
0.99
0.95
1.92
1.01
1.00
9.0 8.5 8.0 7.5 7.0 6.5 6.0 5.5 5.0 4.5 4.0 3.5 3.0 2.5 2.0 1.5 1.0 0.5 0.0 -0.5
f1 (ppm)

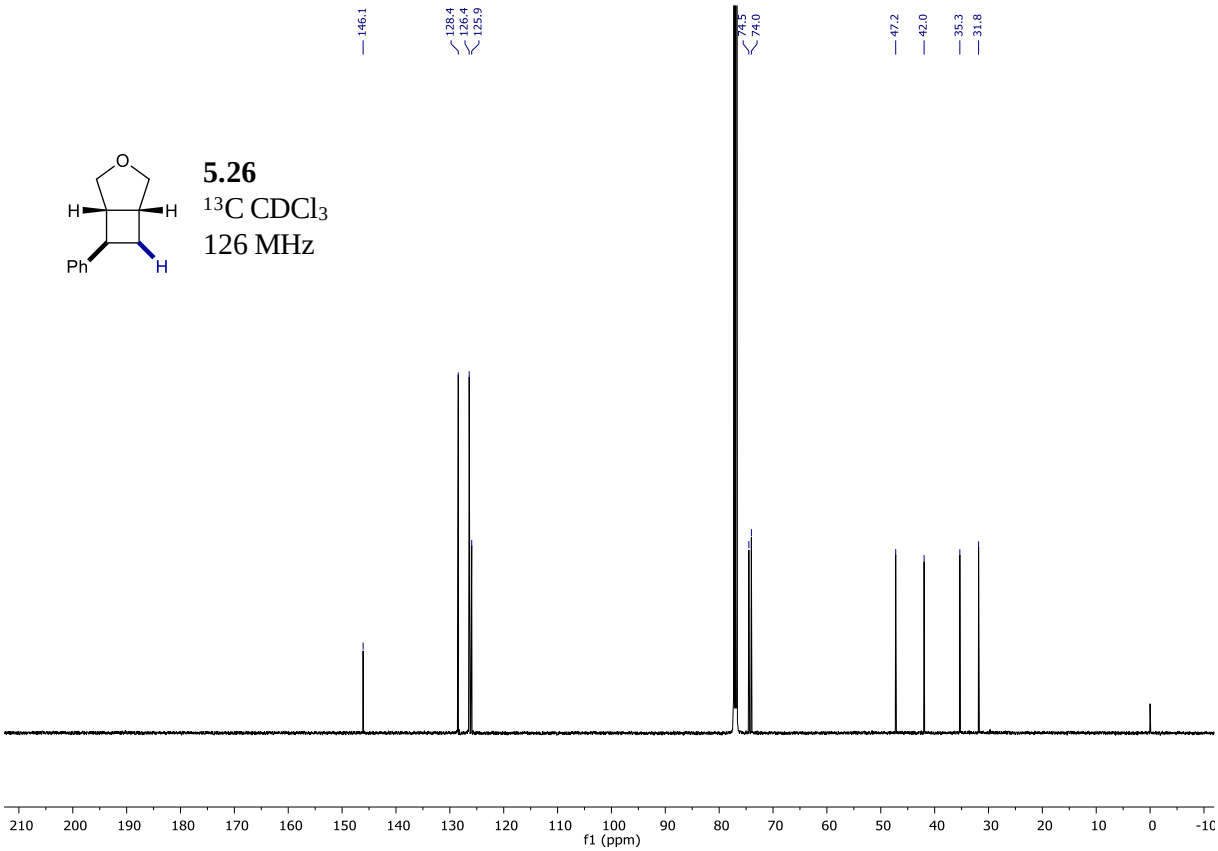
146.1
128.4
126.4
125.9
74.5
74.0
47.2
42.0
35.3
31.8
O
H
H
Ph
H
5.26
13C CDCl3
126 MHz
210 200 190 180 170 160 150 140 130 120 110 100 90 80 70 60 50 40 30 20 10 0 -10
f1 (ppm)

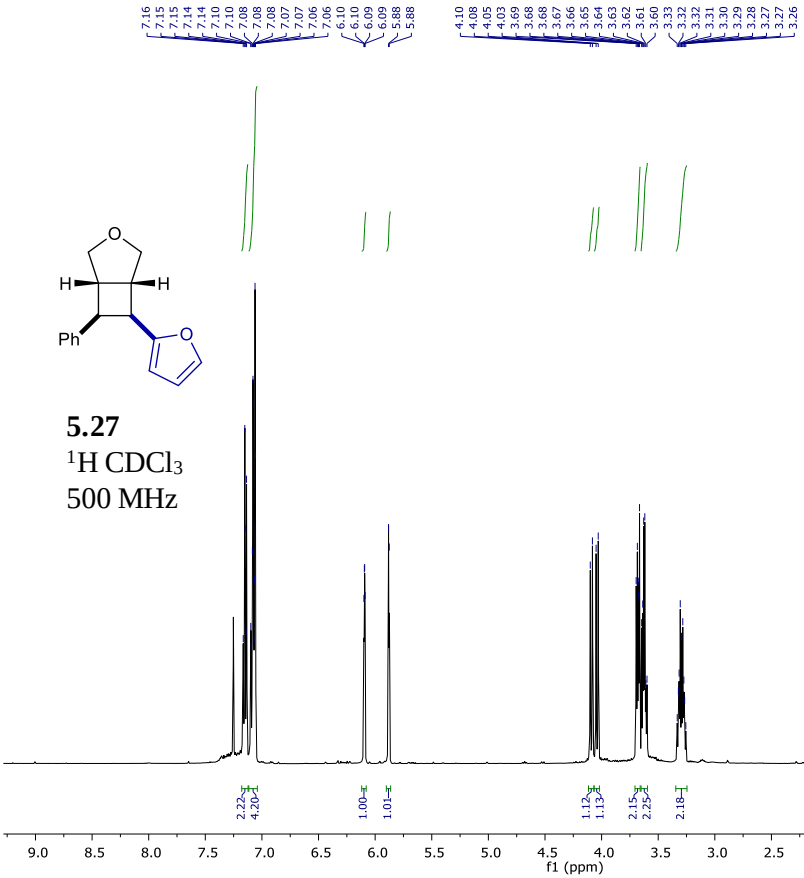

5.27
^{1}H $CDCl_3$
500 MHz

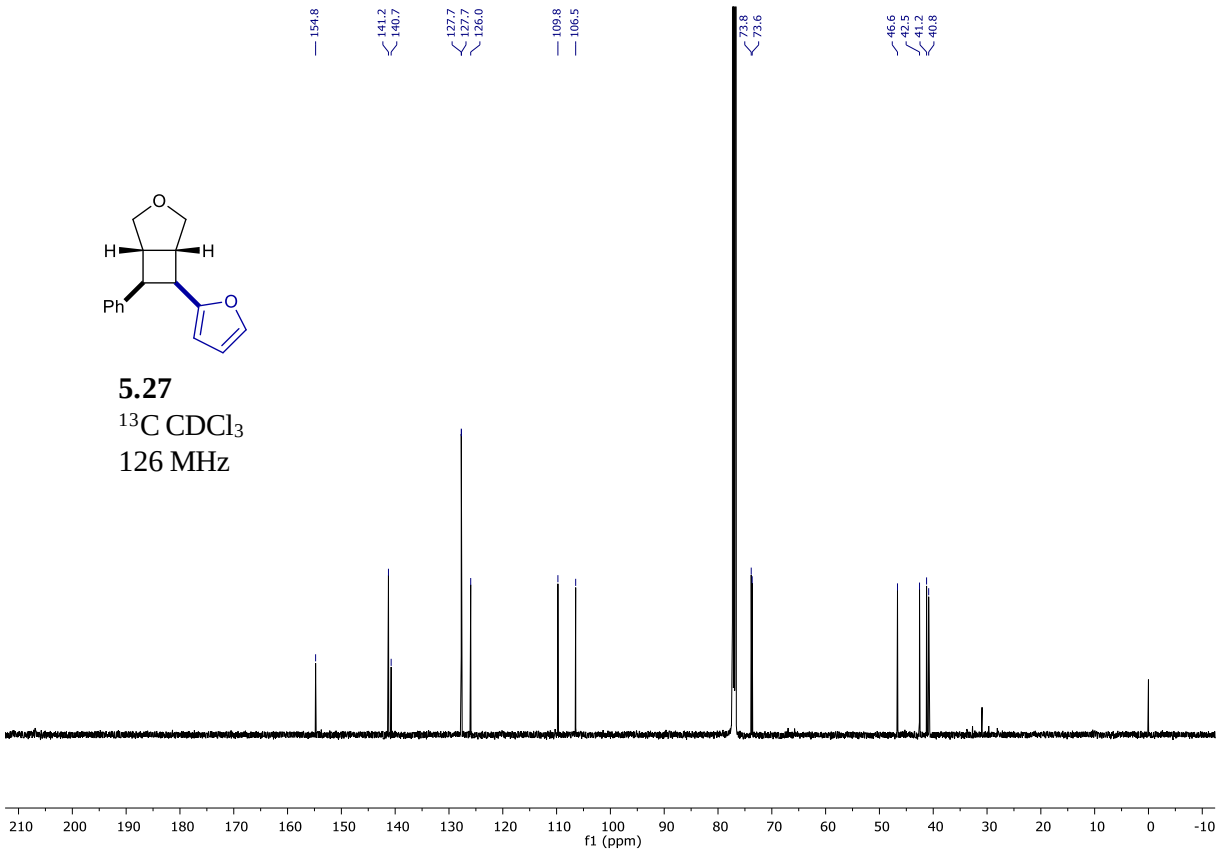

5.27
^{13}C $CDCl_3$
126 MHz

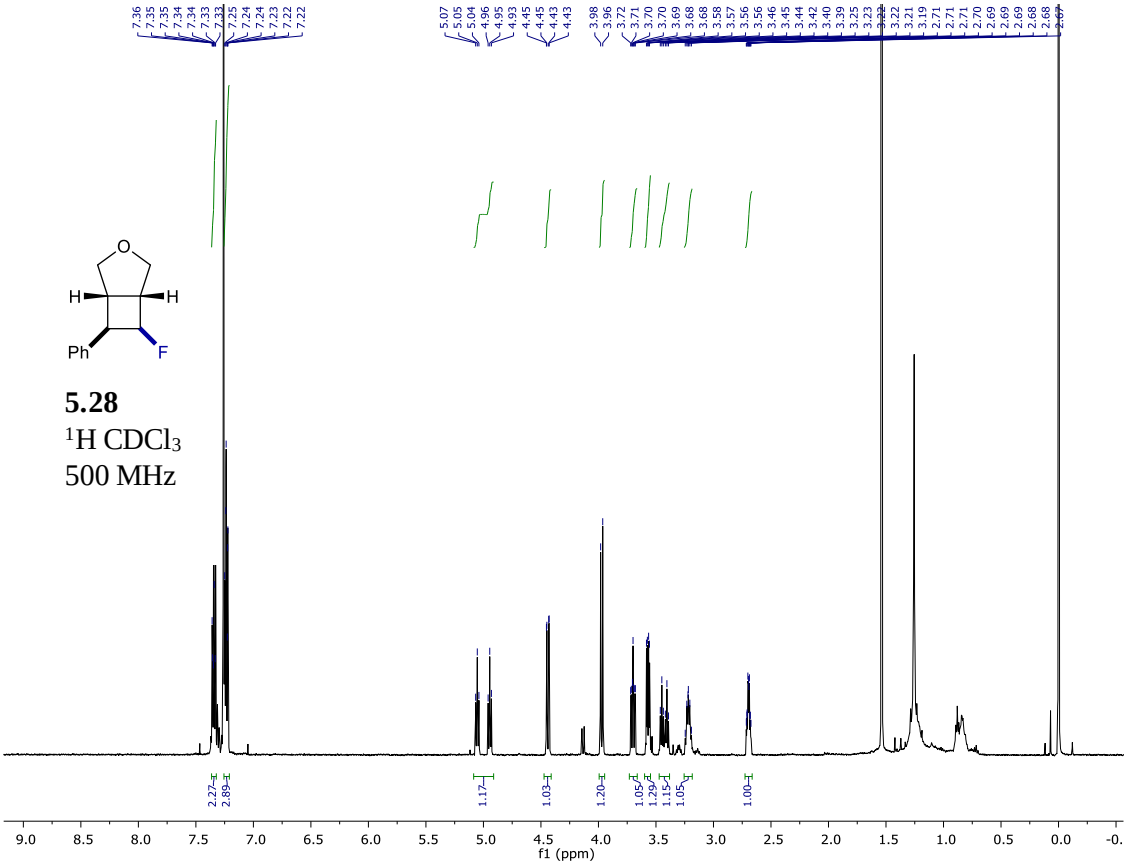
O
H
H
Ph
F
5.28
1H CDCl3
500 MHz
f1 (ppm)

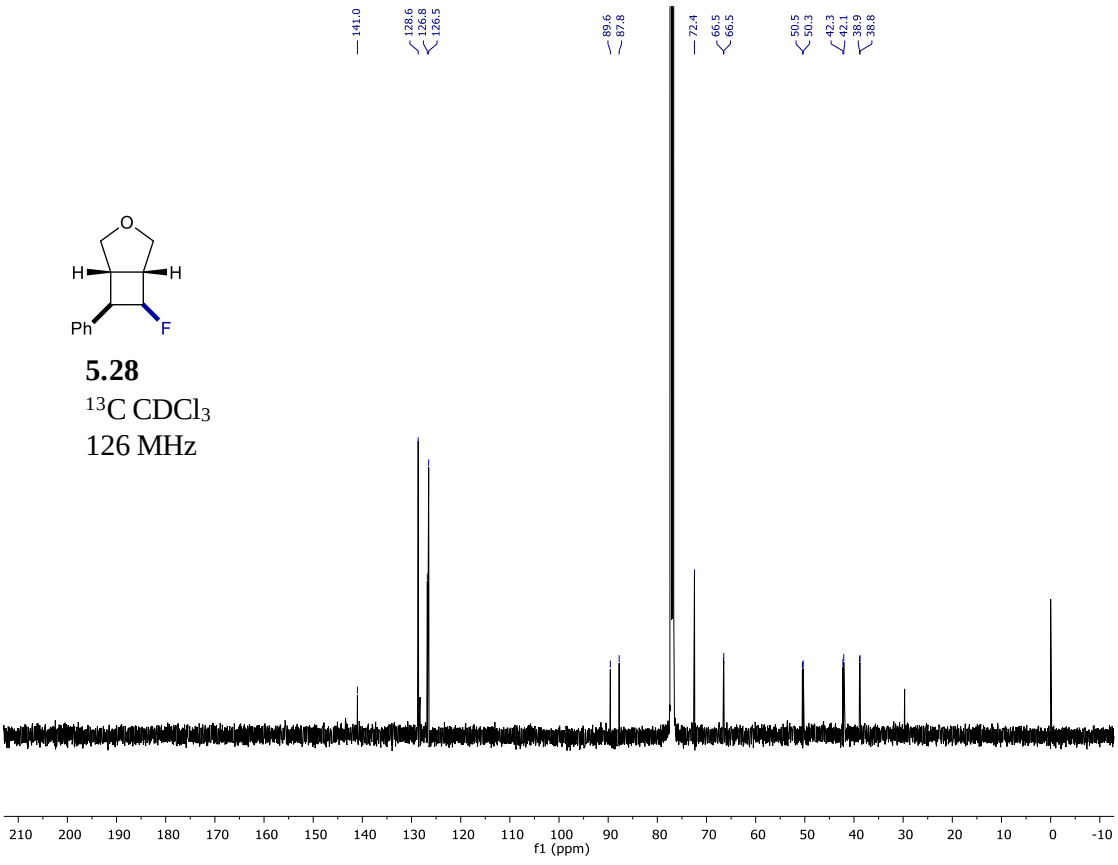
O
H
H
Ph
F
5.28
13C CDCl3
126 MHz
f1 (ppm)

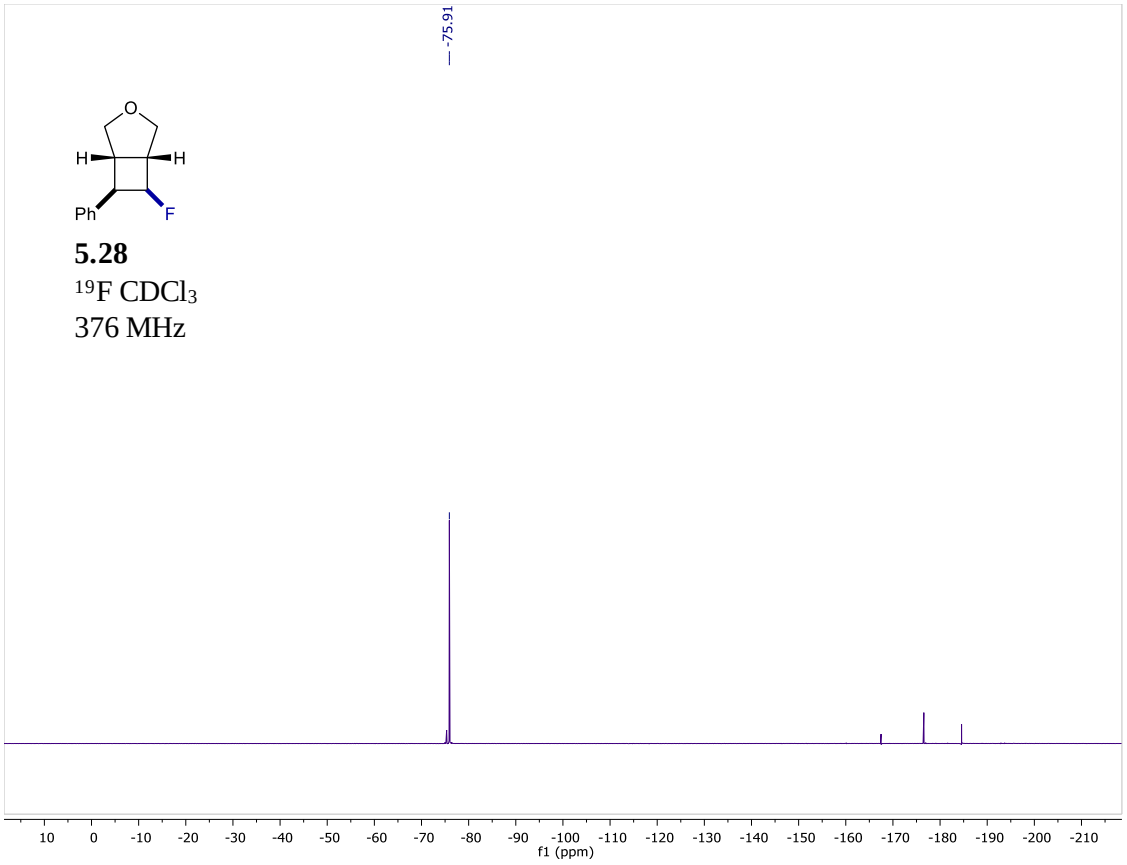

5.28

^{19}F $CDCl_3$

376 MHz

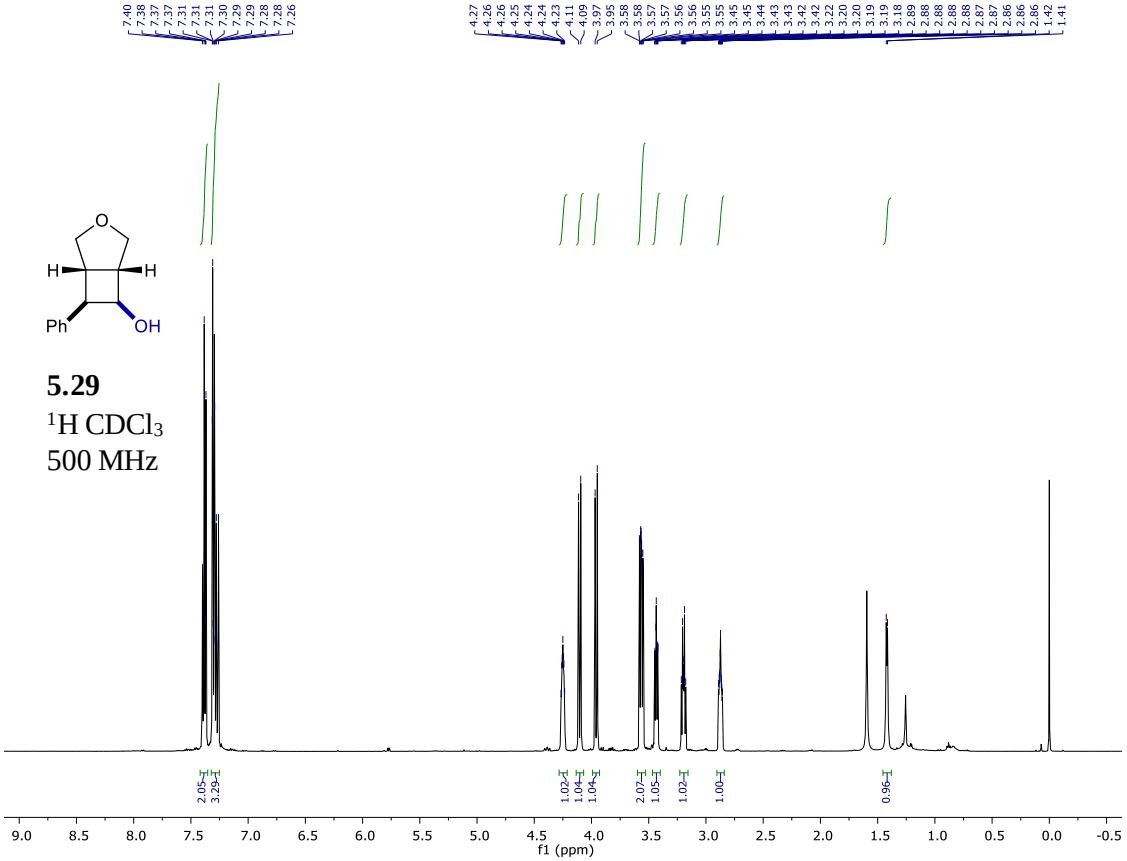
7.40
7.38
7.37
7.37
7.31
7.31
7.31
7.30
7.29
7.29
7.28
7.28
7.26
4.27
4.26
4.26
4.25
4.24
4.24
4.23
4.11
4.09
3.97
3.95
3.58
3.58
3.57
3.57
3.56
3.56
3.55
3.55
3.45
3.44
3.43
3.43
3.42
3.42
3.22
3.20
3.20
3.19
3.19
3.18
2.89
2.88
2.88
2.88
2.88
2.87
2.87
2.86
2.86
2.86
1.42
1.41
O
H
H
Ph
OH
5.29
1H CDCl3
500 MHz
2.05
3.29
1.02
1.04
1.04
2.07
1.05
1.02
1.00
0.96
9.0
8.5
8.0
7.5
7.0
6.5
6.0
5.5
5.0
4.5
4.0
3.5
3.0
2.5
2.0
1.5
1.0
0.5
0.0
-0.5
f1 (ppm)

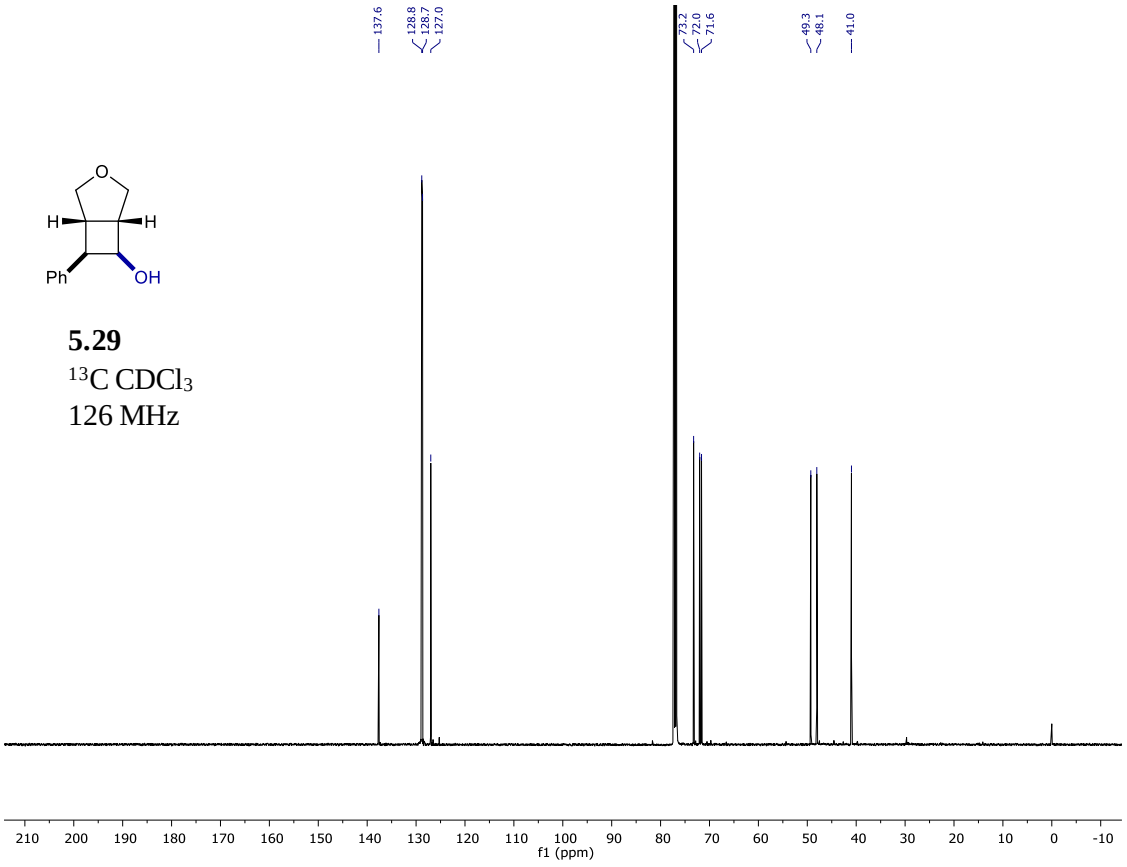
137.6
128.8
128.7
127.0
73.2
72.0
71.6
49.3
48.1
41.0
O
H
H
Ph
OH
5.29
13C CDCl3
126 MHz
210
200
190
180
170
160
150
140
130
120
110
100
90
80
70
60
50
40
30
20
10
0
-10
f1 (ppm)

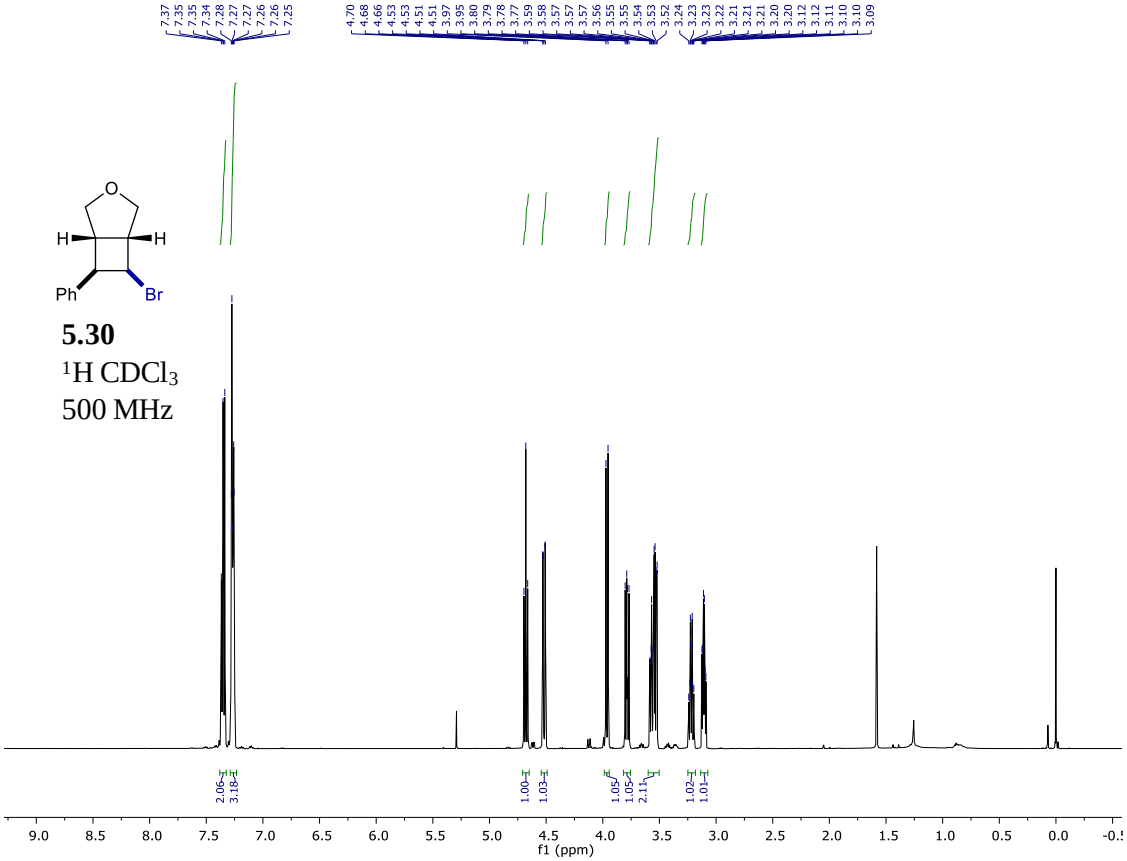
7.37 7.35 7.35 7.34 7.28 7.27 7.27 7.26 7.26 7.25
4.70 4.68 4.66 4.53 4.53 4.51 4.51 3.97 3.95 3.80 3.79 3.78 3.77 3.59 3.58 3.57 3.57 3.57 3.56 3.55 3.55 3.54 3.53 3.52 3.24 3.23 3.23 3.22 3.21 3.21 3.21 3.20 3.20 3.12 3.12 3.11 3.10 3.10 3.09
O
H
H
Ph
Br
5.30
1H CDCl3
500 MHz
2.06
3.18
1.00
1.03
1.05
1.05
2.11
1.02
1.01
9.0 8.5 8.0 7.5 7.0 6.5 6.0 5.5 5.0 4.5 4.0 3.5 3.0 2.5 2.0 1.5 1.0 0.5 0.0
f1 (ppm)

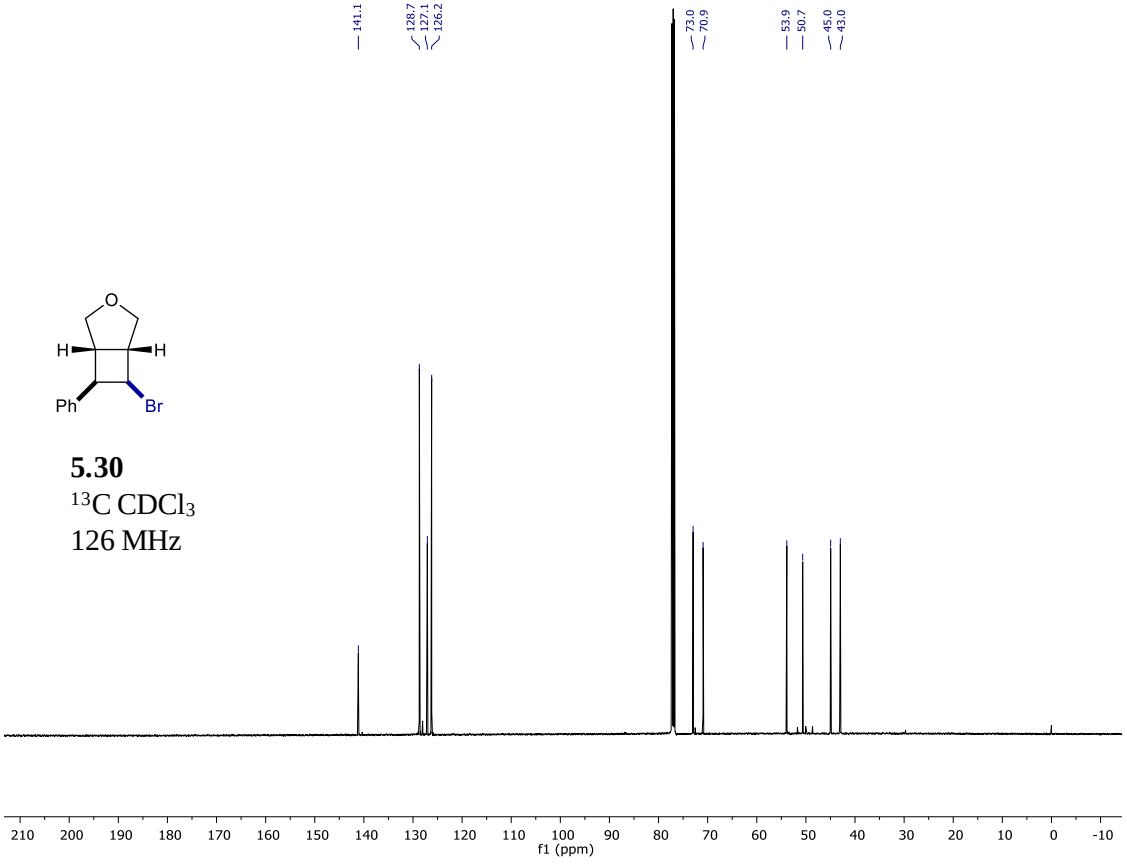
141.1
128.7
127.1
126.2
73.0
70.9
53.9
50.7
45.0
43.0
O
H
H
Ph
Br
5.30
13C CDCl3
126 MHz
210 200 190 180 170 160 150 140 130 120 110 100 90 80 70 60 50 40 30 20 10 0 -10
f1 (ppm)

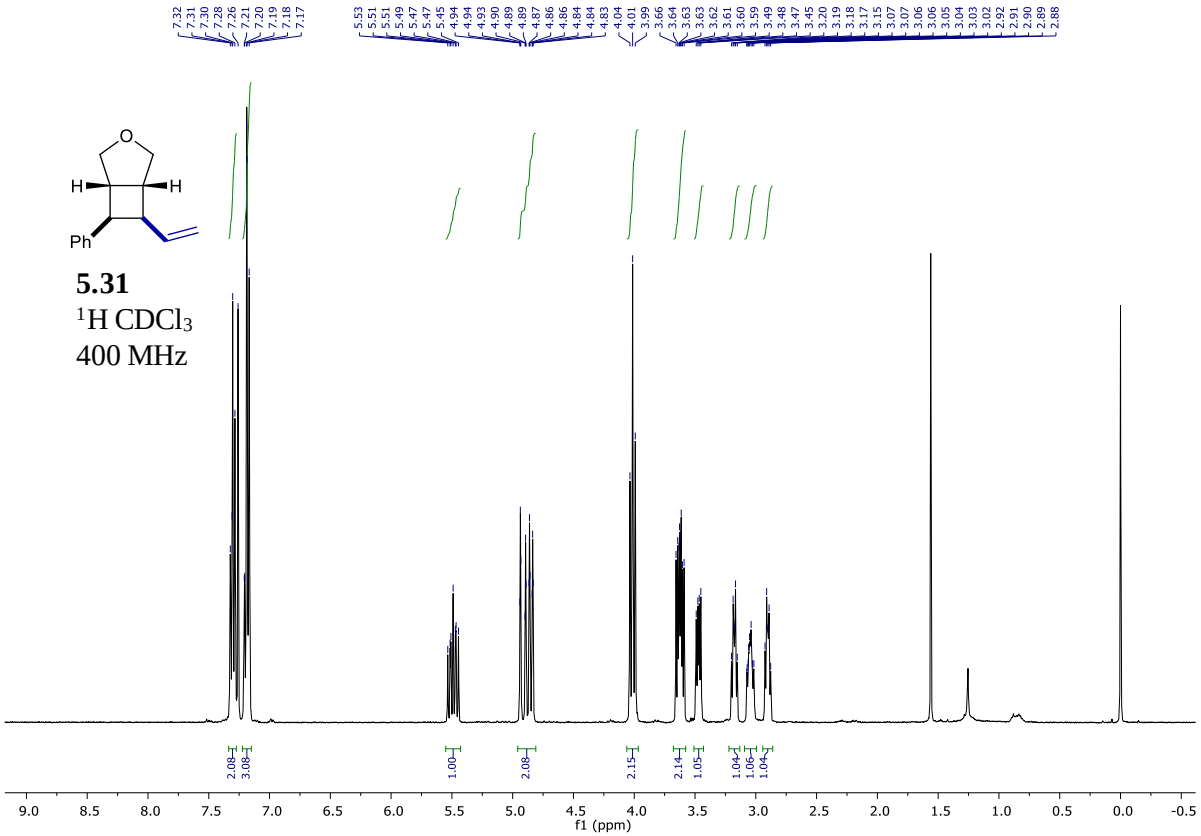
7.32 7.31 7.30 7.28 7.26 7.21 7.20 7.19 7.18 7.17
5.53 5.51 5.51 5.49 5.47 5.47 5.45 4.94 4.94 4.93 4.90 4.89 4.89 4.87 4.86 4.86 4.84 4.84 4.83 4.04 4.01 3.99 3.66 3.64 3.63 3.63 3.62 3.61 3.60 3.59 3.49 3.48 3.47 3.45 3.20 3.19 3.18 3.17 3.15 3.07 3.07 3.06 3.06 3.05 3.04 3.03 3.02 2.92 2.91 2.90 2.89 2.88
O
H
H
Ph
5.31
1H CDCl3
400 MHz
2.08 3.08 1.00 2.08 2.15 2.14 1.05 1.04 1.06 1.04
9.0 8.5 8.0 7.5 7.0 6.5 6.0 5.5 5.0 4.5 4.0 3.5 3.0 2.5 2.0 1.5 1.0 0.5 0.0 -0.5
f1 (ppm)

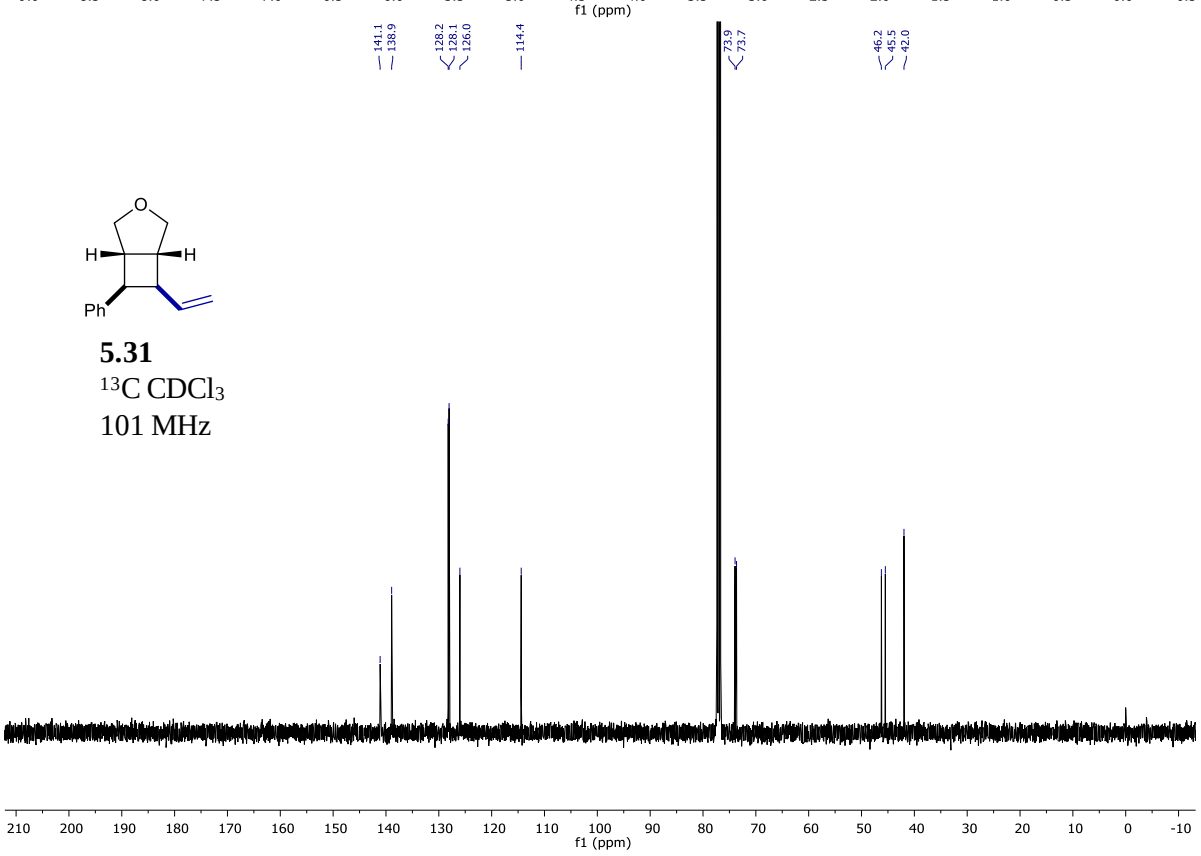
141.1 138.9 128.2 128.1 126.0 114.4 73.9 73.7 46.2 45.5 42.0
O
H
H
Ph
5.31
13C CDCl3
101 MHz
210 200 190 180 170 160 150 140 130 120 110 100 90 80 70 60 50 40 30 20 10 0 -10
f1 (ppm)

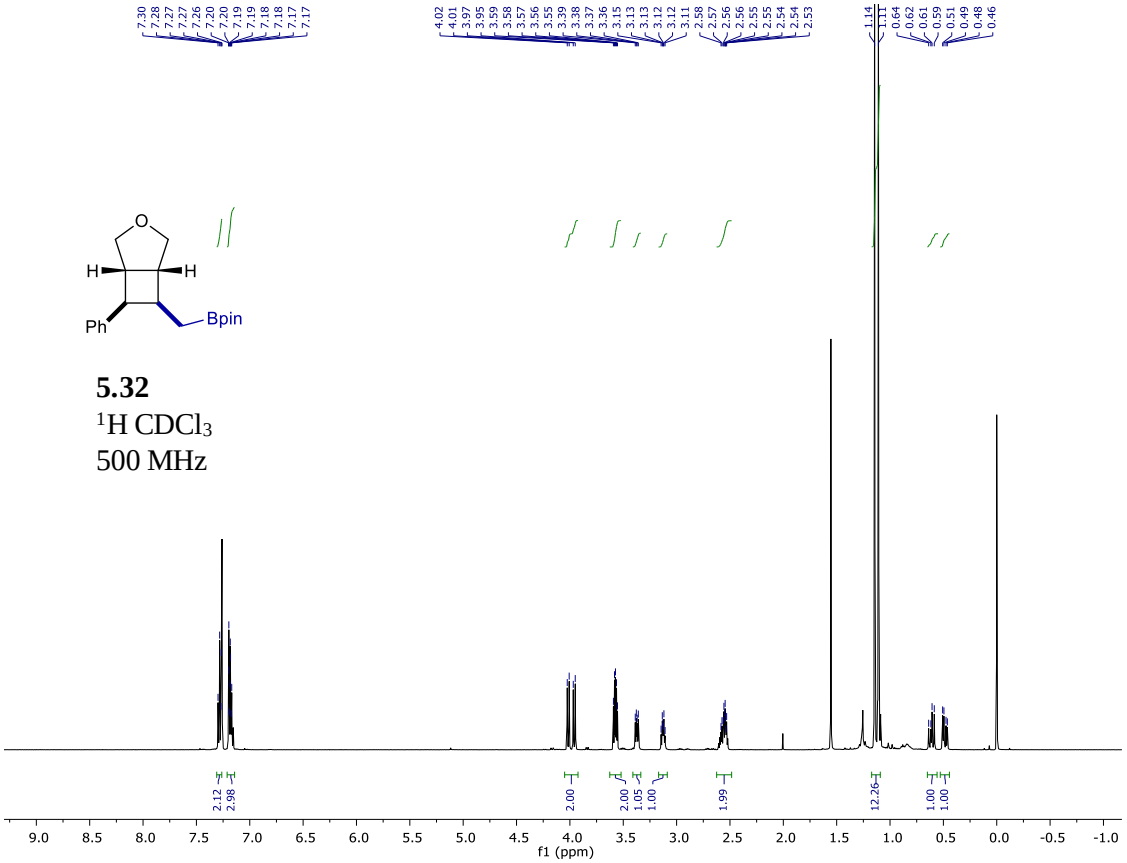

5.32
^{1}H $CDCl_3$
500 MHz

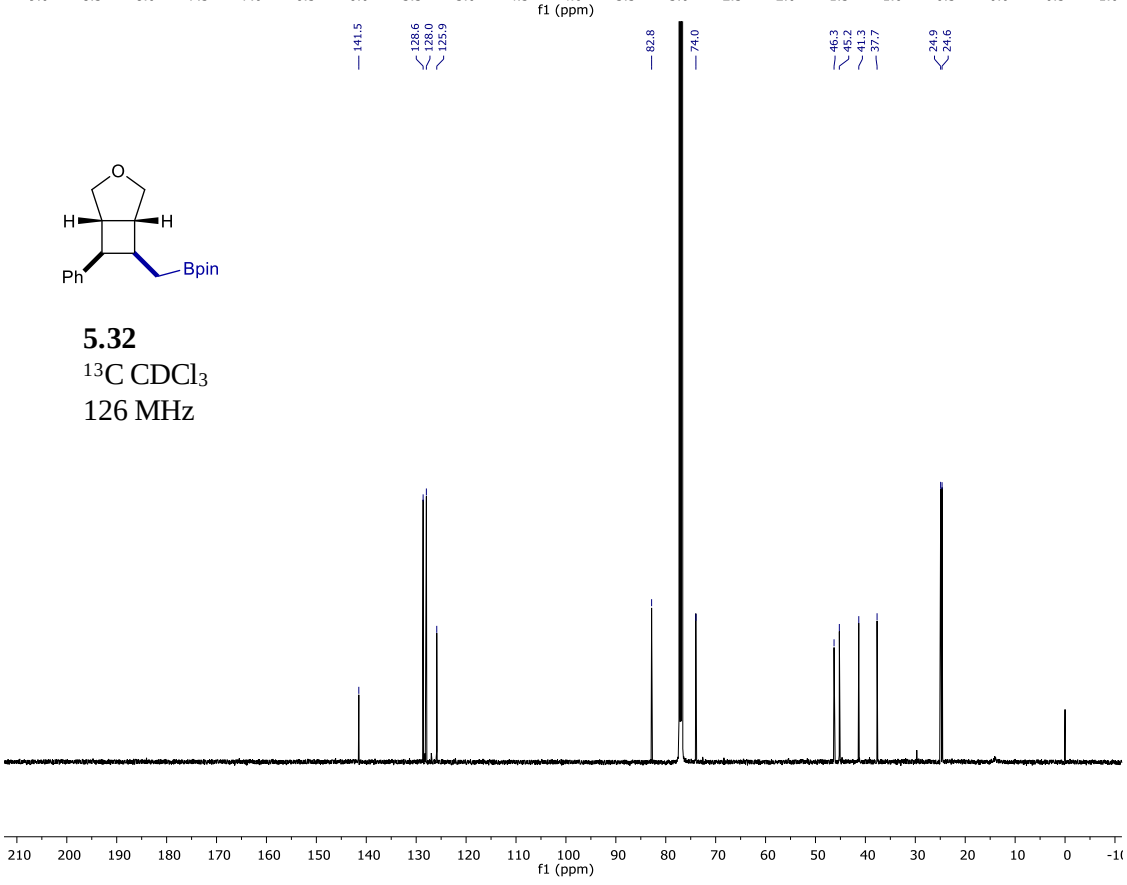

5.32
^{13}C $CDCl_3$
126 MHz

5.32
^{11}B $CDCl_3$
128 MHz

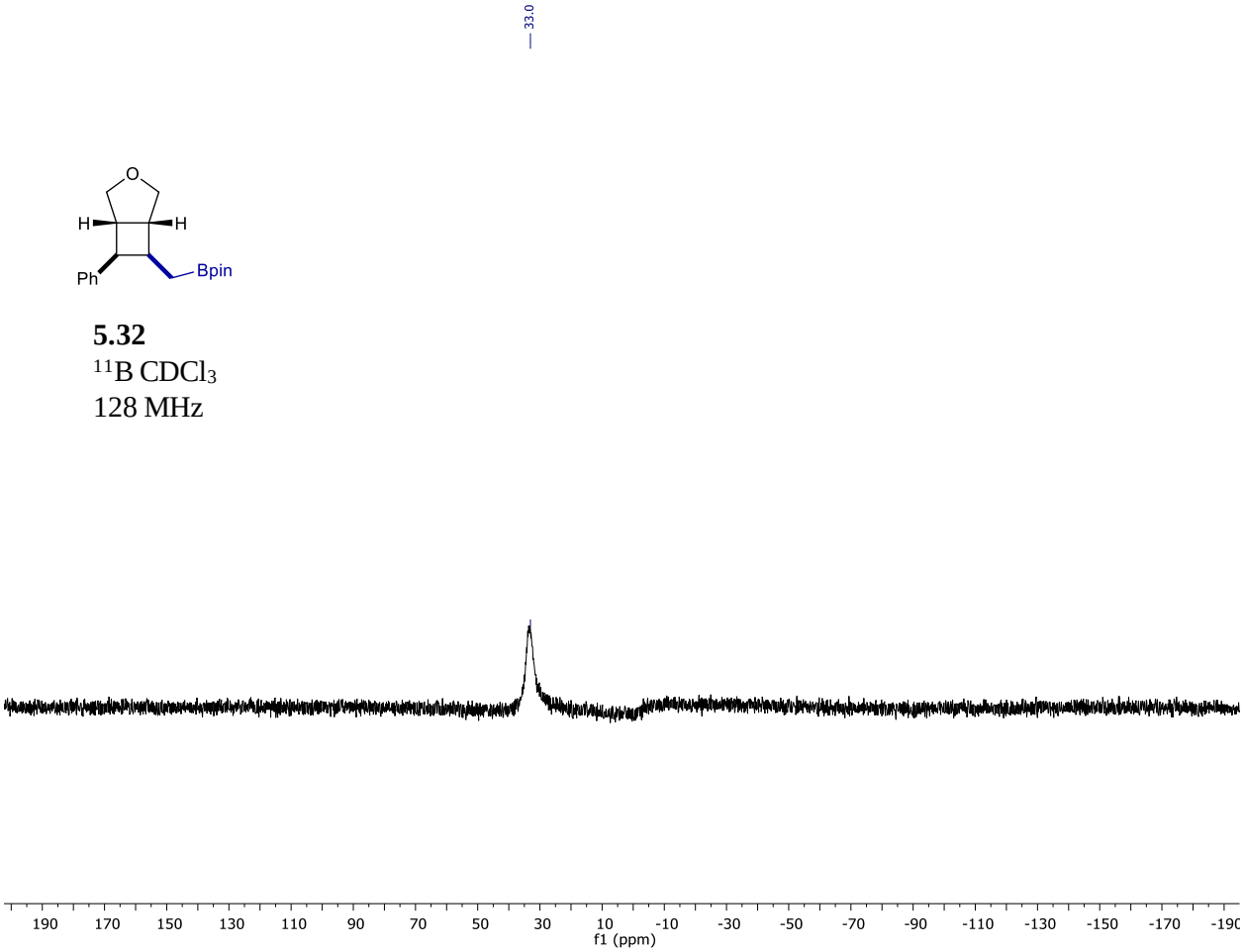

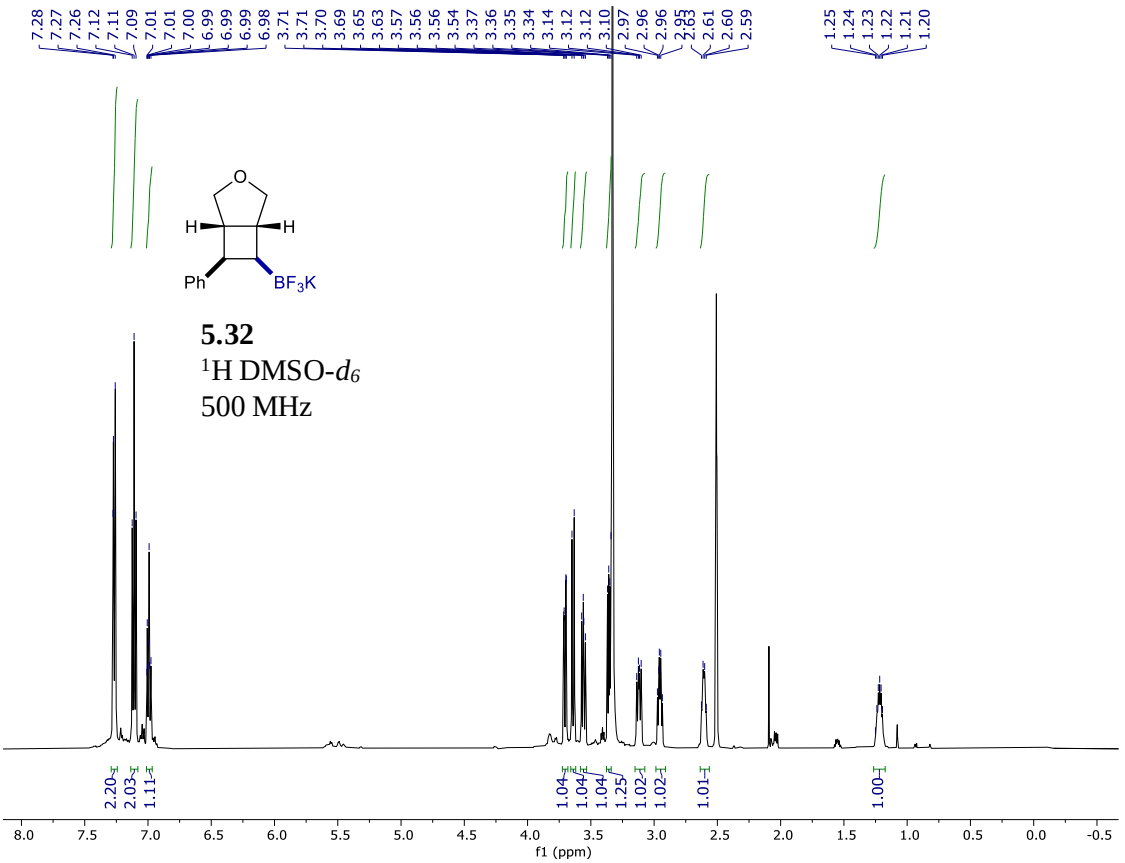

5.32
^{1}H DMSO-*d*$_6$
500 MHz

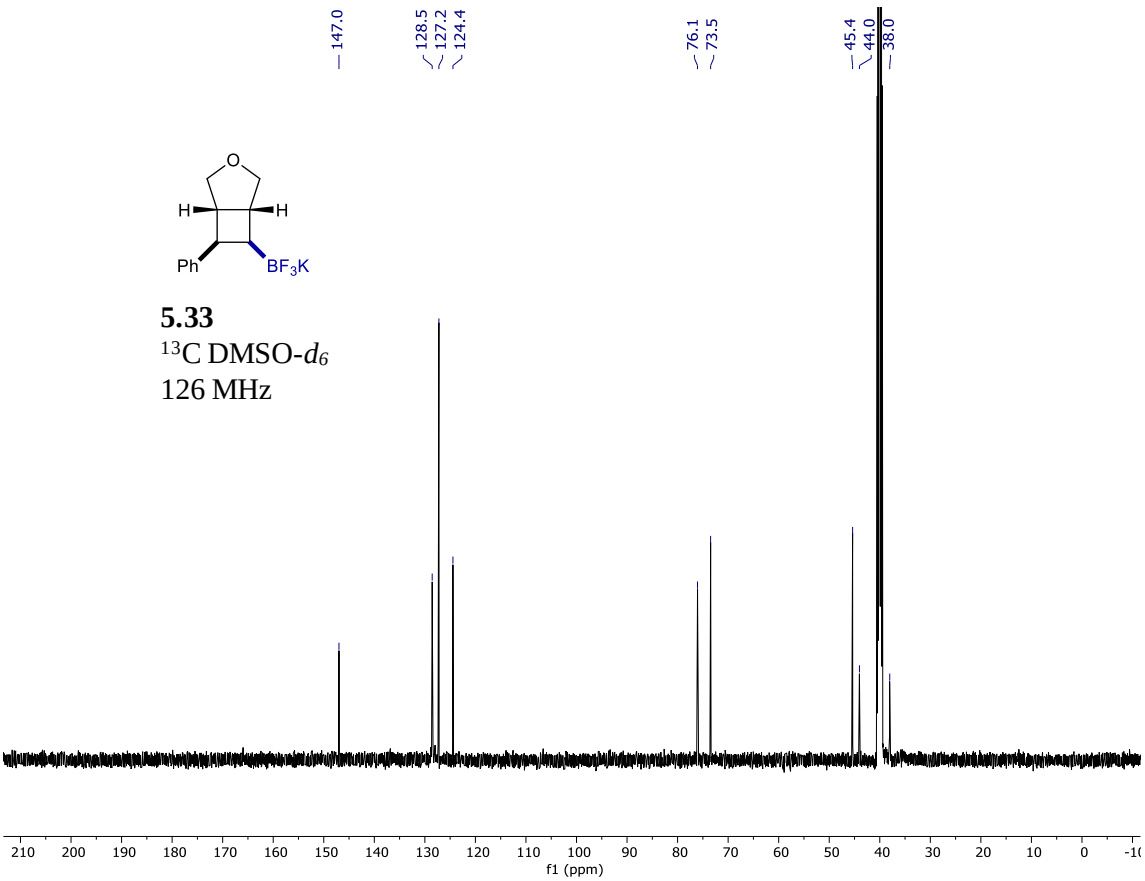

5.33
^{13}C DMSO-*d*$_6$
126 MHz

5.33
^{19}F DMSO-d_6
376 MHz

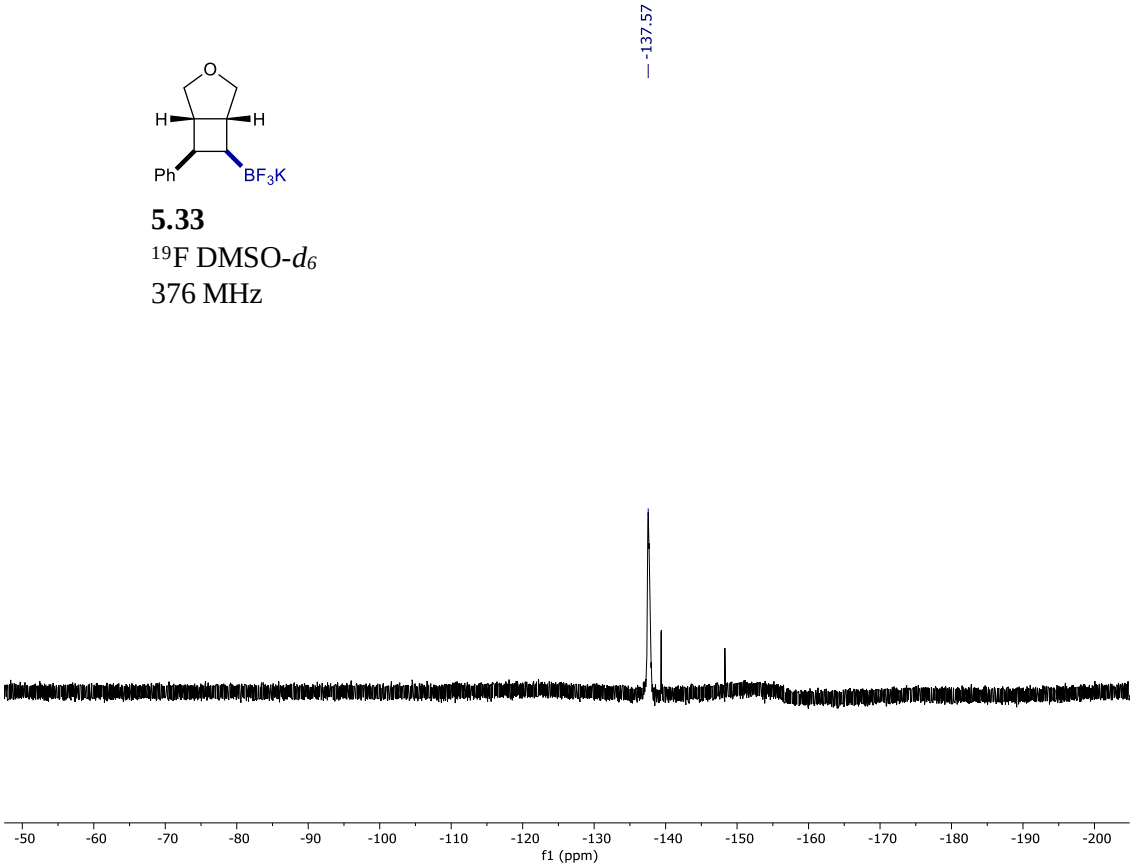

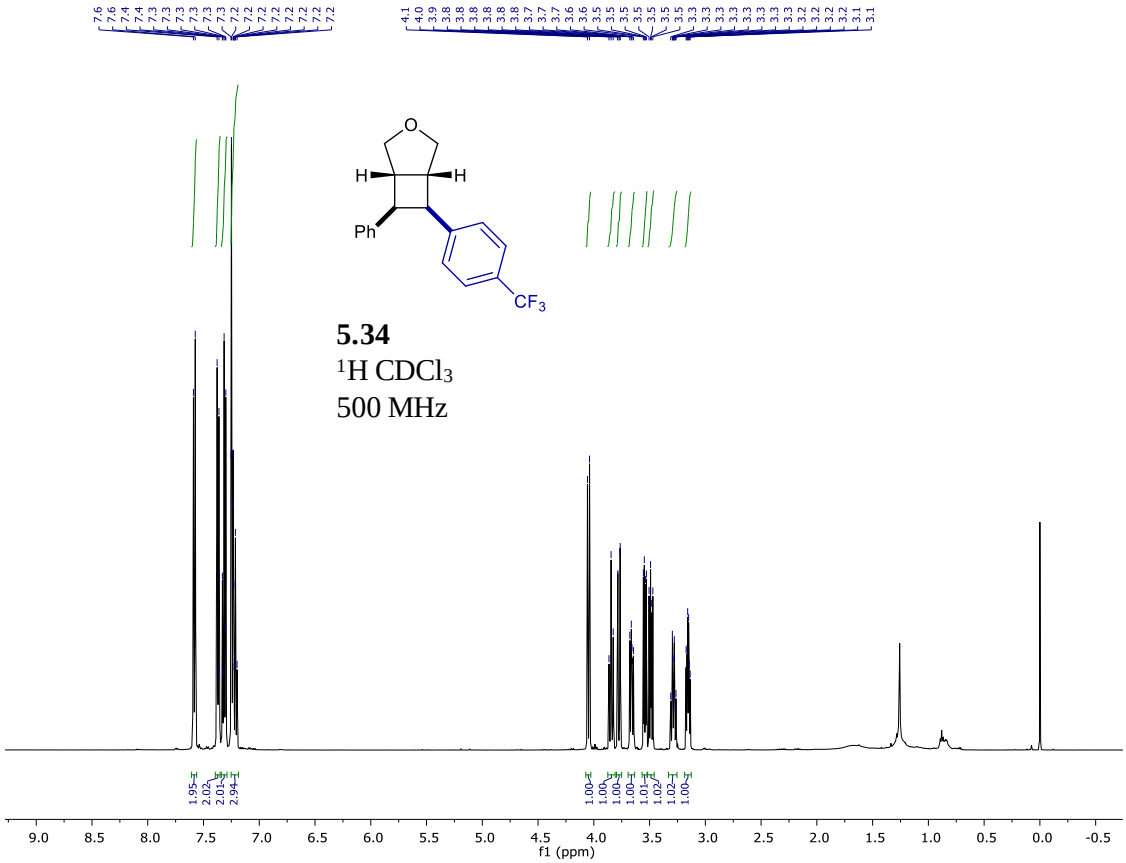

5.34
^{1}H $CDCl_3$
500 MHz

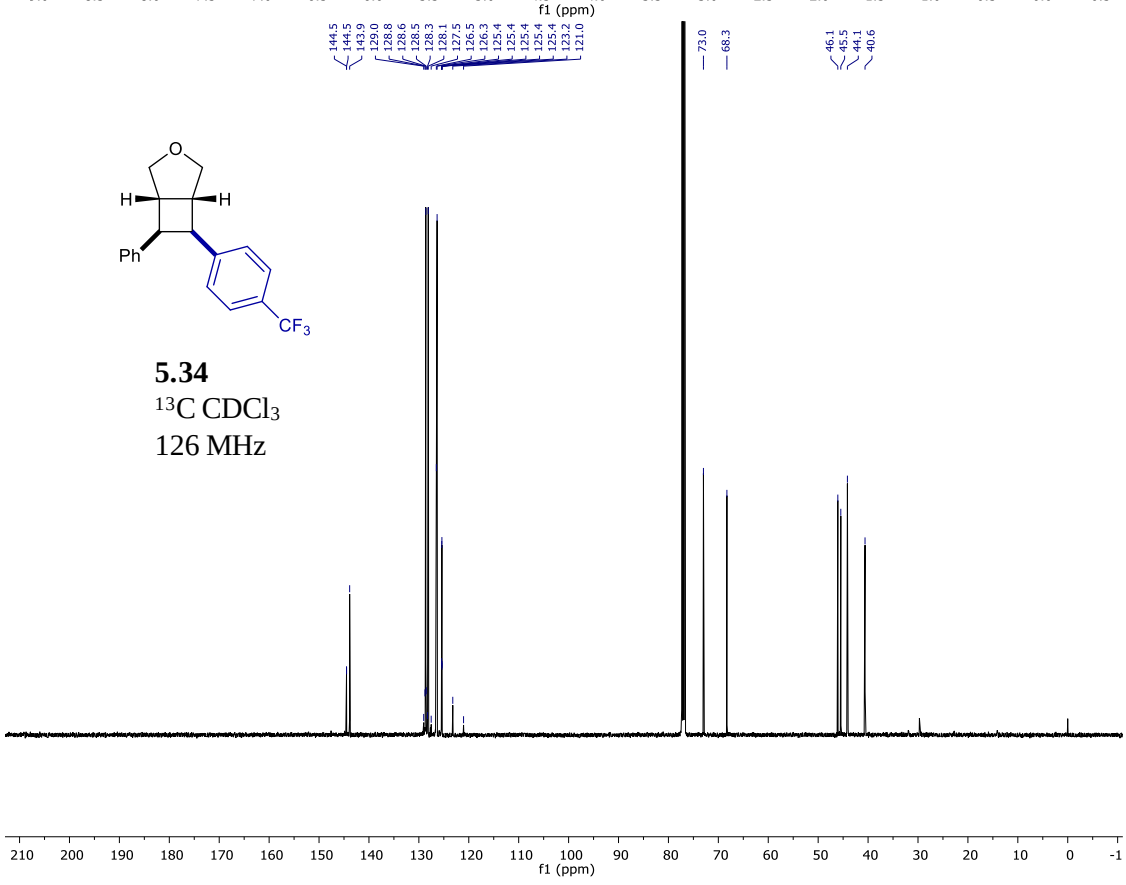

5.34
^{13}C $CDCl_3$
126 MHz

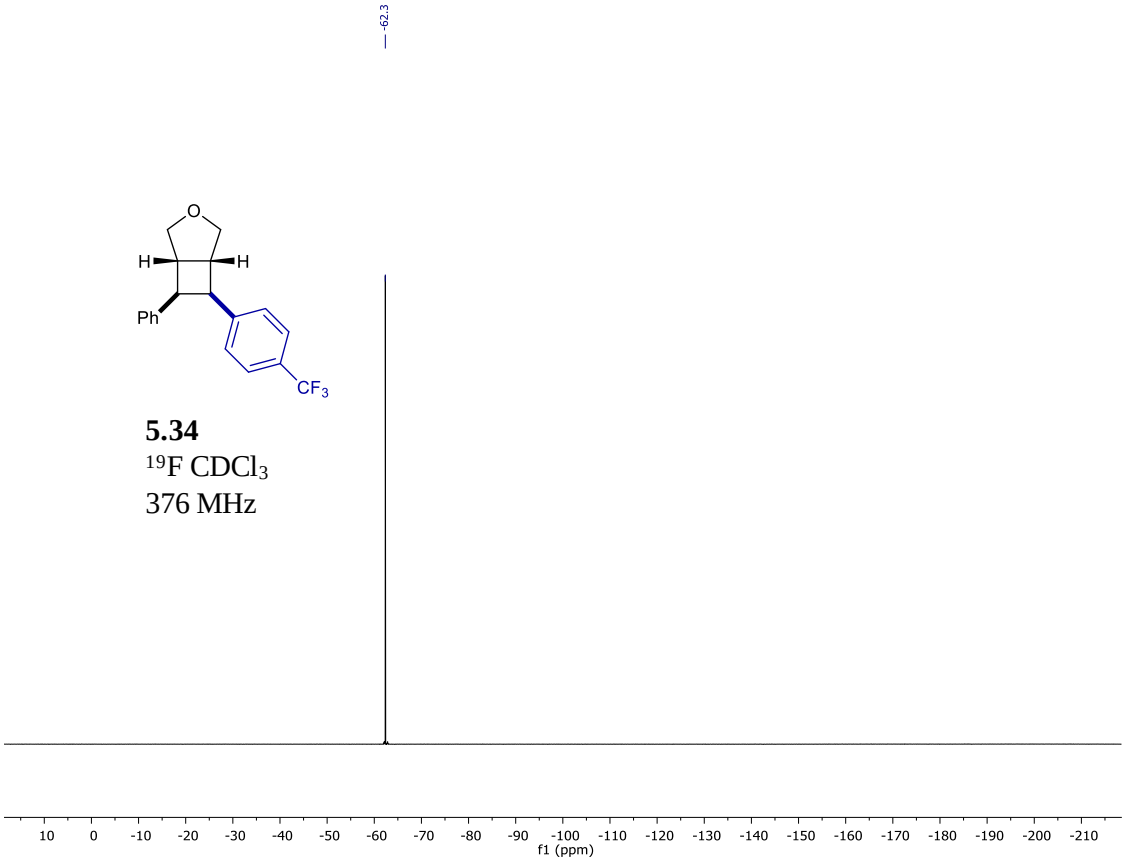

5.34
^{19}F $CDCl_3$
376 MHz

Appendix C. SFC and HPLC Chromatograms for New Compounds

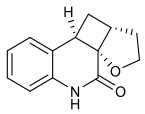

2.29a

Racemic (Daicel CHIRALCEL® OD-H, 70% *i*-PrOH, 30% Hexanes, 1 mL/min, 258.1 nm)

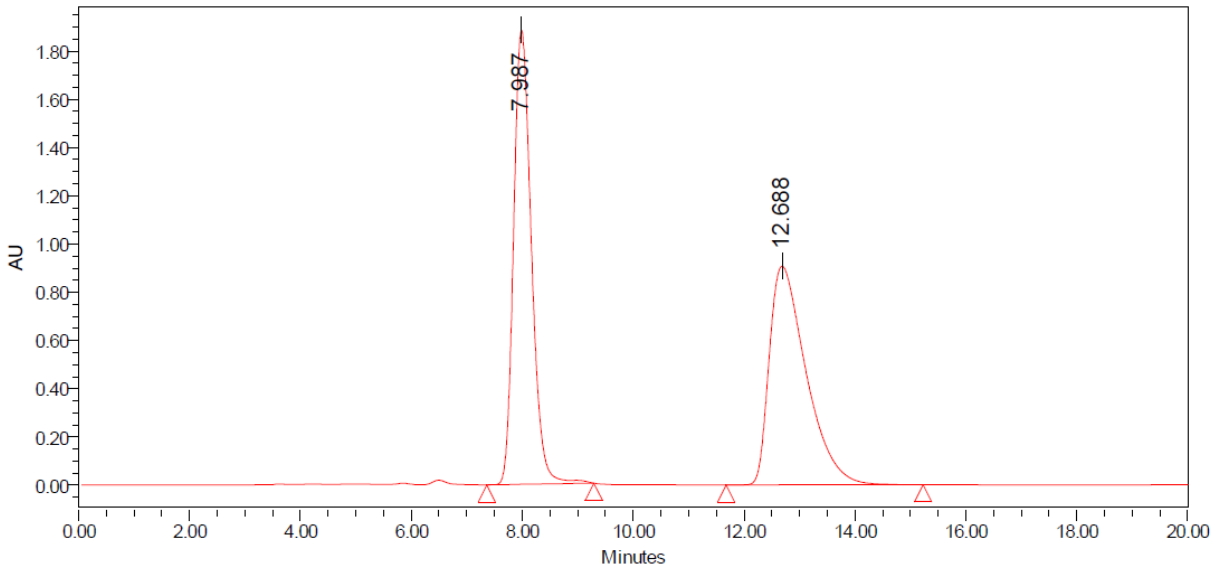

Peak No	RT (min)	Area	Height	% Area
1	7.987	42003659	1884473	50.10
2	12.688	41844116	907816	49.90

Enantioenriched

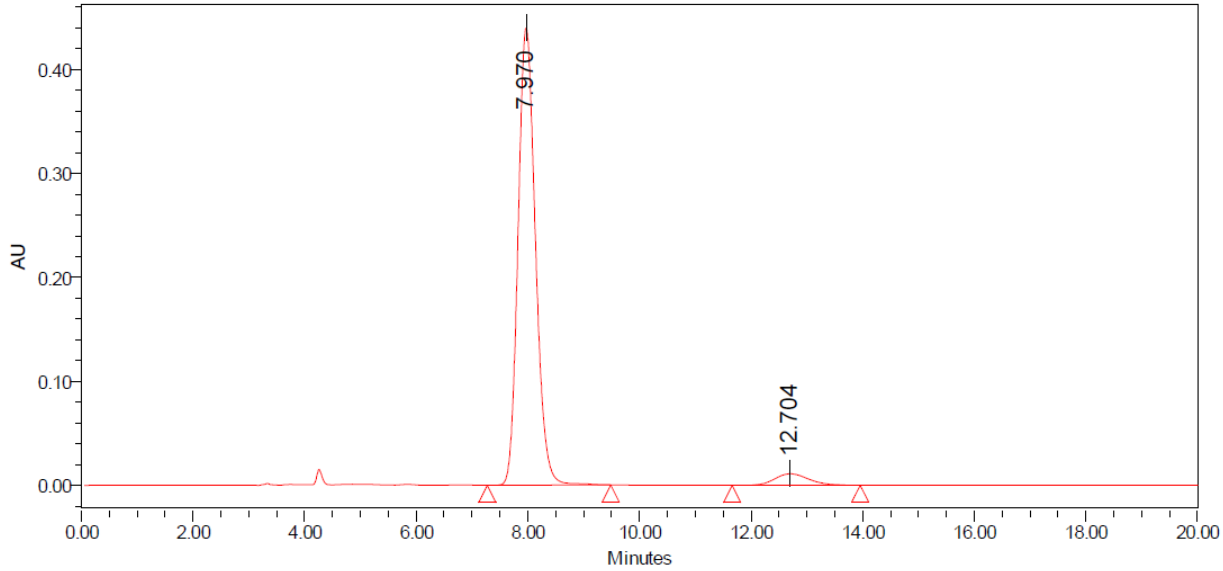

Peak No	RT (min)	Area	Height	% Area
1	7.970	9520832	439595	95.31
2	12.704	468778	11167	4.69

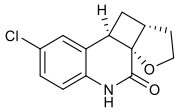

2.29b

Racemic (Daicel CHIRALCEL® OD-H, 70% *i*-PrOH, 30% Hexanes, 1 mL/min, 261.6 nm)

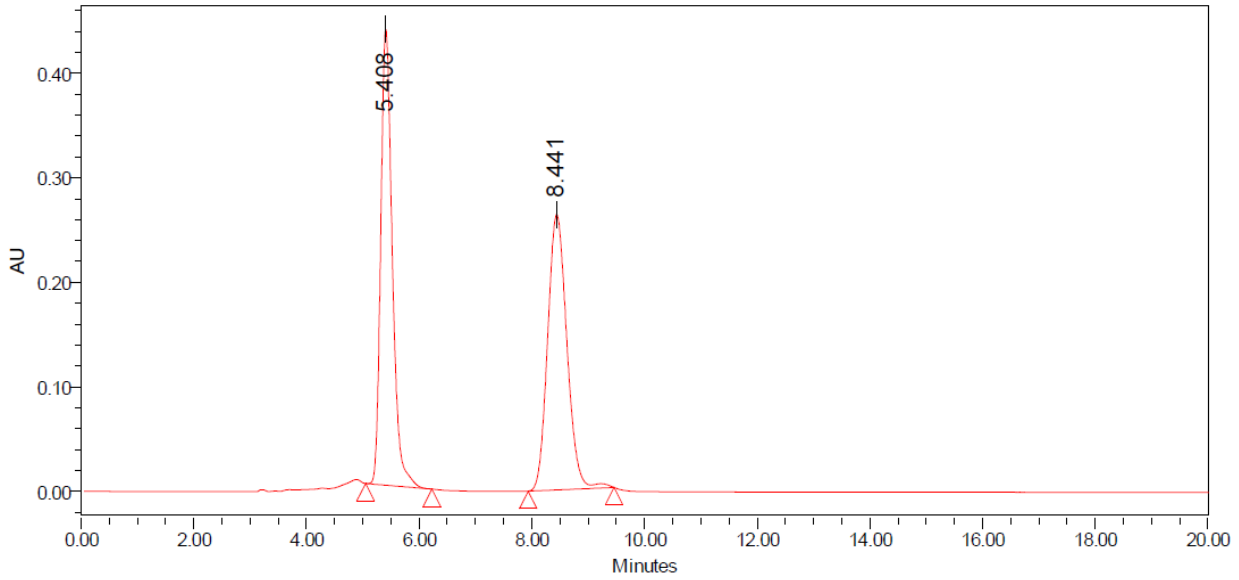

Peak No	RT (min)	Area	Height	% Area
1	5.408	6222500	436070	49.84
2	8.441	6261811	263612	50.16

Enantioenriched

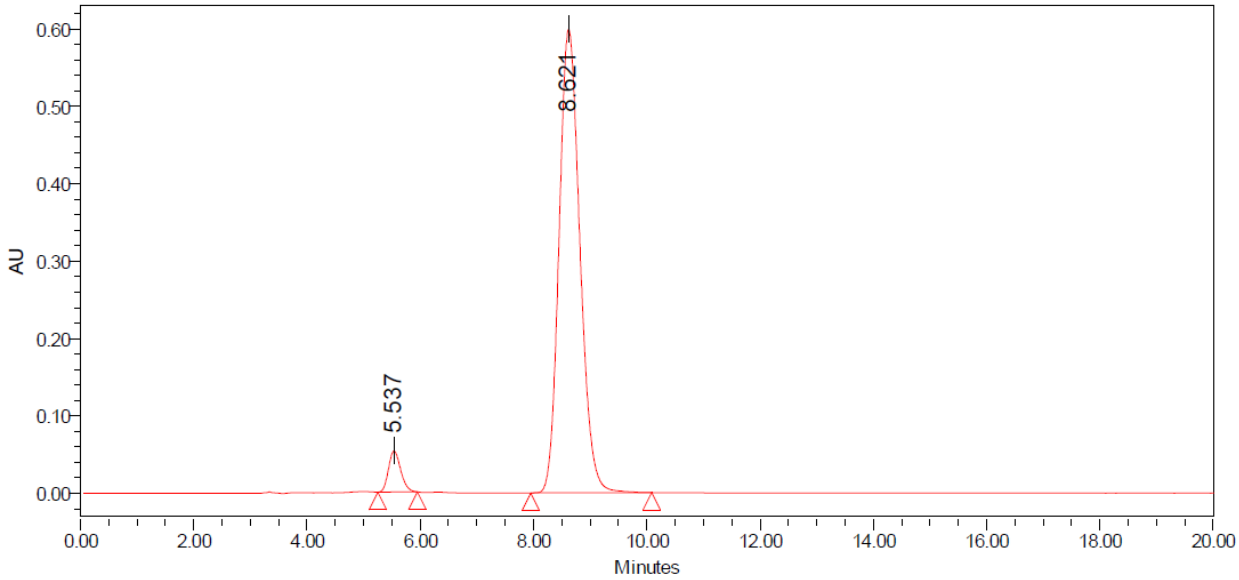

Peak No	RT (min)	Area	Height	% Area
1	5.537	798289	53038	4.95
2	8.621	15332115	599219	95.05

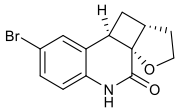

2.29c

Racemic (Daicel CHIRALCEL® OD-H, 70% *i*-PrOH, 30% Hexanes, 1 mL/min, 262.8 nm)

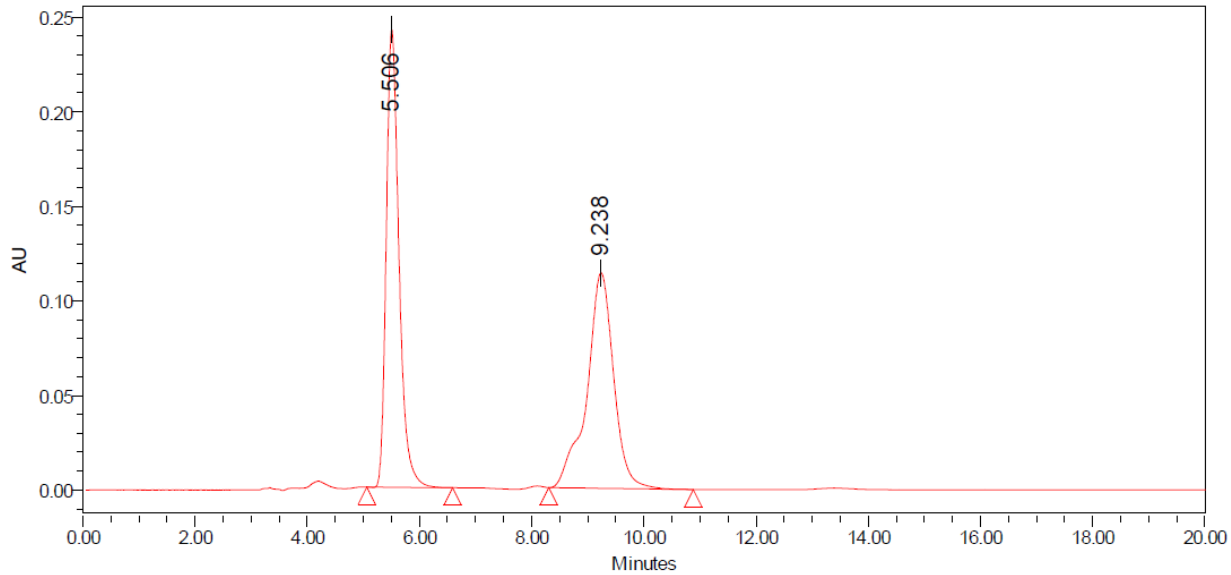

Peak No	RT (min)	Area	Height	% Area
1	5.506	3814752	241922	50.09
2	9.238	3800761	113979	49.91

Enantioenriched

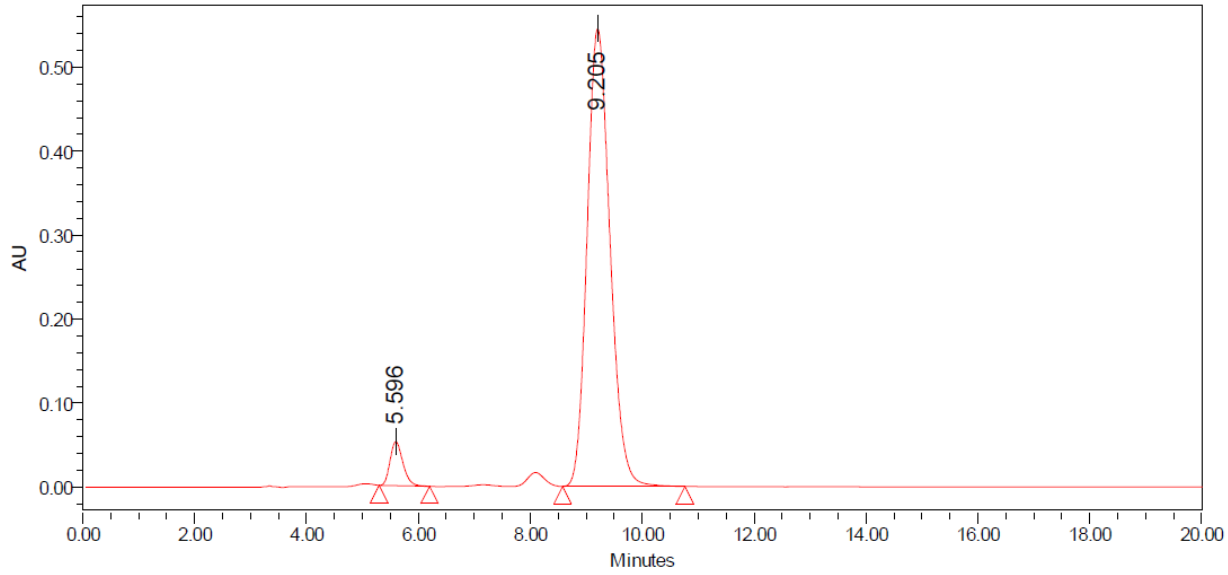

Peak No	RT (min)	Area	Height	% Area
1	5.596	838376	52356	5.15
2	9.205	15445681	544824	94.85

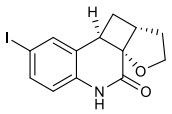

2.29d

Racemic (Daicel CHIRALCEL® OD-H, 70% *i*-PrOH, 30% Hexanes, 1 mL/min, 266.4 nm)

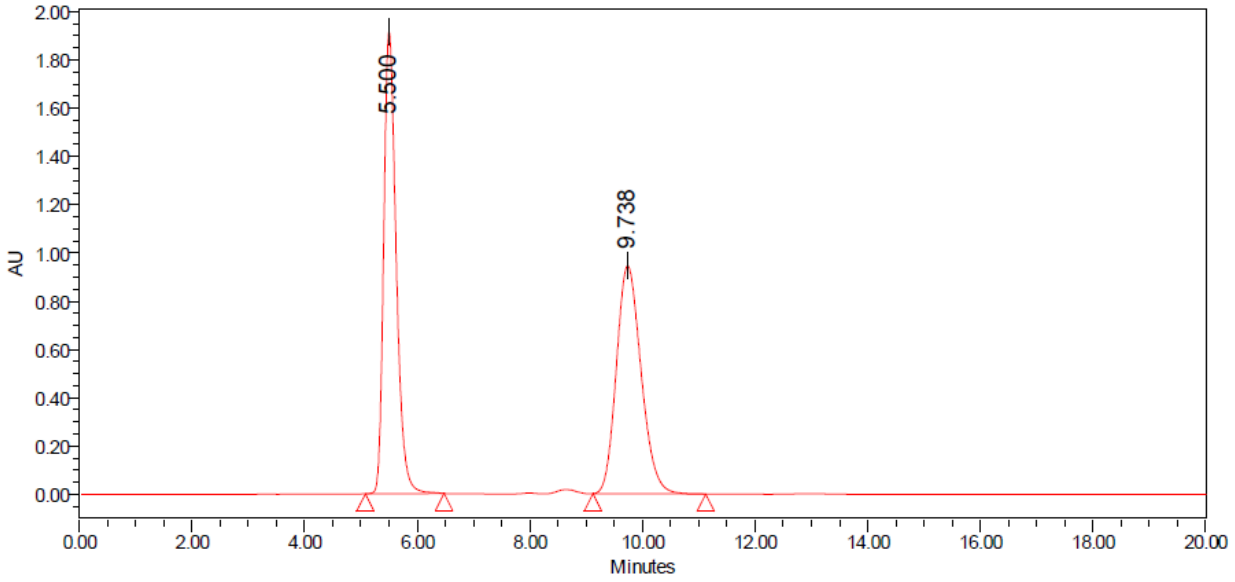

Peak No	RT (min)	Area	Height	% Area
1	5.500	29297259	1912873	50.38
2	9.738	28856648	944476	49.62

Enantioenriched

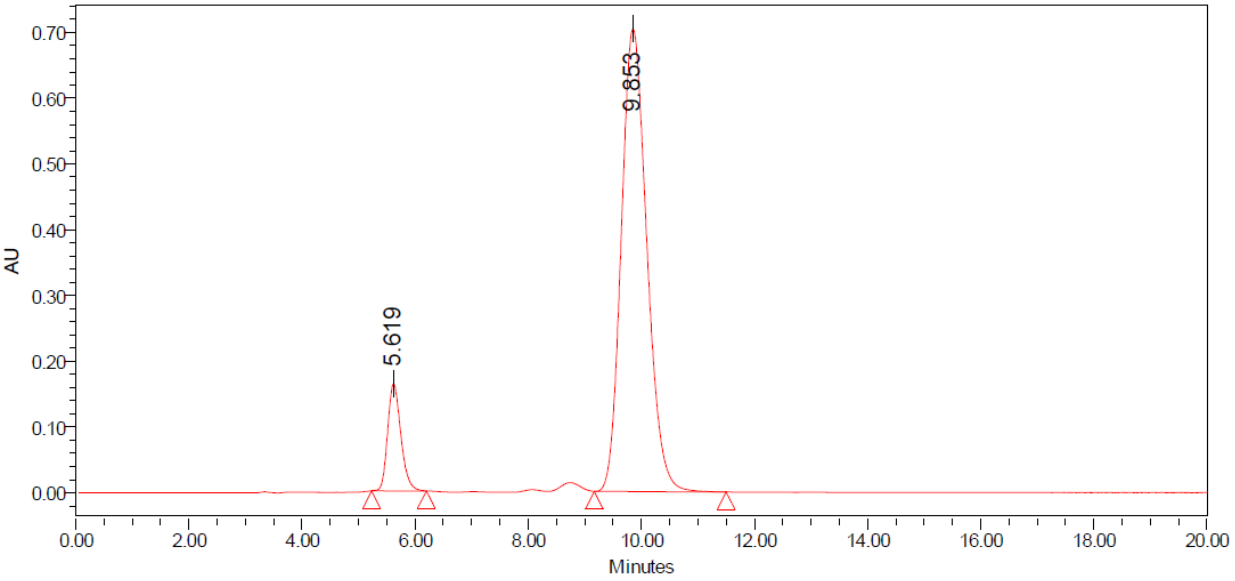

Peak No	RT (min)	Area	Height	% Area
1	5.619	2645705	162791	10.71
2	9.853	22059247	703594	89.29

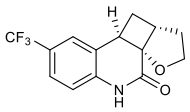

2.29e

Racemic (Daicel CHIRALCEL® OD-H, 70% *i*-PrOH, 30% Hexanes, 1 mL/min, 260.4 nm)

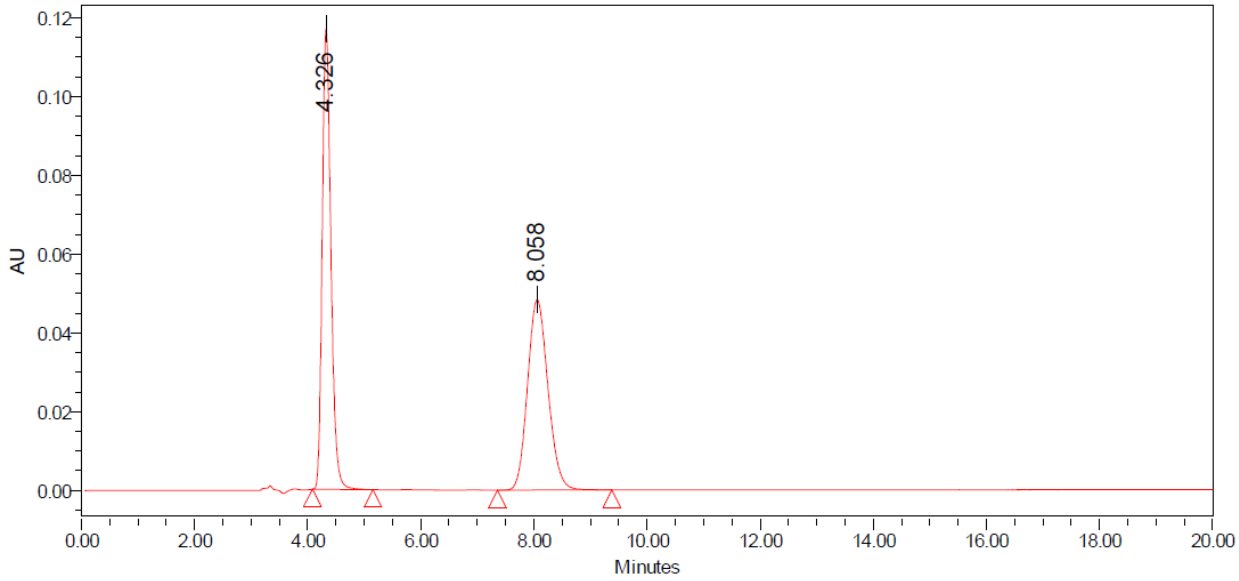

Peak No	RT (min)	Area	Height	% Area
1	4.326	1246759	116782	50.63
2	8.058	1215679	48317	49.37

Enantioenriched

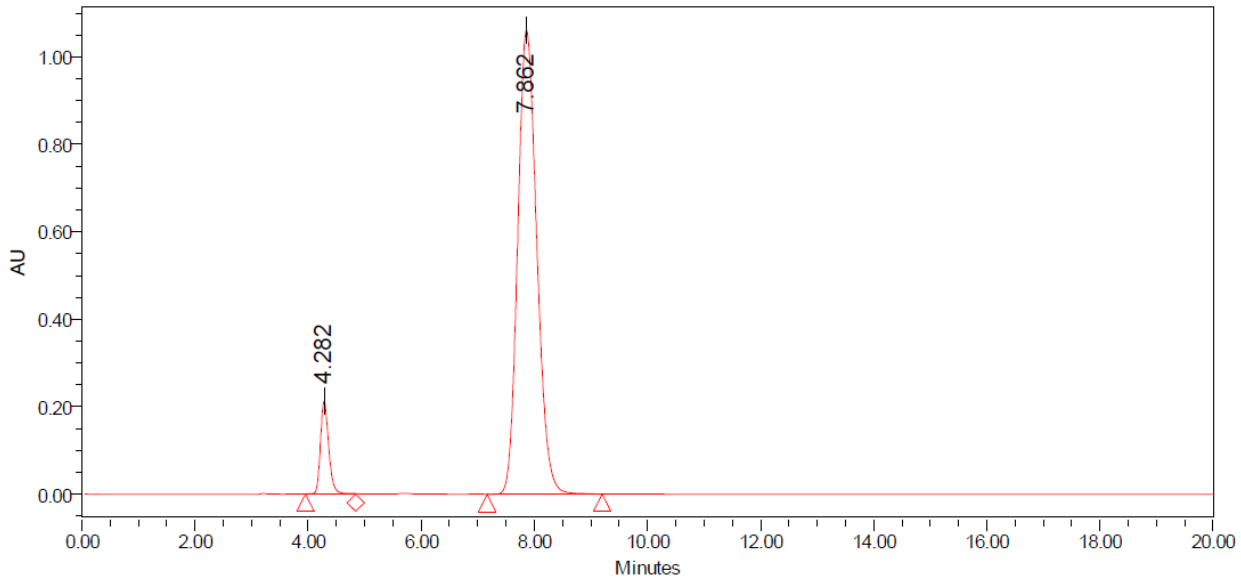

Peak No	RT (min)	Area	Height	% Area
1	4.282	2153077	211873	7.97
2	7.862	24865030	1059840	92.03

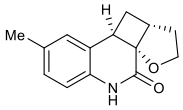

2.29f

Racemic (Daicel CHIRALCEL® OD-H, 70% *i*-PrOH, 30% Hexanes, 1 mL/min, 261.6 nm)

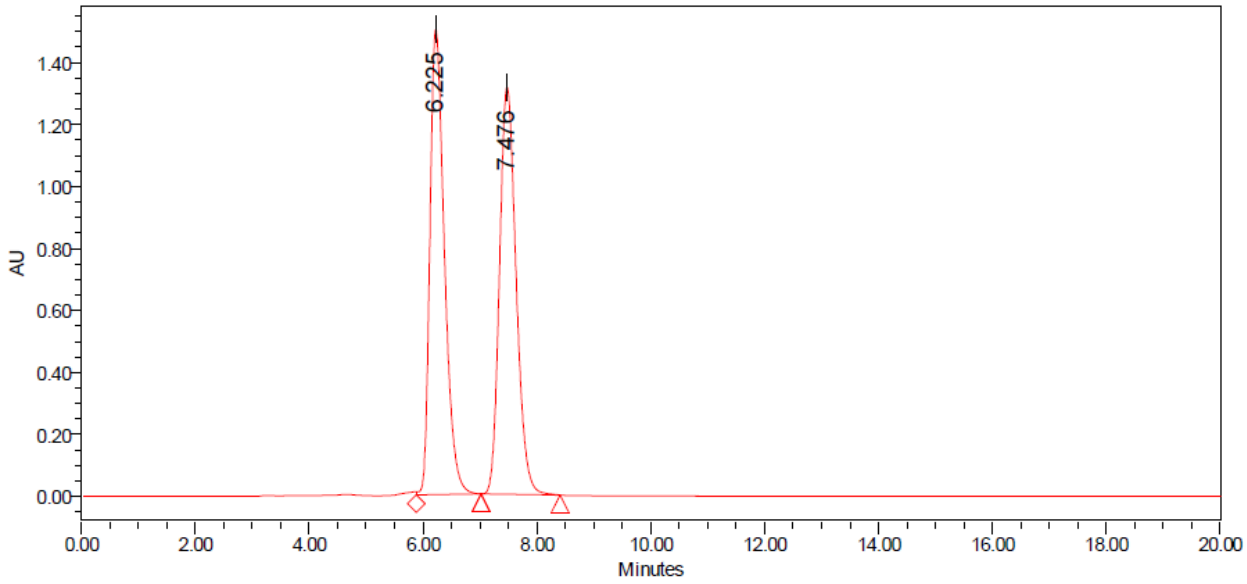

Peak No	RT (min)	Area	Height	% Area
1	6.225	26523909	1502481	49.90
2	7.476	26631499	1314278	50.10

Enantioenriched

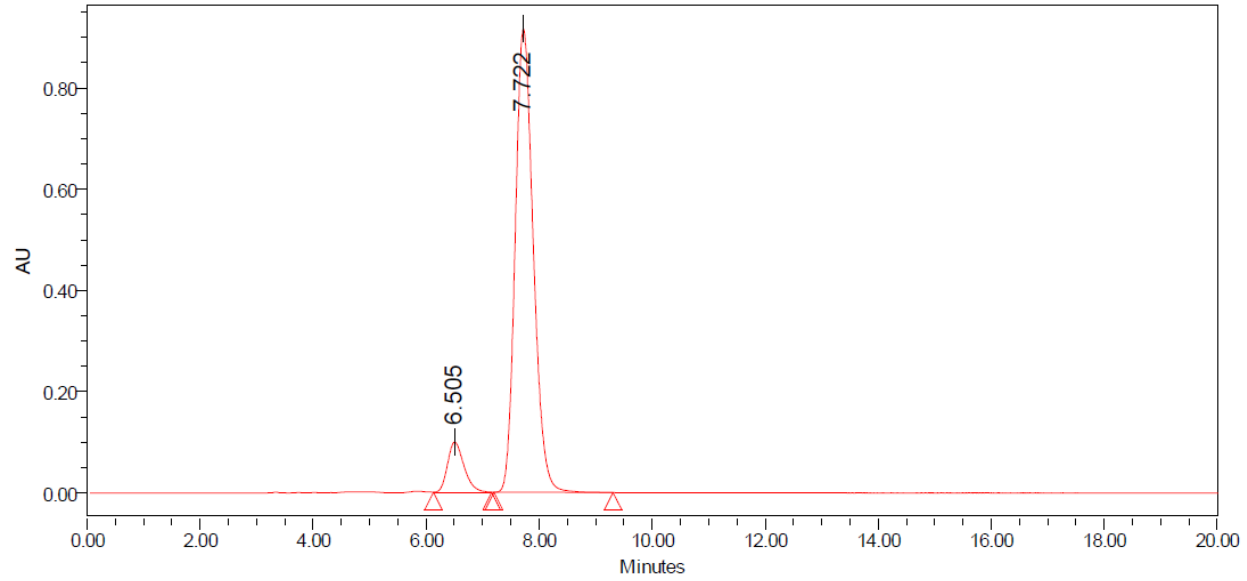

Peak No	RT (min)	Area	Height	% Area
1	6.505	1994677	98766	8.92
2	7.722	20372894	915086	91.08

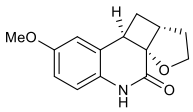

2.29g

Racemic (Daicel CHIRALCEL® OD-H, 70% *i*-PrOH, 30% Hexanes, 1 mL/min, 265.2 nm)

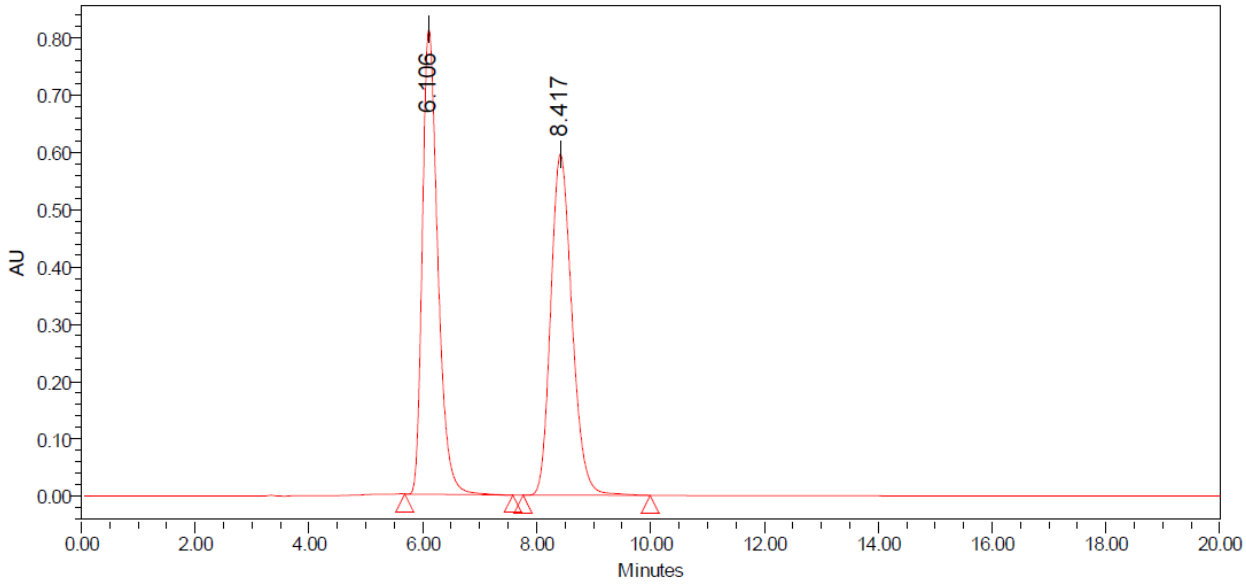

Peak No	RT (min)	Area	Height	% Area
1	6.106	15286501	811627	49.73
2	8.417	15450210	595676	50.27

Enantioenriched

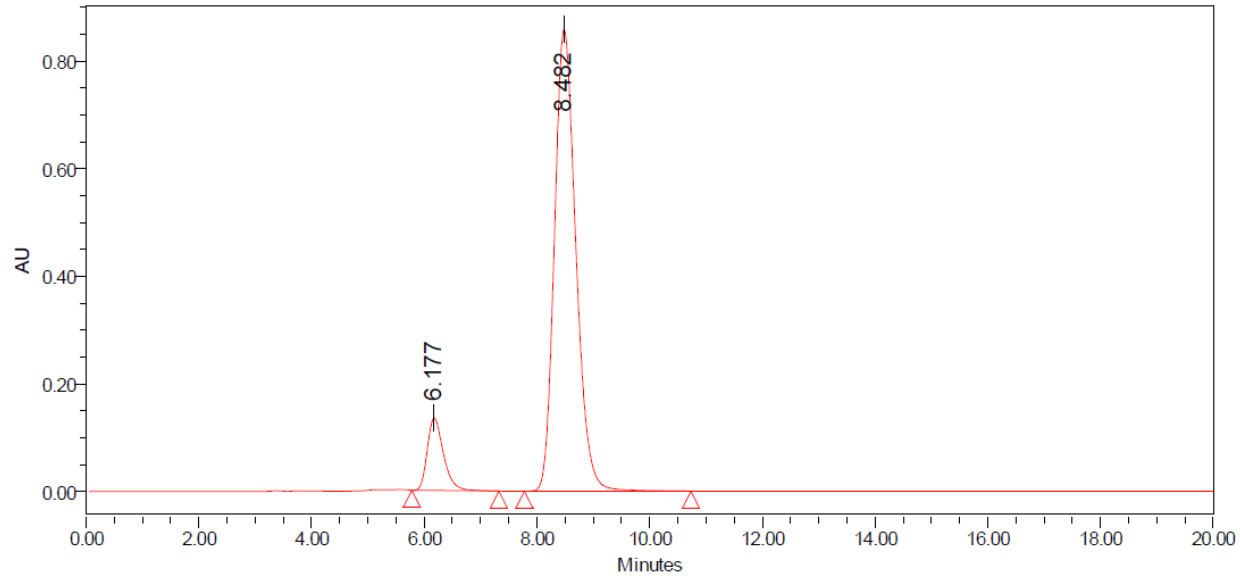

Peak No	RT (min)	Area	Height	% Area
1	6.177	2681624	134584	10.59
2	8.482	22636230	858220	89.41

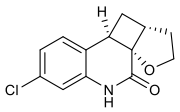

2.29h

Racemic (Daicel CHIRALCEL® OD-H, 70% *i*-PrOH, 30% Hexanes, 1 mL/min, 261.6 nm)

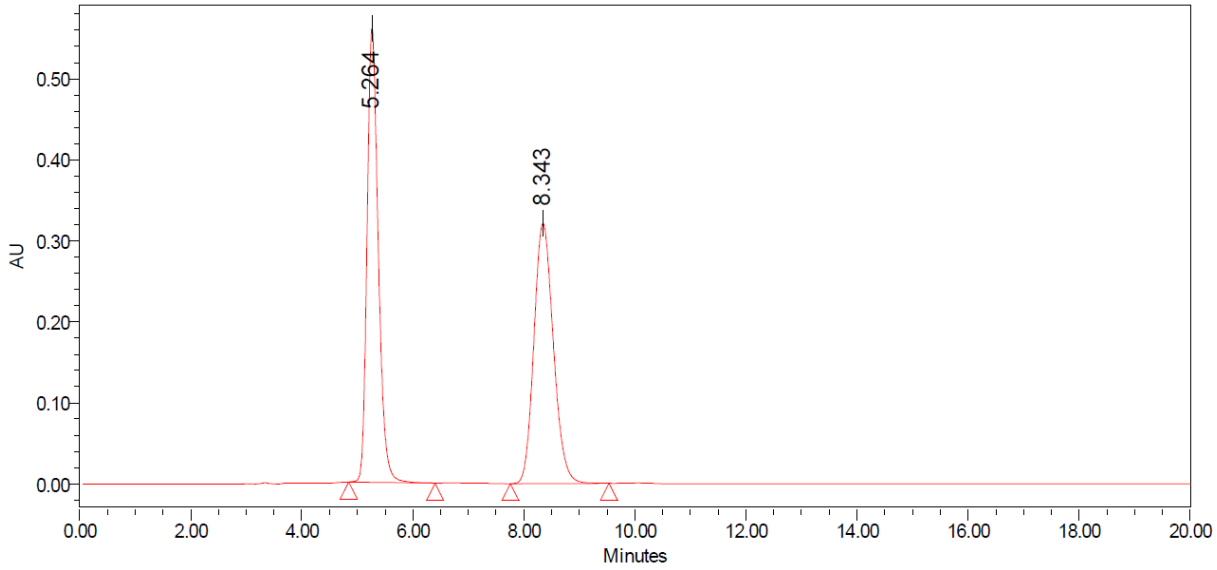

Peak No	RT (min)	Area	Height	% Area
1	5.264	7856093	560482	50.20
2	8.343	7792066	321217	49.80

Enantioenriched

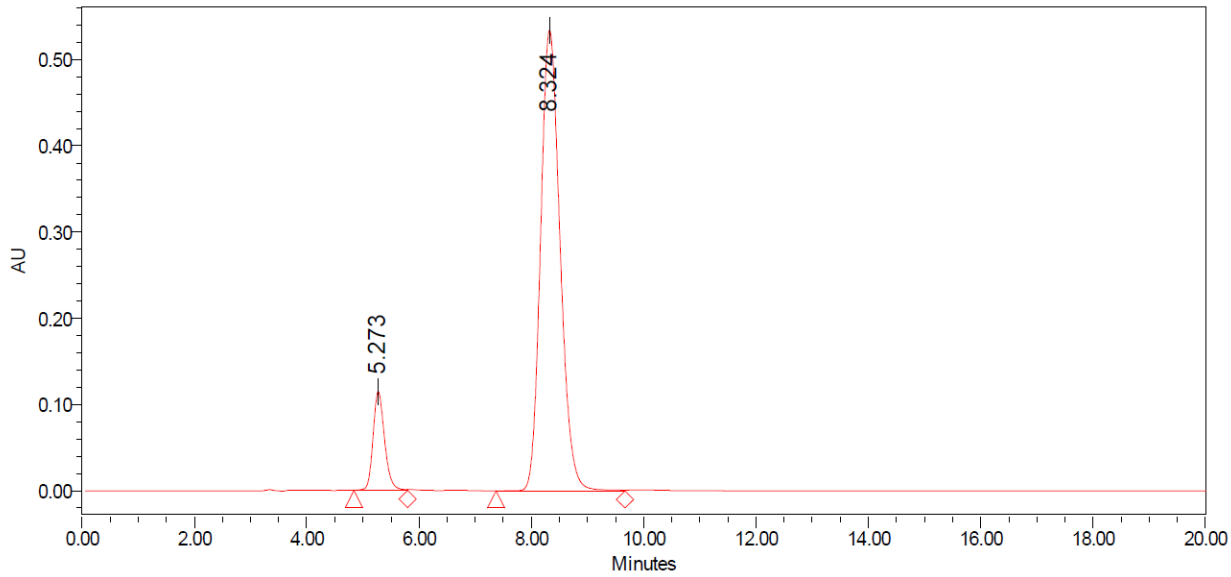

Peak No	RT (min)	Area	Height	% Area
1	5.273	1629790	114551	11.28
2	8.324	12822532	533911	88.72

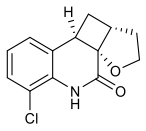

2.29i

Racemic (Daicel CHIRALCEL® OD-H, 70% *i*-PrOH, 30% Hexanes, 1 mL/min, 258.1 nm)

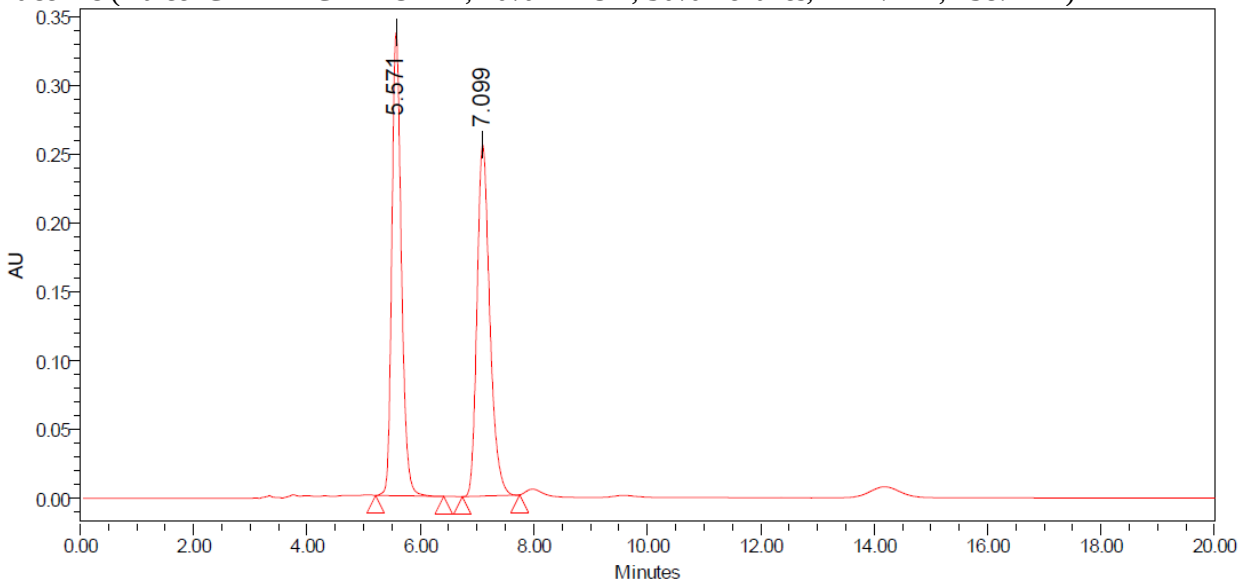

Peak No	RT (min)	Area	Height	% Area
1	5.571	3910910	336288	49.53
2	7.099	3985829	255115	50.47

Enantioenriched

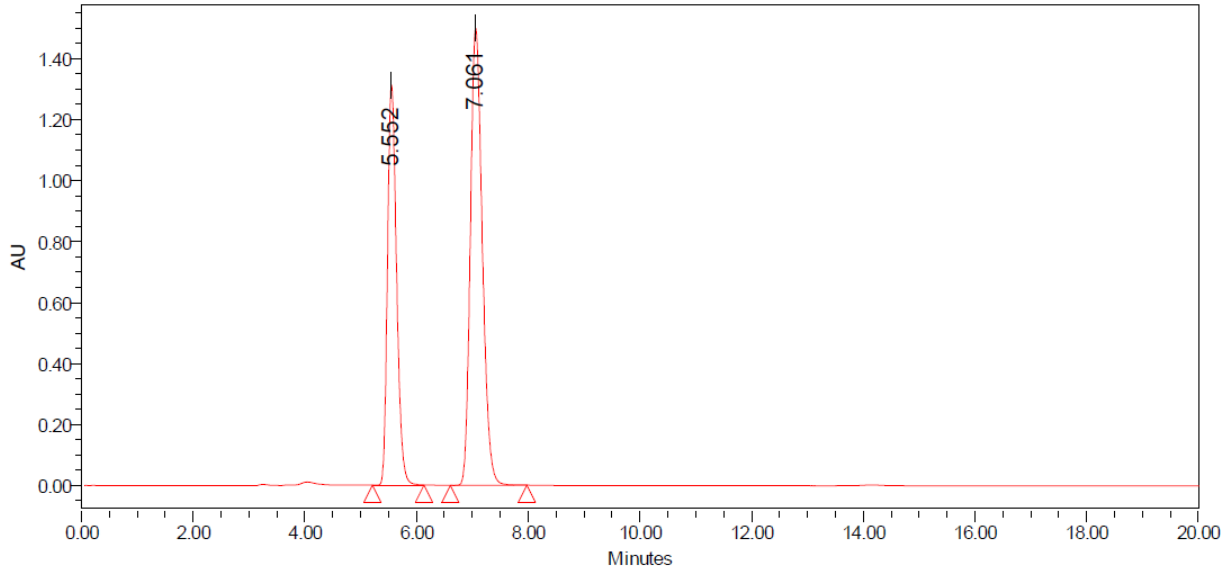

Peak No	RT (min)	Area	Height	% Area
1	5.552	14785623	1312608	39.92
2	7.061	22253299	1499346	60.08

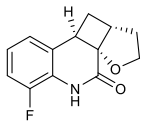

2.29j

Racemic (Daicel CHIRALCEL® OD-H, 70% *i*-PrOH, 30% Hexanes, 1 mL/min, 253.3 nm)

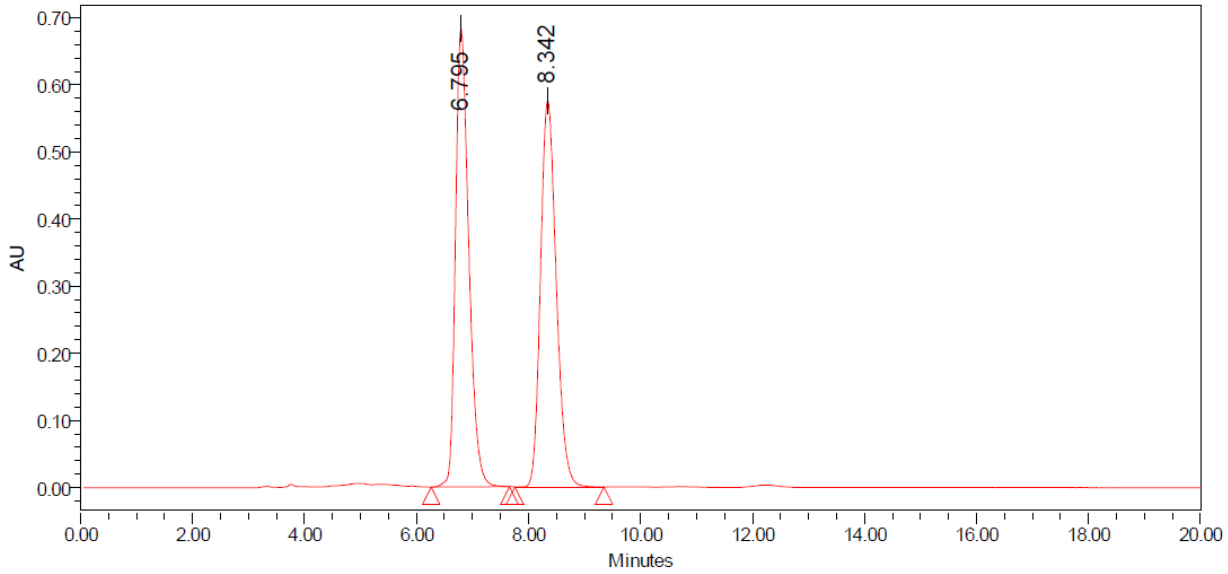

Peak No	RT (min)	Area	Height	% Area
1	6.795	11271325	682039	50.23
2	8.342	11167558	574700	49.77

Enantioenriched

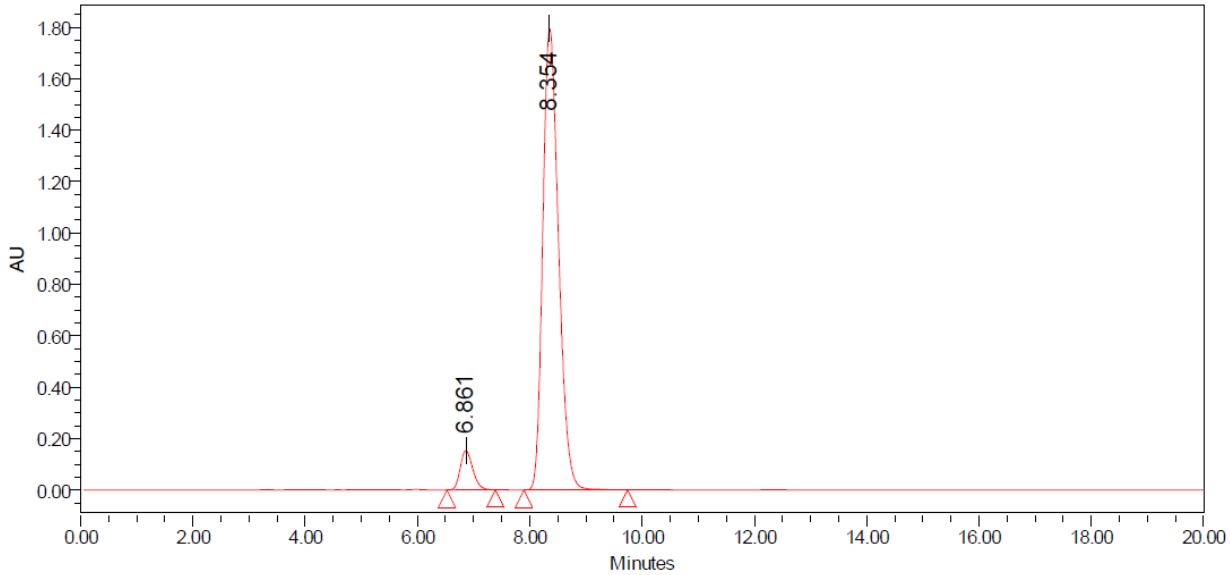

Peak No	RT (min)	Area	Height	% Area
1	6.861	2385252	153465	6.41
2	8.354	34818752	1793459	93.59

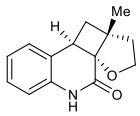

2.29m

Racemic (Daicel CHIRALCEL® OD-H, 70% *i*-PrOH, 30% Hexanes, 1 mL/min, 258.1 nm)

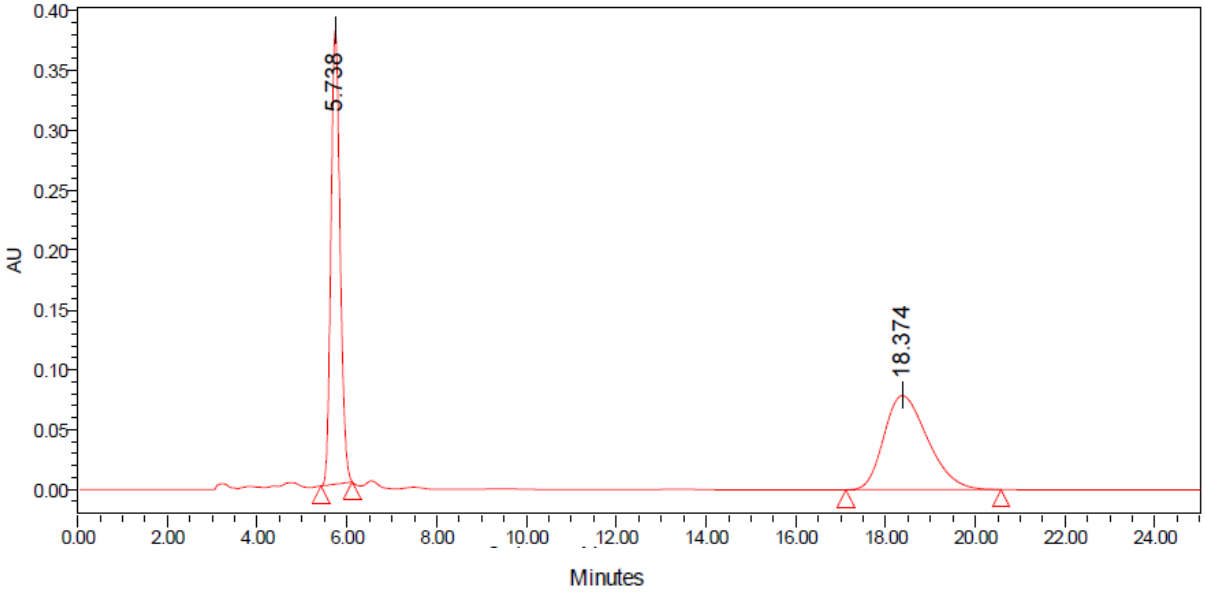

Peak No	RT (min)	Area	Height	% Area
1	5.738	5365063	379260	50.21
2	18.374	5320245	78632	49.78

Enantioenriched

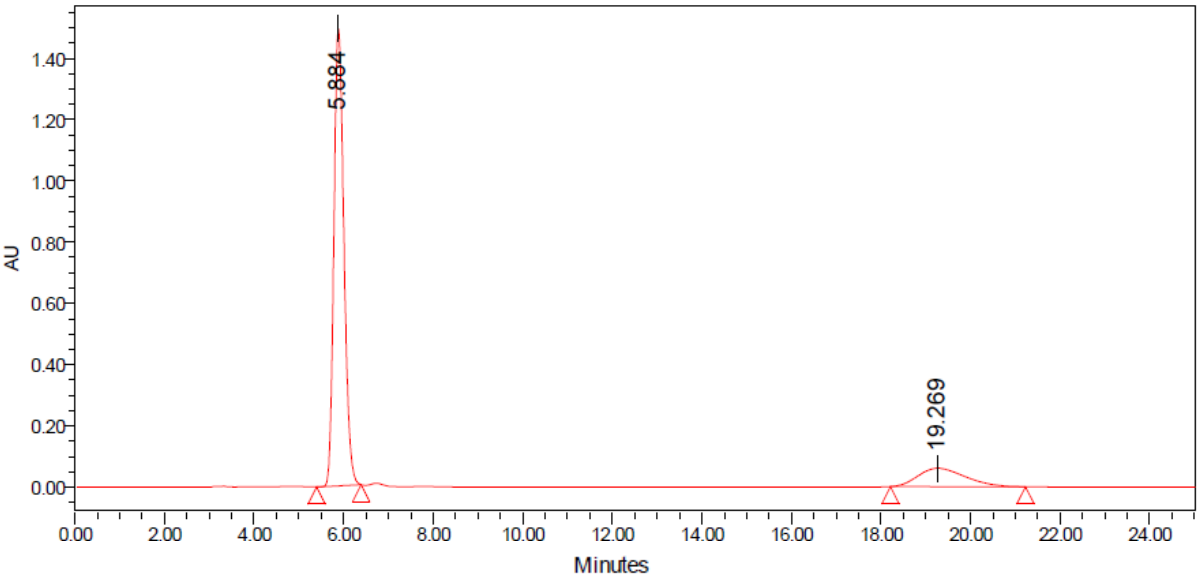

Peak No	RT (min)	Area	Height	% Area
1	5.884	23264485	1493371	84.04
2	19.269	4418706	59981	15.96

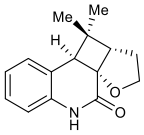

2.29n

Racemic (Daicel CHIRALCEL® OD-H, 70% *i*-PrOH, 30% Hexanes, 1 mL/min, 259.3 nm)

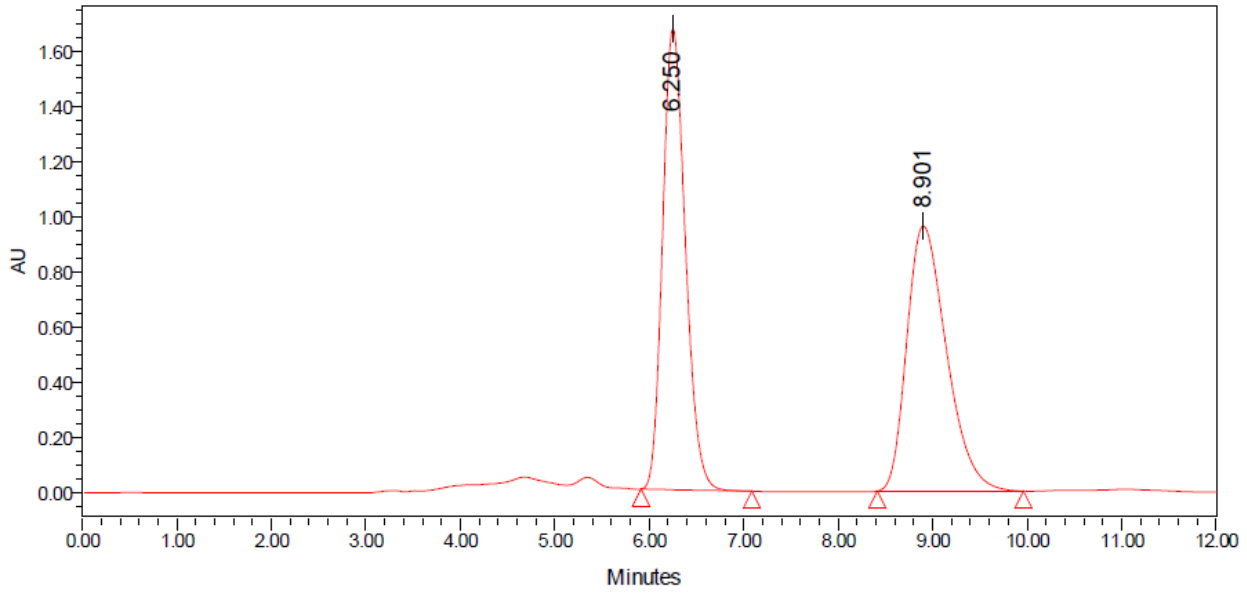

Peak No	RT (min)	Area	Height	% Area
1	6.250	27847373	1669053	49.86
2	8.901	28007810	960398	50.14

Enantioenriched

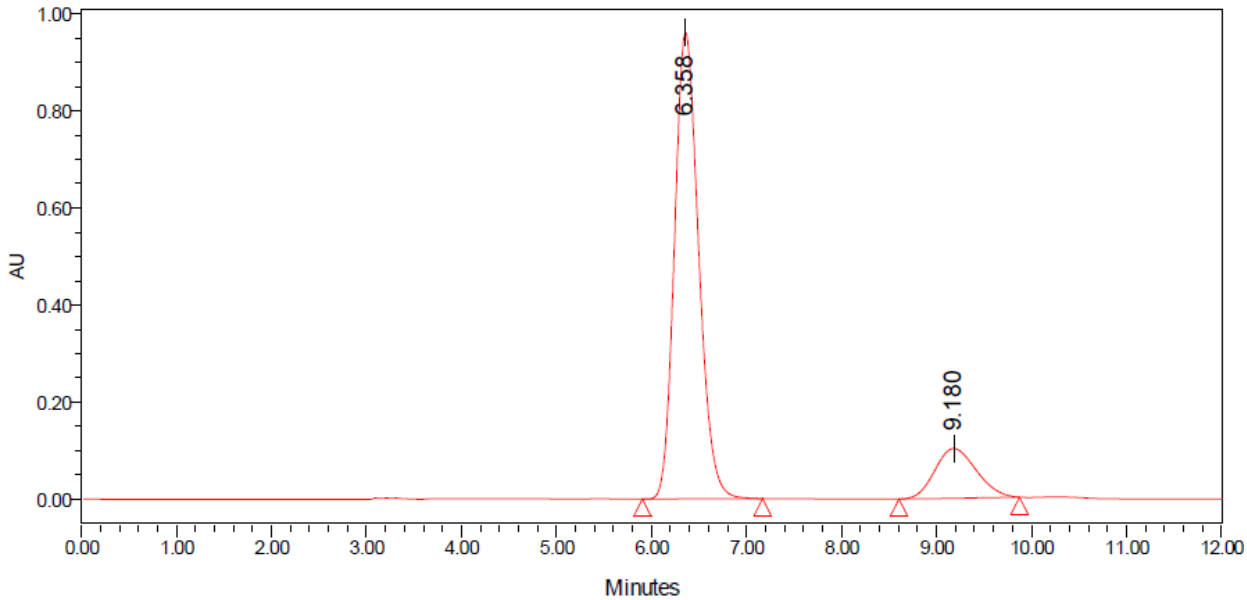

Peak No	RT (min)	Area	Height	% Area
1	6.358	16905672	960550	84.50
2	9.180	3100832	102239	15.50

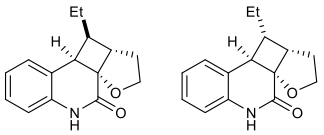

2.29o (from (*E*)-**2.28o**)

Racemic (Daicel CHIRALCEL® OD-H, 10% *i*-PrOH, 90% MTBE, 1 mL/min, 256.9 nm)

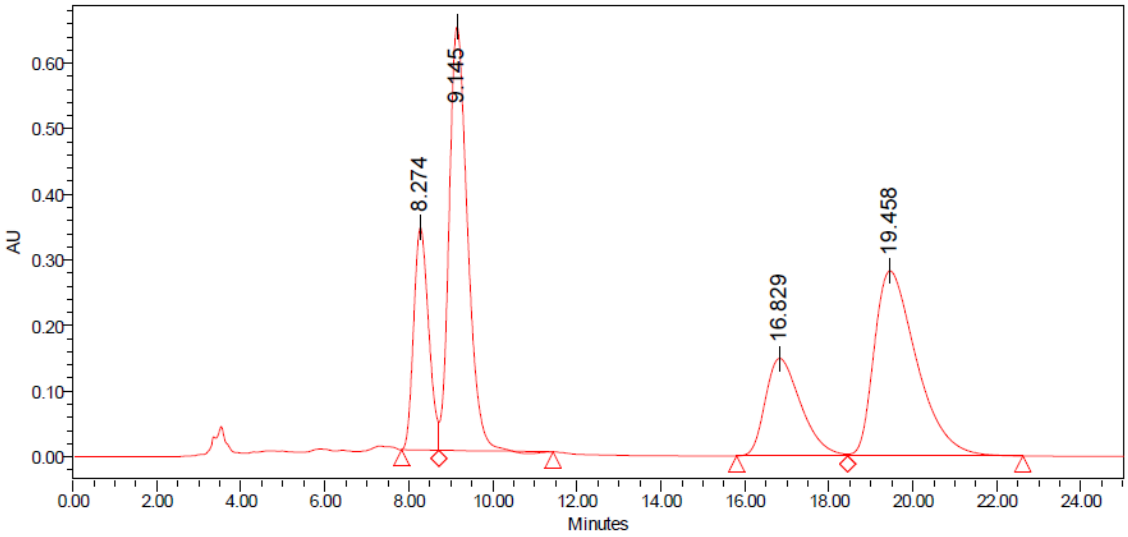

Peak No	RT (min)	Area	Height	% Area
1	8.274	8392993	338867	14.80
2	9.145	19747664	646227	34.82
3	16.829	8750623	148832	15.43
4	19.458	19827835	282181	34.96

Enantioenriched

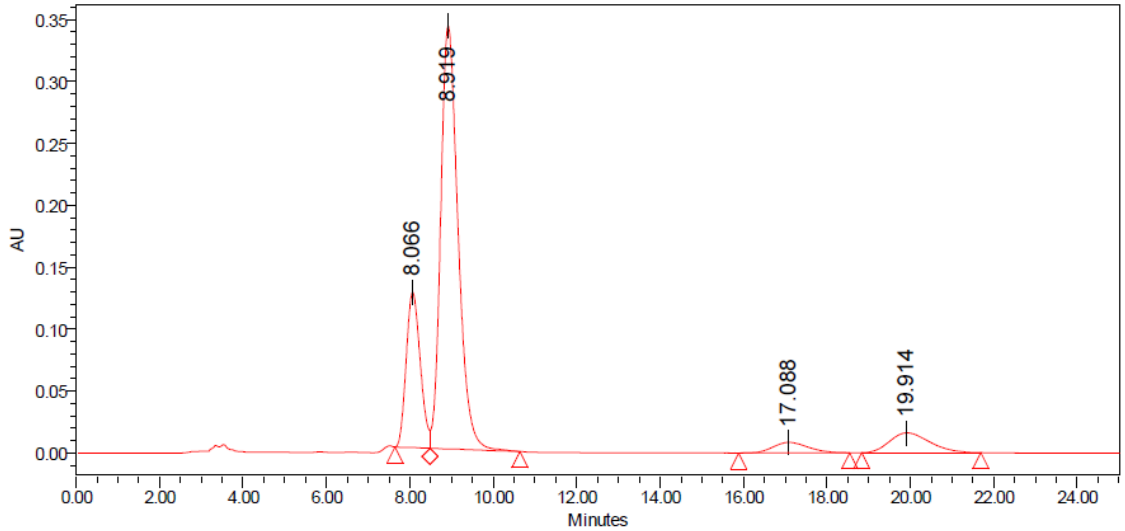

Peak No	RT (min)	Area	Height	% Area
1	8.066	2921893	125406	20.37
2	8.919	341672	68.70	34.82
3	17.088	497220	8468	3.47
4	19.914	1070025	16007	7.46

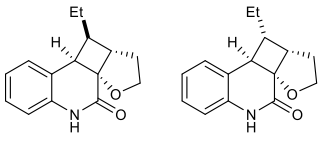

2.29o (from (*Z*)-**2.28o**)

Racemic (Daicel CHIRALCEL® OD-H, 10% *i*-PrOH, 90% MTBE, 1 mL/min, 256.9 nm)

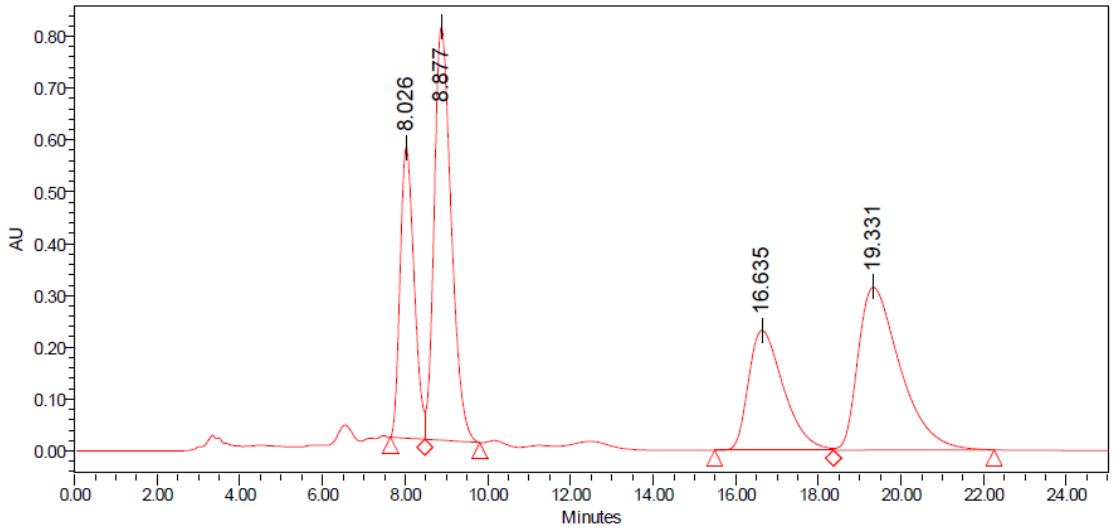

Peak No	RT (min)	Area	Height	% Area
1	8.026	13172874	560564	18.35
2	8.877	22877589	797603	31.86
3	16.635	13582896	231171	18.92
4	19.331	22168081	314225	30.87

Enantioenriched

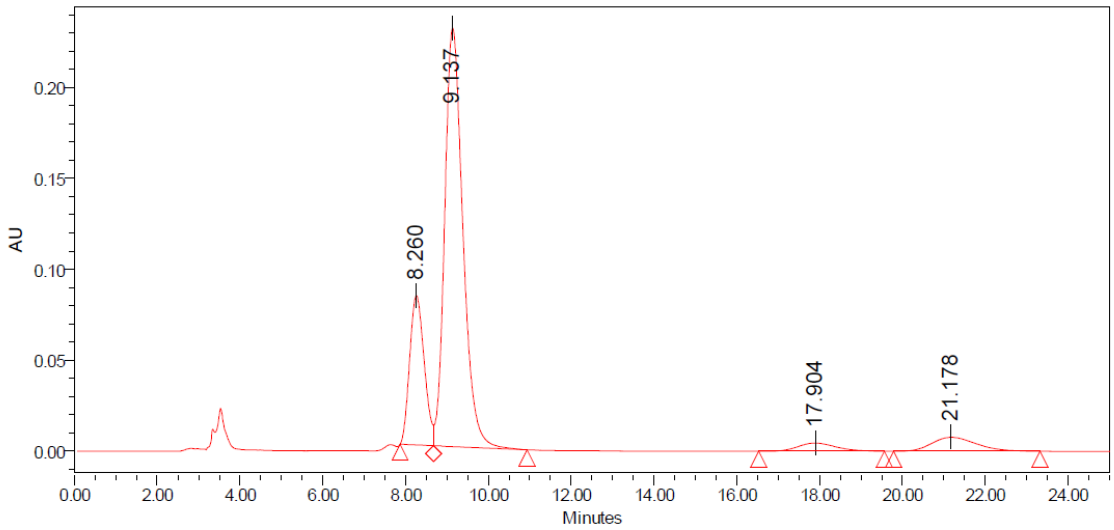

Peak No	RT (min)	Area	Height	% Area
1	8.260	2003433	82110	20.30
2	9.137	7008372	230163	71.02
3	17.904	285844	4441	2.90
4	21.178	570634	7681	5.78

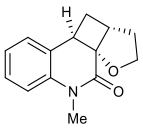

2.29k

Racemic (Daicel CHIRALCEL® OD-H, 70% *i*-PrOH, 30% Hexanes, 1 mL/min, 260.4 nm)

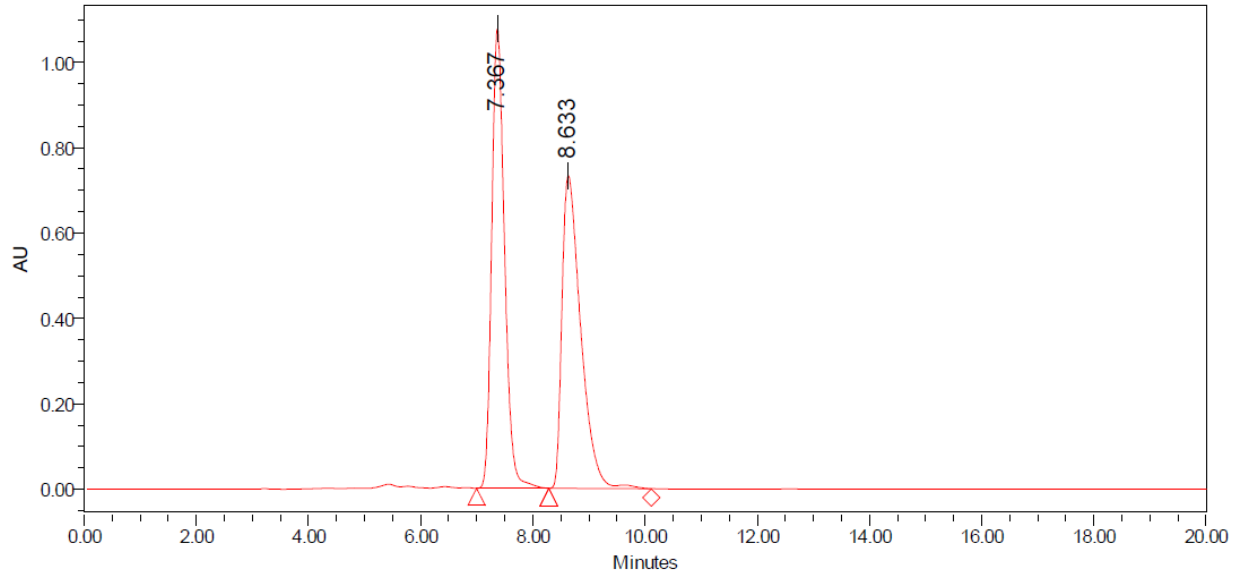

Peak No	RT (min)	Area	Height	% Area
1	7.367	17114233	1075823	50.07
2	8.633	17068252	732528	49.93

Enantioenriched

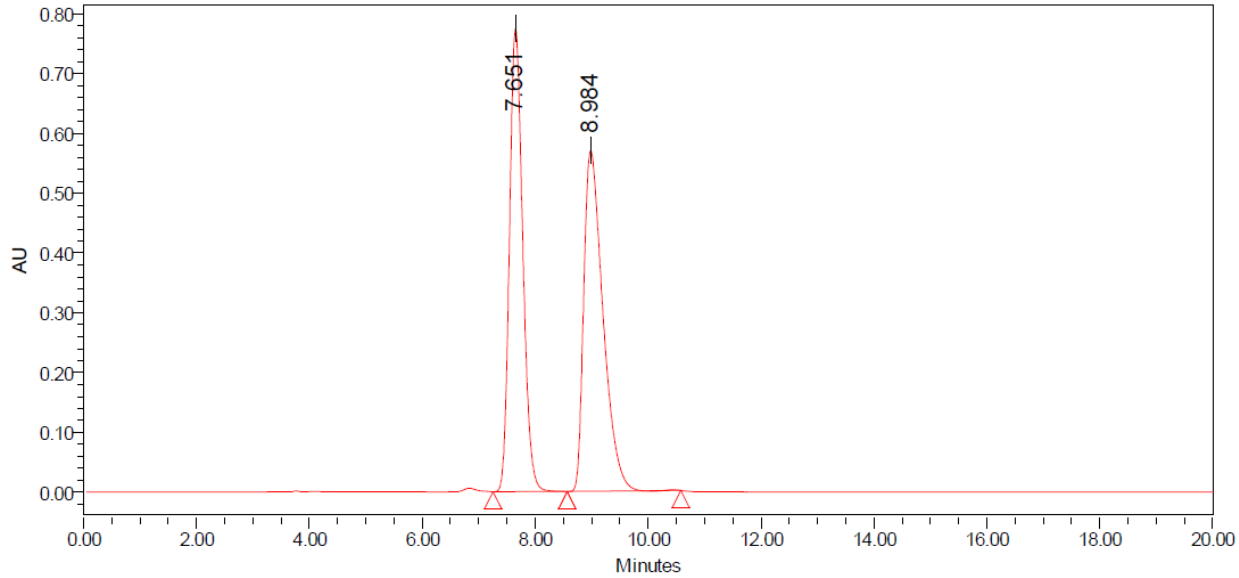

Peak No	RT (min)	Area	Height	% Area
1	7.651	12713546	774282	48.48
2	8.984	13508529	569763	51.52

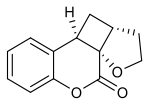

2.29l

Racemic (Daicel CHIRALCEL® OD-H, 70% *i*-PrOH, 30% Hexanes, 1 mL/min, 277.1 nm)

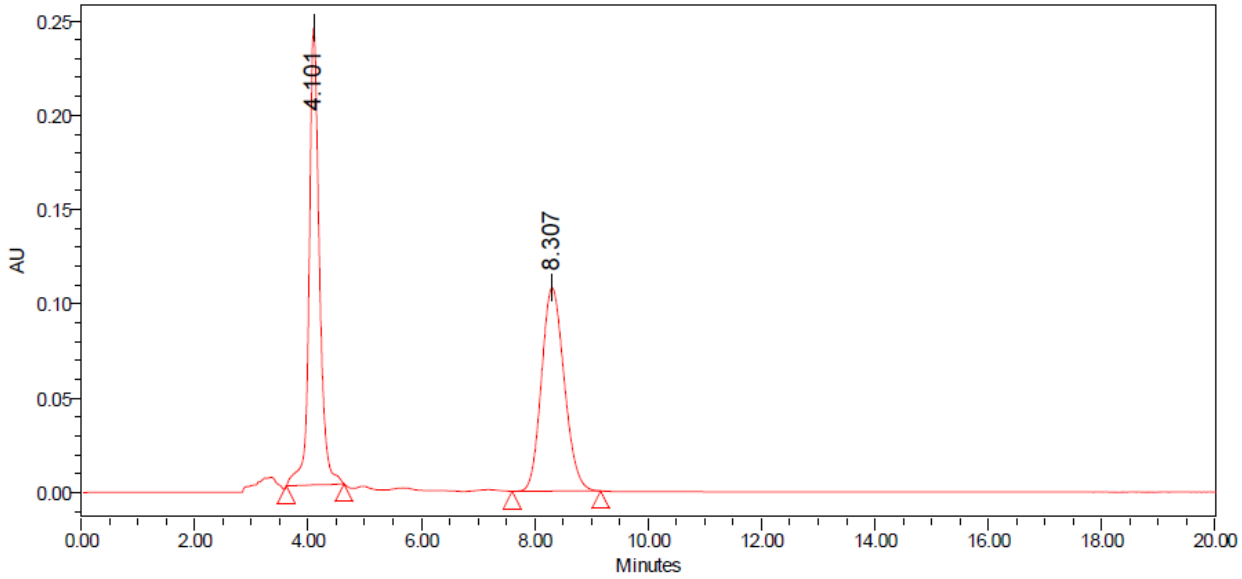

Peak No	RT (min)	Area	Height	% Area
1	4.101	3053759	242367	50.39
2	8.307	3006521	107818	49.61

Enantioenriched

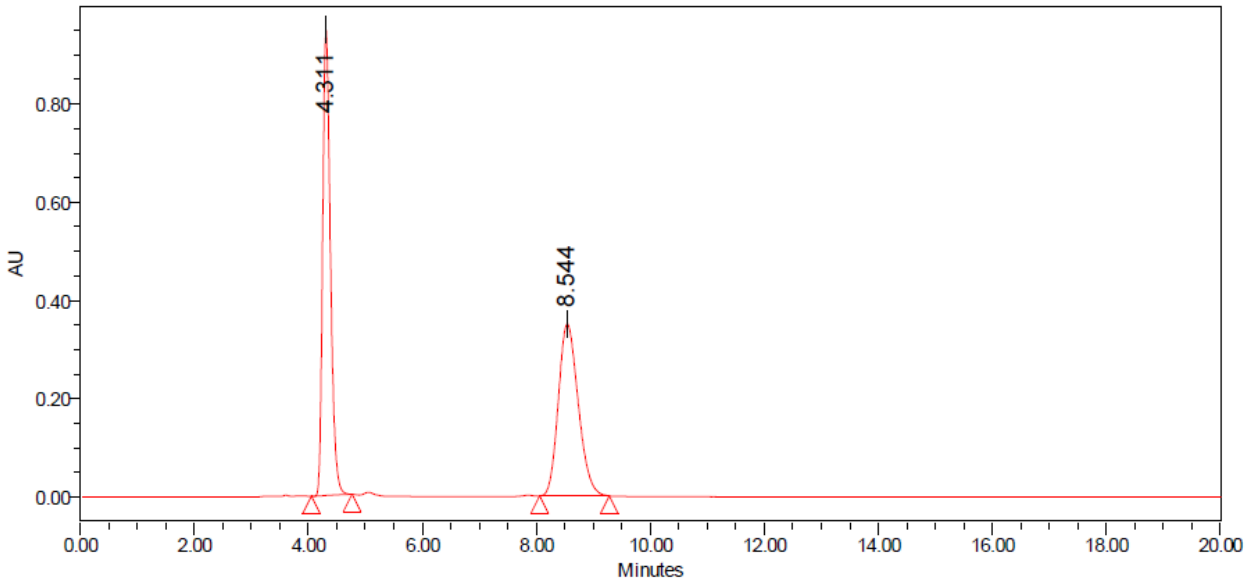

Peak No	RT (min)	Area	Height	% Area
1	4.311	8958208	948218	51.33
2	8.544	8492978	350194	48.67

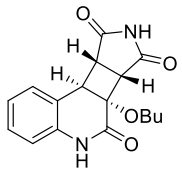

3.27a

Racemic (HPLC, Daicel CHIRALPAK® AD-H, Gradient 5% iPrOH (95% Hexane) to 40% iPrOH (60% Hexane), 1.0 mL/min)

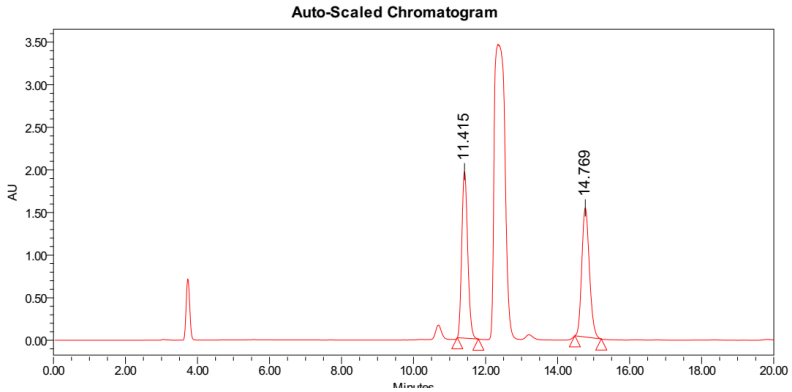

Peak Results

	RT	Area	Height	% Area
1	11.415	22356786	1953516	50.09
2	14.769	22280382	1515989	49.91

Enantioenriched

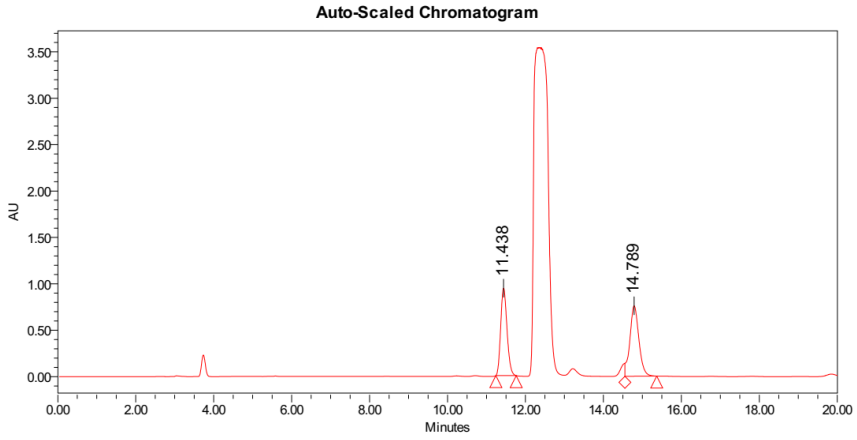

Peak Results

	Name	RT	% Area	Area	Height	Amount	Units
1		11.438	46.38	10562264	941755		
2		14.789	53.62	12213120	759237		

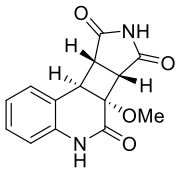

3.27b

Racemic (HPLC, Daicel CHIRALPAK®OD-H, Gradient 5% iPrOH (95% Hexane) to 40% iPrOH (60% Hexane), 1.0 mL/min)

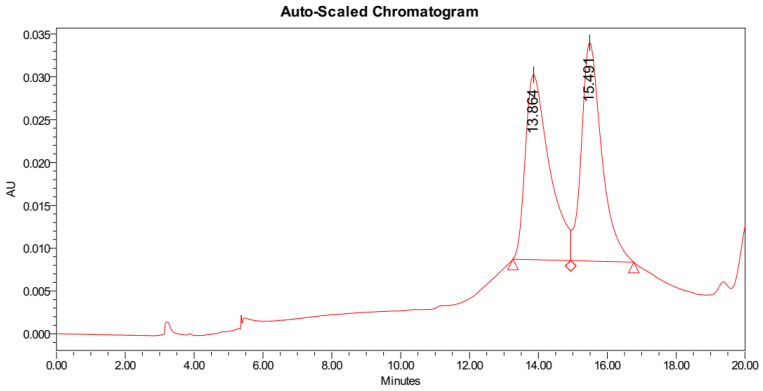

Peak Results

	Name	RT	% Area	Area	Height	Amount	Units
1		13.864	50.01	1051987	21593		
2		15.491	49.99	1051664	25490		

Enantioenriched

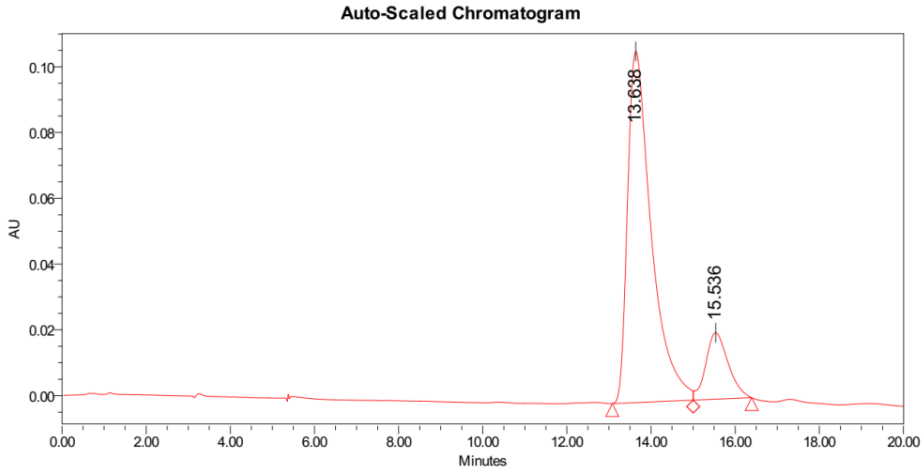

Peak Results

	Name	RT	% Area	Area	Height	Amount	Units
1		13.638	84.81	4189844	106765		
2		15.536	15.19	750234	20224		

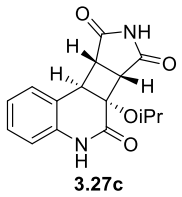

3.27c

Racemic (Daicel CHIRALPAK® AD-H, isocratic 20% MeOH, 3.0 mL/min)

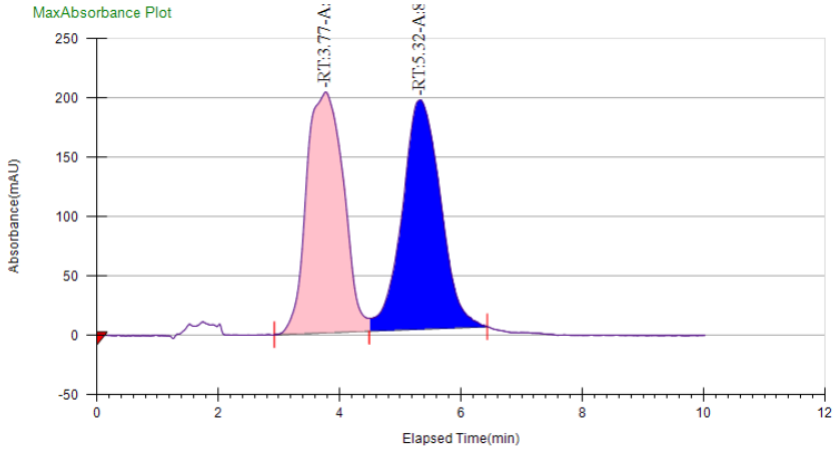

Peak Information

Peak No	% Area	Area	Ret. Time	Height	Cap. Factor
1	50.2078	8546.8427	3.77 min	202.8821	3773.95
2	49.7922	8476.0871	5.32 min	193.2605	5323.9333

Enantioenriched

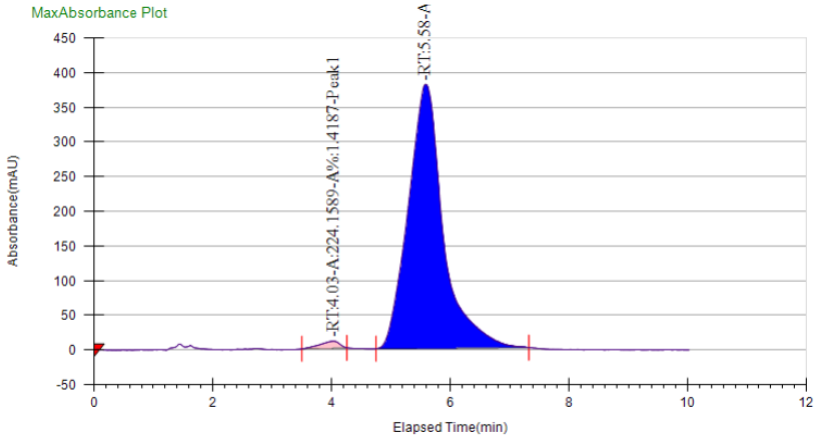

Peak Information

Peak No	% Area	Area	Ret. Time	Height	Cap. Factor
1	1.4187	224.1589	4.03 min	10.0525	4032.2833
2	98.5813	15575.8887	5.58 min	380.7977	5582.25

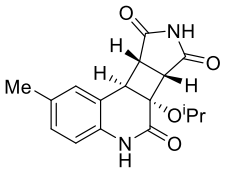

3.27e

Racemic (Daicel CHIRALPAK® OJ-H, isocratic 20% MeOH, 3.0 mL/min)

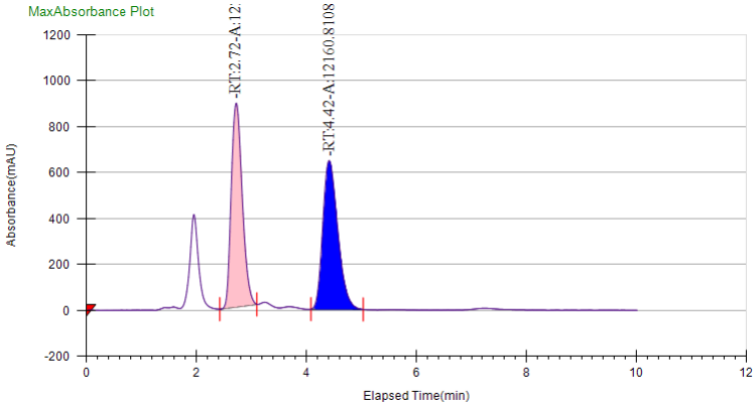

Peak Information

Peak No	% Area	Area	Ret. Time	Height	Cap. Factor
1	50.0965	12207.8381	2.72 min	889.3199	0
2	49.9035	12160.8108	4.42 min	647.833	0

Enantioenriched

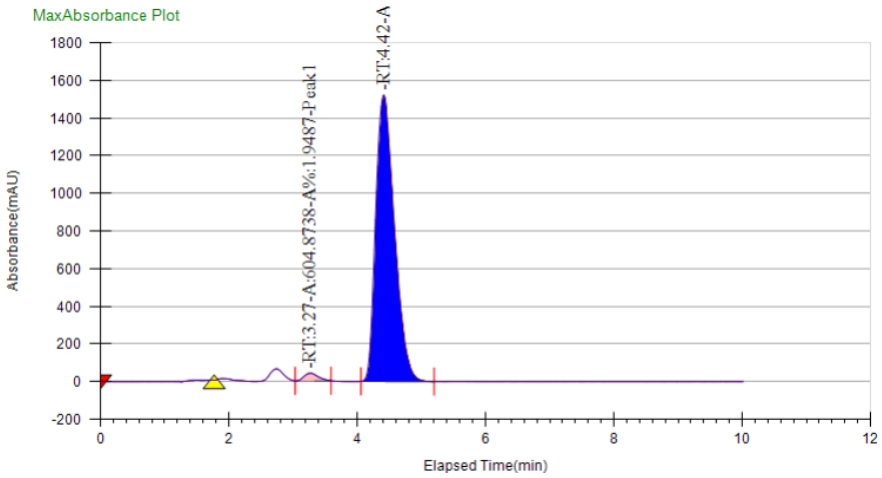

Peak Information

Peak No	% Area	Area	Ret. Time	Height	Cap. Factor
1	1.9487	604.8738	3.27 min	40.7334	3273.95
2	98.0513	30435.7324	4.42 min	1519.2618	4415.6

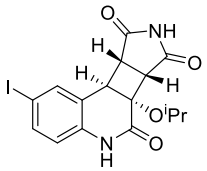

3.27f

Racemic (Daicel CHIRALPAK® OD-H, isocratic 20% MeOH, 3.0 mL/min)

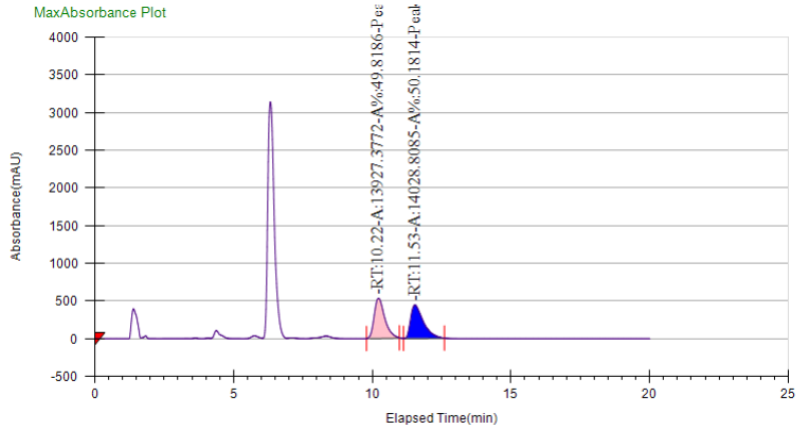

Peak Information

Peak No	% Area	Area	Ret. Time	Height	Cap. Factor
1	49.8186	13927.3772	10.22 min	532.1485	10223.85
2	50.1814	14028.8085	11.53 min	443.0015	11532.1667

Enantioenriched

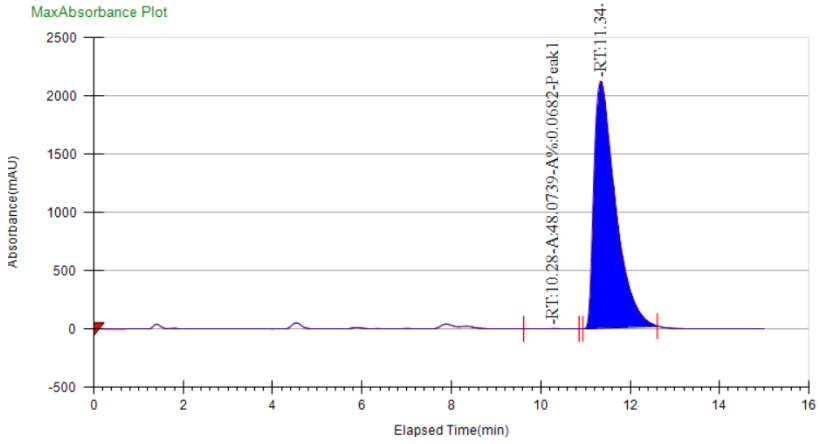

Peak Information

Peak No	% Area	Area	Ret. Time	Height	Cap. Factor
1	0.0682	48.0739	10.28 min	1.9283	10282.1833
2	99.9318	70486.7238	11.34 min	2120.3538	11340.5

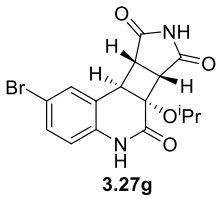

3.27g

Racemic (Daicel CHIRALPAK® OD-H, isocratic 20% MeOH, 3.0 mL/min)

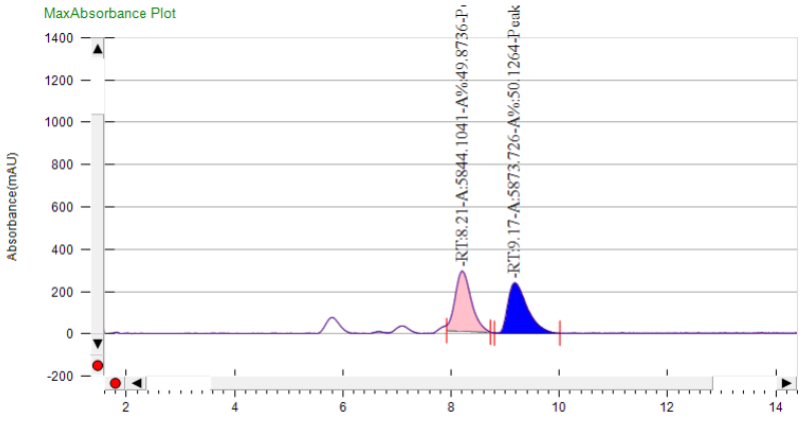

Peak Information

Peak No	% Area	Area	Ret. Time	Height	Cap. Factor
1	49.8736	5844.1041	8.21 min	283.9236	8207.2167
2	50.1264	5873.726	9.17 min	238.1279	9173.8667

Enantioenriched

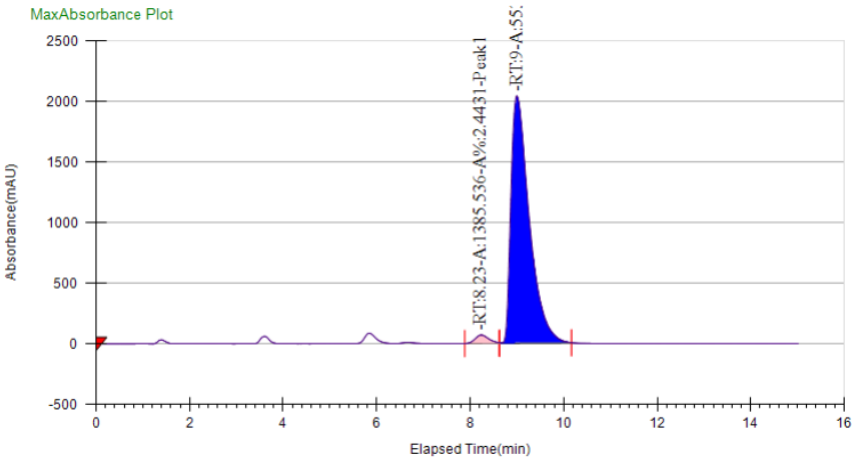

Peak Information

Peak No	% Area	Area	Ret. Time	Height	Cap. Factor
1	2.4431	1385.536	8.23 min	69.7019	8232.2167
2	97.5569	55327.6548	9 min	2040.8461	8998.8667

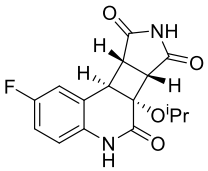

3.27h

Racemic (Daicel CHIRALPAK® OJ-H, isocratic 20% MeOH, 3.0 mL/min)

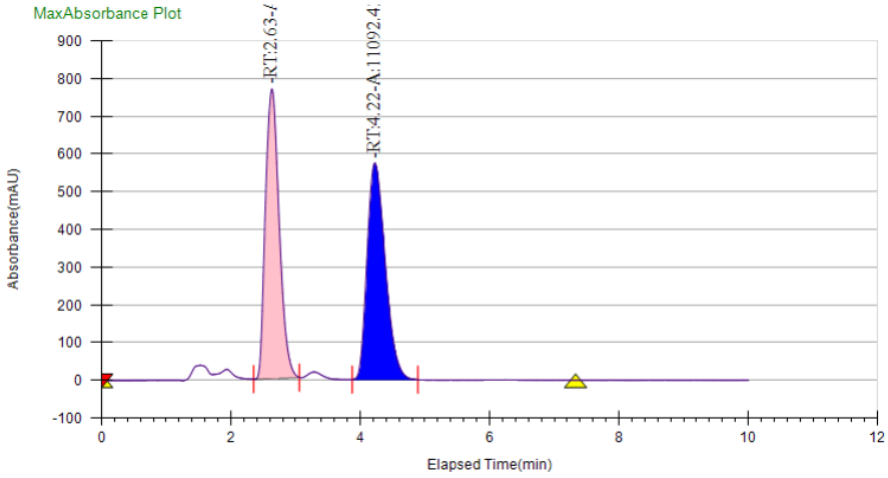

Peak Information

Peak No	% Area	Area	Ret. Time	Height	Cap. Factor
1	50.3347	11241.9581	2.63 min	767.9485	2632.3
2	49.6653	11092.4392	4.22 min	574.149	4223.95

Enantioenriched

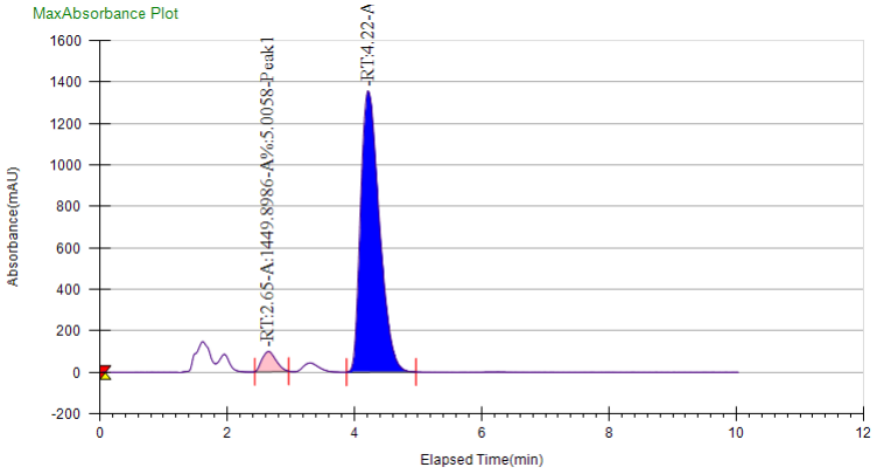

Peak Information

Peak No	% Area	Area	Ret. Time	Height	Cap. Factor
1	5.0058	1449.8986	2.65 min	96.6928	2648.9667
2	94.9942	27514.4409	4.22 min	1355.8644	4215.6167

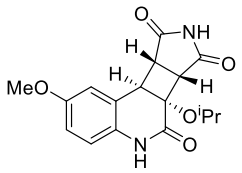

3.27i

Racemic (Daicel CHIRALPAK® OJ-H, isocratic 20% MeOH, 3.0 mL/min)

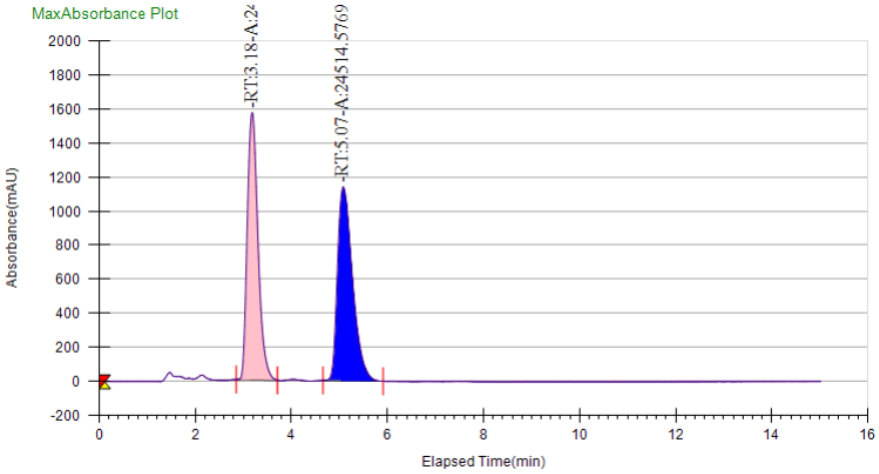

Peak Information

Peak No	% Area	Area	Ret. Time	Height	Cap. Factor
1	49.5496	24076.9125	3.18 min	1570.3162	3182.3
2	50.4504	24514.5769	5.07 min	1137.2063	5073.9333

Enantioenriched

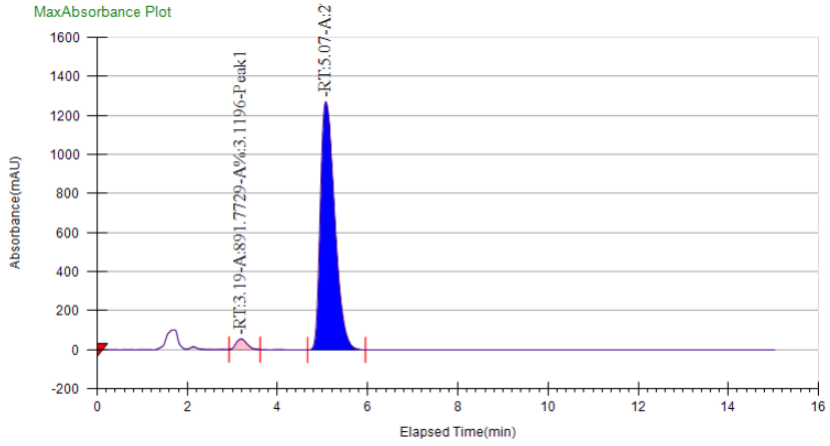

Peak Information

Peak No	% Area	Area	Ret. Time	Height	Cap. Factor
1	3.1196	891.7729	3.19 min	54.1131	3190.6167
2	96.8804	27694.4371	5.07 min	1271.028	5065.6

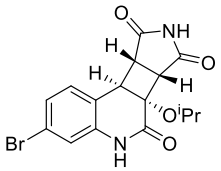

3.27j

Racemic (Daicel CHIRALPAK® OD-H, isocratic 20% MeOH, 3.0 mL/min)

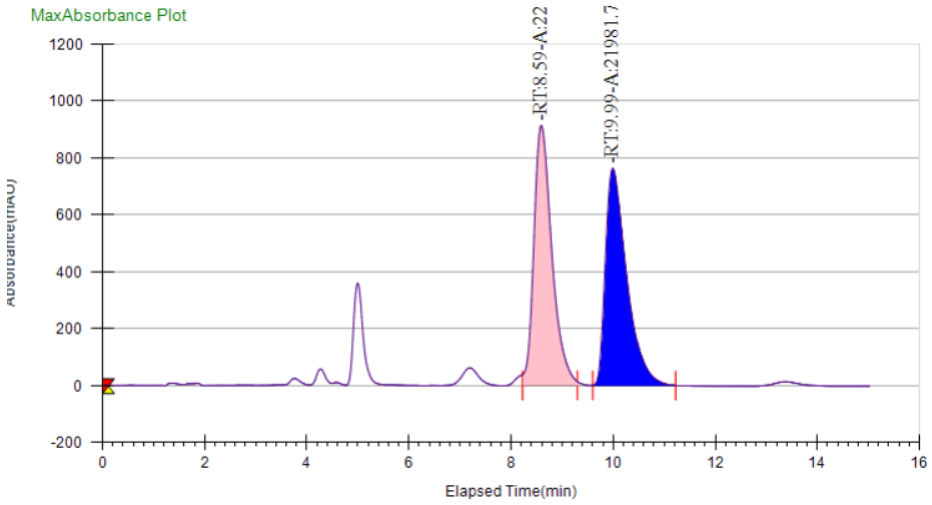

Peak Information

Peak No	% Area	Area	Ret. Time	Height	Cap. Factor
1	50.4107	22345.9182	8.59 min	914.967	8590.55
2	49.5893	21981.7974	9.99 min	762.7972	9990.5167

Enantioenriched

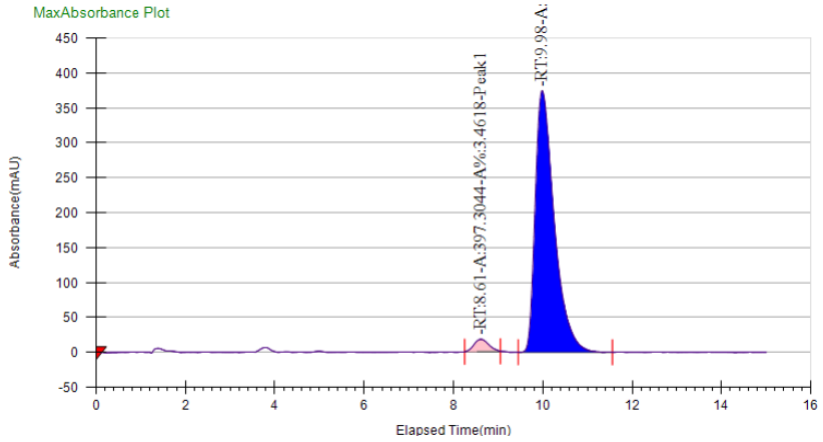

Peak Information

Peak No	% Area	Area	Ret. Time	Height	Cap. Factor
1	3.4618	397.3044	8.61 min	17.593	8607.2167
2	96.5382	11079.4413	9.98 min	374.6226	9982.1833

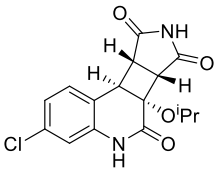

3.27k

Racemic (Daicel CHIRALPAK® OD-H, isocratic 20% MeOH, 3.0 mL/min)

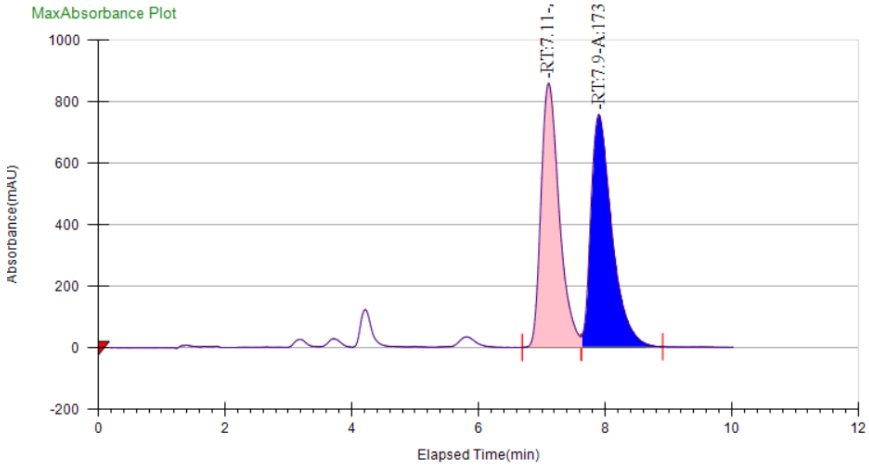

Peak Information

Peak No	% Area	Area	Ret. Time	Height	Cap. Factor
1	49.5784	17040.6438	7.11 min	859.1194	7107.2333
2	50.4216	17330.4324	7.9 min	756.1548	7898.8833

Enantioenriched

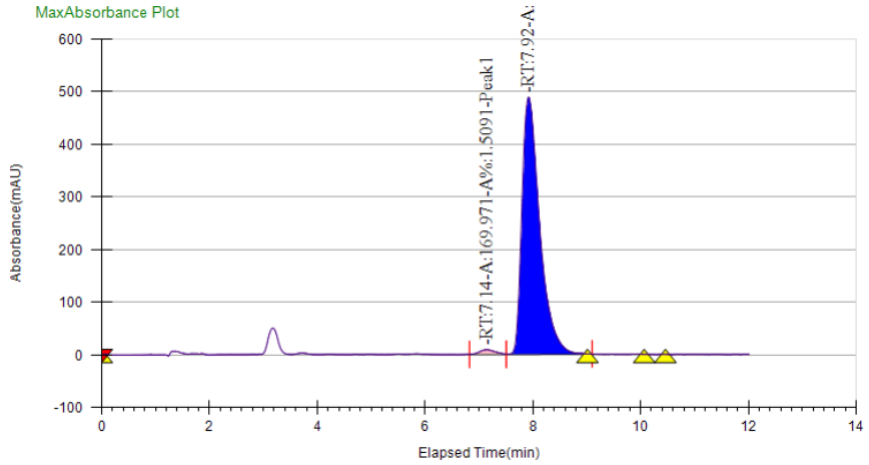

Peak Information

Peak No	% Area	Area	Ret. Time	Height	Cap. Factor
1	1.5091	169.971	7.14 min	8.7985	7140.5667
2	98.4909	11093.091	7.92 min	488.4023	7915.55

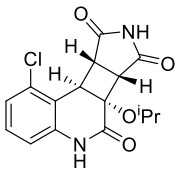

3.27l

Racemic (Daicel CHIRALPAK® OD-H, isocratic 20% MeOH, 3.0 mL/min)

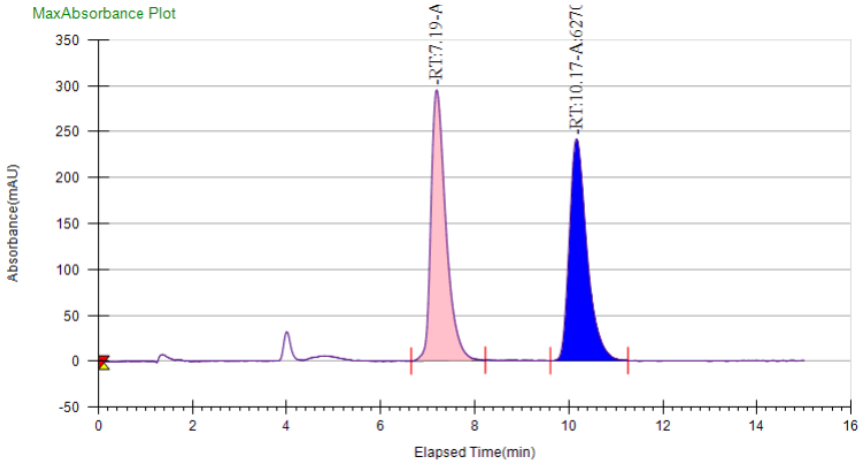

Peak Information

Peak No	% Area	Area	Ret. Time	Height	Cap. Factor
1	50.9116	6503.5032	7.19 min	295.0747	7190.5667
2	49.0884	6270.6008	10.17 min	241.7064	10165.5167

Enantioenriched

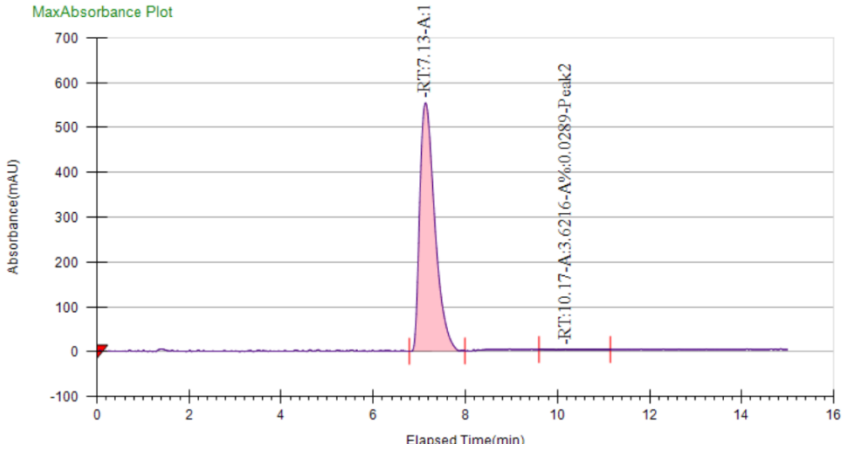

Peak Information

Peak No	% Area	Area	Ret. Time	Height	Cap. Factor
1	99.9711	12525.7192	7.13 min	554.1727	0
2	0.0289	3.6216	10.17 min	0.9375	0

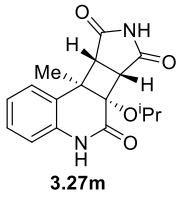

3.27m

Racemic (Daicel CHIRALPAK® AD-H, isocratic 20% MeOH, 3.0 mL/min)

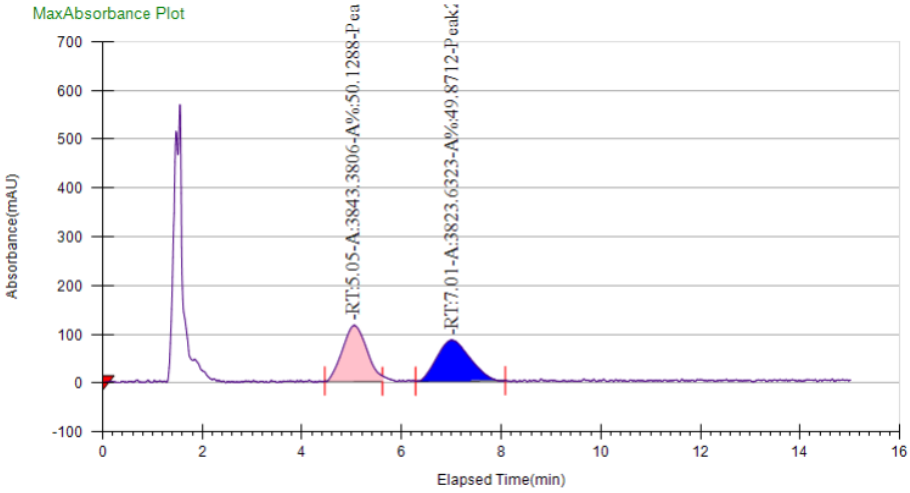

Peak Information

Peak No	% Area	Area	Ret. Time	Height	Cap. Factor
1	50.1288	3843.3806	5.05 min	114.3053	5048.9333
2	49.8712	3823.6323	7.01 min	83.9513	7007.2333

Enantioenriched

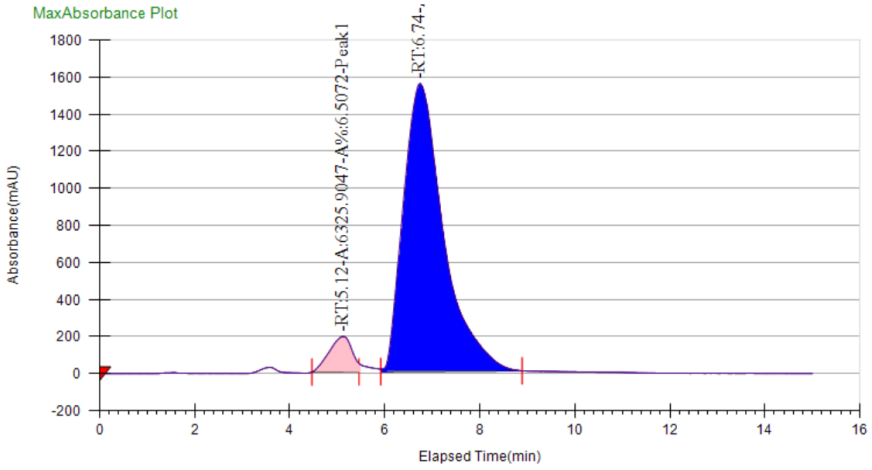

Peak Information

Peak No	% Area	Area	Ret. Time	Height	Cap. Factor
1	6.5072	6325.9047	5.12 min	191.0788	5123.9333
2	93.4928	90888.4781	6.74 min	1553.0837	6740.5667

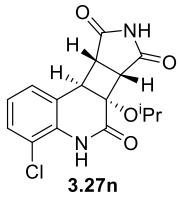

3.27n

Racemic (Daicel CHIRALPAK® OD-H, isocratic 20% MeOH, 3.0 mL/min)

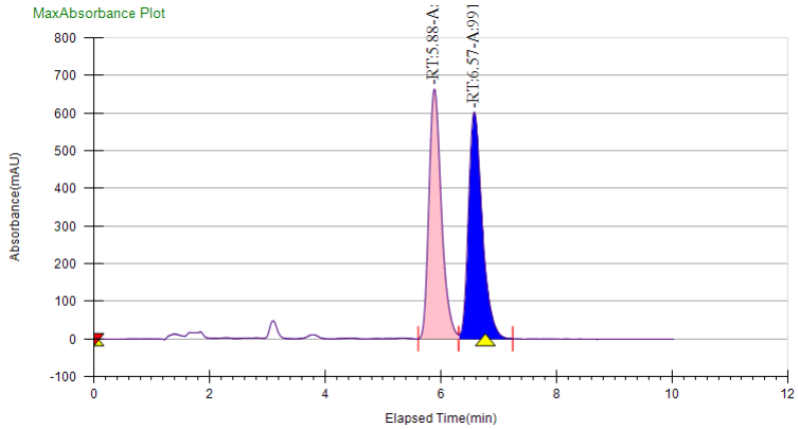

Peak Information

Peak No	% Area	Area	Ret. Time	Height	Cap. Factor
1	49.901	9872.46	5.88 min	663.1358	0
2	50.099	9911.6356	6.57 min	602.386	0

Enantioenriched

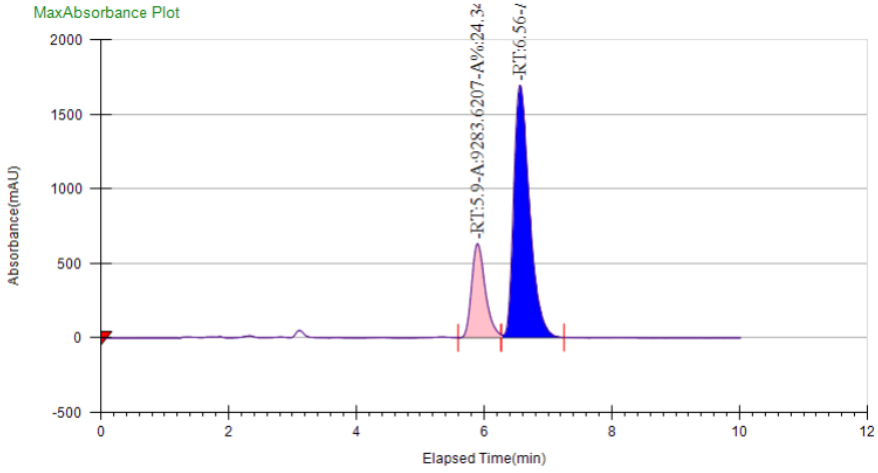

Peak Information

Peak No	% Area	Area	Ret. Time	Height	Cap. Factor
1	24.3493	9283.6207	5.9 min	629.5085	5898.9167
2	75.6507	28843.2057	6.56 min	1692.4888	6557.2333

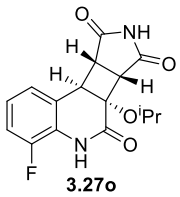

3.27o

Racemic (Daicel CHIRALPAK® OD-H, isocratic 20% MeOH, 3.0 mL/min)

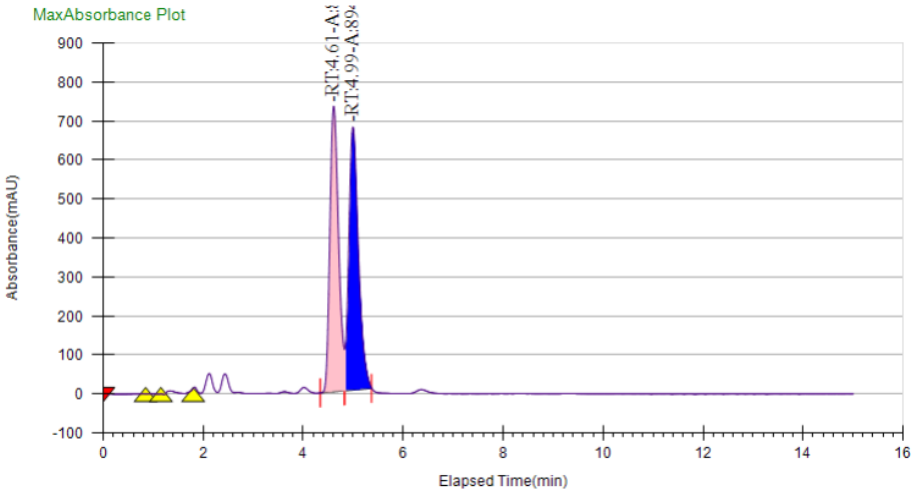

Peak Information

Peak No	% Area	Area	Ret. Time	Height	Cap. Factor
1	49.3293	8711.6116	4.61 min	732.0155	4607.2667
2	50.6707	8948.4957	4.99 min	674.6575	4990.6

Enantioenriched

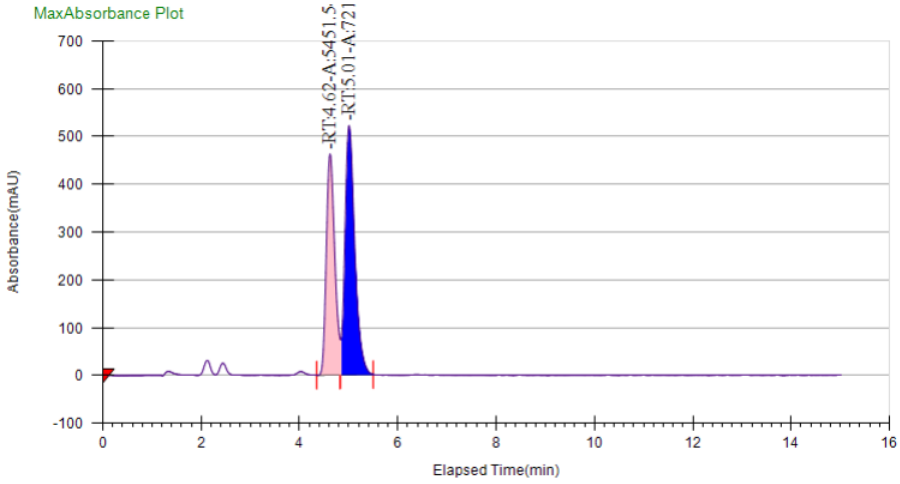

Peak Information

Peak No	% Area	Area	Ret. Time	Height	Cap. Factor
1	43.0234	5451.5485	4.62 min	462.7003	4623.9333
2	56.9766	7219.5699	5.01 min	521.8705	5007.2667

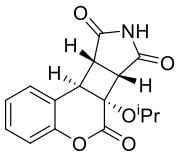

3.27p

Racemic (Daicel CHIRALPAK® OD-H, isocratic 20% MeOH, 3.0 mL/min)

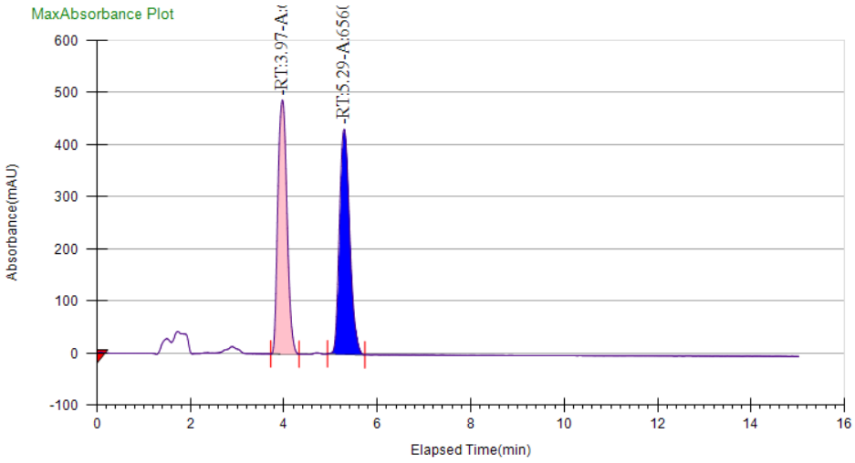

Peak Information

Peak No	% Area	Area	Ret. Time	Height	Cap. Factor
1	49.9619	6550.5045	3.97 min	487.7592	0
2	50.0381	6560.5032	5.29 min	432.034	0

Enantioenriched

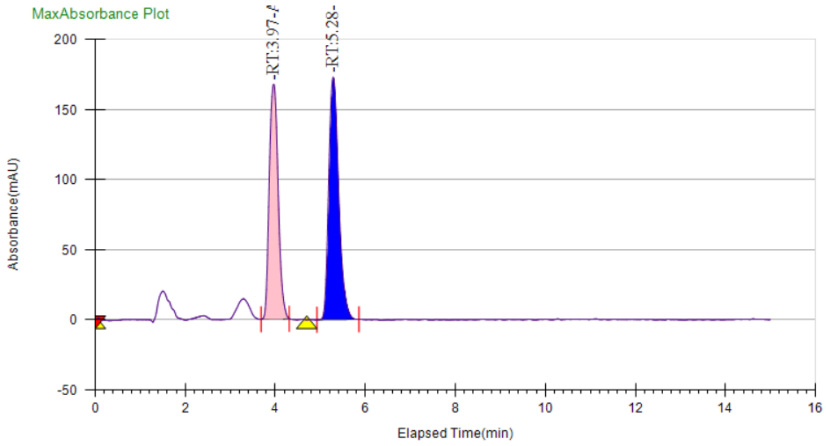

Peak Information

Peak No	% Area	Area	Ret. Time	Height	Cap. Factor
1	46.4422	2271.4897	3.97 min	167.4073	0
2	53.5578	2619.5099	5.28 min	172.7807	0

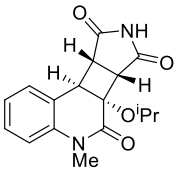

3.27q

Racemic (Daicel CHIRALPAK® OD-H, isocratic 20% MeOH, 3.0 mL/min)

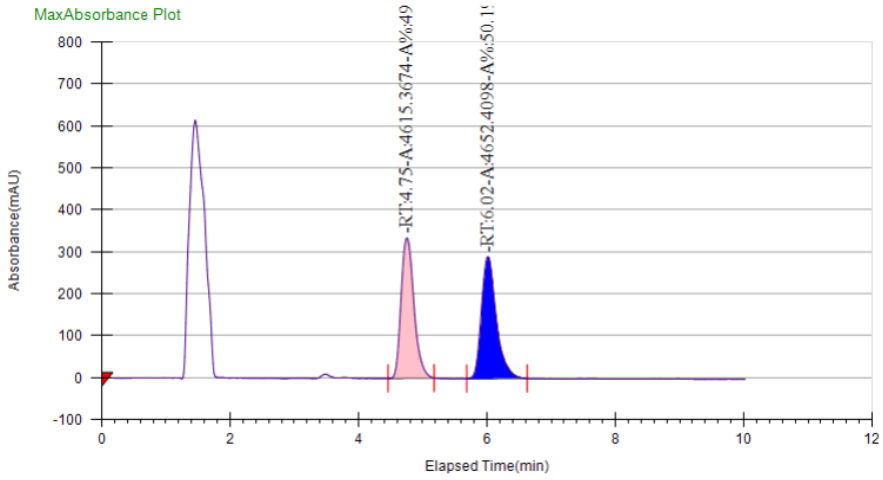

Peak Information

Peak No	% Area	Area	Ret. Time	Height	Cap. Factor
1	49.8002	4615.3674	4.75 min	334.2987	4748.9333
2	50.1998	4652.4098	6.02 min	290.982	6015.5833

Enantioenriched

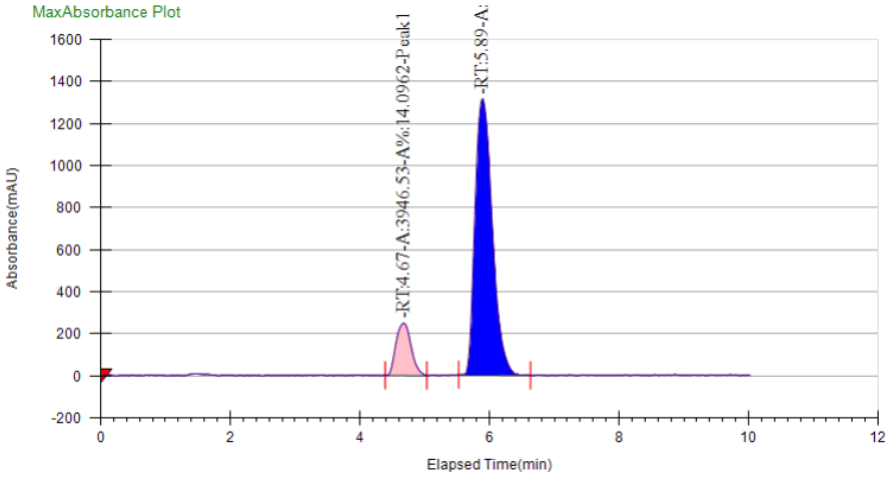

Peak Information

Peak No	% Area	Area	Ret. Time	Height	Cap. Factor
1	14.0962	3946.53	4.67 min	247.9067	4673.9333
2	85.9038	24050.5519	5.89 min	1312.9553	5890.5833

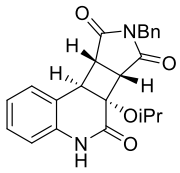

3.27r

Racemic (Daicel CHIRALPAK® OD-H, isocratic 20% MeOH, 3.0 mL/min)

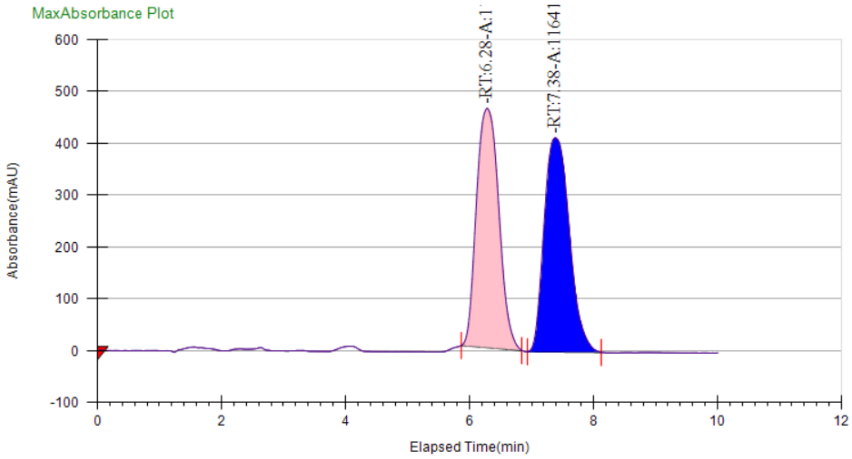

Peak Information

Peak No	% Area	Area	Ret. Time	Height	Cap. Factor
1	49.6997	11502.5157	6.28 min	461.9003	6282.25
2	50.3003	11641.539	7.38 min	413.2681	7382.2333

Enantioenriched

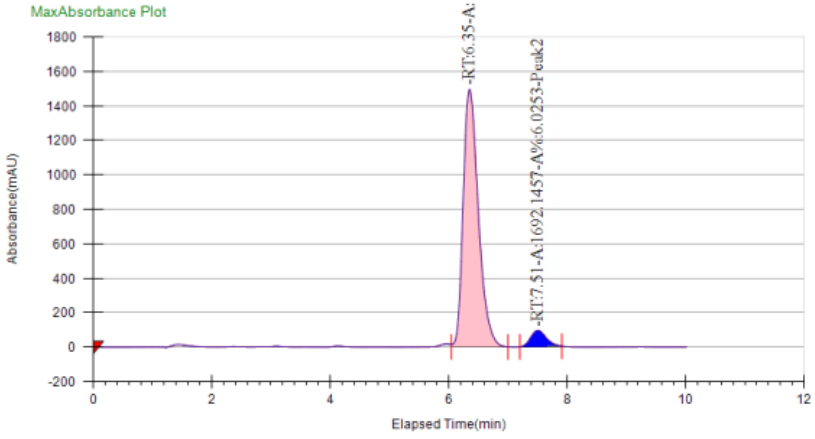

Peak Information

Peak No	% Area	Area	Ret. Time	Height	Cap. Factor
1	93.9747	26391.9521	6.35 min	1494.3521	6348.9167
2	6.0253	1692.1457	7.51 min	93.9479	7507.2333

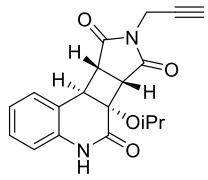

3.27s

Racemic (HPLC, Daicel CHIRALPAK® AD-H, Gradient 5% iPrOH (95% Hexane) to 40% iPrOH (60% Hexane), 1.0 mL/min)

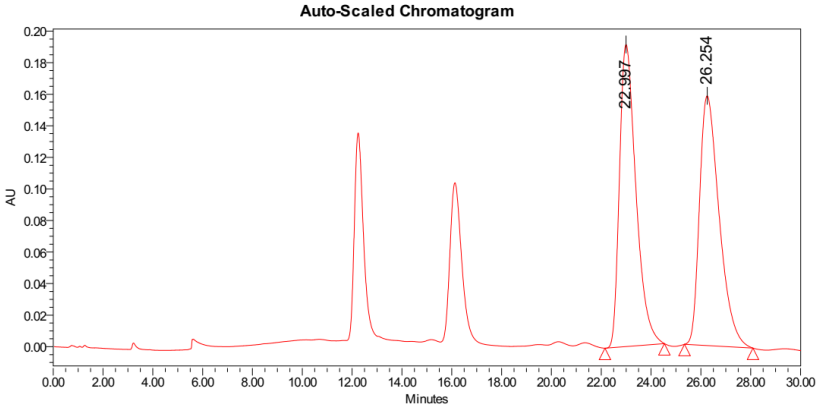

Peak Results

	RT	Area	Height	% Area
1	22.997	8781325	191488	50.29
2	26.254	8679006	158274	49.71

Enantioenriched

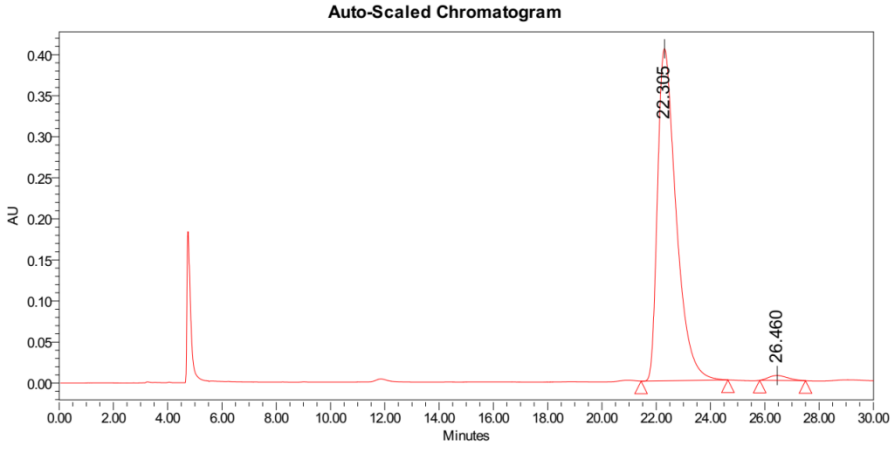

Peak Results

	RT	Area	Height	% Area
1	22.305	19213782	404446	98.48
2	26.460	296053	6030	1.52

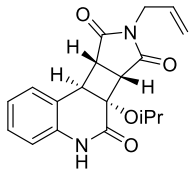

3.27t

Racemic (Daicel CHIRALPAK® OD-H, isocratic 20% MeOH, 3.0 mL/min)

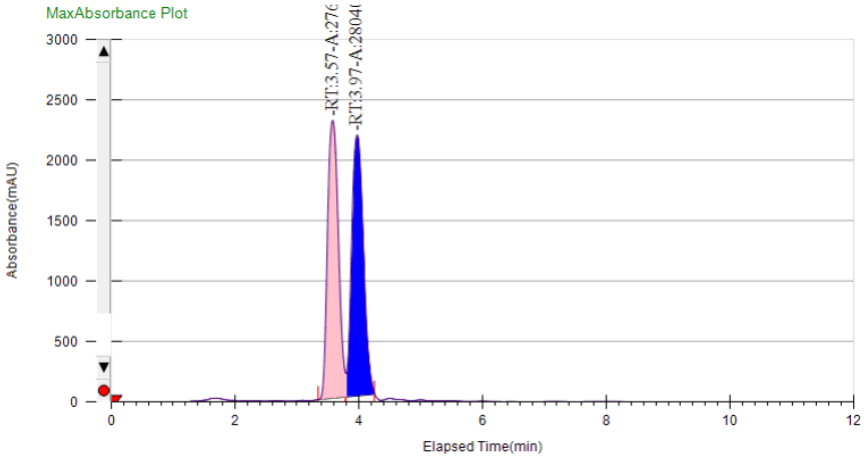

Peak Information

Peak No	% Area	Area	Ret. Time	Height	Cap. Factor
1	49.6657	27668.4083	3.57 min	2299.687	3573.95
2	50.3343	28040.904	3.97 min	2156.4579	3973.95

Enantioenriched

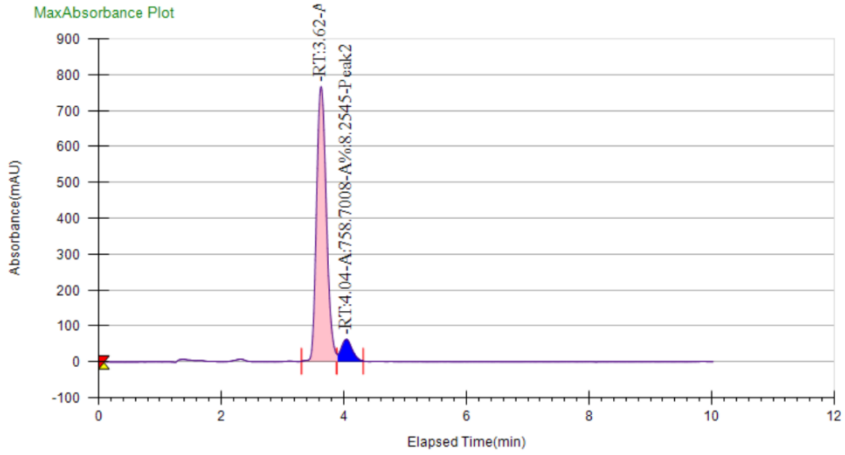

Peak Information

Peak No	% Area	Area	Ret. Time	Height	Cap. Factor
1	91.7455	8432.6091	3.62 min	765.2103	3623.95
2	8.2545	758.7008	4.04 min	60.7419	4040.6167

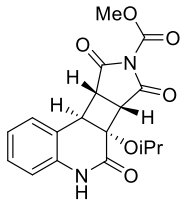

3.27u

Racemic (Daicel CHIRALPAK® OD-H, isocratic 20% MeOH, 3.0 mL/min)

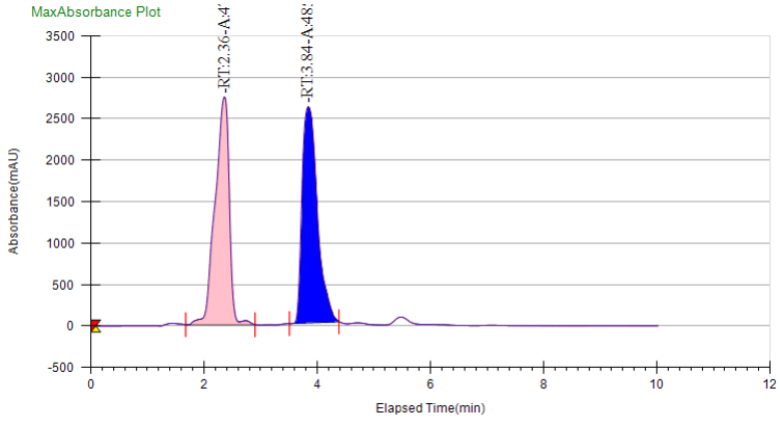

Peak Information

Peak No	% Area	Area	Ret. Time	Height	Cap. Factor
1	49.5785	47777.3214	2.36 min	2749.646	2357.3
2	50.4215	48589.7592	3.84 min	2609.6966	3840.6167

Enantioenriched

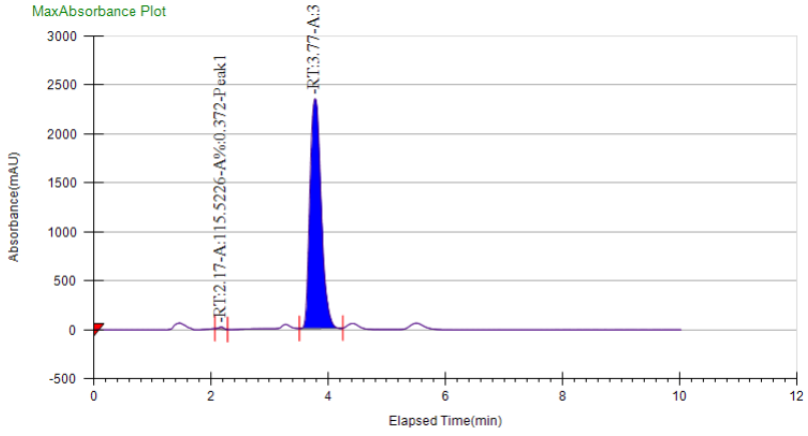

Peak Information

Peak No	% Area	Area	Ret. Time	Height	Cap. Factor
1	0.372	115.5226	2.17 min	20.5205	2173.9667
2	99.628	30940.5044	3.77 min	2346.5626	3773.95

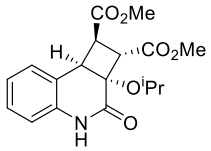

3.27v

Racemic (Daicel CHIRALPAK® OD-H, isocratic 20% MeOH, 3.0 mL/min)

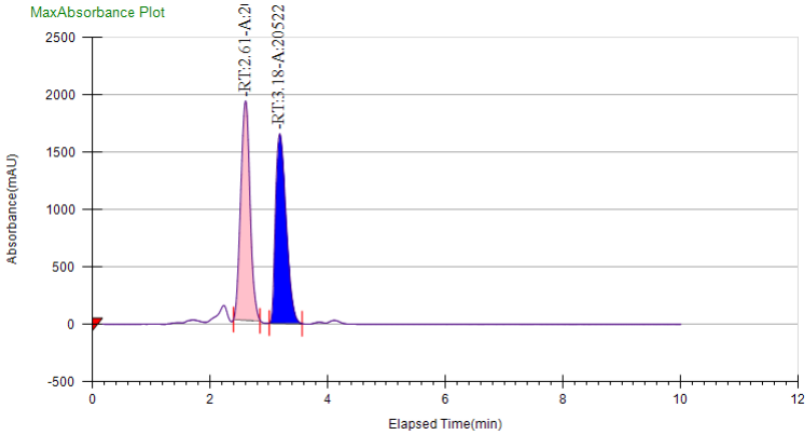

Peak Information

Peak No	% Area	Area	Ret. Time	Height	Cap. Factor
1	50.3225	20788.8897	2.61 min	1910.7564	2607.3
2	49.6775	20522.4072	3.18 min	1649.4834	3182.3

Enantioenriched

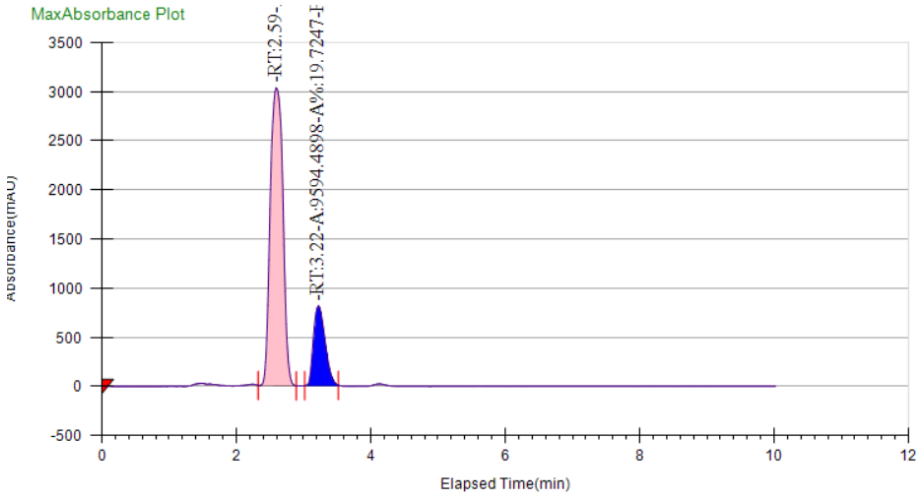

Peak Information

Peak No	% Area	Area	Ret. Time	Height	Cap. Factor
1	80.2753	39047.4459	2.59 min	3034.5262	2590.6333
2	19.7247	9594.4898	3.22 min	809.8666	3215.6167

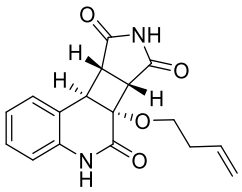

3.27w

Racemic (HPLC, Daicel CHIRALPAK®OD-H, Gradient 5% iPrOH (95% Hexane) to 50% iPrOH (50% Hexane), 1.0 mL/min)

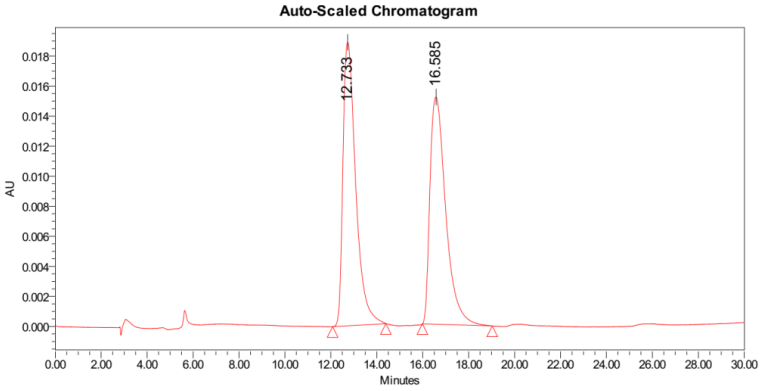

Peak Results

	Name	RT	% Area	Area	Height	Amount	Units
1		12.733	50.24	728494	18872		
2		16.585	49.76	721629	15128		

Enantioenriched

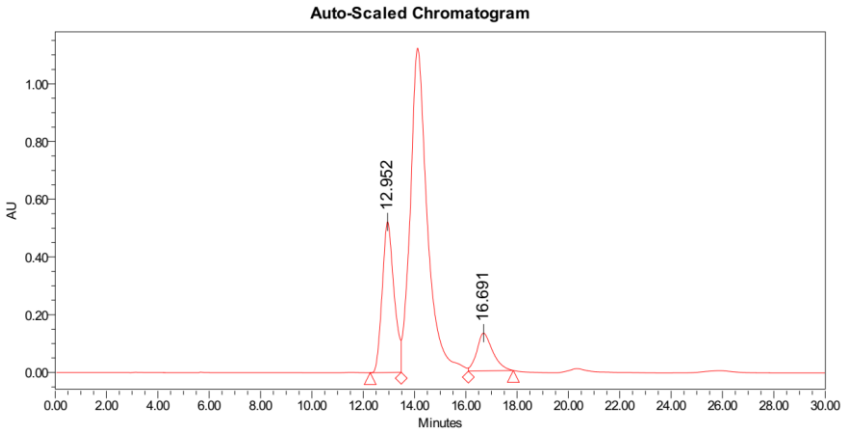

Peak Results

	Name	% Area	RT	Area	Height	Amount	Units
1		74.73	12.952	16663695	521729		
2		25.27	16.691	5634896	131122		

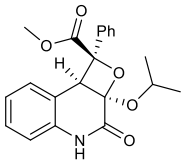

4.48a *endo*

Racemic (Daicel CHIRALCEL® AS-H, 10% EtOH, 90% Hexanes, 1 mL/min, 246.2 nm)

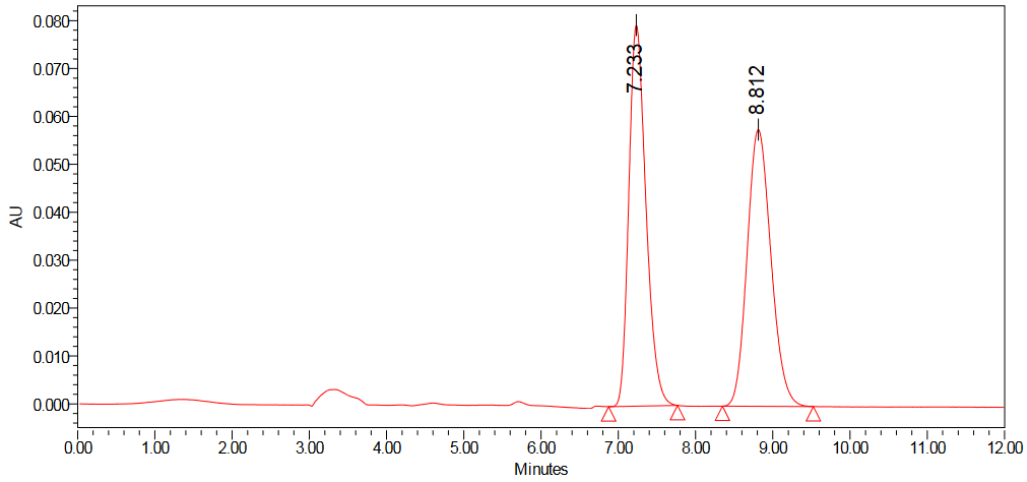

Peak No	RT (min)	Area	Height	% Area
1	7.233	1227276	79538	49.81
2	8.812	1236843	57756	50.19

Enantioenriched (Daicel CHIRALCEL® IC, 30% *i*-PrOH, 70% Hexanes, 1 mL/min, 287.2 nm)

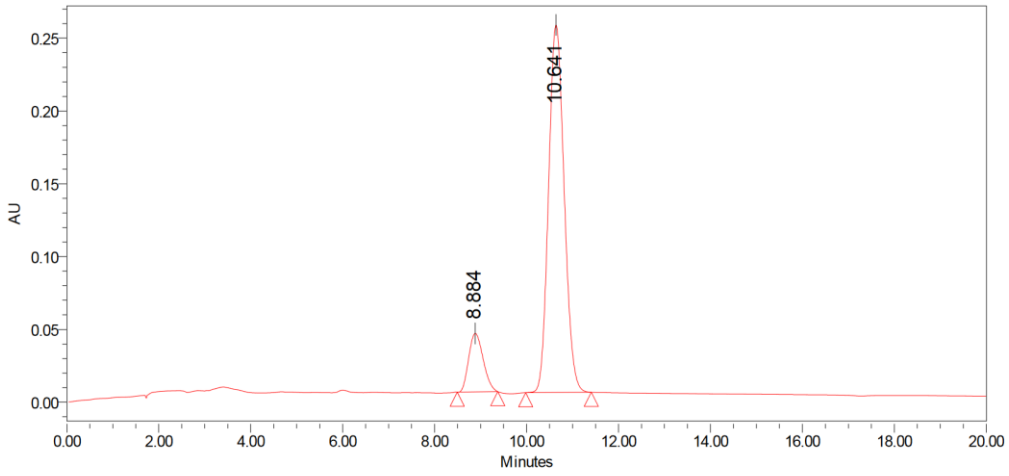

Peak No	RT (min)	Area	Height	% Area
1	8.884	876861	40120	12.84
2	10.641	5951182	252426	87.16

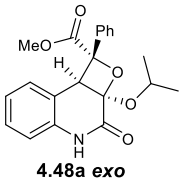

4.48a *exo*

Enantioenriched (Daicel CHIRALCEL® IC, 30% *i*-PrOH, 70% Hexanes, 1 mL/min, 287.2 nm)

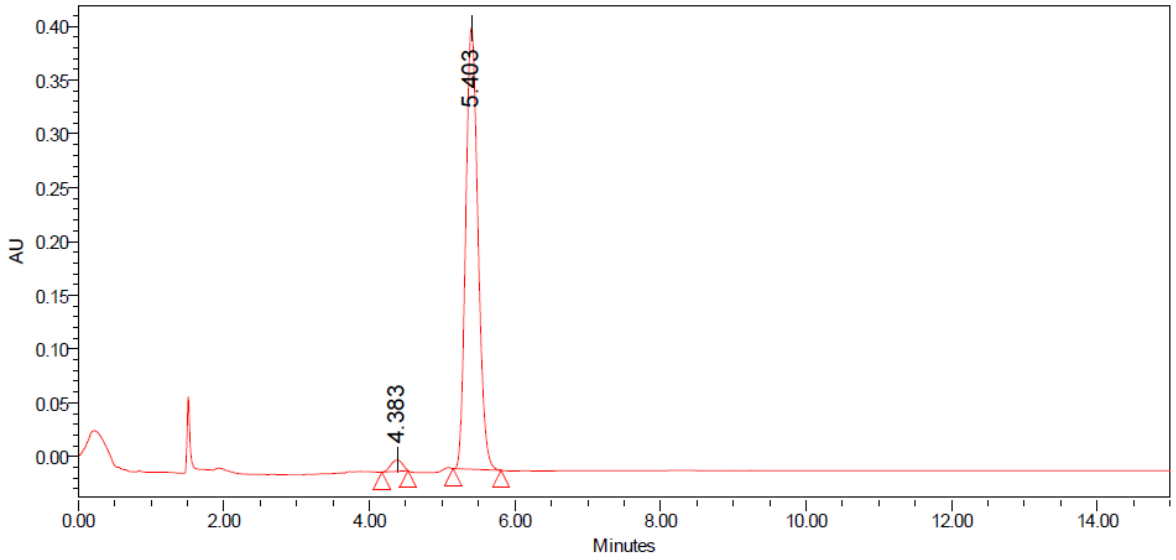

Peak No	RT (min)	Area	Height	% Area
1	4.383	113773	10461	2.31
2	5.403	4801268	410610	97.69

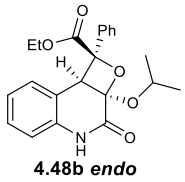

4.48b *endo*

Enantioenriched (Daicel CHIRALCEL® AS–H, 10% EtOH, 90% Hexanes, 1 mL/min, 250.0 nm)

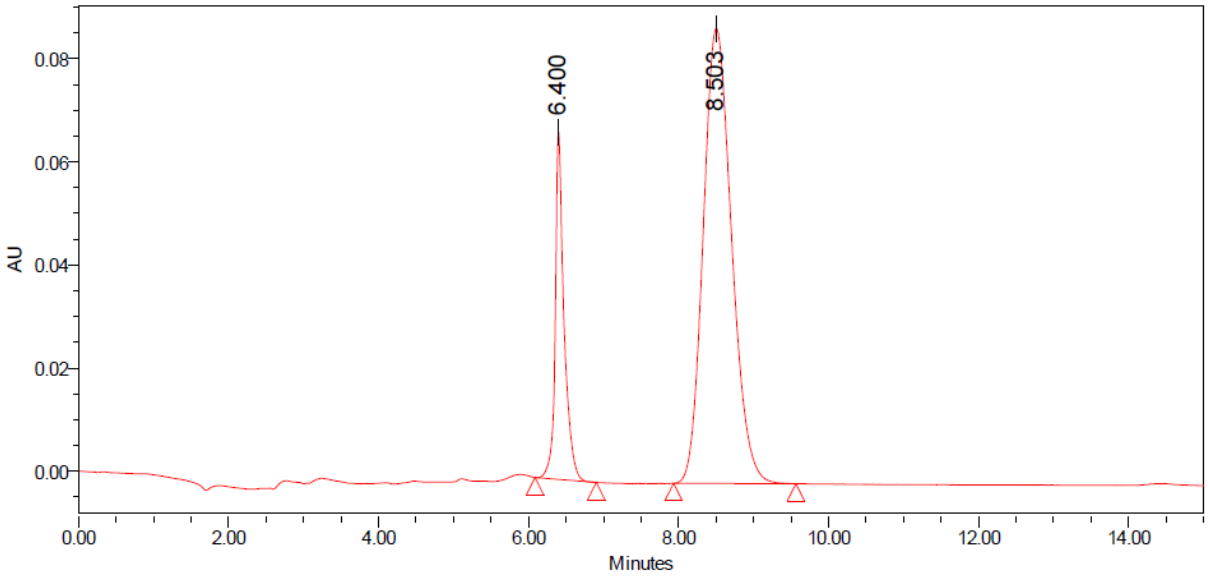

Peak No	RT (min)	Area	Height	% Area
1	6.400	548114	67462	19.12
2	8.503	2318410	88254	80.88

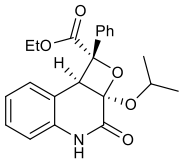

4.48b *exo*

Enantioenriched (Daicel CHIRALCEL® IC, 30% *i*-PrOH, 70% Hexanes, 1 mL/min, 250.0 nm)

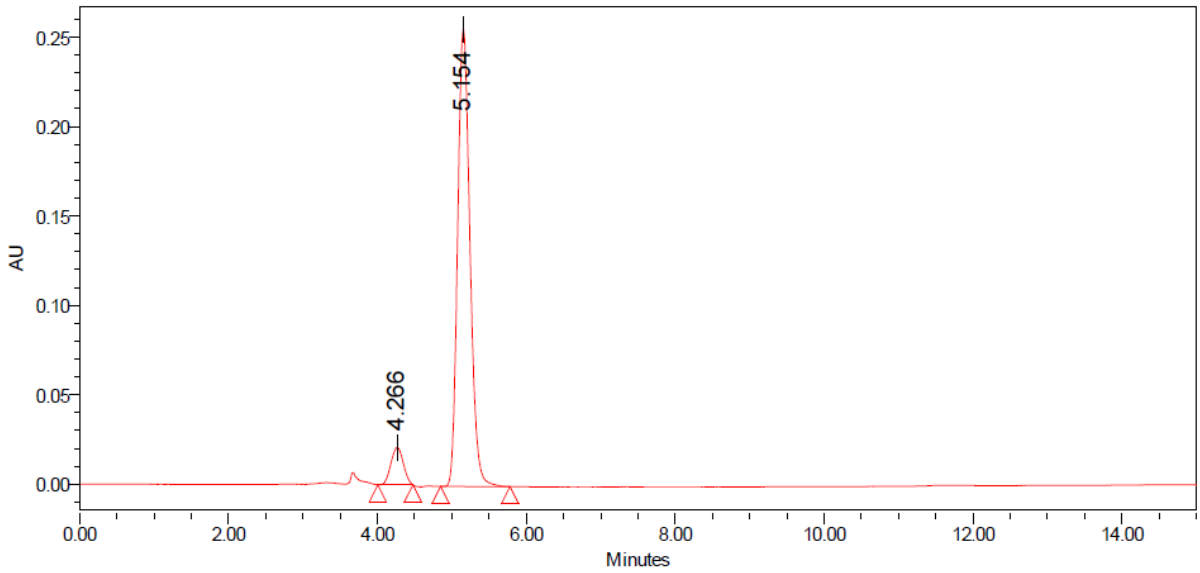

Peak No	RT (min)	Area	Height	% Area
1	4.266	241878	20846	7.61
2	5.154	2936275	255756	92.39

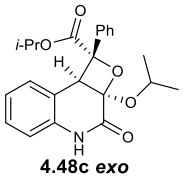

4.48c *exo*

Enantioenriched (Daicel CHIRALCEL® IC, 30% *i*-PrOH, 70% Hexanes, 1 mL/min, 250.0 nm)

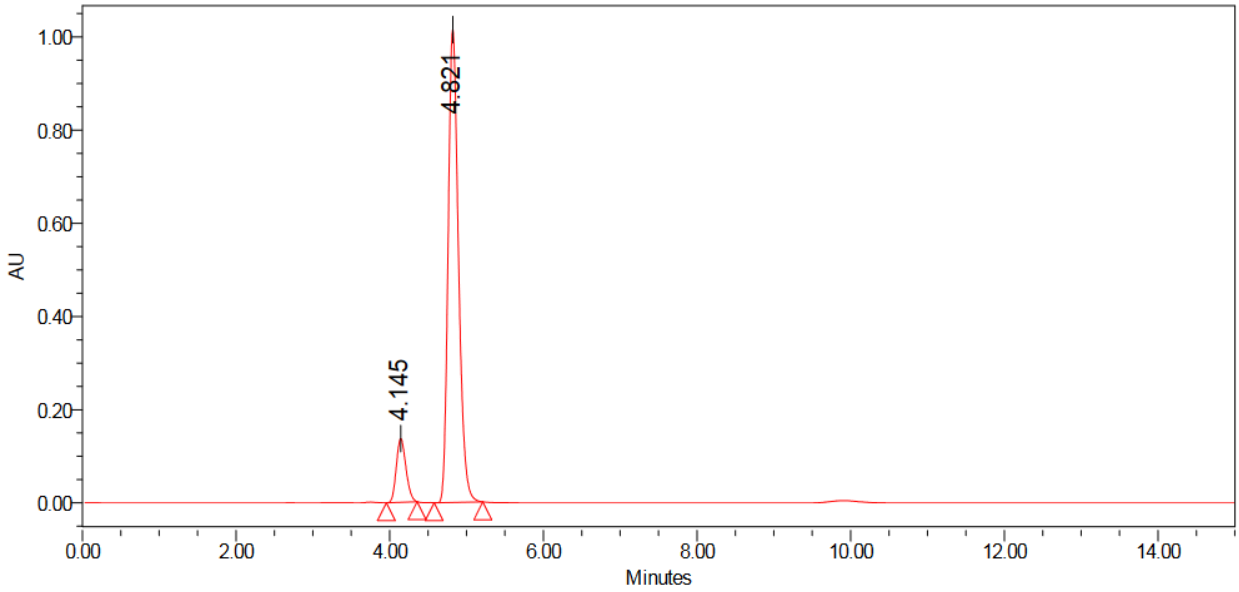

Peak No	RT (min)	Area	Height	% Area
1	4.145	1187268	136604	11.15
2	4.821	9463886	1014867	88.85

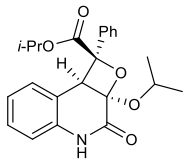

4.48c *endo*

Enantioenriched (Daicel CHIRALCEL® AS–H, 10% EtOH, 90% Hexanes, 1 mL/min, 250.0 nm)

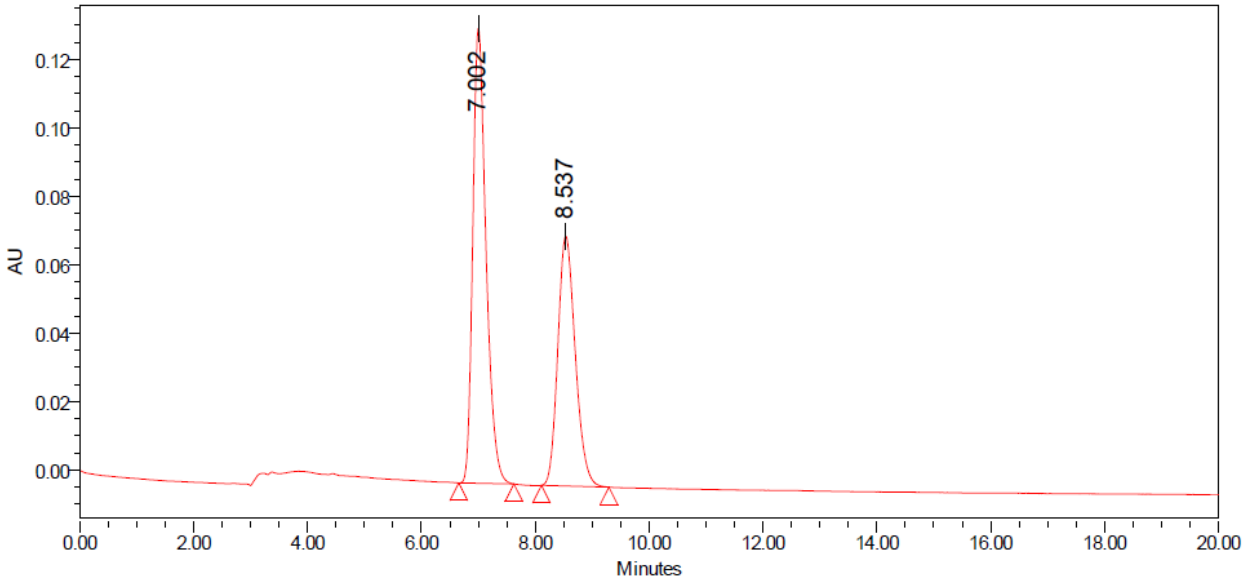

Peak No	RT (min)	Area	Height	% Area
1	7.002	2141988	132945	58.00
2	8.537	1551313	72976	42.00

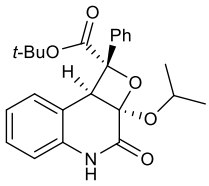

4.48d

Enantioenriched (Daicel CHIRALCEL® IC, 30% *i*-PrOH, 70% Hexanes, 1 mL/min, 250.0 nm)

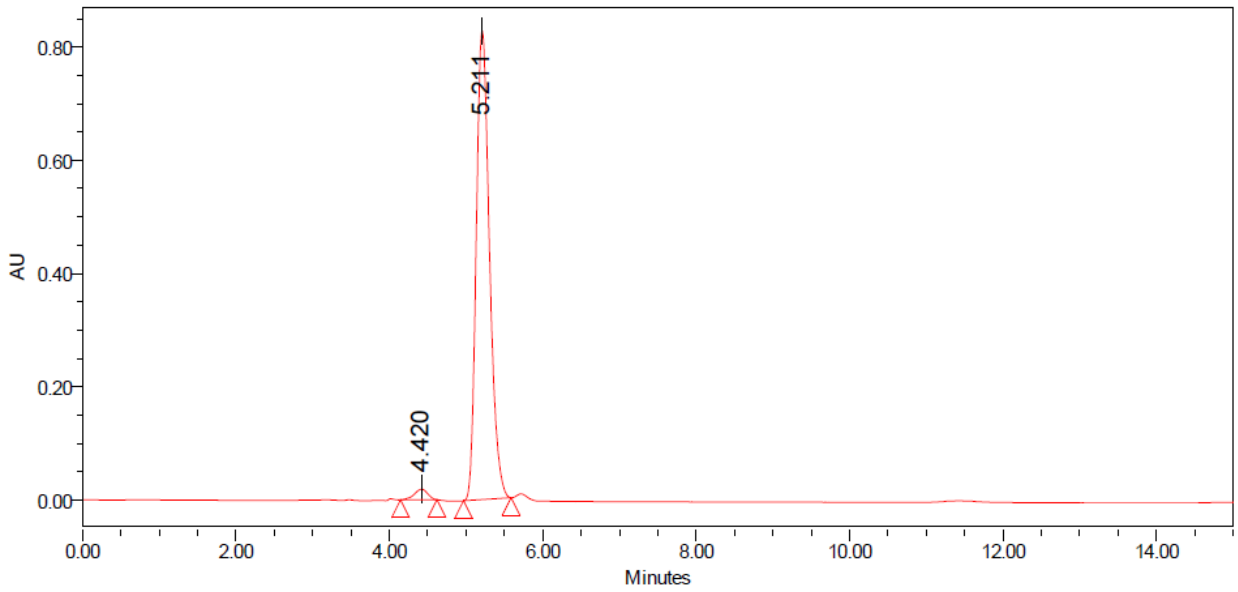

Peak No	RT (min)	Area	Height	% Area
1	4.420	226872	18666	2.23
2	5.21	9941254	828126	97.77

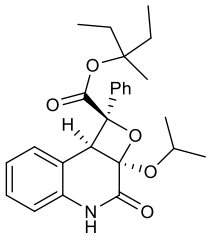

4.48e

Enantioenriched (Daicel CHIRALCEL® IC, 20% *i*-PrOH, 80% Hexanes, 1 mL/min, 250.0 nm)

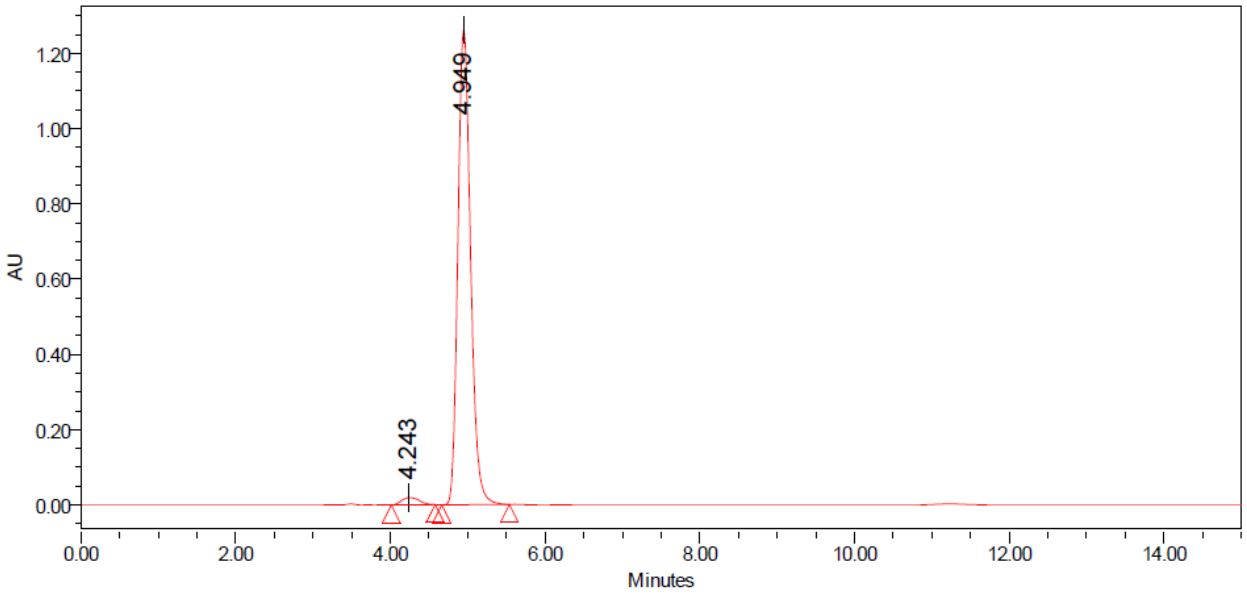

Peak No	RT (min)	Area	Height	% Area
1	4.243	305208	19254	2.09
2	4.949	14326090	1262802	97.91

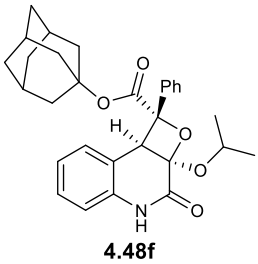

4.48f

Enantioenriched (Daicel CHIRALCEL® IC, 20% *i*-PrOH, 80% Hexanes, 1 mL/min, 250.0 nm)

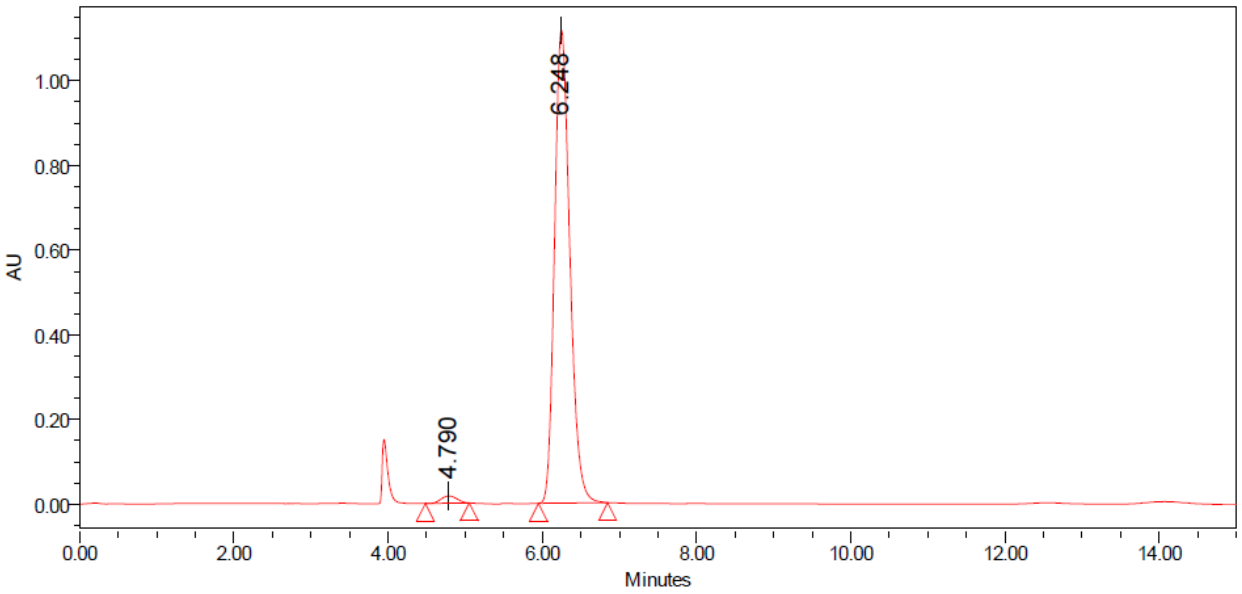

Peak No	RT (min)	Area	Height	% Area
1	4.790	244833	16892	1.56
2	6.248	15409312	1117648	98.44

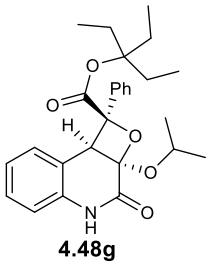

4.48g

Enantioenriched (Daicel CHIRALCEL® IC, 20% *i*-PrOH, 80% Hexanes, 1 mL/min, 250.0 nm)

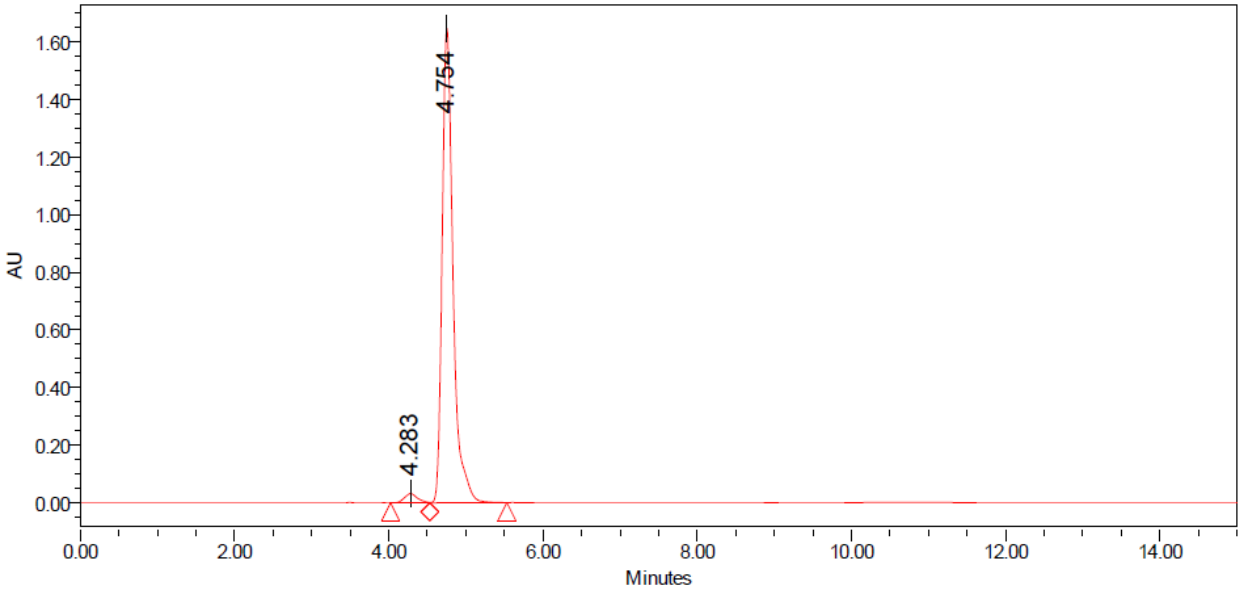

Peak No	RT (min)	Area	Height	% Area
1	4.283	373851	32034	2.26
2	4.754	16138029	1646267	97.74

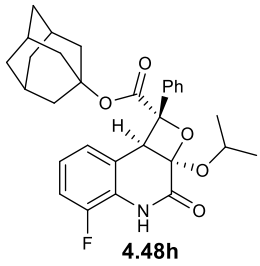

4.48h

Enantioenriched (Daicel CHIRALCEL® IC, 20% *i*-PrOH, 80% Hexanes, 1 mL/min, 250.0 nm)

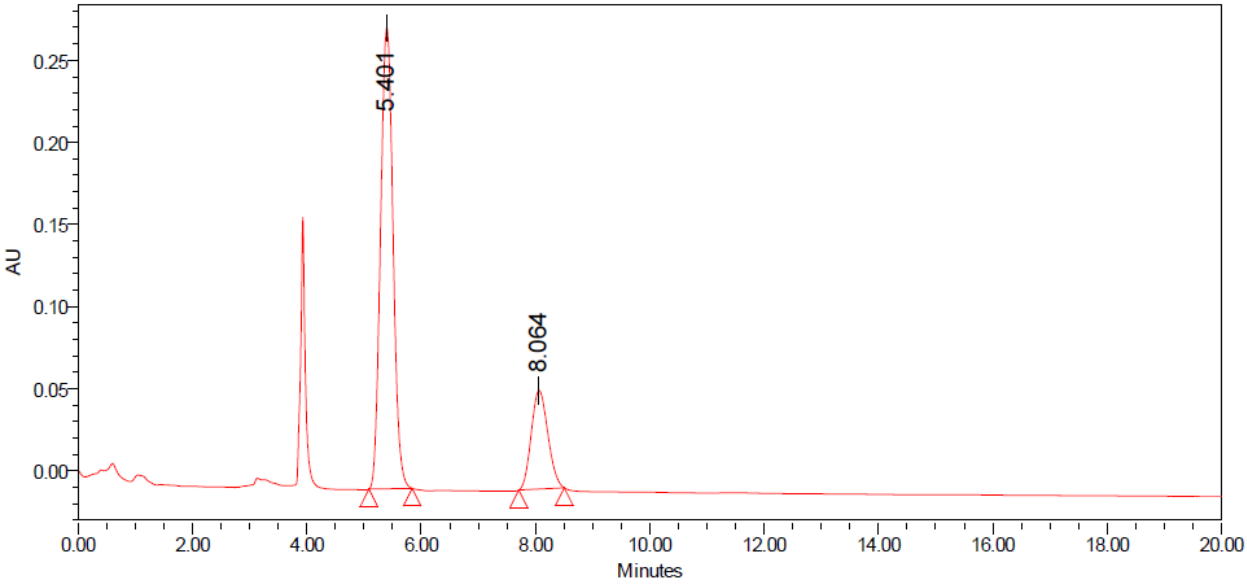

Peak No	RT (min)	Area	Height	% Area
1	5.401	4267429	280876	77.84
2	8.064	1214838	60108	22.16

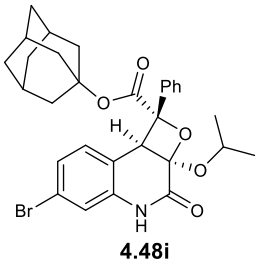

4.48i

Enantioenriched (Daicel CHIRALCEL® IC, 20% *i*-PrOH, 80% Hexanes, 1 mL/min, 250.0 nm)

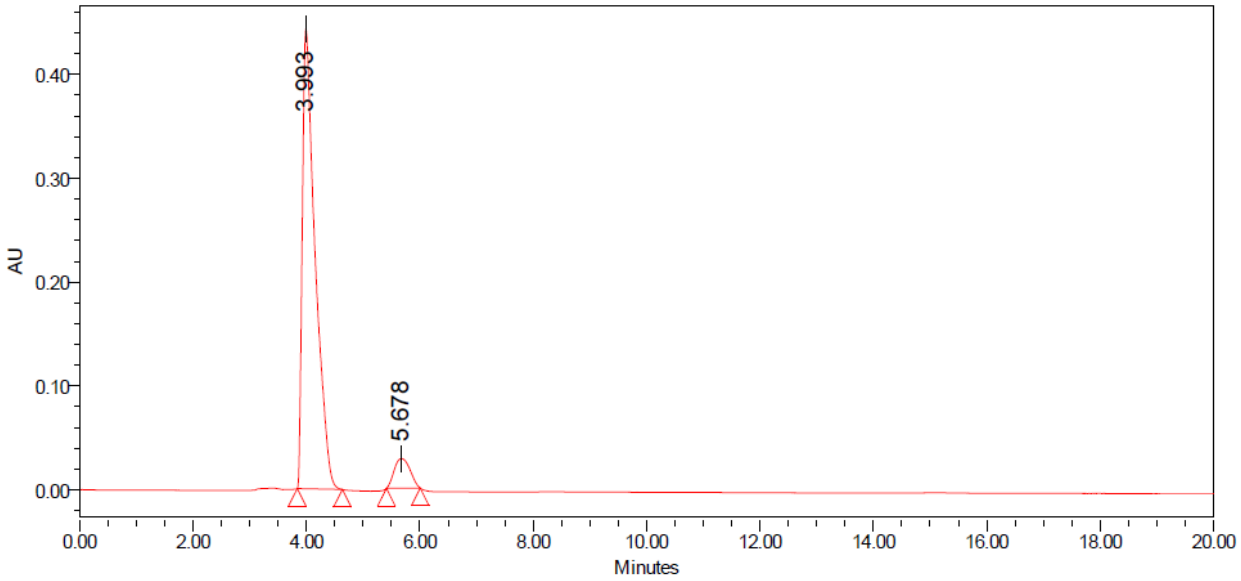

Peak No	RT (min)	Area	Height	% Area
1	3.993	6955738	443295	92.62
2	5.678	554246	28487	7.38

Appendix D. X-Ray Crystallographic Data

D.1 X-Ray Data for Compound Λ-2.32

D.1.1 Data Collection

A yellow crystal with approximate dimensions 0.078 x 0.057 x 0.040 mm^3 was selected under oil under ambient conditions and attached to the tip of a MiTeGen MicroMount©. The crystal was mounted in a stream of cold nitrogen at 100(1) K and centered in the X-ray beam by using a video camera.

The crystal evaluation and data collection were performed on a Bruker Quazar SMART APEXII diffractometer with Mo K_α (λ = 0.71073 Å) radiation and the diffractometer to crystal distance of 4.96 cm.[1]

The initial cell constants were obtained from three series of ω scans at different starting angles. Each series consisted of 12 frames collected at intervals of 0.5º in a 6º range about ω with the exposure time of 10 seconds per frame. Thse reflections were successfully indexed by an automated indexing routine built in the APEXII program suite. The final cell constants were calculated from a set of 9202 strong reflections from the actual data collection.

The data were collected by using the full sphere data collection routine to survey the reciprocal space to the extent of a full sphere to a resolution of 0.70 Å. A total of 131360 data were harvested by collecting 5 sets of frames with 0.5º scans in ω and φ with exposure times of 60 sec per frame. These highly redundant datasets were corrected for Lorentz and polarization effects. The absorption correction was based on fitting a function to the empirical transmission surface as sampled by multiple equivalent measurements.[2]

D.1.2 Structure Solution and Refinement

The systematic absences in the diffraction data were consistent for the space groups $P2_1$ and $P2_1/m$. The *E*-statistics strongly suggested the non-centrosymmetric space group $P2_1$ that yielded chemically reasonable and computationally stable results of refinement.[3–8]

A successful solution by the direct methods provided most non-hydrogen atoms from the *E*-map. The remaining non-hydrogen atoms were located in an alternating series of least-squares cycles and difference Fourier maps. All non-disordered non-hydrogen atoms were refined with anisotropic displacement coefficients. All hydrogen atoms were included in the structure factor calculation at idealized positions and were allowed to ride on the neighboring atoms with relative isotropic displacement coefficients.

The asymmetric unit contains two symmetry-independent Ir complexes, two symmetry-independent counterions, and 1.68 molecules of solvent ethanol.

There is extensive positional disorder in the structure. In the Ir1 complex atoms the ring containing N5 is disordered over two positions with the major component contribution of 67(3)%. In the Ir2 complex the CF_3 group at C62 is disordered over three positions in a 34.1(4):37.1(4):28.8(4) ratio. In the B1 counterion the CF_3 groups at C77, C83 and C85 are disordered over two positions with the major component contributing 55(2), 53(2), and 51(3)%; the C89 ring is disordered over two positions with the major component contributing 55.9(15)%. The entire B2 counterion is disordered over two positions the major component contributing 53.4(7)%. One solvent ethanol molecule is fully occupied, the other is 69.0(19)% occupied. The disordered atoms were refined isotropically with similarity restraints and constraints.

The final least-squares refinement of 1780 parameters against 29402 data resulted in residuals *R* (based on F^2 for $I \geq 2\sigma$) and *wR* (based on F^2 for all data) of 0.0429 and 0.1121, respectively. The final difference Fourier map was featureless.

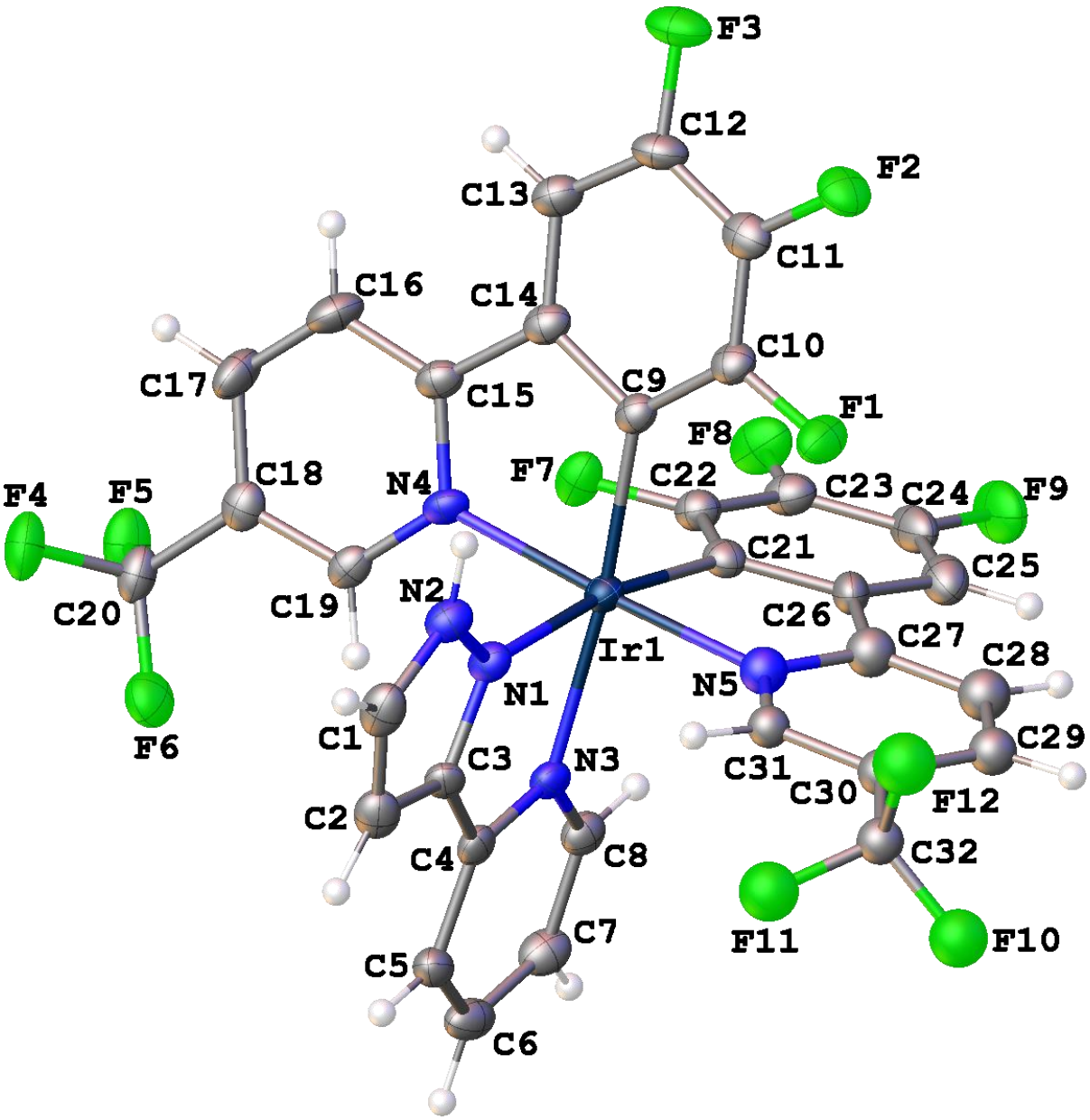

Figure D.1. A molecular drawing of the Ir1 complex shown with 40% probability ellipsoids. Only one position of the disordered components is shown.

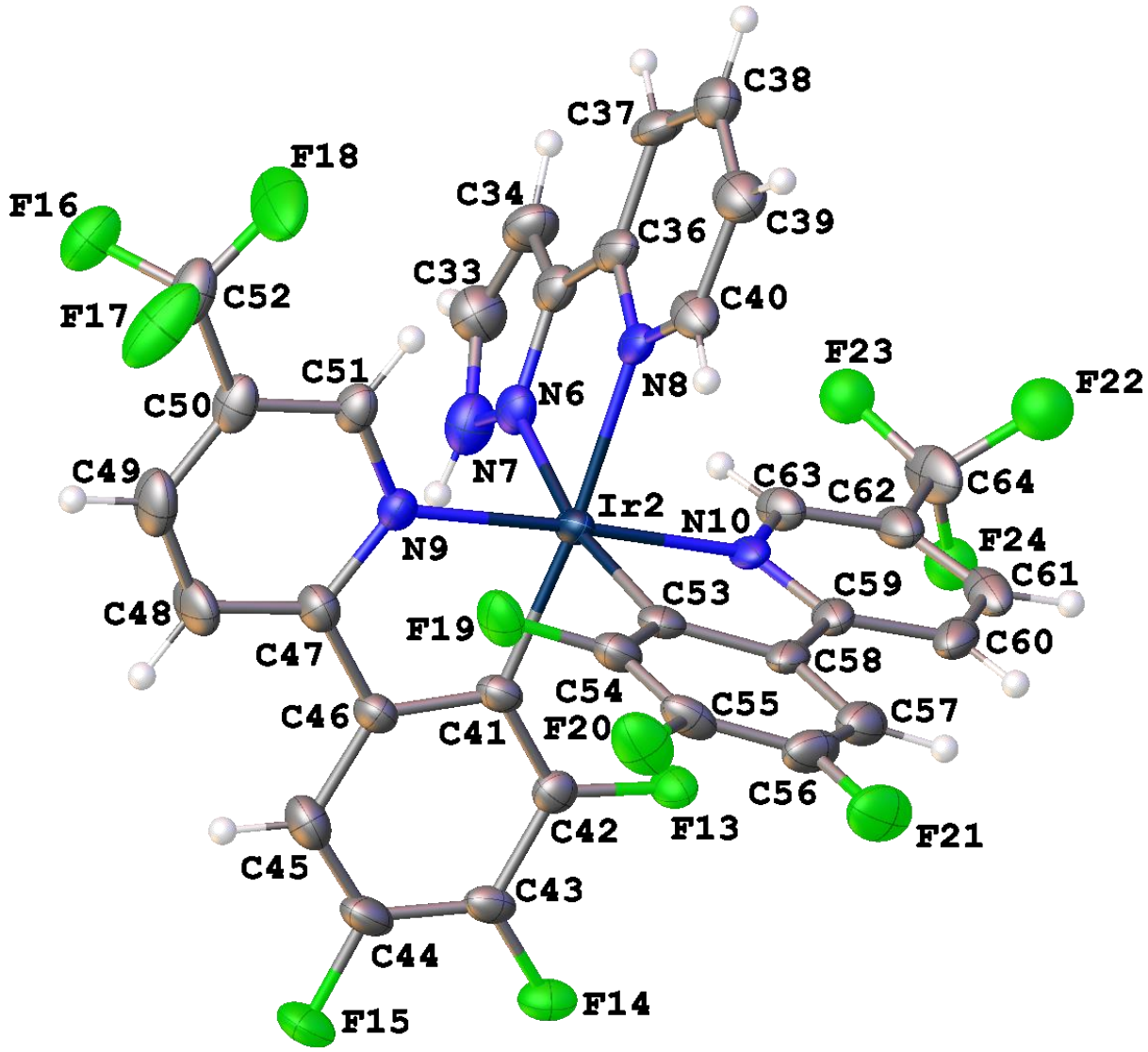

Figure D.2. A molecular drawing of the Ir2 complex shown with 40% probability ellipsoids. Only one position of the disordered components is shown.

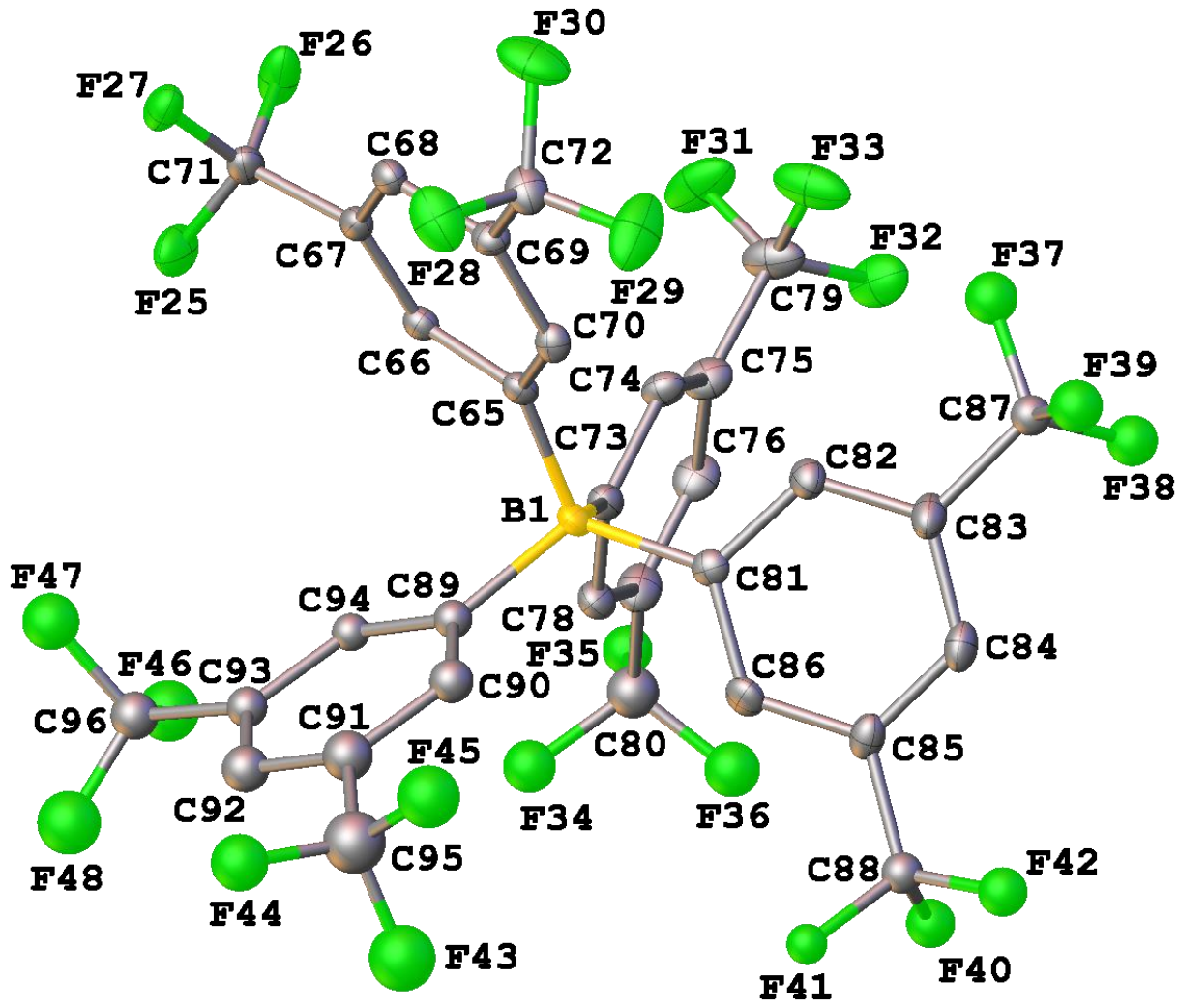

Figure D.3. A molecular drawing of the B1 anion shown with 30% probability ellipsoids. Only one position of the disordered components is shown. All H atoms are omitted.

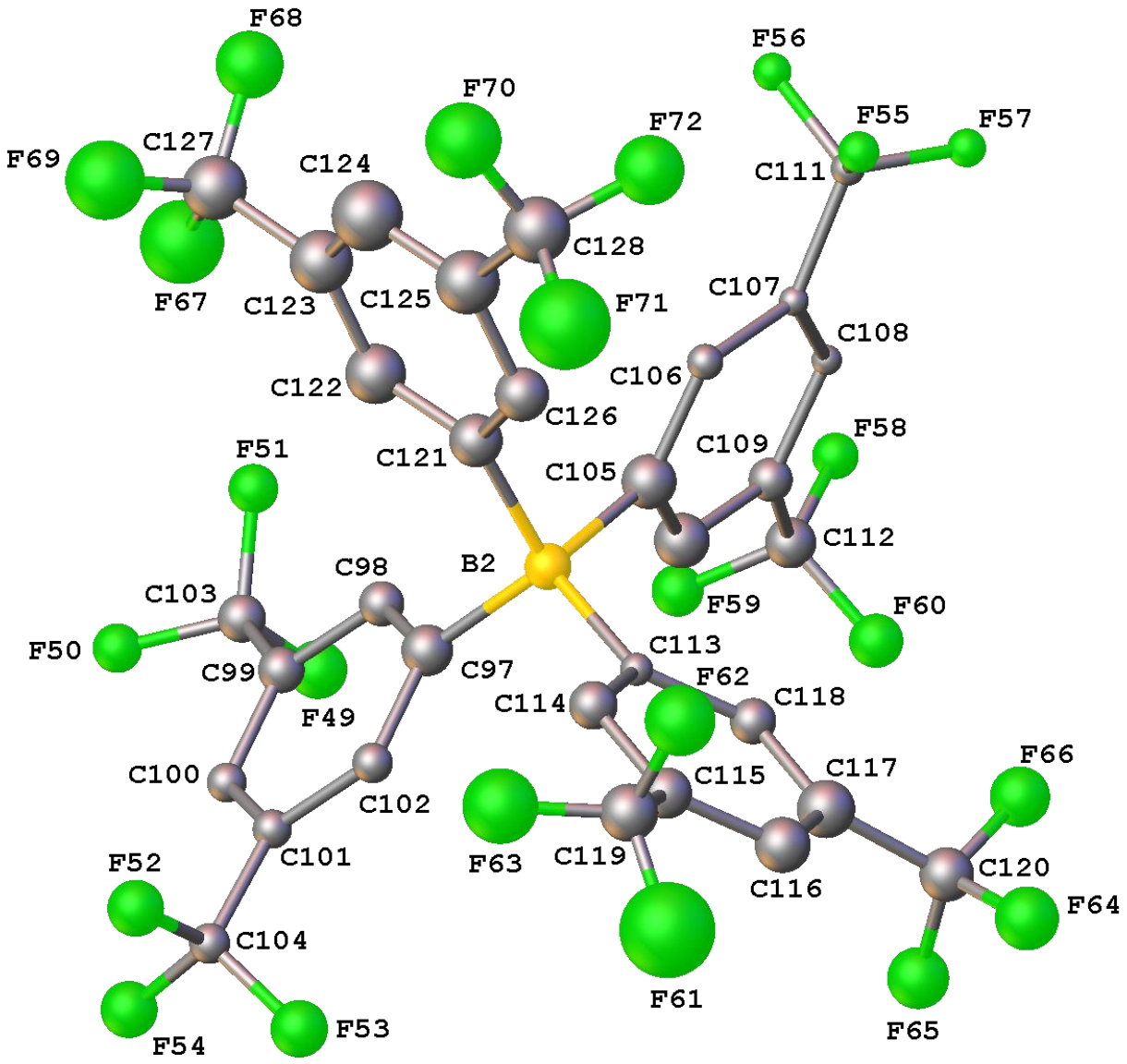

Figure D.4. A molecular drawing of the B2 anion shown with 30% probability ellipsoids. Only one position of the disordered components is shown. All H atoms are omitted.

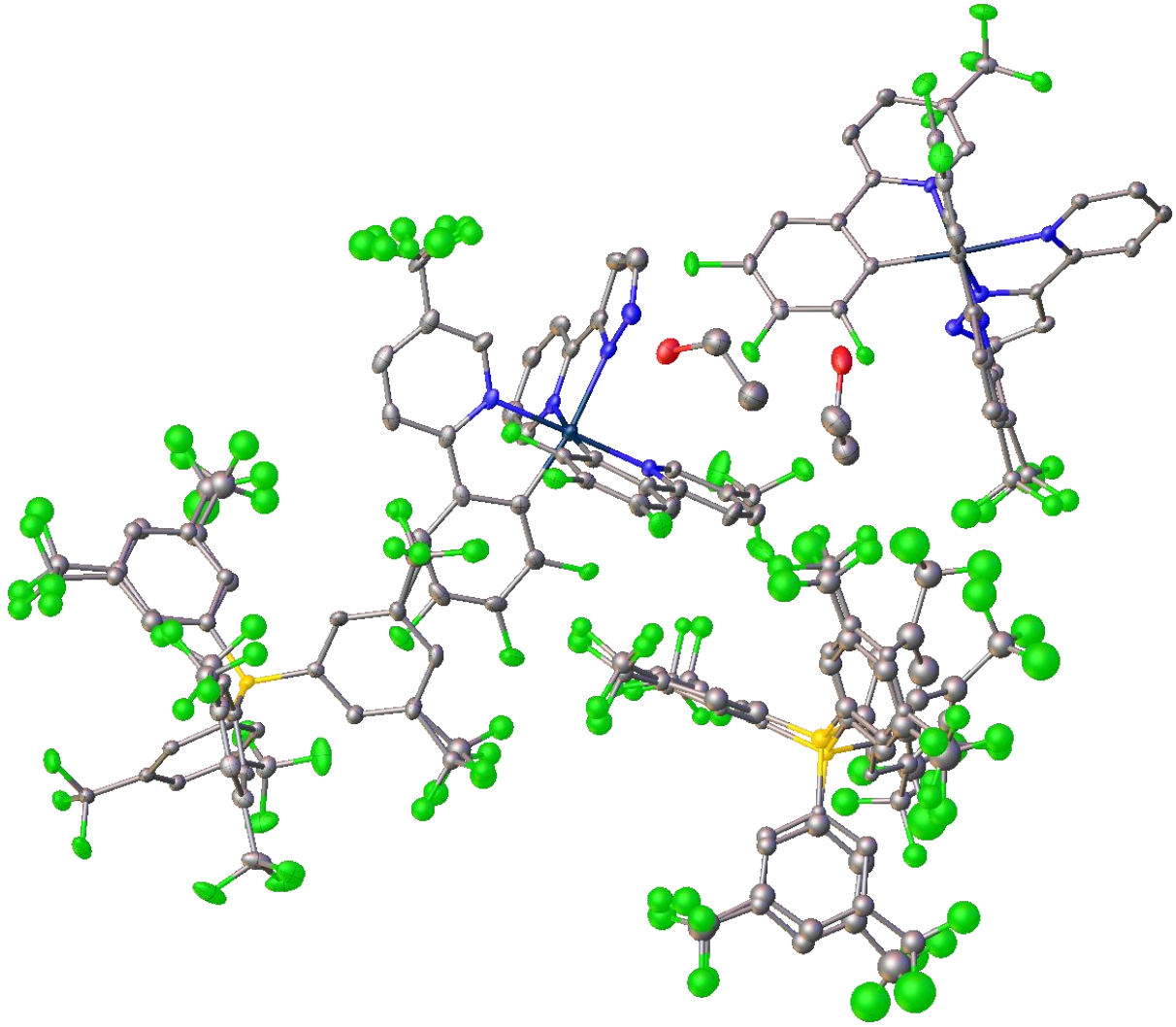

Figure D.5. The content of the asymmetric unit shown with 30% probability ellipsoids. All disordered atoms are shown. All H atoms are omitted.

Table D.1. Crystal data and structure refinement for **2.32**.

Identification code	yoon51	
Empirical formula	$[C_{32}H_{15}F_{12}IrN_5][C_{32}H_{12}BF_{24}].0.84EtOH$	
Formula weight	1791.84	
Temperature	100(2) K	
Wavelength	0.71073 Å	
Crystal system	Monoclinic	
Space group	$P2_1$	
Unit cell dimensions	a = 18.606(7) Å	α= 90°.
	b = 18.804(8) Å	β= 90.89(3)°.
	c = 19.121(7) Å	γ = 90°.
Volume	6689(5) $Å^3$	
Z	4	
Density (calculated)	1.779 Mg/m^3	
Absorption coefficient	2.145 mm^{-1}	
F(000)	3496	
Crystal size	0.078 x 0.057 x 0.040 mm^3	
Theta range for data collection	1.515 to 27.118°.	
Index ranges	-23<=h<=23, -24<=k<=24, -24<=l<=24	
Reflections collected	131360	
Independent reflections	29402 [R(int) = 0.0373]	
Completeness to theta = 25.000°	99.8 %	
Absorption correction	Numerical with SADABS	

Max. and min. transmission	.43 and .39
Refinement method	Full-matrix least-squares on F^2
Data / restraints / parameters	29402 / 4716 / 1780
Goodness-of-fit on F^2	1.010
Final R indices [I>2sigma(I)]	R1 = 0.0429, wR2 = 0.1089
R indices (all data)	R1 = 0.0474, wR2 = 0.1121
Absolute structure parameter	-0.0247(15)
Extinction coefficient	n/a
Largest diff. peak and hole	1.408 and -1.072 e.$Å^{-3}$

Table D.2. Atomic coordinates (x 10^4) and equivalent isotropic displacement parameters ($Å^2$x 10^3) for **2.32**. U(eq) is defined as one third of the trace of the orthogonalized U^{ij} tensor.

	x	y	z	U(eq)
Ir(1)	8895(1)	7131(1)	268(1)	24(1)
F(1)	8194(3)	6506(3)	1798(3)	40(1)
F(2)	7155(2)	7084(3)	2554(2)	40(1)
F(3)	6447(3)	8252(3)	2126(3)	45(1)
N(1)	8393(3)	6405(3)	-414(4)	26(1)
N(2)	7747(4)	6071(4)	-464(4)	30(1)
N(3)	9704(3)	6903(3)	-497(3)	27(1)
N(4)	8413(4)	7922(3)	-314(4)	26(1)

C(1)	7740(5)	5613(5)	-993(5)	37(2)
C(2)	8381(5)	5629(4)	-1316(5)	35(2)
C(3)	8784(4)	6141(4)	-940(4)	25(2)
C(4)	9514(4)	6435(4)	-996(4)	27(2)
C(5)	9981(4)	6234(5)	-1528(4)	31(2)
C(6)	10659(5)	6546(5)	-1527(5)	38(2)
C(7)	10855(4)	7031(5)	-1018(5)	36(2)
C(8)	10362(4)	7190(4)	-513(4)	30(2)
C(9)	8068(4)	7386(4)	905(4)	26(2)
C(10)	7868(3)	7100(5)	1538(4)	30(2)
C(11)	7323(4)	7374(5)	1937(4)	35(2)
C(12)	6954(4)	7974(5)	1710(5)	36(2)
C(13)	7111(4)	8273(5)	1066(5)	34(2)
C(14)	7654(4)	7978(4)	681(4)	29(2)
C(15)	7841(4)	8247(4)	-14(4)	28(2)
C(16)	7471(5)	8774(5)	-372(5)	41(2)
C(17)	7666(5)	8968(5)	-1031(5)	40(2)
C(19)	8603(4)	8103(4)	-961(4)	26(2)
C(18)	8242(4)	8605(4)	-1341(3)	31(2)
C(20)	8468(4)	8814(4)	-2061(4)	35(2)
F(4)	7907(3)	8807(3)	-2521(3)	46(1)
F(5)	8735(3)	9473(3)	-2080(3)	48(1)
F(6)	8964(3)	8382(3)	-2318(3)	45(1)

F(7)	9385(3)	8855(3)	325(3)	37(1)
F(8)	10273(3)	9502(3)	1238(3)	51(1)
F(9)	10947(3)	8778(4)	2260(3)	58(2)
C(21)	9532(4)	7737(5)	893(4)	28(2)
C(22)	9685(4)	8461(4)	839(4)	31(2)
C(23)	10151(4)	8803(5)	1299(5)	36(2)
C(24)	10491(5)	8414(6)	1828(5)	43(2)
C(25)	10383(5)	7707(6)	1894(5)	42(2)
C(26)	9895(4)	7368(5)	1433(4)	31(2)
C(27)	9752(19)	6595(6)	1427(14)	38(12)
C(28)	10025(12)	6093(8)	1894(11)	41(7)
C(29)	9878(9)	5393(7)	1835(10)	35(5)
C(30)	9459(7)	5156(6)	1261(11)	34(4)
C(31)	9180(9)	5666(5)	806(11)	27(5)
C(32)	9306(4)	4384(6)	1128(6)	34(3)
N(5)	9333(11)	6363(5)	881(10)	35(8)
F(10)	9865(5)	3970(5)	1264(9)	52(3)
F(11)	9144(5)	4245(5)	462(7)	54(3)
F(12)	8738(5)	4160(6)	1478(8)	60(4)
C(27A)	9790(30)	6616(8)	1470(20)	20(18)
C(28A)	10068(18)	6166(10)	1987(16)	24(11)
C(29A)	9915(18)	5470(10)	1987(17)	39(11)
C(30A)	9473(11)	5204(7)	1446(15)	24(8)

C(31A)	9202(17)	5663(7)	935(17)	24(11)
C(32A)	9274(7)	4434(7)	1393(13)	32(7)
N(5A)	9330(16)	6359(6)	966(15)	13(10)
F(10A)	9828(8)	4010(8)	1519(15)	45(6)
F(11A)	9004(14)	4258(11)	771(16)	95(10)
F(12A)	8764(10)	4259(12)	1839(19)	86(9)
Ir(2)	6292(1)	7273(1)	5269(1)	27(1)
F(13)	6825(3)	7817(3)	6900(2)	35(1)
F(14)	7886(3)	7289(3)	7702(2)	41(1)
F(15)	8770(3)	6277(4)	7228(3)	55(2)
F(16)	7229(3)	5487(3)	2575(3)	58(2)
F(17)	6534(4)	4751(3)	3078(3)	80(3)
F(18)	6152(4)	5790(4)	2804(4)	89(3)
F(19)	5825(3)	5542(3)	5386(3)	44(1)
F(20)	4888(3)	4933(3)	6249(4)	58(2)
F(21)	4156(3)	5722(4)	7179(3)	63(2)
F(22)	5205(6)	10433(6)	5972(12)	60(5)
F(23)	6207(10)	10165(7)	5485(7)	47(4)
F(24)	6169(10)	10329(6)	6591(6)	43(4)
F(22A)	5298(10)	10459(7)	6344(11)	90(7)
F(23A)	5807(11)	10209(7)	5374(5)	54(4)
F(24A)	6431(8)	10241(8)	6331(12)	95(8)
F(22B)	5350(10)	10361(8)	5611(11)	64(6)

F(23B)	6472(7)	10133(8)	5763(12)	54(5)
F(24B)	5830(14)	10422(7)	6635(7)	71(7)
N(6)	6828(4)	8016(4)	4632(4)	36(2)
N(7)	7426(5)	8395(5)	4664(5)	48(2)
N(8)	5521(4)	7501(4)	4461(3)	33(2)
N(9)	6792(4)	6467(4)	4727(4)	30(2)
N(10)	5824(4)	8066(4)	5850(3)	30(2)
C(33)	7417(7)	8929(7)	4171(6)	57(3)
C(34)	6806(6)	8893(6)	3819(5)	48(2)
C(35)	6427(5)	8308(5)	4110(5)	39(2)
C(36)	5724(6)	8008(5)	3994(5)	40(2)
C(37)	5242(6)	8217(5)	3456(4)	40(2)
C(38)	4577(6)	7909(6)	3403(5)	47(2)
C(39)	4357(6)	7392(6)	3876(5)	50(2)
C(40)	4863(4)	7210(5)	4386(4)	40(2)
C(41)	7089(4)	7023(4)	5965(4)	31(2)
C(42)	7227(4)	7301(5)	6626(4)	31(2)
C(43)	7780(4)	7025(5)	7055(4)	34(2)
C(44)	8216(5)	6496(6)	6803(5)	45(2)
C(45)	8114(5)	6217(6)	6164(6)	49(2)
C(46)	7537(5)	6466(5)	5754(4)	35(2)
C(47)	7380(5)	6177(5)	5054(5)	38(2)
C(48)	7765(6)	5636(6)	4736(6)	51(3)

C(49)	7549(6)	5407(6)	4080(7)	53(3)
C(50)	6963(5)	5704(4)	3756(3)	39(2)
C(51)	6588(5)	6233(4)	4085(5)	34(2)
C(52)	6714(4)	5441(4)	3052(4)	48(2)
C(53)	5620(4)	6684(5)	5867(4)	32(2)
C(54)	5488(5)	5963(5)	5848(5)	39(2)
C(55)	5010(5)	5641(5)	6290(5)	39(2)
C(56)	4630(5)	6049(6)	6759(5)	47(2)
C(57)	4728(5)	6767(6)	6804(5)	44(2)
C(58)	5215(4)	7091(5)	6350(4)	33(2)
C(59)	5345(5)	7853(5)	6325(4)	35(2)
C(60)	4992(5)	8367(6)	6744(5)	45(2)
C(61)	5144(6)	9073(6)	6653(5)	48(3)
C(62)	5648(5)	9274(3)	6163(4)	44(2)
C(63)	5985(5)	8768(5)	5771(5)	37(2)
C(64)	5813(4)	10045(4)	6054(4)	60(3)
B(1)	3624(5)	6200(4)	9562(5)	27(2)
C(65)	2910(4)	5729(4)	9377(4)	24(2)
C(66)	2349(4)	5715(4)	9865(4)	24(1)
C(67)	1684(4)	5425(4)	9700(4)	27(2)
C(68)	1542(4)	5096(4)	9071(4)	29(2)
C(69)	2102(4)	5085(4)	8591(4)	28(2)
C(70)	2763(4)	5407(4)	8732(4)	26(2)

C(71)	1097(5)	5478(5)	10225(4)	32(2)
C(72)	1948(5)	4742(5)	7888(5)	39(2)
C(73)	3932(4)	6040(4)	10356(4)	28(2)
C(74)	3946(4)	5338(5)	10616(4)	31(2)
C(75)	4294(5)	5169(5)	11235(5)	38(2)
C(76)	4641(5)	5680(5)	11627(5)	38(2)
C(77)	4633(4)	6368(4)	11391(4)	42(2)
C(78)	4294(4)	6540(5)	10761(4)	32(2)
C(79)	4317(6)	4409(6)	11476(6)	50(3)
F(25)	1103(3)	6092(3)	10579(3)	50(1)
F(26)	1114(3)	4961(4)	10697(3)	54(2)
F(27)	435(3)	5438(3)	9923(3)	41(1)
F(28)	1492(4)	5130(4)	7498(3)	58(2)
F(29)	2523(3)	4614(5)	7525(4)	75(2)
F(30)	1610(4)	4104(3)	7969(4)	68(2)
F(31)	3867(3)	4280(4)	11995(4)	75(2)
F(32)	4971(3)	4214(4)	11719(3)	58(2)
F(33)	4154(4)	3944(3)	10964(4)	69(2)
C(80)	5033(6)	6891(6)	11835(6)	53(6)
F(34)	4735(7)	7545(4)	11788(7)	55(5)
F(35)	5059(6)	6718(5)	12516(4)	49(3)
F(36)	5704(4)	6968(7)	11625(7)	60(4)
C(80A)	5046(6)	6990(6)	11694(7)	47(6)

F(34A)	4596(7)	7536(5)	11832(8)	49(6)
F(35A)	5361(8)	6818(7)	12309(6)	58(5)
F(36A)	5564(7)	7236(8)	11296(8)	66(5)
C(81)	4319(4)	6026(4)	9082(4)	26(2)
C(82)	4485(4)	5316(5)	8911(5)	32(2)
C(83)	5111(4)	5136(3)	8579(5)	38(2)
C(84)	5619(4)	5663(5)	8403(5)	37(2)
C(85)	5473(3)	6366(3)	8577(4)	33(2)
C(86)	4833(4)	6537(4)	8903(4)	31(2)
C(87)	5286(5)	4359(5)	8493(6)	33(4)
F(37)	4812(5)	3918(5)	8792(7)	54(4)
F(38)	5934(5)	4189(6)	8760(7)	51(4)
F(39)	5307(6)	4170(6)	7823(5)	54(4)
C(87A)	5293(7)	4418(6)	8301(7)	58(7)
F(37A)	4720(6)	3981(6)	8343(9)	63(5)
F(38A)	5825(7)	4111(7)	8676(8)	70(7)
F(39A)	5495(7)	4412(7)	7641(6)	59(4)
C(88)	6003(5)	6912(5)	8358(7)	34(6)
F(40)	6440(6)	7079(7)	8905(7)	47(4)
F(41)	5695(6)	7525(5)	8160(8)	33(6)
F(42)	6423(7)	6701(6)	7846(8)	48(4)
C(88A)	6002(6)	6959(6)	8472(7)	47(8)
F(40A)	6241(8)	7260(7)	9074(6)	49(4)

F(41A)	5713(8)	7489(6)	8089(8)	56(10)
F(42A)	6589(6)	6760(6)	8135(10)	52(4)
C(89)	3293(8)	7026(5)	9438(6)	30(6)
C(90)	3297(8)	7313(6)	8768(5)	38(5)
C(91)	2977(7)	7969(6)	8640(5)	50(5)
C(92)	2653(7)	8338(5)	9180(6)	44(5)
C(93)	2649(6)	8050(5)	9850(5)	32(4)
C(94)	2969(7)	7394(6)	9979(4)	28(4)
C(95)	3097(7)	8352(7)	7970(6)	77(9)
C(96)	2269(6)	8428(6)	10424(7)	45(5)
F(43)	3693(6)	8764(7)	7998(7)	87(5)
F(44)	2549(5)	8779(6)	7807(6)	65(4)
F(45)	3187(7)	7910(6)	7440(5)	77(4)
F(46)	2586(7)	8318(8)	11051(6)	74(4)
F(47)	1582(5)	8224(7)	10473(7)	64(4)
F(48)	2246(7)	9128(5)	10332(8)	79(5)
C(89A)	3354(11)	7052(6)	9505(8)	30(7)
C(90A)	3351(9)	7404(7)	8865(6)	28(5)
C(91A)	3021(8)	8064(7)	8799(5)	31(5)
C(92A)	2694(7)	8373(5)	9372(7)	32(5)
C(93A)	2696(8)	8021(7)	10012(6)	33(5)
C(94A)	3026(10)	7361(7)	10078(6)	44(7)
C(95A)	2968(8)	8364(7)	8074(6)	58(8)

C(96A)	2297(6)	8329(7)	10615(7)	33(5)
F(43A)	2838(9)	9070(6)	8090(8)	81(6)
F(44A)	2420(9)	8086(11)	7694(9)	129(10)
F(45A)	3549(8)	8264(9)	7698(7)	80(6)
F(46A)	2611(7)	8153(8)	11234(6)	59(4)
F(47A)	1629(6)	8077(8)	10655(8)	53(4)
F(48A)	2270(8)	9031(5)	10599(9)	59(4)
B(2)	8532(6)	2815(6)	5694(6)	40(6)
C(97)	9329(6)	3171(7)	5961(11)	49(7)
C(98)	9417(6)	3905(6)	5941(10)	38(5)
C(99)	10069(7)	4206(4)	6147(8)	40(5)
C(100)	10632(5)	3773(6)	6372(7)	29(4)
C(101)	10544(5)	3040(5)	6392(7)	28(4)
C(102)	9892(7)	2739(4)	6186(9)	30(4)
C(103)	10115(6)	4996(6)	6145(7)	43(5)
C(104)	11150(6)	2550(6)	6577(6)	31(5)
C(105)	7819(6)	3371(9)	5803(8)	55(8)
C(106)	7234(7)	3381(7)	5342(6)	24(4)
C(107)	6644(5)	3810(6)	5481(5)	16(3)
C(108)	6640(5)	4230(6)	6079(6)	17(4)
C(109)	7226(7)	4220(7)	6540(6)	36(6)
C(110)	7815(7)	3791(9)	6401(8)	57(9)
C(111)	6035(5)	3863(5)	4969(6)	21(3)

C(112)	7294(7)	4703(7)	7156(6)	48(7)
C(113)	8388(8)	2020(6)	6098(6)	20(3)
C(114)	8695(7)	1392(7)	5864(6)	43(5)
C(115)	8584(8)	761(6)	6225(7)	49(5)
C(116)	8165(10)	757(6)	6820(7)	57(7)
C(117)	7858(9)	1386(8)	7055(7)	62(11)
C(118)	7969(8)	2017(6)	6694(7)	39(6)
C(119)	8820(8)	76(7)	5894(8)	62(6)
C(120)	7455(7)	1375(7)	7730(7)	54(12)
C(121)	8542(9)	2758(8)	4808(5)	52(6)
C(122)	8841(9)	3328(7)	4452(8)	67(7)
C(123)	8802(9)	3352(7)	3726(8)	74(8)
C(124)	8465(10)	2807(9)	3356(5)	93(10)
C(125)	8167(8)	2237(8)	3712(7)	76(7)
C(126)	8205(8)	2212(7)	4438(7)	54(5)
C(127)	9111(8)	3968(7)	3336(8)	76(8)
C(128)	7701(8)	1681(8)	3369(8)	82(9)
F(49)	9886(8)	5269(8)	6755(6)	64(4)
F(50)	10787(5)	5228(7)	6061(8)	45(4)
F(51)	9713(6)	5294(6)	5645(7)	45(3)
F(52)	11413(6)	2198(7)	6018(5)	59(4)
F(53)	10953(6)	2047(6)	7032(6)	60(4)
F(54)	11708(6)	2894(6)	6859(7)	60(4)

F(55)	5943(6)	3246(4)	4617(5)	31(3)
F(56)	6135(5)	4385(5)	4501(5)	27(2)
F(57)	5411(4)	4008(6)	5265(5)	28(2)
F(58)	6845(6)	5261(6)	7096(7)	40(3)
F(59)	7959(6)	4969(8)	7214(7)	50(4)
F(60)	7148(8)	4372(7)	7747(6)	54(4)
F(61)	8952(14)	-430(9)	6371(10)	170(20)
F(62)	8334(9)	-195(9)	5430(9)	91(6)
F(63)	9417(8)	142(10)	5530(10)	105(7)
F(64)	7193(8)	723(6)	7873(8)	75(5)
F(65)	7864(7)	1571(9)	8282(7)	71(5)
F(66)	6895(7)	1815(8)	7742(8)	67(4)
F(67)	9407(11)	4466(9)	3764(9)	130(9)
F(68)	8615(8)	4322(8)	2964(8)	84(5)
F(69)	9616(9)	3776(10)	2897(9)	116(8)
F(70)	7816(10)	1633(10)	2675(7)	106(7)
F(71)	7822(11)	1028(7)	3628(11)	152(11)
F(72)	7003(7)	1803(9)	3433(9)	89(5)
B(3)	8497(5)	2624(6)	5670(5)	26(4)
C(129)	8333(10)	1882(6)	6137(8)	61(7)
C(130)	8523(9)	1224(8)	5866(6)	68(7)
C(131)	8367(9)	606(6)	6234(7)	64(6)
C(132)	8023(8)	647(5)	6872(7)	51(5)

C(133)	7833(8)	1305(7)	7143(6)	40(6)
C(134)	7989(9)	1923(5)	6776(8)	39(6)
C(135)	8463(8)	-138(7)	5972(7)	111(12)
C(136)	7404(7)	1364(7)	7794(7)	83(16)
C(137)	8566(4)	2405(5)	4819(3)	15(2)
C(138)	8043(4)	1966(5)	4523(4)	21(3)
C(139)	8047(4)	1823(5)	3809(4)	38(4)
C(140)	8574(6)	2119(6)	3392(3)	55(5)
C(141)	9097(5)	2558(7)	3688(5)	69(6)
C(142)	9093(5)	2701(6)	4402(5)	51(5)
C(143)	7467(6)	1342(6)	3534(6)	44(4)
C(144)	9696(7)	2859(7)	3256(7)	71(7)
C(145)	7839(5)	3229(7)	5800(6)	18(3)
C(146)	7302(6)	3268(7)	5288(5)	39(5)
C(147)	6732(5)	3737(7)	5365(5)	36(5)
C(148)	6698(5)	4168(6)	5954(6)	39(5)
C(149)	7235(6)	4130(7)	6466(5)	29(5)
C(150)	7806(5)	3660(7)	6389(5)	20(4)
C(151)	6150(6)	3766(6)	4814(6)	37(4)
C(152)	7212(6)	4568(7)	7122(5)	37(4)
C(153)	9264(6)	3024(7)	5936(10)	37(4)
C(154)	9819(7)	2583(5)	6165(9)	51(6)
C(155)	10462(6)	2876(7)	6408(9)	70(8)

C(156)	10550(6)	3609(7)	6420(9)	59(6)
C(157)	9995(8)	4050(5)	6191(9)	55(6)
C(158)	9352(6)	3758(6)	5949(10)	52(6)
C(159)	11094(7)	2437(7)	6637(7)	107(14)
C(160)	10092(7)	4836(6)	6259(8)	61(6)
F(73)	8750(10)	-132(8)	5326(6)	96(5)
F(74)	7846(7)	-501(9)	5931(11)	154(9)
F(75)	8901(7)	-514(7)	6372(6)	57(4)
F(76)	7711(8)	1822(8)	8245(7)	80(5)
F(77)	6740(6)	1598(8)	7636(8)	83(5)
F(78)	7346(8)	756(6)	8135(8)	83(5)
F(79)	6816(5)	1547(7)	3739(7)	78(4)
F(80)	7548(6)	671(5)	3762(6)	57(3)
F(81)	7455(6)	1315(6)	2840(4)	58(3)
F(82)	9783(9)	3562(6)	3369(9)	115(6)
F(83)	10330(6)	2560(10)	3417(10)	142(9)
F(84)	9595(9)	2785(9)	2576(5)	114(6)
F(85)	5497(5)	3884(6)	5085(6)	44(3)
F(86)	6269(6)	4278(5)	4347(6)	49(3)
F(87)	6100(6)	3166(5)	4455(6)	52(3)
F(88)	7028(7)	4169(7)	7679(6)	66(4)
F(89)	6721(6)	5090(6)	7088(7)	57(4)
F(90)	7836(6)	4868(7)	7285(7)	54(4)

F(91)	11559(7)	2343(9)	6115(7)	81
F(92)	10891(7)	1786(6)	6842(8)	81
F(93)	11460(7)	2734(7)	7161(7)	81
F(94)	10769(7)	5043(8)	6113(9)	72(5)
F(95)	9974(10)	5070(9)	6913(8)	104(7)
F(96)	9658(9)	5214(8)	5846(10)	114(9)
O(1)	6649(4)	6232(4)	451(5)	70(2)
C(1S)	6515(8)	5588(6)	827(5)	89(4)
C(2S)	6074(8)	5104(6)	355(8)	92(5)
O(2)	8522(5)	8011(6)	5565(6)	55(3)
C(3S)	9289(5)	7964(8)	5548(12)	80(6)
C(4S)	9488(9)	7183(9)	5533(14)	103(8)

Table D.3. Bond lengths [Å] and angles [°] for **2.32**

Ir(1)-C(21)	2.023(8)	F(1)-C(10)	1.362(10)
Ir(1)-N(5)	2.024(12)	F(2)-C(11)	1.340(10)
Ir(1)-C(9)	2.035(7)	F(3)-C(12)	1.350(9)
Ir(1)-N(4)	2.054(7)	N(1)-C(3)	1.345(11)
Ir(1)-N(1)	2.097(6)	N(1)-N(2)	1.359(9)
Ir(1)-N(5A)	2.124(15)	N(2)-C(1)	1.329(12)
Ir(1)-N(3)	2.157(6)	N(2)-H(2)	0.8800

N(3)-C(8)	1.340(10)	C(13)-H(13)	0.9500
N(3)-C(4)	1.342(10)	C(14)-C(15)	1.470(12)
N(4)-C(19)	1.336(11)	C(15)-C(16)	1.382(12)
N(4)-C(15)	1.361(10)	C(16)-C(17)	1.366(14)
C(1)-C(2)	1.350(14)	C(16)-H(16)	0.9500
C(1)-H(1)	0.9500	C(17)-C(18)	1.408(12)
C(2)-C(3)	1.409(11)	C(17)-H(17)	0.9500
C(2)-H(2A)	0.9500	C(19)-C(18)	1.363(10)
C(3)-C(4)	1.471(11)	C(19)-H(19)	0.9500
C(4)-C(5)	1.400(11)	C(18)-C(20)	1.499(8)
C(5)-C(6)	1.392(13)	C(20)-F(6)	1.329(8)
C(5)-H(5)	0.9500	C(20)-F(5)	1.336(7)
C(6)-C(7)	1.380(13)	C(20)-F(4)	1.354(7)
C(6)-H(6)	0.9500	F(7)-C(22)	1.346(10)
C(7)-C(8)	1.374(11)	F(8)-C(23)	1.340(11)
C(7)-H(7)	0.9500	F(9)-C(24)	1.359(10)
C(8)-H(8)	0.9500	C(21)-C(22)	1.393(12)
C(9)-C(10)	1.381(11)	C(21)-C(26)	1.407(11)
C(9)-C(14)	1.415(11)	C(22)-C(23)	1.385(12)
C(10)-C(11)	1.379(11)	C(23)-C(24)	1.393(14)
C(11)-C(12)	1.387(13)	C(24)-C(25)	1.350(15)
C(12)-C(13)	1.388(13)	C(25)-C(26)	1.408(12)
C(13)-C(14)	1.377(11)	C(25)-H(25)	0.9500

C(26)-C(27A)	1.430(15)	C(31A)-N(5A)	1.331(13)
C(26)-C(27)	1.478(14)	C(31A)-H(31A)	0.9500
C(27)-N(5)	1.364(18)	C(32A)-F(10A)	1.323(9)
C(27)-C(28)	1.390(16)	C(32A)-F(11A)	1.325(9)
C(28)-C(29)	1.350(19)	C(32A)-F(12A)	1.328(9)
C(28)-H(28)	0.9500	Ir(2)-C(41)	2.032(7)
C(29)-C(30)	1.41(2)	Ir(2)-C(53)	2.036(9)
C(29)-H(29)	0.9500	Ir(2)-N(10)	2.061(7)
C(30)-C(31)	1.392(18)	Ir(2)-N(9)	2.066(7)
C(30)-C(32)	1.501(15)	Ir(2)-N(6)	2.112(8)
C(31)-N(5)	1.347(11)	Ir(2)-N(8)	2.136(7)
C(31)-H(31)	0.9500	F(13)-C(42)	1.337(10)
C(32)-F(10)	1.322(8)	F(14)-C(43)	1.344(10)
C(32)-F(12)	1.329(8)	F(15)-C(44)	1.366(10)
C(32)-F(11)	1.330(9)	F(16)-C(52)	1.336(8)
C(27A)-N(5A)	1.37(2)	F(17)-C(52)	1.341(8)
C(27A)-C(28A)	1.392(17)	F(18)-C(52)	1.317(8)
C(28A)-C(29A)	1.34(2)	F(19)-C(54)	1.348(11)
C(28A)-H(28A)	0.9500	F(20)-C(55)	1.353(11)
C(29A)-C(30A)	1.40(2)	F(21)-C(56)	1.350(11)
C(29A)-H(29A)	0.9500	F(22)-C(64)	1.354(8)
C(30A)-C(31A)	1.39(2)	F(23)-C(64)	1.340(9)
C(30A)-C(32A)	1.498(17)	F(24)-C(64)	1.325(8)

F(22A)-C(64)	1.360(9)	C(37)-H(37)	0.9500
F(23A)-C(64)	1.337(9)	C(38)-C(39)	1.394(15)
F(24A)-C(64)	1.311(9)	C(38)-H(38)	0.9500
F(22B)-C(64)	1.339(9)	C(39)-C(40)	1.387(12)
F(23B)-C(64)	1.365(9)	C(39)-H(39)	0.9500
F(24B)-C(64)	1.319(9)	C(40)-H(40)	0.9500
N(6)-N(7)	1.321(12)	C(41)-C(42)	1.388(11)
N(6)-C(35)	1.354(12)	C(41)-C(46)	1.401(12)
N(7)-C(33)	1.378(15)	C(42)-C(43)	1.404(11)
N(7)-H(7A)	0.8800	C(43)-C(44)	1.376(14)
N(8)-C(40)	1.346(11)	C(44)-C(45)	1.340(15)
N(8)-C(36)	1.364(12)	C(45)-C(46)	1.401(12)
N(9)-C(51)	1.354(11)	C(45)-H(45)	0.9500
N(9)-C(47)	1.364(11)	C(46)-C(47)	1.468(13)
N(10)-C(59)	1.344(12)	C(47)-C(48)	1.391(13)
N(10)-C(63)	1.363(12)	C(48)-C(49)	1.380(16)
C(33)-C(34)	1.314(17)	C(48)-H(48)	0.9500
C(33)-H(33)	0.9500	C(49)-C(50)	1.365(14)
C(34)-C(35)	1.424(14)	C(49)-H(49)	0.9500
C(34)-H(34)	0.9500	C(50)-C(51)	1.374(11)
C(35)-C(36)	1.439(15)	C(50)-C(52)	1.500(8)
C(36)-C(37)	1.410(13)	C(51)-H(51)	0.9500
C(37)-C(38)	1.369(15)	C(53)-C(54)	1.378(13)

C(53)-C(58)	1.424(12)	C(66)-H(66)	0.9500
C(54)-C(55)	1.377(13)	C(67)-C(68)	1.374(11)
C(55)-C(56)	1.384(15)	C(67)-C(71)	1.498(11)
C(56)-C(57)	1.363(16)	C(68)-C(69)	1.399(11)
C(57)-C(58)	1.403(13)	C(68)-H(68)	0.9500
C(57)-H(57)	0.9500	C(69)-C(70)	1.393(11)
C(58)-C(59)	1.455(14)	C(69)-C(72)	1.514(12)
C(59)-C(60)	1.422(13)	C(70)-H(70)	0.9500
C(60)-C(61)	1.369(16)	C(71)-F(26)	1.327(10)
C(60)-H(60)	0.9500	C(71)-F(25)	1.340(10)
C(61)-C(62)	1.388(14)	C(71)-F(27)	1.355(10)
C(61)-H(61)	0.9500	C(72)-F(29)	1.307(11)
C(62)-C(63)	1.369(12)	C(72)-F(28)	1.338(10)
C(62)-C(64)	1.497(7)	C(72)-F(30)	1.364(12)
C(63)-H(63)	0.9500	C(73)-C(78)	1.386(11)
B(1)-C(81)	1.629(11)	C(73)-C(74)	1.411(11)
B(1)-C(65)	1.630(11)	C(74)-C(75)	1.379(12)
B(1)-C(73)	1.642(12)	C(74)-H(74)	0.9500
B(1)-C(89A)	1.683(9)	C(75)-C(76)	1.374(12)
B(1)-C(89)	1.686(8)	C(75)-C(79)	1.501(14)
C(65)-C(70)	1.398(11)	C(76)-C(77)	1.371(13)
C(65)-C(66)	1.412(11)	C(76)-H(76)	0.9500
C(66)-C(67)	1.384(10)	C(77)-C(78)	1.388(12)

C(77)-C(80)	1.492(9)	C(85)-C(88A)	1.503(9)
C(77)-C(80A)	1.509(9)	C(86)-H(86)	0.9500
C(78)-H(78)	0.9500	C(87)-F(39)	1.331(10)
C(79)-F(31)	1.330(13)	C(87)-F(38)	1.341(9)
C(79)-F(33)	1.343(13)	C(87)-F(37)	1.344(9)
C(79)-F(32)	1.347(11)	C(87A)-F(39A)	1.322(10)
C(80)-F(36)	1.325(10)	C(87A)-F(38A)	1.343(10)
C(80)-F(35)	1.342(10)	C(87A)-F(37A)	1.350(10)
C(80)-F(34)	1.351(10)	C(88)-F(42)	1.322(10)
C(80A)-F(36A)	1.321(10)	C(88)-F(41)	1.340(9)
C(80A)-F(35A)	1.346(10)	C(88)-F(40)	1.353(10)
C(80A)-F(34A)	1.354(10)	C(88A)-F(42A)	1.331(10)
C(81)-C(86)	1.402(11)	C(88A)-F(41A)	1.344(10)
C(81)-C(82)	1.410(11)	C(88A)-F(40A)	1.352(10)
C(82)-C(83)	1.378(11)	C(89)-C(90)	1.3900
C(82)-H(82)	0.9500	C(89)-C(94)	1.3900
C(83)-C(84)	1.414(12)	C(90)-C(91)	1.3900
C(83)-C(87A)	1.492(9)	C(90)-H(90)	0.9500
C(83)-C(87)	1.507(9)	C(91)-C(92)	1.3900
C(84)-C(85)	1.390(12)	C(91)-C(95)	1.489(10)
C(84)-H(84)	0.9500	C(92)-C(93)	1.3900
C(85)-C(86)	1.390(11)	C(92)-H(92)	0.9500
C(85)-C(88)	1.489(9)	C(93)-C(94)	1.3900

C(93)-C(96)	1.495(9)	C(96A)-F(47A)	1.333(9)
C(94)-H(94)	0.9500	C(96A)-F(46A)	1.352(10)
C(95)-F(45)	1.323(10)	B(2)-C(121)	1.697(10)
C(95)-F(44)	1.331(10)	B(2)-C(97)	1.698(10)
C(95)-F(43)	1.353(10)	B(2)-C(105)	1.704(10)
C(96)-F(48)	1.328(10)	B(2)-C(113)	1.707(10)
C(96)-F(47)	1.338(9)	C(97)-C(98)	1.3900
C(96)-F(46)	1.343(10)	C(97)-C(102)	1.3900
C(89A)-C(90A)	1.3900	C(98)-C(99)	1.3900
C(89A)-C(94A)	1.3900	C(98)-H(98)	0.9500
C(90A)-C(91A)	1.3900	C(99)-C(100)	1.3900
C(90A)-H(90A)	0.9500	C(99)-C(103)	1.488(9)
C(91A)-C(92A)	1.3900	C(100)-C(101)	1.3900
C(91A)-C(95A)	1.499(9)	C(100)-H(100)	0.9500
C(92A)-C(93A)	1.3900	C(101)-C(102)	1.3900
C(92A)-H(92A)	0.9500	C(101)-C(104)	1.494(9)
C(93A)-C(94A)	1.3900	C(102)-H(102)	0.9500
C(93A)-C(96A)	1.497(9)	C(103)-F(51)	1.329(10)
C(94A)-H(94A)	0.9500	C(103)-F(50)	1.336(10)
C(95A)-F(45A)	1.321(10)	C(103)-F(49)	1.350(10)
C(95A)-F(44A)	1.347(10)	C(104)-F(54)	1.331(9)
C(95A)-F(43A)	1.350(10)	C(104)-F(53)	1.340(10)
C(96A)-F(48A)	1.321(10)	C(104)-F(52)	1.355(9)

C(105)-C(106)	1.3900	C(116)-C(117)	1.3900
C(105)-C(110)	1.3900	C(116)-H(116)	0.9500
C(106)-C(107)	1.3900	C(117)-C(118)	1.3900
C(106)-H(106)	0.9500	C(117)-C(120)	1.503(10)
C(107)-C(108)	1.3900	C(118)-H(118)	0.9500
C(107)-C(111)	1.490(8)	C(119)-F(63)	1.325(10)
C(108)-C(109)	1.3900	C(119)-F(61)	1.338(10)
C(108)-H(108)	0.9500	C(119)-F(62)	1.356(10)
C(109)-C(110)	1.3900	C(120)-F(66)	1.330(10)
C(109)-C(112)	1.491(10)	C(120)-F(65)	1.344(10)
C(110)-H(110)	0.9500	C(120)-F(64)	1.350(10)
C(111)-F(57)	1.327(9)	C(121)-C(122)	1.3900
C(111)-F(56)	1.342(9)	C(121)-C(126)	1.3900
C(111)-F(55)	1.349(9)	C(122)-C(123)	1.3900
C(112)-F(60)	1.323(10)	C(122)-H(122)	0.9500
C(112)-F(59)	1.338(10)	C(123)-C(124)	1.3900
C(112)-F(58)	1.345(10)	C(123)-C(127)	1.497(10)
C(113)-C(114)	1.3900	C(124)-C(125)	1.3900
C(113)-C(118)	1.3900	C(124)-H(124)	0.9500
C(114)-C(115)	1.3900	C(125)-C(126)	1.3900
C(114)-H(114)	0.9500	C(125)-C(128)	1.501(10)
C(115)-C(116)	1.3900	C(126)-H(126)	0.9500
C(115)-C(119)	1.503(9)	C(127)-F(69)	1.320(10)

C(127)-F(68)	1.336(10)	C(136)-F(78)	1.321(10)
C(127)-F(67)	1.354(10)	C(136)-F(76)	1.340(10)
C(128)-F(72)	1.326(10)	C(136)-F(77)	1.341(10)
C(128)-F(71)	1.341(10)	C(137)-C(138)	1.3900
C(128)-F(70)	1.351(10)	C(137)-C(142)	1.3900
B(3)-C(153)	1.685(9)	C(138)-C(139)	1.3900
B(3)-C(137)	1.686(9)	C(138)-H(138)	0.9500
B(3)-C(129)	1.686(9)	C(139)-C(140)	1.3900
B(3)-C(145)	1.693(9)	C(139)-C(143)	1.498(9)
C(129)-C(130)	1.3900	C(140)-C(141)	1.3900
C(129)-C(134)	1.3900	C(140)-H(140)	0.9500
C(130)-C(131)	1.3900	C(141)-C(142)	1.3900
C(130)-H(130)	0.9500	C(141)-C(144)	1.508(9)
C(131)-C(132)	1.3900	C(142)-H(142)	0.9500
C(131)-C(135)	1.497(10)	C(143)-F(81)	1.327(9)
C(132)-C(133)	1.3900	C(143)-F(79)	1.336(9)
C(132)-H(132)	0.9500	C(143)-F(80)	1.343(10)
C(133)-C(134)	1.3900	C(144)-F(84)	1.319(10)
C(133)-C(136)	1.493(10)	C(144)-F(83)	1.338(10)
C(134)-H(134)	0.9500	C(144)-F(82)	1.349(10)
C(135)-F(75)	1.314(10)	C(145)-C(146)	1.3900
C(135)-F(74)	1.338(10)	C(145)-C(150)	1.3900
C(135)-F(73)	1.354(10)	C(146)-C(147)	1.3900

C(146)-H(146)	0.9500	C(157)-C(160)	1.494(9)
C(147)-C(148)	1.3900	C(158)-H(158)	0.9500
C(147)-C(151)	1.498(9)	C(159)-F(93)	1.326(10)
C(148)-C(149)	1.3900	C(159)-F(92)	1.342(10)
C(148)-H(148)	0.9500	C(159)-F(91)	1.344(10)
C(149)-C(150)	1.3900	C(160)-F(96)	1.326(10)
C(149)-C(152)	1.501(9)	C(160)-F(95)	1.348(10)
C(150)-H(150)	0.9500	C(160)-F(94)	1.351(10)
C(151)-F(87)	1.323(10)	O(1)-C(1S)	1.4311
C(151)-F(86)	1.335(9)	O(1)-H(1S)	0.8400
C(151)-F(85)	1.346(9)	C(1S)-C(2S)	1.5147
C(152)-F(90)	1.324(10)	C(1S)-H(1S1)	0.9900
C(152)-F(89)	1.341(9)	C(1S)-H(1S2)	0.9900
C(152)-F(88)	1.352(10)	C(2S)-H(2S1)	0.9800
C(153)-C(154)	1.3900	C(2S)-H(2S2)	0.9800
C(153)-C(158)	1.3900	C(2S)-H(2S3)	0.9800
C(154)-C(155)	1.3900	O(2)-C(3S)	1.4298
C(154)-H(154)	0.9500	O(2)-H(2S)	0.8400
C(155)-C(156)	1.3900	C(3S)-C(4S)	1.5146
C(155)-C(159)	1.496(10)	C(3S)-H(3S1)	0.9900
C(156)-C(157)	1.3900	C(3S)-H(3S2)	0.9900
C(156)-H(156)	0.9500	C(4S)-H(4S1)	0.9800
C(157)-C(158)	1.3900	C(4S)-H(4S2)	0.9800

C(4S)-H(4S3)	0.9800		
C(21)-Ir(1)-N(5)	80.4(4)	N(2)-N(1)-Ir(1)	136.8(6)
C(21)-Ir(1)-C(9)	87.4(3)	C(1)-N(2)-N(1)	110.5(7)
N(5)-Ir(1)-C(9)	97.0(7)	C(1)-N(2)-H(2)	124.8
C(21)-Ir(1)-N(4)	99.2(3)	N(1)-N(2)-H(2)	124.8
N(5)-Ir(1)-N(4)	177.0(7)	C(8)-N(3)-C(4)	118.6(7)
C(9)-Ir(1)-N(4)	80.0(3)	C(8)-N(3)-Ir(1)	125.7(5)
C(21)-Ir(1)-N(1)	170.3(3)	C(4)-N(3)-Ir(1)	115.7(5)
N(5)-Ir(1)-N(1)	93.8(4)	C(19)-N(4)-C(15)	119.7(7)
C(9)-Ir(1)-N(1)	101.1(3)	C(19)-N(4)-Ir(1)	124.4(5)
N(4)-Ir(1)-N(1)	87.1(2)	C(15)-N(4)-Ir(1)	115.8(6)
C(21)-Ir(1)-N(5A)	78.4(4)	N(2)-C(1)-C(2)	109.6(8)
C(9)-Ir(1)-N(5A)	93.9(10)	N(2)-C(1)-H(1)	125.2
N(4)-Ir(1)-N(5A)	173.6(10)	C(2)-C(1)-H(1)	125.2
N(1)-Ir(1)-N(5A)	96.2(4)	C(1)-C(2)-C(3)	104.4(8)
C(21)-Ir(1)-N(3)	96.0(3)	C(1)-C(2)-H(2A)	127.8
N(5)-Ir(1)-N(3)	88.4(7)	C(3)-C(2)-H(2A)	127.8
C(9)-Ir(1)-N(3)	174.1(3)	N(1)-C(3)-C(2)	110.1(7)
N(4)-Ir(1)-N(3)	94.6(3)	N(1)-C(3)-C(4)	115.2(7)
N(1)-Ir(1)-N(3)	76.0(3)	C(2)-C(3)-C(4)	134.7(8)
N(5A)-Ir(1)-N(3)	91.6(10)	N(3)-C(4)-C(5)	122.3(7)
C(3)-N(1)-N(2)	105.3(6)	N(3)-C(4)-C(3)	115.3(7)
C(3)-N(1)-Ir(1)	117.7(5)	C(5)-C(4)-C(3)	122.4(7)

C(6)-C(5)-C(4)	117.3(8)	C(11)-C(12)-C(13)	119.9(8)
C(6)-C(5)-H(5)	121.4	C(14)-C(13)-C(12)	118.5(8)
C(4)-C(5)-H(5)	121.4	C(14)-C(13)-H(13)	120.8
C(7)-C(6)-C(5)	120.6(8)	C(12)-C(13)-H(13)	120.8
C(7)-C(6)-H(6)	119.7	C(13)-C(14)-C(9)	123.8(8)
C(5)-C(6)-H(6)	119.7	C(13)-C(14)-C(15)	122.1(8)
C(8)-C(7)-C(6)	117.9(8)	C(9)-C(14)-C(15)	114.2(7)
C(8)-C(7)-H(7)	121.1	N(4)-C(15)-C(16)	120.0(8)
C(6)-C(7)-H(7)	121.1	N(4)-C(15)-C(14)	115.0(7)
N(3)-C(8)-C(7)	123.3(8)	C(16)-C(15)-C(14)	124.9(8)
N(3)-C(8)-H(8)	118.3	C(17)-C(16)-C(15)	120.7(8)
C(7)-C(8)-H(8)	118.3	C(17)-C(16)-H(16)	119.6
C(10)-C(9)-C(14)	114.7(7)	C(15)-C(16)-H(16)	119.6
C(10)-C(9)-Ir(1)	130.6(6)	C(16)-C(17)-C(18)	118.3(8)
C(14)-C(9)-Ir(1)	114.6(6)	C(16)-C(17)-H(17)	120.9
F(1)-C(10)-C(11)	115.6(7)	C(18)-C(17)-H(17)	120.9
F(1)-C(10)-C(9)	121.0(7)	N(4)-C(19)-C(18)	122.3(7)
C(11)-C(10)-C(9)	123.4(8)	N(4)-C(19)-H(19)	118.8
F(2)-C(11)-C(10)	121.2(8)	C(18)-C(19)-H(19)	118.8
F(2)-C(11)-C(12)	119.1(7)	C(19)-C(18)-C(17)	118.9(7)
C(10)-C(11)-C(12)	119.7(8)	C(19)-C(18)-C(20)	121.9(7)
F(3)-C(12)-C(11)	118.5(8)	C(17)-C(18)-C(20)	119.1(7)
F(3)-C(12)-C(13)	121.6(8)	F(6)-C(20)-F(5)	107.3(6)

F(6)-C(20)-F(4)	106.6(6)	C(21)-C(26)-C(27)	113.3(9)
F(5)-C(20)-F(4)	106.0(5)	C(25)-C(26)-C(27)	124.3(10)
F(6)-C(20)-C(18)	112.7(6)	N(5)-C(27)-C(28)	118.2(12)
F(5)-C(20)-C(18)	112.2(6)	N(5)-C(27)-C(26)	114.9(10)
F(4)-C(20)-C(18)	111.6(6)	C(28)-C(27)-C(26)	126.8(15)
C(22)-C(21)-C(26)	116.1(7)	C(29)-C(28)-C(27)	122.5(17)
C(22)-C(21)-Ir(1)	128.6(6)	C(29)-C(28)-H(28)	118.7
C(26)-C(21)-Ir(1)	115.2(6)	C(27)-C(28)-H(28)	118.7
F(7)-C(22)-C(23)	117.1(8)	C(28)-C(29)-C(30)	118.9(12)
F(7)-C(22)-C(21)	120.7(7)	C(28)-C(29)-H(29)	120.6
C(23)-C(22)-C(21)	122.2(8)	C(30)-C(29)-H(29)	120.6
F(8)-C(23)-C(22)	120.4(8)	C(31)-C(30)-C(29)	117.8(10)
F(8)-C(23)-C(24)	120.3(8)	C(31)-C(30)-C(32)	119.6(13)
C(22)-C(23)-C(24)	119.3(9)	C(29)-C(30)-C(32)	122.7(10)
C(25)-C(24)-F(9)	122.1(9)	N(5)-C(31)-C(30)	121.9(14)
C(25)-C(24)-C(23)	121.2(8)	N(5)-C(31)-H(31)	119.1
F(9)-C(24)-C(23)	116.6(9)	C(30)-C(31)-H(31)	119.1
C(24)-C(25)-C(26)	118.8(9)	F(10)-C(32)-F(12)	110.1(9)
C(24)-C(25)-H(25)	120.6	F(10)-C(32)-F(11)	103.9(10)
C(26)-C(25)-H(25)	120.6	F(12)-C(32)-F(11)	104.5(9)
C(21)-C(26)-C(25)	122.2(8)	F(10)-C(32)-C(30)	112.9(8)
C(21)-C(26)-C(27A)	117.5(11)	F(12)-C(32)-C(30)	111.8(10)
C(25)-C(26)-C(27A)	120.1(11)	F(11)-C(32)-C(30)	113.1(10)

C(31)-N(5)-C(27)	120.7(12)	F(12A)-C(32A)-C(30A)	112.0(12)
C(31)-N(5)-Ir(1)	123.3(11)	C(31A)-N(5A)-C(27A)	119.2(13)
C(27)-N(5)-Ir(1)	115.8(7)	C(31A)-N(5A)-Ir(1)	125.3(12)
N(5A)-C(27A)-C(28A)	120.5(14)	C(27A)-N(5A)-Ir(1)	115.5(7)
N(5A)-C(27A)-C(26)	113.4(11)	C(41)-Ir(2)-C(53)	87.3(3)
C(28A)-C(27A)-C(26)	126.0(17)	C(41)-Ir(2)-N(10)	97.1(3)
C(29A)-C(28A)-C(27A)	121.1(18)	C(53)-Ir(2)-N(10)	79.7(3)
C(29A)-C(28A)-H(28A)	119.4	C(41)-Ir(2)-N(9)	80.1(3)
C(27A)-C(28A)-H(28A)	119.4	C(53)-Ir(2)-N(9)	99.6(3)
C(28A)-C(29A)-C(30A)	118.1(14)	N(10)-Ir(2)-N(9)	177.3(3)
C(28A)-C(29A)-H(29A)	121.0	C(41)-Ir(2)-N(6)	100.7(3)
C(30A)-C(29A)-H(29A)	121.0	C(53)-Ir(2)-N(6)	169.4(3)
C(31A)-C(30A)-C(29A)	119.9(12)	N(10)-Ir(2)-N(6)	92.3(3)
C(31A)-C(30A)-C(32A)	117.7(15)	N(9)-Ir(2)-N(6)	88.6(3)
C(29A)-C(30A)-C(32A)	122.5(12)	C(41)-Ir(2)-N(8)	174.6(3)
N(5A)-C(31A)-C(30A)	121.0(16)	C(53)-Ir(2)-N(8)	95.9(3)
N(5A)-C(31A)-H(31A)	119.5	N(10)-Ir(2)-N(8)	87.7(2)
C(30A)-C(31A)-H(31A)	119.5	N(9)-Ir(2)-N(8)	95.1(3)
F(10A)-C(32A)-F(11A)	107.3(13)	N(6)-Ir(2)-N(8)	76.6(3)
F(10A)-C(32A)-F(12A)	107.2(12)	N(7)-N(6)-C(35)	105.6(8)
F(11A)-C(32A)-F(12A)	104.5(13)	N(7)-N(6)-Ir(2)	137.3(7)
F(10A)-C(32A)-C(30A)	112.3(10)	C(35)-N(6)-Ir(2)	115.7(7)
F(11A)-C(32A)-C(30A)	113.1(12)	N(6)-N(7)-C(33)	111.2(9)

N(6)-N(7)-H(7A)	124.4	C(38)-C(37)-C(36)	120.0(9)
C(33)-N(7)-H(7A)	124.4	C(38)-C(37)-H(37)	120.0
C(40)-N(8)-C(36)	118.4(8)	C(36)-C(37)-H(37)	120.0
C(40)-N(8)-Ir(2)	126.5(6)	C(37)-C(38)-C(39)	121.4(10)
C(36)-N(8)-Ir(2)	115.1(6)	C(37)-C(38)-H(38)	119.3
C(51)-N(9)-C(47)	119.9(8)	C(39)-C(38)-H(38)	119.3
C(51)-N(9)-Ir(2)	124.7(6)	C(40)-C(39)-C(38)	115.2(10)
C(47)-N(9)-Ir(2)	115.3(6)	C(40)-C(39)-H(39)	122.4
C(59)-N(10)-C(63)	120.9(7)	C(38)-C(39)-H(39)	122.4
C(59)-N(10)-Ir(2)	116.1(6)	N(8)-C(40)-C(39)	125.5(10)
C(63)-N(10)-Ir(2)	123.0(6)	N(8)-C(40)-H(40)	117.2
C(34)-C(33)-N(7)	108.3(11)	C(39)-C(40)-H(40)	117.2
C(34)-C(33)-H(33)	125.9	C(42)-C(41)-C(46)	116.2(7)
N(7)-C(33)-H(33)	125.9	C(42)-C(41)-Ir(2)	129.2(6)
C(33)-C(34)-C(35)	105.6(10)	C(46)-C(41)-Ir(2)	114.5(6)
C(33)-C(34)-H(34)	127.2	F(13)-C(42)-C(41)	122.2(7)
C(35)-C(34)-H(34)	127.2	F(13)-C(42)-C(43)	116.6(7)
N(6)-C(35)-C(34)	109.4(9)	C(41)-C(42)-C(43)	121.1(8)
N(6)-C(35)-C(36)	116.4(9)	F(14)-C(43)-C(44)	120.7(7)
C(34)-C(35)-C(36)	134.1(9)	F(14)-C(43)-C(42)	119.8(8)
N(8)-C(36)-C(37)	119.5(10)	C(44)-C(43)-C(42)	119.5(8)
N(8)-C(36)-C(35)	115.7(8)	C(45)-C(44)-F(15)	121.3(9)
C(37)-C(36)-C(35)	124.7(9)	C(45)-C(44)-C(43)	121.7(8)

F(15)-C(44)-C(43)	116.9(9)	F(18)-C(52)-F(17)	107.3(7)
C(44)-C(45)-C(46)	118.5(9)	F(16)-C(52)-F(17)	105.6(6)
C(44)-C(45)-H(45)	120.8	F(18)-C(52)-C(50)	113.1(6)
C(46)-C(45)-H(45)	120.8	F(16)-C(52)-C(50)	112.2(6)
C(45)-C(46)-C(41)	122.8(8)	F(17)-C(52)-C(50)	111.1(6)
C(45)-C(46)-C(47)	121.8(8)	C(54)-C(53)-C(58)	116.7(8)
C(41)-C(46)-C(47)	115.4(7)	C(54)-C(53)-Ir(2)	129.1(7)
N(9)-C(47)-C(48)	120.4(9)	C(58)-C(53)-Ir(2)	114.1(6)
N(9)-C(47)-C(46)	114.6(7)	F(19)-C(54)-C(55)	117.0(9)
C(48)-C(47)-C(46)	124.9(8)	F(19)-C(54)-C(53)	120.7(8)
C(49)-C(48)-C(47)	118.7(9)	C(55)-C(54)-C(53)	122.2(9)
C(49)-C(48)-H(48)	120.6	F(20)-C(55)-C(54)	120.5(9)
C(47)-C(48)-H(48)	120.6	F(20)-C(55)-C(56)	119.8(8)
C(50)-C(49)-C(48)	120.3(9)	C(54)-C(55)-C(56)	119.7(9)
C(50)-C(49)-H(49)	119.9	F(21)-C(56)-C(57)	120.2(10)
C(48)-C(49)-H(49)	119.9	F(21)-C(56)-C(55)	118.5(10)
C(49)-C(50)-C(51)	119.8(8)	C(57)-C(56)-C(55)	121.3(9)
C(49)-C(50)-C(52)	120.4(8)	C(56)-C(57)-C(58)	118.6(10)
C(51)-C(50)-C(52)	119.8(7)	C(56)-C(57)-H(57)	120.7
N(9)-C(51)-C(50)	120.8(8)	C(58)-C(57)-H(57)	120.7
N(9)-C(51)-H(51)	119.6	C(57)-C(58)-C(53)	121.4(9)
C(50)-C(51)-H(51)	119.6	C(57)-C(58)-C(59)	123.9(8)
F(18)-C(52)-F(16)	107.2(7)	C(53)-C(58)-C(59)	114.7(8)

N(10)-C(59)-C(60)	119.7(9)	F(22B)-C(64)-F(23B)	105.2(8)
N(10)-C(59)-C(58)	115.3(7)	F(24A)-C(64)-C(62)	113.4(8)
C(60)-C(59)-C(58)	125.0(9)	F(24B)-C(64)-C(62)	113.9(8)
C(61)-C(60)-C(59)	119.3(9)	F(24)-C(64)-C(62)	112.5(7)
C(61)-C(60)-H(60)	120.4	F(23A)-C(64)-C(62)	111.1(7)
C(59)-C(60)-H(60)	120.4	F(22B)-C(64)-C(62)	112.7(8)
C(60)-C(61)-C(62)	119.6(8)	F(23)-C(64)-C(62)	113.1(7)
C(60)-C(61)-H(61)	120.2	F(22)-C(64)-C(62)	111.4(7)
C(62)-C(61)-H(61)	120.2	F(22A)-C(64)-C(62)	110.5(8)
C(63)-C(62)-C(61)	120.0(7)	F(23B)-C(64)-C(62)	111.2(7)
C(63)-C(62)-C(64)	120.0(7)	C(81)-B(1)-C(65)	114.8(6)
C(61)-C(62)-C(64)	120.0(7)	C(81)-B(1)-C(73)	102.4(6)
N(10)-C(63)-C(62)	120.6(9)	C(65)-B(1)-C(73)	111.9(6)
N(10)-C(63)-H(63)	119.7	C(81)-B(1)-C(89A)	113.1(8)
C(62)-C(63)-H(63)	119.7	C(65)-B(1)-C(89A)	105.1(9)
F(24A)-C(64)-F(23A)	108.8(8)	C(73)-B(1)-C(89A)	109.5(8)
F(24B)-C(64)-F(22B)	107.5(8)	C(81)-B(1)-C(89)	113.4(7)
F(24)-C(64)-F(23)	106.8(8)	C(65)-B(1)-C(89)	100.1(8)
F(24)-C(64)-F(22)	106.2(8)	C(73)-B(1)-C(89)	114.8(7)
F(23)-C(64)-F(22)	106.3(8)	C(70)-C(65)-C(66)	116.0(7)
F(24A)-C(64)-F(22A)	107.0(8)	C(70)-C(65)-B(1)	125.1(7)
F(23A)-C(64)-F(22A)	105.6(8)	C(66)-C(65)-B(1)	118.4(7)
F(24B)-C(64)-F(23B)	105.6(8)	C(67)-C(66)-C(65)	121.6(7)

C(67)-C(66)-H(66)	119.2	F(29)-C(72)-C(69)	113.9(7)
C(65)-C(66)-H(66)	119.2	F(28)-C(72)-C(69)	111.8(7)
C(68)-C(67)-C(66)	122.4(7)	F(30)-C(72)-C(69)	110.8(8)
C(68)-C(67)-C(71)	118.9(7)	C(78)-C(73)-C(74)	115.5(7)
C(66)-C(67)-C(71)	118.6(7)	C(78)-C(73)-B(1)	123.5(7)
C(67)-C(68)-C(69)	116.5(7)	C(74)-C(73)-B(1)	120.1(7)
C(67)-C(68)-H(68)	121.8	C(75)-C(74)-C(73)	121.6(8)
C(69)-C(68)-H(68)	121.8	C(75)-C(74)-H(74)	119.2
C(70)-C(69)-C(68)	122.1(7)	C(73)-C(74)-H(74)	119.2
C(70)-C(69)-C(72)	120.7(7)	C(76)-C(75)-C(74)	121.2(9)
C(68)-C(69)-C(72)	117.1(7)	C(76)-C(75)-C(79)	119.2(8)
C(69)-C(70)-C(65)	121.3(7)	C(74)-C(75)-C(79)	119.6(8)
C(69)-C(70)-H(70)	119.4	C(77)-C(76)-C(75)	118.6(8)
C(65)-C(70)-H(70)	119.4	C(77)-C(76)-H(76)	120.7
F(26)-C(71)-F(25)	106.7(7)	C(75)-C(76)-H(76)	120.7
F(26)-C(71)-F(27)	105.1(7)	C(76)-C(77)-C(78)	120.5(6)
F(25)-C(71)-F(27)	105.3(7)	C(76)-C(77)-C(80)	115.6(8)
F(26)-C(71)-C(67)	113.5(7)	C(78)-C(77)-C(80)	123.9(8)
F(25)-C(71)-C(67)	113.3(7)	C(76)-C(77)-C(80A)	127.0(8)
F(27)-C(71)-C(67)	112.3(7)	C(78)-C(77)-C(80A)	112.0(8)
F(29)-C(72)-F(28)	108.7(8)	C(73)-C(78)-C(77)	122.5(8)
F(29)-C(72)-F(30)	106.4(8)	C(73)-C(78)-H(78)	118.7
F(28)-C(72)-F(30)	104.7(7)	C(77)-C(78)-H(78)	118.7

F(31)-C(79)-F(33)	106.7(8)	C(81)-C(82)-H(82)	119.0
F(31)-C(79)-F(32)	105.6(7)	C(82)-C(83)-C(84)	120.7(6)
F(33)-C(79)-F(32)	105.4(10)	C(82)-C(83)-C(87A)	125.8(8)
F(31)-C(79)-C(75)	112.8(10)	C(84)-C(83)-C(87A)	113.1(7)
F(33)-C(79)-C(75)	113.0(8)	C(82)-C(83)-C(87)	118.4(7)
F(32)-C(79)-C(75)	112.7(8)	C(84)-C(83)-C(87)	120.5(7)
F(36)-C(80)-F(35)	107.6(8)	C(85)-C(84)-C(83)	118.4(7)
F(36)-C(80)-F(34)	105.6(9)	C(85)-C(84)-H(84)	120.8
F(35)-C(80)-F(34)	107.0(8)	C(83)-C(84)-H(84)	120.8
F(36)-C(80)-C(77)	111.3(8)	C(86)-C(85)-C(84)	119.9(6)
F(35)-C(80)-C(77)	113.7(8)	C(86)-C(85)-C(88)	122.8(7)
F(34)-C(80)-C(77)	111.2(8)	C(84)-C(85)-C(88)	117.1(7)
F(36A)-C(80A)-F(35A)	106.0(9)	C(86)-C(85)-C(88A)	117.1(7)
F(36A)-C(80A)-F(34A)	107.8(9)	C(84)-C(85)-C(88A)	122.9(8)
F(35A)-C(80A)-F(34A)	105.9(9)	C(85)-C(86)-C(81)	123.0(7)
F(36A)-C(80A)-C(77)	115.0(9)	C(85)-C(86)-H(86)	118.5
F(35A)-C(80A)-C(77)	111.2(8)	C(81)-C(86)-H(86)	118.5
F(34A)-C(80A)-C(77)	110.5(8)	F(39)-C(87)-F(38)	105.4(8)
C(86)-C(81)-C(82)	116.0(7)	F(39)-C(87)-F(37)	105.9(8)
C(86)-C(81)-B(1)	123.5(7)	F(38)-C(87)-F(37)	106.5(8)
C(82)-C(81)-B(1)	119.9(7)	F(39)-C(87)-C(83)	111.9(8)
C(83)-C(82)-C(81)	122.0(8)	F(38)-C(87)-C(83)	112.6(8)
C(83)-C(82)-H(82)	119.0	F(37)-C(87)-C(83)	114.0(8)

F(39A)-C(87A)-F(38A)	106.7(9)	C(91)-C(90)-H(90)	120.0
F(39A)-C(87A)-F(37A)	106.7(9)	C(92)-C(91)-C(90)	120.0
F(38A)-C(87A)-F(37A)	106.4(9)	C(92)-C(91)-C(95)	118.1(8)
F(39A)-C(87A)-C(83)	114.7(9)	C(90)-C(91)-C(95)	120.8(8)
F(38A)-C(87A)-C(83)	111.6(9)	C(93)-C(92)-C(91)	120.0
F(37A)-C(87A)-C(83)	110.2(8)	C(93)-C(92)-H(92)	120.0
F(42)-C(88)-F(41)	107.8(9)	C(91)-C(92)-H(92)	120.0
F(42)-C(88)-F(40)	106.7(8)	C(92)-C(93)-C(94)	120.0
F(41)-C(88)-F(40)	105.6(8)	C(92)-C(93)-C(96)	120.1(8)
F(42)-C(88)-C(85)	113.7(8)	C(94)-C(93)-C(96)	119.8(8)
F(41)-C(88)-C(85)	113.0(8)	C(93)-C(94)-C(89)	120.0
F(40)-C(88)-C(85)	109.6(8)	C(93)-C(94)-H(94)	120.0
F(42A)-C(88A)-F(41A)	105.7(9)	C(89)-C(94)-H(94)	120.0
F(42A)-C(88A)-F(40A)	105.6(8)	F(45)-C(95)-F(44)	107.8(9)
F(41A)-C(88A)-F(40A)	106.0(9)	F(45)-C(95)-F(43)	106.1(9)
F(42A)-C(88A)-C(85)	113.5(8)	F(44)-C(95)-F(43)	106.7(9)
F(41A)-C(88A)-C(85)	111.5(8)	F(45)-C(95)-C(91)	112.2(9)
F(40A)-C(88A)-C(85)	113.8(8)	F(44)-C(95)-C(91)	111.6(9)
C(90)-C(89)-C(94)	120.0	F(43)-C(95)-C(91)	112.1(9)
C(90)-C(89)-B(1)	118.7(8)	F(48)-C(96)-F(47)	105.3(8)
C(94)-C(89)-B(1)	121.1(8)	F(48)-C(96)-F(46)	106.5(9)
C(89)-C(90)-C(91)	120.0	F(47)-C(96)-F(46)	107.5(9)
C(89)-C(90)-H(90)	120.0	F(48)-C(96)-C(93)	112.8(8)

F(47)-C(96)-C(93)	112.2(8)	F(45A)-C(95A)-C(91A)	114.0(9)
F(46)-C(96)-C(93)	112.1(8)	F(44A)-C(95A)-C(91A)	113.0(9)
C(90A)-C(89A)-C(94A)	120.0	F(43A)-C(95A)-C(91A)	111.0(9)
C(90A)-C(89A)-B(1)	120.5(9)	F(48A)-C(96A)-F(47A)	108.7(9)
C(94A)-C(89A)-B(1)	118.7(9)	F(48A)-C(96A)-F(46A)	106.2(9)
C(89A)-C(90A)-C(91A)	120.0	F(47A)-C(96A)-F(46A)	104.7(9)
C(89A)-C(90A)-H(90A)	120.0	F(48A)-C(96A)-C(93A)	112.8(9)
C(91A)-C(90A)-H(90A)	120.0	F(47A)-C(96A)-C(93A)	112.4(8)
C(90A)-C(91A)-C(92A)	120.0	F(46A)-C(96A)-C(93A)	111.5(8)
C(90A)-C(91A)-C(95A)	116.3(9)	C(121)-B(2)-C(97)	107.6(11)
C(92A)-C(91A)-C(95A)	123.3(9)	C(121)-B(2)-C(105)	100.5(10)
C(93A)-C(92A)-C(91A)	120.0	C(97)-B(2)-C(105)	113.5(9)
C(93A)-C(92A)-H(92A)	120.0	C(121)-B(2)-C(113)	113.6(9)
C(91A)-C(92A)-H(92A)	120.0	C(97)-B(2)-C(113)	110.6(9)
C(92A)-C(93A)-C(94A)	120.0	C(105)-B(2)-C(113)	110.7(10)
C(92A)-C(93A)-C(96A)	120.0(9)	C(98)-C(97)-C(102)	120.0
C(94A)-C(93A)-C(96A)	119.9(9)	C(98)-C(97)-B(2)	119.1(9)
C(93A)-C(94A)-C(89A)	120.0	C(102)-C(97)-B(2)	120.9(9)
C(93A)-C(94A)-H(94A)	120.0	C(99)-C(98)-C(97)	120.0
C(89A)-C(94A)-H(94A)	120.0	C(99)-C(98)-H(98)	120.0
F(45A)-C(95A)-F(44A)	105.7(9)	C(97)-C(98)-H(98)	120.0
F(45A)-C(95A)-F(43A)	107.5(9)	C(100)-C(99)-C(98)	120.0
F(44A)-C(95A)-F(43A)	105.1(9)	C(100)-C(99)-C(103)	122.8(8)

C(98)-C(99)-C(103)	117.1(8)	C(106)-C(105)-B(2)	122.3(9)
C(99)-C(100)-C(101)	120.0	C(110)-C(105)-B(2)	117.6(9)
C(99)-C(100)-H(100)	120.0	C(105)-C(106)-C(107)	120.0
C(101)-C(100)-H(100)	120.0	C(105)-C(106)-H(106)	120.0
C(102)-C(101)-C(100)	120.0	C(107)-C(106)-H(106)	120.0
C(102)-C(101)-C(104)	117.9(8)	C(108)-C(107)-C(106)	120.0
C(100)-C(101)-C(104)	121.9(8)	C(108)-C(107)-C(111)	119.3(8)
C(101)-C(102)-C(97)	120.0	C(106)-C(107)-C(111)	120.5(8)
C(101)-C(102)-H(102)	120.0	C(109)-C(108)-C(107)	120.0
C(97)-C(102)-H(102)	120.0	C(109)-C(108)-H(108)	120.0
F(51)-C(103)-F(50)	107.0(9)	C(107)-C(108)-H(108)	120.0
F(51)-C(103)-F(49)	106.2(9)	C(108)-C(109)-C(110)	120.0
F(50)-C(103)-F(49)	106.8(8)	C(108)-C(109)-C(112)	123.2(9)
F(51)-C(103)-C(99)	113.1(8)	C(110)-C(109)-C(112)	116.5(9)
F(50)-C(103)-C(99)	112.3(9)	C(109)-C(110)-C(105)	120.0
F(49)-C(103)-C(99)	111.0(9)	C(109)-C(110)-H(110)	120.0
F(54)-C(104)-F(53)	107.5(8)	C(105)-C(110)-H(110)	120.0
F(54)-C(104)-F(52)	105.6(8)	F(57)-C(111)-F(56)	105.3(8)
F(53)-C(104)-F(52)	105.9(8)	F(57)-C(111)-F(55)	106.5(8)
F(54)-C(104)-C(101)	112.2(8)	F(56)-C(111)-F(55)	108.4(8)
F(53)-C(104)-C(101)	112.0(8)	F(57)-C(111)-C(107)	113.2(8)
F(52)-C(104)-C(101)	113.2(8)	F(56)-C(111)-C(107)	112.0(7)
C(106)-C(105)-C(110)	120.0	F(55)-C(111)-C(107)	111.0(8)

F(60)-C(112)-F(59)	107.9(9)	C(113)-C(118)-H(118)	120.0
F(60)-C(112)-F(58)	107.7(9)	F(63)-C(119)-F(61)	106.2(9)
F(59)-C(112)-F(58)	106.7(9)	F(63)-C(119)-F(62)	104.3(9)
F(60)-C(112)-C(109)	111.9(9)	F(61)-C(119)-F(62)	107.0(10)
F(59)-C(112)-C(109)	111.1(8)	F(63)-C(119)-C(115)	113.1(9)
F(58)-C(112)-C(109)	111.3(9)	F(61)-C(119)-C(115)	112.0(9)
C(114)-C(113)-C(118)	120.0	F(62)-C(119)-C(115)	113.6(9)
C(114)-C(113)-B(2)	122.0(9)	F(66)-C(120)-F(65)	104.6(9)
C(118)-C(113)-B(2)	118.0(9)	F(66)-C(120)-F(64)	106.0(9)
C(113)-C(114)-C(115)	120.0	F(65)-C(120)-F(64)	107.0(9)
C(113)-C(114)-H(114)	120.0	F(66)-C(120)-C(117)	114.1(9)
C(115)-C(114)-H(114)	120.0	F(65)-C(120)-C(117)	112.8(9)
C(114)-C(115)-C(116)	120.0	F(64)-C(120)-C(117)	111.8(9)
C(114)-C(115)-C(119)	118.4(9)	C(122)-C(121)-C(126)	120.0
C(116)-C(115)-C(119)	120.8(10)	C(122)-C(121)-B(2)	116.8(10)
C(117)-C(116)-C(115)	120.0	C(126)-C(121)-B(2)	122.9(10)
C(117)-C(116)-H(116)	120.0	C(121)-C(122)-C(123)	120.0
C(115)-C(116)-H(116)	120.0	C(121)-C(122)-H(122)	120.0
C(118)-C(117)-C(116)	120.0	C(123)-C(122)-H(122)	120.0
C(118)-C(117)-C(120)	121.1(9)	C(124)-C(123)-C(122)	120.0
C(116)-C(117)-C(120)	118.7(9)	C(124)-C(123)-C(127)	119.4(10)
C(117)-C(118)-C(113)	120.0	C(122)-C(123)-C(127)	120.6(10)
C(117)-C(118)-H(118)	120.0	C(123)-C(124)-C(125)	120.0

C(123)-C(124)-H(124)	120.0	C(153)-B(3)-C(145)	105.5(8)
C(125)-C(124)-H(124)	120.0	C(137)-B(3)-C(145)	111.8(7)
C(124)-C(125)-C(126)	120.0	C(129)-B(3)-C(145)	109.9(9)
C(124)-C(125)-C(128)	123.7(10)	C(130)-C(129)-C(134)	120.0
C(126)-C(125)-C(128)	115.7(10)	C(130)-C(129)-B(3)	119.3(9)
C(125)-C(126)-C(121)	120.0	C(134)-C(129)-B(3)	120.6(9)
C(125)-C(126)-H(126)	120.0	C(131)-C(130)-C(129)	120.0
C(121)-C(126)-H(126)	120.0	C(131)-C(130)-H(130)	120.0
F(69)-C(127)-F(68)	106.9(9)	C(129)-C(130)-H(130)	120.0
F(69)-C(127)-F(67)	106.7(9)	C(130)-C(131)-C(132)	120.0
F(68)-C(127)-F(67)	104.4(9)	C(130)-C(131)-C(135)	125.8(9)
F(69)-C(127)-C(123)	112.8(9)	C(132)-C(131)-C(135)	113.8(9)
F(68)-C(127)-C(123)	112.5(9)	C(131)-C(132)-C(133)	120.0
F(67)-C(127)-C(123)	112.9(9)	C(131)-C(132)-H(132)	120.0
F(72)-C(128)-F(71)	106.4(9)	C(133)-C(132)-H(132)	120.0
F(72)-C(128)-F(70)	105.7(9)	C(132)-C(133)-C(134)	120.0
F(71)-C(128)-F(70)	105.8(9)	C(132)-C(133)-C(136)	121.3(9)
F(72)-C(128)-C(125)	113.5(9)	C(134)-C(133)-C(136)	118.5(9)
F(71)-C(128)-C(125)	112.5(9)	C(133)-C(134)-C(129)	120.0
F(70)-C(128)-C(125)	112.2(9)	C(133)-C(134)-H(134)	120.0
C(153)-B(3)-C(137)	108.9(9)	C(129)-C(134)-H(134)	120.0
C(153)-B(3)-C(129)	111.6(10)	F(75)-C(135)-F(74)	106.5(9)
C(137)-B(3)-C(129)	109.1(8)	F(75)-C(135)-F(73)	106.6(9)

F(74)-C(135)-F(73)	107.5(9)	C(142)-C(141)-C(144)	118.7(7)
F(75)-C(135)-C(131)	112.6(9)	C(140)-C(141)-C(144)	121.2(7)
F(74)-C(135)-C(131)	113.0(9)	C(141)-C(142)-C(137)	120.0
F(73)-C(135)-C(131)	110.4(9)	C(141)-C(142)-H(142)	120.0
F(78)-C(136)-F(76)	106.0(9)	C(137)-C(142)-H(142)	120.0
F(78)-C(136)-F(77)	108.2(9)	F(81)-C(143)-F(79)	107.7(8)
F(76)-C(136)-F(77)	108.4(9)	F(81)-C(143)-F(80)	106.8(8)
F(78)-C(136)-C(133)	113.3(9)	F(79)-C(143)-F(80)	105.9(8)
F(76)-C(136)-C(133)	110.9(9)	F(81)-C(143)-C(139)	112.0(8)
F(77)-C(136)-C(133)	109.8(9)	F(79)-C(143)-C(139)	111.9(8)
C(138)-C(137)-C(142)	120.0	F(80)-C(143)-C(139)	112.1(8)
C(138)-C(137)-B(3)	118.4(6)	F(84)-C(144)-F(83)	107.1(9)
C(142)-C(137)-B(3)	121.4(6)	F(84)-C(144)-F(82)	106.0(9)
C(139)-C(138)-C(137)	120.0	F(83)-C(144)-F(82)	105.8(9)
C(139)-C(138)-H(138)	120.0	F(84)-C(144)-C(141)	113.9(9)
C(137)-C(138)-H(138)	120.0	F(83)-C(144)-C(141)	111.9(9)
C(140)-C(139)-C(138)	120.0	F(82)-C(144)-C(141)	111.5(9)
C(140)-C(139)-C(143)	123.4(6)	C(146)-C(145)-C(150)	120.0
C(138)-C(139)-C(143)	116.6(6)	C(146)-C(145)-B(3)	116.4(7)
C(139)-C(140)-C(141)	120.0	C(150)-C(145)-B(3)	123.5(7)
C(139)-C(140)-H(140)	120.0	C(145)-C(146)-C(147)	120.0
C(141)-C(140)-H(140)	120.0	C(145)-C(146)-H(146)	120.0
C(142)-C(141)-C(140)	120.0	C(147)-C(146)-H(146)	120.0

C(148)-C(147)-C(146)	120.0	F(88)-C(152)-C(149)	111.4(9)
C(148)-C(147)-C(151)	120.5(8)	C(154)-C(153)-C(158)	120.0
C(146)-C(147)-C(151)	119.5(8)	C(154)-C(153)-B(3)	116.8(9)
C(147)-C(148)-C(149)	120.0	C(158)-C(153)-B(3)	123.2(9)
C(147)-C(148)-H(148)	120.0	C(153)-C(154)-C(155)	120.0
C(149)-C(148)-H(148)	120.0	C(153)-C(154)-H(154)	120.0
C(148)-C(149)-C(150)	120.0	C(155)-C(154)-H(154)	120.0
C(148)-C(149)-C(152)	122.0(7)	C(156)-C(155)-C(154)	120.0
C(150)-C(149)-C(152)	118.0(7)	C(156)-C(155)-C(159)	116.8(9)
C(149)-C(150)-C(145)	120.0	C(154)-C(155)-C(159)	123.2(9)
C(149)-C(150)-H(150)	120.0	C(155)-C(156)-C(157)	120.0
C(145)-C(150)-H(150)	120.0	C(155)-C(156)-H(156)	120.0
F(87)-C(151)-F(86)	106.2(8)	C(157)-C(156)-H(156)	120.0
F(87)-C(151)-F(85)	106.5(8)	C(158)-C(157)-C(156)	120.0
F(86)-C(151)-F(85)	107.3(8)	C(158)-C(157)-C(160)	121.5(9)
F(87)-C(151)-C(147)	112.3(8)	C(156)-C(157)-C(160)	118.3(9)
F(86)-C(151)-C(147)	111.7(8)	C(157)-C(158)-C(153)	120.0
F(85)-C(151)-C(147)	112.4(8)	C(157)-C(158)-H(158)	120.0
F(90)-C(152)-F(89)	107.1(9)	C(153)-C(158)-H(158)	120.0
F(90)-C(152)-F(88)	106.4(8)	F(93)-C(159)-F(92)	108.0(9)
F(89)-C(152)-F(88)	105.3(8)	F(93)-C(159)-F(91)	106.7(9)
F(90)-C(152)-C(149)	113.2(8)	F(92)-C(159)-F(91)	106.6(9)
F(89)-C(152)-C(149)	113.0(8)	F(93)-C(159)-C(155)	112.4(9)

F(92)-C(159)-C(155)	111.4(9)	C(1S)-C(2S)-H(2S3)	109.5
F(91)-C(159)-C(155)	111.5(9)	H(2S1)-C(2S)-H(2S3)	109.5
F(96)-C(160)-F(95)	105.8(9)	H(2S2)-C(2S)-H(2S3)	109.5
F(96)-C(160)-F(94)	106.5(9)	C(3S)-O(2)-H(2S)	109.5
F(95)-C(160)-F(94)	105.4(9)	O(2)-C(3S)-C(4S)	107.8
F(96)-C(160)-C(157)	114.0(9)	O(2)-C(3S)-H(3S1)	110.1
F(95)-C(160)-C(157)	112.4(9)	C(4S)-C(3S)-H(3S1)	110.1
F(94)-C(160)-C(157)	112.2(9)	O(2)-C(3S)-H(3S2)	110.1
C(1S)-O(1)-H(1S)	109.5	C(4S)-C(3S)-H(3S2)	110.1
O(1)-C(1S)-C(2S)	107.8	H(3S1)-C(3S)-H(3S2)	108.5
O(1)-C(1S)-H(1S1)	110.1	C(3S)-C(4S)-H(4S1)	109.5
C(2S)-C(1S)-H(1S1)	110.1	C(3S)-C(4S)-H(4S2)	109.5
O(1)-C(1S)-H(1S2)	110.1	H(4S1)-C(4S)-H(4S2)	109.5
C(2S)-C(1S)-H(1S2)	110.1	C(3S)-C(4S)-H(4S3)	109.5
H(1S1)-C(1S)-H(1S2)	108.5	H(4S1)-C(4S)-H(4S3)	109.5
C(1S)-C(2S)-H(2S1)	109.5	H(4S2)-C(4S)-H(4S3)	109.5
C(1S)-C(2S)-H(2S2)	109.5		
H(2S1)-C(2S)-H(2S2)	109.5		

Symmetry transformations used to generate equivalent atoms:

Table D.4. Anisotropic displacement parameters ($Å^2 x\ 10^3$) for **2.32**. The anisotropic displacement factor exponent takes the form: $-2\pi^2[\ h^2\ a^{*2}U^{11} + ...\ + 2\ h\ k\ a^*\ b^*\ U^{12}\ ]$

	U^{11}	U^{22}	U^{33}	U^{23}	U^{13}	U^{12}
Ir(1)	21(1)	25(1)	26(1)	0(1)	0(1)	2(1)
F(1)	33(2)	44(3)	42(3)	13(2)	8(2)	5(2)
F(2)	33(2)	52(3)	36(2)	2(2)	11(2)	-6(2)
F(3)	31(2)	52(3)	53(3)	-19(3)	15(2)	-4(2)
N(1)	22(3)	25(3)	32(4)	-4(3)	-3(3)	-1(2)
N(2)	25(3)	28(3)	39(4)	1(3)	1(3)	-1(3)
N(3)	27(3)	24(3)	28(3)	3(3)	1(2)	7(2)
N(4)	23(3)	20(3)	35(4)	-6(3)	1(3)	2(2)
C(1)	42(5)	27(4)	42(5)	-3(4)	-12(4)	-1(4)
C(2)	44(5)	24(4)	36(5)	-3(3)	-5(4)	1(3)
C(3)	31(4)	19(3)	26(4)	-3(3)	0(3)	6(3)
C(4)	31(4)	23(4)	28(4)	3(3)	-4(3)	8(3)
C(5)	35(4)	33(4)	25(4)	0(3)	1(3)	10(3)
C(6)	41(5)	34(4)	39(5)	11(4)	12(4)	12(4)
C(7)	29(4)	33(4)	46(5)	7(4)	5(3)	0(3)
C(8)	30(3)	25(4)	34(4)	5(3)	1(3)	2(3)
C(9)	22(3)	26(4)	30(4)	-3(3)	-3(3)	0(3)
C(10)	21(3)	33(4)	34(4)	-1(4)	-1(3)	-1(3)
C(11)	26(3)	43(5)	35(4)	-9(4)	-1(3)	-7(3)

C(12)	29(4)	38(5)	41(5)	-12(4)	10(3)	0(3)
C(13)	29(4)	30(4)	42(5)	-5(4)	1(3)	3(3)
C(14)	22(3)	28(4)	37(4)	-4(3)	-1(3)	-1(3)
C(15)	25(4)	24(4)	36(4)	-6(3)	0(3)	1(3)
C(16)	32(4)	36(5)	56(6)	0(4)	4(4)	12(4)
C(17)	32(4)	38(5)	49(6)	15(4)	-1(4)	9(4)
C(19)	25(4)	19(3)	36(4)	-3(3)	-5(3)	-1(3)
C(18)	31(4)	27(4)	35(5)	-1(3)	-7(3)	-5(3)
C(20)	34(4)	32(4)	37(5)	8(4)	-12(3)	-5(3)
F(4)	46(3)	51(3)	41(3)	16(2)	-17(2)	-9(2)
F(5)	58(3)	39(3)	46(3)	15(2)	-13(3)	-16(3)
F(6)	48(3)	53(3)	35(3)	9(2)	5(2)	-1(3)
F(7)	41(3)	25(2)	45(3)	-3(2)	-13(2)	-2(2)
F(8)	45(3)	38(3)	68(4)	-19(3)	-15(3)	-4(2)
F(9)	48(3)	77(4)	47(3)	-21(3)	-18(3)	-5(3)
C(21)	24(4)	34(4)	27(4)	-3(3)	4(3)	0(3)
C(22)	27(4)	31(4)	33(4)	-4(3)	0(3)	1(3)
C(23)	28(4)	36(5)	43(5)	-8(4)	1(3)	1(3)
C(24)	29(4)	64(6)	35(5)	-18(4)	-7(4)	2(4)
C(25)	31(4)	60(6)	34(5)	-1(4)	-1(4)	0(4)
C(26)	30(4)	40(5)	22(3)	0(3)	-3(3)	6(3)
Ir(2)	34(1)	26(1)	22(1)	0(1)	-1(1)	8(1)
F(13)	39(3)	36(3)	29(2)	-6(2)	-8(2)	4(2)

F(14)	43(2)	48(3)	33(2)	3(2)	-11(2)	-4(2)
F(15)	44(3)	73(4)	48(3)	13(3)	-14(3)	19(3)
F(16)	70(4)	58(4)	46(3)	-8(3)	18(3)	-11(3)
F(17)	120(6)	60(4)	60(4)	-29(4)	40(4)	-48(4)
F(18)	86(5)	114(7)	66(5)	-61(5)	-24(4)	39(5)
F(19)	46(3)	29(3)	56(3)	8(2)	7(3)	10(2)
F(20)	50(3)	48(3)	78(5)	26(3)	9(3)	-1(3)
F(21)	44(3)	88(5)	57(4)	27(4)	10(3)	-7(3)
N(6)	44(4)	27(4)	35(4)	-2(3)	7(3)	9(3)
N(7)	47(5)	47(5)	52(5)	-4(4)	13(4)	0(4)
N(8)	46(4)	31(4)	22(3)	-4(3)	6(3)	16(3)
N(9)	35(4)	30(4)	26(4)	2(3)	6(3)	6(3)
N(10)	39(4)	35(4)	16(3)	-7(3)	-7(3)	12(3)
C(33)	54(6)	63(7)	53(7)	2(6)	2(5)	7(5)
C(34)	65(7)	43(6)	37(5)	11(4)	10(5)	5(5)
C(35)	53(6)	33(5)	30(5)	-4(4)	7(4)	11(4)
C(36)	60(6)	32(4)	26(4)	-3(3)	3(4)	16(4)
C(37)	62(6)	40(5)	18(4)	2(3)	1(4)	10(4)
C(38)	60(6)	44(5)	37(5)	-3(4)	6(4)	17(5)
C(39)	55(5)	52(6)	41(5)	-11(5)	-8(4)	11(5)
C(40)	44(4)	40(5)	35(4)	-15(4)	-11(3)	9(4)
C(41)	33(4)	32(4)	29(4)	7(3)	-4(3)	4(3)
C(42)	30(3)	34(4)	29(4)	5(4)	4(3)	-1(3)

C(43)	31(3)	41(5)	30(4)	13(4)	-3(3)	-2(3)
C(44)	36(5)	59(6)	40(5)	17(5)	-6(4)	12(4)
C(45)	43(5)	50(6)	53(6)	2(5)	0(4)	20(4)
C(46)	39(4)	36(5)	30(4)	5(4)	-2(3)	13(4)
C(47)	39(5)	37(5)	38(5)	2(4)	2(4)	12(4)
C(48)	57(6)	38(5)	58(6)	-8(5)	-4(5)	25(5)
C(49)	57(6)	37(5)	67(8)	-7(5)	17(5)	14(5)
C(50)	48(5)	25(4)	45(5)	-7(4)	13(4)	-4(4)
C(51)	42(5)	27(4)	34(5)	-4(3)	7(4)	3(3)
C(52)	48(5)	41(5)	55(6)	-19(5)	16(5)	-7(4)
C(53)	32(4)	40(5)	24(4)	5(3)	-9(3)	5(3)
C(54)	36(4)	45(5)	34(5)	11(4)	-4(4)	9(4)
C(55)	33(4)	35(5)	50(6)	20(4)	-7(4)	0(3)
C(56)	36(5)	73(7)	32(5)	16(5)	3(4)	-5(5)
C(57)	33(4)	65(7)	34(5)	7(4)	-2(4)	5(4)
C(58)	27(3)	53(5)	18(3)	1(4)	-5(3)	6(4)
C(59)	40(4)	43(5)	21(4)	-6(3)	-6(3)	13(4)
C(60)	35(5)	77(7)	23(4)	-5(4)	-3(4)	12(4)
C(61)	52(6)	52(6)	39(5)	-23(5)	-22(4)	22(5)
C(62)	54(5)	48(6)	30(5)	-8(4)	-12(4)	20(4)
C(63)	53(5)	28(4)	32(4)	-4(3)	-7(4)	10(4)
C(64)	85(8)	36(5)	57(7)	-22(5)	-17(6)	28(5)
B(1)	30(4)	18(4)	32(5)	-3(3)	3(3)	1(3)

C(65)	29(4)	19(3)	25(4)	3(3)	0(3)	0(3)
C(66)	28(4)	21(3)	23(4)	1(3)	-2(3)	1(3)
C(67)	25(4)	23(4)	34(4)	5(3)	2(3)	3(3)
C(68)	27(4)	24(4)	34(4)	1(3)	-1(3)	3(3)
C(69)	27(4)	27(4)	31(4)	-1(3)	-4(3)	-3(3)
C(70)	28(4)	29(4)	21(4)	3(3)	-2(3)	4(3)
C(71)	35(4)	29(4)	33(4)	7(3)	9(3)	3(3)
C(72)	39(4)	41(5)	36(5)	-8(4)	-9(4)	4(4)
C(73)	28(4)	27(4)	29(4)	1(3)	3(3)	0(3)
C(74)	30(4)	33(4)	29(4)	8(3)	-2(3)	-7(3)
C(75)	37(5)	47(5)	30(4)	-3(4)	-8(4)	-10(4)
C(76)	35(4)	51(6)	29(4)	-8(4)	-10(3)	-4(4)
C(77)	37(5)	49(6)	41(5)	-18(4)	-5(4)	-2(4)
C(78)	33(4)	27(4)	35(4)	-4(3)	2(3)	1(3)
C(79)	53(6)	49(6)	48(6)	22(5)	-22(5)	-16(5)
F(25)	46(3)	56(4)	49(3)	-16(3)	17(3)	-1(3)
F(26)	44(3)	70(4)	49(3)	34(3)	16(3)	20(3)
F(27)	27(2)	49(3)	47(3)	12(2)	3(2)	4(2)
F(28)	78(4)	64(4)	32(3)	-6(3)	-20(3)	19(3)
F(29)	51(4)	125(7)	48(4)	-46(4)	-4(3)	4(4)
F(30)	102(5)	40(3)	60(4)	-6(3)	-29(4)	-15(3)
F(31)	54(4)	99(6)	70(4)	57(4)	-12(3)	-18(4)
F(32)	50(3)	69(4)	55(4)	22(3)	-18(3)	-6(3)

F(33)	101(5)	43(3)	61(4)	19(3)	-43(4)	-18(3)
C(81)	26(4)	28(4)	23(4)	4(3)	-4(3)	1(3)
C(82)	26(4)	32(4)	38(5)	-3(4)	-4(3)	3(3)
C(83)	27(4)	40(5)	49(6)	-14(4)	1(4)	3(3)
C(84)	27(4)	48(5)	36(5)	-7(4)	2(3)	9(4)
C(85)	27(4)	43(5)	30(4)	7(4)	2(3)	7(3)
C(86)	35(4)	25(4)	32(4)	10(3)	-2(3)	5(3)
O(1)	52(4)	69(5)	89(6)	-28(5)	21(4)	-13(4)
C(1S)	85(7)	111(8)	72(7)	6(6)	6(6)	-13(6)
C(2S)	84(9)	93(10)	100(10)	-5(8)	21(8)	-4(8)
O(2)	42(5)	57(7)	65(7)	-8(5)	-15(5)	8(5)
C(3S)	86(9)	75(9)	79(9)	3(7)	7(7)	1(7)
C(4S)	93(12)	90(13)	126(14)	12(12)	18(11)	10(12)

Table D.5. Hydrogen coordinates (x 10^4) and isotropic displacement parameters ($Å^2$x 10^3) for **2.32**.

	x	y	z	U(eq)
H(2)	7383	6147	-184	36
H(1)	7346	5319	-1125	45
H(2A)	8527	5357	-1707	41
H(5)	9840	5899	-1876	38
H(6)	10990	6423	-1881	45

H(7)	11316	7248	-1016	44
H(8)	10496	7520	-158	36
H(13)	6849	8673	896	41
H(16)	7077	9003	-158	49
H(17)	7420	9337	-1274	48
H(19)	9005	7874	-1163	32
H(25)	10631	7443	2246	50
H(28)	10326	6250	2269	50
H(29)	10055	5065	2174	42
H(31)	8872	5520	432	33
H(28A)	10372	6356	2344	29
H(29A)	10101	5166	2342	47
H(31A)	8921	5477	558	29
H(7A)	7783	8316	4961	58
H(33)	7789	9266	4098	68
H(34)	6650	9193	3447	58
H(37)	5380	8571	3130	48
H(38)	4258	8051	3036	56
H(39)	3894	7179	3852	60
H(40)	4735	6850	4709	48
H(45)	8426	5859	5994	58
H(48)	8170	5428	4966	61
H(49)	7809	5041	3853	64

H(51)	6180	6438	3858	41
H(57)	4473	7041	7135	53
H(60)	4655	8222	7084	54
H(61)	4906	9423	6923	57
H(63)	6335	8908	5441	45
H(66)	2430	5909	10318	29
H(68)	1088	4887	8968	34
H(70)	3121	5406	8383	31
H(74)	3708	4973	10358	37
H(76)	4881	5559	12053	46
H(78)	4311	7018	10602	38
H(82)	4154	4951	9027	39
H(84)	6050	5540	8171	44
H(86)	4741	7021	9009	37
H(90)	3519	7062	8399	46
H(92)	2434	8786	9092	52
H(94)	2966	7198	10436	34
H(90A)	3575	7193	8473	33
H(92A)	2468	8824	9327	38
H(94A)	3028	7121	10515	52
H(98)	9032	4200	5787	45
H(100)	11078	3979	6513	35
H(102)	9831	2237	6200	36

H(106)	7236	3095	4933	29
H(108)	6238	4523	6174	20
H(110)	8215	3784	6716	68
H(114)	8981	1394	5456	52
H(116)	8090	326	7067	68
H(118)	7759	2446	6855	47
H(122)	9071	3701	4705	80
H(124)	8439	2823	2859	111
H(126)	8001	1823	4681	64
H(130)	8758	1196	5430	82
H(132)	7917	225	7123	61
H(134)	7859	2373	6961	47
H(138)	7683	1763	4808	26
H(140)	8577	2022	2905	66
H(142)	9450	3001	4604	61
H(146)	7325	2973	4885	47
H(148)	6309	4489	6007	47
H(150)	8173	3634	6739	25
H(154)	9759	2081	6157	61
H(156)	10990	3810	6586	70
H(158)	8973	4059	5792	62
H(1S)	6258	6402	305	105
H(1S1)	6250	5693	1260	107

H(1S2)	6975	5355	958	107
H(2S1)	5597	5313	275	138
H(2S2)	6022	4638	578	138
H(2S3)	6316	5048	-94	138
H(2S)	8401	8267	5904	82
H(3S1)	9504	8195	5967	96
H(3S2)	9471	8207	5127	96
H(4S1)	9429	6978	5999	154
H(4S2)	9990	7133	5392	154
H(4S3)	9175	6933	5197	154

Table D.6. Torsion angles [°] for **2.32**.

C(3)-N(1)-N(2)-C(1)	0.7(9)	C(8)-N(3)-C(4)-C(5)	0.5(11)
Ir(1)-N(1)-N(2)-C(1)	-175.4(6)	Ir(1)-N(3)-C(4)-C(5)	180.0(6)
N(1)-N(2)-C(1)-C(2)	-0.3(10)	C(8)-N(3)-C(4)-C(3)	179.7(7)
N(2)-C(1)-C(2)-C(3)	-0.3(10)	Ir(1)-N(3)-C(4)-C(3)	-0.8(8)
N(2)-N(1)-C(3)-C(2)	-0.9(9)	N(1)-C(3)-C(4)-N(3)	2.8(10)
Ir(1)-N(1)-C(3)-C(2)	176.1(5)	C(2)-C(3)-C(4)-N(3)	-176.8(8)
N(2)-N(1)-C(3)-C(4)	179.4(6)	N(1)-C(3)-C(4)-C(5)	-177.9(7)
Ir(1)-N(1)-C(3)-C(4)	-3.6(9)	C(2)-C(3)-C(4)-C(5)	2.5(14)
C(1)-C(2)-C(3)-N(1)	0.8(10)	N(3)-C(4)-C(5)-C(6)	-0.6(11)
C(1)-C(2)-C(3)-C(4)	-179.6(9)	C(3)-C(4)-C(5)-C(6)	-179.8(7)

C(4)-C(5)-C(6)-C(7)	0.1(12)	C(10)-C(9)-C(14)-C(15)	-176.1(7)
C(5)-C(6)-C(7)-C(8)	0.5(12)	Ir(1)-C(9)-C(14)-C(15)	7.1(8)
C(4)-N(3)-C(8)-C(7)	0.2(11)	C(19)-N(4)-C(15)-C(16)	-1.5(11)
Ir(1)-N(3)-C(8)-C(7)	-179.3(6)	Ir(1)-N(4)-C(15)-C(16)	-178.4(6)
C(6)-C(7)-C(8)-N(3)	-0.6(12)	C(19)-N(4)-C(15)-C(14)	176.6(7)
C(14)-C(9)-C(10)-F(1)	176.4(7)	Ir(1)-N(4)-C(15)-C(14)	-0.3(9)
Ir(1)-C(9)-C(10)-F(1)	-7.4(11)	C(13)-C(14)-C(15)-N(4)	176.9(7)
C(14)-C(9)-C(10)-C(11)	-1.8(11)	C(9)-C(14)-C(15)-N(4)	-4.4(10)
Ir(1)-C(9)-C(10)-C(11)	174.4(6)	C(13)-C(14)-C(15)-C(16)	-5.0(13)
F(1)-C(10)-C(11)-F(2)	2.7(11)	C(9)-C(14)-C(15)-C(16)	173.6(8)
C(9)-C(10)-C(11)-F(2)	-179.0(7)	N(4)-C(15)-C(16)-C(17)	0.9(13)
F(1)-C(10)-C(11)-C(12)	-179.2(7)	C(14)-C(15)-C(16)-C(17)	-177.1(9)
C(9)-C(10)-C(11)-C(12)	-0.9(12)	C(15)-C(16)-C(17)-C(18)	1.5(14)
F(2)-C(11)-C(12)-F(3)	1.3(11)	C(15)-N(4)-C(19)-C(18)	-0.3(11)
C(10)-C(11)-C(12)-F(3)	-176.8(7)	Ir(1)-N(4)-C(19)-C(18)	176.3(6)
F(2)-C(11)-C(12)-C(13)	-178.7(7)	N(4)-C(19)-C(18)-C(17)	2.8(12)
C(10)-C(11)-C(12)-C(13)	3.2(12)	N(4)-C(19)-C(18)-C(20)	178.8(7)
F(3)-C(12)-C(13)-C(14)	177.5(7)	C(16)-C(17)-C(18)-C(19)	-3.3(13)
C(11)-C(12)-C(13)-C(14)	-2.5(12)	C(16)-C(17)-C(18)-C(20)	-179.5(8)
C(12)-C(13)-C(14)-C(9)	-0.4(12)	C(19)-C(18)-C(20)-F(6)	10.7(10)
C(12)-C(13)-C(14)-C(15)	178.1(8)	C(17)-C(18)-C(20)-F(6)	-173.3(7)
C(10)-C(9)-C(14)-C(13)	2.5(11)	C(19)-C(18)-C(20)-F(5)	-110.6(8)
Ir(1)-C(9)-C(14)-C(13)	-174.3(6)	C(17)-C(18)-C(20)-F(5)	65.4(9)

C(19)-C(18)-C(20)-F(4)	130.6(7)	C(24)-C(25)-C(26)-C(27A)	178(3)
C(17)-C(18)-C(20)-F(4)	-53.4(9)	C(24)-C(25)-C(26)-C(27)	177(2)
C(26)-C(21)-C(22)-F(7)	177.6(7)	C(21)-C(26)-C(27)-N(5)	4(4)
Ir(1)-C(21)-C(22)-F(7)	1.1(12)	C(25)-C(26)-C(27)-N(5)	-172(2)
C(26)-C(21)-C(22)-C(23)	-1.7(12)	C(21)-C(26)-C(27)-C(28)	-179(3)
Ir(1)-C(21)-C(22)-C(23)	-178.1(6)	C(25)-C(26)-C(27)-C(28)	5(5)
F(7)-C(22)-C(23)-F(8)	1.9(12)	N(5)-C(27)-C(28)-C(29)	-1(5)
C(21)-C(22)-C(23)-F(8)	-178.8(8)	C(26)-C(27)-C(28)-C(29)	-178(3)
F(7)-C(22)-C(23)-C(24)	-178.1(8)	C(27)-C(28)-C(29)-C(30)	3(4)
C(21)-C(22)-C(23)-C(24)	1.2(13)	C(28)-C(29)-C(30)-C(31)	-4(3)
F(8)-C(23)-C(24)-C(25)	-179.1(8)	C(28)-C(29)-C(30)-C(32)	176.2(17)
C(22)-C(23)-C(24)-C(25)	0.9(14)	C(29)-C(30)-C(31)-N(5)	4(3)
F(8)-C(23)-C(24)-F(9)	-0.5(13)	C(32)-C(30)-C(31)-N(5)	-176.3(18)
C(22)-C(23)-C(24)-F(9)	179.5(8)	C(31)-C(30)-C(32)-F(10)	141.0(15)
F(9)-C(24)-C(25)-C(26)	179.2(8)	C(29)-C(30)-C(32)-F(10)	-39.0(19)
C(23)-C(24)-C(25)-C(26)	-2.3(14)	C(31)-C(30)-C(32)-F(12)	-94.2(17)
C(22)-C(21)-C(26)-C(25)	0.3(12)	C(29)-C(30)-C(32)-F(12)	85.8(15)
Ir(1)-C(21)-C(26)-C(25)	177.2(6)	C(31)-C(30)-C(32)-F(11)	23.4(17)
C(22)-C(21)-C(26)-C(27A)	-176(3)	C(29)-C(30)-C(32)-F(11)	-156.6(14)
Ir(1)-C(21)-C(26)-C(27A)	1(3)	C(30)-C(31)-N(5)-C(27)	-2(4)
C(22)-C(21)-C(26)-C(27)	-175.5(19)	C(30)-C(31)-N(5)-Ir(1)	-176.3(15)
Ir(1)-C(21)-C(26)-C(27)	1.4(19)	C(28)-C(27)-N(5)-C(31)	1(5)
C(24)-C(25)-C(26)-C(21)	1.7(13)	C(26)-C(27)-N(5)-C(31)	178(2)

C(28)-C(27)-N(5)-Ir(1)	175(2)	C(28A)-C(27A)-N(5A)-Ir(1)	176(4)
C(26)-C(27)-N(5)-Ir(1)	-7(4)	C(26)-C(27A)-N(5A)-Ir(1)	0(6)
C(21)-C(26)-C(27A)-N(5A)	-1(6)	C(35)-N(6)-N(7)-C(33)	0.1(11)
C(25)-C(26)-C(27A)-N(5A)	-177(3)	Ir(2)-N(6)-N(7)-C(33)	-164.7(8)
C(21)-C(26)-C(27A)-C(28A)	-176(4)	N(6)-N(7)-C(33)-C(34)	0.0(13)
C(25)-C(26)-C(27A)-C(28A)	8(7)	N(7)-C(33)-C(34)-C(35)	-0.1(13)
N(5A)-C(27A)-C(28A)-C(29A)	2(8)	N(7)-N(6)-C(35)-C(34)	-0.2(10)
C(26)-C(27A)-C(28A)-C(29A)	178(4)	Ir(2)-N(6)-C(35)-C(34)	168.4(6)
C(27A)-C(28A)-C(29A)-C(30A)	1(6)	N(7)-N(6)-C(35)-C(36)	-176.9(8)
C(28A)-C(29A)-C(30A)-C(31A)	-1(5)	Ir(2)-N(6)-C(35)-C(36)	-8.3(10)
C(28A)-C(29A)-C(30A)-C(32A)	180(3)	C(33)-C(34)-C(35)-N(6)	0.2(12)
C(29A)-C(30A)-C(31A)-N(5A)	-3(5)	C(33)-C(34)-C(35)-C(36)	176.1(11)
C(32A)-C(30A)-C(31A)-N(5A)	177(3)	C(40)-N(8)-C(36)-C(37)	0.7(11)
C(31A)-C(30A)-C(32A)-F(10A)	137(3)	Ir(2)-N(8)-C(36)-C(37)	-177.7(6)
C(29A)-C(30A)-C(32A)-F(10A)	-43(3)	C(40)-N(8)-C(36)-C(35)	178.9(7)
C(31A)-C(30A)-C(32A)-F(11A)	15(3)	Ir(2)-N(8)-C(36)-C(35)	0.5(9)
C(29A)-C(30A)-C(32A)-F(11A)	-165(3)	N(6)-C(35)-C(36)-N(8)	5.1(11)
C(31A)-C(30A)-C(32A)-F(12A)	-102(3)	C(34)-C(35)-C(36)-N(8)	-170.6(10)
C(29A)-C(30A)-C(32A)-F(12A)	77(3)	N(6)-C(35)-C(36)-C(37)	-176.8(8)
C(30A)-C(31A)-N(5A)-C(27A)	6(6)	C(34)-C(35)-C(36)-C(37)	7.5(16)
C(30A)-C(31A)-N(5A)-Ir(1)	-176(2)	N(8)-C(36)-C(37)-C(38)	-0.2(13)
C(28A)-C(27A)-N(5A)-C(31A)	-6(8)	C(35)-C(36)-C(37)-C(38)	-178.3(9)
C(26)-C(27A)-N(5A)-C(31A)	178(4)	C(36)-C(37)-C(38)-C(39)	0.5(14)

C(37)-C(38)-C(39)-C(40)	-1.1(14)	Ir(2)-C(41)-C(46)-C(47)	2.6(10)
C(36)-N(8)-C(40)-C(39)	-1.5(13)	C(51)-N(9)-C(47)-C(48)	-0.9(14)
Ir(2)-N(8)-C(40)-C(39)	176.6(7)	Ir(2)-N(9)-C(47)-C(48)	-179.3(8)
C(38)-C(39)-C(40)-N(8)	1.7(14)	C(51)-N(9)-C(47)-C(46)	-178.8(8)
C(46)-C(41)-C(42)-F(13)	-177.8(7)	Ir(2)-N(9)-C(47)-C(46)	2.8(10)
Ir(2)-C(41)-C(42)-F(13)	-1.1(12)	C(45)-C(46)-C(47)-N(9)	178.8(9)
C(46)-C(41)-C(42)-C(43)	-0.9(12)	C(41)-C(46)-C(47)-N(9)	-3.6(12)
Ir(2)-C(41)-C(42)-C(43)	175.7(6)	C(45)-C(46)-C(47)-C(48)	1.1(16)
F(13)-C(42)-C(43)-F(14)	-0.7(11)	C(41)-C(46)-C(47)-C(48)	178.6(10)
C(41)-C(42)-C(43)-F(14)	-177.7(7)	N(9)-C(47)-C(48)-C(49)	1.1(17)
F(13)-C(42)-C(43)-C(44)	-179.6(8)	C(46)-C(47)-C(48)-C(49)	178.8(10)
C(41)-C(42)-C(43)-C(44)	3.3(13)	C(47)-C(48)-C(49)-C(50)	-0.7(18)
F(14)-C(43)-C(44)-C(45)	179.0(9)	C(48)-C(49)-C(50)-C(51)	0.1(16)
C(42)-C(43)-C(44)-C(45)	-2.1(15)	C(48)-C(49)-C(50)-C(52)	-178.2(10)
F(14)-C(43)-C(44)-F(15)	-2.5(13)	C(47)-N(9)-C(51)-C(50)	0.3(13)
C(42)-C(43)-C(44)-F(15)	176.4(8)	Ir(2)-N(9)-C(51)-C(50)	178.5(6)
F(15)-C(44)-C(45)-C(46)	-179.8(9)	C(49)-C(50)-C(51)-N(9)	0.1(14)
C(43)-C(44)-C(45)-C(46)	-1.4(16)	C(52)-C(50)-C(51)-N(9)	178.4(7)
C(44)-C(45)-C(46)-C(41)	3.9(16)	C(49)-C(50)-C(52)-F(18)	-178.8(9)
C(44)-C(45)-C(46)-C(47)	-178.7(10)	C(51)-C(50)-C(52)-F(18)	2.9(11)
C(42)-C(41)-C(46)-C(45)	-2.7(14)	C(49)-C(50)-C(52)-F(16)	-57.4(11)
Ir(2)-C(41)-C(46)-C(45)	-179.9(8)	C(51)-C(50)-C(52)-F(16)	124.3(8)
C(42)-C(41)-C(46)-C(47)	179.8(8)	C(49)-C(50)-C(52)-F(17)	60.6(11)

C(51)-C(50)-C(52)-F(17)	-117.8(9)	C(63)-N(10)-C(59)-C(58)	179.3(7)
C(58)-C(53)-C(54)-F(19)	177.3(7)	Ir(2)-N(10)-C(59)-C(58)	-1.2(9)
Ir(2)-C(53)-C(54)-F(19)	0.0(12)	C(57)-C(58)-C(59)-N(10)	-179.1(7)
C(58)-C(53)-C(54)-C(55)	-2.4(12)	C(53)-C(58)-C(59)-N(10)	0.2(10)
Ir(2)-C(53)-C(54)-C(55)	-179.6(6)	C(57)-C(58)-C(59)-C(60)	-0.9(13)
F(19)-C(54)-C(55)-F(20)	-0.5(12)	C(53)-C(58)-C(59)-C(60)	178.5(7)
C(53)-C(54)-C(55)-F(20)	179.2(8)	N(10)-C(59)-C(60)-C(61)	0.5(12)
F(19)-C(54)-C(55)-C(56)	-177.9(8)	C(58)-C(59)-C(60)-C(61)	-177.7(8)
C(53)-C(54)-C(55)-C(56)	1.8(13)	C(59)-C(60)-C(61)-C(62)	-1.2(13)
F(20)-C(55)-C(56)-F(21)	1.7(13)	C(60)-C(61)-C(62)-C(63)	0.5(13)
C(54)-C(55)-C(56)-F(21)	179.1(8)	C(60)-C(61)-C(62)-C(64)	179.4(7)
F(20)-C(55)-C(56)-C(57)	-178.7(8)	C(59)-N(10)-C(63)-C(62)	-1.7(12)
C(54)-C(55)-C(56)-C(57)	-1.3(14)	Ir(2)-N(10)-C(63)-C(62)	178.8(6)
F(21)-C(56)-C(57)-C(58)	-178.9(8)	C(61)-C(62)-C(63)-N(10)	0.9(13)
C(55)-C(56)-C(57)-C(58)	1.4(14)	C(64)-C(62)-C(63)-N(10)	-178.0(7)
C(56)-C(57)-C(58)-C(53)	-2.1(12)	C(63)-C(62)-C(64)-F(24A)	-76.3(14)
C(56)-C(57)-C(58)-C(59)	177.2(8)	C(61)-C(62)-C(64)-F(24A)	104.8(14)
C(54)-C(53)-C(58)-C(57)	2.5(11)	C(63)-C(62)-C(64)-F(24B)	-142.5(14)
Ir(2)-C(53)-C(58)-C(57)	-179.8(6)	C(61)-C(62)-C(64)-F(24B)	38.6(15)
C(54)-C(53)-C(58)-C(59)	-176.8(7)	C(63)-C(62)-C(64)-F(24)	-110.9(12)
Ir(2)-C(53)-C(58)-C(59)	0.9(8)	C(61)-C(62)-C(64)-F(24)	70.2(12)
C(63)-N(10)-C(59)-C(60)	1.0(12)	C(63)-C(62)-C(64)-F(23A)	46.6(12)
Ir(2)-N(10)-C(59)-C(60)	-179.5(6)	C(61)-C(62)-C(64)-F(23A)	-132.3(11)

C(63)-C(62)-C(64)-F(22B)	94.7(14)	C(71)-C(67)-C(68)-C(69)	177.7(7)
C(61)-C(62)-C(64)-F(22B)	-84.2(14)	C(67)-C(68)-C(69)-C(70)	-1.7(11)
C(63)-C(62)-C(64)-F(23)	10.2(13)	C(67)-C(68)-C(69)-C(72)	-178.4(7)
C(61)-C(62)-C(64)-F(23)	-168.6(12)	C(68)-C(69)-C(70)-C(65)	2.9(12)
C(63)-C(62)-C(64)-F(22)	130.0(12)	C(72)-C(69)-C(70)-C(65)	179.6(7)
C(61)-C(62)-C(64)-F(22)	-48.9(13)	C(66)-C(65)-C(70)-C(69)	-0.7(11)
C(63)-C(62)-C(64)-F(22A)	163.5(13)	B(1)-C(65)-C(70)-C(69)	-172.2(7)
C(61)-C(62)-C(64)-F(22A)	-15.4(14)	C(68)-C(67)-C(71)-F(26)	95.4(9)
C(63)-C(62)-C(64)-F(23B)	-23.2(14)	C(66)-C(67)-C(71)-F(26)	-85.0(10)
C(61)-C(62)-C(64)-F(23B)	157.9(13)	C(68)-C(67)-C(71)-F(25)	-142.7(8)
C(81)-B(1)-C(65)-C(70)	-23.9(10)	C(66)-C(67)-C(71)-F(25)	36.8(10)
C(73)-B(1)-C(65)-C(70)	-140.1(7)	C(68)-C(67)-C(71)-F(27)	-23.6(10)
C(89A)-B(1)-C(65)-C(70)	101.1(9)	C(66)-C(67)-C(71)-F(27)	156.0(7)
C(89)-B(1)-C(65)-C(70)	97.8(8)	C(70)-C(69)-C(72)-F(29)	16.9(12)
C(81)-B(1)-C(65)-C(66)	164.7(6)	C(68)-C(69)-C(72)-F(29)	-166.4(8)
C(73)-B(1)-C(65)-C(66)	48.5(8)	C(70)-C(69)-C(72)-F(28)	-106.9(9)
C(89A)-B(1)-C(65)-C(66)	-70.3(9)	C(68)-C(69)-C(72)-F(28)	69.9(10)
C(89)-B(1)-C(65)-C(66)	-73.5(8)	C(70)-C(69)-C(72)-F(30)	136.7(8)
C(70)-C(65)-C(66)-C(67)	-2.7(11)	C(68)-C(69)-C(72)-F(30)	-46.5(10)
B(1)-C(65)-C(66)-C(67)	169.4(7)	C(81)-B(1)-C(73)-C(78)	86.4(8)
C(65)-C(66)-C(67)-C(68)	4.1(11)	C(65)-B(1)-C(73)-C(78)	-150.1(7)
C(65)-C(66)-C(67)-C(71)	-175.5(7)	C(89A)-B(1)-C(73)-C(78)	-33.9(12)
C(66)-C(67)-C(68)-C(69)	-1.8(11)	C(89)-B(1)-C(73)-C(78)	-36.9(12)

C(81)-B(1)-C(73)-C(74)	-82.8(8)	C(74)-C(75)-C(79)-F(32)	136.2(9)
C(65)-B(1)-C(73)-C(74)	40.7(9)	C(76)-C(77)-C(80)-F(36)	92.7(11)
C(89A)-B(1)-C(73)-C(74)	156.9(10)	C(78)-C(77)-C(80)-F(36)	-84.5(12)
C(89)-B(1)-C(73)-C(74)	153.9(9)	C(76)-C(77)-C(80)-F(35)	-29.0(12)
C(78)-C(73)-C(74)-C(75)	0.3(12)	C(78)-C(77)-C(80)-F(35)	153.8(9)
B(1)-C(73)-C(74)-C(75)	170.4(8)	C(76)-C(77)-C(80)-F(34)	-149.9(10)
C(73)-C(74)-C(75)-C(76)	0.4(14)	C(78)-C(77)-C(80)-F(34)	32.9(13)
C(73)-C(74)-C(75)-C(79)	-177.6(9)	C(76)-C(77)-C(80A)-F(36A)	111.2(13)
C(74)-C(75)-C(76)-C(77)	0.2(14)	C(78)-C(77)-C(80A)-F(36A)	-60.5(12)
C(79)-C(75)-C(76)-C(77)	178.2(9)	C(76)-C(77)-C(80A)-F(35A)	-9.3(14)
C(75)-C(76)-C(77)-C(78)	-1.4(14)	C(78)-C(77)-C(80A)-F(35A)	179.0(10)
C(75)-C(76)-C(77)-C(80)	-178.8(9)	C(76)-C(77)-C(80A)-F(34A)	-126.5(12)
C(75)-C(76)-C(77)-C(80A)	-172.5(9)	C(78)-C(77)-C(80A)-F(34A)	61.7(12)
C(74)-C(73)-C(78)-C(77)	-1.6(12)	C(65)-B(1)-C(81)-C(86)	148.3(7)
B(1)-C(73)-C(78)-C(77)	-171.2(7)	C(73)-B(1)-C(81)-C(86)	-90.2(8)
C(76)-C(77)-C(78)-C(73)	2.2(13)	C(89A)-B(1)-C(81)-C(86)	27.6(12)
C(80)-C(77)-C(78)-C(73)	179.3(8)	C(89)-B(1)-C(81)-C(86)	34.2(11)
C(80A)-C(77)-C(78)-C(73)	174.5(8)	C(65)-B(1)-C(81)-C(82)	-41.1(9)
C(76)-C(75)-C(79)-F(31)	77.7(11)	C(73)-B(1)-C(81)-C(82)	80.4(8)
C(74)-C(75)-C(79)-F(31)	-104.3(10)	C(89A)-B(1)-C(81)-C(82)	-161.8(10)
C(76)-C(75)-C(79)-F(33)	-161.3(9)	C(89)-B(1)-C(81)-C(82)	-155.2(9)
C(74)-C(75)-C(79)-F(33)	16.8(14)	C(86)-C(81)-C(82)-C(83)	-0.7(12)
C(76)-C(75)-C(79)-F(32)	-41.8(14)	B(1)-C(81)-C(82)-C(83)	-172.0(8)

C(81)-C(82)-C(83)-C(84)	0.6(13)	C(84)-C(83)-C(87A)-F(38A)	76.1(12)
C(81)-C(82)-C(83)-C(87A)	-172.1(9)	C(82)-C(83)-C(87A)-F(37A)	7.3(14)
C(81)-C(82)-C(83)-C(87)	172.9(8)	C(84)-C(83)-C(87A)-F(37A)	-165.9(10)
C(82)-C(83)-C(84)-C(85)	0.5(13)	C(86)-C(85)-C(88)-F(42)	-156.0(10)
C(87A)-C(83)-C(84)-C(85)	174.1(9)	C(84)-C(85)-C(88)-F(42)	20.0(13)
C(87)-C(83)-C(84)-C(85)	-171.6(8)	C(86)-C(85)-C(88)-F(41)	-32.7(14)
C(83)-C(84)-C(85)-C(86)	-1.4(12)	C(84)-C(85)-C(88)-F(41)	143.2(11)
C(83)-C(84)-C(85)-C(88)	-177.5(8)	C(86)-C(85)-C(88)-F(40)	84.7(11)
C(83)-C(84)-C(85)-C(88A)	174.5(9)	C(84)-C(85)-C(88)-F(40)	-99.3(11)
C(84)-C(85)-C(86)-C(81)	1.2(12)	C(86)-C(85)-C(88A)-F(42A)	-177.7(10)
C(88)-C(85)-C(86)-C(81)	177.1(8)	C(84)-C(85)-C(88A)-F(42A)	6.2(14)
C(88A)-C(85)-C(86)-C(81)	-174.9(8)	C(86)-C(85)-C(88A)-F(41A)	-58.5(13)
C(82)-C(81)-C(86)-C(85)	-0.1(11)	C(84)-C(85)-C(88A)-F(41A)	125.5(12)
B(1)-C(81)-C(86)-C(85)	170.8(7)	C(86)-C(85)-C(88A)-F(40A)	61.4(12)
C(82)-C(83)-C(87)-F(39)	116.8(10)	C(84)-C(85)-C(88A)-F(40A)	-114.6(11)
C(84)-C(83)-C(87)-F(39)	-70.9(11)	C(81)-B(1)-C(89)-C(90)	36.5(11)
C(82)-C(83)-C(87)-F(38)	-124.8(10)	C(65)-B(1)-C(89)-C(90)	-86.3(9)
C(84)-C(83)-C(87)-F(38)	47.6(13)	C(73)-B(1)-C(89)-C(90)	153.8(7)
C(82)-C(83)-C(87)-F(37)	-3.4(12)	C(81)-B(1)-C(89)-C(94)	-148.6(8)
C(84)-C(83)-C(87)-F(37)	169.0(9)	C(65)-B(1)-C(89)-C(94)	88.7(9)
C(82)-C(83)-C(87A)-F(39A)	127.8(11)	C(73)-B(1)-C(89)-C(94)	-31.3(12)
C(84)-C(83)-C(87A)-F(39A)	-45.4(13)	C(94)-C(89)-C(90)-C(91)	0.0
C(82)-C(83)-C(87A)-F(38A)	-110.7(12)	B(1)-C(89)-C(90)-C(91)	175.0(13)

C(89)-C(90)-C(91)-C(92)	0.0	C(65)-B(1)-C(89A)-C(90A)	-86.1(12)
C(89)-C(90)-C(91)-C(95)	167.9(11)	C(73)-B(1)-C(89A)-C(90A)	153.5(9)
C(90)-C(91)-C(92)-C(93)	0.0	C(81)-B(1)-C(89A)-C(94A)	-150.3(8)
C(95)-C(91)-C(92)-C(93)	-168.2(11)	C(65)-B(1)-C(89A)-C(94A)	83.7(11)
C(91)-C(92)-C(93)-C(94)	0.0	C(73)-B(1)-C(89A)-C(94A)	-36.7(12)
C(91)-C(92)-C(93)-C(96)	-176.9(10)	C(94A)-C(89A)-C(90A)-C(91A)	0.0
C(92)-C(93)-C(94)-C(89)	0.0	B(1)-C(89A)-C(90A)-C(91A)	169.6(16)
C(96)-C(93)-C(94)-C(89)	176.9(10)	C(89A)-C(90A)-C(91A)-C(92A)	0.0
C(90)-C(89)-C(94)-C(93)	0.0	C(89A)-C(90A)-C(91A)-C(95A)	-173.0(12)
B(1)-C(89)-C(94)-C(93)	-174.9(13)	C(90A)-C(91A)-C(92A)-C(93A)	0.0
C(92)-C(91)-C(95)-F(45)	-159.8(9)	C(95A)-C(91A)-C(92A)-C(93A)	172.5(13)
C(90)-C(91)-C(95)-F(45)	32.1(13)	C(91A)-C(92A)-C(93A)-C(94A)	0.0
C(92)-C(91)-C(95)-F(44)	-38.7(12)	C(91A)-C(92A)-C(93A)-C(96A)	-175.5(12)
C(90)-C(91)-C(95)-F(44)	153.2(10)	C(92A)-C(93A)-C(94A)-C(89A)	0.0
C(92)-C(91)-C(95)-F(43)	81.0(11)	C(96A)-C(93A)-C(94A)-C(89A)	175.5(12)
C(90)-C(91)-C(95)-F(43)	-87.2(12)	C(90A)-C(89A)-C(94A)-C(93A)	0.0
C(92)-C(93)-C(96)-F(48)	-28.4(12)	B(1)-C(89A)-C(94A)-C(93A)	-169.8(16)
C(94)-C(93)-C(96)-F(48)	154.7(10)	C(90A)-C(91A)-C(95A)-F(45A)	-40.6(14)
C(92)-C(93)-C(96)-F(47)	90.4(11)	C(92A)-C(91A)-C(95A)-F(45A)	146.7(12)
C(94)-C(93)-C(96)-F(47)	-86.6(12)	C(90A)-C(91A)-C(95A)-F(44A)	80.2(14)
C(92)-C(93)-C(96)-F(46)	-148.6(9)	C(92A)-C(91A)-C(95A)-F(44A)	-92.6(14)
C(94)-C(93)-C(96)-F(46)	34.4(12)	C(90A)-C(91A)-C(95A)-F(43A)	-162.1(12)
C(81)-B(1)-C(89A)-C(90A)	39.9(14)	C(92A)-C(91A)-C(95A)-F(43A)	25.1(15)

C(92A)-C(93A)-C(96A)-F(48A)	-30.6(14)	B(2)-C(97)-C(102)-C(101)	179.0(16)
C(94A)-C(93A)-C(96A)-F(48A)	153.9(11)	C(100)-C(99)-C(103)-F(51)	150.2(11)
C(92A)-C(93A)-C(96A)-F(47A)	92.7(13)	C(98)-C(99)-C(103)-F(51)	-32.7(13)
C(94A)-C(93A)-C(96A)-F(47A)	-82.7(13)	C(100)-C(99)-C(103)-F(50)	29.0(14)
C(92A)-C(93A)-C(96A)-F(46A)	-150.0(11)	C(98)-C(99)-C(103)-F(50)	-154.0(11)
C(94A)-C(93A)-C(96A)-F(46A)	34.5(13)	C(100)-C(99)-C(103)-F(49)	-90.5(12)
C(121)-B(2)-C(97)-C(98)	82.1(12)	C(98)-C(99)-C(103)-F(49)	86.6(12)
C(105)-B(2)-C(97)-C(98)	-28.1(15)	C(102)-C(101)-C(104)-F(54)	-171.0(10)
C(113)-B(2)-C(97)-C(98)	-153.2(9)	C(100)-C(101)-C(104)-F(54)	13.7(13)
C(121)-B(2)-C(97)-C(102)	-96.8(13)	C(102)-C(101)-C(104)-F(53)	-50.1(12)
C(105)-B(2)-C(97)-C(102)	152.9(11)	C(100)-C(101)-C(104)-F(53)	134.7(11)
C(113)-B(2)-C(97)-C(102)	27.8(15)	C(102)-C(101)-C(104)-F(52)	69.6(12)
C(102)-C(97)-C(98)-C(99)	0.0	C(100)-C(101)-C(104)-F(52)	-105.6(11)
B(2)-C(97)-C(98)-C(99)	-179.0(16)	C(121)-B(2)-C(105)-C(106)	31.7(14)
C(97)-C(98)-C(99)-C(100)	0.0	C(97)-B(2)-C(105)-C(106)	146.2(12)
C(97)-C(98)-C(99)-C(103)	-177.2(12)	C(113)-B(2)-C(105)-C(106)	-88.7(13)
C(98)-C(99)-C(100)-C(101)	0.0	C(121)-B(2)-C(105)-C(110)	-152.6(9)
C(103)-C(99)-C(100)-C(101)	177.0(13)	C(97)-B(2)-C(105)-C(110)	-38.0(14)
C(99)-C(100)-C(101)-C(102)	0.0	C(113)-B(2)-C(105)-C(110)	87.0(11)
C(99)-C(100)-C(101)-C(104)	175.2(12)	C(110)-C(105)-C(106)-C(107)	0.0
C(100)-C(101)-C(102)-C(97)	0.0	B(2)-C(105)-C(106)-C(107)	175.7(16)
C(104)-C(101)-C(102)-C(97)	-175.4(11)	C(105)-C(106)-C(107)-C(108)	0.0
C(98)-C(97)-C(102)-C(101)	0.0	C(105)-C(106)-C(107)-C(111)	175.9(11)

C(106)-C(107)-C(108)-C(109)	0.0	C(121)-B(2)-C(113)-C(118)	-142.8(10)
C(111)-C(107)-C(108)-C(109)	-175.9(11)	C(97)-B(2)-C(113)-C(118)	96.1(12)
C(107)-C(108)-C(109)-C(110)	0.0	C(105)-B(2)-C(113)-C(118)	-30.6(12)
C(107)-C(108)-C(109)-C(112)	174.1(13)	C(118)-C(113)-C(114)-C(115)	0.0
C(108)-C(109)-C(110)-C(105)	0.0	B(2)-C(113)-C(114)-C(115)	177.7(12)
C(112)-C(109)-C(110)-C(105)	-174.5(12)	C(113)-C(114)-C(115)-C(116)	0.0
C(106)-C(105)-C(110)-C(109)	0.0	C(113)-C(114)-C(115)-C(119)	170.1(13)
B(2)-C(105)-C(110)-C(109)	-175.9(15)	C(114)-C(115)-C(116)-C(117)	0.0
C(108)-C(107)-C(111)-F(57)	-32.3(12)	C(119)-C(115)-C(116)-C(117)	-169.8(13)
C(106)-C(107)-C(111)-F(57)	151.8(10)	C(115)-C(116)-C(117)-C(118)	0.0
C(108)-C(107)-C(111)-F(56)	86.6(11)	C(115)-C(116)-C(117)-C(120)	-175.4(14)
C(106)-C(107)-C(111)-F(56)	-89.3(11)	C(116)-C(117)-C(118)-C(113)	0.0
C(108)-C(107)-C(111)-F(55)	-152.1(9)	C(120)-C(117)-C(118)-C(113)	175.3(14)
C(106)-C(107)-C(111)-F(55)	32.0(12)	C(114)-C(113)-C(118)-C(117)	0.0
C(108)-C(109)-C(112)-F(60)	102.9(12)	B(2)-C(113)-C(118)-C(117)	-177.8(12)
C(110)-C(109)-C(112)-F(60)	-82.8(12)	C(114)-C(115)-C(119)-F(63)	35.3(15)
C(108)-C(109)-C(112)-F(59)	-136.4(11)	C(116)-C(115)-C(119)-F(63)	-154.7(12)
C(110)-C(109)-C(112)-F(59)	37.9(13)	C(114)-C(115)-C(119)-F(61)	155.2(13)
C(108)-C(109)-C(112)-F(58)	-17.6(14)	C(116)-C(115)-C(119)-F(61)	-34.8(16)
C(110)-C(109)-C(112)-F(58)	156.6(10)	C(114)-C(115)-C(119)-F(62)	-83.4(14)
C(121)-B(2)-C(113)-C(114)	39.5(14)	C(116)-C(115)-C(119)-F(62)	86.6(14)
C(97)-B(2)-C(113)-C(114)	-81.6(13)	C(118)-C(117)-C(120)-F(66)	38.6(15)
C(105)-B(2)-C(113)-C(114)	151.7(9)	C(116)-C(117)-C(120)-F(66)	-146.0(12)

C(118)-C(117)-C(120)-F(65)	-80.4(14)	C(122)-C(123)-C(127)-F(69)	120.6(14)
C(116)-C(117)-C(120)-F(65)	94.9(13)	C(124)-C(123)-C(127)-F(68)	60.6(14)
C(118)-C(117)-C(120)-F(64)	158.9(12)	C(122)-C(123)-C(127)-F(68)	-118.4(13)
C(116)-C(117)-C(120)-F(64)	-25.7(14)	C(124)-C(123)-C(127)-F(67)	178.5(12)
C(97)-B(2)-C(121)-C(122)	-40.6(12)	C(122)-C(123)-C(127)-F(67)	-0.5(16)
C(105)-B(2)-C(121)-C(122)	78.3(12)	C(124)-C(125)-C(128)-F(72)	-96.8(14)
C(113)-B(2)-C(121)-C(122)	-163.4(9)	C(126)-C(125)-C(128)-F(72)	74.3(14)
C(97)-B(2)-C(121)-C(126)	146.1(10)	C(124)-C(125)-C(128)-F(71)	142.2(13)
C(105)-B(2)-C(121)-C(126)	-94.9(13)	C(126)-C(125)-C(128)-F(71)	-46.7(15)
C(113)-B(2)-C(121)-C(126)	23.4(15)	C(124)-C(125)-C(128)-F(70)	23.0(15)
C(126)-C(121)-C(122)-C(123)	0.0	C(126)-C(125)-C(128)-F(70)	-166.0(12)
B(2)-C(121)-C(122)-C(123)	-173.5(14)	C(153)-B(3)-C(129)-C(130)	-97.9(12)
C(121)-C(122)-C(123)-C(124)	0.0	C(137)-B(3)-C(129)-C(130)	22.5(13)
C(121)-C(122)-C(123)-C(127)	179.0(14)	C(145)-B(3)-C(129)-C(130)	145.4(9)
C(122)-C(123)-C(124)-C(125)	0.0	C(153)-B(3)-C(129)-C(134)	84.4(13)
C(127)-C(123)-C(124)-C(125)	-179.0(14)	C(137)-B(3)-C(129)-C(134)	-155.2(9)
C(123)-C(124)-C(125)-C(126)	0.0	C(145)-B(3)-C(129)-C(134)	-32.2(14)
C(123)-C(124)-C(125)-C(128)	170.7(14)	C(134)-C(129)-C(130)-C(131)	0.0
C(124)-C(125)-C(126)-C(121)	0.0	B(3)-C(129)-C(130)-C(131)	-177.7(15)
C(128)-C(125)-C(126)-C(121)	-171.4(13)	C(129)-C(130)-C(131)-C(132)	0.0
C(122)-C(121)-C(126)-C(125)	0.0	C(129)-C(130)-C(131)-C(135)	172.7(14)
B(2)-C(121)-C(126)-C(125)	173.1(15)	C(130)-C(131)-C(132)-C(133)	0.0
C(124)-C(123)-C(127)-F(69)	-60.4(15)	C(135)-C(131)-C(132)-C(133)	-173.6(12)

C(131)-C(132)-C(133)-C(134)	0.0	C(145)-B(3)-C(137)-C(142)	100.1(9)
C(131)-C(132)-C(133)-C(136)	174.3(13)	C(142)-C(137)-C(138)-C(139)	0.0
C(132)-C(133)-C(134)-C(129)	0.0	B(3)-C(137)-C(138)-C(139)	174.5(8)
C(136)-C(133)-C(134)-C(129)	-174.5(12)	C(137)-C(138)-C(139)-C(140)	0.0
C(130)-C(129)-C(134)-C(133)	0.0	C(137)-C(138)-C(139)-C(143)	179.7(9)
B(3)-C(129)-C(134)-C(133)	177.6(15)	C(138)-C(139)-C(140)-C(141)	0.0
C(130)-C(131)-C(135)-F(75)	121.1(13)	C(143)-C(139)-C(140)-C(141)	-179.7(10)
C(132)-C(131)-C(135)-F(75)	-65.8(13)	C(139)-C(140)-C(141)-C(142)	0.0
C(130)-C(131)-C(135)-F(74)	-118.3(13)	C(139)-C(140)-C(141)-C(144)	177.0(11)
C(132)-C(131)-C(135)-F(74)	54.8(14)	C(140)-C(141)-C(142)-C(137)	0.0
C(130)-C(131)-C(135)-F(73)	2.1(15)	C(144)-C(141)-C(142)-C(137)	-177.1(11)
C(132)-C(131)-C(135)-F(73)	175.2(11)	C(138)-C(137)-C(142)-C(141)	0.0
C(132)-C(133)-C(136)-F(78)	11.5(15)	B(3)-C(137)-C(142)-C(141)	-174.3(9)
C(134)-C(133)-C(136)-F(78)	-174.1(11)	C(140)-C(139)-C(143)-F(81)	-8.9(12)
C(132)-C(133)-C(136)-F(76)	130.6(12)	C(138)-C(139)-C(143)-F(81)	171.4(8)
C(134)-C(133)-C(136)-F(76)	-55.0(14)	C(140)-C(139)-C(143)-F(79)	-130.0(9)
C(132)-C(133)-C(136)-F(77)	-109.6(13)	C(138)-C(139)-C(143)-F(79)	50.3(11)
C(134)-C(133)-C(136)-F(77)	64.8(13)	C(140)-C(139)-C(143)-F(80)	111.2(9)
C(153)-B(3)-C(137)-C(138)	169.5(7)	C(138)-C(139)-C(143)-F(80)	-68.5(10)
C(129)-B(3)-C(137)-C(138)	47.5(11)	C(142)-C(141)-C(144)-F(84)	-170.4(10)
C(145)-B(3)-C(137)-C(138)	-74.3(10)	C(140)-C(141)-C(144)-F(84)	12.6(14)
C(153)-B(3)-C(137)-C(142)	-16.0(10)	C(142)-C(141)-C(144)-F(83)	68.0(13)
C(129)-B(3)-C(137)-C(142)	-138.1(9)	C(140)-C(141)-C(144)-F(83)	-109.1(12)

C(142)-C(141)-C(144)-F(82)	-50.4(13)	C(146)-C(147)-C(151)-F(86)	-95.0(11)
C(140)-C(141)-C(144)-F(82)	132.6(11)	C(148)-C(147)-C(151)-F(85)	-34.8(12)
C(153)-B(3)-C(145)-C(146)	140.6(9)	C(146)-C(147)-C(151)-F(85)	144.3(9)
C(137)-B(3)-C(145)-C(146)	22.4(11)	C(148)-C(149)-C(152)-F(90)	-135.2(10)
C(129)-B(3)-C(145)-C(146)	-98.9(10)	C(150)-C(149)-C(152)-F(90)	46.6(12)
C(153)-B(3)-C(145)-C(150)	-41.3(13)	C(148)-C(149)-C(152)-F(89)	-13.4(13)
C(137)-B(3)-C(145)-C(150)	-159.4(8)	C(150)-C(149)-C(152)-F(89)	168.5(10)
C(129)-B(3)-C(145)-C(150)	79.2(12)	C(148)-C(149)-C(152)-F(88)	104.9(11)
C(150)-C(145)-C(146)-C(147)	0.0	C(150)-C(149)-C(152)-F(88)	-73.2(11)
B(3)-C(145)-C(146)-C(147)	178.2(11)	C(137)-B(3)-C(153)-C(154)	-86.4(11)
C(145)-C(146)-C(147)-C(148)	0.0	C(129)-B(3)-C(153)-C(154)	34.1(13)
C(145)-C(146)-C(147)-C(151)	-179.1(11)	C(145)-B(3)-C(153)-C(154)	153.5(10)
C(146)-C(147)-C(148)-C(149)	0.0	C(137)-B(3)-C(153)-C(158)	95.2(12)
C(151)-C(147)-C(148)-C(149)	179.0(11)	C(129)-B(3)-C(153)-C(158)	-144.3(11)
C(147)-C(148)-C(149)-C(150)	0.0	C(145)-B(3)-C(153)-C(158)	-25.0(14)
C(147)-C(148)-C(149)-C(152)	-178.1(12)	C(158)-C(153)-C(154)-C(155)	0.0
C(148)-C(149)-C(150)-C(145)	0.0	B(3)-C(153)-C(154)-C(155)	-178.5(14)
C(152)-C(149)-C(150)-C(145)	178.2(11)	C(153)-C(154)-C(155)-C(156)	0.0
C(146)-C(145)-C(150)-C(149)	0.0	C(153)-C(154)-C(155)-C(159)	-177.5(14)
B(3)-C(145)-C(150)-C(149)	-178.1(12)	C(154)-C(155)-C(156)-C(157)	0.0
C(148)-C(147)-C(151)-F(87)	-154.9(9)	C(159)-C(155)-C(156)-C(157)	177.7(13)
C(146)-C(147)-C(151)-F(87)	24.2(12)	C(155)-C(156)-C(157)-C(158)	0.0
C(148)-C(147)-C(151)-F(86)	85.9(11)	C(155)-C(156)-C(157)-C(160)	175.8(14)

C(156)-C(157)-C(158)-C(153)	0.0	C(156)-C(155)-C(159)-F(91)	-83.1(13)
C(160)-C(157)-C(158)-C(153)	-175.7(14)	C(154)-C(155)-C(159)-F(91)	94.5(14)
C(154)-C(153)-C(158)-C(157)	0.0	C(158)-C(157)-C(160)-F(96)	-24.0(16)
B(3)-C(153)-C(158)-C(157)	178.4(15)	C(156)-C(157)-C(160)-F(96)	160.2(12)
C(156)-C(155)-C(159)-F(93)	36.6(14)	C(158)-C(157)-C(160)-F(95)	96.4(14)
C(154)-C(155)-C(159)-F(93)	-145.8(12)	C(156)-C(157)-C(160)-F(95)	-79.4(14)
C(156)-C(155)-C(159)-F(92)	157.9(11)	C(158)-C(157)-C(160)-F(94)	-145.1(12)
C(154)-C(155)-C(159)-F(92)	-24.5(15)	C(156)-C(157)-C(160)-F(94)	39.1(14)

Symmetry transformations used to generate equivalent atoms:

Table D.7. Hydrogen bonds for **2.32** [Å and °].

D-H...A	d(D-H)	d(H...A)	d(D...A)	<(DHA)
N(2)-H(2)...O(1)	0.88	1.85	2.726(11)	174.5
N(7)-H(7A)...O(2)	0.88	1.87	2.746(14)	171.8

Symmetry transformations used to generate equivalent atoms:

D.2 X-Ray Data for Compound 3.27f

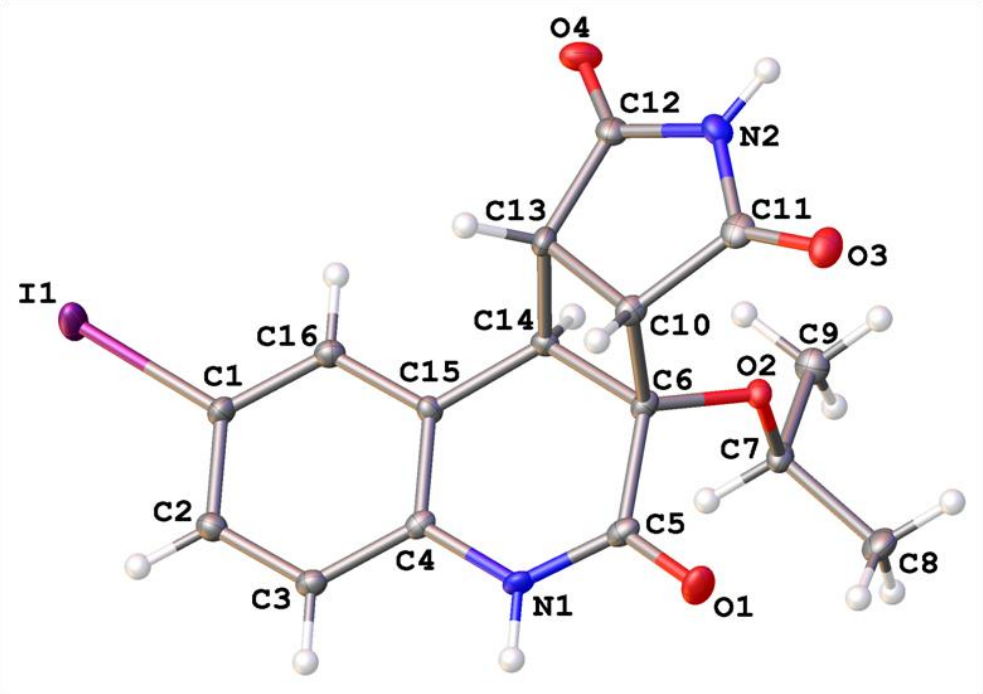

D.2.1 Data Collection

A colorless crystal with approximate dimensions 0.035 x 0.091 x 0.269 mm^3 was selected under oil under ambient conditions and attached to the tip of a MiTeGenMicroMount©. The crystal was mounted in a stream of cold nitrogen at 100(1) K and centered in the X-ray beam by using a video camera.

The crystal evaluation and data collection were performed on a Bruker QuazarSMART APEXII diffractometer with Mo K_α(λ = 0.71073 Å) radiation and the diffractometer to crystal distance of 4.96 cm.

The initial cell constants were obtained from three series of ω scans at different starting angles. Each series consisted of 12 frames collected at intervals of 0.5º in a 6º range about ω with the exposure time of 10 seconds per frame. The reflections were successfully indexed by an automated

indexing routine built in the APEXII program suite. The final cell constants were calculated from a set of 9245 strong reflections from the actual data collection.

The data were collected by using the full sphere data collection routine to survey the reciprocal space to the extent of a full sphere to a resolution of 0.709 Å. A total of 18225 data were harvested by collecting 5 sets of frames with 0.7° scans in ω and φ with exposure times of 26 sec per frame. These highly redundant datasets were corrected for Lorentz and polarization effects. The absorption correction was based on fitting a function to the empirical transmission surface as sampled by multiple equivalent measurements.

D.2.2 Structure Solution and Refinement

The systematic absences in the diffraction data were consistent for the space groups $P2_1$ and $P2_1/m$. The *E*-statistics strongly suggested the non-centrosymmetric space group $P2_1$ that yielded chemically reasonable and computationally stable results of refinement.

A successful solution by the direct methods provided most non-hydrogen atoms from the *E*-map. The remaining non-hydrogen atoms were located in an alternating series of least-squares cycles and difference Fourier maps. All non-hydrogen atoms were refined with anisotropic displacement coefficients. All hydrogen atoms were included in the structure factor calculation at idealized positions and were allowed to ride on the neighboring atoms with relative isotropic displacement coefficients.

The absolute configuration was unequivocally assigned based on anomalous dispersion: C6 – *R*, C10 – *S*, C13 – *S*, C14– *R*.

The final least-squares refinement of 210 parameters against 4520 data resulted in residuals *R* (based on F^2 for $I \geq 2\sigma$) and *wR* (based on F^2 for all data) of 0.0196 and 0.0474, respectively. The final difference Fourier map was featureless.

D.2.3 Summary

Crystal Data for $C_{16}H_{15}IN_2O_4$ (*M* =426.20 g/mol): monoclinic, space group $P2_1$ (no. 4), *a* =9.094(3) Å, *b* =7.248(2) Å, *c* =11.749(3) Å, *V* =769.3(4) $Å^3$, *Z* = 2, *T* = 100.0 K, μ(MoKα) = 2.104 mm^{-1}, *Dcalc* = 1.840 g/cm^3, 18225 reflections measured ($3.49° \leq 2\Theta \leq 60.264°$), 4520 unique ($R_{int}$ = 0.0255, R_{sigma} = 0.0238) which were used in all calculations. The final R_1 was 0.0196 ($I > 2\sigma(I)$) and wR_2 was 0.0474 (all data).

Table D.8. Crystal data and structure refinement for Yoon53.

Identification code	Yoon53
Empirical formula	$C_{16}H_{15}IN_2O_4$
Formula weight	426.20
Temperature/K	100.02
Crystal system	monoclinic
Space group	$P2_1$
a/Å	9.094(3)
b/Å	7.248(2)
c/Å	11.749(3)
α/°	90
β/°	96.62(2)

γ/°	90
Volume/Å^3	769.3(4)
Z	2
ρ_{calc}g/cm^3	1.840
μ/mm^{-1}	2.104
F(000)	420.0
Crystal size/mm^3	0.269 × 0.091 × 0.035
Radiation	MoKα (λ = 0.71073)
2Θ range for data collection/°	3.49 to 60.264
Index ranges	-12 ≤ h ≤ 12, -10 ≤ k ≤ 10, -16 ≤ l ≤ 16
Reflections collected	18225
Independent reflections	4520 [R_{int} = 0.0255, R_{sigma} = 0.0238]
Data/restraints/parameters	4520/1/210
Goodness-of-fit on F^2	1.074
Final R indexes [I>=2σ (I)]	R_1 = 0.0196, wR_2 = 0.0472
Final R indexes [all data]	R_1 = 0.0207, wR_2 = 0.0474
Largest diff. peak/hole / e Å^{-3}	0.69/-0.42
Flack parameter	-0.045(7)

Table D.9. Fractional Atomic Coordinates (×10^4) and Equivalent Isotropic Displacement Parameters (Å^2×10^3) for Yoon53. U_{eq} is defined as 1/3 of of the trace of the orthogonalised U_{IJ} tensor.

Atom	***x***	***y***	***z***	**U(eq)**
I1	7873.3(2)	375.5(3)	1909.6(2)	22.66(6)
O1	-212(2)	5934(3)	945.8(17)	19.2(4)

O2	961(2)	6411(2)	3249.0(16)	10.9(4)
O3	1499(2)	10501(4)	2786.7(16)	19.2(4)
O4	5498(2)	7502(3)	4644.1(18)	19.3(4)
N1	1481(3)	3693(3)	838(2)	12.5(4)
N2	3561(3)	9332(3)	3866(2)	14.4(5)
C1	5724(3)	1428(4)	1561(2)	12.5(5)
C2	4796(3)	842(3)	595(2)	13.3(5)
C3	3385(3)	1593(4)	373(2)	12.1(5)
C4	2903(3)	2932(3)	1099(2)	11.0(5)
C5	959(3)	5205(5)	1329(2)	13.0(5)
C6	1873(3)	5987(4)	2399(2)	11.0(5)
C7	276(3)	4840(3)	3756(2)	12.6(5)
C8	-1390(3)	5060(4)	3536(3)	18.3(6)
C9	816(3)	4842(4)	5028(2)	16.2(5)
C10	2759(3)	7762(4)	2162(2)	12.4(5)
C11	2472(3)	9373(4)	2927(2)	14.9(5)
C12	4535(3)	7880(4)	3864(2)	13.6(5)
C13	4187(3)	6839(4)	2744(2)	12.7(5)
C14	3347(3)	4984(3)	2839(2)	10.7(5)
C15	3823(3)	3510(3)	2059(2)	10.0(5)
C16	5236(3)	2740(4)	2285(2)	12.5(5)

Table D.10. Anisotropic Displacement Parameters ($Å^2 \times 10^3$) for Yoon53. The Anisotropic displacement factor exponent takes the form: $-2\pi^2[h^2a^{*2}U_{11}+2hka^*b^*U_{12}+\ldots]$.

Atom	**U_{11}**	**U_{22}**	**U_{33}**	**U_{23}**	**U_{13}**	**U_{12}**

I1	16.79(9)	31.07(10)	18.46(9)	-9.19(9)	-5.07(6)	12.14(9)
O1	13.8(10)	26.5(11)	16.3(9)	0.4(7)	-2.5(7)	7.3(7)
O2	10.8(9)	9.7(8)	12.6(9)	0.2(7)	3.3(7)	0.0(7)
O3	16.7(8)	14.0(9)	27.2(9)	2.8(11)	4.3(7)	2.7(11)
O4	19.2(10)	16.1(9)	20.8(11)	-1.6(8)	-6.3(8)	-1.0(8)
N1	8.9(11)	17.1(10)	10.6(11)	-1.5(8)	-2.8(8)	-0.6(8)
N2	16.7(12)	10.5(10)	16.0(12)	-2.1(8)	2.1(9)	0.2(8)
C1	9.4(12)	13.9(12)	13.9(12)	-0.3(9)	-0.4(9)	1.6(9)
C2	14.0(12)	13.3(13)	12.4(12)	-1.4(8)	0.7(9)	-0.4(9)
C3	11.3(12)	13.9(11)	10.9(12)	0.4(9)	-0.1(9)	-1.2(9)
C4	9.5(12)	12.0(11)	11.2(12)	3.8(9)	0.5(9)	-0.8(9)
C5	9.9(10)	17.5(13)	11.5(10)	3.2(12)	0.3(8)	-2.5(12)
C6	9.1(11)	12.3(10)	11.6(11)	2.7(8)	1.1(9)	0.6(8)
C7	11.3(12)	9.9(11)	16.8(13)	0.0(8)	3.4(10)	0.0(8)
C8	11.9(12)	19.7(18)	23.7(13)	-0.4(10)	3.5(10)	-3.2(10)
C9	17.9(13)	17.3(12)	13.9(13)	2.5(9)	3.3(10)	-0.1(9)
C10	12.2(13)	11.1(11)	13.7(12)	2.9(9)	0.6(9)	0.3(9)
C11	15.0(13)	12.1(12)	18.4(14)	4.3(10)	4.8(10)	-2.3(10)
C12	13.4(12)	10.9(11)	16.6(13)	-0.9(9)	1.7(10)	-2.3(9)
C13	8.8(12)	13.1(11)	16.7(14)	-1.6(10)	2.9(10)	0.7(9)
C14	11.1(11)	11.7(14)	9.2(11)	-0.9(8)	0.3(8)	-0.4(8)
C15	11.1(12)	9.2(10)	9.6(12)	0.2(9)	0.3(9)	1.8(9)
C16	11.9(12)	13.5(11)	11.7(12)	-0.1(9)	-0.5(9)	-0.3(9)

Table D.11. Bond Lengths for Yoon53.

Atom	Atom	Length/Å	Atom	Atom	Length/Å
I1	C1	2.095(3)	C3	C4	1.396(4)
O1	C5	1.227(3)	C4	C15	1.389(4)
O2	C6	1.403(3)	C5	C6	1.533(4)
O2	C7	1.458(3)	C6	C10	1.560(4)
O3	C11	1.202(4)	C6	C14	1.560(4)
O4	C12	1.223(3)	C7	C8	1.516(4)
N1	C4	1.406(3)	C7	C9	1.518(4)
N1	C5	1.350(4)	C10	C11	1.514(4)
N2	C11	1.395(4)	C10	C13	1.548(4)
N2	C12	1.376(3)	C12	C13	1.518(4)
C1	C2	1.399(4)	C13	C14	1.557(4)
C1	C16	1.383(4)	C14	C15	1.504(3)
C2	C3	1.391(4)	C15	C16	1.398(4)

Table D.12. Bond Angles for Yoon53.

Atom	Atom	Atom	Angle/°	Atom	Atom	Atom	Angle/°
C6	O2	C7	115.81(19)	O2	C7	C9	107.3(2)
C5	N1	C4	125.8(2)	C8	C7	C9	111.8(2)
C12	N2	C11	114.4(2)	C11	C10	C6	113.7(2)
C2	C1	I1	120.66(19)	C11	C10	C13	105.3(2)
C16	C1	I1	119.24(19)	C13	C10	C6	89.36(19)
C16	C1	C2	120.1(2)	O3	C11	N2	124.5(3)
C3	C2	C1	119.4(2)	O3	C11	C10	128.1(3)

C2	C3	C4	120.4(2)	N2	C11	C10	107.3(2)
C3	C4	N1	119.0(2)	O4	C12	N2	125.1(3)
C15	C4	N1	120.7(2)	O4	C12	C13	126.7(3)
C15	C4	C3	120.2(2)	N2	C12	C13	108.1(2)
O1	C5	N1	121.7(2)	C10	C13	C14	90.7(2)
O1	C5	C6	120.5(3)	C12	C13	C10	104.4(2)
N1	C5	C6	117.8(2)	C12	C13	C14	115.0(2)
O2	C6	C5	110.8(2)	C13	C14	C6	89.07(18)
O2	C6	C10	107.8(2)	C15	C14	C6	115.2(2)
O2	C6	C14	115.0(2)	C15	C14	C13	113.0(2)
C5	C6	C10	113.6(2)	C4	C15	C14	121.3(2)
C5	C6	C14	117.6(2)	C4	C15	C16	119.2(2)
C14	C6	C10	90.09(19)	C16	C15	C14	119.4(2)
O2	C7	C8	108.3(2)	C1	C16	C15	120.7(2)

Table D.13. Hydrogen Bonds for Yoon53.

D	**H**	**A**	**d(D-H)/Å**	**d(H-A)/Å**	**d(D-A)/Å**	**D-H-A/°**
N1	H1	O1[1]	0.88	2.21	3.027(3)	154.9
N2	H2	O4[2]	0.88	2.13	2.955(3)	156.1

[1]-X,-1/2+Y,-Z; [2]1-X,1/2+Y,1-Z

Table D.14. Torsion Angles for Yoon53.

A	**B**	**C**	**D**	**Angle/°**	**A**	**B**	**C**	**D**	**Angle/°**
I1	C1	C2	C3	-178.7(2)	C5	C6	C14	C15	8.6(3)
I1	C1	C16	C15	178.1(2)	C6	O2	C7	C8	-119.9(2)

O1	C5	C6	O2	44.7(3)	C6	O2	C7	C9	119.3(2)
O1	C5	C6	C10	-76.9(3)	C6	C10	C11	O3	-86.0(4)
O1	C5	C6	C14	179.8(2)	C6	C10	C11	N2	93.7(3)
O2	C6	C10	C11	3.0(3)	C6	C10	C13	C12	-109.2(2)
O2	C6	C10	C13	109.5(2)	C6	C10	C13	C14	6.8(2)
O2	C6	C14	C13	-103.0(2)	C6	C14	C15	C4	-8.4(3)
O2	C6	C14	C15	141.8(2)	C6	C14	C15	C16	169.9(2)
O4	C12	C13	C10	172.9(3)	C7	O2	C6	C5	67.3(3)
O4	C12	C13	C14	75.2(4)	C7	O2	C6	C10	-167.8(2)
N1	C4	C15	C14	-1.0(4)	C7	O2	C6	C14	-69.1(3)
N1	C4	C15	C16	-179.2(2)	C10	C6	C14	C13	6.8(2)
N1	C5	C6	O2	-134.7(2)	C10	C6	C14	C15	-108.3(2)
N1	C5	C6	C10	103.7(3)	C10	C13	C14	C6	-6.9(2)
N1	C5	C6	C14	0.3(3)	C10	C13	C14	C15	110.3(2)
N2	C12	C13	C10	-6.3(3)	C11	N2	C12	O4	-174.0(3)
N2	C12	C13	C14	-104.0(3)	C11	N2	C12	C13	5.2(3)
C1	C2	C3	C4	0.6(4)	C11	C10	C13	C12	5.2(3)
C2	C1	C16	C15	-0.6(4)	C11	C10	C13	C14	121.3(2)
C2	C3	C4	N1	178.7(2)	C12	N2	C11	O3	178.1(3)
C2	C3	C4	C15	-0.8(4)	C12	N2	C11	C10	-1.7(3)
C3	C4	C15	C14	178.5(2)	C12	C13	C14	C6	99.4(2)
C3	C4	C15	C16	0.2(4)	C12	C13	C14	C15	-143.5(2)
C4	N1	C5	O1	169.5(3)	C13	C10	C11	O3	177.8(3)
C4	N1	C5	C6	-11.0(4)	C13	C10	C11	N2	-2.5(3)
C4	C15	C16	C1	0.5(4)	C13	C14	C15	C4	-108.8(3)

C5	N1	C4	C3	-167.6(3)	C13	C14	C15	C16	69.4(3)
C5	N1	C4	C15	11.8(4)	C14	C6	C10	C11	-113.3(2)
C5	C6	C10	C11	126.3(2)	C14	C6	C10	C13	-6.8(2)
C5	C6	C10	C13	-127.3(2)	C14	C15	C16	C1	-177.8(2)
C5	C6	C14	C13	123.7(2)	C16	C1	C2	C3	0.1(4)

Table D.15. Hydrogen Atom Coordinates (Å×10⁴) and Isotropic Displacement Parameters (Å²×10³) for Yoon53.

Atom	***x***	***y***	***z***	**U(eq)**
H1	878.8	3134.79	306.84	15
H2	3619.88	10166.27	4413.39	17
H2A	5127.25	-60.37	96.54	16
H3	2745.4	1192.26	-276.93	15
H7	581.88	3669.59	3399.86	15
H8A	-1689.49	6175.25	3920.95	27
H8B	-1870.67	3981.93	3834.88	27
H8C	-1687.23	5165.16	2709.95	27
H9A	1885.85	4616.93	5137.67	24
H9B	307.94	3868.03	5409.2	24
H9C	603.82	6041.14	5357.42	24
H10	2771.34	8074.62	1333.87	15
H13	5019.79	6784.74	2258.93	15
H14	3367.88	4552.66	3649.49	13
H16	5868.02	3122.57	2942.57	15

D.3 X-Ray Data for Compound Δ-4.49f

D.3.1 Data Collection

A yellow crystal with approximate dimensions 0.195 x 0.112 x 0.101 mm^3 was selected under oil under ambient conditions and attached to the tip of a MiTeGen MicroMount©. The crystal was mounted in a stream of cold nitrogen at 100(1) K and centered in the X-ray beam by using a video camera.

The crystal evaluation and data collection were performed on a Bruker Quazar SMART APEXII diffractometer with Mo K_α (λ = 0.71073 Å) radiation and the diffractometer to crystal distance of 4.96 cm.[1]

The initial cell constants were obtained from three series of ω scans at different starting angles. Each series consisted of 12 frames collected at intervals of 1º in a 12º range about ω with an exposure time of 2 seconds per frame. The reflections were successfully indexed by an automated indexing routine built in the APEX3 program suite. The final cell constants were calculated from a set of 9358 strong reflections from the actual data collection.

The data were collected by using a full sphere data collection routine to survey reciprocal space to the extent of a full sphere to a resolution of 0.70 Å. A total of 117023 data were harvested by collecting 6 sets of frames with 0.4º scans in ω and φ with an exposure time of 20 sec per frame. These highly redundant datasets were corrected for Lorentz and polarization effects. The absorption correction was based on fitting a function to the empirical transmission surface as sampled by multiple equivalent measurements.[2]

D.3.2 Structure Solution and Refinement

The systematic absences in the diffraction data were consistent for the space groups $P2_1$ and $P2_1/m$. The *E*-statistics strongly suggested the non-centrosymmetric space group $P2_1$ that yielded chemically reasonable and computationally stable results of refinement.[3–8]

A successful solution by intrinsic phasing provided most non-hydrogen atoms from the *E*-map. The remaining non-hydrogen atoms were located with an alternating series of least-squares cycles and difference Fourier maps. Unless otherwise specified, all non-hydrogen atoms were refined with anisotropic displacement coefficients. All hydrogen atoms (except those bound to N atoms) were included in the structure factor calculation at idealized positions and allowed to ride on the neighboring atoms with relative isotropic displacement coefficients.

The absolute structure of the compound was unequivocally established by anomalous dispersion effects.

There is one molecule of pentane and two molecules of ether per Ir complex in the asymmetric unit. One of the molecules of solvent ether was positionally disordered with a major disorder component occupancy of 55.6(7)%. The atoms in both disorder components were refined with atomic displacement parameter constraints.

Several CF_3 groups belonging to the $[C_{32}H_{12}BF_{24}]^-$ anion exhibit positional disorder.

Atoms F11–F13 are disordered over four positions with component occupancy ratios of 54.0(4):25.4(4):14.9(3):5.7(2)%. Atoms F23–F25 are also disordered over four positions with component occupancy ratios of 40.1(4):25.5(4):23.9(4):10.5(3)%. These atoms were refined isotropically with geometric restraints and atomic displacement parameter constraints.

Atoms F14–F16, F26–F28, and F32–F34 are disordered over 2 positions with major disorder component occupancies equal to 64(6)%, 57(3)%, and 68(2)% respectively. These atoms were refined with geometric and atomic displacement parameter restraints.

The final least-squares refinement of 1199 parameters against 24179 data resulted in residuals R (based on F^2 for $I \geq 2\sigma$) and wR (based on F^2 for all data) of 0.0211 and 0.0523, respectively. The final difference Fourier map contains peaks of residual electron density (ca. 1.0 e$^-$/ Å^3) in the vicinity of Ir1. These peaks were in chemically unreasonable positions and were considered noise.

D.3.3 Summary

Crystal Data for $[C_{31}H_{18}F_{10}IrN_6][C_{32}H_{12}BF_{24}] \cdot 2(C_4H_{10}O)(C_5H_{12})$ (M =1940.32 g/mol): monoclinic, space group $P2_1$ (no. 4), a = 15.292(4) Å, b = 15.479(4) Å, c = 17.574(4) Å, β = 106.332(7)°, V = 3992.1(18) Å^3, Z = 2, T = 99.94 K, μ(Mo Kα) = 1.801 mm^{-1}, *Dcalc* = 1.614 g/cm^3, 116505 reflections measured (2.414° ≤ 2Θ ≤ 61.118°), 24179 unique (R_{int} = 0.0308, R_{sigma} = 0.0231) which were used in all calculations. The final R_1 was 0.0211 (I > 2σ(I)) and wR_2 was 0.0523 (all data).

Acknowledgement

The Bruker Quazar APEX2 was purchased by UW–Madison Department of Chemistry with a portion of a generous gift from Paul J. and Margaret M. Bender.

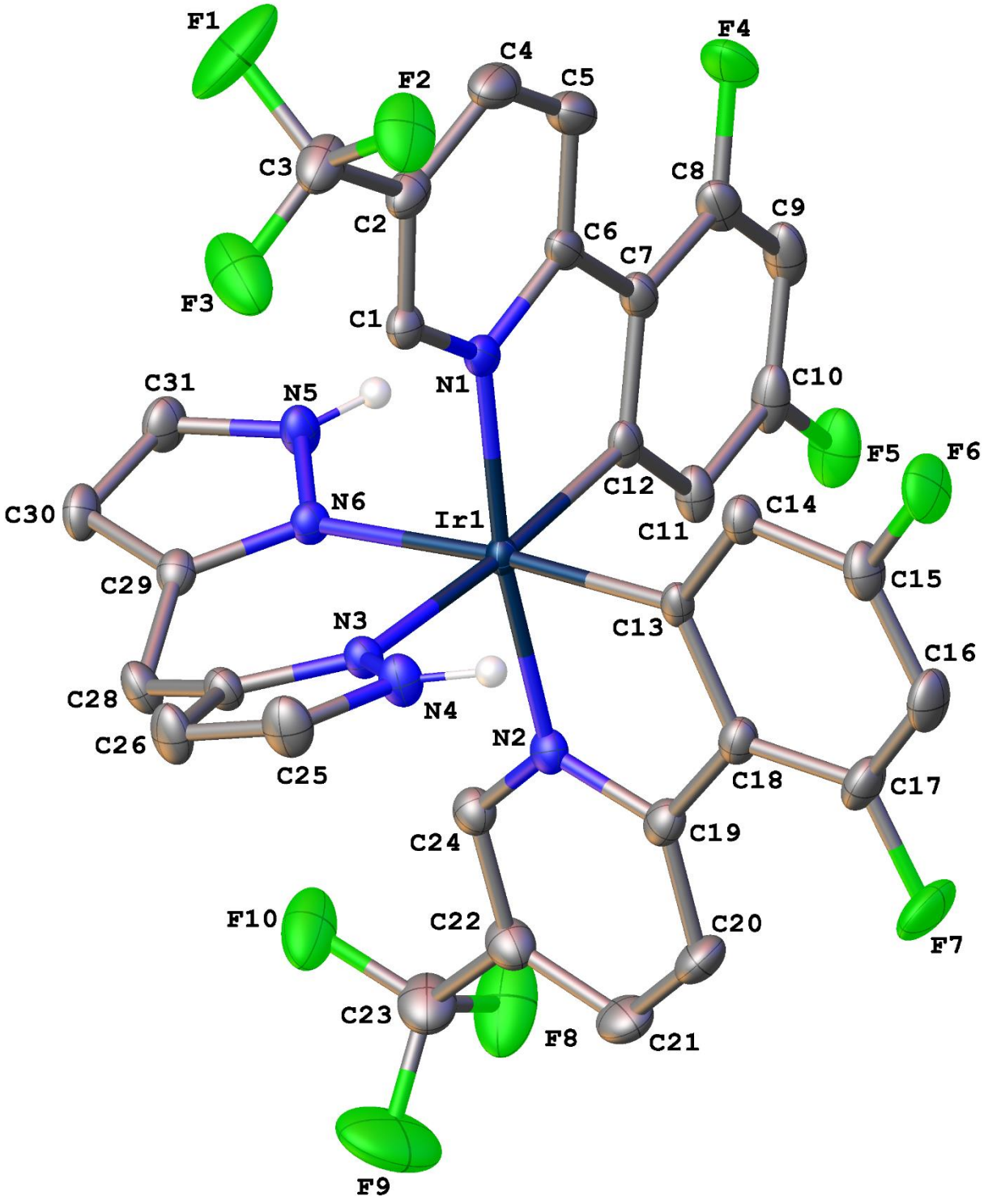

Figure D.6. A molecular drawing of the $C_{31}H_{18}F_{10}IrN_6$ complex in Δ-**4.49f** shown with 50% probability ellipsoids. All H atoms are omitted, except those bound to N atoms.

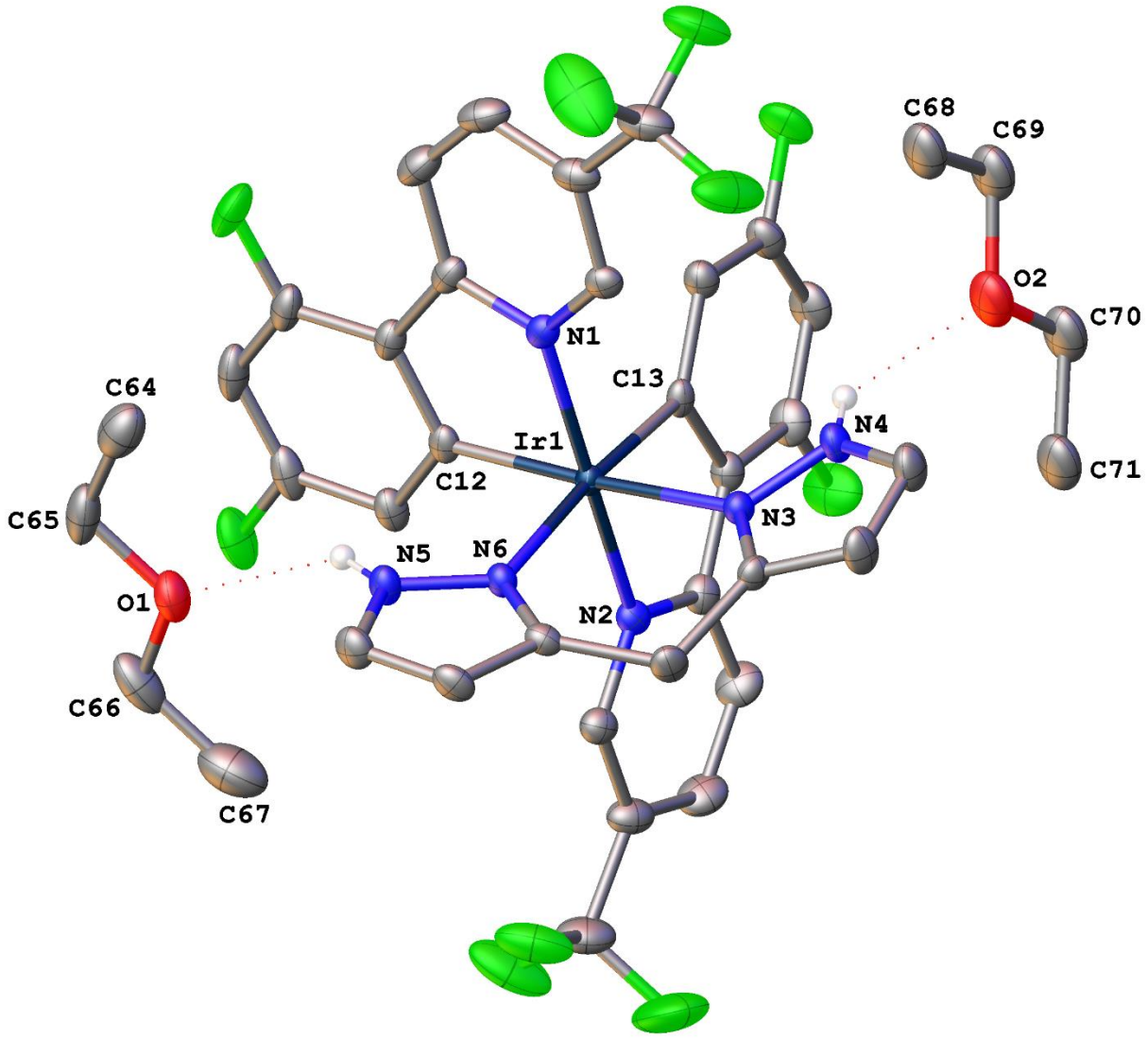

Figure D.7. A molecular drawing highlighting the H-bonding interactions between the Ir complex and the two ether molecules in Δ-**4.49f** shown with 50% probability ellipsoids. All H atoms (except those participating in H-bonding) and minor disorder components are omitted.

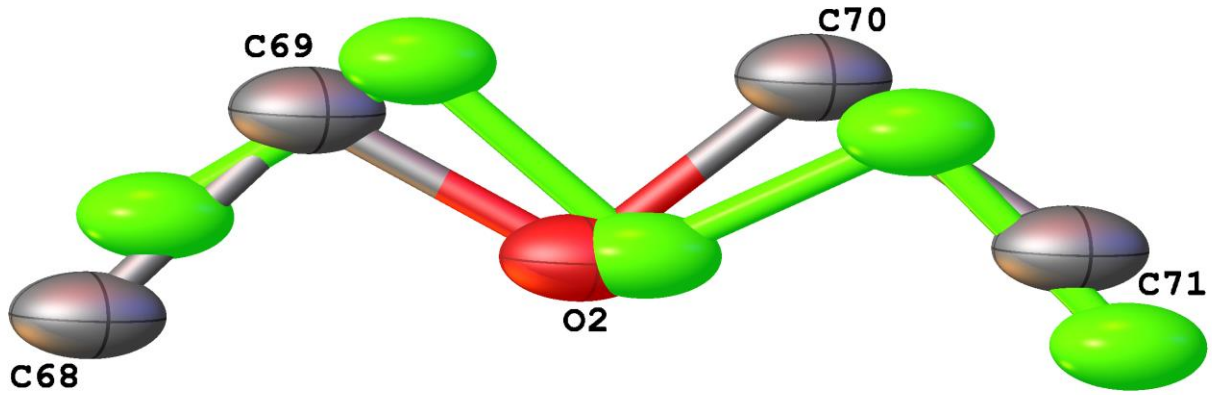

Figure D.8. A molecular drawing of the disordered ether molecule in Δ-**4.49f** shown with 50% probability ellipsoids. All H atoms are omitted, and the minor disorder component is shown in green.

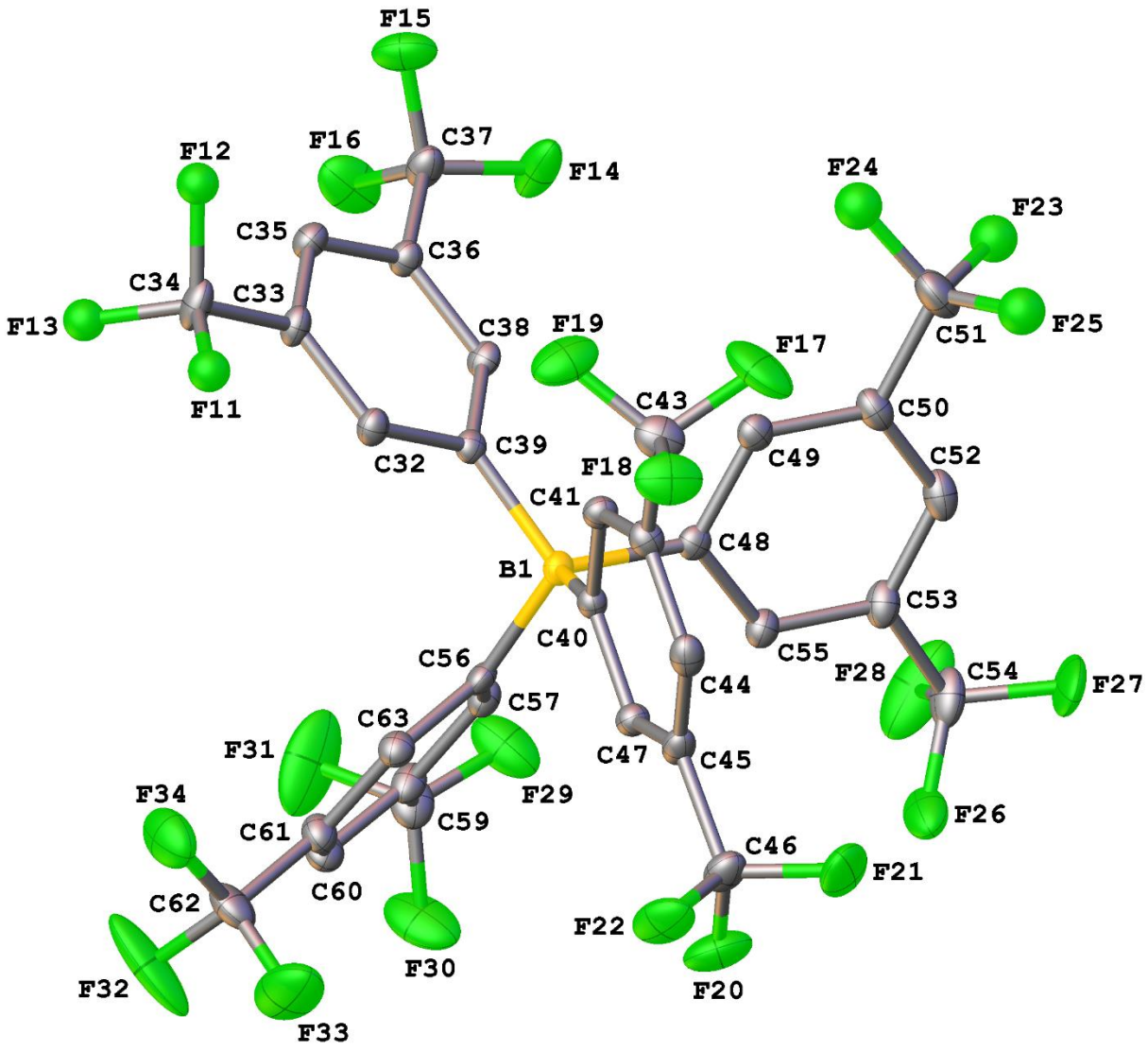

Figure D.9. A molecular drawing of the $[C_{32}H_{12}BF_{24}]^-$ anion in Δ-**4.49f** shown with 50% probability ellipsoids. All H atoms and minor disorder components are omitted. Atoms shown as spheres are refined isotropically.

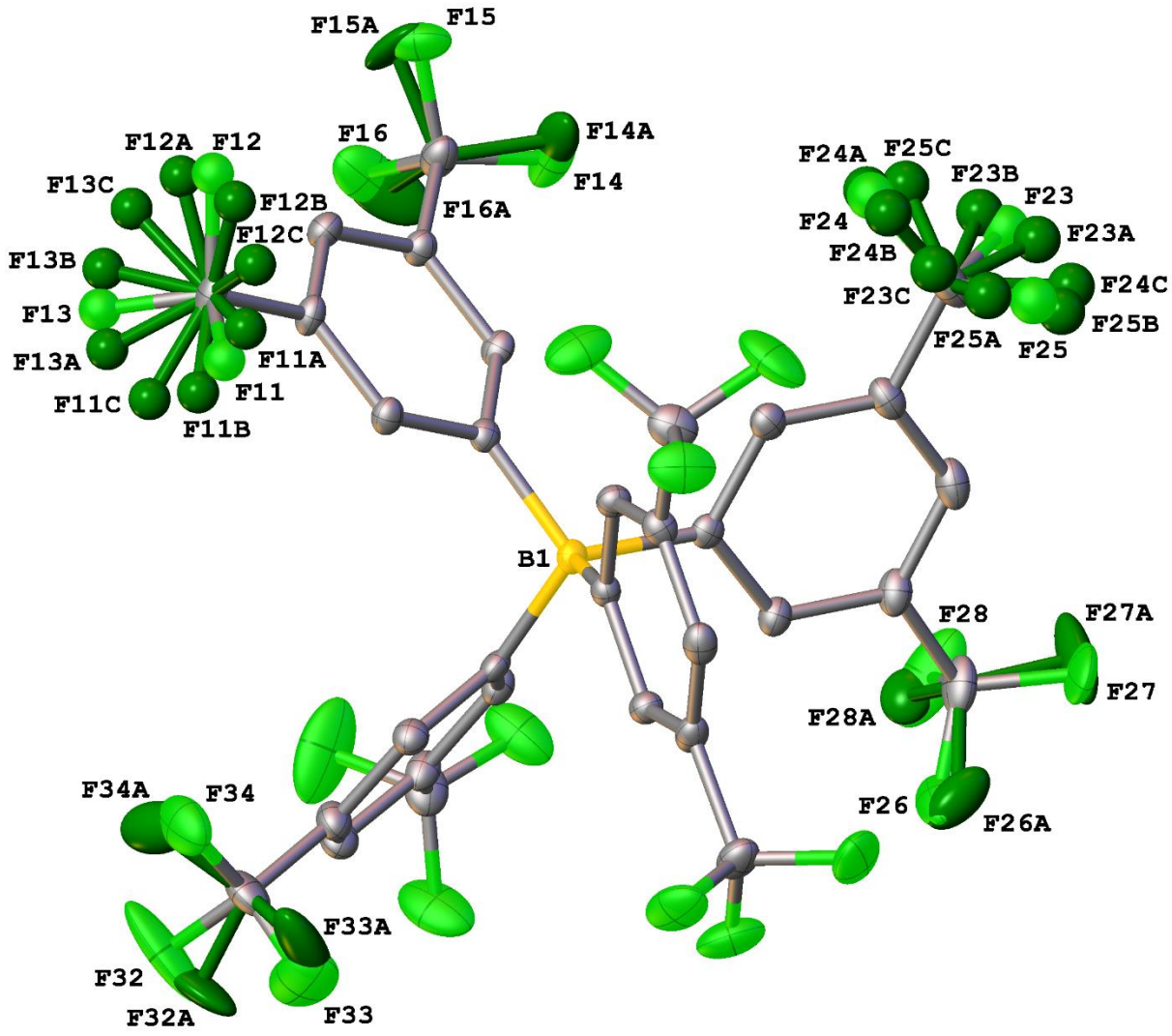

Figure D.10. A molecular drawing of the $[C_{32}H_{12}BF_{24}]^-$ anion with 50% probability ellipsoids and all components of the disordered CF_3 groups shown. All H atoms are omitted, and all minor disorder components are shown in dark green. Atoms represented as spheres are refined isotropically.

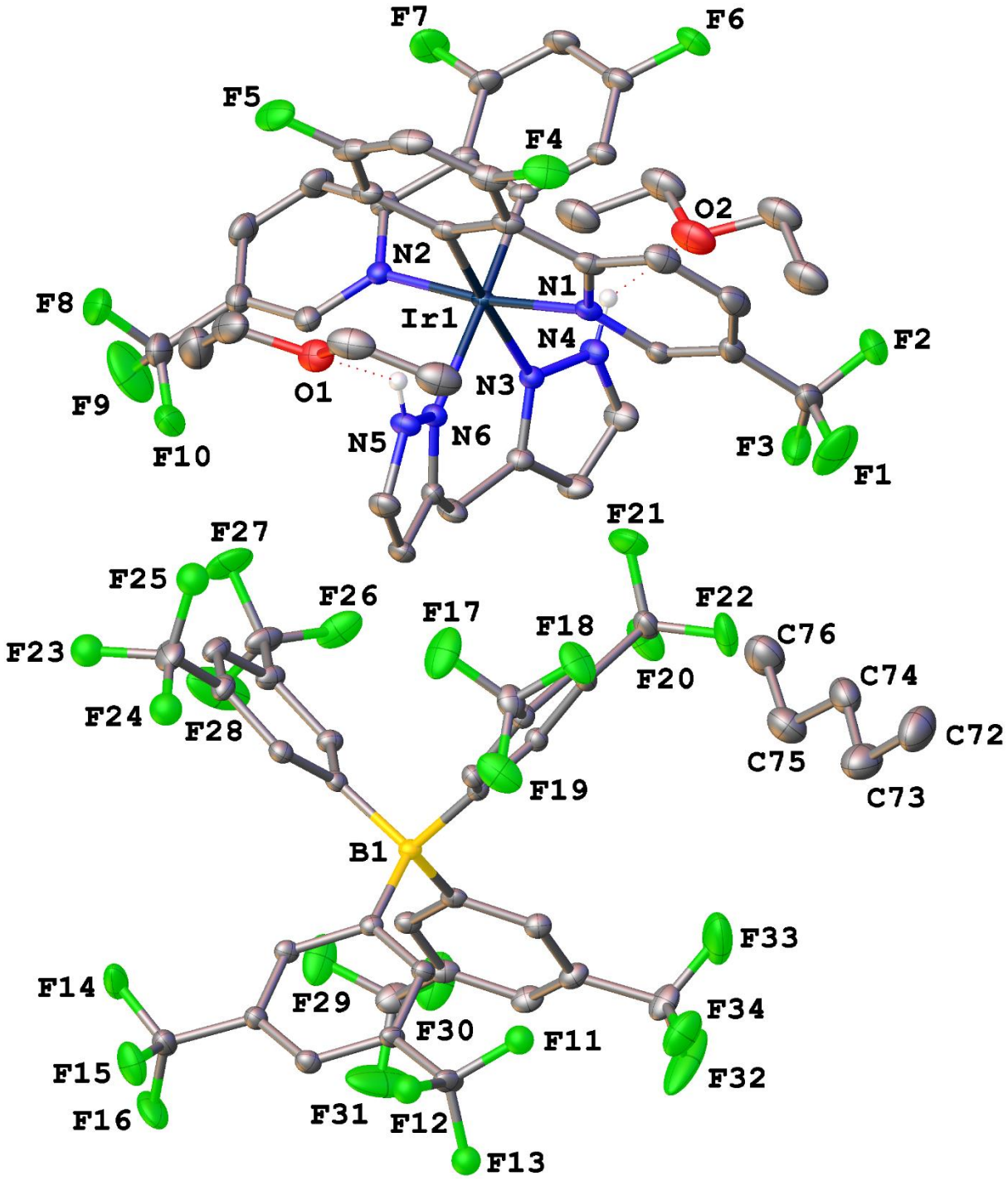

Figure D.11. A molecular drawing of Δ-**4.49f** shown with 50% probability ellipsoids and selected atoms labeled. All H atoms (except those bound to N atoms) and any minor disorder components are omitted. Atoms shown as spheres are refined isotropically.

Table D.16. Crystal data and structure refinement for Δ-**4.49f**.

Identification code	Yoon78
Empirical formula	$[C_{31}H_{18}F_{10}IrN_6][C_{32}H_{12}BF_{24}] \cdot 2(C_4H_{10}O)(C_5H_{12})$
Formula weight	1940.32
Temperature/K	99.94
Crystal system	monoclinic
Space group	$P2_1$
a/Å	15.292(4)
b/Å	15.479(4)
c/Å	17.574(4)
α/°	90
β/°	106.332(7)
γ/°	90
Volume/Å^3	3992.1(18)
Z	2
ρ_{calc}g/cm^3	1.614
μ/mm^{-1}	1.801
F(000)	1928.0
Crystal size/mm^3	0.195 × 0.112 × 0.101
Radiation	Mo Kα (λ = 0.71073)
2Θ range for data collection/°	2.414 to 61.118
Index ranges	$-21 \le h \le 21$, $-21 \le k \le 22$, $-25 \le l \le 25$
Reflections collected	116505
Independent reflections	24179 [R_{int} = 0.0308, R_{sigma} = 0.0231]
Data/restraints/parameters	24179/1013/1199
Goodness-of-fit on F^2	1.022

Final R indexes [I>=2σ (I)]	R_1 = 0.0211, wR_2 = 0.0517
Final R indexes [all data]	R_1 = 0.0225, wR_2 = 0.0523
Largest diff. peak/hole / e Å^{-3}	1.01/-0.72
Flack parameter	-0.0141(13)

Table D.17. Fractional Atomic Coordinates (×10^4) and Equivalent Isotropic Displacement Parameters (Å^2×10^3) for Δ-**4.49f**. U_{eq} is defined as 1/3 of the trace of the orthogonalized U_{IJ} tensor**.**

Atom	***x***	***y***	***z***	**U(eq)**
Ir1	2391.7(2)	6703.9(2)	2387.0(2)	12.71(2)
F1	5633.2(19)	9277(2)	4090.5(19)	67.9(10)
F2	6099.3(15)	8722.4(18)	3165.7(14)	42.9(6)
F3	5756.6(15)	7906.7(19)	4020.8(15)	49.0(7)
F4	1548.9(17)	9827.3(12)	1230.4(13)	35.4(5)
F5	-828.4(13)	7847.8(16)	473.0(12)	35.9(5)
F6	4216.6(13)	6861.6(15)	163.6(11)	32.9(5)
F7	2156.7(17)	4606.4(15)	-16.5(14)	39.7(5)
F8	-1076.7(16)	4492(2)	2120.5(16)	59.2(8)
F9	-170(3)	3530(2)	2762(3)	76.3(11)
F10	-155.0(17)	4803.6(19)	3246.0(15)	47.8(7)
F11	3197(3)	9261(3)	9309(2)	22.6(4)
F12	1965(2)	9378(2)	9668(3)	22.6(4)
F13	3081(3)	8654(2)	10390.9(18)	22.6(4)
F11A	2943(6)	9382(4)	9188(4)	22.6(4)
F12A	2052(4)	9246(5)	9913(5)	22.6(4)
F13A	3321(4)	8608(4)	10287(4)	22.6(4)

Table D.17. Fractional Atomic Coordinates ($\times 10^4$) and Equivalent Isotropic Displacement Parameters ($Å^2 \times 10^3$) for Δ-**4.49f**. U_{eq} is defined as 1/3 of the trace of the orthogonalized U_{IJ} tensor**.**

Atom	***x***	***y***	***z***	**U(eq)**
F11B	3446(6)	9040(8)	9490(7)	22.6(4)
F12B	2127(7)	9514(5)	9435(7)	22.6(4)
F13B	2810(9)	8740(7)	10410(3)	22.6(4)
F11C	3569(4)	8744(11)	9885(13)	22.6(4)
F12C	2506(16)	9529(6)	9191(9)	22.6(4)
F13C	2363(15)	8973(12)	10260(9)	22.6(4)
F14	-178(7)	6039(9)	8422(5)	41.0(19)
F15	-266(6)	7075(4)	9198(9)	34.4(17)
F16	525(5)	5964(7)	9656(6)	38.9(19)
F14A	-282(13)	6220(20)	8366(7)	46(4)
F15A	-167(14)	7032(10)	9370(20)	41(4)
F16A	524(10)	5822(16)	9518(19)	59(5)
F17	1464.3(16)	9493.6(17)	5630.6(18)	45.9(7)
F18	2719.6(15)	10203.3(13)	5836.4(14)	36.0(5)
F19	2159.6(17)	9940.5(13)	6795.5(15)	39.0(5)
F23	-1168(3)	6051(3)	5309(4)	28.6(4)
F24	-634(4)	7204(3)	5920(3)	28.6(4)
F25	-494(4)	6988(4)	4733(3)	28.6(4)
F23A	-1166(4)	6149(4)	5054(5)	28.6(4)
F24A	-703(5)	7053(5)	5999(4)	28.6(4)
F25A	-303(5)	7264(5)	4961(5)	28.6(4)
F23B	-1173(4)	6127(5)	5484(5)	28.6(4)
F24B	-526(5)	7367(4)	5728(5)	28.6(4)

Table D.17. Fractional Atomic Coordinates ($\times 10^4$) and Equivalent Isotropic Displacement Parameters ($Å^2 \times 10^3$) for Δ-**4.49f**. U_{eq} is defined as 1/3 of the trace of the orthogonalized U_{IJ} tensor**.**

Atom	***x***	***y***	***z***	**U(eq)**
F25B	-603(5)	6656(7)	4623(2)	28.6(4)
F23C	-262(8)	7448(4)	5309(9)	28.6(4)
F24C	-900(8)	6323(9)	4700(5)	28.6(4)
F25C	-1000(7)	6587(10)	5886(7)	28.6(4)
F26	2500(3)	4077(7)	5352(7)	38.1(17)
F27	1131(6)	4025(7)	4640(3)	44(2)
F28	1494(12)	3449(4)	5798(7)	72(3)
F26A	2431(6)	4135(8)	5207(10)	42(3)
F27A	1006(9)	3902(9)	4732(7)	76(5)
F28A	1706(8)	3481(5)	5906(6)	32(2)
F29	3212.6(15)	3395.4(13)	8421.3(17)	43.8(6)
F30	4647.5(16)	3213.6(14)	8723.8(19)	50.8(7)
F31	4034(3)	3645.6(18)	9605.2(16)	73.3(11)
F32	6572(5)	5835(5)	9688(6)	81(3)
F33	6457(5)	6400(7)	8558(4)	62.6(19)
F34	5964(4)	7067(3)	9409(5)	43.4(15)
F32A	6679(7)	5731(7)	9429(12)	59(4)
F33A	6303(9)	6692(14)	8541(6)	63(4)
F34A	6025(9)	6896(11)	9643(11)	55(4)
N1	3155.9(16)	7805.5(15)	2572.4(14)	16.4(4)
N2	1597.7(16)	5634.7(16)	2050.8(15)	16.8(4)
N3	3421.7(15)	5929.0(15)	3157.9(14)	15.7(4)
N4	4192(2)	5678(2)	2979.7(19)	20.1(6)

Table D.17. Fractional Atomic Coordinates ($\times 10^4$) and Equivalent Isotropic Displacement Parameters ($Å^2 \times 10^3$) for Δ-**4.49f**. U_{eq} is defined as 1/3 of the trace of the orthogonalized U_{IJ} tensor**.**

Atom	***x***	***y***	***z***	**U(eq)**
N5	1376.0(17)	7604.6(16)	3474.9(15)	19.5(4)
N6	1957.3(15)	6958.7(14)	3421.6(14)	15.8(4)
C1	4025(2)	7852(2)	3033(2)	18.0(6)
C2	4548(2)	8585(2)	3069.3(18)	23.8(6)
C3	5508(2)	8616(2)	3588(2)	30.7(7)
C4	4178(3)	9295(2)	2611(2)	29.5(7)
C5	3287(2)	9263(2)	2150(2)	27.8(6)
C6	2772(2)	8514.0(18)	2135.0(17)	19.4(5)
C7	1826(2)	8373(2)	1680.9(19)	19.7(6)
C8	1245(3)	9008(3)	1244(3)	25.2(8)
C9	356(2)	8848(2)	836.6(19)	29.8(7)
C10	46(2)	8017(2)	867.0(18)	27.0(6)
C11	584.9(19)	7354(2)	1279.8(17)	21.6(5)
C12	1487.1(19)	7523.9(19)	1703.7(17)	17.4(5)
C13	2785.4(18)	6357.1(18)	1434.4(15)	15.7(4)
C14	3423.3(17)	6782(3)	1128.9(15)	19.4(5)
C15	3602(2)	6449(2)	457.9(18)	23.5(6)
C16	3187(2)	5727(2)	62.2(19)	27.7(6)
C17	2572(2)	5313(2)	371.1(18)	25.4(6)
C18	2360.5(19)	5596.3(19)	1054.8(16)	18.9(5)
C19	1707(2)	5193(2)	1410.0(19)	19.8(6)
C20	1210(3)	4435(3)	1165(3)	27.9(8)
C21	581(2)	4160(2)	1535(2)	29.9(7)

Table D.17. Fractional Atomic Coordinates ($\times 10^4$) and Equivalent Isotropic Displacement Parameters ($Å^2 \times 10^3$) for Δ-**4.49f**. U_{eq} is defined as 1/3 of the trace of the orthogonalized U_{IJ} tensor**.**

Atom	***x***	***y***	***z***	**U(eq)**
C22	463(2)	4631(2)	2170.2(19)	25.5(6)
C23	-234(3)	4367(3)	2583(2)	34.7(8)
C24	987.7(19)	5357.9(19)	2418.9(17)	20.0(5)
C25	4782(2)	5305(2)	3607(2)	27.1(6)
C26	4394(2)	5313(2)	4220.3(18)	25.4(6)
C27	3547.6(18)	5712.6(18)	3915.2(16)	17.5(5)
C28	2823(2)	5825(2)	4332.3(18)	21.7(5)
C29	2234.7(16)	6611(2)	4148.9(15)	17.2(5)
C30	1822.4(19)	7033(2)	4661.9(17)	21.4(5)
C31	1276(2)	7651(2)	4210.9(18)	23.6(6)
C32	2618.6(18)	7695.4(17)	8589.8(16)	15.6(5)
C33	2257.6(18)	8018.5(15)	9175.4(15)	16.2(5)
C34	2652.7(18)	8813.5(16)	9633.3(15)	23.2(6)
C35	1509.7(18)	7633.5(17)	9334.7(16)	17.1(5)
C36	1124.4(16)	6920.2(15)	8883.5(15)	15.9(5)
C37	308.0(17)	6499.1(16)	9035.2(15)	22.0(6)
C38	1481.3(16)	6597.2(18)	8293.9(15)	14.8(5)
C39	2236.2(17)	6976.8(16)	8122.6(15)	13.6(4)
C40	3028.6(16)	7356.1(16)	6952.7(15)	13.7(4)
C41	2605.3(17)	8167.2(17)	6815.9(16)	15.1(5)
C42	2805.1(18)	8765.1(18)	6295.0(16)	16.9(5)
C43	2291(2)	9602(2)	6140(2)	24.8(6)
C44	3431.9(18)	8576.9(19)	5886.2(17)	18.9(5)

Table D.17. Fractional Atomic Coordinates ($\times 10^4$) and Equivalent Isotropic Displacement Parameters ($Å^2 \times 10^3$) for Δ-**4.49f**. U_{eq} is defined as 1/3 of the trace of the orthogonalized U_{IJ} tensor**.**

Atom	***x***	***y***	***z***	**U(eq)**
C45	3866.5(17)	7778.5(18)	6017.6(15)	17.7(5)
C46	4531.9(17)	7577.1(17)	5560.1(15)	23.8(6)
F20	4887.4(14)	6781.5(17)	5702.7(13)	39.3(5)
F21	4147.8(15)	7616.1(18)	4773.7(11)	43.9(6)
F22	5229.0(13)	8131.6(14)	5719.1(14)	38.7(5)
C47	3668.0(17)	7186.7(17)	6535.3(16)	15.1(5)
C48	1928.1(17)	6079.2(16)	6750.6(15)	14.0(4)
C49	1073.4(18)	6471.1(17)	6423.9(16)	16.7(5)
C50	428.5(17)	6130.9(18)	5775.3(16)	19.6(5)
C51	-444.4(17)	6608(2)	5424.6(15)	30.6(7)
C52	598(2)	5365.2(19)	5422.4(18)	22.7(6)
C53	1434(2)	4968.4(16)	5731.1(16)	20.5(5)
C54	1639(2)	4127.5(18)	5389.3(17)	28.8(6)
C55	2091.2(19)	5321.9(17)	6377.8(16)	16.8(5)
C56	3539.3(18)	5988.2(17)	7946.6(15)	14.9(4)
C57	3425.9(19)	5122.9(17)	8143.0(16)	16.8(5)
C58	4131(2)	4647.4(17)	8631.7(16)	18.5(5)
C59	3998(2)	3730(2)	8843(2)	27.8(6)
C60	4984(2)	5016.2(19)	8962.8(18)	21.8(5)
C61	5111.3(17)	5866.3(18)	8781.2(17)	20.2(5)
C62	6018(2)	6290(2)	9106.5(19)	27.5(6)
C63	4405.0(18)	6342.0(18)	8281.0(16)	17.3(5)
B1	2689.9(18)	6591(2)	7451.0(16)	13.8(6)

Table D.17. Fractional Atomic Coordinates ($\times 10^4$) and Equivalent Isotropic Displacement Parameters ($Å^2 \times 10^3$) for Δ-**4.49f**. U_{eq} is defined as 1/3 of the trace of the orthogonalized U_{IJ} tensor**.**

Atom	***x***	***y***	***z***	**U(eq)**
O1	-178.9(16)	8544.6(17)	2748.1(16)	29.9(5)
C64	744(3)	9798(2)	3068(2)	39.2(8)
C65	-181(3)	9459(3)	2662(2)	37.1(9)
C66	-1057(2)	8175(3)	2411(2)	41.0(9)
C67	-1017(3)	7233(4)	2575(3)	53.5(12)
O2	5263(7)	5284(5)	1999(6)	40.3(7)
C68	6088(5)	6577(5)	2471(4)	40.3(7)
C69	5944(6)	5907(6)	1861(5)	40.3(7)
C70	5127(6)	4542(6)	1493(5)	40.3(7)
C71	4457(6)	3957(5)	1709(5)	40.3(7)
O2A	5161(9)	5107(7)	1959(8)	40.3(7)
C68A	6063(7)	6369(7)	2179(7)	40.3(7)
C69A	5846(7)	5570(8)	1711(6)	40.3(7)
C70A	4933(8)	4266(7)	1598(6)	40.3(7)
C71A	4250(7)	3844(7)	1904(6)	40.3(7)
C72	7440(3)	8509(3)	6769(3)	51.8(11)
C73	7248(3)	7615(3)	7029(3)	45.0(10)
C74	7211(2)	6933(2)	6404(2)	36.8(9)
C75	6980(3)	6038(3)	6634(3)	41.3(9)
C76	6862(3)	5382(3)	5967(3)	47.6(10)

Table D.18. Anisotropic Displacement Parameters ($Å^2 \times 10^3$) for Δ-**4.49f**. The Anisotropic displacement factor exponent takes the form: $-2\pi^2[h^2a^{*2}U_{11}+2hka^*b^*U_{12}+\ldots]$.

Atom	**U_{11}**	**U_{22}**	**U_{33}**	**U_{23}**	**U_{13}**	**U_{12}**
Ir1	14.54(4)	13.88(4)	10.07(4)	0.36(5)	4.05(2)	1.86(5)
F1	46.9(15)	88(2)	61.1(19)	-54.5(17)	2.5(13)	-11.7(15)
F2	31.9(11)	65.0(16)	36.1(12)	1.6(11)	16.7(9)	-16.8(10)
F3	28.5(11)	69.0(17)	42.6(14)	19.6(12)	-1.4(9)	-17.0(11)
F4	56.7(13)	17.7(9)	32.5(11)	7.3(8)	13.7(10)	12.1(9)
F5	23.9(9)	54.2(13)	25.4(10)	0.5(9)	-0.2(8)	16.6(9)
F6	34.7(9)	46.8(16)	24.4(8)	-0.8(8)	20.2(7)	-3.3(9)
F7	54.0(14)	38.2(12)	31.5(11)	-22.4(9)	19.3(10)	-13.1(10)
F8	25.6(11)	114(3)	36.5(13)	-7.1(15)	6.5(10)	-23.6(13)
F9	95(3)	45.2(17)	108(3)	14.9(18)	60(2)	-21.2(17)
F10	44.4(13)	73.6(18)	28.9(12)	-5.7(11)	16.1(10)	-30.1(12)
F14	36(3)	59(4)	35(3)	-25(2)	22(2)	-30(3)
F15	28(2)	29(3)	54(4)	0(3)	24(3)	0(2)
F16	34(3)	45(3)	41(4)	22(2)	15(2)	-6(2)
F14A	23(5)	78(10)	38(5)	-30(5)	11(4)	-24(5)
F15A	39(6)	52(7)	47(8)	-29(5)	36(6)	-20(4)
F16A	37(6)	37(6)	102(12)	32(7)	15(6)	-13(4)
F17	25.4(11)	32.1(13)	67.8(19)	10.6(12)	-7.3(11)	7.1(9)
F18	41.5(11)	22.1(9)	50.4(13)	17.1(9)	22.9(10)	4.1(8)
F19	56.0(14)	22.4(10)	47.3(13)	6.9(9)	28.7(11)	13.1(9)
F26	41(2)	30(4)	35(4)	-14(3)	-3(2)	14(2)
F27	52(3)	49(4)	24(2)	-23(2)	-1(2)	4(3)
F28	151(10)	22(3)	57(4)	-8(2)	52(5)	-26(4)

Table D.18. Anisotropic Displacement Parameters ($Å^2 \times 10^3$) for Δ-**4.49f**. The Anisotropic displacement factor exponent takes the form: $-2\pi^2[h^2a^{*2}U_{11}+2hka^*b^*U_{12}+\ldots]$.

Atom	**U_{11}**	**U_{22}**	**U_{33}**	**U_{23}**	**U_{13}**	**U_{12}**
F26A	76(5)	24(4)	40(5)	3(3)	35(5)	2(4)
F27A	87(7)	41(5)	59(5)	-28(4)	-47(6)	20(5)
F28A	44(5)	14(3)	36(4)	1(2)	10(3)	0(2)
F29	33.2(11)	20.6(10)	68.6(17)	12.7(10)	-0.1(11)	-2.6(8)
F30	37.9(12)	17.8(10)	89(2)	0.1(11)	4.8(12)	8.9(9)
F31	155(3)	32.9(13)	32.3(14)	11.8(11)	27.2(18)	-15.2(17)
F32	47(3)	48(3)	106(5)	45(3)	-48(3)	-18(2)
F33	35(3)	88(4)	74(3)	-31(3)	30(3)	-23(3)
F34	36(2)	33(2)	52(3)	-14(2)	-4(2)	-3.0(18)
F32A	20(4)	37(5)	99(9)	-2(5)	-16(5)	14(3)
F33A	22(4)	118(11)	42(5)	23(6)	-3(3)	-19(7)
F34A	38(5)	47(7)	84(8)	-31(6)	22(6)	-11(4)
N1	22.0(10)	16.2(10)	12.9(10)	-0.7(8)	8.0(8)	1.1(8)
N2	16.2(10)	19.4(11)	13.8(11)	1.5(9)	2.6(8)	1.0(8)
N3	16.3(10)	16.3(10)	15.0(10)	1.0(8)	5.2(8)	2.0(8)
N4	17.9(12)	24.4(13)	19.0(13)	3.1(10)	6.7(10)	6.6(10)
N5	22.2(11)	22.5(12)	15.8(11)	1.7(9)	8.4(9)	6.5(9)
N6	16.6(9)	17.1(10)	15.0(10)	-0.2(7)	6.4(8)	2.4(7)
C1	22.1(14)	20.1(14)	14.1(13)	-0.8(10)	8.5(11)	-1.5(11)
C2	26.8(14)	28.0(15)	19.4(13)	-5.8(11)	11.2(11)	-8.4(11)
C3	31.9(16)	38.3(18)	24.5(15)	-7.2(13)	12.3(13)	-14.8(14)
C4	42.4(18)	23.3(15)	27.5(16)	-4.1(12)	17.6(14)	-11.7(13)
C5	43.0(18)	17.9(13)	25.6(15)	0.5(11)	14.8(14)	-0.7(12)

Table D.18. Anisotropic Displacement Parameters ($Å^2 \times 10^3$) for Δ-**4.49f**. The Anisotropic displacement factor exponent takes the form: $-2\pi^2[h^2a^{*2}U_{11}+2hka^*b^*U_{12}+\ldots]$.

Atom	U_{11}	U_{22}	U_{33}	U_{23}	U_{13}	U_{12}
C6	30.1(14)	15.7(12)	15.3(12)	-0.1(9)	11.0(10)	2.6(10)
C7	26.7(14)	18.8(14)	14.7(14)	1.6(11)	7.8(11)	6.7(11)
C8	37(2)	20.9(17)	21.0(18)	2.6(14)	12.7(14)	11.8(15)
C9	38.9(17)	32.1(16)	18.4(14)	4.7(12)	8.0(12)	20.8(14)
C10	24.4(14)	41.4(18)	14.3(13)	-0.7(12)	4.2(11)	15.1(13)
C11	21.2(12)	29.0(14)	15.0(12)	2.2(10)	5.9(10)	7.4(11)
C12	21.3(12)	20.6(13)	12.1(12)	0.2(10)	7.6(10)	5.7(10)
C13	19.2(11)	16.9(11)	10.9(11)	1.3(9)	4.0(9)	6.4(9)
C14	22.1(10)	22.2(15)	15.1(10)	0.6(13)	6.9(8)	3.1(13)
C15	23.6(12)	32.1(15)	17.2(13)	2.1(10)	9.5(10)	4.9(10)
C16	32.7(15)	36.1(17)	17.3(14)	-4.7(12)	11.8(12)	5.9(13)
C17	30.5(15)	27.0(15)	18.1(14)	-8.2(11)	5.9(11)	1.8(12)
C18	21.3(12)	20.3(13)	14.7(12)	-1.2(9)	4.5(10)	3.4(10)
C19	20.0(13)	21.1(14)	16.3(14)	-1.8(11)	1.7(11)	1.3(10)
C20	35(2)	24.1(18)	23.2(19)	-9.4(15)	5.2(15)	-5.9(15)
C21	30.4(15)	25.4(15)	29.7(17)	-4.5(12)	1.7(13)	-10.1(12)
C22	22.2(13)	28.3(15)	24.2(15)	3.3(12)	3.5(11)	-6.2(11)
C23	30.9(17)	40(2)	32.5(19)	-0.6(17)	8.2(14)	-16.1(17)
C24	19.2(12)	21.9(13)	17.9(13)	1.3(10)	3.7(10)	-0.1(10)
C25	24.3(14)	31.8(16)	25.3(15)	5.2(12)	7.0(12)	11.9(12)
C26	25.8(14)	31.6(16)	17.7(13)	7.3(11)	4.3(11)	11.9(12)
C27	20.1(12)	16.7(12)	15.7(12)	3.0(9)	4.8(9)	2.8(9)
C28	24.4(13)	24.9(14)	17.7(13)	7.7(10)	8.8(10)	4.4(11)

Table D.18. Anisotropic Displacement Parameters ($Å^2 \times 10^3$) for Δ-**4.49f**. The Anisotropic displacement factor exponent takes the form: $-2\pi^2[h^2a^{*2}U_{11}+2hka^*b^*U_{12}+\ldots]$.

Atom	U_{11}	U_{22}	U_{33}	U_{23}	U_{13}	U_{12}
C29	15.1(9)	22.0(16)	14.8(10)	-0.9(11)	4.9(8)	-2.2(11)
C30	21.2(12)	31.1(13)	14.3(12)	-0.4(10)	8.8(10)	-0.7(10)
C31	26.6(14)	28.3(15)	19.0(14)	-2.4(11)	11.4(11)	3.9(11)
C32	18.2(11)	15.9(11)	13.1(11)	-0.3(9)	4.9(9)	-2.5(9)
C33	21.6(12)	14.7(11)	12.3(11)	-2.2(9)	5.1(9)	-3.7(9)
C34	33.4(15)	22.1(13)	15.2(13)	-6.1(10)	8.6(11)	-9.3(11)
C35	20.3(11)	16.7(12)	15.6(12)	-1.6(9)	7.1(9)	0.1(9)
C36	17.4(10)	16.0(13)	15.1(11)	-1.1(8)	5.8(9)	-2.2(7)
C37	22.3(12)	26.0(16)	19.7(12)	-4.3(9)	9.0(10)	-6.9(9)
C38	19.1(9)	10.8(15)	14.8(10)	-1.5(9)	5.3(8)	-0.9(9)
C39	15.5(10)	12.6(10)	12.2(11)	1.2(8)	2.8(8)	1.0(8)
C40	13.3(10)	14.8(11)	12.3(11)	-0.3(9)	2.4(8)	-0.9(8)
C41	14.8(11)	16.1(11)	15.4(12)	0.4(9)	5.8(9)	-0.4(9)
C42	16.5(11)	16.7(12)	16.7(12)	2.0(9)	3.4(9)	-1.1(9)
C43	24.8(14)	18.8(13)	31.6(16)	6.5(11)	9.1(12)	-0.2(11)
C44	18.5(11)	22.3(13)	15.8(12)	0.5(10)	4.5(9)	-6.1(10)
C45	16.1(11)	23.5(13)	14.8(12)	-2.6(10)	6.5(9)	-4.5(9)
C46	23.6(13)	28.4(15)	23.1(14)	-4.6(11)	12.8(11)	-5.3(11)
F20	42.7(9)	34.1(11)	53.5(11)	-1.0(13)	34.1(9)	5.7(12)
F21	41.0(12)	74.7(17)	22.0(10)	-5.9(10)	18.5(9)	-2.1(11)
F22	28.1(10)	42.5(12)	54.0(14)	-13.6(10)	25.8(10)	-15.0(9)
C47	14.9(10)	15.5(12)	15.5(12)	-0.9(9)	5.1(9)	-0.3(8)
C48	16.5(11)	13.4(11)	13.2(11)	1.7(8)	5.7(9)	-1.4(8)

Table D.18. Anisotropic Displacement Parameters ($Å^2 \times 10^3$) for Δ-**4.49f**. The Anisotropic displacement factor exponent takes the form: $-2\pi^2[h^2a^{*2}U_{11}+2hka^*b^*U_{12}+\ldots]$.

Atom	U_{11}	U_{22}	U_{33}	U_{23}	U_{13}	U_{12}
C49	18.0(11)	17.6(12)	15.4(11)	2.4(8)	6.0(9)	-0.7(8)
C50	16.4(11)	20.8(12)	19.1(13)	3.7(10)	0.8(10)	-2.3(9)
C51	19.4(11)	41(2)	27.2(13)	6.8(16)	-0.9(9)	0.7(15)
C52	25.6(13)	21.5(13)	17.2(13)	1.8(10)	-0.2(10)	-6.7(11)
C53	27.5(13)	15.4(12)	16.5(12)	-0.8(9)	2.9(10)	-4.0(10)
C54	44.1(16)	17.6(14)	19.5(14)	-4.3(10)	0.6(12)	-6.0(13)
C55	20.8(12)	15.1(11)	14.5(12)	-0.4(9)	4.7(10)	-1.0(9)
C56	19.3(11)	15.2(11)	11.3(11)	-1.9(8)	6.1(9)	2.4(9)
C57	21.7(12)	15.2(12)	13.6(11)	-0.7(9)	5.4(9)	0.2(9)
C58	26.5(13)	13.4(11)	15.1(12)	0.5(9)	4.7(10)	4.2(10)
C59	36.3(16)	17.6(13)	25.5(15)	3.6(11)	2.3(12)	3.5(12)
C60	23.2(13)	19.6(13)	19.9(13)	1.8(10)	1.7(10)	7.0(10)
C61	20.3(12)	19.5(12)	18.1(13)	-0.7(10)	0.9(10)	3.3(10)
C62	19.5(14)	22.6(14)	33.1(18)	3.2(12)	-4.5(11)	3.9(11)
C63	19.8(12)	14.9(11)	17.1(12)	0.0(9)	4.8(10)	2.1(9)
B1	15.4(9)	13.9(18)	11.8(10)	0.9(10)	3.3(8)	-0.1(10)
O1	26.3(11)	34.8(13)	28.6(13)	1.7(10)	7.8(9)	11.3(10)
C64	59(2)	29.3(18)	33.1(19)	0.8(14)	18.5(17)	7.6(16)
C65	51(2)	34(2)	28.8(19)	5.6(16)	15.6(16)	23.3(19)
C66	22.7(15)	72(3)	27.8(18)	-3.2(18)	5.9(13)	9.0(16)
C67	41(2)	74(3)	50(3)	-12(2)	19(2)	-16(2)
O2	46.8(14)	46.8(19)	35.6(12)	3.7(12)	25.1(11)	15.6(13)
C68	46.8(14)	46.8(19)	35.6(12)	3.7(12)	25.1(11)	15.6(13)

Table D.18. Anisotropic Displacement Parameters ($Å^2 \times 10^3$) for Δ-**4.49f**. The Anisotropic displacement factor exponent takes the form: $-2\pi^2[h^2a^{*2}U_{11}+2hka^*b^*U_{12}+\ldots]$.

Atom	U_{11}	U_{22}	U_{33}	U_{23}	U_{13}	U_{12}
C69	46.8(14)	46.8(19)	35.6(12)	3.7(12)	25.1(11)	15.6(13)
C70	46.8(14)	46.8(19)	35.6(12)	3.7(12)	25.1(11)	15.6(13)
C71	46.8(14)	46.8(19)	35.6(12)	3.7(12)	25.1(11)	15.6(13)
O2A	46.8(14)	46.8(19)	35.6(12)	3.7(12)	25.1(11)	15.6(13)
C68A	46.8(14)	46.8(19)	35.6(12)	3.7(12)	25.1(11)	15.6(13)
C69A	46.8(14)	46.8(19)	35.6(12)	3.7(12)	25.1(11)	15.6(13)
C70A	46.8(14)	46.8(19)	35.6(12)	3.7(12)	25.1(11)	15.6(13)
C71A	46.8(14)	46.8(19)	35.6(12)	3.7(12)	25.1(11)	15.6(13)
C72	47(2)	45(2)	55(3)	6(2)	0(2)	-15.4(19)
C73	50(2)	45(2)	35(2)	4.7(18)	5.2(18)	-5.5(19)
C74	28.9(15)	46(2)	37.2(18)	6.6(14)	12.4(14)	-2.7(13)
C75	46(2)	45(2)	38(2)	3.6(18)	20.6(18)	-0.5(18)
C76	50(2)	52(3)	47(2)	-7(2)	24(2)	-4.2(19)

Table D.19. Bond Lengths for Δ-**4.49f**.

Atom	Atom	Length/Å	Atom	Atom	Length/Å
Ir1	N1	2.041(2)	C7	C8	1.401(5)
Ir1	N2	2.039(2)	C7	C12	1.418(4)
Ir1	N3	2.134(2)	C8	C9	1.369(6)
Ir1	N6	2.141(2)	C9	C10	1.377(5)
Ir1	C12	2.008(3)	C10	C11	1.387(4)
Ir1	C13	2.005(3)	C11	C12	1.396(4)
F1	C3	1.330(4)	C13	C14	1.402(4)
F2	C3	1.331(4)	C13	C18	1.418(4)

Table D.19. Bond Lengths for Δ-**4.49f**.

Atom	Atom	Length/Å	Atom	Atom	Length/Å
F3	C3	1.330(5)	C14	C15	1.383(4)
F4	C8	1.352(5)	C15	C16	1.374(5)
F5	C10	1.347(4)	C16	C17	1.370(5)
F6	C15	1.353(3)	C17	C18	1.400(4)
F7	C17	1.349(4)	C18	C19	1.459(4)
F8	C23	1.330(5)	C19	C20	1.399(5)
F9	C23	1.330(5)	C20	C21	1.371(5)
F10	C23	1.324(5)	C21	C22	1.388(5)
F11	C34	1.328(3)	C22	C23	1.503(5)
F12	C34	1.381(4)	C22	C24	1.380(4)
F13	C34	1.331(4)	C25	C26	1.368(4)
F11A	C34	1.333(4)	C26	C27	1.398(4)
F12A	C34	1.337(4)	C27	C28	1.500(4)
F13A	C34	1.343(4)	C28	C29	1.494(4)
F11B	C34	1.353(5)	C29	C30	1.399(4)
F12B	C34	1.336(5)	C30	C31	1.367(4)
F13B	C34	1.323(5)	C32	C33	1.391(4)
F11C	C34	1.350(5)	C32	C39	1.408(4)
F12C	C34	1.336(5)	C33	C34	1.501(3)
F13C	C34	1.321(5)	C33	C35	1.386(4)
F14	C37	1.331(4)	C35	C36	1.390(4)
F15	C37	1.337(4)	C36	C37	1.497(3)
F16	C37	1.335(4)	C36	C38	1.393(3)
F14A	C37	1.336(5)	C38	C39	1.401(3)

Table D.19. Bond Lengths for Δ-**4.49f**.

Atom	Atom	Length/Å	Atom	Atom	Length/Å
F15A	C37	1.336(5)	C39	B1	1.641(4)
F16A	C37	1.330(5)	C40	C41	1.402(4)
F17	C43	1.338(4)	C40	C47	1.402(3)
F18	C43	1.334(3)	C40	B1	1.641(4)
F19	C43	1.331(4)	C41	C42	1.395(4)
F23	C51	1.372(4)	C42	C43	1.500(4)
F24	C51	1.354(4)	C42	C44	1.381(4)
F25	C51	1.334(4)	C44	C45	1.392(4)
F23A	C51	1.320(4)	C45	C46	1.496(3)
F24A	C51	1.369(4)	C45	C47	1.384(4)
F25A	C51	1.357(4)	C46	F20	1.341(3)
F23B	C51	1.368(4)	C46	F21	1.343(3)
F24B	C51	1.310(4)	C46	F22	1.335(3)
F25B	C51	1.362(4)	C48	C49	1.409(4)
F23C	C51	1.358(5)	C48	C55	1.399(4)
F24C	C51	1.343(5)	C48	B1	1.641(4)
F25C	C51	1.330(5)	C49	C50	1.384(4)
F26	C54	1.338(4)	C50	C51	1.498(3)
F27	C54	1.337(4)	C50	C52	1.395(4)
F28	C54	1.325(4)	C52	C53	1.384(4)
F26A	C54	1.337(5)	C53	C54	1.503(3)
F27A	C54	1.329(5)	C53	C55	1.400(4)
F28A	C54	1.337(5)	C56	C57	1.406(4)
F29	C59	1.326(4)	C56	C63	1.400(4)

Table D.19. Bond Lengths for Δ-**4.49f**.

Atom	Atom	Length/Å	Atom	Atom	Length/Å
F30	C59	1.337(4)	C56	B1	1.637(4)
F31	C59	1.332(4)	C57	C58	1.386(4)
F32	C62	1.330(4)	C58	C59	1.496(4)
F33	C62	1.330(4)	C58	C60	1.393(4)
F34	C62	1.327(4)	C60	C61	1.381(4)
F32A	C62	1.330(5)	C61	C62	1.495(3)
F33A	C62	1.344(5)	C61	C63	1.396(4)
F34A	C62	1.328(5)	O1	C65	1.423(5)
N1	C1	1.349(4)	O1	C66	1.426(5)
N1	C6	1.373(4)	C64	C65	1.490(6)
N2	C19	1.367(4)	C66	C67	1.485(7)
N2	C24	1.346(4)	O2	C69	1.488(11)
N3	N4	1.358(3)	O2	C70	1.432(11)
N3	C27	1.333(3)	C68	C69	1.463(11)
N4	C25	1.343(4)	C70	C71	1.494(11)
N5	N6	1.358(3)	O2A	C69A	1.434(14)
N5	C31	1.346(4)	O2A	C70A	1.447(14)
N6	C29	1.341(4)	C68A	C69A	1.470(15)
C1	C2	1.380(4)	C70A	C71A	1.457(13)
C2	C3	1.494(5)	C72	C73	1.512(6)
C2	C4	1.386(5)	C73	C74	1.512(6)
C4	C5	1.377(5)	C74	C75	1.512(6)
C5	C6	1.398(4)	C75	C76	1.522(6)
C6	C7	1.459(4)			

Table D.20. Bond Angles for Δ-**4.49f**.

Atom	Atom	Atom	Angle/°	Atom	Atom	Atom	Angle/°
N1	Ir1	N3	94.65(9)	F15	C37	C36	112.2(4)
N1	Ir1	N6	90.63(9)	F16	C37	F15	105.5(4)
N2	Ir1	N1	172.68(10)	F16	C37	C36	112.8(4)
N2	Ir1	N3	90.04(10)	F14A	C37	F15A	105.5(7)
N2	Ir1	N6	95.39(9)	F14A	C37	C36	112.0(6)
N3	Ir1	N6	85.08(9)	F15A	C37	C36	113.0(6)
C12	Ir1	N1	80.48(11)	F16A	C37	F14A	107.0(7)
C12	Ir1	N2	94.93(12)	F16A	C37	F15A	106.1(7)
C12	Ir1	N3	174.98(11)	F16A	C37	C36	112.7(6)
C12	Ir1	N6	93.75(10)	C36	C38	C39	121.9(2)
C13	Ir1	N1	93.68(10)	C32	C39	B1	121.1(2)
C13	Ir1	N2	80.50(11)	C38	C39	C32	116.0(2)
C13	Ir1	N3	92.19(10)	C38	C39	B1	122.9(2)
C13	Ir1	N6	175.08(10)	C41	C40	C47	115.7(2)
C13	Ir1	C12	89.31(11)	C41	C40	B1	122.5(2)
C1	N1	Ir1	124.3(2)	C47	C40	B1	121.0(2)
C1	N1	C6	119.2(3)	C42	C41	C40	122.1(2)
C6	N1	Ir1	116.28(19)	C41	C42	C43	119.4(2)
C19	N2	Ir1	116.3(2)	C44	C42	C41	120.9(3)
C24	N2	Ir1	123.8(2)	C44	C42	C43	119.5(3)
C24	N2	C19	119.9(3)	F17	C43	C42	111.2(3)
N4	N3	Ir1	123.20(19)	F18	C43	F17	107.3(3)
C27	N3	Ir1	130.44(18)	F18	C43	C42	112.6(3)

Table D.20. Bond Angles for Δ-**4.49f**.

Atom	Atom	Atom	Angle/°	Atom	Atom	Atom	Angle/°
C27	N3	N4	105.5(2)	F19	C43	F17	106.5(3)
C25	N4	N3	111.1(3)	F19	C43	F18	106.4(3)
C31	N5	N6	111.1(2)	F19	C43	C42	112.4(3)
N5	N6	Ir1	124.02(18)	C42	C44	C45	118.0(2)
C29	N6	Ir1	130.18(19)	C44	C45	C46	117.5(2)
C29	N6	N5	105.5(2)	C47	C45	C44	121.0(2)
N1	C1	C2	122.1(3)	C47	C45	C46	121.6(2)
C1	C2	C3	120.8(3)	F20	C46	C45	113.1(2)
C1	C2	C4	119.2(3)	F20	C46	F21	105.7(2)
C4	C2	C3	119.9(3)	F21	C46	C45	112.1(2)
F1	C3	F2	106.3(3)	F22	C46	C45	112.2(2)
F1	C3	C2	111.3(3)	F22	C46	F20	107.1(2)
F2	C3	C2	111.7(3)	F22	C46	F21	106.2(2)
F3	C3	F1	106.9(3)	C45	C47	C40	122.3(2)
F3	C3	F2	106.9(3)	C49	C48	B1	118.6(2)
F3	C3	C2	113.3(3)	C55	C48	C49	115.9(2)
C5	C4	C2	119.3(3)	C55	C48	B1	125.0(2)
C4	C5	C6	119.9(3)	C50	C49	C48	122.4(2)
N1	C6	C5	120.2(3)	C49	C50	C51	119.8(2)
N1	C6	C7	112.9(2)	C49	C50	C52	120.7(2)
C5	C6	C7	126.9(3)	C52	C50	C51	119.4(2)
C8	C7	C6	125.0(3)	F23	C51	C50	109.8(3)
C8	C7	C12	119.1(3)	F24	C51	F23	102.4(3)
C12	C7	C6	115.9(3)	F24	C51	C50	113.5(3)

Table D.20. Bond Angles for Δ-**4.49f**.

Atom	Atom	Atom	Angle/°	Atom	Atom	Atom	Angle/°
F4	C8	C7	120.0(4)	F25	C51	F23	107.8(3)
F4	C8	C9	117.2(3)	F25	C51	F24	108.6(4)
C9	C8	C7	122.8(4)	F25	C51	C50	114.0(3)
C8	C9	C10	116.9(3)	F23A	C51	F24A	105.0(4)
F5	C10	C9	117.7(3)	F23A	C51	F25A	111.0(5)
F5	C10	C11	118.9(3)	F23A	C51	C50	117.5(4)
C9	C10	C11	123.4(3)	F24A	C51	C50	110.7(4)
C10	C11	C12	119.5(3)	F25A	C51	F24A	101.2(4)
C7	C12	Ir1	114.0(2)	F25A	C51	C50	110.0(3)
C11	C12	Ir1	127.7(2)	F23B	C51	C50	110.5(4)
C11	C12	C7	118.3(3)	F24B	C51	F23B	106.5(5)
C14	C13	Ir1	126.8(2)	F24B	C51	F25B	111.2(5)
C14	C13	C18	119.0(3)	F24B	C51	C50	116.8(4)
C18	C13	Ir1	114.2(2)	F25B	C51	F23B	101.3(4)
C15	C14	C13	118.5(3)	F25B	C51	C50	109.4(4)
F6	C15	C14	118.4(3)	F23C	C51	C50	109.7(5)
F6	C15	C16	117.5(3)	F24C	C51	F23C	104.3(6)
C16	C15	C14	124.1(3)	F24C	C51	C50	113.1(5)
C17	C16	C15	116.8(3)	F25C	C51	F23C	108.0(6)
F7	C17	C16	117.2(3)	F25C	C51	F24C	108.7(6)
F7	C17	C18	119.9(3)	F25C	C51	C50	112.7(5)
C16	C17	C18	122.9(3)	C53	C52	C50	118.0(3)
C13	C18	C19	115.6(2)	C52	C53	C54	120.1(3)
C17	C18	C13	118.6(3)	C52	C53	C55	121.2(2)

Table D.20. Bond Angles for Δ-**4.49f**.

Atom	Atom	Atom	Angle/°	Atom	Atom	Atom	Angle/°
C17	C18	C19	125.8(3)	C55	C53	C54	118.7(2)
N2	C19	C18	113.3(3)	F26	C54	C53	112.9(4)
N2	C19	C20	119.5(3)	F27	C54	F26	104.6(4)
C20	C19	C18	127.2(3)	F27	C54	C53	111.6(4)
C21	C20	C19	120.4(4)	F28	C54	F26	107.3(5)
C20	C21	C22	119.1(3)	F28	C54	F27	107.4(5)
C21	C22	C23	121.0(3)	F28	C54	C53	112.6(5)
C24	C22	C21	119.2(3)	F26A	C54	C53	113.2(6)
C24	C22	C23	119.8(3)	F27A	C54	F26A	106.3(6)
F8	C23	F9	106.3(4)	F27A	C54	F28A	107.0(6)
F8	C23	C22	111.2(3)	F27A	C54	C53	113.1(5)
F9	C23	C22	111.4(4)	F28A	C54	F26A	105.6(5)
F10	C23	F8	107.2(4)	F28A	C54	C53	111.2(5)
F10	C23	F9	107.8(4)	C48	C55	C53	121.7(3)
F10	C23	C22	112.6(3)	C57	C56	B1	122.7(2)
N2	C24	C22	121.8(3)	C63	C56	C57	115.9(2)
N4	C25	C26	107.6(3)	C63	C56	B1	121.0(2)
C25	C26	C27	105.2(3)	C58	C57	C56	122.0(3)
N3	C27	C26	110.6(2)	C57	C58	C59	121.5(3)
N3	C27	C28	122.7(2)	C57	C58	C60	121.0(3)
C26	C27	C28	126.5(3)	C60	C58	C59	117.5(3)
C29	C28	C27	118.1(2)	F29	C59	F30	106.0(3)
N6	C29	C28	122.8(2)	F29	C59	F31	107.3(3)
N6	C29	C30	110.4(3)	F29	C59	C58	113.4(3)

Table D.20. Bond Angles for Δ-**4.49f**.

Atom	Atom	Atom	Angle/°	Atom	Atom	Atom	Angle/°
C30	C29	C28	126.5(3)	F30	C59	C58	111.8(3)
C31	C30	C29	105.4(3)	F31	C59	F30	106.0(3)
N5	C31	C30	107.6(3)	F31	C59	C58	111.9(3)
C33	C32	C39	122.0(2)	C61	C60	C58	118.0(2)
C32	C33	C34	120.5(2)	C60	C61	C62	120.4(2)
C35	C33	C32	121.1(2)	C60	C61	C63	120.9(2)
C35	C33	C34	118.3(2)	C63	C61	C62	118.7(2)
F11	C34	F12	105.4(3)	F32	C62	F33	106.4(5)
F11	C34	F13	109.5(3)	F32	C62	C61	112.5(4)
F11	C34	C33	113.8(3)	F33	C62	C61	112.4(4)
F12	C34	C33	110.2(2)	F34	C62	F32	105.7(5)
F13	C34	F12	103.9(3)	F34	C62	F33	106.0(4)
F13	C34	C33	113.2(3)	F34	C62	C61	113.3(4)
F11A	C34	F12A	105.2(4)	F32A	C62	F33A	104.5(6)
F11A	C34	F13A	111.1(4)	F32A	C62	C61	112.9(6)
F11A	C34	C33	112.1(4)	F33A	C62	C61	112.3(5)
F12A	C34	F13A	103.8(4)	F34A	C62	F32A	107.7(6)
F12A	C34	C33	113.2(4)	F34A	C62	F33A	105.0(6)
F13A	C34	C33	111.1(4)	F34A	C62	C61	113.7(6)
F11B	C34	C33	111.1(5)	C61	C63	C56	122.1(3)
F12B	C34	F11B	104.3(6)	C39	B1	C40	112.5(2)
F12B	C34	C33	113.8(5)	C39	B1	C48	111.1(2)
F13B	C34	F11B	107.6(6)	C40	B1	C48	102.3(2)
F13B	C34	F12B	105.0(6)	C56	B1	C39	104.9(2)

Table D.20. Bond Angles for Δ-**4.49f**.

Atom	Atom	Atom	Angle/°	Atom	Atom	Atom	Angle/°
F13B	C34	C33	114.3(5)	C56	B1	C40	111.9(2)
F11C	C34	C33	109.5(6)	C56	B1	C48	114.4(2)
F12C	C34	F11C	104.2(7)	C65	O1	C66	112.4(3)
F12C	C34	C33	113.1(7)	O1	C65	C64	109.1(3)
F13C	C34	F11C	107.6(7)	O1	C66	C67	109.3(3)
F13C	C34	F12C	106.8(7)	C70	O2	C69	113.9(7)
F13C	C34	C33	114.9(7)	C68	C69	O2	107.9(6)
C33	C35	C36	117.9(2)	O2	C70	C71	108.6(6)
C35	C36	C37	119.0(2)	C69A	O2A	C70A	115.1(9)
C35	C36	C38	121.2(2)	O2A	C69A	C68A	108.7(8)
C38	C36	C37	119.8(2)	O2A	C70A	C71A	110.6(8)
F14	C37	F15	106.2(5)	C72	C73	C74	113.0(4)
F14	C37	F16	106.5(5)	C75	C74	C73	114.2(3)
F14	C37	C36	113.1(4)	C74	C75	C76	113.1(4)

Table D.21. Hydrogen Bonds for Δ-**4.49f**.

D	H	A	d(D-H)/Å	d(H-A)/Å	d(D-A)/Å	D-H-A/°
N4	H4	O2	0.88(4)	2.13(4)	2.758(10)	128(3)
N4	H4	O2A	0.88(4)	2.15(4)	2.773(12)	128(3)
N5	H5	O1	0.85(4)	2.13(4)	2.774(3)	133(4)

Table D.22. Torsion Angles for Δ-**4.49f**.

A	B	C	D	Angle/°	A	B	C	D	Angle/°
Ir1	N1	C1	C2	172.4(2)	C36	C38	C39	C32	0.9(4)

Table D.22. Torsion Angles for Δ-**4.49f**.

A	B	C	D	Angle/°	A	B	C	D	Angle/°
Ir1	N1	C6	C5	-172.1(2)	C36	C38	C39	B1	178.0(2)
Ir1	N1	C6	C7	7.2(3)	C37	C36	C38	C39	179.1(2)
Ir1	N2	C19	C18	-2.4(3)	C38	C36	C37	F14	-21.4(9)
Ir1	N2	C19	C20	177.6(3)	C38	C36	C37	F15	-141.5(7)
Ir1	N2	C24	C22	179.8(2)	C38	C36	C37	F16	99.6(8)
Ir1	N3	N4	C25	171.1(2)	C38	C36	C37	F14A	-36.4(18)
Ir1	N3	C27	C26	-170.2(2)	C38	C36	C37	F15A	-155.4(17)
Ir1	N3	C27	C28	14.8(4)	C38	C36	C37	F16A	84.3(19)
Ir1	N6	C29	C28	-11.6(4)	C38	C39	B1	C40	142.1(2)
Ir1	N6	C29	C30	174.34(19)	C38	C39	B1	C48	28.1(3)
Ir1	C13	C14	C15	-179.4(2)	C38	C39	B1	C56	-96.0(3)
Ir1	C13	C18	C17	178.4(2)	C39	C32	C33	C34	-176.8(2)
Ir1	C13	C18	C19	0.4(3)	C39	C32	C33	C35	1.2(4)
F4	C8	C9	C10	-178.6(3)	C40	C41	C42	C43	176.6(3)
F5	C10	C11	C12	-178.8(3)	C40	C41	C42	C44	0.3(4)
F6	C15	C16	C17	179.5(3)	C41	C40	C47	C45	-0.4(4)
F7	C17	C18	C13	-177.9(3)	C41	C40	B1	C39	-29.7(3)
F7	C17	C18	C19	-0.1(5)	C41	C40	B1	C48	89.5(3)
N1	C1	C2	C3	179.8(3)	C41	C40	B1	C56	-147.5(2)
N1	C1	C2	C4	-0.9(5)	C41	C42	C43	F17	-78.5(4)
N1	C6	C7	C8	173.7(3)	C41	C42	C43	F18	161.0(3)
N1	C6	C7	C12	-5.6(4)	C41	C42	C43	F19	40.9(4)
N2	C19	C20	C21	3.6(6)	C41	C42	C44	C45	-0.8(4)
N3	N4	C25	C26	-0.4(4)	C42	C44	C45	C46	179.0(2)

Table D.22. Torsion Angles for Δ-**4.49f**.

A	B	C	D	Angle/°	A	B	C	D	Angle/°
N3	C27	C28	C29	-38.2(4)	C42	C44	C45	C47	0.8(4)
N4	N3	C27	C26	-0.7(3)	C43	C42	C44	C45	-177.1(3)
N4	N3	C27	C28	-175.7(3)	C44	C42	C43	F17	97.8(3)
N4	C25	C26	C27	-0.1(4)	C44	C42	C43	F18	-22.7(4)
N5	N6	C29	C28	174.5(3)	C44	C42	C43	F19	-142.8(3)
N5	N6	C29	C30	0.5(3)	C44	C45	C46	F20	-177.5(2)
N6	N5	C31	C30	1.4(4)	C44	C45	C46	F21	-58.1(3)
N6	C29	C30	C31	0.4(3)	C44	C45	C46	F22	61.3(3)
C1	N1	C6	C5	1.9(4)	C44	C45	C47	C40	-0.2(4)
C1	N1	C6	C7	-178.8(3)	C46	C45	C47	C40	-178.3(2)
C1	C2	C3	F1	-124.3(4)	C47	C40	C41	C42	0.3(4)
C1	C2	C3	F2	117.1(3)	C47	C40	B1	C39	160.3(2)
C1	C2	C3	F3	-3.8(4)	C47	C40	B1	C48	-80.4(3)
C1	C2	C4	C5	2.1(5)	C47	C40	B1	C56	42.5(3)
C2	C4	C5	C6	-1.2(5)	C47	C45	C46	F20	0.7(4)
C3	C2	C4	C5	-178.6(3)	C47	C45	C46	F21	120.1(3)
C4	C2	C3	F1	56.4(4)	C47	C45	C46	F22	-120.5(3)
C4	C2	C3	F2	-62.3(4)	C48	C49	C50	C51	-176.2(2)
C4	C2	C3	F3	176.9(3)	C48	C49	C50	C52	1.1(4)
C4	C5	C6	N1	-0.8(4)	C49	C48	C55	C53	-1.4(4)
C4	C5	C6	C7	-179.9(3)	C49	C48	B1	C39	46.1(3)
C5	C6	C7	C8	-7.0(5)	C49	C48	B1	C40	-74.2(3)
C5	C6	C7	C12	173.7(3)	C49	C48	B1	C56	164.7(2)
C6	N1	C1	C2	-1.1(4)	C49	C50	C51	F23	-132.4(4)

Table D.22. Torsion Angles for Δ-**4.49f**.

A	B	C	D	Angle/°	A	B	C	D	Angle/°
C6	C7	C8	F4	-0.9(5)	C49	C50	C51	F24	-18.5(5)
C6	C7	C8	C9	-178.9(3)	C49	C50	C51	F25	106.5(4)
C6	C7	C12	Ir1	1.4(3)	C49	C50	C51	F23A	-152.8(5)
C6	C7	C12	C11	179.9(3)	C49	C50	C51	F24A	-32.1(5)
C7	C8	C9	C10	-0.5(5)	C49	C50	C51	F25A	78.9(5)
C8	C7	C12	Ir1	-177.9(3)	C49	C50	C51	F23B	-117.6(5)
C8	C7	C12	C11	0.6(4)	C49	C50	C51	F24B	4.3(6)
C8	C9	C10	F5	179.7(3)	C49	C50	C51	F25B	131.7(5)
C8	C9	C10	C11	-0.3(5)	C49	C50	C51	F23C	48.9(8)
C9	C10	C11	C12	1.3(5)	C49	C50	C51	F24C	164.8(8)
C10	C11	C12	Ir1	176.9(2)	C49	C50	C51	F25C	-71.4(8)
C10	C11	C12	C7	-1.4(4)	C49	C50	C52	C53	-1.2(4)
C12	C7	C8	F4	178.4(3)	C50	C52	C53	C54	178.0(3)
C12	C7	C8	C9	0.4(5)	C50	C52	C53	C55	0.0(4)
C13	C14	C15	F6	179.8(3)	C51	C50	C52	C53	176.1(3)
C13	C14	C15	C16	0.6(5)	C52	C50	C51	F23	50.3(4)
C13	C18	C19	N2	1.3(4)	C52	C50	C51	F24	164.2(4)
C13	C18	C19	C20	-178.6(3)	C52	C50	C51	F25	-70.8(5)
C14	C13	C18	C17	-2.1(4)	C52	C50	C51	F23A	29.9(6)
C14	C13	C18	C19	179.9(3)	C52	C50	C51	F24A	150.5(5)
C14	C15	C16	C17	-1.3(5)	C52	C50	C51	F25A	-98.4(5)
C15	C16	C17	F7	179.6(3)	C52	C50	C51	F23B	65.1(5)
C15	C16	C17	C18	0.2(5)	C52	C50	C51	F24B	-173.0(5)
C16	C17	C18	C13	1.5(5)	C52	C50	C51	F25B	-45.6(6)

Table D.22. Torsion Angles for Δ-**4.49f**.

A	B	C	D	Angle/°	A	B	C	D	Angle/°
C16	C17	C18	C19	179.2(3)	C52	C50	C51	F23C	-128.4(8)
C17	C18	C19	N2	-176.5(3)	C52	C50	C51	F24C	-12.5(8)
C17	C18	C19	C20	3.6(5)	C52	C50	C51	F25C	111.3(8)
C18	C13	C14	C15	1.1(4)	C52	C53	C54	F26	141.6(6)
C18	C19	C20	C21	-176.5(3)	C52	C53	C54	F27	24.1(7)
C19	N2	C24	C22	0.2(4)	C52	C53	C54	F28	-96.8(9)
C19	C20	C21	C22	-1.8(6)	C52	C53	C54	F26A	129.3(8)
C20	C21	C22	C23	178.6(4)	C52	C53	C54	F27A	8.3(10)
C20	C21	C22	C24	-0.8(5)	C52	C53	C54	F28A	-112.1(6)
C21	C22	C23	F8	-69.6(5)	C52	C53	C55	C48	1.3(4)
C21	C22	C23	F9	48.7(5)	C54	C53	C55	C48	-176.7(2)
C21	C22	C23	F10	170.0(3)	C55	C48	C49	C50	0.2(4)
C21	C22	C24	N2	1.6(5)	C55	C48	B1	C39	-142.0(3)
C23	C22	C24	N2	-177.8(3)	C55	C48	B1	C40	97.8(3)
C24	N2	C19	C18	177.3(3)	C55	C48	B1	C56	-23.4(3)
C24	N2	C19	C20	-2.8(5)	C55	C53	C54	F26	-40.4(7)
C24	C22	C23	F8	109.7(4)	C55	C53	C54	F27	-157.9(6)
C24	C22	C23	F9	-131.9(4)	C55	C53	C54	F28	81.3(9)
C24	C22	C23	F10	-10.7(5)	C55	C53	C54	F26A	-52.6(8)
C25	C26	C27	N3	0.5(4)	C55	C53	C54	F27A	-173.6(10)
C25	C26	C27	C28	175.3(3)	C55	C53	C54	F28A	66.0(6)
C26	C27	C28	C29	147.6(3)	C56	C57	C58	C59	179.4(3)
C27	N3	N4	C25	0.7(4)	C56	C57	C58	C60	1.1(4)
C27	C28	C29	N6	36.5(4)	C57	C56	C63	C61	-0.3(4)

Table D.22. Torsion Angles for Δ-**4.49f**.

A	B	C	D	Angle/°	A	B	C	D	Angle/°
C27	C28	C29	C30	-150.5(3)	C57	C56	B1	C39	84.7(3)
C28	C29	C30	C31	-173.4(3)	C57	C56	B1	C40	-153.1(2)
C29	C30	C31	N5	-1.1(3)	C57	C56	B1	C48	-37.4(3)
C31	N5	N6	Ir1	-175.5(2)	C57	C58	C59	F29	10.4(4)
C31	N5	N6	C29	-1.2(3)	C57	C58	C59	F30	130.1(3)
C32	C33	C34	F11	14.7(4)	C57	C58	C59	F31	-111.2(4)
C32	C33	C34	F12	132.9(3)	C57	C58	C60	C61	-0.8(4)
C32	C33	C34	F13	-111.2(4)	C58	C60	C61	C62	-178.8(3)
C32	C33	C34	F11A	34.8(5)	C58	C60	C61	C63	0.0(4)
C32	C33	C34	F12A	153.6(5)	C59	C58	C60	C61	-179.1(3)
C32	C33	C34	F13A	-90.1(5)	C60	C58	C59	F29	-171.4(3)
C32	C33	C34	F11B	-10.4(7)	C60	C58	C59	F30	-51.6(4)
C32	C33	C34	F12B	106.9(7)	C60	C58	C59	F31	67.1(4)
C32	C33	C34	F13B	-132.4(7)	C60	C61	C62	F32	-13.4(8)
C32	C33	C34	F11C	-47.6(12)	C60	C61	C62	F33	106.7(6)
C32	C33	C34	F12C	68.2(12)	C60	C61	C62	F34	-133.2(5)
C32	C33	C34	F13C	-168.8(12)	C60	C61	C62	F32A	12.4(11)
C32	C33	C35	C36	-0.8(4)	C60	C61	C62	F33A	130.3(12)
C32	C39	B1	C40	-40.9(3)	C60	C61	C62	F34A	-110.7(12)
C32	C39	B1	C48	-154.9(2)	C60	C61	C63	C56	0.5(4)
C32	C39	B1	C56	81.0(3)	C62	C61	C63	C56	179.4(3)
C33	C32	C39	C38	-1.2(4)	C63	C56	C57	C58	-0.6(4)
C33	C32	C39	B1	-178.4(2)	C63	C56	B1	C39	-87.5(3)
C33	C35	C36	C37	-179.2(2)	C63	C56	B1	C40	34.7(3)

Table D.22. Torsion Angles for Δ-**4.49f**.

A	B	C	D	Angle/°	A	B	C	D	Angle/°
C33	C35	C36	C38	0.5(4)	C63	C56	B1	C48	150.4(2)
C34	C33	C35	C36	177.2(2)	C63	C61	C62	F32	167.7(7)
C35	C33	C34	F11	-163.4(3)	C63	C61	C62	F33	-72.2(6)
C35	C33	C34	F12	-45.2(4)	C63	C61	C62	F34	47.9(5)
C35	C33	C34	F13	70.7(4)	C63	C61	C62	F32A	-166.4(11)
C35	C33	C34	F11A	-143.2(5)	C63	C61	C62	F33A	-48.6(12)
C35	C33	C34	F12A	-24.4(5)	C63	C61	C62	F34A	70.4(12)
C35	C33	C34	F13A	91.9(5)	B1	C40	C41	C42	-170.2(2)
C35	C33	C34	F11B	171.5(7)	B1	C40	C47	C45	170.2(2)
C35	C33	C34	F12B	-71.2(7)	B1	C48	C49	C50	172.9(2)
C35	C33	C34	F13B	49.6(7)	B1	C48	C55	C53	-173.5(2)
C35	C33	C34	F11C	134.4(12)	B1	C56	C57	C58	-173.2(2)
C35	C33	C34	F12C	-109.9(12)	B1	C56	C63	C61	172.5(2)
C35	C33	C34	F13C	13.2(13)	C65	O1	C66	C67	-175.9(3)
C35	C36	C37	F14	158.3(8)	C66	O1	C65	C64	176.8(3)
C35	C36	C37	F15	38.2(8)	C69	O2	C70	C71	178.1(7)
C35	C36	C37	F16	-80.8(8)	C70	O2	C69	C68	-173.8(7)
C35	C36	C37	F14A	143.3(18)	C69A	O2A	C70A	C71A	178.6(9)
C35	C36	C37	F15A	24.2(17)	C70A	O2A	C69A	C68A	-174.9(10)
C35	C36	C37	F16A	-96.1(19)	C72	C73	C74	C75	-177.5(4)
C35	C36	C38	C39	-0.6(4)	C73	C74	C75	C76	174.7(4)

Table D.23. Hydrogen Atom Coordinates (Å×10⁴) and Isotropic Displacement Parameters (Å²×10³) for Δ-**4.49f**.

Atom	***x***	***y***	***z***	**U(eq)**
H4	4220(30)	5730(30)	2490(30)	24
H5	1090(30)	7880(30)	3060(30)	23
H1	4284.81	7363.43	3341.88	22
H4A	4534.94	9798.33	2615.72	35
H5A	3022.04	9750.41	1841.43	33
H9	-28.09	9288.55	546.83	36
H11	342.22	6788.15	1274.21	26
H14	3725.84	7286.77	1377.4	23
H16	3320.14	5524.67	-403.46	33
H20	1308.84	4107.72	738.82	34
H21	231.34	3653.93	1358.91	36
H24	916.82	5671.59	2862.35	24
H25	5363.7	5076.36	3622.79	33
H26	4646.18	5095.14	4741.24	30
H28A	2419.95	5312.48	4212.93	26
H28B	3124.76	5820.26	4910.01	26
H30	1904.74	6915.51	5208.02	26
H31	894.59	8043.29	4385.34	28
H32	3138.69	7967.49	8502.23	19
H35	1268.19	7850.17	9739.42	21
H38	1205.16	6105.52	7999.44	18
H41	2168.67	8314.24	7086.62	18
H44	3562.57	8980.69	5525.93	23

Table D.23. Hydrogen Atom Coordinates (Å×10⁴) and Isotropic Displacement Parameters (Å²×10³) for Δ-**4.49f**.

Atom	***x***	***y***	***z***	**U(eq)**
H47	3975.65	6646.7	6610.56	18
H49	934.29	6988.01	6657.12	20
H52	153.04	5123.63	4983.51	27
H55	2663.11	5040.24	6568.58	20
H57	2848.58	4856.1	7934.24	20
H60	5464.78	4692.16	9303.47	26
H63	4515.07	6924.16	8163.71	21
H64A	907.62	9640.99	3630.51	59
H64B	745.25	10428.8	3016.9	59
H64C	1188.87	9548.88	2823.26	59
H65A	-635.13	9718.25	2898.92	45
H65B	-348.48	9613.12	2092.74	45
H66A	-1251.37	8276.5	1831.58	49
H66B	-1507.27	8451.13	2643.17	49
H67A	-831.56	7136.71	3149.74	80
H67B	-573.03	6962.8	2341.7	80
H67C	-1619.02	6976.88	2343.03	80
H68A	6566.55	6973.04	2415.22	60
H68B	6274.14	6307.75	2996.53	60
H68C	5520.88	6899.26	2409.53	60
H69A	6524.21	5606.97	1891.95	48
H69B	5715.61	6169.18	1327.62	48
H70A	5712.09	4235.68	1560.18	48

Table D.23. Hydrogen Atom Coordinates (Å×10⁴) and Isotropic Displacement Parameters (Å²×10³) for Δ-**4.49f**.

Atom	***x***	***y***	***z***	**U(eq)**
H70B	4892.57	4721.91	932.09	48
H71A	4365.19	3440.91	1373.72	60
H71B	3875.11	4260.4	1628.97	60
H71C	4690.45	3787.7	2267.04	60
H68D	6438.46	6743.57	1949.47	60
H68E	6397.51	6226.26	2727.13	60
H68F	5496.68	6669.38	2173.44	60
H69C	5619.26	5711.45	1140.2	48
H69D	6399.81	5210.5	1794.73	48
H70C	5487.73	3903.48	1711.21	48
H70D	4694.87	4331.52	1015.94	48
H71D	3974.01	3365.44	1553.01	60
H71E	3777.31	4261.71	1928.01	60
H71F	4539.85	3619.64	2437.03	60
H72A	6984.65	8656.51	6270.71	78
H72B	8049.07	8520.4	6688.82	78
H72C	7411.59	8929.3	7177.92	78
H73A	6658.24	7622.59	7158.29	54
H73B	7728.17	7458.52	7517.01	54
H74A	6751.14	7105.83	5909.1	44
H74B	7810.15	6910.85	6292.19	44
H75A	6409.39	6067.08	6793.47	50
H75B	7471.07	5838.84	7098	50

Table D.23. Hydrogen Atom Coordinates (Å×10⁴) and Isotropic Displacement Parameters (Å²×10³) for Δ-**4.49f**.

Atom	***x***	***y***	***z***	**U(eq)**
H76A	6337.57	5544.75	5524.34	71
H76B	6758.61	4808.07	6160.83	71
H76C	7412.59	5371.04	5786.89	71

Table D.24. Atomic Occupancy for Δ-**4.49f**.

Atom	***Occupancy***	**Atom**	***Occupancy***	**Atom**	***Occupancy***
F11	0.540(4)	F12	0.540(4)	F13	0.540(4)
F11A	0.254(4)	F12A	0.254(4)	F13A	0.254(4)
F11B	0.149(3)	F12B	0.149(3)	F13B	0.149(3)
F11C	0.057(2)	F12C	0.057(2)	F13C	0.057(2)
F14	0.64(6)	F15	0.64(6)	F16	0.64(6)
F14A	0.36(6)	F15A	0.36(6)	F16A	0.36(6)
F23	0.401(4)	F24	0.401(4)	F25	0.401(4)
F23A	0.255(4)	F24A	0.255(4)	F25A	0.255(4)
F23B	0.239(4)	F24B	0.239(4)	F25B	0.239(4)
F23C	0.105(3)	F24C	0.105(3)	F25C	0.105(3)
F26	0.57(3)	F27	0.57(3)	F28	0.57(3)
F26A	0.43(3)	F27A	0.43(3)	F28A	0.43(3)
F32	0.68(2)	F33	0.68(2)	F34	0.68(2)
F32A	0.32(2)	F33A	0.32(2)	F34A	0.32(2)
O2	0.556(7)	C68	0.556(7)	H68A	0.556(7)
H68B	0.556(7)	H68C	0.556(7)	C69	0.556(7)
H69A	0.556(7)	H69B	0.556(7)	C70	0.556(7)
H70A	0.556(7)	H70B	0.556(7)	C71	0.556(7)

Table D.24. Atomic Occupancy for Δ-**4.49f**.

Atom	***Occupancy***	**Atom**	***Occupancy***	**Atom**	***Occupancy***
H71A	0.556(7)	H71B	0.556(7)	H71C	0.556(7)
O2A	0.444(7)	C68A	0.444(7)	H68D	0.444(7)
H68E	0.444(7)	H68F	0.444(7)	C69A	0.444(7)
H69C	0.444(7)	H69D	0.444(7)	C70A	0.444(7)
H70C	0.444(7)	H70D	0.444(7)	C71A	0.444(7)
H71D	0.444(7)	H71E	0.444(7)	H71F	0.444(7)

D.4 X-Ray Data for Compound 4.48i

D.4.1 Data Collection

A colorless crystal with approximate dimensions 0.13 × 0.05 × 0.03 mm^3 was selected under oil under ambient conditions and attached to the tip of a MiTeGen MicroMount©. The crystal was mounted in a stream of cold nitrogen at 100(1) K and centered in the X-ray beam by using a video camera.

The crystal evaluation and data collection were performed on a Bruker D8 VENTURE PhotonIII four-circle diffractometer with Cu Kα (λ = 1.54178 Å) radiation and the detector to crystal distance of 4.0 cm.[1]

The initial cell constants were obtained from a 180° φ scan conducted at a 2θ = 50° angle with the exposure time of 1 second per frame. The reflections were successfully indexed by an automated indexing routine built in the APEX3 program. The final cell constants were calculated from a set of 9751 strong reflections from the actual data collection.

The data were collected by using the full sphere data collection routine to survey the reciprocal space to the extent of a full sphere to a resolution of 0.80 Å. A total of 40830 data were harvested by collecting 7 sets of frames with 0.8° scans in ω and φ with an exposure time 1-10 sec per frame. These redundant datasets were corrected for Lorentz and polarization effects. The absorption correction was based on fitting a function to the empirical transmission surface as sampled by multiple equivalent measurements.[2]

D.4.2 Structure Solution and Refinement

The systematic absences in the diffraction data were uniquely consistent for the space group $P2_12_12_1$ that yielded chemically reasonable and computationally stable results of refinement.[3–8]

A successful solution by intrinsic phasing provided most non-hydrogen atoms from the *E*-map. The remaining non-hydrogen atoms were located in an alternating series of least-squares cycles and difference Fourier maps. All non-hydrogen atoms were refined with anisotropic displacement coefficients. All hydrogen atoms (except those attached to N atoms) were included in the structure factor calculation at idealized positions and were allowed to ride on the neighboring atoms with relative isotropic displacement coefficients.

There are two molecules with identical composition and handedness but slightly different conformations in the asymmetric unit.

The absolute structure was unequivocally established by anomalous dispersion effects. The chiral centers have the following handedness: C2, C2a – *S*; C3, C3a, C13, C13a – *R*.

The final least-squares refinement of 677 parameters against 10761 data resulted in residuals *R* (based on F^2 for $I \geq 2\sigma$) and *wR* (based on F^2 for all data) of 0.0318 and 0.0801, respectively. The final difference Fourier map was featureless.

D.4.3 Summary

Crystal Data for $C_{30}H_{32}BrNO_5$ (M =566.47 g/mol): orthorhombic, space group $P2_12_12_1$ (no. 19), a = 10.7859(13) Å, b = 14.119(2) Å, c = 35.824(4) Å, V = 5455.4(13) Å^3, Z = 8, T = 100.0 K, μ(CuKα) = 2.377 mm^{-1}, *Dcalc* = 1.379 g/cm^3, 40830 reflections measured (4.934° ≤ 2Θ ≤ 145.112°), 10761 unique (R_{int} = 0.0562, R_{sigma} = 0.0466) which were used in all calculations. The final R_1 was 0.0318 (I > 2σ(I)) and wR_2 was 0.0801 (all data).

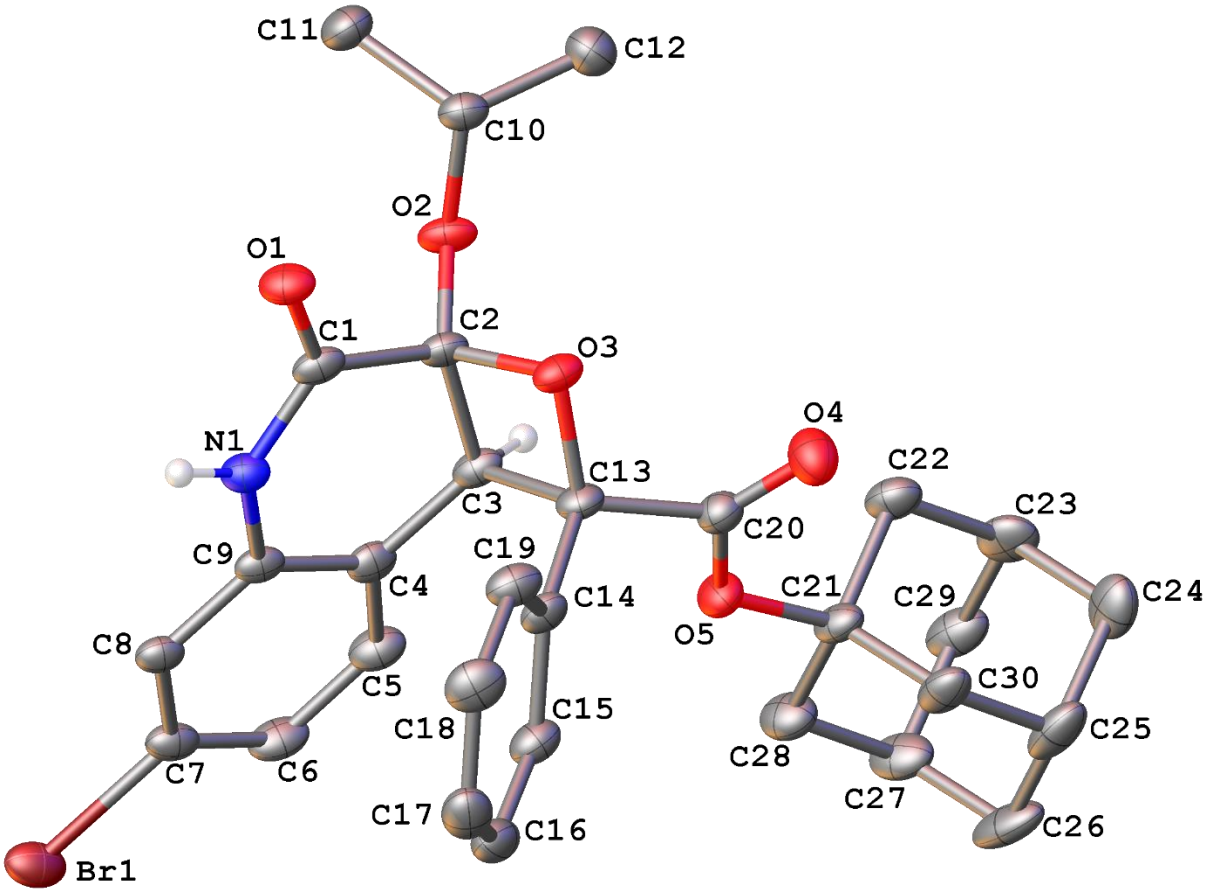

Figure D.12. A molecular drawing of the first symmetry-independent molecule of **4.48i** shown with 50% probability ellipsoids. All H atoms are omitted except on atoms N1 and C3.

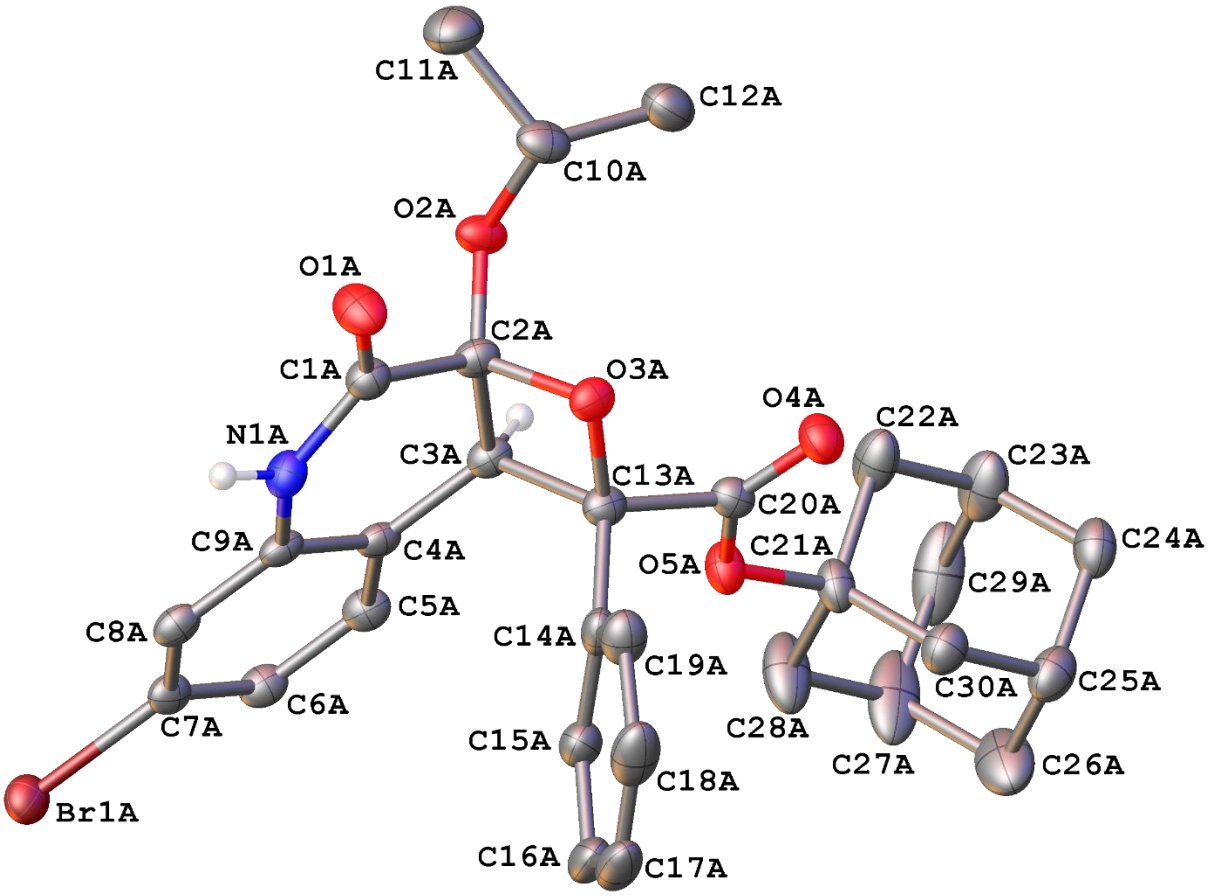

Figure D.13. A molecular drawing of the second symmetry-independent molecule of **4.48i** shown with 50% probability ellipsoids. All H atoms are omitted except on atoms N1a and C3a.

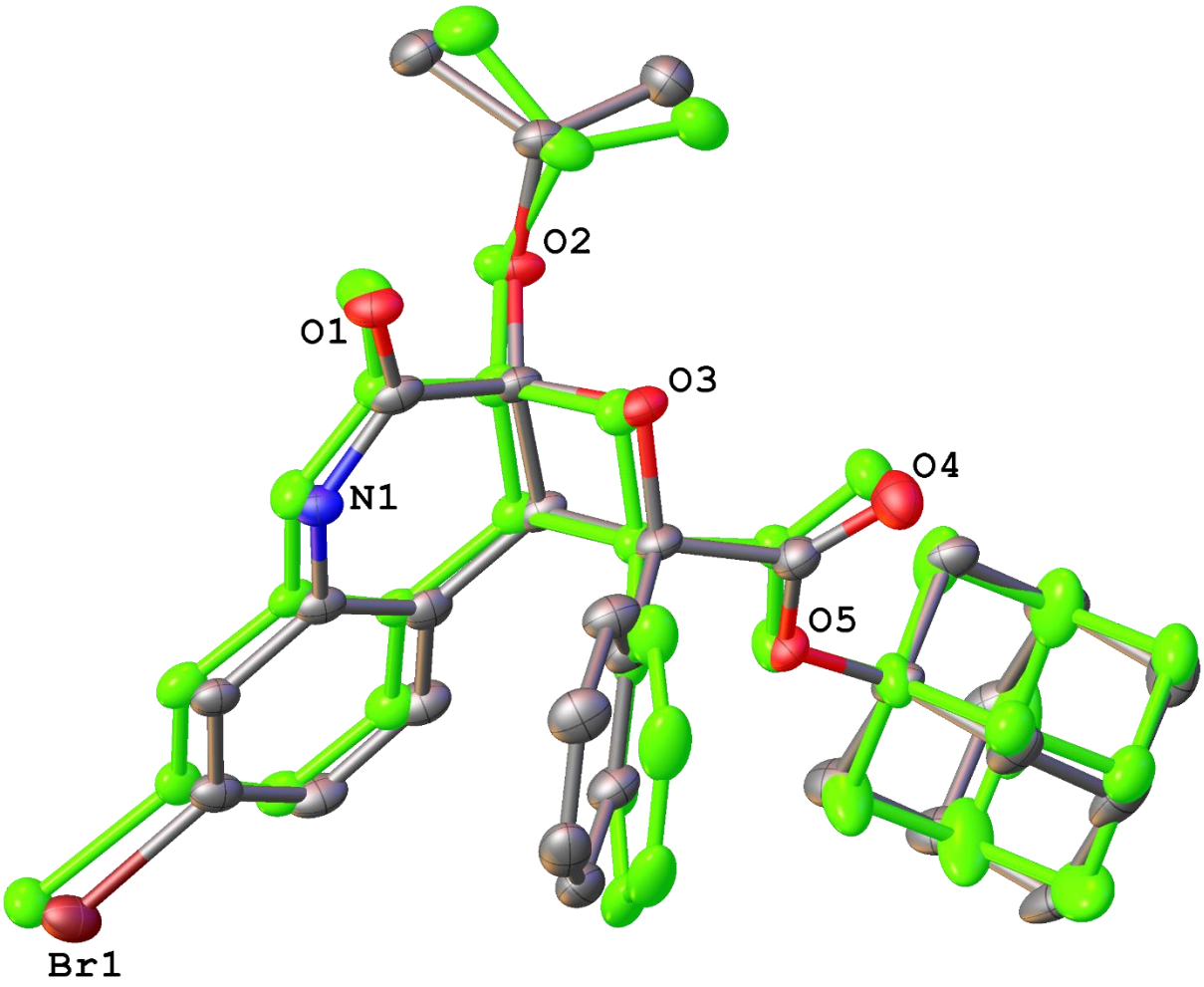

Figure D.14. A molecular drawing of the two symmetry-independent molecule of **4.48i** superimposed. The second molecule is shown in green. All H atoms are omitted.

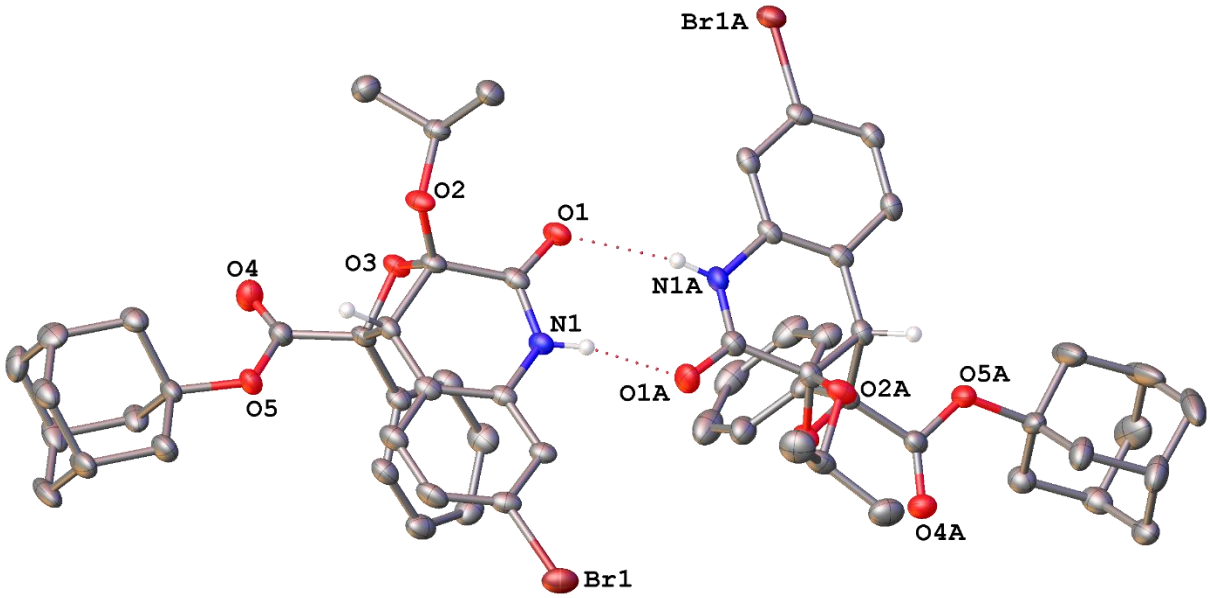

Figure D.15. A molecular drawing of the asymmetric unit of **4.48i** shown with 50% probability ellipsoids. The two molecules are connected by two hydrogen-bonding interactions. All H atoms are omitted except on atoms N1, N1a, C3, C3a.

Table D.25. Crystal data and structure refinement for **4.48i**.

Identification code	Yoon80
Empirical formula	$C_{30}H_{32}BrNO_5$
Formula weight	566.47
Temperature/K	100.0
Crystal system	orthorhombic
Space group	$P2_12_12_1$
a/Å	10.7859(13)
b/Å	14.119(2)
c/Å	35.824(4)
α/°	90
β/°	90
γ/°	90
Volume/Å^3	5455.4(13)
Z	8
ρ_{calc}g/cm^3	1.379
μ/mm^{-1}	2.377
F(000)	2352.0
Crystal size/mm^3	0.13 × 0.05 × 0.03
Radiation	CuKα (λ = 1.54178)
2Θ range for data collection/°	4.934 to 145.112
Index ranges	$-13 \leq h \leq 10$, $-17 \leq k \leq 17$, $-44 \leq l \leq 38$
Reflections collected	40830
Independent reflections	10761 [R_{int} = 0.0562, R_{sigma} = 0.0466]
Data/restraints/parameters	10761/1/677
Goodness-of-fit on F^2	1.043

Final R indexes [I>=2σ (I)]	R_1 = 0.0318, wR_2 = 0.0789
Final R indexes [all data]	R_1 = 0.0337, wR_2 = 0.0801
Largest diff. peak/hole / e Å^{-3}	0.69/-0.59
Flack parameter	-0.014(6)

Table D.26. Fractional Atomic Coordinates (×10^4) and Equivalent Isotropic Displacement Parameters (Å^2×10^3) for **4.48i**. U_{eq} is defined as 1/3 of of the trace of the orthogonalised U_{IJ} tensor.

Atom	***x***	***y***	***z***	**U(eq)**
Br1	6719.0(4)	5730.4(3)	7303.9(2)	30.74(10)
O1	3165(2)	2450.2(19)	6088.1(6)	25.5(5)
O2	3150(2)	1171.3(19)	6746.0(6)	24.3(5)
O3	4915(2)	919.1(18)	6362.5(6)	21.9(5)
O4	6580(3)	-518.4(19)	6573.3(7)	33.4(6)
O5	7232(2)	454.2(18)	7038.4(7)	25.3(5)
N1	4491(3)	3258(2)	6451.1(7)	20.6(5)
C1	3900(3)	2460(3)	6352.9(8)	21.2(7)
C2	4177(3)	1567(3)	6587.0(9)	20.2(7)
C3	5229(3)	1674(3)	6874.7(9)	20.6(7)
C4	5570(3)	2640(3)	6996.5(8)	21.4(6)
C5	6221(3)	2828(3)	7323.9(10)	26.2(7)
C6	6568(3)	3739(3)	7421.6(9)	28.0(8)
C7	6253(3)	4471(3)	7181.5(9)	23.2(7)
C8	5567(3)	4325(3)	6857.9(8)	20.3(6)
C9	5225(3)	3408(3)	6770.3(9)	19.0(7)
C10	2238(3)	717(3)	6502.2(9)	22.2(7)
C11	1028(3)	1215(3)	6573.8(12)	30.7(8)

Table D.26. Fractional Atomic Coordinates ($\times 10^4$) and Equivalent Isotropic Displacement Parameters ($Å^2 \times 10^3$) for **4.48i**. U_{eq} is defined as 1/3 of of the trace of the orthogonalised U_{IJ} tensor.

Atom	*x*	*y*	*z*	U(eq)
C12	2195(4)	-314(3)	6604.1(12)	31.0(8)
C13	6033(3)	1142(3)	6575.4(9)	20.8(7)
C14	6924(3)	1746(3)	6352.9(9)	21.5(7)
C15	7941(3)	2180(3)	6521.7(10)	25.8(7)
C16	8702(3)	2768(3)	6317.1(11)	29.2(8)
C17	8486(3)	2914(3)	5939.4(11)	30.8(8)
C18	7482(3)	2490(3)	5768.6(10)	31.9(8)
C19	6700(3)	1905(3)	5975.7(9)	26.5(7)
C20	6637(3)	242(3)	6720.2(9)	23.4(7)
C21	7868(3)	-261(3)	7267.7(10)	23.7(7)
C22	6967(3)	-1018(3)	7408.3(10)	28.5(8)
C23	7673(4)	-1677(3)	7678.4(11)	32.6(9)
C24	8751(4)	-2133(3)	7471.5(12)	36.6(9)
C25	9641(3)	-1368(3)	7330.2(12)	38.6(10)
C26	10137(3)	-800(4)	7662.3(13)	43.6(11)
C27	9053(4)	-335(3)	7867.9(11)	34.7(9)
C28	8354(4)	313(3)	7595.1(11)	32.0(8)
C29	8158(4)	-1098(3)	8011.7(11)	34.1(9)
C30	8942(3)	-722(3)	7056.8(11)	29.7(8)
Br1A	-598.4(3)	2616.5(3)	4845.1(2)	27.22(10)
O1A	4012(3)	4951(2)	6102.3(7)	31.4(6)
O2A	2972(2)	6708.2(19)	5858.4(7)	25.2(5)
O3A	4575(2)	6176.3(18)	5458.7(6)	22.6(5)

Table D.26. Fractional Atomic Coordinates ($\times 10^4$) and Equivalent Isotropic Displacement Parameters ($Å^2 \times 10^3$) for **4.48i**. U_{eq} is defined as 1/3 of of the trace of the orthogonalised U_{IJ} tensor.

Atom	*x*	*y*	*z*	U(eq)
O4A	5155(2)	7565(2)	4951.4(7)	29.0(6)
O5A	3571(2)	7060.6(19)	4578.2(7)	25.7(5)
N1A	2813(3)	4305(2)	5652.4(8)	21.8(6)
C1A	3411(3)	5039(3)	5812.0(9)	22.6(7)
C2A	3367(3)	6001(2)	5619.8(9)	21.4(7)
C3A	2725(3)	6026(3)	5235.7(9)	20.7(7)
C4A	1917(3)	5210(2)	5139.3(9)	19.5(6)
C5A	1051(3)	5260(3)	4850.2(10)	23.0(7)
C6A	297(3)	4505(3)	4760.5(9)	23.3(7)
C7A	421(3)	3670(3)	4965.3(9)	21.2(7)
C8A	1256(3)	3595(3)	5257.6(9)	21.8(7)
C9A	1993(3)	4371(3)	5342.7(8)	18.9(6)
C10A	3905(3)	7114(3)	6108.6(10)	28.0(8)
C11A	3363(4)	7093(3)	6500.6(11)	39.5(10)
C12A	4193(4)	8100(3)	5970.2(12)	35.5(9)
C13A	4084(3)	6098(3)	5081.5(9)	21.3(7)
C14A	4657(3)	5286(2)	4868.6(10)	23.7(7)
C15A	4123(4)	4961(3)	4537.3(10)	28.5(8)
C16A	4728(4)	4288(3)	4322.6(11)	34.9(9)
C17A	5880(4)	3951(3)	4430.8(12)	38.9(10)
C18A	6409(4)	4260(3)	4762.5(13)	40.5(10)
C19A	5790(3)	4918(3)	4983.3(11)	30.5(8)
C20A	4360(3)	7014(2)	4867.6(9)	21.3(6)

Table D.26. Fractional Atomic Coordinates ($\times 10^4$) and Equivalent Isotropic Displacement Parameters ($Å^2 \times 10^3$) for **4.48i**. U_{eq} is defined as 1/3 of of the trace of the orthogonalised U_{IJ} tensor.

Atom	*x*	*y*	*z*	U(eq)
C21A	3643(3)	7836(3)	4302.8(10)	25.5(8)
C22A	3366(4)	8774(3)	4487.6(12)	34.7(9)
C23A	3331(4)	9544(3)	4182.2(13)	41.6(10)
C24A	4597(4)	9579(3)	3986.4(11)	32.0(8)
C25A	4869(4)	8621(3)	3804.5(11)	32.3(9)
C26A	3858(5)	8387(4)	3522.7(13)	52.4(13)
C27A	2586(5)	8368(5)	3721.4(15)	63.2(18)
C28A	2626(4)	7595(4)	4024.0(13)	49.4(13)
C29A	2333(4)	9327(5)	3897.2(17)	60.6(17)
C30A	4899(3)	7851(3)	4108.2(11)	29.3(8)

Table D.27. Anisotropic Displacement Parameters ($Å^2 \times 10^3$) for **4.48i**. The Anisotropic displacement factor exponent takes the form: $-2\pi^2[h^2a^{*2}U_{11}+2hka^*b^*U_{12}+\ldots]$.

Atom	U_{11}	U_{22}	U_{33}	U_{23}	U_{13}	U_{12}
Br1	28.77(19)	37.7(2)	25.75(18)	-11.37(16)	3.12(15)	-8.26(17)
O1	21.9(11)	34.7(14)	20.0(11)	2.0(10)	-5.3(9)	-4.9(11)
O2	16.7(11)	38.3(14)	17.8(10)	3.9(10)	0.2(9)	-7.6(11)
O3	15.5(11)	31.2(14)	19.1(11)	-2.0(10)	-2.4(8)	0.0(10)
O4	39.8(15)	27.7(15)	32.6(14)	0.1(11)	-8.0(11)	2.0(12)
O5	23.3(12)	26.2(14)	26.5(12)	2.5(10)	-7.9(10)	2.1(10)
N1	19.0(13)	27.0(15)	15.7(12)	1.4(11)	-1.7(11)	-2.9(12)
C1	13.5(13)	35(2)	15.5(14)	0.4(14)	1.5(11)	-1.0(14)
C2	13.0(15)	28.4(18)	19.2(15)	0.2(13)	0.7(11)	-2.7(13)

Table D.27. Anisotropic Displacement Parameters ($Å^2 \times 10^3$) for **4.48i**. The Anisotropic displacement factor exponent takes the form: $-2\pi^2[h^2a^{*2}U_{11}+2hka^*b^*U_{12}+\ldots]$.

Atom	U_{11}	U_{22}	U_{33}	U_{23}	U_{13}	U_{12}
C3	15.0(15)	31.1(19)	15.7(14)	4.9(13)	-0.8(11)	0.1(13)
C4	16.1(14)	30.8(18)	17.3(14)	-2.2(13)	3.3(12)	0.5(15)
C5	20.4(15)	40(2)	18.6(15)	2.0(15)	-2.2(13)	-0.8(15)
C6	20.0(16)	46(2)	18.3(16)	-3.2(15)	-4.0(12)	-1.6(16)
C7	17.0(15)	32(2)	20.3(15)	-5.6(13)	3.2(12)	-4.5(14)
C8	14.5(14)	28.0(17)	18.5(14)	-1.7(13)	2.5(12)	-2.6(14)
C9	13.7(14)	29.9(19)	13.4(14)	-1.5(12)	2.6(11)	-2.2(13)
C10	17.0(15)	28.4(18)	21.2(16)	0.3(14)	-0.1(12)	-3.4(14)
C11	19.7(17)	34(2)	39(2)	1.7(17)	-2.5(14)	1.3(16)
C12	29.9(19)	27(2)	36(2)	-0.2(15)	-0.3(16)	-2.4(16)
C13	15.2(15)	27.8(18)	19.4(15)	0.3(13)	-4.5(12)	-1.4(14)
C14	15.2(15)	28.8(18)	20.4(15)	1.2(13)	2.3(12)	2.0(14)
C15	19.2(16)	35(2)	23.5(17)	-0.8(14)	-2.4(12)	3.1(14)
C16	19.9(16)	30(2)	38(2)	-5.7(15)	0.8(14)	1.3(15)
C17	26.8(19)	30(2)	36(2)	3.7(15)	11.0(15)	0.0(15)
C18	28.8(18)	45(2)	22.2(17)	3.8(16)	5.2(13)	-0.4(18)
C19	19.5(16)	39(2)	21.3(16)	-1.5(14)	0.2(13)	-1.0(16)
C20	19.4(16)	26.4(18)	24.2(16)	2.0(13)	-2.4(13)	0.5(14)
C21	16.4(15)	30.2(19)	24.4(17)	9.4(14)	-4.2(13)	-0.7(14)
C22	19.4(17)	38(2)	28.1(17)	7.1(15)	0.8(13)	-3.4(15)
C23	26.1(18)	40(2)	32(2)	12.6(17)	7.1(16)	-8.4(17)
C24	40(2)	32(2)	37(2)	15.3(17)	4.1(17)	8.1(18)
C25	20.0(18)	53(3)	43(2)	20(2)	8.6(16)	10.6(17)

Table D.27. Anisotropic Displacement Parameters ($Å^2 \times 10^3$) for **4.48i**. The Anisotropic displacement factor exponent takes the form: $-2\pi^2[h^2a^{*2}U_{11}+2hka^*b^*U_{12}+\ldots]$.

Atom	U_{11}	U_{22}	U_{33}	U_{23}	U_{13}	U_{12}
C26	17.4(16)	65(3)	48(2)	28(2)	-7.8(16)	-1.8(19)
C27	27.6(19)	46(2)	31(2)	14.5(17)	-12.7(15)	-5.4(17)
C28	27.0(18)	38(2)	31.1(19)	6.8(16)	-10.2(15)	-1.7(17)
C29	23.9(18)	49(2)	29.5(18)	15.9(17)	-1.1(15)	0.1(18)
C30	17.8(16)	36(2)	35.1(19)	14.2(17)	5.7(14)	0.8(16)
Br1A	21.11(16)	34.6(2)	25.90(17)	0.38(14)	-3.23(13)	-5.48(15)
O1A	37.9(15)	30.2(15)	26.2(13)	4.4(11)	-12.9(11)	-1.4(11)
O2A	19.5(11)	30.1(14)	25.9(12)	-9.0(10)	-2.0(9)	1.6(10)
O3A	16.0(11)	29.4(13)	22.3(11)	-0.6(9)	-1.4(9)	1.3(10)
O4A	28.6(13)	28.8(14)	29.5(12)	0.8(10)	-4.5(10)	-6.8(11)
O5A	22.7(12)	26.3(13)	28.0(12)	6.1(10)	-4.5(9)	-5.2(10)
N1A	19.7(13)	26.0(15)	19.8(13)	6.3(12)	-2.3(10)	1.2(12)
C1A	21.0(16)	26.0(18)	20.7(16)	-0.3(13)	-0.6(13)	1.5(14)
C2A	20.2(15)	24.5(17)	19.4(15)	-1.8(12)	0.4(12)	4.6(14)
C3A	19.2(15)	24.1(17)	18.7(16)	0.7(12)	-0.4(12)	4.7(13)
C4A	16.0(15)	26.2(17)	16.2(14)	-3.8(13)	1.4(12)	3.2(13)
C5A	22.5(16)	24.9(17)	21.6(16)	1.4(14)	-0.9(13)	6.4(13)
C6A	19.4(16)	32(2)	18.9(15)	0.2(13)	-2.6(12)	4.4(14)
C7A	13.4(15)	27.9(18)	22.1(16)	-3.1(13)	1.9(12)	1.1(13)
C8A	18.3(15)	29.0(19)	18.3(16)	1.5(13)	1.8(12)	6.7(14)
C9A	14.7(14)	28.6(18)	13.5(14)	-1.7(12)	0.5(11)	3.0(13)
C10A	22.3(17)	33(2)	28.8(18)	-8.8(15)	-6.2(14)	0.0(15)
C11A	44(2)	47(3)	27.4(19)	-6.1(17)	-1.7(17)	-3(2)

Table D.27. Anisotropic Displacement Parameters ($Å^2 \times 10^3$) for **4.48i**. The Anisotropic displacement factor exponent takes the form: $-2\pi^2[h^2a^{*2}U_{11}+2hka^*b^*U_{12}+\ldots]$.

Atom	U_{11}	U_{22}	U_{33}	U_{23}	U_{13}	U_{12}
C12A	34(2)	33(2)	39(2)	-9.7(17)	2.5(16)	-5.4(17)
C13A	17.2(15)	26.1(18)	20.7(16)	-1.7(13)	-1.7(11)	0.8(13)
C14A	22.1(16)	20.4(16)	28.6(17)	2.9(14)	7.5(14)	-2.1(13)
C15A	28.6(19)	29(2)	27.9(18)	-1.4(15)	7.0(14)	-4.2(15)
C16A	45(2)	30(2)	30.0(18)	-2.2(16)	17.7(16)	-6.6(18)
C17A	48(3)	27(2)	41(2)	-2.4(17)	25.3(19)	0.7(18)
C18A	33(2)	32(2)	56(3)	6(2)	19.0(18)	7.7(18)
C19A	24.8(18)	28(2)	39(2)	3.4(15)	4.4(15)	2.9(15)
C20A	18.2(15)	22.1(16)	23.6(15)	-2.2(13)	-1.9(14)	1.9(13)
C21A	23.1(17)	24.9(19)	28.6(18)	7.2(14)	-5.2(13)	-6.2(14)
C22A	32(2)	30(2)	41(2)	13.4(17)	8.4(17)	6.5(18)
C23A	39(2)	31(2)	54(3)	17.9(19)	11(2)	9.8(19)
C24A	29(2)	36(2)	31.4(19)	11.1(15)	-3.5(15)	-6.8(17)
C25A	23.8(18)	46(2)	27.5(19)	4.9(17)	0.6(14)	-3.2(17)
C26A	69(3)	59(3)	28(2)	13(2)	-17(2)	-21(3)
C27A	41(3)	97(5)	52(3)	37(3)	-30(2)	-36(3)
C28A	38(2)	61(3)	49(3)	24(2)	-22.4(19)	-24(2)
C29A	24(2)	73(4)	84(4)	53(3)	-3(2)	5(2)
C30A	25.4(17)	34(2)	28.7(18)	2.6(15)	1.6(14)	-0.8(15)

Table D.28. Bond Lengths for **4.48i**.

Atom	Atom	Length/Å	Atom	Atom	Length/Å
Br1	C7	1.899(4)	Br1A	C7A	1.899(4)
O1	C1	1.237(4)	O1A	C1A	1.232(4)

Table D.28. Bond Lengths for **4.48i**.

Atom	Atom	Length/Å	Atom	Atom	Length/Å
O2	C2	1.364(4)	O2A	C2A	1.381(4)
O2	C10	1.463(4)	O2A	C10A	1.464(4)
O3	C2	1.455(4)	O3A	C2A	1.446(4)
O3	C13	1.462(4)	O3A	C13A	1.456(4)
O4	C20	1.197(5)	O4A	C20A	1.196(4)
O5	C20	1.342(4)	O5A	C20A	1.343(4)
O5	C21	1.472(4)	O5A	C21A	1.476(4)
N1	C1	1.342(5)	N1A	C1A	1.348(5)
N1	C9	1.407(4)	N1A	C9A	1.422(4)
C1	C2	1.544(5)	C1A	C2A	1.524(5)
C2	C3	1.541(4)	C2A	C3A	1.541(4)
C3	C4	1.479(5)	C3A	C4A	1.484(5)
C3	C13	1.569(5)	C3A	C13A	1.569(4)
C4	C5	1.393(5)	C4A	C5A	1.396(5)
C4	C9	1.403(5)	C4A	C9A	1.394(5)
C5	C6	1.385(6)	C5A	C6A	1.380(5)
C6	C7	1.386(6)	C6A	C7A	1.395(5)
C7	C8	1.391(5)	C7A	C8A	1.385(5)
C8	C9	1.382(5)	C8A	C9A	1.388(5)
C10	C11	1.505(5)	C10A	C11A	1.521(6)
C10	C12	1.502(5)	C10A	C12A	1.511(6)
C13	C14	1.512(5)	C13A	C14A	1.509(5)
C13	C20	1.520(5)	C13A	C20A	1.533(5)
C14	C15	1.394(5)	C14A	C15A	1.397(5)

Table D.28. Bond Lengths for **4.48i**.

Atom	Atom	Length/Å	Atom	Atom	Length/Å
C14	C19	1.391(5)	C14A	C19A	1.391(5)
C15	C16	1.379(5)	C15A	C16A	1.385(6)
C16	C17	1.388(6)	C16A	C17A	1.387(7)
C17	C18	1.381(6)	C17A	C18A	1.388(7)
C18	C19	1.395(5)	C18A	C19A	1.390(6)
C21	C22	1.530(5)	C21A	C22A	1.511(6)
C21	C28	1.519(5)	C21A	C28A	1.522(5)
C21	C30	1.528(5)	C21A	C30A	1.524(5)
C22	C23	1.544(5)	C22A	C23A	1.542(5)
C23	C24	1.521(6)	C23A	C24A	1.536(6)
C23	C29	1.538(6)	C23A	C29A	1.515(8)
C24	C25	1.531(6)	C24A	C25A	1.530(6)
C25	C26	1.532(7)	C25A	C26A	1.523(6)
C25	C30	1.536(5)	C25A	C30A	1.539(6)
C26	C27	1.530(6)	C26A	C27A	1.546(8)
C27	C28	1.537(5)	C27A	C28A	1.539(7)
C27	C29	1.536(6)	C27A	C29A	1.518(10)

Table D.29. Bond Angles for **4.48i**.

Atom	Atom	Atom	Angle/°	Atom	Atom	Atom	Angle/°
C2	O2	C10	118.4(2)	C2A	O2A	C10A	116.7(3)
C2	O3	C13	91.6(2)	C2A	O3A	C13A	91.7(2)
C20	O5	C21	123.0(3)	C20A	O5A	C21A	121.3(3)
C1	N1	C9	127.3(3)	C1A	N1A	C9A	125.3(3)

Table D.29. Bond Angles for **4.48i**.

Atom	Atom	Atom	Angle/°	Atom	Atom	Atom	Angle/°
O1	C1	N1	121.0(3)	O1A	C1A	N1A	122.2(3)
O1	C1	C2	122.1(3)	O1A	C1A	C2A	119.1(3)
N1	C1	C2	116.9(3)	N1A	C1A	C2A	118.6(3)
O2	C2	O3	114.7(3)	O2A	C2A	O3A	113.7(3)
O2	C2	C1	113.9(3)	O2A	C2A	C1A	112.0(3)
O2	C2	C3	111.0(3)	O2A	C2A	C3A	113.4(3)
O3	C2	C1	108.6(3)	O3A	C2A	C1A	107.8(3)
O3	C2	C3	91.6(2)	O3A	C2A	C3A	92.6(2)
C3	C2	C1	115.2(3)	C1A	C2A	C3A	115.9(3)
C2	C3	C13	84.4(2)	C2A	C3A	C13A	84.0(2)
C4	C3	C2	118.1(3)	C4A	C3A	C2A	117.0(3)
C4	C3	C13	120.4(3)	C4A	C3A	C13A	121.1(3)
C5	C4	C3	123.3(3)	C5A	C4A	C3A	121.8(3)
C5	C4	C9	118.2(3)	C9A	C4A	C3A	120.2(3)
C9	C4	C3	118.5(3)	C9A	C4A	C5A	118.0(3)
C6	C5	C4	121.7(3)	C6A	C5A	C4A	121.9(3)
C5	C6	C7	118.0(3)	C5A	C6A	C7A	118.3(3)
C6	C7	Br1	119.3(3)	C6A	C7A	Br1A	119.1(2)
C6	C7	C8	122.5(3)	C8A	C7A	Br1A	119.2(3)
C8	C7	Br1	118.2(3)	C8A	C7A	C6A	121.7(3)
C9	C8	C7	118.0(3)	C7A	C8A	C9A	118.6(3)
C4	C9	N1	120.2(3)	C4A	C9A	N1A	120.0(3)
C8	C9	N1	118.3(3)	C8A	C9A	N1A	118.4(3)
C8	C9	C4	121.5(3)	C8A	C9A	C4A	121.5(3)

Table D.29. Bond Angles for **4.48i**.

Atom	Atom	Atom	Angle/°	Atom	Atom	Atom	Angle/°
O2	C10	C11	106.1(3)	O2A	C10A	C11A	107.1(3)
O2	C10	C12	107.5(3)	O2A	C10A	C12A	107.5(3)
C12	C10	C11	112.6(3)	C12A	C10A	C11A	113.5(3)
O3	C13	C3	90.2(2)	O3A	C13A	C3A	91.0(2)
O3	C13	C14	111.8(3)	O3A	C13A	C14A	112.2(3)
O3	C13	C20	110.6(3)	O3A	C13A	C20A	109.2(3)
C14	C13	C3	116.2(3)	C14A	C13A	C3A	120.8(3)
C14	C13	C20	112.3(3)	C14A	C13A	C20A	108.0(3)
C20	C13	C3	113.8(3)	C20A	C13A	C3A	114.3(3)
C15	C14	C13	121.3(3)	C15A	C14A	C13A	120.7(3)
C19	C14	C13	119.5(3)	C19A	C14A	C13A	119.7(3)
C19	C14	C15	119.2(3)	C19A	C14A	C15A	119.3(3)
C16	C15	C14	120.2(3)	C16A	C15A	C14A	120.2(4)
C15	C16	C17	120.5(3)	C15A	C16A	C17A	120.2(4)
C18	C17	C16	119.9(3)	C16A	C17A	C18A	119.9(4)
C17	C18	C19	119.7(3)	C17A	C18A	C19A	120.0(4)
C14	C19	C18	120.4(3)	C18A	C19A	C14A	120.2(4)
O4	C20	O5	126.7(3)	O4A	C20A	O5A	128.0(3)
O4	C20	C13	125.3(3)	O4A	C20A	C13A	124.2(3)
O5	C20	C13	108.0(3)	O5A	C20A	C13A	107.7(3)
O5	C21	C22	111.5(3)	O5A	C21A	C22A	110.3(3)
O5	C21	C28	103.0(3)	O5A	C21A	C28A	103.6(3)
O5	C21	C30	111.7(3)	O5A	C21A	C30A	111.3(3)
C28	C21	C22	109.7(3)	C22A	C21A	C28A	109.9(4)

Table D.29. Bond Angles for **4.48i**.

Atom	Atom	Atom	Angle/°	Atom	Atom	Atom	Angle/°
C28	C21	C30	110.4(3)	C22A	C21A	C30A	111.3(3)
C30	C21	C22	110.3(3)	C28A	C21A	C30A	110.1(3)
C21	C22	C23	108.2(3)	C21A	C22A	C23A	108.1(3)
C24	C23	C22	109.1(3)	C24A	C23A	C22A	109.0(3)
C24	C23	C29	110.1(3)	C29A	C23A	C22A	110.7(4)
C29	C23	C22	109.5(3)	C29A	C23A	C24A	109.3(4)
C23	C24	C25	110.0(4)	C25A	C24A	C23A	109.6(3)
C24	C25	C26	109.4(3)	C24A	C25A	C30A	109.1(3)
C24	C25	C30	108.8(3)	C26A	C25A	C24A	109.7(4)
C26	C25	C30	110.9(4)	C26A	C25A	C30A	109.3(4)
C27	C26	C25	109.4(3)	C25A	C26A	C27A	109.5(4)
C26	C27	C28	108.9(3)	C28A	C27A	C26A	108.2(5)
C26	C27	C29	109.9(4)	C29A	C27A	C26A	109.6(4)
C29	C27	C28	108.8(3)	C29A	C27A	C28A	110.2(5)
C21	C28	C27	110.0(3)	C21A	C28A	C27A	108.9(4)
C27	C29	C23	109.0(3)	C23A	C29A	C27A	109.4(4)
C21	C30	C25	108.0(3)	C21A	C30A	C25A	108.3(3)

Table D.30. Hydrogen Bonds for **4.48i**.

D	H	A	d(D-H)/Å	d(H-A)/Å	d(D-A)/Å	D-H-A/°
N1	H1	O1A	0.85(4)	1.93(4)	2.746(4)	163(4)
N1A	H1A	O1	0.83(4)	2.26(4)	3.072(4)	165(4)

Table D.31. Torsion Angles for **4.48i**.

A	B	C	D	Angle/°	A	B	C	D	Angle/°
Br1	C7	C8	C9	-179.8(2)	Br1A	C7A	C8A	C9A	-179.9(2)
O1	C1	C2	O2	-57.2(4)	O1A	C1A	C2A	O2A	-54.6(4)
O1	C1	C2	O3	71.9(4)	O1A	C1A	C2A	O3A	71.1(4)
O1	C1	C2	C3	172.9(3)	O1A	C1A	C2A	C3A	173.1(3)
O2	C2	C3	C4	-110.4(3)	O2A	C2A	C3A	C4A	-114.8(3)
O2	C2	C3	C13	128.0(3)	O2A	C2A	C3A	C13A	123.3(3)
O3	C2	C3	C4	132.3(3)	O3A	C2A	C3A	C4A	128.0(3)
O3	C2	C3	C13	10.7(2)	O3A	C2A	C3A	C13A	6.0(2)
O3	C13	C14	C15	168.5(3)	O3A	C13A	C14A	C15A	165.5(3)
O3	C13	C14	C19	-8.9(5)	O3A	C13A	C14A	C19A	-20.7(4)
O3	C13	C20	O4	28.9(5)	O3A	C13A	C20A	O4A	21.0(4)
O3	C13	C20	O5	-150.8(3)	O3A	C13A	C20A	O5A	-159.7(3)
O5	C21	C22	C23	-174.1(3)	O5A	C21A	C22A	C23A	-174.7(3)
O5	C21	C28	C27	179.8(3)	O5A	C21A	C28A	C27A	179.0(4)
O5	C21	C30	C25	173.5(3)	O5A	C21A	C30A	C25A	175.5(3)
N1	C1	C2	O2	122.4(3)	N1A	C1A	C2A	O2A	127.1(3)
N1	C1	C2	O3	-108.5(3)	N1A	C1A	C2A	O3A	-107.2(3)
N1	C1	C2	C3	-7.5(4)	N1A	C1A	C2A	C3A	-5.2(4)
C1	N1	C9	C4	10.3(5)	C1A	N1A	C9A	C4A	11.1(5)
C1	N1	C9	C8	-168.2(3)	C1A	N1A	C9A	C8A	-167.0(3)
C1	C2	C3	C4	20.9(4)	C1A	C2A	C3A	C4A	16.8(4)
C1	C2	C3	C13	-100.7(3)	C1A	C2A	C3A	C13A	-105.1(3)
C2	O2	C10	C11	-122.4(3)	C2A	O2A	C10A	C11A	-129.6(3)
C2	O2	C10	C12	117.0(3)	C2A	O2A	C10A	C12A	108.1(3)

Table D.31. Torsion Angles for **4.48i**.

A	B	C	D	Angle/°	A	B	C	D	Angle/°
C2	O3	C13	C3	11.3(3)	C2A	O3A	C13A	C3A	6.4(3)
C2	O3	C13	C14	-107.2(3)	C2A	O3A	C13A	C14A	-117.7(3)
C2	O3	C13	C20	126.9(3)	C2A	O3A	C13A	C20A	122.6(3)
C2	C3	C4	C5	160.5(3)	C2A	C3A	C4A	C5A	163.1(3)
C2	C3	C4	C9	-19.8(4)	C2A	C3A	C4A	C9A	-15.7(4)
C2	C3	C13	O3	-10.7(2)	C2A	C3A	C13A	O3A	-6.0(2)
C2	C3	C13	C14	103.9(3)	C2A	C3A	C13A	C14A	110.8(3)
C2	C3	C13	C20	-123.4(3)	C2A	C3A	C13A	C20A	-117.7(3)
C3	C4	C5	C6	177.4(3)	C3A	C4A	C5A	C6A	-179.8(3)
C3	C4	C9	N1	4.8(4)	C3A	C4A	C9A	N1A	2.3(5)
C3	C4	C9	C8	-176.8(3)	C3A	C4A	C9A	C8A	-179.6(3)
C3	C13	C14	C15	66.8(4)	C3A	C13A	C14A	C15A	60.1(4)
C3	C13	C14	C19	-110.5(4)	C3A	C13A	C14A	C19A	-126.0(3)
C3	C13	C20	O4	128.7(4)	C3A	C13A	C20A	O4A	121.3(4)
C3	C13	C20	O5	-51.0(4)	C3A	C13A	C20A	O5A	-59.4(4)
C4	C3	C13	O3	-130.1(3)	C4A	C3A	C13A	O3A	-124.1(3)
C4	C3	C13	C14	-15.6(4)	C4A	C3A	C13A	C14A	-7.3(5)
C4	C3	C13	C20	117.2(3)	C4A	C3A	C13A	C20A	124.3(3)
C4	C5	C6	C7	-0.4(5)	C4A	C5A	C6A	C7A	-0.5(5)
C5	C4	C9	N1	-175.5(3)	C5A	C4A	C9A	N1A	-176.6(3)
C5	C4	C9	C8	2.9(5)	C5A	C4A	C9A	C8A	1.5(5)
C5	C6	C7	Br1	-179.6(3)	C5A	C6A	C7A	Br1A	-179.6(3)
C5	C6	C7	C8	2.6(5)	C5A	C6A	C7A	C8A	1.4(5)
C6	C7	C8	C9	-2.0(5)	C6A	C7A	C8A	C9A	-0.9(5)

Table D.31. Torsion Angles for **4.48i**.

A	B	C	D	Angle/°	A	B	C	D	Angle/°
C7	C8	C9	N1	177.6(3)	C7A	C8A	C9A	N1A	177.5(3)
C7	C8	C9	C4	-0.8(5)	C7A	C8A	C9A	C4A	-0.6(5)
C9	N1	C1	O1	171.4(3)	C9A	N1A	C1A	O1A	172.7(3)
C9	N1	C1	C2	-8.2(5)	C9A	N1A	C1A	C2A	-9.1(5)
C9	C4	C5	C6	-2.3(5)	C9A	C4A	C5A	C6A	-1.0(5)
C10	O2	C2	O3	-56.9(4)	C10A	O2A	C2A	O3A	-40.5(4)
C10	O2	C2	C1	69.0(4)	C10A	O2A	C2A	C1A	81.9(4)
C10	O2	C2	C3	-159.1(3)	C10A	O2A	C2A	C3A	-144.6(3)
C13	O3	C2	O2	-125.6(3)	C13A	O3A	C2A	O2A	-123.5(3)
C13	O3	C2	C1	105.8(3)	C13A	O3A	C2A	C1A	111.8(3)
C13	O3	C2	C3	-11.5(3)	C13A	O3A	C2A	C3A	-6.5(3)
C13	C3	C4	C5	-98.8(4)	C13A	C3A	C4A	C5A	-97.0(4)
C13	C3	C4	C9	80.9(4)	C13A	C3A	C4A	C9A	84.1(4)
C13	C14	C15	C16	-176.5(3)	C13A	C14A	C15A	C16A	172.9(3)
C13	C14	C19	C18	177.4(4)	C13A	C14A	C19A	C18A	-171.3(4)
C14	C13	C20	O4	-96.7(4)	C14A	C13A	C20A	O4A	-101.2(4)
C14	C13	C20	O5	83.6(3)	C14A	C13A	C20A	O5A	78.1(3)
C14	C15	C16	C17	-1.7(6)	C14A	C15A	C16A	C17A	-1.5(6)
C15	C14	C19	C18	0.0(6)	C15A	C14A	C19A	C18A	2.6(6)
C15	C16	C17	C18	1.8(6)	C15A	C16A	C17A	C18A	2.5(6)
C16	C17	C18	C19	-1.0(6)	C16A	C17A	C18A	C19A	-0.9(6)
C17	C18	C19	C14	0.1(6)	C17A	C18A	C19A	C14A	-1.6(6)
C19	C14	C15	C16	0.8(5)	C19A	C14A	C15A	C16A	-1.0(5)
C20	O5	C21	C22	-61.0(4)	C20A	O5A	C21A	C22A	-64.1(4)

Table D.31. Torsion Angles for **4.48i**.

A	B	C	D	Angle/°	A	B	C	D	Angle/°
C20	O5	C21	C28	-178.6(3)	C20A	O5A	C21A	C28A	178.3(3)
C20	O5	C21	C30	63.0(4)	C20A	O5A	C21A	C30A	60.0(4)
C20	C13	C14	C15	-66.6(4)	C20A	C13A	C14A	C15A	-74.1(4)
C20	C13	C14	C19	116.1(4)	C20A	C13A	C14A	C19A	99.8(4)
C21	O5	C20	O4	-3.2(6)	C21A	O5A	C20A	O4A	2.9(5)
C21	O5	C20	C13	176.6(3)	C21A	O5A	C20A	C13A	-176.4(3)
C21	C22	C23	C24	-59.7(4)	C21A	C22A	C23A	C24A	-60.1(5)
C21	C22	C23	C29	60.9(4)	C21A	C22A	C23A	C29A	60.2(5)
C22	C21	C28	C27	61.0(4)	C22A	C21A	C28A	C27A	61.1(5)
C22	C21	C30	C25	-61.9(4)	C22A	C21A	C30A	C25A	-61.0(4)
C22	C23	C24	C25	60.7(4)	C22A	C23A	C24A	C25A	60.8(5)
C22	C23	C29	C27	-61.0(4)	C22A	C23A	C29A	C27A	-58.9(5)
C23	C24	C25	C26	59.8(4)	C23A	C24A	C25A	C26A	59.2(4)
C23	C24	C25	C30	-61.4(5)	C23A	C24A	C25A	C30A	-60.5(4)
C24	C23	C29	C27	59.0(4)	C24A	C23A	C29A	C27A	61.1(5)
C24	C25	C26	C27	-59.9(4)	C24A	C25A	C26A	C27A	-58.5(5)
C24	C25	C30	C21	60.9(5)	C24A	C25A	C30A	C21A	59.4(4)
C25	C26	C27	C28	-58.9(5)	C25A	C26A	C27A	C28A	-60.8(6)
C25	C26	C27	C29	60.3(4)	C25A	C26A	C27A	C29A	59.4(5)
C26	C25	C30	C21	-59.4(4)	C26A	C25A	C30A	C21A	-60.5(5)
C26	C27	C28	C21	59.7(4)	C26A	C27A	C28A	C21A	60.5(6)
C26	C27	C29	C23	-59.4(4)	C26A	C27A	C29A	C23A	-60.7(5)
C28	C21	C22	C23	-60.7(4)	C28A	C21A	C22A	C23A	-61.1(4)
C28	C21	C30	C25	59.5(4)	C28A	C21A	C30A	C25A	61.2(4)

Table D.31. Torsion Angles for **4.48i**.

A	B	C	D	Angle/°	A	B	C	D	Angle/°
C28	C27	C29	C23	59.8(5)	C28A	C27A	C29A	C23A	58.2(5)
C29	C23	C24	C25	-59.5(4)	C29A	C23A	C24A	C25A	-60.3(4)
C29	C27	C28	C21	-60.1(4)	C29A	C27A	C28A	C21A	-59.3(5)
C30	C21	C22	C23	61.1(4)	C30A	C21A	C22A	C23A	61.2(4)
C30	C21	C28	C27	-60.8(4)	C30A	C21A	C28A	C27A	-61.9(6)
C30	C25	C26	C27	60.0(4)	C30A	C25A	C26A	C27A	61.1(5)

Table D.32. Hydrogen Atom Coordinates (Å×10⁴) and Isotropic Displacement Parameters (Å²×10³) for **4.48i**.

Atom	*x*	*y*	*z*	U(eq)
H1	4280(40)	3710(30)	6309(11)	25
H3	5076.73	1256.91	7095.64	25
H5	6433.8	2317.7	7484.43	31
H6	7007.92	3859.56	7646.34	34
H8	5339.15	4840	6701.68	24
H10	2486.26	793.52	6234.9	27
H11A	869.59	1236.8	6843.09	46
H11B	355.11	870.79	6449.7	46
H11C	1069.89	1861.93	6475.37	46
H12A	3019.44	-593.86	6571.1	47
H12B	1599.86	-640.86	6442.49	47
H12C	1938.03	-380.39	6865.16	47
H15	8109	2071.02	6778.42	31
H16	9379.24	3076.16	6435.44	35
H17	9028.71	3305.96	5798.66	37

Table D.32. Hydrogen Atom Coordinates (Å×10⁴) and Isotropic Displacement Parameters (Å²×10³) for **4.48i**.

Atom	*x*	*y*	*z*	U(eq)
H18	7324.35	2596.67	5511.09	38
H19	6009.24	1611.77	5858.31	32
H22A	6636.34	-1386.87	7195.47	34
H22B	6261.74	-714.8	7539.08	34
H23	7100.12	-2181.36	7770.75	39
H24A	8432.36	-2505.3	7257.91	44
H24B	9197.16	-2569.35	7640.94	44
H25	10349.96	-1676.13	7197.45	46
H26A	10591.68	-1224.87	7834.33	52
H26B	10719.55	-307.15	7573.05	52
H27	9372.87	46.95	8082.47	42
H28A	7652.59	621.92	7725.61	38
H28B	8917.42	815.09	7503.02	38
H29A	7455.7	-796.97	8144.11	41
H29B	8593.44	-1520.52	8189.12	41
H30A	9506.7	-229.75	6957.91	36
H30B	8621.75	-1098.17	6844.4	36
H1A	2770(40)	3810(30)	5780(12)	26
H3A	2273.34	6637.51	5199.7	25
H5A	979.27	5830.8	4711.41	28
H6A	-292.15	4551.71	4564.21	28
H8A	1321.68	3024.31	5396.91	26
H10A	4673.62	6718.59	6100.71	34

Table D.32. Hydrogen Atom Coordinates (Å×10⁴) and Isotropic Displacement Parameters (Å²×10³) for **4.48i**.

Atom	*x*	*y*	*z*	U(eq)
H11D	2573.34	7436.75	6503.23	59
H11E	3942.66	7395	6674.47	59
H11F	3223.64	6435.1	6576.61	59
H12D	4517.48	8065.22	5715.09	53
H12E	4813.9	8392.5	6133.37	53
H12F	3434.75	8482.47	5972.48	53
H15A	3342.87	5201.27	4458.95	34
H16A	4351.58	4057.4	4100.75	42
H17A	6308.24	3508.31	4278.04	47
H18A	7192.77	4022.36	4838.56	49
H19A	6143.44	5116.08	5213.29	37
H22C	4016.38	8925.04	4673.48	42
H22D	2557.9	8744.36	4617.95	42
H23A	3157.79	10171.91	4299.98	50
H24C	4592.99	10081.98	3793.75	38
H24D	5252.66	9730.86	4170.43	38
H25A	5689.96	8647.01	3675.13	39
H26C	4025.22	7762.41	3407.79	63
H26D	3849.39	8869.52	3322.16	63
H27A	1920.07	8217.32	3536.47	76
H28C	1815.79	7559.72	4153.33	59
H28D	2795.04	6971.63	3908.2	59
H29C	2326.15	9823.22	3701.84	73

Table D.32. Hydrogen Atom Coordinates (Å×10⁴) and Isotropic Displacement Parameters (Å²×10³) for **4.48i**.

Atom	*x*	*y*	*z*	U(eq)
H29D	1510.42	9322.12	4020.05	73
H30C	5070.53	7225.63	3994.17	35
H30D	5562.43	7990.26	4291.1	35

D.5 References

[1] Bruker-AXS (2016). APEX3. Version 2016.5-0. Madison, Wisconsin, USA.

[2] Krause, L., Herbst-Irmer, R., Sheldrick, G. M. & Stalke, D. (2015). J. Appl. Cryst. 48. 3-10.

[3] Sheldrick, G. M. (2013b). XPREP. Version 2013/1. Georg-August-Universität Göttingen, Göttingen, Germany.

[4] Sheldrick, G. M. (2013a). The SHELX homepage, http://shelx.uni-ac.gwdg.de/SHELX/.

[5] Sheldrick, G. M. (2015a). Acta Cryst. A, 71, 3-8.

[6] Sheldrick, G. M. (2015b). Acta Cryst. C, 71, 3-8.

[7] Dolomanov, O. V., Bourhis, L. J., Gildea, R. J., Howard, J. A. K. & Puschmann, H. (2009). J. Appl. Crystallogr. 42, 339-341.

[8] Guzei, I. A. (2007-2013). Programs Gn. University of Wisconsin-Madison, Madison, Wisconsin, USA.